SACO RIVER AND CAMP ELLIS BEACH

SECTION 111 SHORE DAMAGE MITIGATION STUDY

APPENDIX C

DATA COLLECTION AND MODELING REPORT
(Volumes 1 and 2)

FINAL REPORT

Volume I

Saco River and Camp Ellis Beach

Data Collection and Modeling Report

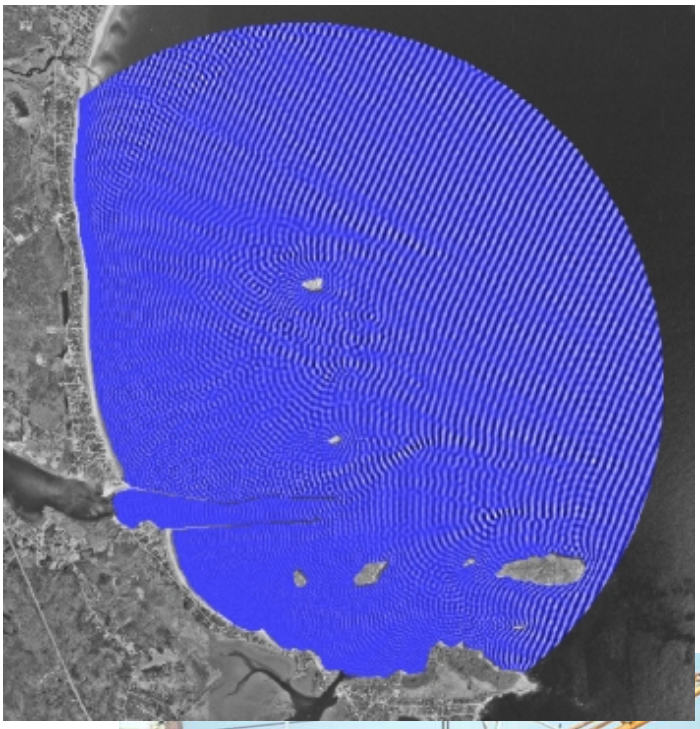

Prepared For:
United States Army Corps of Engineers
New England District
696 Virginia Road
Concord, MA 01742

Prepared By:

Woods Hole Group
Environmental Laboratories

Aubrey Consulting, Inc..
81 Technology Park Drive
East Falmouth, MA 02536

October 2006

SACO RIVER AND CAMP ELLIS BEACH
DATA COLLECTION AND MODELING REPORT

Saco River and Camp Ellis Beach, ME

October 2006

Prepared for:

U.S. Army Corps of Engineers
New England District
696 Virginia Road
Concord, MA 01742

Prepared by:

Woods Hole Group
Environmental Laboratories
375 Paramount Drive, Suite 2
Raynham, MA 02767

Aubrey Consulting, Inc.
81 Technology Park Drive
East Falmouth, MA 02536
(508) 540-8080

Table of Contents

LIST OF FIGURES

LIST OF TABLES

LIST OF ABBREVIATIONS

ACI	Aubrey Consulting, Inc.
ADCP	Acoustic Depth Current Profiler
CERC	Coastal Engineering Research Center
cfs	cubic feet per second
CHL	Coastal Hydraulics Laboratory
cm	centimeter
cy	cubic yard
DGPS	Differential Global Positioning System
DOQ	digital orthophoto quads
E	East
ENE	East Northeast
ESE	East Southeast
ft	feet
GEODAS	Geophysical Data System
GoMOOS	Gulf of Maine Ocean Observing System
in	inch
ka	1,000 calendar years
khz	kilohertz
km	kilometers
kts	knots
m	meter
mi	statute mile
mm	millimeter
MHW	Mean High Water
MLW	Mean Low Water
MSL	Mean Sea Level
MTL	Mean Tide Level
MWL	Mean Water Level
N	North
NAD	North American Datum

NASA	National Aeronautics and Space Administration
NAVD	North America Vertical Data
NCDC	National Climatic Data Center
NE	Northeast
NGDC	National Geophysical Data Center
NGVD	National Geodetic Vertical Datum
NNE	North Northeast
NNW	North Northwest
NOAA	National Oceanic and Atmospheric Administration
NOS	National Ocean Service
NW	Northwest
PO.DAAC	Physical Oceanography Distributed Active Archive Center
RMS	root-mean-square
S	South
s	second
SE	Southeast
SOWM	Navy's Spectral Ocean Wave Model
SSE	South Southeast
SW	Southwest
SSW	South Southwest
USACE	U.S. Army Corps of Engineers
USC&GS	U.S. Coast and Geodetic Survey
UTM	Universal Transverse Mercator
W	West
WIS	Wave Information Study
WNW	West Northwest
WSW	West Southwest
yd	yard
yr	year

1.0 INTRODUCTION

The City of Saco and its Camp Ellis Beach neighborhood, (Figure 1-1), is located on the east bank of the Saco River in York County, Maine. Camp Ellis is located at the River's mouth (discharging into Saco Bay). Camp Ellis Beach lies adjacent to the north jetty, which is part of the Federal Navigation Project for the Saco River. Although the site of numerous geological studies, the Camp Ellis/Saco Bay area represents a complex coastal setting where waves, sediment transport, and other coastal processes have not been well understood. The highly irregular offshore bathymetry, nearby islands, tidal shoals, 3 to 4 m (9.8 to 13.1 ft) tidal range, mile-long coastal structures, and the overall crenulate-shape of Saco Bay all influence wave propagation and resulting sediment transport in the vicinity of Camp Ellis Beach and the Saco River Jetties. Camp Ellis Beach has been subject to shoreline change including significant erosion over the past several decades. Significant studies of the region have been performed, as presented in Chapter 2.0, including physical models, engineering analysis, and geological assessment, but these have provided conflicting viewpoints and left the local community with no resolution to the ongoing erosion. In an effort to mitigate the erosion, the United States Army Corps of Engineers (USACE) decided that a data collection program and more rigorous numerical modeling approach, evaluating waves and sediment transport from a generation-scale to nearshore-scale, was required to provide a definitive resolution to the decade-long controversy. In this particular case, high-level numerical modeling and science functioned not only to understand the physical processes at work, but also provided potential design solutions to an erosion problem plaguing the community.

The impact of waves on the nearshore environment, specifically on shorelines that are highly populated or serve significant recreational and/or economic benefits, requires knowledge of wave propagation, wave transformations, and wave predictions for site-specific areas. The impact of waves on nearshore processes and shoreline change is highly dependent on the offshore wave climate and the transformation of waves propagating to the shoreline. Subsequently, as the waves interact with the coastline, wave-induced currents are a major component of sediment transport and shoreline change. Therefore, a key component of understanding the coastal processes and erosion occurring at Camp Ellis Beach is determining the nature of the wave field both offshore and in the nearshore region of Saco Bay.

The present study was undertaken at the request of the United States Army Corps of Engineers, New England District, Engineering and Planning Division, under Contract DACW33-02-D-0006. The work was in support of the Saco River and Camp Ellis Beach Section 111 Project and was conducted by Aubrey Consulting, Inc., a member of the Woods Hole Group of companies, located in Falmouth, Massachusetts. Aubrey Consulting, Inc. was a subconsultant to Woods Hole Group Environmental Laboratories, which subsequently was purchased by Alpha Analytical Laboratories during the study time period.

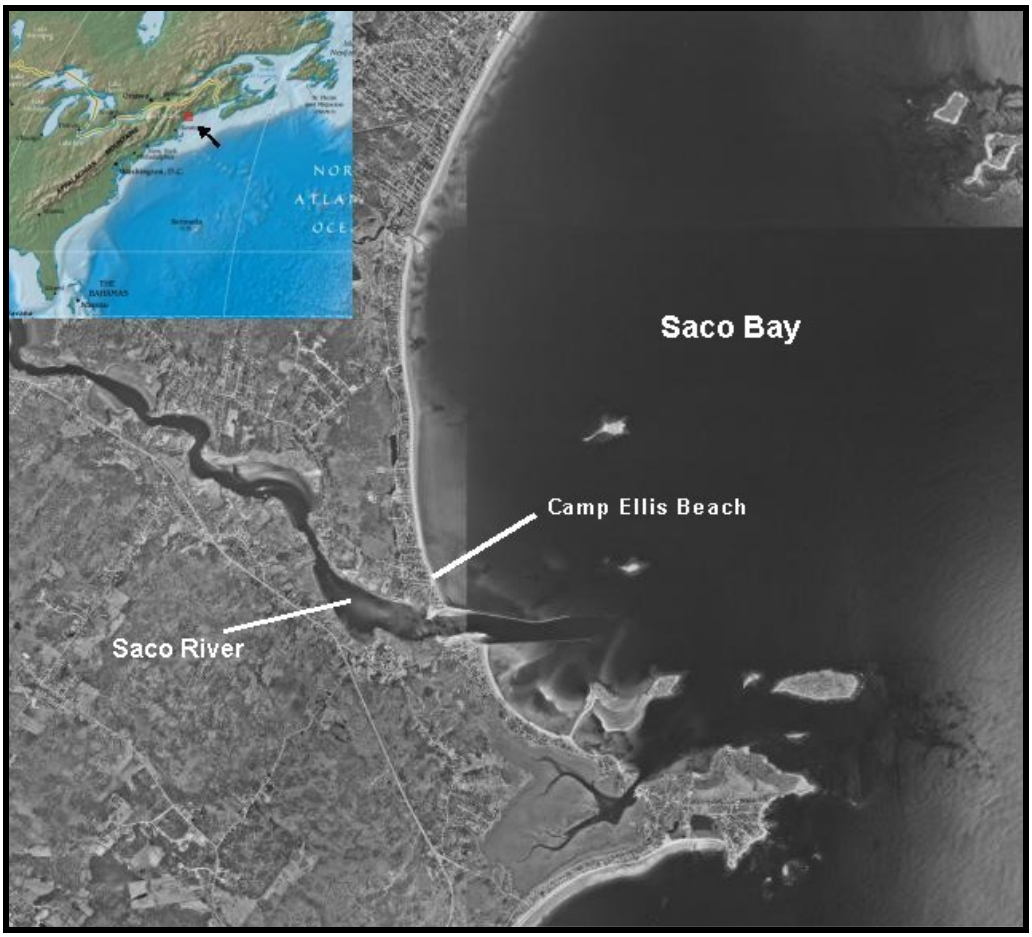

Figure 1-1. Saco Bay, Saco River and Camp Ellis Beach, Maine.

The purpose of this study is to evaluate the likely success of potential engineered alternatives to the ongoing erosion at Camp Ellis Beach, and to identify and evaluate viable solutions. The study focuses on evaluating the physical processes (concentrating on the wave environment) occurring within the vicinity of Saco Bay, and specifically the Camp Ellis Beach region, to assess potential alternatives that may be used to mitigate the erosion along the shoreline. There are two main components of the study: a field data collection component, and a numerical modeling component. The field data collection component consisted of observing the existing site-specific conditions (e.g., waves, currents, tides, bathymetry, etc.) and the historic environment (e.g., shoreline change, offshore wave data, existing studies, etc.) to develop an initial understanding of the ongoing coastal processes that shape the Camp Ellis shoreline. The field data also served to provide the required data for developing predictive models of the Camp Ellis region. More specifically, the data collected during the field program provide the information needed to both drive and verify the numerical models to assure that they accurately represent the coastal processes occurring at Camp Ellis. The numerical modeling component of the study consists of simulating the existing conditions within the vicinity of Camp Ellis, verifying the models' performance with observed data, and subsequently, utilizing the verified models to simulate various alternatives for shoreline protection. The

numerical modeling portion of the study ultimately evaluated the performance of each considered alternative and the ability to sustain a protective beach at Camp Ellis. All elements of the project, both in the field data collection and numerical modeling components, are geared towards arriving at a technically feasible, cost-effective, and long-term solution to this local coastal erosion.

The report follows a logical step-by-step process that presents the data collection and numerical modeling components, describes the screening process used to develop and assess alternatives, and selects final alternatives having the greatest potential for success. The data collection section of the report consists of Chapters 2.0 through 7.0. The numerical modeling section of the report consists of Chapters 8.0 through 12.0. Specific task numbers are also provided for each Chapter. These task numbers correspond to the task numbers presented in the original scope of work provided by the USACE.

1.1 Data Collection

A wide spectrum of field measurements was collected during March to June of 2003, including bathymetry, tides, nearshore currents, and waves. The data collection component of the study was geared towards understanding the physical processes at work, and providing valuable information for building and verifying the numerical modeling system. The data collection portion of the study is organized and divided into the following main chapters.

Chapter 2.0 (Task 1) focuses on the human use history of Saco Bay and Camp Ellis Beach, and presents previous studies that had been completed for the region at the time of this study. This does not included studies that were in-progress or not yet published at the time of this study. This Chapter also provides a brief summary of the local geology and previous observations related to potential sediment sources and transport patterns. In essence, Chapter 2.0 sets the backdrop for the study.

Chapter 3.0 (Task 17) presents a historical shoreline change analysis of the entire Saco Bay littoral system, extending from Prout's Neck and Scarborough River in the north to Saco River and Fletcher's Neck in the south. The analysis used various data sets spanning from 1864 to 1998 to assess the historical shoreline changes within Saco Bay. Utilizing the historical maps, data, and information, the shoreline change analysis was used to interpret the magnitude and direction of sediment transport, monitor the historic impact of engineering modifications to the region, examine geomorphic variations in the coastal zone, and verify the numerical nearshore and sediment transport models. Additional more recent changes to the shorelines have occurred since 1998. But these data were not available at the time of this study.

Chapter 4.0 (Task 3) presents the bathymetric data collection effort for the nearshore area offshore of Camp Ellis Beach. A high-resolution nearshore bathymetric survey was conducted near the mouth of the Saco River to provide up-to-date information for the local and nearshore (local) wave model simulations.

Chapter 5.0 (Task 12) presents the time series of pressure observations (used to calculate water levels) collected from the Saco River region. Time series of water surface

elevation were obtained from 4 locations to the region over approximately 2 (two) months and applied within the numerical wave transformation modeling.

Chapter 6.0 (Task 13) presents tidal current characterization within the Saco River and offshore of Camp Ellis Beach. The current observations define the spatial structure of the currents within the region.

Chapter 7.0 (Task 2) presents the wave data collection component of the project. The wave data were a critical component of the overall project and were used to calibrate and verify the numerical wave transformation models. Chapter 7.0 details the wave data collection procedures, presents the observations and data analysis, and provides comparisons to other offshore wave observations.

1.2 Numerical Modeling

A comprehensive numerical wave modeling system and application were developed for the Saco Bay area. The modeling system is able to simulate wave conditions from wave generation-scale (utilizing satellite wind data), through transformation-scale, to high resolution local scale. Each subsequent model builds on the results from the previous model. Spectral input conditions were passed forward at each transition, with each model progression resulting in an increase in resolution, added complexity, and incorporation of additional wave dynamics and structural interactions. Each model was calibrated, verified, and/or validated. Validated models were then used to evaluate potential alternatives for reducing wave energy, and subsequently sediment erosion in the Camp Ellis region. The entire modeling system, therefore, consists of the integration of multiple validated wave models taking waves from their offshore generation to their interaction at the coastline.

The numerical modeling portion of the study is organized and divided into the following main chapters.

Chapter 8.0 (Task 16) presents the generation-scale wave modeling. Due to many limitations in the temporal availability and parameters observed of the offshore wave data, both regional wind fields and an offshore, spectral, wave generation model were applied to generate directional waves for a wide range of time periods, as well as to provide wave forcing information directly at the boundary of the regional wave model. Chapter 8.0 details the development and utilization of the generation-scale wave modeling effort.

Chapter 9.0 (Task 5) presents the results of the regional wave modeling effort. Wave modeling conducted on a regional scale (Saco Bay) is detailed and utilized to propagate the waves at a transformation-scale level. Wave information is taken from the generation scale results and transformed to the nearshore environment. Chapter 9.0 presents the development, verification, and results of the transformation-scale (regional) modeling effort.

Chapter 10.0 details the development of the engineered alternatives to be evaluated, summarizes the 30 alternatives considered in the alternatives analysis, and presents the

methodology for screening and assessment of the various alternatives. Both the initial screening and final screening processes are presented.

Chapter 11.0 (Task 6A) provides the development, calibration, verification, and results for the nearshore, (local) wave modeling. The local phase-resolving wave modeling uses wave spectra output from the transformation-scale (regional) model and encompasses additional wave processes important in the nearshore vicinity of Camp Ellis. This nearshore (local) phase resolving wave model is used to evaluate the local physical processes, and subsequently the engineering alternatives. Results for both existing conditions and post-alternative conditions are presented. Therefore, Chapter 11.0 also presents the initial screening analysis of the alternatives and the comparison of pre- and post-alternative results.

Chapter 12.0 (Task 8) presents the final results of the alternative analysis through assessment of the sediment transport regime and patterns. The ultimate goal of the overall project is to create a sustainable beach at Camp Ellis Beach through sediment supplied through local maintenance dredging. Therefore, an assessment of the performance of each of the final alternatives, coupled with a beach nourishment program, is presented. This information can be used to guide cost-benefit-analysis and compare the effectiveness of each solution over the design life. Chapter 12.0 also presents a regional sediment transport analysis using the results of the regional wave modeling.

Finally, Chapter 13.0 presents the conclusions of the study and a final summary of the alternatives analysis.

2.0 HISTORY AND PREVIOUS STUDIES (TASK 1)

The chapter provides a brief history and summary of the previous studies conducted in the area. It is not intended to be a comprehensive review of the entire body of work for the region, rather the chapter provides a summary of the area, the history of the inlet, and a backdrop for the current technical analysis. At the time of the study presented herein (2002-2004), there were a number of ongoing studies being conducted (e.g., Brothers, et al., in press) that were either in publication or not yet completed. Personal discussions were conducted with authors of unpublished literature if possible. These more recent studies are not referenced herein since the content was not fully available when this task was being completed. However, discussions were conducted with the authors' during the development of the work presented herein to provide an understanding of the most recent work being conducted. In addition, a significant purpose of this study was to conduct an unbiased technical assessment of the coastal processes influencing the region based on data that had never previously been collected in the area (e.g. nearshore spectral wave data). As such, this section presents only a cursory overview of the history and previous studies to provide background for the reader.

The Saco River estuary is located at the southern end of a sandy barrier system within the Saco embayment, (in southern Maine). The Saco River is one of the largest rivers in southern Maine and gives rise to the state's largest beach and salt marsh system (Kelley et al., 1989; Kelley et al., 1995). Due to the rocky nature of the majority of the northern New England coastline, tidal inlet and barrier island beach development in the region is limited to isolated areas having adequate glacial and riverine sediment supplies. Barriers and tidal inlets in south coastal Maine locations, like Saco Bay, are associated with major river systems due to the abundance of sand transported to the coast by these rivers since the last deglaciation (Fitzgerald et al., 2002). The Saco inlet has been classified as a riverine-associated tidal inlet with significant freshwater discharge, especially in the late winter and early spring (Fitzgerald et al., 2002). Historically, navigation within the inlet has been difficult due to the presence of a significant tidal delta at the inlet mouth. Sediment deposition at the inlet mouth created shallow sandbars and ledges that required cautious piloting in order to navigate the channel. The navigational hazards became more acute during the mid-19th century as the Biddeford and Saco mills began to import coal and export textile goods, requiring larger ships having deeper drafts (Kelley and Anderson, 2000).

As a response to increasing ship traffic and to ensure safe navigation in the Saco River, in 1827 the United States Army Corps of Engineers (USACE) started work to stabilize the inlet, and continued to construct/modify structures in the area until 1969. By the beginning of the 20th century, shortly after the initial construction of coastal engineering structures at the mouth of the Saco River (1866), the erosion of Camp Ellis Beach commenced subsequent to a brief period of accretion (USACE, 1955; Kelley and Anderson, 2000). Presently, the Maine Geological Survey classifies Camp Ellis Beach as "Highly Erosional." Highly Erosional shorelines are defined as those shorelines that have high erosional rates (more than two feet per year if known), have high reinforced seawalls along the frontal dunes, are in need of beach replenishment to replace eroded sand, and have no recreational opportunities for about half the tidal cycle (Maine State

Planning Office, 1998). To date, erosion at Camp Ellis Beach has been responsible for the loss of more than 30 homes and repetitive storm damage to roads and streets (Slovinsky and Dickson, 2003).

2.1 Local Geology

The Saco embayment is framed by a basement of pre-Quaternary igneous and metamorphic rock (Osberg et al., 1985). These formations (Precambrian and Paleozoic Cape Elizabeth and Kittery Formations) have been traced directly from coastal outcrops to the subsurface (Osberg et al., 1985; Belknap et al., 1989; Belknap and Shipp, 1991). Subsequent fluvial erosion and Pleistocene glacial scouring have shaped the basement with an irregular upper surface having abundant narrow ridges and pinnacles. These morphological features are responsible for the offshore islands in the bay, including Ram Island, 520 meters (1,700 feet) north of the northern Saco River breakwater, and Eagle Island, 1980 meters (6,500 feet) east of Ferry Beach. Most of the basement bedrock surface is uncomfortably overlain by late Wisconsinan glacial till and/or glaciomarine silt and clay (Presumpscott Formation), which comprises the majority of the Pleistocene deposits in the region (Bloom, 1963). Shallow subaqueous geology of the bay has been identified using side-scan sonar and shallow subsurface seismic techniques. Kelley et al. (1986) analyzed the seismic stratigraphy of Saco Bay using low-resolution seismic profiles of the outer bay. They inferred that a thick deposit of sand floored Saco Bay, concluding that this sand must have been derived from the Saco River, and this same sand was the source for the beaches in the area. More recent studies (Kelley et al., 1995) using more sophisticated techniques (bottom samples, side-scan sonar records, and seismic reflection profiles) have produced an accurate picture of the geologic framework of the bay. Exposed bedrock covers 8% of the bay, cropping out on the shallow submerged margins of all islands in the Bay seaward of the peninsulas at Biddeford Pool and Prouts Neck. Mixed rock and gravel occupies 30% of the bay bottom and is the most common seafloor environment. Rippled coarse sand and gravel cover 9% of the Saco Bay and are located in extensive fields to the south of Prouts Neck and Richmond Island. Medium-fine sand occurs in water depths less than 15 m (50 ft) directly offshore of many beaches in the region, with a northward fining trend in grain size of the sediment located between 5 and 7 m (16 and 23 ft) in depth (Farrell, 1972; Kelly et al., 1995). Muddy sand covers the previously mapped Shelf Valleys, between Prouts Neck and Cape Elizabeth (Kelly et al., 1995). Seismic records indicate that this large muddy sand area delineates an area where glacial-marine sediment crops out on the seafloor and may be a lag deposit (Kelley et al., 1989).

The geology of the Saco River itself has been investigated with recent sedimentological and hydrological studies (Fitzgerald et al., 2002). The lower (seaward) 10 kilometers (6.2 miles) of the river cuts into bedrock at several locations and its morphology is characterized by relatively deep gorges (5-8 m or 16.4-20.2 ft) separated by wide, shallow reaches (2–4 m or 6.5 -13.1 ft) bordered by marshes and tidal flats (Fitzgerald et al., 2002). Most of the river bottom is covered by medium- to-coarse-grained sand except in the gorges where cobbles and boulders predominate (Manthorp et al., 1994; Manthorp, 1995; Fitzgerald et al., 2002). The river mouth itself is shallow, less than 3.0 m (10 ft) deep naturally, and is currently stabilized by two jetties.

2.2 Estuarine Regime

Several comprehensive studies of the hydrographic regime of the Saco River estuary have been completed since the 1990's (Fitzgerald et al., 1993; Kelley et al., 1995; Manthorp, 1995; Fitzgerald et al., 2002). These studies gathered hydrographic and sedimentological data from the lower 10 km (6.2 miles) of the Saco River and Saco Bay, including profile measurements of current velocities, temperature, and salinity at various locations within the estuary. The surveys were carried out during several years (1991, 1992, 1993) and during varying tidal and freshwater discharge conditions to understand the hydrographic regime of the estuary.

Fitzgerald et al. (2002) found that during normal river stages (majority of the year), the estuary is highly stratified with well-defined thermoclines and haloclines. The upper two-thirds of the estuary is, on average, ebb-dominated (Fitzgerald et al., 2002). However, the lower third of the estuary experiences dominant average ebb flows in the upper portion of the water column, whereas bottom currents are flood dominant (excess flood current of 4 to 16 cm/s), exemplifying the characteristics of a classic salt-wedge estuary. During spring freshet events, the riverine discharge increases by more than an order of magnitude, fully displacing the tidal prism, which is usually greater than ten times the freshwater discharge, resulting in total domination of the estuary by riverine processes (Manthorp et al., 1994; Barber, 1995; Fitzgerald et al., 2002). Under these conditions, estuarine flow is ebb dominant at all stages of the tide throughout the water column, and this condition may persist for days or weeks.

2.3 Offshore Regime

The offshore regime was studied by Dickson et al. (1993a) and Kelley et al. (1995) using current meter arrays deployed at various locations within outer Saco Bay. In both studies, the current meters measured mean currents, tidal currents, wave orbital motion and wind-driven circulation. Fair-weather tidal current velocities were less than 15 cm/s on average and rotary in nature, resulting in a tidal ellipse. The greatest velocities in the ellipse were into and out of Saco Bay (northwest-southeast) along the axis of the shelf valley, but never strong enough to transport sand and gravel (Dickson et al., 1993a). Wave-orbital currents capable of transporting sand and gravel were observed on several occasions. Wave-induced orbital currents reached 48 cm/s, measured beneath 2 m (6.6 ft) storm waves with a period of 10 s during a March 19, 1992 northeaster. However, the reversing nature of these currents (onshore-offshore) probably led to little net sediment movement (Kelley et al., 1995). Kelley et al. (1995) also observed wind-driven circulation that produced current velocities capable of sediment transport. Prolonged offshore-directed bottom currents, lasting up to 12.0 hours and having magnitude of 35 cm/s, were produced during northeasters and Hurricane Bob in 1991. This probably resulted from an onshore wind-driven surface current that induced coastal set-up leading to an offshore-directed downwelling storm current (Kelley et al., 1995).

2.4 History of Saco River Inlet

In response to navigation hazards, USACE has been altering the Saco River Inlet, either by dredging or by the construction of substantial coastal engineering structures, since 1827. A timeline depicting the progression of engineering projects at the inlet is given in

Figure 2-1. Historically, the natural ebb-tidal delta (sandbars and ledges) has inhibited traffic in the lower estuary (Kelley and Anderson, 2000). More recently, chronic shoaling within the jettied channel and the harbor landward of the estuary mouth has necessitated a continual monitoring and dredging program operated by the USACE (Fitzgerald et al., 2002). Currently, the inlet is stabilized by a 2,010 m (6600 ft) jetty to the north of the mouth, and 1,463 m (4800 ft) jetty to the south. A 122 m (400 ft) long spur jetty is located about 30.5 m (100 ft) from the shoreward end of the north jetty and extends parallel to shore. The heights of these structures vary. The shoreward 259 m (850 ft) of the north jetty has an elevation of 5.2 m (17 ft) relative to mean low water (MLW), the seaward 750 m (2460 ft) has an elevation of 1.7 m (5.5 ft) (MLW), and the remainder of the structure has an elevation of 4.5 m (15.0 ft) (MLW). The height of the spur jetty varies from 2.6 m (8.5 ft) (MLW) at the jetty attachment point, to 0.9 m (3.0 ft) (MLW) at the extremes. The south jetty has a crest elevation of 3.4 m (11.0 ft) (MLW) along the 536 m (1759 ft) shoreward portion, with the remainder constructed to an elevation of 1.7 m (5.5 ft) (MLW).

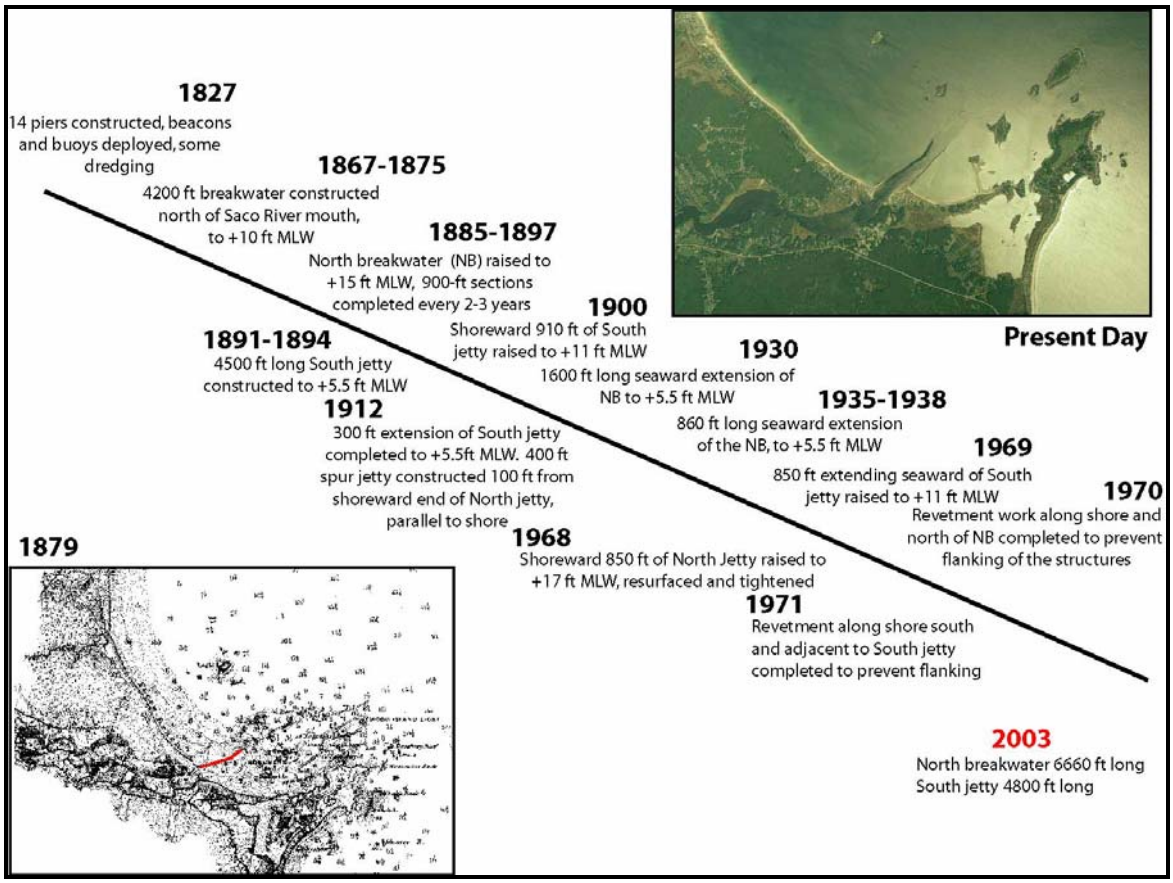

Figure 2-1. Timeline of the structural modifications in the vicinity of Saco River and Camp Ellis Beach.

At the time of the first jetty construction, it was thought that net sediment transport was from the north to the south and that this pattern was responsible for sand deposition at the inlet mouth. The north jetty was constructed to intercept this inferred north-to-south movement of sand in the littoral drift, "…a constant movement of sand from north to south along the beach…which has…deposited material in front of the original entrance channel" (USACE 1910, p.3). This statement was later reiterated in a USACE beach erosion report for Saco published in 1955. The USACE inferred, from general knowledge of local geology, that the source of this sediment was an offshore glacial deposit that moved landward to a nodal point near Old Orchard Beach and then traveled north to Pine Point and south to Camp Ellis. A riverine sediment source for the shoaling estuary/harbor was not considered, although the USACE acknowledged a large amount of sand traveled down the Saco River at least to the estuary, if not the Bay, "The river…during spring freshets carried large quantities of sand…(to) just below Factory Island…whereby the material was deposited" (USACE, 1886, p. 5).

2.5 Sediment Sources

2.5.1 Saco River

Freshwater and sediment discharge rates have been calculated/estimated for the Saco River system. A mean yearly freshwater discharge of 3.1×10^9 m^3 (1.1×10^{11} ft^3) or 100 m^3/s) (3530 cfs) was thought to supply sand to the system particularly during spring freshets (Fitzgerald et al., 1993; Barber, 1995; Manthorp, 1995; Kelley et al., 1994). Detailed studies of the sediments in outer Saco Bay, the Saco River estuary and the beach systems of the bay have provided further evidence to substantiate the claim that the Saco River is the main source of sediment to the region (e.g. Fitzgerald et al., 2002; van Heteren et al., 1996). Additionally, hydrographic surveys have supplied support for this theory by proving that the river is capable of significant sediment transport and discharge to the outer bay.

Fitzgerald et al. (2002) collected extensive hydrographic and sedimentologic data in the Saco River, its estuary and the nearshore region during the summers of 1992 and 1993 to analyze the influence of a major flood during the spring of 1993. Grain size data from 140 stations within the estuary and nearshore region indicated that the dominant sediment type was medium-coarse sand with finer-grained sediments flanking the wider portions of the river (tidal flat and marshes). Beyond the jetties the sediment was uniformly fine sand. Sediment samples collected prior to and after the 1993 spring freshet showed that 76% of the post freshet 1993 sediments were coarser than in 1992 and the locations of consistent or decreasing grain size were in areas adjacent to tidal flats. Hydrographic data showed that during the spring freshet event, river discharge totally overwhelmed tidal flow and controlled net sediment transport directions (Fitzgerald et al., 2002).

Bedform analysis in the mid-summer (low freshwater discharge) and during the spring freshet also confirmed the change in hydrographic regime during these events. Side-scan sonar records showed that in the mid-summer (normal conditions), both flood-and ebb-oriented sandwaves and megaripples existed in the channel, reflecting the dominance of tidal flow. In the jettied channel, symmetrical megaripples were found resulting from bi-

directional currents and shoaling waves (Fitzgerald et al., 2002). However, during the Spring freshet, sandwaves in the channel and the jettied channel became ebb-oriented, with few flood-oriented features, indicating the dominance of the freshwater flow and implying offshore sand transport during that time (Kelley et al., 1995).

The evidence above led Fitzgerald et al. (2002) to conclude that the Saco River contributed sand to the nearshore zone during periods of high riverine discharge. The sediments in the estuary were medium-coarse sand and texturally immature whereas the region seaward contained fine sands. Velocity measurements taken at various times and locations in the study area during the freshet confirmed the predominance of stronger ebb than flood currents. Bedform configuration during the freshet further supported the conclusion that freshwater flow is dominant during these events. The magnitude, direction and persistence of the current velocities indicate that the freshets are important events in supplying coarse-grained sediment to the estuary mouth, and with the current jetty configuration, this sediment was responsible for shoaling within the harbor and jettied channel (Fitzgerald et al., 2002).

2.5.2 Saco Bay

According to the data and bottom classifications of Kelley et al. (1995), the majority of the Saco embayment just seaward of the sandy beaches is covered by Holocene sand with large ripple fields or narrow linear sand bands. Seaward of these sand bedforms, bedrock and gravel are predominant north of Biddeford Pool and Wood Island, rippled gravel is prevalent south of Prouts Neck, and the center of the bay is dominated by muddy sand and bedrock outcrops (Kelley et al., 1995). These observations in Saco Bay contradict the early, unsupported assumptions of the USACE that there is a significant source of glacial sand in the bay. Most of the existing sand is part of the shoreface profile and does not provide a new source of sand to contribute to the shoaling Saco River channel or to the beaches (Kelley et al., 1995). Muddy or rocky material outcrops over the rest of the bay, apart from a lag deposit near Prouts Neck, which probably represents a reworked till or glacial-marine deposit that may have once been an important sand/gravel source (Kelly et al., 1995). Side-scan sonar records show reworking of some of the offshore seabed but the potential source area for sand is small (4 km^2 or 988 ac). An unreasonable and unobserved amount of erosion would be required to produce the volume of sand added to Pine Point alone in the last century. Furthermore, the offshore sediments are largely mud at depth (Kelley et al., 1992) and are only covered with a thin veneer of coarser sediments, whereas sand at nearby Pine Point is fine-grained (Farrell, 1972; Barber, 1995).

2.6 Sediment Transport Regime

2.6.1 Geological Observations

Kelley et al. (1995) summarized geologic evidence in support of a net south-to-north sediment transport direction that has occurred in Saco Bay since the late Holocene. Geomorphological interpretation and Ground Penetrating Radar (GPR) have been primary tools used in the discovery of this evidence. The orientation and continuity of paleospits along the southern part of the beach indicate a significant quantity of sand

derived from the Saco River (Kelley et al., 1989a; van Heteren et al., 1994a, 1996; van Heteren, 1996). A small south-oriented spit at Goosefare Brook is paired with a north-oriented spit on the other side of the inlet and is Kelley et al., (1995) presumed this an artifact of local wave refraction. GPR observations at Pine Point also depict the northeastward growth of that spit into the Scarborough River Inlet. In addition, the fining grain sizes from south to north along both the beach and nearshore also suggest net northerly transport (Farrell, 1972).

Historical shoreline change analysis using both historical charts and aerial photographs has also provided strong support for net northward sediment transport as well (Kelley et al., 1995, Kelley and Anderson, 2000). Charts from 1866 depict a large ebb-tidal delta at the mouth of the Saco River, which was destroyed by construction of the north jetty causing the sand to move ashore (Farrell, 1972). The jetty altered the flow out of Saco River from a forked two-channel morphology to a single channel oriented in an east-west direction (Kelley and Anderson, 2000). Bathymetric changes between the 5.5 m isobath and the MHW line, documented by the USACE, indicate the loss of 5.95×10^6 m^3 (7.78 x 10^6 cy) of sand from the southern part of the bay from 1859 to 1955 (USACE, 1955). Concurrently the Little River Inlet closed (between 1871 and 1877), Pine Point continued to build out and the flood-tidal delta of Scarborough River accreted sand. Aerial photographs from the past 40 years have documented this continued erosion at Camp Ellis Beach and simultaneous accretion at Pine Point. The photographs also confirm the growth of the spit at Pine Point by 40–80 (130-260 ft) meters in a seaward direction (Kelley et al., 1995).

Although the 1955 USACE Report offered little explanation for the loss of sand at Camp Ellis Beach, Kelley et al. (1995) used seismic profiles and GPR to estimate sand volumes within the Saco Bay beach system. They concluded that at the same time as the sand was lost from southern Saco Bay, 1.3×10^6 m^3 (1.7 x 10^6 cy) of sand were added to the sub-aerial beach and dunes at Pine Point. If the sand deposit offshore of Pine Point, which is presently the largest single deposit in Saco Bay, accreted only 0.5–1.0m (1.6-3.2 ft) vertically during the same period, it would account for an additional 3.5×10^6 m^3 (4.6 x 10^6 cy) of sand. Additional sand also exists in the relic flood deltas of Little River and Scarborough River (Farrell, 1972). Visual observations following dredging events at the Camp Ellis anchorage in 1992 substantiate this northward movement of sand. In one particular event, 65,000 m^3 (85,000 cy) of dredged sand were placed on Camp Ellis Beach for renourishment purposes. Subsequent to the renourishment, the woody, shelly, estuarine sand was rapidly eroded from Camp Ellis Beach and transported to the north congesting the Goosefare Brook inlet and deposited along other northern beaches (Kelley et al., 1995).

Evidence supporting *north-to-south* sediment movement includes the orientation of a small modern spit on the northern side of Goosefare Brook, which indicated southerly sand transport (Kelley et al., 1995). Hindcast meteorological and oceanographic data also supported this hypothesis (USACE, 1955, Jensen, 1983). These data suggested that the largest wind and wave events approached the outer bay from the northeast-east in the winter, and that summer waves are derived from the southeast-southwest. The USACE assumed that the summer waves were insignificant compared to the winter waves and

were most likely blocked by Biddeford Pool and the north jetty. Additionally, shoaling on the northern side of the north jetty and the lack of shoaling in the navigation channel have been cited as evidence for contemporary north-to-south littoral sand transport. Furthermore, geological evidence in the form of unfilled depressions in the Saco River estuary and dams on the river were used to suggest a lack of a present-day riverine sediment source to the bay (Maine State Planning Office, 1979).

The north-to-south hypothesis, and the evidence listed above has formed the basis for USACE reports and subsequent construction effects in the Saco River inlet for more than a century. However, no initial study was performed from which to derive this hypothesis, and no continuous, long-term measurements of wave characteristics, littoral and onshore/offshore sediment transport, or bottom profiling have since been performed by the USACE. Shoreline change analyses performed by USACE in 1955 indicated that more than six million cubic meters of sand had disappeared from Camp Ellis from 1859 to 1955 (61,933 m^3/yr or 81,000 cy/yr), but the USACE offered no explanation for this loss of sand (USACE, 1955; Kelley and Anderson, 2000). By 1995, the USACE reported erosion rates of 0.9 m/yr (3.0 ft/yr) on the 457 m (1500 ft) of shore immediately adjacent to the north jetty, and 0.6 m/yr (2.0 ft/yr) for 305 m (1000 ft) farther north. This erosion was attributed to the assumption that the entire area lacked nourishment and that material removed by storm waves was not being naturally replenished (USACE, 1995). The USACE also noted that historical records showed an increased rate of change of the Mean High Water (MHW) line around the time of completion of an inshore segment of the breakwater in 1895-1897, an observation that implicates jetty construction as a cause for the alteration of natural coastal processes (USACE, 1991; 1995). The USACE stated that the north jetty had partially contributed to erosion at Camp Ellis Beach by affecting the local wave field, although they maintained that this structure could not be solely responsible for erosion at Camp Ellis as the source of sediment was the offshore glacial deposit (USACE, 1995; Saco Bay Regional Beach Management Plan, 2000).

2.6.2 Previous Modeling Studies

In order to study the hydrodynamic and sediment transport regimes of Saco Bay, and to test a number of construction alternatives with the purpose of reducing erosion on Camp Ellis Beach, the USACE performed a study using a scaled model of the area in 1995 (USACE, 1995). The study involved the construction of a 1:100 scale fixed-bed model of the Saco inlet and the beach directly to the north. The model reproduced 2,438 m (8000 ft) of shoreline, an area of 1,952 m^2 (21,011 ft^2), and extended to an offshore depth of about -13.7 m (45 ft) (MLW). A cement base was modeled to accurately depict bathymetry within the model bounds. The model was calibrated using an existing conditions scenario, and modified to analyze the effects of nine engineering alternatives. Remolding of the fixed-bed model to historical bathymetric conditions prior to and during initial jetty construction/modification allowed for the analysis of the wave, current, and sediment transport patterns prior to engineering activities in the area.

The model used a unidirectional spectral, electrohydraulic, wave generator to create waves at the eastern extent of the model for a period of up to 32 hours for each engineering alternative tested. WIS hindcast data were utilized to simulate wave heights

and choose conservative directions for wind/wave approach. These data were then converted from deepwater to shallow water heights and directions. A variety of shallow-water wave directions (101°, 88°, 75°, 56°) were used to simulate normal conditions, of which 101° and 88° were determined to be the most critical; an 88° approach was used to simulate storm conditions. The model area included the morphology of the Saco inlet but only used a river discharge in one of the alternatives and the historical tests. Although the USACE used a mean discharge of water ($91 m^3/s$ or 3213 cfs) in some of these tests, it never accounted for sediment discharge from the river. The model was calibrated by comparing wave heights and current patterns and magnitudes with hindcast-spawned data. No long-term, continuous measurements of wave characteristics, littoral and onshore/offshore transportation or bottom profiling data were collected in order to calibrate the model. This absence of data was attributed to economic limitations (USACE, 1995). Sediment tracer tests were also conducted where an appropriate sediment tracer, in this case crushed coal, was placed along the Camp Ellis shoreline and its transport patterns recorded as the physical model was run.

The results of this model included a series of wave heights and current data for each alternative and the historical tests. In addition, visual observations of wave patterns were made and recorded. Wave heights were adjusted using Keugelan coefficients to reduce the effect of excessive bottom friction in the model. In all alternatives tested by the model, the net current direction and sediment transport were to the *north*, and without renourishment, all model scenarios experienced erosion of Camp Ellis Beach. The model did not predict any southerly sediment transport; the only sediment entering the navigation channel from the north would be that washed over the jetty during storms. The results also indicated that the north jetty had little effect on the hydrodynamic regime in front of Camp Ellis Beach and therefore the presence of the structure should have had minimal effect on the northerly migration of sediment.

In general the results of the model analysis revealed that the assumption of north-to-south sediment transport, as advocated by the USACE since 1886, was fundamentally flawed. Additionally, the model indirectly indicates the importance of the Saco River as a source of sediment to the system. For example, if the 1897 jetty was so effective at preventing sand from entering the channel, as was predicted by a model scenario, then why was a continuous monitoring and dredging program implemented to counteract chronic shoaling? If the sand infilling the jettied channel and Camp Ellis anchorage did not come from the north, it must have come either from the south, or from the Saco River itself.

2.7 Sediment Budget

Continuing erosion at Camp Ellis has led to an imbalance in the sand resources in Saco Bay, where erosion at Camp Ellis is coupled with accretion at Pine Point (Saco Bay Regional Beach Management Plan, 2000). In response to a growing number of complaints made by Camp Ellis property owners, the Maine Geological Survey in cooperation with the University of Maine and Boston University initiated a study in 1991 (Kelley and Anderson, 2000). This Maine-New Hampshire Sea Grant Program-funded study involved the collection of hydrographic and sedimentological data within the Saco River and the outer Saco Bay with the purpose of increasing knowledge of the estuarine and offshore regimes and sediment budget.

The term "imbalance" was used above in regards to the sand resources because a sediment budget for the Saco Bay coastal system was never clearly identified. The volume of the coastal zone sediments, from dunes to the subaqueous deposits offshore (the sink in this budget), is known, but the sources capable of providing sediment to the coastal system have remained relatively uncertain. Estimates of the sediment discharge rate for the Saco River have shown that this sediment source is capable of providing most, if not all, of the sand in the modern coastal system (Barber, 1995). Barber (1995) estimated that the mean annual sand and gravel discharge of the Saco River is 8,000 to 12,000 m^3 (10,463-15,695 cy). Van Heteren et al. (1996) performed a volumetric analysis of the entire Saco barrier system using GPR and coring techniques, and confirmed that the Saco River has provided 40 to 60×10^6 m^3 (52 to 78 x 10^6 cy) of sand to the coastal area in the last 4,500 years, assuming constant fluvial input rates. Van Heteren et al. (1996) reiterated that this fluvial input has been more important to the development and maintenance of the Saco Bay shoreline than onshore transport of sediment reworked from offshore sand/gravel (Barber, 1995).

Kelley et al. (1995) estimated a new sediment discharge rate using the suspended sand content in riverine discharge at a gauging station 35 km (21.75 miles) above the head of the tide. They regressed the suspended sand volume, from the times of observations to all stages of river discharge, and calculated an estimate of 6,100 m^3/yr (7,978 cy/yr) of suspended load transport. This estimate was taken as a minimum discharge rate as it does not account for bedload discharge. They also utilized the infilling rate of the Camp Ellis anchorage as another estimate of sand discharge by the Saco River. The average historical infilling rate was 6,300 m^3/yr (8240 cy/yr) (1872–1994) and the modern infilling rate is 8,500 m^3/yr (11,117 cy/yr) (1984-1994), but these were also assumed to be minimum estimates as additional sand may have been transported out into the outer bay during freshets (Kelley et al., 1995). Sand transported into the bay from the Saco River is thought to be the predominant sediment source to the bay (Barber, 1995; Fitzgerald et al., 2002; Kelley et al., 1995). Therefore the sediment discharge from the Saco River should account for a portion of the infilling sand at Biddeford Pool (3600-4800 m^3/yr or 4,708 to 6,218 cy/yr) and Scarborough River anchorage (17,000 m^3/yr or 22,235 cy/yr) (Kelley et al., 1995). Using this reasoning, Kelley et al. (1995) estimated a sediment discharge rate from the Saco River of between 10,000 and 16,000 m^3/yr (13,080 and 20,927 cy/yr).

Kelley et al. (1995) used these new estimates of sediment discharge along with volumetric estimates of the different sand bodies in the coastal system to construct sand budgets for Saco Bay for three time periods: 1) 7,000 yr to 130 yr Before Project, 2) 1859 to 1955, and 3) 1955 to 1991. They considered the only possible source of offshore sand, a 4 km^2 (988 ac) rippled sand and gravel deposit south of Prouts Neck, and its capability of providing sand to the system. Using the sand content of this deposit (58%) and sand content for average Maine glacial-marine sediment (33%), they estimated this deposit was capable of contributing between 3.3 and 6.0×10^7 m^3 (4.3 and 7.8 x 10^7 cy) of sand (using 33% and 58% respectively), assuming the deposit eroded from 5 m (16.5 ft) above MSL to its current depth of 20 m (65.6 ft) below MSL). However, the Prouts Neck sand is coarse-grained (2.8 phi) whereas the sand in all the nearshore deposits is fine-grained (3.2 phi). This comparison implies that the Prouts Neck sand body is unlikely to have

provided the sand in the current barrier system. If the principal source of sand to the Saco Bay barrier system is sediment discharge from the Saco River, this process has likely been acting since the last deglaciation (Fitzgerald et al., 2002). Using estimated sediment discharge rates and extrapolating back in time, the volume of sand required to create the entire coastal system (the eventual sediment sink) would have been delivered to the bay in the last 7800 to 4900 years (Kelley et al., 1995). Evidence supporting this scenario includes radiocarbon dates of 6-7 ka, from back-barrier fauna; as well as recent reconstructions suggesting the Wells barrier beaches formed within that interval (Kelley et al., 1995a), in response to a slowdown of the regional rate of sea level rise at that time (Barnhardt et al., 1995). All this evidence indicates that the Saco River has been, and continues to be, the primary sediment source for the Saco Bay beaches.

3.0 HISTORICAL SHORELINE CHANGE (TASK 17)

In a physical system like that of Saco Bay, the geologic and historical perspective is important for understanding the coastal processes of the region, as well as providing insight into the future. Although micro-scale processes, such as turbulence, wave-induced currents, tidal currents, and individual wave orbital velocities determine the magnitude and direction of individual grain motion, variations in these processes are considered noise at a regional scale. Regional geomorphic change describes the evolution of depositional environments for coastal stretches over extended periods of time. An underlying premise of modeling long-term morphologic change is that a dynamic equilibrium may be eventually reached as a final stage of coastal evolution. However, the interaction between region's response to driving forces causing change may result in a net sediment deficit or surplus within a system, causing disequilibria, and preventing a dynamic equilibrium.

Aerial photographs and topographic and hydrographic surveys of coastal and nearshore morphology provide data for quantifying regional geomorphology and change. Comparison of analysis of coastal shoreline change developed from aerial photographs and digital bathymetric data for the same region, but collected at different time periods, produces a method for calculating historical sediment movement within a region. Utilizing the historical maps, data, and information collected during Task 1, a shoreline change analysis was performed for the entire Saco Bay region. This information was used to provide a historical perspective and qualitative assessment of the magnitude and direction of sediment transport, assessment of the engineering modifications to the region, examining geomorphic variations in the coastal zone, and ground-truthing numerical sediment transport models.

3.1 Geographic Setting

Saco Bay, Maine (Figure 1-1) is an 8-mile long arcuate stretch of shoreline bound to the south by Fletcher's Neck and the Saco River, and to the north by Scarborough River and Prout's Neck (Figure 3-1). The majority of Saco Bay's coastline is densely developed consisting of small beachfront communities. As discussed in the previous chapter, the Bay represents the largest sand beach and salt marsh system in Maine and the Saco River has been considered one of the primary historical sources of sediment to the beaches within the Bay (Kelley et al., 1995; Slovinsky and Dickson, 2003). The Saco River estuary is located at the southern end of the sandy coastal system within the Saco embayment. Current day tidal influences extend 10 km upstream to the base of two dams at Factory Island. The Saco River mouth is shallow (< 3.0m or 10 ft) and is currently stabilized by two jetties. Recurring shoaling between the two jetties and in the harbor landward of the estuary mouth has necessitated a continual maintenance dredging program operated by the USACE.

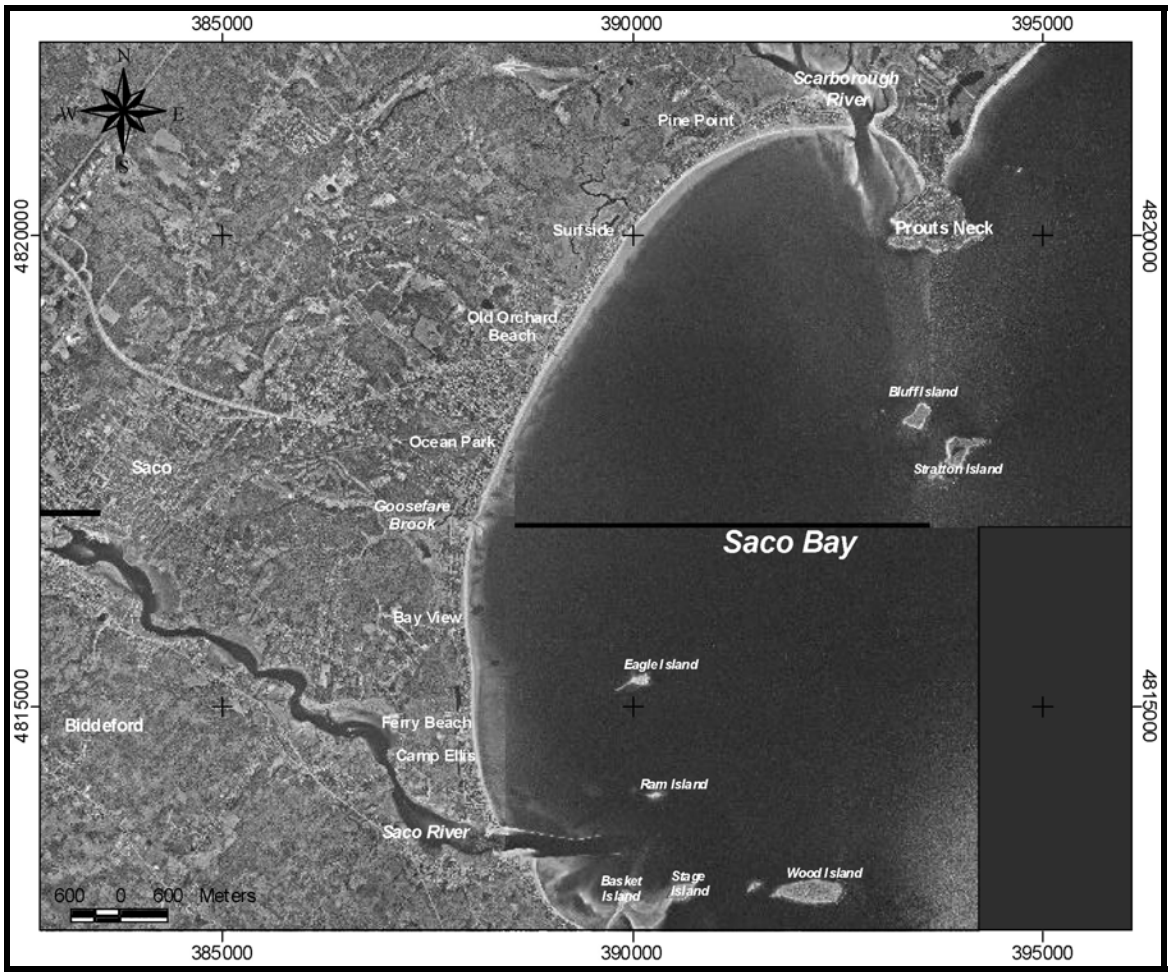

Figure 3-1. Aerial photograph from 1998 identifying the important areas within the Saco Bay study area including Saco River, Goose Fare Brook, and Scarborough River (projection in UTM NAD83 meters).

In the 19th century, navigation at the mouth of the Saco River became difficult due to the presence of tidal deltas (ledges and sandbars) in front of the inlet. In response to increasing marine traffic in the 19th century, the United States Army Corps of Engineers (USACE) began altering the inlet in 1827. In 1867, a 1,280m (4,200 ft) long breakwater north of the river mouth was constructed in order to maintain a clear navigation channel at the inlet and to provide wave energy reduction in the harbor and channel entrance. This construction altered the flow out of Saco River from a forked two-channel morphology to a single channel oriented in an east-west direction. Between 1885 to 1969, the northern breakwater was extended and heightened to a maximum length of approximately 2,010 m (6,600 ft) with a varying crest elevation of between 0.3 m (1 ft) (seaward end) to 3.8 m (12.5 ft) (landward end) relative to Mean Tide Level (MTL). In addition, a jetty was constructed on the south side of the river entrance in 1894, which was eventually lengthened to approximately 1,463 m (4,800 ft) and heightened with a varying crest elevation between 0.3 m (1 ft) (seaward end) and 2.0 m (6.6 ft) (landward end).

To identify resulting shoreline changes that took place along the Saco Bay shoreline since 1864, an analysis of historical shoreline change was performed. As part of this analysis, rates of long-term shoreline change were calculated throughout the Saco Bay littoral cell, with specific focus on the Camp Ellis Beach region. Evaluating the historical shoreline change provides a good understanding of the overall time-averaged physical processes that are active within Saco Bay. Based on comparison of different time periods, temporal variability can also be determined. The analysis also serves as a pre-cursor to the wave and sediment transport analysis that is presented in Chapters 8 through 12 of this report. Magnitudes and trends in shoreline change can be compared to wave and sediment transport modeling results in order to provide a qualitative verification of model performance. For example, areas of coastline that have experienced historical erosion may correlate to regions that have increased wave energy and/or sediment transport divergence.

The integration of map and photographic data allowed for the evaluation of morphologic changes along the 8-mile long embayment through time. For Saco Bay, the earliest maps suitable for analysis of shoreline change date back to 1864. A representative selection of aerial photographs and charts representing different time periods was used to quantify changes in shoreline position during the 1800 and 1900s. The map and photographic data provided information on the stability of the Saco Bay complex, and helped to identify trends of accretion and erosion within the Bay since 1864. Since the publication of this document, additional, more recent aerial photographic data may have been available to provide additional contemporary analysis.

3.1.1 Coastal Environment

The Saco Bay shoreline forms a littoral cell in the southeastern coastline of Maine. This embayment contains the largest sand beach and salt marsh system in Maine and has a mean tidal range of approximately 2.7 m (9 ft), with a spring range of 3.5 m (11.6 ft). The shoreline reach is classified as a mesotidal shoreline according to the Hayes (1975) tidal classification, which groups coastal areas according to tidal range. The coast is characterized by three tidal inlets: the Saco River Inlet, Goose Fare Brook Inlet, and Scarborough Inlet, with sandy pocket beaches that provide economic, environmental, and recreational benefits (Slovinsky and Dickson, 2003).

3.1.2 Coastal Geology

The Saco embayment of Maine is considered a riverine-derived sandy barrier shoreline, which is defined as a barrier that has developed from the onshore and alongshore reworking of sediment deposited on the inner continental shelf by rivers (Fitzgerald, et al., 1994). Complete details on the local geology can be found in Chapter 2.0.

Grain size data from samples taken at 140 stations throughout the estuary and nearshore region indicate that the dominant sediment type is medium-to-coarse grained sand with finer-grained sediment flanking the wider portions of the river (tidal flats and marshes, which are long-term sediment accumulation areas). South of the jetties the sediment is uniformly fine sand (Fitzgerald et al., 2002). Grain size within the Saco Bay system is finer in the northern reaches of the system than in the south. Fining grain sizes were

found by Kelley et al. (1995), and more recently by Woods Hole Group sediment analysis (Chapter 12.0).

Riverine-associated inlets like that of Saco, contribute sand to the nearshore zone during periods of high riverine discharge. Sediment texture and bedforms show that larger spring freshet events overwhelm tidal flow in the estuaries and control net sediment transport directions. The magnitude, direction, and persistence of the current velocities indicate that freshets are important events in supplying coarse-grained sediment to the estuary mouth, filling harbor regions and/or shoaling jettied channels as in Saco (Fitzgerald et al., 2002).

3.2 Historical Shoreline Change Analysis

A computer-based mapping methodology, within a Geographic Information System (GIS) framework, was used to compile and analyze changes in the historical shoreline position between 1864 (T-Sheet compiled from 1849 to 1879) and 1998 for Saco Bay. The purpose of this task was to quantify changes in shoreline position using the most accurate data sources and compilation procedures available, and to characterize areas of erosion and accretion. This chapter provides a detailed description of the of the methods and data sources used, quantifies the confidence level of the data sources, provides the historic shoreline change rates, and provides a discussion of the results of the analysis.

3.2.1 Data Sources

Shoreline change can be determined by accurately overlaying historical shoreline positions as obtained from the U.S. Coast and Geodetic Survey (USC&GS) historical T-sheets, the National Oceanographic Atmospheric Administration (NOAA) National Ocean Service (NOS) T-sheets, vertical aerial photography, and digital orthophoto quads (DOQ). The NOS T-sheets, which are compiled from results of field surveys, are the most accurate historical maps available for the coastal zone, exceeding the accuracy of United States Geological Survey (USGS) topographic maps (Shalowitz, 1964). Topographic surveys have been conducted by USC&GS (NOAA's predecessor) since the 1830s, and at that time the high water line was determined to be the best field indicator of the land-sea interface (e.g., the shoreline) and that is what is shown on the T-sheets. Therefore, since the high water line is the only available shoreline on the historic T-sheets, the high water line is required to be used as the shoreline identifier on the aerial photographs in order to be comparable to the historical T-sheet data. As such, the high water line can link historical shoreline maps to more recent shoreline data since the same indicator is used. Fortunately, the high water line is evidenced by a change in gray tone on black and white aerial photographs, and the position of this wetted boundary (represented by the last high tide or the non-storm wrack line on the aerial photography) is identifiable on aerial photographs (Stafford, 1971). Although there is some debate over the best shoreline indicator when determining shoreline position, of all the shoreline indicators, the high water line is considered the best shoreline indicator by many (but not all) researchers (Crowell, 1991; Leatherman and Buckley, 1991). Other shoreline indicators (e.g., dune crest, dune toe, berm crest, vegetation line, scarp edge, etc.) have been less commonly used in shoreline change analysis; however, these identifiers were not consistently available in the aerial photographs, nor would they correspond to the

historical (T-sheet) shoreline identifier. For example, a vegetation line is not available along the entire stretch of the coastline (e.g. at the Camp Ellis shoreline where no vegetation exists).

One of the major disadvantages to the historical T-sheets is that the shoreline field studies used to produce them were so time consuming that long periods elapsed between successive maps. Such infrequent data collection can make trends in historical shoreline change difficult to interpret because of the paucity of data. More recently, vertical aerial photographs, which have the benefit of a relatively synoptic view and potentially frequent collection and analysis, have been used to update historical maps. However, if aerial photos are to be treated as maps, the images must be rectified to eliminate the effects of distortions in the photographic process. In addition, before the photographic data can be compared with historical cartographic data for quantitative studies of shoreline change, the shoreline position information must be geo-referenced.

For this project, four primary sources of data were used to evaluate changes in shoreline position during the period 1864 (1849-1879) to 1998. Shoreline data from 1864 (1849-1879) and 1944 were obtained from U.S. Coast and Geodetic Survey (USC&GS) historical T-sheets. Data for the 1864 T-sheet was collected over a period of time ranging from 1849-1879 and 1864 was chosen as a mid-point timeframe for this data. The shoreline data shown on these historical maps were surveyed using standard planetable surveying techniques. The 1965 and 1977 shoreline data were obtained from aerial photography flown by Col-East, Inc and James W. Sewall Company, respectively, and were obtained as overlapping 9x9 inch images covering the Saco Bay study area. The 1977, 1986, and 1995 shoreline data were obtained from aerial photography provided by the Maine Geological Survey and were obtained as overlapping 9x9 inch images covering Saco Bay. Digital USGS orthophoto quadrangle (DOQ) from 1998 obtained from the Maine Geological GIS data website was used as the basemap for this shoreline change analysis.

The time series of photographs selected for this study represents the highest quality and most evenly spaced photographic data available. If the aerial photography was taken during an elevated high tide or storm time period, such that the high water line could be accurately delineated, that set of photograph was not used in the analysis. For example, aerial photography from 2002 was available for use in this shoreline change analysis; however, because the photos were taken during a spring high tide (tidal range of +11.69 ft or 3.56m), the mean high water line could not be delineated accurately. Therefore, the 2002 were not used in the analysis. A significant number of additional aerial photographs, covering additional time periods, were also available for inclusion in the shoreline change analysis. Only the shorelines that provided high quality and visible shoreline identifiers were used. In addition, every attempt was made to select a set of shorelines representing an evenly-spaced temporal distribution to adequately resolve the historic changes along the coast. Seasonal changes that occur in the beach profile (i.e., the winter to summer beach profile change) can be important on a short-term basis; however, over the 130+ years of evaluated shoreline change and with a number of times used, these seasonal trends are irrelevant to the long-term trend of the shoreline. Seasonal changes will result in small fluctuations compared to the overall total error

(Section 3.2.3.3), and are insignificant over the long-term. Details regarding each of the data sources are given in Table 3-1. This time series of shoreline data provides a high-resolution history of shoreline response along Saco Bay shoreline since approximately 1864.

3.2.2 Data Compilation and Analysis Methods

Each set date of aerial photographs listed in Table 3-1 provides a synoptic view of the Saco Bay coastline. These data however, are not tied to a geographic coordinate system, and thus cannot be directly compared with historical map data or with each other without additional processing. In addition, the photographs contain a variety of distortions intrinsic to air photos, such as radial distortion, tilt and pitch of the aircraft, and scale variations. Thus, before shoreline position data from various years can be compared for quantitative analysis of shoreline change, the photographs (or shoreline positions) must be geo-referenced and corrected for distortion. These corrections were accomplished utilizing computer aided cartographic mapping software.

The 9x9 inch air photos were scanned to produce a digital raster-based image. The high-resolution images provided greater accuracy in locating control points for geo-referencing the photos. The initial part of the analysis involved identification of a reference shoreline on each of the digital images. Air photo interpretation along a shoreline is improved by familiarity with the area and its processes, and includes a certain amount of error and interpretative subjectivity. Delineation of the reference shoreline is the most important and most subjective part of shoreline change analysis, particularly in areas where relief distortion can compound interpretation. The horizontal position of the high-water shoreline as recognized on the beach and on photography (i.e., the position of the wetted boundary) was determined using a hierarchy of criteria dependent on morphologic features present on the subaerial beach. The primary criterion was a well-marked limit of uprush by waves associated with high tide. This generally was recognized as a beach scarp or debris line, marking the upper limit of the foreshore. If a scarp could not be identified, a debris line usually was identified.

These criteria for delineating the high water line are consistent with those used by field topographers and NOS photo interpreters (Shalowitz, 1964). A single interpreter familiar with the morphology of Saco Bay was assigned to the aerial photo analysis so that all interpretations remained consistent. Reference shorelines for each photograph were captured through heads-up digitizing, and stored digitally in a Geographic Information System (GIS).

Geo-referencing was accomplished by identifying a series of evenly spaced ground control points on the images for which real world x, y coordinates were known. The 1998 USGS digital orthophoto quadrangles were utilized to obtain the ground control. These maps contained a variety of features that were easily visible on the scanned images. The DOQs were previously referenced to the UTM (meter) Coordinate System (NAD 1983) Zone 19 by the USGS. Suitable control point positions visible on both the imagery and the DOQ were identified, and marked on the scanned images. Cartographic mapping software was then used to geo-reference the vector data representing the reference shorelines according to the appropriate transformation algorithm (least-squares,

affine, or projective). Shorelines from the early USC&GS historical maps were captured using the same technique described above.

Table 3-1. Summary of shoreline source data characteristics for Saco Bay, Maine.

Date	Data Source	Comments
1864 (1849-1879)	USC&GS Historical T-sheet with a scale of 1:80,000	First surveyed shoreline using standard planetable surveying techniques. Coast Chart No.106
1944	USC&GS Historical T-sheet with a scale of 1:20,000	Surveyed shoreline using standard planetable surveying techniques. T-sheets # 8517, 8518, 8520 and 8521
1965	Col-East, Inc. Aerial Survey with a scale of 1:400	Shoreline interpreted from 9x9 inch scanned and rectified images
1977	James W. Sewall, Co. Aerial Survey, provided by the Maine Geological Survey with a scale of 1:12,000	Shoreline interpreted from 9x9 inch scanned and rectified images
1986	Aerial Photography provided by the Maine Geological Survey with a scale of 1:6,238	Shoreline interpreted from 9x9 inch scanned and rectified images
1995	Aerial Photography provided by the Maine Geological Survey with a scale of 1:12,000	Shoreline interpreted from 9x9 inch scanned and rectified images
1998	USGS DOQ, from the state of Maine GIS data website	1998 DOQ utilized as the basemap for the shoreline change analysis

Once the shoreline position data were compiled accurately, spatial and temporal changes in the data were quantified. This identification was accomplished by identifying a series of shore-normal transects along Saco Bay where shoreline change could be measured through time, and where rates of shoreline change could be computed. Two hundred and sixty five shore-normal transects were established at evenly spaced 50 foot intervals (see Appendix 3-A for maps entitled "Historical Shoreline Change Saco Bay, Maine, Transect Locations"). For graphical purposes, only every third transect rate was displayed on the maps for clarity. At each transect, distances of shoreline movement were calculated, and annual rates of shoreline change were determined using the various time intervals between shorelines. A matrix of long-term and incremental shoreline change rates was developed using all of the available shoreline data. Appendix 3-B shows the incremental and long-term rates of shoreline change, where positive values indicate shoreline accretion (ft/yr), and negative values indicate shoreline erosion (ft/yr).

The rates of shoreline change shown in Appendix 3-B were calculated using two different methods. The incremental rates of change were calculated using the end-point method, which is calculated based on the distance over which the shoreline position changed (measured along each transect), divided by the number of years during which the change occurred. This method was used to compare successive shoreline dates. A second method, the linear regression method, was used to determine the long-term rates of change (e.g., from 1864 to 1998). In this method, an average rate of change is based on a best-fit line to a series of points, each representing shoreline position at a period of time. The linear regression method is the most applicable method when looking at long-term averages in the rates of shoreline change, although both methods can reveal valuable information regarding the history of the shoreline.

3.2.3 Error Analysis

A certain level of error is inherent in all measurements of shoreline position using historical data sources. Potential errors in shoreline change rates can be characterized in three ways: accuracy, precision, and resolution. Accuracy refers to the degree to which a recorded value conforms to a known standard. In the case of mapping, this term relates to how well a position on a map is represented relative to actual ground location (e.g., infrastructure, high-water shoreline). Precision, on the other hand, refers to how well a measurement taken from this map or an aerial photograph can be reproduced (Anders and Byrnes, 1991). Resolution refers to the ability to distinguish detail in the original data source, and is highly dependent on scale. Higher resolution maps or photos have smaller scales allowing finer and more accurate depiction of the data. All three types of error were evaluated to gauge the significance of calculated changes relative to inherent inaccuracies. These errors arise in spite of the fact that this analysis used standard methods that are widely accepted within the industry and with Government. Although every attempt is made to eliminate error, some error persists. The key is to minimize the error, and then account for it so interpretations are supported by the analysis. The following discussion addresses these factors in terms of data sources, operator procedures, and equipment limitations.

3.2.3.1 Cartographic Errors

All maps of shoreline position, whether created from engineering survey or from aerial photographic sources, have inherent errors. For example, using a 1:10,000 scale T-sheet national standards allow up to ±28 ft of error for a stable point, but the location of these points may be more accurate (Shalowitz, 1964; Anders and Byrnes, 1991; Crowell et al., 1991). Non-stable points are located with less accuracy; however, features critical to safe marine navigation are mapped to accuracies stricter than national standards (Ellis, 1978). Historical T-sheet shorelines are mapped to within ± 0.02 inches (at map scale) of true position, which (for example) at a scale of 1:10,000 represents survey error of ±16 ft on the ground (Crowell et al., 1991).

Additional cartographic errors such as digitizer error, digitizer operator error, line thickness and relative location of control points on a map can be evaluated to provide an estimate of potential inaccuracy for source information. The parameters outlined above are assumed constant for all field surveys, and then were incorporated into this project's

error estimates to provide a conservative estimate of those potential errors. Crowell et al. (1991) assume a conservative digitizer error of ± 0.01 inch, which at a map scale of 1:10,000 converts to a ground distance of ± 8.3 ft. Line thickness of the plotted High Water Line (HWL) on the original production and photo reproduction of a T-Sheet can be estimated at 0.02 in., or ± 16.7 ft ground distance for a 1:10,000 scale (Crowell et al., 1991). The precision at which an operator can visualize and move the cursor along a line can lead to errors up to 0.01 in., or ± 8.3 ft at a 1:10,000 scale (Crowell et al., 1991). Fortunately, improper tracking associated with shoreline digitizing is random and may be dampened when averaged over finite distances of shoreline (Tanner, 1978). Table 3-2 displays the potential error associated with data sources originating from T-Sheets used in this analysis. The potential errors associated with these data sources are 1) traditional field survey error, and 2) cartographic processes error.

3.2.3.2 Aerial Survey Errors

Two potential sources of error were considered for this analysis of aerial photographs: 1) photograph scale, and 2) georectification or georeferencing. Error associated with photographic scale is directly related to the elevation from which the photograph was taken; in general, given the same camera, the higher the aircraft's elevation, the greater the error is when trying to delineate features on the earth's surface. Georeferencing introduces error to a spatial analysis when a transformation algorithm warps the photograph to conform to the earth's surface and to a geographic coordinate system. Although the scale of the photograph remains static, georeferencing errors can vary depending upon the condition of the photo and the method of transformation. Recently, high-quality alternative approaches have become available to rectify photographs for production of metric-quality photomaps (e.g., image processing/mapping software for georeferencing photos with ground based horizontal control of DOQs). The data compiled from aerial photographs for this study utilized the DOQ georeferencing technique. This method involves linking control points on the photographs with control points identified on the DOQs. The USGS DOQ was originally created from an aerial photograph, therefore there are varying amounts of error associated with the production of the 1998 DOQ, error associated with georeferencing the other photographs to the 1998 DOQ, and error associated with delineating the high water line position on the photographs (photo-scale dependant).

Table 3-2 displays the potential error associated with the aerial photo and DOQ data sources used in this analysis. The potential errors associated with these data sources are 1) position of the measured points (the location of the control points relative to their true location or horizontal accuracy), and 2) the delineation of the high water line on the photograph. Aerial photograph errors associated with the position of the measured points were calculated by the GIS software, by which the aerial photograph was georeferenced. Aerial photograph errors associated with the delineation of the high water line is scale dependant, and these values were determined using a linear relationship from established standard errors (Crowell et al., 1991).

Table 3-2. Estimates of error associated with acquiring shoreline position from data sources (error in feet).

USC&GS Historical T-Sheet (1864)			
Error: Traditional Field Survey		± 16.7 ft	
Error: Cartographic Processes		± 54.6 ft	
Aerial Survey / Photos			
Year	Scale	Error: Position of Measured Points	Error: Delineation of HWL
1944	1:20,000	± 7.8 ft	± 33.0 ft
1965	1:400	± 1.4 ft	± 2.0 ft
1977	1:12,000	± 2.4 ft	± 4.0 ft
1986	1:6,238	± 1.6 ft	± 5.2 ft
1995	1:12,000	± 0.8 ft	± 10.0 ft
Digital Orthophotograph Quad Basemap (USGS)			
Year	Scale	Error: Position of Measured Points	Error: Delineation of HWL
1998	1:40,000	± 3.6 ft	± 17.0 ft
Sources: Shalowitz, 1964; Ellis, 1978; Anders and Byrnes, 1991; Crowell et al., 1991			

3.2.3.3 Total Error

From the several sources of errors inherent in using historical maps and aerial photographs as shoreline position data sources, a total error can be calculated from the root-mean-square (RMS) of these various errors. Table 3-3 provides a summary of the total RMS error that pertains to the data sources for each shoreline. In other words, the errors presented in Table 3-3 list the relative precision of any point along the shorelines compiled from the data sources.

Here it is assumed that individual errors represent standard deviations, so a root-mean-square (RMS) approach was applied to provide a more realistic assessment of combined potential for different data sources (Merchant, 1987; Crowell et al., 1991; Byrnes and

Hiland, 1994 Table 3-4. The RMS errors in Table 3-4 were calculated by taking the square root of the sum of the mean squares of all potential errors between the data sources being compared. The relatively large error associated with the 1864 data source is a result of the low resolution scale (1:80,000). Likewise, the relatively small error associated with the 1965 data source is a result of the high resolution scale (1:400).

Table 3-3. Estimates of total error associated with shoreline positions (error in feet).

Shoreline Year	Total Error
1864	± 57.1 ft
1944	± 33.9 ft
1965	± 2.4 ft
1977	± 4.7 ft
1986	± 5.4 ft
1995	± 10.0 ft
1998	± 17.4 ft

Table 3-4. Maximum Root-Mean-Square (RMS) potential error for shoreline change data.

Date	1944	1965	1977	1986	1995	1998
1864	±66.4[1]	±57.1	±57.3	±57.4	±57.9	±59.7
	±0.83[2]	±0.56	±0.51	±0.47	±0.44	±0.44
1944		±33.9	±34.2	±34.3	±35.3	±38.1
		±1.61	±1.04	±0.82	±0.69	±0.71
1965			±5.3	±5.9	±10.3	±17.6
			±0.44	±0.28	±0.34	±0.53
1977				±7.2	±11.0	±18.2
				±0.80	±0.61	±0.87
1986					±11.4	±20.1
					±1.27	±01.52
1995						±20.1
						±6.69

1.Magnitude of potential error associated with high-water shoreline position change (ft)
2 Rate of potential error associated with high-water shoreline position change (ft/yr)

The potential RMS error calculated for the rates of shoreline change shown in Table 3-4 were used to help gauge the significance of the magnitude of the shoreline change. In general, where the RMS errors are greater than or equal to the rates of shoreline change, the uncertainty in the magnitude of the shoreline change is high. This usually occurs in areas where the annual rates of shoreline changes are low. For this study, the RMS errors are limited and the uncertainty in the magnitude of shoreline change is excessive only for data spans of short time periods (e.g., 1995 to 1998). For longer time periods of interest, the associated error rates are less than or equal to the rate of change for that time period. Therefore, each of these longer time periods has a higher level of confidence. Although the error shows that there is some uncertainty in the magnitude of the shoreline change, the trends in shoreline position are accurate. For example, the shoreline erosion trend exhibited for the 1864-1998 time period directly north of the Saco River would indicate significant erosion even with the error rate applied. Therefore, the long-term shoreline change trends (i.e., shoreline retreat, shoreline advance) are accurate.

3.3 Discussion of Shoreline Change

To evaluate trends in shoreline change at Saco Bay, various graphical representations have been developed. Shoreline positions for each of the available dates between the period of 1864 and 1998 are shown in Figures 3-2 through 3-5. The transect locations used for computation of shoreline change rates are shown in Appendix 3-A on the maps entitled "Historical Shoreline Change Saco Bay, Maine, 1864-1998, Transect Locations."

Figure 3-2 shows the southernmost part of Saco Bay. Each historic shoreline position is presented by color code as presented in the legend. The transect lines are indicated by the black lines (perpendicular to the shoreline) and associated transect numbers are shown in red. An associated shoreline change rate is presented (in white) for every third transect. Negative values correspond to shoreline erosion, whereas positive values correspond to shoreline accretion. These values represent the historic average shoreline change rate over the 134-year period.

Figure 3-2 indicates that the area directly north of the Saco River (Camp Ellis Beach) has experienced significant erosion for a distance of approximately 2,500 to 3,000 feet north of the northern jetty. This erosion remained significant until approximately 1986. Subsequently, this region has remained relatively stable due to the placement of rock revetment and shoreline structures during the 1970s and 1980s. Currently, Maine state law does not allow shore attached structures and these revetments were placed in response to the emergency conditions. It is expected that without these structures, the erosion would continue. The shoreline north of this 2,500 to 3,000 foot stretch has been stable throughout the time period evaluated; however in more recent times (after 1998) this area has also shown erosion likely due to increased storm events and the lack of available sediments from beaches to the south (Camp Ellis). A sandbar emanating from the north jetty melds to the shoreline at the approximate location where the shoreline erosion begins to taper off. This bar, formed since the construction of the jetties, may be a potential sediment transport pathway for sand moving from south-to-north around the jetty.

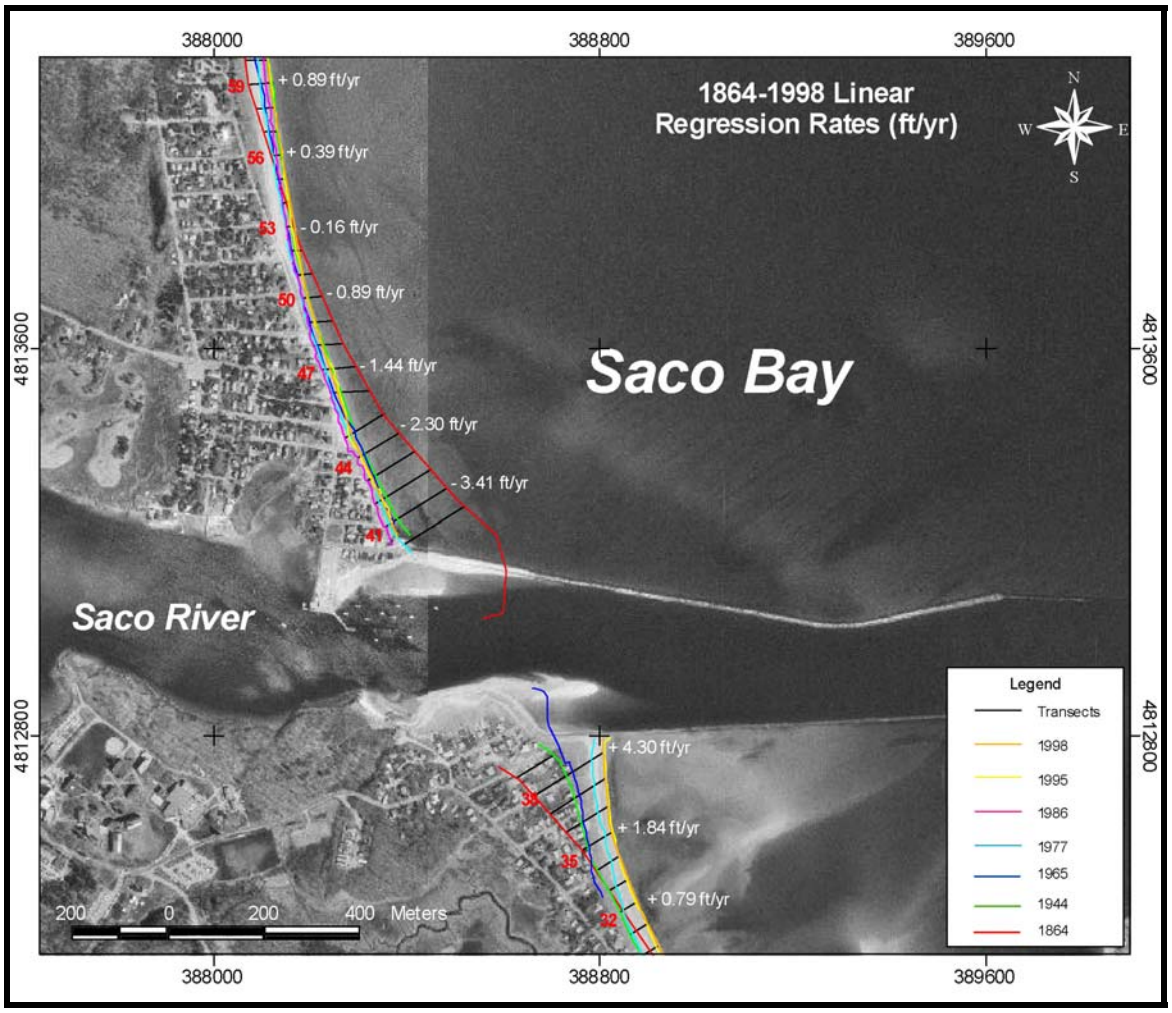

Figure 3-2. Historical shoreline positions and change rates (linear regression) from 1864-1998 for the region near the Saco River.

Figure 3-3 presents the shoreline positions and change rates for the area north of Camp Ellis Beach, containing Ferry Beach and Bay View. Although this stretch of shoreline has been relatively stable during the time period evaluated (up to 1998), erosion in this area has increased recently due to storm events and the lack of available sediment from the beaches directly to the south (Camp Ellis). Shoreline change rates indicate slight accretion, with a stable point at the salient landward of Eagle Island. This salient feature may also reduce wave energy on both sides of the salient, producing areas more susceptible to accretion.

Figure 3-4 presents the next stretch of shoreline to the north, featuring the inlet at Goosefare Brook. This reach of shoreline also indicates a fairly stable history. Shoreline change rates show consistent accretion, averaging around 1-1.5 ft/yr. Shoreline advancement is most significant in the areas directly adjacent to the inlet at Goosefare Brook. The orientation of the ebb shoal complex at Goosefare Brook would seem to indicate a small, localized net southward sediment transport direction.

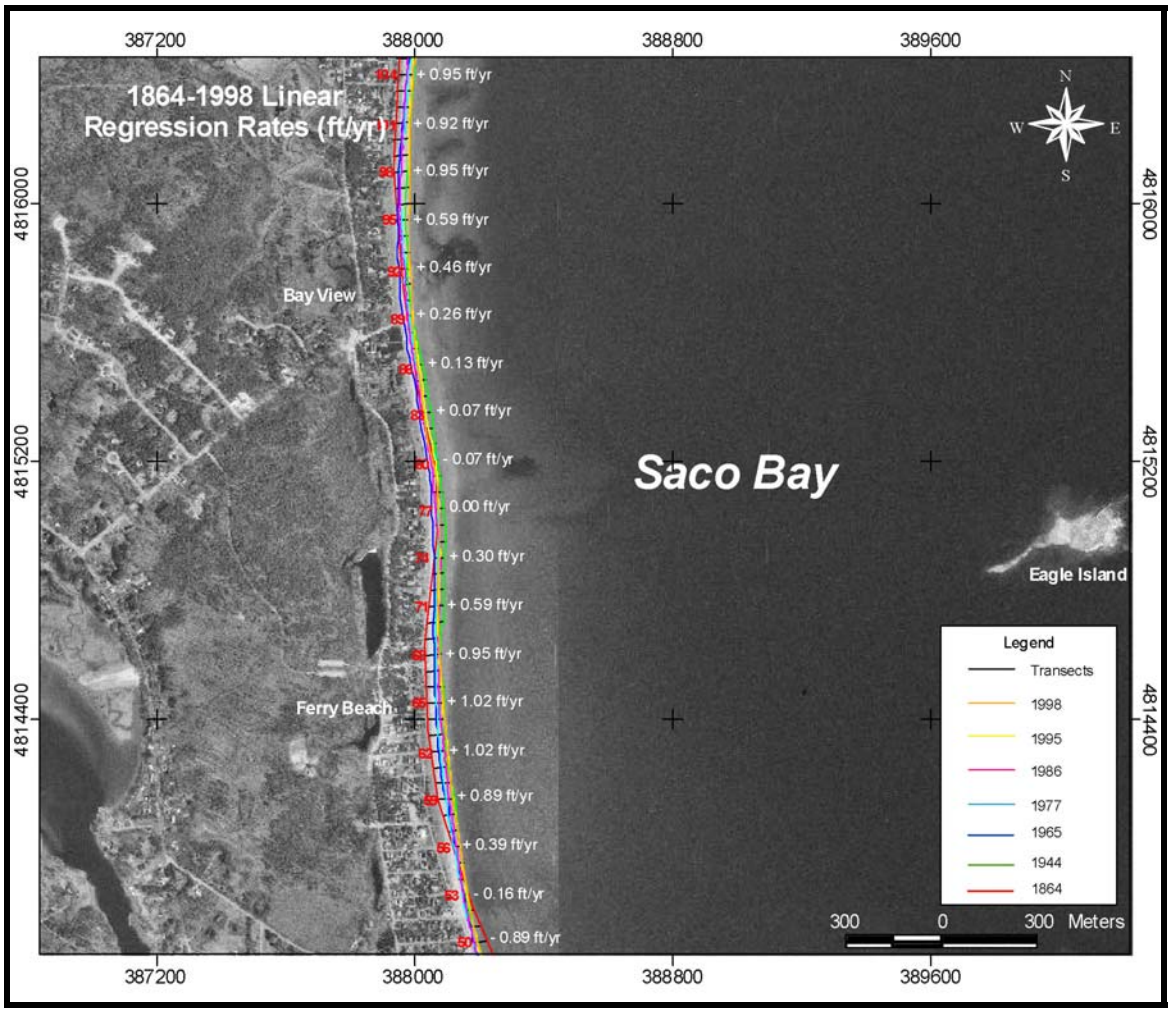

Figure 3-3. Historical shoreline positions and change rates (linear regression) from 1864-1998 for the region near Ferry Beach and Bay View in Saco Bay.

Figure 3-5 presents the northern portion of the Saco Bay shoreline, near Scarborough River. This reach of shoreline (to the west of Scarborough Inlet) indicates significant accretion. Shoreline change rates show approximately 2-3 ft/yr shoreline advancement, although this trend has approached a more stable condition in recent years. A consistent pattern of moderate to moderately high accretion has existed throughout this portion of the shoreline. Sediment transport in this region is clearly to the east/northeast. A more detailed shoreline change assessment of the shoreline regions near the Scarborough River, including a specific focus on Western Beach, as discussed in Aubrey Consulting, Inc/Woods Hole Group (2004). The analysis of shoreline change for Western Beach (Woods Hole Group, 2004) evaluated the shoreline response for time periods pre and post project construction (dredging, widening, and structures at the Scarborough River).

Figure 3-6 displays the rates of shoreline change computed using the end-point (dotted line) and linear regression (solid line) methods for the entire time period of 1864 to 1998. The x-axis indicates the rate of shoreline change, where positive values indicate

accretion, and negative values indicate erosion. The y-axis indicates the transect number corresponding to the maps of transects presented in Appendix 3-A. In general, the transect numbers increment from south to north and Figure 3-6 presents the shoreline change rates for the entire Saco Bay region. The figure shows that the end-point and linear regression methods yield similar rates of change. This similarity is an indication that the changes in shoreline position have been linear and steady through time and that there is little temporal variability in the data throughout the 134-year period at a given location. The only significant erosion within the entire Bay is at Camp Ellis Beach. Moderate accretion is evident at Goosefare Brook, the region directly south of the Saco River, and the area directly west of the Scarborough River.

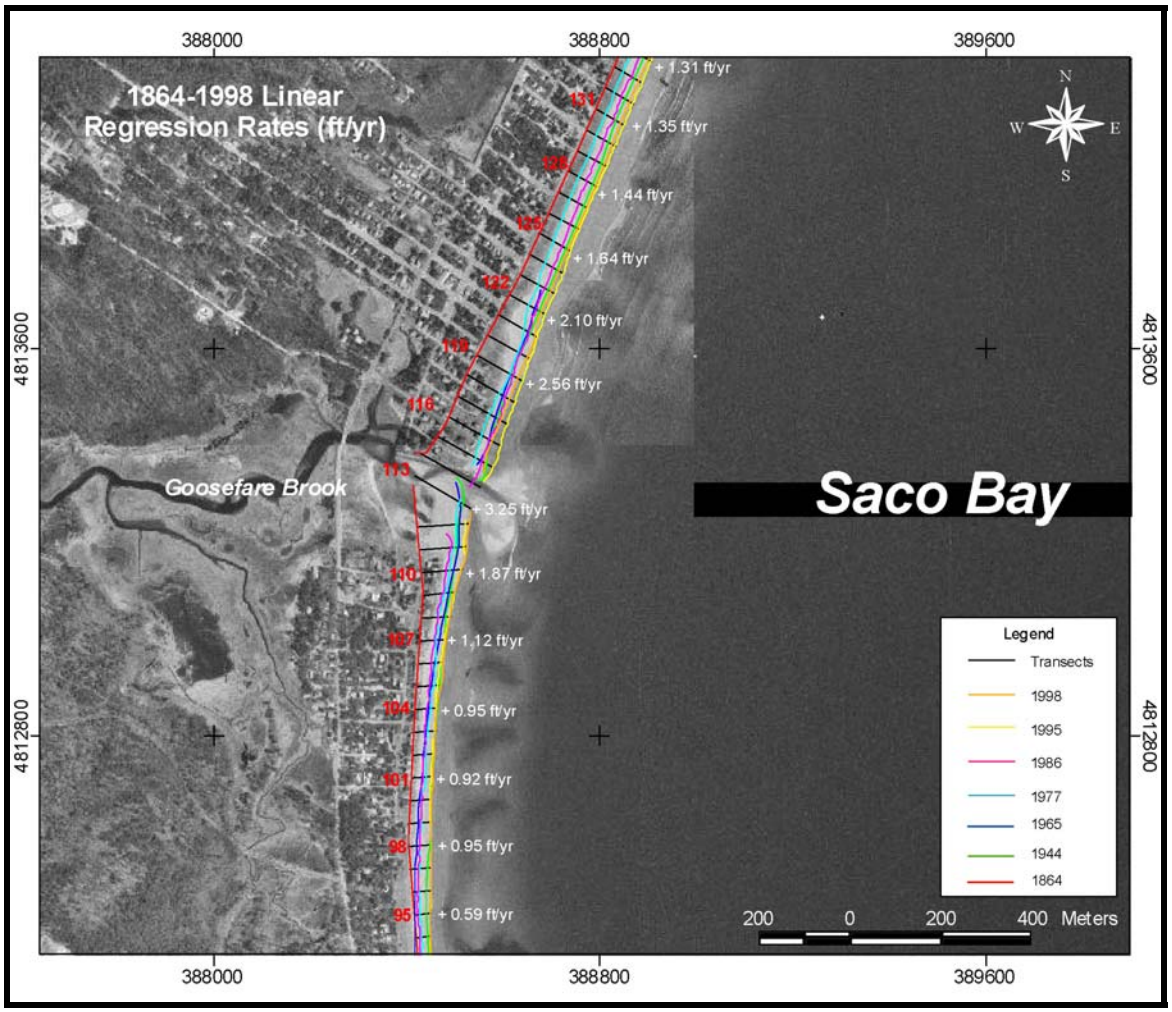

Figure 3-4. Historical shoreline positions and change rates (linear regression) from 1864-1998 for the region near Goosefare Brook in Saco Bay.

The potential RMS errors calculated for the rates of shoreline change shown in Table 3-4 were used to help gauge the significance of the magnitude of shoreline change. In

general, where the RMS errors are greater than or equal to the rates of shoreline change, the uncertainty in the magnitude of shoreline change is high. This usually occurs in areas where the annual rates of shoreline change are low. Although the error bands show the uncertainty in the magnitude of shoreline change, the trends in shoreline position are accurate. For example, areas that show a trend for shoreline retreat still indicate shoreline retreat even with the error bounds applied. Therefore, the interpretation of the shoreline change rates is not controlled by potential errors. RMS bands have been plotted in Figure 3-7 to show the range in computed shoreline change rates (error bands shown for end-point method only). The solid line indicates the calculated shoreline change rate, while the dashed lines show the upper and lower bounds after the error had been added to the calculated rates.

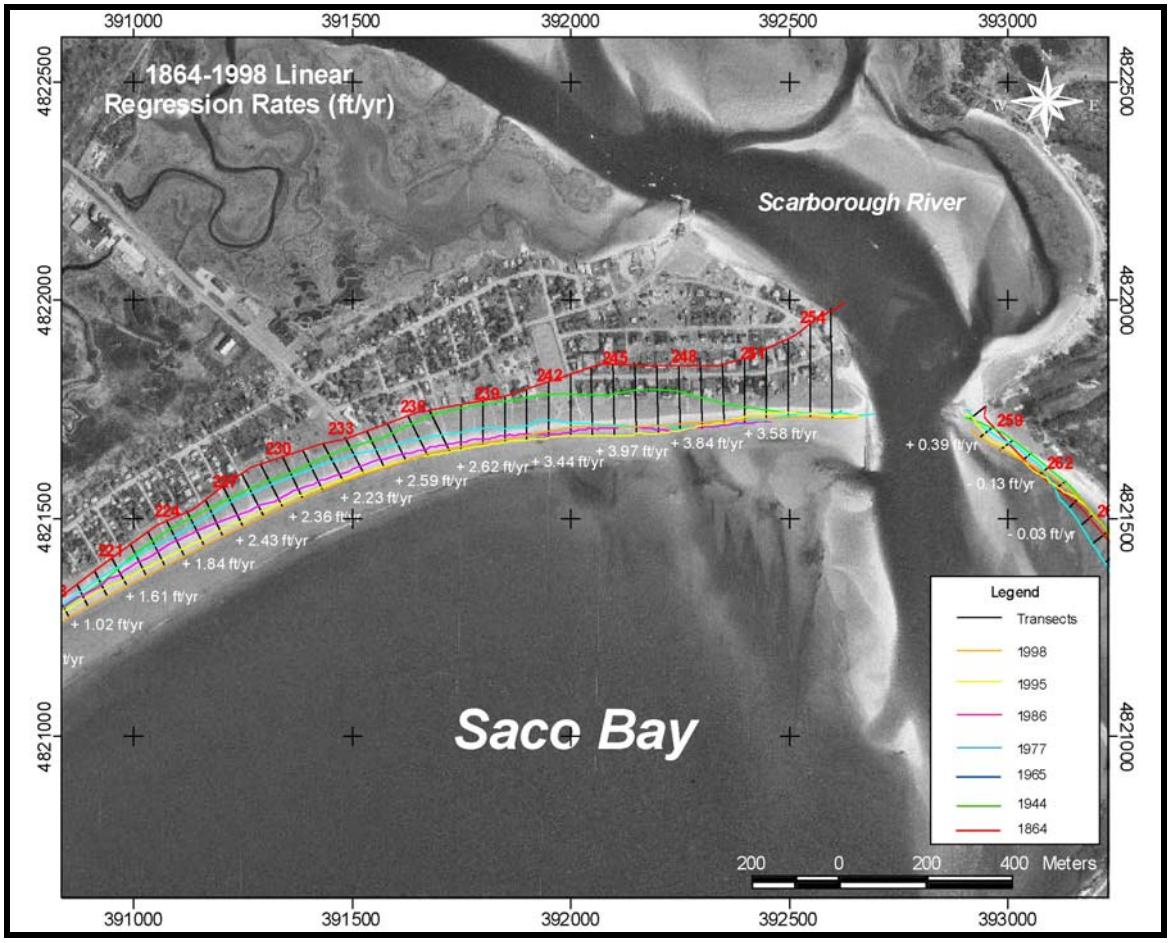

Figure 3-5. Historical shoreline positions and change rates (linear regression) from 1864-1998 for the region near Scarborough River in Saco Bay.

To evaluate the historical development of the Saco Bay shoreline, the response of the shoreline was examined during different time intervals. The discussion of the historical shoreline change analysis was broken into both a historical (1864-1944) and

contemporary (1944-1998) time period to compare the shoreline response to the overall shoreline change trends (1864-1998). This segregation was used to evaluate potential differences in shoreline change between historic and more recent times. Figure 3-8 presents the historic (red line), contemporary (green line), and overall (blue line) shoreline change rates for Saco Bay. In general, patterns and trends of erosion and accretion remain the same over all three time periods.

3.3.1 Overall Shoreline Changes (1864-1998)

Between 1864 and 1998, a number of important changes took place around the southern portion of the Saco embayment, in particular in the area to the north and to the south of the USACE jetties. One of the most notable changes was the erosion that has occurred on the northern side of the jetties near Camp Ellis from 1864-1998, with localized erosion rates in excess of -3.41 ft/yr. Concurrently, adjacent to the southern jetty accretion has occurred over this time period in excess of +4.0 ft/yr. The construction of the two jetties have clearly resulted in a net accretion on the southern side of the jetties, and conversely, net erosion to the north (Camp Ellis Beach).

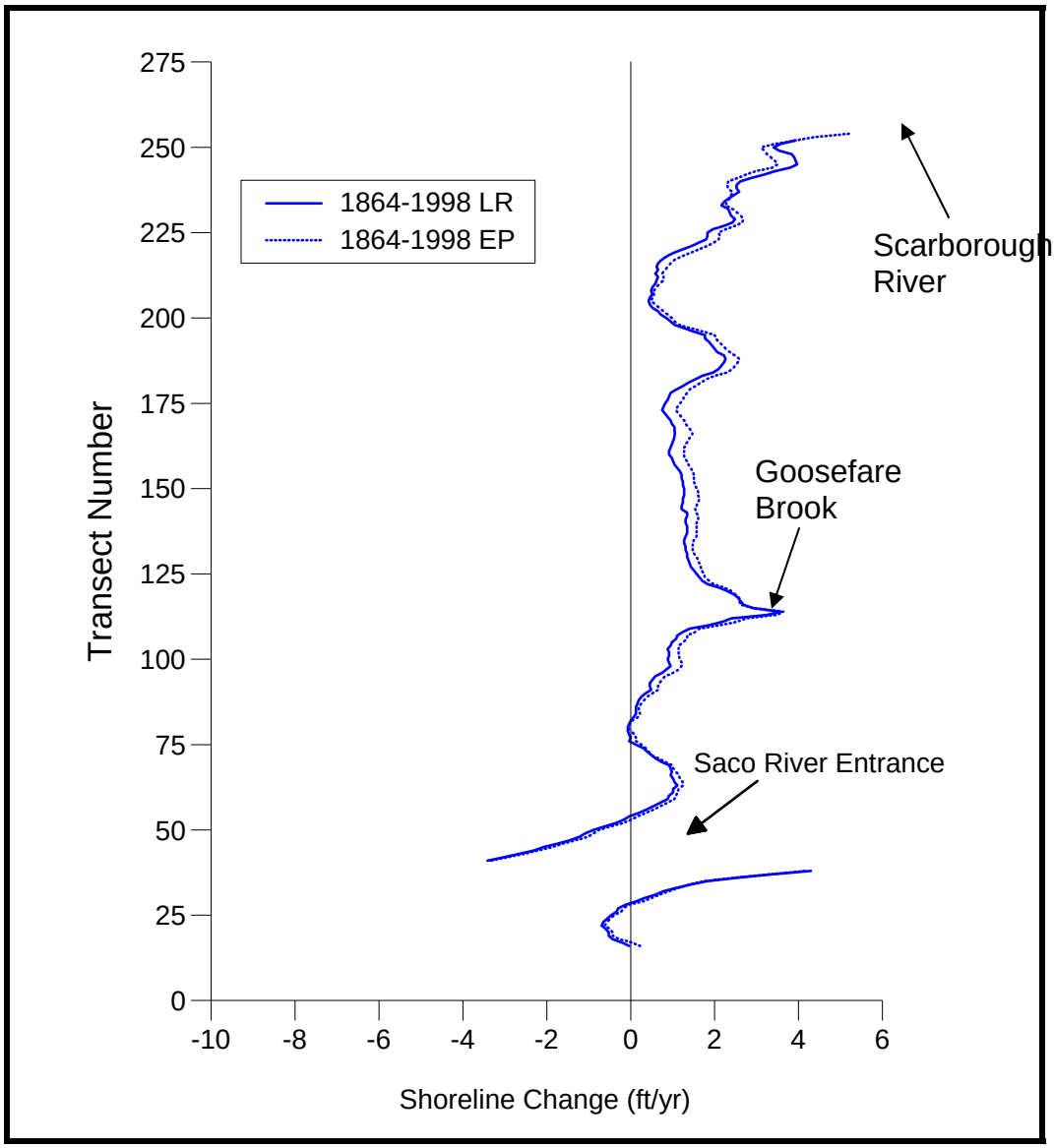

Figure 3-6. Shoreline change rates calculated using the linear regression (solid line) and end point methods (dotted line) for the period of 1864-1998. For transect locations, see Appendix 3-A.

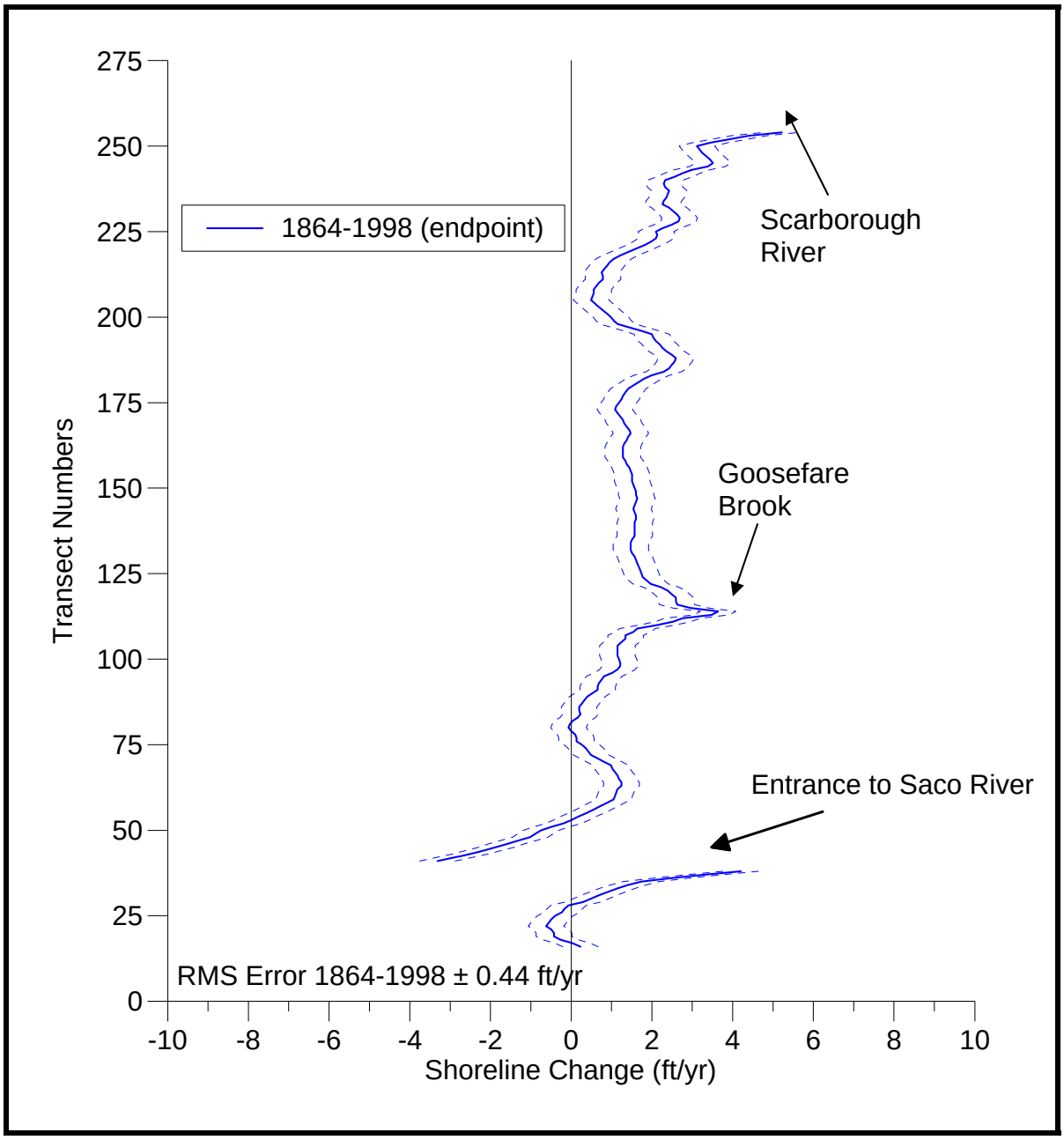

Figure 3-7. Shoreline change rates calculated using the end point method (solid line) for the period of 1864-1998. Dotted lines represent the upper and lower estimated rates of change after adding the error bounds (± 0.44 ft/yr). For transect locations, see Appendix 3-A.

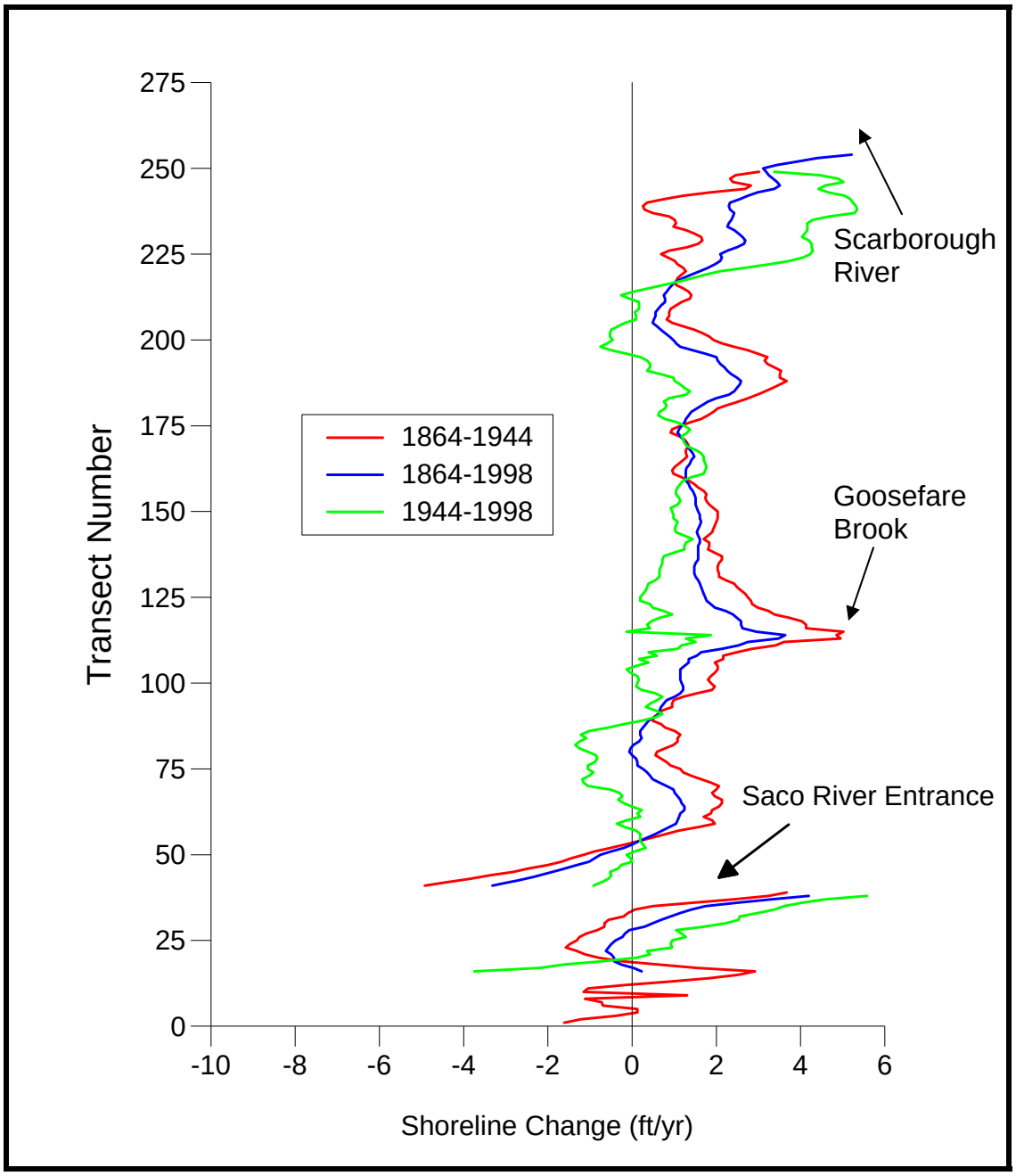

Figure 3-8. Shoreline change rates calculated using the end point method for the time periods of 1864-1944 (red), 1944-1998 (green), and 1864-1998 (blue). For transect locations, see Appendix 3-A.

Modifications to the Saco River continued after the initiation of the northern jetty in 1869 through 1937-1958. During this time the jetty was extended an additional 860 feet and the height of the landward end of the northern jetty was increased. Erosion continued throughout this time period, and not until shoreline protection was introduced in the 1970s and 1980s does erosion lessen. This reduction in the erosion rate is likely a

temporary state caused by the emergency shore protection measures (revetments, sand placement, geotubes, etc.).

Between transects 53 and 101 (in the area between Ferry Beach and Bay View), a generally stable section of shoreline persists (Figure 3-6). Shoreline change rates range from -0.16 ft/yr to +0.92 ft/yr in this region. Rates of accretion begin to increase close to the area of Goosefare Brook, and rates reach in excess of +2.0 ft/yr at some locations in the vicinity of the Goosefare Brook inlet. Average rates of shoreline change between Ocean Park and Surfside are +1.2 ft/yr and are relatively stable to moderately accretional. Although this section was generally stable over the entire 1864-1998 period of analysis, the area directly north of Camp Ellis Beach experienced erosion in the order of -1 ft/yr during the 1944-1998 time period (Figure 3-8).

Another significant change that occurred between 1864 and 1998 was the seaward growth or accretion of the shoreline in the northern portion of Saco Bay. The beach west of Scarborough River has experienced accretion throughout the entire 134-year study period, with accretion rates reaching +3.5 ft/yr. Previous work (Kelley et al., 1995) have assumed a general northerly sediment transport direction for this embayment with the major sediment source being the Saco River. Slovinsky and Dickson (2003) determined that this particular zone appears to be outside the direct influence of the Saco River; however it is likely heavily influenced by the Scarborough River and its jetty. Sediment from the Scarborough River being transported by tidal currents may have a large effect on the accretion rates in the northern portion of the bay. The increase in accretion in this area is thought to be a result of sediments trapped in the Scarborough River ebb-tidal delta and a decrease in tidal currents from the river. It is also likely that a significant portion of Saco Bay has a net south to north sediment transport direction as inferred from the direction of shoreline advancement at the Scarborough River.

Throughout Saco Bay there are significant variations in beach profile shapes as presented by Slovinsky and Dickson (2003). They discovered that in general, low profile elevations and relatively steep slopes dominate the southern portion of the Saco embayment (from the Jetties to Ferry Beach). To the north, near Goosefare Brook, the beach profiles tend to flatten and attain higher elevations, this pattern continues to the southern area of Old Orchard Beach. At Old Orchard Beach the profile elevations decrease dramatically, and the profile slopes flatten substantially. At Scarborough Inlet the profiles shallow seaward, but increase in overall elevation. These variations in shoreline profiles may coincide with changes in rates at which the shorelines change in Saco Bay (Slovinsky and Dickson, 2003). The trends are generally in agreement with beach shape associated with erosional and accretional beaches world-wide.

3.3.2 Historic Data (1864-1944)

The historic data range (1864-1944) illustrates a similar pattern of shoreline changes as compared to the overall time period (1864-1998).

The magnitude of erosion at Camp Ellis Beach is increased, since this historic time period immediately follows the initial construction of the Saco River northern jetty. Rates of shoreline erosion have maximum values of approximately -5 ft/yr.

In addition, the magnitude of the accretion in the Goosefare Brook inlet region is also increased when compared to the overall time period. The average long-term rate is approximately 3.5 ft/yr, while the historic period rate approached 5 ft/yr.

The magnitude of the accretion adjacent to the Scarborough River is reduced when compared to the overall time period. Shoreline accretion averages 1 to 2 ft/yr, while the overall time period indicated rates of between 2 to 4 ft/yr.

3.3.3 Contemporaneous Data (1944-1998)

The contemporary data period (1994-1998) shows similar patterns to the overall and historic time periods; however, there are some significant differences in magnitudes, and in some cases reversals of trends.

The contemporary data show continued accretion immediately to the south of Saco River, with rates between 2 to 6 ft/yr. All time periods indicate this region (immediately south of the Saco River) as an area undergoing shoreline advance. There have been time periods of erosion in the coastline further south of Saco River. For example, the Hills Beach region has shown time periods of erosion (approximately -1 ft/yr).

There is reduced erosion over the 2,500 to 3,000 foot stretch of coast just north of the northern jetty (Camp Ellis Beach). This stretch of shoreline was the most prone for erosion historically; however, during the contemporary time period it appears to have temporarily stabilized. This stabilization is likely a result of a combination of armoring of the shoreline (revetments, seawalls, etc.) and the more contemporary practice of placing sand dredged from the Saco River navigation project on Camp Ellis Beach.

The area directly north of Camp Ellis Beach, which over the entire time period has been stable, has experienced erosion over the more recent time period. This may be due to the armoring of the neighboring beach (directly to the south) and/or the reduction in sediment available at Camp Ellis Beach due to the significant erosion at Camp Ellis Beach, With this significant reduction in sediment supply at Camp Ellis Beach, this area can no longer provide sediment to the beaches to the north. Rates of erosion during the recent time period are approximately -1 ft/yr.

Overall, the contemporary time period shows less accretion over the middle section of the Saco Bay shoreline. Rates have decreased considerably in some stretches, and a few locations have switched from accretion to erosion.

Increased accretion is shown at Scarborough River over a greater distance of beach. Significant accretion rates occur between transects 225 and 250.

3.4 Summary

An analysis of historical shoreline change was performed for an 8-mile shoreline segment along Saco Bay, Maine. The data used to compile the analyses were derived from aerial photography, historical maps, and digital orthophotographic quads. Rates of historical shoreline change were calculated at 265 shore-normal transects from Biddeford Pool to Prouts Neck.

Between 1864 and 1998, the shoreline accreted adjacent to the southern jetty in Saco Bay. Accretion rates along this stretch ranged from +0.74 ft/yr at transect 32 to +4.3 ft/yr at transect 38, adjacent to the southern jetty. Between 1944 and 1998 the shoreline accreted more rapidly at rates exceeding 5 ft/yr. A small erosional area exists at Hills Beach (at approximately transect 25). Rates of erosion in this region are approximately -1 ft/yr.

The shoreline adjacent to the northern jetty (Camp Ellis Beach) experienced significant erosion. The shoreline between 1864 and 1998 eroded at rates between -3.4 ft/yr (at transect 41) and -0.2 ft/yr (at transect 53). The more contemporary time period (1944-1998) shows continued erosion, but at a reduced rate (approximately -1.0 ft/yr and less). This relative stabilization is primarily due to man-made intervention in the form of heavy structural stabilization (seawalls, revetments, etc.) and sand nourishment efforts in this area (placing sand dredged from the Saco River in the beach).

Between transects 53 and 101, the area between Ferry Beach and Bay View, there is a relatively stable section of shoreline from 1864 to 1998. Here shoreline change rates range from -0.2 ft/yr to +0.9 ft/yr. However, in the more contemporary time period, the shoreline becomes erosive, with rates averaging approximately -1 ft/yr. This may be due to the reduced sediment supply that is available for transport to this region from Camp Ellis Beach.

Between 1864 and 1998, a seaward growth of the shoreline occurred in the northern portion of the bay, and most notably closer to the area of Scarborough Inlet. This region has experienced accretion throughout the entire 134-year study period with accretion rates reaching +3.5 ft/yr. For recent history (1944-1998) a similar trend, with an increased magnitude, exists.

In general, in more recent history (1977-1998) the entire Saco embayment is experiencing shoreline accretion at reduced rates than during the historical time-period from 1864 to 1998. This may indicate a paucity of sediment supply compared to historic time periods, as less sand has been delivered from the Saco River to the beaches since the jetties (specifically the northern jetty) does not allow the sediment to be transported to the beach.

4.0 BATHYMETRIC DATA COLLECTION (TASK 3)

A significant amount of bathymetric information was required to simulate the sea state from the large, coarser grids of the generation-scale model to the smaller, finer grids of the nearshore (local) wave models. Existing data sources were used extensively and supplemented with new surveys for the nearshore region. The generation-scale modeling used 30 arc-second bathymetry constructed by the Coastal and Marine Geology Program of the United States Geological Survey. The digital bathymetry was constructed using various data sources:

- NOAA Hydrographic Survey Data and NGDC Marine Trackline Geophysics Data
- Naval Oceanographic Office Digital Bathymetric Data Base - Variable Resolution gridded bathymetry
- Supplemental Datasets from Bedford Institute of Oceanography and Brookhaven National Laboratory
- NOAA Medium resolution digital Shoreline and DMA World Vector Shoreline
- Defense Mapping Agency ETOPO5 Digital relief of the Surface of the Earth
- GEBCO General Bathymetric Chart of the Oceans
- USGS North American 30 arc-second Digital Elevation Model (DEM)

The transformation-scale (or regional) modeling used digital bathymetry from the National Ocean Service (NOS), combined with 1 m LIDAR data (Irish and Lillycrop, 1999), as shown in Figure 4-1. In addition, a high-resolution nearshore bathymetric survey conducted near the mouth of the Saco River on May 13 and 15, 2003 was also included. The LIDAR and new nearshore bathymetric data were also used in the local and nearshore (local) wave model simulations.

Details on the bathymetric extents, sources, and grid development are discussed in each specific model chapter. For example, the bathymetry and model grid used for the regional wave modeling are presented in Chapter 9.0. This chapter focuses on the bathymetric data set collected as part of this study, in the nearshore region of Camp Ellis Beach.

4.1 Survey Methodology

CR Environmental, Inc. (CR) conducted a bathymetric survey of portions of Saco Bay and Wood Island Harbor near the mouth of the Saco River on May 13 and 15, 2003, for Aubrey Consulting, Inc. The survey was conducted from CR's 22-foot R/V C-Hawk. The boat was equipped with safety gear, multiple 12-volt power supplies, and a laptop computer equipped with navigation and data-logging software.

4.1.1 Survey Extent and Spacing

Figure 4-2 presents the survey extent and spacing for the 2003 survey. Proposed track lines are indicated by the white lines and are spaced at approximately 50 meters.

Additional data exceeding that planned were also collected within the throat of the Saco River Inlet (between the jetties). The survey extent was selected to focus on the region that was most critical for wave transformations in the nearshore vicinity of Camp Ellis Beach. In addition, this nearshore region had the most potential for recent physical changes. Therefore, in this region it was critical to get the most recent and accurate bathymetric information.

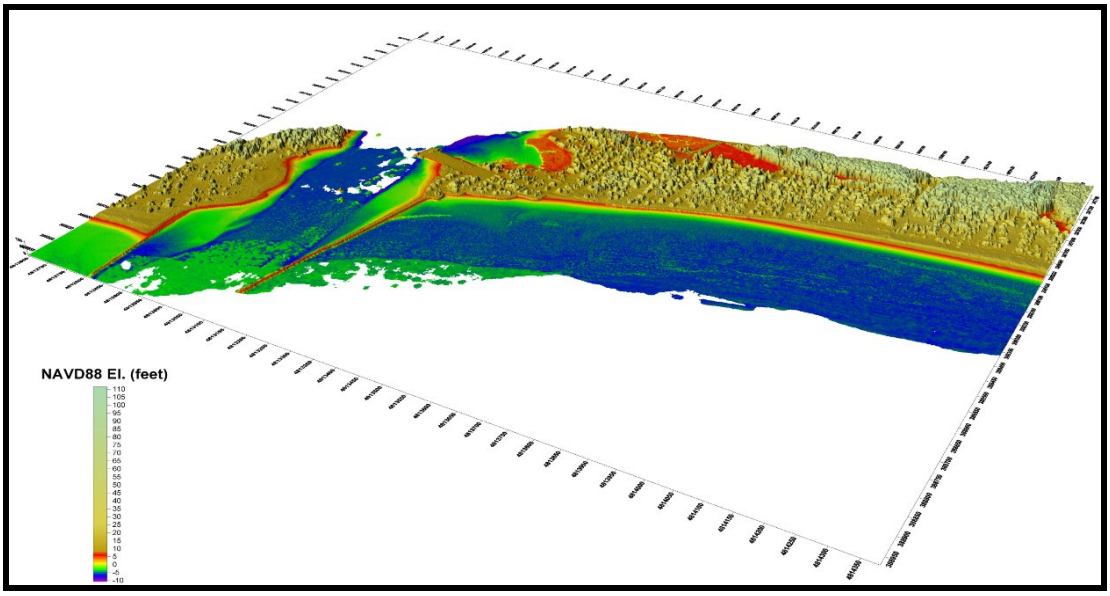

Figure 4-1. 1-meter LIDAR data of Camp Ellis region.

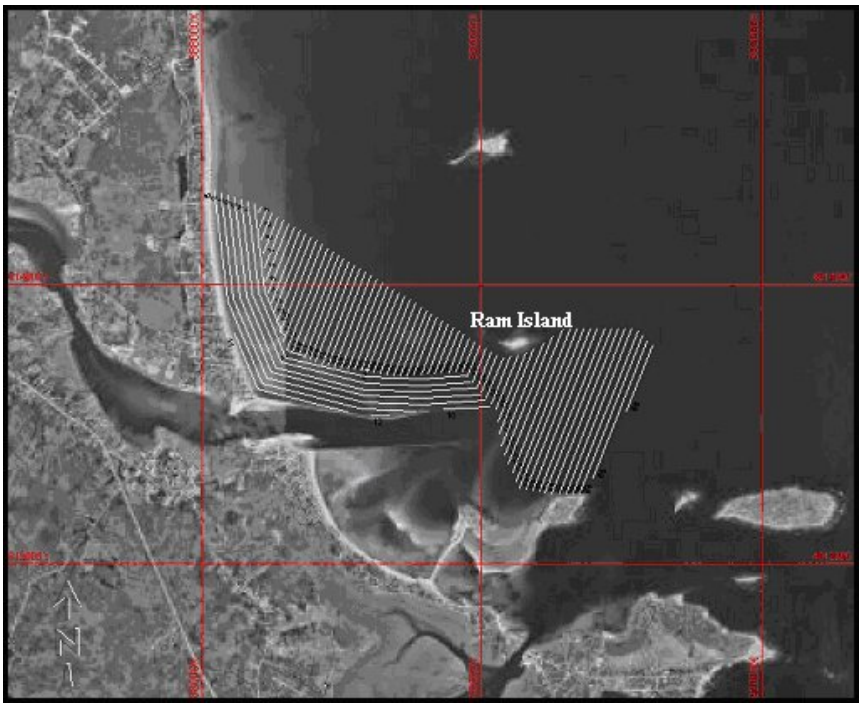

Figure 4-2. Survey extent and line spacing for the 2003 bathymetric survey.

4.1.2 Equipment Description and Operation

Real-time horizontal position accuracy of less than 1-meter was achieved during the survey using a Trimble Navigation Pro-XRS Differential Global Positioning System (DGPS). United States Coast Guard differential correction beacons were used to provide real-time corrections to satellite data. DGPS signal quality and satellite geometry were continuously monitored and filtered during the survey.

Water depth measurements were collected using a DE719D MK2 precision survey echo sounder (Raytheon Electronics, Inc.). The echo sounder was retrofitted by Ocean Data Equipment Corporation (ODEC) of Providence, Rhode Island with circuitry specifically designed for work in water as shallow as 1.5 feet (below the transducer). The echo sounder was equipped with an 8-degree 200-kHz transducer having an accuracy of 0.5% of the indicated depth. The echo sounder outputs depth measurements at a rate between 2 to 10 soundings per second, depending on water depth.

Prior to survey work, the echo sounder was calibrated for site-specific water sound velocity by measuring the water temperature to estimate sound velocity, by using the bar-check method, and by comparison with manual soundings conducted in flat areas. The fathometer consistently reported depths to within 0.1 feet of the manual soundings throughout the range of depths encountered in the survey area.

The Trimble DGPS and the fathometer were interfaced to a shipboard computer running Coastal Oceanographic's HYPACK MAX™ hydrographic surveying software. During the survey, HYPACK calculated meter scale XY positions, recorded the depth and navigation data, and provided a steering display for the vessel helmsman.

4.1.3 Data Processing and Mapping

Raw (unaltered) bathymetric data for each transect line were evaluated using Hypack's Editing program. Outlying data points (spikes) caused by biological interference (e.g., fish or vegetation) were deleted. Tide corrections were applied using water elevation data as discussed in Chapter 5.0. Corrected soundings were exported from Hypack as a single ASCII formatted XYZ file. Sounding data were converted to the Maine State Plane grid, referenced to the North American Vertical Datum of 1929, using the most recent release of the U.S. Army Corps of Engineers CORPSCON program (V. 5.11.08).

4.2 Bathymetric Observations and Summary

Figure 4-3 presents the post-processed bathymetric data collected in May 2003. The contours indicate 2-foot elevation swaths relative to NGVD 1929. The color contours are presented as red (shallow) to dark purple (approximately –56 feet). Figure 4-4 presents a closer view. A number of relevant features are shown in the bathymetric data that likely impact wave propagation and transformation in the vicinity of Camp Ellis Beach:

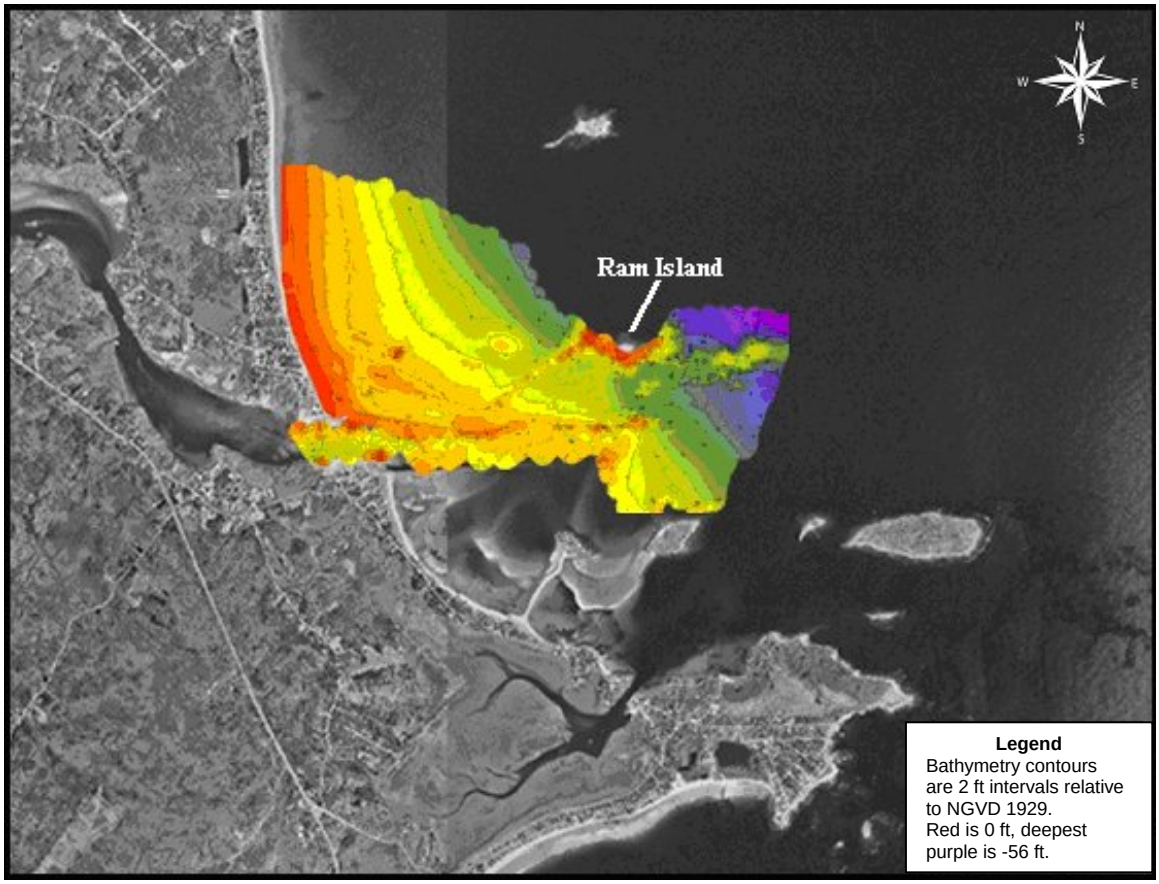

Figure 4-3. Nearshore bathymetric data collected in May, 2003.

Seal Rock is clearly identifiable in the bathymetry, as indicated in Figure 4-4, and is a feature that becomes exposed during low tide. Although Seal Rock does have some impact on wave focusing and transformations and provides some wave breaking ability, it does not play a significant role in the overall sea state in the nearshore region. Seal Rock does serve as an important landmark and some of the alternatives were designed to help utilize the natural ability of Seal Rock to provide some level of wave protection. For example, the segmented breakwater alternatives were spaced such that Seal Rock was located in the gaps between breakwater segments.

A salient has formed between Ram Island and the northern jetty. A salient is a coastal accumulation of sediment typically formed by wave refraction and diffraction and currents, leading from shallow water out towards an offshore island or breakwater. Typically salients form between an offshore island or breakwater and the shoreline; however, in this case the salient has formed between the island and the northern jetty.

A significant shore-and-jetty attached sand bar has formed extending in the northwest-southeast orientation between the northern jetty and Camp Ellis Beach. This feature likely serves as a natural wave dissipater for waves approaching the beach. The bar has a significant impact on the wave energy reaching the beach, and alternative layouts and

designs consider this feature as an important natural formation. All alternatives were designed to minimize the impact and work in concert with this natural feature.

An offshore shoal formation is evident seaward of Ram Island. This formation influences wave propagation and transformation seaward of the Eagle and Ram Island complex and is a key feature in the local wave modeling assessment.

The Saco River Inlet contained between the jetties features some complex bathymetry and shoals. As expected, the depths increase in the more constricted area near the landward end of the structures.

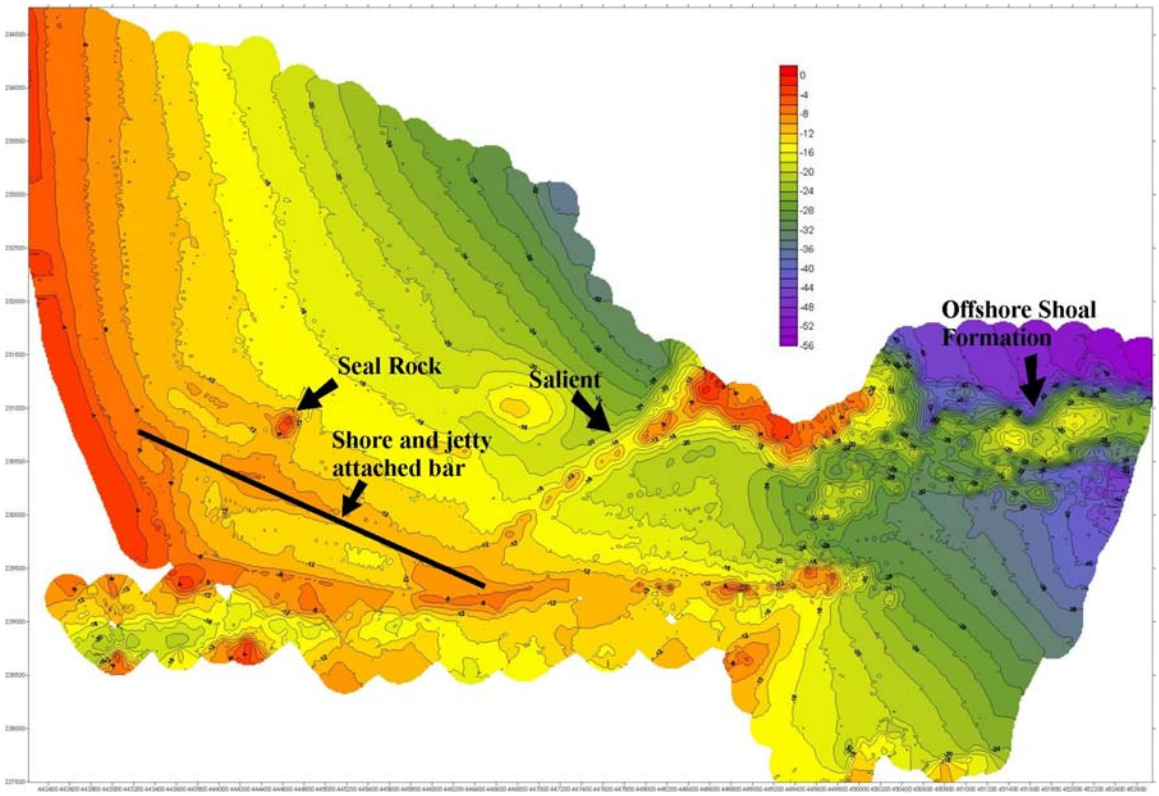

Figure 4-4. Bathymetric contour data and relevant features in the bathymetry offshore of Camp Ellis Beach.

5.0 TIDE DATA COLLECTION (TASK 12)

This chapter presents the time series of water surface observations collected from the Saco River region as part of Task 12 of the Saco River and Camp Ellis Beach Section 111 Project. Time-series of water surface elevation (calculated from pressure measurements) were obtained at four (4) locations (Figure 5-1) within the region during an interval of approximately two (2) months. The two (2) month deployment period allows for adequate characterization of all of the primary tidal constituents. Whereas short tidal records may be biased by climatic events, such as surges, wind, rainfall, atmospheric pressure, etc., this longer deployment samples a range of tidal events and is more representative of average tidal conditions within the estuary. This chapter briefly presents the data, including data collection procedures and instrumentation. These observations are analyzed to define the tidal fluctuations in the region and subsequently were applied in the numerical wave transformation modeling.

These data were also collected within the Saco River estuary in case the USACE decided modeling of nearshore circulation, hydrodynamics, and tidal driven sediment transport modeling was eventually warranted. For example, with the collection of these long-term tidal measurements, the ability to calibrate a hydrodynamic model of the Saco River system was feasible. However, in the process of the study, it was determined that although the Saco river delivered sediment to the system the hydrodynamics of the Saco River had little influence on the sediment transport dynamics occurring at Camp Ellis Beach, where waves were the primary forcing mechanism for sand movement. This conclusion is discussed in greater detail in Chapter 6.0, where direct measurements of the tidal currents are presented.

5.1 Instrument Setup

River deployment locations were chosen to measure the tide at the entrance to the river (near the Saco pier), as well as characterize adequately the tidal changes that occur through the lower portion of the river itself to provide calibration information for a river hydrodynamic model (near Saco Yacht Club). Redundant gauges were deployed at each of these two locations to ensure adequate data coverage, provide backup systems in case of failure, and provide accurate measurements.

Additionally, the two (2) wave measurement systems (Chapter 7.0 - Task 2) collected tidal observations in the offshore vicinity of the Saco River. Figure 5-1 shows the location of each of the tidal stations. The tide gauges were installed by securing each gauge to a pipe anchor and subsequently driving the anchor into the seafloor at each of the locations. Table 5-1 presents the recording interval and frequency of the deployed tide gauges. Even though one of the gauges (gauge #52020) was frozen for a portion of the deployment, due to the deployment of redundant gauges, 100% data return was achieved at each of the observation stations.

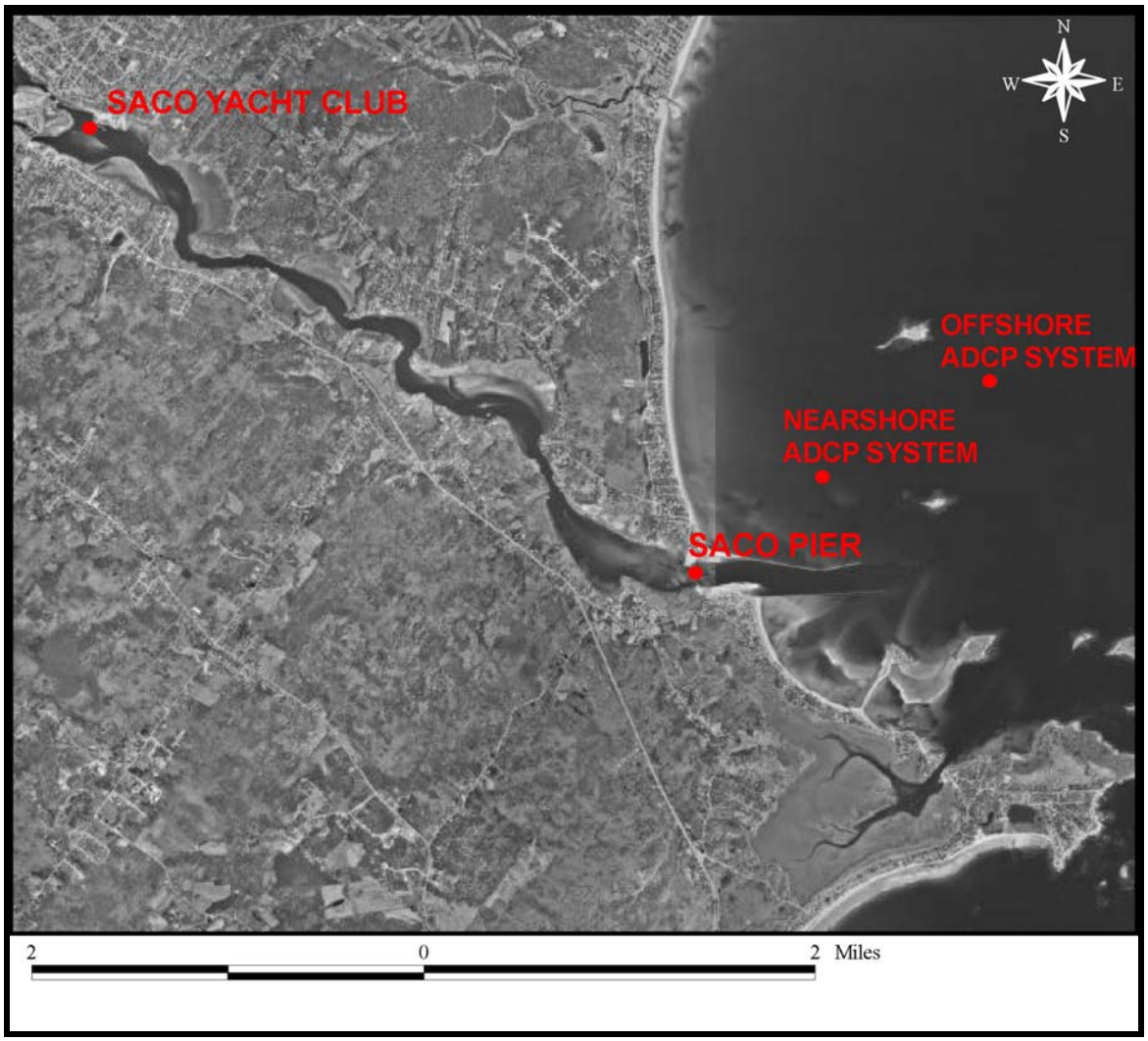

Figure 5-1. Tide gauge locations within the study area.

Table 5-1. Instrument deployment summary.

Tide Station Location (gauge #)	Recording Frequency (minutes)	Logging Interval	
		Began Recording	Ended Recording
Saco Pier (52017)	3.75	3/12/2003	5/23/2003
Saco Pier (52020)	3.75	4/21/2003*	5/23/2003
Yacht Club (52019)	3.75	3/12/2003	5/23/2003
Yacht Club (52021)	3.75	3/12/2003	5/23/2003
Nearshore Wave Station	60	3/12/2003	5/23/2003
Offshore Wave Station	60	3/12/2003	5/23/2003

* Gauge 52020 was frozen for the first half of the deployment period

Tidal elevations were measured using Woods Hole Group Seapac 2100 pressure gauges deployed within the River (Saco Pier and Yacht Club). Each tide gauge contained a Paroscientific DigiQuartz pressure sensor (0.015% accuracy and 0.0015% resolution) coupled to a data logger. Each of these instruments measured pressure continuously, recording the average pressure over 3.75 minute intervals. Pressure data were downloaded using a personal computer and associated software packages.

The two offshore wave stations recorded tidal elevations every hour averaged over a 20 minute burst via a Workhorse Sentinel ADCP fitted with a pressure sensor. Time resolution of tide observations at the offshore sites was reduced compared to River gauges due to battery and memory requirements of the *in situ* wave and current observations. However, this reduced resolution did not affect the analysis.

5.2 Tidal Observations

Each tide gauge measured the water and atmospheric pressure above the instrument. In order to estimate the water level (gauge pressure), the atmospheric pressure was removed from the measured signal. The data were corrected using regional atmospheric pressure data from National Climatic Data Center (NCDC) Portland International Airport station, presented in Figure 5-2. Subsequently, pressure data were converted to water surface elevation using the hydrostatic relationship based on the density of water. In order to reference the tide gauges to a common vertical datum, tide data from each gauge were referenced to the NAVD 1988 vertical datum. The tide gauges were surveyed to the instruments' pressure port via a local benchmark. Additionally, water surface elevation measurements were taken to provide a secondary means of referencing the water surface to NAVD 1988.

Figures 5-3 through 5-8 show the tidal observations from each instrument. Figure 5-9 shows a portion of the measured tidal observations during the deployment period for both locations within the Saco River. The data show two high tides and two low tides each day due to the influence of the moon and the sun. During a typical day, one of the high tides is higher than the other, and one of the low tides is lower. The spring and neap tides are also easily observed in the signal scale (Figures 5-3, 5-4, 5-5 and 5-6). During spring tide, also known as a moon tide, the tidal range is approximately 11.5 to 12.0 ft (3.5 to 3.7 m). However, during neap tide, the tidal range is reduced to approximately 7.0 ft (2.1 m). The observations at the upstream tide gauges (red line) indicated that only minor tidal attenuation compared to the downstream observations (blue line) as the tide propagates upstream. The tidal range at the upstream gauges is damped less than 0.6 ft (0.2 m), and the average daily reduction is even smaller. The nearshore ADCP shows a slow upward trend in the data likely caused by instrument settling. This trend can be removed by a linear detrend of the data and using the observed MTL at the offshore ADCP if the data are needed for hydrodynamic assessment or modeling.

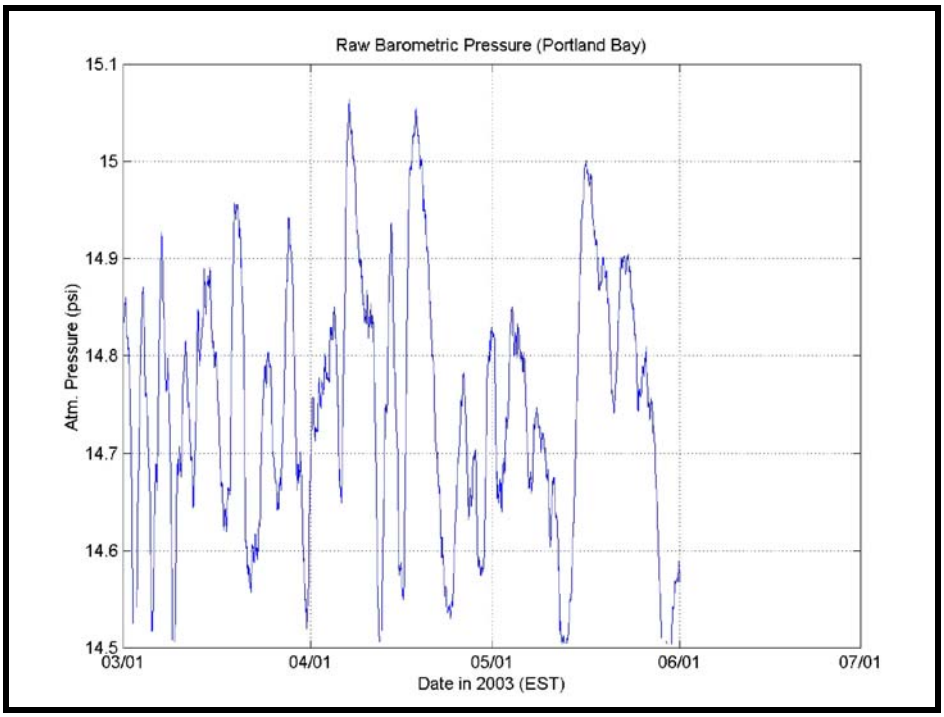

Figure 5-2. Atmospheric pressure data obtained from National Climatic Data Center (NCDC) for Portland International Airport Station.

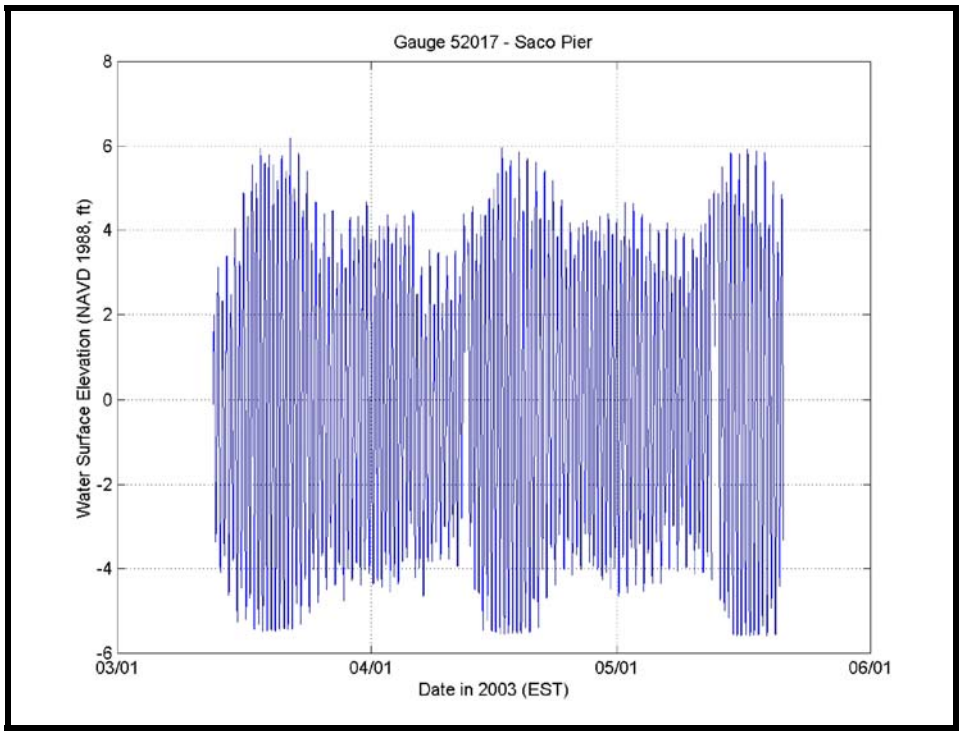

Figure 5-3. Measured water surface elevation at Saco Pier, just inland of the jettied channel (Gauge 52017).

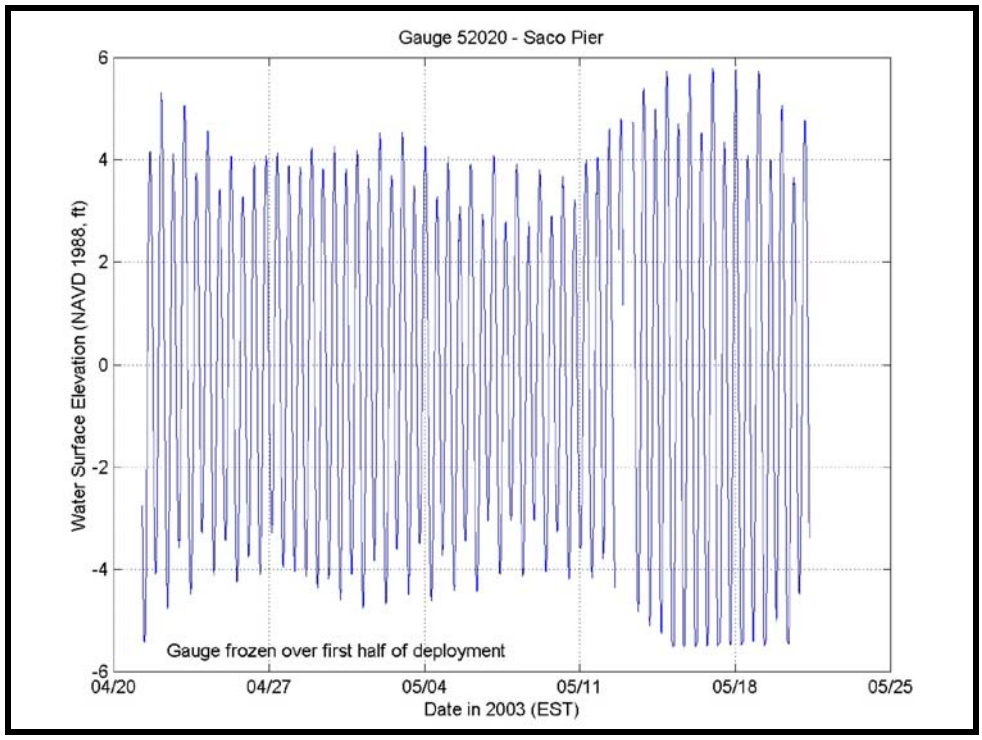

Figure 5-4. Measured water surface elevation at Saco Pier, just inland of the jettied channel (Gauge 52020).

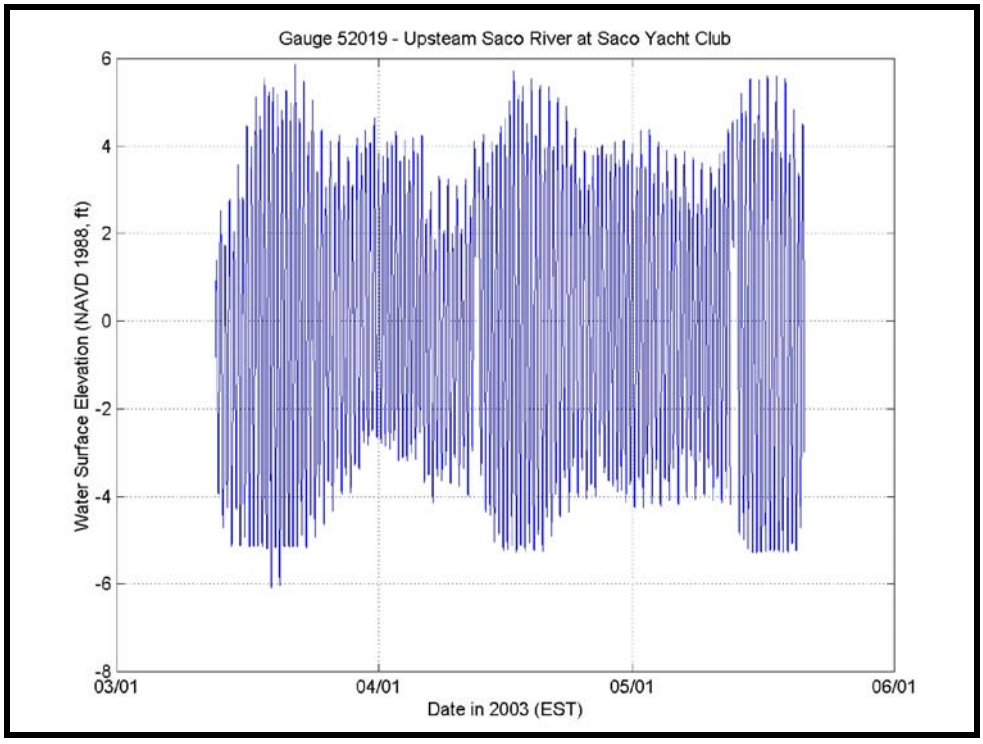

Figure 5-5. Measured water surface elevation at the Yacht Club upstream of the Saco River inlet (Gauge 52019).

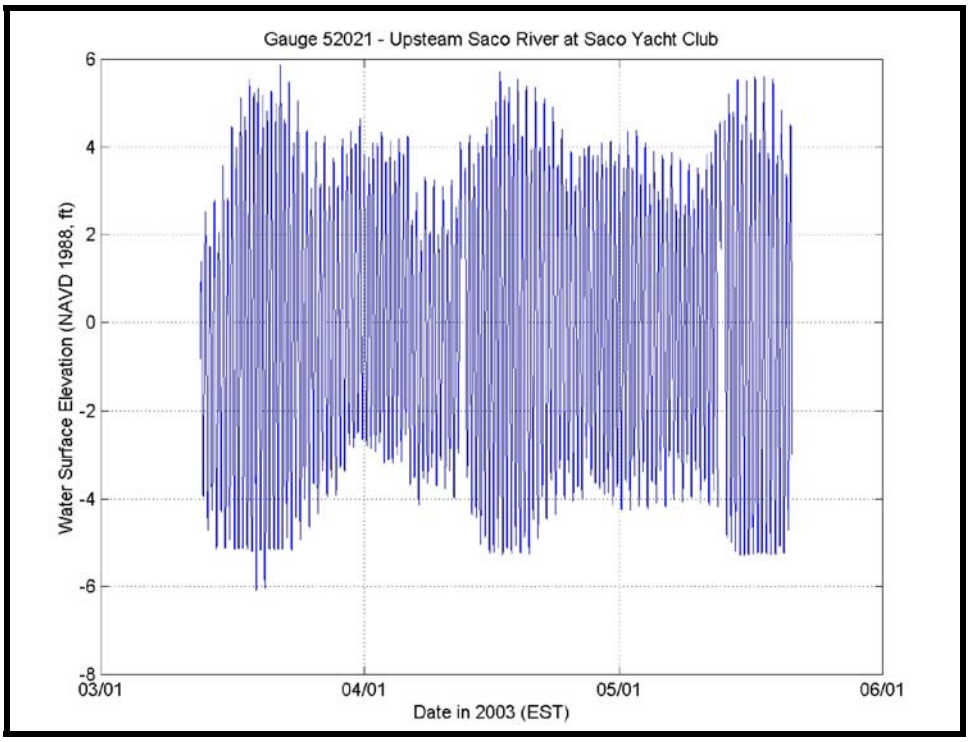

Figure 5-6. Measured water surface elevation at the yacht Club upstream of the Saco River inlet (Gauge 52021).

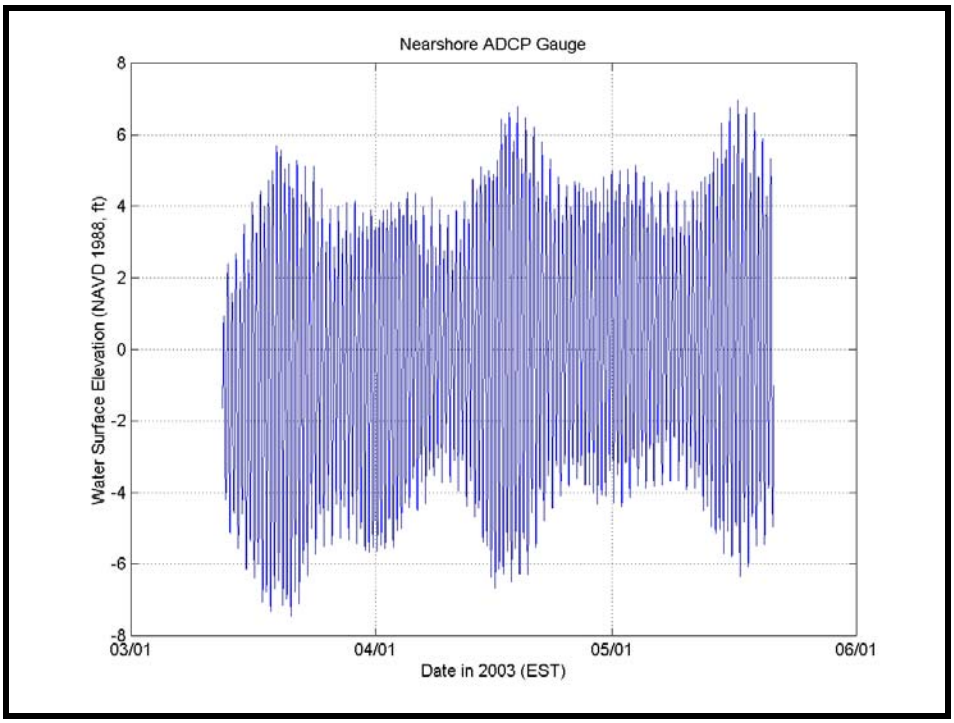

Figure 5-7. Measured water surface elevation at the nearshore ADCP station. The slight upward trend in the data is likely due to slow instrument settling.

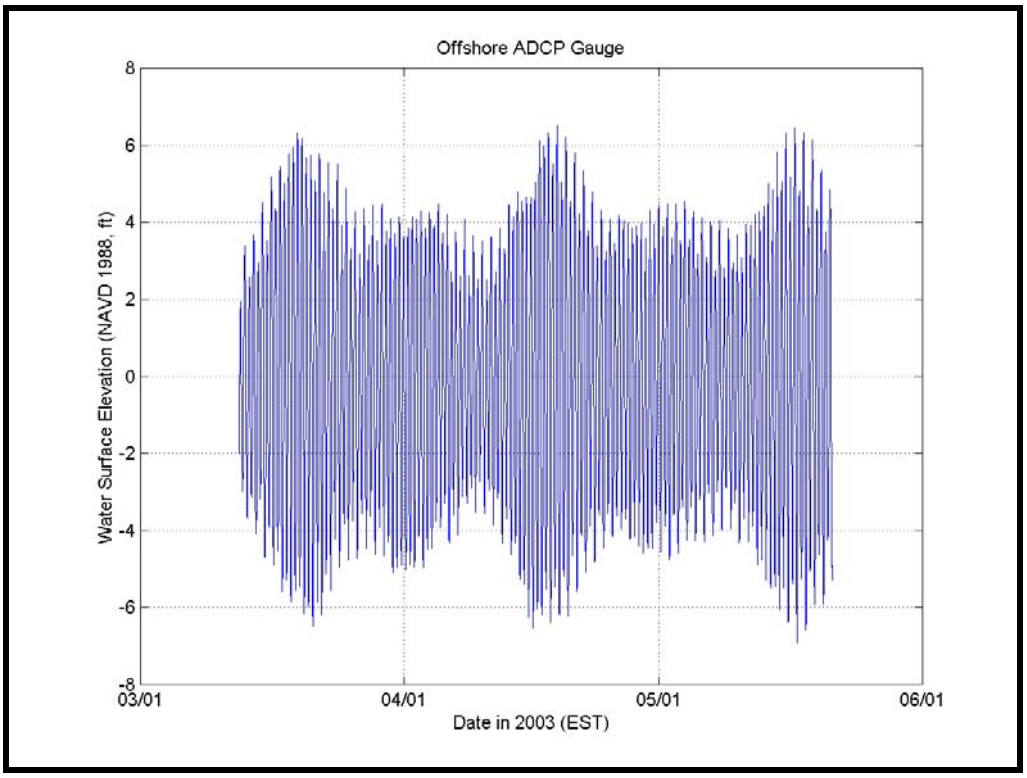

Figure 5-8. Measured water surface elevation at the offshore ADCP station.

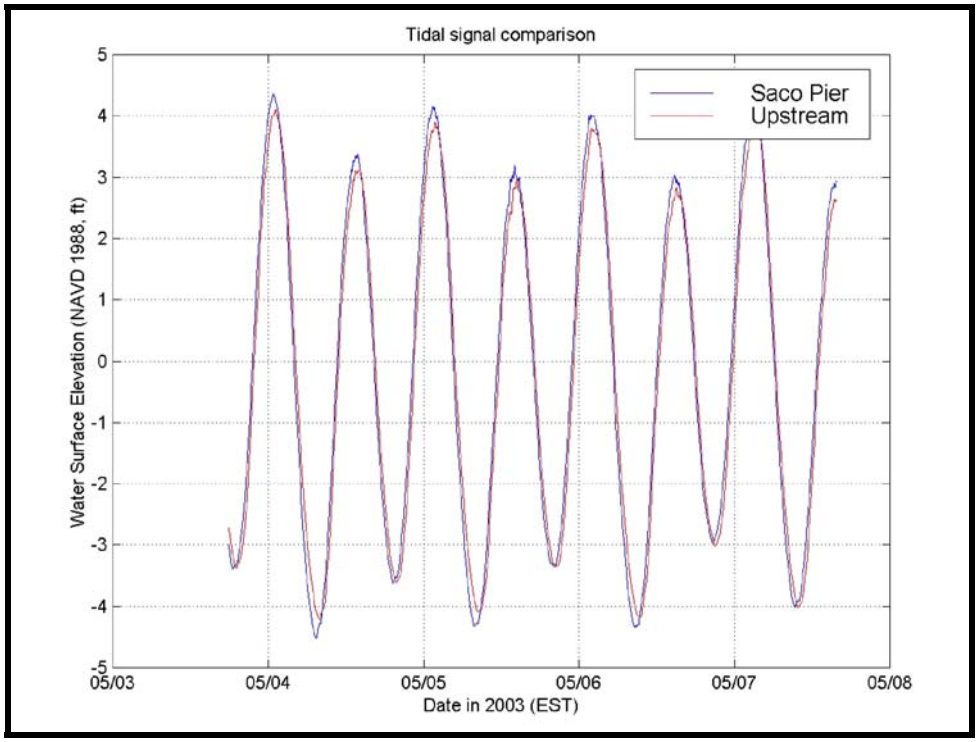

Figure 5-9. Measured water surface elevation of Saco River, inland of the jettied channel and upstream at the Yacht Club (time-zoom).

6.0 ADCP SURVEY (TASK 13)

Aubrey Consulting, Inc. defined the spatial structure of the currents within the Saco River and the region surrounding Camp Ellis Beach by measuring the tidal currents at selected locations in the river and offshore of Camp Ellis Beach during approximately one complete lunar semi-diurnal tidal cycle (12.4 hours) on May 14, 2003. The observations were obtained using an Acoustic Doppler Current Profiler (ADCP) mounted to a survey vessel. Six (6) transects were surveyed repeatedly, providing a resulting data set that provides a view of the temporal variation in spatial structure of tidal currents in the Saco River. The collection of these data served two purposes:

Evaluation of the average tidal current magnitude in the vicinity of Camp Ellis Beach, and thereby the potential influence of tidal currents on the sediment transport rates and patterns in the nearshore zone. If the tidal currents are sufficiently small, then the wave forces might be considered the dominant forcing mechanism for sand transport at Camp Ellis Beach.

Although not being directly evaluated in the present study, the tidal current measurements within the Saco River provide the ability to develop a hydrodynamic and tidal current sediment transport model of the Saco River estuary system. This would include an estimated quantity of the amount of sediment delivered to the coastal region via the river.

6.1 Survey Region

The survey was performed on May 14, 2003. Six (6) transects were surveyed in the jettied channel and surrounding areas: a river transect across the channel inland of the jetties, a transect parallel to the north jetty along its southern side, a transect parallel to the north jetty on its northern side, a shore-parallel transect north of the northern jetty, diagonally from the northern tip of the previous transect to the eastern tip of the northern jetty and a channel-perpendicular transect from the eastern tip of the north jetty to the eastern tip of the south jetty (see Figure 6-1). These six transects formed a contiguous loop to observe the spatial and time varying current regime in the area. Additionally, a seventh transect was surveyed to collect additional information during time periods when the tide level was too low to survey safely transects 3-5. This seventh transect progressed along the jettied channel from east to west (see Figure 6-1). Table 6-1 presents the survey dates, locations, transect repetition period, and temporal coverage for each transect line.

6.2 Equipment Description

Measurements were obtained using a broadband 1200 khz Acoustic Doppler Current Profiler (ADCP) manufactured by RD Instruments of San Diego, CA. The ADCP was mounted rigidly to the starboard rail of the survey vessel, a 22-foot C-Hawk owned by CR Environmental. Position information was provided by a Trimble 4000-series differential GPS (see description in Chapter 4.0).

Table 6-1. Survey dates, locations, repeat interval, and temporal coverage of the ADCP transects.

Location	Transect	Date	Repeat Internal	# of Transects
Inland Jetty	1	May 14	1.5 hrs	9
North Jetty (E-W)	2	May 14	1.5 hrs	9
North Jetty (W-E)	3	May 14	1.5 hrs	6
Alongshore	4	May 14	1.5 hrs	5
Shore to end North Jetty	5	May 14	1.5 hrs	6
North Jetty to South Jetty	6	May 14	1.5 hrs	9
Jettied Channel	7	May 14	1.0 hrs during low tide	2

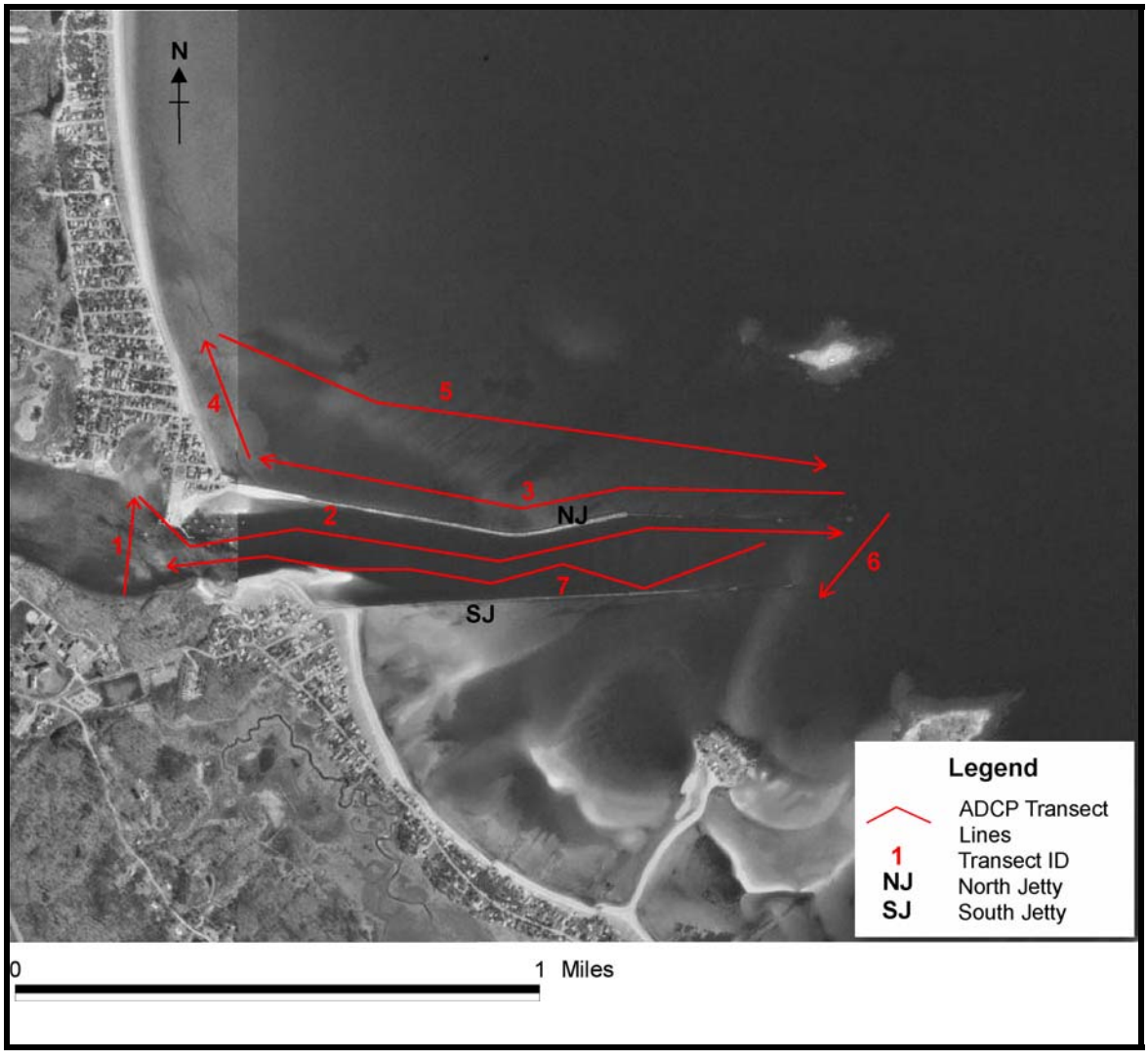

Figure 6-1. Location of ADCP transects.

The ADCP is capable of high resolution measurements of the spatial structure of current flow beneath the instrument transducer. When mounted to a moving platform, such as a small vessel, a detailed picture of the current characteristics can be obtained. Repeating the transects at regular time intervals throughout a complete tidal cycle offers an unparalleled temporal definition of the spatial variability in tidal current structure in the study area.

The ADCP measures currents using acoustic pulses emitted individually from four angled (at 20° from the vertical) acoustic transducers in the instrument. The instrument listens to the backscattered echoes from discrete depth layers in the water column. The returned echoes, reflected from ambient sound scatters (plankton, debris, sediment, etc.), are compared in the frequency domain to the original emitted pulse. The change in frequency (doppler shift) between the emitted versus the reflected pulse is directly proportional to the speed of the water parallel to the individual beam. For example, an echo of lower frequency indicates water moving away from the transducer while an echo of higher frequency indicates water moving toward the transducer. By combining the doppler velocity components for at least three of the four directional beams, the current velocities can be transformed to an orthogonal earth coordinate system in terms of east, north, and vertical components of current velocity.

Vertical resolution is gained using a technique called 'range-gating'. Returning pulses are divided into discrete 'bins' based on discrete time intervals following the emission of the original pulse. Combined with knowledge of the speed of sound in water, the discrete time intervals reflect the range (or depth) of each discrete bin from the transducer face.

Interpretation of current data acquired with an ADCP requires the removal of the speed of the transducer (mounted to the vessel) from the estimates of current velocity. This separation is performed by 'bottom tracking' or, using the doppler shift to measure simultaneously the velocity of the transducer relative to the bottom. Bottom tracking allows the ADCP to record absolute versus relative velocities beneath the transducer.

The accuracy of the current measurements can be compromised by random errors (or noise) inherent to this technology. Improvements in the accuracy of each measurement are achieved by averaging several individual acoustic returns together. These averaged results are termed 'ensembles'; the more pings used in the average, the smaller the standard deviation of the random error.

For this study each ensemble took approximately 1.8 seconds to collect. The vertical resolution was set to 30 cm (11.8 m), or one velocity observation per 30 cm (11.8 in) of water depth. The first measurement bin was centered 0.83 m (32.7 in) from the surface, allowing for the transducer draft as well as an appropriate blanking distance between the transducer and the first measurement. The transducer was set 40 cm (15.7 in) below the surface to prevent the transducer from coming out of the water in the ocean swells.

Position information was collected by Hypack, an integrated navigation software package running on a PC computer, linked to a Trimble 4000-series differential GPS. The position data were read from the device in UTM Zone 19N (meters) coordinate system,

and subsequently transformed to NAD 1927 State Plane Maine West zone (feet). Position updates were available every 1 second, and raw position data were also sent to the ADCP laptop to assist in verifying the clock synchronization between the GPS and ADCP. Data recording was begun as the vessel neared the start of each line and was terminated at the end of each line.

6.3 Survey Technique

Six transect profiles were surveyed to define a contiguous loop within the jettied channel and the surrounding area. This loop was repeated throughout the survey period to depict the changing effects of the current regime through the tidal cycle. Each repetition of the loop was performed in the same sequence to assure consistent results. During low tide, the water depths did not allow for continued transect runs on Transects 3-5. Therefore a seventh transect was performed to assess the central channel current variations, and was also repeated in the same direction (landward towards river).

Transect 1 began on the southern edge of the Saco River close to the inland extent of the jettied channel, and proceeded to the northern side of the river. The transect heading was perpendicular to the channel axis. The second transect heading was in an easterly direction parallel to the northern jetty. The third leg was another transect parallel to the northern jetty heading in a westerly direction on the north side of the structure. The fourth transect ran approximately parallel to the shoreline in a north-west/north direction from the inland extent of the northern jetty. The fifth transect was a diagonal cut from the end of Transect 4 to the eastern extent of the northern jetty. The heading was approximately 100° southeast. The final transect in the loop was another diagonal cut across the entrance of the jettied channel on an approximate heading of 210° southwest. This complete loop was repeated approximately every 1.5 hours and is shown in figure 6-1. The shallow bathymetry prevented Transect 4 from being taken at periods surrounding low tide (around 1510 hours on May 14, 2003). The final three loops surveyed consisted of only Transects 1, 2 and 6 in order to maximize the data obtained within the jettied channel in the time available. Consequently the seventh transect was also taken twice in the latter part of the survey to supplement the data. This transect was taken from the seaward edge of the jettied channel to its inland extent in the central channel. The transect heading varied within the channel but generally was in a westerly direction (see Figure 6-1).

Sea conditions and weather were relatively calm throughout the survey although a persistent rain continued throughout the day. Due to the lack of waves, the survey results show primarily tidal velocities through the Inlet, uncontaminated by ocean wave interactions. Further, the tides during the survey period were in the spring phase, indicating maximum water surface elevation and current fluctuations.

6.4 Data Processing Techniques

The survey resulted in two types of data: current velocity and vessel position. The ADCP data for a single transect consisted of velocity components at every depth bin for every ensemble. In addition, the raw ADCP (binary) files also include ancillary data such as correlation magnitudes, echo amplitudes, percent good pings, and error velocities

(among others). These data can be used to recalculate velocities, as well as assure quality of the results. Each ensemble also includes header information such as the ensemble number, time of the ensemble, and water temperature.

Position data were recorded as time-northing-easting within Hypack. The northing-easting pairs were referenced to UTM Zone 19N (feet). These pairs were subsequently converted to the United States State Plane 1927, Maine West Zone (feet) using Hypack. This transformation was done to maintain consistent projection system within the project. The raw ADCP data were converted to ASCII files using RDI's proprietary software (BBLIST) to a user-defined data format.

Subsequently, the ensemble profiles must be merged with the position data to assign a unique x-y pair to every ensemble. This merging operation is done using time and GPS position as the common link between the Hypack and ADCP data files. By searching for the unique position at a specific time for each of the data sets, an accurate x-y location was assigned to each ensemble.

6.5 Survey Results

Color contour plots of each transect are presented in Appendix 6-A. The color contour plots represent measured conditions at the time of the survey. Each pair of plots present the spatial structure of flow through the transect at a discrete time period. Viewing a series of these plots for sequential intervals through a complete tidal cycle can offer a better understanding of how the spatial structure of flow varies with time.

Each figure consists of two panels: the top panel presents the north/south component of velocity through the transect, whereas the bottom panel presents the east/west component of velocity through the transect. The directions are referenced to magnetic north. For example, positive north velocities represent water flowing in a northerly direction. Negative velocities represent water flowing to the south. Positive east velocities represent water flowing to the east; negative east velocities represent flow to the west.

The vertical axis for each plot is depth (in meters), representing the depth of the water column. The horizontal axis represents distance across the transect line. A distance of zero (0) indicates the start of the line, whereas the end of the transect is indicated by the maximum distance. Refer to Figure 6-1 for the start and end points of each transect line.

The color bar on the extreme right of each plot indicates the magnitude of the north and east current velocities. Strong northerly and easterly flows are indicated by deep red; strong southerly and westerly flows are indicated by deep blue. White areas of each plot indicate regions below the bottom; therefore, a crude indication of the channel bathymetry is outlined by the white areas below the color-filled spaces. The complete data set can be found in Appendix 6-A.

6.5.1 Transect 1

The channel geometry along Transect 1 consists of a single, relatively shallow channel. The transect is located just east of the Saco Pier, where a significant reduction in channel

width occurs. Maximum depths in the channel at this location are approximately 5m (16.4 ft).

The maximum recorded flood velocities were approximately 100-125 cm/s (3.3-4.1 ft/s). The maximum flood currents run in a west to west northwest direction throughout the entire water column. In addition to the westward flow, northward flow occurred on the northern portion of the channel indicating likely eddying around the point on the northern shore. The east/west flow also indicates some eastward flow in the northern extent of the transect, supporting the eddy structure. As the flood tide progressed, the stronger western currents were confined to the southern part of the channel. High tide occurred at 0905 hours and reversal of the flow direction was observed throughout the channel by 1019 hours. The maximum recorded ebb velocities were approximately 100-125 cm/s (3.3-4.1 ft/s) and occurred between 1100 and 1330 hours. These southeasterly ebb currents appear to favor the north side of the channel during the start of the ebb where the strongest currents are confined to the upper 2m of the water column. As the tide progresses, these currents spread to the entire channel area depth and breadth.

During the majority of the ebb and flood phases of the tide, the color contour plots show increased turbulence and related eddy formation adjacent to the north shore (between 500 ft [152 m] and the end of transect). The increased turbulence is a result of the protrusion of the northern point (near Saco Harbor) into the channel. This narrowing prevents direct flow into or out of the river channel producing eddies as water tries to enter or exit the reduced-width channel.

6.5.2 Transect 2

This transect parallels the northern jetty and runs along the length of the jettied channel from west to east. The bathymetry along the transect features a relatively steep drop from 2.25 m to 7 m (7.4-22.9 ft) depth from 0-304 m (0-1000 ft), followed by a fairly consistent water depth of around 5 m (16.4 ft). Several shoals can be identified as the water level drops during low tide.

Flooding currents flow in a west to west northwest direction and occupy the entire water column. A maximum velocity of approximately 100 cm/s (3.3 ft/s) was attained during the flood phase. Approaching high slack tide the velocities were reduced, except within the harbor region, which maintained accelerated flow due to channel contraction. By 1149 hours, the tide had reversed to an ebb flow and the currents in the upper 2 m (6.6 ft) of the water column had started to flow in a northeasterly direction. Elevated velocities near the constriction at the harbor can again be identified, and a transient eddy formed just seaward of this structure. This eddy can be identified on the color contour plots as southeasterly currents followed by strong northeasterly velocities as water passes the jetty (at distance 500 in Figure 6-A13 and 6-A14). This eddy was maintained throughout the ebb phase. Maximum ebb flow was attained by 1327 hours throughout the water column when maximum velocities were approximately 150 cm/s (4.9 ft/s).

Low tide occurred at approximately 1510 hours, but currents do not initially reverse until 1720 hours due to river – tide interactions. At this time, only currents at the seaward end of the transect reversed, (i.e. the offshore currents reverse first). This initial flow reversal

is clearly indicated in Figures 6-A14 and 6-A15. The incoming sea water is more saline (higher density) and the less dense fresh water stays on the surface. The flood flows traveled in a southwesterly direction through the channel, while the ebb flows traveled in a northeasterly direction (aligning with the orientation of the northern jetty). This provides a qualitative indication that potential sediment transport out of the jettied channel would likely be towards the northeast as sediment is delivered to the system from the river.

6.5.3 Transect 3

Transect 3 runs along the north side of the northern jetty, paralleling the jetty's length. The approximate depths of the transect are between 7 m (22.9 ft) at its seaward end and 4 m (13.1 ft) at its landward end. Due to the quiescent conditions on the survey day, minimal currents can be identified on the color contour plots for this transect. Generally, flow is to the northeast (maximum velocities approximately 25 cm/s or 0.8 ft/s) and no significant tidal currents persist along this transect. There are some areas of stronger northeast currents (1025 to 1347 hours) that may represent water overtopping the half-tide portion of the northern jetty. The lack of significant tide-induced currents along this transect suggests that wave processes are the primary driver of sediment movement in the nearshore vicinity of Camp Ellis Beach.

6.5.4 Transect 4

Transect 4 is a transect paralleling the shoreline of Camp Ellis Beach having a maximum water depth of 3 m (9.8 ft). At low tide, significant shoals can be identified reducing the water depth to less than 1 m (3.3 ft). The currents show an alongshore component during the ebb tide. Maximum velocities were attained on the ebb tide and reached approximately 30 cm/s (1.0 ft/s) to the southwest. As with transect 3, the lack of significant tide-induced currents along this transect suggests that wave processes are the primary driver of sediment movement in the nearshore vicinity of Camp Ellis Beach.

6.5.5 Transect 5

The approximate depth of this transect is between 3 m (9.8 ft) at the landward end and 8.5 m (27.9 ft) at the seaward end. Shoals were easily identified during low tide. Transect 5 cut diagonally from the shoreline back to the seaward end of the northern jetty and was surveyed to investigate the possible currents on the outer portion of the northern jetty and in the nearshore vicinity of Camp Ellis Beach. No significant tidal currents could be identified for Transect 5.

6.5.6 Transect 6

Transect 6 is located at the seaward end of the jettied channel, running in a north-south direction across the entrance. The geometry of the transect is dominated by the presence of the two jetties, which can be identified in the color contour plots at low tide. The remaining transect water depth is relatively consistent.

The ebb phase of the tide occurred between 0957 and 1601 hours. At the start of the ebb the northeasterly currents were focused in the bottom 1.5 m (4.9 ft) of the water column,

but soon rapidly spread to the upper water column where they were largely confined during the rest of the ebb phase. Maximum observed velocities were approximately 100 cm/s (3.3 ft/s). Between 1250 and 1433 hours, significant entrainment of water from south of the southern jetty can be seen in the color contour plots. The strong northeasterly ebb currents continue past the end of the southern jetty still confined by the longer northern jetty. As this happens, water is entrained in the flow from south of the southern jetty. This phenomena is transient, coincident with the strongest ebb currents. As this water is entrained, it is forced under the strong northeast currents at the surface to flow in the mid-water column (see Figure 6A-39 and 6A-40).

By 1647 hours, the currents started to reverse as the flood tide begins. The maximum flooding velocities observed were approximately 35 cm/s (1.1 ft/s), which are significantly less than those recorded on the ebb tide or along Transects 1 and 2. Since transect 6 is located seaward of the main jettied channel, and therefore the flood currents are not yet confined (and thus accelerated) by the channel, they are significantly slower than the ebb currents, which flow out of the confined channel. The color contour plots indicate increased turbulence and eddying around the jetty ends throughout the entire water column. The data from this transect confirms that flow, and likely potential suspended sediment, are directed in a northeasterly direction.

6.6 Averaged Velocities

The velocities at selected nodes across each transect were calculated for each time step. Each transect was divided into eight (8) equal-length subsections; the center of each subsection was labeled individually as node 1 through node 8. For each node, vertically- and horizontally-averaged (east and north) velocity components were calculated for each time step. The vertical average of each ensemble consisted of the mean velocity for all valid bins. The validity of the bottom bin measurements was determined by comparing the standard deviation of bottom values to the standard deviation of mid-column measurements. If the standard deviation at the bottom was more than twice the standard deviation of mid-column measurements, the bottom bin was discarded from the calculation. If the bottom value was within the limits defined by adjacent measurements, the value was included in the calculation. The horizontal average included all vertically-averaged ensemble velocities within each nodal subsection.

The result of this averaging procedure was a series of values showing the average velocity magnitude and direction for each loop of transects. In addition, the nodal averages included the average time of all ensembles in the subsection, average water depth of all ensembles in the subsection, and x-y position of each node. The values for each contiguous loop were plotted as arrows on separate geo-referenced maps to show the spatial current characteristics during each time step (see Appendix 6-B).

6.7 Summary

The relative strength of the currents within the jettied channel (≤ 150 cm/s or 4.9 ft/s) exceeded at the seaward end of the channel (≤ 30 cm/s or 1.0 ft/s). This feature is particularly obvious near the inland jetty site where channel-width reduction accelerates the flow (contraction flow) even further. This feature is important in considering

sediment transport within the system and more importantly transport of sediment out of the river system. The flooding currents seem to favor a west to west northwest direction focused in the southern part, of the channel whereas the ebb currents favor a northeasterly direction in the northern part of the channel. Consequent dominant sediment transport out of the system likely removes sediment from the northern part of the channel and transport it to the northeast as it leaves the jettied channel.

Water from south of the southern jetty is entrained between the jetties during ebb tide. This occurs as a result of the shorter length of the south jetty as compared to the northern jetty and results in the introduction of water (and potentially sediment) from outside the jettied channel area into the main ebb flow.

There is also a distinct lag between the change in tidal flow direction at the landward and seaward ends of the jettied channel. This is evident between 1619 and 1647 hours as the tide is changing from ebb to flood. The currents on transect 6 have already altered to westward flow but the currents within the jettied channel are still strongly eastward-flowing. This condition is maintained until 1745 hours, when currents at the inland jetty are just beginning to change.

Finally, the magnitude of the tidal currents in the nearshore vicinity north of the jetties is minimal. This lack of significant tide-induced currents offshore of Camp Ellis Beach suggests that wave processes are the primary driver of sediment movement in the nearshore vicinity of Camp Ellis Beach.

7.0 WAVE DATA COLLECTION (TASK 2)

The wave data were a critical component of the overall project and were used to provide an understanding of wave propagation within the vicinity of Camp Ellis Beach, as well as to provide calibration and verification data for the numerical wave transformation models. Due to the complex bathymetry in the study area, accurate model calibration and verification required on-site information near these complex features (e.g., offshore islands, structures, rock outcrops, etc.). The collection program used two bottom-mounted Acoustic Doppler Current Profilers (ADCP). The ADCPs recorded directional wave information once every hour over a nine-week period. The ADCPs also collected directional current information and water level elevation every 10 minutes. The data collected by the two ADCPs were statistically evaluated and utilized to facilitate calibration and verification of the various wave transformation models (STWAVE, WAVAD, and CGWAVE) used in the numerical modeling portion of the project. This chapter focuses on the basic wave statistics observed by the ADCP systems, including a limited discussion of some of the higher energy wave events observed during the time of the deployment. Specific wave spectra and comparisons to spectral model results are detailed in the modeling chapters (Chapters 8.0 through 12.0).

Chapter 7.0 details the wave data collection procedures, presents the observations and data analysis, and provides comparisons to offshore observations. Specifically, this chapter includes:

- discussion of the setup of two ADCPs,
- the data analysis procedures,
- a brief summary of the wave data gathered by the offshore and nearshore ADCPs,
- a comparison to additional wave data collected by three nearby buoys operated as part of the Gulf of Maine Ocean Observing System (GoMOOS) and as part of NOAA's National Data Buoy Center (NDBC), and
- a brief presentation of the directional current data collected by the ADCP.

This chapter does not discuss the additional data sources used in the development of boundary conditions for the transformation models or the historical data. This information is detailed extensively in Section 9.4.

7.1 Instrument Setup

The two bottom-mounted Acoustic Doppler Current Profilers (ADCPs) were deployed on March 12, 2003 (Figure 7-1). Diving operations were performed off of the local fishing vessel *Susan & Caitlyn*. Each ADCP instrument was secured to the ocean floor using a trawl-resistant mooring system (Figure 7-2). The ADCP trawl mount was anchored to the sea floor via four (approximately 90 cm long) screw anchors. The screw anchors were attached at each of the four corners of the trawl mount and secured via shackle and chain. As an additional measure of security for a worst-case scenario, a Danforth anchor was secured to the sea floor and attached to the grate of the trawl mount with

approximately 1.2 m of heavy gauge chain. In case of a severe storm that might pull the screw anchors from the bottom, the Danforth anchor provided a secondary level of security to keep the system within the region of deployment.

Figure 7-1. Deployment of one of the ADCP systems on March 12, 2003.

Figure 7-2. ADCP fitted in trawl-resistant bottom mount.

The ADCP chosen for deployment was RD Instuments' Workhorse Sentinel ADCP. The Workhorse Sentinel ADCP uses a four-beam array, 20^{o} from vertical, in a convex-upward

mount configuration. Power is provided through a battery pack made of 28-D cell alkaline batteries. Data were stored internally on a 512 MB PC card. A 600 kHz Workhorse Sentinel ADCP was deployed at a location seaward of Eagle and Ram Islands. This placement is referred to as the "Offshore ADCP" location. The second Workhorse Sentinel ADCP was placed landward of Eagle and Ram Islands, and operated at 1200 kHz (the higher frequency was possible due to the shallower water depth). This placement is referred to as the "Nearshore ADCP" location. The use of the trawl mount and the size of the Workhorse Sentinel ADCP result in the transducer head being located 48.3 cm (1/6 ft) off of the sea floor. The instrument locations were selected to help identify the wave transformations that likely occur as waves propagate through the complicated island and bathymetric region offshore of Camp Ellis Beach. The Offshore ADCP observed the waves prior to propagating through the islands, while the Nearshore ADCP observed the waves after they propagated through the island complex. Due to the significant changes that were expected to occur in this region, these locations provided valuable information to ensure the wave models were accurately representing reality.

The Offshore ADCP was placed in the region seaward of Eagle and Ram Islands (43^{o} 28.60' N, 070^{o} 20.48' W) in approximately 17 m (56 ft) of water at Mean Tide Level (Figure 7-3). The ADCP operated at a frequency of 600 kHz and could resolve waves having a 2.9 second period and longer. The deployment diver reported that the sea floor is a flat, featureless gravel bottom. Observations made during retrieval of the ADCP did not indicate any measurable movement of the trawl mount during the recording period.

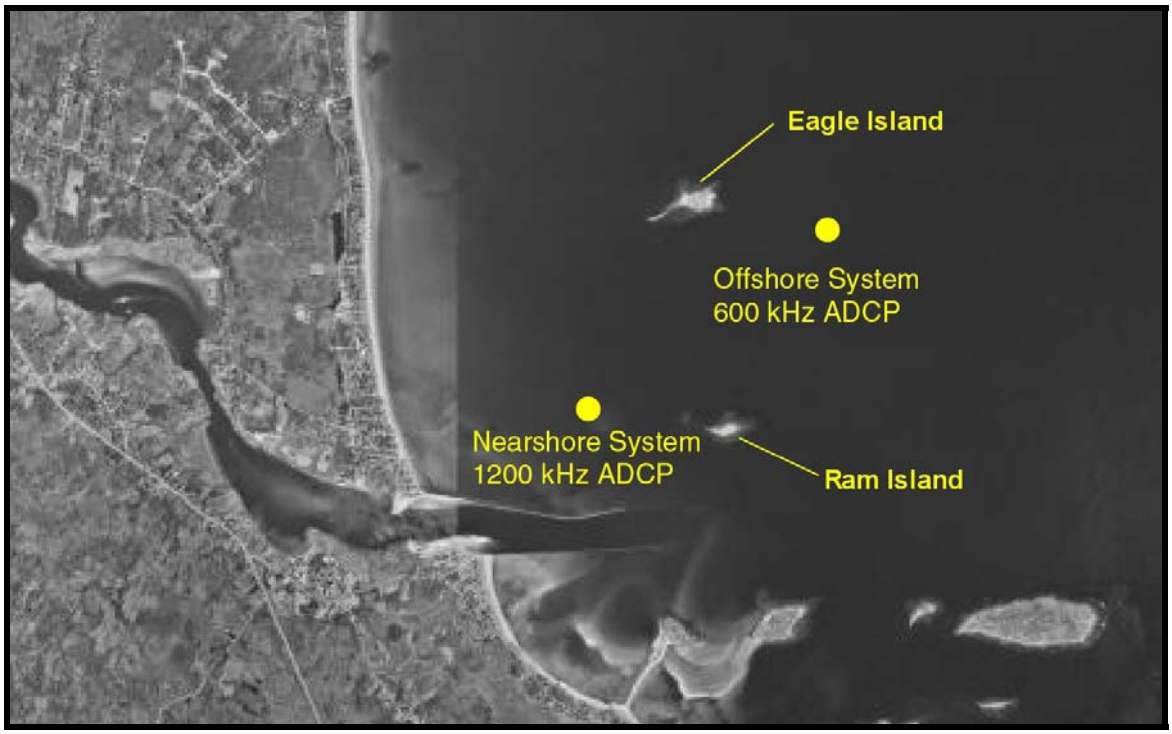

Figure 7-3. Approximate location of ADCP systems deployed offshore of Camp Ellis Beach.

The second ADCP (Nearshore ADCP) was placed in the region landward of Eagle and Ram Islands (43° 28.31' N, 070° 22.42' W) in approximately 4 m (13 ft) water depth (Figure 7-3). The ADCP operated at a frequency of 1200 kHz and could resolve waves having a 1.7 second period or longer. The deployment diver reported that the sea floor was a flat, featureless sand bottom. Observations made during the retrieval of the ADCP showed that the platform was partially buried; however the ADCP head was not covered.

Data were postprocessed from the ADCP using the RD Instruments software "WavesMon" and "WavesView." "WavesMon" allowed the user to automate the processing of the saved data log. Both the Offshore ADCP and Nearshore ADCP data logs were analyzed such that the following information was processed and saved:

- Ambient Velocity Time Series
- Sea Surface Elevation Time Series
- Water pressure Time Series
- Ambient Velocity Spectra
- Sea Surface Spectra
- Water pressure Spectra
- Directional Wave Spectra
- Other Wave Parameters

Some of this information is presented in this chapter, while the rest is presented in the modeling chapters of this report.

The information presented in this chapter was taken from the processed data log using the "WavesView" computer program. "WavesView" used the processed data as input and output a text file containing: significant wave height post-processing (H_{sig}), peak wave period (T_{peak}), peak wave direction, water depth, ambient velocity/current magnitude and current direction. This information was then used as input into a Matlab script that determined the general statistics of the data, and produced data plots. A 40-second peak wave period was chosen as a low frequency cutoff value in the Offshore ADCP and Nearshore ADCP data. During low wave energy time periods (calm conditions), the ADCPs occasionally recorded erroneous values for peak wave period. When an erroneous peak wave period (for instance, the physically impossible situation when T_{peak}>40-seconds corresponding to a insignificant wave height) was recorded, all associated wave information (H_{sig} and peak wave direction) was discarded from the data set.

7.2 Wave Observations

This section presents a basic statistical overview of the wave observations collected during the deployment time period for both the offshore and nearshore ADCP stations. The primary purpose of this section is to present the raw results of the wave observations and provide a first-order evaluation of the wave statistics. Greater evaluation of the observed wave conditions is discussed in context of the calibration and verification of modeling results, in terms of both general statistics and wave spectra. This discussion is

also limited to the time period of the deployment (March - May 2003), and therefore, does not represent the overall wave climate in the vicinity of Camp Ellis Beach, which undergoes significant changes during the winter months versus the summer months. For example, northeasterly storm waves are not identified within the deployment time period; however, they represent a significant process identified in longer time period data records and observations and are included in the modeling effort. Although a complete picture of the temporal wave climate is not available through the observations presented herein, they do serve the purpose of providing nearshore wave data to calibrate the numerical models. Once calibrated, the models are used to simulate a wide range of seasonal situations and storm events.

7.2.1 Offshore Wave Station

The Offshore ADCP made measurements from 1400 hrs March 12, 2003 until 1000 hrs May 21, 2003. There was no data loss during the reporting period (100% data return). About 97.85% of the data were usable. The metadata ('data about the data') statistics for the wave data set are presented in Table 7-1. This table gives a perspective of the data quality and completeness. Wave statistics, specifically the percent of occurrence table for specific value ranges of significant wave height, peak wave period and peak direction, are presented in Table 7-2.

Table 7-1. Wave metadata statistics for Offshore ADCP station.

Start Time of Data Series: March 12, 2003 1400 hrs
End Time of Data Series: May 21, 2003 1000 hrs
Total Number of Samples Possible: 1677
Total Number of Samples Recorded: 1677
Total Percentage Data Return: 100%
Total Wave Records: 1677
Total Valid H_{sig} values: 1641
Total Valid Peak Direction values: 1641
Total Valid Peak Wave Period values (valid if less than 40 seconds): 1641

The data indicate that significant wave height values (Figure 7-4) ranged from 17 to 226 cm (0.6 to 7.4 ft) during the reporting period. Specific events associated with higher significant wave heights are described in Table 7-6. The most common wave heights were in the range between 38 and 50 cm (1.2 and 1.6 ft) (20.0%) and between 50 and 63 cm (1.6 and 2.1 ft) (19.0%). Significant wave heights exceeded 1 m (3.3 ft) 19.2% of the time.

Peak wave periods (Figure 7-5) ranged from 3.0 to 14.2 seconds, with the majority of wave periods (21.1%) located in a band from 8 to 9 seconds. Of the remaining peak wave periods recorded, 48.6% of the time they were less than 8 seconds, and 30.3% of the time they were greater than 9 seconds.

Waves approached the offshore ADCP location primarily from the ESE (Figure 7-6). The largest percentage of waves came from the ESE (43.9%), with the second largest 22-degree band being from the SE (28.0%). These directions are expected for the time of year of the deployment, and based on the geometry of the site location within the Gulf of Maine.

Table 7-2. Wave frequency of occurrence statistics for Offshore ADCP station.

Sig. Wave Height (cm)	Peak Wave Period (sec)	Peak Direction (degrees)
Min-max: total samples\(%)	Min-max: total samples\(%)	Min-max: total samples\(%)
0-25: 41\(2.5)	0-3: 0\(0.0)	-11-11: 0\(0.0)
25-38: 163\(9.9)	3-4: 64\(3.9)	11-34: 0\(0.0)
38-50: 328\(20.0)	4-5: 135\(8.2)	34-56: 9\(0.5)
50-62: 312\(19.0)	5-6: 169\(10.3)	56-79: 52\(3.2)
62-75: 205\(12.5)	6-7: 218\(13.3)	79-101: 350\(21.3)
75-88: 173\(10.5)	7-8: 212\(12.9)	101-124: 720\(43.9)
88-100: 105\(6.4)	8-9: 346\(21.1)	124-146: 459\(28.0)
100-125: 172\(10.5)	9-10: 333\(20.3)	146-169: 46\(2.8)
125-150: 93\(5.7)	10-11: 89\(5.4)	169-191: 0\(0.0)
150-175: 24\(1.5)	11-12: 47\(2.9)	191-214: 0\(0.0)
175-200: 18\(1.1)	12-13: 25\(1.5)	214-236: 2\(0.1)
200-250: 7\(0.4)	13-14: 0\(0.0)	236-259: 2\(0.1)
250-300: 0\(0.0)	14-16: 3\(0.2)	259-281: 0\(0.0)
300-400: 0\(0.0)	16-18: 0\(0.0)	281-304: 0\(0.0)
400-500: 0\(0.0)	18-20: 0\(0.0)	304-326: 1\(0.1)
500-1000: 0\(0.0)	20-40: 0\(0.0)	326-349: 0\(0.0)

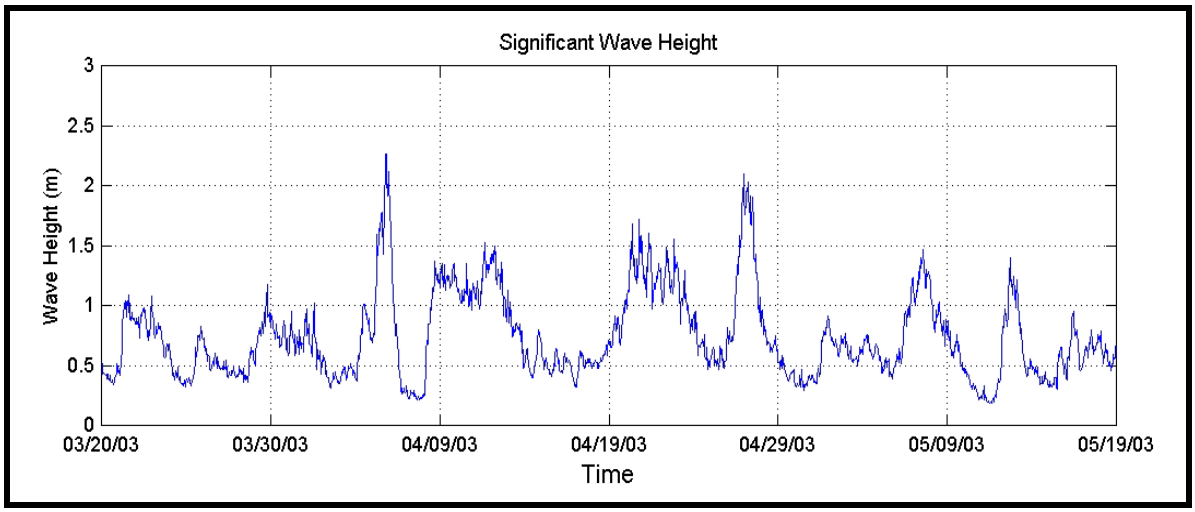

Figure 7-4. Offshore ADCP station significant wave height time series.

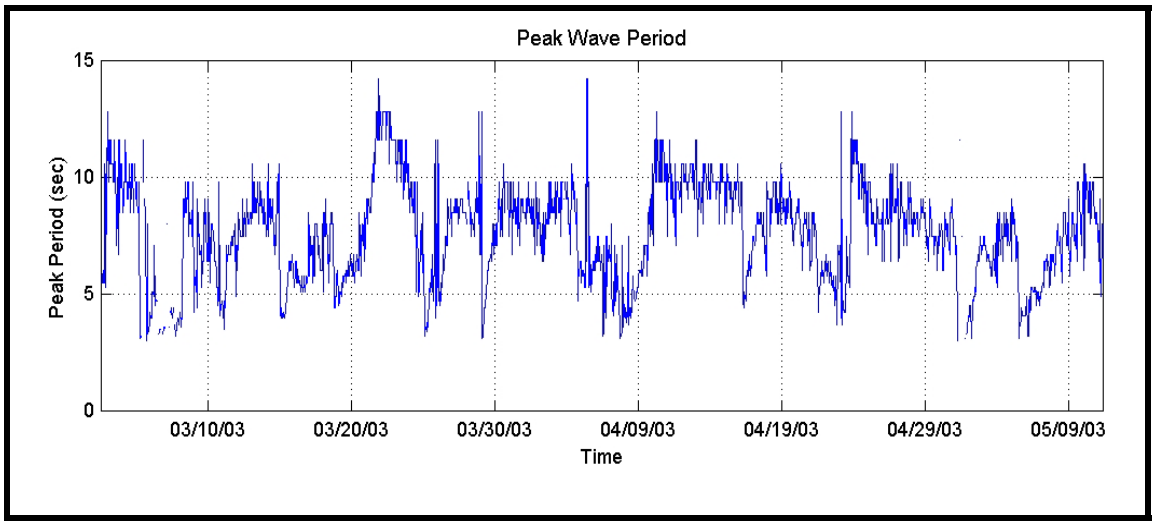

Figure 7-5. Offshore ADCP station peak wave period time series.

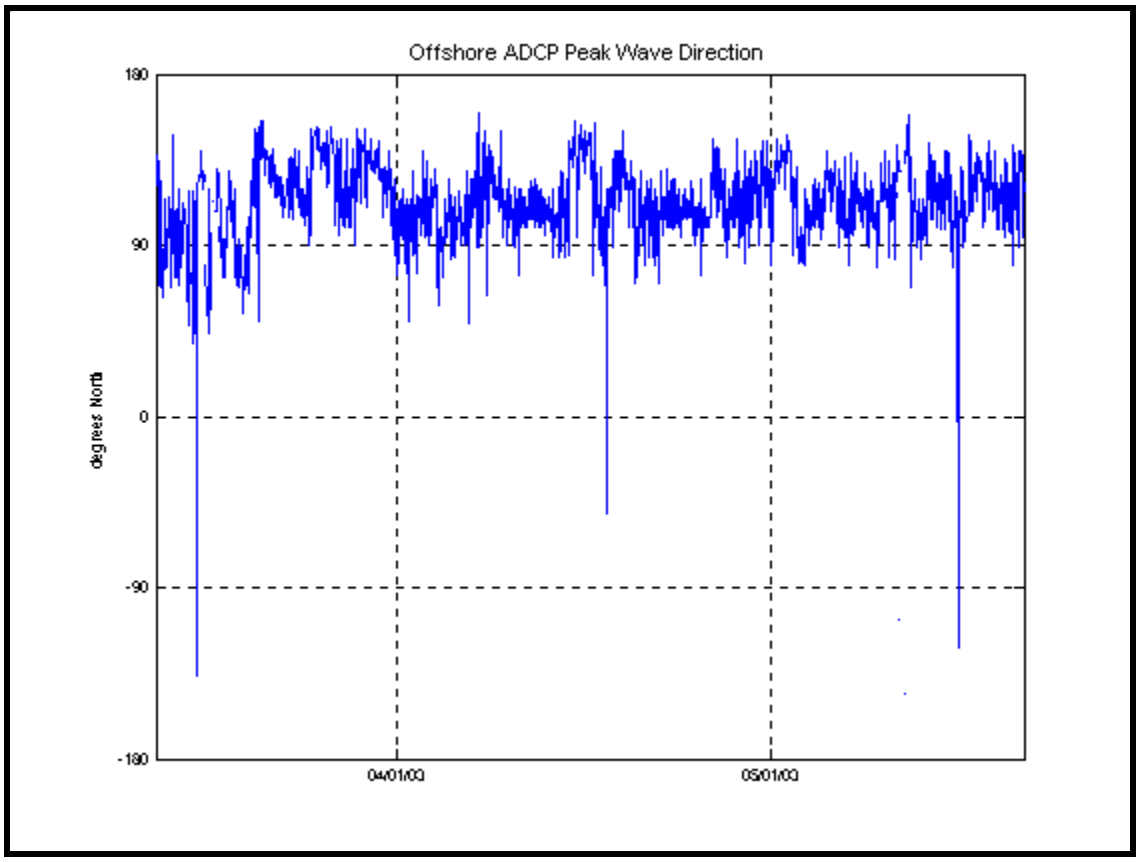

Figure 7-6. Offshore ADCP station peak wave direction time series.

Figure 7-7 presents the directional distribution of wave height (cm) data (illustrated using a wave rose). The gray-scale sidebar indicates the magnitude of wave height, the circular axis represents the direction of wave approach (coming from) relative to North (0

degrees), and the extending radial lines indicate percent occurrence within each magnitude and directional band. The most common wave approach is from the ESE. Figure 7-8 presents a similar rose plot for the directional distribution of the peak wave period.

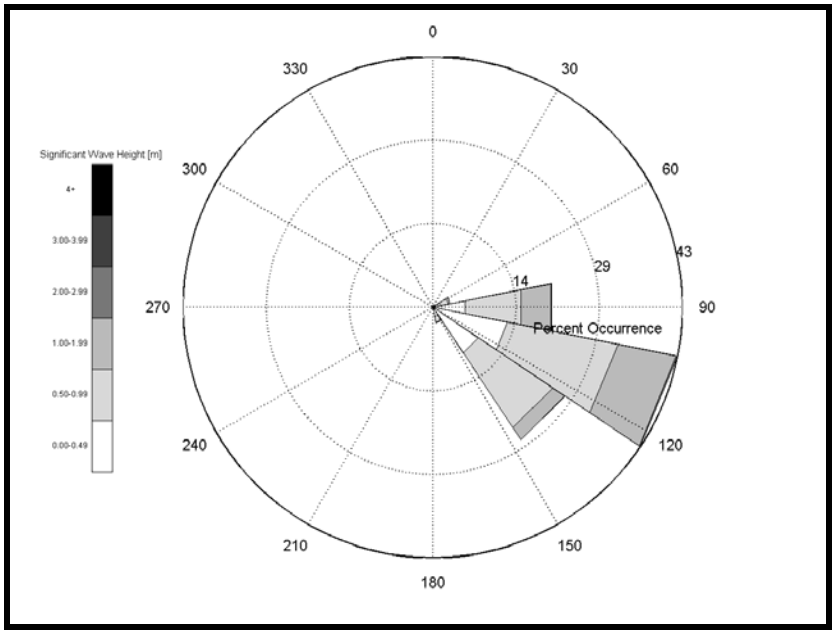

Figure 7-7. Wave rose of wave height data at Offshore ADCP station over deployment time period (March- May 2003).

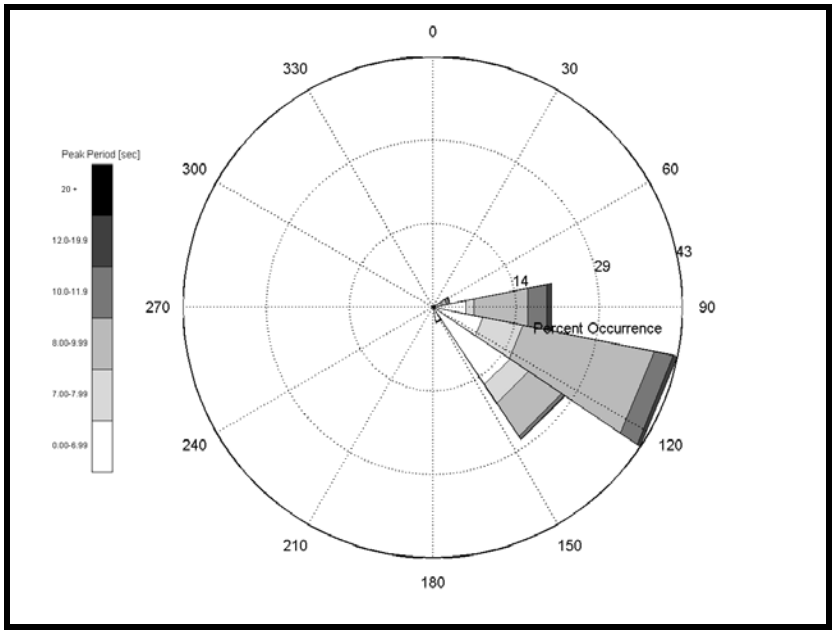

Figure 7-8. Wave rose of peak period data at Offshore ADCP station over deployment time period (March- May 2003).

Table 7-3 presents the percentage frequency of occurrence of significant wave height versus the peak wave direction. The table shows the percentage of occurrence of significant wave height (cm) and directional (degrees from north) cells. The number printed within each cell represents the percentage of occurrence associated with that wave height/directional cell combination. The table is also overlain with contour lines to highlight the location of higher percentages. In addition, total percentages of direction and height bins are shown at the far right and bottom of each table. The table indicates that almost all of the waves arrived between 79 degrees from north and 146 degrees from north (93.18%). The majority of the waves were between 38 and 75 cm (1.2 and 2.5 ft) in height (51.5%). The table also indicates that a most common wave approach was from between 101 and 146 degrees from north (71.85%). A total of 36.88% of the waves were between 101 and 146 degrees and between 38 and 75 cm (1.2 and 2.5 ft) in height. The larger waves (>100 cm) approach from the 101-124 directional bin (or from the east-south-east) as indicated by the secondary peak in the frequency of occurrence at this bin combination (5.55%).

Table 7-3. Percentage frequency of occurrence statistics of significant wave height versus peak wave direction for the offshore ADCP station.

Significant Wave Height (cm)

Peak Wave Direction (deg)	0	25	38	50	63	75	88	100	125	150	175	200	250	300	400	500	1000	All
-11-11	0.00	0.00	0.00	0.00	0.00	0.00	0.00	0.00	0.00	0.00	0.00	0.00	0.00	0.00	0.00	0.00	0.00	0.00
11-34	0.00	0.00	0.00	0.00	0.00	0.00	0.00	0.00	0.00	0.00	0.00	0.00	0.00	0.00	0.00	0.00	0.00	0.00
34-56	0.12	0.24	0.06	0.06	0.00	0.06	0.00	0.00	0.00	0.00	0.00	0.00	0.00	0.00	0.00	0.00	0.00	0.55
56-79	0.24	0.67	0.49	0.67	0.37	0.24	0.18	0.30	0.00	0.00	0.00	0.00	0.00	0.00	0.00	0.00	0.00	3.17
79-101	0.24	1.95	3.60	4.51	2.44	1.83	1.22	3.05	1.46	0.67	0.18	0.18	0.00	0.00	0.00	0.00	0.00	21.33
101-124	0.98	3.47	8.96	7.50	4.94	4.39	2.99	5.55	3.60	0.67	0.67	0.18	0.00	0.00	0.00	0.00	0.00	43.88
124-146	0.73	3.29	5.61	5.42	4.45	3.90	2.01	1.52	0.61	0.12	0.24	0.06	0.00	0.00	0.00	0.00	0.00	27.97
146-169	0.06	0.24	1.28	0.73	0.30	0.12	0.00	0.06	0.00	0.00	0.00	0.00	0.00	0.00	0.00	0.00	0.00	2.80
169-191	0.00	0.00	0.00	0.00	0.00	0.00	0.00	0.00	0.00	0.00	0.00	0.00	0.00	0.00	0.00	0.00	0.00	0.00
191-214	0.00	0.00	0.00	0.00	0.00	0.00	0.00	0.00	0.00	0.00	0.00	0.00	0.00	0.00	0.00	0.00	0.00	0.00
214-236	0.06	0.06	0.00	0.00	0.00	0.00	0.00	0.00	0.00	0.00	0.00	0.00	0.00	0.00	0.00	0.00	0.00	0.12
236-259	0.06	0.00	0.00	0.06	0.00	0.00	0.00	0.00	0.00	0.00	0.00	0.00	0.00	0.00	0.00	0.00	0.00	0.12
259-281	0.00	0.00	0.00	0.00	0.00	0.00	0.00	0.00	0.00	0.00	0.00	0.00	0.00	0.00	0.00	0.00	0.00	0.00
281-304	0.00	0.00	0.00	0.00	0.00	0.00	0.00	0.00	0.00	0.00	0.00	0.00	0.00	0.00	0.00	0.00	0.00	0.00
304-326	0.00	0.00	0.00	0.06	0.00	0.00	0.00	0.00	0.00	0.00	0.00	0.00	0.00	0.00	0.00	0.00	0.00	0.06
326-349	0.00	0.00	0.00	0.00	0.00	0.00	0.00	0.00	0.00	0.00	0.00	0.00	0.00	0.00	0.00	0.00	0.00	0.00
All	2.50	9.93	19.99	19.01	12.49	10.54	6.40	10.48	5.67	1.46	1.10	0.43	0.00	0.00	0.00	0.00		

Table 7-4 presents the percentage frequency of occurrence of peak wave period versus peak wave direction. The table shows the percentage of occurrence of peak wave period in period (seconds) and wave directional (degrees from north) cells. The number printed within each cell represents the percentage of occurrence associated with the particular wave period/wave direction combination. The table is also overlain with contour lines to highlight the location of higher percentages. In addition, total percentages of directional and period bins are shown at the far right and bottom of each table. The table indicates that a majority of the wave periods were between 7 and 10 seconds (54.3%). A total of 41.9% of the waves were between 7 and 10 seconds and approach from between 79 and 124 degrees. A high percentage (23.6%) of the 8-10 second waves were coming from between 101 and 124 degrees (ESE). A secondary peak (7.1%) of waves between 6 and 7 seconds came from between 124 and 146 degrees (SE). Higher frequency waves had a more southerly approach. The directional variability of the waves was limited as indicated by the tightly focused contour lines.

Table 7-4. Percentage frequency of occurrence statistics of peak period versus peak wave direction for the offshore ADCP station.

Peak Wave Period (sec)

Peak Wave Direction (deg)	0	3	4	5	6	7	8	9	10	11	12	13	14	16	18	20	40	All
-11-11	0.00	0.00	0.00	0.00	0.00	0.00	0.00	0.00	0.00	0.00	0.00	0.00	0.00	0.00	0.00	0.00	0.00	0.00
11-34	0.00	0.00	0.00	0.00	0.00	0.00	0.00	0.00	0.00	0.00	0.00	0.00	0.00	0.00	0.00	0.00	0.00	0.00
34-56	0.00	0.12	0.00	0.00	0.06	0.00	0.06	0.24	0.00	0.06	0.00	0.00	0.00	0.00	0.00	0.00	0.00	0.55
56-79	0.00	0.85	0.37	0.18	0.06	0.30	0.18	0.55	0.30	0.30	0.00	0.00	0.06	0.00	0.00	0.00	0.00	3.17
79-101	0.00	1.10	1.77	1.65	1.40	1.52	4.02	5.61	2.01	1.40	0.79	0.00	0.06	0.00	0.00	0.00	0.00	21.33
101-124	0.00	0.79	2.07	2.01	4.08	7.19	12.49	11.09	2.50	0.98	0.67	0.00	0.00	0.00	0.00	0.00	0.00	43.88
124-146	0.00	0.67	2.86	5.67	7.13	3.90	4.27	2.74	0.55	0.06	0.06	0.00	0.06	0.00	0.00	0.00	0.00	27.97
146-169	0.00	0.12	1.16	0.79	0.55	0.00	0.06	0.06	0.06	0.00	0.00	0.00	0.00	0.00	0.00	0.00	0.00	2.80
169-191	0.00	0.00	0.00	0.00	0.00	0.00	0.00	0.00	0.00	0.00	0.00	0.00	0.00	0.00	0.00	0.00	0.00	0.00
191-214	0.00	0.00	0.00	0.00	0.00	0.00	0.00	0.00	0.00	0.00	0.00	0.00	0.00	0.00	0.00	0.00	0.00	0.00
214-236	0.00	0.12	0.00	0.00	0.00	0.00	0.00	0.00	0.00	0.00	0.00	0.00	0.00	0.00	0.00	0.00	0.00	0.12
236-259	0.00	0.06	0.00	0.00	0.00	0.00	0.00	0.00	0.00	0.06	0.00	0.00	0.00	0.00	0.00	0.00	0.00	0.12
259-281	0.00	0.00	0.00	0.00	0.00	0.00	0.00	0.00	0.00	0.00	0.00	0.00	0.00	0.00	0.00	0.00	0.00	0.00
281-304	0.00	0.00	0.00	0.00	0.00	0.00	0.00	0.00	0.00	0.00	0.00	0.00	0.00	0.00	0.00	0.00	0.00	0.00
304-326	0.00	0.06	0.00	0.00	0.00	0.00	0.00	0.00	0.00	0.00	0.00	0.00	0.00	0.00	0.00	0.00	0.00	0.06
326-349	0.00	0.00	0.00	0.00	0.00	0.00	0.00	0.00	0.00	0.00	0.00	0.00	0.00	0.00	0.00	0.00	0.00	0.00
All	0.00	3.90	8.23	10.30	13.28	12.92	21.08	20.29	5.42	2.86	1.52	0.00	0.18	0.00	0.00	0.00		

Table 7-5 presents the percentage frequency of occurrence of significant wave height versus peak wave period. The table shows the percentage of occurrence of peak wave period in height (cm) and wave period (seconds) cells. The number printed within each cell represents the percentage of occurrence associated with the particular wave height/ wave period combination. The table is also overlain with contour lines to highlight the location of higher percentages. In addition, total percentages of period and height bins are shown at the far right and bottom of each table. The largest portion of waves (7.6%) had wave heights between 38 and 50 cm (1.2 and 1.6 ft) and periods between 8 and 10 seconds. The larger waves (>100 cm) had periods between 6 and 11 seconds, and with a primary peak in the 9 to 10 second bin. The smaller wave heights tended to either have a period of 5-6 seconds or 9-10 seconds. Rarely did wave periods exceed 13 seconds.

Table 7-5. Percentage frequency of occurrence statistics of significant wave height versus peak wave period for the offshore ADCP station.

Significant Wave Height (cm)

Peak Wave Period (sec)	0	25	38	50	63	75	88	100	125	150	175	200	250	300	400	500	1000	All
0-3	0.00	0.00	0.00	0.00	0.00	0.00	0.00	0.00	0.00	0.00	0.00	0.00	0.00	0.00	0.00	0.00	0.00	0.00
3-4	0.37	1.22	0.67	1.22	0.43	0.00	0.00	0.00	0.00	0.00	0.00	0.00	0.00	0.00	0.00	0.00	0.00	3.90
4-5	0.06	1.28	2.07	2.50	0.91	0.91	0.37	0.12	0.00	0.00	0.00	0.00	0.00	0.00	0.00	0.00	0.00	8.23
5-6	0.00	0.30	2.13	2.74	1.71	1.77	0.85	0.49	0.18	0.12	0.00	0.00	0.00	0.00	0.00	0.00	0.00	10.30
6-7	0.06	0.73	2.32	2.56	2.62	1.77	0.79	1.34	0.55	0.37	0.18	0.00	0.00	0.00	0.00	0.00	0.00	13.28
7-8	0.30	0.98	3.35	1.83	0.79	1.28	1.10	1.71	0.85	0.12	0.43	0.18	0.00	0.00	0.00	0.00	0.00	12.92
8-9	0.67	3.29	3.78	2.99	2.19	1.89	1.34	2.38	1.58	0.37	0.43	0.18	0.00	0.00	0.00	0.00	0.00	21.08
9-10	0.79	1.22	3.84	3.53	2.19	2.01	1.34	3.05	1.89	0.30	0.06	0.06	0.00	0.00	0.00	0.00	0.00	20.29
10-11	0.06	0.61	0.91	0.85	0.61	0.49	0.37	1.04	0.37	0.12	0.00	0.00	0.00	0.00	0.00	0.00	0.00	5.42
11-12	0.12	0.24	0.61	0.61	0.55	0.06	0.12	0.30	0.18	0.06	0.00	0.00	0.00	0.00	0.00	0.00	0.00	2.86
12-13	0.06	0.06	0.18	0.18	0.43	0.37	0.12	0.06	0.06	0.00	0.00	0.00	0.00	0.00	0.00	0.00	0.00	1.52
13-14	0.00	0.00	0.00	0.00	0.00	0.00	0.00	0.00	0.00	0.00	0.00	0.00	0.00	0.00	0.00	0.00	0.00	0.00
14-16	0.00	0.00	0.12	0.00	0.06	0.00	0.00	0.00	0.00	0.00	0.00	0.00	0.00	0.00	0.00	0.00	0.00	0.18
16-18	0.00	0.00	0.00	0.00	0.00	0.00	0.00	0.00	0.00	0.00	0.00	0.00	0.00	0.00	0.00	0.00	0.00	0.00
18-20	0.00	0.00	0.00	0.00	0.00	0.00	0.00	0.00	0.00	0.00	0.00	0.00	0.00	0.00	0.00	0.00	0.00	0.00
20-40	0.00	0.00	0.00	0.00	0.00	0.00	0.00	0.00	0.00	0.00	0.00	0.00	0.00	0.00	0.00	0.00	0.00	0.00
All	2.50	9.93	19.99	19.01	12.49	10.54	6.40	10.48	5.67	1.46	1.10	0.43	0.00	0.00	0.00	0.00		

In order to evaluate some of the higher energy time periods that occurred during the deployment, wave events were defined. For discussion purposes, higher energy wave events are herein defined as times when significant wave heights exceed 100 cm (3.3 ft) for more than 12 hours. Six higher energy wave events were observed at the offshore ADCP site during the deployment time period, as evidenced in the time series of significant wave height shown in Figure 7-4. Table 3-6 details these events, including some of the pertinent event statistics.

Table 7-6. Summary of wave events at offshore ADCP station (event threshold: H_{sig} > 100 cm for time >12 hours).

Event ID Number	Start of Event	End of Event	Time event exceeded threshold (hours)	Mean H_{sig} during event (cm)	Max H_{sig} during event (cm)	Mean T_{peak} during event (sec)	Mean Peak Wave Direction during event (degrees)
1	4/4/03 12:00:00	4/6/03 06:00:00	42	135	226	7.1	100
2	4/8/03 13:00:00	4/13/03 03:00:00	110	119	152	8.3	110
3	4/19/03 23:00:00	4/23/03 14:00:00	87	125	172	9.9	105
4	4/26/03 12:00:00	4/27/03 22:00:00	34	158	210	7.2	116
5	5/6/03 20:00:00	5/8/03 13:00:00	41	113	147	8.5	109
6	5/12/03 5:00:00	5/13/03 05:00:00	14	115	140	7.0	102

7.2.2 Nearshore Wave Station

The nearshore ADCP made measurements from 1500 hrs March 12, 2003 until 1200 hrs May 21, 2003. There was no data loss during the reporting period. However, only 97.2% of the data were usable, with the unusable data occurring when waves were quite small. The metadata ('data about the data') statistics for the wave data set are presented in Table 7-7. This table gives a perspective of the data quality and completeness. Wave statistics, specifically the percent of occurrence table for specific value ranges of significant wave height, peak wave period and peak direction, are presented in Table 7-8.

The data indicate that significant wave height values (Figure 7-9) ranged from 15 to 117 cm (0.5 to 3.8 ft) during the reporting period. The greatest percentages of wave heights were between 25 and 38 cm (0.8 and 1.2 ft) (35.1%) and between 38 and 50 cm (1.2 ft and 1.6 ft) (20.4%). Wave heights exceeded 75 cm only 6.8% of the time during the deployment time period.

Peak wave periods (Figure 7-10) ranged from 2.0 to 14.2 seconds, with the majority of wave periods (19.1%) located in a band from 8 to 9 seconds. Of the remaining peak wave periods recorded, 40.3% of the time they were less than 8 seconds, and 40.7% of the time they were greater than 9 seconds (but less than 15 seconds).

Table 7-7. Wave metadata statistics for Nearshore ADCP station.

Start Time of Data Series: March 12, 2003 1500 hrs
End Time of Data Series: May 21, 2003 1200 hrs
Total Number of Samples Possible: 1678
Total Number of Samples Recorded: 1678
Total Percentage Data Return: 100%
Total Wave Records: 1677
Total Valid H(sig) values: 1631
Total Valid Peak Direction values: 1631
Total Valid Peak Wave Period values (valid if less than 40 seconds): 1631

The nearshore ADCP depicted a wave environment that had little variation in approach direction over time (Figure 7-10). Waves approached the nearshore station between northeast and east 87.5% of the time. The greatest portion of those waves approached from the E (70.4%). Compared to the offshore ADCP station, which had a relatively consistent wave approach from the ESE, the nearshore ADCP station indicates a consistent E and slightly NE approach direction. Therefore, waves approaching the Camp Ellis region appear to be transformed by the offshore island complex towards the Camp Ellis Beach area.

Table 7-8. Wave frequency of occurrence statistics for Nearshore ADCP station.

Significant Wave Height (cm)	Peak Wave Period (sec)	Peak Direction (degrees)
Min-max: total samples\(%)	Min-max: total samples\(%)	Min-max: total samples\(%)
0-25: 275\(16.9)	0-3: 48\(2.9)	-11-11: 0\(0.0)
25-38: 573\(35.1)	3-4: 60\(3.7)	11-34: 16\(1.0)
38-50: 332\(20.4)	4-5: 63\(3.9)	34-56: 29\(1.8)
50-62: 179\(11.0)	5-6: 87\(5.3)	56-79: 250\(15.3)
62-75: 161\(9.9)	6-7: 202\(12.4)	79-101: 1149\(70.4)
75-88: 72\(4.4)	7-8: 197\(12.1)	101-124: 118\(7.2)
88-100: 15\(0.9)	8-9: 312\(19.1)	124-146: 8\(0.5)
100-125: 24\(1.5)	9-10: 308\(18.9)	146-169: 5\(0.3)
125-150: 0\(0.0)	10-11: 187\(11.5)	169-191: 5\(0.3)
150-175: 0\(0.0)	11-12: 99\(6.1)	191-214: 8\(0.5)
175-200: 0\(0.0)	12-13: 55\(3.4)	214-236: 1\(0.1)
200-250: 0\(0.0)	13-14: 0\(0.0)	236-259: 10\(0.6)
250-300: 0\(0.0)	14-16: 13\(0.8)	259-281: 21\(1.3)
300-400: 0\(0.0)	16-18: 0\(0.0)	281-304: 8\(0.5)
400-500: 0\(0.0)	18-20: 0\(0.0)	304-326: 0\(0.0)
500-1000: 0\(0.0)	20-40: 0\(0.0)	326-349: 0\(0.0)

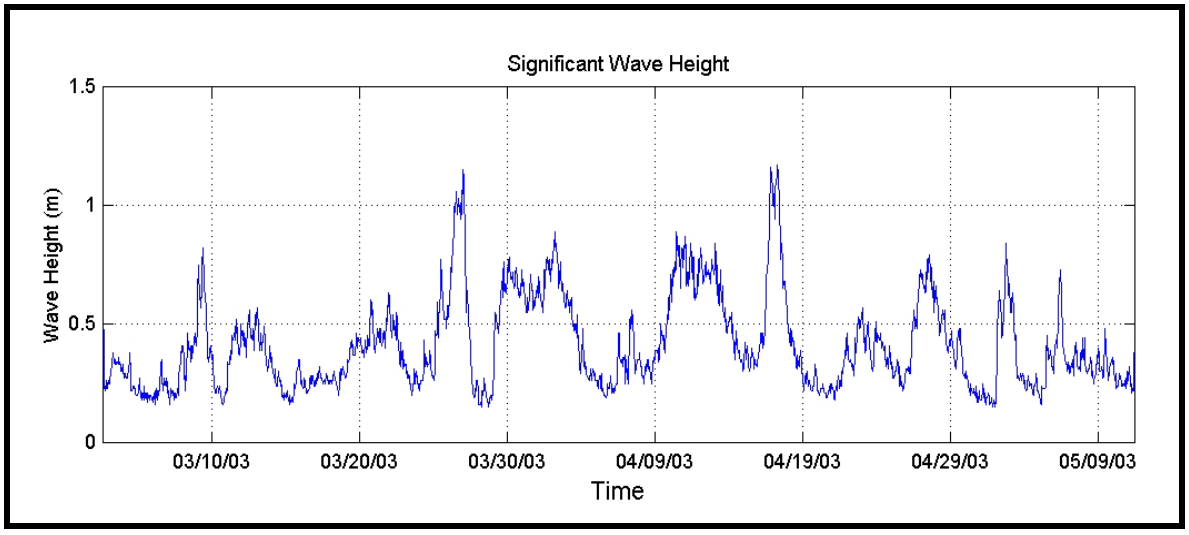

Figure 7-9. Nearshore ADCP station significant wave height time series.

Figure 7-12 presents the directional distribution of wave height (cm) data (illustrated using a wave rose). The gray-scale sidebar indicates the magnitude of wave height, the circular axis represents the direction of wave approach (coming from) relative to North (0 degrees), and the extending radial lines indicate percent occurrence within each magnitude and directional band. The most common wave approach is from the ESE.

Figure 7-13 presents a similar rose plot for the directional distribution of the peak wave period.

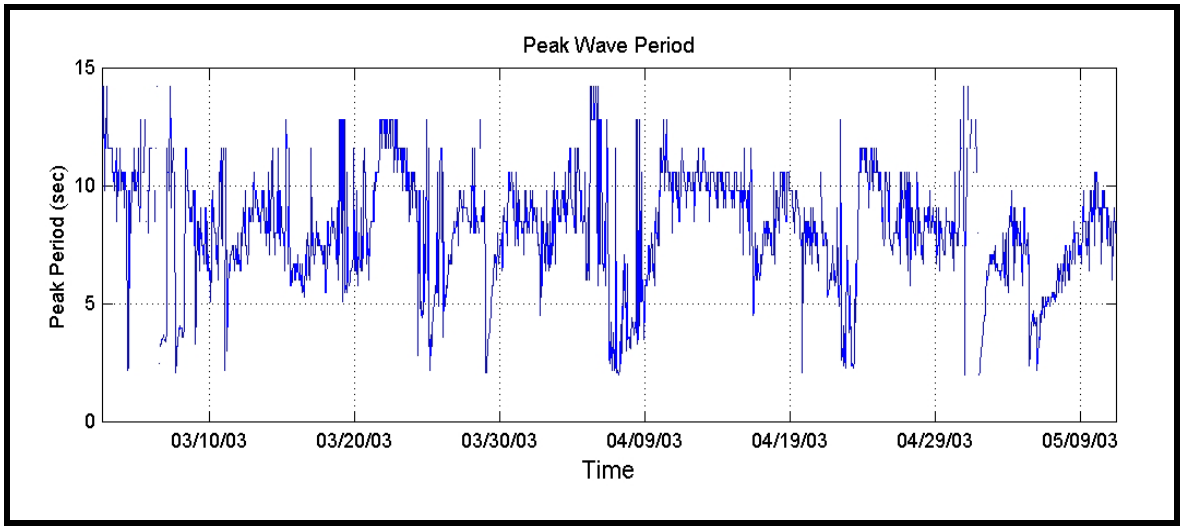

Figure 7-10. Nearshore ADCP station peak wave period time series.

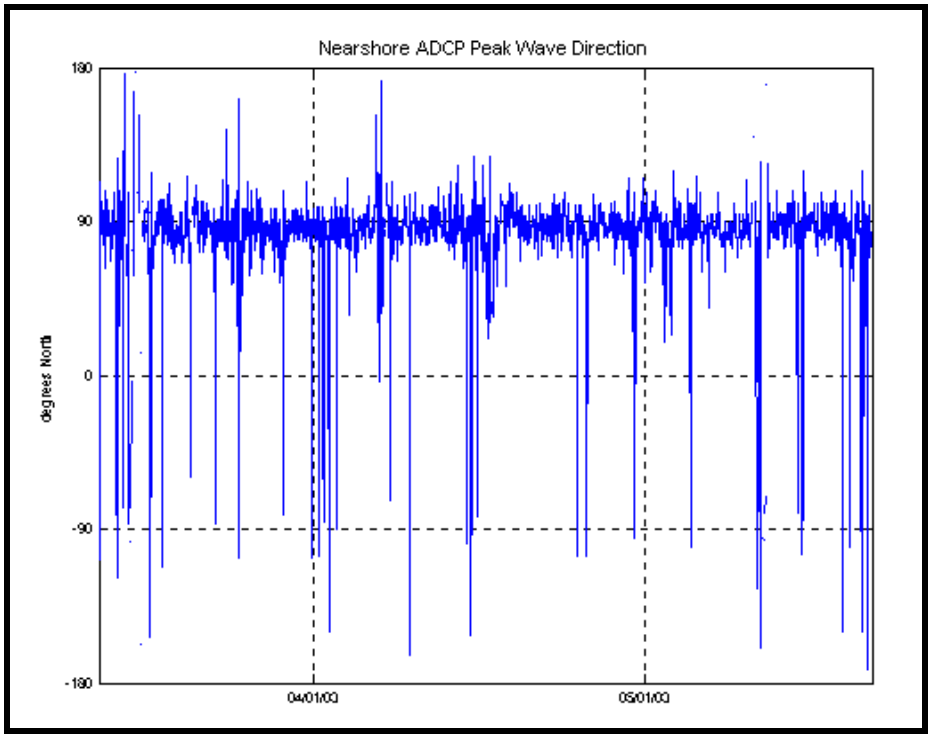

Figure 7-11. Offshore ADCP station peak wave direction time series.

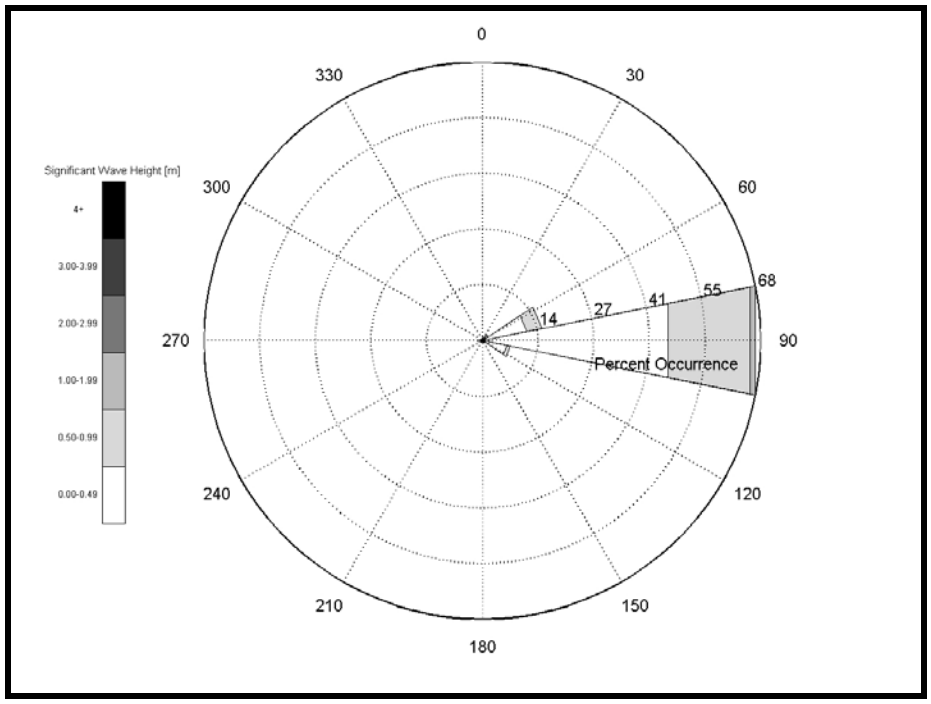

Figure 7-12. Wave rose of wave height data at Nearshore ADCP station over deployment time period (March- May 2003).

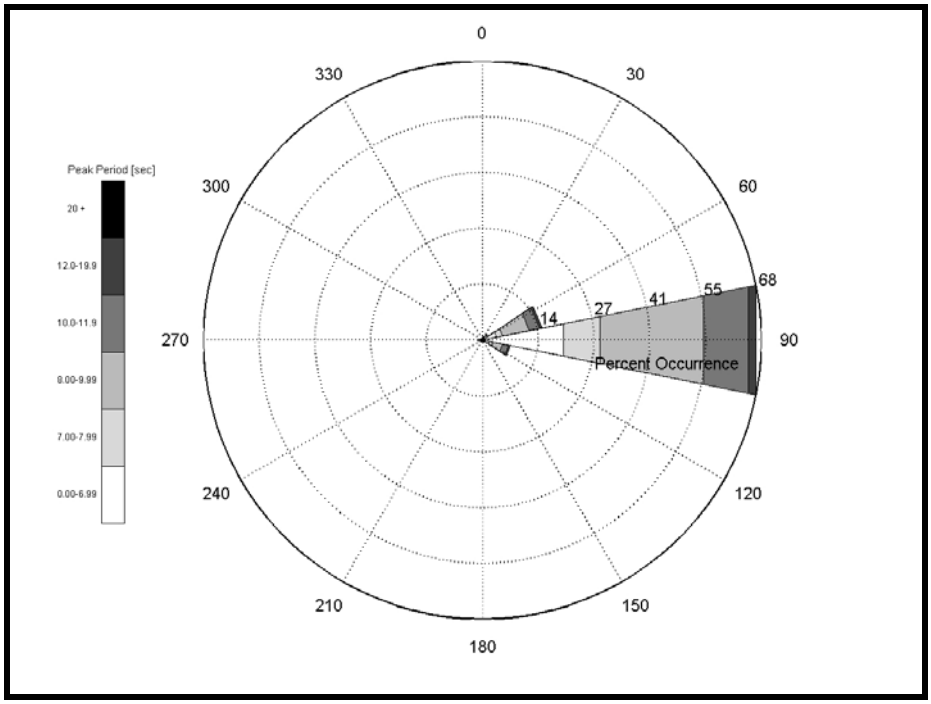

Figure 7-13. Wave rose of peak period data at Nearshore ADCP station during the deployment time period (March- May 2003).

Table 7-9 presents the percentage frequency of occurrence of significant wave height versus peak wave direction. The table shows the percentage of occurrence of significant wave height in height (cm) and directional (degrees from north) cells. The number printed within each cell represents the percentage of occurrence for each height/direction combination. The table is also overlain with contour lines to highlight the location of higher percentages. In addition, total percentages of directional and height bins are shown at the far right and bottom of each table. The table indicates that almost all of the waves arrived in the directional range between 56 degrees from north and 124 degrees from north (93.01%), with the primary approach direction between 79 and 101 degrees from north (70.45%). During the deployment time frame (March- May 2003), the waves were almost unidirectional. The majority of the waves were between 25 and 50 cm (0.8 and 1.6 ft) in height (55.49%). A total of 39.73% of the waves are between 79 and 101 degrees and between 25 and 50 cm 0.8 and 1.6 ft) in height. The larger waves (>75 cm) (2.5 ft) approach from the 79-101 degree directional bin. Wave heights were reduced compared to the offshore ADCP station.

Table 7-10 presents the percentage frequency of occurrence of peak wave period versus peak wave direction. The table shows the percentage of occurrence of peak wave period in period (seconds) and directional (degrees from north) cells. The number printed within each cell represents the percentage of occurrence for that particular period/direction combination. The table is also overlain with contour lines to highlight the location of higher percentages. In addition, total percentages of directional and period bins are shown at the far right and bottom of each table. The table indicates that a majority of the wave periods were between 7 and 10 seconds (50%). A total of 36% of the waves were between 7 and 10 seconds and approached from between 79 and 101 degrees. The directional variability of the waves is limited as indicated by the tightly focused contour lines.

Table 7-11 presents the percentage frequency of occurrence of significant wave height versus peak wave period. The table shows the percentage of occurrence of peak wave period in height (cm) and period (seconds) cells. The number printed within each cell represents the percentage of occurrence for that particular height/period combination. The table is also overlain with contour lines to highlight the location of higher percentages. In addition, total percentages of period and height bins are shown at the far right and bottom of each table. The largest portion of waves (12.1%) had wave heights between 25 and 38 cm (0.8 and 1.2 ft) and periods between 8 and 10 seconds. The larger waves (>75 cm) had periods between 6 and 11 seconds, and had a secondary peak in the 8 to 9 second bin. Rarely did wave periods exceed 13 seconds.

Table 7-9. Percentage frequency of occurrence statistics of significant wave height versus peak wave direction for the nearshore ADCP station.

Significant Wave Height (cm)

Peak Wave Direction (deg)	0	25	38	50	63	75	88	100	125	150	175	200	250	300	400	500	1000	All
-11-11	0.12	0.06	0.00	0.00	0.00	0.00	0.00	0.00	0.00	0.00	0.00	0.00	0.00	0.00	0.00	0.00	0.00	0.18
11-34	0.43	0.25	0.25	0.06	0.00	0.00	0.00	0.00	0.00	0.00	0.00	0.00	0.00	0.00	0.00	0.00	0.00	0.98
34-56	0.25	0.98	0.37	0.18	0.00	0.00	0.00	0.00	0.00	0.00	0.00	0.00	0.00	0.00	0.00	0.00	0.00	1.78
56-79	3.19	5.40	2.82	1.90	1.29	0.67	0.06	0.00	0.00	0.00	0.00	0.00	0.00	0.00	0.00	0.00	0.00	15.33
79-101	8.28	24.10	15.63	8.40	8.15	3.62	0.86	1.41	0.00	0.00	0.00	0.00	0.00	0.00	0.00	0.00	0.00	70.45
101-124	2.27	3.00	1.10	0.31	0.37	0.12	0.00	0.06	0.00	0.00	0.00	0.00	0.00	0.00	0.00	0.00	0.00	7.23
124-146	0.31	0.18	0.00	0.00	0.00	0.00	0.00	0.00	0.00	0.00	0.00	0.00	0.00	0.00	0.00	0.00	0.00	0.49
146-169	0.31	0.00	0.00	0.00	0.00	0.00	0.00	0.00	0.00	0.00	0.00	0.00	0.00	0.00	0.00	0.00	0.00	0.31
169-191	0.25	0.06	0.00	0.00	0.00	0.00	0.00	0.00	0.00	0.00	0.00	0.00	0.00	0.00	0.00	0.00	0.00	0.31
191-214	0.18	0.25	0.00	0.00	0.06	0.00	0.00	0.00	0.00	0.00	0.00	0.00	0.00	0.00	0.00	0.00	0.00	0.49
214-236	0.06	0.00	0.00	0.00	0.00	0.00	0.00	0.00	0.00	0.00	0.00	0.00	0.00	0.00	0.00	0.00	0.00	0.06
236-259	0.18	0.25	0.06	0.12	0.00	0.00	0.00	0.00	0.00	0.00	0.00	0.00	0.00	0.00	0.00	0.00	0.00	0.61
259-281	0.67	0.49	0.12	0.00	0.00	0.00	0.00	0.00	0.00	0.00	0.00	0.00	0.00	0.00	0.00	0.00	0.00	1.29
281-304	0.37	0.12	0.00	0.00	0.00	0.00	0.00	0.00	0.00	0.00	0.00	0.00	0.00	0.00	0.00	0.00	0.00	0.49
304-326	0.00	0.00	0.00	0.00	0.00	0.00	0.00	0.00	0.00	0.00	0.00	0.00	0.00	0.00	0.00	0.00	0.00	0.00
326-349	0.00	0.00	0.00	0.00	0.00	0.00	0.00	0.00	0.00	0.00	0.00	0.00	0.00	0.00	0.00	0.00	0.00	0.00
All	16.86	35.13	20.36	10.97	9.87	4.41	0.92	1.47	0.00	0.00	0.00	0.00	0.00	0.00	0.00	0.00	0.00	

Table 7-10. Percentage frequency of occurrence statistics of peak period versus peak wave direction for the nearshore ADCP station.

Peak Wave Period (sec)

Peak Wave Direction (deg)	0	3	4	5	6	7	8	9	10	11	12	13	14	16	18	20	40	All
-11-11	0.00	0.00	0.00	0.00	0.00	0.00	0.06	0.00	0.00	0.06	0.06	0.00	0.00	0.00	0.00	0.00		0.18
11-34	0.55	0.00	0.00	0.00	0.00	0.12	0.12	0.06	0.00	0.06	0.00	0.00	0.06	0.00	0.00	0.00		0.98
34-56	0.98	0.00	0.00	0.00	0.12	0.00	0.25	0.12	0.06	0.12	0.12	0.00	0.00	0.00	0.00	0.00		1.78
56-79	0.25	0.80	0.43	0.37	1.84	1.47	3.43	3.49	1.66	0.98	0.61	0.00	0.00	0.00	0.00	0.00		15.33
79-101	0.86	2.70	3.19	4.35	9.75	9.44	13.61	12.94	8.22	3.43	1.72	0.00	0.25	0.00	0.00	0.00		70.45
101-124	0.18	0.18	0.25	0.61	0.61	0.86	1.29	1.29	0.80	0.67	0.31	0.00	0.18	0.00	0.00	0.00		7.23
124-146	0.06	0.00	0.00	0.00	0.00	0.00	0.00	0.18	0.00	0.18	0.06	0.00	0.00	0.00	0.00	0.00		0.49
146-169	0.00	0.00	0.00	0.00	0.00	0.00	0.00	0.18	0.00	0.12	0.00	0.00	0.00	0.00	0.00	0.00		0.31
169-191	0.00	0.00	0.00	0.00	0.00	0.06	0.12	0.06	0.00	0.06	0.00	0.00	0.00	0.00	0.00	0.00		0.31
191-214	0.00	0.00	0.00	0.00	0.00	0.00	0.06	0.12	0.06	0.06	0.06	0.00	0.12	0.00	0.00	0.00		0.49
214-236	0.06	0.00	0.00	0.00	0.00	0.00	0.00	0.00	0.00	0.00	0.00	0.00	0.00	0.00	0.00	0.00		0.06
236-259	0.00	0.00	0.00	0.00	0.00	0.00	0.00	0.25	0.06	0.12	0.12	0.00	0.06	0.00	0.00	0.00		0.61
259-281	0.00	0.00	0.00	0.00	0.06	0.12	0.12	0.12	0.43	0.06	0.25	0.00	0.12	0.00	0.00	0.00		1.29
281-304	0.00	0.00	0.00	0.00	0.00	0.00	0.06	0.06	0.18	0.12	0.06	0.00	0.00	0.00	0.00	0.00		0.49
304-326	0.00	0.00	0.00	0.00	0.00	0.00	0.00	0.00	0.00	0.00	0.00	0.00	0.00	0.00	0.00	0.00		0.00
326-349	0.00	0.00	0.00	0.00	0.00	0.00	0.00	0.00	0.00	0.00	0.00	0.00	0.00	0.00	0.00	0.00		0.00
All	2.94	3.68	3.86	5.33	12.39	12.08	19.13	18.88	11.47	6.07	3.37	0.00	0.80	0.00	0.00	0.00		

Again, in order to evaluate some of the higher energy time periods that occurred during the deployment, wave events were defined. For discussion purposes, wave events are herein defined as when significant wave heights exceed 75 cm (2.5 ft) for more than 12 hours. Four higher energy wave events occurred at the study site during the months of recording, as is evidenced in the time series of significant wave height shown in Figure 7-9. Table 7-12 details these events, including some of the pertinent event statistics. These four events are a subset of the six events that were measured at the Offshore ADCP. The offshore ADCP measured two events in May 2003 that did not exceed the required thresholds at the Nearshore ADCP station.

7.2.3 Additional Wave Data

The wave ADCP data collected during this project were compared to other available wave information in the area in order to ensure proper functionality of the observation systems. Section 9.4 presents a complete discussion of all additional wave data and information, including the utilization of existing wave data for modeling purposes and the development of wave input conditions. This section presents a brief comparison of the observed wave data to the NOAA buoy located offshore of Portland. Since the NOAA buoy does not record directional information, comparison is performed only between significant wave height and peak wave period.

Table 7-11. Percentage frequency of occurrence statistics of significant wave height versus peak wave period for the nearshore ADCP station.

Peak Wave Period (sec) \ Significant Wave Height (cm)	0	25	38	50	63	75	88	100	125	150	175	200	250	300	400	500	1000	All
0-3	0.37	1.23	1.04	0.31	0.00	0.00	0.00	0.00	0.00	0.00	0.00	0.00	0.00	0.00	0.00	0.00	0.00	2.94
3-4	0.25	1.96	0.92	0.49	0.06	0.00	0.00	0.00	0.00	0.00	0.00	0.00	0.00	0.00	0.00	0.00	0.00	3.68
4-5	0.00	1.59	0.98	0.92	0.25	0.12	0.00	0.00	0.00	0.00	0.00	0.00	0.00	0.00	0.00	0.00	0.00	3.86
5-6	0.55	2.76	0.92	0.31	0.49	0.25	0.06	0.00	0.00	0.00	0.00	0.00	0.00	0.00	0.00	0.00	0.00	5.33
6-7	1.47	4.29	3.31	1.16	0.86	0.61	0.18	0.49	0.00	0.00	0.00	0.00	0.00	0.00	0.00	0.00	0.00	12.39
7-8	1.78	4.41	2.02	1.23	1.29	0.61	0.43	0.31	0.00	0.00	0.00	0.00	0.00	0.00	0.00	0.00	0.00	12.08
8-9	4.90	6.01	3.00	1.41	2.21	0.80	0.18	0.61	0.00	0.00	0.00	0.00	0.00	0.00	0.00	0.00	0.00	19.13
9-10	3.00	6.13	3.86	2.76	2.45	0.61	0.00	0.06	0.00	0.00	0.00	0.00	0.00	0.00	0.00	0.00	0.00	18.88
10-11	1.35	3.49	2.33	1.47	1.72	1.10	0.00	0.00	0.00	0.00	0.00	0.00	0.00	0.00	0.00	0.00	0.00	11.47
11-12	1.53	2.15	1.29	0.43	0.37	0.25	0.06	0.00	0.00	0.00	0.00	0.00	0.00	0.00	0.00	0.00	0.00	6.07
12-13	1.10	0.92	0.67	0.49	0.12	0.06	0.00	0.00	0.00	0.00	0.00	0.00	0.00	0.00	0.00	0.00	0.00	3.37
13-14	0.00	0.00	0.00	0.00	0.00	0.00	0.00	0.00	0.00	0.00	0.00	0.00	0.00	0.00	0.00	0.00	0.00	0.00
14-16	0.55	0.18	0.00	0.00	0.06	0.00	0.00	0.00	0.00	0.00	0.00	0.00	0.00	0.00	0.00	0.00	0.00	0.80
16-18	0.00	0.00	0.00	0.00	0.00	0.00	0.00	0.00	0.00	0.00	0.00	0.00	0.00	0.00	0.00	0.00	0.00	0.00
18-20	0.00	0.00	0.00	0.00	0.00	0.00	0.00	0.00	0.00	0.00	0.00	0.00	0.00	0.00	0.00	0.00	0.00	0.00
20-40	0.00	0.00	0.00	0.00	0.00	0.00	0.00	0.00	0.00	0.00	0.00	0.00	0.00	0.00	0.00	0.00	0.00	0.00
All	16.86	35.13	20.36	10.97	9.87	4.41	0.92	1.47	0.00	0.00	0.00	0.00	0.00	0.00	0.00	0.00	0.00	

The Portland, Maine NOAA buoy (designator 44007) is located 12 nautical miles southeast of Portland, Maine in approximately 18.9 m (62 ft) of water. The buoy is a 3 m (9.8 ft) discus buoy that records wave heights for 20 minutes every hour and averages the information over that sample period. The buoy is capable of recording waves in the wave height range of 0 to 35 m (0 to 115 ft) and periods spanning 0 to 30 seconds. The buoy can resolve a wave to 0.1 m in height and 1.0 sec of period. The buoy is stated to be accurate to +/- 0.2 m (0.7 ft) in wave height and +/-1.0 sec in period. The wave data for the months of March, April and May 2003, were obtained from the National Data Buoy Center. There was a 98% data return during these three months.

Table 7-12. Summary of wave events at nearshore ADCP station (event threshold: H_{sig} > 75 cm for time >12 hours).

Event ID Number	Start of Event	End of Event	Time event exceeded threshold (hours)	Mean H_{sig} during event (cm)	Max H_{sig} during event (cm)	Mean T_{peak} during event (sec)	Mean Peak Wave Direction during event (degrees)
1	4/4/03 12:00:00	4/6/03 04:00:00	40	81	115	7.5	85
2	4/11/03 15:00:00	4/12/03 12:00:00	23	77	89	7.3	90
3	4/20/03 09:00:00	4/23/03 03:00:00	66	74	89	10.3	86
4	4/26/03 16:00:00	4/27/03 15:00:00	23	99	117	7.4	88

The NOAA buoy recorded a mean significant wave height of 0.91 m (2.9 ft) and a maximum of 2.56 m (8.4 ft) during this time period. The time series of significant wave height as recorded by the NOAA buoy, as well as the Offshore ADCP and Nearshore ADCP, is presented in Figure 7-14. The significant wave heights recorded by the ADCPs indicate a reduced magnitude, as expected due to typical energy losses and dissipation effects as the waves approach the shoreline. Patterns in the significant wave heights are similar at all three locations, providing a good level of confidence in the observed data.

The mean peak wave period recorded by the NOAA buoy was 7.6 seconds with a maximum of 12.5 seconds. Figure 7-15 shows peak period recorded by the NOAA buoy and both the Offshore and Nearshore ADCP. The peak period also tracks well between the three locations. Differences between locations occur when the wave height is small or immeasurable. For example, during the time period between approximately May 11 and May 13, the Nearshore ADCP observed minor wave heights, and subsequently non-representative wave periods.

7.3 Current Observations

Although wave observations were the focus of the field data collection program, the ADCPs were also programmed to resolve the water column into several elevation bins and determine the three components of the ambient current (u,v,w) within each bin. Only the horizontal components of the surface current are analyzed in this report (u,v). The ADCP recorded current information every 10 minutes; however, for the purpose of this report, currents were only analyzed every hour.

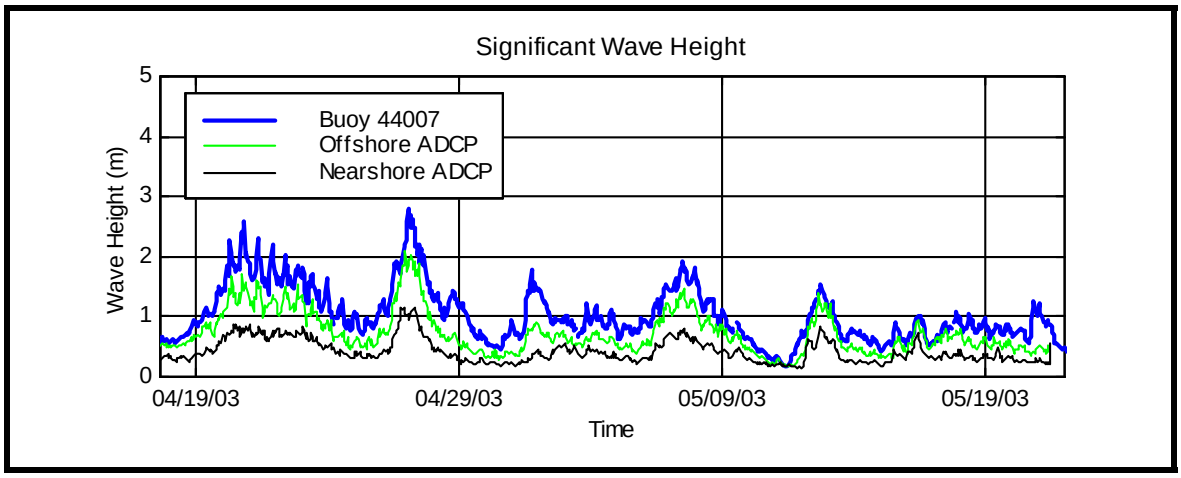

Figure 7-14. Comparison of significant wave height (m) between NOAA buoy 44007 and the two ADCP stations during the deployment time period (March-May 2003).

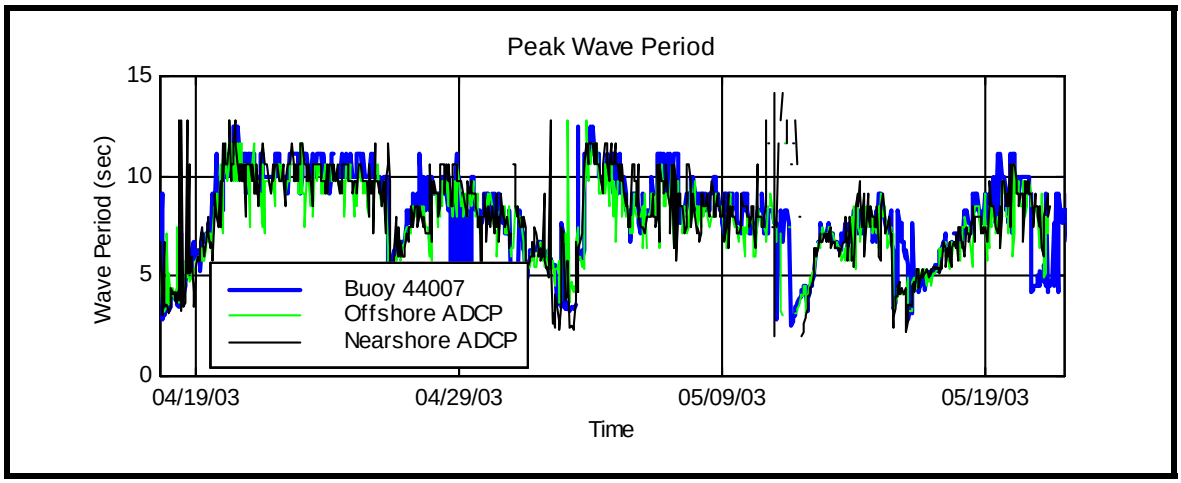

Figure 7-15. Comparison of peak wave period (sec) between NOAA buoy 44007 and the two ADCP stations during the deployment time period (March-May 2003).

The Offshore ADCP is capable of resolving current magnitude to within a standard deviation of 2.2 cm/sec (0.07 ft/s). There was 100% data return during the data collection

period. The average current speed collected at this offshore location was 7.1 cm/sec (0.2 ft/s). The maximum magnitude recorded at this location was 31.5 cm/sec (1.0 ft/s). During the recording period, the mean direction of the current was 214.9°. Figure 7-16 presents the directional distribution of current magnitude (cm/s) data (illustrated using a wave rose). The gray-scale sidebar indicates the magnitude of the current, the circular axis represents the direction of current approach (coming from) relative to North (0 degrees), and the extending radial lines indicate percent occurrence within each magnitude and directional band. The figure depicts a general trend of current flow alternating between flows directed towards the Southwest and the Northeast due to the tidal fluctuations.

The Nearshore ADCP is capable of resolving current magnitude to within a standard deviation of 1.8cm/s (0.06 ft/s). There was 100% data return during the data collection period. The average current magnitude collected at the nearshore location was 5.5 cm/sec (0.2 ft/s). The maximum magnitude recorded at this location was 20.3 cm/sec (0.7 ft/s). During the recording period, the average direction of the current was 184.0° North, or almost due south. The frequency of occurrence rose plot for the Nearshore ADCP is presented in Figure 7-17. The currents are significantly smaller and less organized at the Nearshore ADCP station, than at the offshore ADCP station.

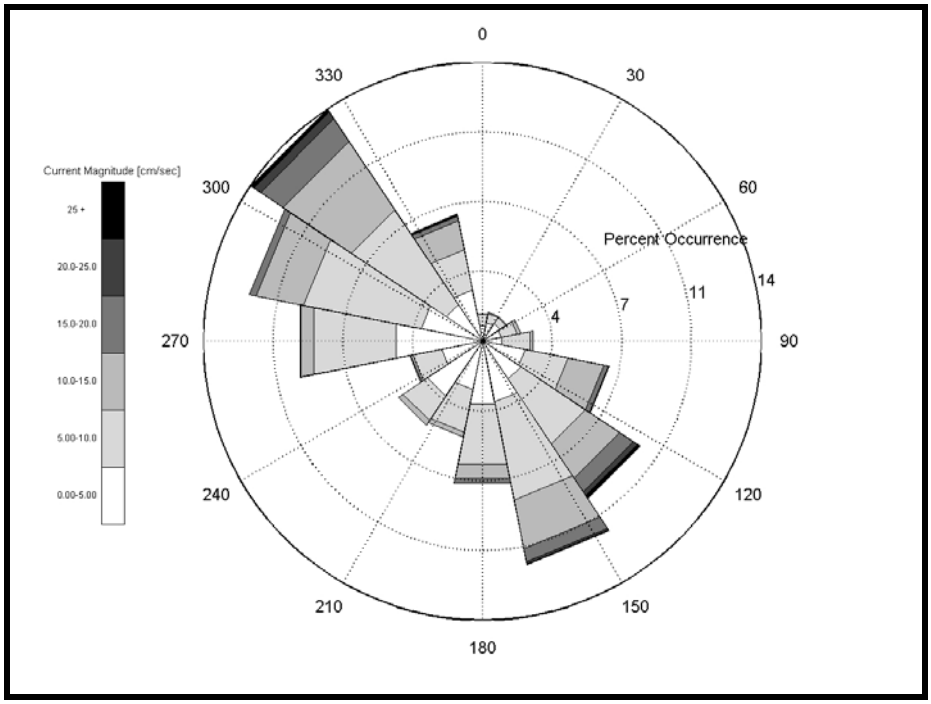

Figure 7-16. Rose plot of current observations at the Offshore ADCP station during the deployment time period (March- May 2003).

7.4 Summary

This chapter presented the wave and current data collected in the nearshore vicinity of Camp Ellis Beach. Wave and current data were collected at target locations seaward and landward of the Eagle/Ram Island complex in order to assess accurately the wave transformations that occur due to the complicated physical nature of the islands and bathymetry in this region. Wave data, at least over the deployment time period, indicate that waves approaching Camp Ellis Beach are primarily unidirectional, approaching from an ENE direction, even when waves approach from the ESE seaward of the islands. The wave ADCP data were compared to existing NOAA buoy data to provide a level of confidence in the observed data. The wave data were a necessity for calibrating and verifying the numerical wave transformation models. Data were used extensively to validate model performance, as presented in Chapters 8.0 through 13.0.

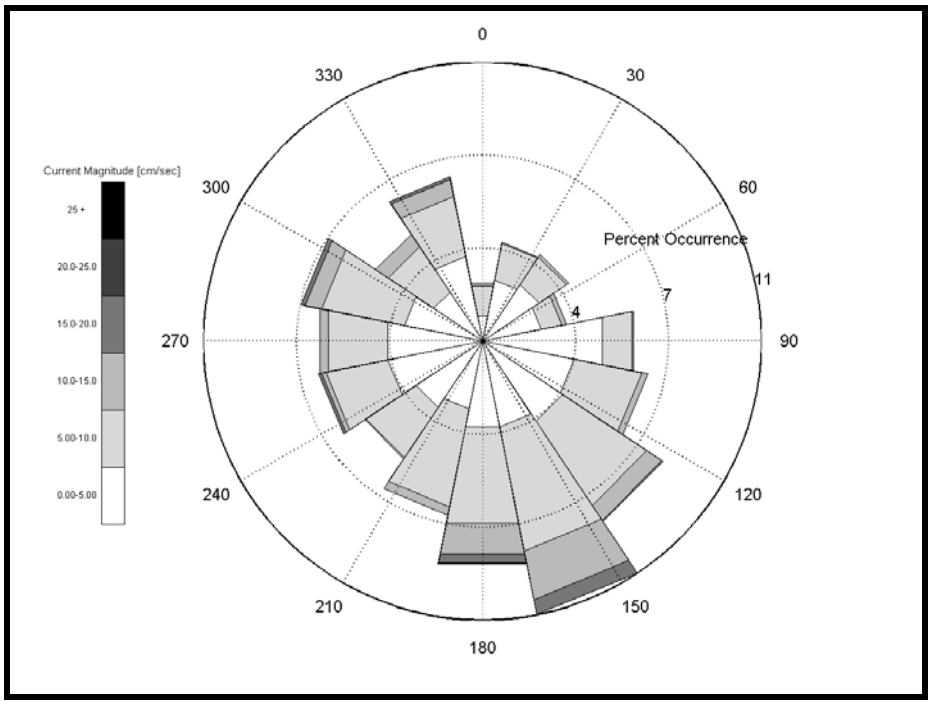

Figure 7-17. Rose plot of current observations at the Nearshore ADCP station during the deployment time period (March- May 2003).

8.0 GENERATION-SCALE WAVE MODELING (TASK 16)

Numerical models are only as good as the quality of the data used to specify boundary conditions, to calibrate, and to verify the model. Data used to calibrate the transformation-scale (regional) wave model were developed from up-to-date, accurate measurements at two locations within Saco Bay (field measurement program, Section 7.0). However, data specified at the boundary had to be developed based on buoys and/or historical hindcast data, which have directional and temporal limitations, respectively.

In many cases, wave input conditions for nearshore wave transformation-scale (regional) modeling can be obtained directly from offshore wave buoys or previously developed hindcast wave data. However, to calibrate, verify, and validate the wave modeling system within Saco Bay, offshore directional wave information was required concurrently with the nearshore wave observations (March - May 2003). Although there are abundant wave observations within the Gulf of Maine (Figure 9-3), the data are all non-directional. Therefore, buoy data have limited use as a boundary condition for calibration of the transformation models. Existing Wave Information System (WIS) wind-wave hindcast data contained directional spectra, but the current database only extends up to 1999, and temporally does not match the nearshore wave observations. Additionally, the location of the existing offshore buoys and hindcast data are spatially limited (i.e., do not correspond directly to the offshore boundary of the wave model). To improve upon these limitations, satellite wind fields and an offshore, spectral, wave generation model was applied for the time period of the field data collection program (March-May 2003) to provide directional, spectral wave input conditions directly at the boundary of the transformation-scale (regional) wave model.

This chapter presents the generation-scale component of the modeling system. This chapter describes:

- the analysis approach applied to simulate waves at this scale,
- the required input data, including the wind and bathymetric information,
- the calibration and verification of the model (compared to wave buoys) during the entire observation period,
- and a discussion of the wave modeling results.

8.1 Analysis Approach

The goal of the generation-scale modeling for Camp Ellis Beach was to simulate wave growth, dissipation and propagation in deep-water for use as input into the regional wave transformation modeling (Chapter 9.0). A spectral wave model, WAVAD (Resio, 1990), was used for the generation-scale modeling. The model used input wind fields as the primary generating force for deep-water waves. The model output included wave spectra at equi-spaced points within the area of interest.

The modeled wave spectra represented the distribution of wave energy across frequency, and were represented as fully three-dimensional spectra in discretized frequency and direction bands. Processes such as propagation effects and source/sink mechanisms were modeled and led to variations for energy levels in each of these frequency-direction elements. All wave parameters, such as significant wave height, frequency of the spectral peak, and mean wave direction, were computed within these discrete elements.

8.2 Wave Model Description

The physics embodied in WAVAD represent the state-of-the-art in our present understanding of wave generation. The model is based on a f^{-4} equilibrium range formulation, as supported by field experiments (Toba, 1978; Forristall 1981; Kahma, 1981; Kitaigorodskii, 1983), and is consistent with energy conservation in the equilibrium range, as calculated from the complete or reduced Boltzmann integrals. In a coordinate system moving with the group velocity of the spectral peak, the governing equation for the evolution of the wave spectrum can be approximated as:

$$\frac{DE(f)}{Dt} = \sum_{i=1}^{5} S_i(f) \quad \text{..... (8-1)}$$

where $S_i(f)$ represents a separate source term:

$S_1(f)$ = shoaling,

$S_2(f)$ = refraction,

$S_3(f)$ = wind effects,

$S_4(f)$ = wave-wave interactions

$S_5(f)$ = bottom interaction effects.

The WAVAD model represents each of these processes using methodologies developed from theory and experiments. The fetch-growth characteristics of the model are similar to the JONSWAP relationships (i.e., wave energy increased linearly with fetch) and the duration-growth characteristics are roughly similar to those of Resio (1981) and the Navy's Spectral Ocean Wave Model (SOWM).

The WAVAD model propagates each frequency-direction element independently using an upstream differencing method, which offers advantages for stability, execution time and set-up simplicity. In a latitude-longitude grid, as used in this model, propagation along meridians (or components of propagation along meridians) is the equivalent of propagation along great circles. Consequently, there is no curvature away from a straight-line propagation along these axes; however, divergence/convergence effects are incorporated for meridional propagation. For propagation along latitudes (parallels), there is no divergence/convergence; however, angular curvature is included in the model. Since a latitude-longitude grid was used in this study, the convergence/divergence effects and angular curvature is included.

Proper simulation of the physics of energy transfer into and out of each element in the directional spectrum is essential for accurate wave modeling. WAVAD uses the following simulated sources and sinks of energy:

- Energy transfer from the atmosphere (winds) to the wave field,
- Energy transfers among wave components (wave-wave interactions),
- Energy losses due to wave breaking,
- Bottom friction

The total energy input into the wave spectra from the wind is given by:

$$\frac{\partial E_o}{\partial t} = \frac{Ru^3}{g} \quad \text{(8-2)}$$

Where R is a dimensionless constant, g is the acceleration of gravity, E_o is the one-dimensional wave spectrum, and u is the wind speed. This equation is consistent with the concept that, at oceanic scales, the coefficient of drag is independent of the wave height; therefore, the total energy transfer rate from the atmosphere to the water is independent of wave height.

Theoretical considerations dictate that certain geometric constraints on wave-wave interactions effectively force the wave spectrum toward a characteristic similarity form. As a result the energy balance between nonlinear fluxes and wind inputs leads to an equilibrium range of the f^{-4} type (Resio, 1987, 1988).

The WAVAD model assumes that wave breaking removes all energy that is transferred into frequencies above some threshold frequency. Other than wave breaking, wave-wave interactions are conservative and do not produce any energy loss.

Bottom friction follows a quadratic formulation, which, following Collins (1972), leads to a rate of energy loss given by:

$$\frac{\partial E(f,\theta)}{\partial t} = -\frac{E(f,\theta)C_f g k^2}{2\pi\omega^2 \cosh(kh)}\langle u \rangle \quad \text{..... (8-3)}$$

where

$$u = \left[\int \frac{E(f) g^2 k^2}{\omega^2 \cosh^2(kh)} df \right]^{1/2} \quad \text{..... (8-4)}$$

and k is the wave number, h is the water depth, $E(f,\theta)$ is the 3-D were spectrum, ω is the angular frequency, and C_f is the bottom friction coefficient.

8.3 Input Conditions

The generation-scale wave model required two primary input files. The first file contained the wind information (wind speed and direction) at each grid point. Wind directions utilized by the model were in vector form. The vectors indicated the direction the winds were blowing towards. Wind angles were referenced such that 0° was equal to 90° true N. The direction of rotation was counter-clockwise; therefore, a wind angle of 180° was equal to 270° true N (Figure 8-1). Wind speeds were supplied to the model in the units of m/s and converted within the model to knots. The winds were assumed to be representative of a 10 m height above the water surface. For the Camp Ellis Beach study, wind fields were input every 12 hours. Details on the input wind field are presented in Section 8.3.1.

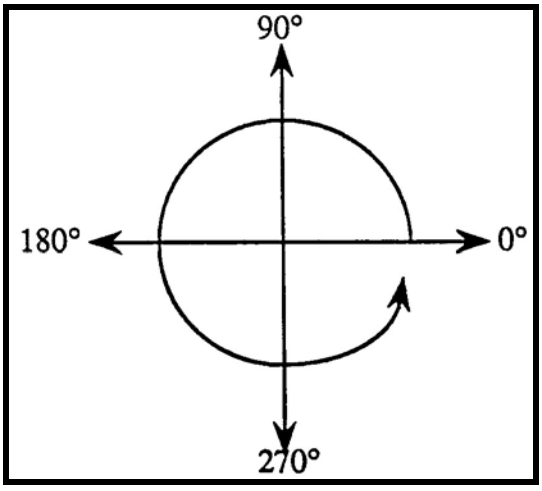

Figure 8-1. Representation of the wind angle notation used in WAVAD.

The second input file contained many of the parameters needed for the wave model. Included in these parameters were the number of columns in the grid, number of rows in

the grid, number of angle bands, number of frequency bands, distance between grid points, model time step, elevation of winds, number of hours between wind updates, options to read/write boundary data, options to write a variety of output files, etc. In general, these parameters remained constant between the model runs; however, it was necessary to vary several parameters between the nested grid runs (i.e., numbers of columns, rows, latitude of lower left grid corner). Included in this file is the depth at each of the grid points. Details on the development of the bathymetric grid, including the nesting of different resolution grids, can be found in Section 8.3.2.

8.3.1 QuikSCAT Satellite Winds

The model used wind fields as the primary generating force for deep-water waves. The wind fields were created using the data from the National Aeronautics and Space Administration's QuikSCAT satellite. This satellite houses a microwave scatterometer (SeaWinds) designed specifically to measure near-surface wind velocity (both speed and direction) over the global oceans under all weather conditions (Jet Propulsion Laboratory, 2001). Scatterometers measure the wind indirectly. The scatterometer transmits microwave pulses and receives backscattered power from the ocean surface. Changes in wind velocity and direction modified the ocean surface roughness, as a modification of the backscattered power (Jet Propulsion Laboratory, 2001).

The NASA Jet Propulsion Laboratory's Physical Oceanography Distributed Active Archive Center (PO.DAAC) Environmental Science Information Partner (ESIP) Tool (POET) was used to obtain the wind fields. An ASCII file containing the meridional and zonal components of the wind was used to define the wind speed and wind direction at each of the grid points. An example of one of the wind fields used is presented in Figure 8-2. The complete set of wind fields is presented in Appendix 8-A. Data gaps within the wind record were filled through interpolation of the average meridional and zonal components of the grid.

Wind vectors in the immediate vicinity of the shoreline cannot be acquired using QuikSCAT imagery. The complex nature of waves in shallow water makes the retrieved vectors inaccurate. The changes in ocean surface roughness near the coastline are not solely attributable to changes in wind. Therefore, wind speeds recorded at the nearshore buoy and the winds recorded at Portland International Jetport, ME were used to fill in the missing wind information in the shallow water regions. The wind from the Jetport was assumed to be the same as the wind at the shoreline, and linear interpolation was performed between the NOAA buoy and the shoreline. The winds for the Jetport were obtained digitally from the National Climatic Data Center. This process allowed for a representation of the nearshore winds and hence the nearshore wind-generated waves. Although ultimately, the nearshore region was more accurately simulated using the higher resolution nearshore transformation models such that the coarse resolution, wave generation model was not used in the nearshore region.

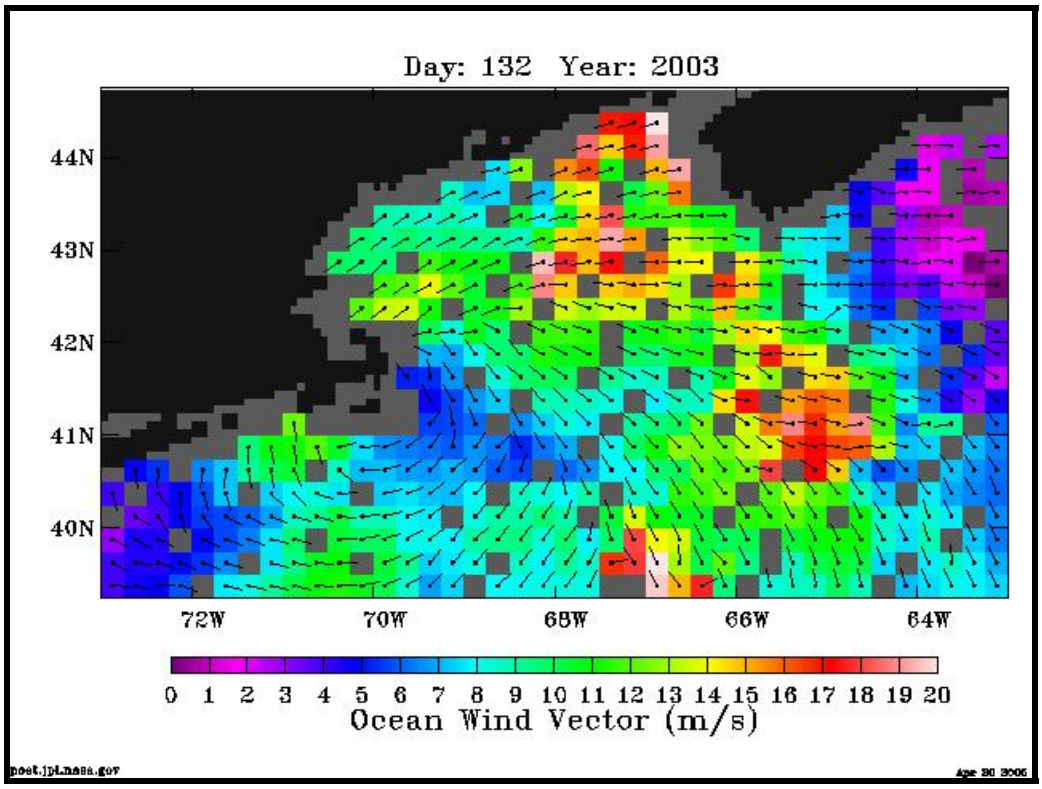

Figure 8-2. Example QuikSCAT wind field. Morning satellite overflight on May 12, 2003. This example represents one of the wind fields used to rectify the input wind during the deployment time period.

Since the satellite passes over the region twice during a 24-hour period, the time between wind field inputs was limited to 12 hours. The satellite passed over the region at approximately 6 AM and 6 PM (GMT) everyday. These wind fields were laced together to form a temporally varying gridded wind field during the time of the nearshore wave observations (March-May 2003).

8.3.2 Bathymetry and Grid Generation

The WAVAD model required specification of bathymetry at each point in the computational grid. A series of two nested grids was applied to simulate the time period spanning the deployment of the two ADCPs. The larger grid has a resolution of 0.25 decimal degrees (17.3 miles), whereas the nested grid has a resolution of 0.05 decimal degrees (3.5 miles). Water depths within the grids were determined from the 30-arc second digital bathymetry constructed by the Coastal and Marine Geology Program of the United States Geological Survey (http://woodshole.er.usgs.gov/project-pages/oracle/gomaine/bathy/). The digital bathymetry was constructed using various data sources:

- NOAA Hydrographic Survey Data and NGDC Marine Trackline Geophysics Data

- Naval Oceanographic Office Digital Bathymetric Data Base - Variable Resolution gridded bathymetry
- Supplemental Datasets from Bedford Institute of Oceanography and Brookhaven National Laboratory
- NOAA Medium resolution digital Shoreline and DMA World Vector Shoreline
- Defense Mapping Agency ETOPO5 Digital relief of the Surface of the Earth
- GEBCO General Bathymetric Chart of the Oceans
- USGS North American 30 arc-second Digital Elevation Model (DEM)

The digital bathymetry (Figure 8-3) contained both positive (land) and negative (sea floor) values in meters, referenced to mean sea level. Since WAVAD required that all values be positive and in meters, all land values were converted to 0 and all ocean values were converted to positive values.

Solutions in the deep-water wave model were computed on a rectangular grid, which had equal sized x and y increments. The axes of the grid were aligned with latitude-longitude lines. Points in the grid were denoted by (I,J) coordinates, where I referenced the columns and J referenced the rows. Grid point (I=1, J=1) is in the lower left corner of the grid.

For simulations requiring finer resolution, the offshore wave model had a nesting capability. This nesting allowed the user to reduce the computational overhead of fine mesh calculations by utilizing a sequence of nested grids, each having a resolution finer than the preceding. The nested grids communicated through transfer of compatible boundary information. There was no limit to the number of nested grids that could be used during a WAVAD simulation.

Two nested grids were applied in the offshore wave generation scale modeling. The larger grid having a resolution of 0.25° (17.3 miles), extended from 39.375° N to 44.625° N and 72.875° W to 63.125° W (Figure 8-4). The maximum depth in the larger grid was 4939 meters (16,205 feet). The nested grid, a resolution of 0.05° (3.5 miles), extended from 42.325° N to 44.675° N and from 71.175° W to 67.825° W (Figure 8-5). The maximum depth in the nested grid was 290 meters (951.5 feet).

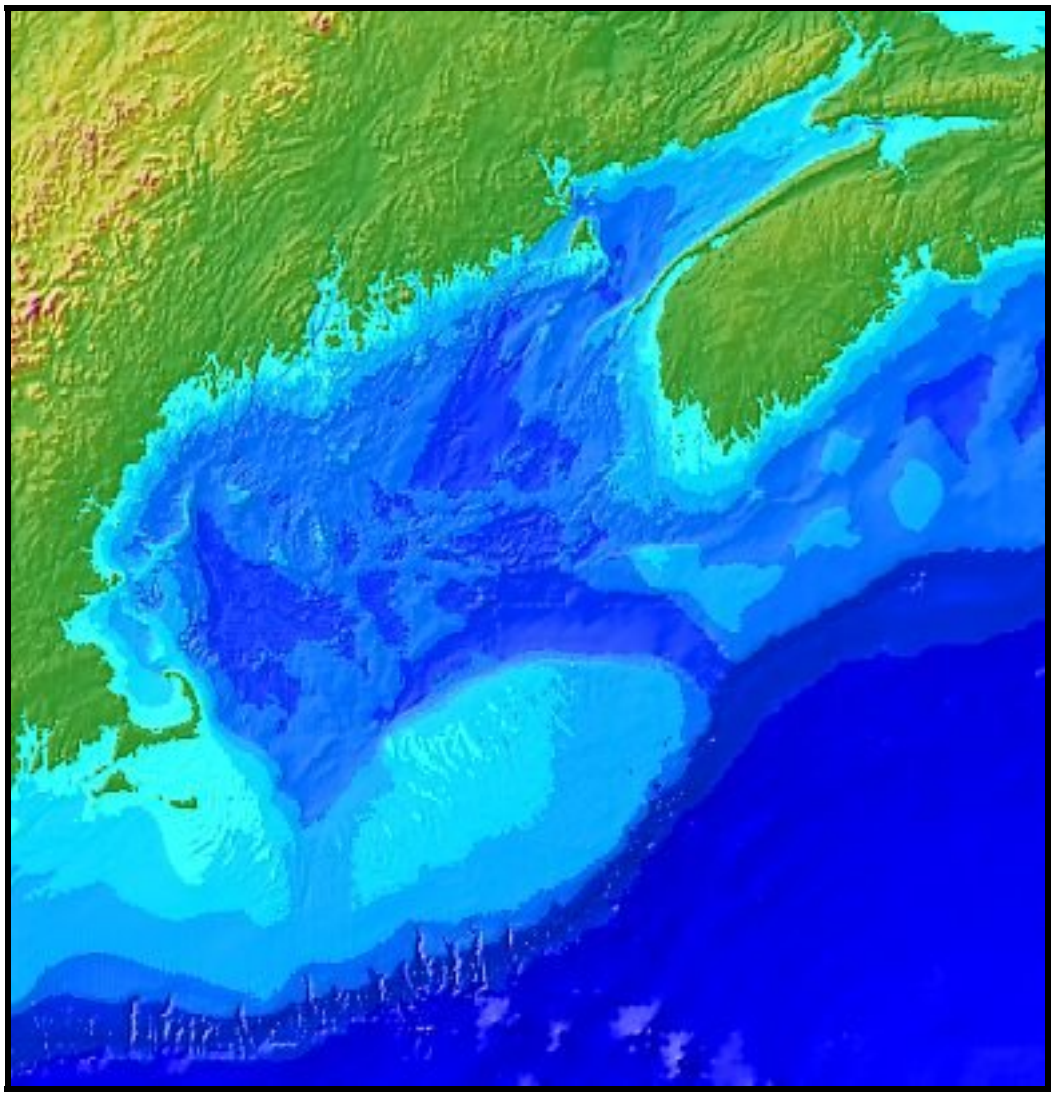

Figure 8-3. Digital bathymetry for the Gulf of Maine used in the generation-scale wave modeling (Image courtesy of USGS).

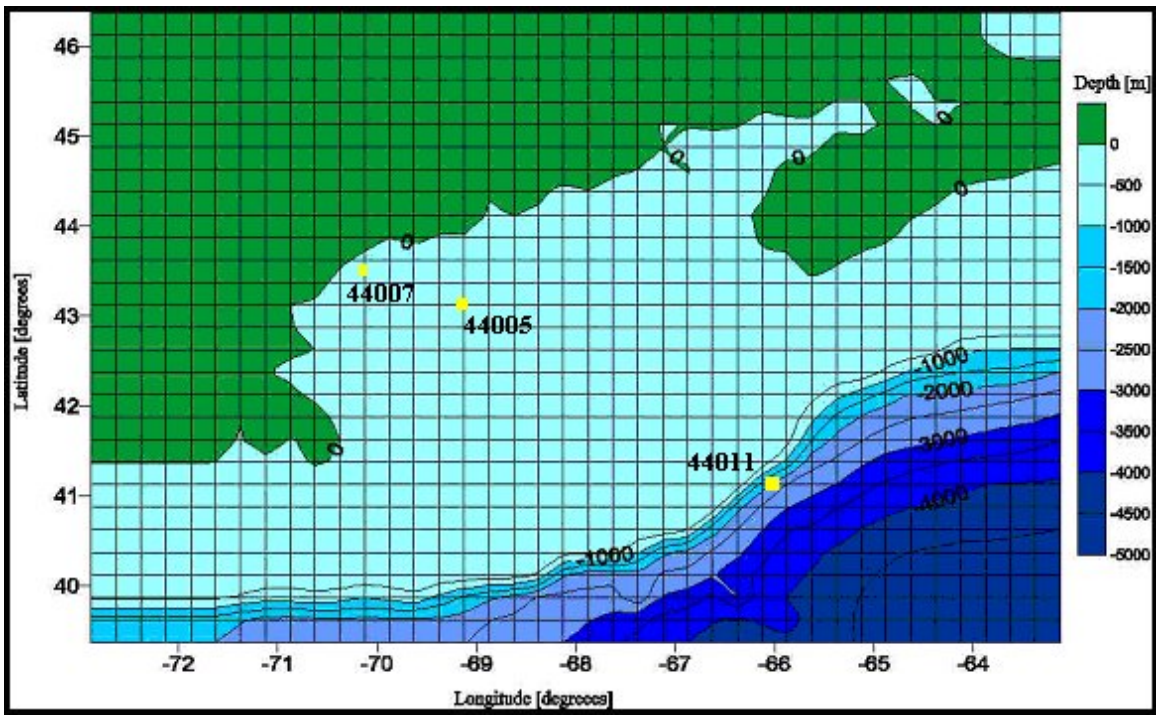

Figure 8-4. Larger WAVAD model grid.

8.4 Model Calibration

Calibration of the wave model required an ability to compare observed wave heights with the modeled wave heights during the same time period. The generation scale model was calibrated through comparison to buoy data (Chapter 7.0) observed within the model region. Table 8-1 presents the NOAA buoys, along with their locations, utilized in the calibration process. Buoy 44011 is located within the large grid, but not within the smaller, nested grid. Buoys 44005 and 44007 are located within both the large and nested grids.

Table 8-1. NOAA Buoys used in calibration of the generation scale model.

NOAA Buoy	Latitude (°N)	Longitude (°W)	Depth (m)
44011	41.11	66.02	88.4
44005	43.18	69.18	21.9
44007	43.53	70.14	18.9

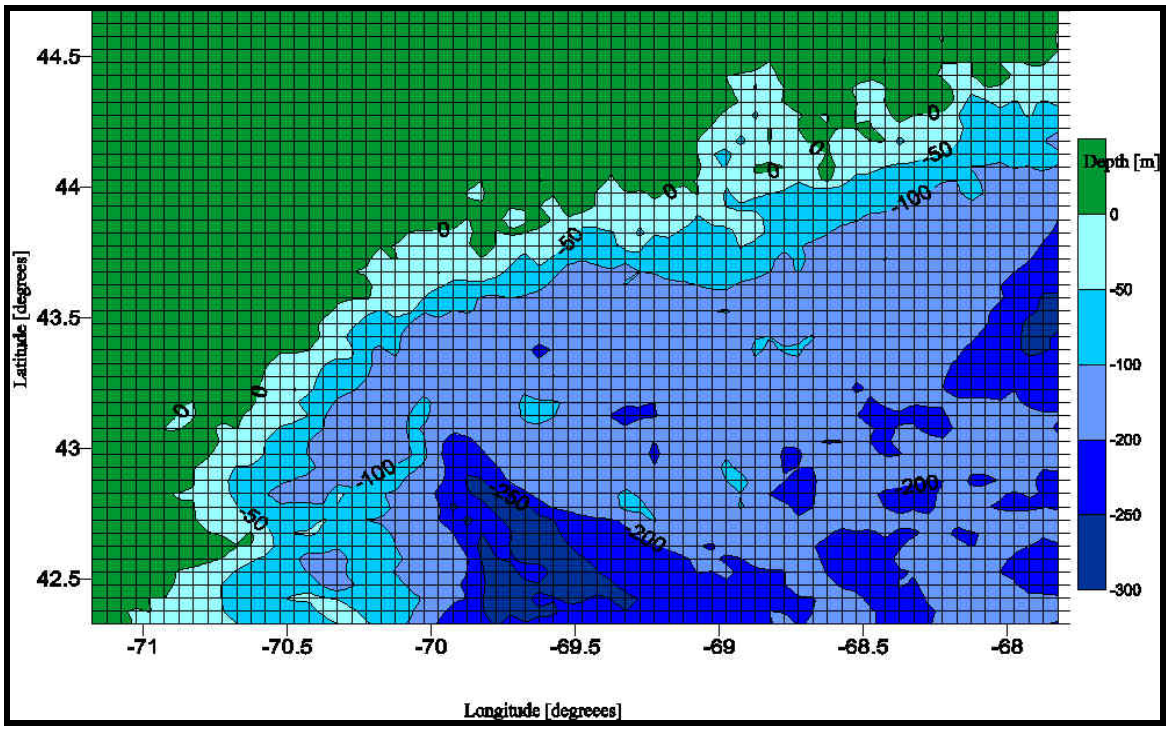

Figure 8-5. Nested WAVAD model grid.

The generation-scale model was calibrated for the entire deployment time period (March-May 2003). An iterative process was completed in order to assure good agreement between the modeled and observed wave data by adjusting the wind speed. Error statistics (bias and RMS error) are used to quantify the performance of the wave model. The bias and root-mean-square (RMS) error are defined as:

$$Bias = \frac{\sum \left(P_{measured} - P_{simulated} \right)}{n} \quad \text{.....(8-5)}$$

$$RMS\ Error = \sqrt{\frac{\sum \left(P_{measured} - P_{simulated} \right)^2}{n}} \quad \text{.....(8-6)}$$

where $P_{measured}$ is the measured wave parameter (NOAA Buoy), $P_{simulated}$ is the modeled wave parameter, and n is the number of values. A positive bias indicates underestimates by the model, while a negative bias indicates an overestimate. In addition, specific higher energy events were evaluated to determine the effectiveness of WAVAD for determination of wave height and spectral evolution during an event passage.

8.5 Model Results

8.5.1 Deployment Period

The model was used to simulate the entire time period corresponding to the deployment measurements from the ADCPs (March 12, 2003 through May 21, 2003). Model results were compared to three different NOAA buoy locations (Table 8-1). The output from the large grid consisted of spectral wave information at 12-hour intervals, whereas output from the nested grid was at 1-hour intervals. Figure 8-6 shows a comparison between the modeled (blue line) and the measured (red line) wave height and the modeled (blue line) and measured (red line) wind speed during the deployment time period for the larger grid results and buoy 44011.

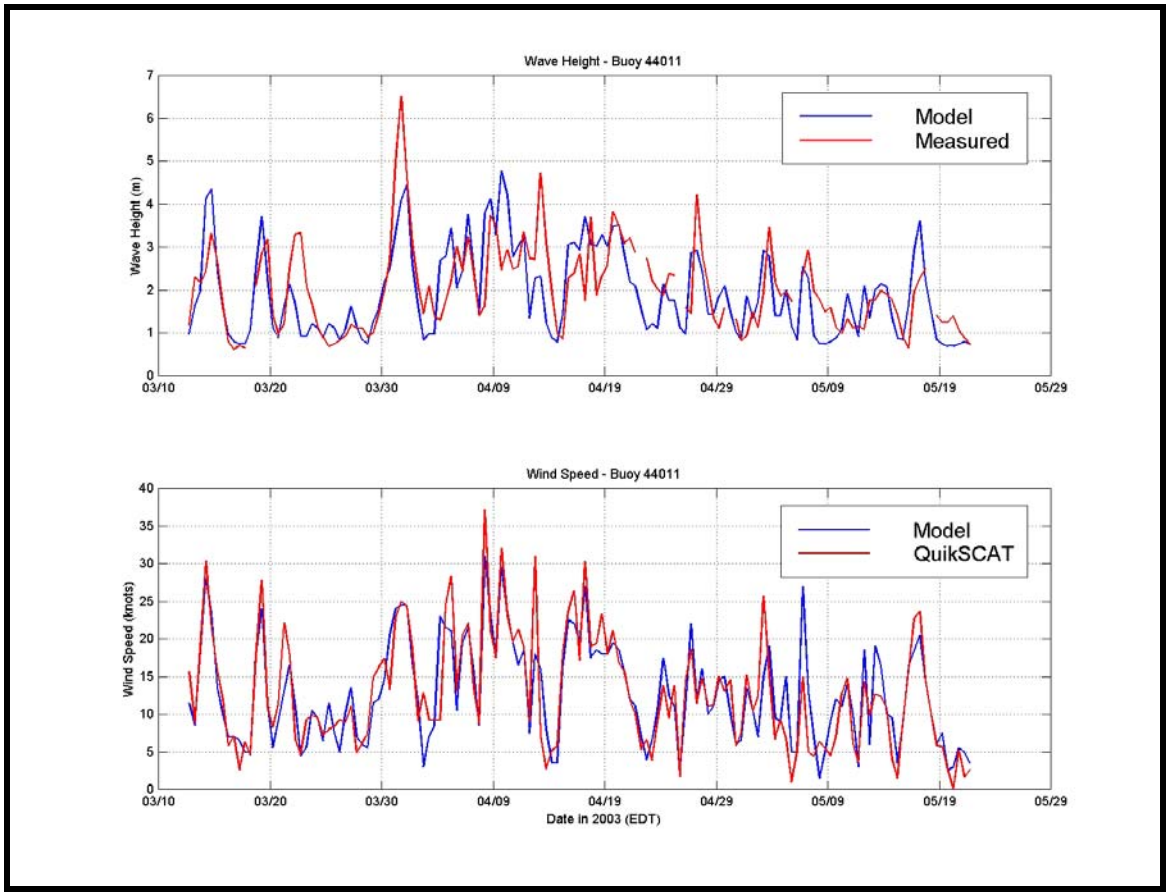

Figure 8-6. Comparison of modeled and measured wave height and wind speed at NOAA Buoy 44011.

Both the wave height and wind speed comparisons at Buoy 44011 show reasonable agreement during the entire time period. The overall trends in wave height are well identified, especially considering the input wind fields are only generated at 12-hour time steps. The computed RMS error between modeled and measured wave height was 0.84

meters with a bias of 0.09 meters. The model slightly underestimated the wave height at this deep-water observation location.

Figure 8-7 presents the calibration results compared to observations at NOAA buoy 44005. Again, the overall trends in wave height are well identified during the entire time period. The generation-scale model does have some difficulty resolving lower wave energies, corresponding to low wind time periods. During relatively calm time periods (i.e., wave heights less than 0.5 meters), the wave model appears unable to dissipate enough energy to reach these calm conditions. Therefore, the model overestimates the wave heights (negative bias) at the observation station in shallower water. This overestimate is considered conservative and is preferred over an underestimate in wave energy. The computed RMS error between modeled and measured wave height was 0.68 meters with a bias of -0.32 meters.

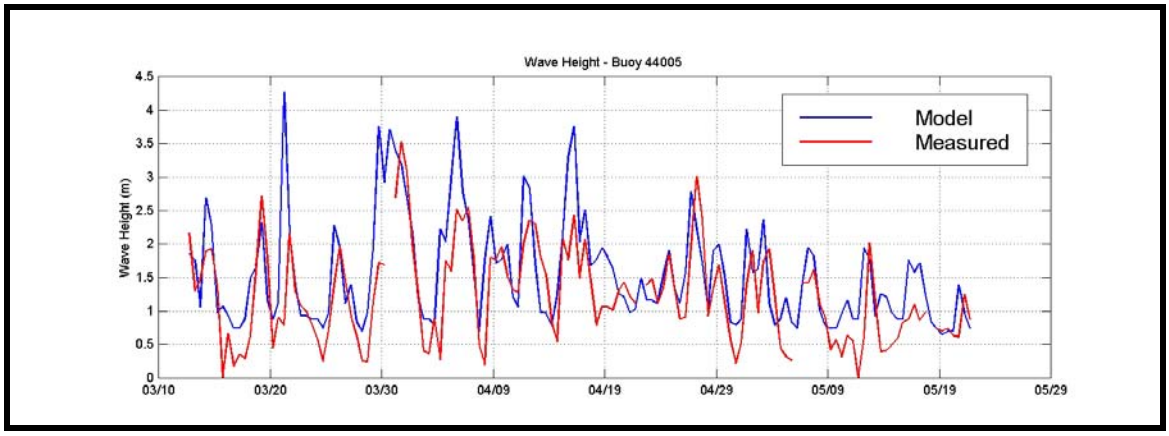

Figure 8-7. Comparison of modeled and measured wave height at NOAA Buoy 44005.

Figure 8-8 presents the calibration results compared to observations at NOAA buoy 44007. Again, at this most shallow observation station, the overall trends in wave height are well identified during the entire time period. At this site, as at buoy 44005, the generation-scale model has difficulty resolving lower wave energies, corresponding to low wind time periods. During relatively calm time periods (i.e., wave heights less than 0.5 meters), the wave model appears unable to dissipate enough energy to reach these calm conditions. Therefore, the model overestimates the wave heights (negative bias) at the observation station in shallower water. Again, this overestimate is considered more desirable than an underestimate in wave energy. The computed RMS error between modeled and measured wave height was 0.62 meters with a bias of -0.24 meters. Table 8-2 presents a summary of the error statistics (bias and RMS error) for the generation-scale wave modeling simulations based on the NOAA buoys. Although the errors appear larger than may be acceptable at the nearshore, high-resolution level (Chapters 9.0 and 11.0) at this coarse temporal and spatial scale the more important benchmark is the correct identification of trends and storm passage in the time series record.

Table 8-2. WAVAD wave height model errors based on NOAA Buoys.

NOAA Buoy	Bias (m)	RMS Error (m)
44011	0.09	0.84
44005	-0.32	0.68
44007	-0.24	0.62

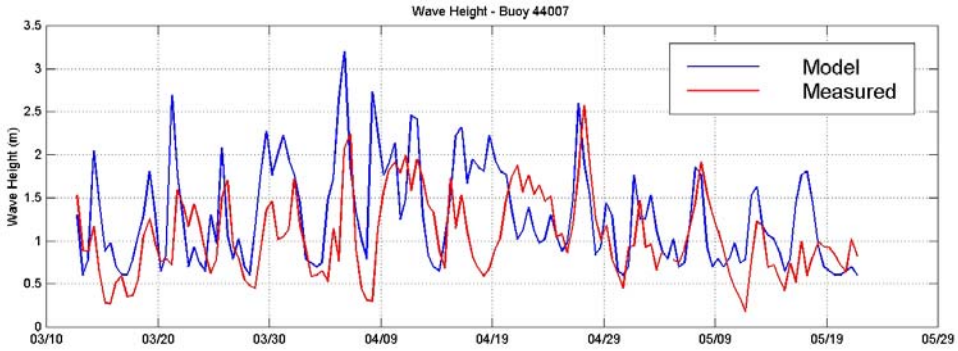

Figure 8-8. Comparison of modeled and measured wave height at NOAA Buoy 44007.

8.5.2 Significant Wave Events

In addition to the overall comparison of waves during the entire deployment time period, two distinct higher energy wave events were evaluated to determine the efficacy of WAVAD in determining wave height and spectra evolution during potential storm events. The time period corresponding to the passage of a storm was extracted from the nested WAVAD output record and compared to the NOAA buoy record. The first time period evaluated as a separate event was from 0000 hours on April 01 until 2300 hours on April 8. Figure 8-9 presents the details on the passage of this event. Four plot panels are represented in the figure. The top two panels present the modeled and measured wave height record at NOAA Buoy 44005 and Buoy 44007 (the buoys located closer to shore) during the specific time period of the event passage. The two bottom panels illustrate two different representations of the modeled frequency spectrum. The plot on the bottom left is the 1D frequency spectra corresponding to the maximum wave height within the event from the model. Wave energy is presented along the y-axis, and the frequency is presented along the x-axis. The plot on the bottom right is a time series of the 1D frequency spectra to show the passage of a storm. The frequency distribution is shown along the y-axis, time along the x-axis, and wave energy is presented as the color mapping. These bottom panels represent data extracted from the location within the generation scale model that corresponds to the edge of the nearshore wave transformation grid (Chapter 9.0).

Both of the modeled buoy locations indicate reasonable and acceptable agreement with the maximum wave height as recorded at the respective NOAA buoys. However, there is a slight difference in the time at which the storm peak occurs. The difference in the peak of the wave event (or the time offset) that occurs between the modeled and measured ware data is likely due to:

1. the inability to resolve the input wind conditions at temporal resolution greater than 12 hours. Satellite wind data are available only during an ascending and descending pass each day. This provides a limited temporal data set that may result in hourly shifts in the response of the model.
2. the time offset associated with the satellite's ascending and descending passes. The ascending pass occurs at 6:00 AM (local standard time of equator crossing), while the descending pass occurs at 6:00 PM (local standard time of equator crossing). The equatorial crossing local time also may result in hourly shifts.

However, based on the shape of the modeled and measured events, the model does represent wave growth and decay at the correct rates and correctly predicting the energy was important. The time series showing the passage of the event indicates that an energetic event is capable of pushing energy into lower frequencies as the event intensity increases. This movement of energy, from higher to lower frequencies, is a good indication that the model is representing spectral development and wave height increases (growth) correctly.

A second time period was evaluated, for another independent event, from 0000 hours on April 24 until 2300 hours on April 29 (Figure 8-10). Again, the figure shows the passage of the higher energy event and is a reasonable representation of the wave heights. In this case, the wave height is slightly under-predicted at the more offshore location (44005), but the model accurately represents the peak wave height at the nearshore location (44007).

8.6 Summary

Because of the lack of temporal and spatial similitude between locally observed wave information and available wave data sources, a generation-scale wave model was required to develop input into the detailed, shallow-water transformation-scale (regional) wave model. The generation-scale model is part of an extensive wave modeling system used to analyze the potential impacts of alternatives to mitigate erosion due to federally constructed and maintained navigational structures in Saco, ME. The generation-scale numerical model used satellite observed wind fields as input and was calibrated and verified using local point wave observations. A nested grid of water depths was used to define the model domain. The calibration between the measured and modeled wave heights was visually successful and quantifiable error statistics were within acceptable bounds for this scale of modeling. In addition, assessment of specific high-energy storms during the deployment time period indicated energy transfer across frequency bands during the passage of an event. Subsequently, spectral wave data were extracted from the generation-scale model at the location coinciding with the offshore boundary of the

regional wave model (Chapter 9.0) for the entire deployment time period. This spectral information was only used as input conditions for validation of the regional-scale modeling effort. Additional wave data sources (e.g., WIS Data) were used to simulate long-term wave impacts on the Camp Ellis shoreline.

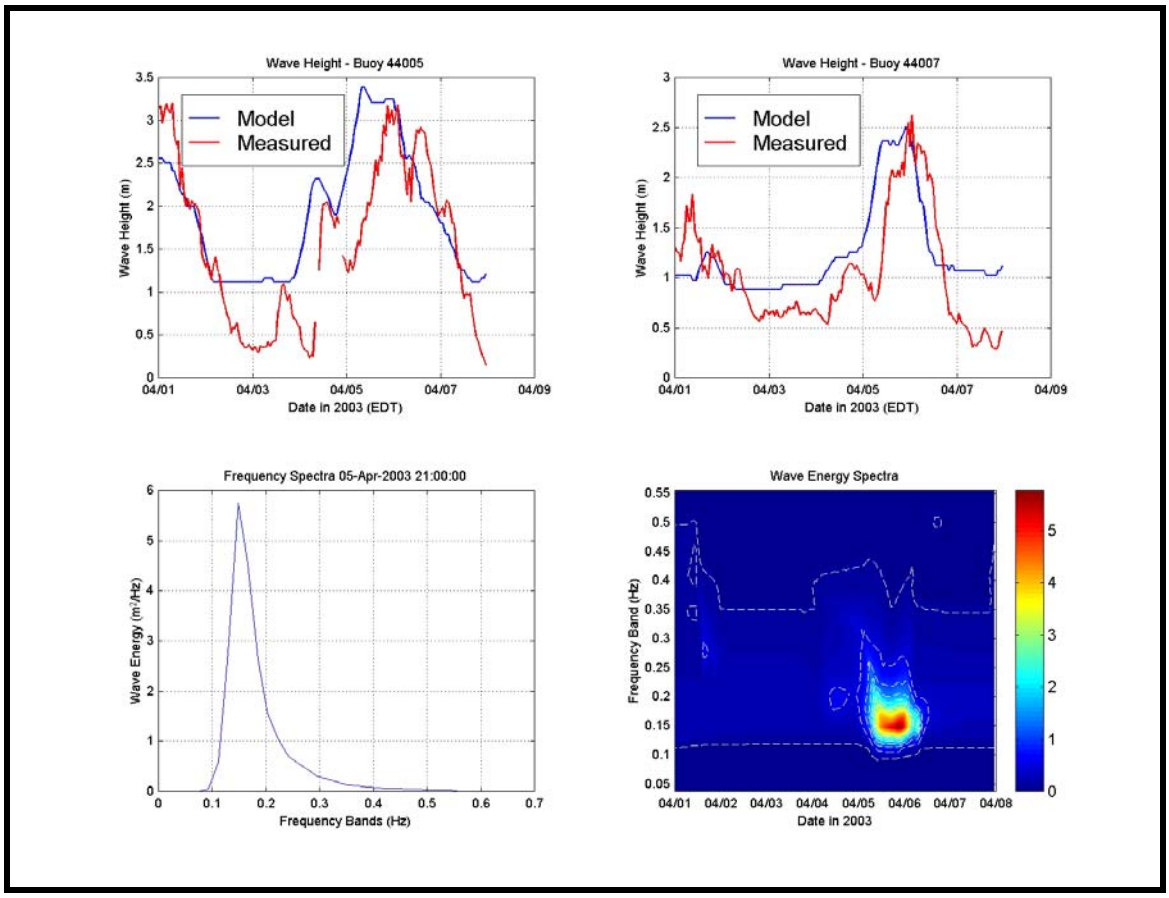

Figure 8-9. Evaluation of a higher energy event spanning April 01, 2003 – April 08, 2003, comparing modeled and measured wave heights and wave energy spectra. Upper left panel shows panel model versus buoy 44005; upper right panel shows model versus buoy 44007; lower left panel shows peak modeled wave spectrum; lower right panel show time series wave energy spectra.

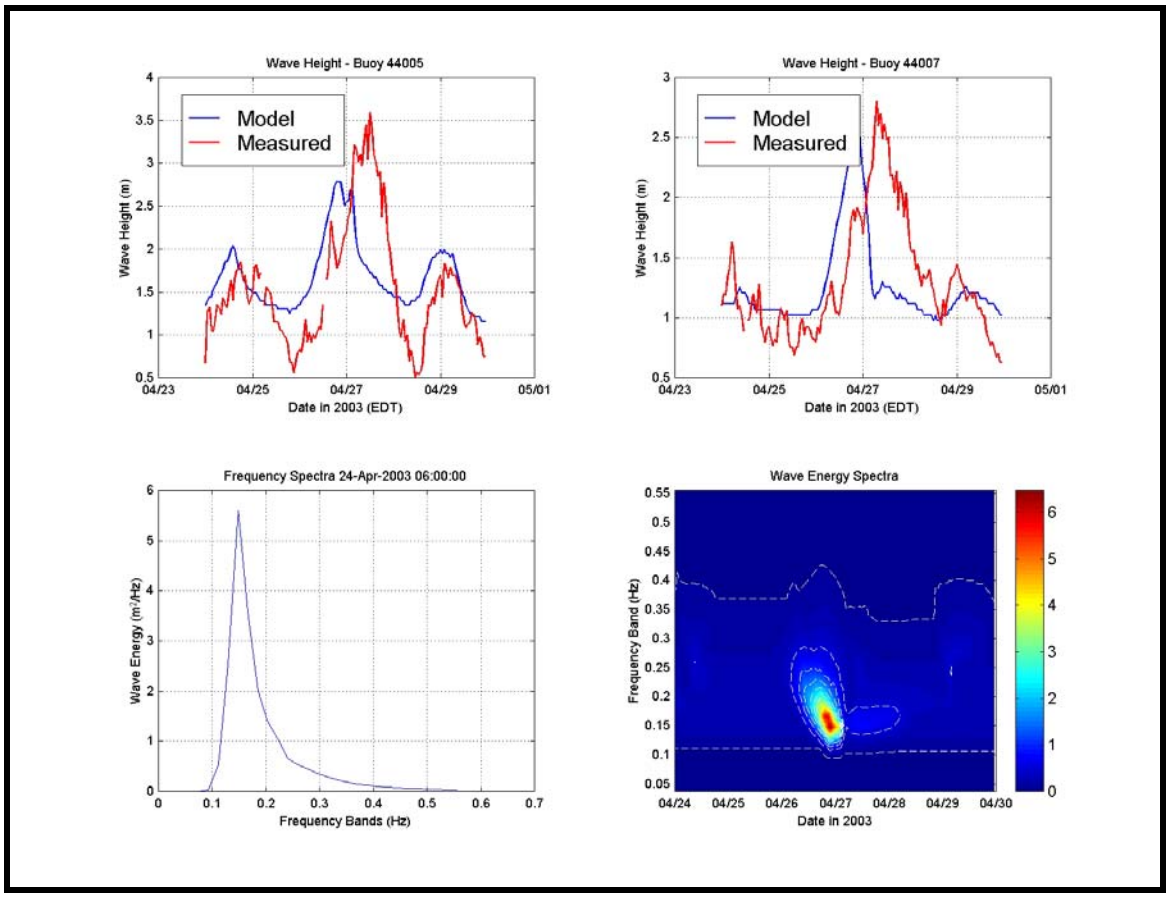

Figure 8-10. Evaluation of a high-energy event spanning April 24, 2003 – April 29, 2003, comparing modeled and measured wave heights and wave energy spectra. Upper left panel shows panel model versus buoy 44005; upper right panel shows model versus buoy 44007; lower left panel shows peak modeled wave spectrum; lower right panel show time series wave energy spectra.

9.0 REGIONAL WAVE MODELING (TASK 5)

The offshore wave climate during the time of the deployment was determined in Chapter 8.0. The offshore wave climate is also known for historical time periods from other data sources (e.g., buoys, wave hindcasting, etc.) However, in order to evaluate local sediment transport pathways, as well as to assess impacts and identify potential alternatives to mitigate the erosion at Camp Ellis Beach, an understanding of the regional wave climate is required. The Camp Ellis Beach region represents a complex coastal setting. The offshore bathymetry, nearby islands, tidal shoals, and crenulate-shape of Saco Bay all influence wave heights and directions in the vicinity of Camp Ellis Beach and the Saco River Jetties. Therefore, before an effective solution can be determined, wave modeling is required to simulate refraction, diffraction, shoaling and breaking of waves at the regional level. Both refraction and diffraction have a significant impact on the effects waves will have on the shoreline. Wave refraction and diffraction produce an uneven distribution of wave energy along the coast and affect sediment transport in the region. Wave modeling allows for quantitative predictions of these processes.

A detailed description of the procedures used to compute the wave conditions within Saco Bay is presented in this chapter. Specifically, this chapter presents the transformation-scale (regional) component of the modeling system. This includes:

- the analysis approach and description of the wave model applied to simulate waves at this scale,
- the generation of the bathymetric grid,
- the development of all the wave input conditions, including the validation time period, the average annual approach cases, and the high-energy events,
- the validation of the model (compared to observations) over the entire observation period,
- and a discussion of the transformation-scale (regional) wave modeling results.

9.1 Analysis Approach

A quantitative understanding of wave characteristics is key to evaluation of nearshore coastal processes and sediment transport. Ocean wave energy is comprised of a large variety of waves moving in different directions and with different frequencies, phases, and heights. These waves undergo significant modifications as they advance into the coastal region, interact with the sea floor, and eventually reach land. The ocean climate also changes temporally with seasonal modulations. The variability in offshore wave climate, the transformations occurring as waves propagate landward, and the temporal modulations, all result in significant fluctuations in the quantity and direction of sediment transport in the coastal zone.

This section evaluates the transformations waves experience as they propagate towards the coastline. To quantify the wave impact along the Saco Bay shorelines, site-specific wave conditions were determined over longer time scales to evaluate both typical and storm conditions. Regional wave transformation models provide predictive tools for evaluating various forces governing wave climate and sediment transport processes. For example, wave refraction and diffraction may have a significant effect on the impacts waves have on a shoreline. Wave refraction and diffraction generally result in an uneven distribution of wave energy along the cost that affects sediment transport in the region. Wave modeling results provide information on wave propagation across the continental shelf and to the shoreline, revealing areas of increased erosion ("hot spots") or areas of increased energy. The refraction and diffraction mechanisms also result in changes in the offshore wave direction that may significantly influence the rate and direction of sand movement. Therefore, the quantitative information provided from the numerical model(s) can be used to explain the physical processes that dominate a region, provide the required input into higher resolution models, and to potentially furnish appropriate recommendations/solutions for each stretch of coast.

A spectral wave model was used to propagate random waves from offshore to the nearshore region and investigate potential changes to the wave field caused by the bathymetry. So while the generation-scale wave model was used to develop the offshore wave climate for the time period when nearshore wave conditions were observed, the transformation-scale (regional) wave model was used to propagate and transform waves into the Saco Bay region for the wave observation time period and longer-term average conditions and storm events. Subsequently, results from the transformation-scale (regional) model are used to drive the nearshore models (Chapters 11.0), which is used to directly evaluate the nature of the waves specifically in the Camp Ellis region.

9.2 Wave Model Description

The spectral wave model STWAVE version 3.0 (Smith, Sherlock, and Resio, 2001), developed by the U.S. Army Corps of Engineers Waterways Experiment Station, was employed to evaluate changes in wave propagation across the nearshore region fronting Saco beaches. STWAVE is a steady state, spectral wave transformation model, based on a form of the wave action balance equation of Jonsson (1990).

$$(C_{ga})_i \frac{\partial}{\partial x_i} \frac{C_a C_{ga} \cos(\mu - \alpha) E(\omega_a, \alpha)}{\omega_r} = \sum \frac{S}{\omega_r} \quad \text{.....(9-1)}$$

where

i = x,y spatial coordinates

C_a = absolute wave celerity

C_{ga} = absolute wave group celerity

μ = current direction

α = propagation direction of spectral component

E = spectral energy density

f = frequency of spectral component

ω_r = relative angular frequency (frequency relative to current or a reference frame to the current)

S = energy source/sink terms

Source and sink terms include wind input, non-linear wave-wave interactions, dissipation in the wind field, and surf-zone breaking. The model can simulate wave refraction and shoaling induced by changes in bathymetry and by wave interactions with currents. The model also includes wave breaking, wave growth, and influences of wave white capping on the distribution and dissipation of energy in the wave spectrum. Model outputs include zero-moment wave height, peak wave period, and mean wave direction at all grid points and two-dimensional spectra at selected grid points.

STWAVE simulates the behavior of a random sea surface by describing wave energy density as a function of direction (directional spectrum) and frequency (frequency spectrum). The two-dimensional wave spectrum is discretized into separate wave components, which constitute an essential part of the input for STWAVE. Through a combination of the various wave directions and frequencies, STWAVE is able to simulate the behavior of a natural, random sea. In addition, detailed analysis and selection of input spectrum allows the model to assess the impact of different seasonal conditions, varying wave approach pathways, and storms. By simulating numerous wave components that propagate towards the Saco Bay shoreline, a spectral wave model is superior to a monochromatic wave model, which would include only one specific wave. A comprehensive discussion of the theoretical background of STWAVE, including model assumptions and limitations, can be found in Smith, Sherlock, and Resio (2001).

Using the generation-scale wave modeling results for validation and existing wave data offshore of Saco Bay for developing appropriate offshore wave conditions, input data was generated to specify the wave boundary conditions. Then, using local bathymetry to create an accurate grid, the model was able to propagate waves within the Saco Bay region.

9.3 Bathymetry and Grid Generation

The transformation-scale (regional) modeling used digital bathymetry from the National Ocean Service (NOS), combined with 1-m LIDAR data, and a high-resolution nearshore bathymetric survey conducted near the mouth of the Saco River on May 13 and 15, 2003 (Chapter 4.0). Existing National Oceanographic and Atmospheric Administration (NOAA) data were obtained from the National Ocean Service (NOS) Office of Coast Survey Hydrographic Survey Geophysical Data System (GEODAS). The GEODAS data can readily be obtained online at http://www.ngdc.noaa.gov/mgg/bathymetry/hydro.html. These bathymetric surveys were combined to define the region offshore of Saco Bay.

The compilation of these surveys was used to provide data for grid creation in the offshore regions. In cases where there were duplicate data points, the most recent data were used. The nearshore and areas adjacent to Camp Ellis Beach and the Saco River used data from the recent bathymetric survey (Chapter 4.0).

In STWAVE, the reference grid consists of a mesh of points with dimensions NI and NJ, as shown in Figure 9-1. At each point within the domain, water depth, as well as ambient current data, can be specified. Reference points are separated by spacing DX (x-direction) and DY (y-direction). The orientation of the reference grid, especially the offshore boundary, was selected to closely represent a shore parallel contour line at a water depth deep enough that waves would not sense the sea floor, and align with the location of the offshore wave information. The reference grid was rotated to be oriented perpendicular to the shoreline, such that a comprehensive range of directional approaches could be simulated. STWAVE is a half plane model (directional approaches relative in a 180 degree half plane). Therefore, rotation of the grid allowed for simulation of all wave approach directions for the Saco Bay shoreline (waves arriving from 30 to 210 degrees relative to true North).

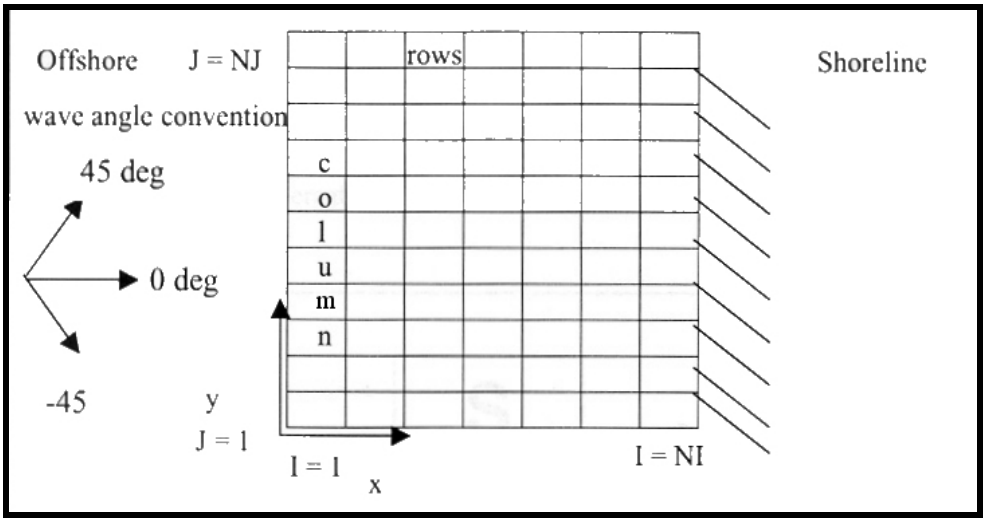

Figure 9-1. Illustration of reference grid notation (Smith, Sherlock, and Resio, 2001).

The model domain consists of one reference grid covering the entire region of Saco Bay. The bathymetric grid is rotated to create an x-axis perpendicular to the shoreline (waves from 120 degrees are parallel to the x-axis) and extends from the shoreline to an offshore node of the WAVAD generation-scale model and WIS Station 99 (for annual average simulations). This offshore boundary corresponded to an approximate depth of 35 to 40 m (115 to 131 ft). The STWAVE grid consists of 290 cells across the shore and 347 cells along the shore with a resolution of 30.5 m (100 ft). Figure 9-2 shows the location and geometry of the reference grid.

9.4 Wave Characteristics and Input Spectra (Task 4)

Transformation wave modeling can only be as accurate as the input data; therefore, a key component of accurate wave modeling is the analysis and selection of input wave data. The results derived from numerical wave transformation modeling, as well as the subsequent movement of sediment in the coastal zone, are controlled by the selected wave input conditions and the transformation to the wave field that occurs over the bathymetric surface. This section evaluates the wave climate offshore of Camp Ellis Beach and describes the selection of input wave parameters for the wave transformation modeling. This includes the assessment of average annual conditions, specific historic storm events, and return-period storms. The data and methodology utilized to develop the wave climate is presented herein.

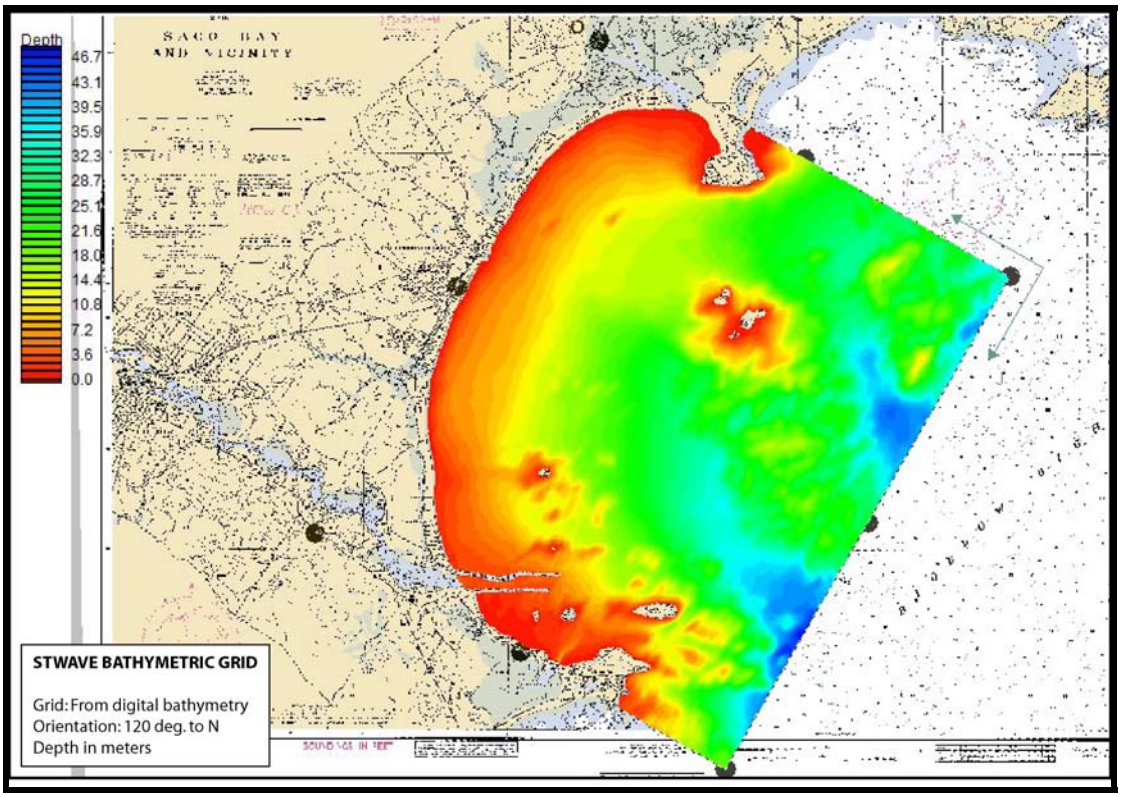

Figure 9-2. Bathymetric grid used for the STWAVE modeling. Depths shown in meters relative to Mean Tide Level (MTL).

9.4.1 Wave Data Analysis and Sources

Long-term time series of wave climate are not available for most shorelines, and although there have been some short-term observations of waves and currents in the nearshore regions (e.g., Heinze, 2001, Chapter 2.0), there are no direct *in situ* measurements offshore of Camp Ellis Beach that record fully directional wave data. Figure 9-3 presents the location of the existing wave data sources in the vicinity of Saco Bay. These data sources include: U.S. Army Corps of Engineers (USACE) Wave Information Study

(WIS) time series of wave data and wind data, National Oceanographic and Atmospheric Administration (NOAA) wave buoys and Gulf of Maine Ocean Observing System (GoMOOS).

Table 9-1 shows the data availability and location of the relevant wave observations from the NOAA and GoMOOS sources. Both these data sources (NOAA and GoMOOS) consist of non-directional wave information, while the GoMOOS system also includes several other parameters (e.g., salinity, temperature, dissolved oxygen, etc.). The benefit of using the NOAA, GoMOOS, or other observed data to describe the offshore wave climate and develop transformation level input conditions is that it is measured rather than predicted (hindcasted). However, because buoys and/or pressure sensors are collecting actual observations, the instruments are subject to severe weather and mechanical problems, and therefore, a consistent long-term wave record is more difficult to attain. In this particular case, the observed data are also limited by the lack of a directional component. Due to the critical nature of the wave direction in the assessment of the Saco Bay region, this data gap made it difficult to use these observations for anything more than ancillary or comparative data (as discussed in Chapter 8.0).

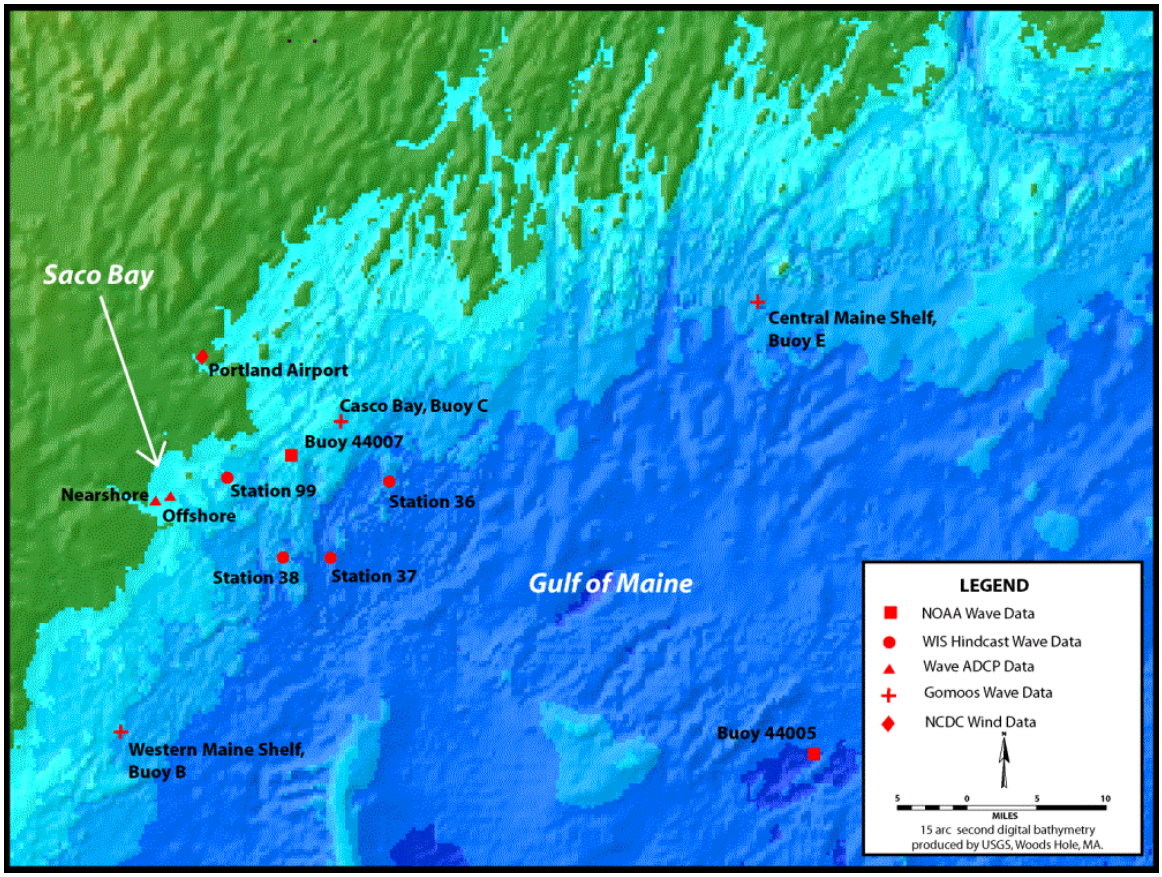

Figure 9-3. Location of existing wave observations and hindcast positions within the Gulf of Maine. The two triangle markers in the nearshore region represent the wave data collected for this study.

Table 9-1. Location and relevant inventory of existing wave observation stations within the vicinity of Saco Bay.

Station ID	Location (St. Pl. NAD27)	Deployment Time*	Wave Height	Wave Period	Wave Direction
NOAA 44007	253917.14N, 507073.29E	1982-present	X	X	O
GoMOOS Buoy C	268313.25N, 529596.90E	2001-present	X	X	O
X = collected; **O** = not collected; *=includes intermittent time gaps					

Due to the directional limitations of the existing buoy information, the Wave Information Study (WIS) time series of wave data and wind data was used to describe the wave climate offshore the Saco Bay region. WIS, performed by the U.S. Army Corps of Engineers (USACE), has met a critical need for wave information in coastal engineering studies since the 1980s and is widely accepted for design purposes for United States shorelines by many coastal engineers and scientists. WIS contains time series information of spectrally-based, significant wave height, peak period, peak direction, and wind speed and direction produced from a computer hindcast (prediction) model. The hindcast wave model, WISWAVE (Resio and Tracy, 1983) is run using wind information (speed and direction) at selected coastal locations around the United States. The model predicts wave climate based on local/regional wind conditions. Wave measurements made by NOAA during the 1980s made verification of the WIS results possible by comparing the statistics and the distributions of wave heights and periods from different time periods (Hubertz et al., 1993). The availability of long-term records makes WIS data attractive when considering average or seasonal wave conditions. Since the data are widespread and continuous, adoption of the generally accepted WIS data for development of spectral wave conditions is applicable. Previous studies and design projects have used WIS data as an accurate measure of wave climate and input to nearshore wave transformation models (Kraus et al., 1988, Byrnes et al., 1999, Byrnes et al. 2000). Although direct, *in situ* measurements might show some difference in detail, the WIS data set provides an accepted and widely used long-term wave data set.

WIS information was originally calculated by hindcasting deepwater waves from historical surface pressure and wind data (Brooks and Corson, 1984). This Phase I-type model used large-scale atmospheric conditions, a large grid size (hundreds of kilometers), and only one type of wave process, air-sea interaction. Phase I results do not include such effects as shoaling, bottom friction, or long waves. Although simplifications are present in Phase I-type modeling, it still provides adequate approximations of time-series results. Improvements have been made through subsequent modeling efforts to increase the accuracy of WIS relative to NOAA measurements. Phase II-type WIS data, which include the effects of shoaling, refraction, diffraction, and bottom friction, were used in the present study. The Phase II WIS data provide wave parameter results every three hours, for a twenty-year time period.

A recent reanalysis of the WIS data using an advanced version of WISWAVE has provided additional WIS data for specific locations on the U.S. coast. This reanalysis effort used more accurate and more highly resolved input winds and better representation of shallow water topographic effects and sheltering by landforms to create more highly resolved model domains. Advancements in weather modeling, increased availability of measured wind data (from buoys and satellites), and improved methods for integrating measured data with model-generated wind fields allowed for significant improvements in the quality of wind input used in this hindcasting. This new WIS data provide wave parameter results every hour and were also used in the current study. Details on the differences between the various Phases of USACE wave generation can be found on the Wave Information System (WIS) website (http://fef.usace.army.mil/wis/wis_main.html). Figure 9-3 presents the location of the WIS stations evaluated for this study, near the offshore boundary of the transformation-scale (regional) modeling domain. Table 9-2 presents a summary of the relevant wave stations. The most recent WIS simulations (Phase II-type and Phase III-type) were used for this study. WIS stations 36 and 37 are located too far offshore to be used for the transformation-scale (regional) wave modeling effort.

Table 9-2. Summary of relevant WIS stations in the modeling domain.

WIS Station	Au2099 (99)	38
Phase	Phase-II	Phase-III
ME State Plane (NAD27) Northing (ft)	242992.25	212455.09
ME State Pane (NAD27) Easting (ft)	477889.15	499901.8
Depth (ft)	59 (18 m)	207 (63 m)
Time Period (yrs)	1976 to 1995	1980 to 1999

Whereas the generation-scale wave modeling presented in Chapter 8.0 provides the wave climate during the time of the instrument deployment, the WIS data sets offers a long-term synopsis of the wave climate offshore of Saco Bay. An examination of the local WIS stations provides details on the wave climate, leads to the development of appropriate input spectra, and identifies the variability in wave approach and the potential impacts on sediment movement. Figures 9-4 and 9-5 present the distribution of significant wave height (illustrated using a wave rose plot) for WIS station Au2099 (99) and 38, respectively. The grayscale colors indicate the magnitude of the wave height, the circular axis represents the direction of wave approach (coming from) relative to True North (0 degree), and the extending radial lines indicate percent occurrence within each magnitude and directional band. The primary clustering of wave directions tends to be propagating towards the shoreline from the east-southeast, with a less frequent, but larger energy component arriving from the northeast and south-southwest, likely due to northeasters and hurricanes, respectively.

The two WIS stations are in significantly different spatial locations and water depths (Figure 9-3). A comparison of the mean wave period distribution (Figure 9-6), the percent occurrence directional distribution (Figure 9-7), and the percent wave energy

directional distribution (Figure 9-8), illustrates the differences between the two data sets. Overall the two stations yield similar trends in wave period, wave occurrence, and wave energy. The energy distribution reveals a more significant component of energy in the peak wave direction, as well as in the northern approach bins predicted at station 99. The geographic location of WIS station 99, which is located in shallower water and closer to the shoreline, likely influences the wave data. It is likely that waves from the northeast and southwest are confined by the shoreline and energy is predominantly from the south and east approach bands. In addition, annual fluctuations in the wave climate also play a role in potential energy distribution differences, and the time period over which station was evaluated is different (1980-1999 for WIS 38, and 1976-1995 for WIS 99). Finally, there are also some potential differences in the Phase-II and Phase-III generation algorithms.

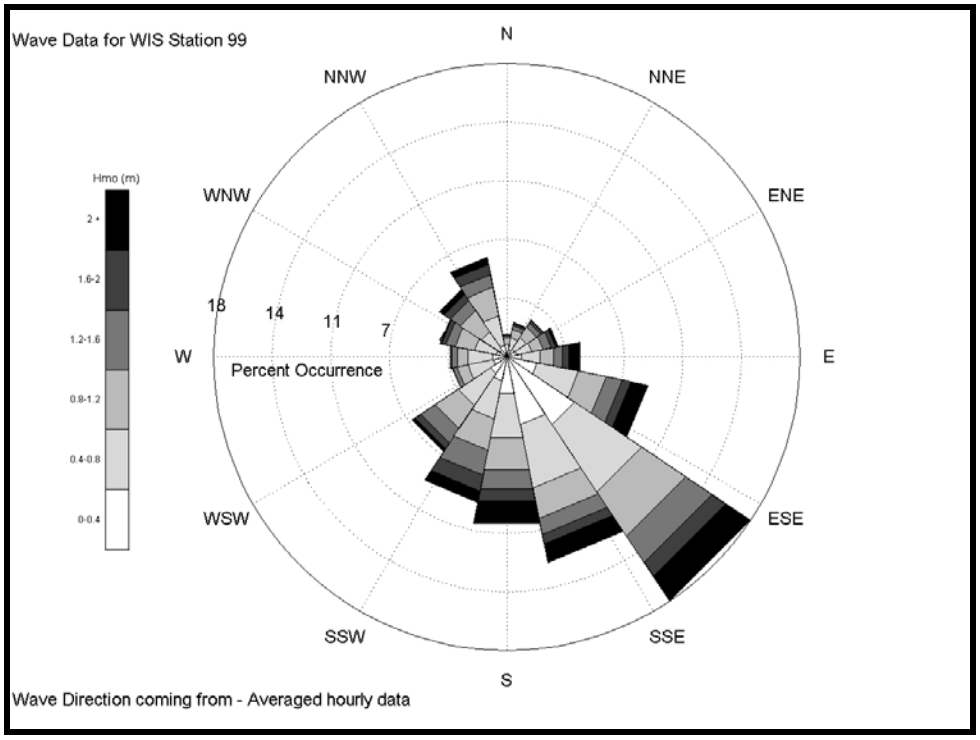

Figure 9-4. Twenty-year averaged wave rose for WIS Station 99.

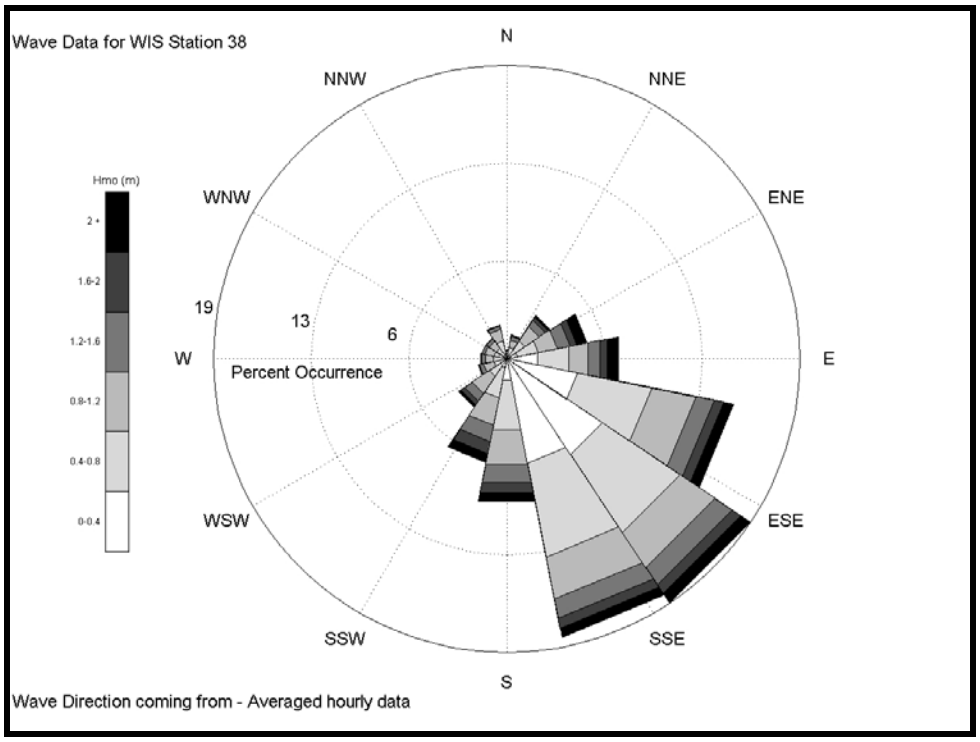

Figure 9-5. Ten-year averaged wave rose for WIS Station 38.

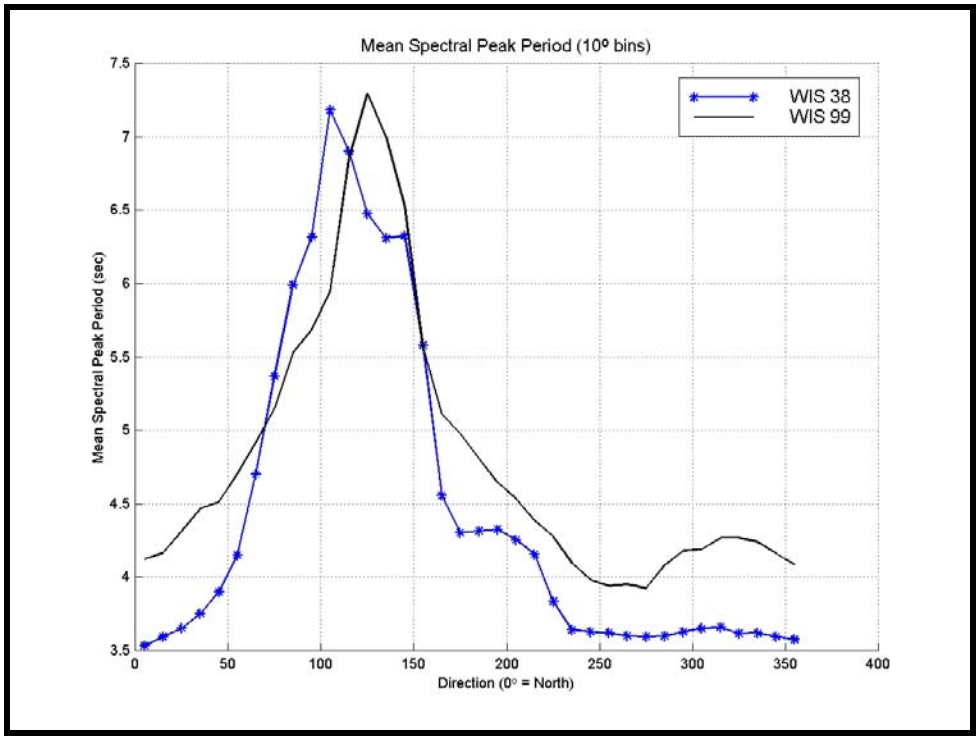

Figure 9-6. Directional distribution (wave directions propagating onshore in 10 degree bins) of mean wave period for WIS Stations 38 and 99.

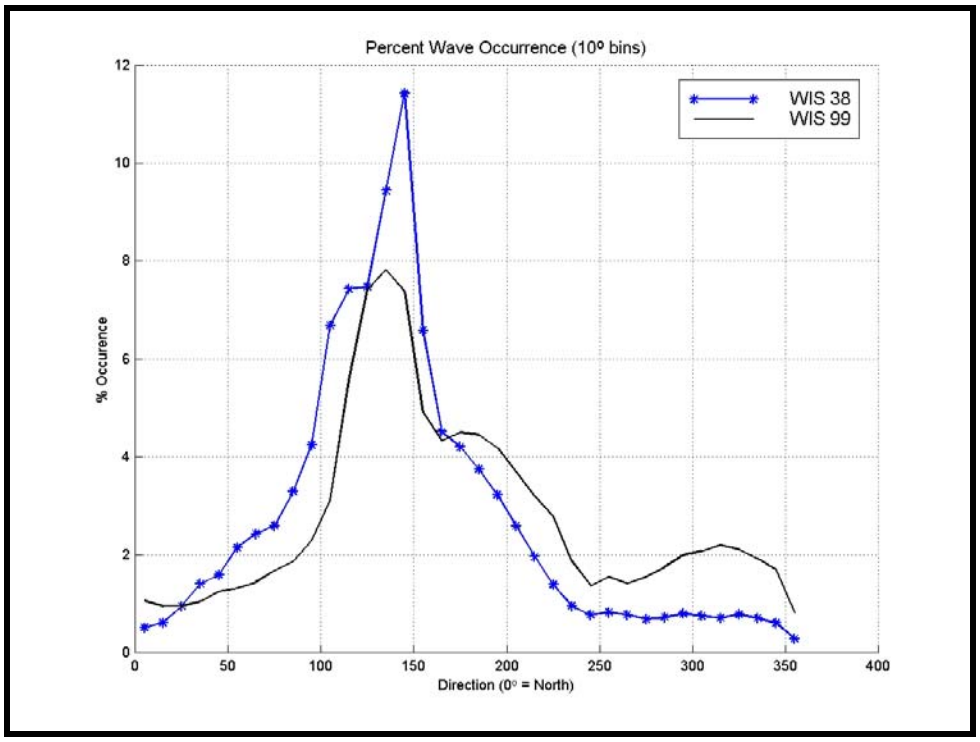

Figure 9-7. Directional distribution (wave directions propagating onshore in 10 degree bins) of percent wave occurrence for WIS Stations 38 and 99.

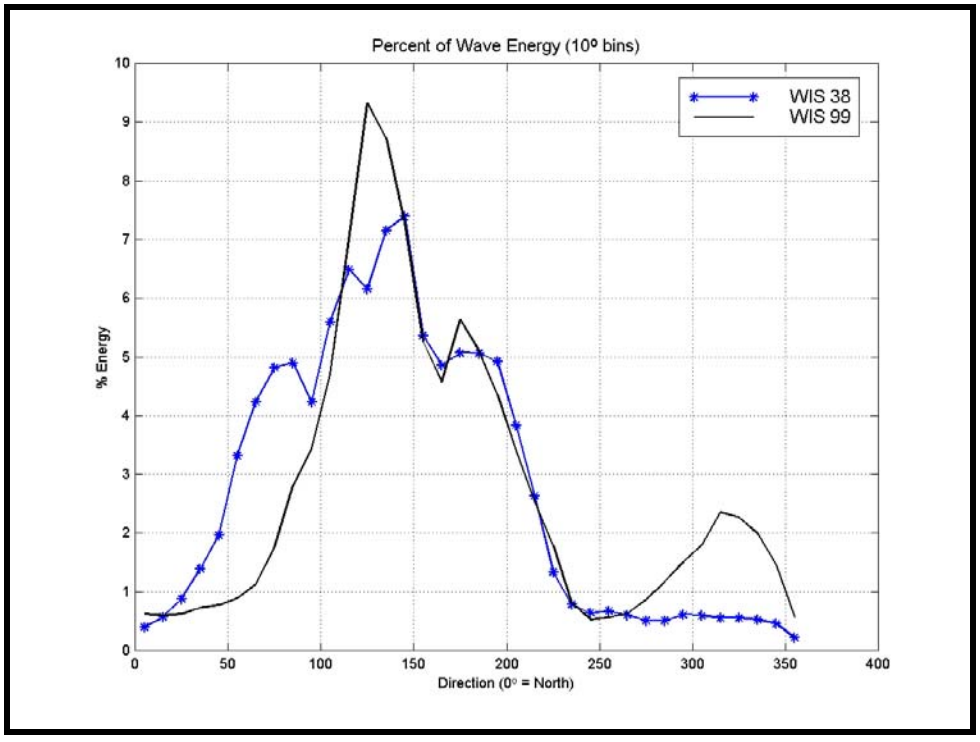

Figure 9-8. Directional distribution (wave directions propagating onshore in 10 degree bins) of percent wave energy for WIS Stations 38 and 99.

Figure 9-9 compares the basic percent occurrence and the percent energy across the directional distribution for WIS station 38. The percent occurrence distribution simply presents the percent of time waves come from each direction, while the percent energy presents the amount of energy coming from each direction. Although most of the waves arrive out of the east-southeast, the energy is more evenly distributed, due to the larger waves from the northeast and southwest directions. The asymmetry indicates the importance of evaluating all directional approaches as well as capturing all the energy associated with annual average wave conditions. Therefore, the longshore sediment transport clearly cannot be defined by one single wave value, but rather is a compilation of a wide variety of waves that drive sediment movement both in the northward and southward directions along the shoreline in Saco Bay. It is also likely that the wave field experiences significant changes as the waves advance towards the coastline from this offshore location. The results of the wave transformation-scale (regional) modeling will explore the changes that occur to the wave distribution as they propagate towards the coast, and specifically in the vicinity of Camp Ellis Beach. The transformation-scale (regional) wave modeling evaluates the propagation of these wave fields into the Saco Bay region.

WIS station 99 is a preferred choice for development of wave input conditions due to the proximity to the shoreline. Since the two WIS stations illustrated limited differences, Station 99, positioned near the offshore boundary of the model domain was used to develop annualized conditions.

9.4.2 Input Wave Conditions

STWAVE simulates the behavior of a random sea surface by describing wave energy density as a function of direction (directional spectrum) and frequency (frequency spectrum). The two-dimensional wave spectrum is discretized into separate wave components, which constitute an essential part of the input for STWAVE. The two-dimensional wave spectrum is given as the product of the energy and directional spectra. Through a combination of the various wave directions and frequencies, STWAVE is able to simulate the behavior of a natural, random sea. In addition, detailed analysis and selection of input spectrum allows the model to assess the impact of different seasonal conditions, varying wave approach pathways, and storms. Spectral results from calibration and verification of WAVAD were used directly as input into STWAVE for model validation purposes, while spectral data were used for representation of longer-term conditions. Bulk wave parameters (parametric methods) were not utilized to generate input conditions in either validation or in average annual wave condition simulations. Spectral conditions derived from parametric methods (e.g., TMA spectra, $\cos^n$ directional distribution) result in larger errors in calculation of peak period and wave direction (Smith and Gravens, 2003). Three distinct types of input conditions were supplied for the transformation-scale (regional) wave modeling:

Wave spectra results taken from the generation-scale wave modeling (Chapter 8.0) that were used for validation of the transformation-scale (regional) wave model during the time period when the nearshore wave systems (Chapter 7.0) were observing the conditions (deployment period).

Energy-conserving annual average directional spectrum developed from the 20 years of WIS data to simulate long-term average conditions.

Storm spectra for site-specific and return period storm events.

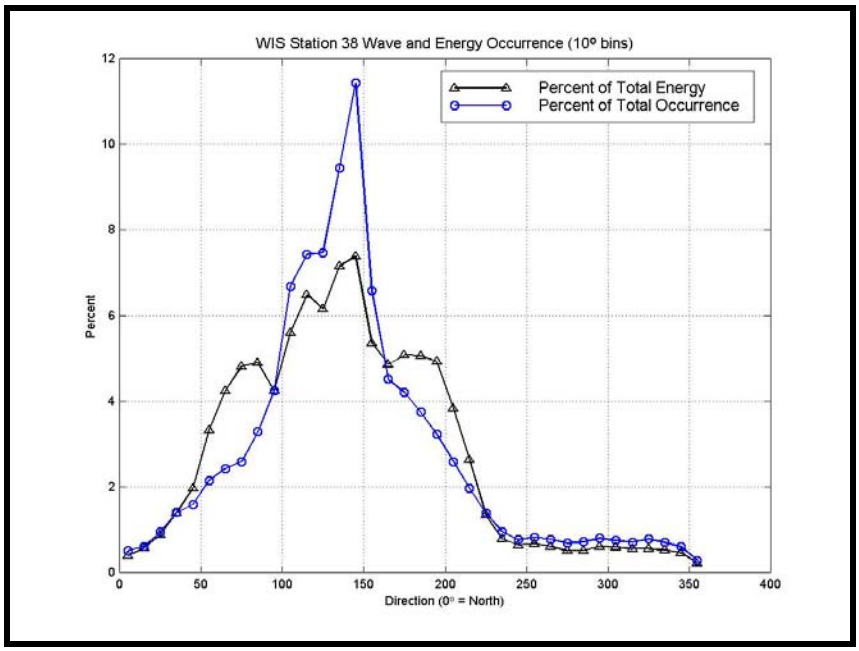

Figure 9-9. Comparison of percent occurrence and the percent energy across the directional distribution for WIS station 38.

9.4.2.1 Deployment Period

Prior to using the model to transform long-term wave climate information into the Saco Bay region, the transformation-scale (regional) model must be validated to ensure adequate performance of the transformation-scale (regional) model. Two-dimensional spectral output from WAVAD (generation-scale) (Chapter 8.0) was used directly as input into STWAVE for validation purposes. STWAVE was used to simulate the entire deployment (March-May 2003) time period (during which the waves were observed). Results of the model validation are presented in Section 9.5.

9.4.2.2 Average Annual Directional Approaches

In order to determine long-term wave conditions and for use in sediment transport calculations, spectral data from WIS station 99 were used to derive energy-conserving annual average directional spectrum. Data are segregated by direction of approach, and an energy distribution, as a function of frequency, is generated from all the waves in each directional bin. The energy associated with each frequency is then summed to create an energy distribution for each approach direction. In essence, a representative two-dimensional spectrum (direction and frequency) is generated for each approach directional bin based on the sum of all the WIS spectra approaching from that mean direction. This is combined with the percentage of occurrence to create a long-term (20 year) evaluation of wave impacts at the shoreline. This energetic directional bin

approach has been successfully utilized in the spectrum transformation modeling (Byrnes et al., 2000) and identifies all potential approach directions, including those that may occur only a small percentage of time during a typical year, but potentially have significant impacts on the shoreline and sediment transport (e.g., the higher wave energy approaches from the northeast).

Table 9-3 presents the directional bin scenarios for WIS station 99 that were simulated in STWAVE to represent the complete wave climate offshore of Saco Bay. The table presents the directional bin scenarios, including the percent occurrence and the percent of the total energy that is contained in each bin, as derived from the WIS data. In addition, STWAVE is a half-plane model, and therefore, only represents waves propagating towards the coast. Waves that may be reflected from the coastline or structures and waves that are generated by winds blowing offshore are not included. Waves headed offshore would represent a calm period along the coastline; therefore, waves propagating offshore were not modeled in the system, and were assimilated into the analysis as calm periods. By conserving energy through the frequency and directional distributions, wave height and direction is not directly input into the wave model. The frequency and directional energy spectra were tailored to match the energy distribution of each approach bin that occurred in the WIS data. Therefore, the directional and frequency distributions matched the data directly. Figure 9-10 presents two examples of the two dimensional spectra (frequency and direction) input generated from the WIS data for representation of annual directional bin conditions. The frequency spectra are presented in the left-hand panel, while the combined frequency-directional spectra are presented in the right-hand panel. The remaining spectra, and the matching to the WIS data, are presented in Appendix 9-A. Each of the directional bins presented in Table 9-3 were simulated in the wave transformation-scale (regional) model.

Table 9-3. Directional simulation cases for WIS station 99.

Directional Case	Directional Bin (0°= True North)	% Occurrence	% Wave Energy
NNE	30 to 55	2.70	2.16
NE	55 to 75	2.85	2.42
ENE	75 to 90	2.77	2.79
E	90 to 110	5.10	3.75
ESE	110 to 130	12.52	7.97
SE	130 to 150	16.69	13.19
SSE	150 to 165	8.79	15.45
S	165 to 185	9.24	8.76
SSW	185 to 210	10.71	10.42
Calm	Wave propagation offshore	27.87	--

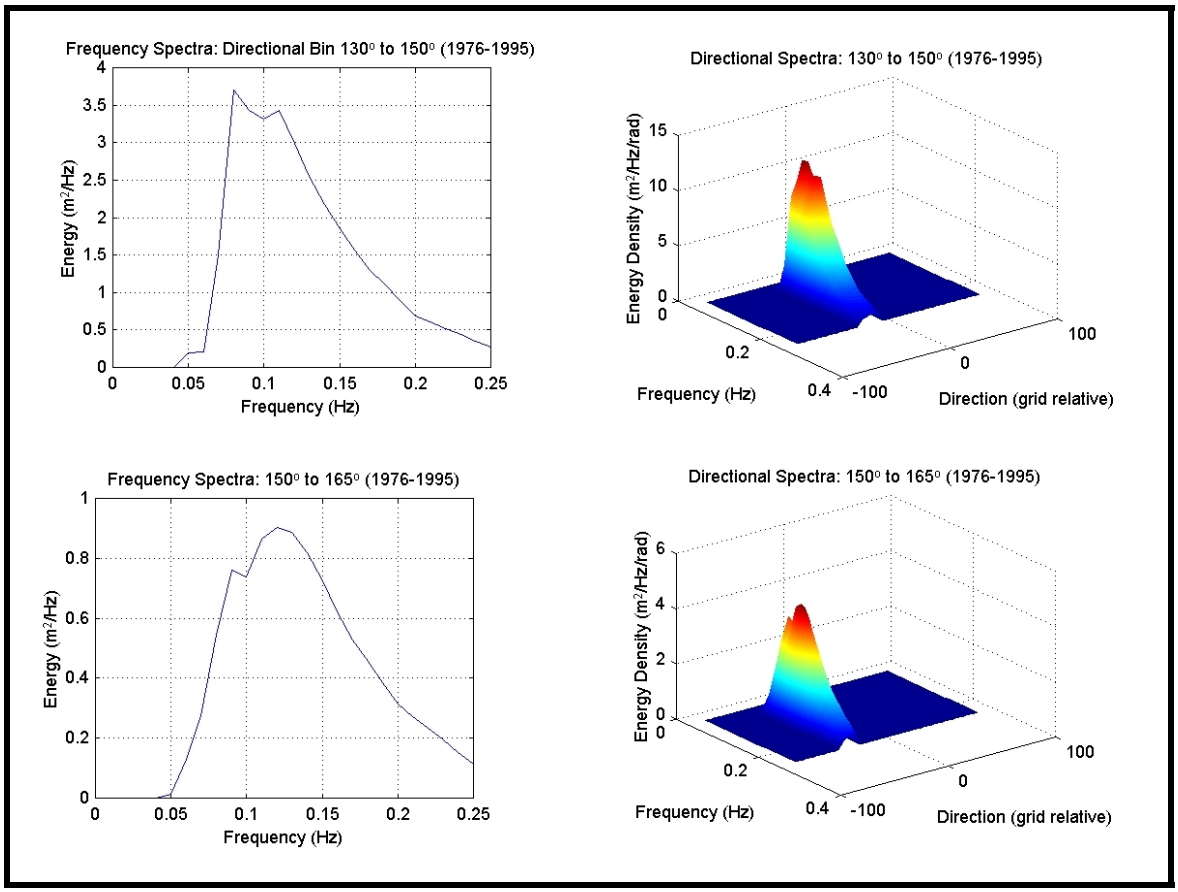

Figure 9-10. Examples of two-dimensional spectra input into STWAVE for annual average directional simulations. The upper two panels are for waves approaching from between 130 to 150 degrees, while the bottom two panels are for waves approaching from 150 to 165 degrees. The frequency spectra are presented in the left-hand panel, while the combined frequency-directional spectra are presented in the right-hand panel.

9.4.2.3 High Energy Events

Since high-energy events have a significant impact on many physical processes (and in most cases, dominate sediment transport), it is crucial to include storm simulations in wave modeling to assess the potential impact of a storm on the shoreline and the potential sediment transport within Saco Bay. WIS data used in this study include the effects of hurricanes and storms; however, the individual effect of an extreme event is represented as a separate model run to quantify the direct impact of a storm event. High energy events were evaluated by reviewing existing literature on hurricanes and northeast storms that affected the southern Maine coastline, investigating the storm tracks, finding the corresponding time period within the buoy and WIS data set and choosing a representative set of wave parameters for a model run.

Two distinct types of storms, northeasters and hurricanes, affect the study area. Northeasters, named after the predominant direction of the associated winds, are large-

scale, low pressure disturbances. Wind speeds associated with a northeast storm are generally less than those of a hurricane, although wind gusts can reach hurricane strength under severe conditions. In addition, northeast storms are typically longer in duration than hurricanes and can result in significant damage to the coastline. Hurricanes are a relatively rare occurrence along the Maine coastline. By the time a hurricane reaches the latitudes of the Maine coast it is typically either far out to sea or in a state of rapid decay. Despite their infrequent occurrence, hurricanes have the potential to produce devastating impacts along the coastline. To represent historical storm conditions in Saco Bay, one historical hurricane event and two historical northeaster storm events were modeled. Historical storm parameters (height, period, and direction) were based on historical data observations and records of storm events. Table 9-4 presents the specific storm events selected, and their associated parameters.

In addition, return-period storm events (10-year, 50-year and 100-year) were developed and simulated in STWAVE to provide varying levels of storm events expected to occur at this location. The return-period storm wave height was developed using the Generalized Extreme Value (GEV) method. This method provides reliable estimates of extremes without assuming the distribution type is known (Resio, 1989). The GEV method uses asymptotic methods to fit sampled maxima to the tail of a parent distribution, whose characteristics are estimated from the original sample. The original sample was taken from the WIS 99 station data set. Table 9-4 presents the wave heights estimated by GEV. The return period storms peak wave periods were estimated using the following relationship (CEM, 2002) for extreme wave parameters:

$$T_p = 12.1\sqrt{\frac{H_o}{g}} \quad \text{..... (9-2)}$$

where H_o is the wave height (in feet). Since the wave direction of extremal events is unknown for return-period storms, a wave direction of 60° (relative to North) was assumed. This direction was chosen to represent wave direction during a typical Northeaster event, and was based on analysis of the larger storm events found within the WIS data.

Storm surge values were also included in the wave modeling simulation to represent the increased water level experienced during the passage of a large storm event. Surge values reported by a variety of sources were used to determine the water level associated with these storm events. For return-period storms, storm surge data were taken from Tidal Flood Profile #11, Station 240, New England Coastline (USACE, 1988). For specific storm events, storm surge was determined from historical observations and published storm surge values for those specific events.

Table 9-4 presents the storm scenarios simulated. Storm spectra were developed from these storm parameters using standard parametric methods (e.g., TMA spectra, $\cos^n$ directional distribution), since the observed spectra during these events are unknown.

Table 9-4. Storm event simulations.

Storm Event	Hs (m)	Tp (sec)	Direction (degrees)	Storm Surge (m above MTL)
10-year	6.2 (20.3 ft)	14.4	60	2.4 (7.9 ft)
50-year	7.1 (23.3 ft)	15.4	60	2.6 (8.5 ft)
100-year	7.5 (24.6 ft)	15.9	60	2.7 (8.9 ft)
Perfect Storm (10/31/1991)	6.9 22.6 ft)	14.3	37	2.4 (7.9 ft)
Hurricane Bob (08/20/1991)	5.8 (19.0 ft)	11.1	-20	1.8 (5.9 ft)
Northeaster March 6-7,2001	5.6 18.4 ft)	11.1	50	2.4 2.9 ft)

9.4.3 Sea Level Rise

Another important consideration in the wave transformation simulations, as well as the long-term planning for Camp Ellis Beach, is potential sea-level rise. The potential impacts of sea-level rise present an additional natural hazard risk for developed areas within the coastal zone. The impacts are similar to those caused by shoreline erosion, and include increased flooding and wave activity in areas previously not affected, as the shoreline moves increasingly further inland.

Scientific research indicates that global (eustatic) sea level has risen approximately 6 to 8 inches (15 to 20 cm) over the last century (EPA, 2000). This eustatic rise in sea level has occurred in part due to glacial isostasy, warming of the world oceans, and melting of continental glaciers. Along most of the US coast, tide gage data show that local sea levels have been rising 2.5 to 3.0 mm/yr, or 10 to 12 inches over the past century. Because the tide gage stations measure sea level relative to the land, which includes changes in the elevations of both water levels and the land, tide gages measure relative sea level rise, and not the absolute change in sea level. Therefore, the rates of relative sea level rise have greater relevance to the evaluation of coastal hazards from sea level rise, than do changes in eustatic sea level.

While the topic of accelerated sea level rise is still heavily debated, the Intergovernmental Panel on Climate Change (IPCC) has undergone a considerable effort to analyze and review the current state of knowledge and provide an estimated range of predicted sea level rise into the next century. For Saco Beach, sea level rise estimates were evaluated from a number of sources, including NOAA and IPCC (2003) estimates. Model simulations were conducted at current sea levels, as well as for predicted sea level rise 50 years in the future. The model simulations were relatively insensitive to the use of various rates of sea level rise (i.e., the results were not impacted by changing the rate of sea level rise). Sea levels based on historical rates of measured sea level rise (NOAA), which provide a reasonable base estimate of sea level rise predictions, were used in all model simulations. At the time of this report, The USACE is currently in the process of developing guidance for incorporating sea-level change considerations in civil works programs; however, in lieu of this documentation, the known, observed sea level rise rate was used. At the time that this study was conducted (2003-2007), the USACE was in the process of developing guidance for incorporating sea-level change considerations in civil

works programs. Since this guidance was unavailable at that time, observed sea level rise was used.

Long-term tide gage data collected at the NOS (National Ocean Service) station in Portland, ME provide the closest measurements to Camp Ellis Beach. Rates of rise computed from the Portland data set spanning the period from 1912 to 2006 indicate a relative rise in sea level of 1.82 mm/year, or 7.2 inches over the past century. This rate of sea level rise (1.82 mm/yr) was included in all model simulations, including assessment of the alternative(s) performance. It is likely that sea level is accelerating; however, site-specific estimates of accelerated sea level rise, nor formal guidance on integrating rates into civil works projects, were available at the time of this work. As such, these estimates help determine potential impacts of rising sea levels on future conditions at Camp Ellis Beach. Ultimately, the range of potential sea level rise scenarios do not have a significant impact on the model results over the expected service life of the various alternatives (both structural and beach nourishment).

9.5 Model Validation

In order to validate the transformation-scale (regional) model, the full deployment time period was simulated using offshore wave data (every hour) generated from the generation-scale wave model, as discussed in Chapter 8.0. Wave model results were compared to the wave measurements from the two nearshore ADCP systems to verify the performance of the model. Figures 9-11 and 9-12 show comparisons of the modeled (green) and measured (black) wave heights at the offshore ADCP site and nearshore ADCP site, respectively. Each panel presents approximately ten days of data. Visually, the wave model compares favorably to the observations, and is able to accurately simulate specific wave height increases, as well as calm periods. For example, the large event around April 27th is accurately predicted, as is the beginning of the deployment in March (smaller waves). Therefore, the wave model does an adequate job of predicting the changes in the wave field due to the transformations from offshore to nearshore.

Figure 9-13 shows a comparison of the modeled (green) and measured (black) wave directions for the nearshore ADCP station. In general, the model predicts the correct directional approach; however, it is unable to rectify sharp changes in wave direction (events when the direction is directed offshore). Since STWAVE is a forward propagating model, if the wave direction was offshore it cannot be simulated by the model. However, periods when wave direction are headed onshore, the model does a reasonable job of predicting the wave direction. This was evident at both the nearshore and offshore ADCP stations. In addition, these differences (both in height and direction) may also develop since STWAVE cannot simulate some of the transformations (diffraction, reflection, etc.) that become important in the presence of coastal structures and nearshore islands. The time shifts and errors introduced in the generation-scale modeling may also transfer into differences in the transformation-scale (regional) wave model. Finally, differences during low-energy (small wave height) time periods add to the overall error, but are not important since when the wave energy is low, the model's performance is not as critical. These differences illustrate the need for a finer scale nearshore, local wave model to accurately predict the wave transformations in the

vicinity of Camp Ellis Beach that can adequately represent important physical processes such as wave diffraction and reflection that will occur in the vicinity of the Camp Ellis shoreline due to the coastal structures and local bathymetry.

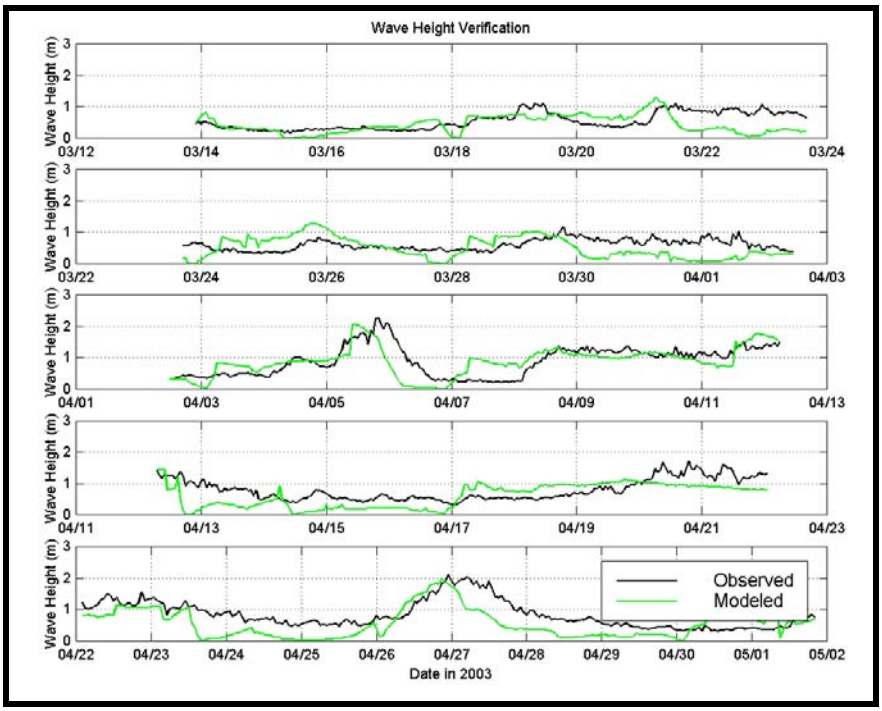

Figure 9-11. Comparison of observed (black line) and modeled (green line) wave height (m) for March (top panel) through April (bottom panel), 2003 at the Offshore ADCP station.

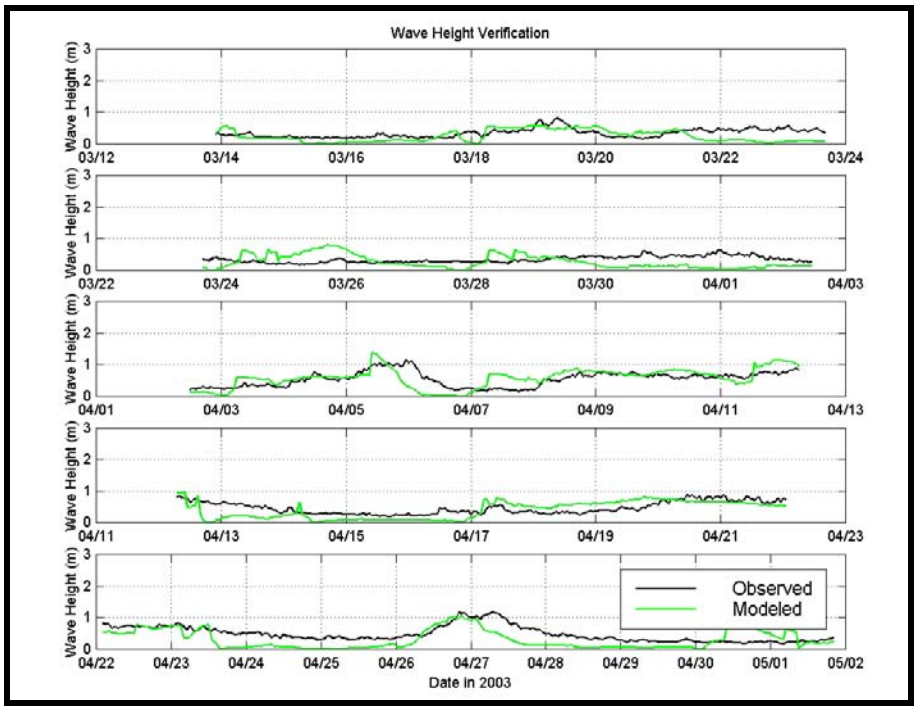

Figure 9-12. Comparison of observed (black line) and modeled (green line) wave height (m) for March (top panel) through April (bottom panel), 2003 at the Nearshore ADCP station.

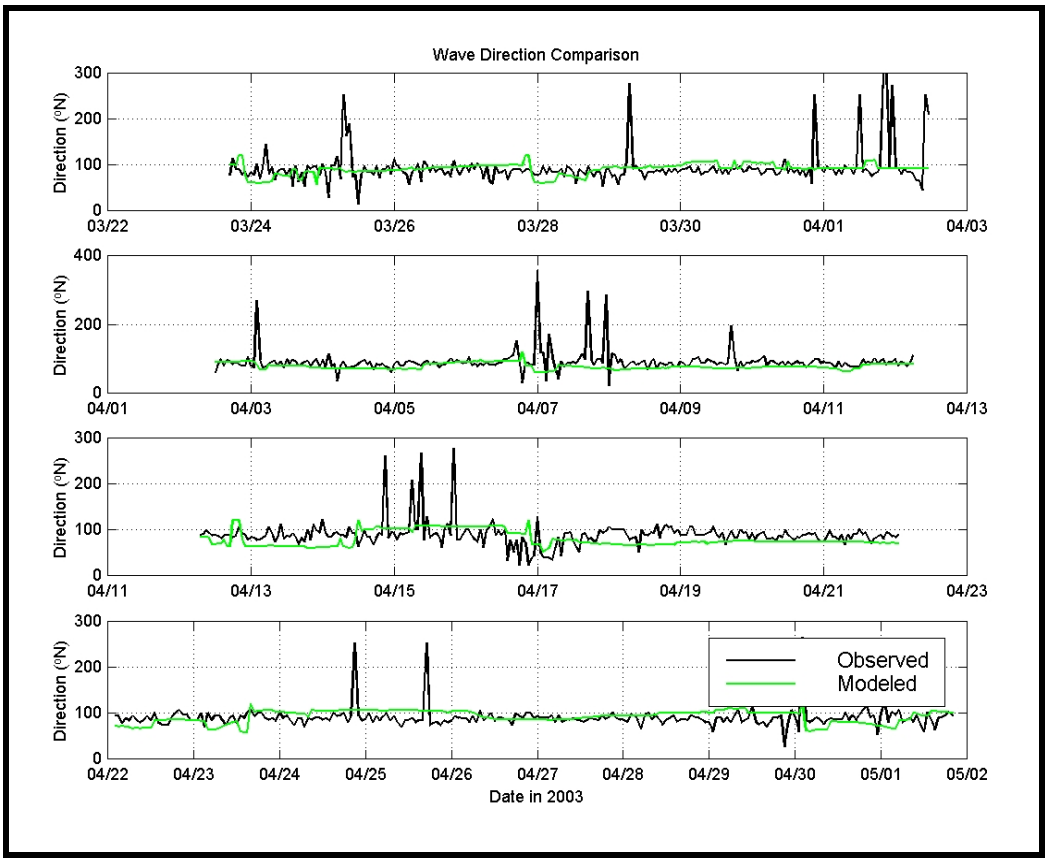

Figure 9-13. Comparison of observed (black line) and modeled (green line) wave direction for March (top panel) through April (bottom panel), 2003 at the Nearshore ADCP station.

Table 9-5 presents error statistics (bias and RMS error) for the STWAVE simulations based on the offshore and nearshore ADCP stations. The bias and RMS errors are similar to errors presented in other STWAVE applications in other coastal regions (Smith and Gravens, 2002). Validation results for STWAVE indicated the model results compare to the observed parameters well. In particular, the wave height bias shows the model is adequately predicting wave heights in the region both seaward (0.11 m) and landward (0.06 m) of the Eagle and Ram island complex. The differences in wave direction may be due to the lack of diffraction processes in the current version of STWAVE (diffraction processes are being added to the STWAVE code, but this version was not completed at the time of this study), which are likely important in the lee of the structures and islands. As a secondary validation, two-dimensional observed spectra from the ADCP stations and two-dimensional spectra output from the STWAVE model were compared. Figure 9-14 shows the visual results of a spectral comparison for April 27, 2003 at 0400 at the offshore ADCP station. The upper panels show the full two-dimension spectra (with the colormap indicating the energy distributed between direction and frequency), while the lower panels shows the frequency spectra. Frequency is shown in Hertz, and energy is shown in m^2/Hz/rad. Modeled spectra are shown in the right panels, while observed data are shown in the left panels. Results of the spectra also showed favorable comparison.

For this particular time, the modeled spectra tend to spread the energy more evenly over a range of frequencies, while the observed data contains more energy at the peak frequency. The total energy; however, matches well. A number of these comparisons were completed at both the nearshore and offshore ADCP stations throughout the deployment time period. Differences in energy between model and observed spectra were 5-15%. Spectral output from the STWAVE validation runs were used to generate input conditions for calibration and verification time periods in the local wave model (Chapter 11.0).

Table 9-5. STWAVE model errors based on ADCP stations.

Wave Parameter	Offshore ADCP Station		Nearshore ADCP Station	
	Bias	**RMS Error**	**Bias**	**RMS Error**
H_S (m)	0.11 m (0.4 ft)	0.39 m (1.2 ft)	0.06 m (0.2 ft)	0.26 m (0.8 ft)
T_p (sec)	2.6 sec	4.4 sec	2.9 sec	4.6 sec
Dir (deg)	10.9 deg	39.3 deg	2.0 deg	20.3 deg

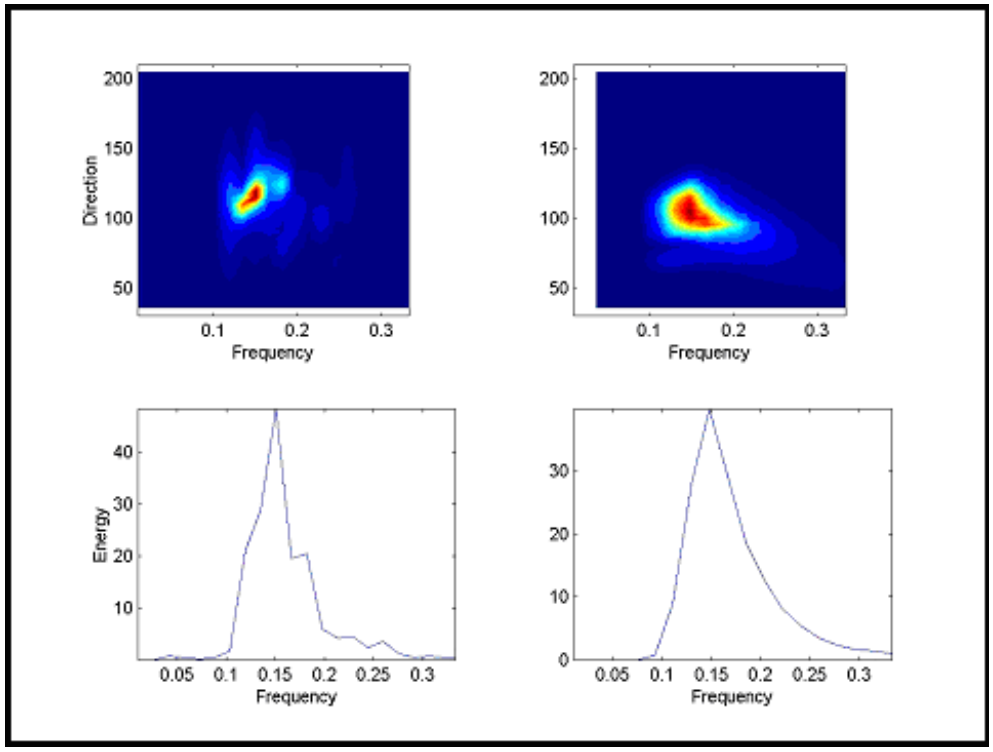

Figure 9-14. Comparison of observed and modeled two-dimensional spectra. Offshore ADCP station spectra are presented in the left panels, while STWAVE output of modeled spectra are presented in the right panels.

9.6 Model Results

Following the validation, the transformation-scale (regional) model (STWAVE) was used to simulate a wide range of annual average directional conditions, return-period storm events, and specific historical storm events.

9.6.1 Average Annual Directional Approaches

Model simulations were performed for the typical wave conditions represented by the directional bin spectra presented in Table 9-3. Wave focusing, and divergence occur at several locations throughout the modeling domain, which results in variations in the wave energy propagating towards the coastline of Saco Bay. Figure 9-15 illustrates STWAVE results for waves approaching from the east-southeast (110 to 130 degree bin), one of the most commonly occurring of the typical condition cases, for the entire modeling domain. The color map corresponds to the distribution of significant wave height (m) throughout the modeling domain. Warm colors (reds and yellows) indicate higher wave height, while cool colors (blues and greens) indicate lower wave height. The model simulation was conducted at depths and shoreline positions corresponding to mean water level since the representative average annual cases represent static time periods. Arrows on the figure represent the modeled wave direction as they propagate and approach the shoreline. The directions become more shore normal as the waves get closer to the coastline and are affected by the irregular bottom bathymetry. The last visible arrow indicates significant redirection towards the coastline, as the waves become more shore normal. In general, the wave height decreases as waves move onshore due to the effect of bottom friction. The offshore islands also significantly influence the waves as they propagate towards the shoreline. Refraction and sheltering processes are clearly evident in the wave height results. There is also a fair amount of wave energy variation along the shoreline. Some areas experience higher wave energy (red areas) due to the focusing of waves in the nearshore zone. The wave energy variation both result in alongshore variability in the direction and magnitude of sediment transport along the shoreline. Figure 9-15 represents an example of the transformation-scale (regional) wave modeling results that were completed for Saco Bay. The results were used to assess the existing wave climate, provide input conditions to the local wave model, and develop regional sediment transport fluxes and divergence. Figures for all approach directions for the entire modeling domain are presented in Appendix 9-B.

On a regional scale, the jetties at the Saco River tend to have a smaller influence than the offshore islands and it is difficult to determine the details of the wave transformations in the vicinity of Camp Ellis Beach. The structures become more important on the local scale (Chapter 11.0), as do the smaller nearshore islands (e.g., Eagle and Ram Islands). Figure 9-16 takes a closer look at the wave modeling results in the vicinity of Camp Ellis Beach, near the entrance to the Saco River. The results are again presented for the east-southeast (110 to 130 degree bin). The colormap again indicates the wave height distribution, and the arrows indicate the direction of wave propagation. The scale of the colormap has been changed to identify more details related to the height distribution. Although the offshore approach direction is east-southeast, the nearshore approach direction in the vicinity of Camp Ellis Beach is from the northeast, a similar trend as seen in the wave observations (Chapter 7.0). Due to the angle of wave approach, in this

scenario fluid transport is predominantly north to south. However, the transformation-scale (regional) model does lack significant physical transformation components, such as reflection of wave energy from the northern jetty and diffraction effects from the structures and islands. The local scale model (Chapter 11.0) will include these important physical processes.

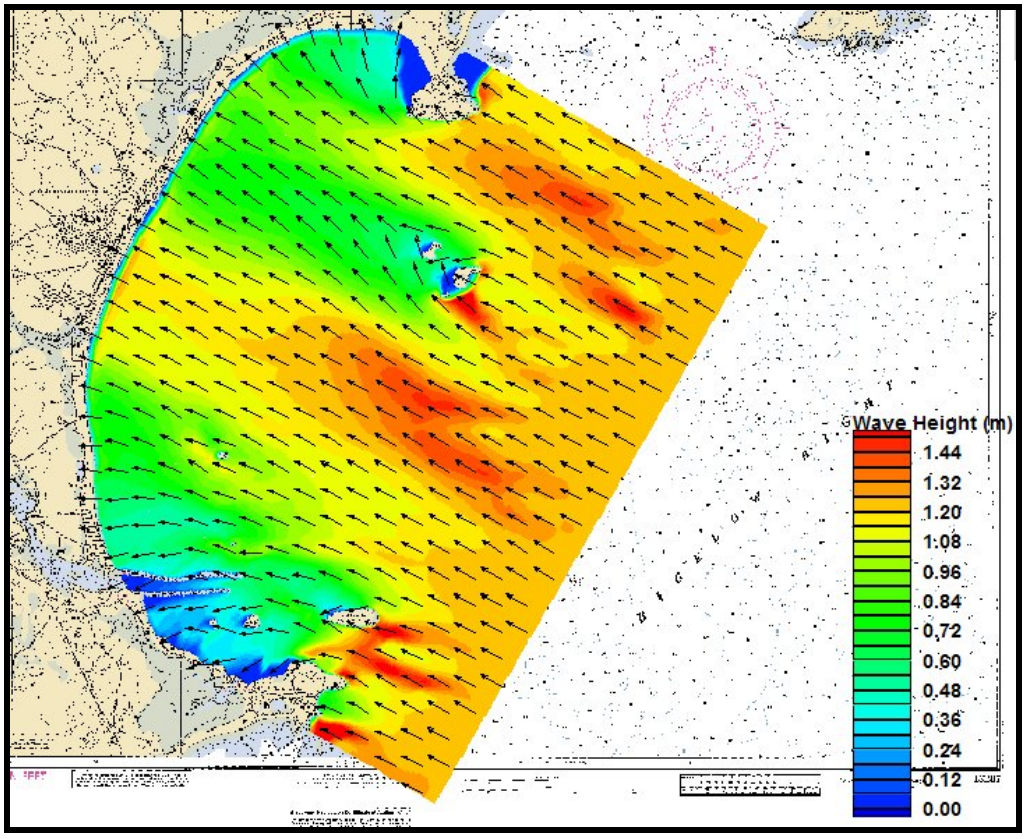

Figure 9-15. Example of STWAVE modeling results for existing conditions using an east-southeast (110 to 130 degree) approach directional spectra bin. The arrows indicate the wave direction.

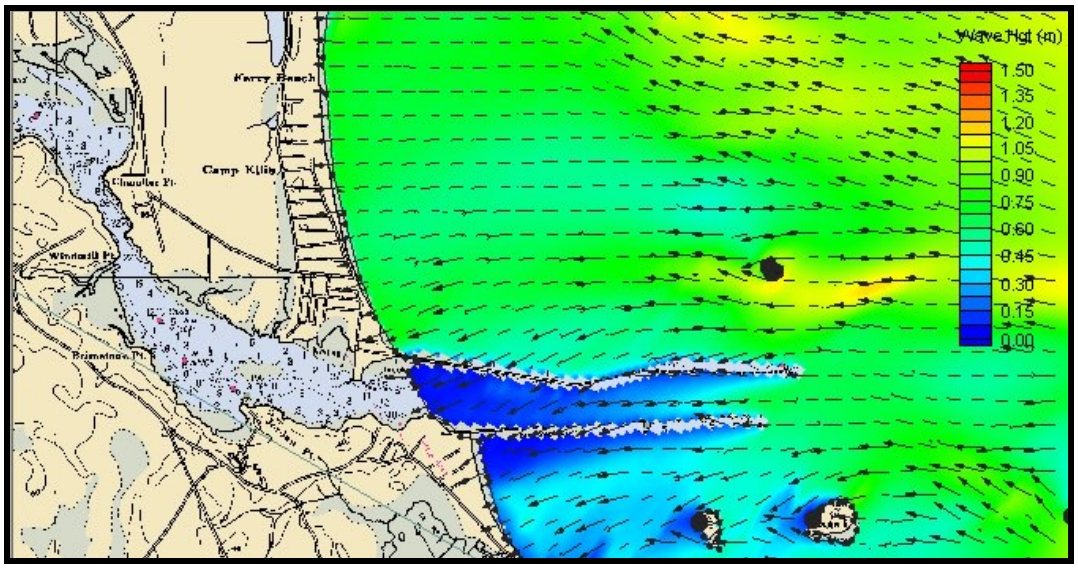

Figure 9-16. Spectral wave modeling results for an east-southeast approach direction (110-130 degree bin) in the Camp Ellis Beach region.

Figures 9-17 and 9-18 present two additional approach directions, from the east-northeast (75 to 90 degree bin) and south-southeast (150 to 165 degree bin), respectively. The variability in the wave climate is clearly indicated by the differences in nearshore wave patterns arising from the various input spectra approach directions. The scale of the colorbar is again adjusted to illustrate distribution changes in wave height. The waves approaching from the east-northeast propagate towards Camp Ellis with little transformation in direction, while even waves that are heading from an almost southerly approach, are redirected to a northeastern approach fronting Camp Ellis Beach.

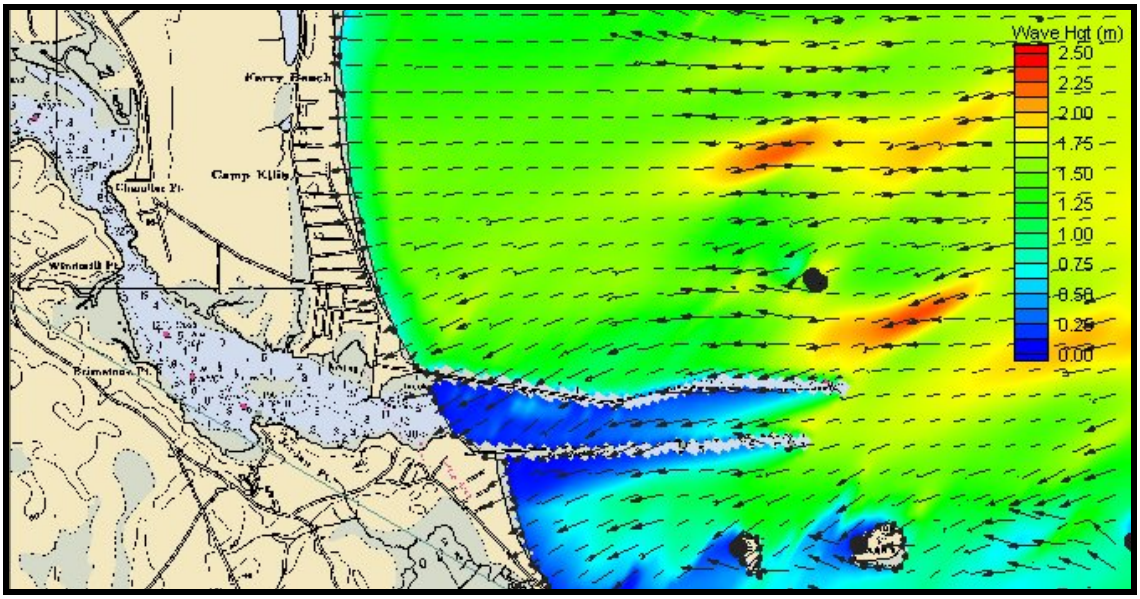

Figure 9-17. Spectral wave modeling results for an east-northeast approach direction (75-90 degree bin) in the Camp Ellis Beach region.

In order to arrive at an accurate estimation of the sediment transport in the region, including the reversals in sediment transport direction that occur, results from the wave model can be used to generate the sediment transport flux. This would include waves coming from all directions and having various wave heights and periods. The combination of all the directional approach cases allows for an assessment of the average annual wave climate. As such, the STWAVE results were used to generate wave-induced currents (from radiation stresses) and regional sediment transport results for the entire Saco Bay Region (from headland to headland), as well as provide input into the nearshore (local) wave model. The results of all the approach directions are used, in concert with the percent occurrence, to compute the annual sediment transport in the region (Chapter 12.0).

9.6.2 High Energy Event Simulations

Specific historical storm events, as well as return-period storms, were also simulated in the validated transformation-scale (regional) model. The simulation of specific storm events was important to quantify the short-term impacts that occur during these energetic scenarios. Sediment transport along the coastline can in many cases be dominated by these short episodic events. Figure 9-19 presents the result from the simulation of the Perfect Storm (10/31/1991). Wave heights are significantly higher than during the annual average directional cases, as the offshore heights are in excess of 7.5 m in locations. Figure 9-20 shows results for a 10-year return period storm event. Figures for all approach directions for the entire modeling domain are presented in Appendix 9-B. The storm event spectral results, as were the annual average directional bin cases, were passed forward to the local scale transformation model (Chapter 11.0) to assess direct impacts on the Camp Ellis Beach region.

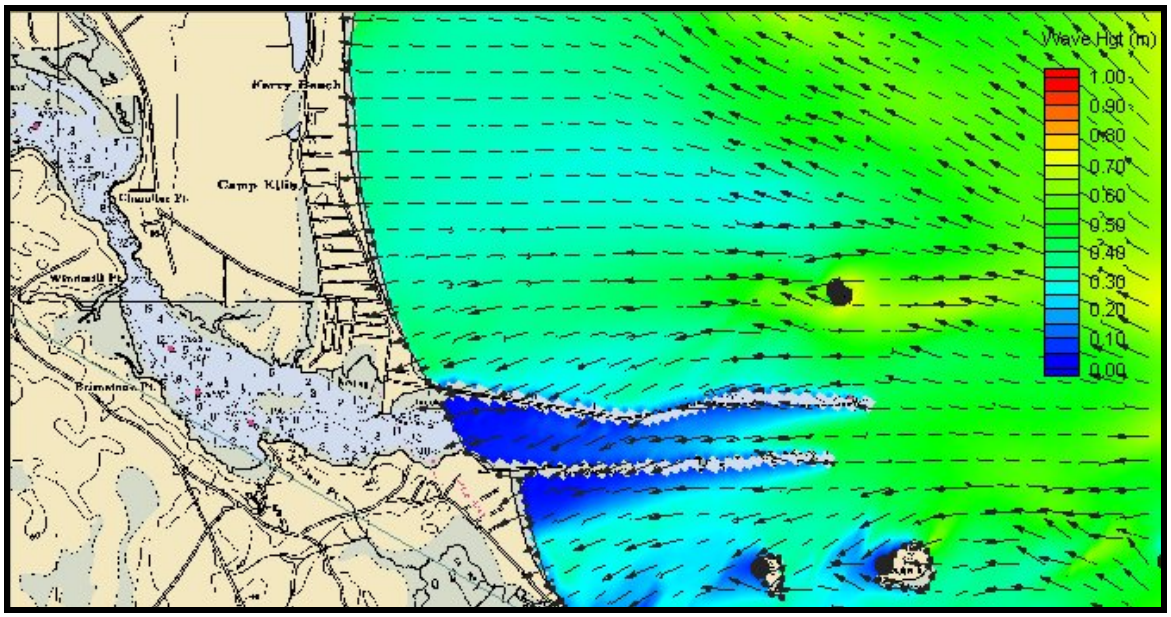

Figure 9-18. Spectral wave modeling results for a south-southeast approach direction (150-165 degree bin) in the Camp Ellis Beach region.

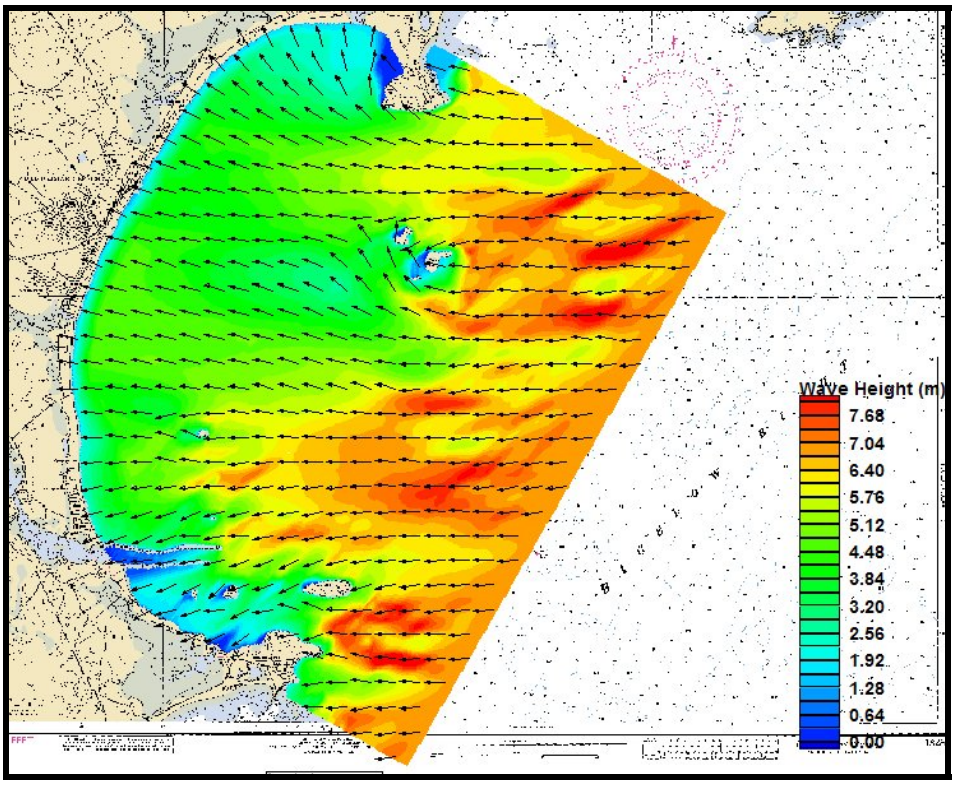

Figure 9-19. STWAVE modeling results for the Perfect Storm (10/31/1991).

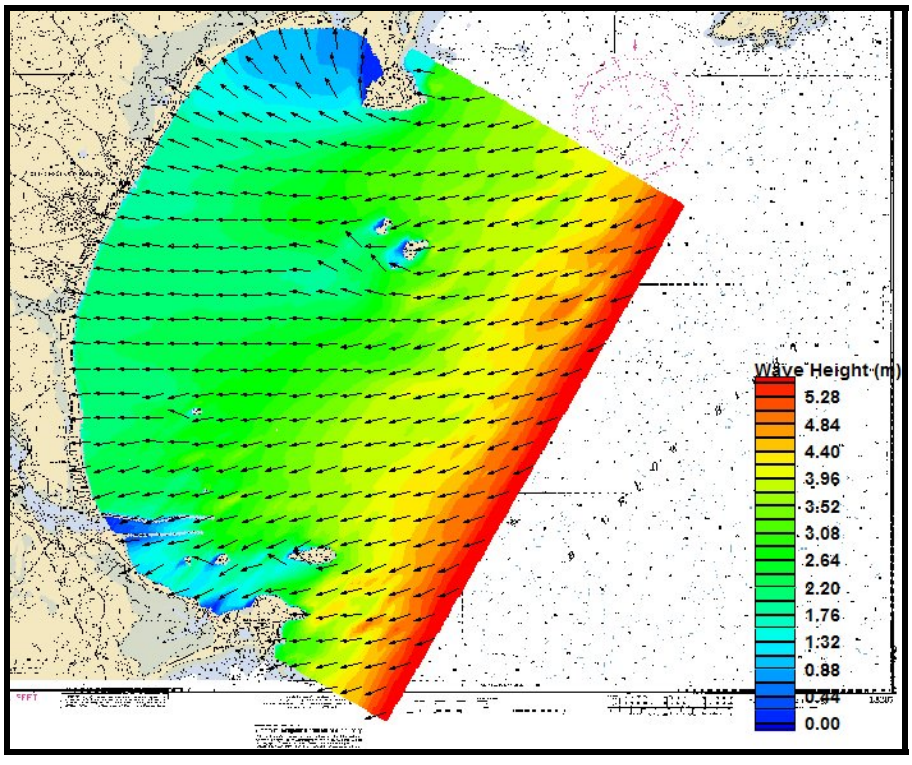

Figure 9-20. STWAVE modeling results for the 10-yr return period storm event.

9.7 Summary

A nearshore, transformation-scale (regional) wave model was used to propagate the offshore wave climate into the Saco Bay region. The model was verified using spectral output from the generation scale modeling results (Chapter 8.0). Once validated, the transformation-scale (regional) model was used to simulate average annual directional cases (developed from WIS data), specific historic storms events, and return-period storms. Results of the transformation-scale (regional) model are used to develop regional sediment transport fluxes and divergence, while providing spectral input for the local wave modeling effort.

10.0 ALTERNATIVE DEVELOPMENT

This study uses a detailed alternatives analysis as the basis for determining the optimal solution to the erosion at Camp Ellis Beach, based partly on an assessment of potential impacts (both physical and environmental). Overall, a variety of factors were considered when evaluating the various alternatives (e.g., cost, feasibility, performance, environmental impacts, constructability, etc.), with the overall objective focused on identifying the optimal solution. However, this technical report primarily focuses on the performance of each alternative in providing protection and maintaining a beach at Camp Ellis. Other factors (e.g., cost, constructability, etc.) are considered, but will be more specifically evaluated directly by the USACE Section 111 Study. The goal of the assessment was to evaluate reasonable, practicable, and feasible alternatives that will achieve the goals and objectives of the project, while minimizing the short and long-term adverse effects (if any). The alternatives analysis procedure developed for the Saco River and Camp Ellis Beach Section 111 Project, as well as a comprehensive list of the alternatives evaluated, is presented in this chapter.

The ultimate application of the modeling system was to evaluate a wide range of potential engineered alternatives to the erosion problem. The alternatives were geared towards mitigating the ongoing erosion occurring at Camp Ellis Beach. More than twenty-five (25) potential solutions, including both structural (e.g., spur jetties, breakwaters, groins, etc.), and non-structural (e.g., partial jetty removal, offshore borrow pits, jetty roughening, etc.) were developed jointly between Woods Hole Group, the USACE New England District, Maine Geological Survey (MGS), and members of the Saco Bay Implementation Team (SBIT).

This chapter is organized as follows. Section 10.1 lays out the methodology for alternative development; Section 10.2 identifies the alternatives; and Section 10.3 discusses the alternatives screening process.

10.1 Development of Alternatives

The identification of the alternatives for consideration is a key first step for any alternatives analysis. The Saco River and Camp Ellis Beach Section 111 Project developed alternatives through a series of meetings and discussions with key stakeholders (USACE New England District, Maine Geological Survey, and members of the Saco Bay Implementation Team). During this iterative process, many viable solutions were discussed and considered, and an initial series of alternatives was selected for the analysis procedure. Careful consideration was given to all factors associated with each alternative. For example, potential impacts on the neighboring shoreline, engineering feasibility, likelihood of success, etc. were all considered in the final selection process. The alternatives that were viewed as the most highly effective were jointly selected for further analysis. Initially, a total of 11 alternatives were considered; however, this was expanded to 17 through the discussion and meeting process. Following some of the initial modeling results, the alternatives were expanded to a total of 23. Subsequent geotechnical evaluation resulted in the addition of 6 more alternatives. All members of the alternative development team (USACE, SBIT, MGS, WHG) agreed upon the final

alternatives that were selected for consideration. These alternatives are presented in greater detail in Section 10.2.

10.2 Alternatives Considered

More than twenty-five (25) alternatives, in addition to the no action alternative, were considered in the evaluation of potential solutions to the erosion occurring at Camp Ellis Beach. Table 10-1 presents a list of the alternatives considered, including the origin of each alternative. The base alternative is a beach nourishment project alone. However, since beach nourishment alone will not sustain an adequate protection level, nor does it directly address the impact caused by the northern jetty (increased energy due to wave reflection and a reduction in sediment supply through pushing sediment further offshore) additional project elements were considered in order to help create a more sustainable beach. Therefore, each alternative presented in Table 10-1 includes a beach nourishment component (to stabilize the shoreline and provide the lost sediment supply), constructed in concert with the alternative. In the table, reference to the northern jetty refers to the northern jetty of the Saco River, which is comprised of three distinct segments. Segment 1 is the shore-attached portion of the jetty that is exposed during all normal tide levels. Segment 1 is approximately 910 m (2,985 ft) in length. Segment 2 represents the northeast/southwest shift in jetty orientation and is approximately 320 m (1,050 ft) long. Segment 3 is comprised of the half-tide (i.e., exposed at low tide and submerged at high tide) portion of the northern jetty and is approximately 700 m (2,300 ft) in length. A spur jetty refers to a structure attached to the existing northern jetty, typically oriented perpendicular to the existing structure. A groin refers to a shore-attached structure that is built perpendicular to the shoreline and intended to trap sand flowing in the alongshore direction. In addition, references to an optimized location in Table 10-1 represent an iterative procedure performed during the modeling effort to identify the optimal performing location, if possible.

10.2.1 No Action Alternative

The no action alternative implies there would be no change to the present conditions at Camp Ellis Beach. This is an unacceptable alternative, as the existing shorefront would continue to be eroded, a sustainable beach and/or any protective action would not be undertaken, and the landward homes and structures would face potential damage/loss. This alternative does not address the required mitigation purview of the Section 111 Authority.

10.2.2 Base Alternative: Beach Nourishment Alone

The base alternative consists of placement of sediment on the beach area fronting Camp Ellis Beach. The current nourishment design consists of approximately 300,000 cubic yards of material extending approximately 910 m (3,000 ft) with the southern end of the project located at the northern jetty. However, as erosion continues, it is likely that the beach nourishment design volume will increase. As such, the final design and dimensions of the beach nourishment will be developed by the USACE, New England District. For the current study, this condition represents the base alternative; however, the beach nourishment is also considered to be a component of every alternative; that is, each alternative incorporates a beach nourishment project that will be constructed in

concert with the other elements in that alternative. The base (beach nourishment alone) alternative is evaluated to determine if beach nourishment alone is an acceptable option for protecting the Camp Ellis Beach region.

10.2.3 Alternative 0: Northern Jetty Removal

This alternative evaluates complete removal of the northern jetty adjacent to the Saco River and would attempt to restore the beach system by removing the jetty. This alternative would also remove the southern jetty at Saco River inlet. The goal of this alternative would be to eliminate reflected wave energy (the energy of the incident wave that is redirected off the structure, in this case towards the beach) from the structure that impacts Camp Ellis Beach, as well as to potentially restore a natural sediment supply to the beach from river sediment flux. However, complete removal of the northern structure has the potential to result in significant negative impacts on Camp Ellis Beach, which has been stabilized by the structure for over 150 years. For example, the construction of the structures likely resulted in a loss of the natural ebb shoal complex that existed at the mouth of the Saco River. This natural shoal complex likely provided stability to the region both north and south of the River, providing natural protection from wave incoming waves. While the coastal structures have had a negative impact on the coastal beaches to the north, they also provide protection and stability to the areas to the south. As such, complete removal of the structures may likely have unintended negative impacts to shorelines on both sides of the Saco River, which is no longer maintains a natural ebb shoal complex.

10.2.4 Alternative 1: Northern Jetty Extension Removal

This alternative (Figure 10-1) would remove the outer 700 m (2,300 ft) of the northern jetty (segment 3), which is comprises the half-tide portion of the structure. This alternative would attempt to reduce a minor portion of the wave energy that reflects off the jetty that impacts Camp Ellis Beach.

10.2.5 Alternative 2: Northern Jetty Extension Removal and Lowering

This alternative (Figure 10-2) couples alternative 1 with the lowering of an additional 600 m (1,970 ft) of the northern jetty. Therefore, at Mean High Water (MHW), the seaward extent of the exposed portion of the northern jetty would be equivalent with the seaward extent of the exposed portion of the southern jetty. This lowered portion of the structure would be reduced to a crest elevation of 0.3 m (1.1 ft) Mean Tide Level. This alternative would attempt to reduce further the reflected wave energy, while creating a somewhat equivalent structure length on both sides of the Saco River Inlet.

Table 10-1. Alternatives considered in the alternative analysis procedure.

Alt. ID	Description	Origin
Base	Beach nourishment alone	Base alternative
0	Northern jetty removal (segments 1, 2, and 3)	Initial alternative set
1	Northern jetty extension (segment 3) removal	Initial alternative set
2	Northern jetty extension (segment 3) removal and additional lowering of 600 m (1,970 ft)	Initial alternative set
3	Seaward location of a 230 m (750 ft) spur jetty	Initial alternative set
4	Optimized location of a 152 m (500 ft) spur jetty	Initial alternative set
5	Optimized location of dual 152 m (500 ft) spur jetties	Initial alternative set
6	Inshore location of a 230 m (750 ft) spur jetty	Initial alternative set
7	Inshore location of a 230 m (750 ft) spur jetty coupled with northern jetty extension (segment 3) removal	Initial alternative set
8	Inshore location of a 230 m (750 ft) spur jetty coupled with shore-based terminal groin	Initial alternative set
9	1st configuration of T-Head Groins	Initial alternative set
10	2nd configuration of T-Head Groins	Initial alternative set
11	Offshore Breakwater (seaward location)	Secondary alternative set
11a	Offshore Breakwater (nearshore location)	Secondary alternative set
11b	Offshore Breakwater (intermediate location)	Secondary alternative set
12	Offshore Breakwater (landward location) coupled with seaward location of a 152 m (500 ft) spur jetty	Secondary alternative set
13	Comb configuration of 15 m (50 ft) spur jetties	Secondary alternative set
14	Offshore borrow pit	Secondary alternative set
15	Seaward location of a 230 m (750 ft) spur jetty with an angled orientation	Secondary alternative set
16	Northern jetty roughening (segments 1, 2, and 3)	Secondary alternative set
17	Submerged shoal/rock outcrop	Secondary alternative set
18	Offshore Breakwater (landward location) coupled with landward location of a 152 m (500 ft) spur jetty	Developed based on highest performing previous alternatives
19	Seaward location of a 230 m (750 ft) spur jetty, northern jetty extension removal, and jetty roughening	Developed based on highest performing previous alternatives
20	Alt. 11a with estimated full salient formation	Estimated based on expected shoreline response
21	Alt. 11a with estimated partial salient formation	Estimated based on expected shoreline response

22	Combination of 230 m (750 ft) spur jetty with two nearshore 114 m (375 ft) segmented breakwater components	Developed based on results of initial geotechnical work
23	Combination of 152 m (500 ft) spur jetty with three 100 m (325 ft) segmented breakwater components	Developed based on results of initial geotechnical work
24	Alt. 23 with additional northern breakwater segment of 100 m (325 ft)	Developed based on results of initial geotechnical work
25	Secondary configuration of 152 m (500 ft) spur jetty with three segmented breakwater components of 125, 120, and 100 m (410, 394, 325 ft), heading south to north, respectively.	Developed based on results of initial geotechnical work
26	Alt. 24 moving the northern most breakwater segment further north	Developed based on results of initial geotechnical work
25A	Modification of Alt. 25, removing northernmost segmented breakwater	Developed based on concern of nearshore proximity of northernmost breakwater

Figure 10-1. Alternative 1: Northern jetty extension removal.

10.2.6 Alternative 3: Seaward Placement of 750-foot Spur Jetty

This alternative (Figure 10-3) would consist of the construction of a 230 m (750 ft) spur jetty that would be attached to the existing northern jetty. The spur would be located approximately 610 m (2,000 ft) from the shoreline (approximately two-thirds the length of segment 1). The spur would be oriented in a shore parallel (jetty perpendicular) orientation. This alternative would attempt to intercept the reflected wave energy, break a portion of the incident wave energy, and block Mach-Stem wave effects from transferring energy along the structure. Mach-Stem waves refer to waves traveling along the structure. When an incident wave reflects off the structure, the reflected wave merges with the incident wave to form a single wave, known as the Mach Stem, propagating along the structure. This Mach Stem effect is the same as occurs with an explosion and associated shock wave. In addition, the spur jetty should assist in reducing cross-shore sediment transport from the beach seaward along the existing northern jetty. Therefore, this alternative might potentially reduce the overall wave energy arriving at Camp Ellis Beach.

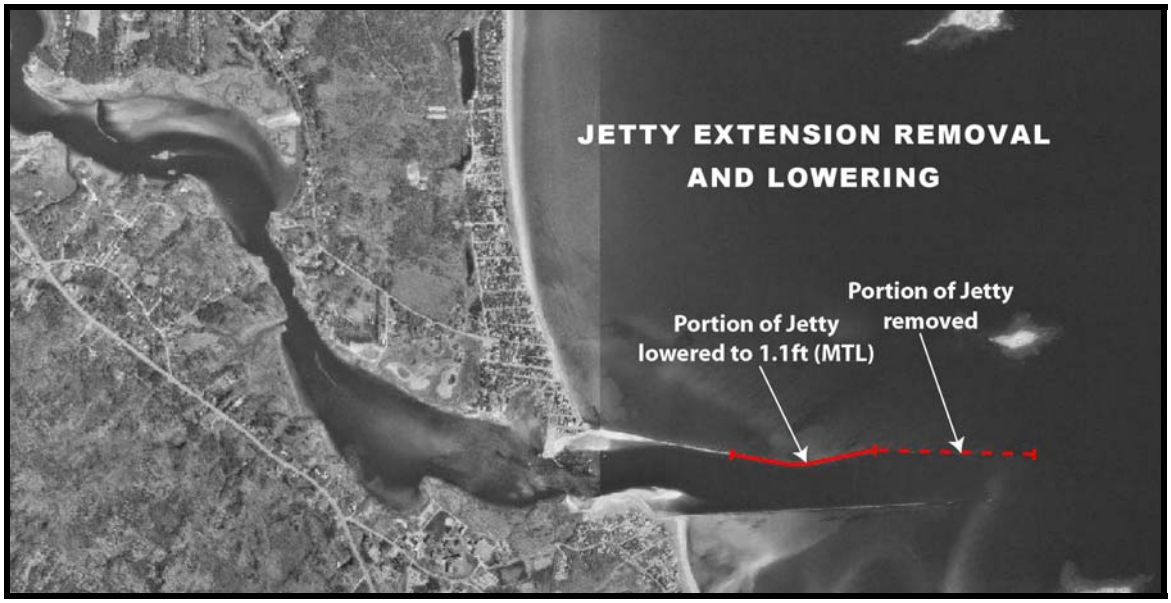

Figure 10-2. Alternative 2: Northern jetty extension removal and lowering.

Figure 10-3. Alternative 3: Seaward placement of 750-foot spur jetty.

10.2.7 Alternative 4: Optimized Location of a 500-foot Spur Jetty

This alternative (Figure 10-4) would consist of the construction of a 152 m (500 ft) spur jetty that would be attached to the existing northern jetty. During the modeling process, an iterative methodology was used to determine the optimal location for the spur. This included evaluation of the existing condition wave energy, and a logical placement of the 500-foot spur. Through this process, the optimal spur would be located at approximately 450 m (1,475 ft) from the shoreline (approximately one-half the length of segment 1). The spur would be oriented in a shore parallel (jetty perpendicular) orientation. As in the case of the Alternative 3, the goal of this alternative would be to intercept the reflected wave energy, break a portion of the incident wave energy, and block Mach-Stem wave effects from transferring energy along the structure. Therefore, this alternative would potentially reduce the overall wave energy arriving at Camp Ellis Beach. In addition, the spur jetty should assist in reducing cross-shore sediment transport from the beach seaward along the existing northern jetty. Additional spur jetty lengths (e.g., Alternative 6) were also evaluated in the analysis.

Figure 10-4. Alternative 4: Placement of 500-foot spur jetty.

10.2.8 Alternative 5: Optimized Location of Dual 500-foot Spur Jetties

This alternative (Figure 10-5) would consist of the construction of two 152 m (500 ft) spur jetties that would be attached to the existing northern jetty. During the modeling process, an iterative methodology was used to determine the optimal location for the spurs. Through this process it was determined that the optimal spurs would be located at approximately 450 m (1,475 ft) from the shoreline (approximately one-half the length of segment 1) and approximately 1,230 m (4,035 ft) from shore (at the seaward end of segment 2). The spurs would be oriented in a shore parallel (jetty perpendicular) orientation. As in previous spur cases, this alternative would attempt to intercept the reflected wave energy, break a portion of the incident wave energy, and block Mach-Stem wave effects from transferring energy along the structure. Therefore, this alternative would potentially reduce the overall wave energy arriving at Camp Ellis Beach. In addition, the spur jetty should assist in reducing cross-shore sediment transport from the beach seaward along the existing northern jetty.

Figure 10-5. Alternative 5: Placement of dual 500-foot spur jetties.

10.2.9 Alternative 6: Inshore Location of a 750-foot Spur Jetty

This alternative (Figure 10-6) would consist of the construction of a 230 m (750 ft) spur jetty that would be attached to the existing northern jetty. The spur would be located approximately 450 m (1,475 ft) from the shoreline (approximately one-half the length of segment 1), determined by optimizing the location through multiple simulations. The spur would be oriented in a shore parallel (jetty perpendicular) orientation. This alternative would attempt to intercept the reflected wave energy, break a portion of the incident wave energy, and block Mach-Stem wave effects from transferring energy along the structure. Therefore, this alternative would potentially reduce the overall wave energy arriving at Camp Ellis Beach. In addition, the spur jetty should assist in reducing cross-shore sediment transport from the beach seaward along the existing northern jetty. This alternative represents the optimal placement location of all spur alternatives, as will be illustrated in Chapter 11.0.

10.2.10 Alternative 7: Alternative 6 with Northern Jetty Extension Removal

This alternative (Figure 10-7) would consist of a combination of alternative 6 and removal of a portion of the existing northern jetty. The removal would extract 230 m (750 ft) of segment 3 for potential beneficial re-use in the construction of the spur jetty. As in other spur alternatives, this alternative would attempt to intercept the reflected wave energy, break a portion of the incident wave energy, and block Mach-Stem wave effects from transferring energy along the structure. Therefore, this alternative would potentially reduce the overall wave energy arriving at Camp Ellis Beach. In addition, the spur jetty should assist in reducing cross-shore sediment transport from the beach seaward along the existing northern jetty.

Figure 10-6. Alternative 6: Inshore placement of 750-foot spur jetty.

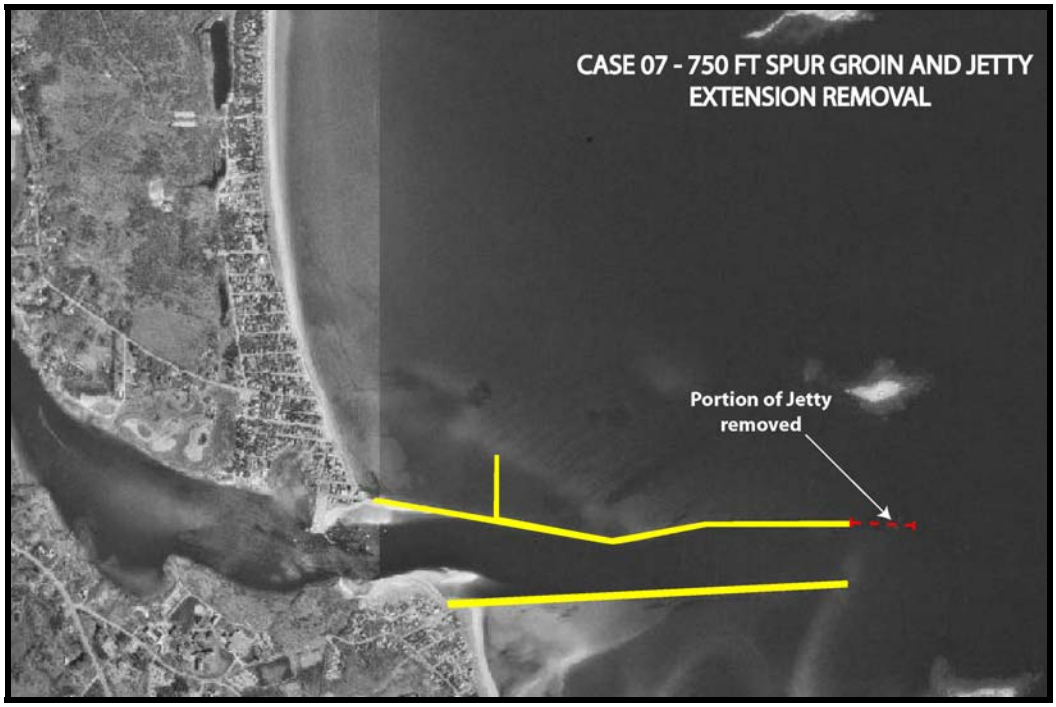

Figure 10-7. Alternative 7: Inshore placement of 750-foot spur jetty coupled with removal of a portion of the northern jetty.

10.2.11 Alternative 8: Alternative 6 with Terminal Groin

This alternative (Figure 10-8) would consist of a combination of alternative 6 and construction of a terminal groin positioned at the approximate location of the northern terminus of the beach nourishment template. The terminal groin would be located approximately 910 m (3,000 ft) north of the existing northern jetty and would extend approximately 75 m (250 ft) offshore. In addition to the potential benefits of the spur jetty, the terminal groin would attempt to prevent the beach nourishment material from being transported to the north and away from the most critical erosional areas of Camp Ellis.

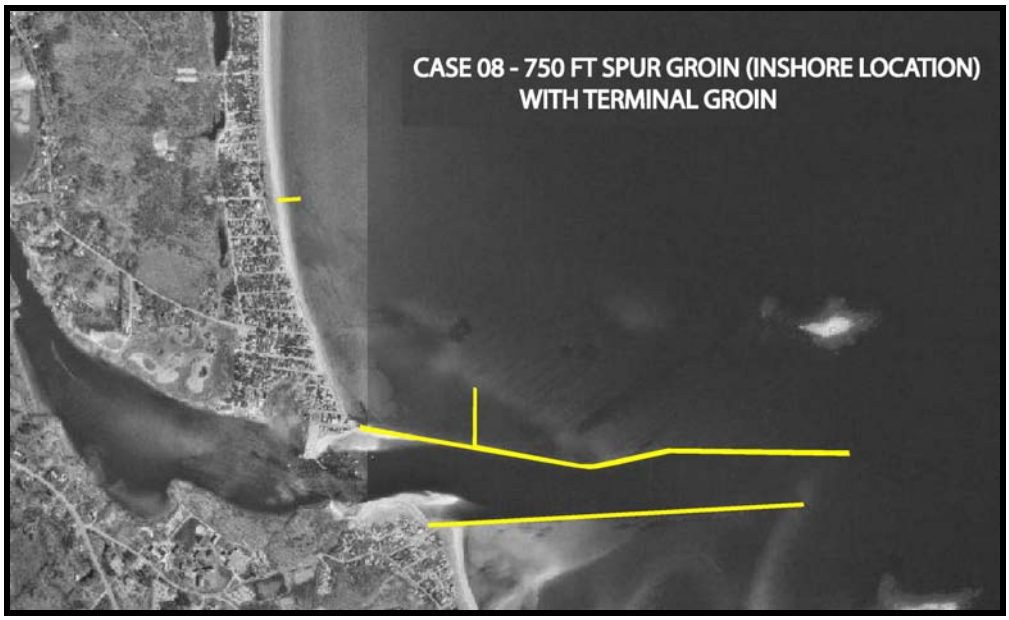

Figure 10-8. Alternative 8: Inshore placement of 750-foot spur jetty coupled with terminal groin positioned north of existing structures.

10.2.12 Alternative 9: Primary Configuration of T-Head Groins

This alternative (Figure 10-9) would consist of the construction of five (5) shore-attached T-head groin structures and a single spur jetty. T-head groins are comprised of a standard shore perpendicular groin fitted with a shore-parallel T-head at their seaward end. The T-head is often built to interrupt the seaward flow of water and sand in rip currents that often develop along a groin's axis. The T-head may also act as a breakwater and shelter a sizeable stretch of beach behind it. In this particular case, the gap spacing and structure lengths are presented in Table 10-2. Table 10-2 presents the structures proceeding from south (1) to north (5). The spur jetty is a shorter structure than the previously presented spurs, and is 30 m (100 ft) in length located approximately 100 m (328 ft) along the North Jetty from shore. The most northerly groin is comprised of a L-head (rather than a T) since it is the last structure in the groin field. This alternative would attempt to hold the beach nourishment in place by preventing losses in both the seaward and alongshore

directions. In addition, the T-heads would afford additional wave protection by breaking wave energy.

Table 10-2. Primary T-head configuration spacing and dimensions.

T-head Groin	Groin Length (m)	T-Head Length (m)	Head-to-Head Spacing (m)
1	83	60	165
2	86	60	90
3	75	60	95
4	75	60	90
5	75	30	90

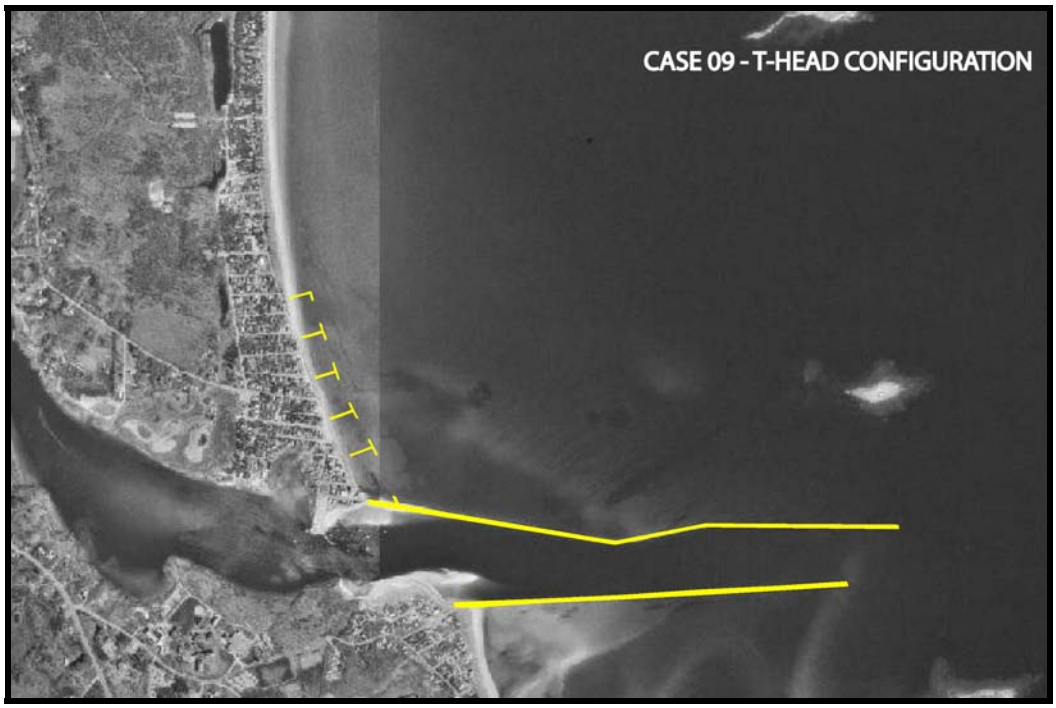

Figure 10-9. Alternative 9: Primary configuration of T-head groins.

10.2.13 Alternative 10: Secondary Configuration of T-Head Groins

This alternative (Figure 10-10) would consist of the construction of seven (7) shore-attached T-head groin structures and a single spur jetty. This is a variation of alternative 9 with an increased number of T-head groins and increased spacing. The function of the layout is intended to be the same, except for covering a longer stretch of coastline and increased spacing. The gap spacing and structure lengths are presented in Table 10-3, proceeding from south (1) to north (7). The spur jetty is a smaller structure than the previously presented spurs, and is 30 m (100 ft) in length located approximately 100 m along the North Jetty from shore. The most northerly groin is comprised of a L-head

(rather than a T) since it is the last structure in the groin field. As with alternative 9, this alternative would attempt to hold the beach nourishment in place by preventing losses in both the seaward and alongshore directions. In addition, the T-heads would afford additional wave protection by breaking wave energy.

Table 10-3. Secondary T-head configuration spacing and dimensions.

T-head Groin	Groin Length (m)	T-Head Length (m)	Head-to-Head Spacing (m)
1	83	60	165
2	75	60	245
3	75	60	240
4	75	60	240
5	75	60	240
6	75	60	240
7	75	30	240

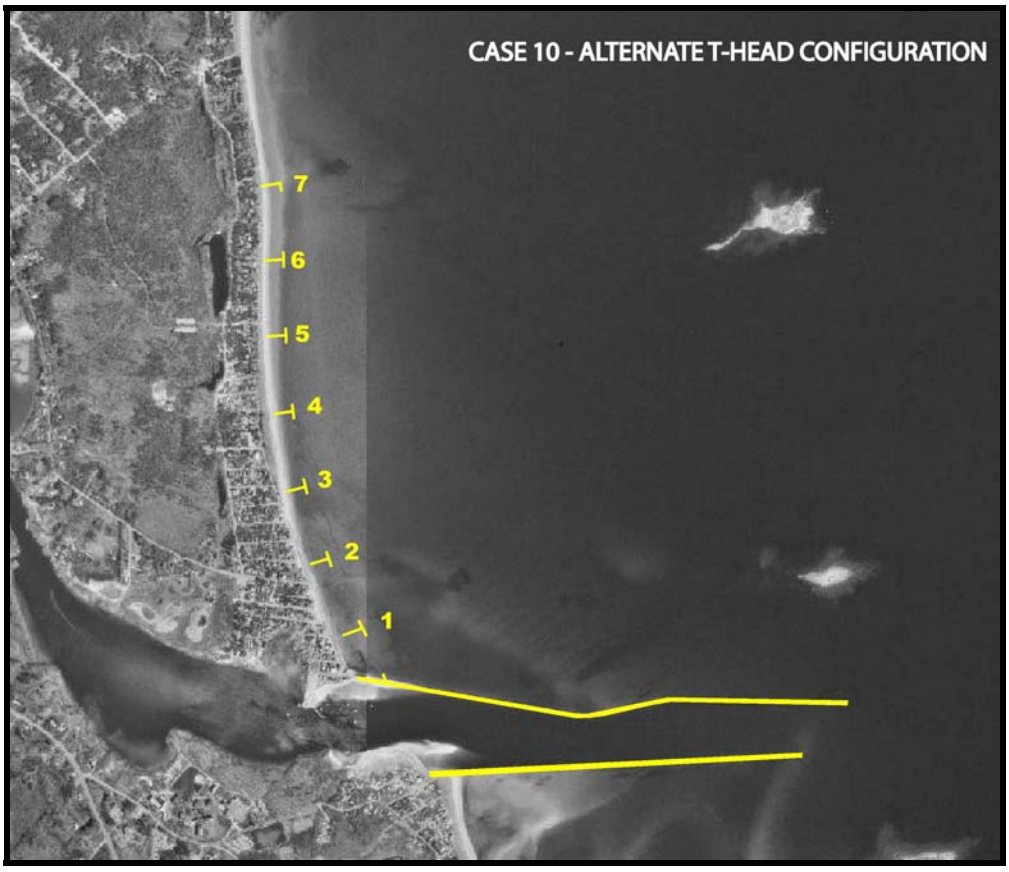

Figure 10-10. Alternative 10: Secondary configuration of T-head groins.

10.2.14 Alternative 11: Offshore Breakwater, Seaward Location

This alternative (Figure 10-11) would consist of the construction of a breakwater located offshore of Camp Ellis Beach and detached from the existing northern jetty. The

breakwater would be 280 m (920 ft) in length and set in approximately 10 m (32 ft) of water depth, relative to MHW. The breakwater would be located approximately 1,450 m (4,755 ft) from the shoreline, with the southern end of the breakwater located approximately 600 m (1,968 ft) north from segment 3 of the northern jetty. The breakwater would be oriented at approximately 45 degrees west of true north. This alternative would attempt to reduce the energy of the incident waves reaching the north jetty and therefore also minimize the amount of incoming and reflected wave energy assaulting Camp Ellis Beach. The breakwater was specifically sited to intercept a commonly present wave train that passes between Eagle and Ram Islands, as illustrated in the existing conditions evaluation and presented in detail in Chapter 11.0.

Figure 10-11. Alternative 11: Seaward location of offshore breakwater.

10.2.15 Alternative 11a: Offshore Breakwater, Inshore Location

This alternative (Figure 10-12) would consist of the construction of a breakwater located offshore of Camp Ellis Beach and detached from the existing northern jetty. This alternative varies from alternative 11 in the location and orientation of the breakwater. The breakwater would be 285 m (935 ft) in length and set in approximately 5.5 m (18 ft) of water depth, relative to MHW. The breakwater would be located approximately 670 m (2,200 ft) from the shoreline, with the southern end of the breakwater located approximately 600 m (1,968 ft) north from segment 1 of the northern jetty. The breakwater would be oriented at approximately 20 degrees west of true north. This alternative would attempt to reduce the incident waves reaching the shoreline, as well as a portion of the reflected wave energy advancing along the northern jetty.

10.2.16 Alternative 11b: Offshore Breakwater, Intermediate Location

This alternative (Figure 10-13) would consist of the construction of a breakwater located offshore of Camp Ellis Beach and detached from the existing northern jetty. This alternative places the breakwater at an intermediate water depth between the positions of alternatives 11 and 11a. . The breakwater would be 285 m (935 ft) in length and set in approximately 7 m (23 ft) of water depth, relative to MHW. The breakwater would be located approximately 1125 m (3,690 ft) from the shoreline, with the southern end of the breakwater located approximately 630 m (2,067 ft) from segment 2 of the northern jetty. The breakwater would be oriented at approximately 35 degrees west of true north.

Figure 10-12. Alternative 11a: Inshore location of offshore breakwater.

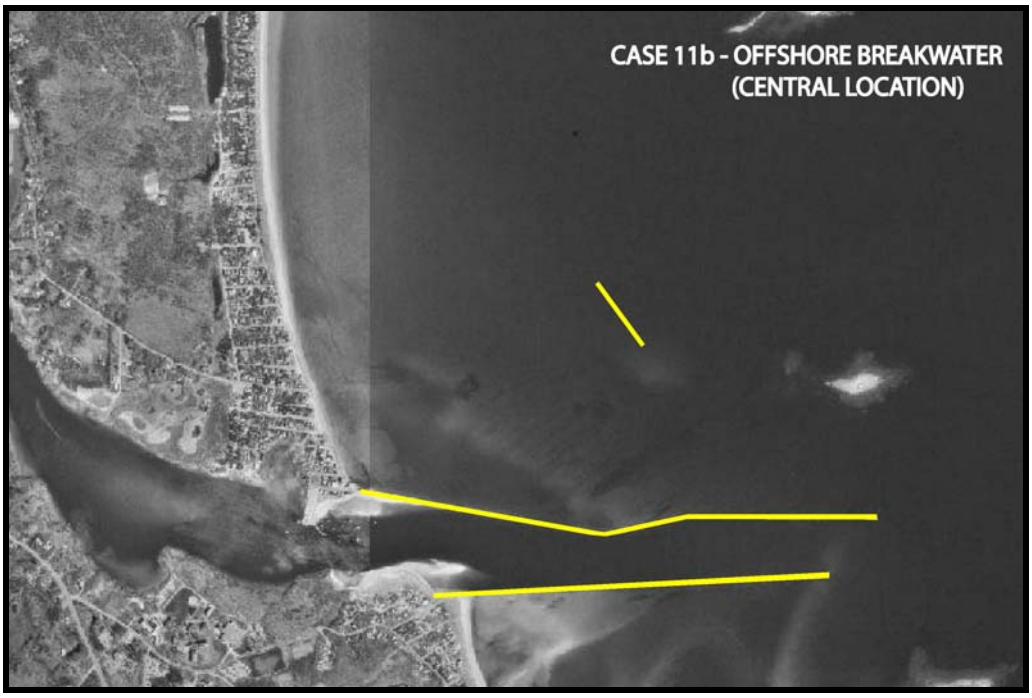

Figure 10-13. Alternative 11b: Central location of offshore breakwater.

10.2.17 Alternative 12: Alternative 11a and Seaward Location of 500-ft Spur Jetty

This alternative (Figure 10-14) would be a combination of the breakwater configuration presented in alternative 11a and a 152 m (500 ft) spur jetty positioned 610 m (2,000 ft) from shore (approximately two-thirds along segment 1). The gap between the breakwater and the northern end of the spur jetty is 490 m (1,607 ft). This alternative would attempt to combine the beneficial effects on wave energy reduction of both the spur jetty and the breakwater. The breakwater is intended to reduce the incident wave energy reaching the shoreline, as well as reducing a portion of the reflected wave energy advancing from the northern jetty. The spur jetty is intended to reduce the reflected wave energy, intercept Mach-Stem effects, and help retain sediment that now advances seaward along the existing northern jetty.

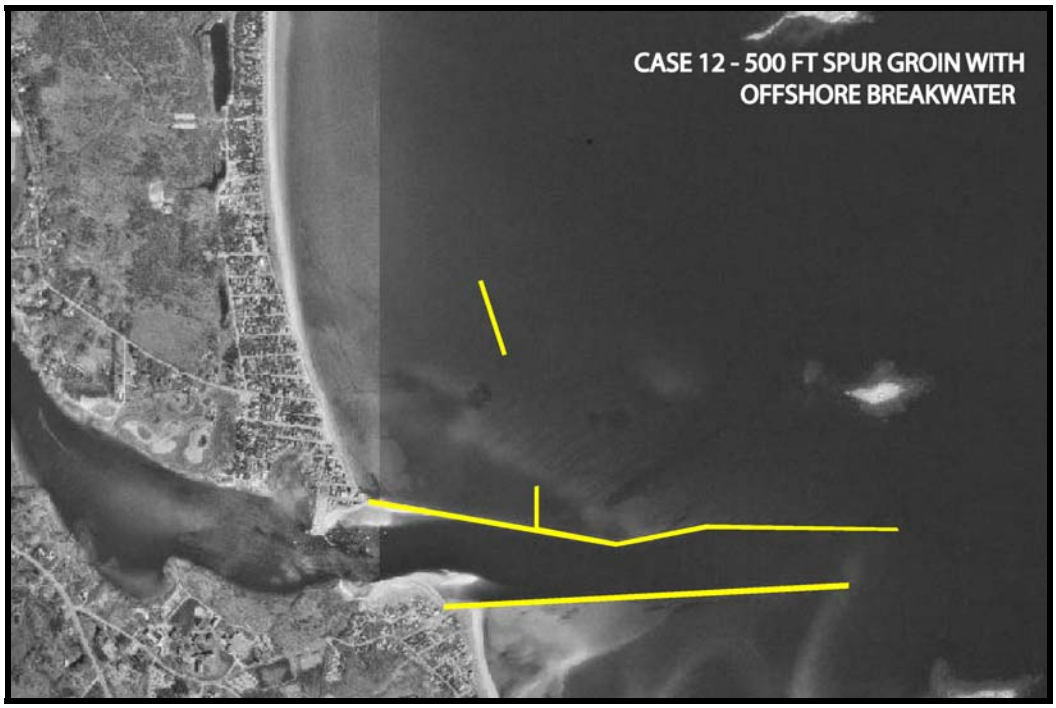

Figure 10-14. Alternative 12: Combined breakwater and 500 foot spur jetty at seaward location.

10.2.18 Alternative 13: Comb Configuration of Spur Jetties

In an effort to cut down on the reflected wave energy and Mach-Stem effect, a configuration of a series of smaller spur jetties was considered. This alternative (Figure 10-15) would consist of 19 small spur jetties attached to the northern jetty. Each spur jetty would be approximately 15 m (50 ft) in length and extend perpendicular to the existing northern jetty. The spurs would be spaced approximately 60 m (200 ft) apart and would extend along segments 1 and 2 of the northern jetty. This alternative would attempt to prevent Mach Stem effects and break the reflected wave energy.

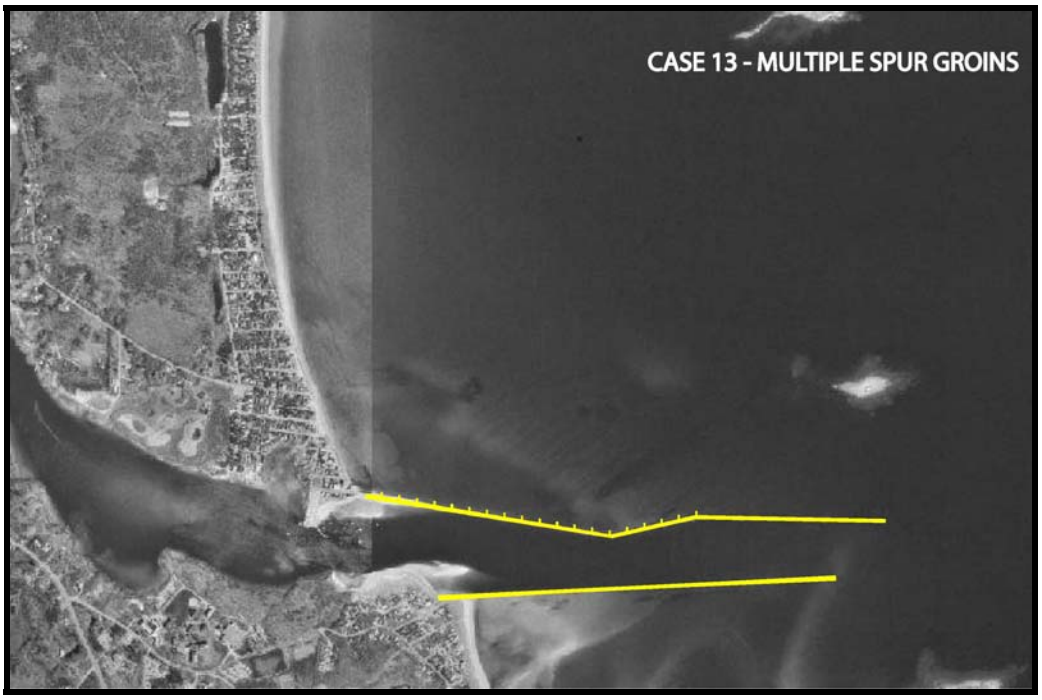

Figure 10-15. Alternative 13: Multiple spur jetties in a comb configuration along northern jetty.

10.2.19 Alternative 14: Offshore Borrow Pit

This alternative (Figure 10-16) would consist of the dredging of an offshore borrow pit in a strategic location offshore of Camp Ellis Beach. The location of the proposed borrow site was sited to intercept the primary wave train advancing between Eagle and Ram Islands. The dredged region would be deepened by approximately 2.5 m (8.2 ft) to a maximum depth of 13.8 m (45 ft) relative to MHW. The dredged material would be used for nourishment of Camp Ellis Beach. This alternative would attempt to diverge wave energy from the Camp Ellis Beach area, while also serving to provide nourishment material. A borrow site, with increased water depth, would create a zone of decreased wave energy behind the sand borrow site and increased energy in areas adjacent to the borrow site. Waves propagating over the borrow site are deflected outward, the opposite of what occurs when waves converge over a shoal.

10.2.20 Alternative 15: Alternative 3 with Angled Orientation

Although various orientations of spur jetties were simulated in the optimization approach, this alternative (Figure 10-17) focused on a specific angled orientation of a spur jetty. The orientation was identified in the existing conditions assessment and was positioned to intercept a primary wave train impacting the northern jetty and Camp Ellis region (see Chapter 11.0). This alternative would consist of the construction of a 230 m (750 ft) spur jetty that would be attached to the existing northern jetty. The spur would be located approximately 610 m (2,000 ft) from the shoreline (approximately two-thirds the length of segment 1). The spur would be oriented approximately 10 degrees west of north. This alternative would attempt to intercept the reflected wave energy, break a portion of the

incident wave energy, and block Mach-Stem wave effects transferring energy along the structure. The angled orientation would be assessed for comparison to other spur jetty alternatives.

Figure 10-16. Alternative 14: Offshore borrow pit.

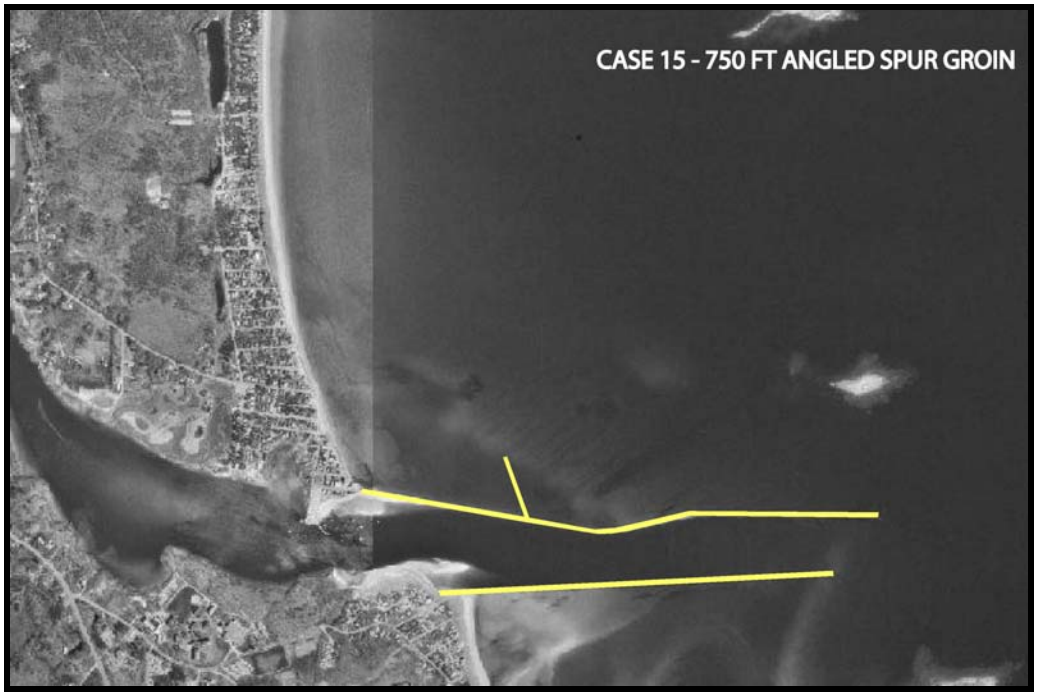

Figure 10-17. Alternative 15: 750 foot angled spur groin.

10.2.21 Alternative 16: Northern Jetty Roughening

This alternative would consist of roughening the northern jetty by repositioning existing armor units in a loose configuration and/or "points out" orientation. Currently, a significant portion of the northern jetty is comprised of well-placed armor units forming a relatively smooth face and increasing its reflectivity. This alternative would attempt to reduce the reflectivity of the structure through roughening of the northern face of the jetty.

10.2.22 Alternative 17: Submerged Breakwater / Rock Outcrop

This alternative would consist of the construction of a submerged detached breakwater, and/or random placement of rocks to form an offshore shoal/outcrop. This is the submerged version of alternative 11. The submerged feature would have a crest elevation equivalent to MTL and would be approximately 280 m (920 ft) in length and located in approximately 10 m (33 ft) water depth (MHW). The structure/feature would be located approximately 1450 m (4,760 ft) from the shoreline and approximately 600 m (183 ft) north of segment 3. The crest width of the submerged breakwater was set to 3 m (10 ft). This alternative would attempt to mimic the protection afforded by typical rock outcrops and submerged features throughout the coastal region of Maine. Therefore, waves would break at this structure prior to reaching the northern jetty and/or Camp Ellis Beach.

10.2.23 Alternative 18: Alternative 11a and Inshore Location of 500-ft Spur Jetty

This alternative (Figure 10-18) would be a combination of the breakwater configuration presented in alternative 11a and a 152 m (500 ft) spur jetty positioned 450 m (1,475 ft) from shore (approximately one-half along the length of segment 1). The gap between the breakwater and the northern end of the spur jetty is 450 m (1,475 ft). This alternative, similar to alternative 12, would attempt to combine the beneficial effects on wave energy reduction of both the spur jetty and the breakwater. The breakwater is intended to reduce the incident wave energy reaching the shoreline, as well as a portion of the reflected wave energy advancing from the northern jetty. The spur jetty is intended to reduce the reflected wave energy, intercept Mach-Stem effects, and help contain sediment from advancing seaward along the existing northern jetty. This alternative represents the second configuration of a combined breakwater and spur jetty.

10.2.24 Alternative 19: 750 foot Spur Jetty, Jetty Roughening, and Jetty Removal

This alternative (Figure 10-19) would be a combination of 230 m (750 ft) spur jetty attached to the existing northern jetty, roughening of the existing northern jetty, and removal of the seaward end of the existing northern jetty. The spur jetty would be located 450 m (1,475 ft) from shore. This alternative would attempt to combine a number of potential alternatives to develop cumulative reductions of wave energy.

10.2.25 Alternative 20 and 21: Alternative 11a with Estimated Salient Formations

Alternative 20 and 21 do not represent specific alternatives, but rather are a subset of expected shoreline response simulations in relation to Alternative 11a. Estimates of salient formation (discussed in detail in Chapter 12.0) are developed to determine the impact of salient formations on wave energy. A salient is a coastal formation of beach

material developed by wave refraction, wave diffraction, and longshore drift producing a bulge in the coastline behind an offshore island of breakwater. If the salient connects to the offshore feature/structure, it is termed a tombolo. Figure 10-20 presents an example of the expected shoreline response to Alternative 11a. These alternatives (20 and 21) helped to gauge the wave changes occurring due to expected shoreline response.

Figure 10-18. Alternative 18: Combined breakwater and 500 foot spur jetty at inshore location.

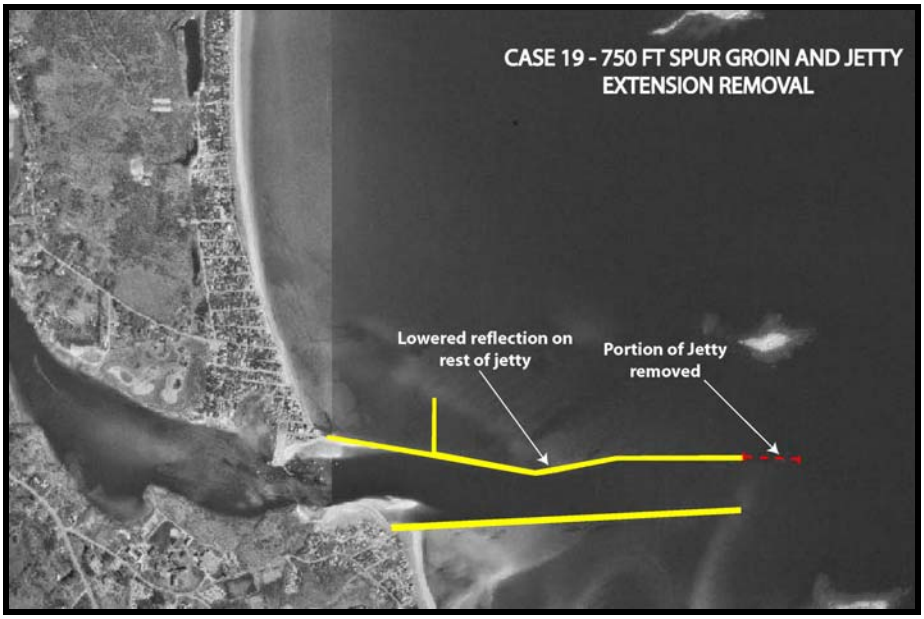

Figure 10-19. Alternative 19: Combined breakwater and 500 foot spur jetty at inshore location.

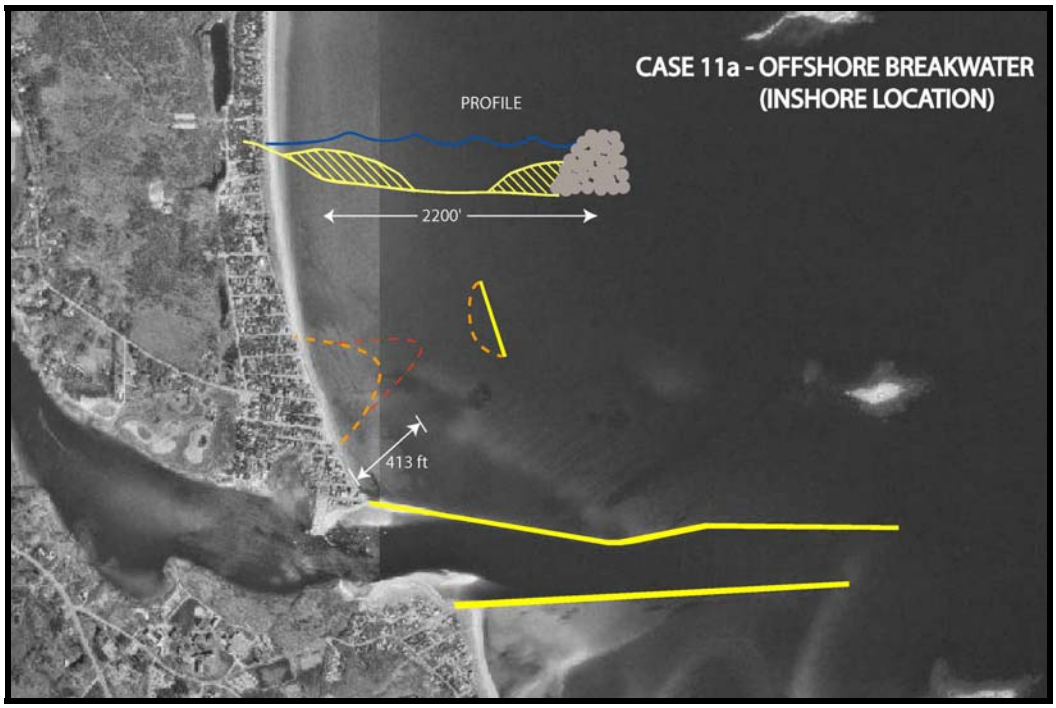

Figure 10-20. Expected shoreline response in salient growth behind offshore breakwater of Alternative 11a (broken red line) and Alternative 18 (broken orange line).

10.2.26 Alternative 22: Segmented Breakwater Configuration 1

The following alternatives (22 – 26) comprise a series of segmented breakwater configurations designed in response to initial geotechnical investigations that identified the soil types (foundation conditions) underlying the seabed in the study area. Of particular concern was the presence of soft clay that underlies the seabed in several areas. Breakwater segments/structures for these alternatives were placed in nearshore locations thought to have adequate soil/sediment bearing capacity. This alternative (Figure 10-21) would consist of 2 detached breakwater segments and a spur jetty. The spur jetty is 230 m (750 ft) in length, 450 m (1,475 ft) from shore, and extends perpendicular to the existing northern jetty. Table 10-4 presents the dimensional details, including structure length, orientation (referenced from 0 degrees equivalent to north), distance from shore, gap distance from adjacent southern structure, and approximate depth, associated with each of the segmented breakwaters. This alternative would attempt to significantly reduce wave energy in the nearshore zone, to impede the reflected wave energy from the existing northern jetty, to extend beach nourishment life, and to produce salient formations that do not create a significant interruption in the littoral transport.

Table 10-4. Segmented breakwater dimensional parameters for Alternative 22.

Breakwater	Approx. Depth (MHW, m)	Length (m)	Distance from Shore (m)	Orientation (from 0° N)	Gap distance from adjacent south structure (m)
1	4	114	330	-20 degrees	25
2	4.5	114	330	-20 degrees	160

Figure 10-21. Alternative 22: Segmented breakwater and spur jetty configuration 1.

10.2.27 Alternative 23: Segmented Breakwater Configuration 2

This alternative (Figure 10-22) would consist of 3 detached breakwater segments and a spur jetty. The spur jetty is 152 m (500 ft) in length, 450 m (1,475 ft) from shore, and extends perpendicular to the existing northern jetty. Table 10-5 presents the dimensional details, including structure length, orientation (referenced from 0 degrees equivalent to north), distance from shore, gap distance from adjacent southern structure, and approximate depth, associated with each of the segmented breakwaters. This alternative would attempt to significantly reduce wave energy in the nearshore zone, to impede the reflected wave energy from the existing northern jetty, to extend beach nourishment life, and to produce salient formations that do not create a significant interruption in the littoral transport.

Table 10-5. Segmented breakwater dimensional parameters for Alternative 23.

Breakwater	Approx. Depth (MHW, m)	Length (m)	Distance from Shore (m)	Orientation (from 0° N)	Gap distance from adjacent south structure (m)
1	4	100	355	-30 degrees	25
2	5	100	320	-27 degrees	150
3	5	100	330	-20 degrees	125

Figure 10-22. Alternative 23: Segmented breakwater and spur jetty configuration 2.

10.2.28 Alternative 24: Segmented Breakwater Configuration 3

This alternative (Figure 10-23) would consist of 4 detached breakwater segments and a spur jetty. The spur jetty is 152 m (750 ft) in length, 450 m (1,475 ft) from shore, and extends perpendicular to the existing northern jetty. Table 10-6 presents the dimensional details, including structure length, orientation (referenced from 0 degrees equivalent to north), distance from shore, gap distance from adjacent southern structure, and approximate depth, associated with each of the segmented breakwaters. This alternative would attempt to significantly reduce wave energy in the nearshore zone, to impede the reflected wave energy from the existing northern jetty, to extend beach nourishment life, and to produce salient formations that do not create a significant interruption in the littoral transport.

Table 10-6. Segmented breakwater dimensional parameters for Alternative 24.

Breakwater	Approx. Depth (MHW, m)	Length (m)	Distance from Shore (m)	Orientation (from 0° N)	Gap distance from adjacent south structure (m)
1	4	100	355	-30 degrees	25
2	5	100	320	-27 degrees	150
3	5	100	330	-20 degrees	125
4	3.75	100	130	-20 degrees	195

Figure 10-23. Alternative 24: Segmented breakwater and spur jetty configuration 3.

10.2.29 Alternative 25: Segmented Breakwater Configuration 4

This alternative (Figure 10-24) would consist of 3 detached breakwater segments and a spur jetty. The spur jetty is 152 m (500 ft) in length, 300 m (985 ft) from shore, and extends perpendicular to the existing northern jetty. Table 10-7 presents the dimensional details, including structure length, orientation (referenced from 0 degrees equivalent to north), distance from shore, gap distance from adjacent southern structure, and approximate depth, associated with each of the segmented breakwaters. This alternative would attempt to significantly reduce wave energy in the nearshore zone, to impede the reflected wave energy from the existing northern jetty, to extend beach nourishment life,

and to produce salient formations that do not create a significant interruption in the littoral transport.

Table 10-7. Segmented breakwater dimensional parameters for Alternative 25.

Breakwater	Approx. Depth (MHW, m)	Length (m)	Distance from Shore (m)	Orientation (from 0° N)	Gap distance from adjacent south structure end point to end point (m)
1	4.75	125	265	-25 degrees	110
2	5	120	280	-22 degrees	105
3	3.75	100	130	-20 degrees	210

Figure 10-24. Alternative 25: Segmented breakwater and spur jetty configuration 4.

10.2.30 Alternative 26: Segmented Breakwater Configuration 5

This alternative (Figure 10-25) would consist of 4 detached breakwater segments and a spur jetty. The spur jetty is 152 m (500 ft) in length, 450 m (1,475 ft) from shore, and extends perpendicular to the existing northern jetty. Table 10-8 presents the dimensional details, including structure length, orientation (referenced from 0 degrees equivalent to north), distance from shore, gap distance from adjacent southern structure, and

approximate depth, associated with each of the segmented breakwaters. This alternative would attempt to significantly reduce wave energy in the nearshore zone, to impede the reflected wave energy from the existing northern jetty, to extend beach nourishment life, and to produce salient formations that do not create a significant interruption in the littoral transport.

Table 10-8. Segmented breakwater dimensional parameters for Alternative 26.

Breakwater	Approx. Depth (MHW, m)	Length (m)	Distance from Shore (m)	Orientation (from 0° N)	Gap distance from adjacent south structure (m)
1	4	100	355	-30 degrees	25
2	5	100	320	-27 degrees	150
3	5	100	330	-20 degrees	125
4	3.75	100	130	-20 degrees	210

Figure 10-25. Alternative 26: Segmented breakwater and spur jetty configuration 5.

10.2.31 Alternative 25a: Segmented Breakwater Configuration 6

This alternative (Figure 10-26) would consist of 2 detached breakwater segments and a spur jetty. The spur jetty is 152 m (500 ft) in length, 300 m (985 ft) from shore, and extends perpendicular to the existing northern jetty. Table 10-9 presents the dimensional

details, including structure length, orientation (referenced from 0 degrees equivalent to north), distance from shore, gap distance from adjacent southern structure, and approximate depth, associated with each of the segmented breakwaters. This alternative would attempt to significantly reduce wave energy in the nearshore zone, to impede the reflected wave energy from the existing northern jetty, to extend beach nourishment life, and to produce salient formations that do not create a significant interruption in the littoral zone. This alternative was created to address the issue of the potential lack of suitable geologic conditions in the northern section of the proposed beach nourishment area for stable structural foundations and to alleviate potential concerns that the northernmost breakwater in Alternative 25 was too close to the shoreline.

Figure 10-26. Alternative 25A: Segmented breakwater and spur jetty configuration 4 (modified).

Table 10-9. Segmented breakwater dimensional parameters for Alternative 25A.

Breakwater	Approx. Depth (MHW,m)	Length (m)	Distance from Shore (m)	Orientation (from 0° N)	Gap distance from adjacent south structure, end point to end point (m)
1	4.75	125	265	-25 degrees	110
2	5	120	280	-25 degrees	105

10.3 Alternatives Screening Process

As part of the alternatives analysis, a process was developed to perform an initial screening of all the alternatives presented above in order to streamline the modeling and analysis evaluation, focusing on only the alternatives that were reasonably meeting the performance goals. This initial screening process focused on wave height changes and energy reduction within the local region. Potential adverse impacts to neighboring beaches, navigation, and the Camp Ellis region were also evaluated. Results of the initial screening and alternatives analysis are presented in Chapter 11.0. The alternatives that indicated the best potential for performance success were passed forward by the project team (WHG, USACE, SBIT, MGS) to a more detailed alternatives analysis and final assessment. The final screening and alternatives analysis consisted of a more detailed level of wave evaluation and assessment of the sediment transport (Chapter 12.0).

11.0 LOCAL WAVE MODELING (TASK 6A)

As discussed, the regional, transformation-scale wave model (STWAVE – Chapter 9.0) is a half-plane model, and therefore, only represents waves propagating towards the coast. Waves that may be reflected from the coastline or structures are not included. In addition, STWAVE does not account for a number of wave transformation processes that are prevalent in the vicinity of Camp Ellis Beach (e.g., diffraction, reflection, etc.). STWAVE, therefore, only represents an intermediate step in the wave modeling system and although is useful for identifying regional sediment transport trends, cannot be used for local sediment transport calculations for the Camp Ellis Beach region. Due to the limitations inherent in STWAVE, it was important to advance to a higher-resolution, phase-resolving model that embodied the reflection processes and could more accurately determine the nearshore structural interactions.

11.1 Analysis Approach

The goal of the local, nearshore wave modeling effort for Camp Ellis Beach was to simulate combined wave refraction/diffraction, wave reflection and wave dissipation by friction and breaking as well as including nonlinear amplitude dispersion. Therefore, two-dimensional spectral output from the transformation-scale (regional) model (which transformed the wave spectral energy from deep water to shallow water) was used as input into the nearshore (local) wave model. The nearshore (local) wave model, CGWAVE, is utilized to evaluate the local physical processes, (e.g., wave reflection, wave-induced currents, wave dispersion, nearshore wave refraction and diffraction, etc.), and subsequently the engineering alternatives.

11.2 Wave Model Description

The physics embodied in CGWAVE represent the state-of-the-science in our present understanding of wave prediction. CGWAVE was developed at the University of Maine for the U.S. Army Corps of Engineers. The model is based on the mild-slope equation with the open boundary condition treated by the classical super-element method and a parabolic approximation (Xu, Panchang and Demirbilek 1996). An iterative procedure (conjugate gradient method) is used to solve the discretized equations.

The two-dimensional elliptic mild-slope wave equation may be written as:

$$\nabla \bullet \left(CC_g \nabla \hat{\eta}\right) + \frac{C_g}{C}\sigma^2 \hat{\eta} = 0 \quad \text{..... (11-1)}$$

where:

$\hat{\eta}$=complex surface elevation function, from which the wave height can be determined

σ=wave frequency under consideration (radians/second)

C=phase velovity= σ/k

C_g=group velocity =$\partial\sigma/\partial k$=nC

$$n = \frac{1}{2}\left(1 + \frac{2kd}{\sinh(2kd)}\right) \quad \text{(11-2)}$$

k=wave number (2π/L), related to the local depth d through the linear dispersion relation:

$$\sigma^2 = (gk)\tanh(kd) \quad \text{(11-3)}$$

Equation 11-1 simulates wave refraction, diffraction and reflection in coastal domains of arbitrary shape. The mild slope equation can be modified to account for the effects of frictional dissipation and wave breaking:

$$\nabla \bullet \left(CC_g \nabla \hat{\eta}\right) + \left(\frac{C_g}{C}\sigma^2 + i\sigma w + iC_g \sigma\gamma\right)\hat{\eta} = 0 \quad \text{(11-4)}$$

where *w* is a friction factor and γ is the wave breaking parameter. The frictional damping factor is found following Dalrymple et al. (1984):

$$w = \left(\frac{2n\sigma}{k}\right)\left(\frac{2f_r}{3\pi}\frac{ak^2}{(2kd + \sinh(2kd))\sinh(kd)}\right) \quad \text{(11-5)}$$

where a is the wave amplitude and f_r is a friction coefficient provided by the user. The wave breaking parameter is found by using the following formulation:

$$\gamma = \frac{\chi}{d}\left(1 - \frac{\Gamma^2 d^2}{4a^2}\right) \quad \text{(11-6)}$$

where χ is a value supplied by the user and Γ is an empirical constant of 0.4.

It is also possible to account for non-linear wave mechanics in CGWAVE. The mild-slope equation is modified by using a non-linear dispersion relation instead of the linear relation (Equation 11-3):

$$\sigma^2 = gk\left\{1 + (ka)^2 F_1 \tanh^5(kd)\tanh(kd + kaF_2)\right\} \quad \text{(11-7)}$$

where:

$$F_1 = \frac{\cosh(4kd) - 2\tanh^2(kd)}{8\sinh^4(kd)} \quad \text{(11-8)}$$

$$F_2 = \left(\frac{kd}{\sinh(kd)}\right)^4 \quad \text{(11-9)}$$

To account for the model domain boundaries that are not open water, the model assumes a reflective boundary condition given by:

$$\frac{\partial \hat{\eta}}{\partial n} = \alpha \hat{\eta} \quad \text{(11-10)}$$

where η is a coordinate normal to boundary and α is a complex coefficient that is generally represented as a function of the reflection coefficient, K_r:

$$\alpha = ik\frac{1 - K_r}{1 + K_r} \quad \text{(11-11)}$$

The reflection coefficient is supplied by the user for each section of the domain boundary.

Along open boundaries where outgoing waves must propagate to infinity, the Sommerfeld radiation condition is applied:

$$\lim_{kr\to\infty} \sqrt{kr}\left(\frac{\partial}{\partial r} - ik\right)\hat{\eta}_s = 0 \quad \text{(11-12)}$$

where $\hat{\eta}_s$ is the scattering wave potential. The solution of the Sommerfeld radiation condition that satisfies the mild-slope equation includes Hankel functions of the first kind, $H_n(kr)$:

$$\hat{\eta}_s = \sum_{n=0}^{\infty} H_n(kr)\left(\alpha_n \cos(n\theta) + \beta_n \sin(n\theta)\right) \quad \text{(11-13)}$$

The scattering wave potential used in solution (Equation 11-13) requires that the exterior domain have a constant depth. Xu, Panchang and Demirbilek (1996) developed an alternative scheme in dealing with the open boundary problem using a parabolic approximation. The parabolic approximation is used in the CGWAVE model:

$$\frac{\partial \hat{\eta}_s}{\partial r} + p\hat{\eta}_s + q\frac{\partial \hat{\eta}_s^2}{\partial \theta^2} = 0 \quad \text{..... (11-14)}$$

where

$$p = \frac{k^2 r^2 + k_0^2 r^2 + ik_0 r + \frac{1}{4}}{2ik_0 r^2} \text{ and } q = \frac{1}{2ik_0 r^2} \quad \text{..... (11-15)}$$

With k_0 being the wave number corresponding to the averaged water depth along the open boundary, Γ. The mild-slope equation is used within the model domain, Ω (Figure 11-1).

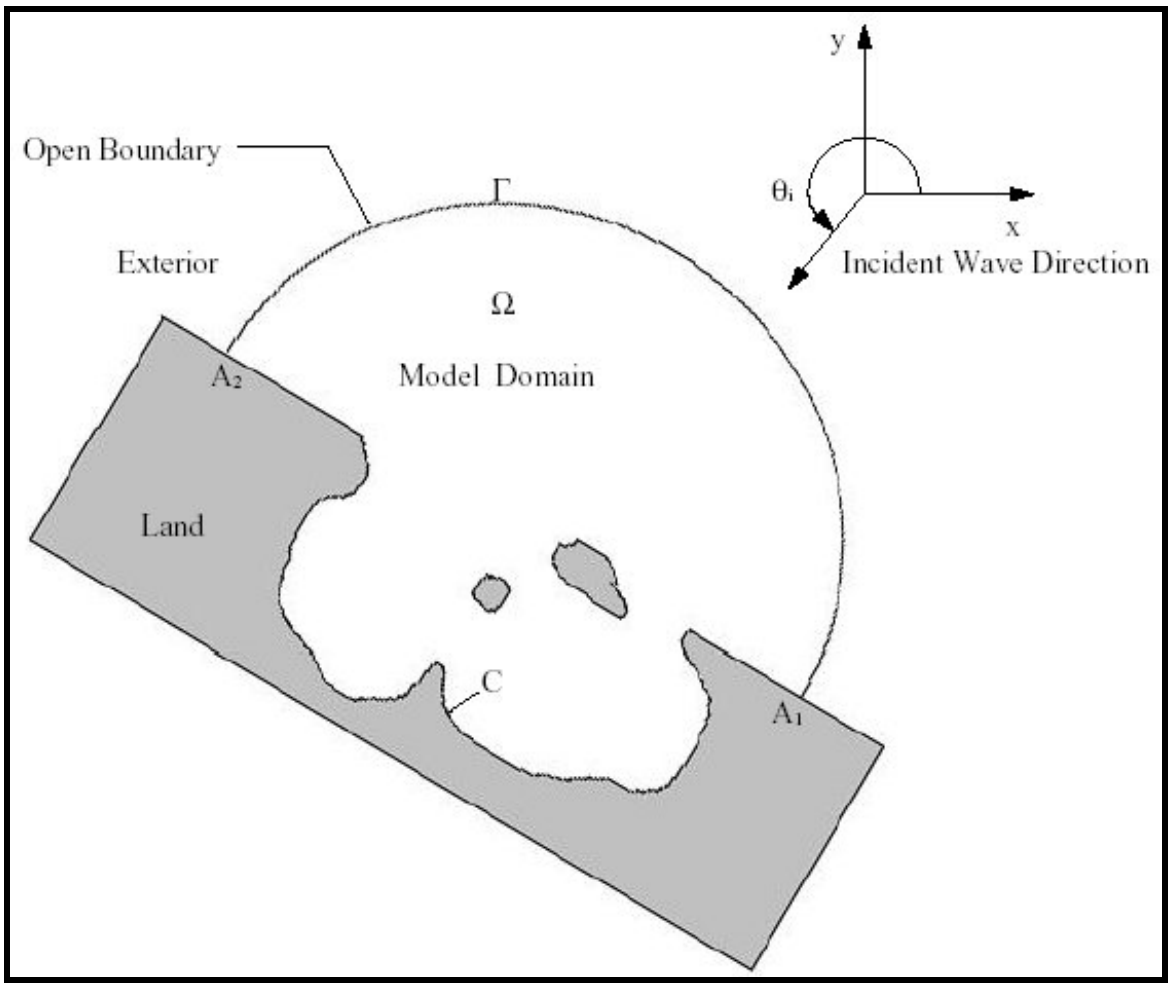

Figure 11-1. Definition sketch of the CGWAVE model domain (Demirbilek and Panchang, 1998).

11.3 Grid Generation

CGWAVE is solved using a finite-element method. The finite-element method is used to model coastal phenomena in a region with complex shapes (the coastal area offshore of Saco Bay certainly represents a significantly complex region). Figure 11-2 presents the modeling grid used for the nearshore (local scale) wave modeling consisting of 262,940 nodes and 523,555 elements. The total model domain has dimensions of approximately 3 nautical miles by 3 nautical miles. The mesh is comprised of triangular elements. The nodal spacing within the mesh is dependent upon the wavelength. In the nearshore zone, resolution is approximately 10 m (32.8 ft) or about 8 nodes per wavelength. Figure 11-3 contains a zoomed in view of the mesh around the navigational structures and Ram Island, illustrating the density of the nodes and elements. The radiation domain, as shown in Figure 11-2, is a half circle and the waves propagate from the outer edge towards the shoreline.

The bathymetric data sources used in the generation of the model domain nodal depths came from three (3) sources (Chapter 4.0). These included, (1) the high spatial resolution bathymetric survey collected in 2003 north of the navigational structures to just south of Ram Island, (2) the LIDAR data collected in 1999, and (3) National Geophysical Data Center's Geophysical Data Systems (GEODAS) hydrographic surveys. Three hydrographic surveys from the GEODAS data were incorporated with the primary data set to generate the nodal depths within the modeling domain.

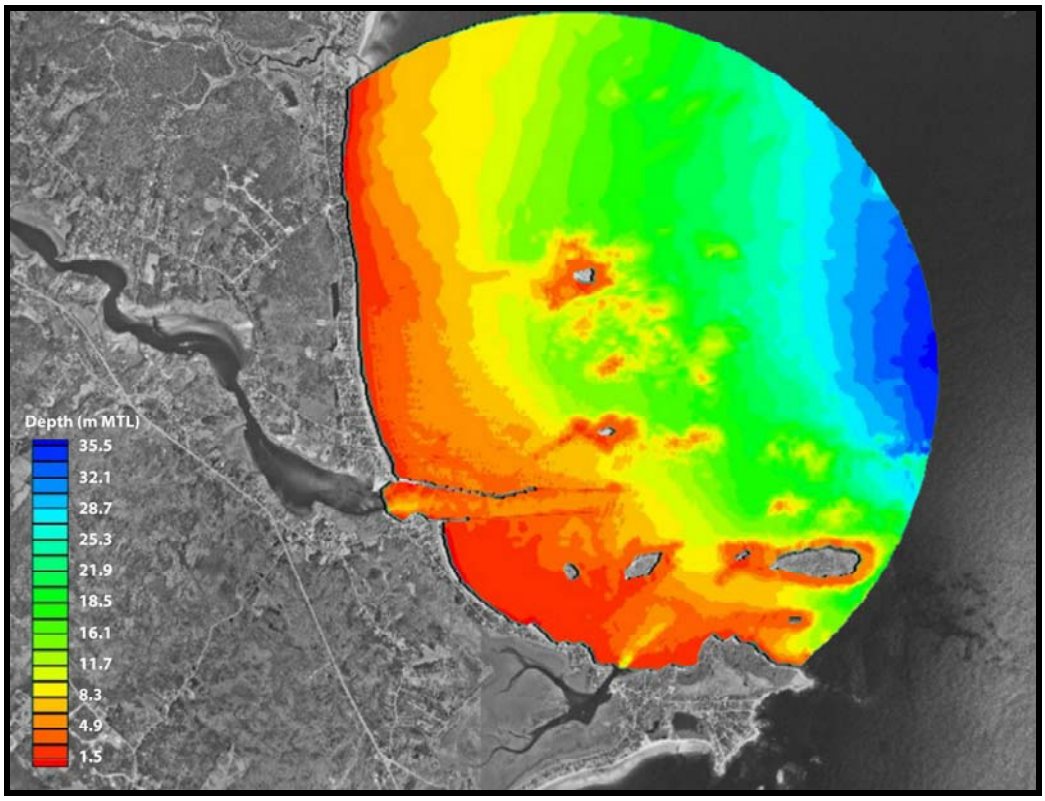

Figure 11-2. CGWAVE model domain for existing conditions. Depths are presented relative to Mean Tide Level (MTL).

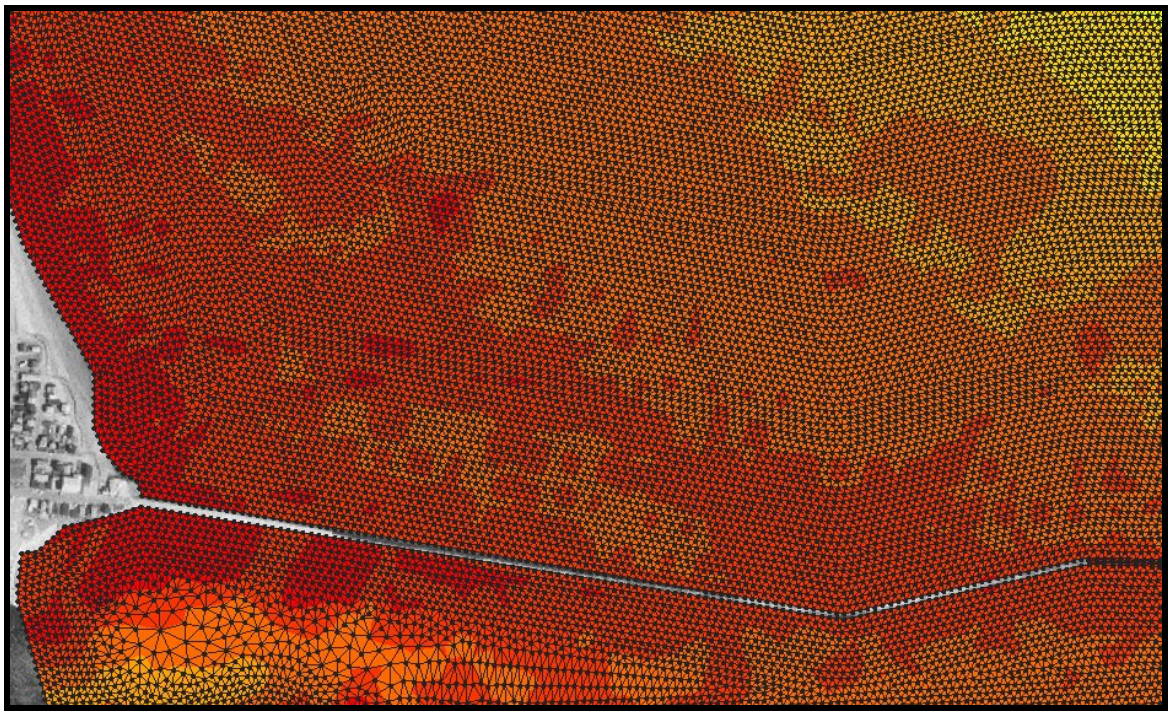

Figure 11-3. Detail of mesh density within the vicinity of the northern jetty. Shallower areas require closer nodal spacing and finer resolution.

11.4 Wave Input Spectra

The nearshore (local) wave model was simulated using the same set of conditions developed for the transformation-scale (regional) modeling (as presented in section 9.4.2). Spectral boundary conditions are specified along the offshore radiating boundary using spectral results from STWAVE in order to calibrate and verify the nearshore (local) wave model, as well as all average annual, directional approach simulations and storm events. The section explains how the spectral information is passed from the transformation-scale (regional) wave model to the nearshore (local) wave model.

CGWAVE does not allow for direct input of a complete wave spectrum; however, spectral input can be simulated through a combination of multiple directional/frequency paired components. Therefore, the two-dimensional wave spectra specified at the offshore boundary was assembled based on the output of the regional model extracted at that same location. These spectra matched the observed data reasonably well, as discussed in section 9.5. As the number of spectral wave components increases, the more resolved the wave spectra, and potentially more accurate the wave results. However, a single direction/frequency pair requires approximately 8-12 hours of simulation time, so each wave climate simulation requires careful selection of the spectral components. As such, selection of the components for each scenario (e.g. quantity, directions, frequencies, etc.) is a key aspect of accurate spectral representation.

Figure 11-4 illustrates the methodology applied to transfer the wave spectra from the regional (transformation-scale) wave model to local (nearshore) wave model, using the

Perfect Storm simulation as an example. For each simulated case, the STWAVE (transformation-scale) spectrum was output at the boundary of the nearshore (local) wave model. The spectra were plotted as a two-dimensional directional spectrum to determine the peak directions and secondary peaks, to identify the frequency spectrum, and evaluate the energy density distribution. In essence, this is simply a course discretization of the input spectra. The upper left hand and lower right hand panels in Figure 11-4 show the directional and frequency spectra output from the transformation-scale (regional) model, respectively. The black cross markers on the upper left hand panel indicate the directional components selected for the directional distribution. The upper right hand panel shows the full two-dimensional spectrum generated from the directional and frequency components. Once the distinct directional/frequency pairs were identified, the directional spectrum was plotted to determine the total energy from that spectrum and the peak wave frequency (Figure 11-5). The associated wave height at the location of the wave spectrum (offshore boundary of the nearshore model) was used as the input wave height. The wave height was proportioned across the directional bands based on the percentage of energy present in each band. Therefore, the energy is conserved within the overall spectra, and is appropriately distributed amongst the directional spread and frequency spectrum. The Perfect Storm example of the wave spectrum reconstruction illustrated in Figures 11-4 and 11-5 produce the associated wave parameters presented in Table 11-1. This methodology was applied for all cases, including calibration and verification time periods, average annual directional approach bins, and storm events.

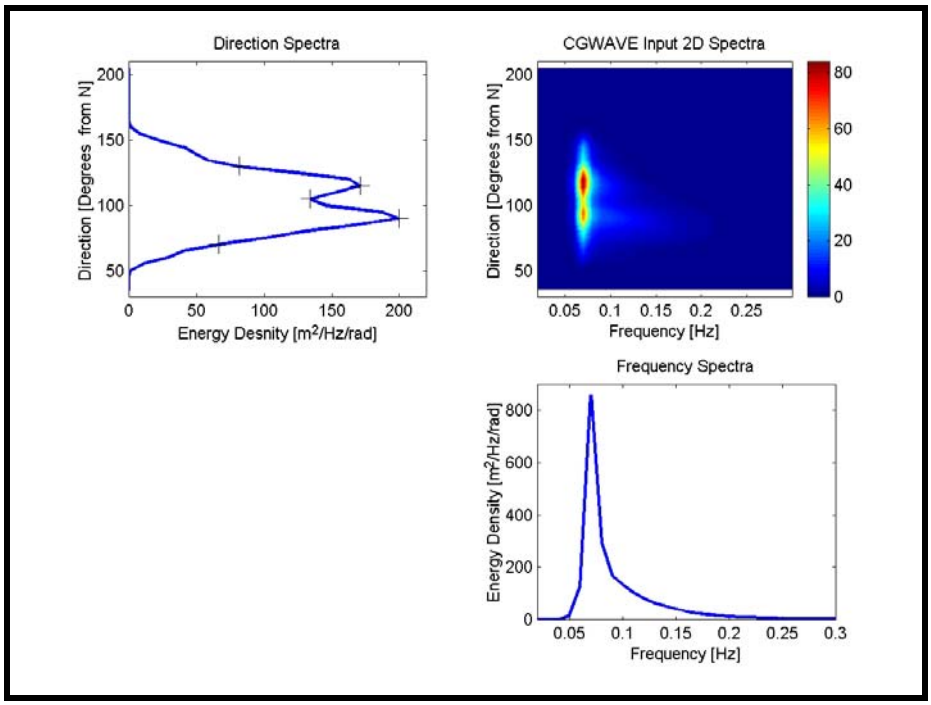

Figure 11-4. Two-dimensional spectral output (lower right hand panel and upper left hand panel) from STWAVE (regional model) and associated input (upper right hand panel) into CGWAVE (nearshore model) for the Perfect Storm scenario. Black cross markers on the directional spectrum indicate locations of selected directional components.

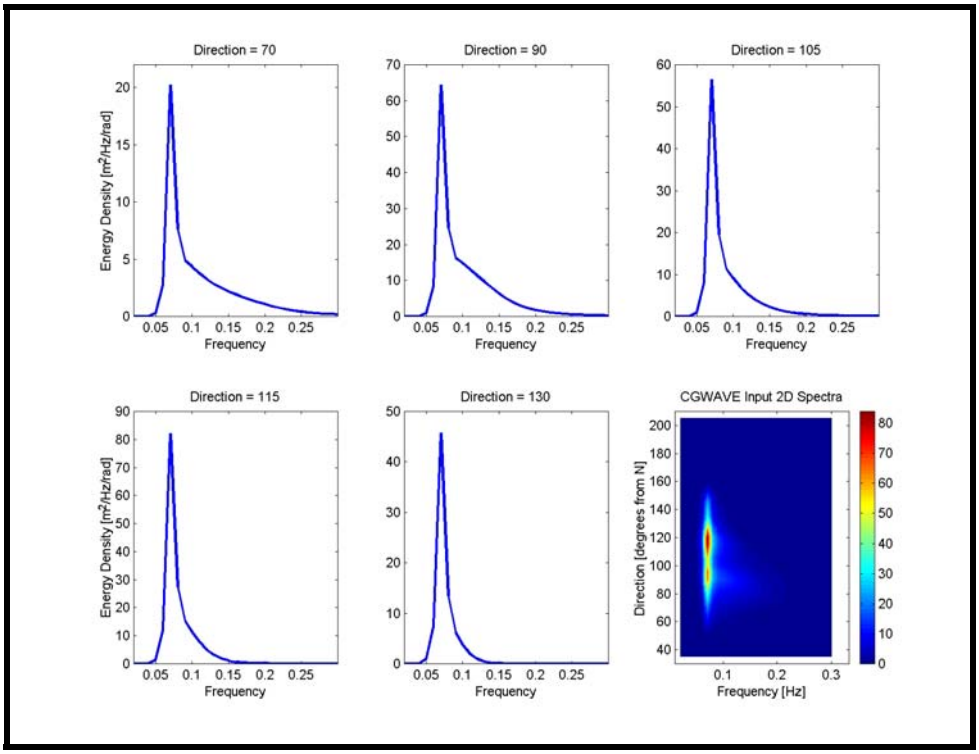

Figure 11-5. Specific spectral components used to generate two-dimensional spectra input for the local, nearshore wave model. Spectral components were developed from the output of the regional, transformation-scale model.

Table 11-1. Spectral components used as input to CGWAVE for Perfect Storm scenario.

Spectral Component	Wave Direction (0° = True North)	Wave Height (m)	Wave Period (seconds)
1	70	1.62 (5.3 ft)	14.29
2	90	2.58 (8.5 ft)	14.29
3	105	1.06 (3.5 ft)	11.11
4	115	1.20 (3.9 ft)	11.11
5	130	0.42 1.2 ft)	11.11

11.5 Model Calibration and Verification

Prior to simulation of the existing conditions scenarios (average annual directional approaches and high energy events), the nearshore model was calibrated and verified to the observed wave data collected during March-May 2003 (Chapter 7.0). Although the entire deployment time period was simulated in the generation scale and transformation-scale models, due to the significant computational time restrictions present in the nearshore (local) wave modeling, the entire deployment time period could not be simulated. Therefore, specific time periods were selected and compared to the observed wave data. The selected time periods represented the passage of higher energy wave periods (relative to the deployment period). These time periods included April 4, 2003 at

0700 hours and April 27, 2003 at 0400 hours. The spectral output from the transformation-scale (regional) model was broken into spectral components following the same methodology presented in section 11.2. Table 11-2 and 11-3 present the spectral components for the April 4 and April 27 time periods, respectively. Figures 11-6 and 11-7 illustrate the spectral components (shown in frequency domain) selected and associated two-dimension input spectra for the April 4 and April 27 time periods, respectively.

Table 11-2. Spectral wave components used to simulate April 4, 2003 at 0700 hours.

Spectral Component	Wave Direction (0° = True North)	Wave Height (m)	Wave Period (seconds)
1	110.07	0.08 (0.3 ft)	7.69
2	100.94	0.34 (1.1 ft)	6.76
3	94.52	0.70 (2.3 ft)	5.99
4	88.28	0.20 (0.7 ft)	5.41
5	84.91	0.14 (0.5 ft)	4.90

Table 11-3. Spectral wave components used to simulate April 27, 2003 at 0400 hours.

Spectral Component	Wave Direction (0° = True North)	Wave Height (m)	Wave Period (seconds)
1	111.76	0.82 (2.7 ft)	6.76
2	114.42	0.66 (2.2 ft)	7.69
3	117.71	0.22 (0.7 ft)	9.01
4	95	0.50 (1.6 ft)	5.99

In order to get reasonable agreement between the observed and modeled results, coefficients within the model were adjusted through an iterative process. This consisted of adjustment to the wave breaking coefficient, the frictional coefficients, and reflection coefficients (as presented in section 11.2) within a reasonable range of bounds, until agreement was achieved between the observed and modeled data. The default wave breaking coefficient is 0.15, but a value of 0.17 was used for the Camp Ellis Beach model domain. The frictional coefficient was set at 0.05, to represent bottom friction within the model domain. A 0.05 value is consistent with existing Manning coefficients presented in literature. The wave reflection coefficient was varied for various boundaries within the model (e.g., structures, shoreline, islands, etc.). The reflection coefficient for the offshore islands, primarily rocky outcrops, was set to 0.25 and to 0.6-0.8 for various portions of the structures, which consist of well-placed smooth faced armor units and are highly reflective. The shoreline was set to fully absorbing (i.e., reflection coefficient of 0). All the coefficients were varied during the calibration process, with the values presented above, selected as the final coefficients based on comparisons to the observed wave data. The model was also applied using non-linear interactions, which was a critical component of the overall model calibration process. Without the non-linear factors, the

model was unable to resolve many of the complex wave interaction in the nearshore region of Camp Ellis Beach (e.g., intersection of incident and reflected wave trains).

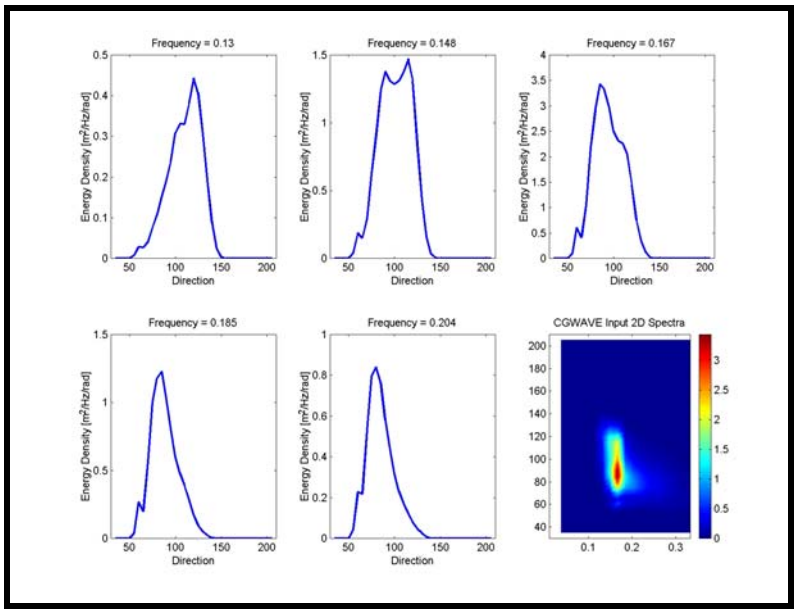

Figure 11-6. Specific spectral components used to generate two-dimensional spectra input for the calibration time period of April 4, 2003 at 0700 hours. Spectral components were developed from the output of the regional, transformation-scale model.

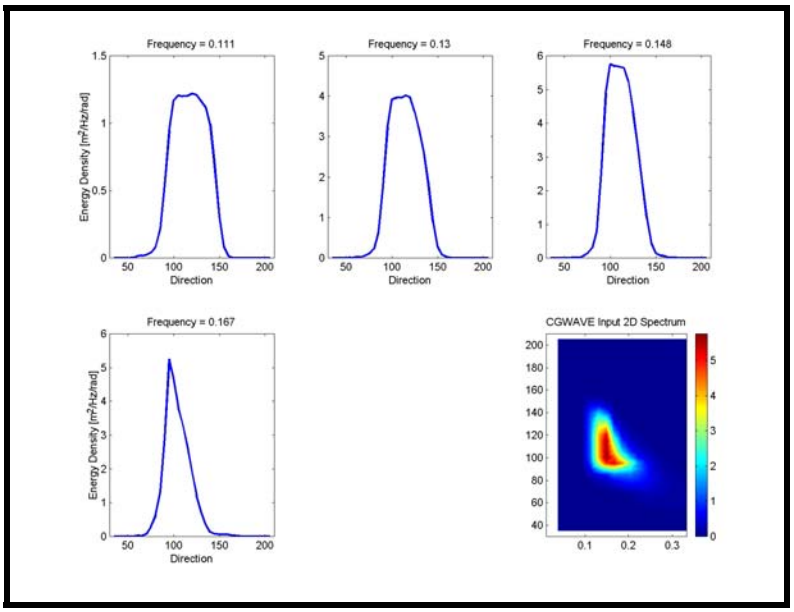

Figure 11-7. Specific spectral components used to generate two-dimensional spectra input for the calibration time period of April 27, 2003 at 0400 hours. Spectral components were developed from the output of the regional, transformation-scale model.

Due to the high resolution of the model domain, similar calibration techniques to those presented in Briggs et al. (2003) were used to calibrate and verify the CGWAVE model. This technique consists of averaging model results within a 30 m (100 ft) box centered on the offshore and nearshore ADCP locations to allow for location anomalies and the contouring algorithm in the model software (Briggs et al., 2003). The wave height and direction at each nodal location within the averaging box were compared to the recorded wave height and wave direction at the corresponding ADCP locations. Table 11-4 contains the comparison between measured and modeled wave height and direction based on the offshore and nearshore ADCP stations for April 4, 2003 at 0700 hours. The percentage error of the modeled values is also presented. A negative percent error represents an under prediction of wave height, while a positive percentage represents an over prediction of the wave height. The model slightly under predicted the wave heights (approximately 10% error), and performed reasonably well in relationship to the wave direction (between 5-8% error).

Table 11-4. Modeled and measured wave height and wave direction for April 4, 2003 at 0700 hours.

	Offshore ADCP Location		Nearshore ADCP Location	
	Wave Height [m]	Wave Direction (0° = True North)	Wave Height [m]	Wave Direction (0° = True North)
Measured	1.59 (5.2 ft)	96	0.86 (2.8 ft)	88
Modeled	1.41 (4.6 ft)	88	0.77 (2.5 ft)	84
% Error	-11.3%	8.3%	-10.4%	4.5%

The April 27, 2003 at 0400 hours time period was subsequently used to verify the model's performance using the same coefficients determined during the calibration time period (April 4, 2003 at 0700 hours). The spectral decomposition of the verification spectrum is in Table 11-3. Table 11-5 contains the comparison between measured and modeled wave height and direction based on the offshore and nearshore ADCP stations for April 27, 2003 at 0400 hours. The verification of the model indicated slight over prediction of the model wave height (approximately 1% error) at the nearshore location and small errors in wave direction (approximately 2% error).

Table 11-5. Modeled and measured wave height and wave direction for April 27, 2003 at 0400 hours.

	Offshore ADCP Location		Nearshore ADCP Location	
	Wave Height [m]	Wave Direction (0° = True North)	Wave Height [m]	Wave Direction (0° = True North)
Measured	1.95 (6.4 ft)	114	1.07 (3.5 ft)	95
Modeled	1.92 (6.3 ft)	112	1.08 (3.5 ft)	97
% Error	-1.5%	1.8%	1.0%	2.1%

The errors from two simulated time periods were combined in order to quantify the overall accuracy of the nearshore model. Table 11-6 presents the percentage error for each of the ADCP locations for both wave height and wave direction. A negative percent error represents an under prediction of wave height, while a positive percentage represents an over prediction of the wave height. These values represent a gauge of the overall performance of the model to simulate the observed wave data. The nearshore model compared favorably to the observed results as long as the number of spectral components remained high. Failure to use non-linear terms or use of a reduced number of spectral components resulted in increased errors. The accuracy is slightly better than the results shown for the regional transformation-scale model (Chapter 9.0), likely due to the increased model resolution in the region.

Table 11-6. Percentage error for the nearshore (local) wave model compared to the offshore and nearshore ADCP (averaged over both simulated calibration time periods).

	Offshore ADCP Location		Nearshore ADCP Location	
	Wave Height	Wave Direction	Wave Height	Wave Direction
Percentage Error	-6.4%	5.1%	-4.7%	3.3%

11.6 Existing Conditions Simulations

The existing conditions simulations were performed on the same grid as that used in the calibration and verification procedures, using the same coefficients and parameters. Both average annual directional spectra and high energy events were simulated. The methodology established during the calibration and verification procedure for developing input spectra was followed for both simulation sets.

11.6.1 Average Annual Directional Approaches

The same average annual directional approaches that were simulated in the regional, transformation-scale wave model were also simulated in the nearshore (local) wave model. The exception was the north-northeast (30 to 55 degree) approach bin, which was not simulated in the nearshore (local) wave model. The north-northeast approach bin contained a minimal amount of the offshore wave energy (approximately 2%), and this amount of energy was reduced further through in the transformation of the waves in the regional model. Therefore, due to the insignificant amount of overall energy arriving at the shoreline, the north-northeast approach bin was not simulated in the nearshore (local) wave modeling effort. Input conditions for the nearshore (local) wave model were established using the same methodology as presented in the previous sections. All of the directional approach simulations were performed on both a grid referenced to MHW and a grid referenced to MLW for sediment transport purposes. The following wave discussion focuses on the MHW simulations, which represent the more energetic cases.

Figure 11-8 shows example sea surface results from the nearshore (local) wave model for a southeastern approach spectrum. Dark blues represent the wave crests, while whites represent the wave troughs. The nearshore (local) wave model simulations can be used to evaluate the interaction of the waves with the complex nearshore bathymetry, the navigational structures, the islands, and the shoreline. The impact of the nearshore islands, shoals, and structures, as well as diffraction/refraction patterns and the crossing of various wave trains, is clearly evident in the sea surface results. Of particular interest are the wave patterns in the vicinity of Eagle and Ram Islands, which have considerable influence on the propagation of the wave field. The complex bathymetric area between the two islands also results in a significant modification to the offshore wave trains. At this scale (Figure 11-8), it is difficult to identify wave processes occurring in the nearshore region of Camp Ellis Beach. As such, detailed close-ups of the Camp Ellis area are presented for existing conditions and alternative cases throughout this Chapter.

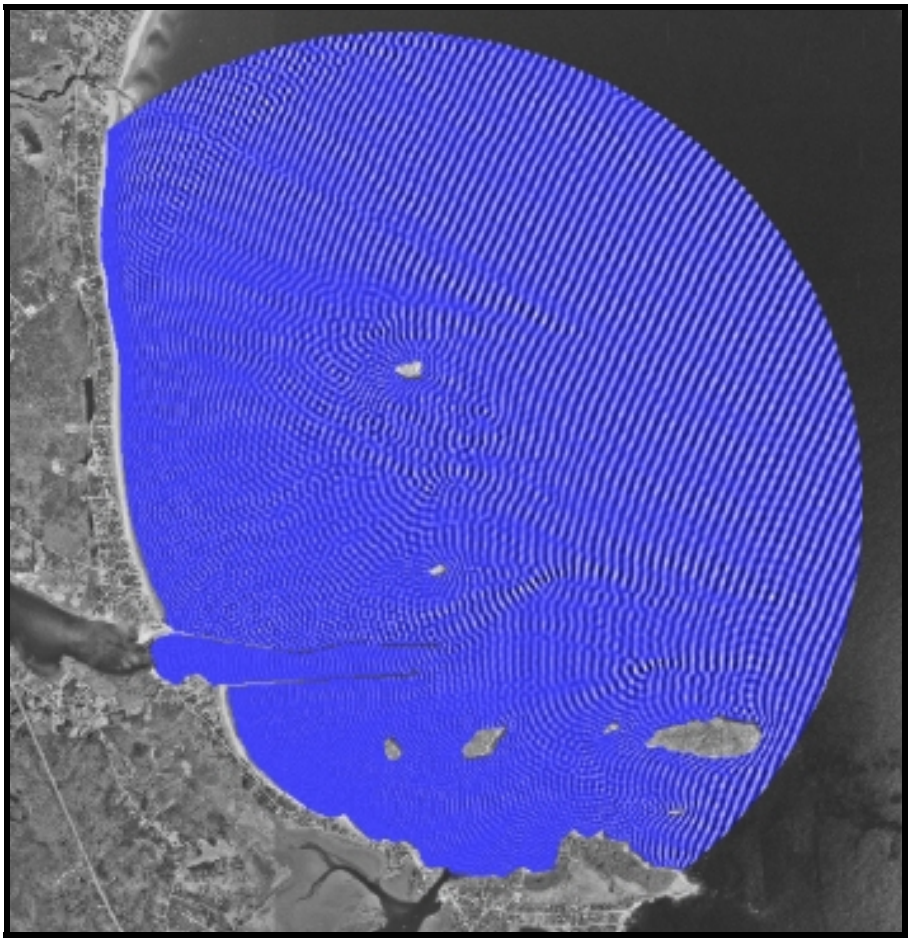

Figure 11-8. Example results of seas surface output from the nearshore (local) wave model (CGWAVE). The simulation is for a southeastern approach spectrum at Mean Tide Level. Dark blues represent wave crests, while the whites represent wave troughs. Patterns of refraction and diffraction throughout the domain are clearly visible.

Figure 11-9 presents similar sea surface results for the east-southeast (110 to 130 degree) approach bin in the direct vicinity of Camp Ellis Beach. This region extends from approximately Eagle Island to the northeast down to the intersection of the northern navigational structure and the shoreline. The color map was modified to represent an entire spectrum of color in order to facilitate visual identification of wave train interaction. The blues indicate wave crests, while the reds and yellows indicate wave troughs. The scale in the upper left corner of the figure presents the sea surface disturbance in meters. In addition, Figure 11-10 presents sea surface results for the east-northeast (75 to 90 degree) approach bin scenario, while Figure 11-11 presents sea surface results for the southeast (130 to 150 degree) approach bin scenario. All average annual directional approach sea surface results are presented in Appendix 11-A. Additionally, wave animations for each scenario are contained on the corresponding data and wave animation DVD provided with this report.

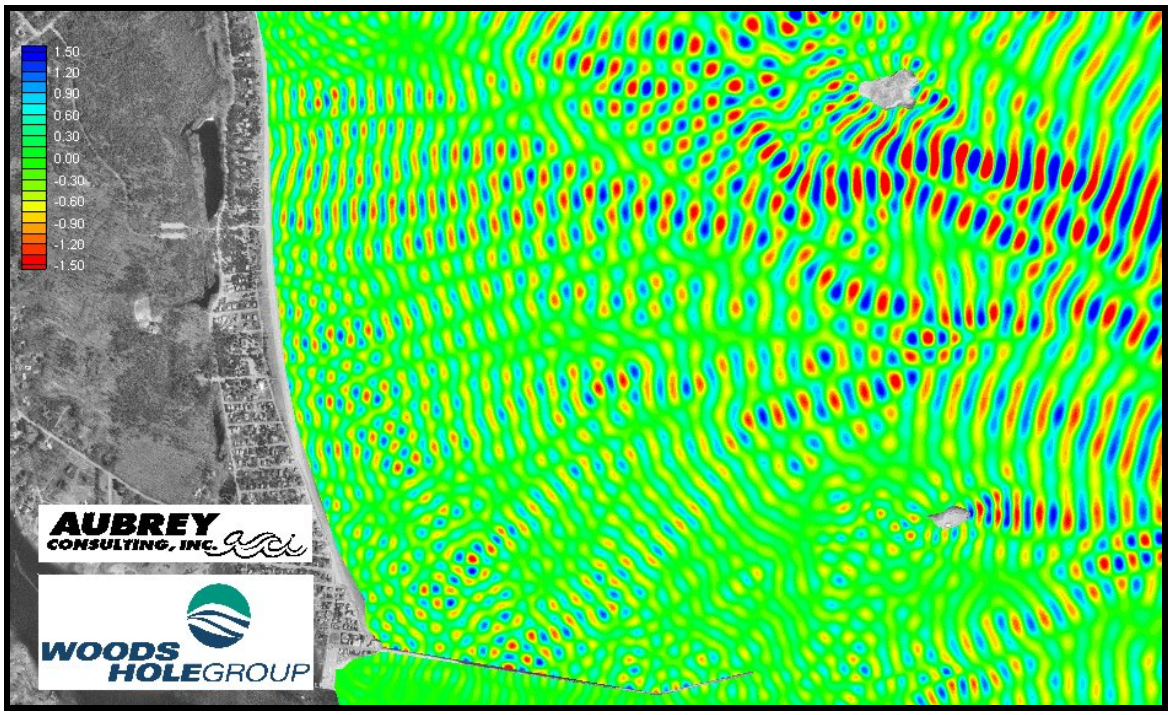

Figure 11-9. Sea surface results from the nearshore (local) wave model for the east-southeast (110-130 degree) approach bin. Blues indicate wave crests, while reds and yellows indicate wave troughs.

Evaluation of the sea surface results for the existing conditions average annual approach directions reveal some important wave transformation aspects:

The significant wave reflection off of the northern jetty is identified as the waffle type sea surface north of the structure. These waffle-like patterns are formed due to the interaction of the incident and reflected wave trains. Upon impacting the structure, the

incident waves are reflected back towards Camp Ellis Beach. Therefore, for a portion of the shoreline directly adjacent to the northern jetty, the beach is impacted not only by the incident wave energy, but also by the reflected wave energy. As such, approximately 610-914 m (2,000-3,000 ft) of shoreline experiences a significant increase in energy. In certain cases, portions of the reflected wave train can be seen in the model simulations as far north as Bay View.

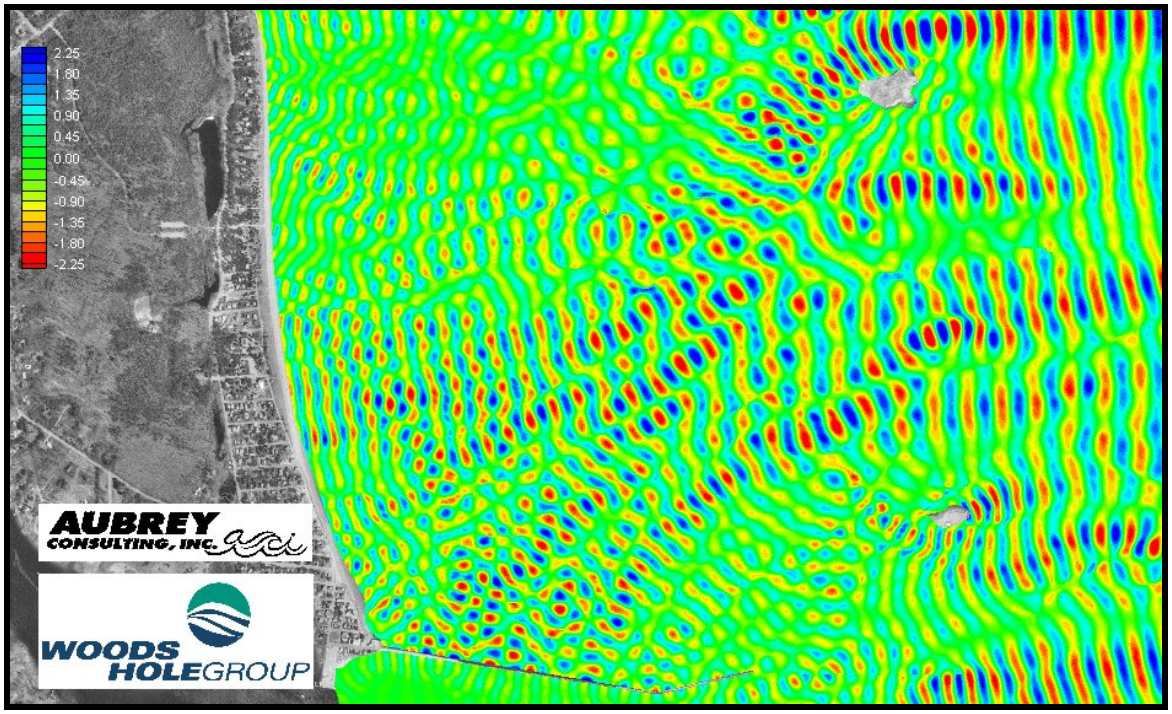

Figure 11-10. Sea surface results from the nearshore (local) wave model for the east-northeast (75 to 90 degree) approach bin. Blues indicate wave crests, while reds and yellows indicate wave troughs.

In nearly all cases, independent of offshore direction of approach, the nearshore waves propagated directly towards the Camp Ellis Beach region and the northern jetty. The transformations due to the complex bathymetry between the islands, and the islands themselves, resulted in a nearly uniform approach towards the region of highest erosion and reflection. This was evident in both the observed data collected at the nearshore ADCP station and the nearshore (local) wave modeling results. The processes causing the waves to be redirected towards the structure are complex, and due to both diffraction and refraction mechanisms through the gap between Ram and Eagle Islands, as well as the highly irregular bathymetry between the islands. The presence of a deep channel and various submerged shoals/outcrops in the region produce a nearly unidirectional wave approach landward of the islands. The amount of energy redirected towards the Camp Ellis region varies based on the offshore direction of approach, but this channeling effect is evident in all average annual approach cases. For example, east and northeast offshore approach bins results in more energy at Camp Ellis Beach, yet even southeast approach

directions produce a significant amount of incident and reflected wave energy at Camp Ellis.

Mach-Stem waves (waves traveling along the structure) propagating along the northern jetty can be seen in most cases. Although this does not represent a large amount of energy, it does produce an additional wave process that impacts the coastline, and specifically the corner where the shoreline and northern jetty meet. The Mach-Stem wave can be readily viewed in the animation files provided on the corresponding DVD.

Since the bottom contours near the northern jetty run almost parallel to the structure (Figure 11-2), waves are refracted towards the structure. As waves align themselves with the bottom contours, a portion of the wave energy is directed toward the structure creating both Mach-Stem effects and reflected wave energy.

Although for a majority of the cases the wave energy is propagating directly towards Camp Ellis Beaches, variations between various annual average approach directions can be important. For example, in the eastern (90-110 degree) approach bin, a significant wave train advances directly parallel to the northern jetty. The importance of simulating all approach directions, and not just the most common, is key.

Results from the nearshore (local) wave model were utilized to produce local sediment transport estimates, generate energetics based performance evaluations, and provide an initial screening of the proposed engineering alternatives (as presented in Chapter 10.0). Results from the directional approach simulations were used as part of the alternative analyses.

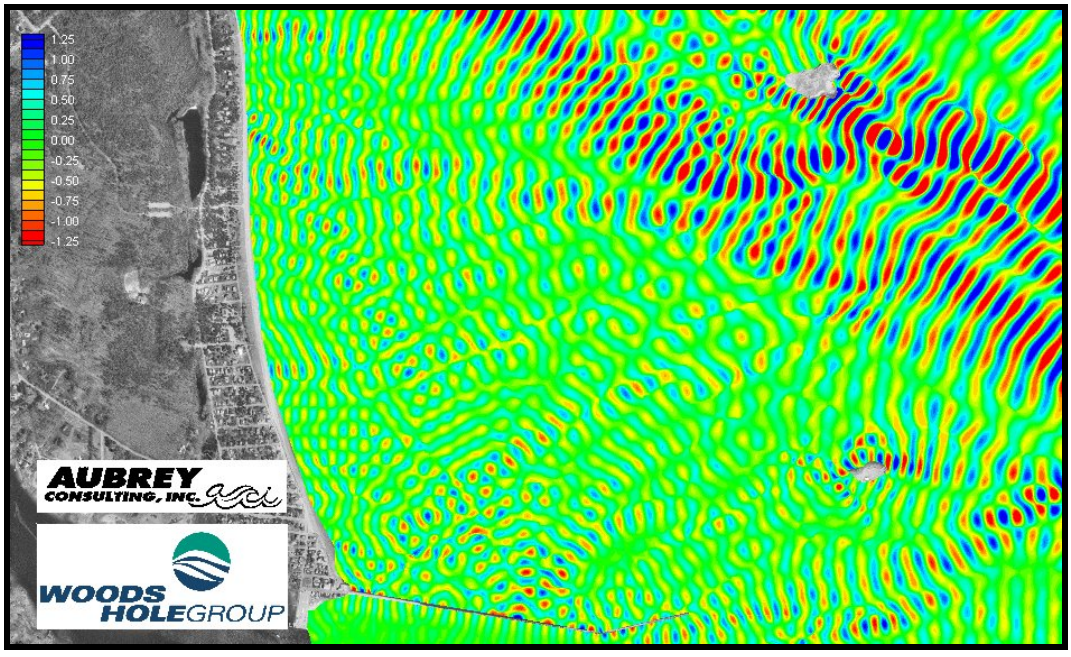

Figure 11-11. Sea surface results from the nearshore (local) wave model for the southeast (130 to 150 degree) approach bin. Blues indicate wave crests, while reds and yellows indicate wave troughs.

11.6.2 High Energy Event Simulations

In addition to the average annual approach directions, high-energy events were also simulated to provide a more complete picture of the existing conditions impacting Camp Ellis Beach. These simulations consisted of both return period design storms (10-, 50- and 100-year) and historical storm events (Hurricane Bob, Nor'easter of 2001 and "The Perfect Storm"). Input conditions for the storm scenarios were established using the same spectral component methodology presented in section 11.4. Each return period simulation was executed on a model grid that had increased water depth due to increased storm surge elevations, as were presented in Table 9-4. It was assumed that under all conditions, the portions of the existing structure that were emergent at MHW would remain emergent for the storm conditions.

Figure 11-12 presents the sea surface results for the 10-year return period storm in the direct vicinity of Camp Ellis Beach. The blues indicate wave crests, while the reds and yellows indicate wave troughs. The scale in the upper left corner of the figure presents the sea surface disturbance in meters. The storm case, consisting of increased wave heights and water depths in the vicinity of the shoreline, presents a more well-structured wave field when compared to the average annual approach directions. The interaction and shoreline impact of the incident and reflected wave trains is clearly evident. Many of the same wave transformation features discussed for the average annual approach cases are also evident in the storm scenarios.

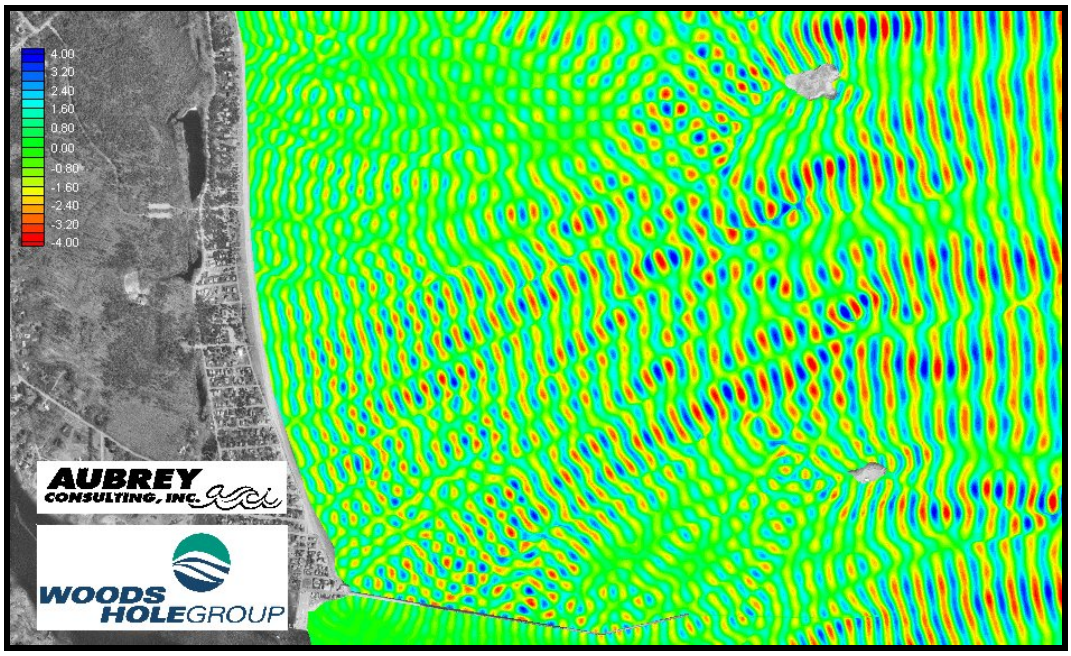

Figure 11-12. Sea surface results from the nearshore (local) wave model for the 10-year return period storm event. Blues indicate wave crests, while reds and yellows indicate wave troughs.

Figures 11-13 and 11-14 present similar sea surface results for the Perfect Storm and Hurricane Bob, respectively. These events represent some of the largest historical storms for this location. The significant impact on the Camp Ellis region can be seen in both cases, again independent of offshore wave approach direction. Northeasters likely have a greater impact than southeast approaching storms (e.g., Hurricane Bob), but both approach directions focus energy directly on the Camp Ellis region and the northern jetty. All storm scenario sea surface results are presented in Appendix 11-A. Additionally, wave animations for each storm scenario are contained on the corresponding wave animation DVD provided with this report.

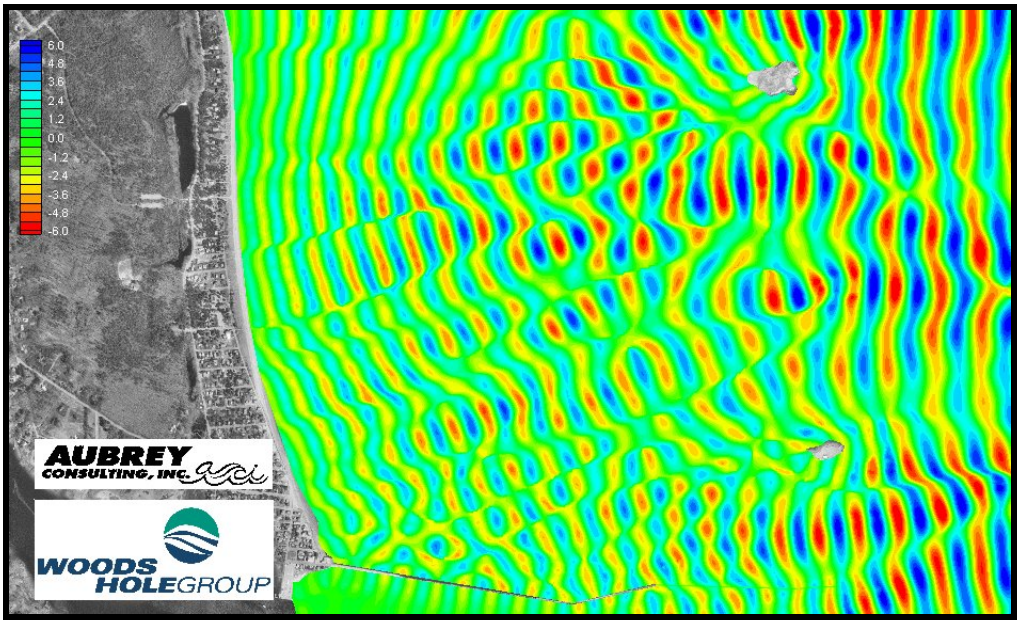

Figure 11-13. Sea surface results from the nearshore (local) wave model for the Perfect Storm. Blues indicate wave crests, while reds and yellows indicate wave troughs.

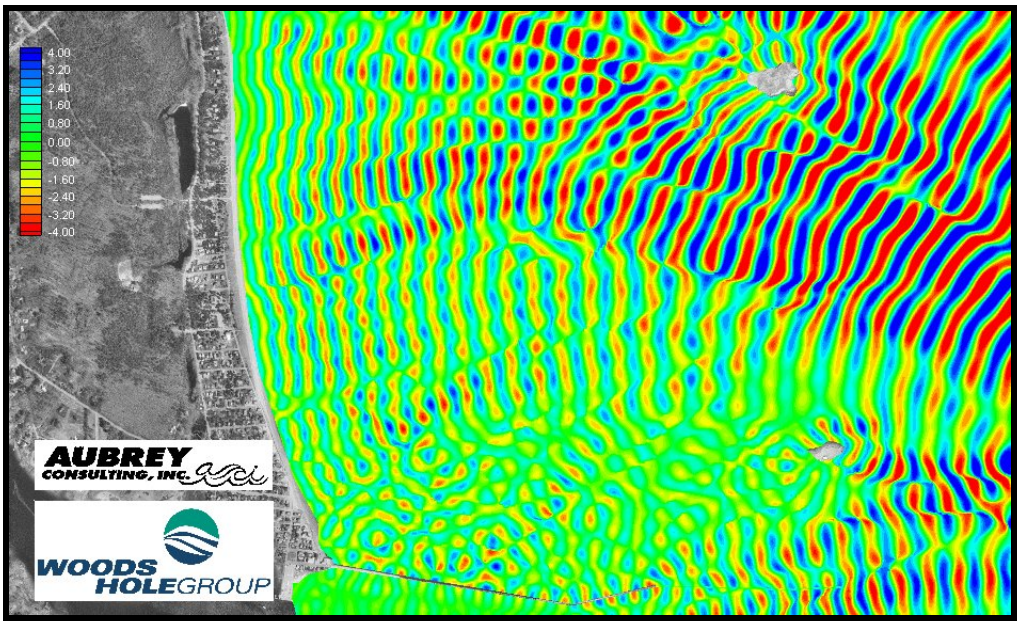

Figure 11-14. Sea surface results from the nearshore (local) wave model for Hurricane Bob. Blues indicate wave crests, while reds and yellows indicate wave troughs.

The results from the nearshore storm simulations were used to quantify storm impacts on sediment transport and beach nourishment performance, as well as provide critical assessment of the alternatives (e.g., alternative performance during a significant storm event).

11.7 Alternative Simulations

The ultimate goal of the overall modeling system was application towards the evaluation of the wide range of alternatives presented in Chapter 10.0. The alternatives were geared towards mitigation of the ongoing erosion occurring at Camp Ellis Beach. The resolution of the local nearshore model allows for the simulation of these alternatives with accurate dimensions and layouts. In order to simulate the alternatives, the existing conditions model grid was numerically modified to include the proposed layouts. This included a variety of modifications based on the proposed alternatives:

Removal and/or lowering of portions of the jetties from the model grid. This consisted of lowering the nodes comprising the existing structure to the depth of the surrounding bathymetry. In cases where the structure was lowered, rather than removed, the nodes were set at the desired elevation for the structure.

Addition of proposed structures (e.g., T-Head groins, breakwaters, spur jetties, etc.) through modification of nodes within the model domain. Typically, this consisted of removing of the nodes from the model domain to create a land/island type feature.

Raising or lowering of the bathymetric surface to represent proposed submerged outcrops/shoals or proposed dredging scenarios. This consisted of numerical changing the elevations of corresponding nodes to represent the proposed modification.

Modification to the reflection coefficients for proposed alternatives that consist of jetty roughening or structural modifications. For jetty roughening, the reflection coefficient was reduced to account for a decreased ability to reflect the wave energy.

Specific alternative layouts, sizes, and grid modifications are presented in Chapter 10 and in the following section. The layouts were ultimately decided based on the results of the existing condition scenarios. For example, spur jetties and breakwaters were positioned to intercept significant wave trains shown in the existing conditions. Layouts were designed to attempt to optimize the amount of wave energy reduction along the most erosive parts of Camp Ellis Beach, while minimizing the impacts to adjacent shores, islands, and the navigability of the Saco River. The modified model grids (for each alternative) were simulated for the same set of wave conditions run on the existing conditions grid (i.e., average annual approach directional bins and high energy events). These simulation results were used in the initial screening analysis in order to evaluate the overall performance of each alternative and, in concert with the existing conditions simulations for each scenario, to generate differences in wave energy within the vicinity of Camp Ellis Beach.

Figures 11-15 through 11-18 present examples of the modified grid results for some of the alternatives. Figure 11-15 shows sea surface results for Alternative 2, the northern jetty extension removal and jetty lowering, under the eastern wave approach condition. With the removal of the northern jetty extension, waves are allowed to propagate directly into the navigation channel. In addition, a significant amount of wave reflection is still evident from the remaining northern structure. Figure 11-16 presents seas surface results for Alternative 6, consisting of a 750-foot spur jetty, for a 10-year return period storm scenario. The spur jetty intercepts a significant part of both the incident and reflected wave energy impacting Camp Ellis Beach. The area seaward of the spur experiences significant wave turbulence, due to reflected wave energy from both the spur and the existing northern jetty. Figure 11-17 presents sea surface results for Alternative 18, a combined offshore breakwater and 500-foot spur jetty case. The breakwater intercepts a significant portion of the incoming wave energy, while the spur captures a portion of the reflected wave energy. Overall, a significant wave energy reduction is seen along the most erosive portion of Camp Ellis Beach. Figure 11-18 presents sea surface results for Alternative 25, one of the segmented breakwater alternatives. This alternative indicates significant wave energy reduction along the shoreline, while intercepting a majority of the reflected wave energy off of the existing northern jetty.

Visual observations from these figures were one component of the initial screening analysis. Detailed discussions of the results for each alternative are presented in the following section as part of the initial screening analysis. Selected wave animations for some of the proposed alternatives and selected scenarios are presented on the corresponding wave animation DVD provided with this report. The selected alternatives

consist of those that indicated reasonable performance at reducing the wave energy with minimal negative impacts (as discussed in detail in the following section).

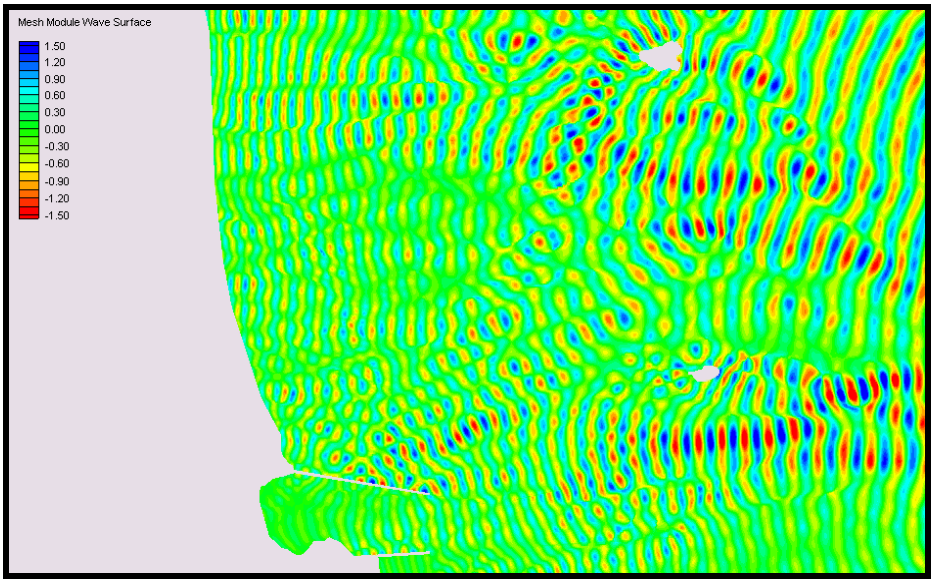

Figure 11-15. Sea surface results for Alternative 2 (northern jetty extension removal and additional lowering) for an east approach directional bin. Blues indicate wave crests, while reds and yellows indicate wave troughs.

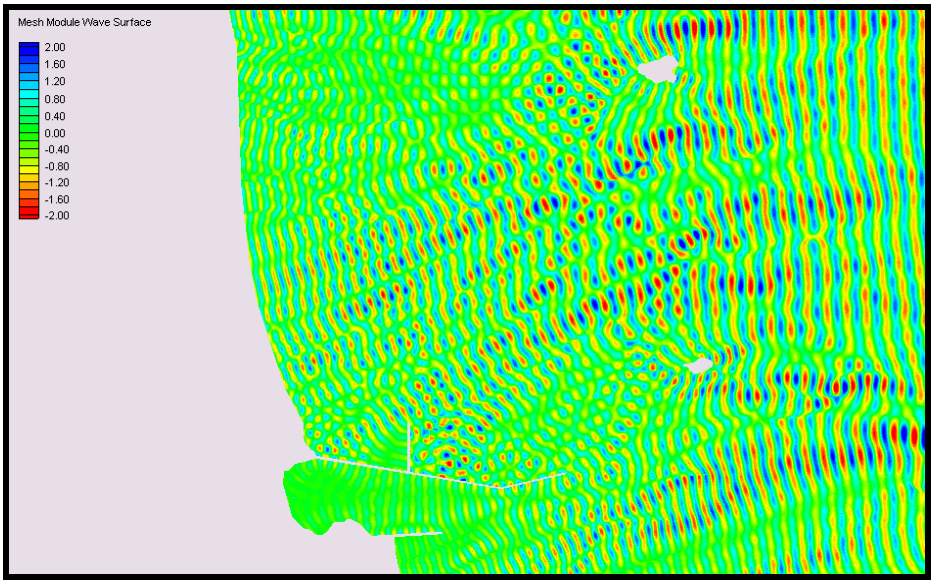

Figure 11-16. Sea surface results for Alternative 6 (750-foot spur jetty) for a 10-year return period storm. Blues indicate wave crests, while reds and yellows indicate wave troughs.

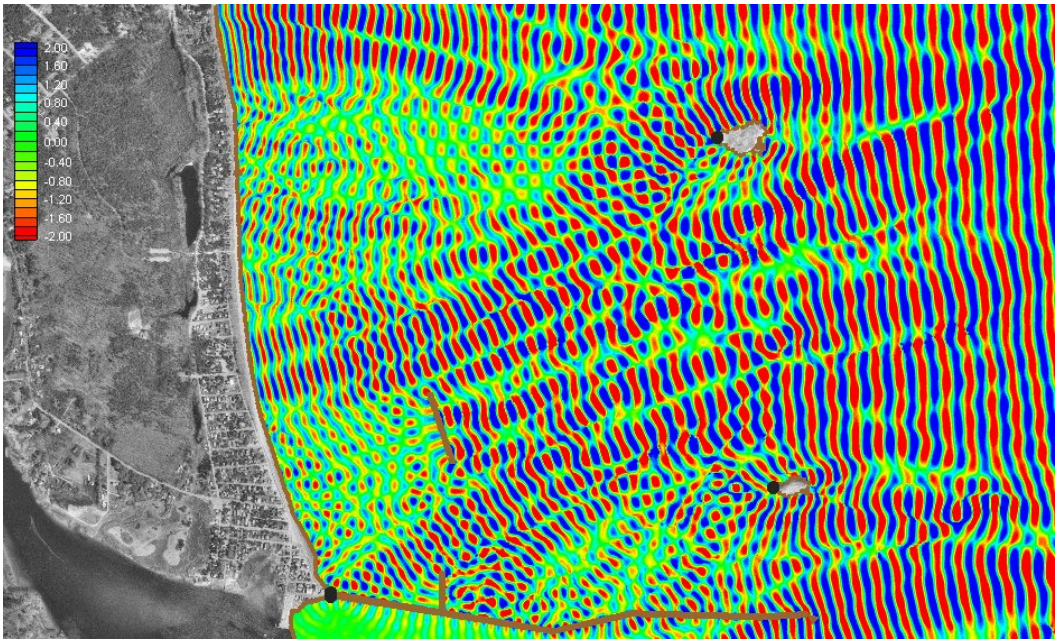

Figure 11-17. Sea surface results for Alternative 18 (combined offshore breakwater and 500-foot spur) for a 10-year return period storm. Blues indicate wave crests, while reds and yellows indicate wave troughs.

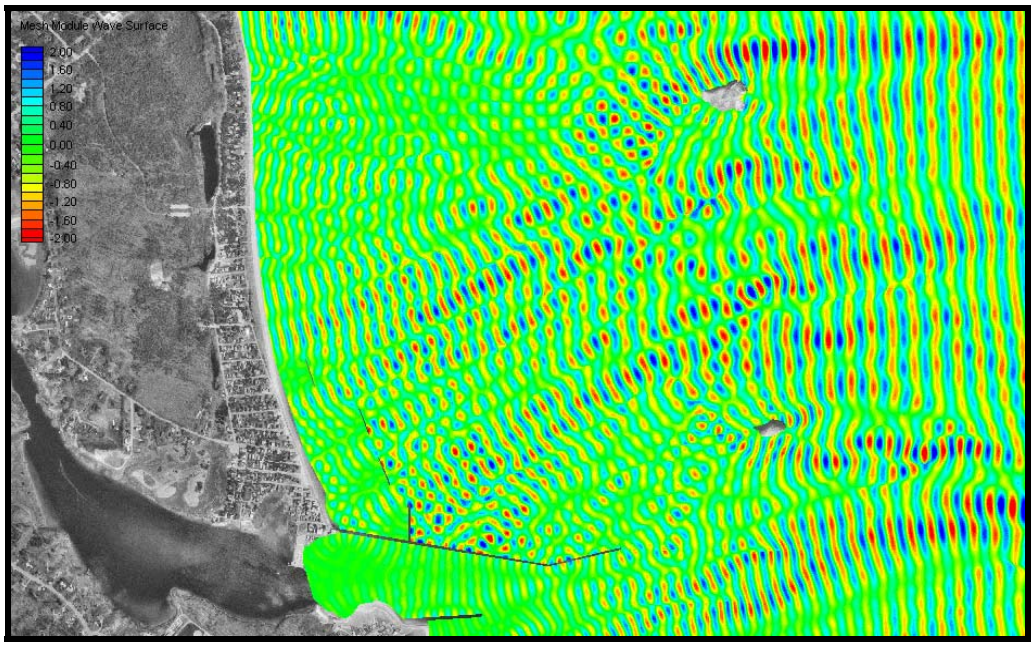

Figure 11-18. Sea surface results for Alternative 25 (one of the segmented breakwater alternatives) for a 10-year return period storm. Blues indicate wave crests, while reds and yellows indicate wave troughs.

11.8 Initial Screening Analysis

Due to the number of simulations required to evaluate all potential solutions, the alternatives analysis consisted of an initial and final screening process. With approximately 30 alternatives, eight (8) average annual directional approach bins, and six (6) high-energy events, there is no reasonable way to simulate all scenarios for all alternatives. Therefore, the nearshore (local) wave model was used as the initial screening tool through evaluation of changes in wave energy, wave height, and wave direction prior to performing all simulations and associated sediment transport calculations. All alternatives were simulated for the 10-year return period storm and an eastern average annual wave approach directional bin. If an alternative was not adequately performing in these cases, it is likely that it would be ineffective in the other more energetic storm scenarios. From these two scenarios, an initial screening process (preliminary alternatives analysis) was conducted. The initial screening process consisted of the following elements:

The wave results figures and animations (examples presented in section 11.7). Visual assessment of the figures and animations provided an overview of the modifications to the nearshore wave climate and wave propagation in the vicinity of Camp Ellis Beach.

Wave height changes caused by the proposed alternative. Differences in wave heights (between existing conditions and alternative cases) were computed at each node within the model domain. Difference plots were then created (subtracting alternative wave heights from existing) that indicate regions of increased and/or decreased wave heights and assessed to determine the overall impact of the alternative on the wave height in the region. Figure 11-19 presents an example of the wave height change plots for Alternative 11a (an offshore breakwater) for a 10-year return period storm scenario. Positive values (yellows and reds) of wave height change (m) indicate an increase in wave energy, while negative values (blues and purples) of wave height change (m) indicate a decrease in wave energy. These difference plots are discussed throughout this section, and presented in full (all alternatives, 10-year return period storm and eastern average annual approach) in Appendix 11-B.

Wave energy reduction was evaluated in specific zones in the vicinity of Camp Ellis and the existing structures. Figure 11-20 shows the zones within which wave energy between existing conditions and alternative cases were compared. The results in Figure 11-20 show wave heights (m) for Alternative 11 (offshore breakwater) as a colormap behind the evaluation zones. The zones were selected to identify specific regions of potential concern, for example, zones A and B represent the most erosive portions of the Camp Ellis shoreline. It is critical to reduce the amount of wave energy in these two zones if there is any chance for the alternative to perform effectively. Zone C represents a region where the coastline is more historically stable; however, it was important that any alternative did not increase the wave energy in zone C. Zone H represents the entrance channel to the Saco River. It is also important that the alternative does not increase wave energy in this region due to potential navigational and maintenance concerns. Zones D through G provide a complete picture of potential wave energy changes adjacent to the northern structure. These zones allow for a more detailed assessment of wave energy

changes resulting from each proposed alternative, and are referred to throughout the initial screening analysis discussion. The energy changes for all zones, all alternatives, and the two evaluated scenarios are presented in Appendix 11-C.

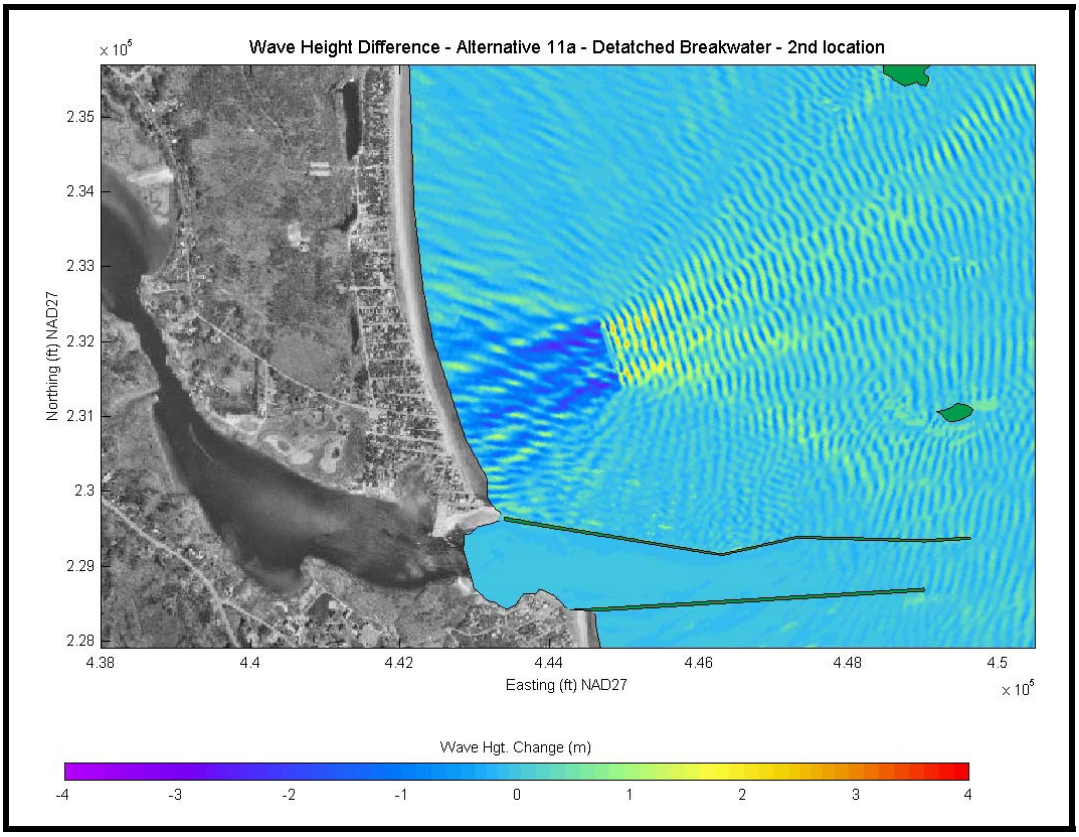

Figure 11-19. Wave height changes for Alternative 11a for a 10-year return period storm scenario.

Assessment of impacts on adjacent shores, the navigation, maintenance concerns, etc. An important aspect of any potential alternative and/or solution is the potential negative impacts that may be associated with the alternative. This may include, increased wave energy in other shoreline regions (e.g., Hills Beach or north of Camp Ellis), increased wave energy in the navigational channel, or alternatives that result in significant maintenance concerns.

Alternatives demonstrating the greatest potential for successfully reducing wave energy (and thus sediment transport), without resulting in negative impacts, were passed forward to the final screening analysis. The alternatives that were recommended for more in depth analysis were then simulated for all approach directions and storm cases to identify energy changes and to calculate sediment transport and beach nourishment performance. This section details the initial screening process and presents a discussion related to each alternative, including recommendations of alternatives that should be passed through to

the more detailed analysis. It should be noted that the alternative screening process is focused solely on the overall functional performance of the alternatives. Complete details on the configuration and layout of each alternative are presented in Chapter 10.0.

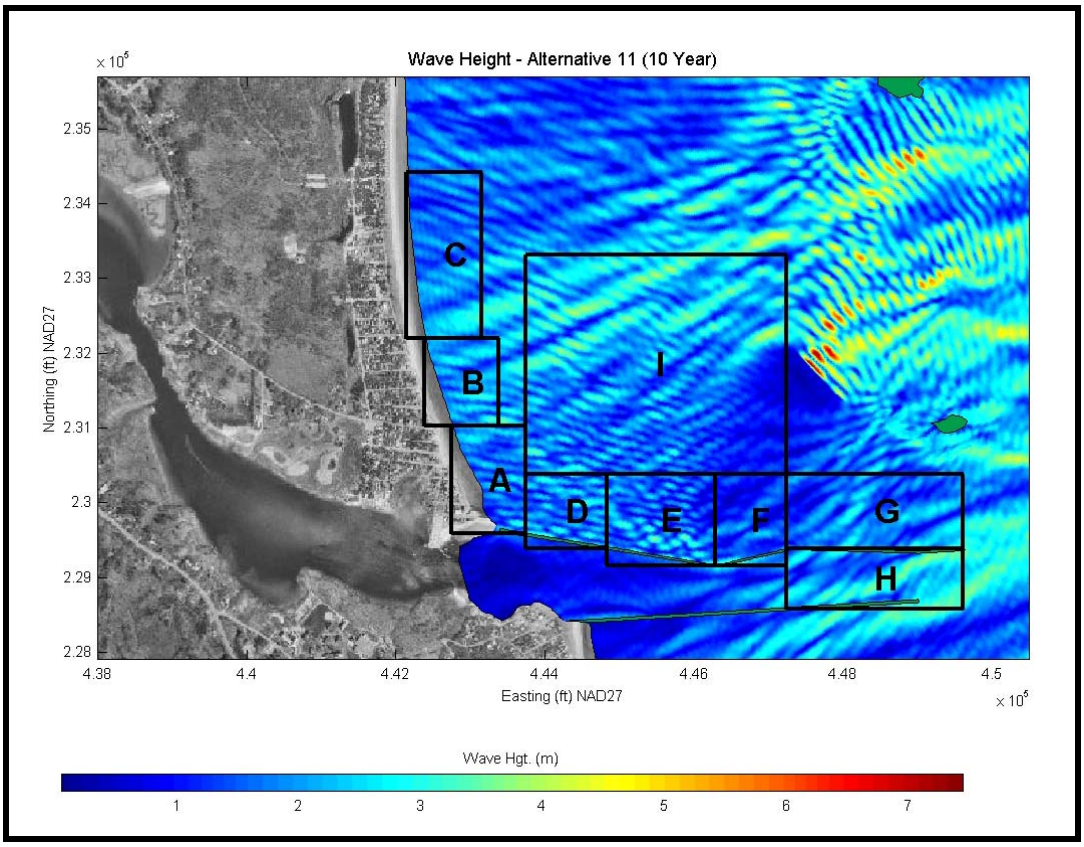

Figure 11-20. Zones used to evaluate changes in wave energy in the vicinity of Camp Ellis Beach and the Saco River Jetties.

11.8.1 No Action

As discussed, the no action alternative implies there would be no change to the present conditions at Camp Ellis Beach. This is clearly an unacceptable alternative, as the existing shorefront would continue to be eroded, a sustainable beach and/or any protective action would not be taken, and the landward homes and structures would face potential damage/loss. This alternative does not address the required mitigation purview of the Section 111 Authority. This alternative is not recommended.

11.8.2 Base Alternative: Beach Nourishment Alone

The base alternative plan was not simulated directly as an alternative. The plan does not meet the criteria of a true alternative as it is not considered complete or effective due to a significant risk of failure during repeat storms, and it does not mitigate for the north jetty's effect on the local wave field. Beach nourishment efforts have been conducted in the past with little success, as material has quickly eroded due to the exacerbated wave

energy on the Camp Ellis region. Existing conditions simulations were used to assess the potential performance of this plan, and it was included in further analyses from the standpoint of being a comparative measure for the other alternatives. The potential lifetime of beach nourishment alone can be used to assess the relative performance of other alternatives, as the same level of beach nourishment, is included in every alternative. However, based on the historical performance of beach nourishment alone efforts, and the lack of mitigation to the jetty induced wave energy increase, beach nourishment along is likely not a preferred option. This alternative does not fully address all the causes of the increased erosion at the project location.

11.8.3 Alternative 0: Northern Jetty Removal

Figure 11-21 presents the wave height difference plot for Alternative 0 under the average annual eastern (90-110 degree) approach bin. Although reflected wave energy is reduced, indicated by the dark blue bands extending to the north, there is significant wave height and energy increases in the navigation channel. These wave height increases were even greater during the 10-year return period storm event (Appendix 11-B). So while this alternative does eliminate reflected wave energy from the structure, there are some significant negative impacts associated with this alternative, including a plausible increase to the erosion at Camp Ellis Beach.

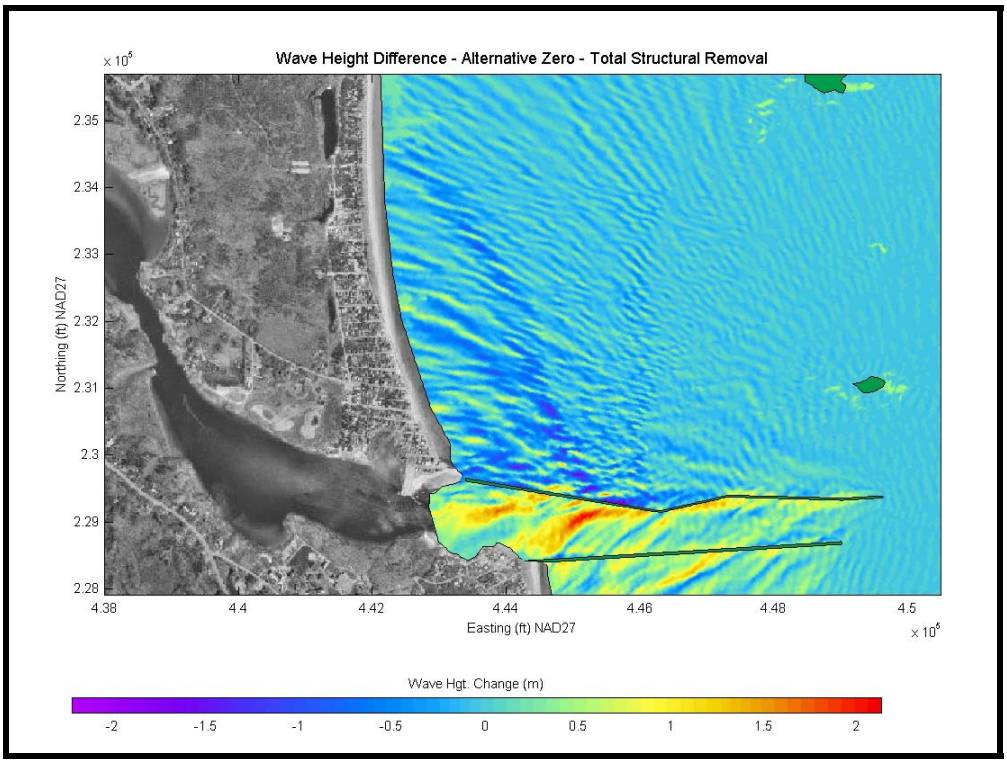

Figure 11-21. Wave height changes for Alternative 0 for an eastern (90-110 degree) wave approach bin. A negative wave height change indicates a reduction in wave height, while a positive wave height change indicates an increase in wave height.

The increased wave energy at the entrance to the Saco River will result in significant navigation and maintenance concerns related to the navigational channel.

Wave energy would increase significantly at Hills Beach under all wave approach scenarios.

The removal of all existing structures would also remove some protection that is afforded Camp Ellis Beach from the southeastern approach directions and hurricanes.

Removal of the northern structure would destabilize the Camp Ellis shoreline. The northern jetty has been in place for over 150 years, and although it likely the structure has removed a significant sediment supply to Camp Ellis Beach (by directing the sediment laden Saco River discharge much further offshore), the shoreline has had the structures in place for 150 years and re-adjusted to their presence. It is likely that complete removal of the northern jetty may actually exacerbate erosion at Camp Ellis Beach through destabilization of the shoreline (communications with MGS, 2005). The southern terminus of the beach would be exposed to significant tidal currents and due to the lack of sediment supplied over the last 150 years, and it is very likely the entire southern portion of Camp Ellis Beach would be flooded, eroded, or completely severed.

Removal of the structures would allow the Saco River Inlet to migrate (i.e., shift its position to either the north of south) and could results in the loss of a significant portion of Camp Ellis Beach.

Although the Saco River is a principal supplier of sediment to the nearshore region, a portion of the sediment flux may have been reduced due to the dams that have been constructed upstream along the River. It is expected that the dams have minimal impact on the sediment flux, but due to both natural and anthropogenic changes to the River system, the sediment flux may not be as high as it had been a century ago.

This alternative was not recommended by the project team (WHG, USACE, SBIT, MGS).

11.8.4 Alternative 1: Northern Jetty Extension Removal

Figure 11-22 presents the wave height difference plot for Alternative 1 under the average annual eastern (90-110 degree) approach bin. Wave height differences for the 10-year return period storm event are presented in Appendix 11-B, while percent energy changes are presented in Appendix 11-C.

For average annual eastern approach scenario – No major changes in much of the region, with the exception of a major wave energy increase in the entrance channel (42.8% energy increase, 0.25 m (0.8 ft) wave height increase), and a bit of an increase (15% energy) in Area F (which would become the new outer portion of the structure. There were no other significant changes or loss of energy.

- For the 10-yr storm case – The same increase zones as in the annual eastern approach case. In the entrance channel wave heights increase 0.14 m (0.5 ft) and

energy increase 12.1 %. Due to the approach direction difference (more NE and directly at the structure) there are more energy increases along the length of the structure (areas D-F) than in the annual case. This leads to greater reflection and a slight increase in wave height/energy along the shoreline as well.

- Overall, this alternative warrants little further study or consideration, the wave energy/heights only show increases in the navigational channel or along the remaining structure length. The key problem with this alternative is that the primary goal of reducing reflected wave energy does not occur. Wave energy is not reduced at zones A and B, so no significant improvement over existing conditions is expected. This alternative is not recommended.

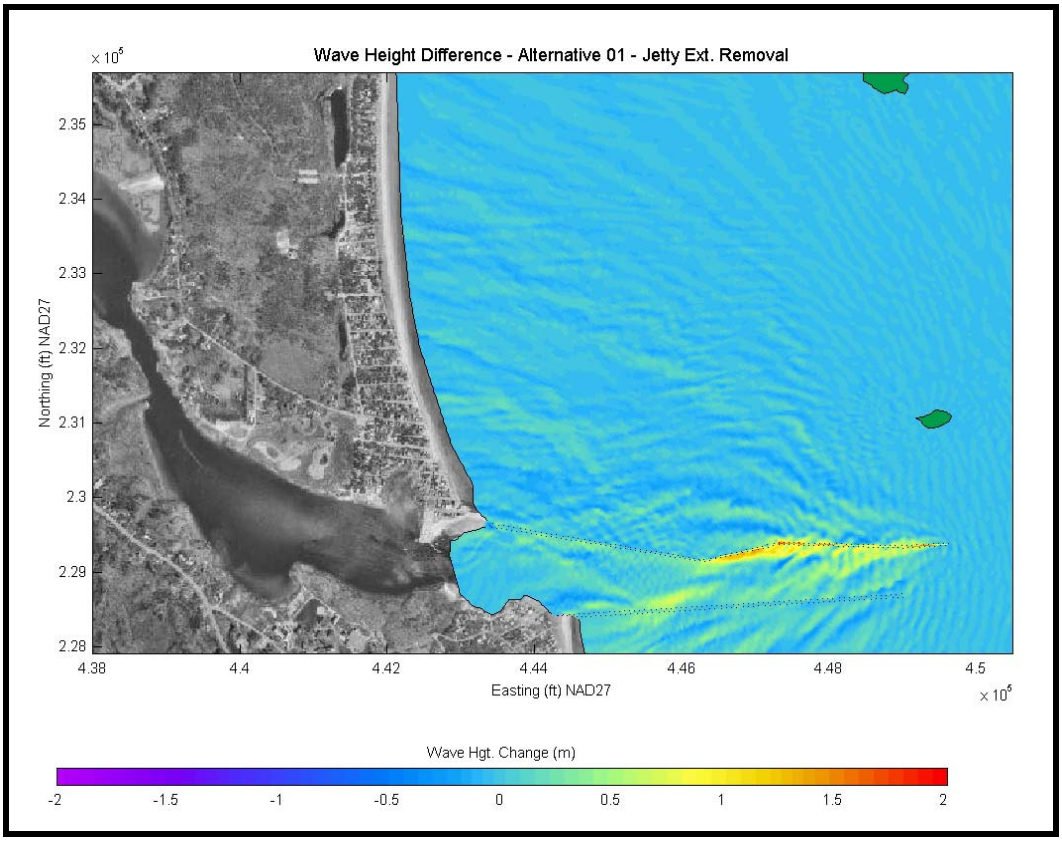

Figure 11-22. Wave height changes for Alternative 1 for an eastern (90-110 degree) wave approach bin. A negative wave height change indicates a reduction in wave height, while a positive wave height change indicates an increase in wave height.

11.8.5 Alternative 2: Northern Jetty Extension Removal and Lowering

Figure 11-23 presents the wave height difference plot for Alternative 2 under the average annual eastern (90-110 degree) approach bin. Wave height differences for the 10-year return period storm event are presented in Figure 11-24, while percent energy changes are presented in Appendix 11-C.

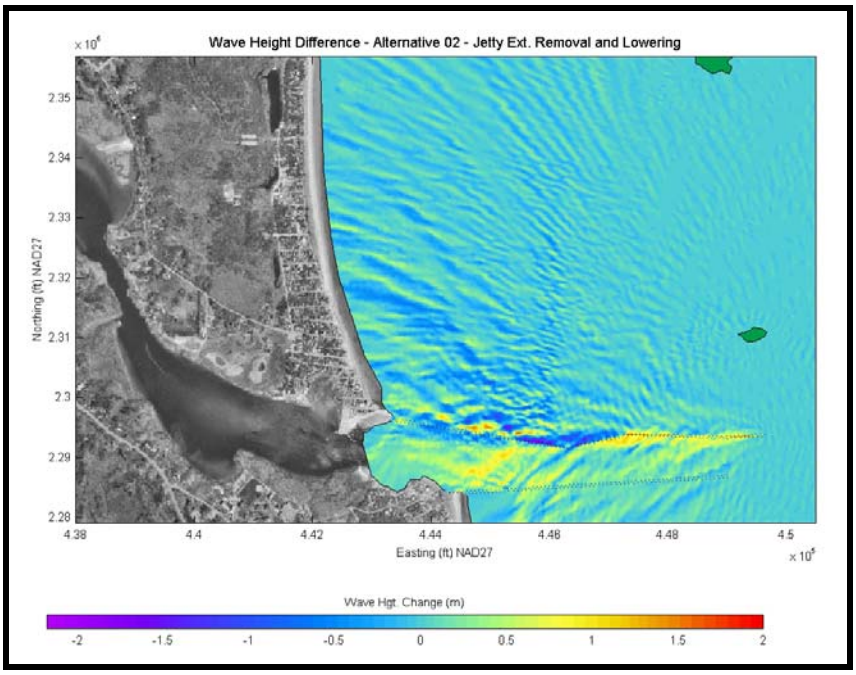

Figure 11-23. Wave height changes for Alternative 2 for an eastern (90-110 degree) wave approach bin. A negative wave height change indicates a reduction in wave height, while a positive wave height change indicates an increase in wave height.

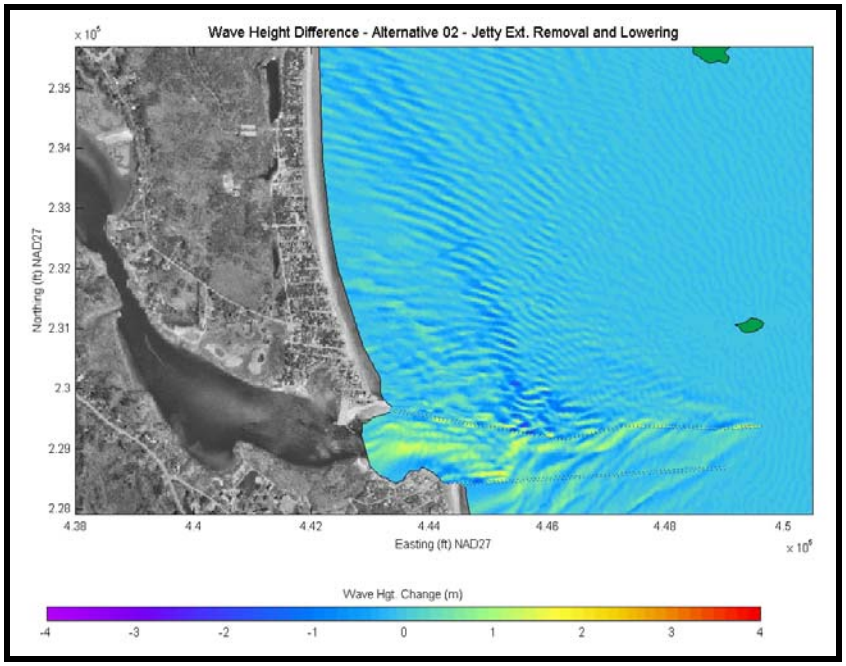

Figure 11-24. Wave height changes for Alternative 2 for a 10-year return period storm. A negative wave height change indicates a reduction in wave height, while a positive wave height change indicates an increase in wave height.

For average annual eastern approach scenario – Again, as was the case for Alternative 1, there are major wave energy increases in the entrance channel (42.8% energy increase, 0.25 m (0.8 ft) wave height increase). There are two locations that indicate wave energy reduction for the eastern approach direction. The first is the actual area of the lowering (Area E) on the northern jetty, which was expected due to reduced wave reflection off the structure in this region (12.5% reduction in energy). The second area that indicates a decease is Area B (12.5% reduction in energy) along the shoreline. Waves from this approach direction that were reflected off the structure onto the beach in this region are now eliminated. This is indicated by the blue bands that represented wave trains that were reflected off this portion of the structure under existing conditions.

- For the 10-yr storm case – The storm simulation indicates a 10.4% wave energy increase in the channel. The model also indicates a similar decrease (15% energy reduction) in Area E (the section of jetty lowered) due to the lack of reflection. However, due to the more northeast wave approach, the 10-yr storm case does not have a significant reduction along the shoreline in any area (zones A, B, or C), as indicated in Appendix 11-C. Therefore, this alternative is not as effective during the northeast prevalent storm cases.
- Overall, this alternative warrants little further study or consideration. The wave energy/heights in the entrance channel during both annual and storm conditions increases and although some benefit to the shoreline regions is apparent for the eastern average annual approach direction, other directional approaches; and storm cases, exhibit little to no benefit. This alternative is not recommended.

11.8.6 Alternative 3: Seaward Placement of 750-foot Spur Jetty

The next six (6) alternatives discuss variations in spur jetty configurations extending off the northern jetty. This includes length, location along the structure, number of spurs, and orientation of the spur. Although the possibilities are endless, the alternatives are narrowed through evaluation of the existing condition wave fields and focusing on permutations of the most effective baseline cases.

Figure 11-25 presents the wave height difference plot for Alternative 3 under a 10-year return period storm scenario. The average annual eastern (90-110 degree) approach bin wave height differences are presented in Appendix 11-B, while percent energy changes are presented in Appendix 11-C.

For average annual eastern approach scenario – Zone D, which lies directly landward of the spur experiences significant energy reductions (approximately 18%), while critical zones A and B indicate minor energy reductions, 9% and 8%, respectively. Increased wave energy occurs in zone F on the order of approximately 20%. For this approach simulation, the alternative is minimally effective.

- For the 10-yr storm case – Wave height reduction is significant directly landward of the structure (approximately 2 m (6.6 ft)), but wave height reduction is small for zones A and B along the coast (less than 0.1 meters). The position of the spur jetty does not intercept a majority of the waves that are reflected back towards

Camp Ellis Beach. Wave energy is reduced approximately 5% in the A and B region. A significant increase in wave energy is also visible in the animations and quantified in Appendix 11-C in zone F (approximately 26%). This increase may result in some structural maintenance concerns during storm events.

- Although this alternative does intercept a portion of the wave energy that is reflected off of the northern jetty, its layout and location does not significantly improve the wave energy acting on zones A and B. Therefore, this alternative warrants little further study or consideration, and is not recommended.

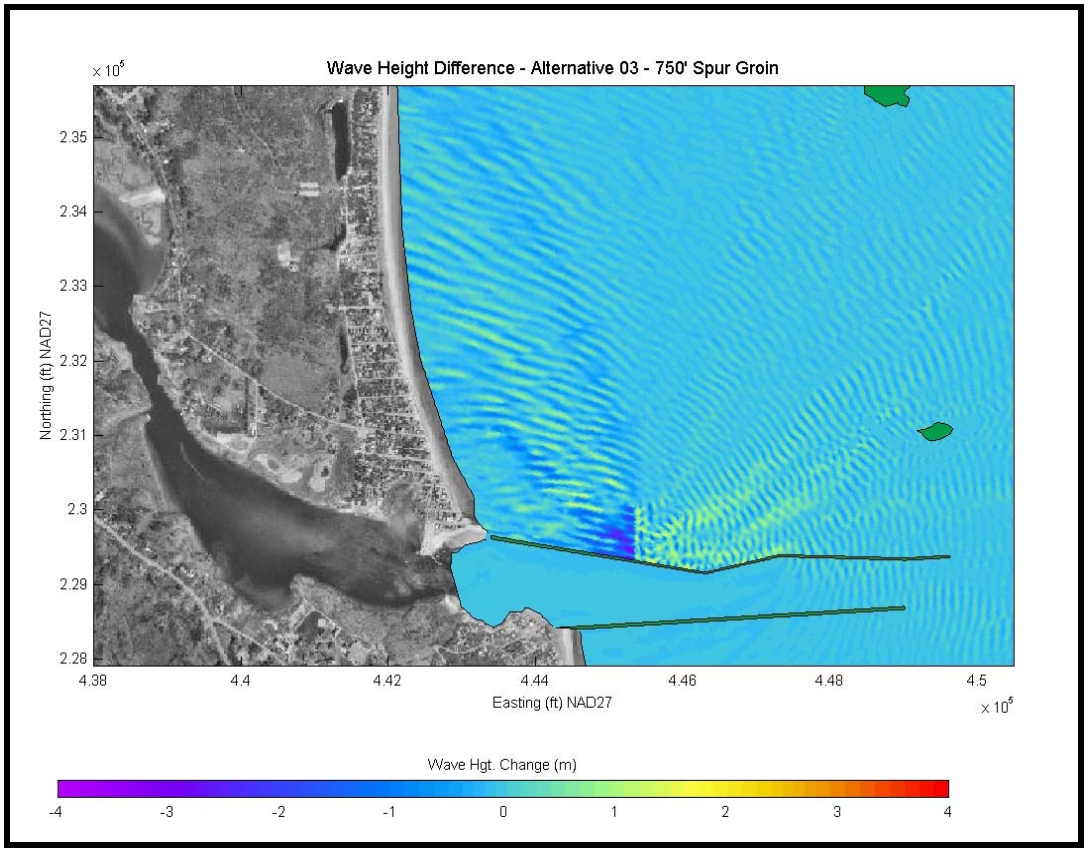

Figure 11-25. Wave height changes for Alternative 3 for a 10-year return period storm. A negative wave height change indicates a reduction in wave height, while a positive wave height change indicates an increase in wave height.

11.8.7 Alternative 4: Optimized Location of a 500-foot Spur Jetty

Figure 11-26 presents the wave height difference plot for Alternative 4 under a 10-year return period storm scenario. The average annual eastern (90-110 degree) approach bin wave height differences are presented in Appendix 11-B, while percent energy changes are presented in Appendix 11-C.

For the average annual eastern approach scenario – Similar results to Alternative 3, with a significant energy decrease in zone D (approximately 30%), moderate increases in

zones E and F (approximately 10%), and minimal decreases in energy in zones A and B (less than 10%). There is a slight increase in wave energy (3%) in zone C for this approach scenario, as well.

- For the 10-yr storm case – The storm case indicated similar results to the average annual eastern approach scenario. Wave height reduction is significant directly landward of the structure (approximately 2 m (6.6 ft)), but wave height reduction is small for zones A and B along the coast (less than 0.1 meters (0.3 ft)). The length of the spur jetty does not intercept a majority of the waves that are reflected back towards Camp Ellis Beach. Wave energy is reduced approximately 10% in zone A and 9% in zone B.
- Overall, results for this alternative are similar to Alternative 3, with a slight improvement during storm events. This alternative indicates the location is far improved over alternative 3; however, the reduction in the length of the structure (152 m from 228 m or 500 ft from 750 ft) decreases the effectiveness of Alternative 4. Although an improvement, in relation to the improved spur jetty alternatives, this alternative warrants little further study or consideration, and is not recommended.

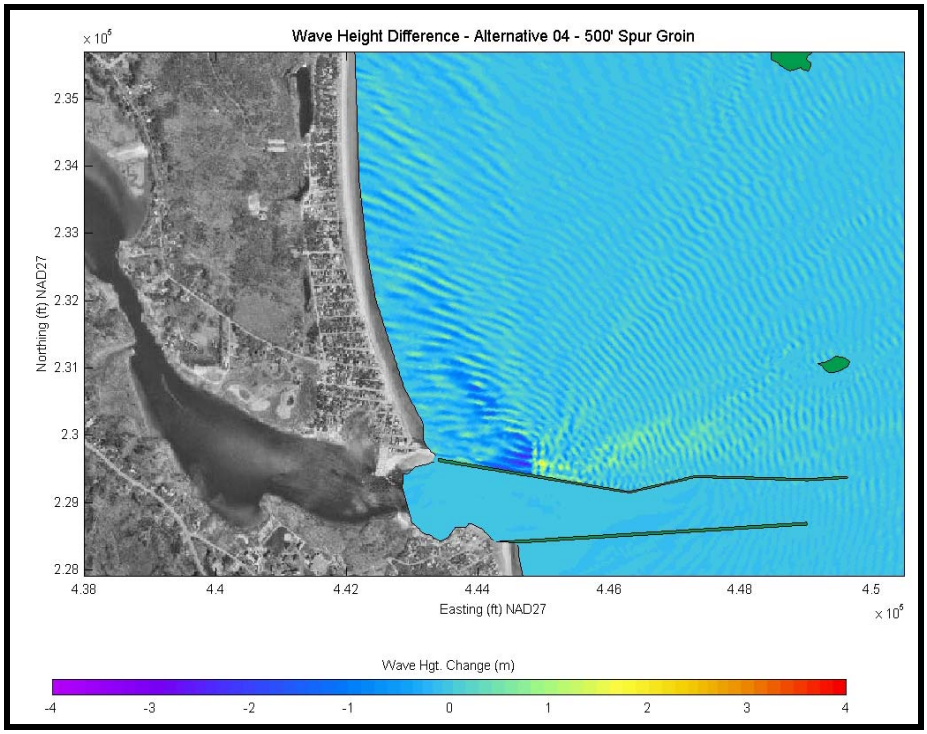

Figure 11-26. Wave height changes for Alternative 4 for a 10-year return period storm. A negative wave height change indicates a reduction in wave height, while a positive wave height change indicates an increase in wave height.

11.8.8 Alternative 5: Optimized Location of Dual 500-foot Spur Jetties

In an attempt to improve the spur jetty performance a second spur was added to Alternative 4. Figure 11-27 presents the wave height difference plot for Alternative 5 under a 10-year return period storm scenario. The average annual eastern (90-110 degree) approach bin wave height differences are presented in Appendix 11-B, while percent energy changes are presented in Appendix 11-C.

For average annual eastern approach scenario – Similar results to Alternative 4, with increased energy reduction within zone F due to the shadow zone caused by the second spur jetty.

For the 10-yr storm case – The reflected wave energy reduction can be clearly seen in Figure 11-27, but it is approximately the same amount of wave energy reduction as was present in Alternative 4. The only significant differences between the wave energy and wave height differences between Alternatives 4 and 5 occur along the northern jetty, where the dual spur jetties create a complex wave interaction.

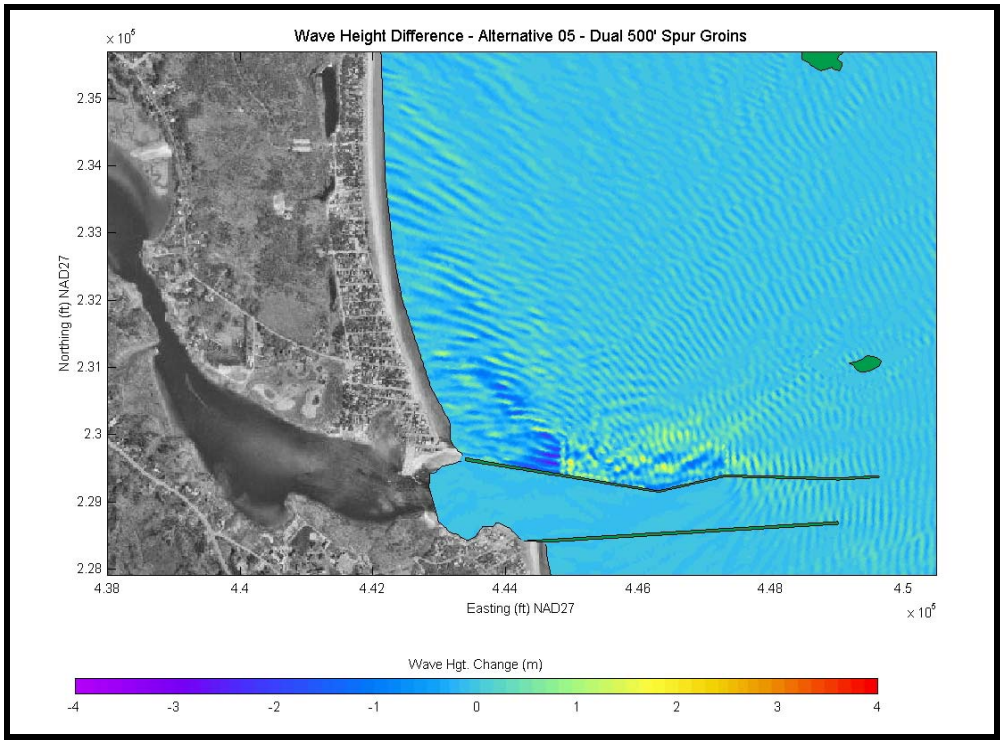

Figure 11-27. Wave height changes for Alternative 5 for a 10-year return period storm. A negative wave height change indicates a reduction in wave height, while a positive wave height change indicates an increase in wave height.

- Overall, the dual spur option shows little improvement over a single spur alternative, and also creates a region of significant wave turbulence in between the two spurs, along the length of the northern jetty. Although this alternative

eliminates the Mach-Stem wave and reduces a portion of the reflected wave energy, it doesn't offer significant improvement over the single spur cases, nor does it result in a significant energy reduction in zones A and B. This alternative is not recommended.

11.8.9 Alternative 6: Inshore Location of a 750-foot Spur Jetty

This alternative was build off the success of Alternative 4 and attempted to take advantage of an increased spur length at an optimized location. Figure 11-28 presents the wave height difference plot for Alternative 6 under the average annual eastern (90-110 degree) approach bin. Wave height differences for the 10-year return period storm event are presented in Figure 11-29, while percent energy changes are presented in Appendix 11-C.

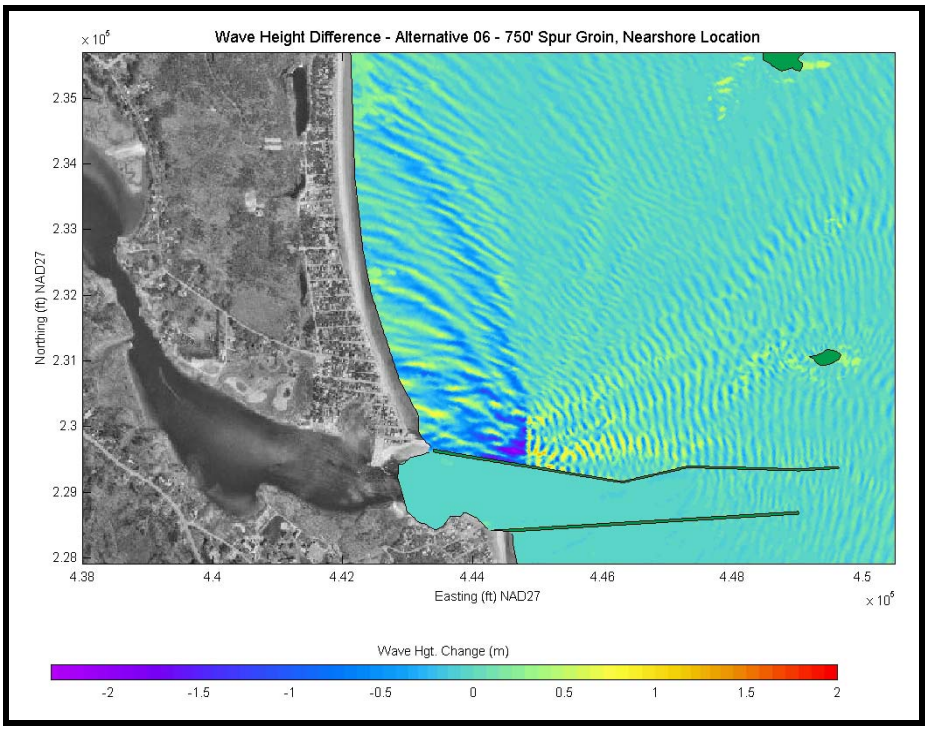

Figure 11-28. Wave height changes for Alternative 6 for an eastern (90-110 degree) wave approach bin. A negative wave height change indicates a reduction in wave height, while a positive wave height change indicates an increase in wave height.

For average annual eastern approach scenario – This is the first alternative that has shown significant wave energy reduction in zone A (17%), as well as wave energy reduction in both zones B and C (5%). The large reduction in wave energy in zone D (52%) also makes this alternative the best performing spur alternative that was simulated. Zones E and F show moderate energy increases (12-15%), as expected seaward of the spur. There also was no change in wave energy at the entrance to the navigational channel (zone H). Figure 11-28 clearly shows the interception of a good portion of the reflected wave

energy throughout the directional array. Waves are intercepted that would propagate to a significant stretch of Camp Ellis Beach.

For the 10-yr storm case – Alternative 6 also reduces wave energy within the same zones during the 10-year return period storm scenario. The percentage of reduction is not as great, but the overall wave height reduction is still significant. Again, reduced energy is indicated for zones A-D.

- Overall, Alternative 6 was the best performing spur alternative. A significant amount of the reflected wave is intercepted, it reduces wave energy in critical zones A, B, and D, while it does not negatively impact zone C or the entrance to the navigational channel (zone H). It is recommended that Alternative 6 be considered for further detailed assessment, including simulation of all wave approach directions and sediment transport assessment.

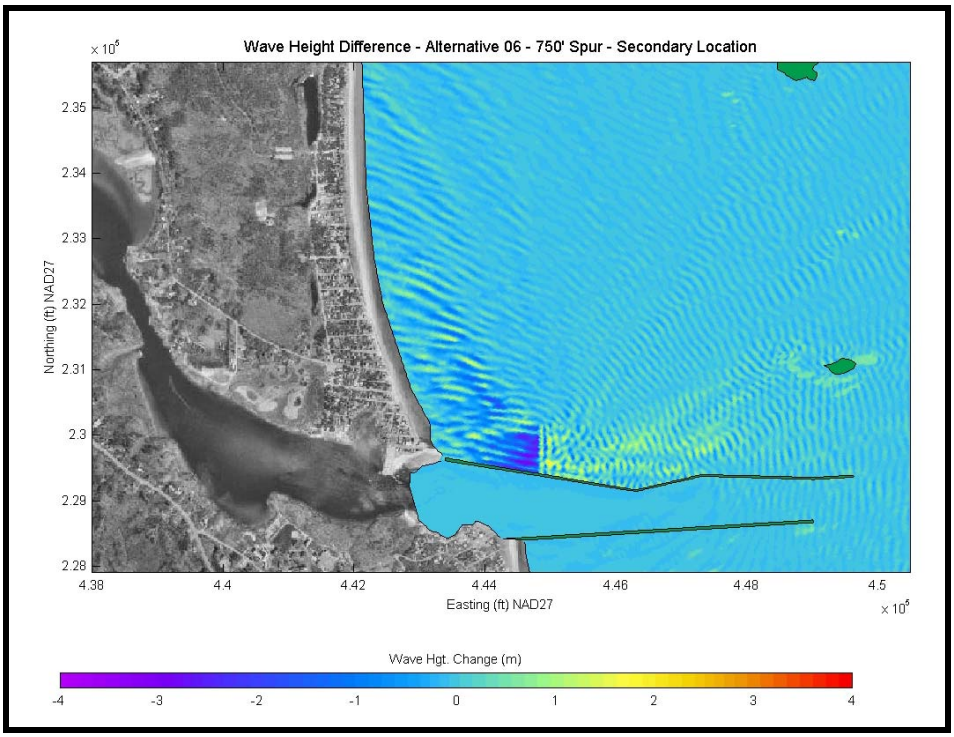

Figure 11-29. Wave height changes for Alternative 6 for a 10-year return period storm. A negative wave height change indicates a reduction in wave height, while a positive wave height change indicates an increase in wave height.

11.8.10 Alternative 7: Alternative 6 with Northern Jetty Extension Removal

Alternative 7 combined the best performing spur alternative (Alternative 6) with removal of the northern jetty extension. Wave height difference plots for Alternative 7 for both a 10-year return period storm scenario and the average annual eastern (90-110 degree) approach bin are presented in Appendix 11-B, while percent energy changes are presented in Appendix 11-C.

The results of this alternative were the same as Alternative 6 with the only difference related to an approximately 20% increase of wave energy at the entrance to the navigational channel (zone H). Additionally, no significant improvement on shoreline protection is added by removing the northern jetty extension. This alternative warrants little further study or consideration, and is not recommended.

11.8.11 Alternative 8: Alternative 6 with Terminal Groin

Alternative 8 combined the best performing spur alternative (Alternative 6) with inclusion of a terminal groin located approximately 910 m (3,000 ft) north of the northern jetty along Camp Ellis Beach (approximately at the northern end of zone B). Percent energy changes for Alternative 8 are presented in Appendix 11-C.

The terminal groin does not have any significant influence on the wave transformation in the vicinity of Camp Ellis Beach. The primary purpose of the terminal groin is to help contain sand within the beach nourishment project region and minimize the amount of sand escaping northward. The terminal groin will also likely have a negative influence on the adjacent northerly coastline by cutting off a sediment source and not allowing sand to be transported into the area. As the sediment supply from Camp Ellis Beach continues to be depleted, it is likely that erosion may continue to advance northward as no sediment will be supplied from Camp Ellis to the beaches to the north. Therefore, this terminal groin would likely have a negative impact in the future. It may be feasible that the overall benefit of the terminal groin can be much better accomplished through the use of T-Head groins, which are presented in the next two alternatives. If shore-attached structures are potentially required or were recommended, the T-Head groins would be a better performing alternative than a single terminal groin. As such, Alternative 8 is not recommended for further consideration.

11.8.12 Alternative 9 and 10: T-Head Groin Configurations

Figure 11-30 presents the wave height difference plot for Alternative 9 under the average annual eastern (90-110 degree) approach bin, while Figure 11-31 presents the wave height difference plot for Alternative 10 under the average annual eastern (90-110 degree) approach bin. Wave height differences for the 10-year return period storm event for both alternatives are presented in Appendix 11-B, while percent energy changes are presented in Appendix 11-C.

Both Alternative 9 and 10 represent additional cases with shore-attached structures that are difficult to directly assess in terms of wave energy reduction. The primary purpose of the T-head groins is to contain sand in the nearshore region fronting Camp Ellis Beach. The wave energy changes show some reduction in wave energy in zones A (6-13%) and B (1-4%) for Alternative 9, located behind the head of the structures. Wave energy changes for Alternative 10 are local only, behind each individual structure. Comparing Alternative 9 and 10, Alternative 9 clearly has the better layout configuration. No additional wave changes occur throughout the entire domain. The T-head groins would likely be effective at holding sand in place from a beach nourishment scenario, but also likely may have significant impacts on neighboring beaches by only allowing minimal sand movement. The assessment of the T-head groins is primarily based on their

influence on sediment transport processes. Therefore, the best T-head groin alternative (Alternative 9) is recommended for consideration in the sediment transport assessment (Chapter 12.0) to assess impact on beaches to the north.

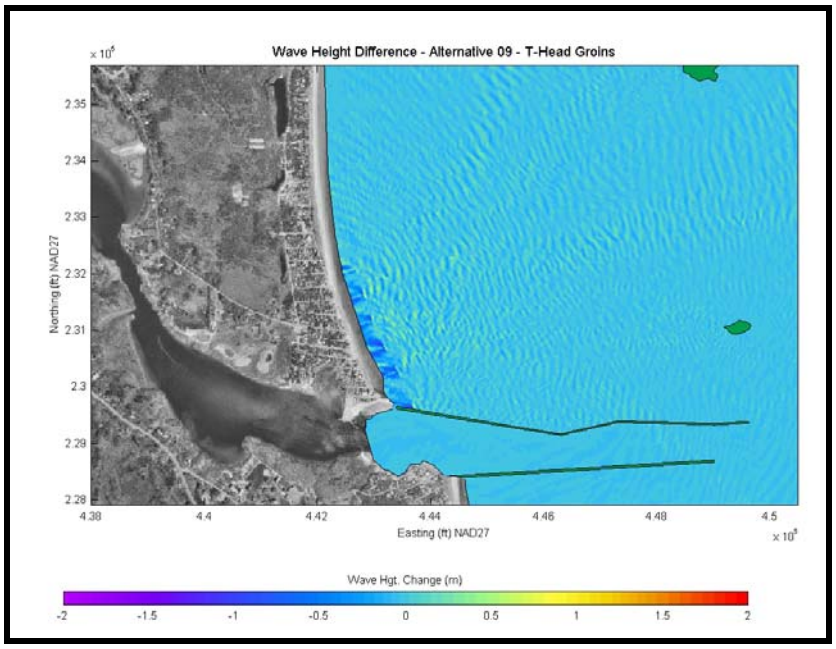

Figure 11-30. Wave height changes for Alternative 9 for an eastern (90-110 degree) wave approach bin. A negative wave height change indicates a reduction in wave height, while a positive wave height change indicates an increase in wave height.

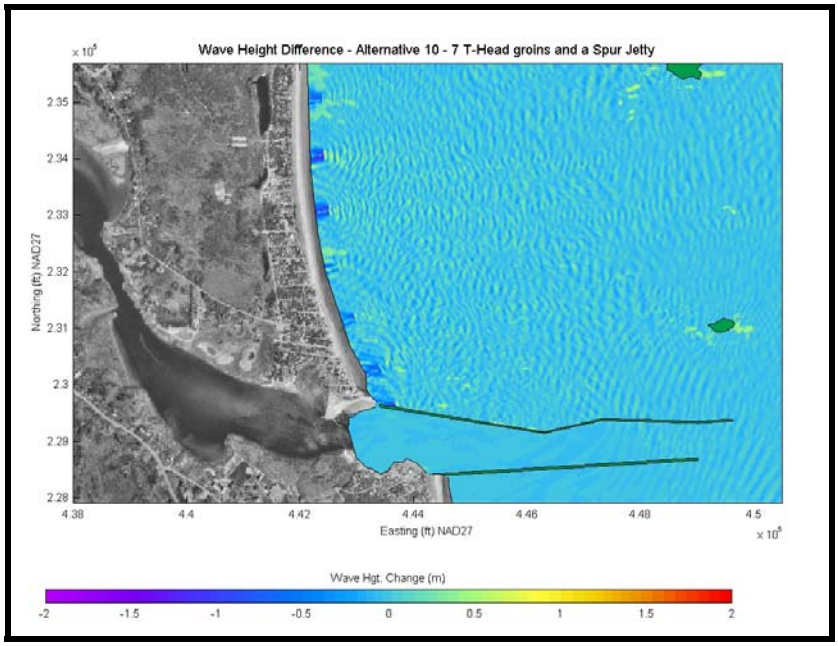

Figure 11-31. Wave height changes for Alternative 10 for an eastern (90-110 degree) wave approach bin. A negative wave height change indicates a reduction in wave height, while a positive wave height change indicates an increase in wave height.

11.8.13 Alternative 11: Offshore Breakwater, Seaward Location

The following three alternatives assess the feasibility of using an offshore breakwater to mitigate the erosion at Camp Ellis Beach. The breakwaters were positioned based on the results of the existing conditions model by intercepting a significant amount of wave energy impacting both Camp Ellis Beach and the northern structure. Three different locations, placing the breakwater at different water depths were simulated.

The Alternative 11 breakwater was specifically sited to intercept a consistent wave train that passes between Eagle and Ram Islands, as illustrated in the existing conditions evaluation. Figure 11-32 presents the wave height difference plot for Alternative 11 for a 10-year return period storm scenario. The average annual eastern (90-110 degree) approach bin wave height difference plot is presented in Figure 11-33, while percent energy changes are presented in Appendix 11-C.

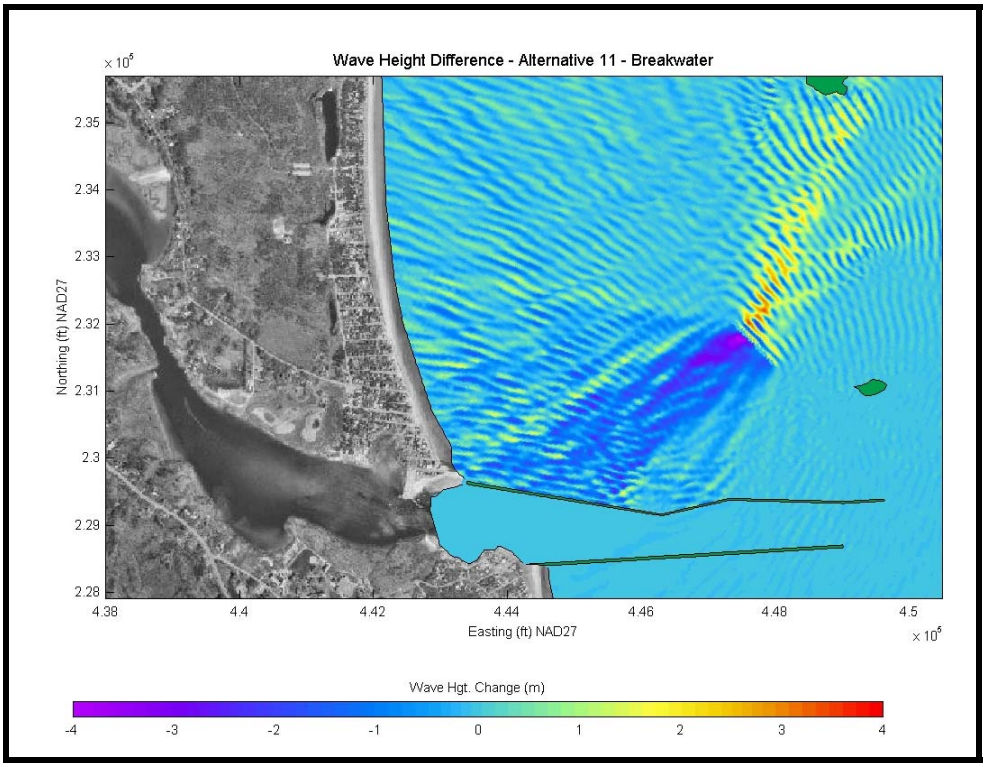

Figure 11-32. Wave height changes for Alternative 11 for a 10-year return period storm. A negative wave height change indicates a reduction in wave height, while a positive wave height change indicates an increase in wave height.

For average annual eastern approach scenario – The offshore breakwater, located at the seaward position, produces a significant reduction in wave energy throughout the local area. Wave heights are reduced by up to 2 m (6.6 ft) in this average annual approach direction. Wave energy is reduced in almost all zones, and significantly in zone B (28%). However, for this approach direction, the offshore breakwater fails to reduce the wave

energy in zone A. This is due to the wave train that propagates nearly parallel to the northern jetty and is able to bypass the influence of the offshore breakwater. So although the Alternative 11 breakwater is able to reduce a significant amount of wave energy arriving from between Eagle and Ram Islands, this alternative misses the wave propagating along the structure.

- For the 10-yr storm case – With a more northeastern approach, the Alternative 11 breakwater intercepts a majority of the wave energy. Wave heights are reduced by up to 4 m (13.1 ft) in the shadow zone of the breakwater and approximately 2 m (6.6 ft) for a significant region behind the structure. The wave energy is reduced in every zone, with significant reductions in zones A (19%), D (40%), and E (47%). Zone B (9%) and C (2%) also experience reduced wave energy for the 10-year storm.

- Overall, the Alternative 11 breakwater performs well; however, it also has significant limitations under the average annual eastern approach conditions and does not produce consistent wave energy reduction in the critical regions. The increased water depth also adds significant difficulty in construction and maintenance. These factors, coupled with the improved performance of some of the other breakwater alternatives, render Alternative 11 unworthy of further consideration, and it is not recommended.

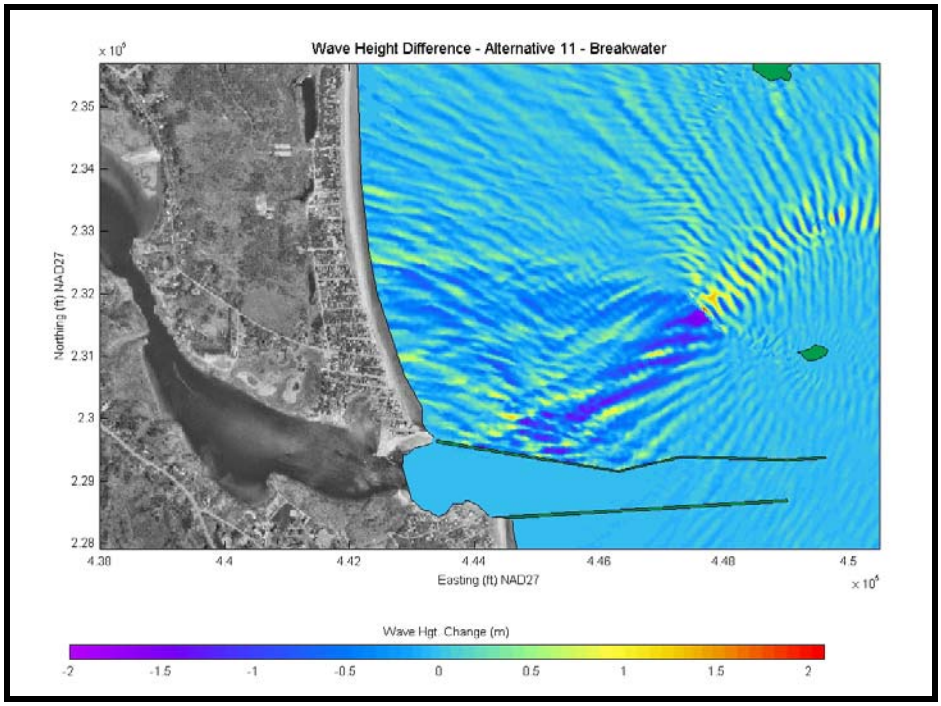

Figure 11-33. Wave height changes for Alternative 11 for an eastern (90-110 degree) wave approach bin. A negative wave height change indicates a reduction in wave height, while a positive wave height change indicates an increase in wave height.

11.8.14 Alternative 11a: Offshore Breakwater, Inshore Location

Figure 11-34 presents the wave height difference plot for Alternative 11a under a 10-year return period storm scenario. The average annual eastern (90-110 degree) approach bin wave height differences are presented in Appendix 11-B, while percent energy changes are presented in Appendix 11-C. The location of the breakwater for this alternative was shifted landward and oriented to provide direct protection to zones A and B along Camp Ellis Beach.

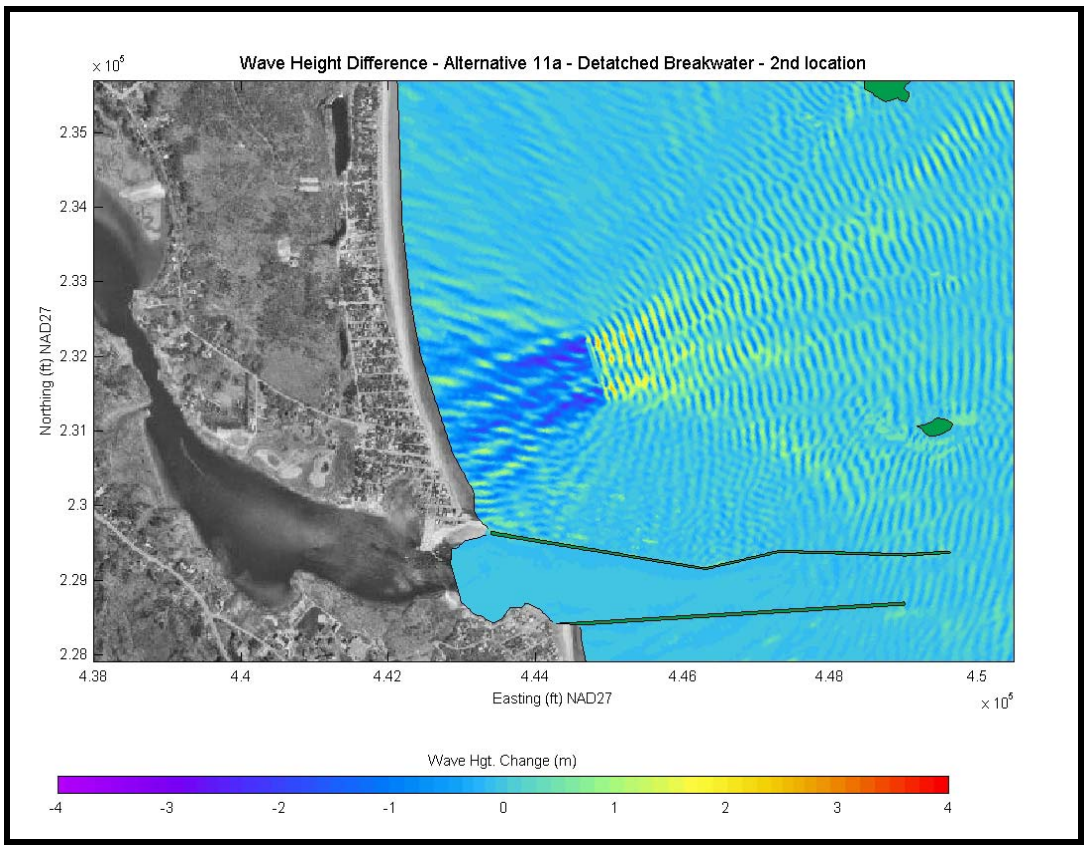

Figure 11-34. Wave height changes for Alternative 11a for a 10-year return period storm. A negative wave height change indicates a reduction in wave height, while a positive wave height change indicates an increase in wave height.

For average annual eastern approach scenario – The Alternative 11a breakwater, located at the inshore position, focuses on wave energy reduction in zones A and B. Wave heights are reduced by up to 2 m (6.6 ft) in this average annual approach direction. Wave energy is reduced by 12% in zone A and 52% in zone B. There is also no negative impact on zone C, which shows a wave energy reduction of 2.5%. Insignificant wave energy changes occur throughout the rest of the local domain.

- For the 10-yr storm case – Alternative 11a consistently reduces wave energy in zones A and B. The 10-year return period storm case shows energy reduction of

22% in zone A and 37.5% in zone B. Wave heights are reduced by up to 3 m (9.8 ft) in the shadow zone of the breakwater and approximately 2 m (6.6 ft) for a significant region behind the structure.

- Overall, the Alternative 11a breakwater is the best performing breakwater alternative. It consistently reduced wave energy in the most critical areas, without negative influence on adjacent shores. The breakwater is also located in shallower water, reducing construction, cost, and maintenance concerns. It is recommended that Alternative 11a be considered for further detailed assessment, including simulation of all wave approach directions and sediment transport assessment.

11.8.15 Alternative 11b: Offshore Breakwater, Intermediate Location

Figure 11-35 presents the wave height difference plot for Alternative 11b under a 10-year return period storm scenario. The average annual eastern (90-110 degree) approach bin wave height differences are presented in Appendix 11-B, while percent energy changes are presented in Appendix 11-C. The location of the breakwater for this alternative was selected in an intermediate water depth between Alternative 11 and 11a.

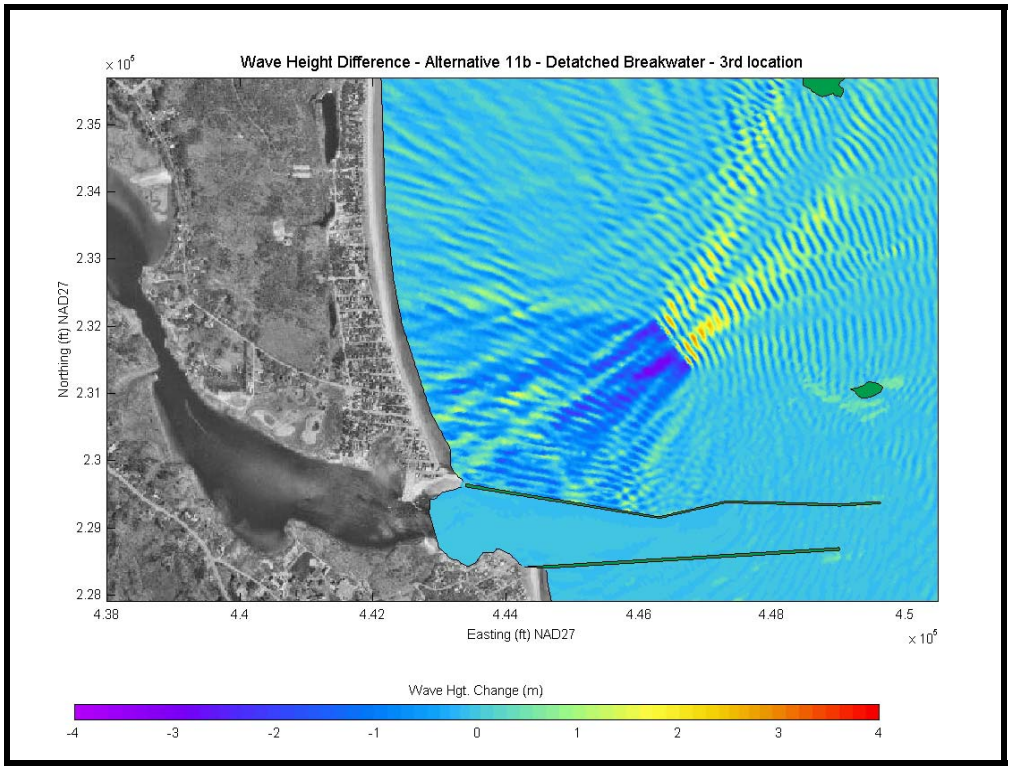

Figure 11-35. Wave height changes for Alternative 11b for a 10-year return period storm. A negative wave height change indicates a reduction in wave height, while a positive wave height change indicates an increase in wave height.

The Alternative 11b breakwater did not perform as well as Alternative 11a. The reduction in wave energy was significantly less for every zone in both scenarios simulated. Therefore, this alternative warrants little further study or consideration, and is not recommended since there is a better performing breakwater alternative.

11.8.16 Alternative 12: Alternative 11a and Seaward Location of 500-ft Spur Jetty

Alternative 12 and 18 represent combinations of the best performing breakwater configuration and a spur jetty. Figure 11-36 presents the wave height difference plot for Alternative 12 under a 10-year return period storm scenario. The average annual eastern (90-110 degree) approach bin wave height differences are presented in Appendix 11-B, while percent energy changes are presented in Appendix 11-C.

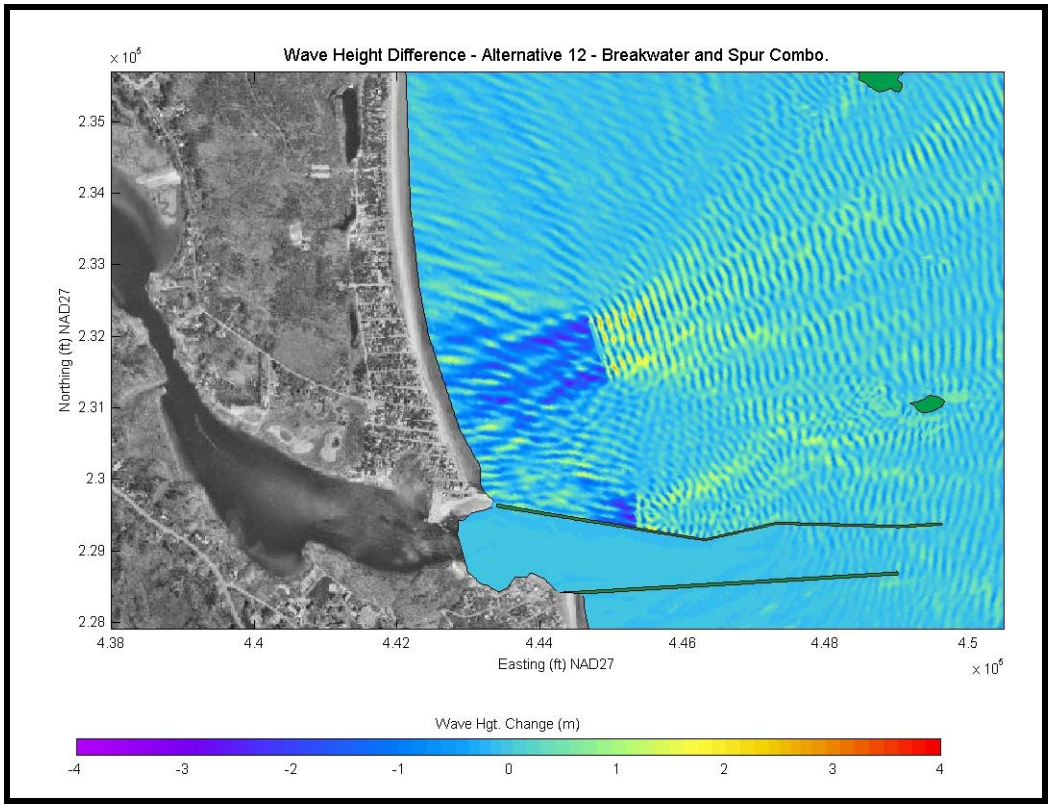

Figure 11-36. Wave height changes for Alternative 12 for a 10-year return period storm. A negative wave height change indicates a reduction in wave height, while a positive wave height change indicates an increase in wave height.

Alternative 12 improves on Alternative 11a by eliminating a portion of the reflected wave energy from the nearshore region through use of a spur jetty. Increases in energy reduction (Appendix 11-C) occur for all of the critical zones; however, Alternative 18 exceeds the performance of Alternative 12 by repositioning the spur jetty to the optimal

location. Therefore, although Alternative 12 indicates effective performance, it is not recommended for further analysis since Alternative 18 outperformed it.

11.8.17 Alternative 13: Comb Configuration of Spur Jetties

Figure 11-37 presents the wave height difference plot for Alternative 13 under a 10-year return period storm scenario. The average annual eastern (90-110 degree) approach bin wave height differences are presented in Appendix 11-B, while percent energy changes are presented in Appendix 11-C.

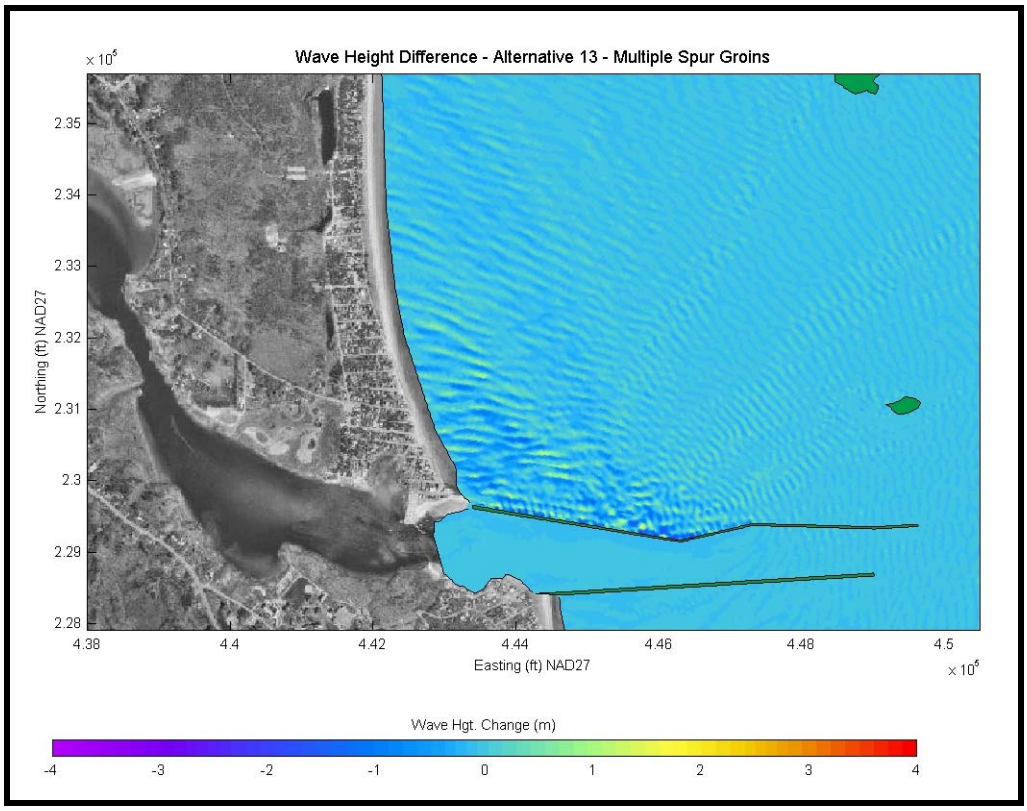

Figure 11-37. Wave height changes for Alternative 13 for a 10-year return period storm. A negative wave height change indicates a reduction in wave height, while a positive wave height change indicates an increase in wave height.

Alternative 13 was effective at diminishing the reflective wave energy and Mach-Stem effects, but only to a minimal to moderate level. Energy reduction in both the average annual approach and 10-year return period storm were approximately 2-10% for zones along the structure. When compared to some of the better performing alternatives, and considering the logistical hurdles associated with installing 19 small individual structures, Alternative 13 is not recommended for further analysis.

11.8.18 Alternative 14: Offshore Borrow Pit

Figure 11-38 presents the wave height difference plot for Alternative 14 under a 10-year return period storm. The average annual eastern (90-110 degree) approach bin wave height differences are presented in Appendix 11-B, while percent energy changes are presented in Appendix 11-C.

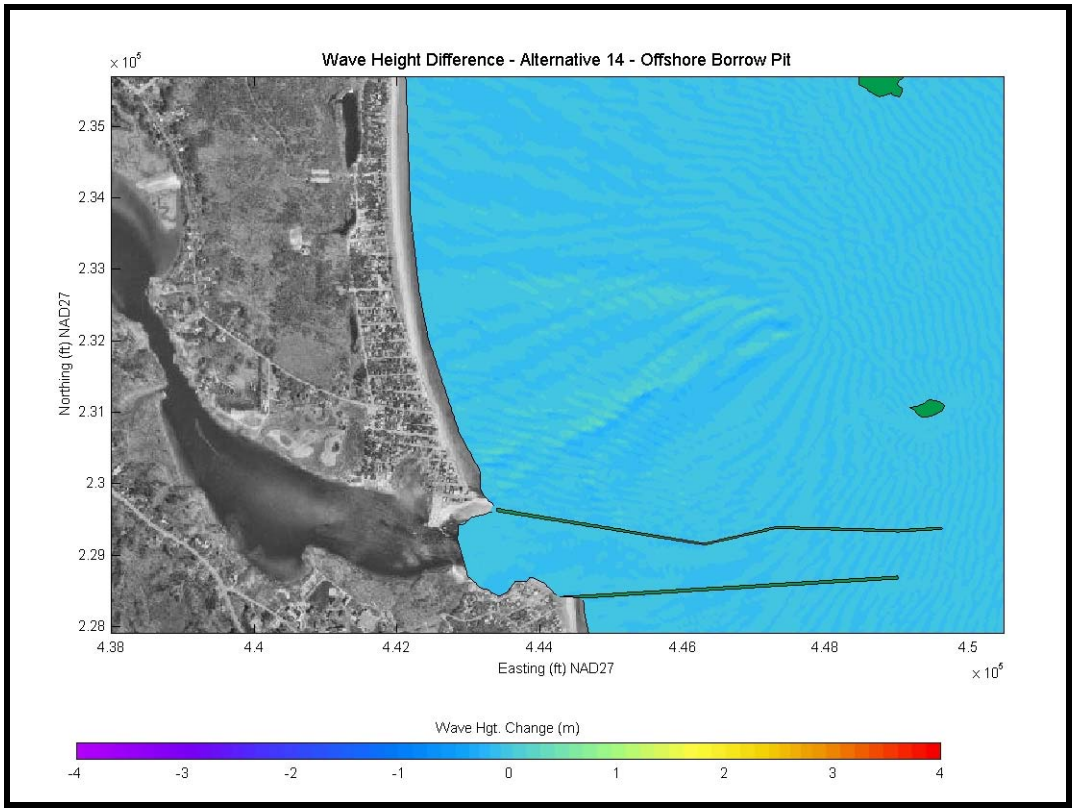

Figure 11-38. Wave height changes for Alternative 14 for a 10-year return period storm. A negative wave height change indicates a reduction in wave height, while a positive wave height change indicates an increase in wave height.

As shown in Figure 11-38, the offshore borrow pit had minimal influence on the wave field and transformation. Wave height changes were only a maximum of 0.4 m (1.3 ft) during the 10-year return period storm case, and there were no significant wave energy changes within the entire region. The net result is that an offshore borrow site, at least one of reasonable depth and dimensions, would not improve conditions at Camp Ellis Beach over existing conditions. Based on the minimal changes and underperformance, the offshore borrow pit is not recommended.

11.8.19 Alternative 15: Alternative 3 with Angled Orientation

Figure 11-39 presents the wave height difference plot for Alternative 15 under a 10-year return period storm scenario. The average annual eastern (90-110 degree) approach bin

wave height differences are presented in Appendix 11-B, while percent energy changes are presented in Appendix 11-C.

In the 10-year return period scenario, maximum wave height decrease was 3 m (9.8 ft), located directly in the shadow of the angled spur. Wave energy reduction was most significant in zone D (18%), while zone B showed minor reduction (6%). There was a significant increase in wave energy in zone F (+36%). Alternative 15 showed no change in wave energy in zone A, and did not perform as well as Alternative 6, which was the best performing straight spur jetty alternative. In the wave transformation animation, it was evident that the angled spur was not as effective at intercepting the important wave trains that were reflected off of the northern jetty and directed at Camp Ellis Beach. Therefore, this alternative warrants little further study or consideration, and is not recommended.

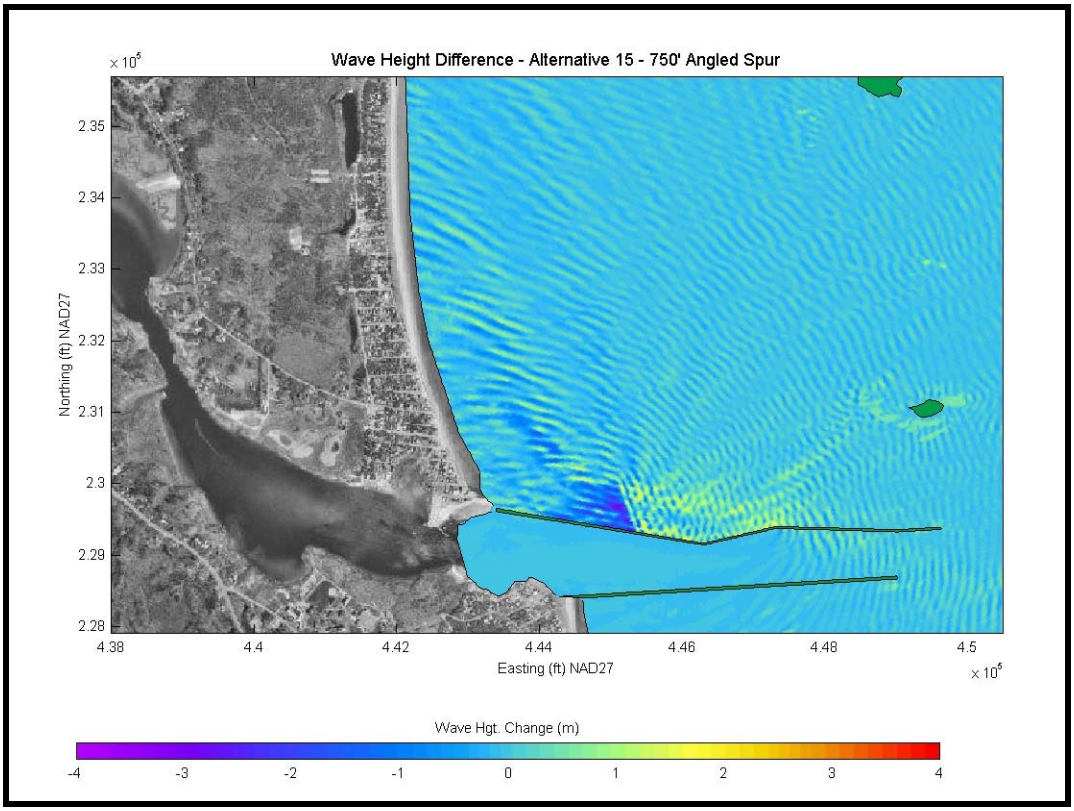

Figure 11-39. Wave height changes for Alternative 15 for a 10-year return period storm. A negative wave height change indicates a reduction in wave height, while a positive wave height change indicates an increase in wave height.

11.8.20 Alternative 16: Northern Jetty Roughening

Figure 11-40 presents the wave height difference plot for Alternative 16 under a 10-year return period storm scenario. The average annual eastern (90-110 degree) approach bin wave height differences are presented in Appendix 11-B, while percent energy changes

are presented in Appendix 11-C. The northern jetty was numerically roughened by reducing the reflection coefficient for the northern jetty by approximately 40%. It is debatable if the jetty could potentially be roughened to that extent, considering the existing size and length of the structure. It would likely require a nearly complete reconstruction of a significant portion of the jetty. However, this level of roughening was simulated in the model to determine if Alternative 16 was viable even under the best roughening conditions.

The jetty roughening alternative indicated moderate wave height and zone energy reductions throughout the domain. Jetty roughening does impact the amount of reflected wave energy that is directed back toward the Camp Ellis Beach shoreline and the development of the Mach-stem effects. Wave energy reductions ranged from 3 to 17% for the critical zones along the shoreline. Although indicating moderate success at reducing wave energy, jetty roughening did not produce the same level of energy loss as some of the other alternatives. Therefore, this alternative warrants little further study or consideration, and is not recommended.

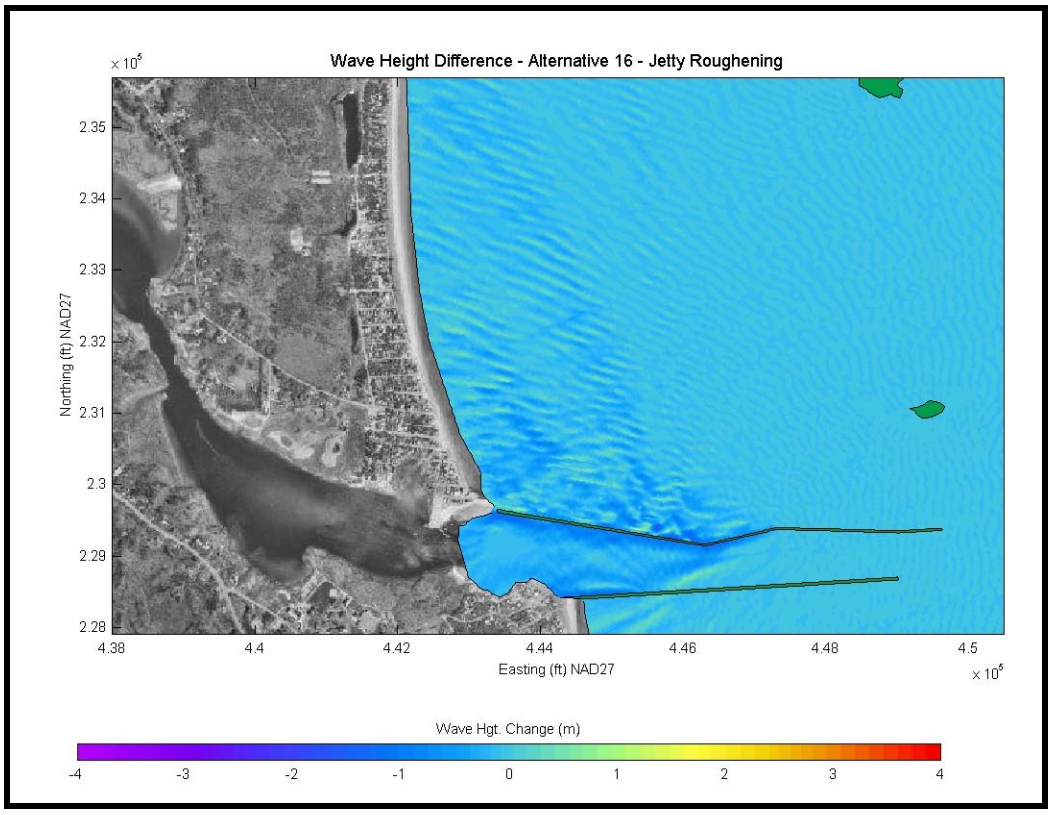

Figure 11-40. Wave height changes for Alternative 16 for a 10-year return period storm. A negative wave height change indicates a reduction in wave height, while a positive wave height change indicates an increase in wave height.

11.8.21 Alternative 17: Submerged Breakwater / Rock Outcrop

Figure 11-41 presents the wave height difference plot for Alternative 17 under a 10-year return period storm scenario. The average annual eastern (90-110 degree) approach bin wave height differences are presented in Appendix 11-B, while percent energy changes are presented in Appendix 11-C.

The submerged breakwater/rock outcrop alternative performed similar to the offshore borrow pit alternative. The amount of wave energy reduction was minimal (less than 3% in critical areas) and wave height reduction was less than a meter, even in areas directly adjacent to the submerged feature. The submerged feature does have some benefits, but it lags behind the emergent structures in terms of performance. The potential significant maintenance requirements and difficulties associated with maintaining a submerged structure, as well as the hindrance to navigation, are also significant concerns when considering a submerged solution at this location. Although beneficial, it does not perform well enough to solve the problem at Camp Ellis Beach. Therefore, this alternative warrants little further study or consideration, and is not recommended.

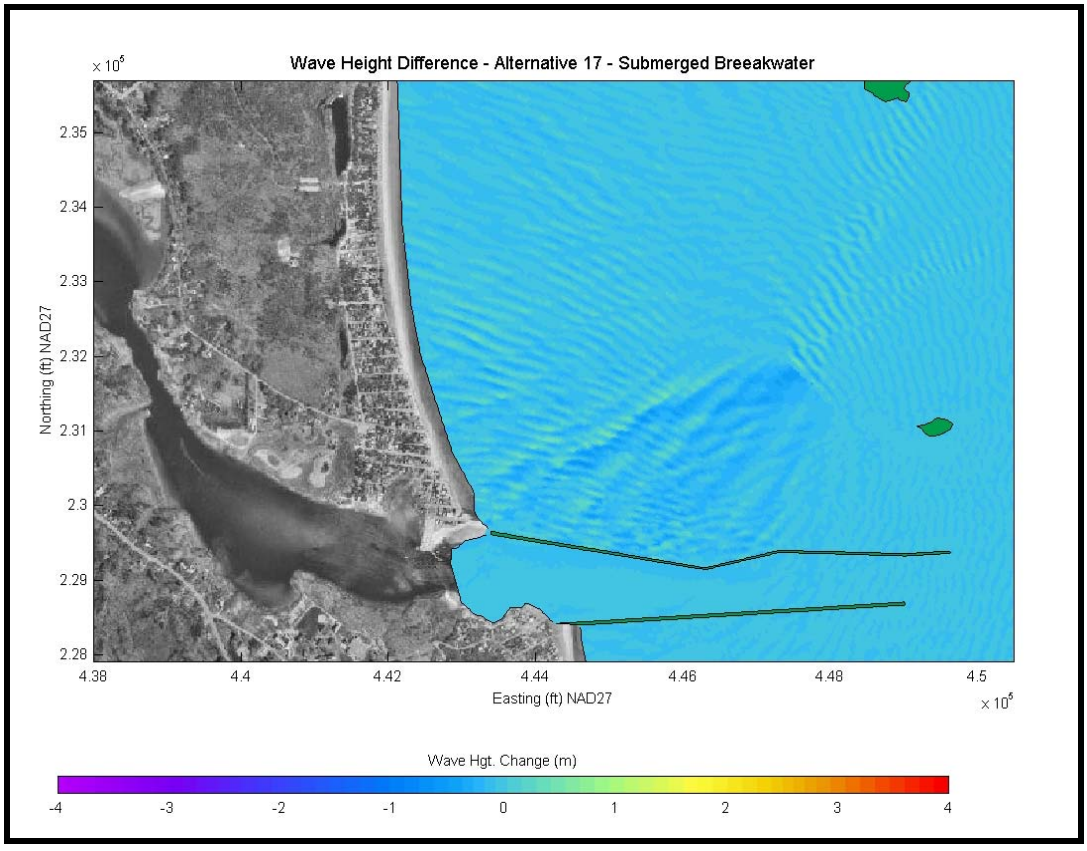

Figure 11-41. Wave height changes for Alternative 17 for a 10-year return period storm. A negative wave height change indicates a reduction in wave height, while a positive wave height change indicates an increase in wave height.

11.8.22 Alternative 18: Alternative 11a and Inshore Location of 500-ft Spur Jetty

Figure 11-42 presents the wave height difference plot for Alternative 18 under a 10-year return period storm scenario. The average annual eastern (90-110 degree) approach bin wave height differences are presented in Appendix 11-B, while percent energy changes are presented in Appendix 11-C. This alternative builds on the performance of 11a and adds a spur jetty. Alternative 12 presented a similar option; however, alternative 18 repositions the spur jetty at the same location as in Alternative 6, which proved to be the best performing spur jetty alternative.

For the average annual eastern approach scenario – Alternative 18 indicates high performance, with wave height reductions of 1 to 2 m (3.3 to 6.6 ft) in the regions landward of the proposed structures. The wave energy for the average annual eastern approach case is significant in the three most critical zones. Zone A is reduced by over 26%, zone B is reduced by over 56%, and zone D is reduced by nearly 30%. There are no negative impacts to zone C, which also show a decrease in wave energy of over 3%. Wave energy is increased seaward of the proposed structures from 2–11%.

- For the 10-yr storm case – Alternative 18 shows similar performance to the average annual eastern approach scenario. The wave heights are decreased by 2 to 3 m (3.3 to 6.6 ft) landward of the proposed structures, with average reductions of approximately 0.5 to 0.6 m (1.6 to 2.0 ft) in zones along the shoreline (A and B). The 10-year return period storm case shows energy reduction of approximately 35% in zone A, approximately 51% in zone B, and approximately 28% in zone D. Again, there are no negative impacts to zone C, which also show a decrease in wave energy of approximately 3%. Wave energy is increased seaward of the proposed structures to approximately 11-18%.

- Overall, the Alternative 18 combination is the best performing breakwater/spur alternative. The animations of wave propagation show the scenario intercepts a majority of the wave energy, missing only a single wave train that passes between the two structures. Alternative 18 consistently reduced wave energy in the most critical areas, without negative influence on adjacent shores. It is recommended that Alternative 18 be considered for further detailed assessment, including simulation of all wave approach directions and sediment transport assessment.

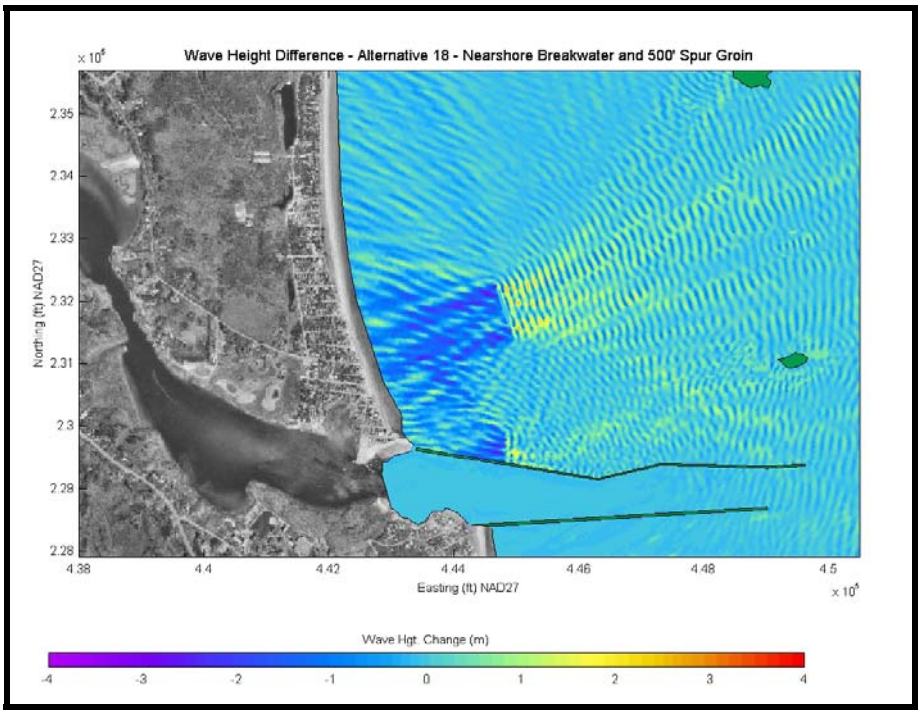

Figure 11-42. Wave height changes for Alternative 18 for a 10-year return period storm. A negative wave height change indicates a reduction in wave height, while a positive wave height change indicates an increase in wave height.

11.8.23 Alternative 19: 750 foot Spur Jetty, Jetty Roughening, and Jetty Removal

Figure 11-43 presents the wave height difference plot for Alternative 19 under a 10-year return period storm scenario. The average annual eastern (90-110 degree) approach bin wave height differences are presented in Appendix 11-B, while percent energy changes are presented in Appendix 11-C. This alternative attempts to build on the beneficial performance of Alternative 6 through jetty roughening and removal.

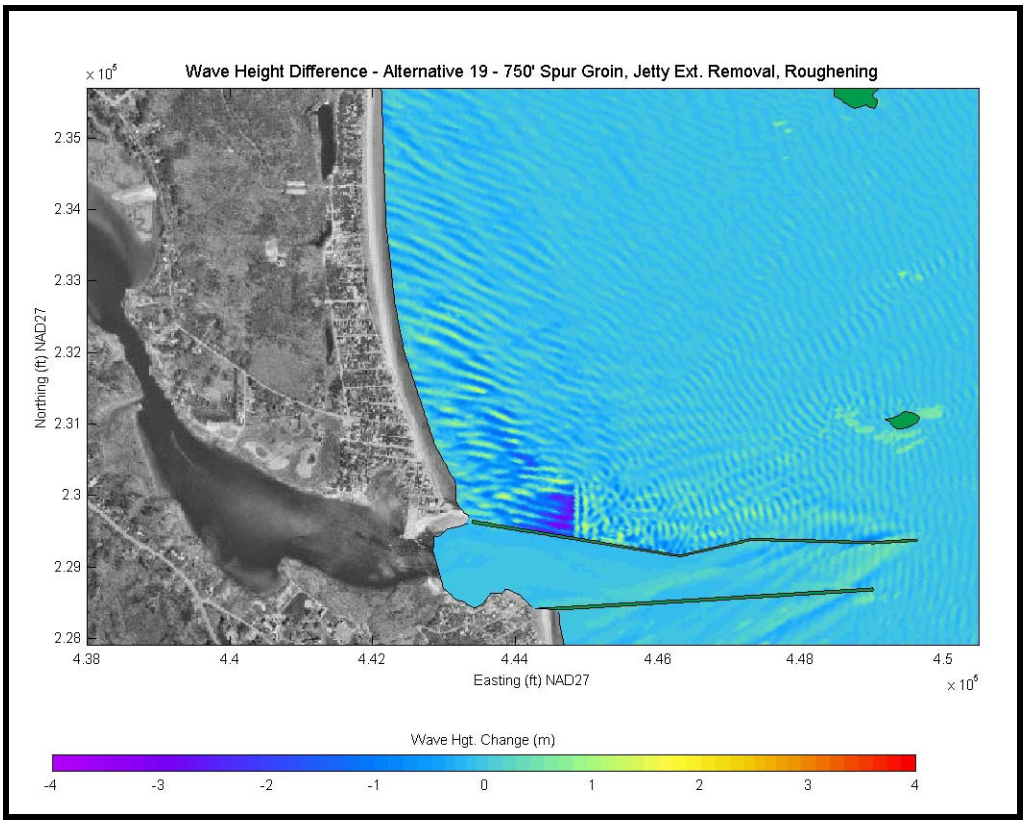

Figure 11-43. Wave height changes for Alternative 19 for a 10-year return period storm. A negative wave height change indicates a reduction in wave height, while a positive wave height change indicates an increase in wave height.

- Alternative 19 shows minimal performance gains over Alternative 6. Wave energy reduction for both the 10-year return period storm remains under 10% for the shoreline areas, while the average annual eastern directional approach performs significantly better due to the spur jetties ability to intercept the wave train propagating directly parallel to the northern jetty. Although there are some improvements over Alternative 6, they are not great enough to warrant the significant construction component of the added roughening and removal. In addition, as is the case for any removal option, there is an increase in wave energy at the entrance to the navigational channel, impacting both vessel traffic and maintenance requirements. Alternative 19 is not recommended for further analysis.

11.8.24 Alternative 20 and 21: Alternative 11a with Estimated Salient Formations

As presented in Chapter 10.0, Alternative 20 and 21 do not represent specific alternatives, rather are a subset of expected shoreline response simulations in relation to alternative 11a and other offshore breakwater scenarios. Estimates of salient formation (discussed in detail in Chapter 12.0) are developed to determine the impact of salient formations on wave energy. A salient is a coastal formation of beach material developed by wave refraction, wave diffraction, and longshore drift producing a bulge in the coastline behind

an offshore island or breakwater. If the salient connects to the offshore feature/structure, it is termed a tombolo. Figure 10-20 presents an example of the expected shoreline response to alternative 11a. These alternatives (20 and 21) helped to gauge the wave changes occurring due to expected shoreline response and are discussed in Chapter 12.0.

11.8.25 Alternatives 22-26: Segmented Breakwater Configurations

The following alternatives (22–26) comprise a series of segmented breakwater configurations, as presented in Chapter 10.0. The configuration and dimensions of the segmented breakwaters were designed based on the existing wave conditions in the regions, as well as the geotechnical (foundation condition) limitations. Figures 11-44 through 11-49 presents the wave height difference plot for Alternatives 22-26, respectively, for a 10-year return period storm scenario. The average annual eastern (90-110 degree) approach bin wave height differences are presented in Appendix 11-B, while percent energy changes are presented in Appendix 11-C.

Due to the proximity of the segmented breakwater alternatives to the shoreline, zone B was divided such that the presence of the segmented breakwaters did not divide the energy zone. This was required so that the energy zone wasn't identifying both the reduced energy landward of the structure, and the increased energy seaward of the structure. Ultimately, the concern is related to the wave energy at the shoreline. The smaller zone B is defined as B2. Figure 11-50 presents the adjusted energy zones used to assess the segmented breakwater alternatives. The results in Figure 11-50 show wave heights (m) for Alternative 25 as a color-map behind the evaluation zones. The numbers in each zone represent the overall energy change in that zone. Negative values indicate a decrease in energy, while positive values indicate an increase in energy. In order to readily compare the segmented breakwater alternatives, Table 11-7 presents the wave energy changes for selected zones (A-D, a portion of Appendix 11-C) for both the average annual eastern approach direction and the 10-year return period storm. Zones seaward of the structure indicate wave energy increase.

The energy reduction values shown in Table 11-7 indicate the energy within zone A is decreased approximately the same amount for all cases. Likewise, zone C indicates minor changes, and actually results in beneficial changes during storm events, such that adjacent shores are relatively uninfluenced for all alternatives. The significant differentiator is zone B2, which experiences significant differences between alternatives. The lack of the most northern breakwater in Alternatives 22, 23 and 25A, result in minimal protection of the shoreline within zone B2. Accordingly, the ability to maintain a beach along this stretch would be more difficult. Therefore, Alternatives 22, 23 and 25A would normally not be recommended. However, due to geotechnical data indicating poor foundation materials in the area of the proposed northern breakwater, as well as the concern with the relative close proximity to the shoreline, Alternative 25A is recommended for further analysis due to its performance within zone A for average annual conditions. Alternatives 24, 25 and 26 all perform better in terms of zone B2, with Alternatives 25 and 26 experiencing the most significant reductions. Therefore Alternative 24 is not recommended.

The difference in zone D for Alternatives 25 and 25A is due to the more landward location of the spur jetty. As shown in figure 11-49, the spur jetty for these alternatives bisects zone D, and therefore averages both the shadow zone and the reflected wave energy from the spur. When evaluating the shadow region only, a similar reduction (approximately 35%) is obtained. Based on visual observations of the wave results, geotechnical data, and the energy changes presented in Table 11-7, Alternatives 25, 25A and 26 are recommended for further analysis.

Table 11-7. Comparison of energy changes for the segmented breakwater alternatives.

Alternative	Avg. Annual Eastern Approach				10-yr return period storm			
	% Energy Reduction in Zone				% Energy Reduction in Zone			
	A	B2	C	D	A	B2	C	D
22	-44.4	-4.2	-3.8	-56.6	-36.0	-1.0	-3.7	-50.3
23	-44.9	-6.3	3.3	-38.0	-46.9	-0.9	-3.1	-34.9
24	-44.6	-44.0	4.9	-38.2	-46.4	-23.4	-3.2	-34.7
25	-46.4	-50.2	3.5	-14.4	-42.8	-41.2	-2.2	-12.8
26	-44.8	-52.8	4.2	-37.6	-47.1	-40.0	-2.9	-35.3
25A	-47.3	-4.7	1.3	-14.6	-42.0	-0.9	-2.7	-13.0

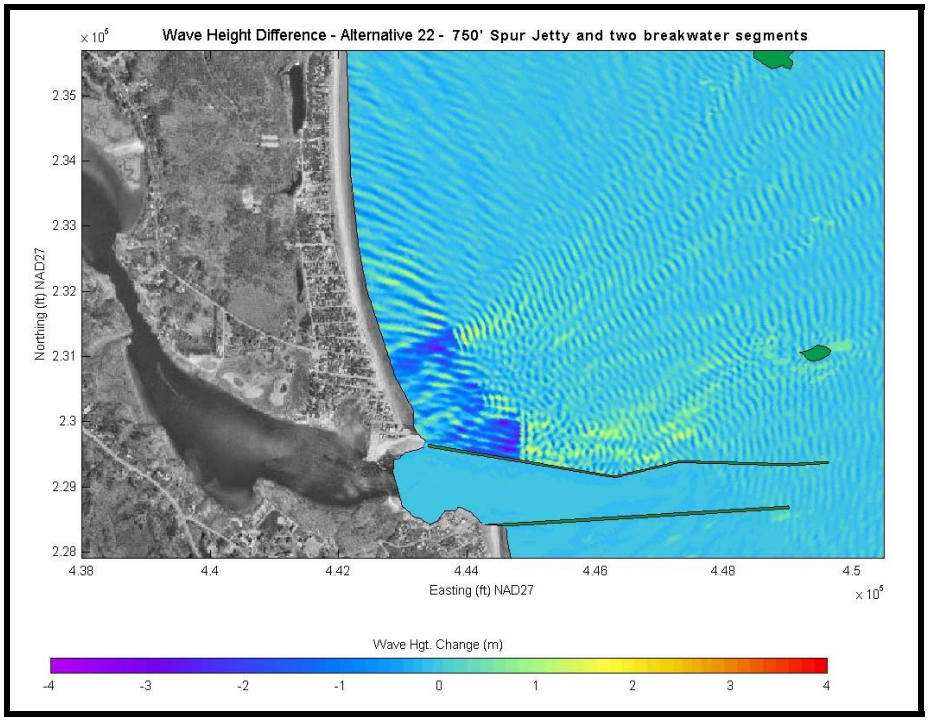

Figure 11-44. Wave height changes for Alternative 22 for a 10-year return period storm. A negative wave height change indicates a reduction in wave height, while a positive wave height change indicates an increase in wave height.

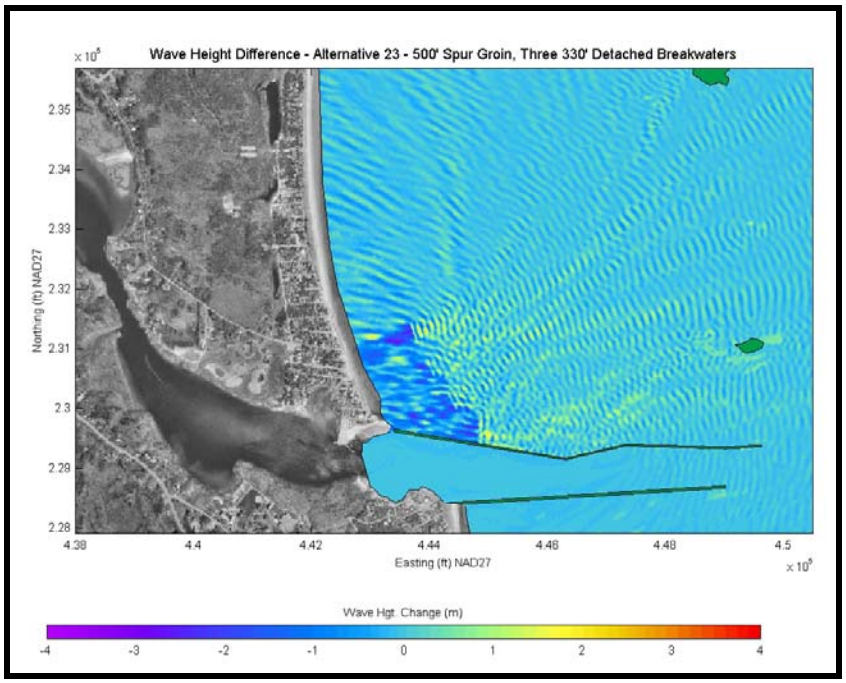

Figure 11-45. Wave height changes for Alternative 23 for a 10-year return period storm. A negative wave height change indicates a reduction in wave height, while a positive wave height change indicates an increase in wave height.

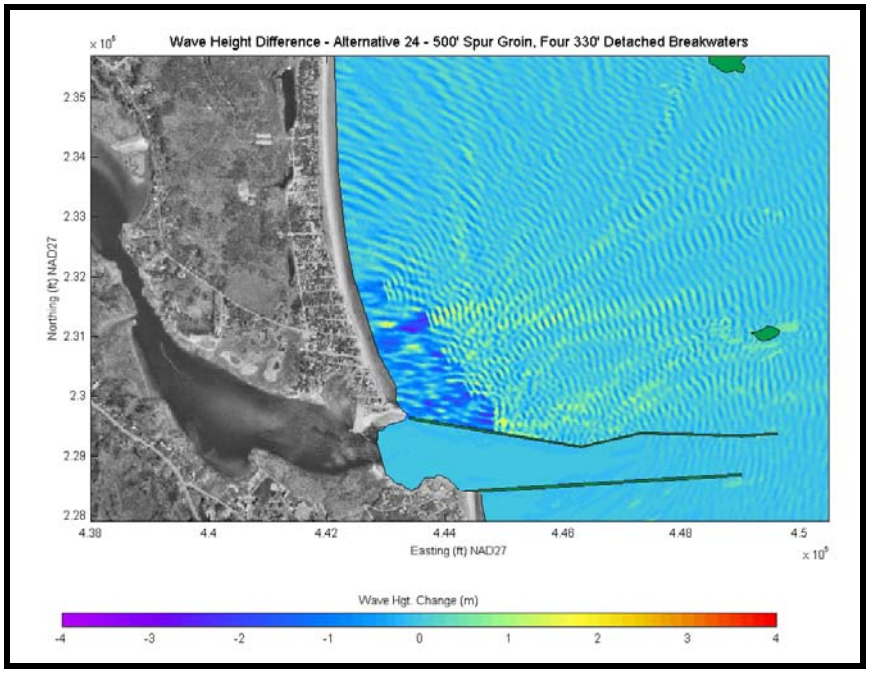

Figure 11-46. Wave height changes for Alternative 24 for a 10-year return period storm. A negative wave height change indicates a reduction in wave height, while a positive wave height change indicates an increase in wave height.

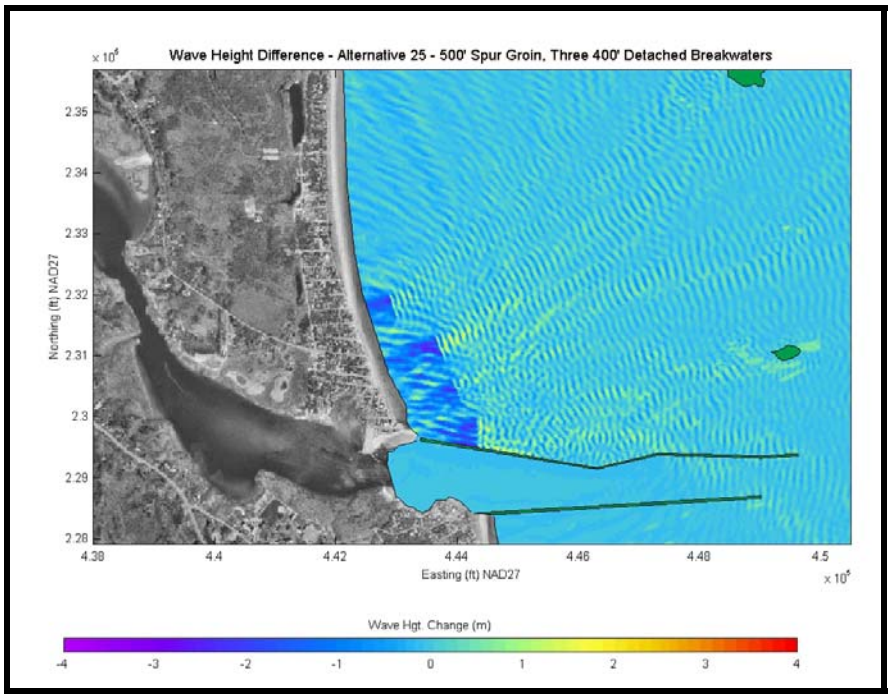

Figure 11-47. Wave height changes for Alternative 25 for a 10-year return period storm. A negative wave height change indicates a reduction in wave height, while a positive wave height change indicates an increase in wave height.

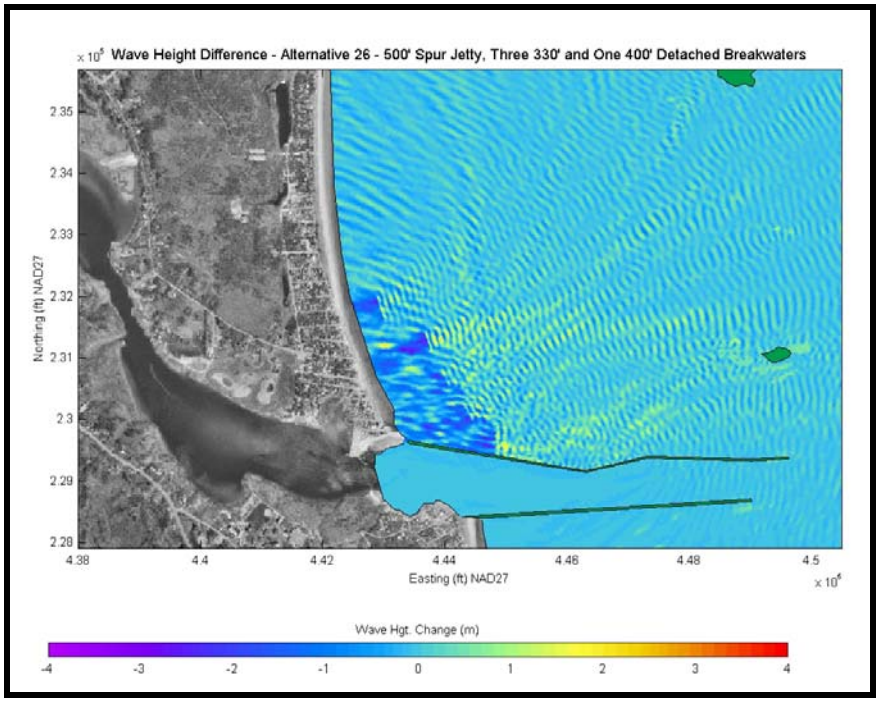

Figure 11-48. Wave height changes for Alternative 26 for a 10-year return period storm. A negative wave height change indicates a reduction in wave height, while a positive wave height change indicates an increase in wave height.

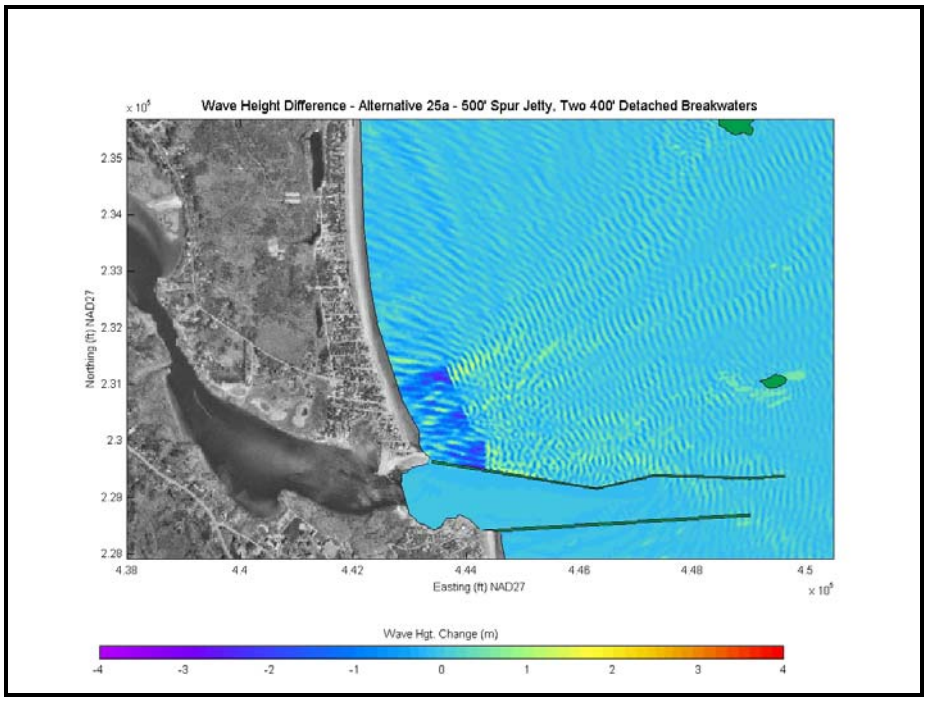

Figure 11-49. Wave height changes for Alternative 25A for a 10-year return period storm. A negative wave height change indicates a reduction in wave height, while a positive wave height change indicates an increase in wave height.

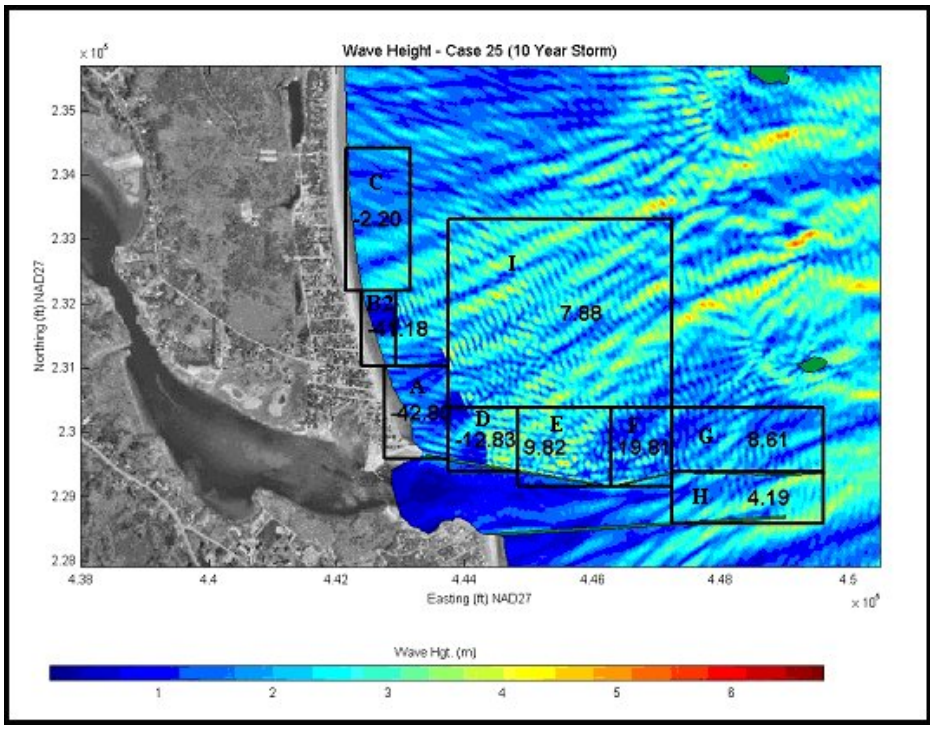

Figure 11-50. Redefined zones used to evaluate changes in wave energy in the vicinity of Camp Ellis Beach and the Saco River Jetties for the segmented breakwater alternatives.

11.9 Summary

The regional model (STWAVE) presented in chapter 9.,0, only represents an intermediate step in the wave modeling system and although useful for identifying regional sediment transport trends, cannot be used for local sediment transport calculations for the Camp Ellis Beach region. Therefore, it was important to advance to higher-resolution models that embodied the reflection processes and could more accurately determine the nearshore structural interactions. The goal of the local, nearshore wave modeling effort for Camp Ellis Beach was to simulate the local physical processes, (e.g., wave reflection, wave-induced currents, wave dispersion, nearshore wave refraction and diffraction, etc.), and subsequently the engineering alternatives.

The nearshore (local) wave model was simulated using the same set of conditions developed for the transformation-scale (regional) modeling. Spectral boundary conditions are specified along the offshore radiating boundary using spectral results from STWAVE in order to calibrate and verify the nearshore (local) wave model, as well as all average annual, directional approach simulations and storm events. CGWAVE does not allow for direct input of a complete wave spectrum; however, spectral input can be simulated through combination of multiple directional/frequency paired components. Therefore, the two-dimensional wave spectra specified at the offshore boundary was assembled based on the output of the regional model extracted at that same location. These spectra matched the observed data well, as discussed in section 9.5. The nearshore (local) wave model was calibrated using two simulated time periods were in order to quantify the overall accuracy. The nearshore model compared favorably to the observed results and accuracy is slightly better than the results presented for the regional transformation-scale model.

Evaluation of the sea surface results for the existing conditions revealed: (1) the significant wave reflection off of the northern jetty indicating the beach is impacted not only by the incident wave energy, but also by the reflected wave energy, (2) independent of offshore direction of approach, the nearshore waves propagated directly towards the Camp Ellis Beach region and the northern jetty, (3) Mach-Stem waves propagating along the northern jetty can be seen in most cases, (4) waves are refracted towards the northern jetty due to the jetty-parallel bottom contours, and (5) variations between annual average approach directions are important to understand the processes occurring at Camp Ellis Beach.

Due to the number of simulations required to evaluate all potential solutions, the alternatives analysis consisted of an initial and final screening process. The nearshore (local) wave model was used as the initial screening tool through evaluation of results (figures and animations), wave height changes, wave energy reduction, and assessment of potential impacts. Table 11-8 summarizes the results for all the alternatives. Appendix 11-C also provides an overall summary of the wave modifications caused by each alternative. More complete discussions of each alternative are presented within this chapter in the preceding sections. The initial screening process identified seven (7) alternatives that warranted evaluation in terms of sediment transport changes and beach performance. These alternatives (fully detailed in Chapter 10.0) are listed below. This

included a beach nourishment alone plan, which was used to compare the relative performance of the ability of each alternative to help sustain a beach in front of Camp Ellis.

Beach nourishment alone:

- Alternative 6: Inshore location of a 750-foot spur jetty
- Alternative 9: Primary T-head groin configuration
- Alternative 11a: Offshore breakwater, inshore location
- Alternative 18: Alternative 11a and inshore location of 500-ft spur jetty
- Alternative 25: Segmented breakwater configuration 4
- Alternative 26: Segmented breakwater configuration 5
- Alternative 25A. Segmented breakwater configuration 6

Table 11-8. Summary of results for all alternatives. The final (fourth) column indicates whether or the alternative warranted further study (**), or was relatively ineffective (--). Details of each alternative are presented in the proceeding text of Chapter 11.0.

Alt. ID	Description	Summary	
Base	Beach nourishment alone	Base alternative	**
0	Northern jetty removal (segments 1, 2, and 3)	Increased wave energy in channel, reduce protection, and destabilized the entire Camp Ellis shoreline	--
1	Northern jetty extension (segment 3) removal	Increased wave energy in channel and did not reduce reflected wave energy	--
2	Northern jetty extension (segment 3) removal and additional lowering of 600 m (1,970 ft)	Increased wave energy in channel and offered limited energy reduction along shoreline	--
3	Seaward location of a 230 m (750 ft) spur jetty	Reduces portion of reflected wave energy, but offers limited protection to most of historically eroding shoreline.	--
4	Optimized location of a 152 m (500 ft) spur jetty	Similar results to Alt. 3 with improvements due to location of spur. Not as effective as the improved spur alternative (Alt. 6).	--
5	Optimized location of dual 152 m (500 ft) spur jetties	Shows little improvement over a single spur, while creating a region of significant wave turbulence.	--
6	Inshore location of a 230 m (750 ft) spur jetty	Best performing spur alternative, recommended for further assessment.	**
7	Inshore location of a 230 m (750 ft) spur jetty coupled with northern jetty extension (segment 3) removal	Same results as Alt. 6 with an increase in wave energy in the navigational channel.	--
8	Inshore location of a 230 m (750 ft) spur jetty coupled with shore-based terminal groin	Same results as Alt. 6. Since T-head groins would be more effective as shore-attached structures, this alternative is not recommended.	--
9	1st configuration of T-Head Groins	Best performing T-head groin scenario, recommended for further analysis.	**
10	2nd configuration of T-Head Groins	Since Alt. 9 performed better, not recommended.	--
11	Offshore Breakwater (seaward location)	Performs well under storm scenarios, has limitations with some average conditions. Other breakwater alternatives perform better.	--
11a	Offshore Breakwater (nearshore	Best performing offshore breakwater	**

	location)	scenarios, recommended for further analysis.	
11b	Offshore Breakwater (intermediate location)	Alt 11a indicated improved performance.	--
12	Offshore Breakwater (landward location) coupled with seaward location of a 152 m (500 ft) spur jetty	Outperformed by Alt. 18	--
13	Comb configuration of 15 m (50 ft) spur jetties	Effectively eliminated a portion of the reflected and Mach-Stem wave energy, but only minimally. Logistically difficult. Not recommended.	--
Alt. ID	Description	Summary	
14	Offshore borrow pit	No significant energy reduction with reasonable depth and dimensions. Not recommended.	--
15	Seaward location of a 230 m (750 ft) spur jetty with an angled orientation	Angled spur did not improve performance compared to Alt. 6. Not recommended.	--
16	Northern jetty roughening (segments 1, 2, and 3)	Moderated wave height and energy reductions, but not as effective as other alternatives.	--
17	Submerged shoal/rock outcrop	Similar performance to Alt. 14. Significantly outperformed by emergent structures.	--
18	Offshore Breakwater (landward location) coupled with landward location of a 152 m (500 ft) spur jetty	Best performing spur and offshore breakwater alternative. Reduces wave energy in all critical areas and does not negatively influence adjacent shores.	**
19	Seaward location of a 230 m (750 ft) spur jetty, northern jetty extension removal, and jetty roughening	Minimal performance improvement over Alt. 6 with increased wave energy in channel. Not recommended.	--
20	Alt. 11a with estimated full salient formation	N/A	--
21	Alt. 11a with estimated partial salient formation	N/A	--
22	Combination of 230 m (750 ft) spur jetty with two 114 m (375 ft) segmented breakwater components	Outperformed by Alt. 25 and 26.	--
23	Combination of 152 m (500 ft) spur jetty with three 100 m (325 ft) segmented breakwater components	Outperformed by Alt. 25 and 26.	--

24	Alt. 23 with additional northern breakwater segment of 100 m (325 ft)	Outperformed by Alt. 25 and 26.	--
25	Secondary configuration of 152 m (500 ft) spur jetty with three 100 m (325 ft) segmented breakwater components	Significant wave energy reduction in all critical areas. Recommended for further analysis.	**
26	Alt. 24 moving the northern breakwater segment further north	Significant wave energy reduction in all critical areas. Recommended for further analysis.	**
25A	Alt. 25 with removal of northernmost breakwater segment	Wave energy reduction in most critical areas recommended for further analysis	**

12.0 SEDIMENT TRANSPORT (TASK 8)

Understanding the wave transformations is a critical step in the determination of shoreline processes and changes, and this wave information is required in order to provide an estimate on how sediment moves in the nearshore region. Ultimately, however, the goal of the overall project is to mitigate the increased erosion induced by the federally constructed Saco River structures by (1) reducing the increased wave energy caused by the reflected waves from the northern structure, and (2) provide, at some level, a sediment source to the beach that was once provided by the Saco River sediment flux that discharged in the nearshore region. As a secondary consideration, if an alternative is able to reduce the erosion to a level that allows for reasonable maintenance of the beach, then there is a higher likelihood that a long-term sustainable beach can be attained. For example, approximately 80,000 cubic yards of sediment is dredged from the Saco River approximately every 10 years. This material may be used as a direct source to replenish the beach. Therefore, if a proposed alternative is able to reduce the erosion to the point that this influx of material is able to maintain a beach capable of stabilizing the shoreline, it would be considered a potential long-term solution. The wave modeling system results were the key input into the sediment transport modeling and beach nourishment performance evaluation.

This chapter evaluates the regional sediment transport within Saco Bay, the local sediment transport in the vicinity of Camp Ellis Beach, and the performance of the beach nourishment in relationship to the final alternatives. The performance of the beach nourishment is the final step in the alternatives analysis evaluation.

12.1 Grain Size Analysis

During a site visit to the Saco Bay region on October 7, 2003, sediments samples were collected along the coastline of Saco Bay and analyzed to determine the sediment distribution throughout the region. A total of seven (7) surface grab samples were collected. The first sample was collected at low tide north of the Saco River Northern Jetty, landward of the spur jetty. The second sample was collected at low tide in the Saco River near the Pier. The third sample was collected in the Saco River during low tide at the easternmost end of the accretion fillet next to the Northern Jetty. The fourth sample was collected at low tide along Camp Ellis Beach. The fifth sample was collected on the southern side of Goosefare Brook. The sixth sample was collected on the northern side of Goosefare Brook. The seventh sample was collected south of the Scarborough marsh inlet.

The results of the grain size analysis are presented in Appendix 12-A. To determine potential spatial variability in the sediment, Figure 12-1 presents a comparison of some of the sediment samples in the region. A general fining of sediment is observed from south to north (as discussed in Chapter 2.0). As such, the median grain size is finer at the northern end of littoral cell (Scarborough) than it is at the southern end (Camp Ellis). In order to further characterize the sediments, five specific grain size parameters were evaluated. These included d_5, d_{16}, d_{50}, d_{84} and d_{95}; corresponding to the grain diameter that 5, 16, 50, 84 or 95% passes during the sieve analysis. The mean grain size, d_{50}, is used to provide a general classification to the sample. For the case of the Saco Bay

samples, the mean grain size indicates that all of the samples are sands, with all of the samples being medium grained sands except for the Scarborough sample, which is fine grained sand. The four other grain diameters are used to define the standard deviation, σ_φ:

$$\sigma_\phi = \frac{(\phi_{84} - \phi_{16})}{4} + \frac{(\phi_{95} - \phi_5)}{6} \quad \text{..... (12-1)}$$

with the resultant value being in units of phi. The standard deviation is used to determine the sorting of the material. The procedure from the US Army Corps of Engineers Coastal Engineering Manual (2002) was used to determine the sorting of the samples, as presented in Table 12-1. Table 12-2 contains the grain size information for the seven samples collected in 2003, as well as the standard deviation measurement.

Figure 12-1. Comparison of sediment samples from locations along Saco Bay shoreline. The lower x-axis indicate the grain size in mm, while the upper x-axis shows the standard sieve sizes.

Table 12-1. Quantitative Terminology for Sample Sorting

(σ)	Description
<0.35	Very well sorted
0.35-0.50	Well sorted
0.50-0.71	Moderately well sorted
0.71-1.00	Moderately sorted
1.00-2.00	Poorly sorted
2.00-4.00	Very poorly sorted
>4.00	Extremely poorly sorted

Table 12-2. Table of Sediment Properties for Saco Bay samples.

Sample	Location	d_5 [mm]	d_{16} [mm]	d_{50} [mm]	d_{84} [mm]	d_{95} [mm]	□ □
1	Adjacent to existing spur jetty	0.58	0.63	1.08	1.73	1.91	+0.65
2	South of northern jetty	0.15	0.28	0.63	0.97	1.54	+1.01
3	North of northern jetty	0.19	0.30	0.60	0.90	1.34	+0.87
4	Camp Ellis Beach	0.37	0.60	1.43	2.63	3.54	+1.08
5	South of Goosefare Brook	0.51	0.56	0.74	1.15	1.71	+0.55
6	North of Goosefare Brook	0.28	0.37	0.55	0.96	1.48	+0.74
7	Scarborough	0.14	0.17	0.29	0.46	0.60	+0.71

12.2 Methodology

Sediment movement in the coastal zone, as well as the effects of coastal structures on shoreline processes, can be estimated by using various types of sediment transport models. These models may differ in their detail, in their degree of representation of the physics, in their complexity, and in other manners. All models also have a certain level of uncertainty since predicting sediment transport in a dynamic coastal environment is inherently difficult. Although no single model of sediment transport may be fully representative of all conditions, these sediment transport models still provide a useful tool for analyzing the effects of structures on local coastal processes.

Shore perpendicular structures, such as the Saco River jetties, are known to influence the movement of sand along the shore, rather than its movement across the shore, in general. Therefore, models evaluating the effects of structures on sediment transport are normally focused on clarifying the physics of this alongshore component of sediment transport. In the specific case of the Saco River jetties, however, the length of the jetty, especially on the northern side, has created a nearshore region along the onshore-offshore length of the structure. In some respects, this behaves like an alongshore stretch of coastline –albeit unnatural, that contains a significant curvature, as evident by the offshore contours (see Chapter 4.0). This is somewhat inconsequential at the regional scale, which does not adequately represent the wave processes in the vicinity of the structure. However, although onshore-offshore movement is not directly considered in this study (but is considered by the USACE in the final assessment of alternatives), due to orientation of

the nearshore contours along the northern jetty, this stretch of shoreline is incorporated into the sediment transport modeling through alongshore sediment transport modeling. Essentially, the northern structure interacts with the wave field as a continuation of the shoreline in terms of the potential sediment movement. In addition onshore/offshore movement and assessment is being conducted by the USACE for this project.

Various types of sediment transport models have been used to estimate the effects of shore perpendicular structures on sediment transport. Process-based sediment transport models (those that address directly the fundamental physics of waves and sediment transport) may focus on those essential physics that capture the variable wave field. Such sediment transport models may not represent all aspects of physical processes accurately, but they can be used to demonstrate the regional sediment transport trends and spatial influence of coastal structures on adjacent shorelines. The sediment transport model presented herein is a process-based model of the regional sediment transport trends in the presence of time-variable (in direction and height) waves.

The goal of the model is to provide a physically-based representation of alongshore currents and sediment transport driven by breaking waves in the surf zone. The specific objective is to obtain physically-based estimates of the alongshore sediment flux integrated across the surf zone. To achieve this physically-based representation, it is important to understand what alongshore sediment processes may cause erosion or accretion. Typically, a section of shoreline can be represented as a cell, having finite length along the shore. A certain amount of sediment enters this cell from the updrift side (direction from which the waves advance), and a certain amount leaves the cell from the downdrift side. This sediment balance may vary depending on the height of the wave, the direction of the wave, and the period of the wave. If the effects of a particular wave passing a cell are examined, there are three possibilities that may be observed:

- The same amount of sediment enters a cell as leaves the cell, for that wave condition.
- More sediment enters a cell than leaves the cell, for that wave condition.
- More sediment leaves a cell than enters the cell, for that wave condition.

The first possibility leads to a stable shoreline. The shoreline neither erodes nor accretes. The second possibility leads to an accumulation of sand in the cell, which is a situation causing accretion (building out of the shoreline) to occur. This possibility is referred to as sediment convergence, as sediment converges in the cell. The final possibility leads to a net loss of sediment in the cell, which is a situation causing erosion. This possibility is referred to as sediment divergence, as sediment diverges from that cell. Thus, shoreline erosion or accretion can be thought of as a simple divergence or convergence of sediment moving alongshore.

Of course, storms also can move sand offshore, and other waves may move sand onshore; however, as discussed, this onshore-offshore process is not directly modeled here and the

focus is on the alongshore movement of sand in the region. Onshore and offshore movement of sediment may be an important factor in the overall assessment of the impacts of the alternatives on sediment movement in the region; however, this was not included in the required scope of work provided to Aubrey Consulting/

Woods Hole Group. Cross-shore sediment transport assessment was being conducted by the USACE for the final recommended alternatives. In general, cross-shore movement is primarily caused by seasonal variations in the wave field, with smaller, less energetic summer waves moving sand onshore, and larger, more energetic winter waves moving sand offshore. As such, longshore sediment processes that move sand directly out of the Camp Ellis region are more critical in understanding the overall performance of a beach nourishment or alternative. This doesn't mean cross-shore sediment movement is insignificant, rather that sand moving alongshore is a key predictor in the performance of a nourishment effort.

The regional sediment transport model requires as input the results of the wave field presented in Chapter 9.0. The sediment transport model itself consists of a hydrodynamic component (to determine the wave-induced currents) and a sediment transport component (to quantify the amount of sediment moved by the wave-induced currents). The hydrodynamic component is based on a standard set of equations that are widely accepted and generally used, more specifically known as the steady-state depth-averaged mass and momentum equations for a fluid of constant density. These equations are standard in many surf zone applications (*e.g.,* Mei, 1983) and provide a state-of-the-art representation of the alongshore current. The sediment transport component is based on a recent peer-reviewed and published formulation by Haas & Hanes (2004), which has been shown to be consistent with recent complex formulae for wave-driven sediment transport and with the Coastal Engineering Research Center (CERC) formula for the total (laterally-integrated) alongshore sediment flux in the limit of a long straight beach subject to waves that are uniform alongshore.

12.3 Model Description

12.3.1 Hydrodynamic Component

12.3.1.1 Boundary Conditions

The wave-averaged, depth-integrated, mass-conservation equation for a constant-density fluid with a rigid lid is

$$\frac{\partial(Hu)}{\partial x}+\frac{\partial(Hv)}{\partial y}=0, \quad \text{.....(12-2)}$$

and the wave-averaged, depth-averaged momentum equations for a non-rotating system are

$$\frac{\partial u}{\partial t}+u\frac{\partial u}{\partial x}+v\frac{\partial u}{\partial y}=-g\frac{\partial \eta}{\partial x}-\frac{ru}{H}+\frac{\tau_x}{(\rho H)} \quad \text{..... (12-3)}$$

and

$$\frac{\partial v}{\partial t}+u\frac{\partial v}{\partial x}+v\frac{\partial v}{\partial y}=-g\frac{\partial \eta}{\partial y}-\frac{rv}{H}+\frac{\tau_y}{(\rho H)} \quad \text{..... (12-4)}$$

Here x and y are the horizontal coordinates, t is time, u and v are the x and y components of the wave-averaged and depth-averaged horizontal velocity, g is the gravitational acceleration, η is the surface displacement, r is the bottom resistance coefficient, H is the water depth, ρ is the fluid density, and τ_x and τ_y are $-(1/H)\partial S_{xx}/\partial x - (1/H)\partial S_{xy}/\partial y$ and $-(1/H)\partial S_{xy}/\partial x - (1/H)\partial S_{yy}/\partial y$, respectively, where S_{xx}, S_{xy}, and S_{yy} are the components of the wave-induced radiation stress tensor (e.g. Mei 1983).

A stream function ψ can be defined by

$$(u,v)=H^{-1}\left(\frac{\partial \psi}{\partial y},-\frac{\partial \psi}{\partial x}\right), \quad \text{..... (12-5)}$$

which satisfies (12-2) identically, and an equation for the wave-averaged potential vorticity ξ, defined by

$$\xi=\frac{1}{H}\left(\frac{\partial v}{\partial x}-\frac{\partial u}{\partial y}\right)=-\frac{1}{H}\frac{\partial}{\partial x}\left(\frac{1}{H}\frac{\partial \psi}{\partial x}\right)-\frac{1}{H}\frac{\partial}{\partial y}\left(\frac{1}{H}\frac{\partial \psi}{\partial y}\right), \quad \text{..... (12-6)}$$

is obtained by taking the curl of (12-3) and (12-4) and dividing the result by H, which yields

$$\frac{\partial \xi}{\partial t}+u\frac{\partial \xi}{\partial x}+v\frac{\partial \xi}{\partial y}+\lambda\xi=\lambda\xi_0+\frac{v_0-v}{H}\frac{\partial \lambda}{\partial x}-\frac{u_0-u}{H}\frac{\partial \lambda}{\partial y} \quad \text{..... (12-7)}$$

where $\lambda=r/H$, $u_0=\tau_x/(\rho r)$, $v_0=\tau_y/(\rho r)$, and $\xi_0=H^{-1}(\partial v_0/\partial x - \partial u_0/\partial y)$.

In the present application, H is known, r is assumed to be given in the linear long wave approximation by $c_d[H_s/(4H)](gH)^{1/2}$ (e.g. Mei 1983), and τ_x and τ_y are output from the wave transformation-scale (regional) model. Here $c_d = 0.003$ is the drag coefficient for the surf zone under breaking waves (Feddersen *et al.,* 1998) and H_s is the significant wave height, defined to be four times the standard deviation of the wave-induced

oscillatory surface displacements, which is also given by the wave model. With this information, (12-5), (12-6) and (12-7) determine the coupled evolution of ξ, ψ, u and v.

12.3.1.2 Boundary Conditions

The coordinate system is defined so that x is positive onshore, $x = 0$ defines the offshore boundary of the computational domain, $y = 0$ and $y = L_y$ denote the alongshore boundaries of the computational domain, and the shoreline is a potentially irregular boundary in $x > 0$. In the present version of the model, there can be only one shoreline, and H is restricted to be positive and nonzero everywhere in the domain. Boundary conditions are required for ψ on all boundaries and for ξ on inflow boundaries. The following boundary conditions are intended for applications in which the offshore boundary is well seaward of the surf zone and the shoreline at the alongshore boundaries is approximately straight and parallel to the y axis.

At the offshore boundary, the forcing and velocity fields are assumed to weak, so that the alongshore velocity and potential vorticity are negligibly small and the offshore boundary conditions become

$$\frac{\partial \psi}{\partial x} = 0 \text{ and } \xi = 0 \text{ at } x = 0. \quad \text{(12-8)}$$

At the alongshore boundaries, the velocity field is assumed to be approximately confined to the y direction and approximately independent of y, so that the alongshore boundary conditions become

$$\frac{\partial \psi}{\partial y} = 0 \text{ and } \frac{\partial \xi}{\partial y} = 0 \text{ at } y = 0, L_y. \quad \text{(12-9)}$$

The shoreline is a streamline, so that ψ on the shoreline must be a constant, which may without loss of generality be set to zero:

$$\psi = 0 \text{ on the shoreline.} \quad \text{(12-10)}$$

The shoreline is not an inflow boundary, so that the shoreline potential vorticity does not affect the solution.

12.3.1.3 Numerical Solution

Equations (12-5), (12-6) and (12-7) are solved by means of a standard numerical procedure described, for example, by Roache (1998). Spatial derivatives are represented using finite differences on a rectangular grid with equal spacing dx in the x and y directions. The representation of the spatial derivatives is second-order-accurate except that the advective terms in (12-7) are represented by a first-order upwind scheme. The time derivative in (12-7) is represented by an explicit first-order scheme with time step dt. The solution for each application begins from rest and advances in time until it

reaches an asymptotic steady state. At each time step, the potential vorticity ξ is advanced according to (12-7), the elliptic equation (12-6) is then solved for the streamfunction ψ using Jacobi iteration (e.g., Lynch 2004), and finally the velocities u and v are calculated according to (12-5). Attainment of an approximate steady state requires that the solution advance until t is approximately equal to 3 times the maximum value of λ. Stability requires that the Courant number $(u^2+v^2)^{1/2}dt/dx$ based on the maximum flow speed be less than approximately unity.

12.3.2 Sediment Transport Component

Haas & Hanes (2004) proposed a simple formula for the alongshore sediment flux, which is, in the present notation,

$$q_s = \left(\frac{2c_1 c_d}{g} \right) < |\boldsymbol{u}|^2 > u_s \quad \text{..... (12-11)}$$

where q_s is the alongshore component of the sediment flux, c_1 is an empirical constant approximately equal to 1.3, brackets denote an average over many wave periods, $\boldsymbol{u}$ is the instantaneous velocity vector (including both the wave-induced oscillatory velocity and the current), and u_s is the alongshore component of the current velocity.

In the present application, $\boldsymbol{u}$ is assumed to be dominated by wave-induced oscillatory velocities and to be related to wave-induced surface displacement by linear long wave theory, so that $<|\boldsymbol{u}|^2>$ approximates $[H_s/(4H)]^2 gH$. In addition, a right-handed coordinate system (s,n,z) is defined so that s is locally alongshore, n is locally shore-normal, and z is vertical and positive upward. In this coordinate system, $Hu_s = \partial\psi/\partial n$. Equation (12-11) can therefore be written

$$q_s = 2c_1 c_d \left[\frac{H_s}{4H} \right]^2 \frac{\partial \psi}{\partial n} \quad \text{..... (12-12)}$$

In the surf zone, H_s/H is approximately constant ($H_s/H < 0.63$ is explicitly assumed by STWAVE), so that (12-12) can be integrated with respect to n across the surf zone to yield

$$Q = \frac{c_1 c_d}{8} \left[\frac{H_{sb}}{H_b} \right]^2 \psi_b \quad \text{..... (12-13)}$$

where Q is the alongshore sediment flux integrated across the surf zone and subscript b denotes evaluation at the break point (*i.e.* at the seaward edge of the surf zone). In the present application, (12-13) is used to determine the sediment flux integrated across the surf zone after the stream function has been computed from the hydrodynamic component.

12.4 Regional Sediment Transport

In order to understand the nature of the localized alongshore erosion occurring at Camp Ellis Beach, the regional (within Saco Bay) sediment transport patterns were evaluated as an initial step to better understand the overall sediment transport fluxes. This section uses the results of the regional wave model, as presented in Chapter 9.0, to determine the nearshore hydrodynamics, and subsequently, the sediment flux (representing the rate of sediment moving along the coast) and divergence (indicating potential areas of erosion/deposition) within Saco Bay (between Biddeford and Prout's Neck).

The regional wave modeling results (Chapter 9.0) were used as input into the non-linear sediment transport model. Wave results from each of the average annual directional spectra bin simulations were used to develop the complete summary of sediment movement for various wave conditions. Sediment transport results were also combined to define the average annual sediment transport regime throughout the Saco Bay region.

Model simulations were performed for the wave conditions represented by the directional bin spectra presented in Table 9-3. Output from the wave model was used as input into the sediment transport model described in section 12.3. Figures 12-2 and 12-3 illustrate the sediment transport results for waves approaching from the eastern (90 to 110 degree) approach bin. Figure 12-2 presents the resultant wave height (left panel) from the regional wave transformation-scale model and the associated stream function from equation 12-5 (right panel). The stream function represents the hydrodynamic forcing (i.e., wave-induced currents) that determines the sediment flux along the coastline. Figure 12-3 presents the associated sediment flux and sediment divergence for the eastern (90- to 110 degree) approach bin case. The sediment flux represents the rate of sediment moving along the coast, where negative values indicate movement towards the north (from bottom to top of the figure) and positive values indicate movement towards the south (from top to bottom of the figure). This rate is presented in units of m^3/yr and can be used to quantify the annual sediment transport in reaches within Saco Bay. Subsequently the flux divergence is calculated, and indicates areas of erosion and/or deposition. A flux divergence represents erosion, while a flux convergence represents accretion. A convergence is defined as -dQ/dy and the figure presents units of convergence and divergence as m^2/yr. These calculations all assume that sediment is available for transport on the beach. If the shoreline is armored, or doesn't have a sediment source readily available, then the sediment transport rates are meaningless. Therefore the rates are likely conservatively high as they assume an infinite supply of sediment, and do not account for morphologic changes to the shoreline.

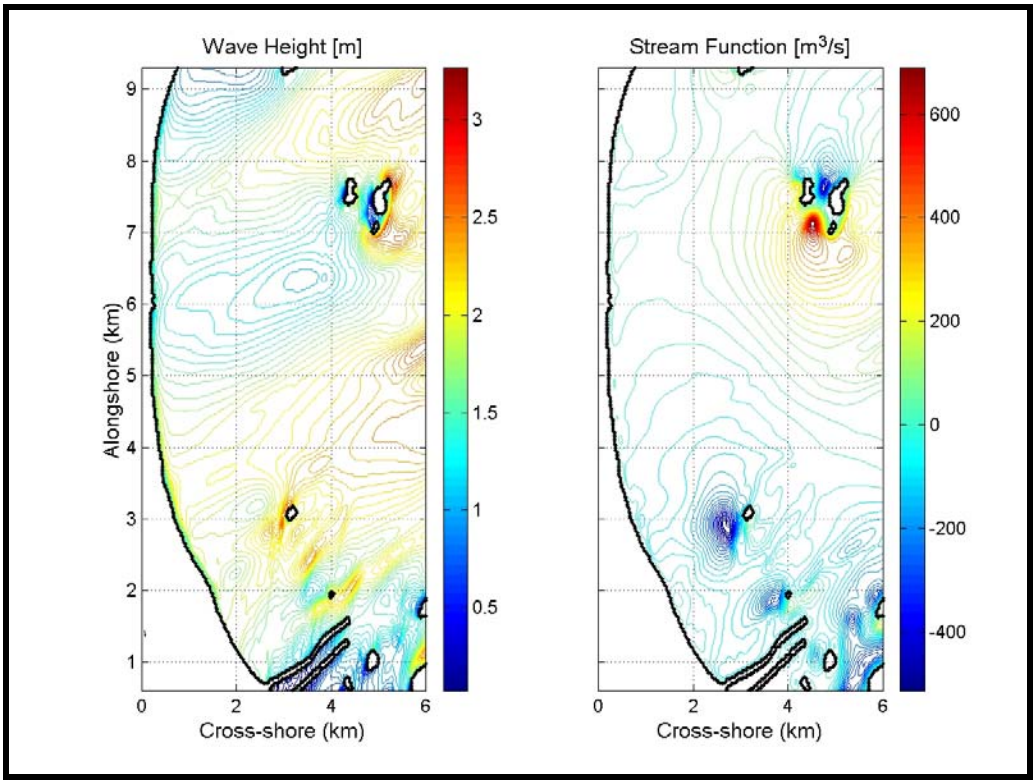

Figure 12-2. Wave height and stream function for an eastern (90 to 110 degree) approach condition.

For this approach scenario, the sediment flux (middle panel) in Figure 13-2 shows sediment transport towards the north in the southern portion of Saco Bay (Camp Ellis). Directly adjacent to the northern jetty, the sediment transport rate is approximately 250,000 m^3/yr towards the north. A region of decreased transport rate is located directly to the north, as the rate slows to less than 25,000 m^3/yr towards the north for a stretch of the more stable shoreline (as presented in Chapter 3.0). The northward rate increases along the shoreline landward of Eagle Island (300,000 m^3/yr) at the 3 km alongshore location. The center and northern portions of Saco Bay (under these conditions), except for a relatively stable section near Scarborough, indicates sediment transport towards the south. The rate of sediment transport averages between 150,000 to 200,000 m^3/yr towards the south. Under these conditions, a nodal point (change in transport direction) is located approximately 3.5 to 4.0 km (2.2 to 2.5 miles) north of the jetties. With a spectral peak wave direction coming from the east and the curved orientation of the shoreline, this shift in directionality of transport would be expected under these conditions. These rates (presented in the paragraph above) are for only a single approach scenario and should not be confused with the overall yearly average sediment transport rates, which are presented later (last paragraph in this section). For example, the rates of 300,000 m^3/yr presented above are not the net rates of sediment transport for the region, rather they represent the sediment transport potential that occurs during a specific approach scenario occurring over a small portion of the year. The net rates, for example just north of the Saco River structures, are 25,000 to 50,000 cubic yards per year.

The flux divergence (right hand panel) in Figure 13-2 indicates areas of convergence/divergence in the sediment transport rate corresponding to areas of erosion or accretion. As sediment flux decreases, less sediment is moved out of an area and remains at a location, this produces a positive divergence. Positive valued flux divergence indicates areas of expected accretion, while negative valued flux divergence indicates areas of expected erosion. For this wave scenario, potential accretion/erosion coupling is evident behind the Eagle and Ram Island complex, and specifically in the shadow zone of Eagle Island. A similar, but muted, erosion/accretion fluctuation is visible landward of the Bluff and Stratton Island complex in the northern section of the Bay. Erosion potential is evident directly north of the Saco River jetties, and the majority of the center portion of the bay shoreline remains relatively stable.

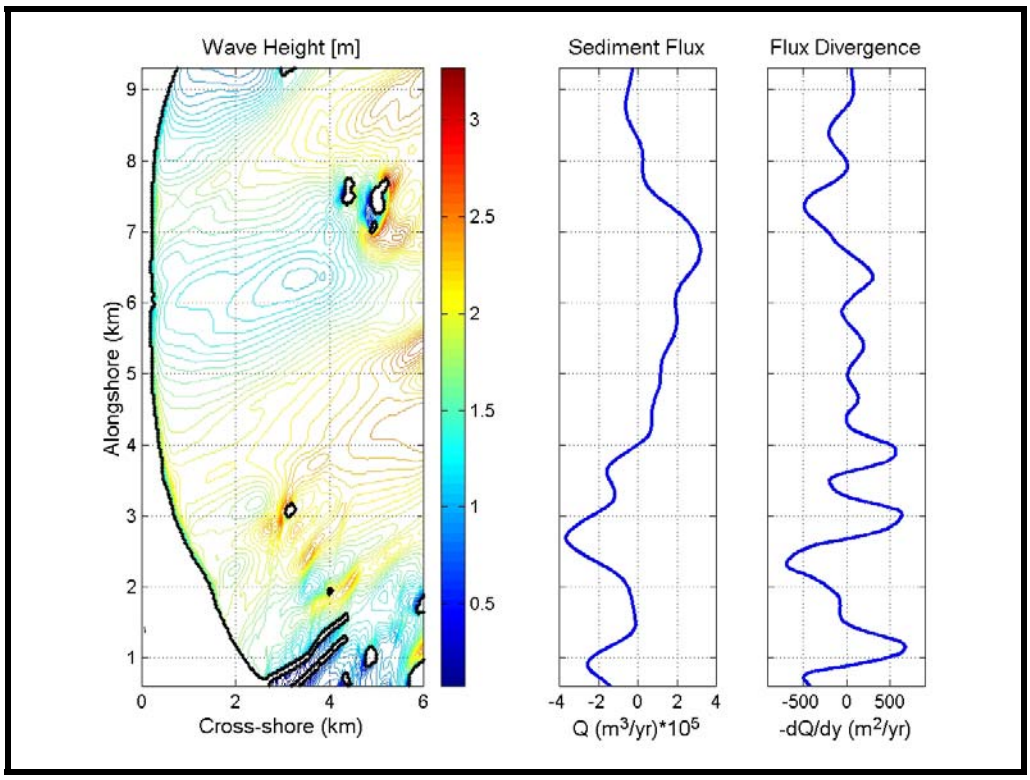

Figure 12-3. Sediment flux and flux divergence for an eastern (90 to 110 degree) wave directional approach simulation.

Figure 13-2 presents a single wave scenario (wave spectra approaching from the east). Appendix 12-B contains results for the remaining average annual wave approach directions. The figures in Appendix 12-B indicate similar sediment transport regimes with southward transport being dominant for wave spectra centered about a northeast approach and northward transport being dominant for wave spectra centered about a southeast approach. However, in all cases, independent of approach direction, the region adjacent to the Saco River navigation structures indicates northward transport. Even for approach directions consisting of a peak northerly wave (i.e., 55 to 75 and 75 to 90)

approach, an area approximately 1-3 km (0.6 to 1.9 miles) of northward transport is evident adjacent to the northern jetty. Additionally, the influence of the islands is evident in every scenario, influencing sediment transport in regions landward of the islands. Specifically, the Bluff and Stratton Island complex affects the flux divergence in cases with a southeastern approach. The current sediment transport model does not include bathymetric evolution. Therefore, the bathymetry stays fixed even though the flux convergence and divergence indicate erosion and deposition that would modify the bathymetry.

The various wave scenarios (Appendix 12-B) can also be combined to represent an average annual year of wave climate. Using the percent occurrence of wave approach (Chapter 9.0), the average annual approach directions were normalized and combined to determine the net longshore transport rate. Figure 12-4 presents the average yearly sediment flux and flux divergence. The sediment flux indicates an average annual longshore transport rate to the north. However, the magnitude of the transport varies throughout the domain. A region extending from just north of the navigational structures to approximately 3 km to the north, averages approximately 25,000 to 50,000 m^3/yr (32,700 to 65,000 cubic yards) towards the north. Increases in flux can be seen directly adjacent to the northern jetty, and landward of Eagle Island at the 3 km alongshore location. The flux divergence in this area would indicate a general trend towards shoreline erosion over this reach. In the center of the bay, extending approximately 3 km, the average annual sediment flux rate is small. This is a region that gross transport direction shifts depending on the angle of the incoming wave field, and generally are equivalent. There is a small net northward transport rate of 10,000 to 20,000 m^3/yr (13,000 to 27,000 cubic yards) and the flux divergence indicates a stable stretch of coastline. This reach of shoreline is generally not prone to erosion or accretion, and remains relatively stable under average annual conditions. This was also indicated in the historical shoreline change analysis (Chapter 3). The northernmost region of the bay is strongly influenced by the Bluff and Stratton Island complex and there are major fluctuations in both the sediment flux and divergence. The average sediment transport rate in this region is 40,000 m^3/yr (52,000 cubic yards) towards the north, with peaks of 70,000 m^3/yr (92,000 cubic yards) towards the north. However, these regions of sediment flux (and subsequently, accretion and erosion) likely change daily based on the incoming wave climate, and some of this fluctuation may be minimized (i.e., these smaller fluctuations might not be real). Gross sediment transport rates vary significantly for the various average annual approach directions, and reach maximums of 300,000 to 350,000 m^3/yr (392,000 to 450,000 cubic yards). The magnitudes of the gross sediment transport rates provide an indicator of the wave energy associated within each wave approach direction (Appendix 12-B).

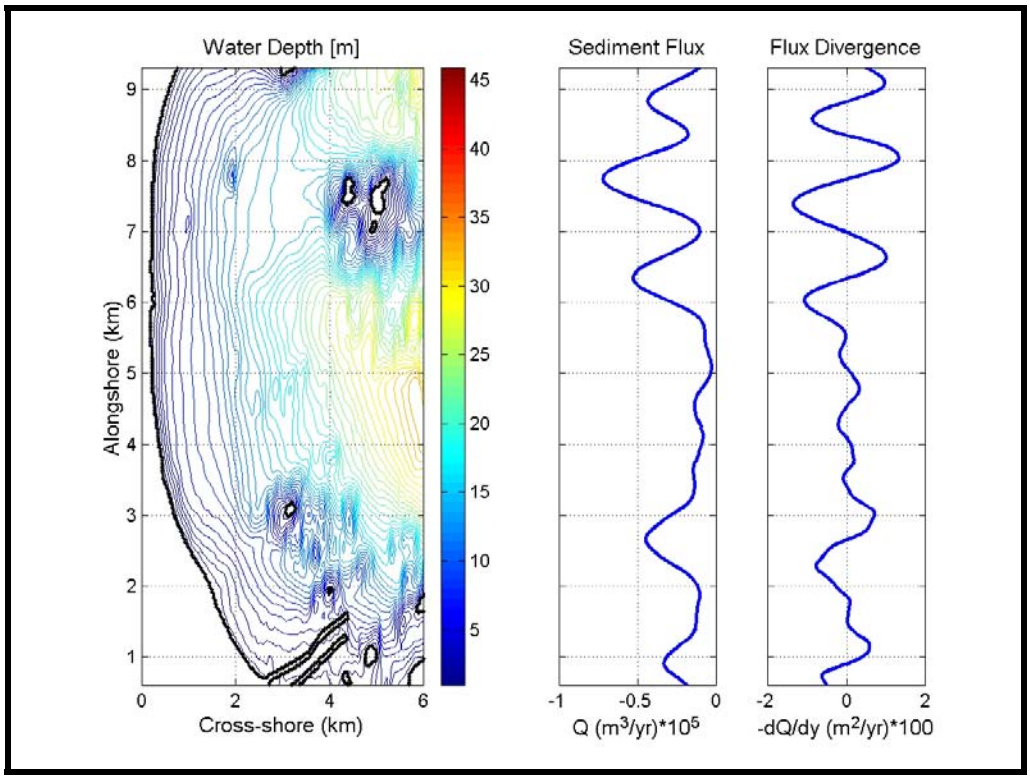

Figure 12-4. Annualized sediment flux and divergence for Saco Bay.

12.5 Final Alternative Screening

At the heart of the final alternative analysis is alteration to the sediment transport and beach nourishment performance. The alternatives passed forward from the initial screening analysis are evaluated herein to determine relative performance in terms of their ability to maintain a stable shoreline at Camp Ellis. This section compares the relative performance of the final alternatives and presents the information to allow the reader to determine, from a purely performance standpoint, the relative merit of each alternative.

12.5.1 Methodology

In order to determine the more complicated local sediment transport regime, including the potential ability of each alternative to maintain a healthy beach, the same zones as used in the wave energy reduction assessment were used to provide a local assessment of sediment transport. Specifically, the nearshore region zones of A, B, and C (Figure 11-20) were used. The values of sediment transport computed within these three boxes act as the basis for comparison to the alternative sediment transport results. It was the goal of all alternatives to reduce erosion (sediment transport) within zone A and B and to have limited impact upon the sediment transport within zone C. Areas represented by zones A and B, which are 300 m (1,000 ft) zones, have historically experienced significant erosion. Zone C, a 600 m (1970 ft) zone, is a region that has exhibited more stable shoreline conditions.

Subsequently, the potential influence on sediment transport occurring on the northern side of the Saco River inlet was evaluated in terms of the performance of the proposed nourishment for all of the final alternatives. One of the key considerations when evaluating the effectiveness of an alternative and sand placement is the ability of an alternative to maintain the beach. If the placed material is quickly removed or eroded from the region, the project will require frequent maintenance. To adequately assess the performance of the beach nourishment many factors need to be considered. At Saco River, the required factors include the effect of the inlet, the effect of the structures (both existing and proposed), dispersion of the nourishment material, and the effect of ongoing background erosion.

Results from the nearshore (local) wave model were used to drive the local sediment transport analysis. These wave results capture the most physical processes in the vicinity of Camp Ellis each and provide high resolution (approximately 10 m or 30 ft) results. Therefore, the nearshore (local) wave model results provide the most accurate and detailed wave data to drive the sediment flux.

Alternative 9, the T-Head groin case, represents an alternative that is significantly different than the other final alternatives. While the other alternatives are focused on reducing the wave energy, and subsequently reducing the ability of the wave to move the sediment, the T-Head groins primary function is to hold the sand in place by eliminating nearly all of the alongshore sediment transport. T-Head groins have proven successful in other sand-rich environments (USACE, 2001) such as Florida, but have not been applied in the New England region or significant tidal variations (such as the 3.7 m (12 ft) tidal range in Saco, Maine). However, it is assumed that T-Head groins will be effective at containing sand in the region where they are placed, and will likely mitigate the chronic erosion that has occurred at Camp Ellis Beach. Currently, however, there is a significant lack of data, research, and analyses techniques to adequately assess the overall performance of T-Heads, as well as their potential impact on downdrift shorelines along northern Atlantic coastlines where the tide range is reasonably large. The T-Head groins are considered separately from the other alternatives throughout this section, due to the inherent differences in their operational nature, and relative lack of proven analytical techniques for assessing their impact.

12.5.2 Wave Reflection

As an initial step in the evaluation of the local processes for the final screening assessment, the wave field within each nearshore zone was dissected in terms of incident and reflected wave energy. As illustrated in the nearshore (local) wave modeling results, the sea surface in the nearshore zone directly adjacent to the northern jetty is complex. In this region, there is significant merging between various waves reflected off of the structure, and incident wave propagating from the offshore domain. The complex nature of this region and this interaction makes it unreasonable to select a single wave height and direction for each location along the coastline, since there are clearly multiple waves (with varying directions) acting to move the sediment along the shoreline. Therefore, the waves within each nearshore zone (A, B, and C) were separated in terms of direction (relative to the coastline), and evaluated to determine the associated wave energy in the

incident and reflected bands. Waves propagating to the north or northwest relative to shore-perpendicular were considered reflective, while waves propagating towards the south or southwest relative to shore-perpendicular were considered incident.

Figure 12-5 presents the segregated wave energy for existing conditions, Alternative 6 (spur jetty), Alternative 11a (offshore breakwater), and Alternative 18 (combined offshore breakwater and spur jetty) within zone A. The blue color indicates the portion of wave energy within zone A that is considered incident wave energy, the maroon color indicates the portion of wave energy within zone A that is considered reflected wave energy, and the off white color indicates the portion of spurious (primarily waves heading offshore) wave energy. The bar plots present total wave energy for existing conditions, and each alternative. The smaller the bar height is for each alternative, the smaller the wave energy within zone A. Figure 12-5 shows that the spur jetty alternative (Alternative 6) reduces the amount of reflected wave energy within zone A, as well as a small portion of the incident wave energy. The breakwater alternative (Alternative 11a) primarily reduces the incident wave energy in zone A, but does not reduce any of the reflected wave energy. The breakwater is able to reduce the incident wave energy to such a degree that in the shadow zone behind the breakwater the reflective wave energy becomes dominant. In terms of overall energy in zone A, the spur jetty alternative and the breakwater alternative are similar. The combined breakwater and spur jetty alternative (Alternative 18) reduces both the reflected and incident wave energy.

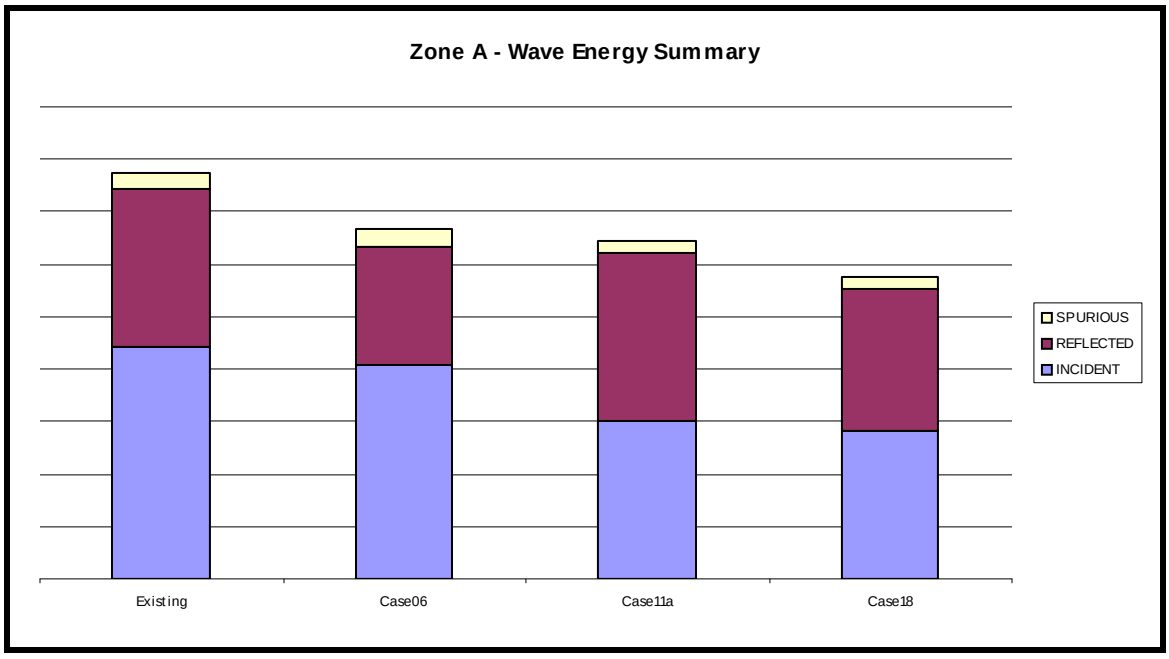

Figure 12-5. Summary of reflected and incident wave energy within zone A for existing conditions, Alternative 6 (spur jetty), Alternative 11a (breakwater), and Alternative 18 (combined breakwater and spur jetty).

Figures 12-6 and 12-7 present similar wave energy bar plots for zones B and C, respectively. The spur jetty alternative (Alternative 6) has less influence on the wave field in zone B, as only a minimal reduction in the reflected wave energy is shown. A majority of the reflected wave energy found within zone B is not intercepted by the spur jetty. The alternatives that include the breakwater show significant influence in the zone B region, primarily through the reduction of the incident wave energy. The combined breakwater and spur jetty alternative (Alternative 18) shows the greatest impact, reducing the total energy by almost 50%. A slight reduction in wave energy is seen in zone C for the alternatives that include a spur jetty (6 and 18). Overall, there is minimal change in energy in zone C, indicating that sediment transport potential should remain the same within zone C.

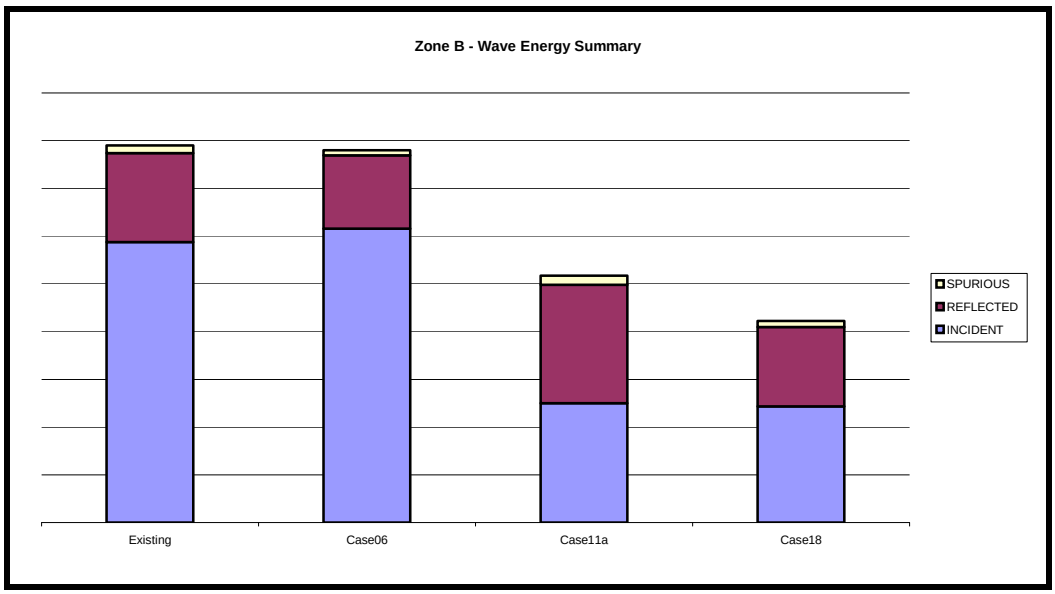

Figure 12-6. Summary of reflected and incident wave energy within zone C for existing conditions, Alternative 6 (spur jetty), Alternative 11a (breakwater), and Alternative 18 (combined breakwater and spur jetty).

Figures 12-8 through 12-10 present similar reflection/incident energy bar plots comparing existing conditions to three of the segmented breakwater alternatives (25A, 25, and 26). The segmented breakwater alternatives all perform similarly within zone A, and outperform the previous alternatives (Figure 12-5). The lack of the northern most breakwater segment in Alternative 25A is evident in the energy within zone B, as Alternatives 25 and 26 outperform Alternative 25A. As in the previous alternatives, there is minimal change in energy in zone C, indicating that sediment transport potential should remain the same within zone C.

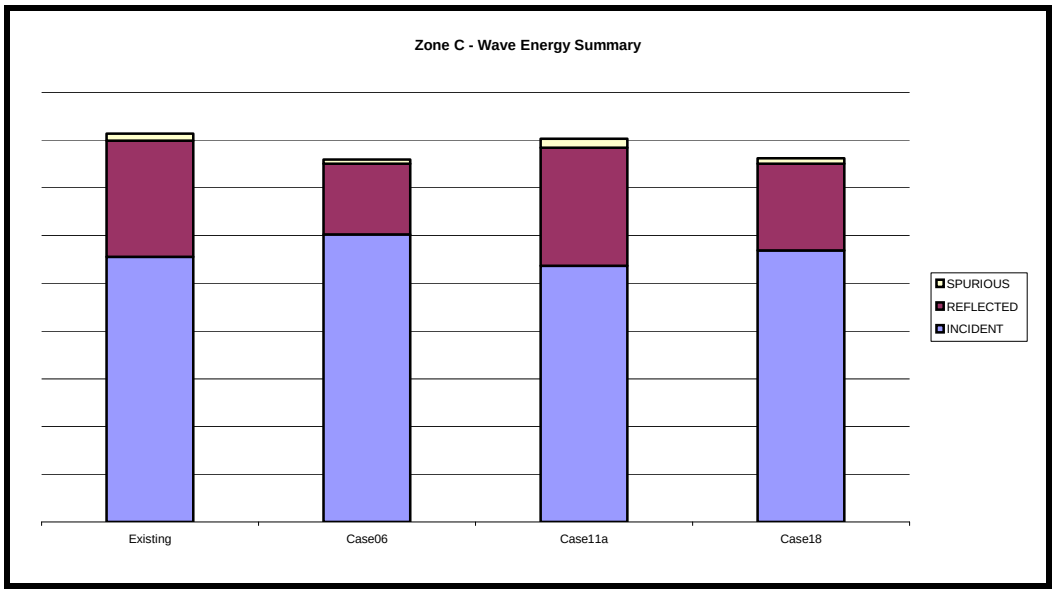

Figure 12-7. Summary of reflected and incident wave energy within zone C for existing conditions, Alternative 6 (spur jetty), Alternative 11a (breakwater), and Alternative 18 (combined breakwater and spur jetty).

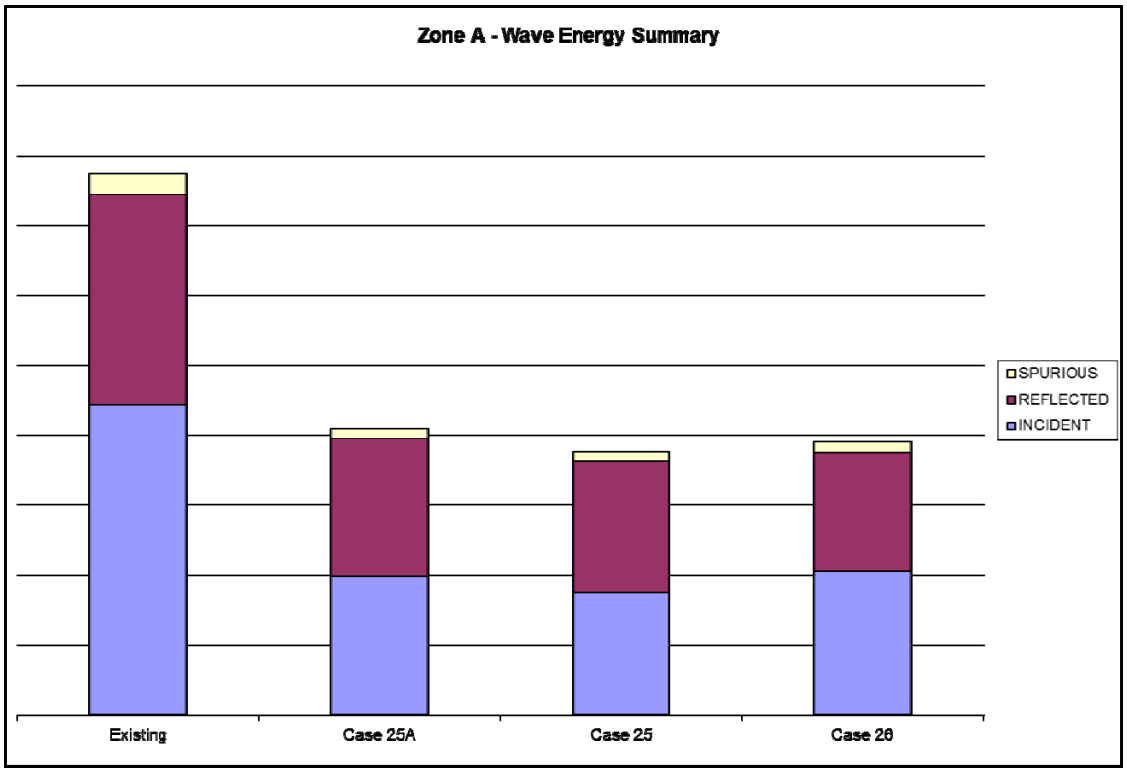

Figure 12-8. Summary of reflected and incident wave energy within zone A for existing conditions, and three segmented breakwater alternatives (Alternative 25A, 25 and 26.

12.5.3 Sediment Transport Reduction

Changes in potential sediment transport flux were also evaluated for each alternative, within each zone. Figures 12-11 and 12-12 present the change in potential sediment transport flux for the final alternatives. The numbers represent the percent reduction in potential sediment transport rate when compared to the existing potential sediment transport rate. A greater reduction in potential sediment transport means that a smaller amount of material would be leaving the region in the alongshore direction. Alternatives 25 and 26 show the greatest reduction, exceeding 50% for both zones A and B. In all alternatives, there is a minimal amount of change in zone C. This means that there will be a potential decrease in sediment entering zone C from A and B; however, currently (and approximately over the last 40 years) there has been little to no sediment available for transport in these areas due to the severe historic erosion and revetment construction, as evident that Zone C has begun to experience significant erosion under existing conditions for recent times (periods after 1998). Therefore, even with a reduced transport rate from zones A and B, zone C will experience a net increase in sediment with the influx from the beach nourishment program. This is important, since the overall project will have a net benefit on the shorelines to the north for most final alternatives considered (except for the T-groin alternative) as (1) currently there is a deficit of sand available for transport to the region such that erosion is expected to develop in this area with no action, and (2) the addition of sand to the system can only benefit the regions to the north, since even with a reduced transport rate, the net sand moving to the northern beaches would be greater than currently exists.

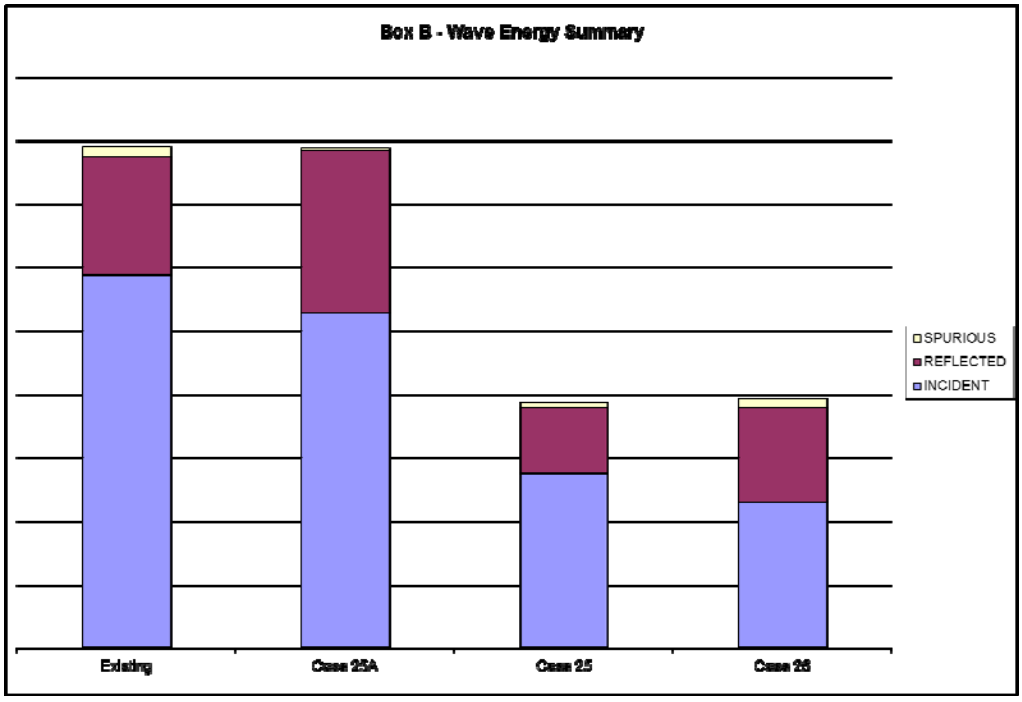

Figure 12-9. Summary of reflected and incident wave energy within zone B for existing conditions, and three segmented breakwater alternatives (Alternative 25A, 25 and 26.

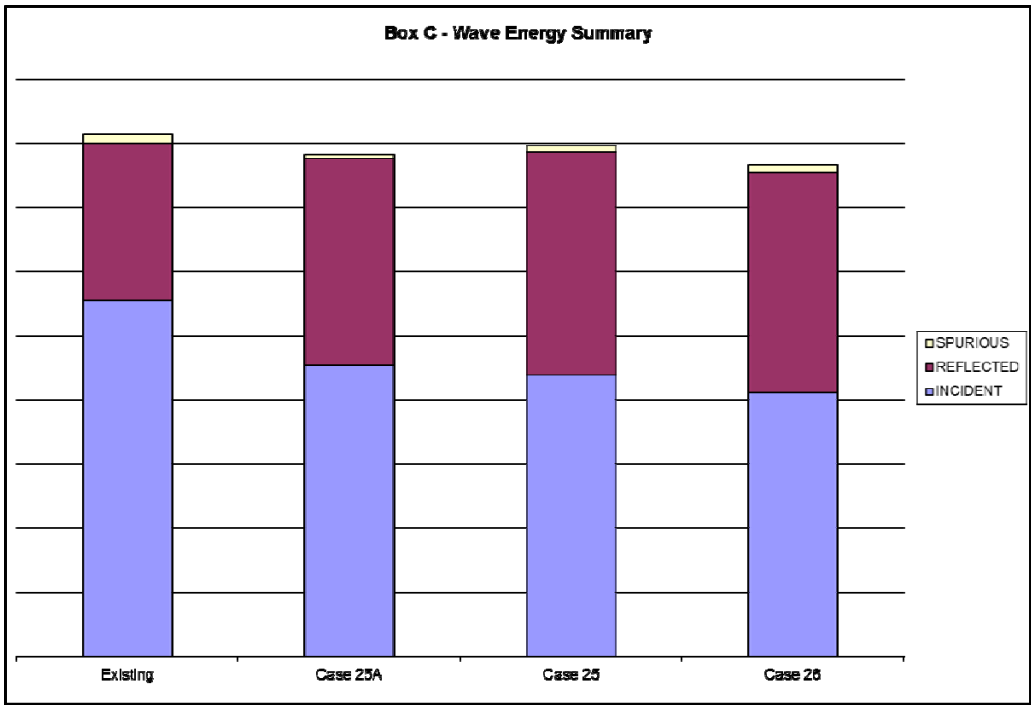

Figure 12-10. Summary of reflected and incident wave energy within zone C for existing conditions, and three segmented breakwater alternatives (Alternative 25A, 25 and 26.

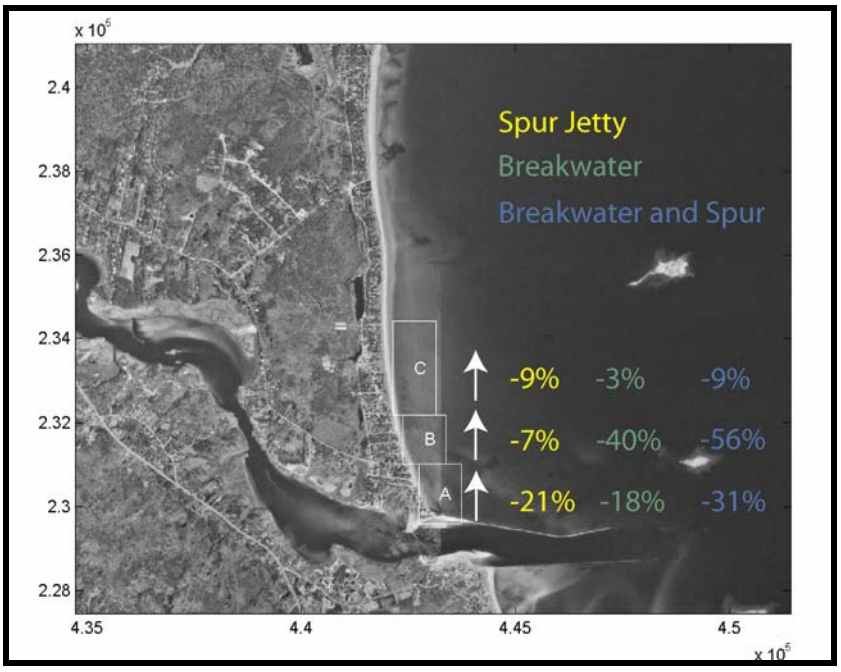

Figure 12-11. Changes in sediment transport flux for Alternatives 6, 11a, and 18. The numbers indicate the percent reduction in sediment transport rate for each corresponding alternative.

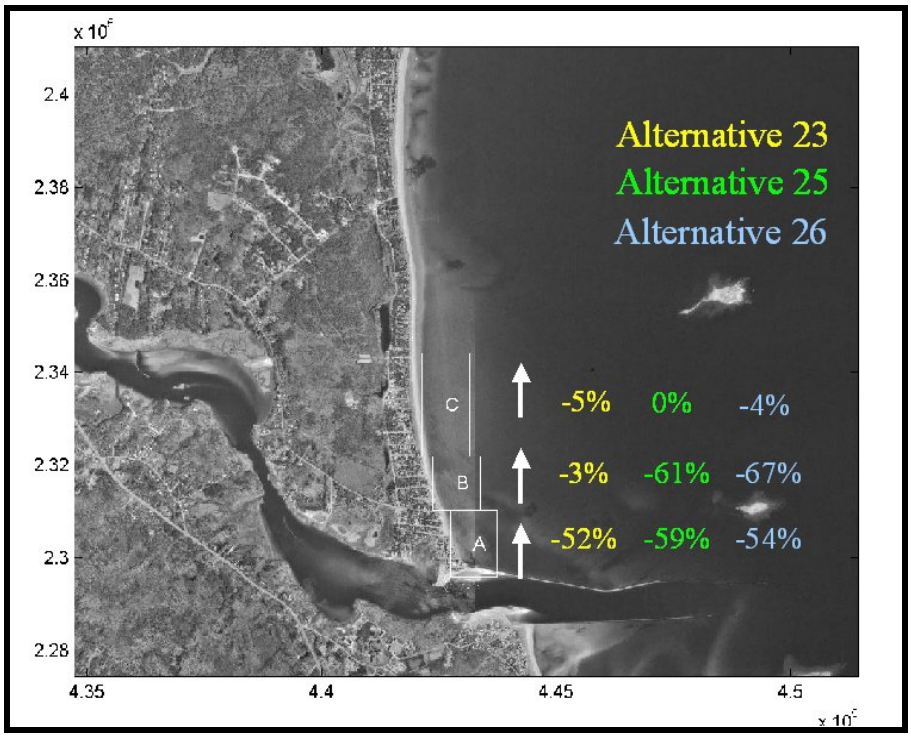

Figure 12-12. Changes in sediment transport flux for Alternatives 23, 25, and 26. The numbers indicate the percent reduction in sediment transport rate for each corresponding alternative.

12.5.4 Salient Formation

For the alternatives that involve the proposed instillation of an offshore breakwater, or segmented breakwaters, estimates of shoreline response are developed to determine the impact of potential salient formation on wave energy and coastal processes. A salient is a coastal formation of beach material developed by wave refraction, wave diffraction, and longshore drift producing a bulge in the coastline behind an offshore island or breakwater. If the salient connects to the offshore feature/structure, it is termed a tombolo. Salient growth was determined to ensure that a tombolo would not form behind the proposed breakwater(s), and subsequently severely inhibit alongshore transport to the north. Finally, estimates of the volume of sediment that would comprise the salient are provided, and thus provide an estimate of how much material would be sacrificed from the beach nourishment to eventually form the equilibrium salient.

To determine the amplitude and shape of the salient formation, recent studies completed by Suh and Dalrymple (1987), Seiji, Uda, and Tanaka (1987), Aherns and Cox (1990), Noble (1978), and Hsu and Silvester (1990) that evaluated the formation of salients behind breakwaters were used.

For the single breakwater case proposed in Alternative 11a and 18, the growth of the salient was determined using the work of Suh and Dalrymple (1987) and Hsu and Silvester (1990). Suh and Dalrymple (1987) found that a tombolo will form if the distance from the shoreline to the breakwater is smaller than half the length of the

breakwater. For the Saco alternatives, this is not the case, and no tombolo is expected to form. Subsequently, Hsu and Silvester (1990) used experimental data to derive the following empirical relationship for the dimensionless ratio $(y_B-y_s)/L_B$, which is the dimensionless distance from the breakwater to the salient:

$$\frac{(y_B - y_s)}{L_B} = 0.678\left(\frac{y_B}{L_B}\right)^{1.215} \quad \text{..... (12-14)}$$

where y_s the amplitude of the equilibrium salient, y_B is the distance from the original shoreline to the breakwater, and L_B is the length of the breakwater. Equation 12-14 was used to determine the amplitude of the equilibrium salient. The volume of the depositional feature was then determined by assuming a parabolic salient shape and integrating over the actual bathymetric region where the salient would form.

For the multiple segmented breakwater cases proposed in Alternatives 25, 25A, and 26, Ahrens and Cox (1990) arrived at the following empirical relationship for a multiple breakwater scenario:

$$I_s = e^{\left(1.72-0.41\left(L_B/y_B\right)\right)} \quad \text{..... (12-15)}$$

where if,

$I_s \approx 1$, then there is permanent tombolo formation

$I_s \approx 2$, then there are periodic tombolo formations

$I_s \approx 3$, then there are well-developed salients

$I_s \approx 4$, then there are subdued salients

$I_s \approx 5$, then there is little sinuosity on the shoreline planform

Alternative 25, 25A, and 26 consist of subdued to well-developed salients behind each of the breakwaters. Gap erosion potential, defined as the retreat of the shoreline landward of the original shoreline position in the lee of the segmented breakwater gaps, was also calculated using the following relationships defined by Seiji, Uda, and Tanaka (1987):

$$\frac{L_g}{y_s} < 0.8 \quad \text{no erosion in lee of gap..... (12-16)}$$

$$0.8 \le \frac{L_g}{y_s} \le 1.3 \quad \text{possible erosion in lee of gap} \quad \text{(12-17)}$$

$$\frac{L_g}{y_s} \ge 1.3 \quad \text{certain erosion in lee of gap} \quad \text{(12-18)}$$

where L_g is the gap distance between adjacent breakwater segments. The proposed segmented breakwaters of Alternative 25 and 26 would expect to see minor gap erosion in the gap between the northernmost breakwater segment and the breakwater segment to the south (segment 2 in Alternative 25, and segment 3 in Alternative 26). The remaining gaps should produce no erosion in the lee.

Suh and Dalrymple (1987) developed the following relationship for the prediction of salient amplitude for segmented breakwaters:

$$y_s = 14.8 y_B \frac{L_g y_s}{{L_B}^2} e^{\left(-2.83\sqrt{\frac{L_g y_s}{{L_B}^2}}\right)} \quad \text{(12-19)}$$

Equation 12-19 was used to determine the amplitude of the equilibrium salients landward of the segmented breakwaters. The volume of the depositional feature was then determined by assuming a parabolic salient shape and integrating over the actual bathymetric region where the salient would form.

Figure 12-13 presents the salient formation expected for the breakwater associated with Alternatives 11a and 18. The salient would extent a distance of approximately 415 feet offshore, and consist of a total volume of approximately 41,650 cubic yards. Figures 12-14 and 12-15 present the salient formations for the segmented breakwater configurations of Alternatives 25 and 26, respectively. Alternative 25A would not have the northernmost salient. The schematic shows the estimated amplitudes and shapes of the salient formations behind the breakwater segments and provides a reasonable estimate of the potential shoreline modification. The total volumetric value (highlighted in the white box) is the summation of all the salients in these cases. Since the final beach nourishment template and width was unknown at the time of this report, this analysis was completed without including the shoreline advancement associated with the proposed beach nourishment. This would push the salient formations further seaward and would also results in slightly different amplitudes and volumes.

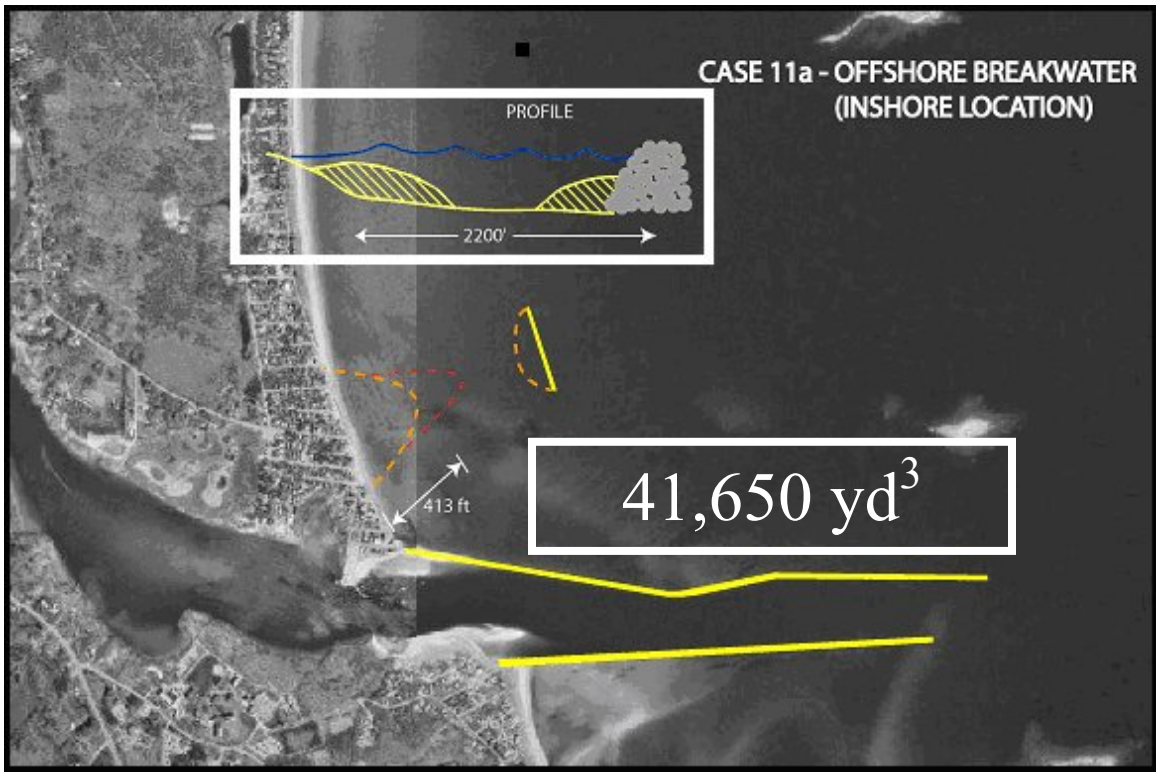

Figure 12-13. Estimated salient formation for the breakwater associated with Alternative 11a (broken red line) and 18 (broken orange line). Insert not to scale.

In all of the final breakwater alternatives, theory does not predict the formation of tombolos. Therefore, the effect on the natural longshore sediment transport will not be severe. In addition, the total volume of sediment estimated for full salient formation is less than $1/6^{th}$ of the overall initial fill volume for Alternatives 11a and 18, and less than $1/5^{th}$ of the initial fill volume for Alternatives 25A, 25, and 26.

For the Alternative 11a and 18 salient formations, salient formation distances and volumes were used in the nearshore (local) wave model (as Alternatives 20 and 21) to provide an estimate of the wave energy changes due to the salient formation in the nearshore zone. The salients were numerically added to the model domain and were simulated for the full range of wave climate scenarios. Alternative 20 simulates a full salient formation, while Alternative 21 simulates a partial salient formation. The effect on the wave energy, coupled with the proposed structure, is presented in Appendix 11-C. These wave results were used in the development of the beach nourishment performance estimates presented in the section 12.5.5 for the breakwater alternatives.

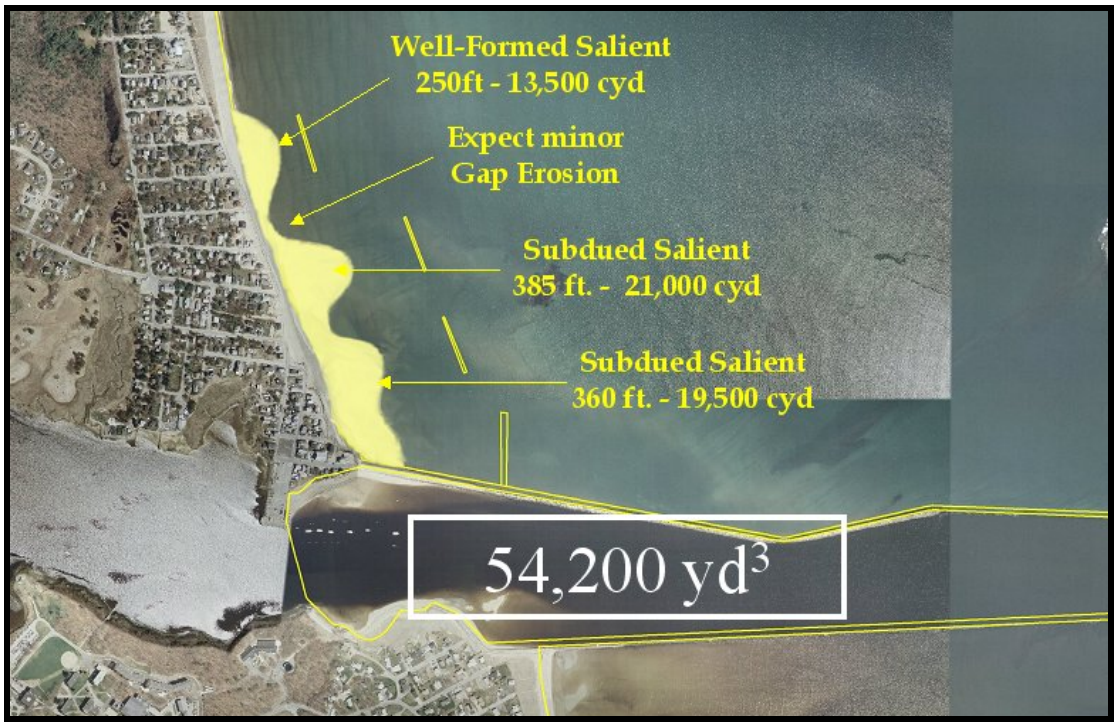

Figure 12-14. Estimated salient formation for the segmented breakwater configuration of Alternative 25.

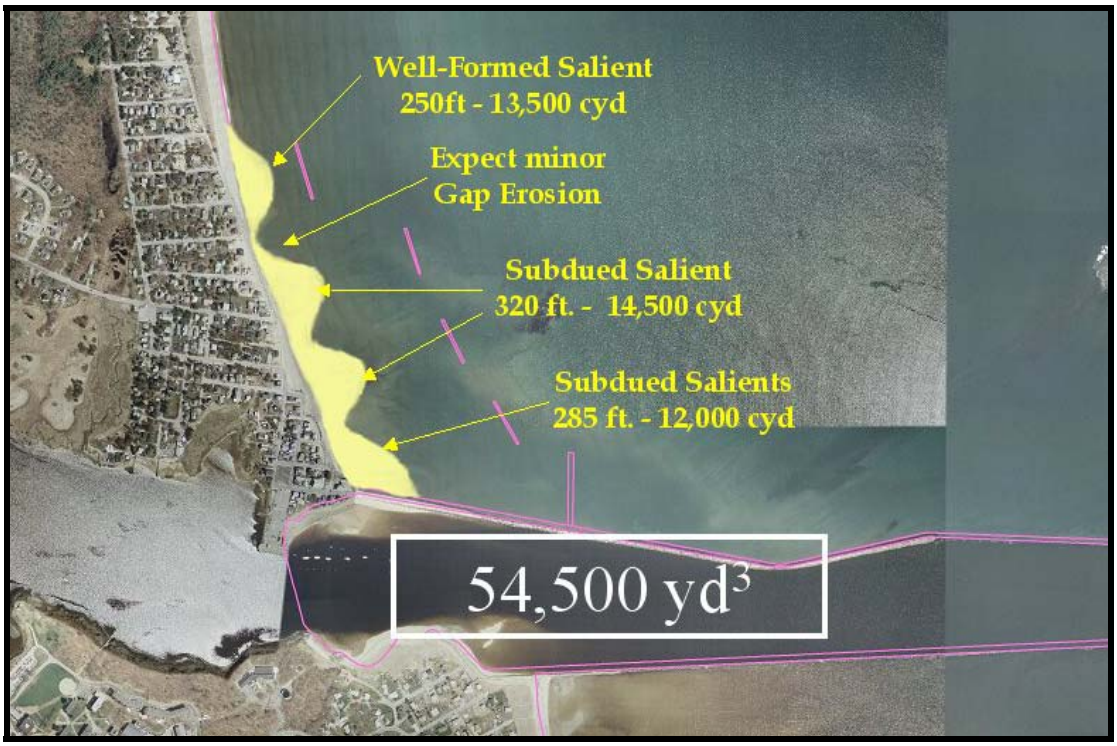

Figure 12-15. Estimated salient formation for the segmented breakwater configuration of Alternative 26.

12.5.5 Beach Nourishment Performance

The basic fundamentals usually used to evaluate the performance of the nourishment program do not necessarily apply to the conditions at Saco Harbor. Typically, nourishment performance is evaluated on an open coastline and does not include the effects of a neighboring inlet or coastal structures. The standard evaluation combines the conservation of sediment equation with the linearized transport equation. This formulation, called the Pelnard-Considére (1956) equation (Equation 12-20), is used in providing theoretical results to establish design and performance standards for nourishments. A more detailed description of the derivation of the equations and their applications can be found in Dean (2002).

$$M(t) = \frac{2\sqrt{Gt}}{l\sqrt{\pi}}\left(e - \left(\frac{1}{2\sqrt{Gt}} \right)^2 - 1 \right) + erf\left(\frac{l}{2\sqrt{Gt}} \right) \quad \text{(12-20)}$$

where *M(t)* is the proportion of sand remaining in the placed location, *G* is the alongshore diffusivity parameter, *t* is time, and *l* is the project (nourishment) length. The alongshore diffusivity is presented by Pelnard-Considére (1956) as:

$$G = \frac{KH_b^{5/2}\sqrt{g/\kappa}}{8(s-1)(1-p)(h_* + B)} \quad \text{(12-21)}$$

where K is the sediment transport coefficient (a function of sediment size), B is the berm elevation, H_b is the breaking wave height, h_* is the depth of closure (in this case 8.7 m or 28.5 ft) , p is the *in-situ* sediment porosity (approximately 0.35 to 0.40), s is the sediment specific gravity (approximately 2.65), and κ is the ratio of wave height to water depth within the surf zone (approximately 0.78).

The Pelnard-Considére equation can be applied to determine the performance of a beach nourishment project. For example, Figure 12-16 presents a typical nourishment on an open coast beach without any structures or inlets. Figure 12-16 contains a series of lines depicting the temporal planform evolution of a rectangular nourishment on a long straight beach. The resulting planform is symmetrical about the centerline of the nourishment. Therefore, only one-half of the resulting planform is shown in Figure 12-16. The solid black line indicates the initial fill template, and subsequent lines indicate the temporal progression of the nourishment. The vertical axis indicates the nourishment width (or distance seaward from the original shoreline), while the horizontal axis indicates the alongshore distance from the center of the nourishment. Within 1-year of placement of the nourishment, the shoreline excursion at the center of the project has already retreated over (30 m or 100 ft), as sand has been transported in both directions due to the perturbation that is created on the shoreline. However, as shown by the lines corresponding to temporal changes in fill, the material diffuses onto the adjacent

properties and is not lost from the local system immediately. The conditions that exist around the Saco River inlet will not allow for this type of spreading pattern to occur. The presence of an inlet and/or shore-perpendicular (jetties and groins) structures modify how material will be transported over time. In order to evaluate the performance and sediment transport to the north of the Saco River inlet for the alternatives, a variety of conditions need to be applied.

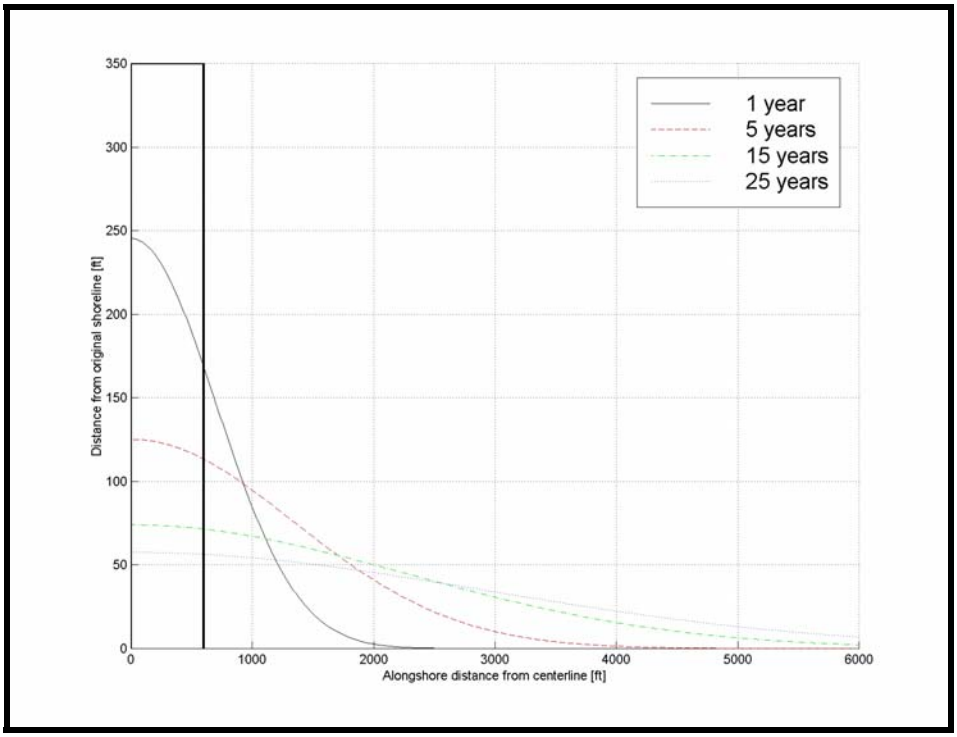

Figure 12-16. Temporal evolution of an example nourishment placed along an open coast (without the influence of an inlet and/or structures). Since the nourishment spreading is symmetrical, only half the fill distance is presented.

The Pelnard-Considére equation can be applied to many different scenarios by adjusting the boundary conditions. Dean (2002) has adapted the equations to evaluate sand movement in regions with inlets and/or structural influences. To evaluate the beach nourishment performance in the region surrounding Saco River inlet, where there are significant coastal structures, another boundary condition is applied to account for the impact of coastal structures (Dean, 2002). In this case, the Pelnard-Considére equation is modified to include the spreading of the nourishment, and the erosion of the shoreline downdrift of a littoral barrier (coastal structure). In an open coast situation, the nourishment will spread symmetrically about the centerline of the project as material is transported to both sides of the nourishment. However, placing the fill adjacent to a littoral barrier only allows the nourishment to move in one direction (to the north when considering placement of material next to the northern structure), compared to the initial planform. Therefore, nourishment placed next to a littoral barrier can only spread in a single direction (Dean, 2002). In effect, the littoral barrier increases the time with which sediment must remain in the fill region. However, this does not mean that the lifetime of

a nourishment placed next to a structure will be increased, since the downdrift impact of the coastal structures must also be considered. Superimposed on top of the solution for the nourishment spreading is the solution for shoreline displacement at a littoral barrier (i.e., groin, jetty, etc.).

Table 12-3 presents the adjusted length of the nourishment for each alternative based on the influence of the structures (both existing and proposed). These adjusted lengths do not represent an actual physical extension of the nourishment; however, the adjustment is used to represent the influence of structures on the rate of dispersion in the sediment transport model. As discussed, the inclusion of structures will limit the spreading of the nourishment to one direction, as opposed to an open coast situation where spreading occurs in both directions. Typically, a structure such as the northern jetty at Saco River would limit the spreading to a single direction and the nourishment length would be doubled to account for this influence (Dean 2002). However, in the specific case of the Saco River northern jetty; the length of the jetty, especially on the northern side, has created nearshore contours along the onshore-offshore length of the structure. In some respects, this behaves like an alongshore stretch of coastline that contains a significant curvature, as evident by the contours and the way the waves refract into the structure. Waves approach a portion of the structure like a shoreline, increasing wave reflection and producing physical sediment transport that is more alongshore physics based in the cross-shore direction. Therefore, the existing northern jetty is considered to provide less of a boundary to the dispersion of sand, which will likely spread along the structure in the offshore direction. As such, doubling the nourishment length to account for the presence of the northern jetty (i.e., allowing no dispersion in the southern direction) does not seem realistic. In cases where a spur jetty is included, however, the combined ability of the northern jetty and spur to contain sand within the nourished zone is highly probable, and therefore, doubling of the nourishment length is advised. The selection of these lengths is based on engineering judgment and based on the results of the existing condition sediment transport along the northern structure.

Table 12-3. Adjusted nourishment lengths for assessment of beach nourishment performance at Camp Ellis Beach.

Alternative	Adjusted Nourishment Length
Beach Nourishment Alone	990 m (3,250 ft)
6 – Spur Jetty	1,440 m (4,125 ft)
11a – Breakwater	1440 m (4,125 ft)
18 – Combined Spur Jetty and Breakwater	1440 m (4,125 ft)
25 - Segmented Breakwater Configuration 4	1440 m (4,125 ft)
26 – Segmented Breakwater Configuration 5	1440 m (4,125 ft)

In addition, since the wave environment at Camp Ellis Beach is complex, as presented in section 12.5.2, calculation of the alongshore diffusivity was completed based on the wave distribution (incident and reflected) for each average annual directional approach bin. For example, each directional approach bin was segregated into waves that would move sediment to the north and waves that would move sediment to the south, based on the

shoreline orientation. The percent occurrence of each of these wave types (for each directional bin) was also computed. Values of alongshore diffusivity were then computed for each wave type, in each directional bin, and for both MHW and MLW cases. Finally, based on the overall percent occurrence for each wave type and each directional bin, a representative alongshore diffusivity was computed within each alongshore zone. For breakwater alternatives, this also included the calculation of alongshore diffusivity for both full and partial salient formations, and these formations were included in the nourishment performance. Salients were expected to form within 3 years following breakwater construction in all cases. This methodology produces a much more representative alongshore diffusivity value than the selection of the most commonly occurring wave height and direction, or averaged wave height and direction.

In all cases a nourishment of 300,000 cubic yards and (762 m or 2,500 ft) in length was evaluated as the initial nourishment project. Although the final template of the nourishment, including berm height and width, was unknown at the time of the report, a berm elevation of (3.0 m or 10 ft) was used based on a preliminary engineering analysis performed by the USACE.

Since the material diffuses (spreads) over time, it is possible to evaluate the longevity of the nourishment by looking at the amount of material (by percent) left in the project area. Subsequently, alternatives can be compared to one another based on their ability to maintain a beach at Camp Ellis. Figure 12-17 presents the performance of a 300,000 cubic yard fill in terms of amount of material remaining, as a function of time, for the beach nourishment alone alternative (black line), Alternative 6 (blue line), and Alternative 18 (green line). This includes background erosion corresponding to 2 ft/yr (0.6 m/yr). That is, in addition to the dispersion that is occurring, an additional 2 ft/yr (0.6 m/yr) is eroded due to the natural erosion of the beach (as indicated in the historical data analysis for the region directly north of the northern jetty – Chapter 3.0). The percent of initial material remaining is presented along the left hand axis, while the time (in years) is presented along the bottom axis. The upward spike in each alternative on a ten-year interval represents the beneficial re-use of the dredged material (80,000 cubic yards) from the Saco River. Approximately 80,000 cubic yards of sediment is removed from the Saco River approximately every 10 years. This material may be used as a direct source to replenish the beach. The slight upward trend in the combined spur jetty and breakwater alternative (18 – green line) indicates the potential ability to sustain a reasonable beach width and volume through time. Although the performance curves are presented for a estimated 300,000 cubic yard nourishment, they can be scaled to represent any volume of proposed nourishment that the USACE designs as the rate of dispersion is not a function of total volume, but is representative of the percent of the initial volume nourished.

Figure 12-18 presents the performance of a 300,000 cubic yard fill in terms of amount of material remaining, as a function of time, for the beach nourishment alone alternative (black line), Alternative 26 (blue line), Alternative 25 (red line) and Alternative 25A (purple line). Again, this includes background erosion corresponding to 2 ft/yr (0.6 m/yr) and includes the beneficial re-use of the dredged material (80,000- cubic yards) from the

Saco River. The segmented breakwater alternatives, specifically alternative 25 and 25A, perform well in terms of sustaining a beach at Camp Ellis.

Due to the inherent unknowns within the coastal zone (e.g., being able to predict the storm frequency or wave energy in any given year), Figure 12-19 presents three (3) selected alternatives (beach nourishment alone, Alternative 6, and Alternative 25A) with associated error bounds. The error bounds are determined by assuming ±25% change in the background erosion rate. This fluctuation accounts for variations in the average annual year that may be more/less energetic. As the time scale increases, the level of certainty decreases, and the associated error range increases accordingly. Therefore, as expected, the long-term predictability is less certain due to both the extended look into the future and the probability associated with the number of years that may be more/less energetic than the average year. On a 50-year time horizon, the ±25% variation in background erosion rate, results in approximately a ±10% variation from the average performance curve. The high performing alternatives (e.g., Alternative 25A) still perform well, even at the lower bound of the confidence interval.

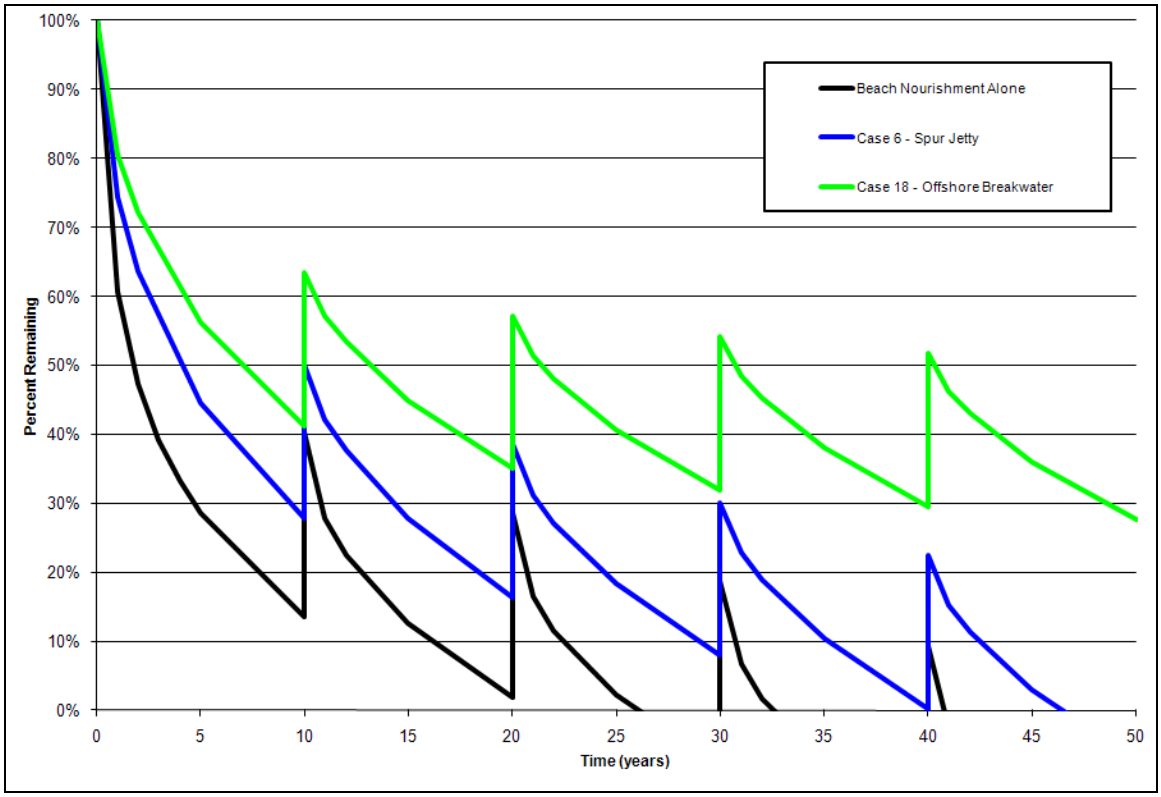

Figure 12-17. Nourishment performance in zones A and B for beach nourishment alone, Alternative 6, and Alternative 18.

Another method for evaluating the performance of the beach nourishment is to allow the nourishment to erode until a critical threshold is reached. This critical threshold is

typically defined as the minimal amount of material to resist a certain level return-period storm event (e.g., 10-year storm). Figure 12-20 presents an example of this performance evaluation by allowing the beach nourishment to erode to 30% (90,000 cubic yards) remaining before replenishing the beach template to 100% (300,000 cubic yards). With 30% of the material remaining, it was roughly estimated that an adequate defense can be provided against a moderate storm event (10-year); however, this is being assessed through additional storm modeling by the USACE. Under this scenario, the number of renourishments required over a given time horizon can be estimated. For example, in a 50-year time horizon, the beach nourishment alone alternative would have to be replenished 11 times, Alternative 6 (spur jetty) would have to be replenished 5 times, and Alternative 25A would have to be replenished 3 times. Appendix 12-C presents all the beach nourishment performance data in tabular format, including amount of material required for each replenishment, time of replenishment, and percent remaining as a function of time. This includes both evaluation methods (e.g., 80,000 replenishment every 10-years, and 30% threshold).

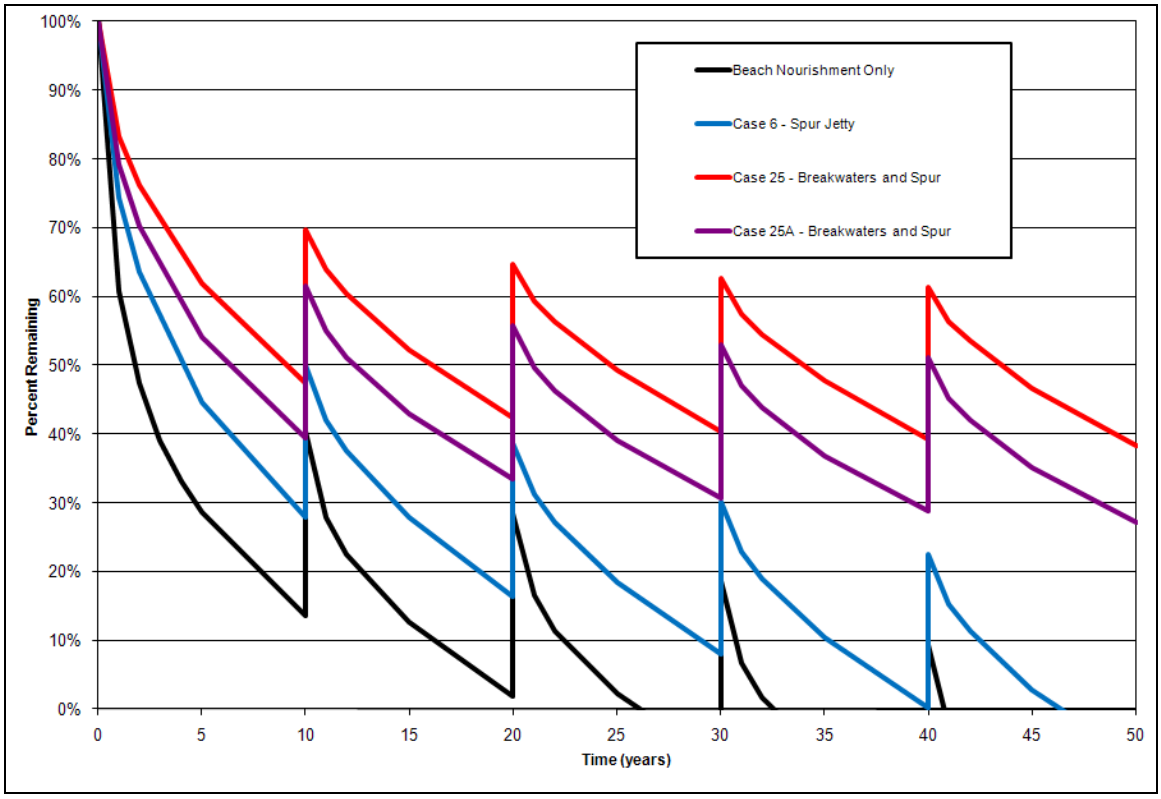

Figure 12-18. Nourishment performance in zones A and B for beach nourishment alone, Alternative 23, Alternative 25, and Alternative 25A.

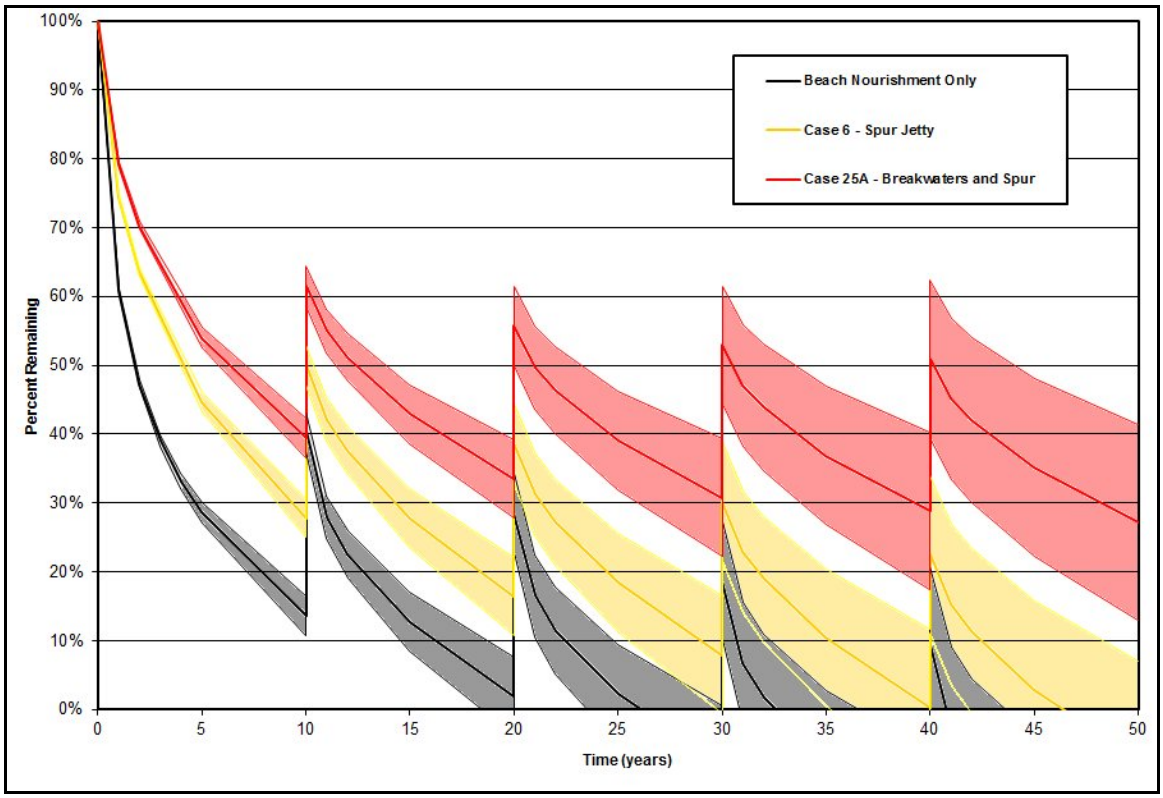

Figure 12-19. Nourishment performance in zones A and B for beach nourishment alone, Alternative 6, and Alternative 25A. The shaded regions present the confidence levels for each alternative, providing upper and lower bounds on the performance.

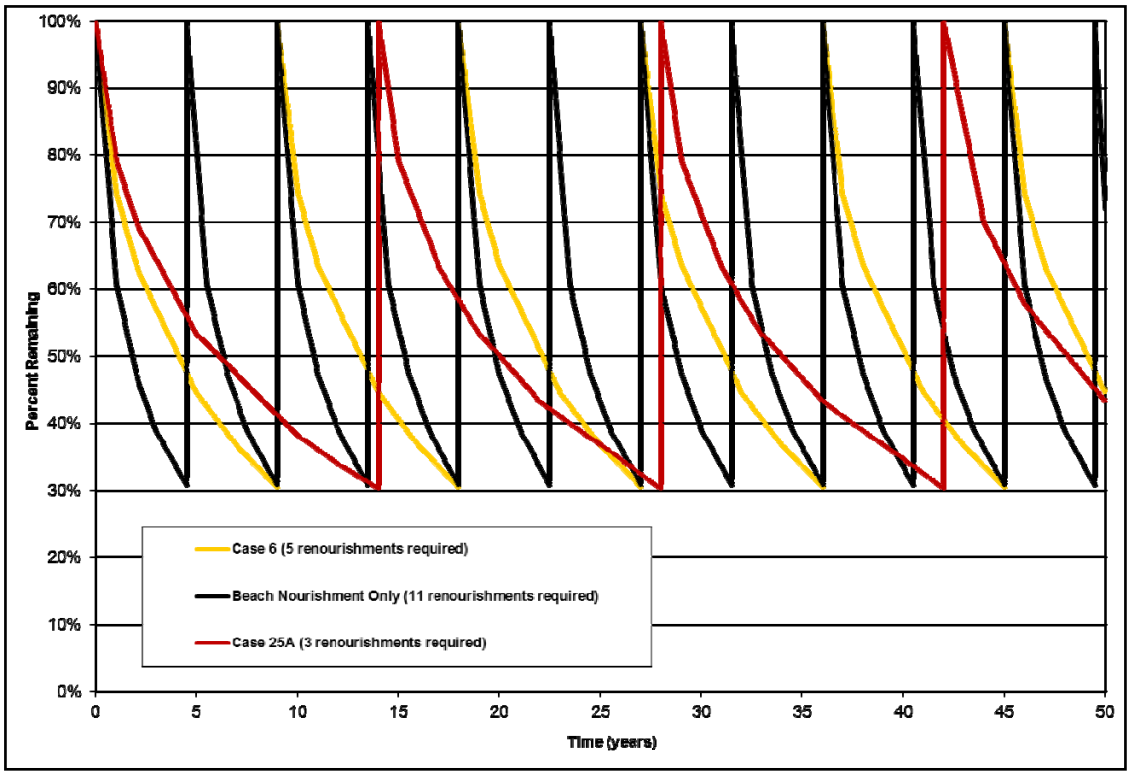

Figure 12-20. Nourishment performance in zones A and B for beach nourishment alone, Alternative 6, and Alternative 25A. The initial nourishment is allowed to erode until only 30% is remaining in the existing template region. The nourishment area is then replenished to 100%.

As discussed at the beginning of this section, Alternative 9, the T-Head groin case, represents an alternative that is significantly different than the other final alternatives. While the other alternatives are focused on reducing the wave energy, and subsequently reducing the ability of the wave to move the sediment, the T-Head groins primary function is to hold the sand in place by eliminating nearly all of the alongshore sediment transport. It is assumed that T-Head groins will be effective at containing sand in the region where they are placed, and will likely mitigate the chronic erosion that has occurred at Camp Ellis Beach. Currently, however, there is a significant lack of data, research, and analyses techniques to adequately assess the overall performance of T-Heads, as well as their potential impact on downdrift shorelines in the northern Atlantic coastlines with a significant tide range. In order to provide an estimate on the potential downdrift impact of the T-Head system proposed in Alternative 9, the potential impact on downdrift beaches is presented in Figure 12-21. This analysis assumes that the region donwdrift of the groin field is also nourished and that minimal bypassing is occurring around the groin field. After approximately 6 years, the shoreline begins to erode beyond its current location and experiences additional erosion. Therefore, after every six years, the region down drift of the T-Head groin field would require replenishment.

In order to put this in perspective with the other alternatives, the amount of sediment required to be placed downdrift of the groins can also be determined from Figure 12-21. Under existing conditions, and assuming that sediment is readily available for transport along the beach approximately 33,000 to 65,000 cy/yr is transported to the north for this region (as determined earlier in this chapter). Therefore, the loss of 300,000 cubic yards over one time span of six years (~ 50,000 cy/yr) is reasonable assuming no sand is able to migrate from the T-head region. This produces a required nourishment of approximately 50,000 cy/yr to keep the downdrift shoreline at its current location.

Alternative 25, on the other hand, requires approximately 75,000 to 90,000 cubic yards of nourishment every ten years (Figure 12-18), or 7.500 to 9,000 cy/yr. The downdrift impacts associated with the other alternatives are substantially less and also allow a portion of material to naturally be transported into the northerly area (Box C). If the region of Box C is assumed to be reasonably stable (as historically has been shown), but in more recent times unlikely. Additional sand from nourishment of Camp Ellis should provide a supply of material that may not currently be available. Tabular data for the T-Head groin case is also presented in Appendix 12-C.

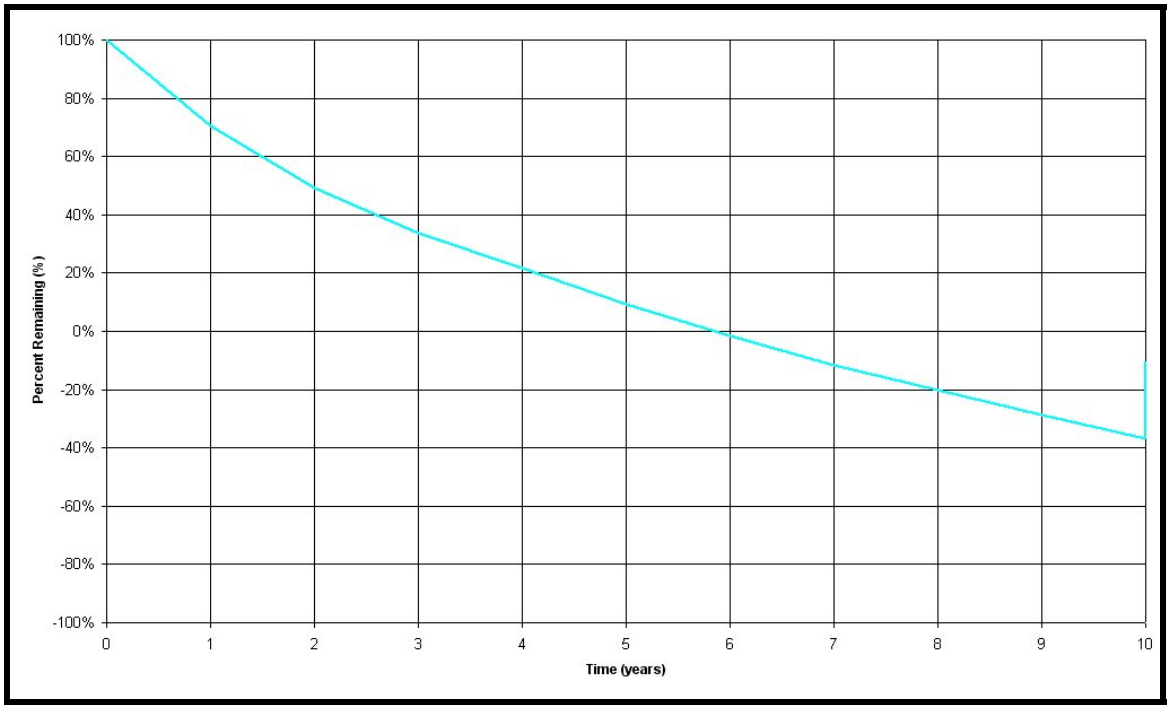

Figure 12-21. Potential impact on downdrift beaches due to the Alternative 9, T-Head groin alternative.

13.0 CONCLUSIONS

13.1 Summary

The Saco-Camp Ellis Beach area, located adjacent to the Saco River federal jetties, represents a complex coastal setting that has not been well understood. Camp Ellis Beach has undergone significant shoreline changes over the past 150 years, including significant erosion over the past several decades. The purpose of this study was to evaluate potential alternatives that may be viable solutions to the ongoing erosion at Camp Ellis Beach. The study focuses on evaluating the physical processes (concentrating on the wave environment) occurring within the vicinity of Saco Bay, and specifically the Camp Ellis Beach area, to assess potential alternatives that may be used to mitigate the erosion along the shoreline.

There were two main components of the study, a field data collection component, and a numerical modeling component. The field data collection component consists of observing the existing site-specific conditions (e.g., waves, currents, tides, bathymetry, etc.) and the historic environment (e.g., shoreline change, offshore wave data, existing studies, etc.) to develop an initial understanding of the ongoing coastal processes that shape the Camp Ellis shoreline. The field data also serve to provide the required data for developing predictive models of the Camp Ellis region. The numerical modeling component of the study consists of accurately simulating the existing conditions within the vicinity of Camp Ellis, verifying the models performance with observed data, and subsequently, utilizing the verified models to simulate various alternatives for shoreline protection. The numerical modeling portion of the study ultimately evaluates the performance of each of the alternatives and the ability to sustain a beach at Camp Ellis, while focusing on the ability of the alternatives to rectify the potential causes of erosion at Camp Ellis caused by the federally maintained structures. Specifically, the paucity of sediment supplied to the region by the direction of the sediment laden Saco River discharge a significant distance offshore and the structural impact producing increased wave energy exerted on the Camp Ellis coastline.

The existing environmental conditions within the region were studied extensively in preparation for evaluating the potential alternatives. Where possible, information from existing studies was used to describe the system. Not every study or conversation is discussed directly herein; however, a vast amount of material was reviewed regarding the historical and current status of the Saco Bay region. In other cases, site-specific field investigations were undertaken to evaluate the physical conditions within the project area. A summary of the major components of the field data collection program is given below.

Historical shoreline change – An analysis of historical shoreline change was performed for the Saco Bay littoral cell (approximately an 8-mile shoreline segment). The data used to compile the analyses were derived from aerial photography, historical maps, and digital orthophotographic quads. Rates of historical shoreline change were calculated at 265 shore-normal transects from Biddeford Pool to Prouts Neck. The shoreline adjacent to the northern jetty (Camp Ellis Beach) experienced significant erosion. The shoreline between 1864 and 1998 eroded at rates between –3.41 ft/yr (at transect 41) and –0.16

ft/yr (at transect 53). The more contemporary time period (1944-1998) shows continued erosion, but at a reduced rate (approximately 1.0 ft/yr and less). This stabilization is likely the result man-made intervention in the form of heavy structural stabilization (seawalls, revetments, etc.). Currently, Maine State Law does not allow shore attached structures and these revetments were placed in response to the emergency conditions. It is expected that without these structures, the erosion would continue. With the lack of sediment supply that currently exists at the Camp Ellis shoreline, erosion has begun to occur to the shorelines north of the historical erosion area as less sediment is available for northerly transport into these once stable regions.

Bathymetry – Bathymetric information was obtained from existing sources and a bathymetric survey performed of the nearshore region of Camp Ellis Beach in 2003. The nearshore bathymetry is complex, with rock outcrops, linear shoals, and irregular contours. The data collected was used extensively in the modeling of the Camp Ellis region.

Tides and Currents – Tide and current information was collected in the vicinity of Camp Ellis Beach. During a spring tide, the tidal range is approximately 11.5 to 12.0 feet (ft). However, during a neap tide the tidal range is reduced to approximately 7.0 ft. Only minor tidal damping occurs as water propagates upstream. The relative strength of the currents (≤ 150cm/s) within the jettied channel compared with flow at the seaward end of the channel (≤ 30 cm/s). As the flooding currents seem to favor a south-westerly direction focused in the southern part if the channel and the ebb currents favor a northeasterly direction in the northern part of the channel, dominant sediment transport out of the system is likely to remove sediment from the northern part of the channel and transport it to the northeast as it leaves the jettied channel. The magnitude of the tidal currents in the nearshore vicinity north of the jetties is minimal. This lack of significant tide-induced currents offshore of Camp Ellis Beach suggests that wave processes are the primary driver of sediment movement in the nearshore vicinity of Camp Ellis Beach.

Wave Climate – Wave data were gathered from existing buoys, existing hindcast model nodes, and data observations associated with this study. Offshore data sources included, NOAA buoys, GOMOOS Buoys, and USACE WIS hindcast data. Wave data were also collected at target locations seaward and landward of the Eagle/Ram Island complex in order to accurately assess the wave transformations that occur due to the complicated physical nature of the islands and bathymetry in this region. Wave data, at least over the deployment time period, indicate that waves approaching Camp Ellis Beach are primarily unidirectional, approaching from an ENE direction, even when waves approach from the ESE seaward of the islands. The wave ADCP data were compared to existing NOAA buoy data to provide a level of confidence in the observed data. The wave data were a necessity for calibrating and verifying the numerical wave transformation models.

Sediments - A total of seven (7) surface grab samples were collected within the Saco Bay region. A general fining of sediment is observed from south to north (as discussed in Chapter 2.0). As such, the median grain size is finer at the northern end of the Bay (Scarborough) than it is at the southern end (Camp Ellis).

Armed with the data observations and historical information, the modeling effort was calibrated in order to ensure that it was appropriately simulating reality within reasonable error bounds. The models were then used to simulate existing conditions, and finally, to assess a wide range of alternatives. A summary of the major components of the numerical modeling program is given below.

Generation Scale Wave Modeling - Because of the lack of temporal and spatial similitude between locally observed wave information and available data sources, a generation scale wave model was used to develop input into the detailed, shallow-water transformation-scale wave model. The generation-scale model is part of an extensive wave modeling system used to analyze the potential impacts of alternatives to mitigate erosion due to federally constructed and maintained navigational structure in Saco, Maine. The generation scale numerical model used satellite observed wind fields as input and was calibrated and verified using local point wave observations. A nested grid of water depths was used to define the model domain. The calibration between the measured and modeled wave heights was visually successful and quantifiable error statistics were within acceptable bounds. In addition, assessment of specific higher energy events during the deployment time period indicated energy transfer across frequency bands during the passage of an event. Subsequently, spectral wave data were extracted from the generation scale model at the location coinciding with the offshore boundary of the regional wave model for the entire deployment time period. This spectral information were used as input conditions for validation of the regional scale modeling effort.

- ***Transformation-Scale Wave Modeling*** - A nearshore, transformation-scale (regional) wave model was used to propagate the offshore wave climate into the Saco Bay region and evaluates the transformations waves experience as they propagate towards the coastline. The model was verified using spectral output from the generation scale modeling results, and the error estimates were within acceptable bounds. Once validated, the transformation-scale (regional) model was used to simulate average annual directional cases (developed from WIS data), specific historic storms events, and return-period storms. Regional wave transformation models provide predictive tools for evaluating various forces governing wave climate and sediment transport processes. The transformation-scale (regional) model identified transformation effects that produced an uneven distribution of wave energy along the coast that affects sediment transport in the region, revealing areas of increased erosion ("hot spots") or areas of increased energy. The transformation mechanisms also result in changes in the offshore wave direction that may significantly influence the rate and direction of sand movement. Therefore, the quantitative information provided from the numerical model(s) can be used to explain the physical processes that dominate a region, provide the required input into higher resolution models, and to potentially furnish appropriate recommendations/solutions for each stretch of coast. Results of the transformation-scale (regional) model are used to develop regional sediment transport fluxes and divergence, while providing spectral input for the local wave modeling effort.

Local Scale Wave Modeling - The regional model only represents an intermediate step in the wave modeling system and although is useful for identifying regional sediment transport trends, cannot be used for local sediment transport calculations for the Camp Ellis Beach area. Therefore, it was important to advance to higher-resolution models that embodied the reflection processes and could more accurately determine the nearshore structural interactions. The nearshore (local) wave model was simulated using the same set of conditions developed for the transformation-scale (regional) modeling. Spectral boundary conditions are specified along the offshore radiating boundary using spectral results from the transformation-scale (regional) model in order to calibrate and verify the nearshore (local) wave model, as well as all average annual, directional approach simulations and storm events. The nearshore (local) wave model was calibrated using two simulated time periods to quantify the overall accuracy. The nearshore (local) model compared favorably to the observed results and was slightly more accurate when compared to the results presented for the regional, transformation-scale model.

Evaluation of the sea surface results for the existing conditions revealed: (1) the significant wave reflection off of the northern jetty indicating the beach is impacted not only by the incident wave energy, but also by the reflected wave energy, (2) independent of offshore direction of approach, the nearshore waves propagated directly towards the Camp Ellis Beach area and the northern jetty, (3) Mach-Stem waves propagating shoreward along the northern jetty can be seen in most cases, (4) waves are refracted towards the northern jetty due to the jetty-parallel bottom contours, and (5) variations between annual average approach directions are important to understand the processes occurring at Camp Ellis Beach.

Sediment Transport Assessment - Understanding the wave transformations is a critical step in determination of shoreline processes and changes, and this wave information is required in order to provide an estimate on how sediment moves in the nearshore region. Ultimately, however, the goal of the overall project is to create a sustainable beach at Camp Ellis. The wave modeling system results were the key input into the sediment transport modeling and beach nourishment performance evaluation. The various wave scenarios were also combined to represent an average annual year of wave climate. The sediment flux indicates an average annual longshore transport rate to the north. However, the magnitude of the transport varies throughout the domain. A region extending from just north of the navigational structures to approximately 3 km to the north, averages approximately 25,000 to 50,000 m^3/yr (32,700 to 65,000 cubic yards) towards the north. In the center of the bay, extending approximately 3 km to the north, the average annual sediment flux rate is small. This is a region that gross transport direction shifts depending on the angle of the incoming wave field, and generally are equivalent. There is a small net northward transport rate of 10,000 to 20,000 m^3/yr (13,000 to 27,000 cubic yards) and the flux divergence indicates a stable stretch of coastline. The northernmost region of the bay is strongly influenced by the Bluff and Stratton Island complex and there are major fluctuations in both the sediment flux and divergence. The average sediment transport rate in this region is 40,000 m^3/yr (52,000 cubic yards) towards the north.

A variety of alternatives were considered for addressing the chronic erosion at Camp Ellis Beach. Over twenty-five (25) potential solutions, including both structural (e.g., spur jetties, breakwaters, groins, jetty roughening, etc.) and non-structural (e.g., partial jetty removal, offshore borrow pits, jetty roughening, etc.) were determined jointly between Woods Hole Group, the USACE New England District, Maine Geological Survey (MGS), and members of the Saco Bay Implementation Team (SBIT). These alternatives were detailed in Chapter 10.0.

Due to the number of simulations required to evaluate all potential solutions, the alternatives analysis consisted of an initial and final screening process. The nearshore (local) wave model was used as the initial screening tool through evaluation of results, wave height changes, wave energy reduction, and assessment of potential impacts. Potential adverse impacts to neighboring beaches, navigation, and the Camp Ellis region were also evaluated. The initial screening process identified six (6) alternatives that warranted further evaluation in terms of sediment transport changes and beach performance. These alternatives, each of which includes beach nourishment to restore the beach to a useable (and more importantly protective) width are listed below. Included in the final analysis was a beach nourishment alone plan, that was used to compare relative performance of the alternatives ability to help sustain a beach in front of Camp Ellis.

Beach nourishment alone (evaluation baseline):

- Alternative 6: Inshore location of a 750-foot spur jetty
- Alternative 9: Primary T-head groin configuration
- Alternative 11a: Offshore breakwater, inshore location
- Alternative 18: Alternative 11a and inshore location of 500-ft spur jetty
- Alternative 25: Segmented breakwater configuration 4
- Alternative 26: Segmented breakwater configuration 5
- Alternative 25A: Segmented breakwater configuration 6

The final alternative analysis was an assessment of sediment transport and beach nourishment performance. The relative performance of each alternative was compared in terms of their ability to sustain a protective beach at Camp Ellis and reduce wave energy at the shoreline. Changes to the wave reflection wave energy, the reduction of sediment transport, the potential influence of salient formations, and the overall beach performance over a 50-year time horizon were assessed (section 12.5).

13.2 Final Screening Summary and Conclusions

The final alternative that is selected must address the increased erosion caused by the federally maintained navigational structures. The data, modeling, and analysis indicate that the federal structures at Saco River have created increased wave energy to the north of the Saco River inlet and significantly reduced the amount of sediment supplied to the beach by the Saco River by channeling the discharge a greater distance offshore. Therefore, the preferred alternative should (1) mitigate the increased wave energy caused

by wave reflection off of the northern jetty and (2) replenish, to a feasible level, the sediment that would naturally be supplied to the system by the Saco River discharge. A preferred alternative is not provided in this report, which focuses on the technical performance and the physical processes associated with each alternative, and narrows the alternatives on purely a performance and environmental impact basis. Although other factors (e.g., cost, constructability, etc.) were considered in the alternatives assessment, the weight of these additional factors, in concert with the performance, will be determined by the USACE. As such, this report provides technical guidance for the USACE in making a decision on the alternative that meets the required elements of the Section 111 authority. The bullets presented below provide some conclusions based solely on the scientific and engineering results presented herein.

- Beach nourishment alone is not a viable solution without the inclusion of a significant maintenance component. Lacking any additional wave energy reduction, a standalone beach would be quickly eroded. The beach nourishment alone alternative also does not mitigate any of the reflected wave energy that impacts Camp Ellis Beach. Therefore, it would not be possible for beach nourishment alone to meet the project purpose of mitigating the erosive effect of the jetty and preventing further retreat of the Camp Ellis shoreline.

- Each of the final alternatives, coupled with beach nourishment, performs with relative levels of improvement. Therefore, each alternative can be effective depending on the level of maintenance expected and success criteria.

- The geology at the offshore breakwater location (Alternatives 11a and 18) is not suitable to support the weight of the structure. There is considerable concern related to settlement at this location, as such these final alternatives are not recommended.

- Alternative 6 provides a reduction in the reflected wave energy caused by the northern jetty, and coupled with beach nourishment provides a reasonable solution for consideration. However, increased maintenance, as compared to the segmented breakwater and spur jetty combinations would be expected.

- From a purely performance perspective, Alternatives 25 and 26 are unmatched. There are subtle differences between the two alternatives in performance, but overall there is no measurable distinction. However, as subsurface explorations determined that soft marine clay underlies the northernmost breakwater for both alternatives, constructing a stable structure at this location would be costly.

- Alternatives 25 and 26 do show some potential for salient formation in terms of amplitude at the northernmost breakwaters, but this would not significantly impact the shorelines to the north due to the increased sediment supply provided by the beach nourishment. Alternative 25A provides an alternative segmented

breakwater solution that removes the northernmost breakwater and still provides reasonable performance.

- It is critical that the final alternative selected includes a beach nourishment component. Shoreline erosion is continuing to occur north of the structure and erosion is extending a further distance north of the structure due to the lack of sediment supply available for transport. In order to provide a functional solution at Camp Ellis, the wave energy must be reduced, this will also reduce the rate of sediment transport to the north. As such, all the final recommended solutions indicate a net reduction in sediment transport to the north. However, the proposed alternative will have a net benefit to the shorelines to the north due to the increased sediment supply provided by the beach nourishment. Currently, there is little to no sediment supply in the Camp Ellis shoreline/dune system to be transported to the north. Therefore, erosion will continue to occur both at Camp Ellis and the shorelines to the north. However, a significant nourishment will replenish the sediment supply to the coastline and this additional sediment can only benefit the regions to the north. Even at a reduced sediment transport rate, the net sand moving to the northern beaches will be far greater than currently exists.

14.0 REFERENCES

Ahrens, J.P. and Cox, J. 1990. Design and Performance of Reef Breakwaters. Journal of Coastal Research. p. 61-75.

Anders, F.J. and M.R. Byrnes. 1991. Accuracy of Shoreline Change Rates as Determined from Maps and Aerial Photographs. Shore and Beach, 59(1): p. 17-26.

Barber, D.C. 1995. Holocene Depositional History and Modern Sand Budget of Inner Saco Bay, Maine: Unpub. M.S. Thesis, University, Maine, Orono, 178 pp.

Barnhardt, W.A., W.R. Gehrels, D.F. Belknap, and J.T. Kelley. 1995. Late Quaternary Relative Sea-Level change in the Western Gulf of Maine; Evidence for a Migrating Glacial Forebulge. Geology, v 23, no. 4, p. 317-320.

Belknap, D.F., R.C. Shipp, J.T. Kelley, and D. Schnitker. 1989. Depositional Seqence Modeling of the Late Quaternary Geologic History, West Central Maine Coast, In Tucker, R.D., and Marvinney, R.G., eds., Studies in Maine Geology, Volume 5: Quaternary Geology: Augusta, Maine Geol. Survey, Dept. of Conservation, p. 29-46.

Belknap, D.F. and R.C. Shipp. 1991. Seismic Stratigraphy of Glacial Marine Units, Maine Inner Shelf, in Anderson, J.B. and Ashley, G.M. (editors), Glacial Marine Sedimentation; Paleoclimatic Significance: Geological Society of America, Special Paper 261, p. 137-157.

Bloom, A.L. 1963. Late-Pleistocene Fluctuations of Sea Level and Postglacial and Crustal Rebound in Coastal Maine: American Journal of Science, v. 261, p. 862-879.

Briggs, M.J., B.P. Donnell, Z. Demirbilek, and R.D. Carver. 2003. Tediuos Creek Small Craft Harbor: CGWAVE Model Comparisons Between Existing and Authorized Breakwater Configurations. U.S. Army Corps of Engineers ERDC/CHL CHETN-I-67.

Brooks, R.M. and W.D. Corson. 1984. Summary of Archived Study Pressure, Wind, Wave, and Water Level Data. U.S. Army Engineer Waterways Experiment Station, Wave Information Study, Vicksburg, MS, WIS Report 13.

Brothers, L., in press, Nearshore sedimentary pathways and their social implications, Saco Bay, Maine. MS degree, University of Maine.

Byrnes, M.R. and M.W. Hiland. 1994. Compilation and Analysis of Shoreline and Bathymetry Data (Appendix B). In: N.C. Kraus, L.T. Gorman, and J. Pope (editors), Kings Bay Coastal and Estuarine Monitoring and Evaluation Program: Coastal Studies. Technical Report CERC-94-09, U.S. Army Engineer Waterways Experiment Station, Coastal Engineering Research Center, Vicksburg, MS, p. B1-B89.

Byrnes, M.R., R.M. Hammer, B.A. Vittor, J.S. Ramsey, D.B. Snyder, K.F. Bosma, J.D. Wood, T.D. Thibaut, and N.W. Phillips. 1999. Environmental Study of

Identified Sand Resource Areas Offshore Alabama: Volume I: Main Text, Volume II: Appendices. U.S. Department of the Interior, Minerals Management Service, International Activities and Marine Minerals Division (INTERMAR), Herndon, VA. OCS Report MMS 99-0052, 326 pp. + 132 pp. appendices.

Byrnes, M.R, R.M. Hammer, B.A. Vittor, J.S. Ramsey, D.B. Snyder, J.D. Wood, K.F. Bosma, T.D. Thibaut, N.W. Phillips. 2000. Environmental Survey of Potential Sand Resource Sites: Offshore New Jersey. U.S. Department of the Interior, Minerals Management Service, International Activities and Marine Minerals Division (INTERMAR), Herndon, VA. OCS Report MMS 2000-052, Volume I: Main Test 380 pp. + Volume II: appendices 291 pp.

Brooks, R.M. and W.D. Corson. 1984. Summary of Archived Study Pressure, wind, Wave, and Water Level Data. U.S. Army Engineer Waterways Experiment Station, Wave Information Study, Vicksburg, MS, WIS Report 13.

Coastal and Marine Geology Program of the United States Geological Survey (http://woodshole.er.usgs.gov/project-pages/oracle/gomaine/bathy/)

Collins, J. 1972. Prediction of Shallow-Water Spectra. Journal of Geophysical Research, Vol. 77, p. 2693-2707.

Crowell, Mark, Stephen P., Leatherman, and Michael K. Buckley. 1991. Historical Shoreline Change: Error Analysis and mapping Accuracy. Journal of Coastal Research, 7(3): p. 839-852.

Dalrymple, R. A., J.T. Kirby, and P.A. Hwang. 1984. Wave Diffraction Due to Areas of High Energy Dissipation. J. Waterway, Port, Coastal and Ocean Eng.,110, p. 67-79.

Dean, Robert G. 2002. Beach Nourishment theory and Practice. Advanced Series on Ocean Engineering – Volume 18. World Scientific.

Demirbilek, Z. and V.Panchang. 1998. CGWAVE: A Coastal Surface Water Wave Model of the Mild Slope Equation. U.S. Army Corps of Engineers technical Report CHL-98-xx.

Dickson, S.K., J.T. Kelley, D.F. Belknap, L.K. Fink, D.C. Barber, D.M. FitzGerald, S. van Heteren, and P.A. Manthorp. 1993a. A Sediment Budget for Saco Bay, Maine, and an Evaluation of the Long- and Short-Term Geologic and Oceanographic Processes: In List, J.H., ed., Large-Scale Coastal Behavior '93: U.S. Geol. Survey Open-file Rept. 93-381, p. 48-51.

Ellis M.Y. 1978. Coastal Mapping Handbook. U.S. Department of the Interior, Geological Survey, U.S. Department of Commerce, National Ocean Service, U.S. Government Printing Office, Washington, D.C., 199 pp.

EPA (U.S. Environmental Protection Agency). 2000. Global Warming – climate, Sea Level. http://yosemite.epa.gov/OAR/globalwarming.nsf/content/ClimateTrendsSeaLevel.html

Farrell, S.C. 1972. Present Coastal Processes, Recorded Changes, and the Post-Pleistocene Geologic Record of Saco Bay, Maine: Unpub. Ph.D. Dissertation, Univ. Massachusetts, Amherst, 296 pp.

Feddersen, F., R. T. Guza, S. Elgar, and T. H. C. Herbers. 1998. Alongshore Momentum Balances in the Nearshore. J. Geophys. Res., v. 103, p. 15,667-15,676.

FitzGerald, D.M., P.A. Manthorp, C. Kuo, and S. van Heteren. 1993. Estuarine Circulation and Sediment Transport Trends in the Lower Saco River. Abstr. Programs, Northeast Sect. Meet., Geol. Soc. Am., 25.

FitzGerald, D.M., S. van Heteren and R.M. Montello. 1994. Shoreline Processes and Damage Resulting from the Halloween Eve Storm of 1991 Along the North and South Shores of Massachusetts Bay. U.S.A. Journal of Coastal Research, 10, p. 113-132.

FitzGerald, D.M., I.V. Buynevich, R.A. Davis Jr., and M.S. Fenser. 2002. New England Tidal Inlets with Special Reference to Riverine-Associated Inlet Systems. Geomorphology 48, p. 179-208.

Forristall, G.Z. 1981. Measurements of a Saturated Range in Ocean Wave Spectra. Journal of Geophysical Research, v. 86, p. 8075-8094.

Haas, K. A. and Hanes, D. M. 2004. Process Based Modeling of Total Longshore Sediment Transport. J. Coastal Res. v. 20, p. 853-861.

Hayes, M.O. 1975. Morphology of Sand Accumulations in Estuaries. In: Cronin, L.E. (Eds.), Estuarine Research, Vol. 2. Academic Press, New York, p. 3-22.

Heinze, Heather W. 2001. Anthropogenic Influences and Meteorological Effects: How They are changing the Sand Beaches in Southern Maine. Unpublished MA Thesis, The Graduate School, the University of Maine. 167 pp.

Hsu, J.R.C. and R. Silvester. 1990. Accretion Behind Single Offshore Breakwater. Journal Waterway, Port, Coastal, and Ocean Eng., ASCE, Vol. 116, No. 3, p. 362-380.

Hubertz, J.M., R.M. Brooks, W.A. Brandon, and B.A. Tracy. 1993. Hindcast Wave Information for the U.S. Atlantic Coast. WIS Report 30, U.S. Army Engineer Waterways Experiment Station, Coastal Engineering Research Center, Wave Information Study, Vicksburg, MS.

IPPC. 2003. ttp://www.ipcc.ch/publications_and_data/publications_ipcc_third_ assessment_ report_synthesis_report.htm.

Irish, J.L. and W.J. Lillycrop. 1999. Scanning Laser Mapping of the Coastal Zone: The SHOALS System: ISPRS Journal of Photogrammetry and Remote Sensing, v. 54, p. 123-129.

Jensen, X.E. 1983. Atlantic Coast Hindcasting Shallow Water Significant Wave Information. WIS Report, 8, Vicksburg, MS, 75 pp.

Jet Propulsion Laboratory. 2002. SeaWinds Science Data Product: User's Manual. Ed. Ted Lungu, California Institute of Technology.

Jonsson, I.G. 1990. Wave-Current Interactions. The Sea. Vol. 9, Part A, B. LeMehaute and D.M. Hanes, ed., John Wiley & Sons, Inc., New York.

Kahma, K.K. 1981. A Study of the Growth of the Wave Spectrum with Fetch. Journal of Physical Oceanography, v. 11, p. 1503-1515.

Kelley, J.T. and W.A. Anderson. 2000. The Maine Shore and the Army Corps; A Tale of Two Harbors, Camp Ellis and Wells, Maine. Maine Policy Review, 9,p. 20-35.

Kelley, J.T., A.R. Kelley. D.F. Belknap, and R.C. Shipp. 1986. Variability in the Evolution of Two Adjacent Bedrock-Framed Estuaries in Maine, In Wolfe, D.A. (Editor), Estuarine Variability: Academic Press, Orlando, p. 21-42.

Kelley, J.T., A.R. Kelley and O.H. Pilkey. 1989. Living with the Coast of Maine. Durham, NC: Duke University Press, 174 pp.

Kelley, J.T., S.M. Dickson, D.F. Belknap, and R. Stuckenrath. 1992. Sea-Level Change and Late Quaternary Sediment Accumulation on the Southern Maine Inner Continental Shelf, in Fletcher, C.H., III, and Wehmiller, J.F. (Editors), Quaternary Coastal Systems of the United States: Society of Economic Paleontologists and Mineralogists, Special Publication 48, p. 23-34.

Kelley, J.T., D.M. FitzGerald, P.A. Manthorp, and D.C. Barber. 1994. Seasonal Variation in the Direction of Estuarine Sediment and Water Movement, Saco Bay, ME. Geol. Soc. Am, Abstr. Programs, 1994 Annual Meeting 26, A68.

Kelley, J.T., D.F. Belknap, D.M. FitzGerald, D.C. Barber, S.M. Dickson, S. van Heteren, P.A. Manthorp, and L.K. Fink. 1995. A Sand Budget for Saco Bay, Maine. Maine Geological survey Open-file Report 95-1, Maine Geological Survey, Augusta, ME., 59 pp.

Kitaigorodskii, S.A. 1983. On the Theory of the Equilibrium Range in the Spectrum of Wind-Generated Gravity Waves. Journal of Physical Oceanography, v. 13, p. 816-827.

Kraus, S.D., A.R. Knowlton, and J.H. Prescott. 1988. Surveys for Wintering Right Whales (*Eubalaena glacialis*) Along the Southeastern United States, 1984-1988. Final Report to the Department of the Interior, Minerals Management Service, Branch of Environmental Studies, Washington, DC, 19 pp. + app.

Lynch, D. R. 2004. Numerical Partial Differential Equations for Environmental Scientists and Engineers. Springer.

Maine State Planning Office. 1979. A Study of Beach Processes and Management Alternatives for Saco Bay: Maine State Planning Office Report, Augusta, Maine, 82 pp.

Maine State Planning Office. 1998. Improving Maine's Beaches: Recommendations of the Southern Maine Beach Stakeholder Group, Maine State Planning Office Report, Augusta, Maine.

Manthorp, P.A., D.M. FitzGerald, P.A. McKinlay, S. van Heteren, and J.T. Kelley. 1994. The Effects of Spring Freshets in the Lower Saco River, Maine: Geological Society of America, Abstracts with Programs, v. 26, no 3, p. 58.

Manthorp, P.A. 1995. Estuarine Circulation and Sediment Transport in the Saco River Estuary, ME. Unpublished MA Thesis, Department of Geology, Boston University, Boston, MA. 230 pp.

Mei, C. C. 1983. The Applied Dynamics of Ocean Surface Waves. Wylie.

Merchant, D.C. 1987. Spatial Accuracy Specification for Large-Scale Topographic Maps. Photogrammetry Eng. Remote Sensing, 53: p. 958-961.

Noble, R.M. 1978. Coastal Structures' Effects on Shorelines, Proc 17th Intl. Conf. Coastal Eng. ASCE, Sydney, p. 2069-2085.

Osberg, P.H., A.M. Hussey II, and G.M. Boone. 1985. Bedrock Geologic Map of Maine: Augusta, Maine Geol. Survey, Scale 1:500,000.

Pelnard-Considère, R. 1956. Essai de Théorie de l'Evolution des Formes de Rivage en Plages de Sable et de Galets, 4th Journees de l'Hydraulique Les Energies de la Mer, Question III, Rapport No. 1.

Resio, D.T. 1981. The Estimation of Wind Wave Generation in a Discrete Model. Journal of Physical Oceanography, v. 11, p. 510-525.

Resio, D. 1987. Shallow-Water Waves-Part I: Theory. Journal of Waterway, Port, Coastal and Ocean Engineering, Vol. 113, p. 266-283.

Resio, D. 1988. Shallow-Water Waves-Part II: Data Comparison. Journal of Waterways, Port, Coastal and Ocean Engineering, Vol. 114, p. 50-65.

Resio, D.T. 1989. EXTRM2 Extremes Program User's Guide. Offshore & Coastal Technologies, Inc. (OCTI).

Resio, D.T. 1990. Program WAVAD: Global/Regional Wave Model for Wave Prediction in Deep and/or Shallow Water, Offshore & Coastal Technologies, Inc.

Resio, D.T. and B.A. Tracy. 1983. A Numerical Model for Wind-Wave Prediction in Deepwater, WIS Report 12, U.S. Army Engineer Waterways Experiment Station, Coastal Engineering Research Center, Wave Information Study, Vicksburg, MS.

Roache, P. J. 1998. Fundamentals of Computational Fluid Dynamics. Hermosa Publishers.

Saco Bay Regional Beach Management Plan. 2000. http://smrpc.org/landuse/Coastal/Saco%20Bay%20Plan%20Final.pdf

Seiji, M., T. Uda, and S. Tanaka. 1987. Statistical Study on the Effect and Stability of Detached Breakwaters, Coastal Eng. In Japan, Vol. 30, No. 1, p. 131-141.

Shalowitz, A.L. 1964. Shoreline and Sea Boundaries, Volume 2. U.S. Department of Commerce Publication 10-1, U.S. Government Printing Office, Washington, DC, 420 pp.

Slovinsky, Peter A. and Stephen M. Dickson. 2003. Variation of Beach Morphology Along the Saco Bay Littoral Cell. An Analysis of Recent Trends and Management Alternatives. Open-File Report 03-78, Maine Geological Survey Department of Conservation.

Smith, J.M. and M.B. Gravens. 2002. Incident Boundary Conditions for Wave Transformation. 7th International Workshop on Wave Hindcasting and Forecasting, Banff, Alberta.

Smith, J.M. and M.B. Gravens. 2003. Incident Boundary Conditions for Wave Transformation. 7th International Workshop on Wave Hindcasting and Forecasting, Banff, Alberta.

Smith, J.M, A.R. Sherlock, and D.T. Resio. 2001. STWAVE: Steady-State Spectral Wave Model User's Manual for STWAVE, Version 3.0. U.S. Army Corps of Engineers, Vicksburg, MS.

Stafford, D.B. 1971. An Aerial Photographic Technique for Beach Erosion Surveys in North Carolina, CERC Technical Memo No. 36, 115 pp.

Suh, K. and R.A. Dalrymple. 1987. Offshore Breakwaters in Laboratory and Field. Journal Waterway, Port, Coastal, and Ocean Eng., ASCE, Vol. 113, No. 2, p. 105-121.

Tanner, W.F. 1978. Standards for Measuring Shoreline Changes: A Study of the Precision Obtainable and Needed in making Measurements of Changes (Erosion and Accretion). Proceedings of a Workshop, Florida State University, Tallahassee, FL. 89 pp.

Toba, Y. 1978. Stochastic Form of the Growth of Wind Waves in a Single-Parameter Representation with Physical Implications. Journal of Physical Oceanography, v. 8, p. 494-507.

U.S. Army Corps of Engineers. 2002. Coastal Engineering Manual. Engineer Manual 1110-2-1100, U.S. Army Corps of Engineers, Washington, D.C. (in 6 volumes).

USACE. 1886. Report of the Acting Chief of the Engineers of a Survey of the Saco River. Executive Document 37, 49th Congress, p. 5.

USACE. 1910. Reports of the Examination and Survey of the Saco River, Maine. Document 752, 61st Congress, p.3.

USACE. 1955. Beach Erosion Control Report on Cooperative Study of Saco, Maine. Waltham.

USACE. 1984. Shore Protection Manual Volume II.

USACE. 1988. Tidal Flood Profile #11, Station 240, New England Coastline.

USACE. 1991. Assessment of Coastal Processes in Saco Bay, Maine, with Emphasis on Camp Ellis Beach: U.S. Army Corps of Engineers, Coastal Engineering Research Center, Vicksburg, MS, 39 pp. and Appendices.

USACE. 1995. Camp Ellis Beach, Saco Bay, Maine, Model Study of Beach Erosion. Coastal Model Investigation. Technical Report CERC-95-11.

USACE. 2001. Saco River and Camp Ellis Beach, Saco Maine Beach Erosion Study: Section 111 Shoreline Damage Mitigation Study, Initial Appraisal (DRAFT), U.S. Army Corps of Engineers, New England District, Waltham, MA, 15 pp.

van Heteren, S., D.M. FitzGerald, D.C. Barber, J.T. Kelley, and D.F. Belknap. 1994a. Bedrock Control on the Development of the Saco Bay, Maine, Barrier System: Geological Society of America, Abstracts with Programs, v. 26, no. 3, p.77.

van Heteren, S., D.M. FitzGerald, D.C. Barber. J.T. Kelley, and D.F. Belknap. 1996. Volumetric Analysis of a New England Barrier System Using Ground-Penetrating –Radar and Coring Techniques: Journal of Geology, v. 104, p. 471-483.

Woods Hole Group. 2004. Final Report Analysis of shoreline Change for Western Beach, Saco, Maine, 16 pp.

Xu, Bingyi, Vijay Panchang and Zeki Demirbilek. 1996. Exterior Reflections in Elliptic Harbor Wave Models. Journal of Waterway, Port, Coastal, and Ocean Engineering, May/June, p. 118-126.

FINAL REPORT Appendices
Volume II
Saco River and Camp Ellis Beach
Data Collection and Modeling Report

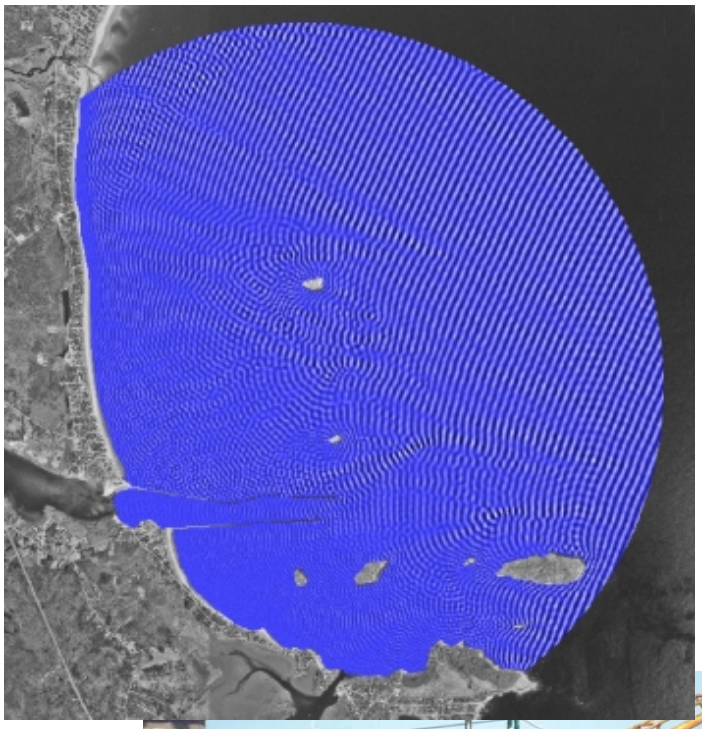

Prepared For:
United States Army Corps of Engineers
New England District
696 Virginia Road
Concord, MA 01742

Prepared By:

Woods Hole Group
Environmental Laboratories

Aubrey Consulting, Inc..
81 Technology Park Drive
East Falmouth, MA 02536

October 2006

Woods Hole Group, Inc.
81 Technology Park Drive
East Falmouth, MA 02536

Tel: (508) 540-8080
Fax: (508) 540-1001
Web: www.woodsholegroup.com

Houston Office
10615 Shadow Wood Drive, Ste 100
Houston, TX 77043-2844
Tel: (713) 468-5075
Fax: (713) 468-1115

Delaware Office
100 Carlson Way, Suite 9
Capital City Business Park
Dover, DE 19901-2365
Tel: (302) 734-1434
Fax: (302) 734-1434

Woods Hole Group Middle East
Ibn Zahar
P.O. Box 94704
Riyadh 11614
Kingdom of Saudi Arabia
Tel: 966 1 483 2080
Fax: 966 1 483 2090

APPENDIX 3-A

Figure 3-A1. Historical shoreline change at Saco Bay, Maine, 1864-1998, Transect Locations. Map 1.

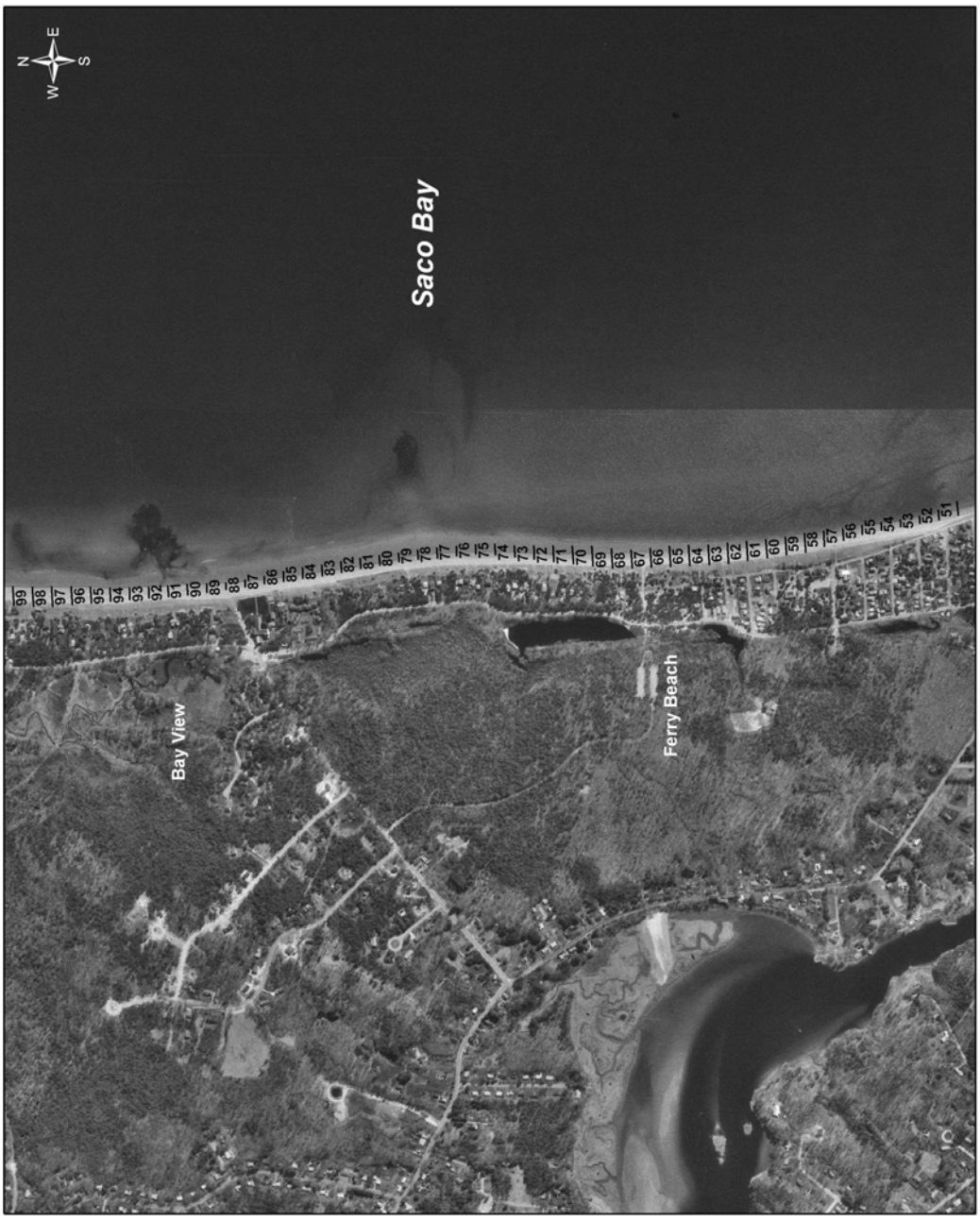

Figure 3-A2. Historical shoreline change at Saco Bay, Maine, 1864-1998, Transect Locations. Map 2.

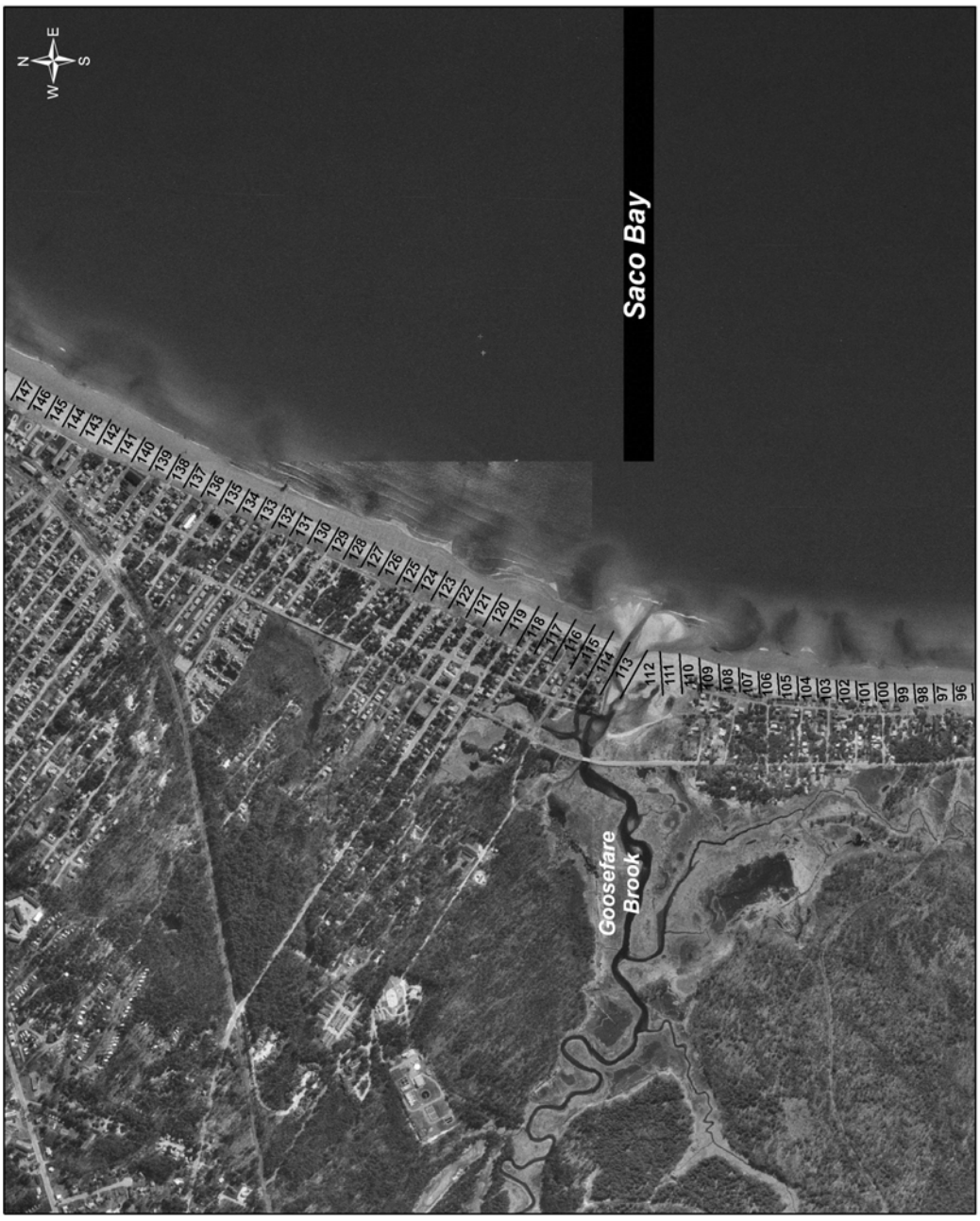

Figure 3-A3. Historical shoreline change at Saco Bay, Maine, 1864-1998, Transect Locations. Map 3.

Figure 3-A4. Historical shoreline change at Saco Bay, Maine, 1864-1998, Transect Locations. Map 4.

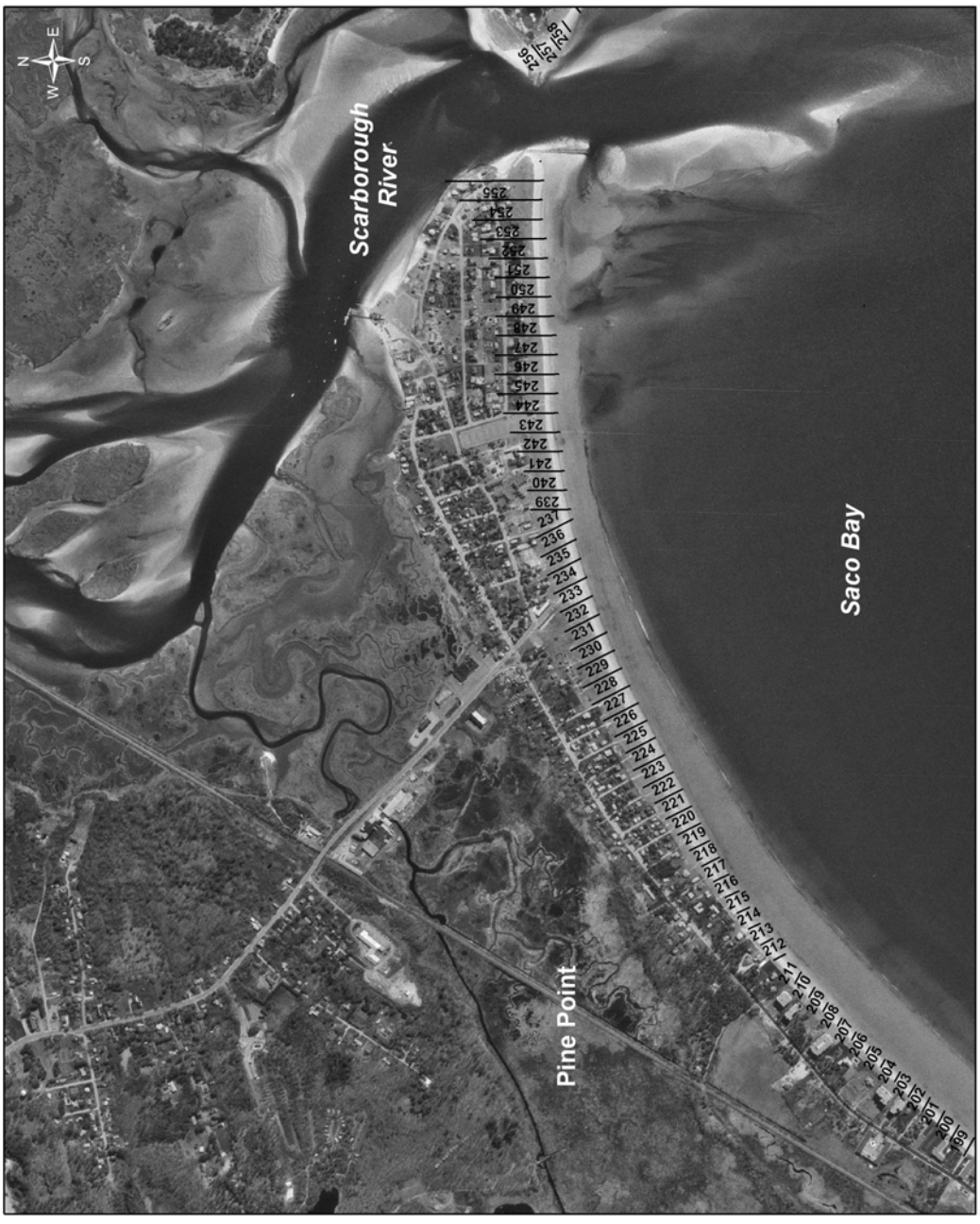

Figure 3-A5. Historical shoreline change at Saco Bay, Maine, 1864-1998, Transect Locations. Map 5.

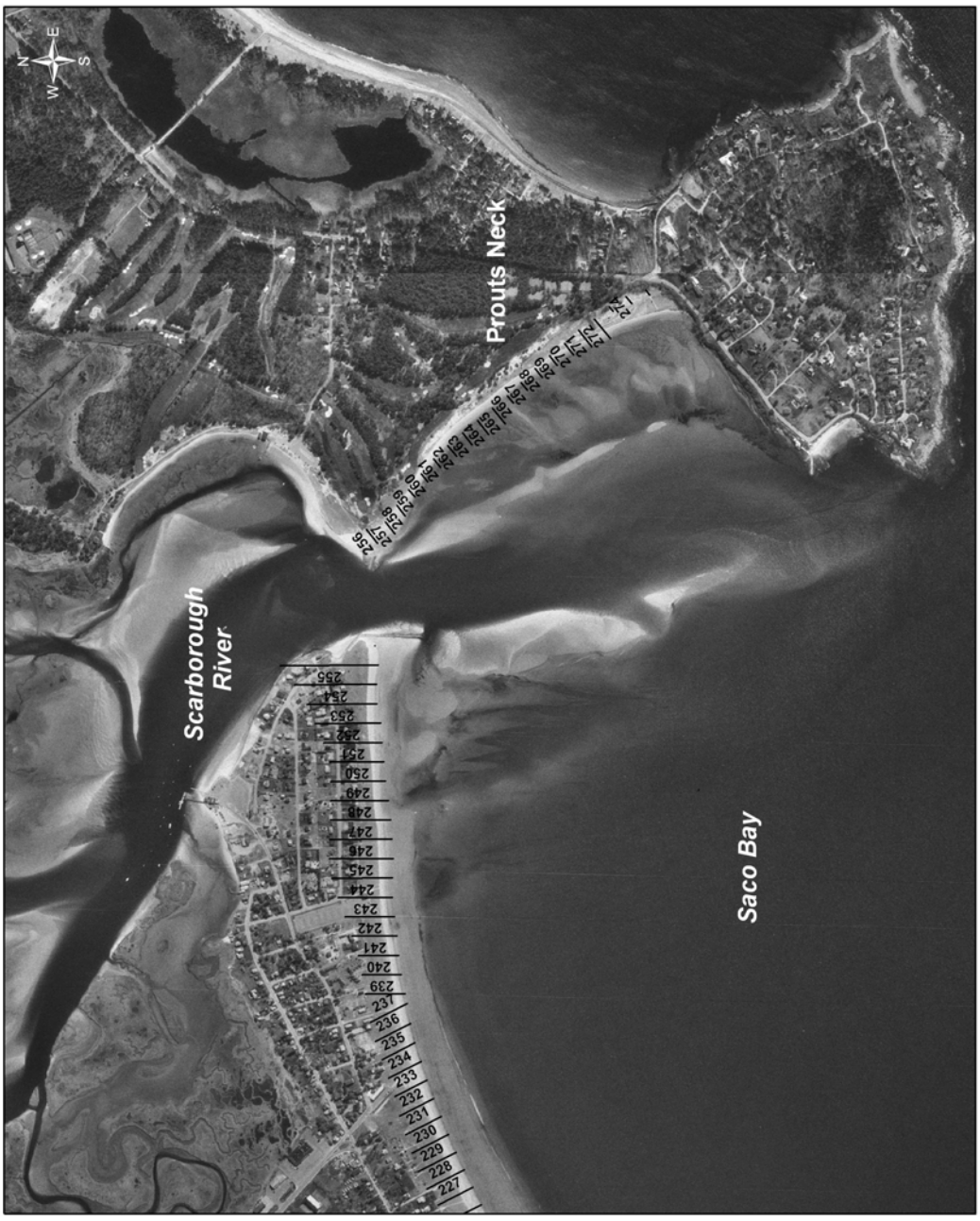

Figure 3-A6. Historical shoreline change at Saco Bay, Maine, 1864-1998, Transect Locations. Map 6.

APPENDIX 6-A

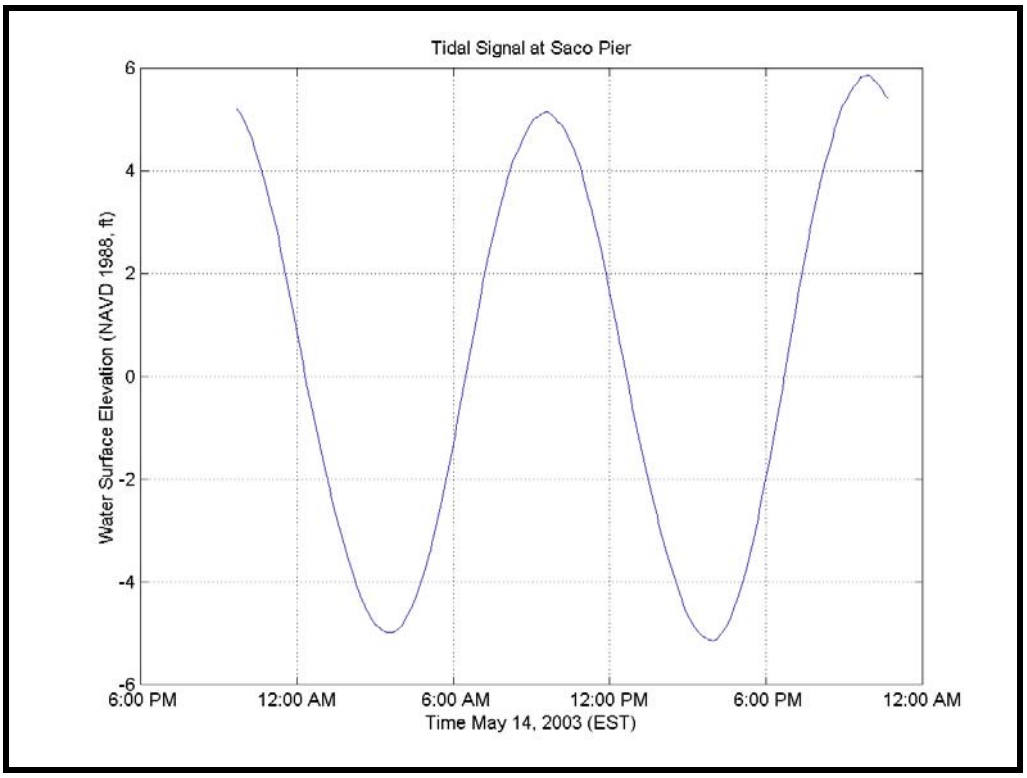

Figure 6-A0. Tidal plot for May 14, 2003.

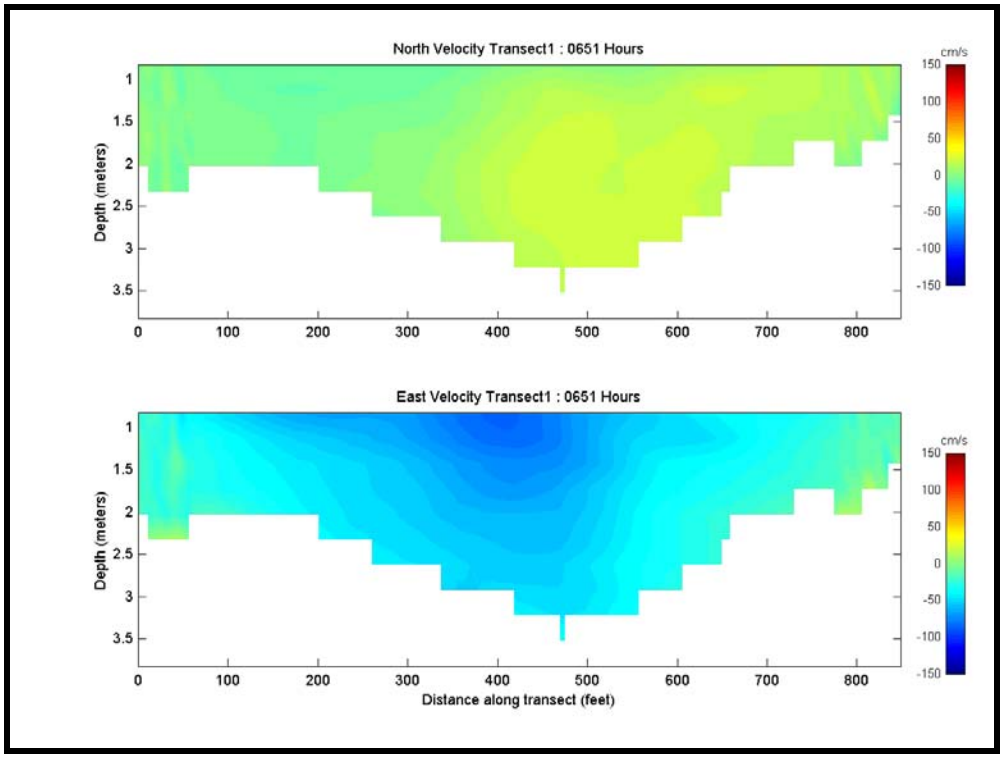

Figure 6-A1. Color contour plots of north-south and east-west velocity for Transect 1 at 6:51 AM on May 14, 2003.

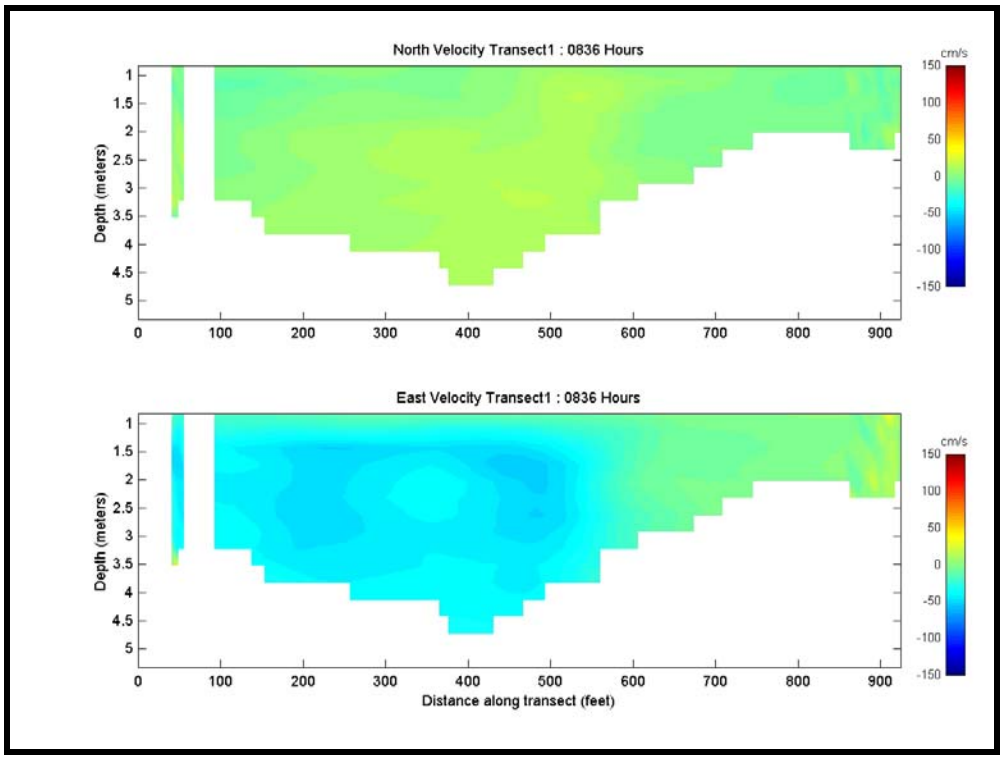

Figure 6-A2. Color contour plots of north-south and east-west velocity for Transect 1 at 8:36 AM on May 14, 2003.

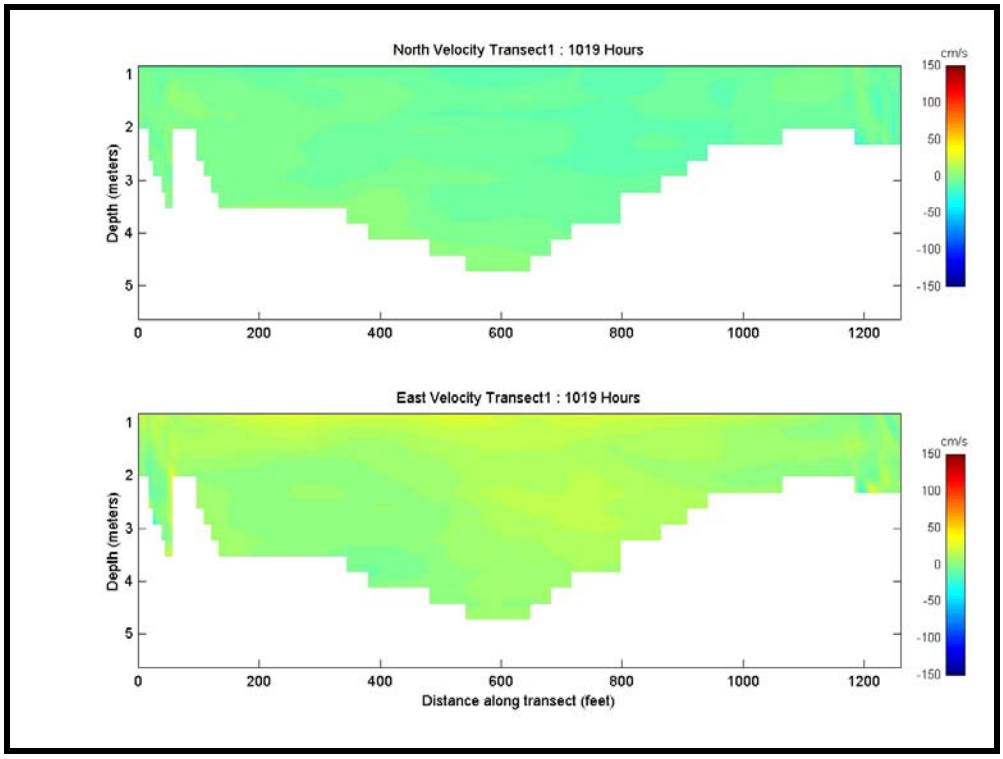

Figure 6-A3. Color contour plots of north-south and east-west velocity for Transect 1 at 10:19 AM on May 14, 2003.

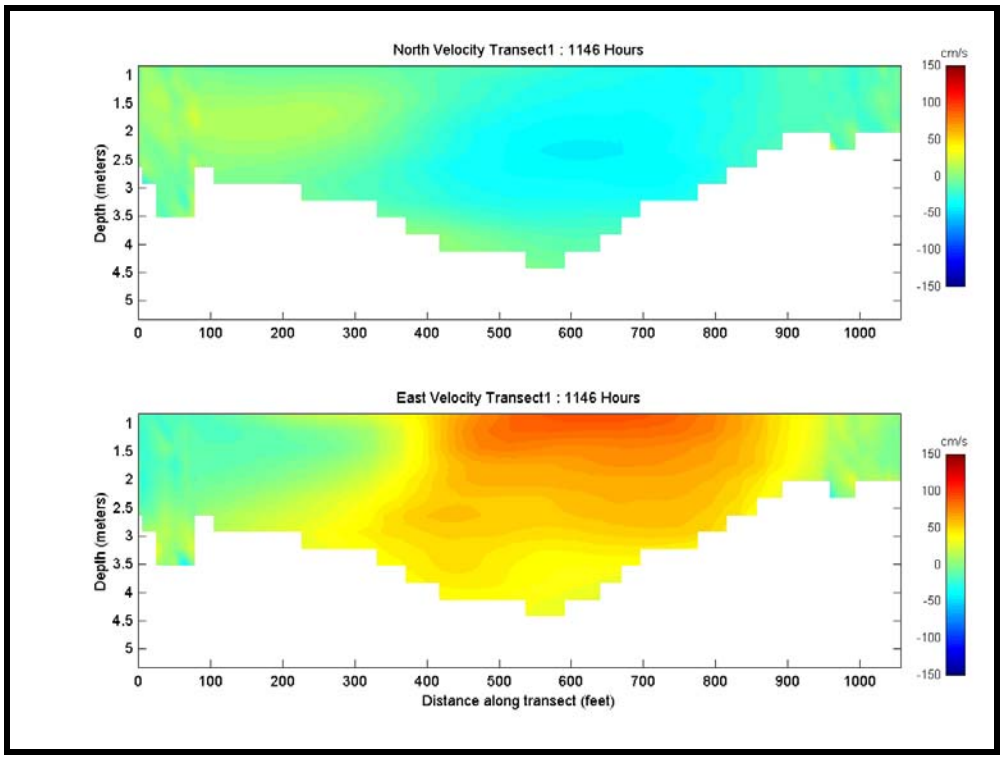

Figure 6-A4. Color contour plots of north-south and east-west velocity for Transect 1 at 11:46 AM on May 14, 2003.

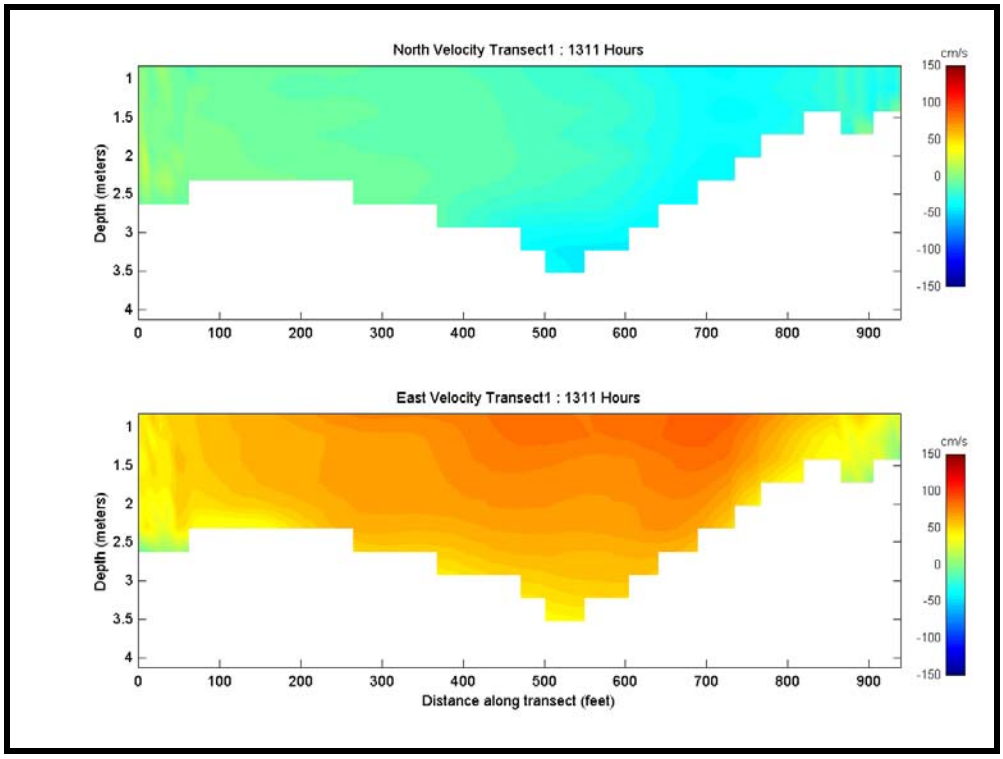

Figure 6-A5. Color contour plots of north-south and east-west velocity for Transect 1 at 1:11 PM on May 14, 2003.

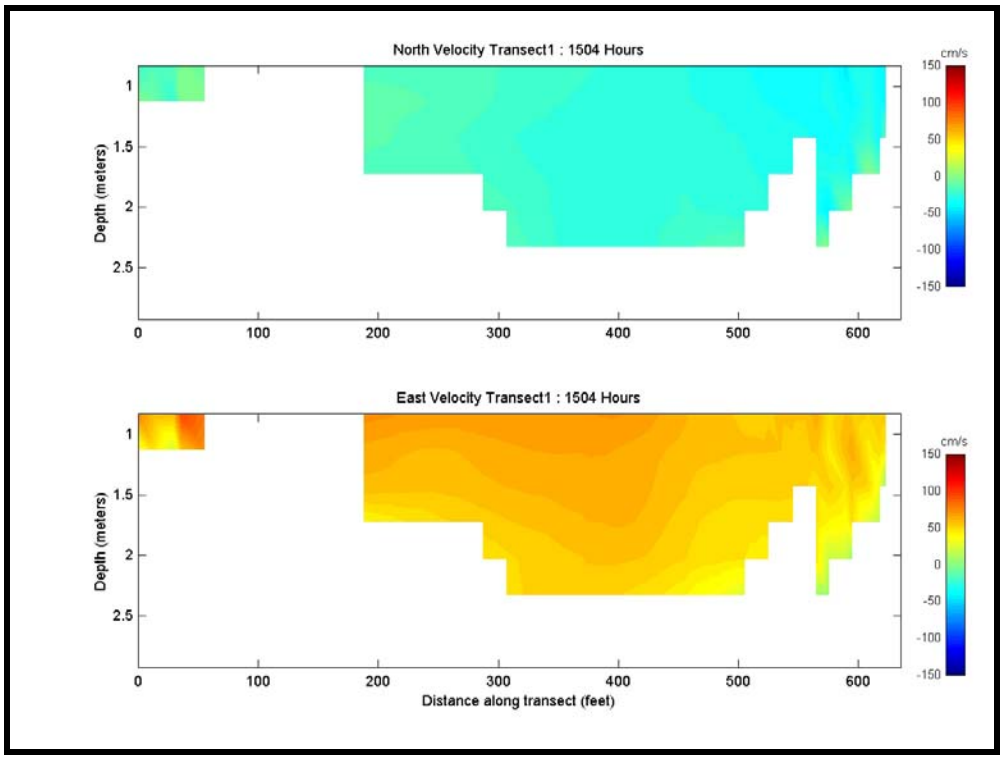

Figure 6-A6. Color contour plots of north-south and east-west velocity for Transect 1 at 3:04 PM on May 14, 2003.

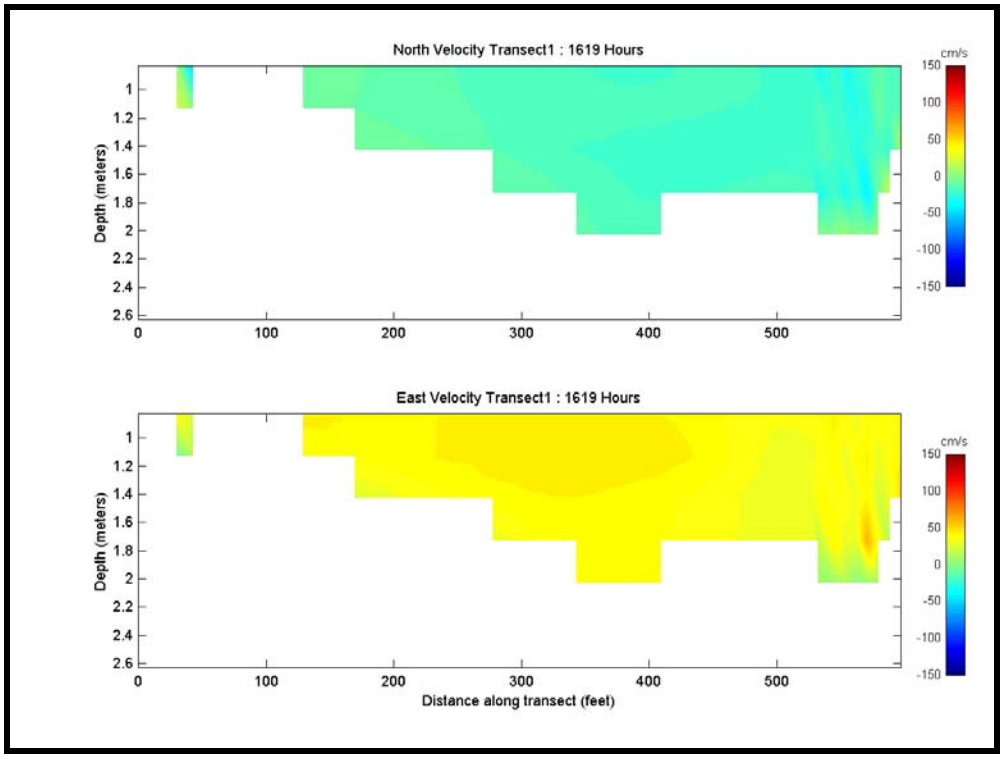

Figure 6-A7. Color contour plots of north-south and east-west velocity for Transect 1 at 4:19 PM on May 14, 2003.

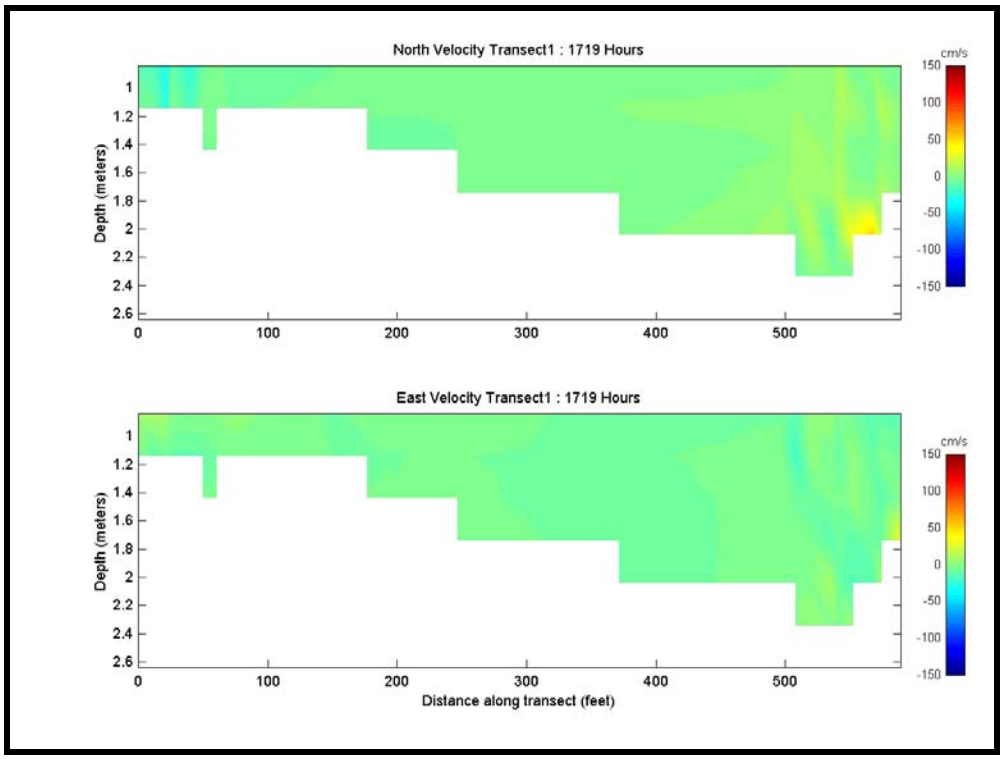

Figure 6-A8. Color contour plots of north-south and east-west velocity for Transect 1 at 5:19 PM on May 14, 2003.

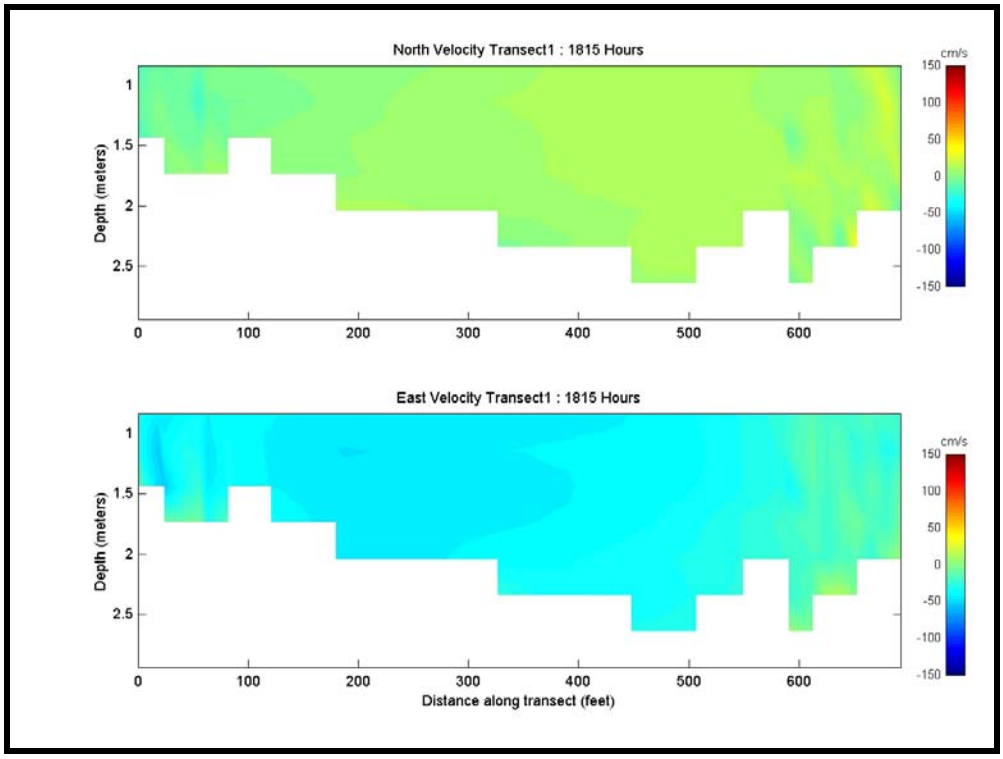

Figure 6-A9. Color contour plots of north-south and east-west velocity for Transect 1 at 6:15 PM on May 14, 2003.

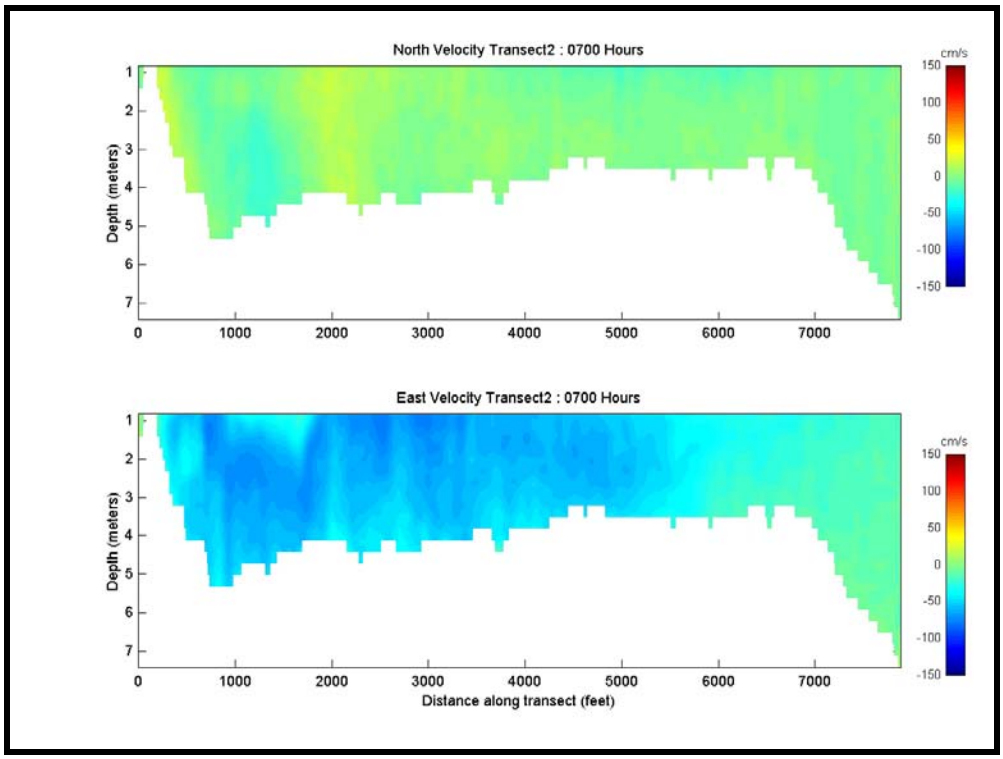

Figure 6-A10. Color contour plots of north-south and east-west velocity for Transect 2 at 7:00 AM on May 14, 2003.

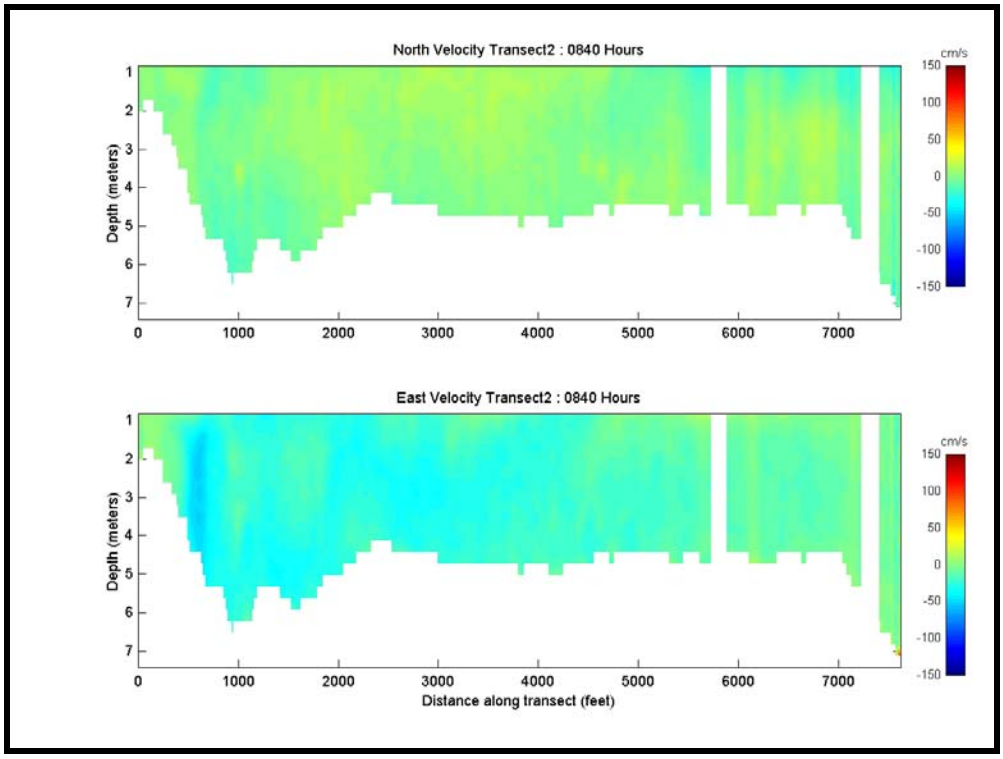

Figure 6-A11. Color contour plots of north-south and east-west velocity for Transect 2 at 8:40 AM on May 14, 2003.

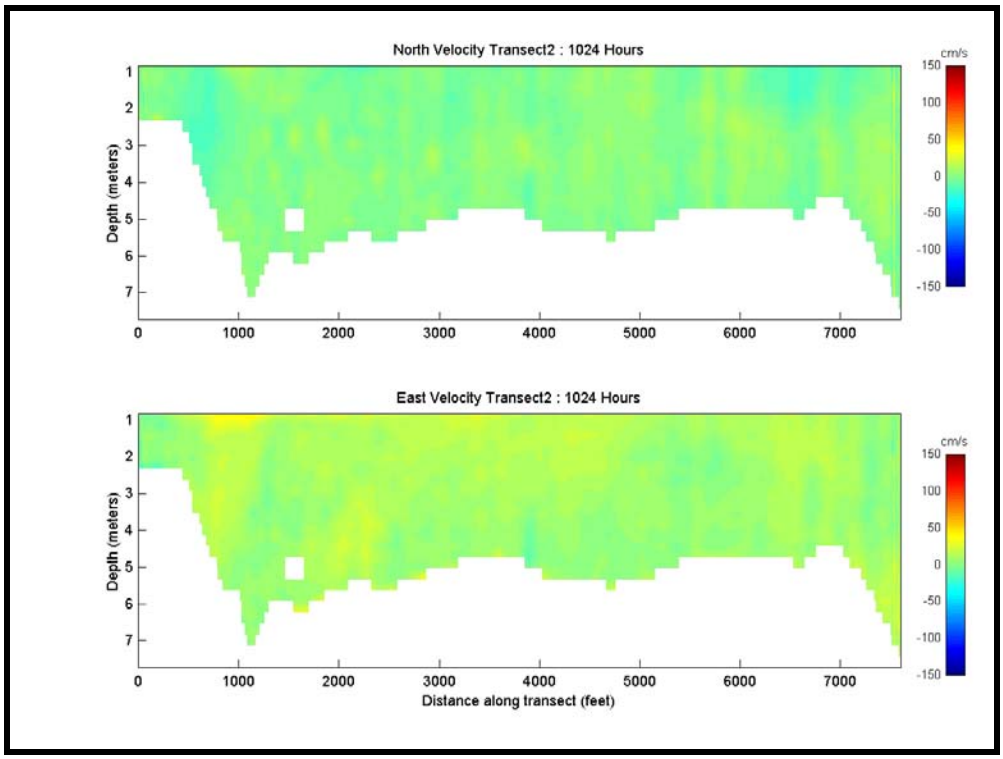

Figure 6-A12. Color contour plots of north-south and east-west velocity for Transect 2 at 10:24 AM on May 14, 2003.

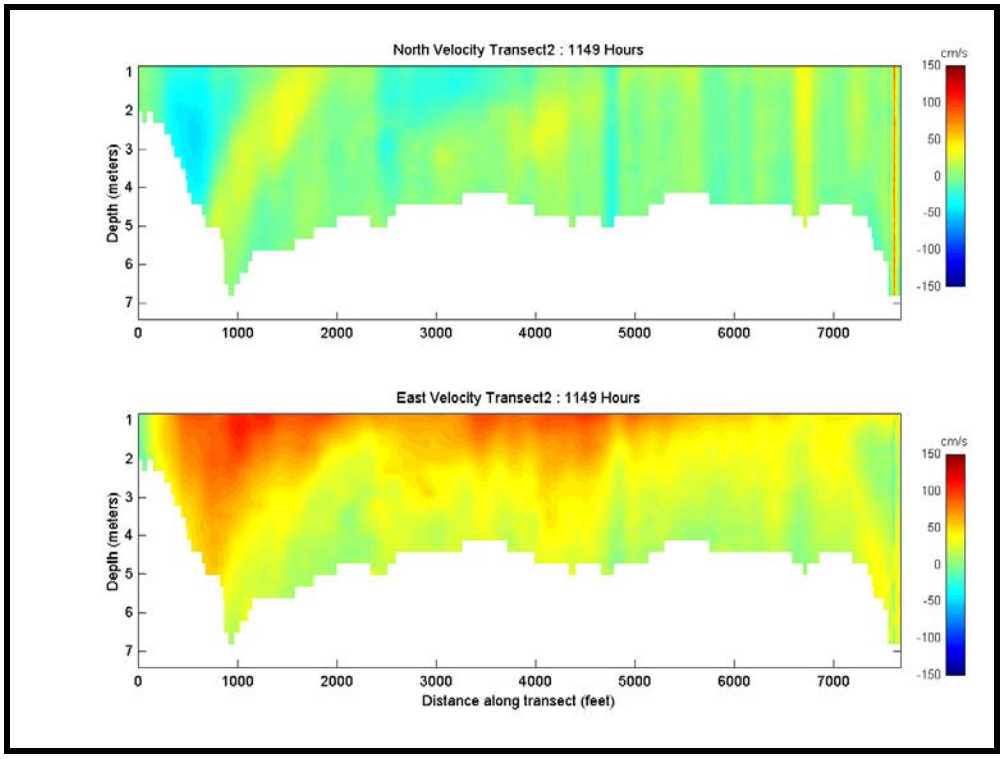

Figure 6-A13. Color contour plots of north-south and east-west velocity for Transect 2 at 11:49 AM on May 14, 2003.

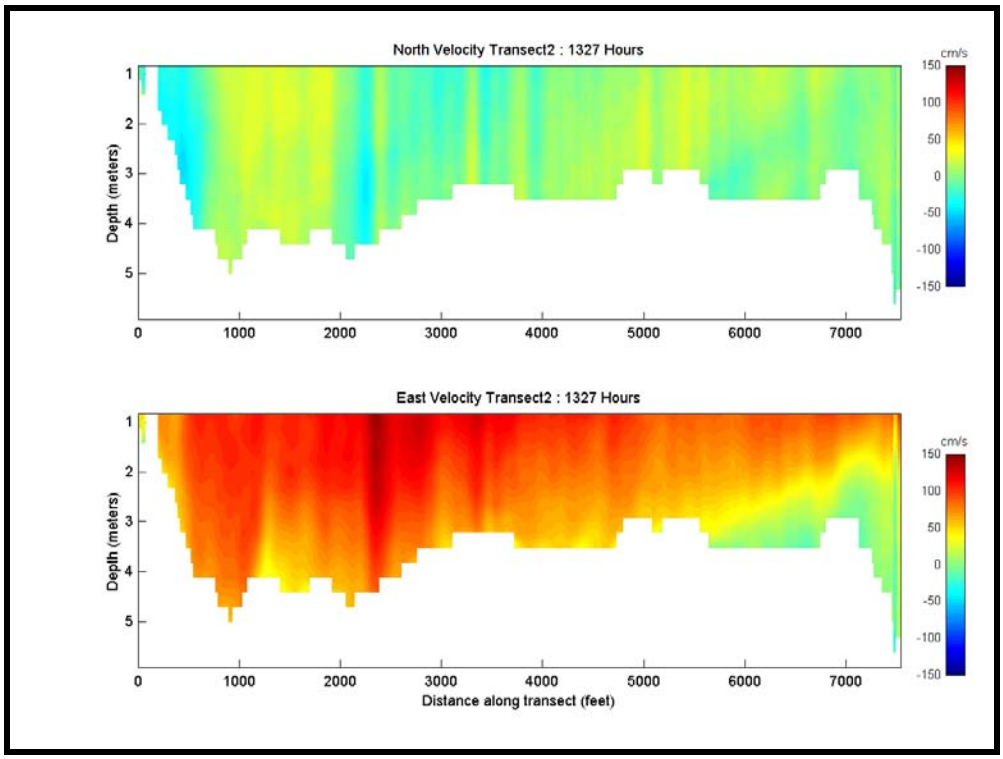

Figure 6-A14. Color contour plots of north-south and east-west velocity for Transect 2 at 1:27 PM on May 14, 2003.

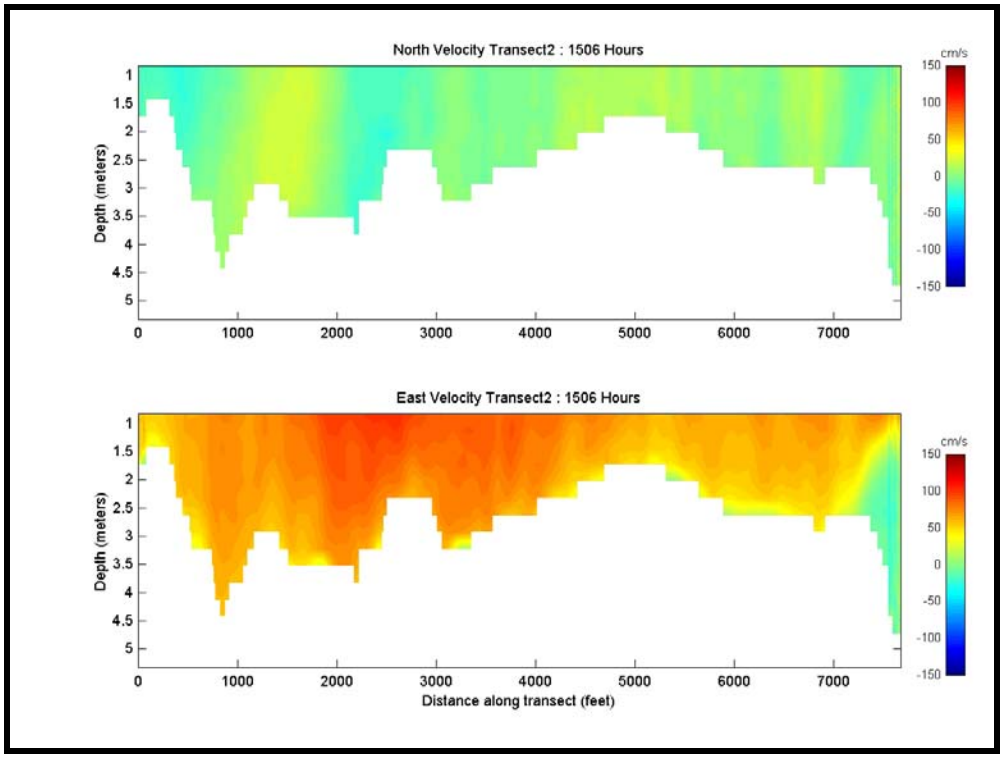

Figure 6-A15. Color contour plots of north-south and east-west velocity for Transect 2 at 3:06 PM on May 14, 2003.

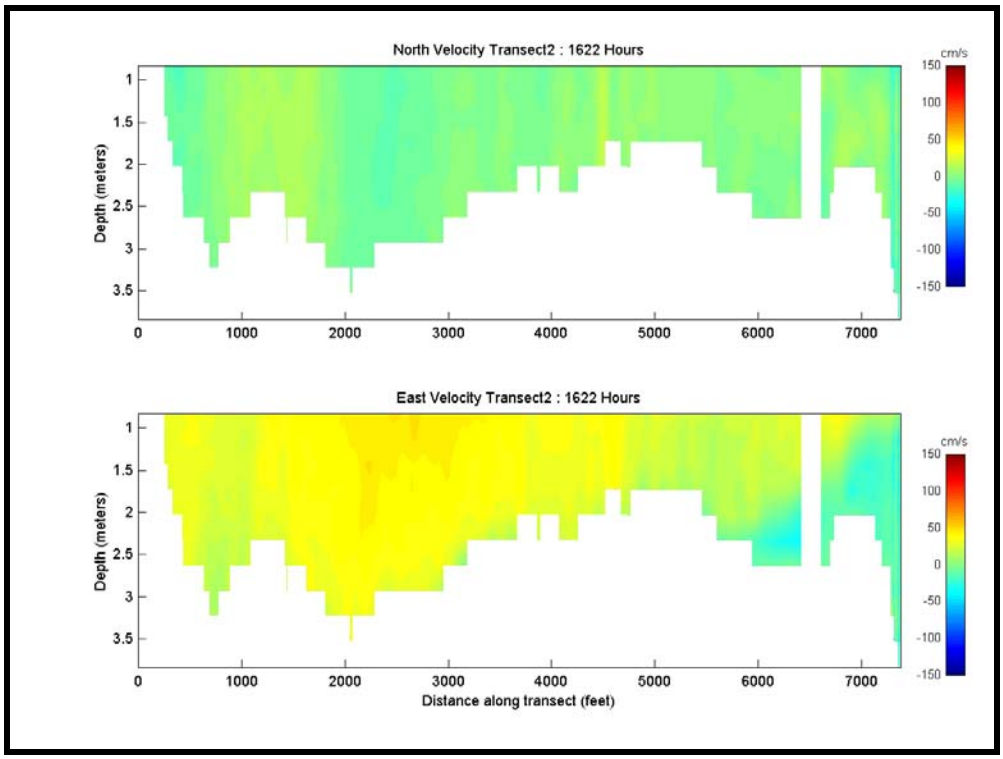

Figure 6-A16. Color contour plots of north-south and east-west velocity for Transect 2 at 4:22 PM on May 14, 2003.

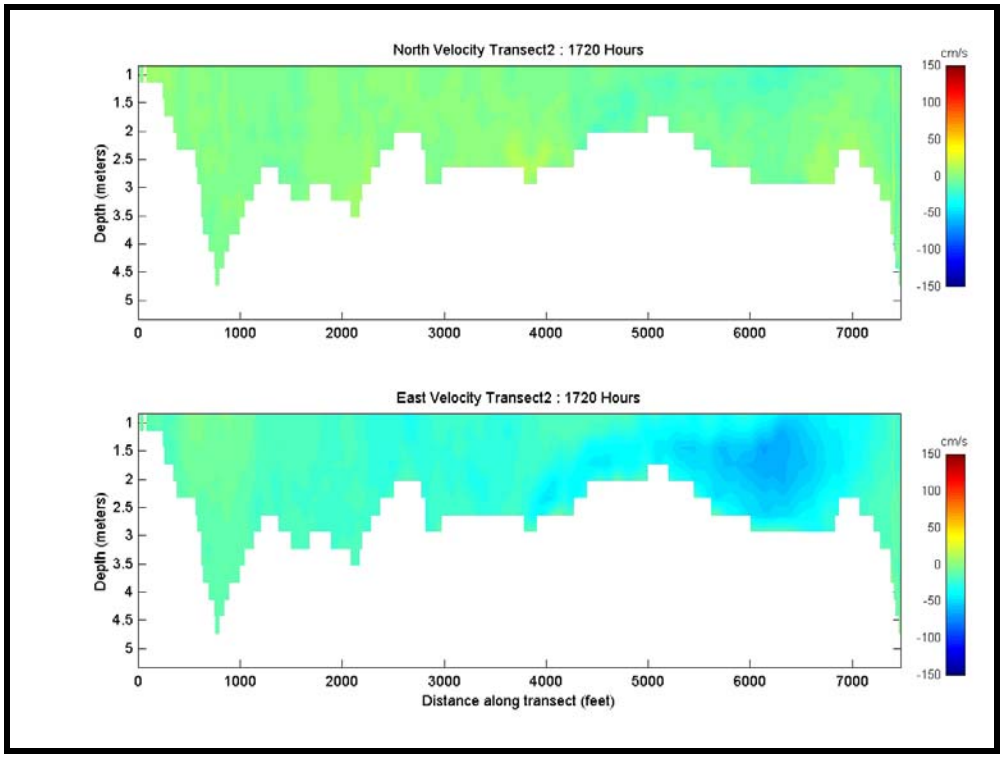

Figure 6-A17. Color contour plots of north-south and east-west velocity for Transect 2 at 5:20 PM on May 14, 2003.

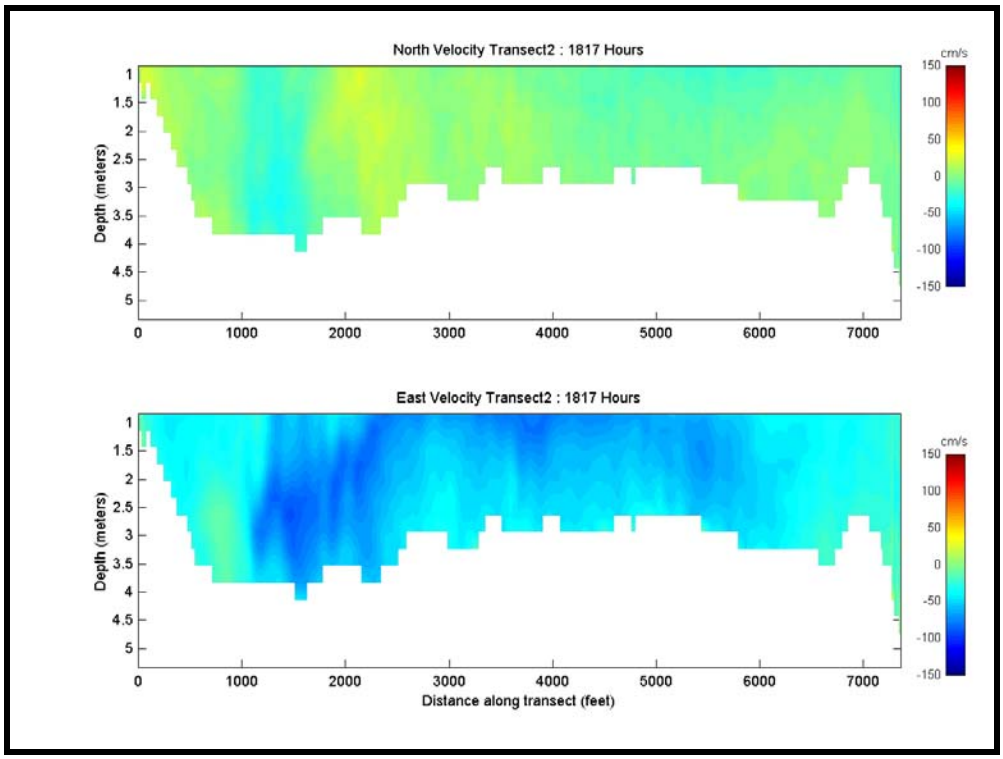

Figure 6-A18. Color contour plots of north-south and east-west velocity for Transect 2 at 6:17 PM on May 14, 2003.

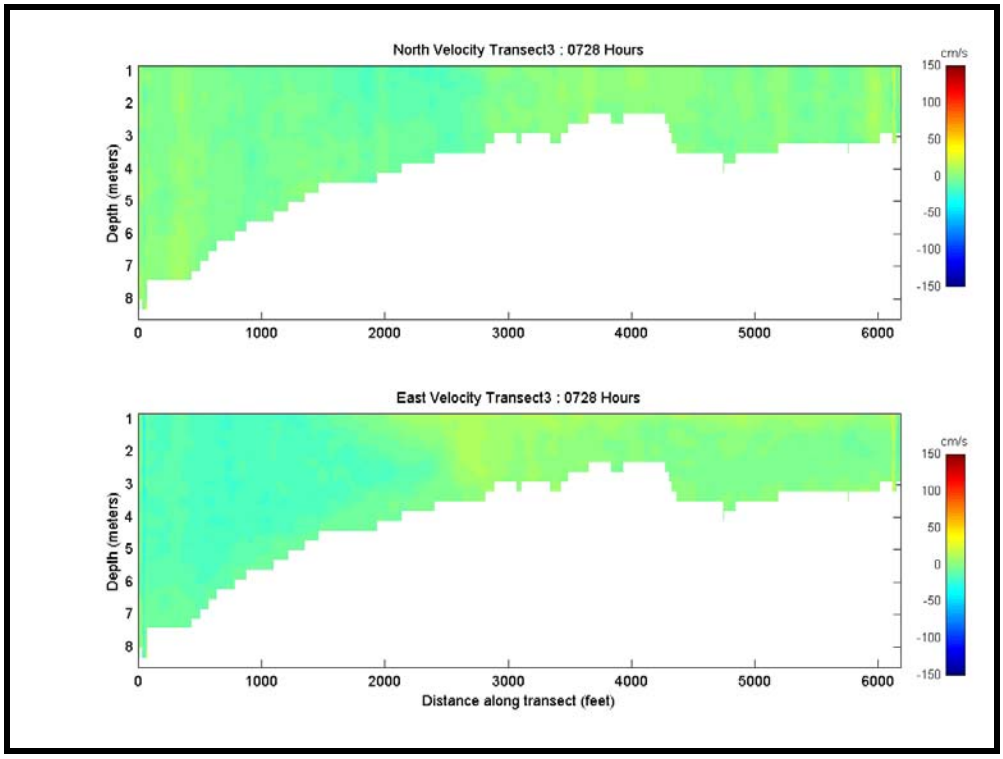

Figure 6-A19. Color contour plots of north-south and east-west velocity for Transect 3 at 7:28 AM on May 14, 2003.

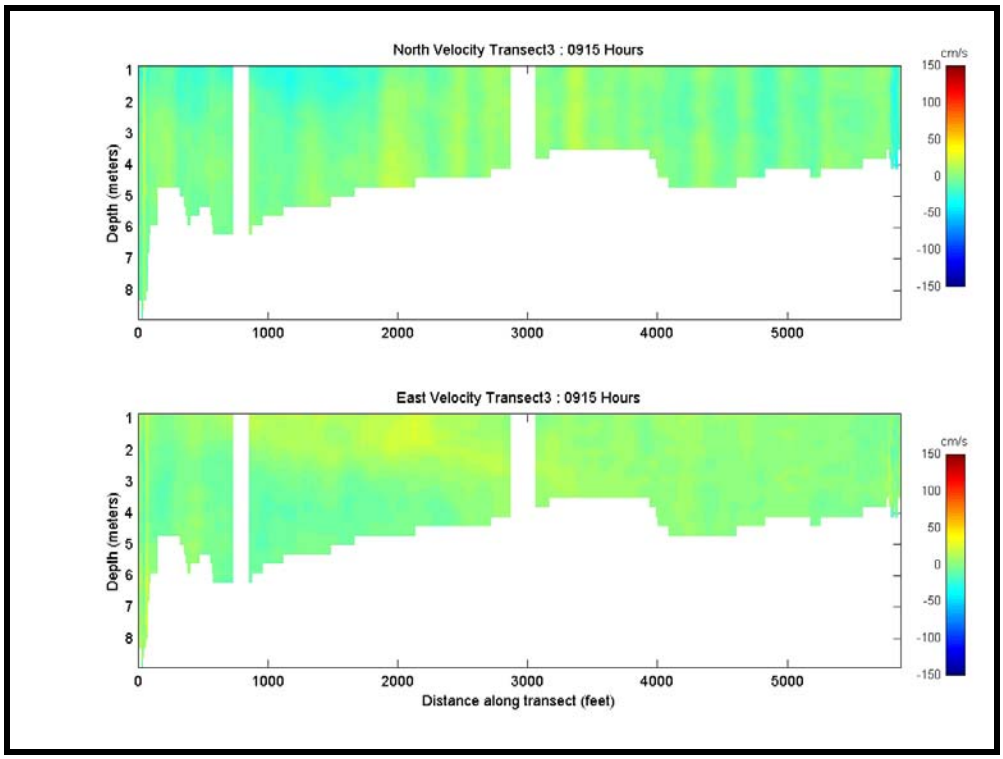

Figure 6-A20. Color contour plots of north-south and east-west velocity for Transect 3 at 9:15 AM on May 14, 2003.

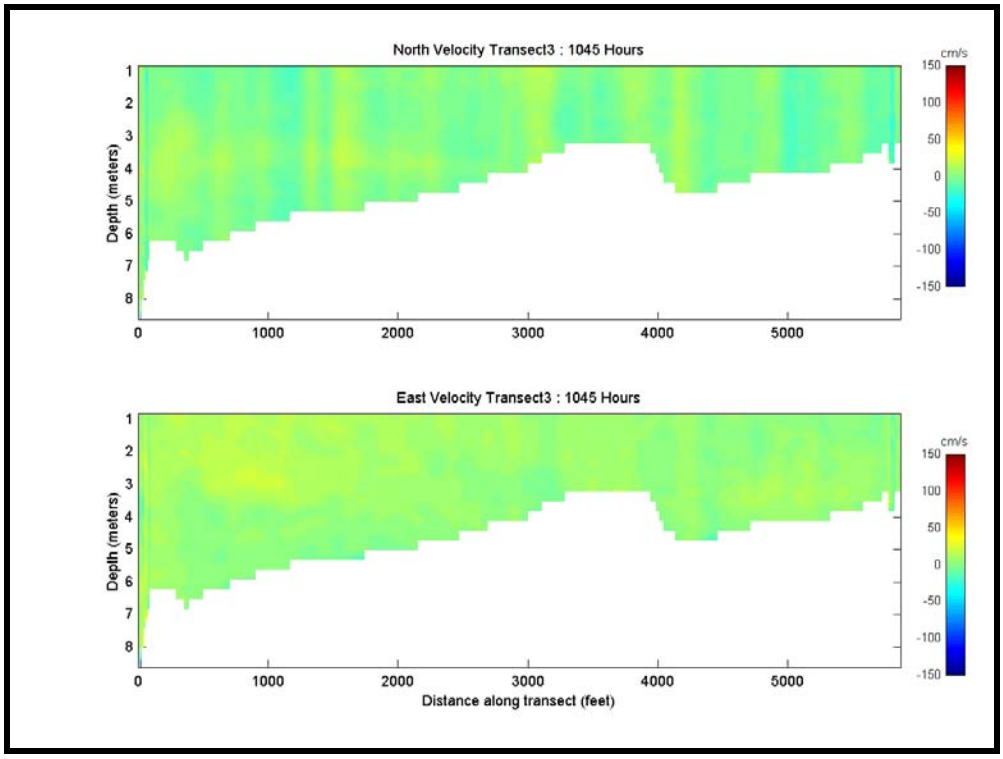

Figure 6-A21. Color contour plots of north-south and east-west velocity for Transect 3 at 10:45 AM on May 14, 2003.

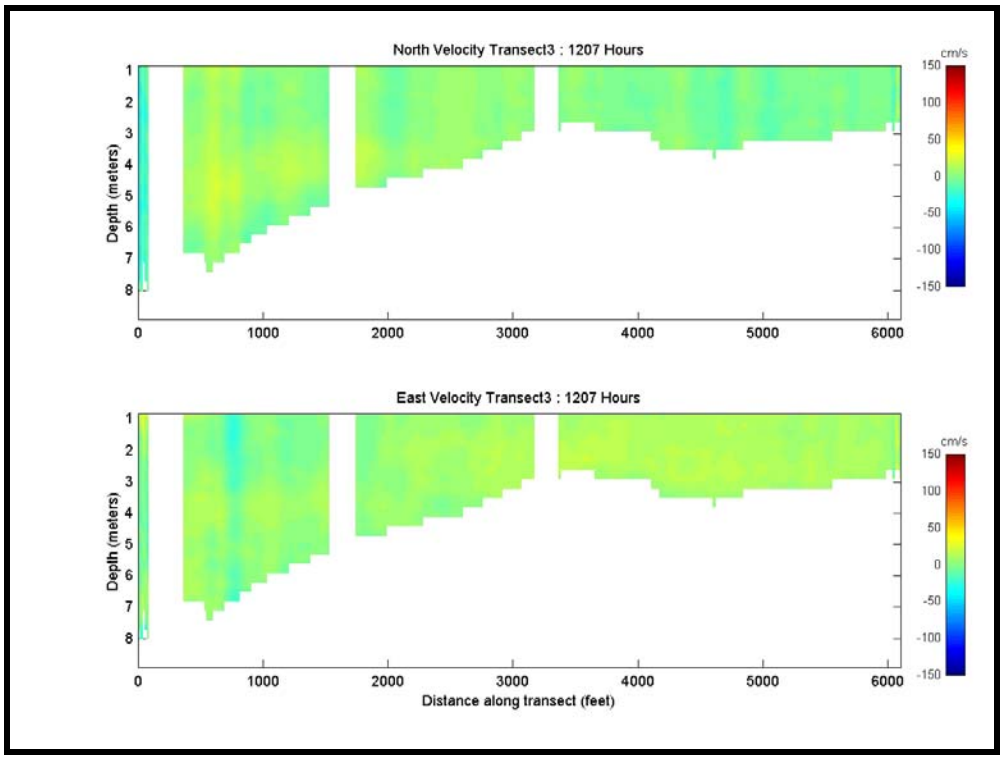

Figure 6-A22. Color contour plots of north-south and east-west velocity for Transect 3 at 12:07 PM on May 14, 2003.

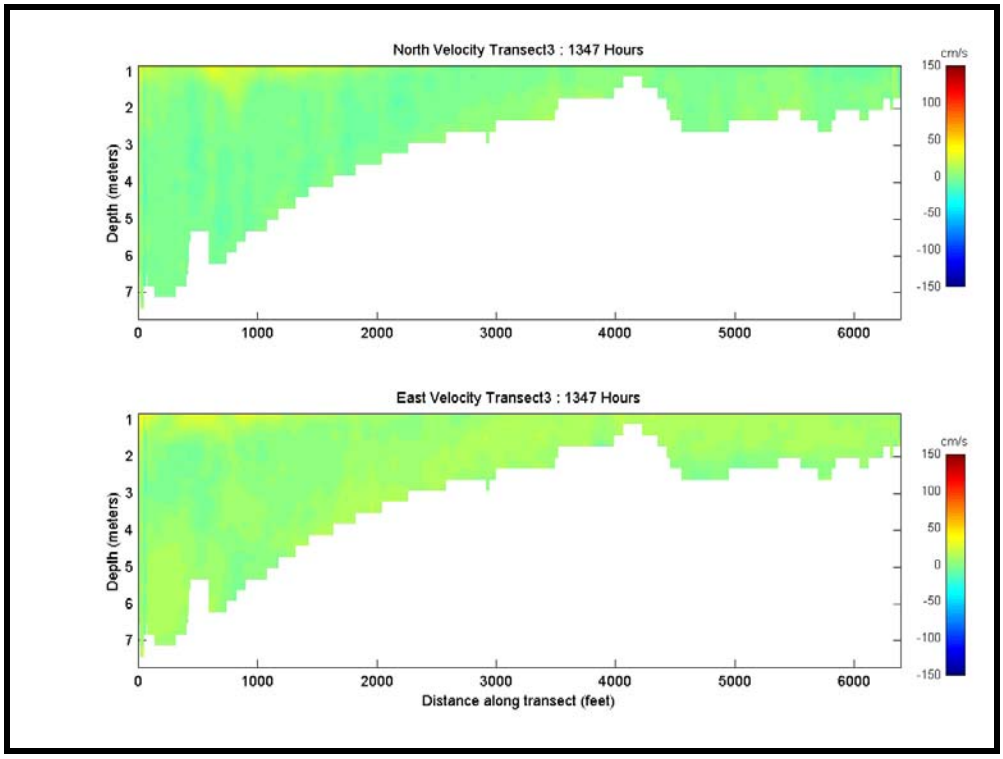

Figure 6-A23. Color contour plots of north-south and east-west velocity for Transect 3 at 1:47 PM on May 14, 2003.

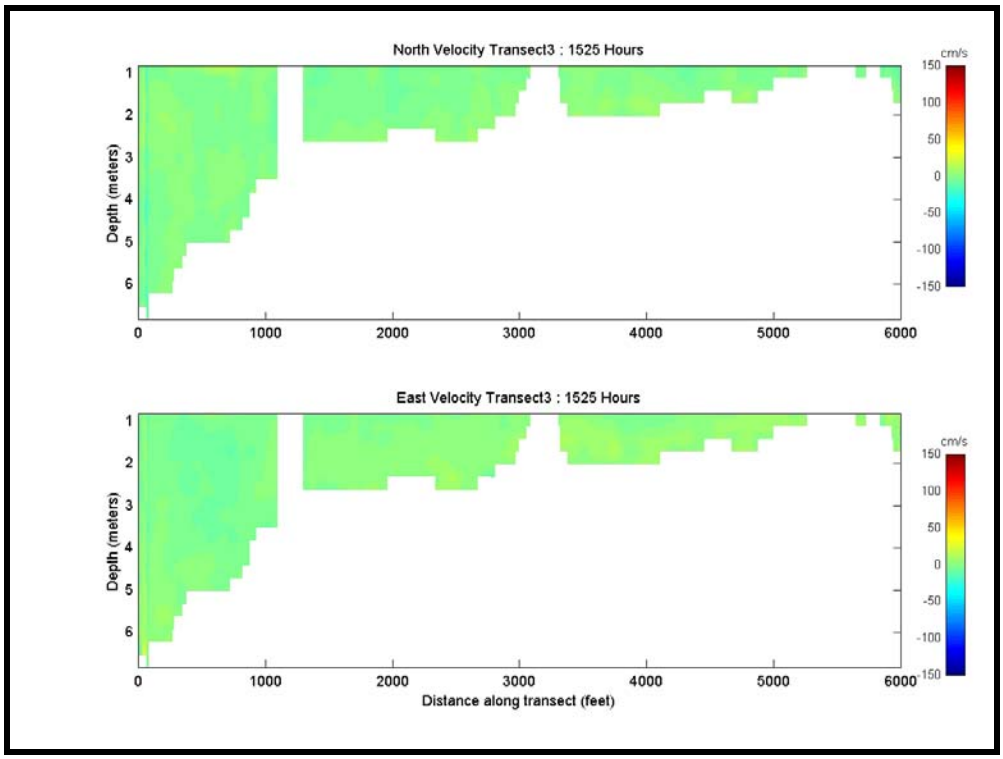

Figure 6-A24. Color contour plots of north-south and east-west velocity for Transect 3 at 3:25 PM on May 14, 2003.

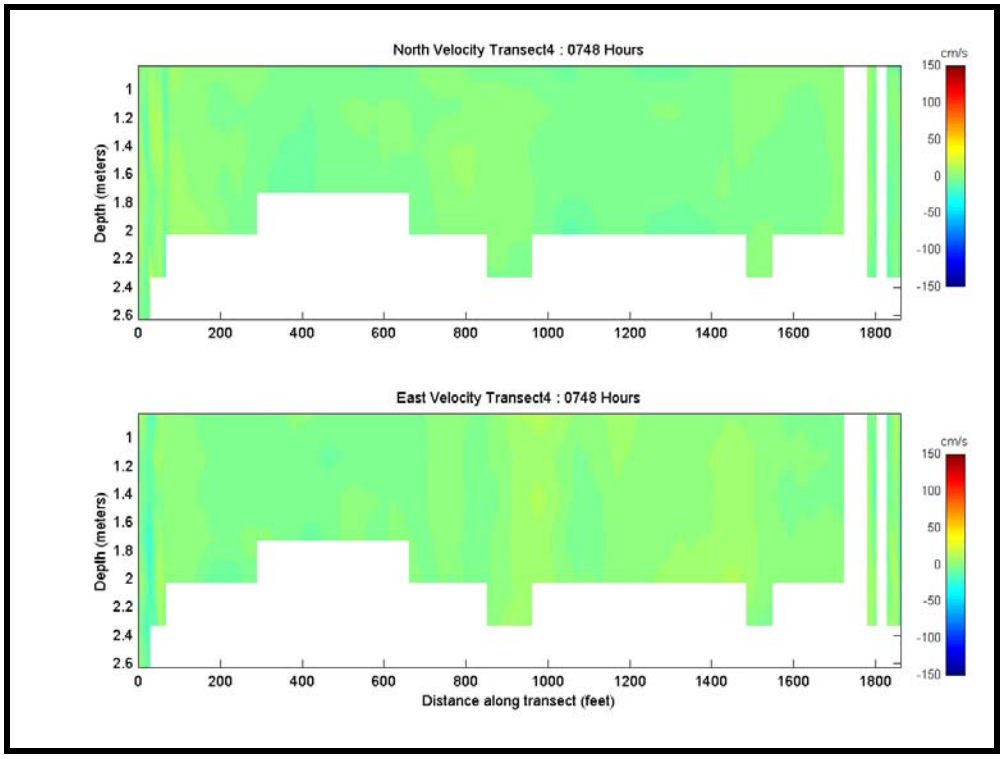

Figure 6-A25. Color contour plots of north-south and east-west velocity for Transect 4 at 7:48 AM on May 14, 2003.

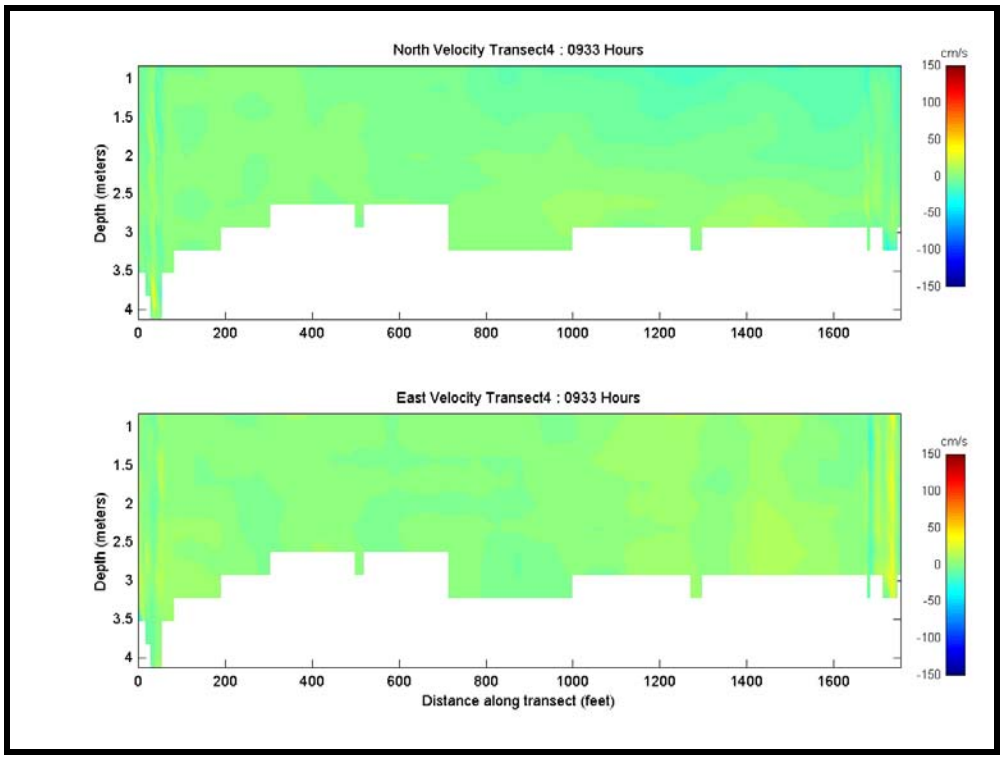

Figure 6-A26. Color contour plots of north-south and east-west velocity for Transect 4 at 9:33 AM on May 14, 2003.

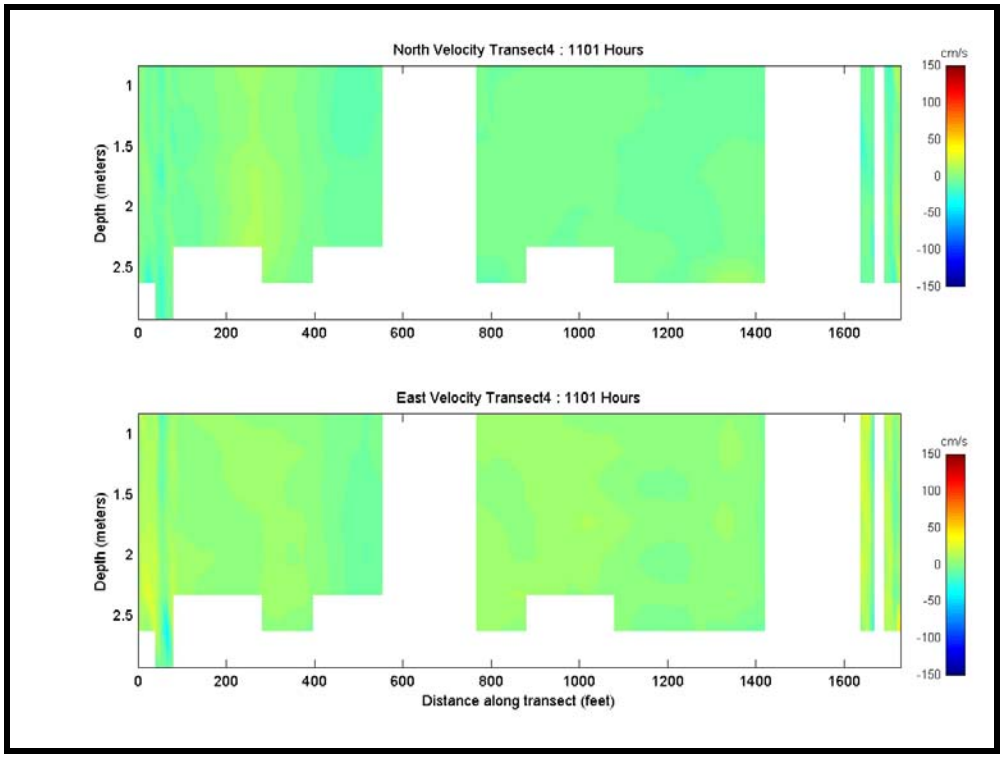

Figure 6-A27. Color contour plots of north-south and east-west velocity for Transect 4 at 11:01 AM on May 14, 2003.

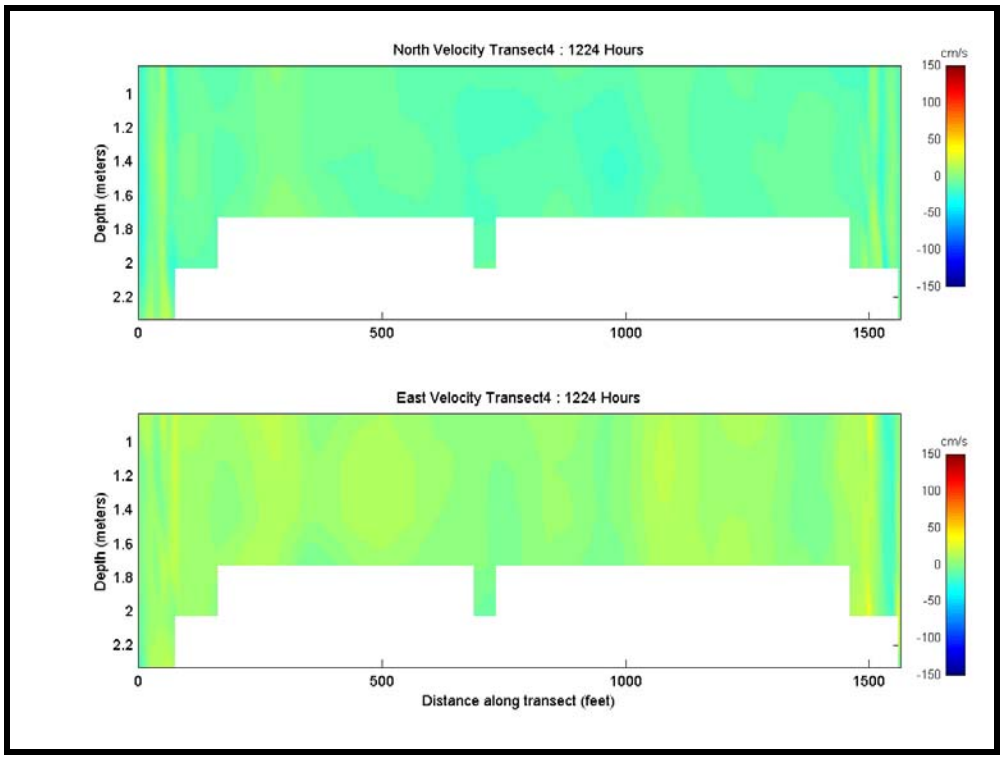

Figure 6-A28. Color contour plots of north-south and east-west velocity for Transect 4 at 12:24 PM on May 14, 2003.

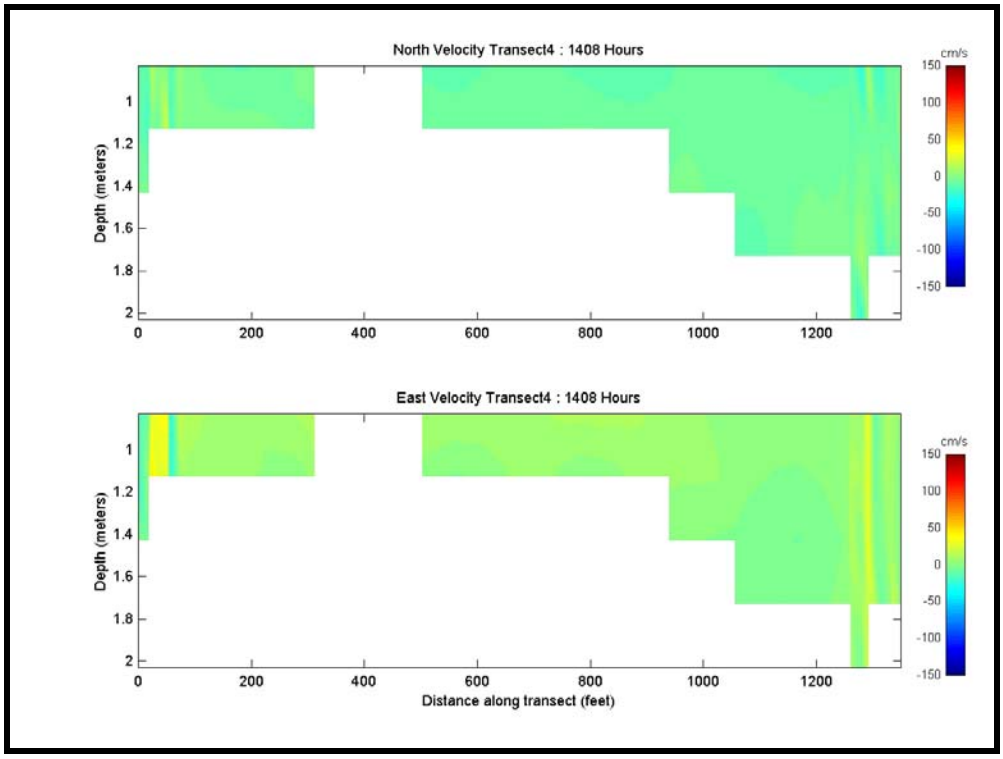

Figure 6-A29. Color contour plots of north-south and east-west velocity for Transect 4 at 2:08 PM on May 14, 2003.

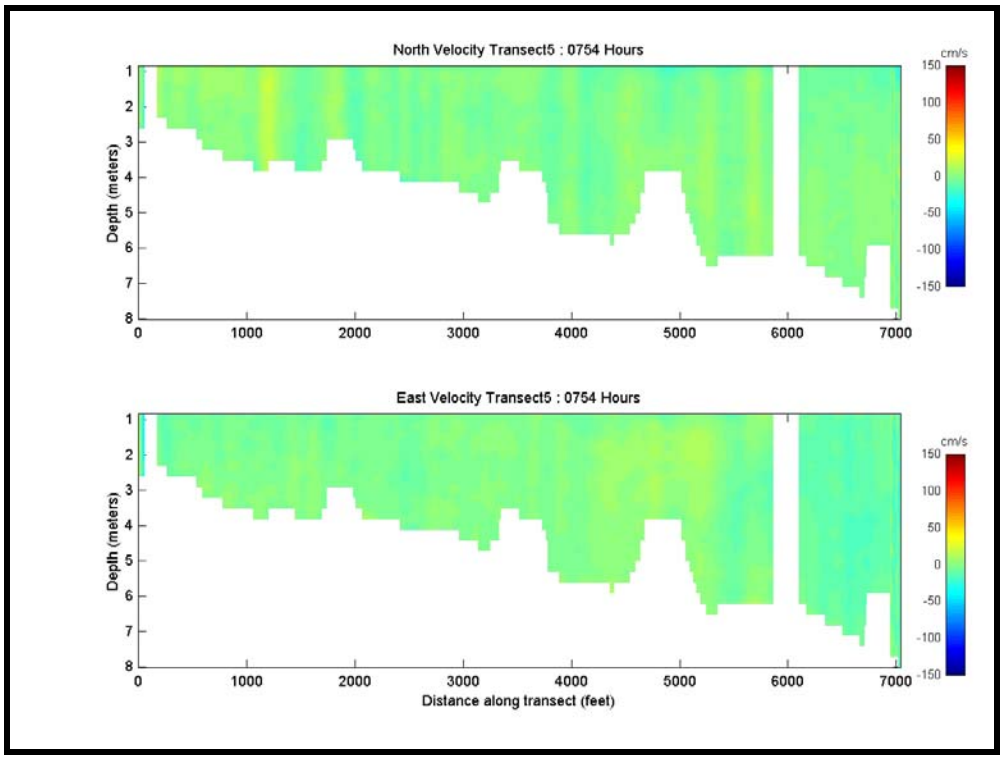

Figure 6-A30. Color contour plots of north-south and east-west velocity for Transect 5 at 7:54 AM on May 14, 2003.

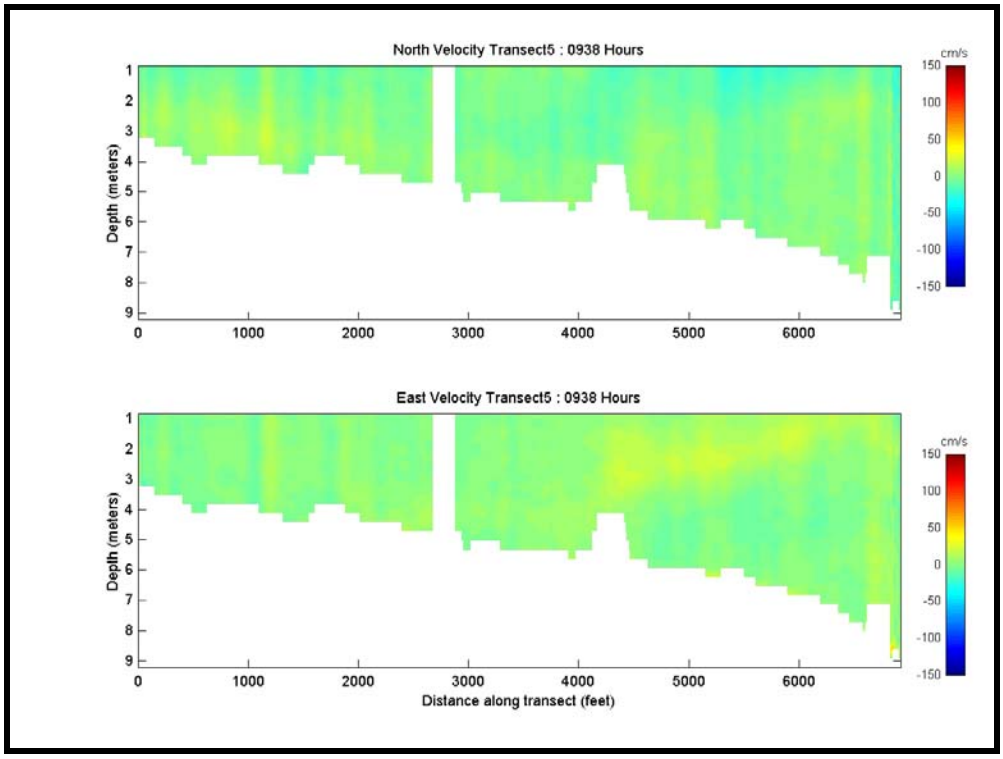

Figure 6-A31. Color contour plots of north-south and east-west velocity for Transect 5 at 9:38 AM on May 14, 2003.

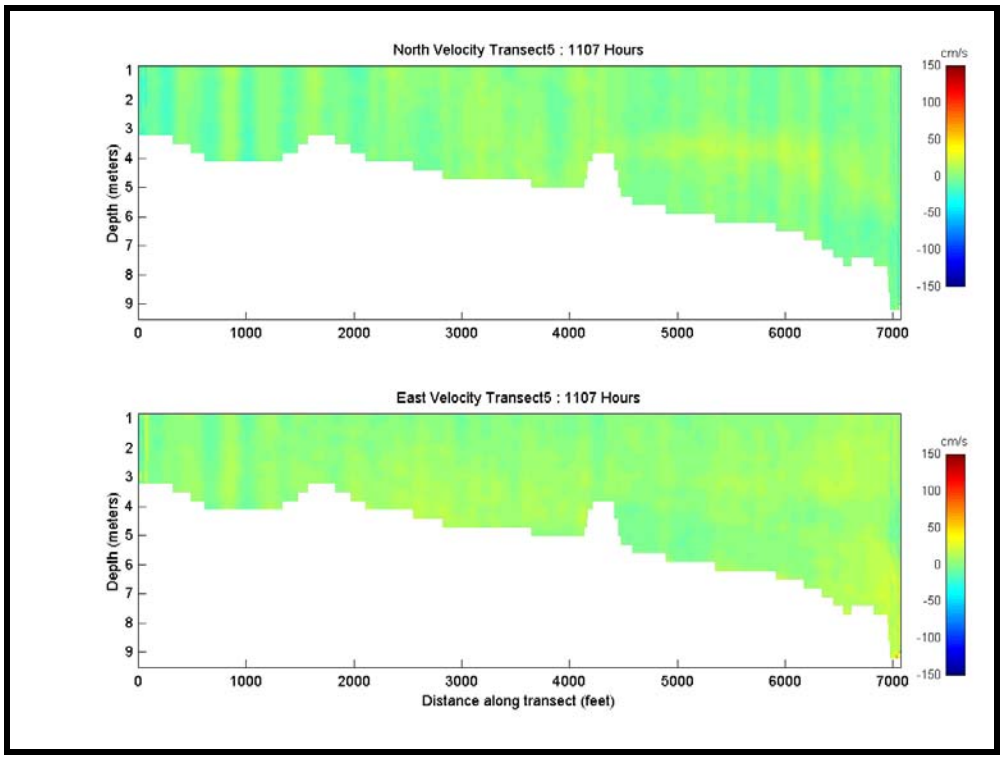

Figure 6-A32. Color contour plots of north-south and east-west velocity for Transect 5 at 11:07 AM on May 14, 2003.

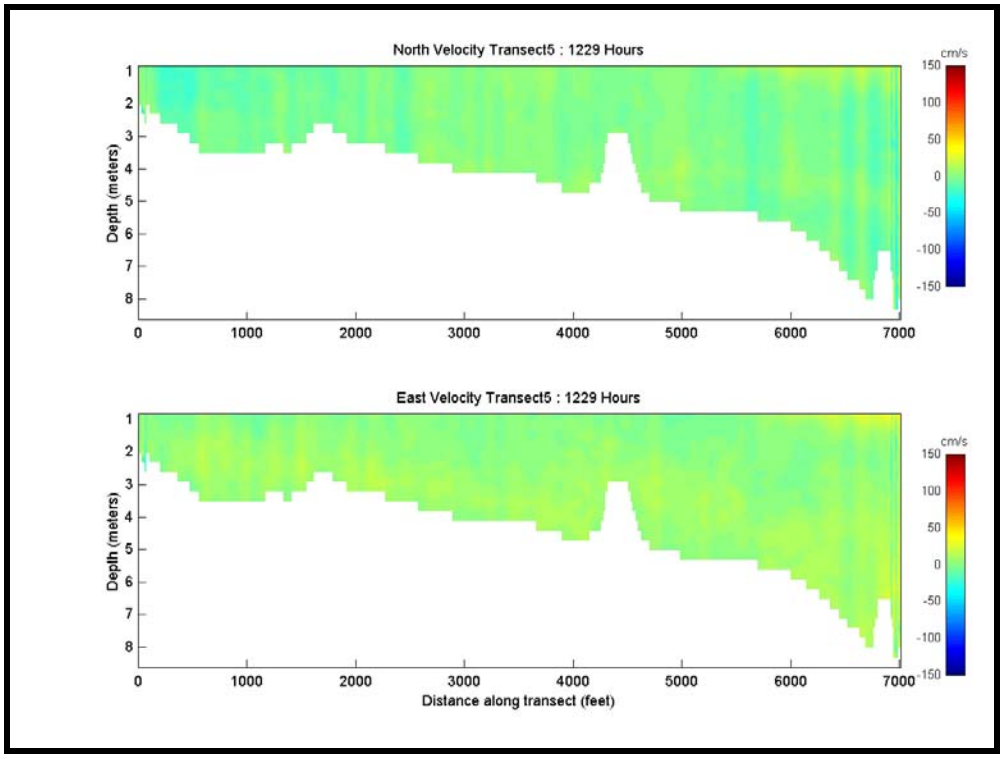

Figure 6-A33. Color contour plots of north-south and east-west velocity for Transect 5 at 12:29 PM on May 14, 2003.

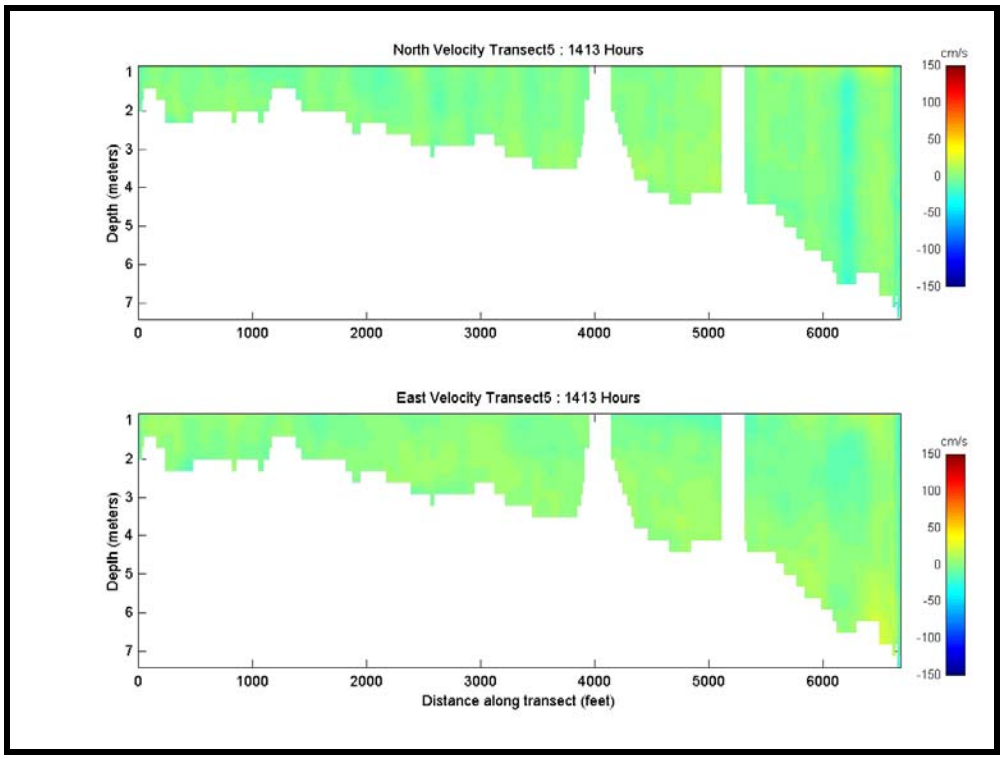

Figure 6-A34. Color contour plots of north-south and east-west velocity for Transect 5 at 2:13 PM on May 14, 2003.

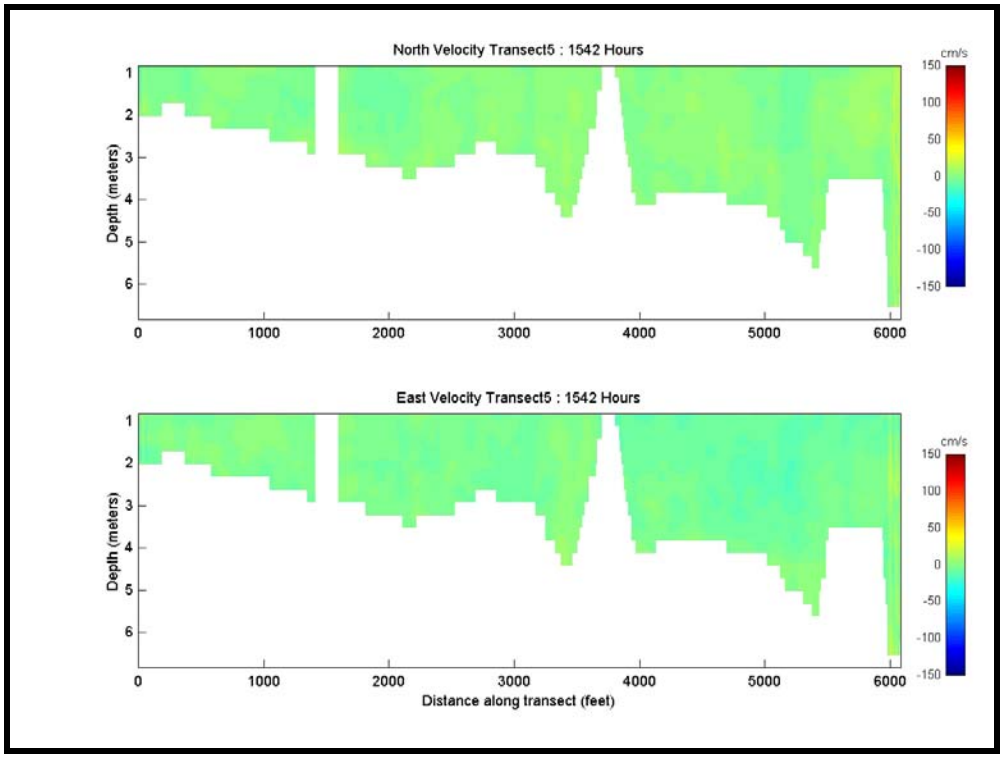

Figure 6-A35. Color contour plots of north-south and east-west velocity for Transect 5 at 3:42 PM on May 14, 2003.

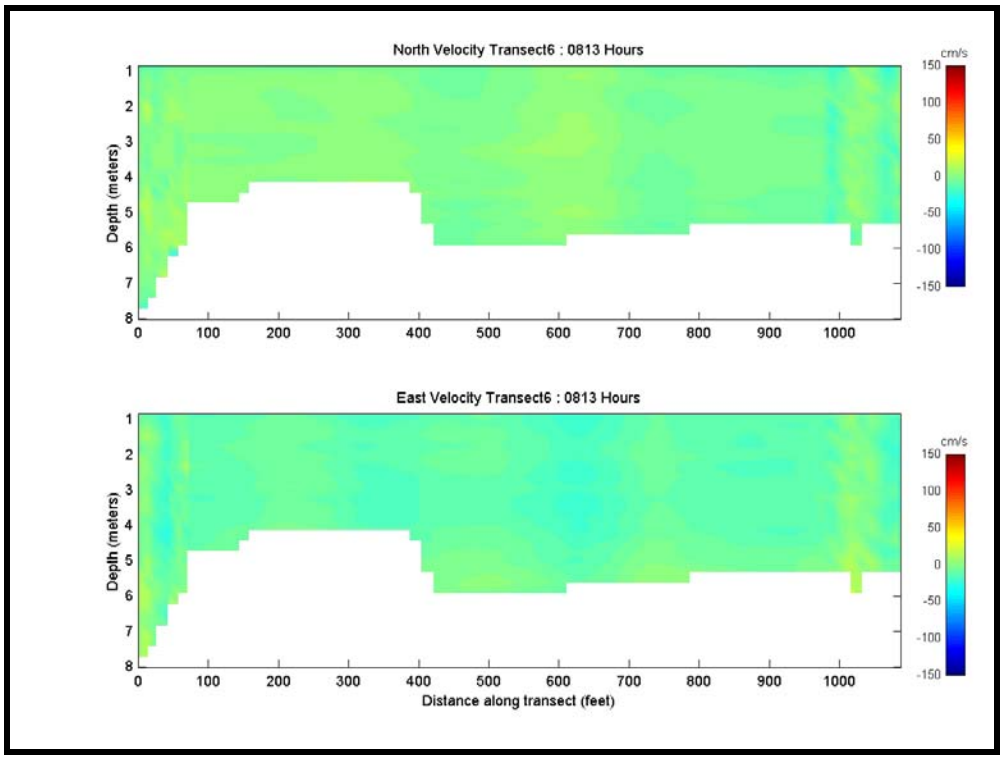

Figure 6-A36. Color contour plots of north-south and east-west velocity for Transect 6 at 8:13 AM on May 14, 2003.

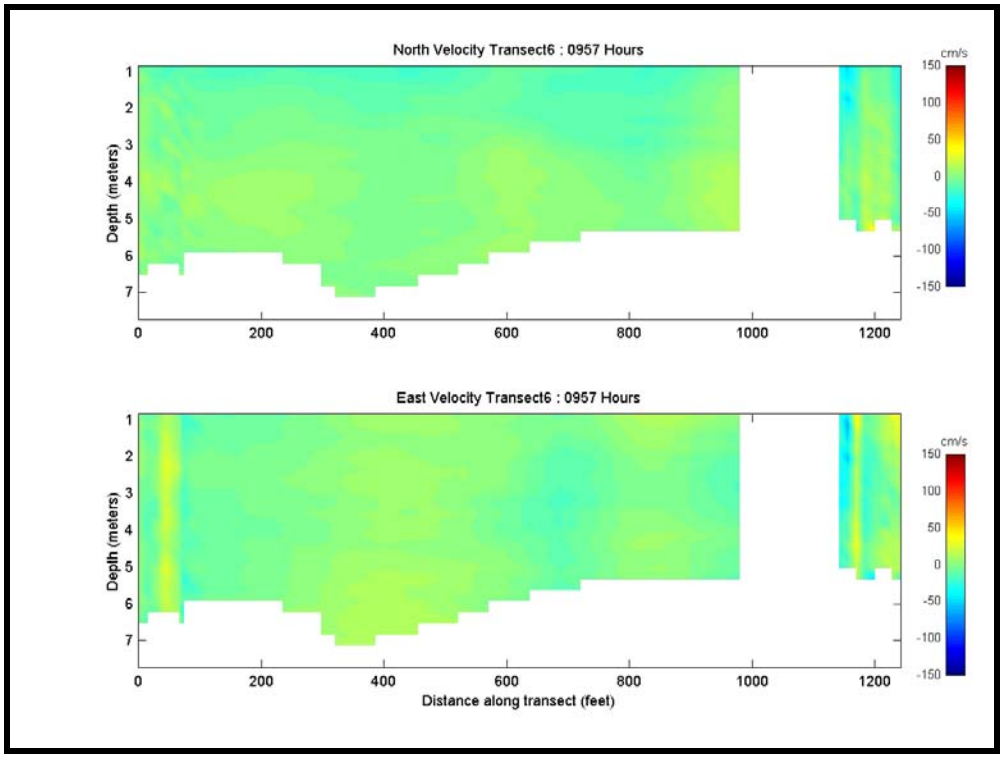

Figure 6-A37. Color contour plots of north-south and east-west velocity for Transect 6 at 9:57 AM on May 14, 2003.

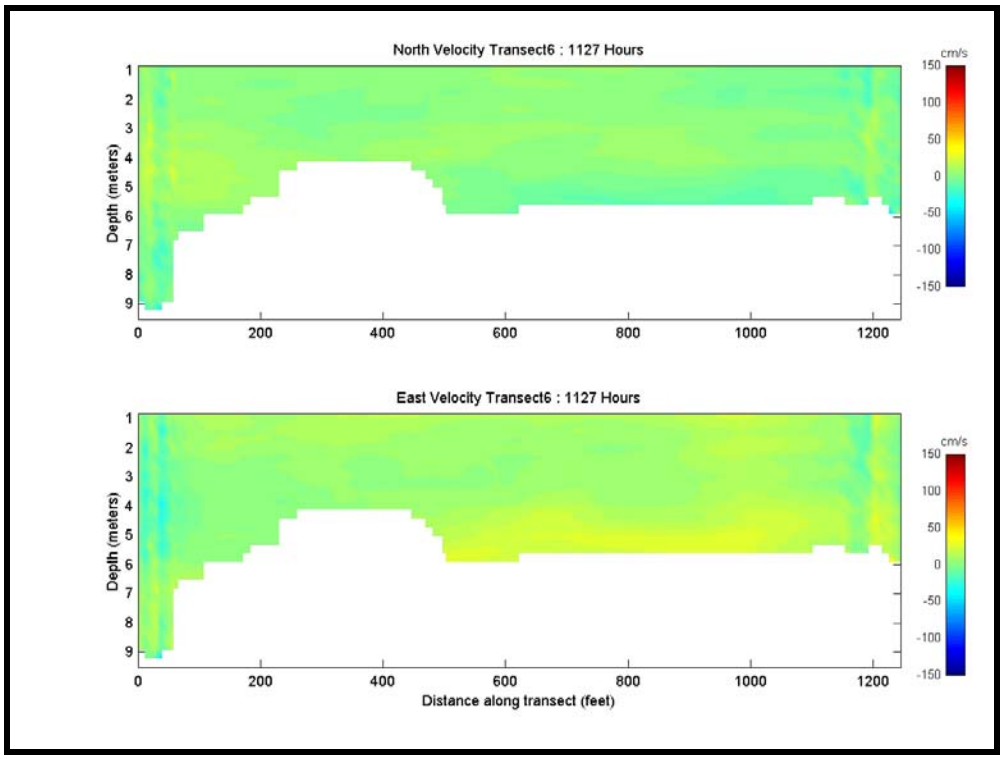

Figure 6-A38. Color contour plots of north-south and east-west velocity for Transect 6 at 11:27 AM on May 14, 2003.

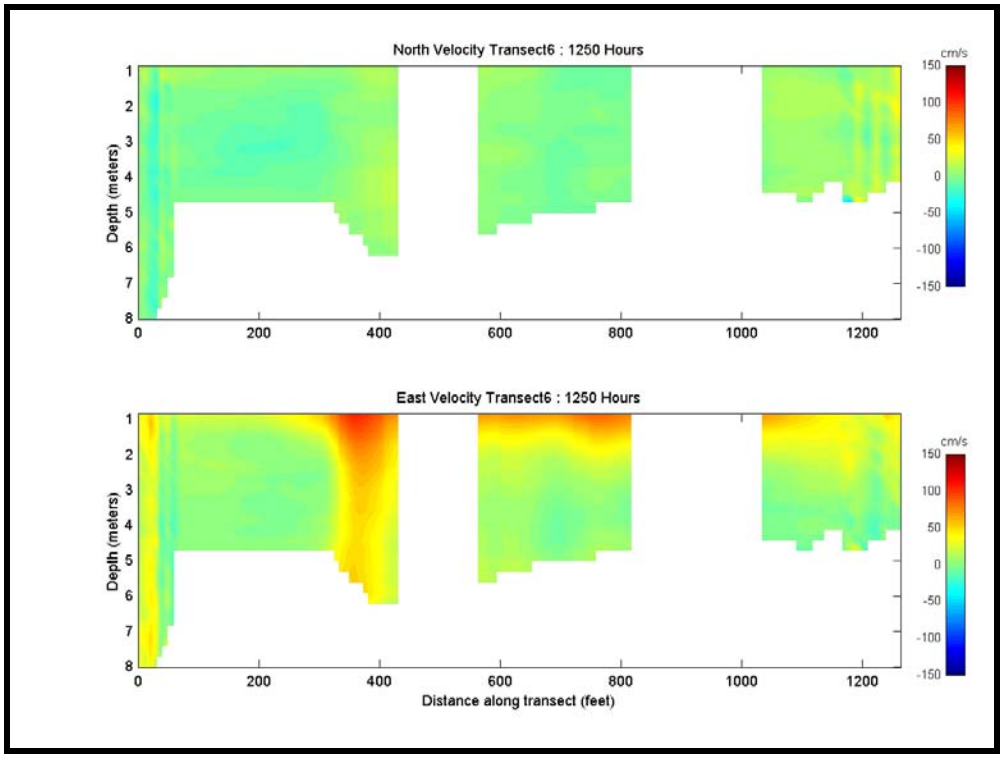

Figure 6-A39. Color contour plots of north-south and east-west velocity for Transect 6 at 12:50 PM on May 14, 2003.

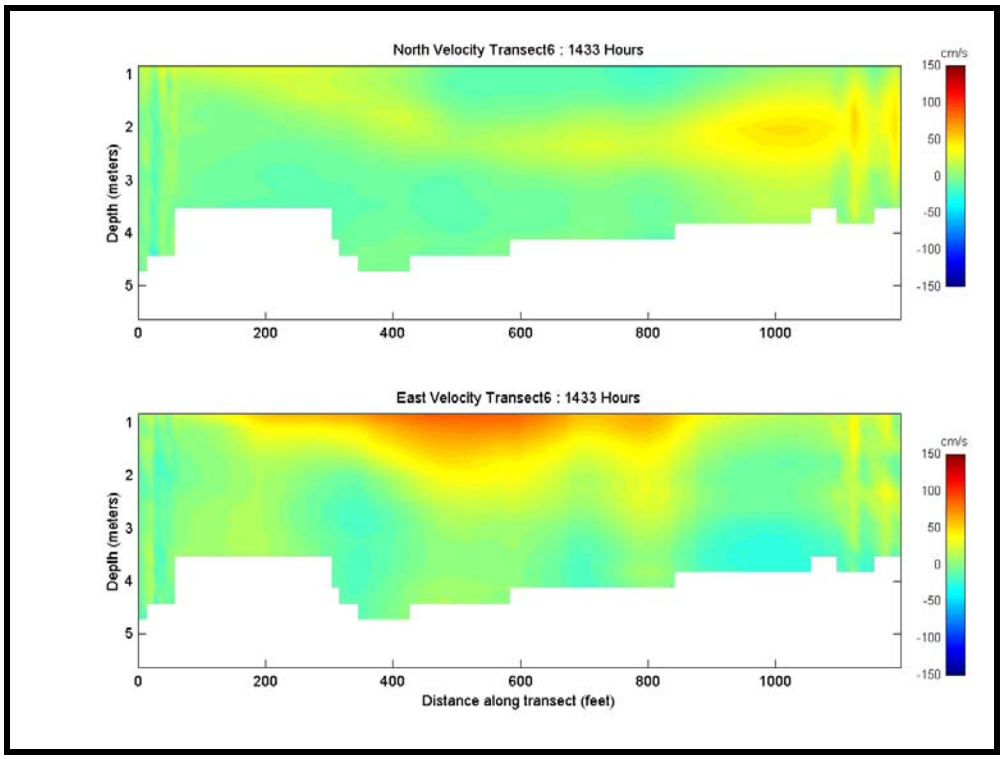

Figure 6-A40. Color contour plots of north-south and east-west velocity for Transect 6 at 2:33 PM on May 14, 2003.

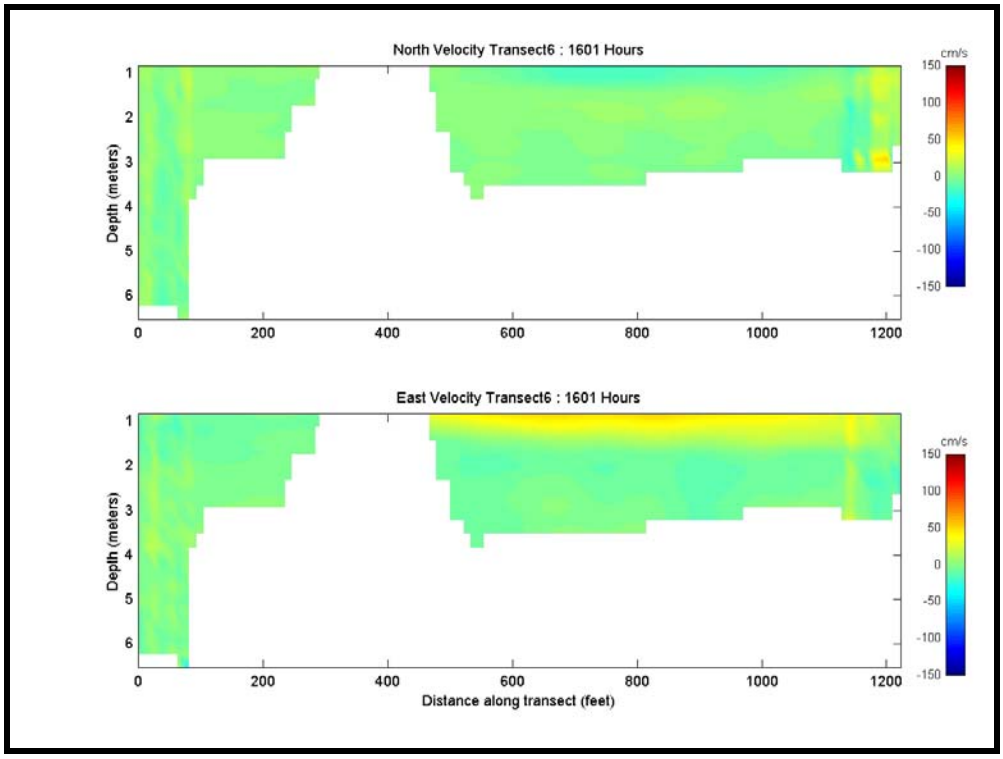

Figure 6-A41. Color contour plots of north-south and east-west velocity for Transect 6 at 4:01 PM on May 14, 2003.

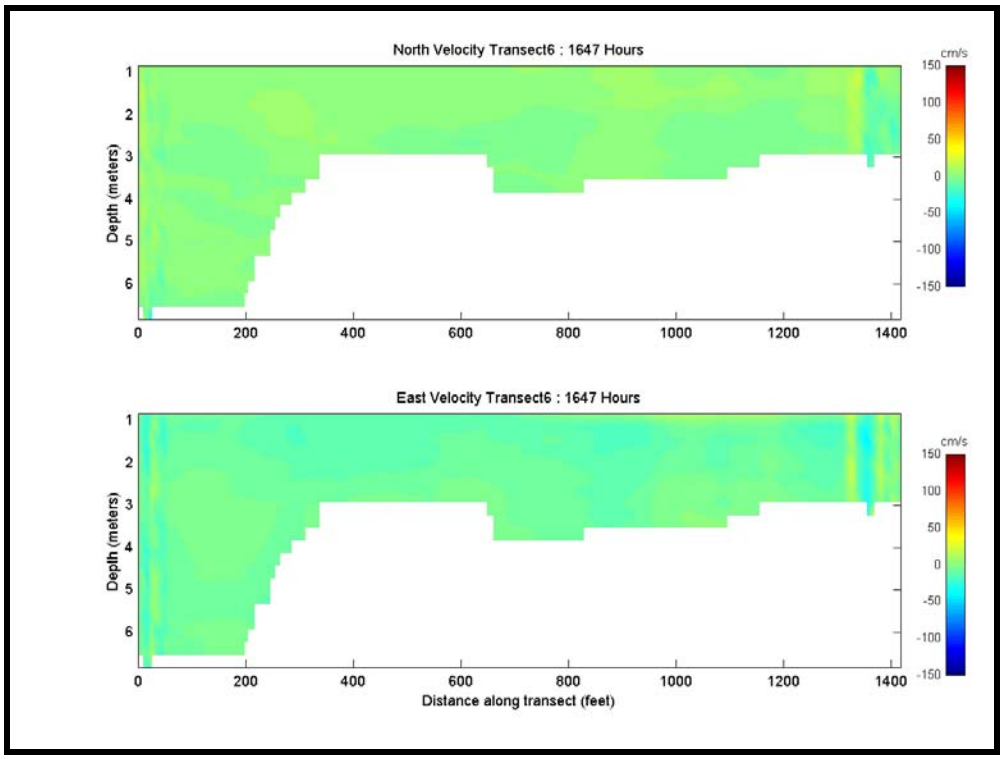

Figure 6-A42. Color contour plots of north-south and east-west velocity for Transect 6 at 4:47 PM on May 14, 2003.

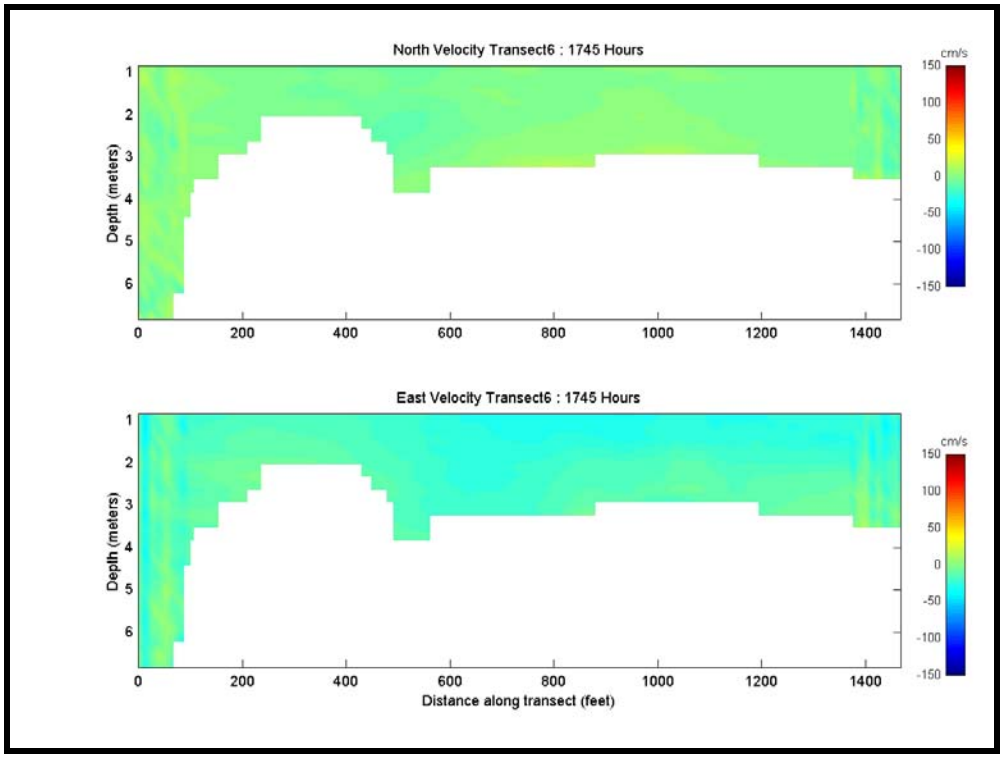

Figure 6-A43. Color contour plots of north-south and east-west velocity for Transect 6 at 5:45 PM on May 14, 2003.

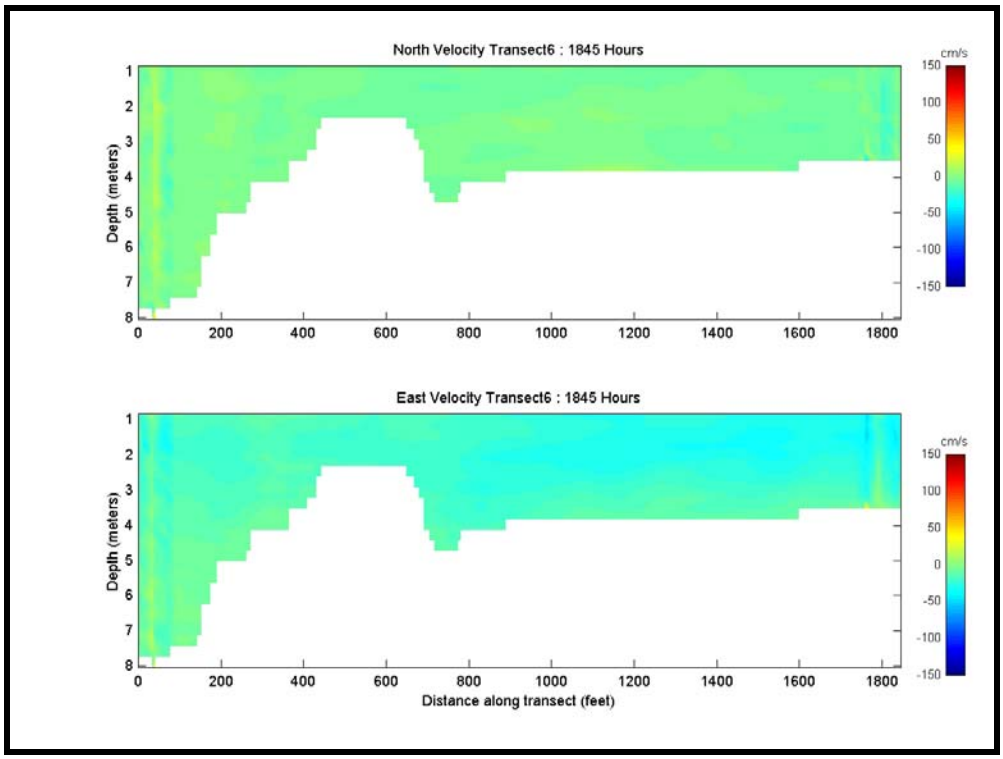

Figure 6-A44. Color contour plots of north-south and east-west velocity for Transect 6 at 6:45 PM on May 14, 2003.

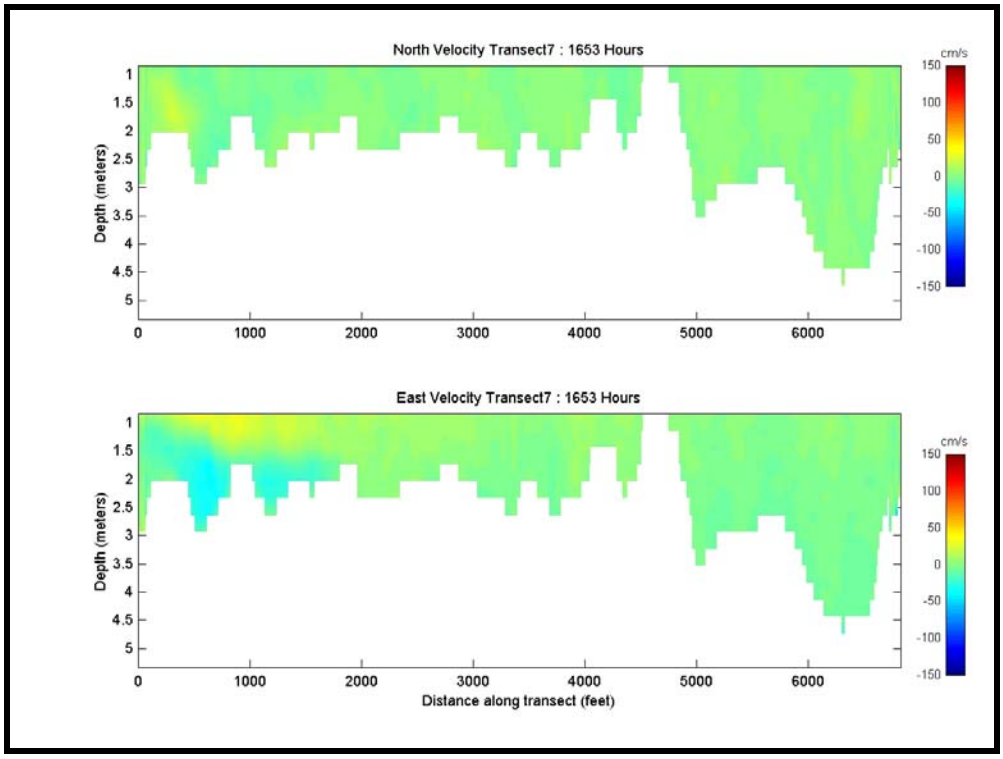

Figure 6-A45. Color contour plots of north-south and east-west velocity for Transect 7 at 4:53 PM on May 14, 2003.

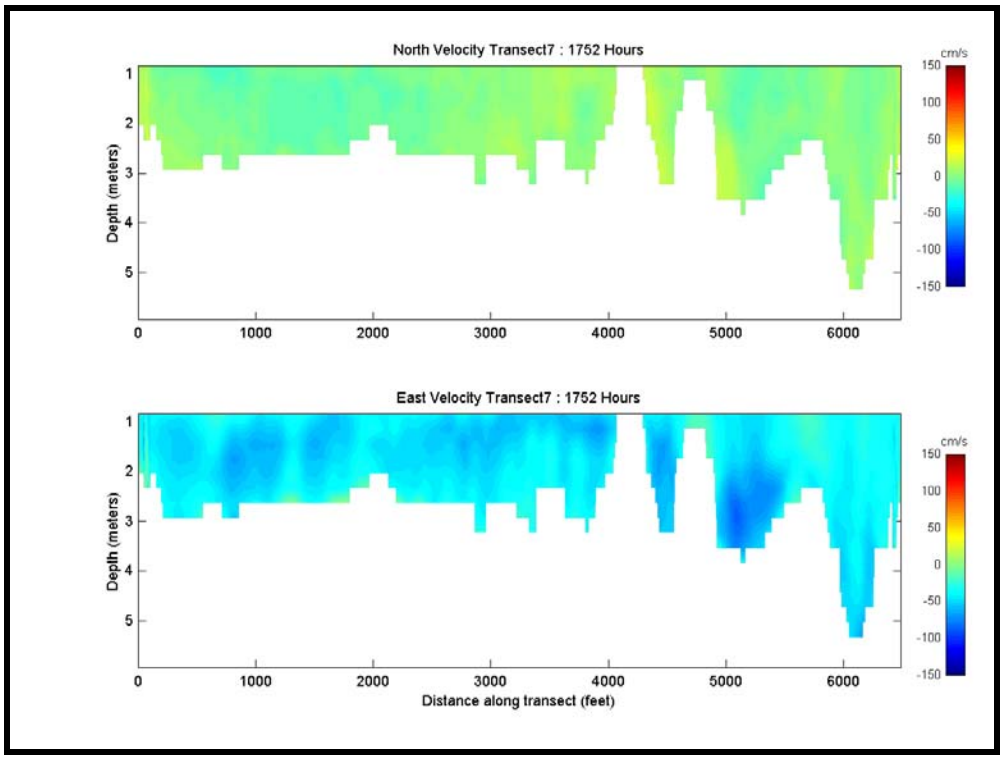

Figure 6-A46. Color contour plots of north-south and east-west velocity for Transect 7 at 5:52 PM on May 14, 2003.

APPENDIX 8-A

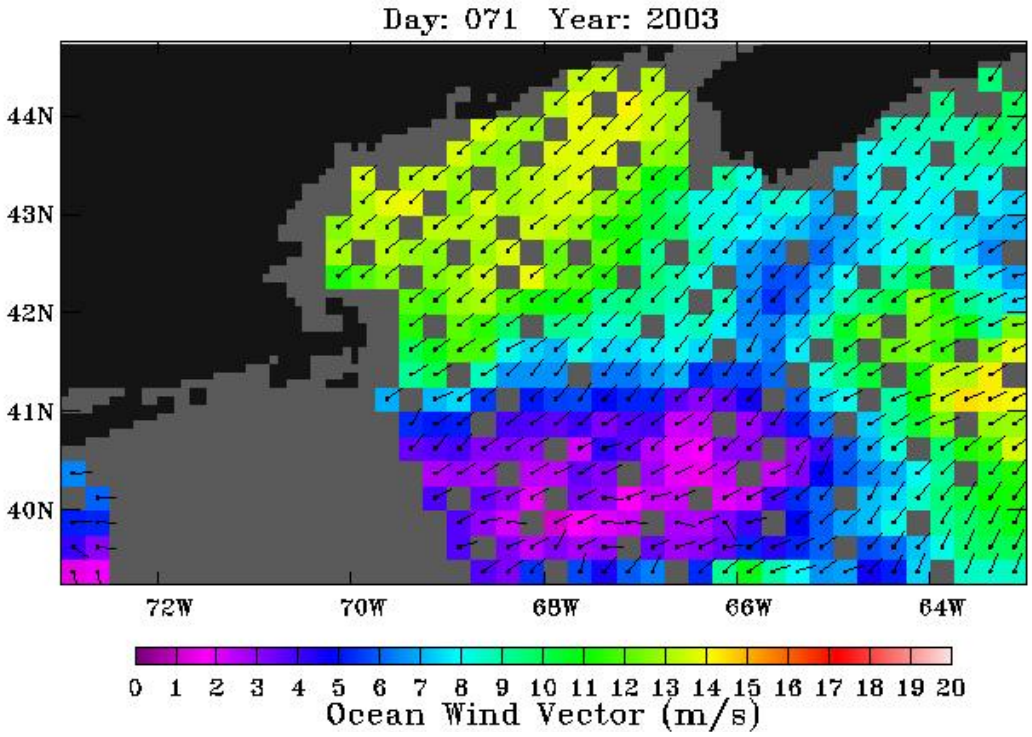

Figure 8-A1. QuikSCAT wind field. Morning satellite overpass on March 12, 2003.

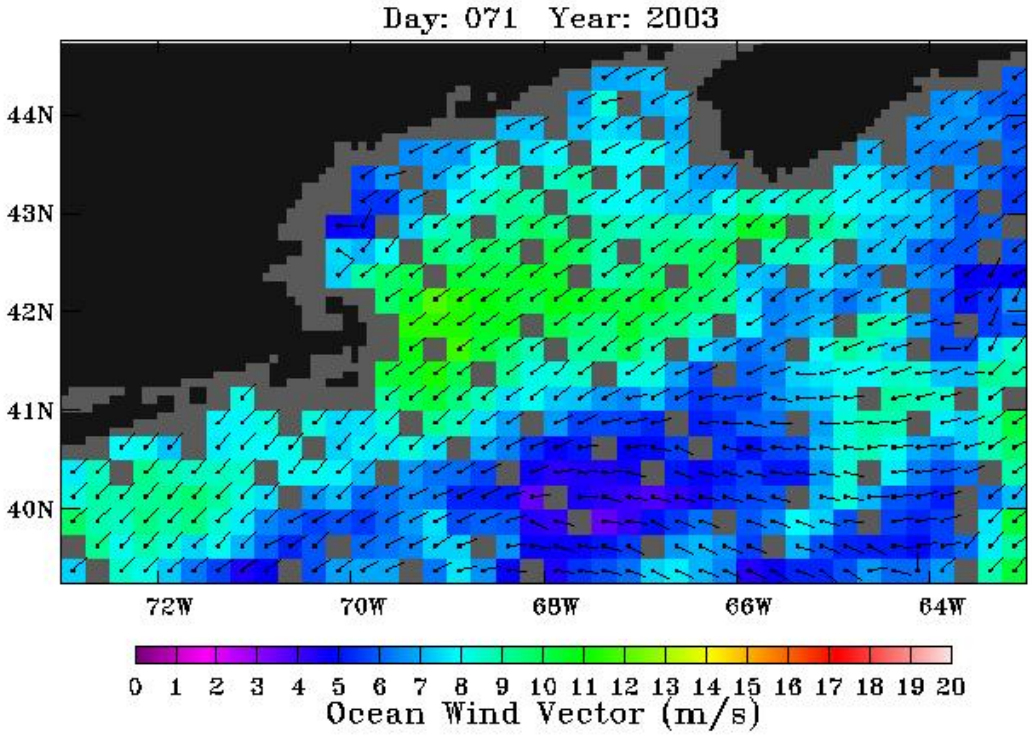

Figure 8-A2. QuikSCAT wind field. Evening satellite overpass on March 12, 2003.

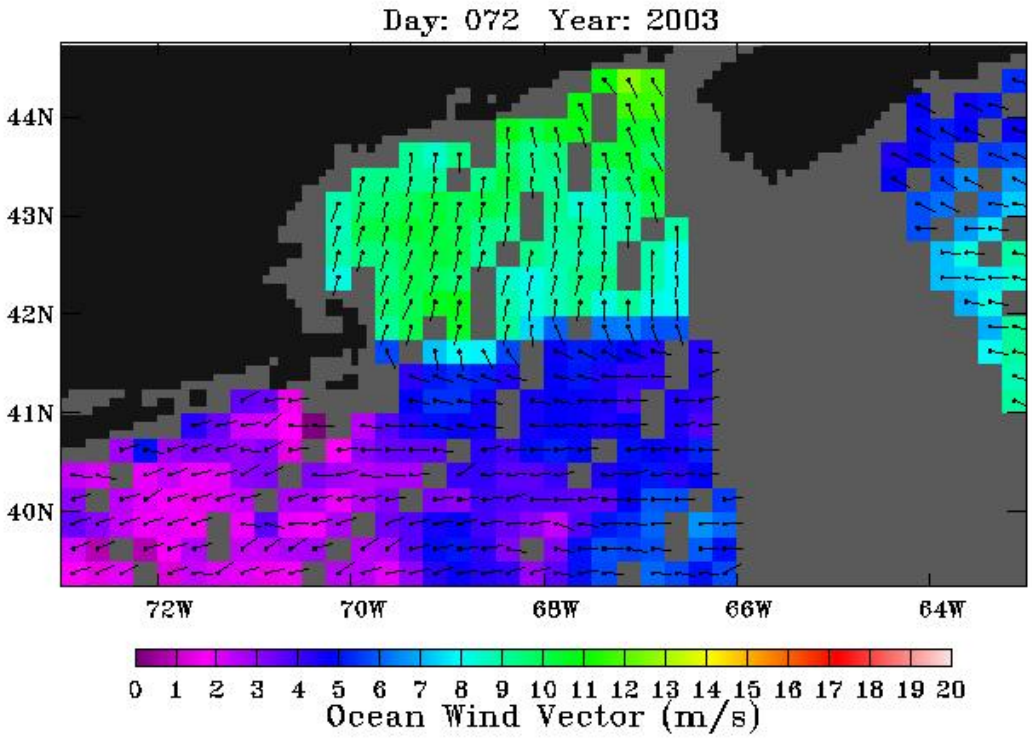

Figure 8-A3. QuikSCAT wind field. Morning satellite overpass on March 13, 2003.

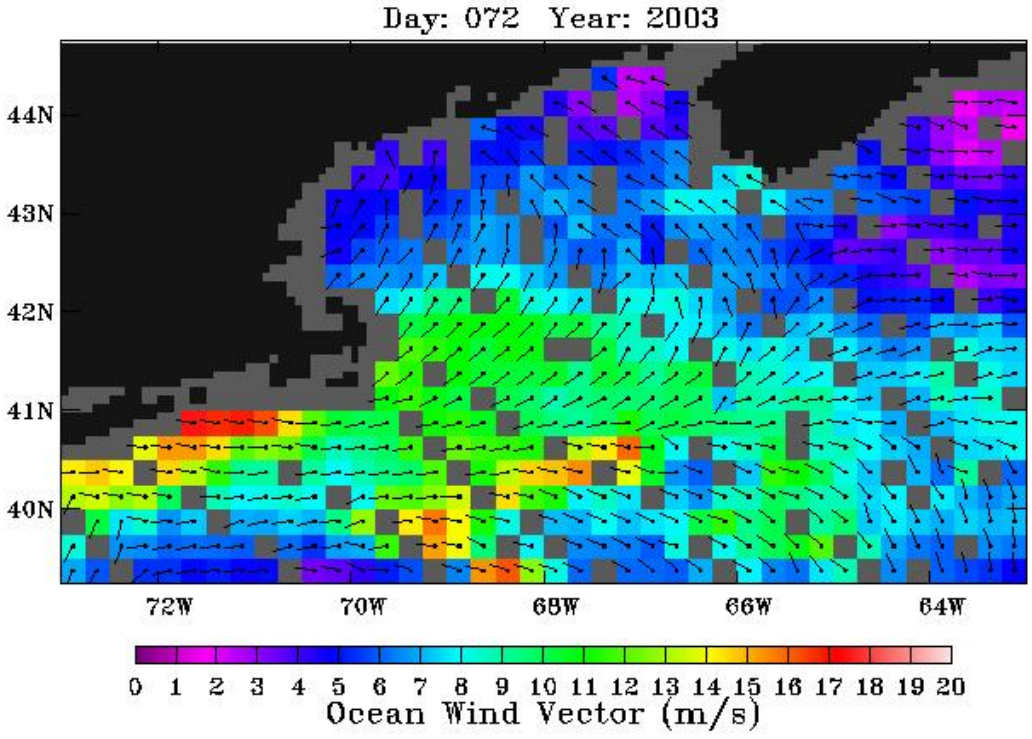

Figure 8-A4. QuikSCAT wind field. Evening satellite overpass on March 13, 2003.

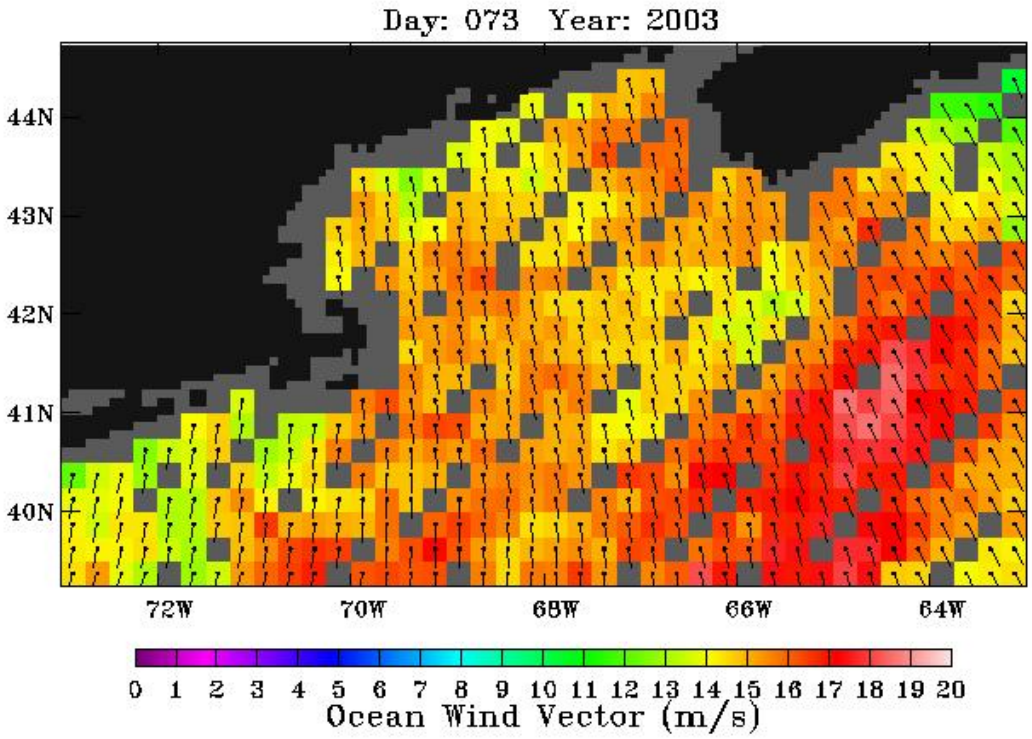

Figure 8-A5. QuikSCAT wind field. Morning satellite overpass on March 14, 2003.

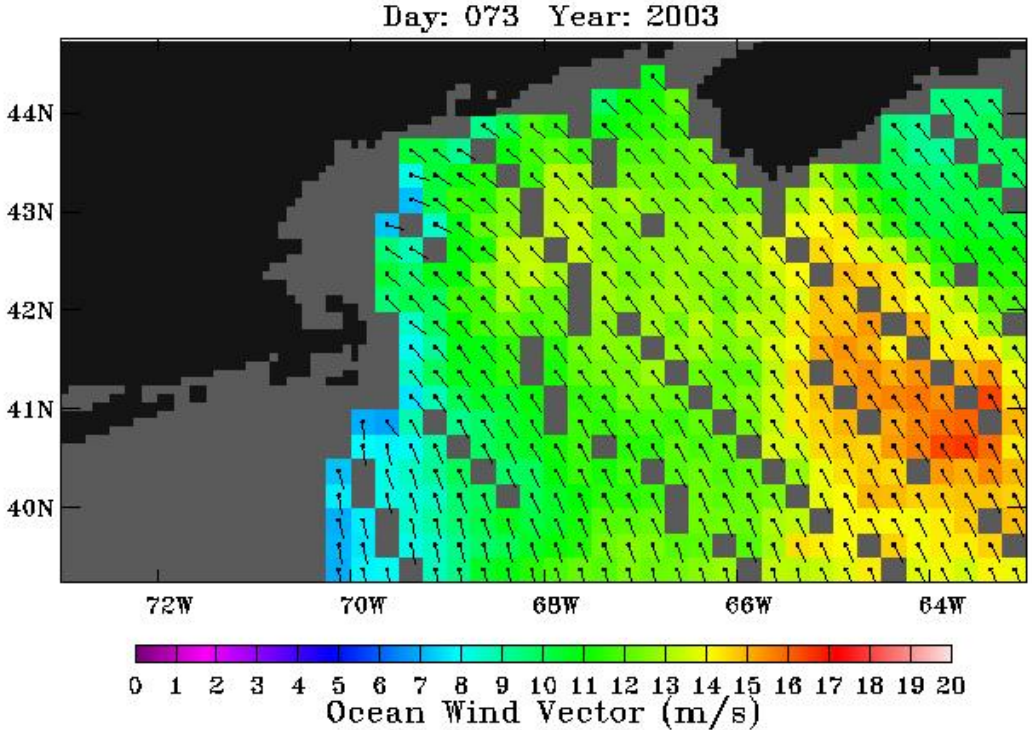

Figure 8-A6. QuikSCAT wind field. Evening satellite overpass on March 14, 2003.

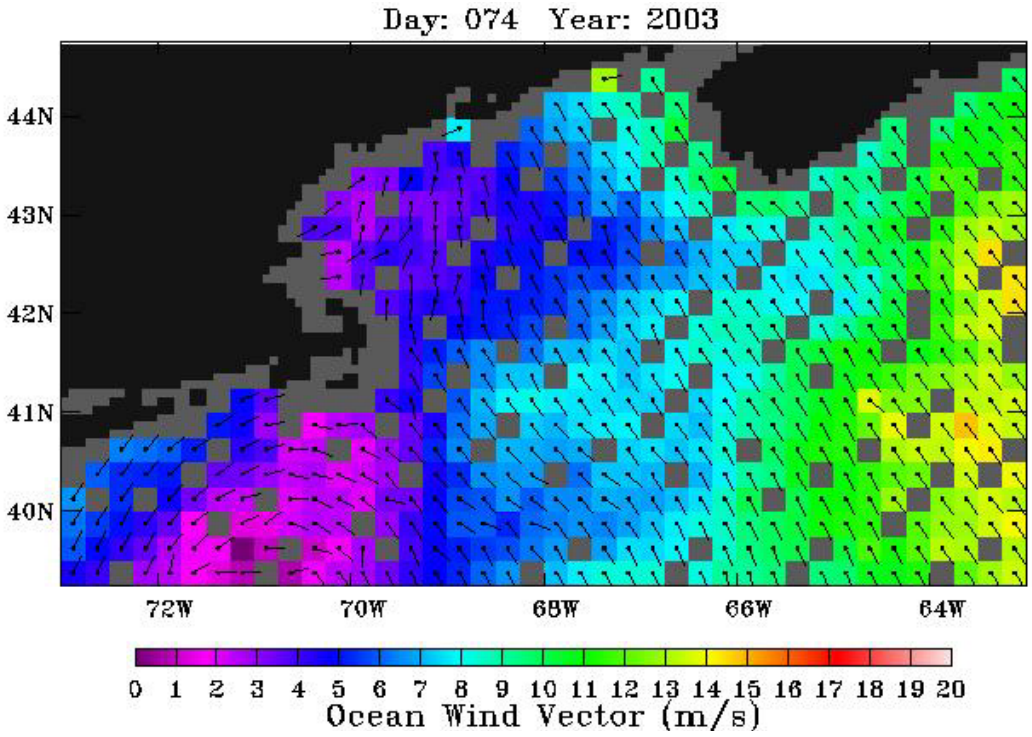

Figure 8-A7. QuikSCAT wind field. Morning satellite overpass on March 15, 2003.

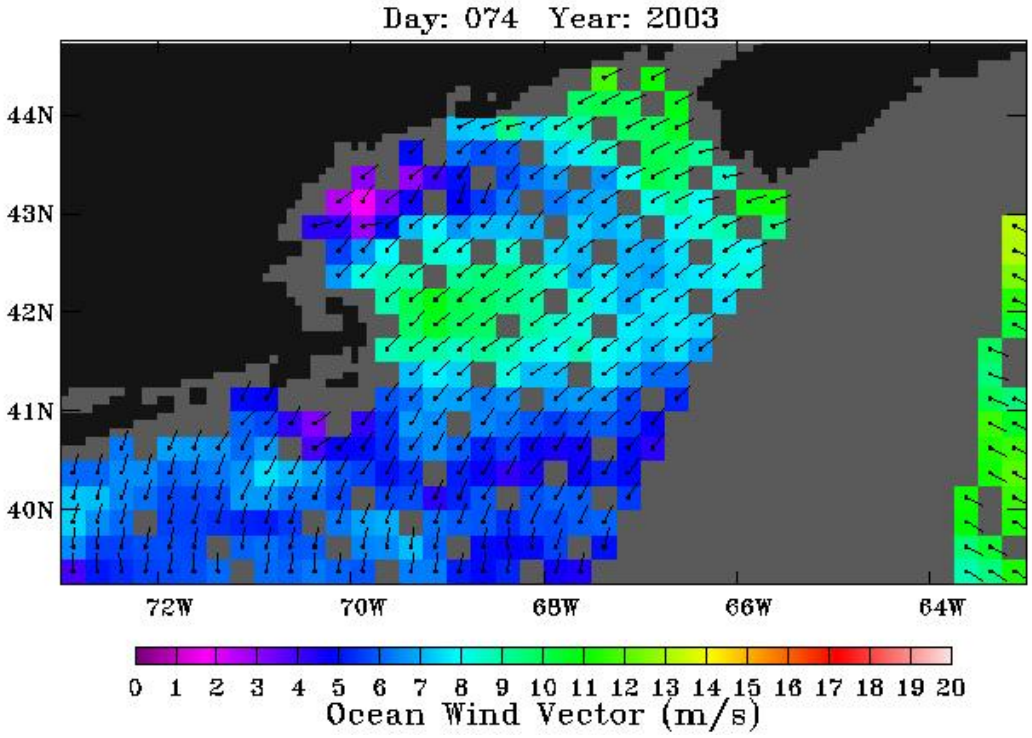

Figure 8-A8. QuikSCAT wind field. Evening satellite overpass on March 15, 2003.

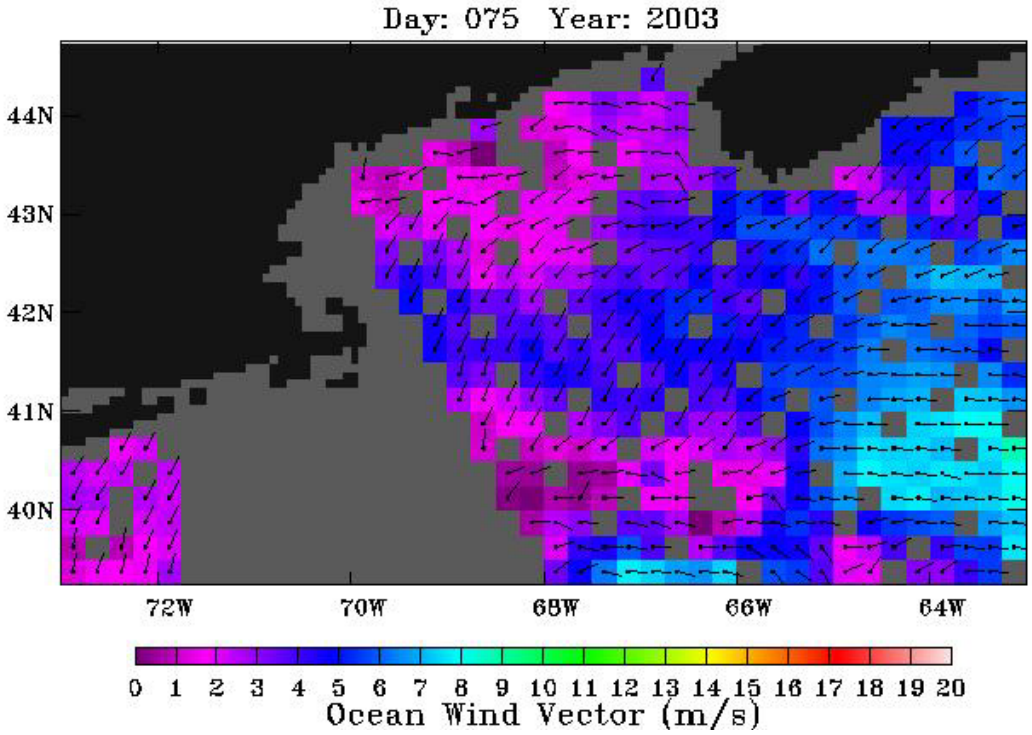

Figure 8-A9. QuikSCAT wind field. Morning satellite overpass on March 16, 2003.

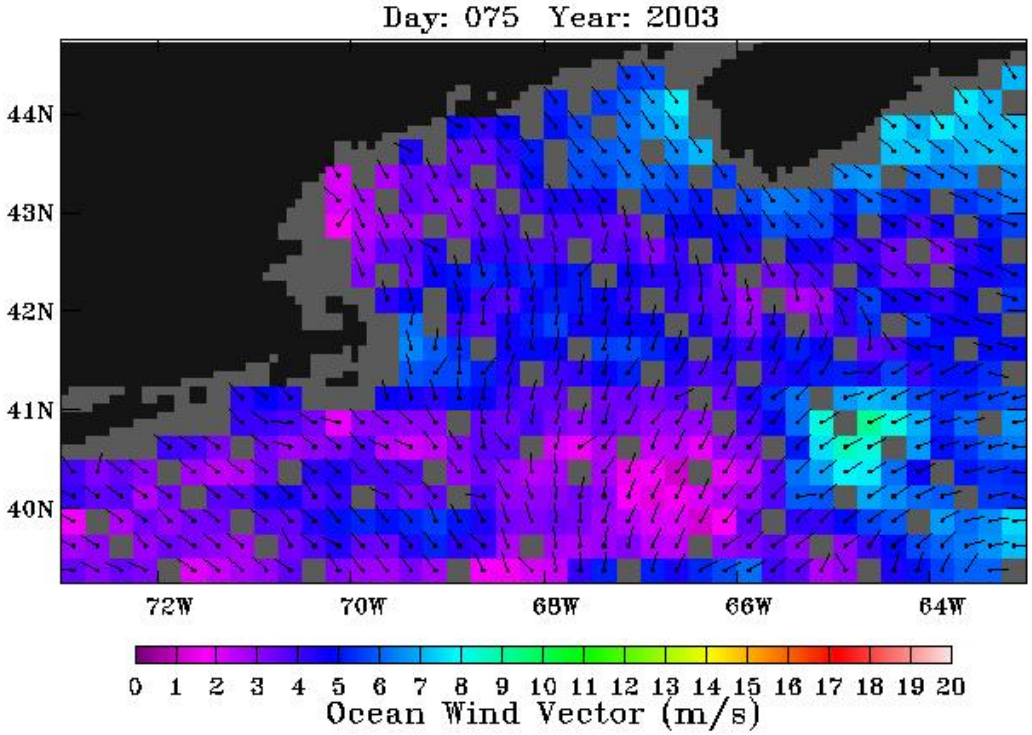

Figure 8-A10. QuikSCAT wind field. Evening satellite overpass on March 16, 2003.

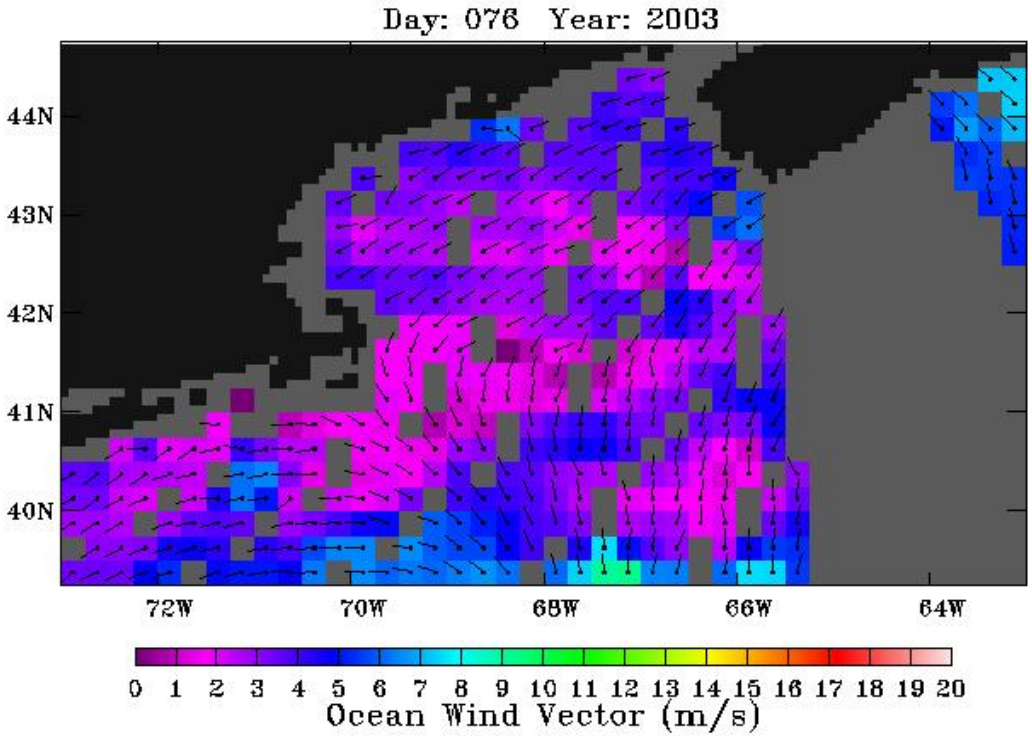

Figure 8-A11. QuikSCAT wind field. Morning satellite overpass on March 17, 2003.

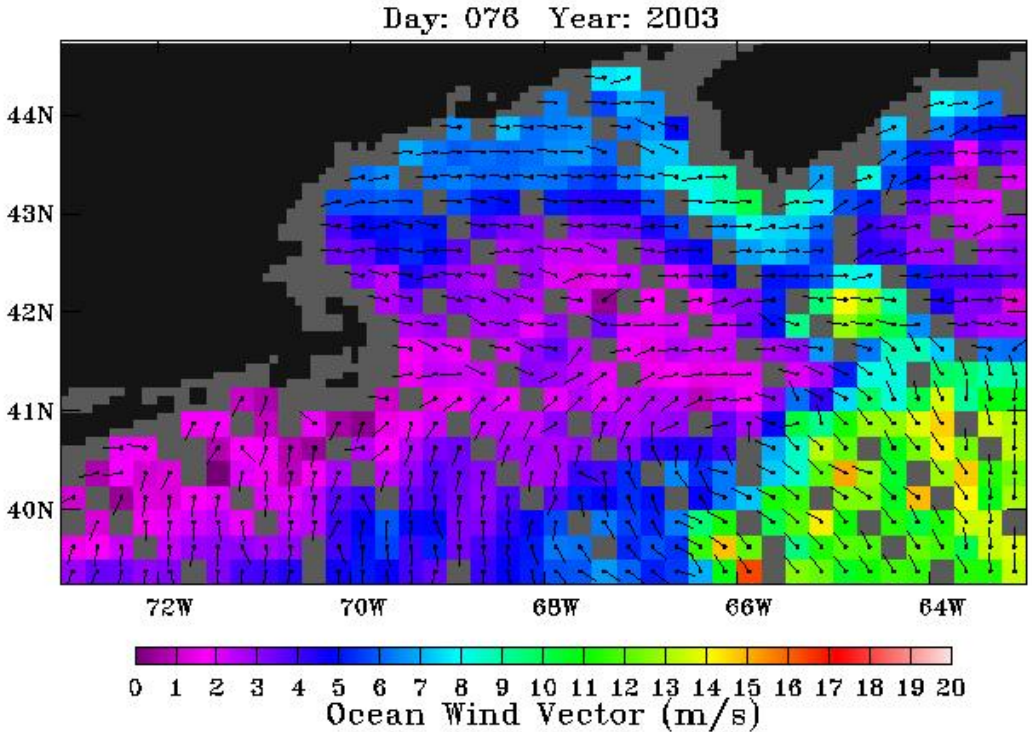

Figure 8-A12. QuikSCAT wind field. Evening satellite overpass on March 17, 2003.

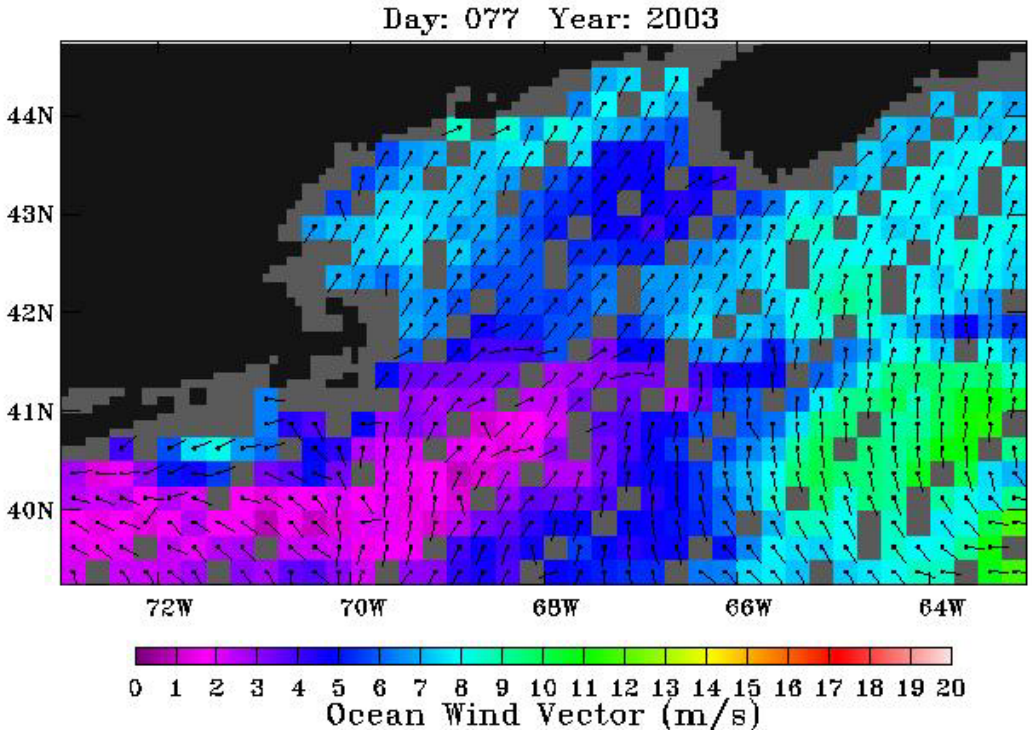

Figure 8-A13. QuikSCAT wind field. Morning satellite overpass on March 18, 2003.

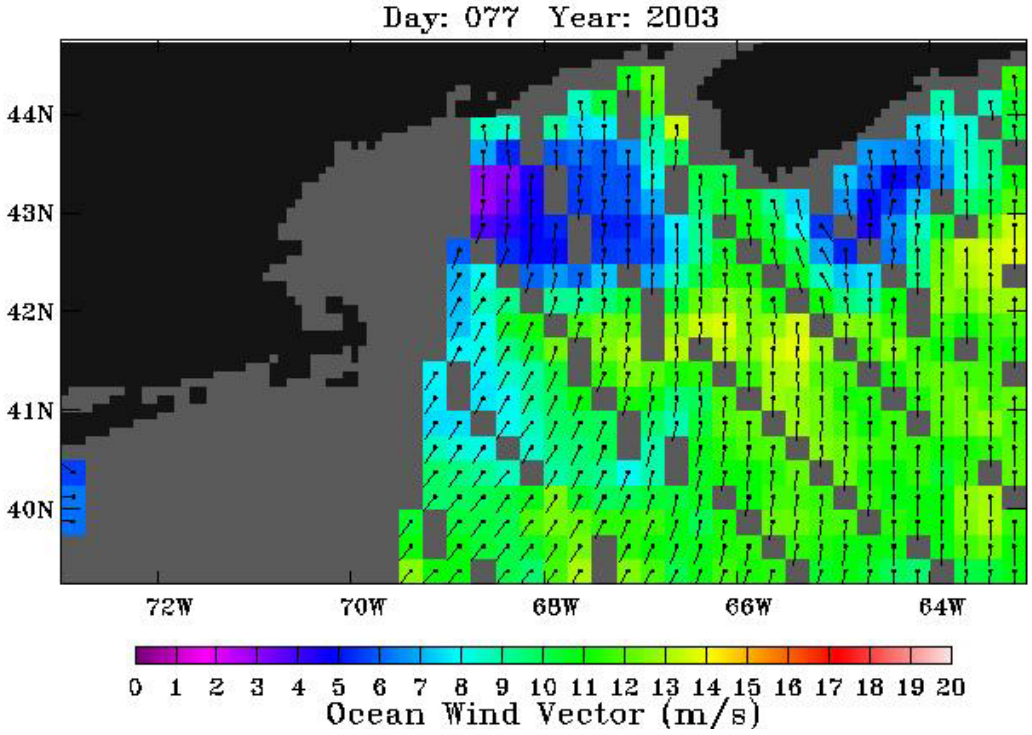

Figure 8-A14. QuikSCAT wind field. Evening satellite overpass on March 18, 2003.

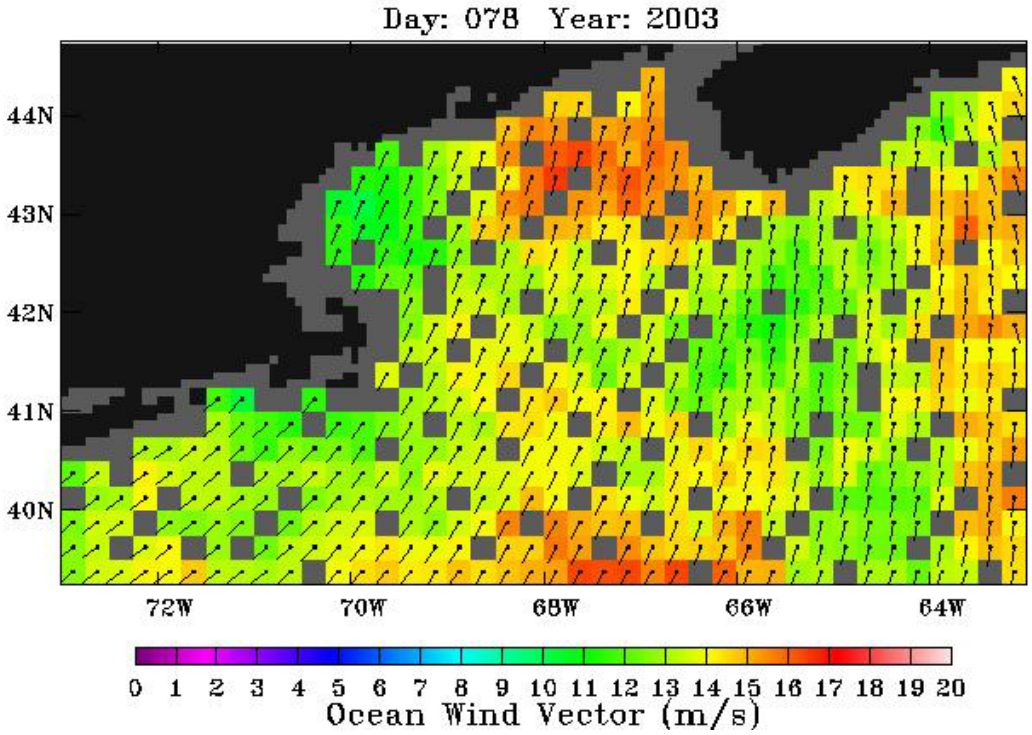

Figure 8-A15. QuikSCAT wind field. Morning satellite overpass on March 19, 2003.

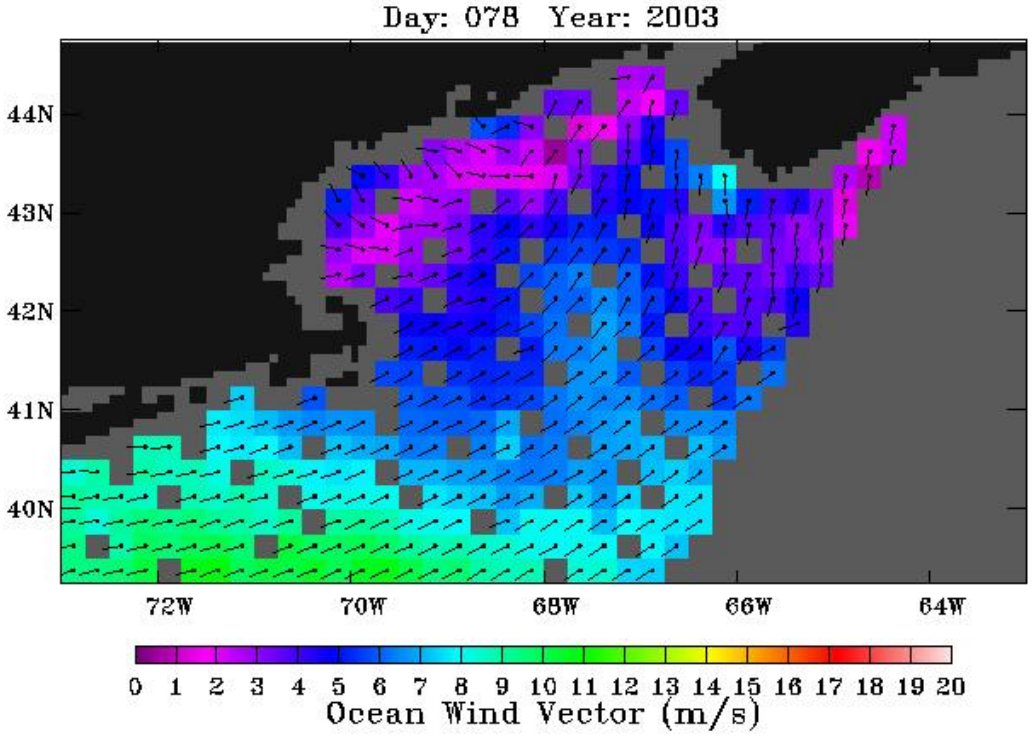

Figure 8-A16. QuikSCAT wind field. Evening satellite overpass on March 19, 2003.

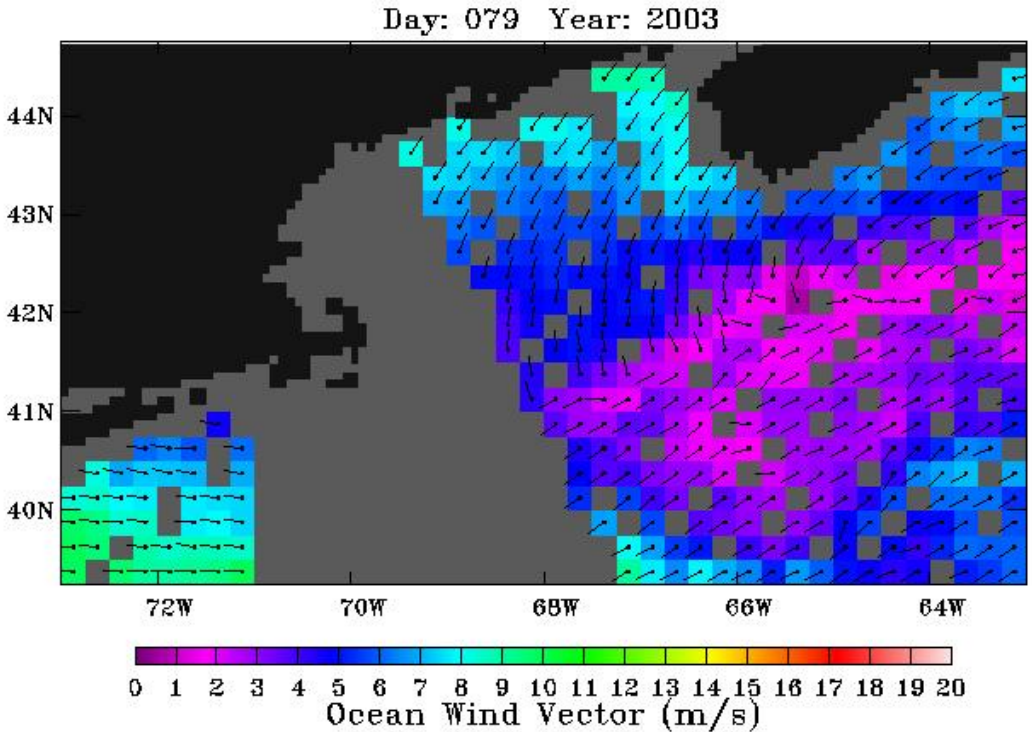

Figure 8-A17. QuikSCAT wind field. Morning satellite overpass on March 20, 2003.

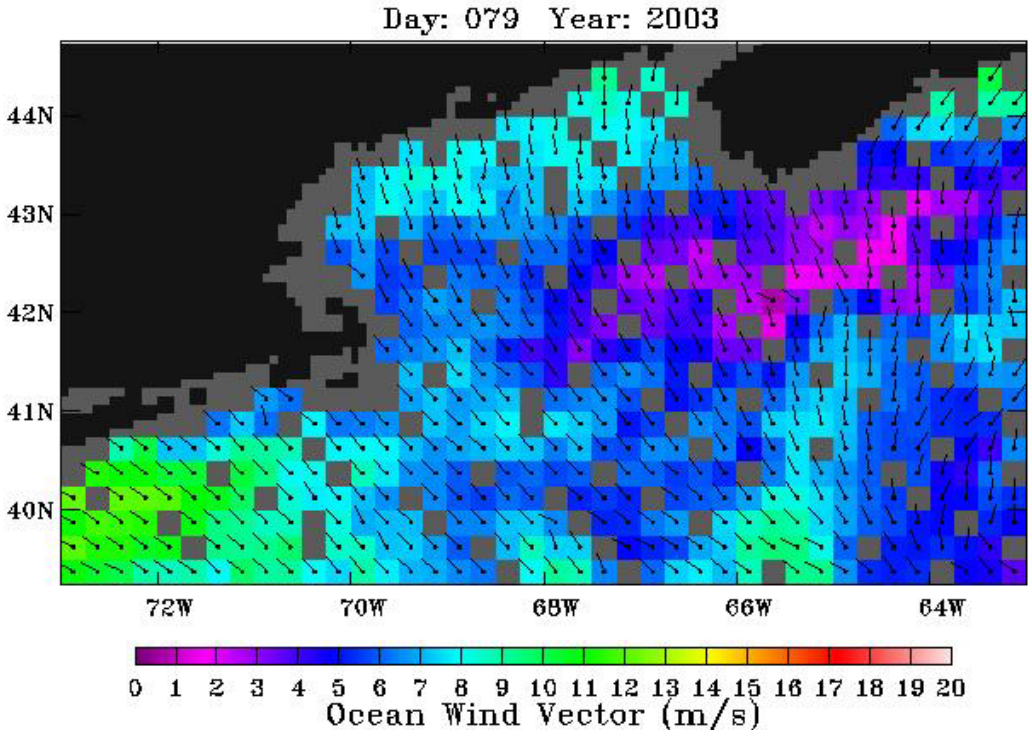

Figure 8-A18. QuikSCAT wind field. Evening satellite overpass on March 20, 2003.

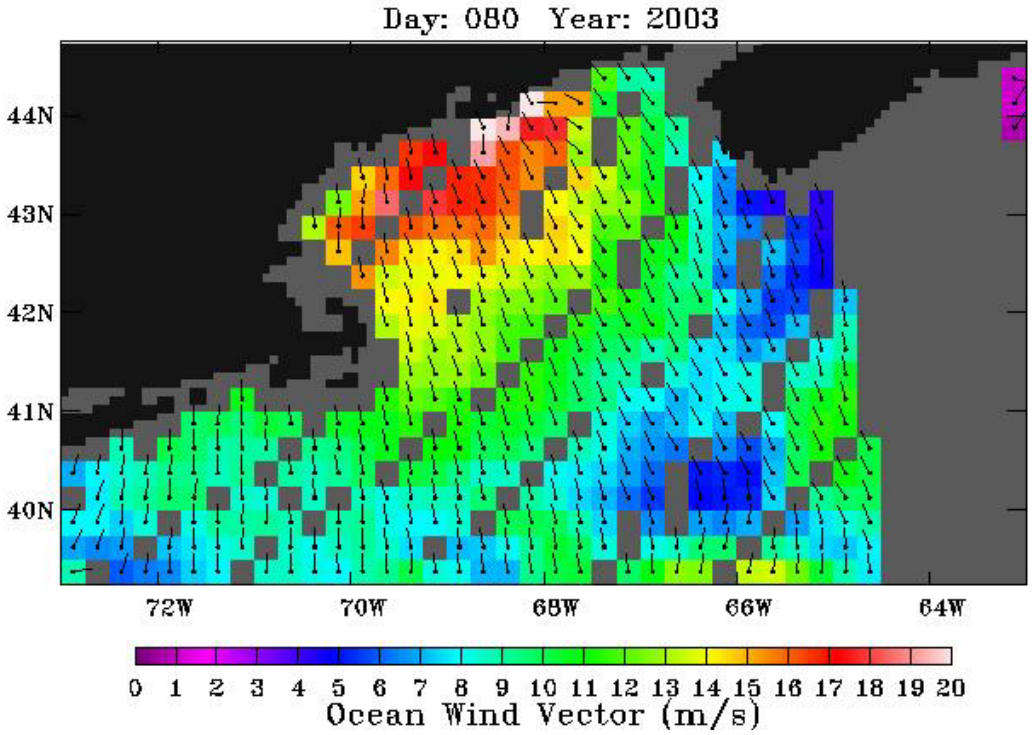

Figure 8-A19. QuikSCAT wind field. Morning satellite overpass on March 21, 2003.

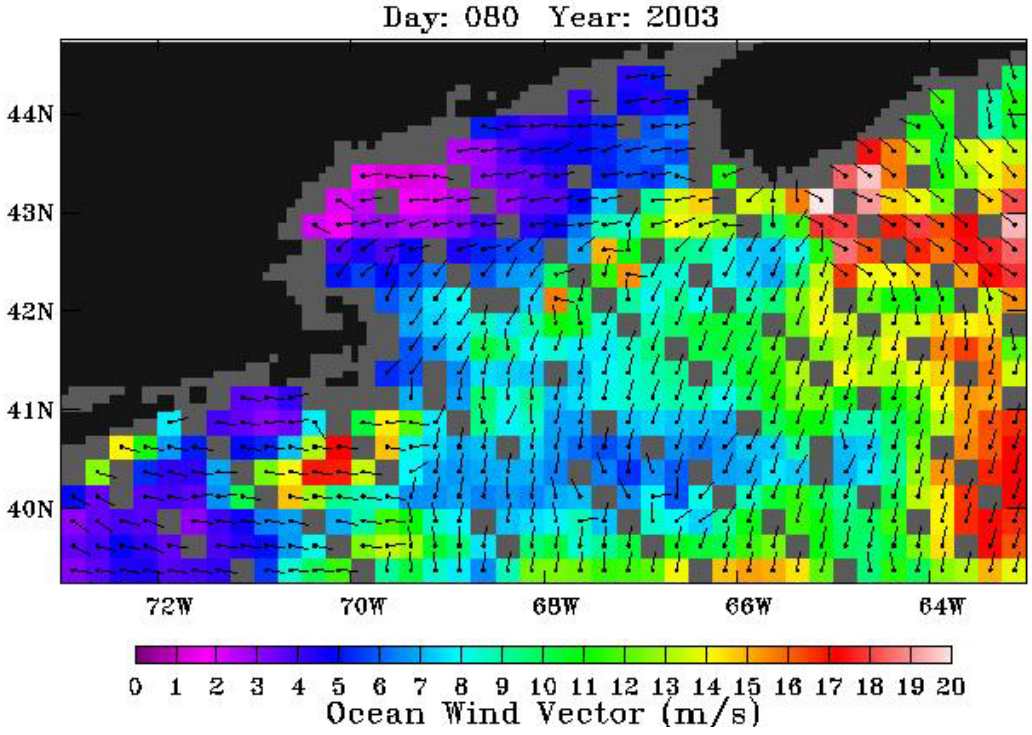

Figure 8-A20. QuikSCAT wind field. Evening satellite overpass on March 21, 2003.

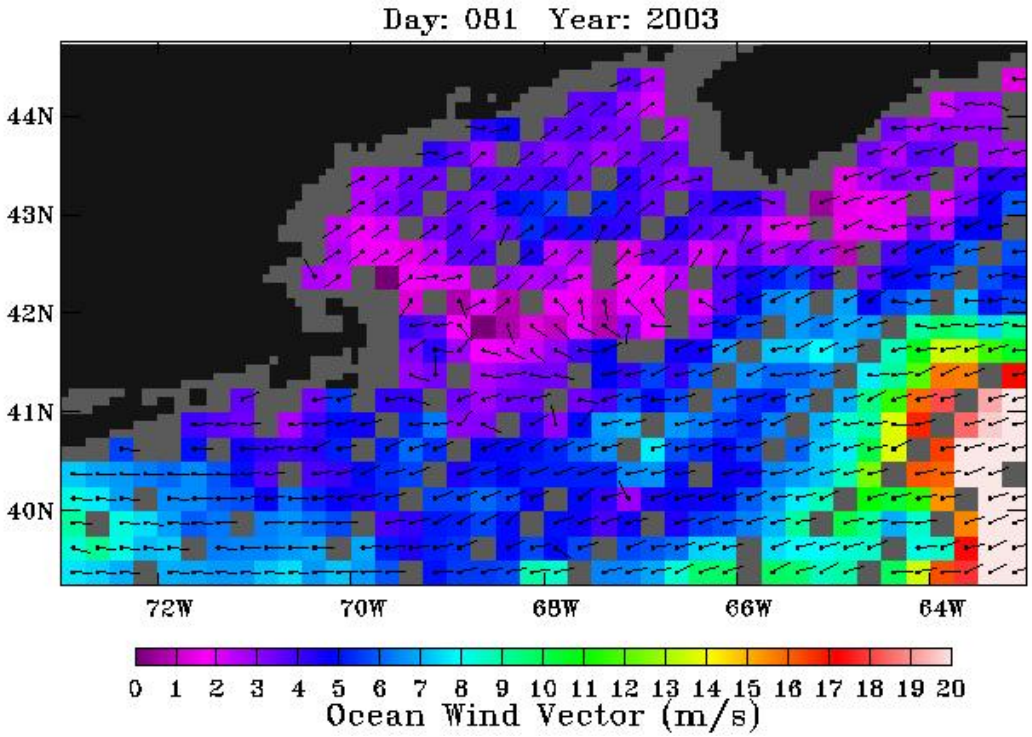

Figure 8-A21. QuikSCAT wind field. Morning satellite overpass on March 22, 2003.

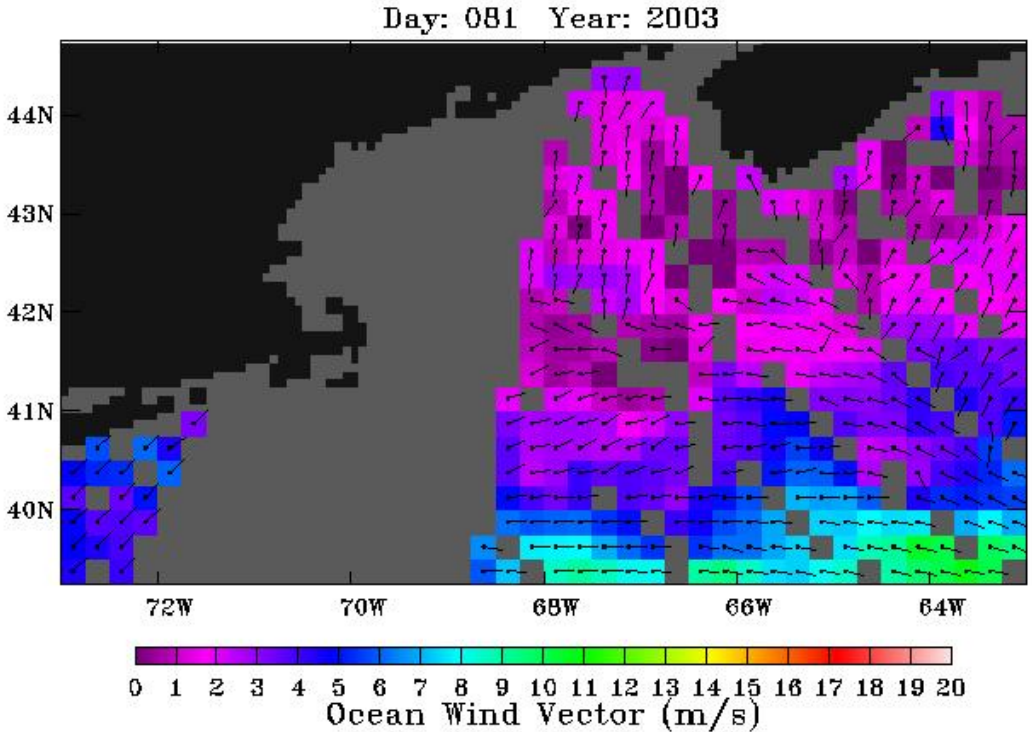

Figure 8-A22. QuikSCAT wind field. Evening satellite overpass on March 22, 2003.

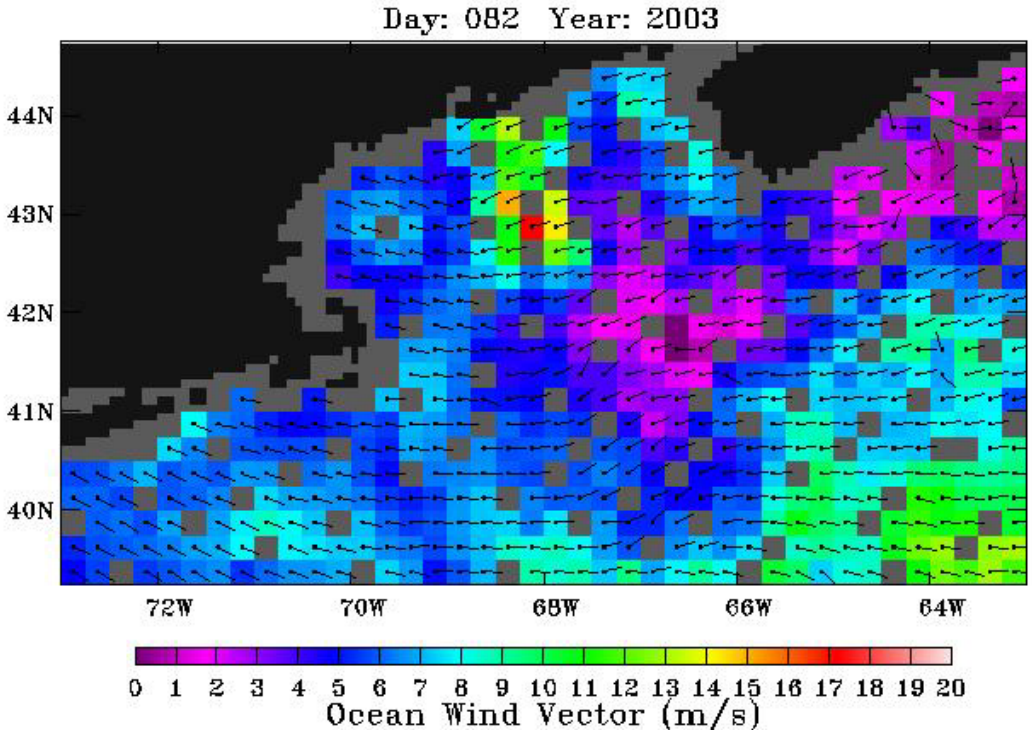

Figure 8-A23. QuikSCAT wind field. Morning satellite overpass on March 23, 2003.

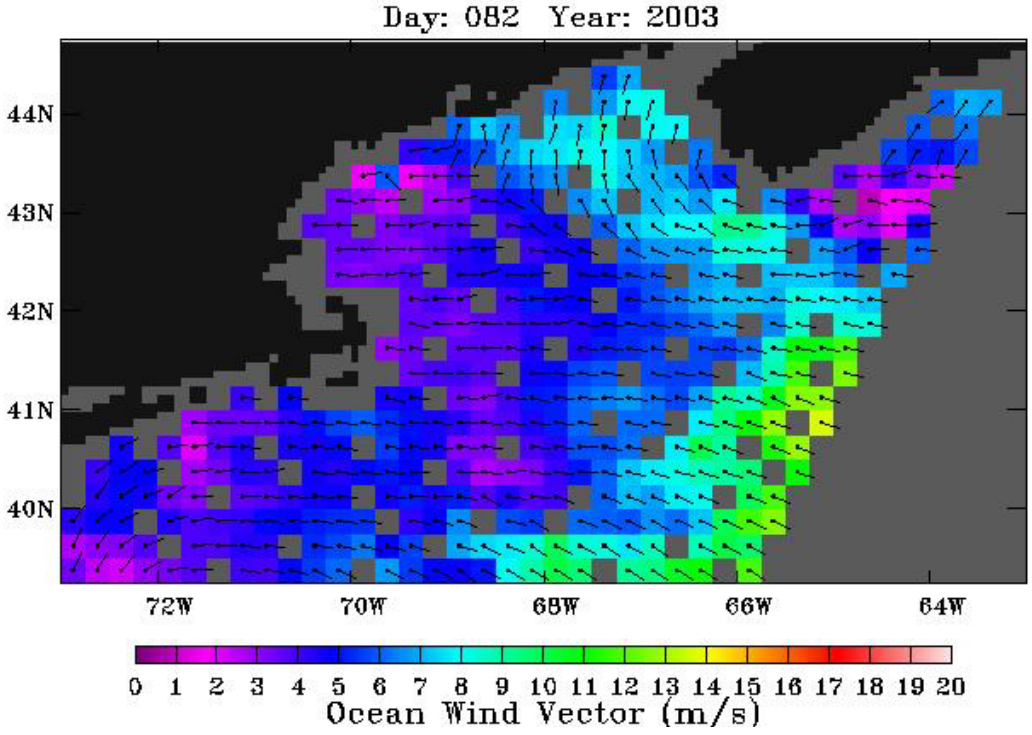

Figure 8-A24. QuikSCAT wind field. Evening satellite overpass on March 23, 2003.

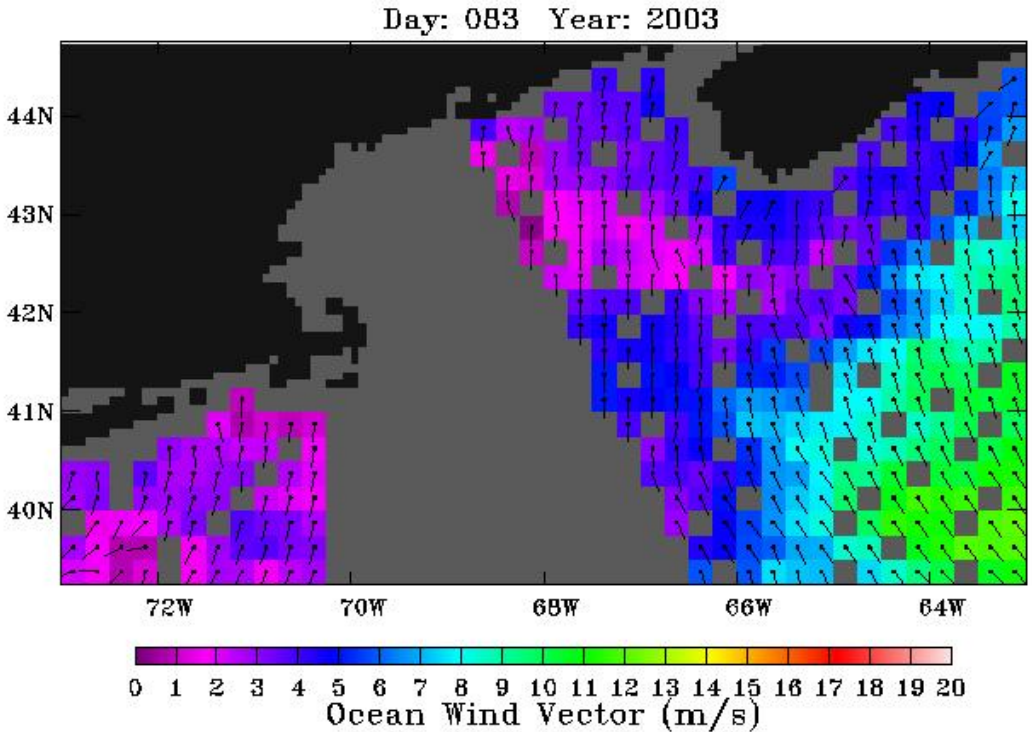

Figure 8-25. QuikSCAT wind field. Morning satellite overpass on March 24, 2003.

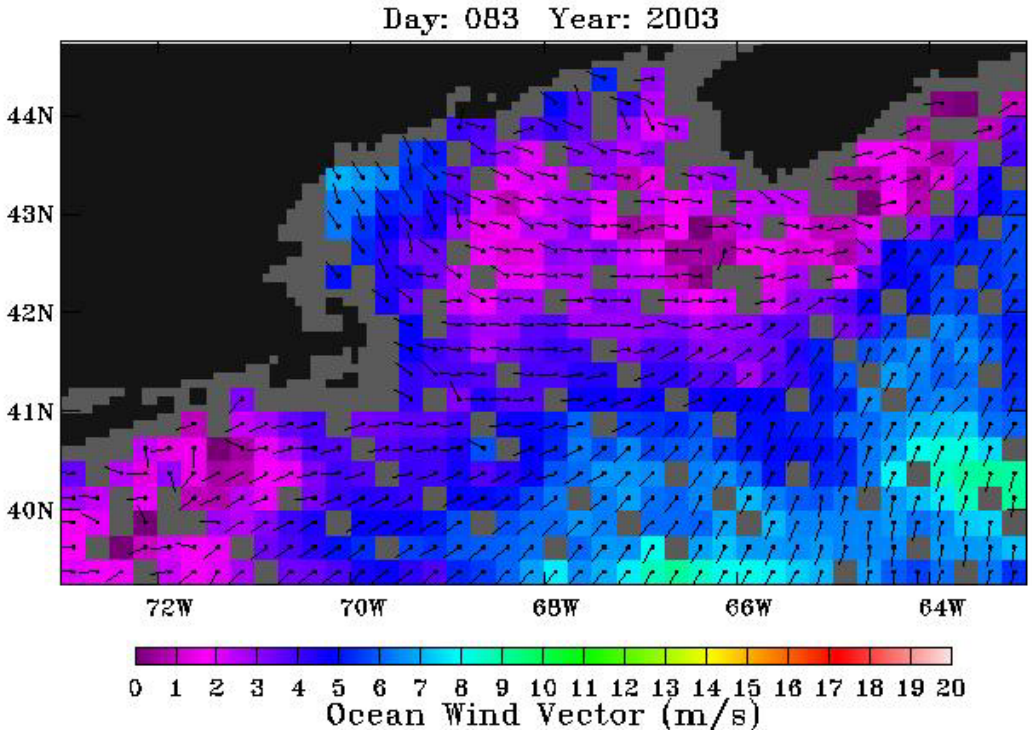

Figure 8-A26. QuikSCAT wind field. Evening satellite overpass on March 24, 2003.

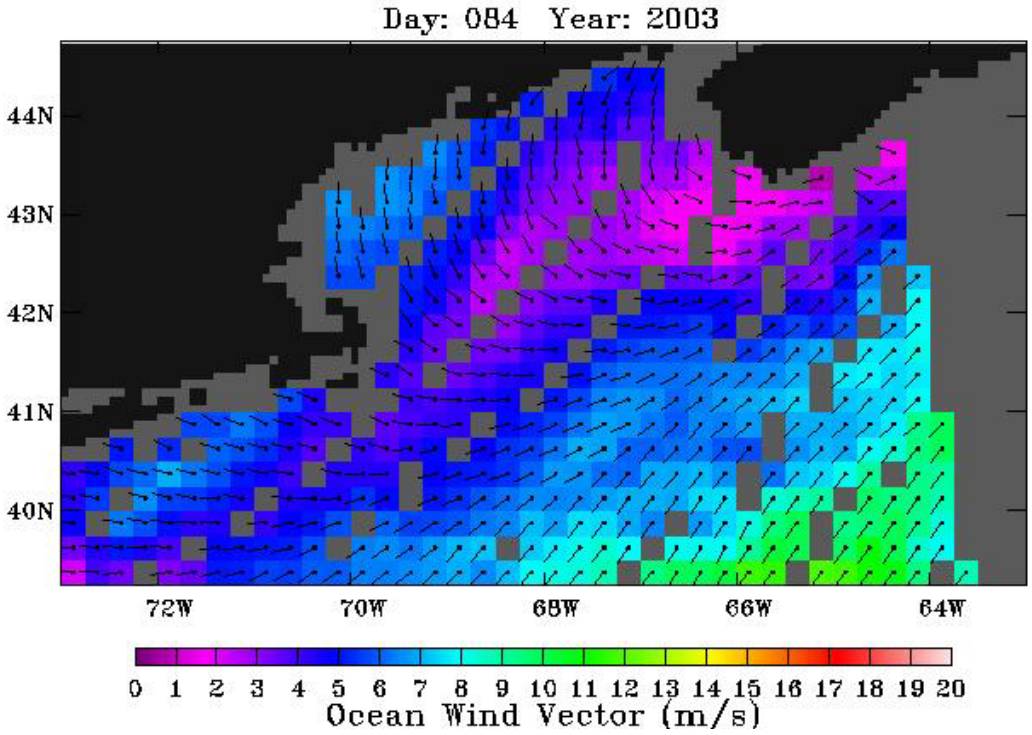

Figure 8-27. QuikSCAT wind field. Morning satellite overpass on March 25, 2003.

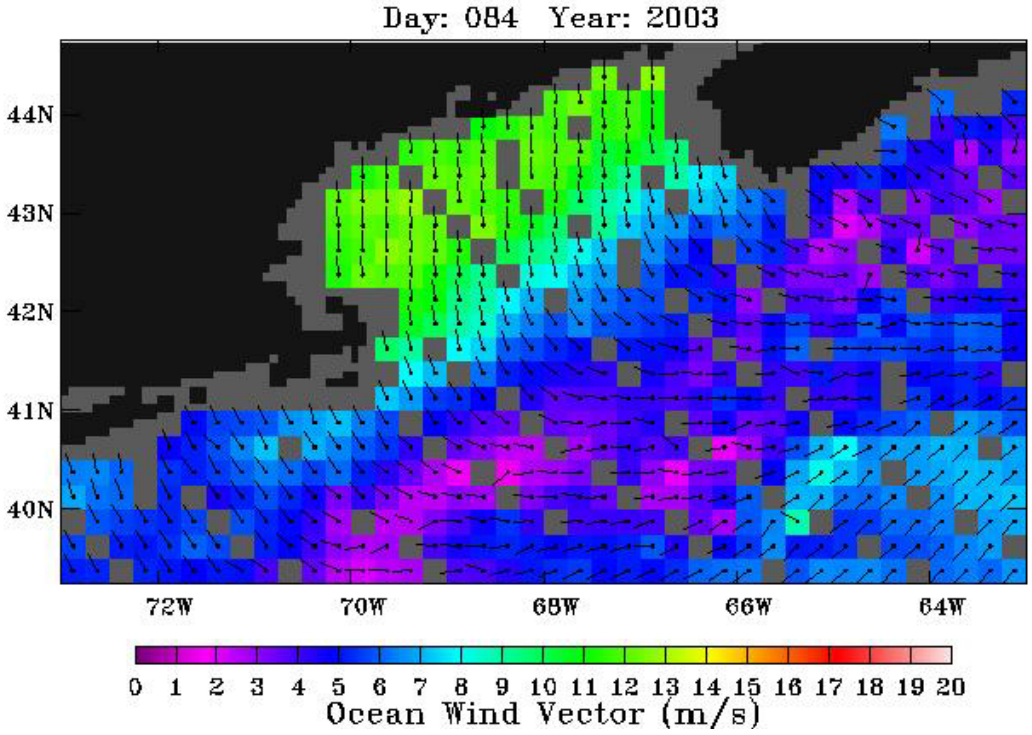

Figure 8-A28. QuikSCAT wind field. Evening satellite overpass on March 25, 2003.

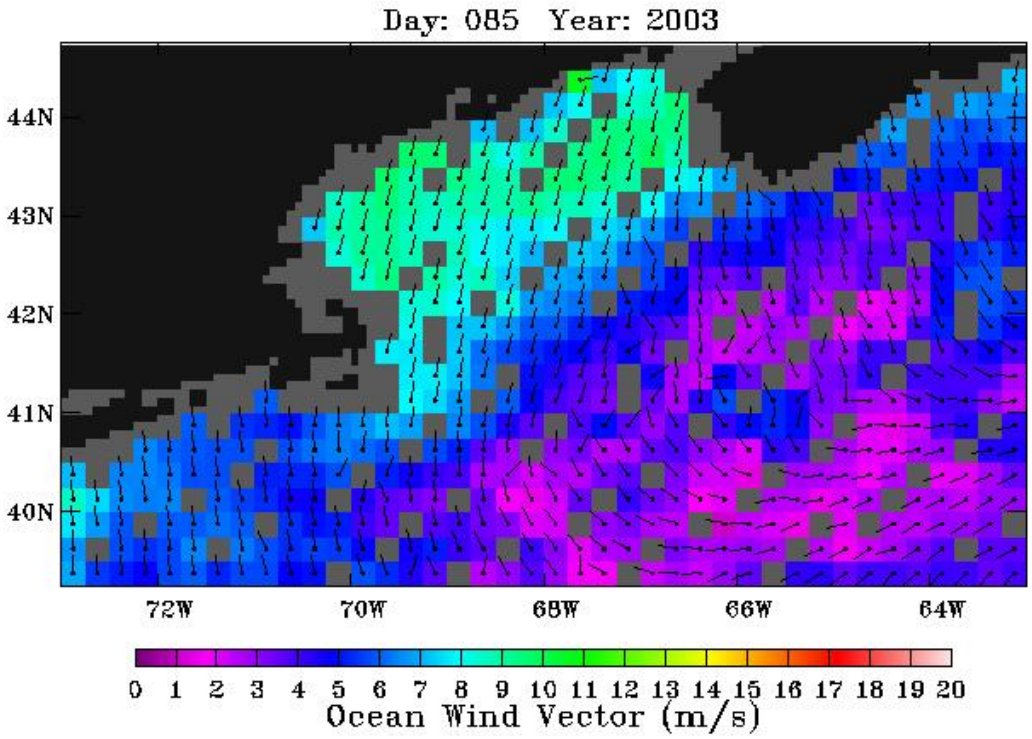

Figure 8-A29. QuikSCAT wind field. Morning satellite overpass on March 26, 2003.

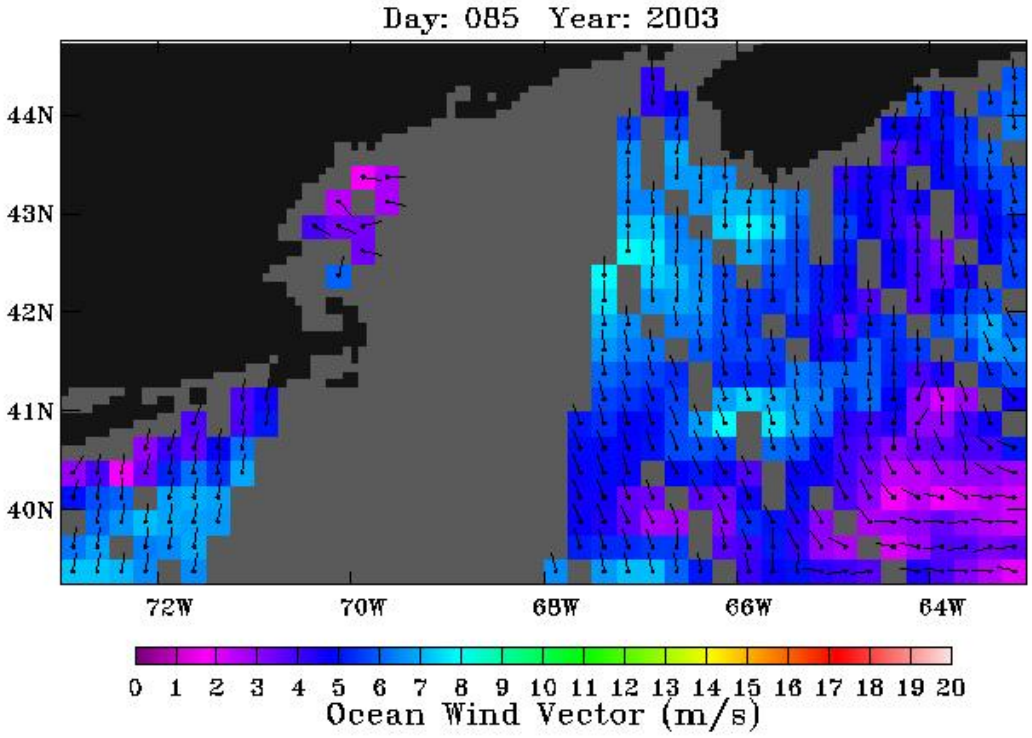

Figure 8-A30. QuikSCAT wind field. Evening satellite overpass on March 26, 2003.

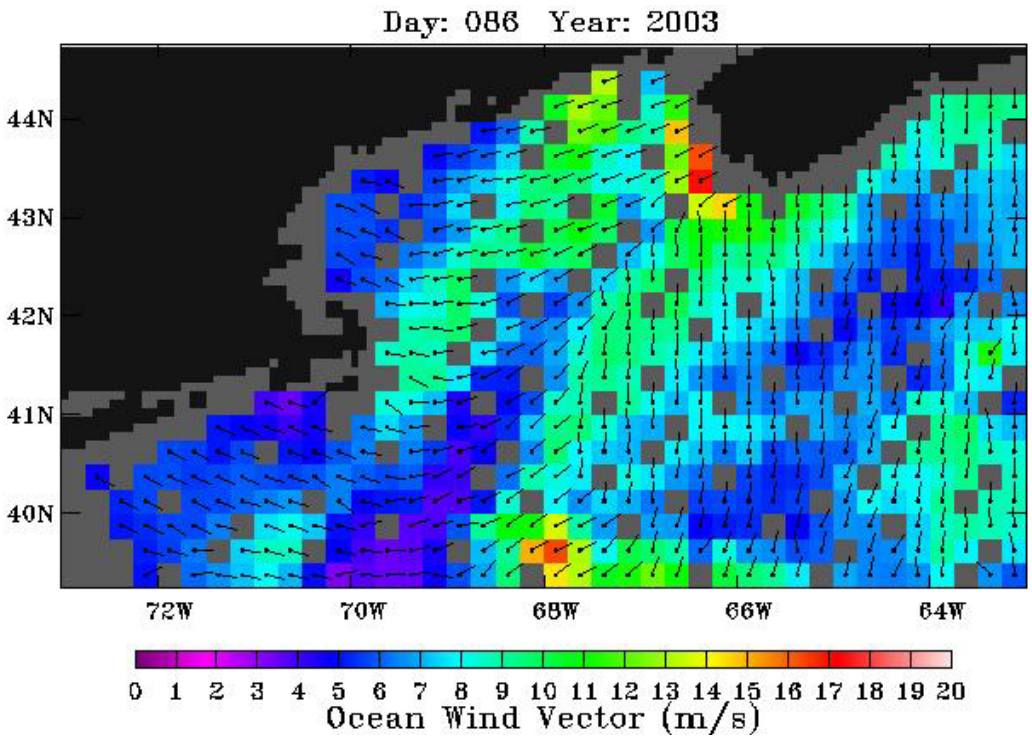

Figure 8-A31. QuikSCAT wind field. Morning satellite overpass on March 27, 2003.

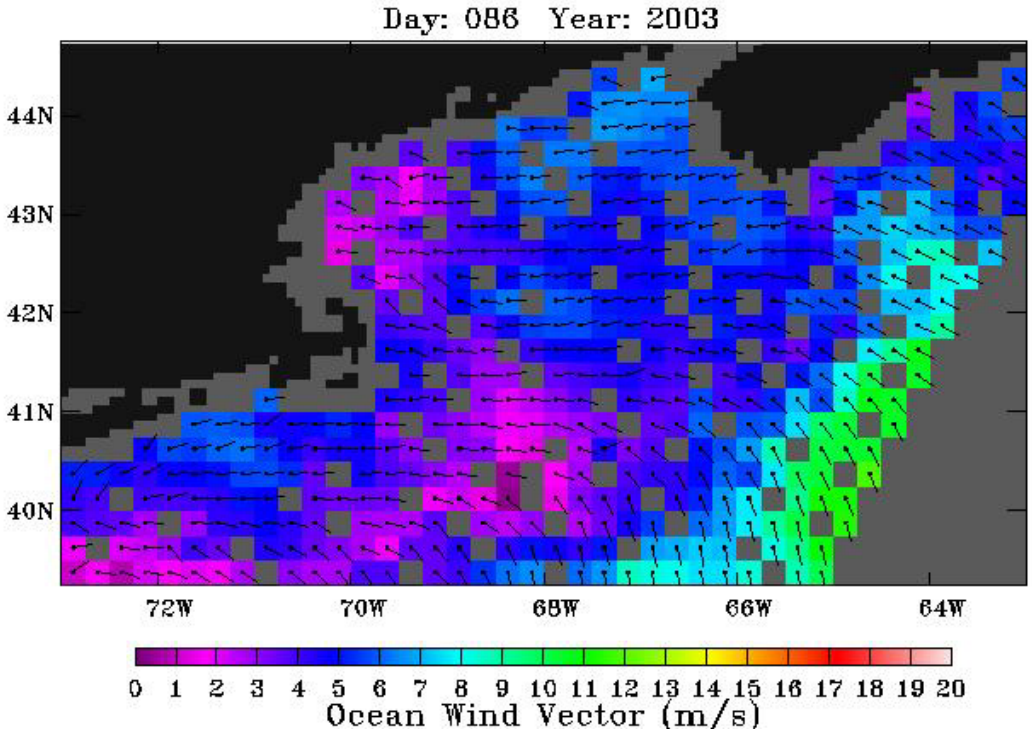

Figure 8-A32. QuikSCAT wind field. Evening satellite overpass on March 27, 2003.

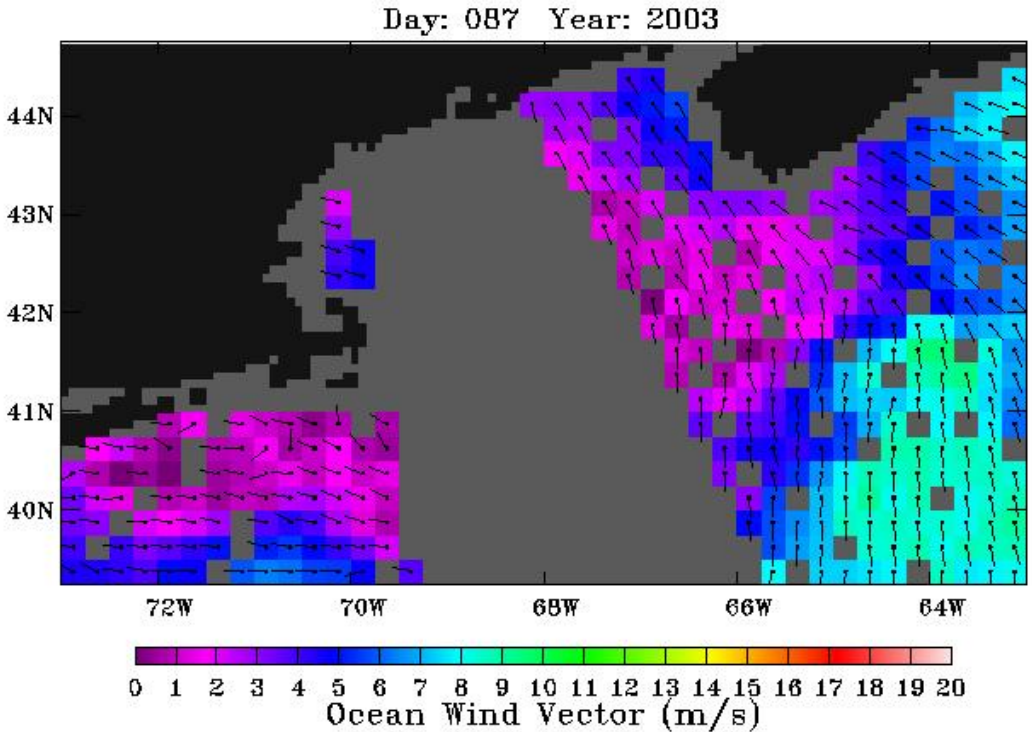

Figure 8-33. QuikSCAT wind field. Morning satellite overpass on March 28, 2003.

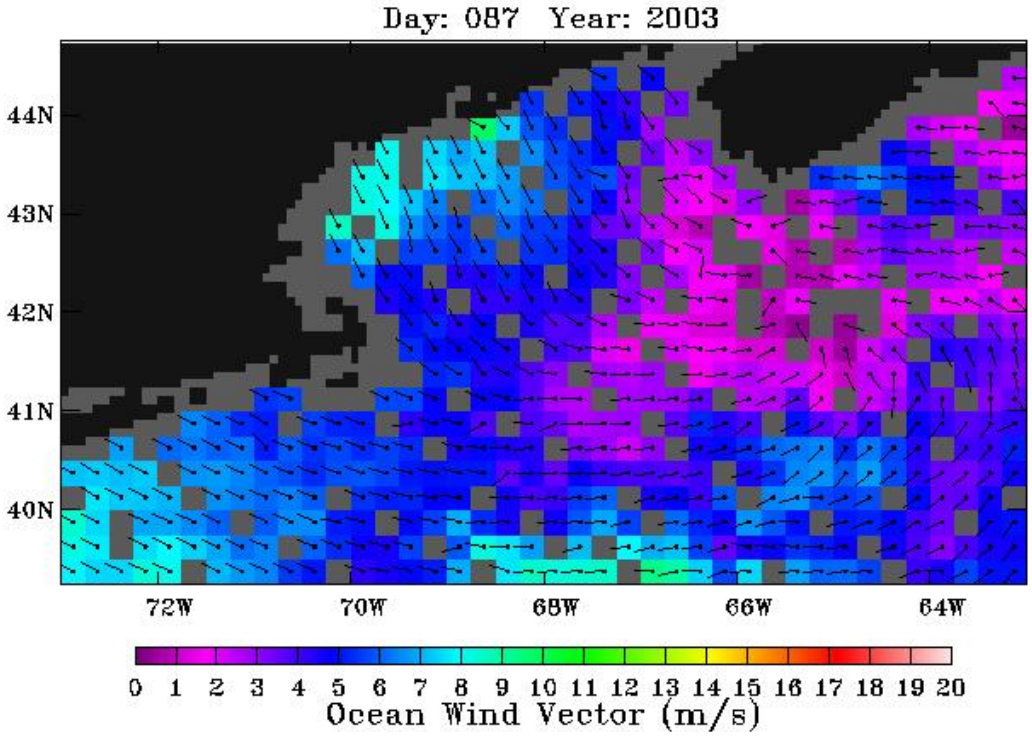

Figure 8-A34. QuikSCAT wind field. Evening satellite overpass on March 28, 2003.

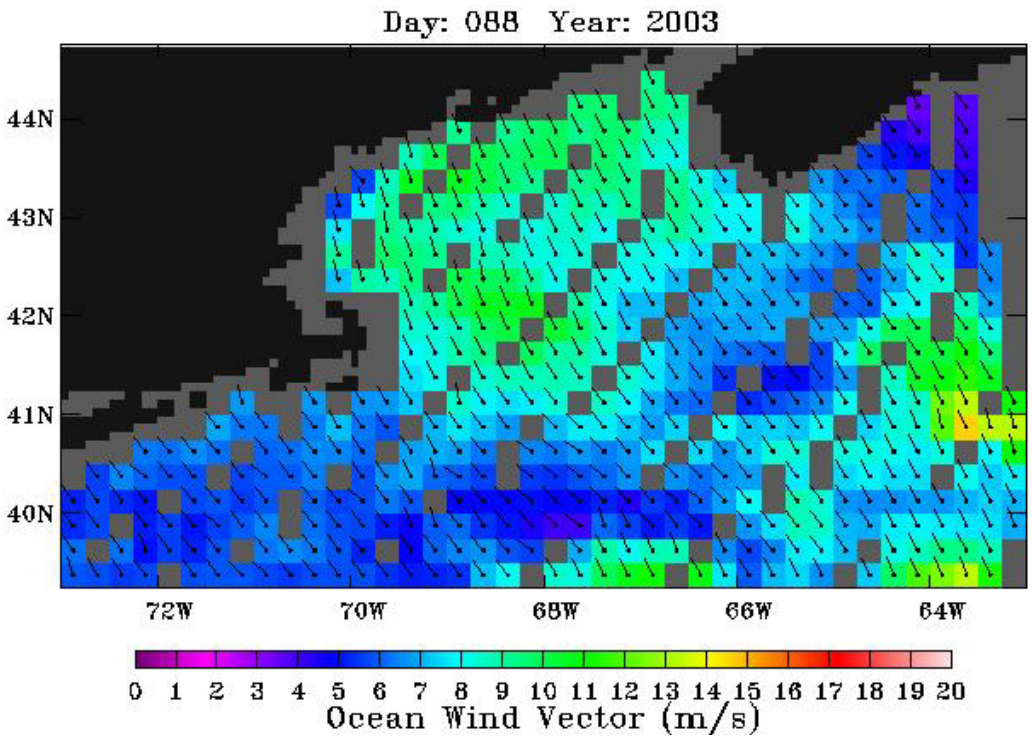

Figure 8-A35. QuikSCAT wind field. Morning satellite overpass on March 29, 2003.

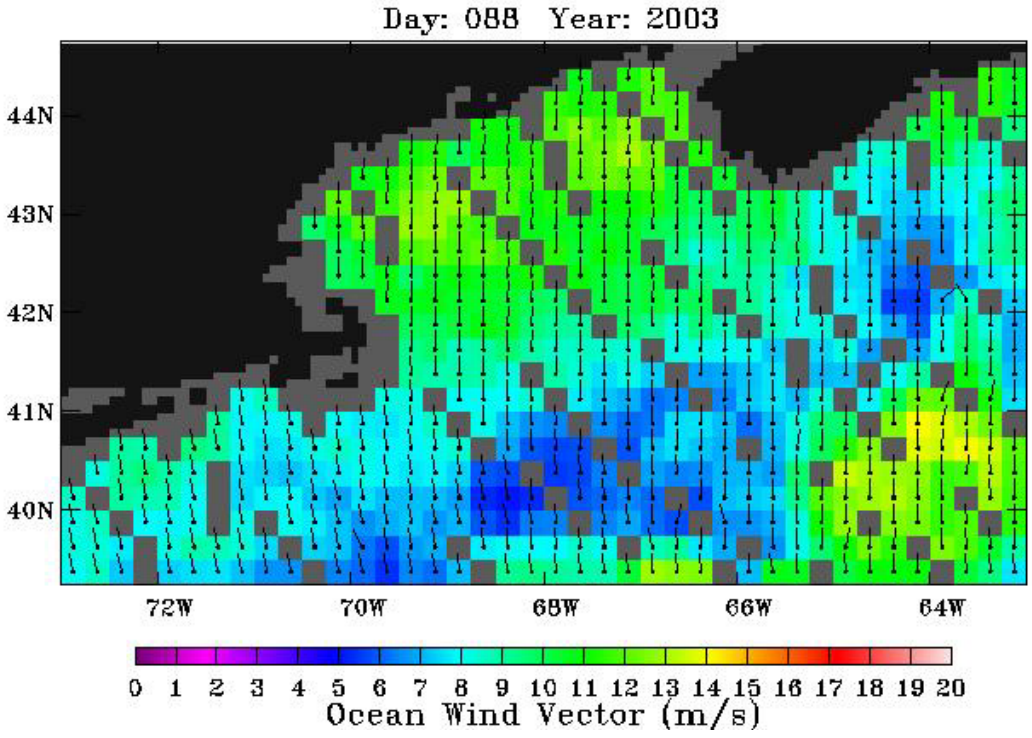

Figure 8-A36. QuikSCAT wind field. Evening satellite overpass on March 29, 2003.

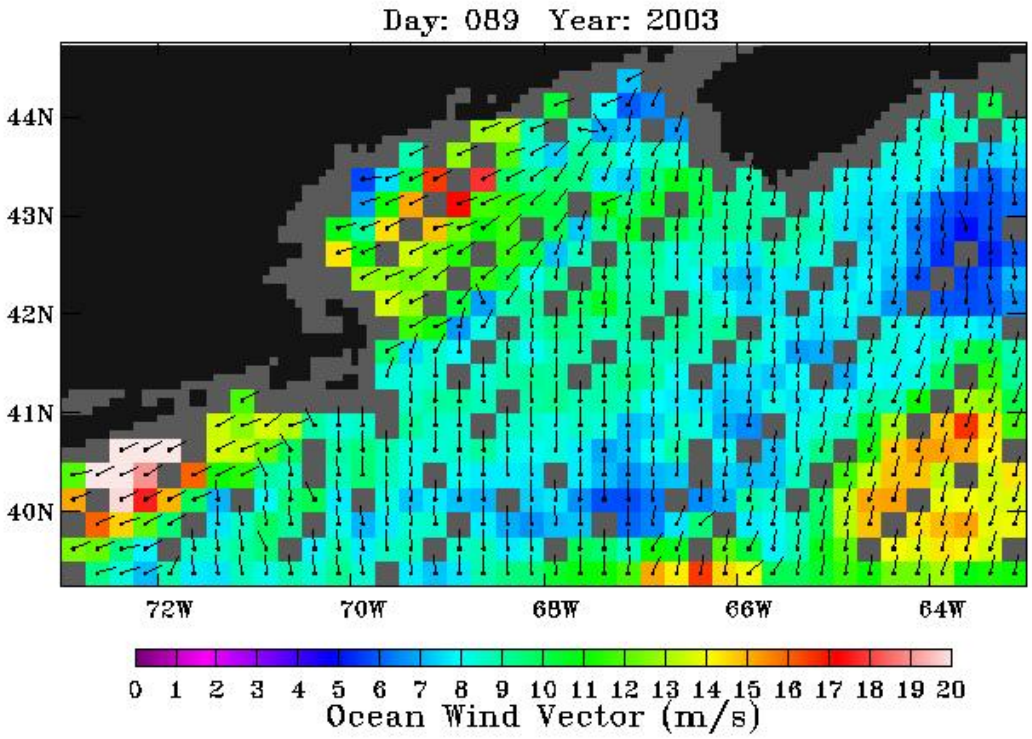

Figure 8-A37. QuikSCAT wind field. Morning satellite overpass on March 30, 2003.

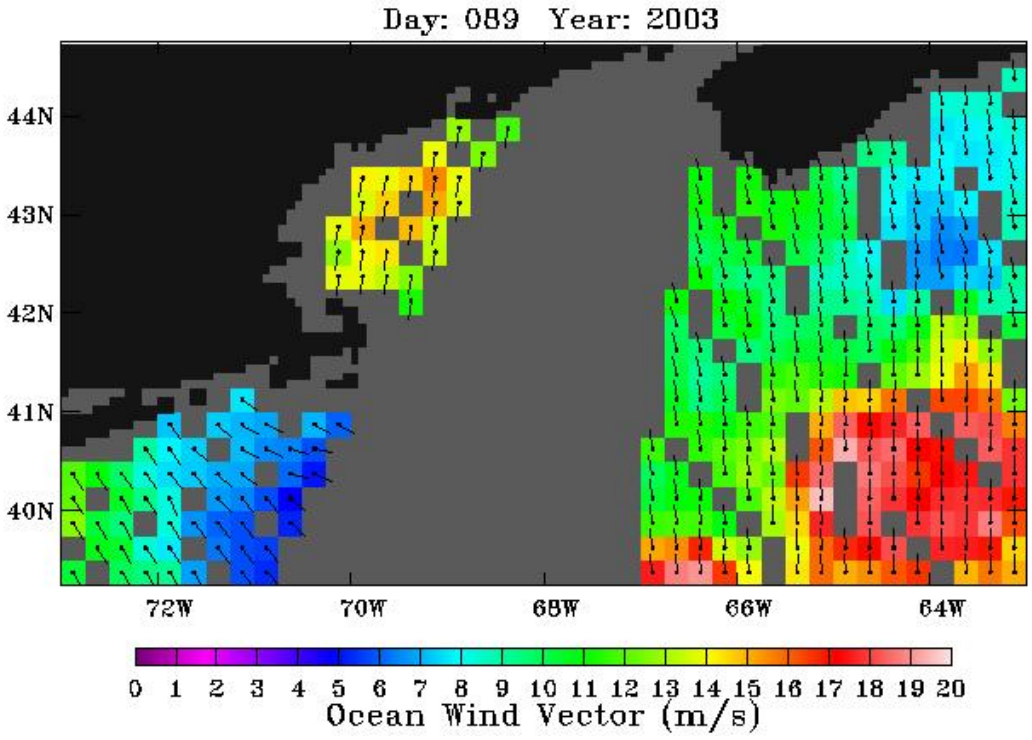

Figure 8-A38. QuikSCAT wind field. Evening satellite overpass on March 30, 2003.

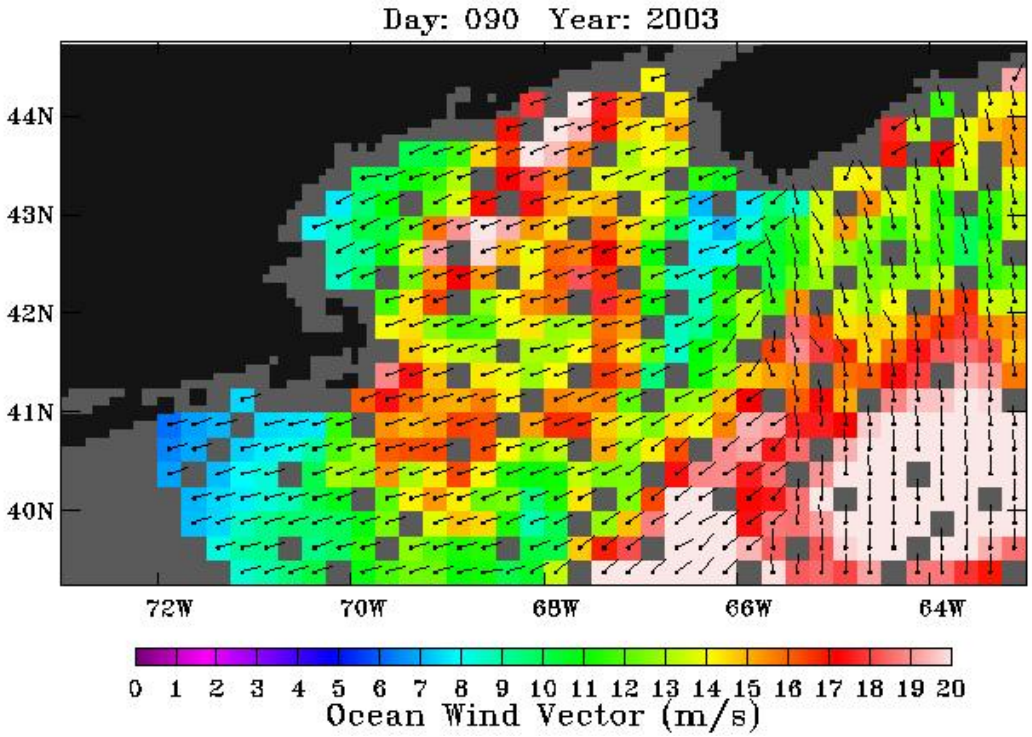

Figure 8-A39. QuikSCAT wind field. Morning satellite overpass on March 31, 2003.

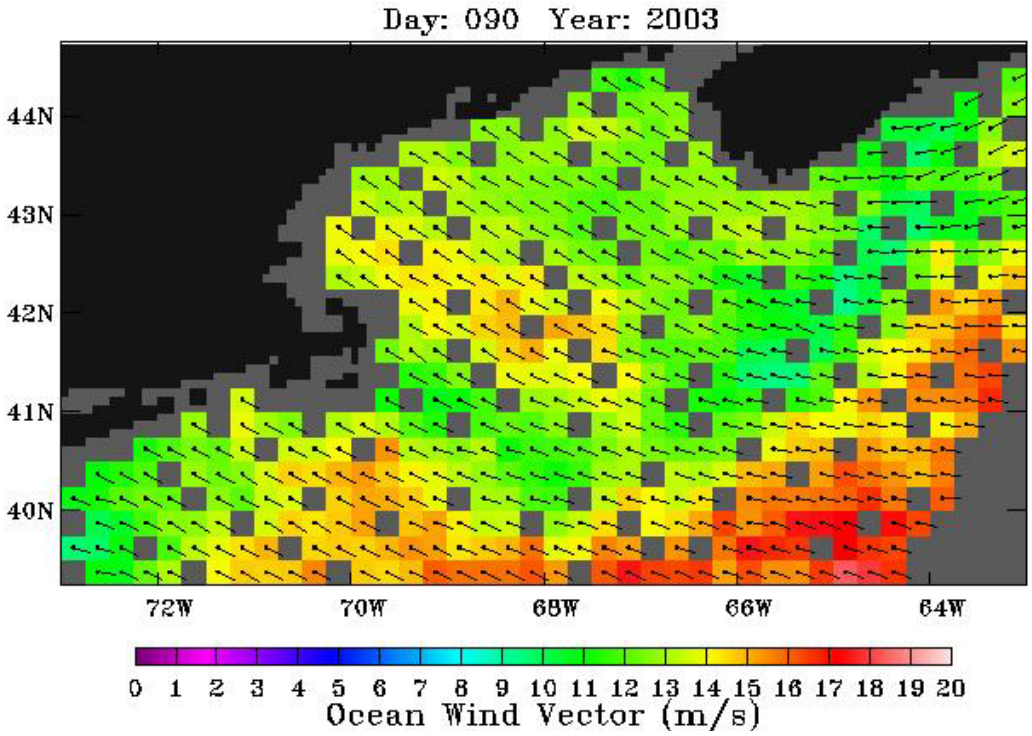

Figure 8-A40. QuikSCAT wind field. Evening satellite overpass on March 31, 2003.

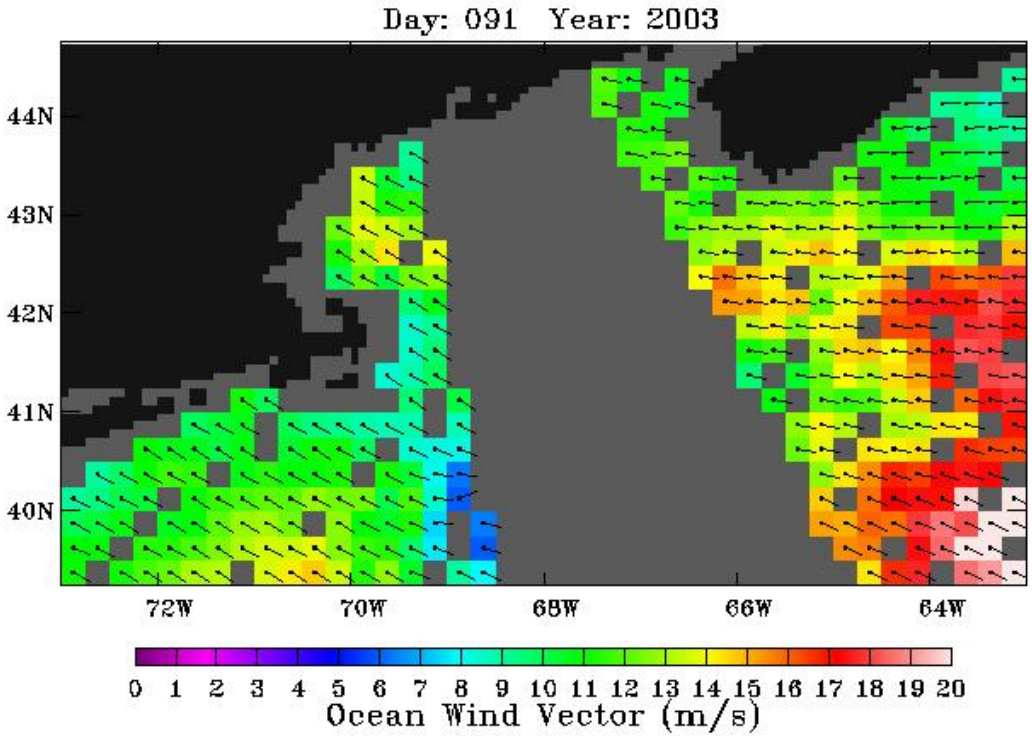

Figure 8-A41. QuikSCAT wind field. Morning satellite overpass on April 1, 2003.

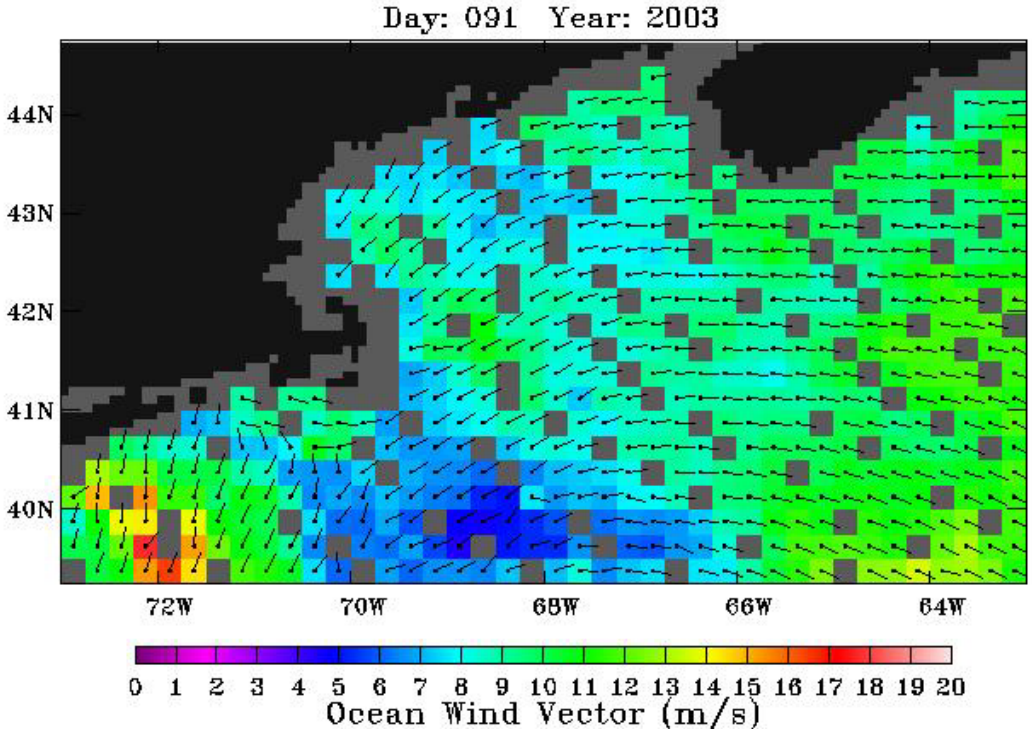

Figure 8-A42. QuikSCAT wind field. Evening satellite overpass on April 1, 2003.

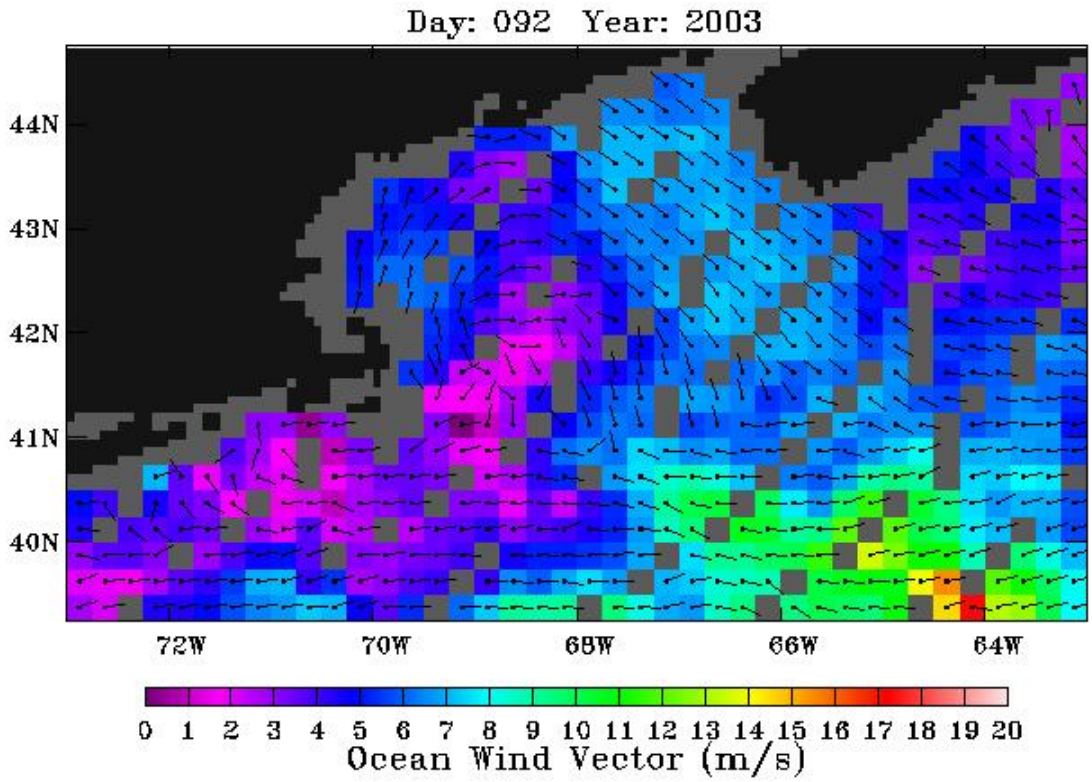

Figure 8-A43. QuikSCAT wind field. Morning satellite overpass on April 2, 2003.

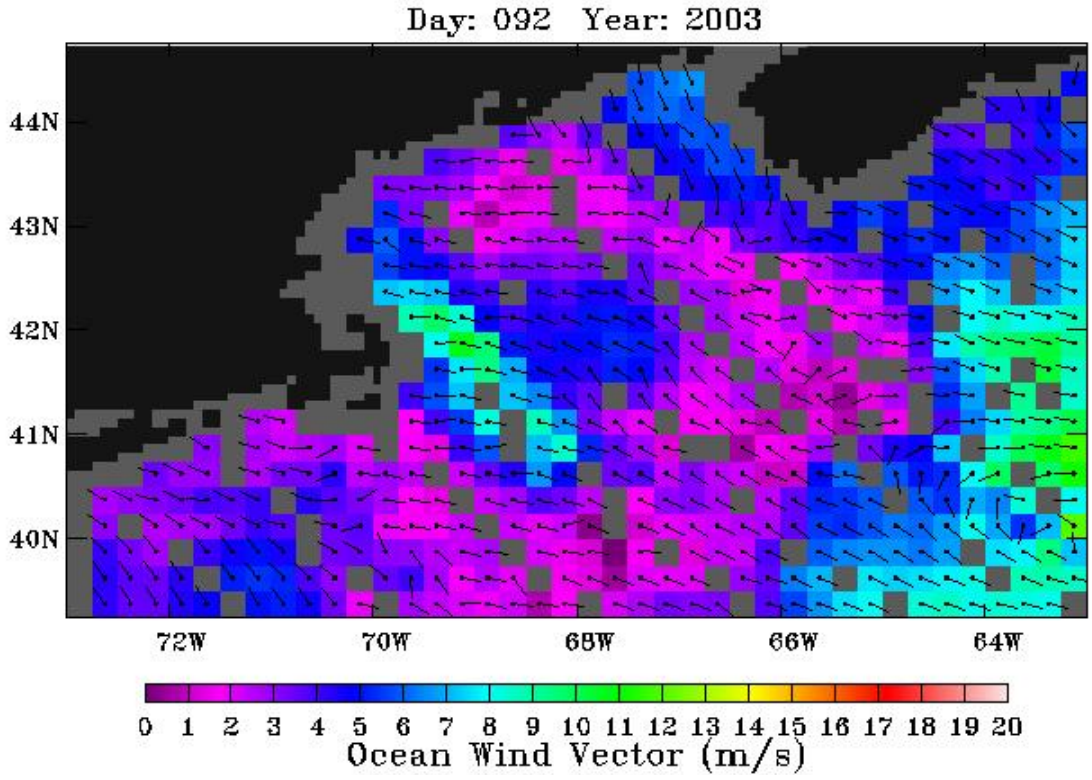

Figure 8-A44. QuikSCAT wind field. Evening satellite overpass on April 2, 2003.

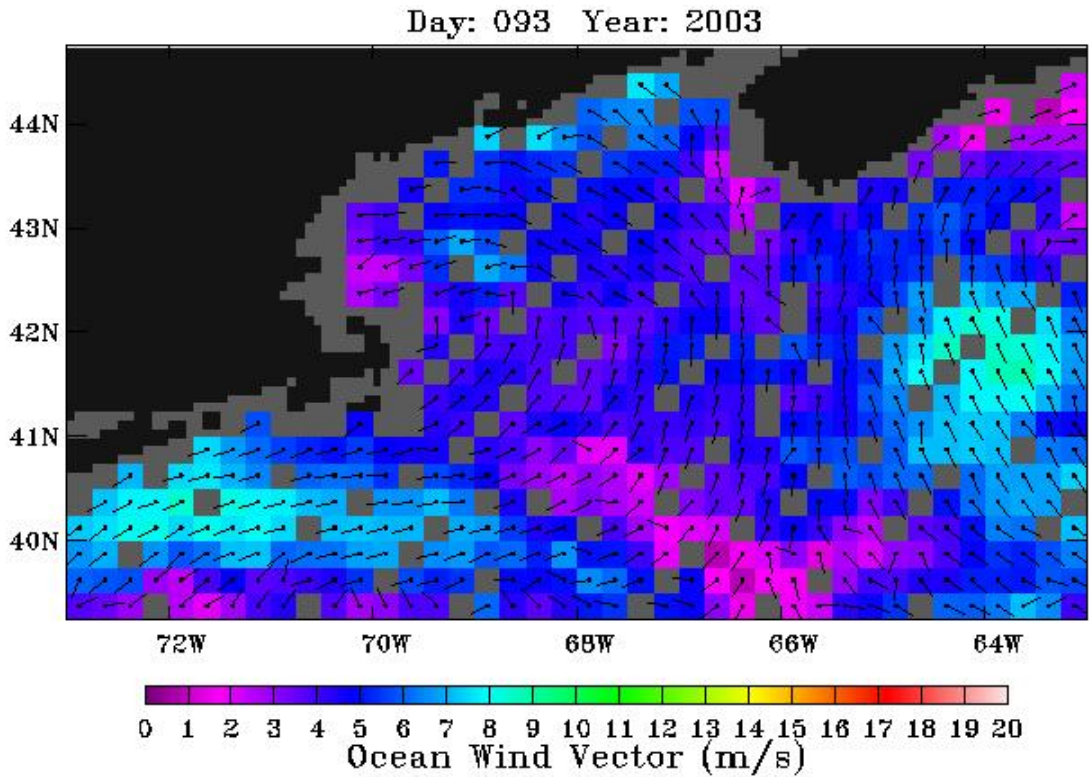

Figure 8-A45. QuikSCAT wind field. Morning satellite overpass on April 3, 2003.

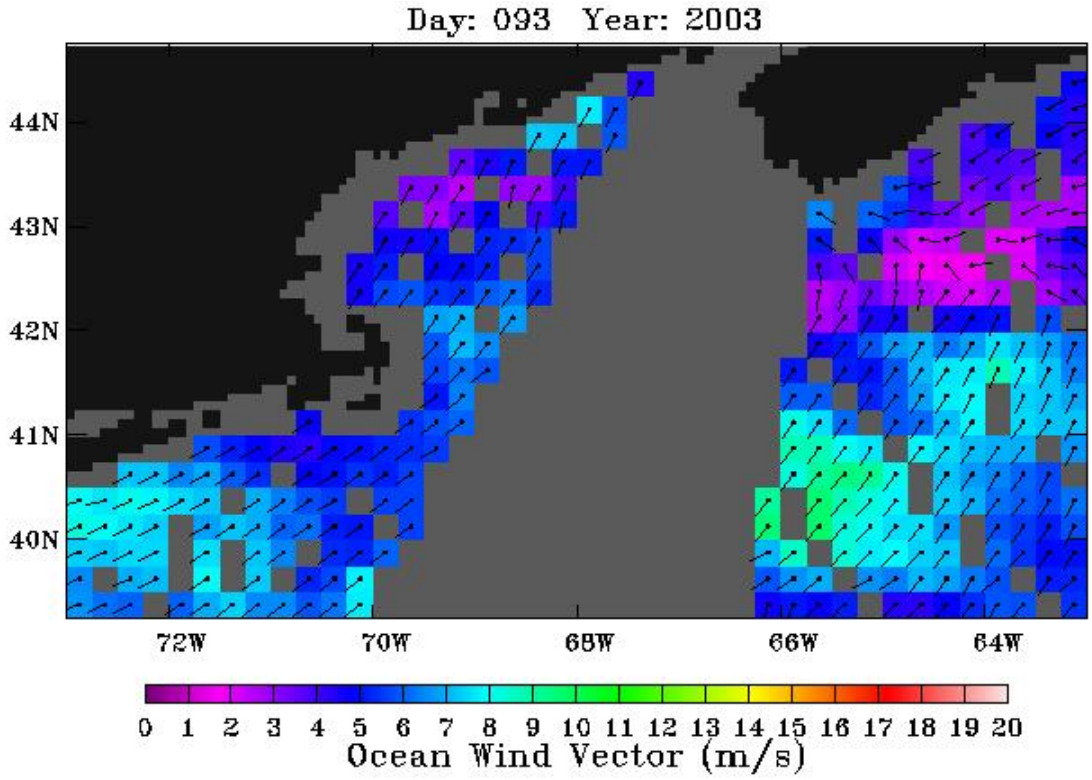

Figure 8-A46. QuikSCAT wind field. Evening satellite overpass on April 3, 2003.

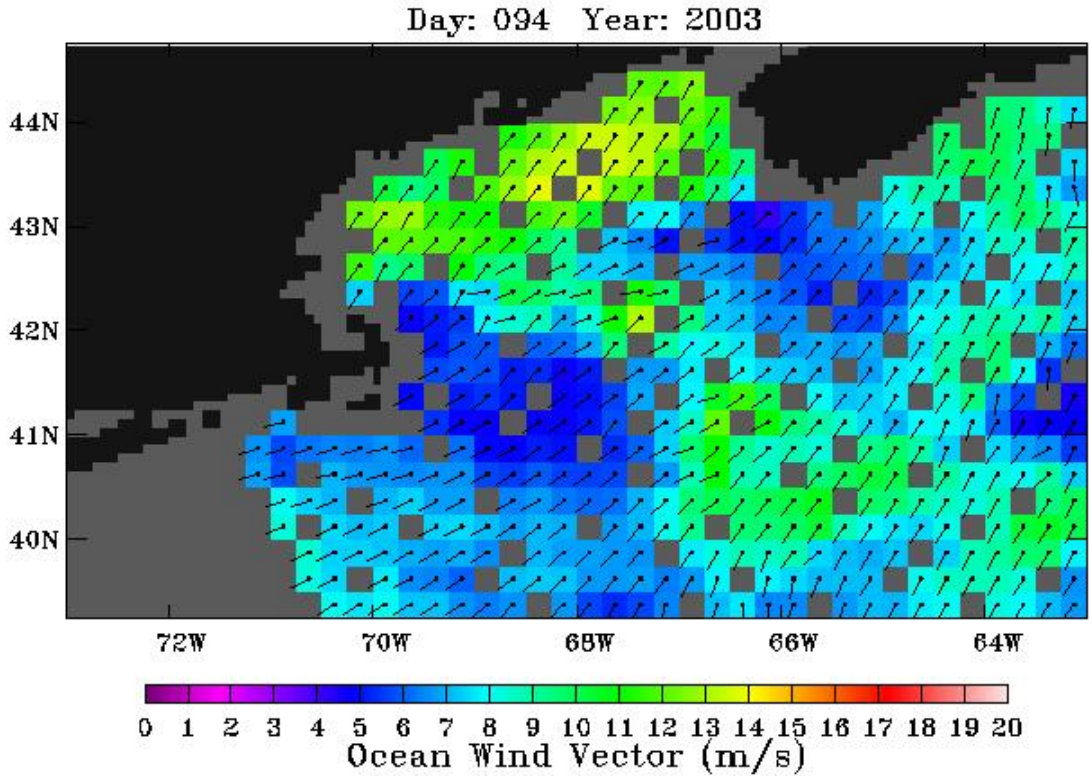

Figure 8-A47. QuikSCAT wind field. Morning satellite overpass on April 4, 2003.

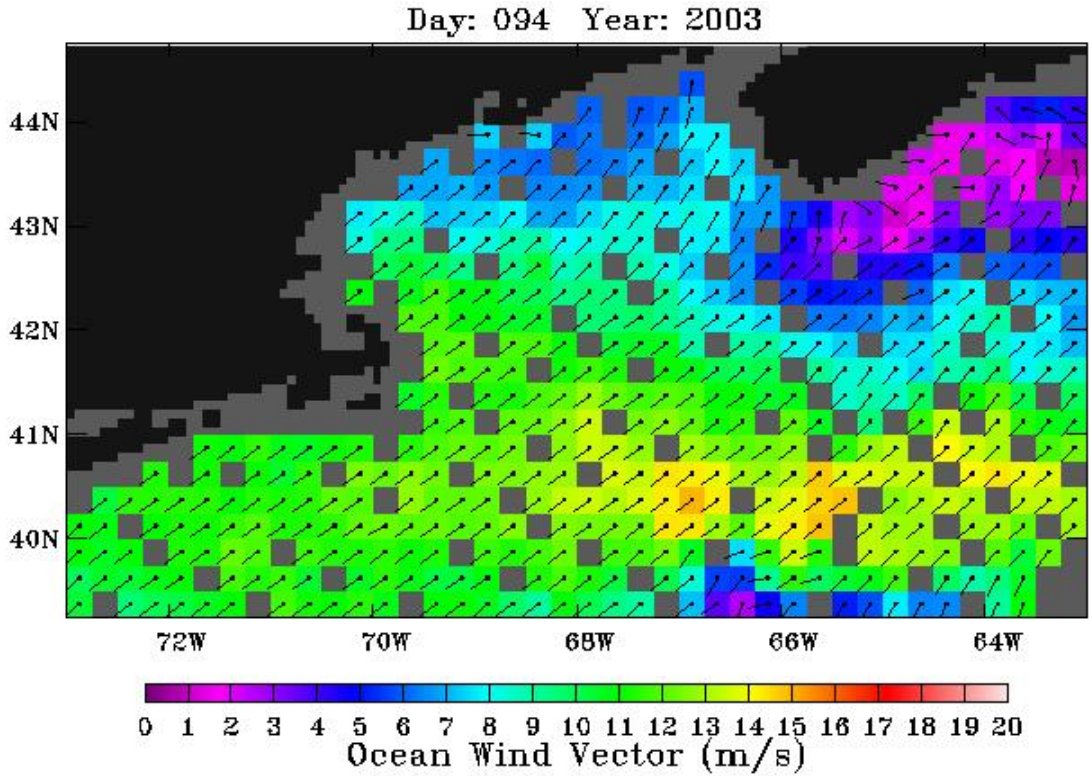

Figure 8-A48. QuikSCAT wind field. Evening satellite overpass on April 4, 2003.

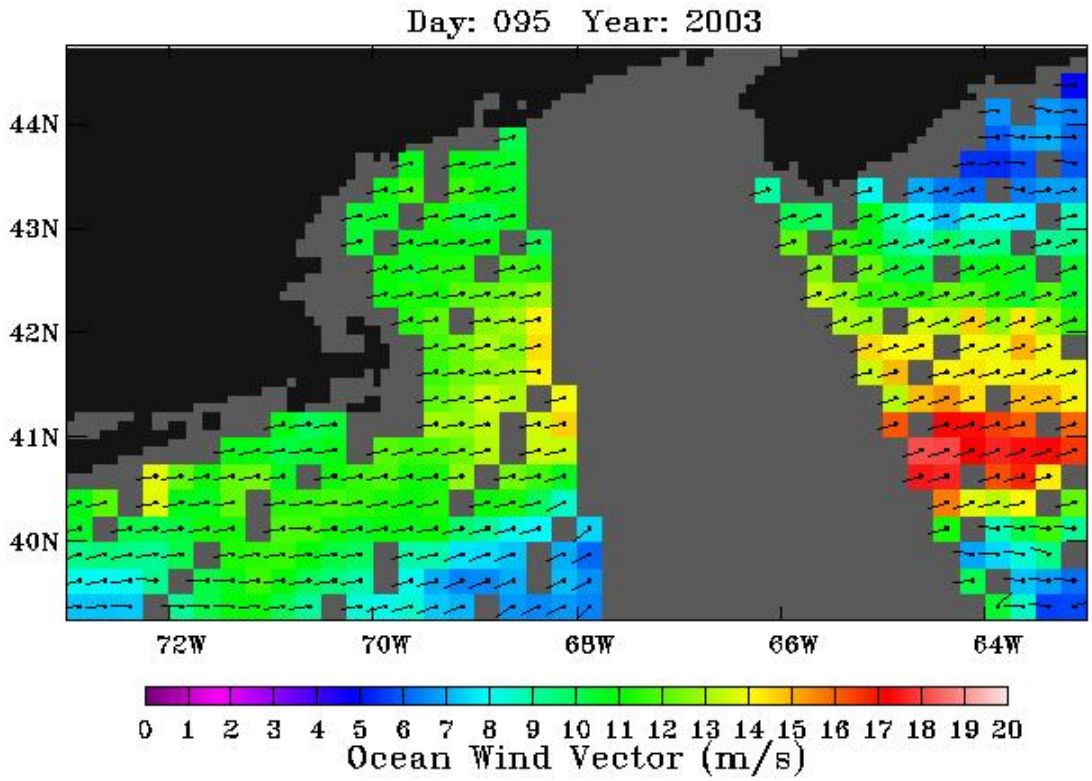

Figure 8-A49. QuikSCAT wind field. Morning satellite overpass on April 5, 2003.

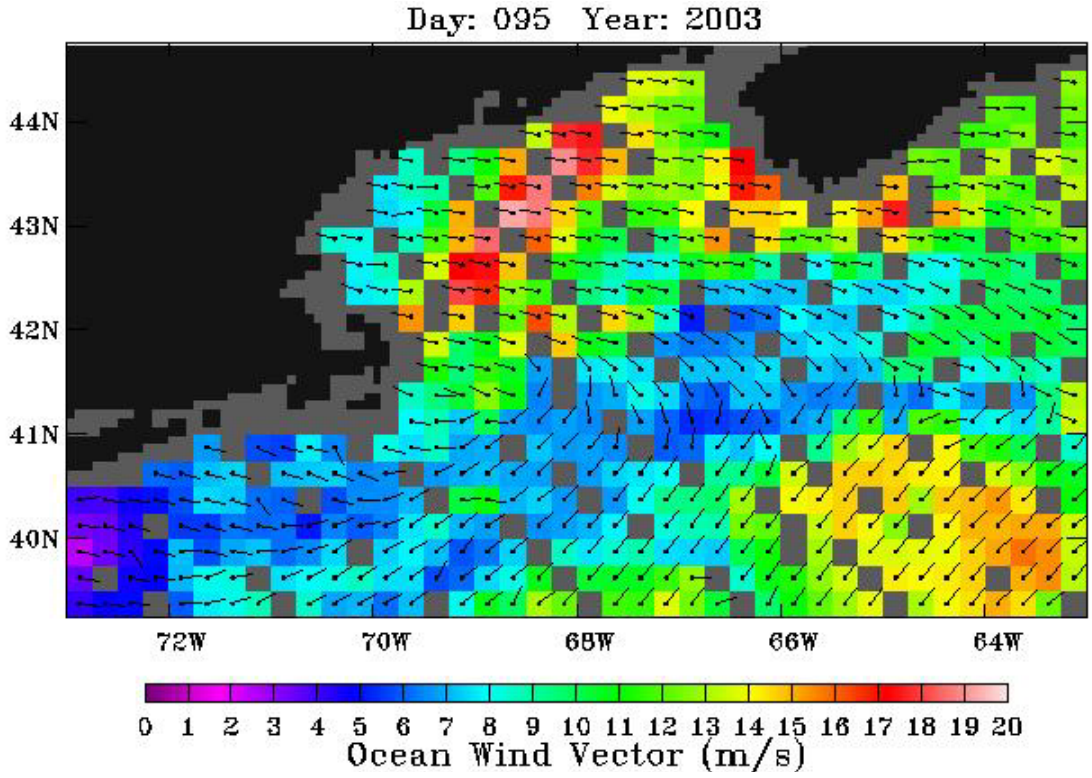

Figure 8-A50. QuikSCAT wind field. Evening satellite overpass on April 5, 2003.

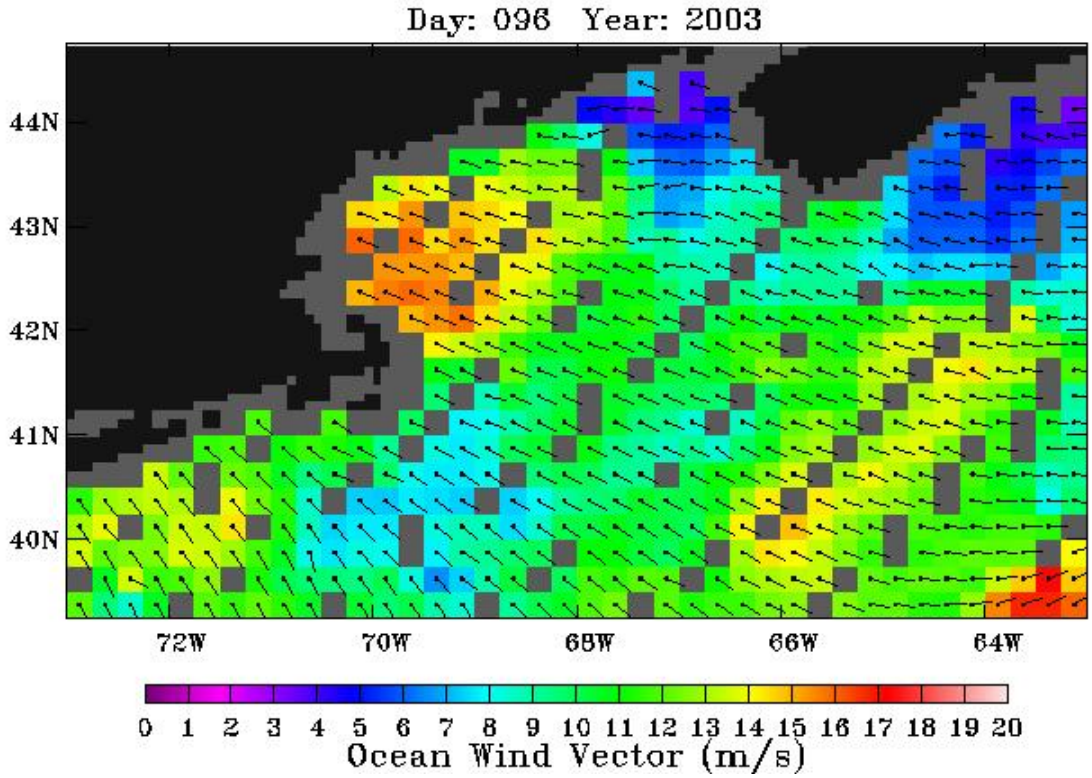

Figure 8-A51. QuikSCAT wind field. Morning satellite overpass on April 6, 2003.

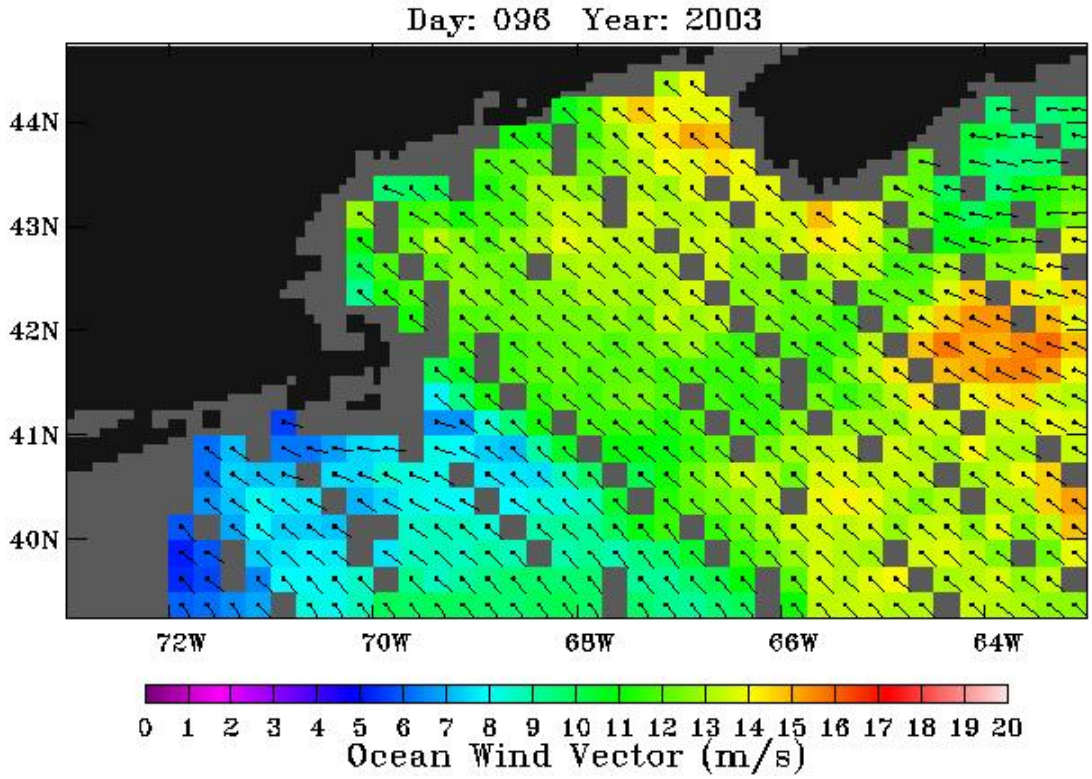

Figure 8-A52. QuikSCAT wind field. Evening satellite overpass on April 6, 2003.

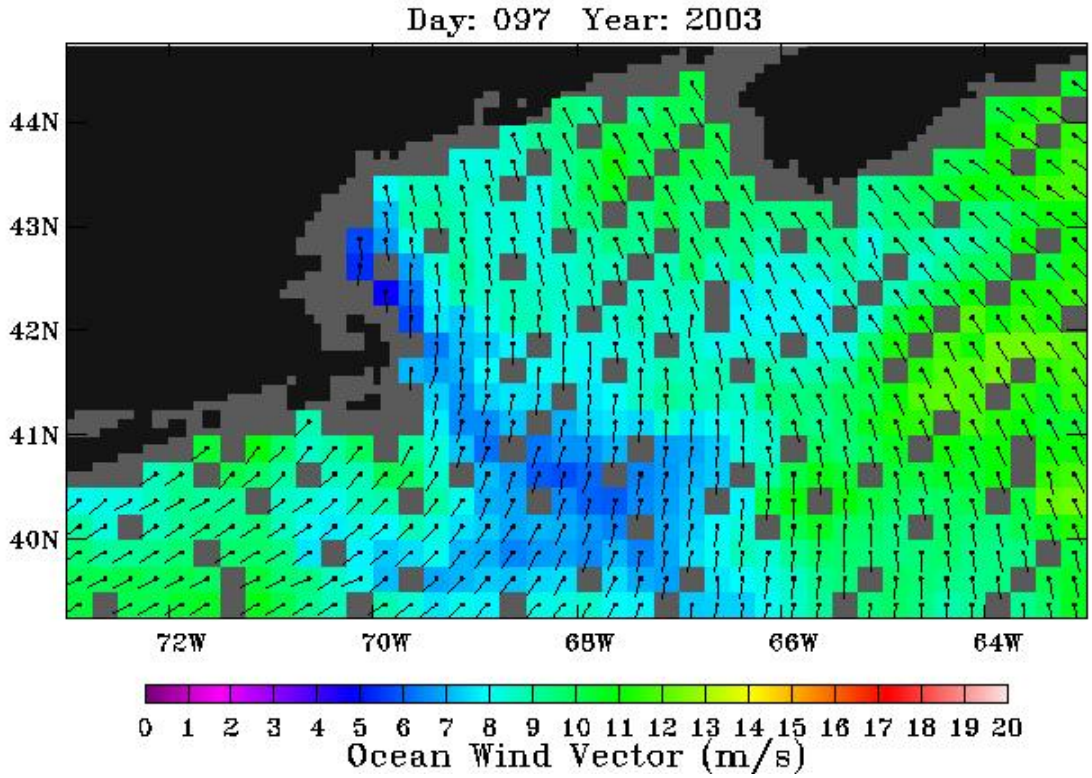

Figure 8-A53. QuikSCAT wind field. Morning satellite overpass on April 7, 2003.

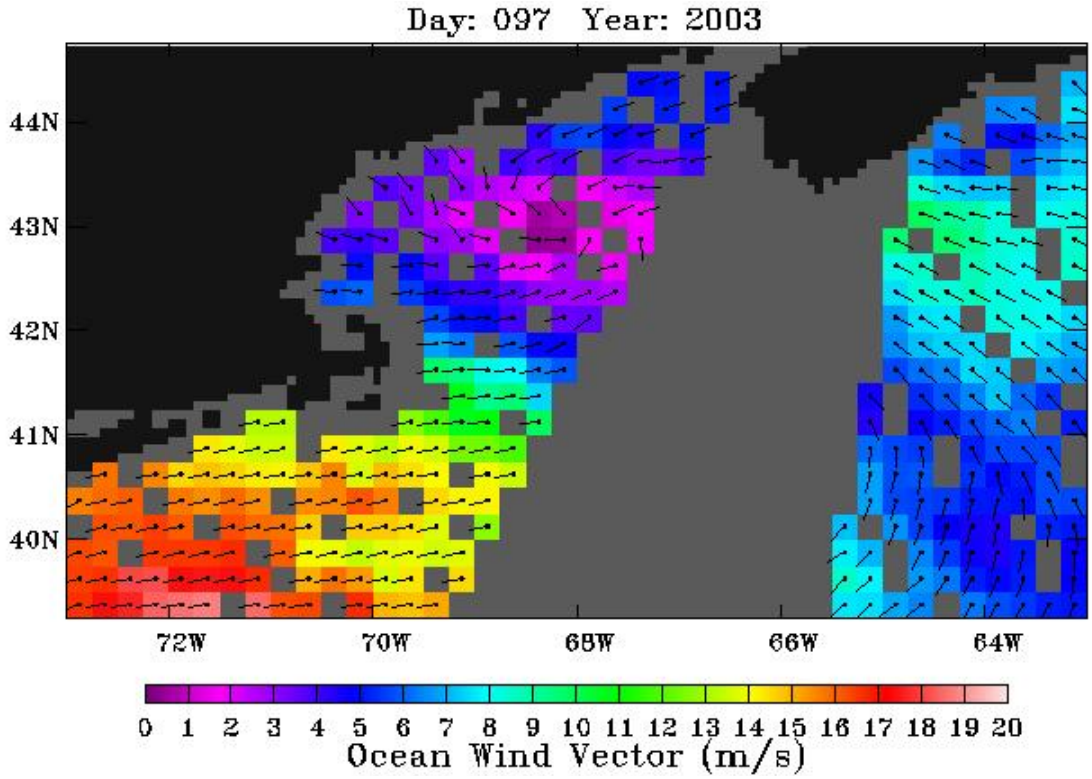

Figure 8-A54. QuikSCAT wind field. Evening satellite overpass on April 7, 2003.

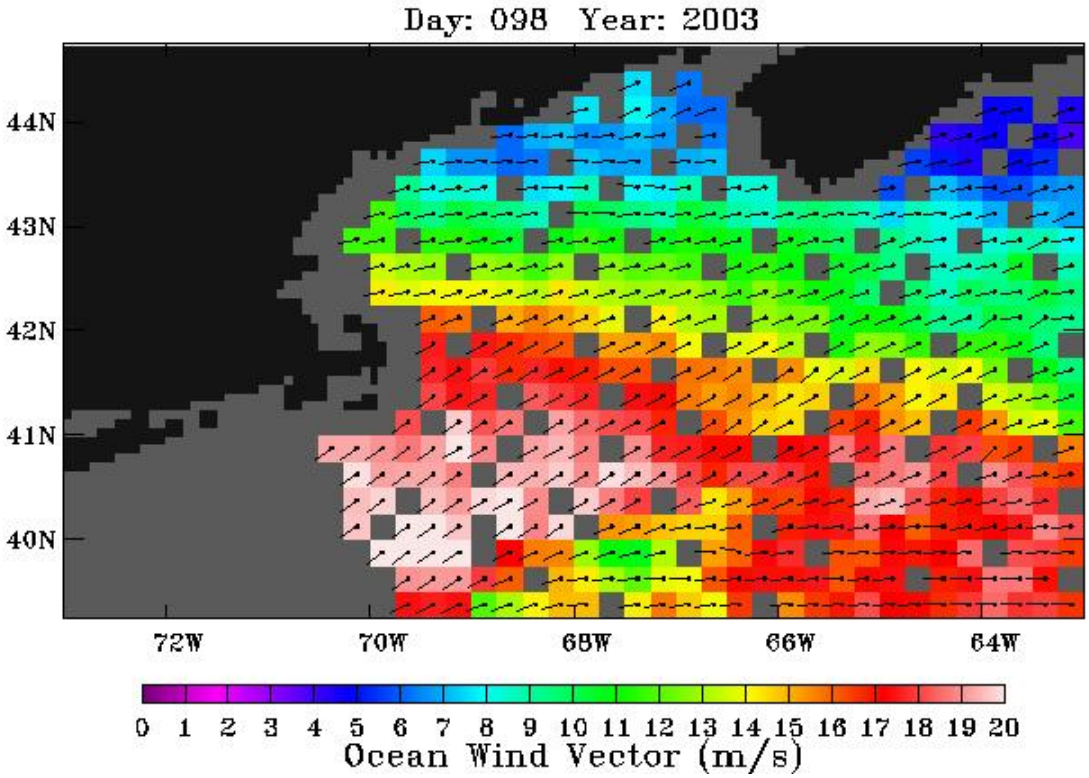

Figure 8-A55. QuikSCAT wind field. Morning satellite overpass on April 8, 2003.

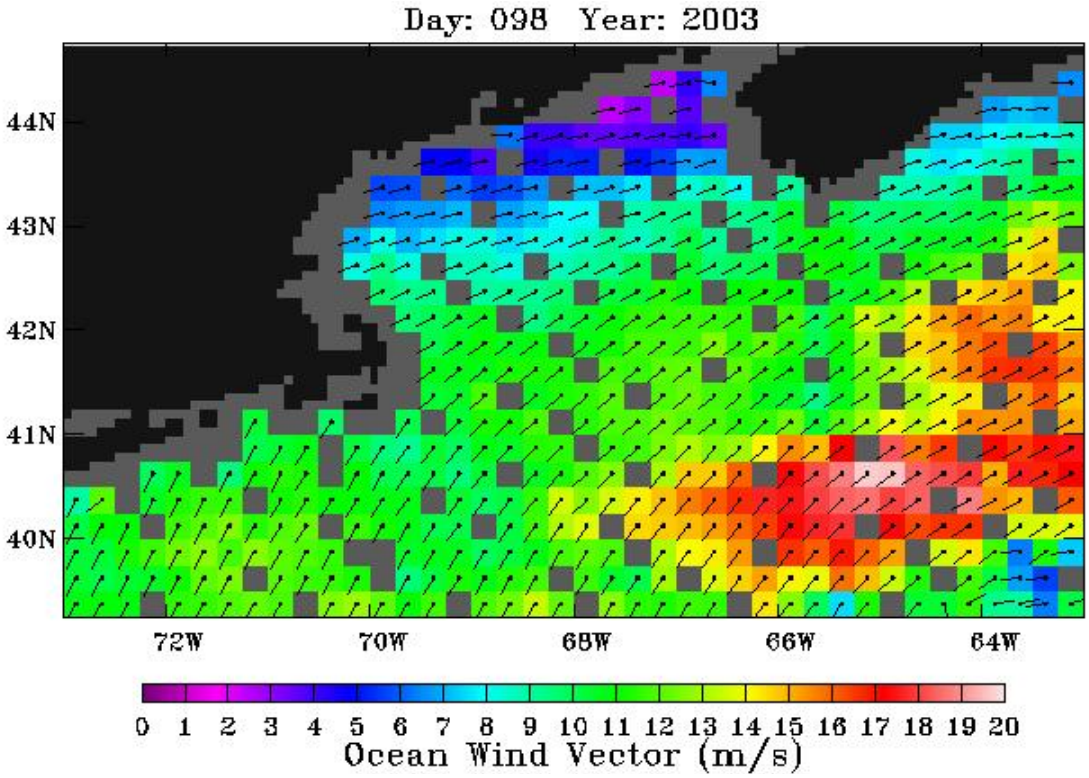

Figure 8-A56. QuikSCAT wind field. Evening satellite overpass on April 8, 2003.

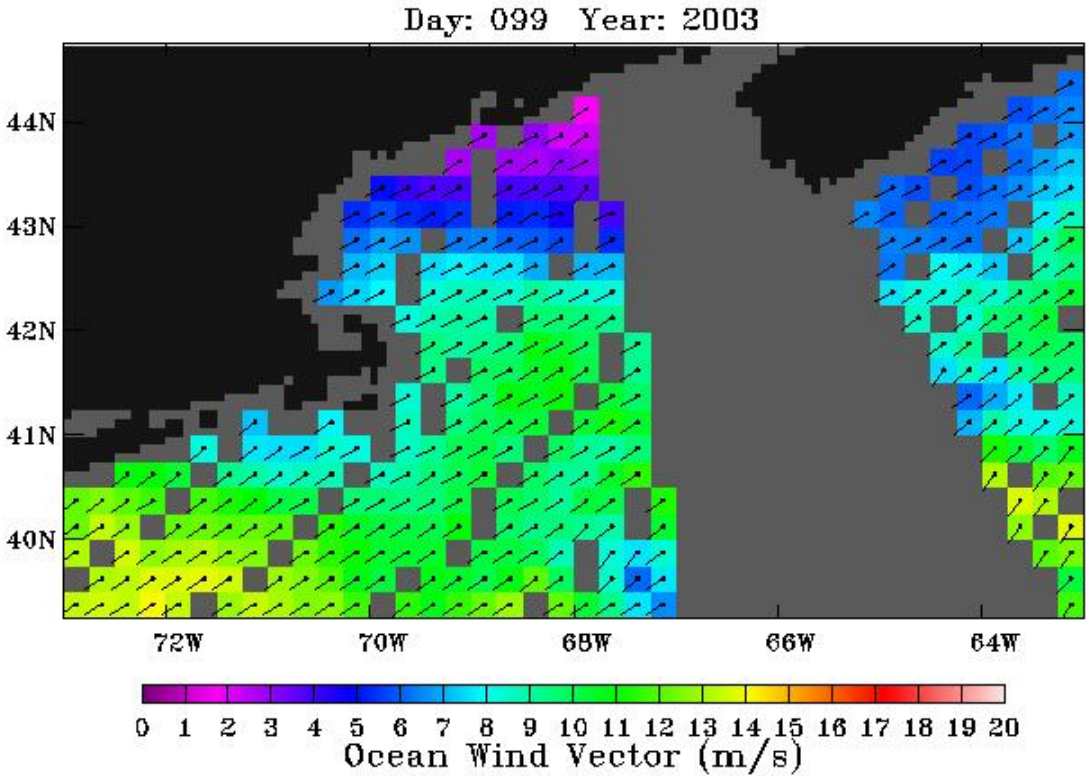

Figure 8-A57. QuikSCAT wind field. Morning satellite overpass on April 9, 2003.

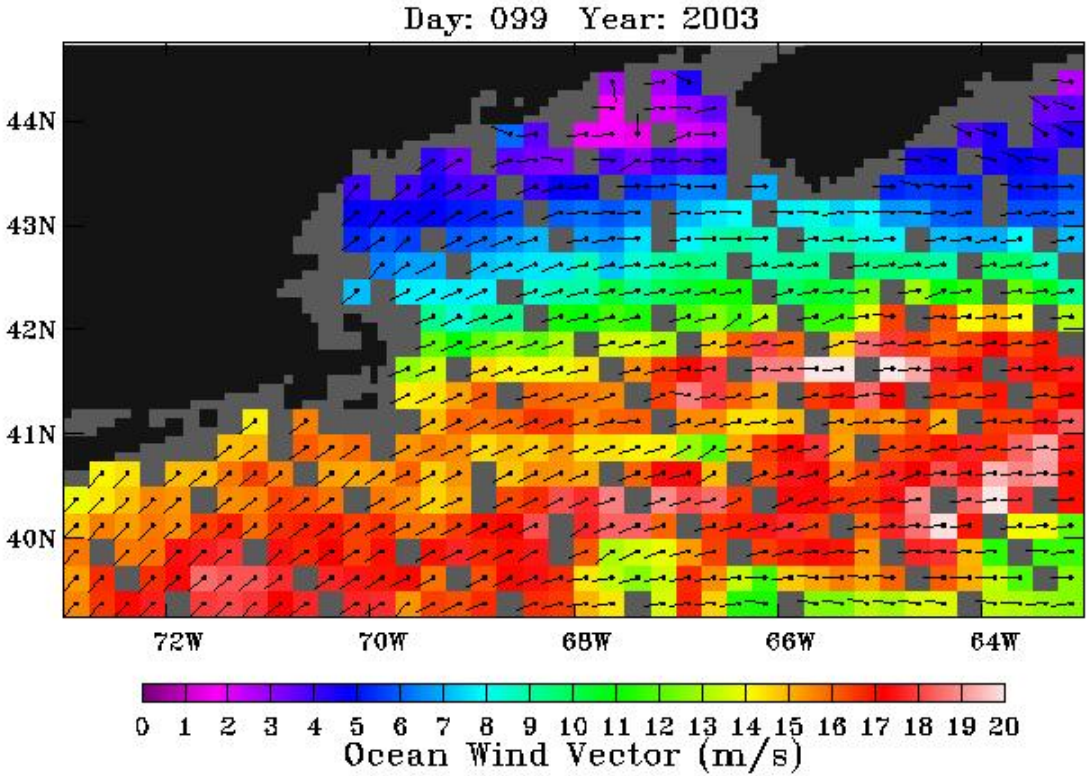

Figure 8-A58. QuikSCAT wind field. Evening satellite overpass on April 9, 2003.

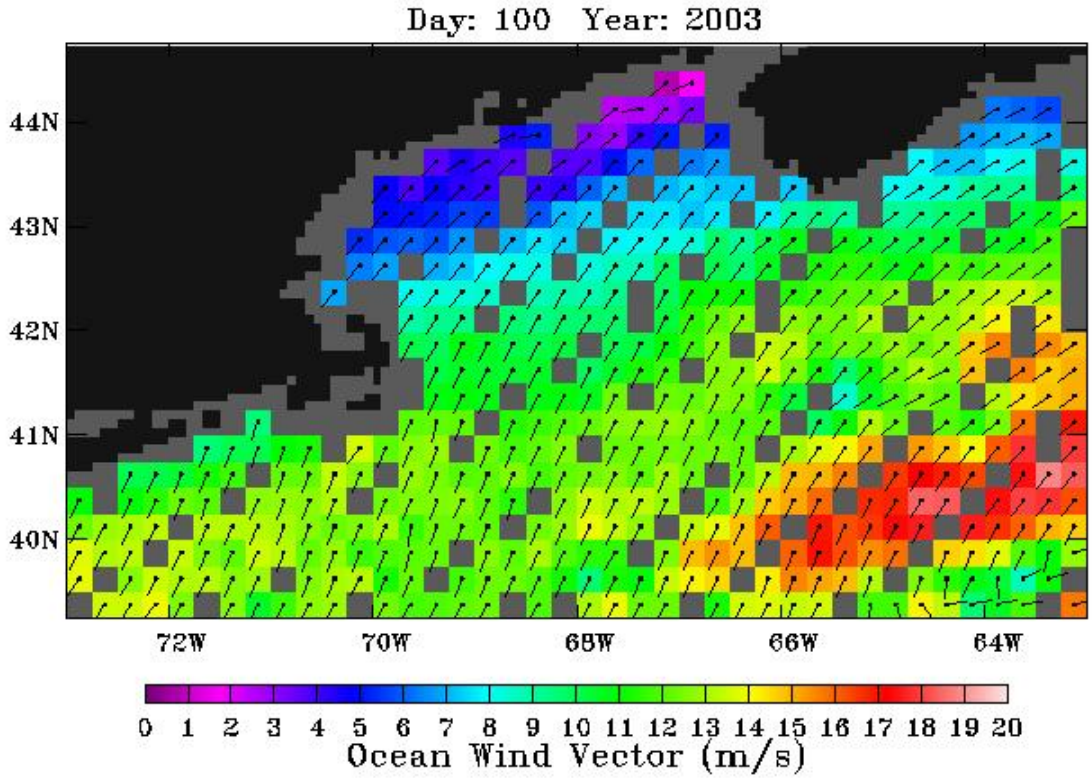

Figure 8-A59. QuikSCAT wind field. Morning satellite overpass on April 10, 2003.

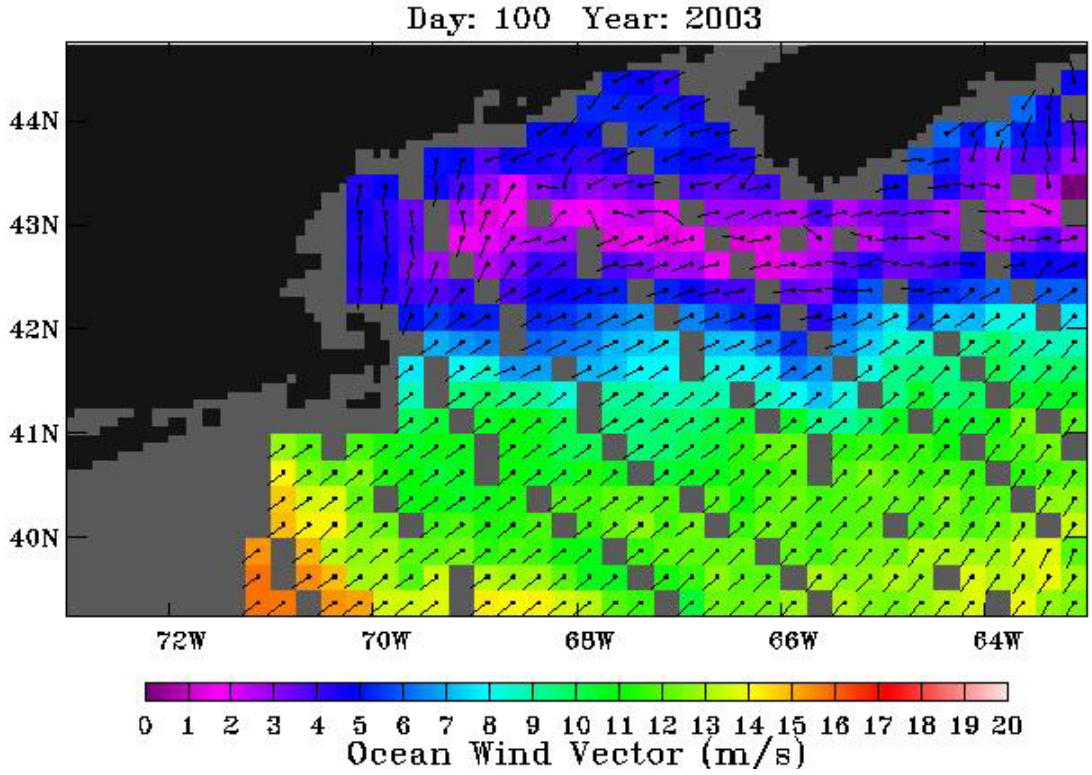

Figure 8-A60. QuikSCAT wind field. Evening satellite overpass on April 10, 2003.

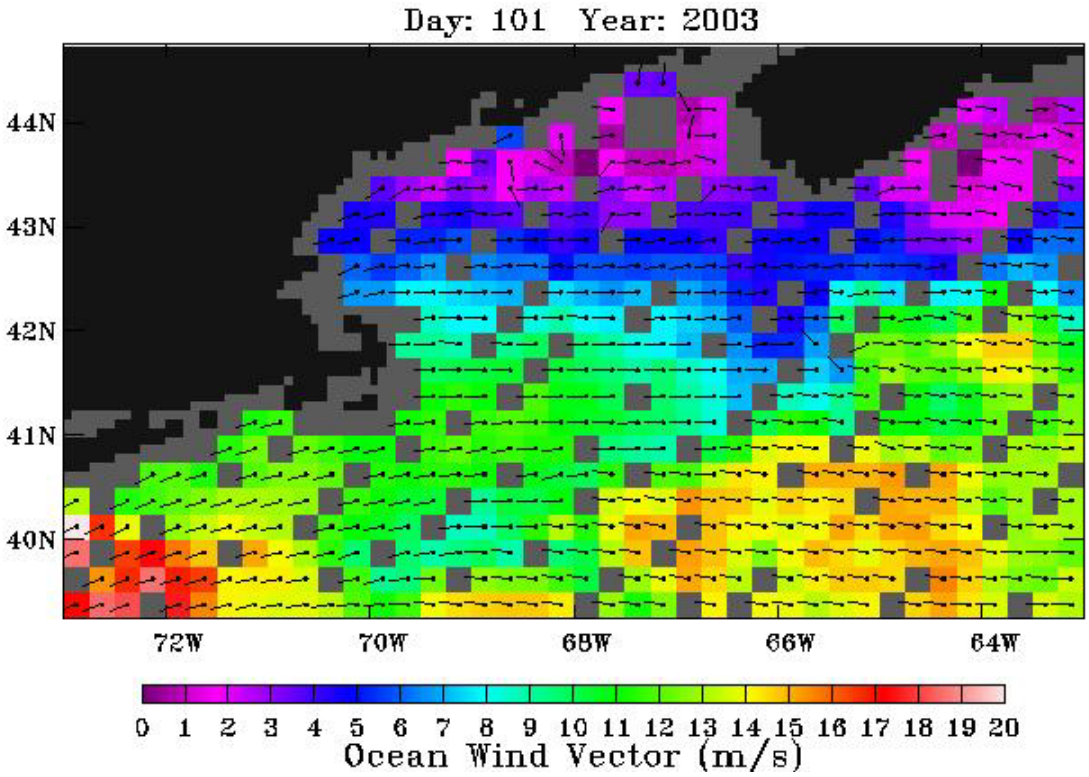

Figure 8-A61. QuikSCAT wind field. Morning satellite overpass on April 11, 2003.

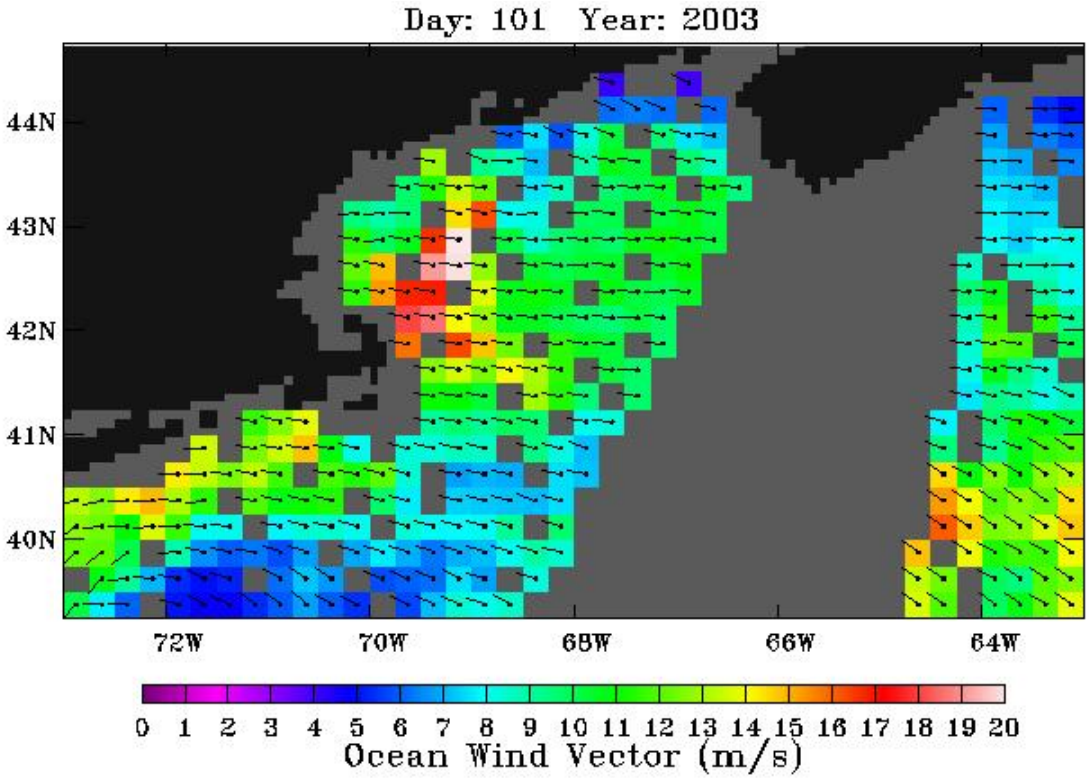

Figure 8-A62. QuikSCAT wind field. Evening satellite overpass on April 11, 2003.

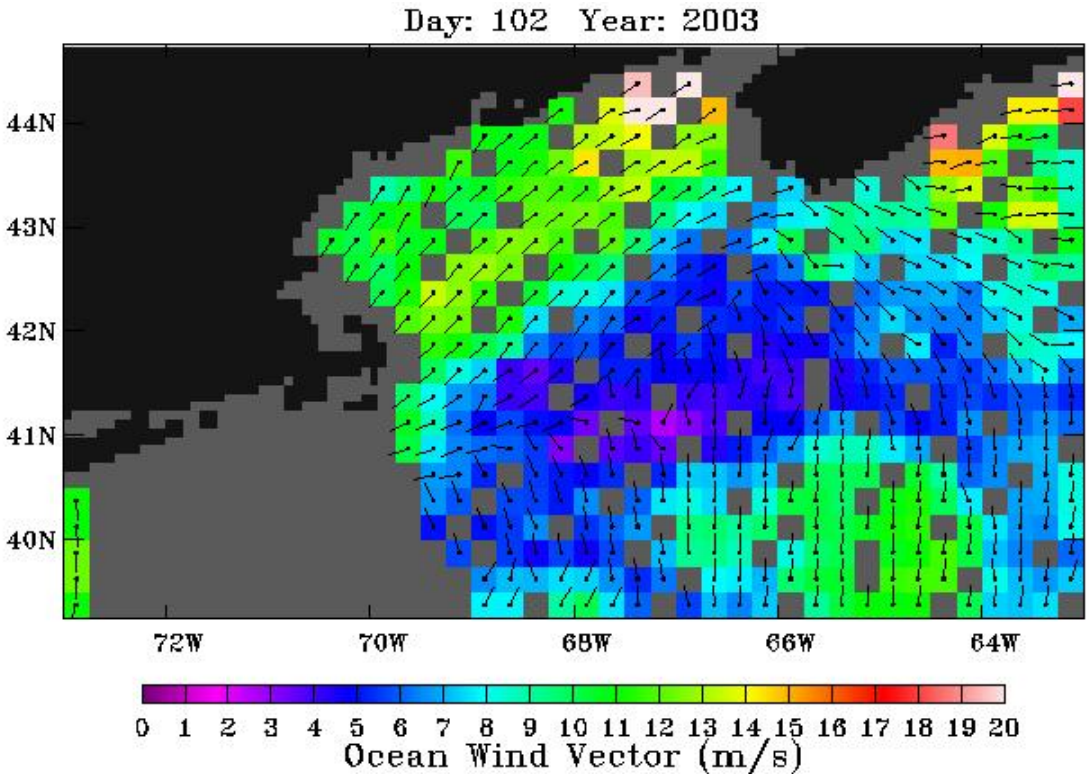

Figure 8-A63. QuikSCAT wind field. Morning satellite overpass on April 12, 2003.

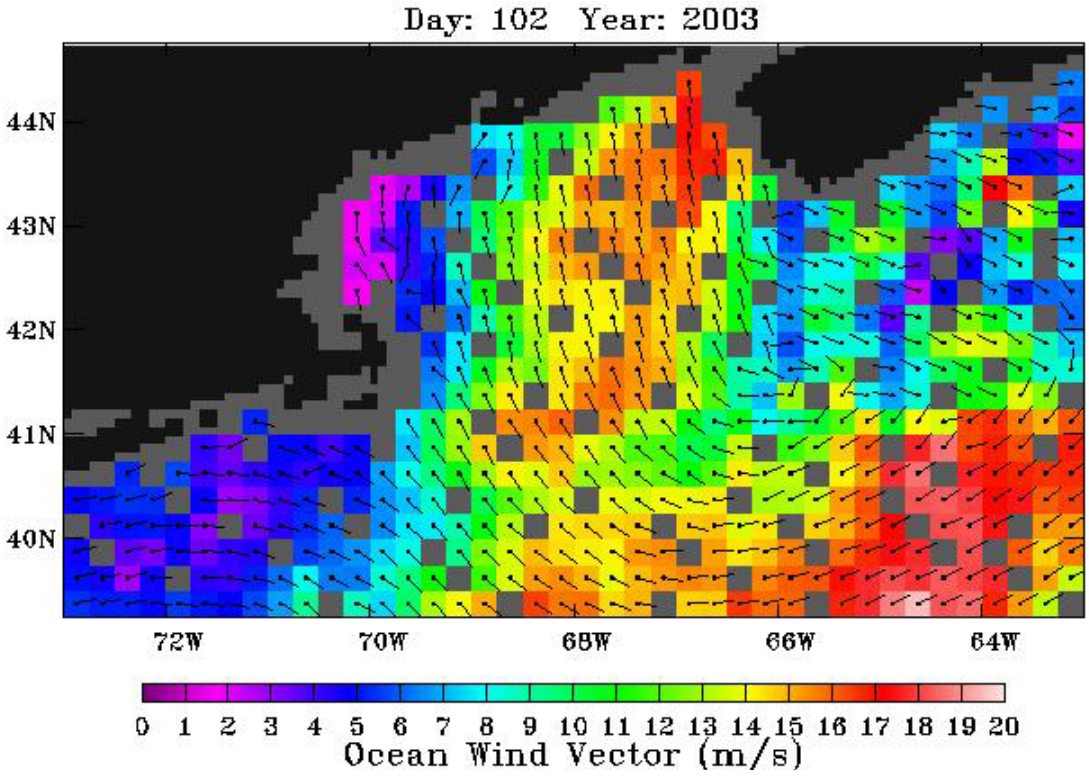

Figure 8-A64. QuikSCAT wind field. Evening satellite overpass on April 12, 2003.

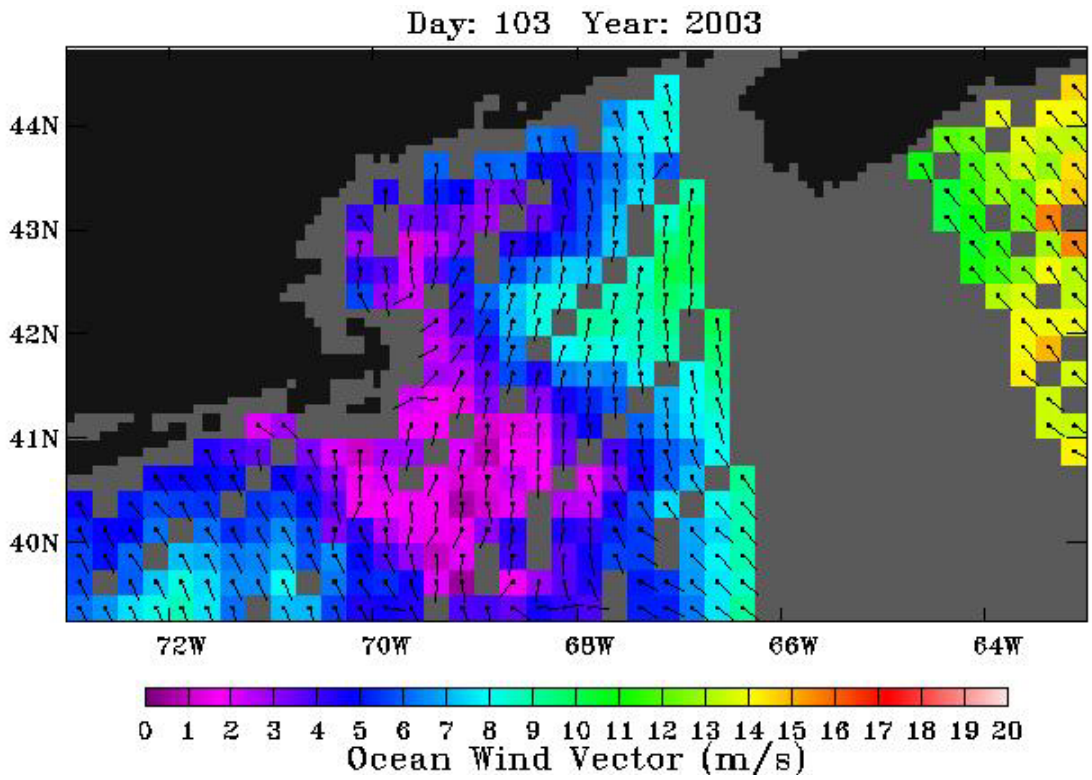

Figure 8-A65. QuikSCAT wind field. Morning satellite overpass on April 13, 2003.

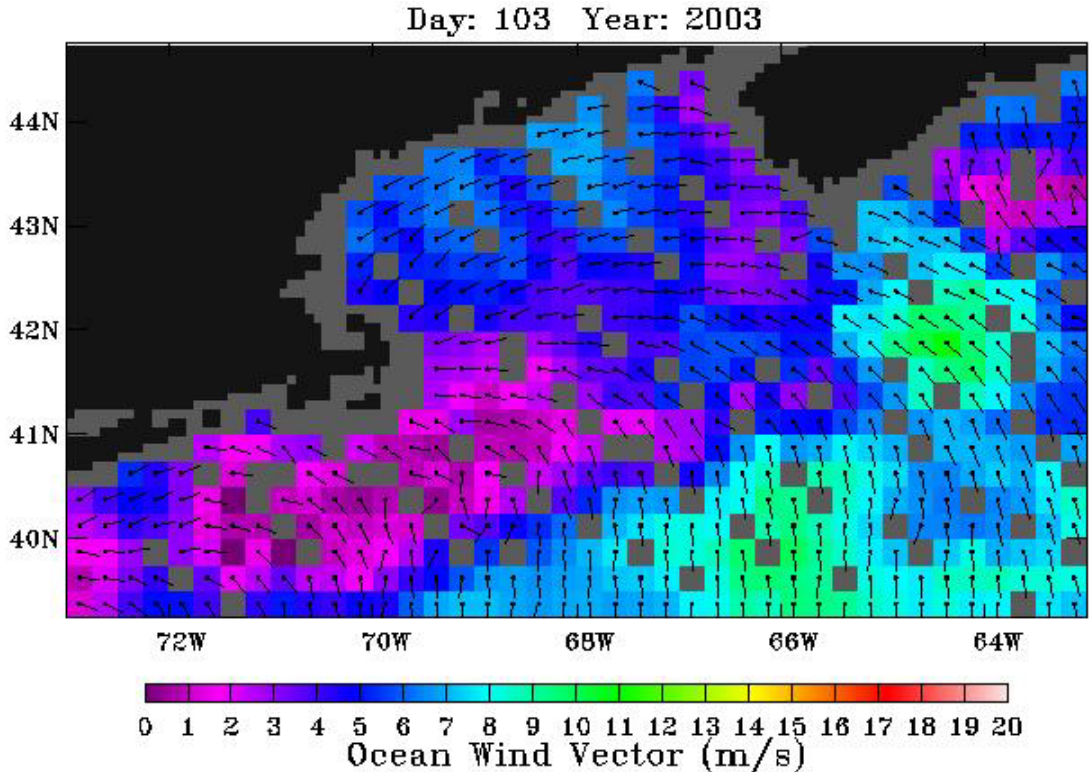

Figure 8-A66. QuikSCAT wind field. Evening satellite overpass on April 13, 2003.

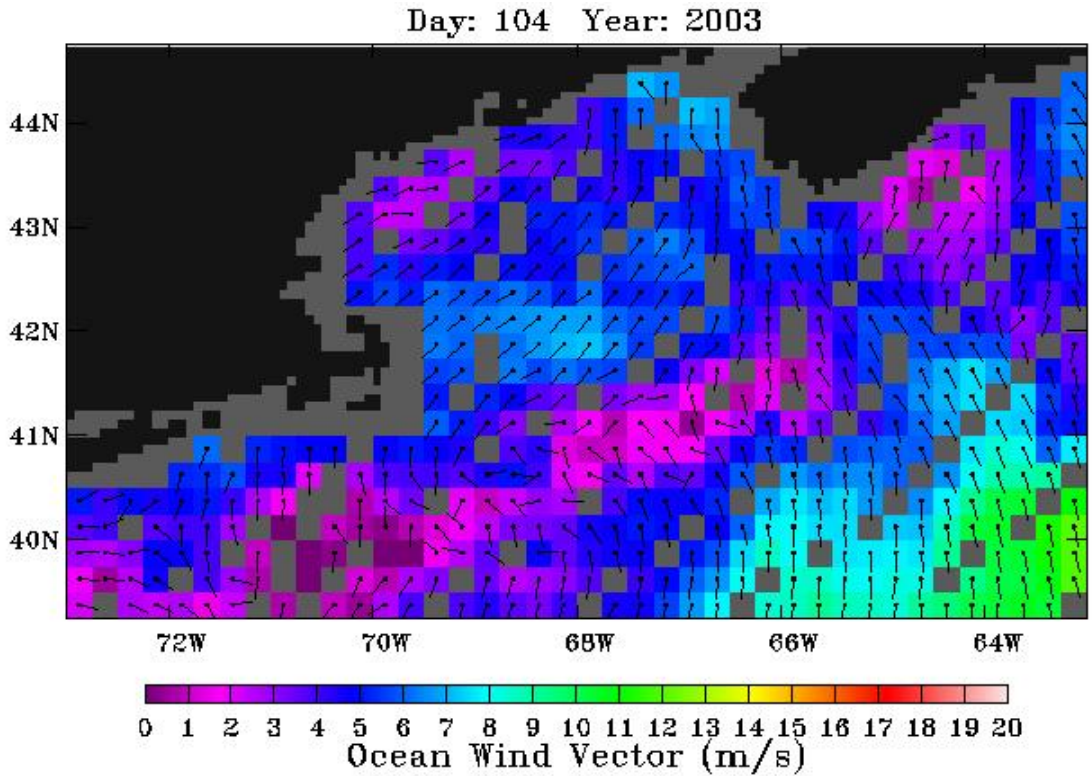

Figure 8-A67. QuikSCAT wind field. Morning satellite overpass on April 14, 2003.

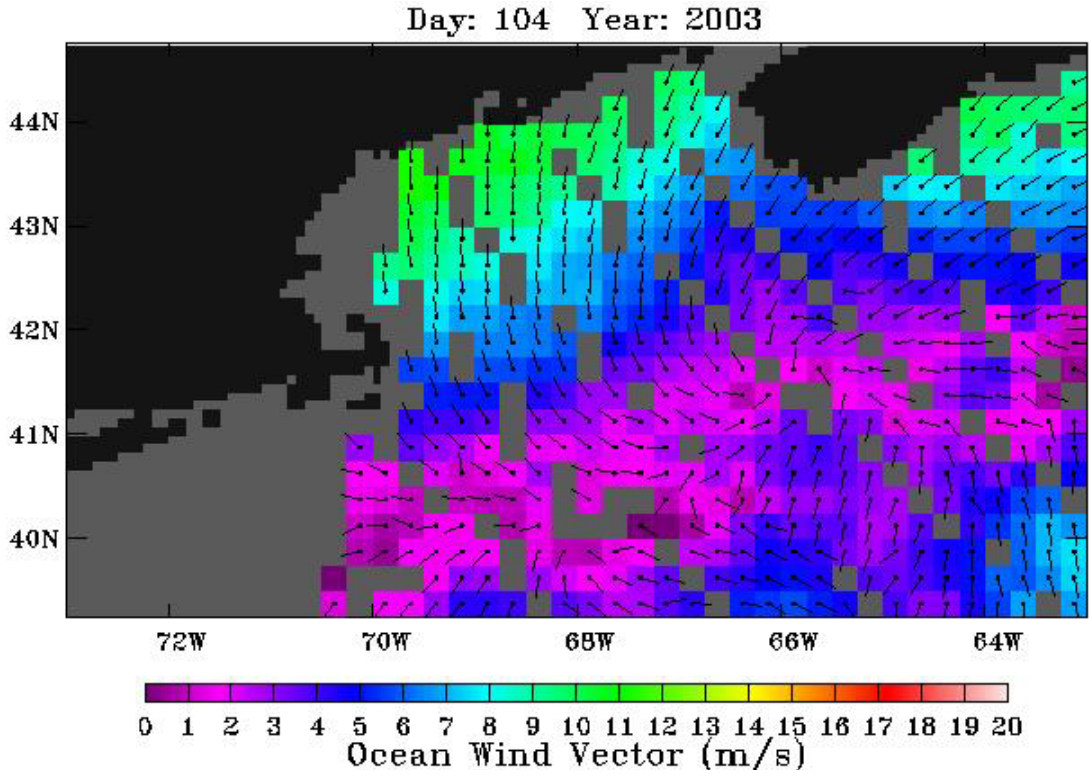

Figure 8-A68. QuikSCAT wind field. Evening satellite overpass on April 14, 2003.

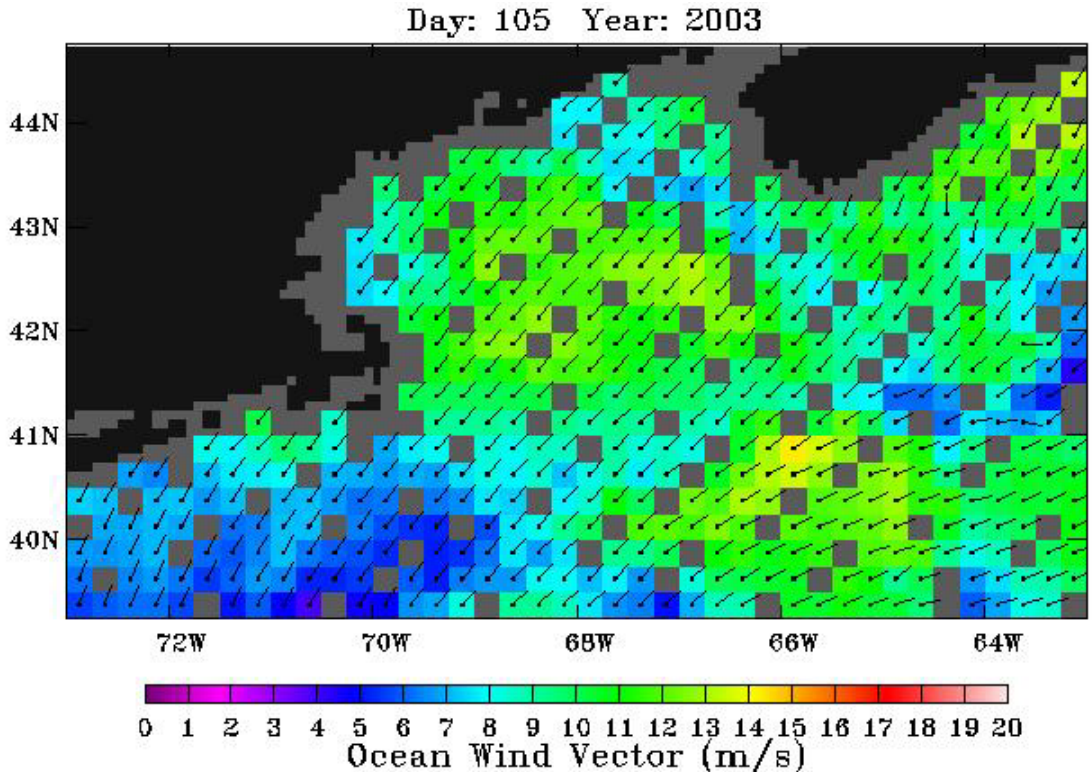

Figure 8-A69. QuikSCAT wind field. Morning satellite overpass on April 15, 2003.

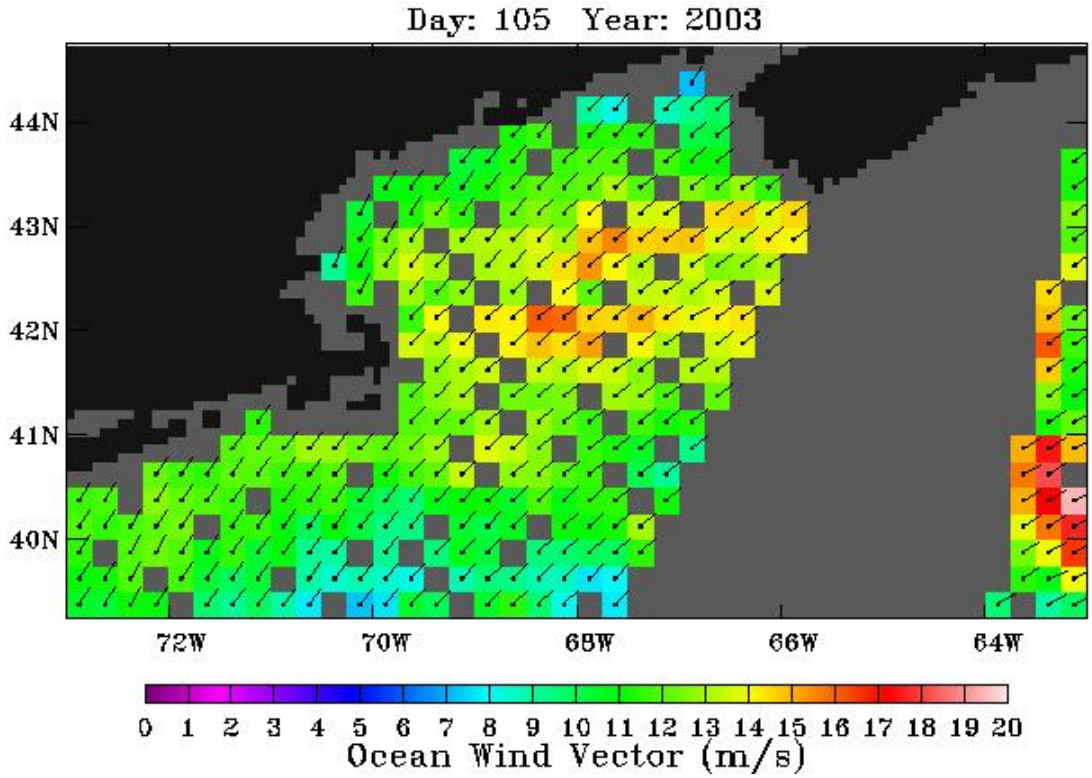

Figure 8-A70. QuikSCAT wind field. Evening satellite overpass on April 15, 2003.

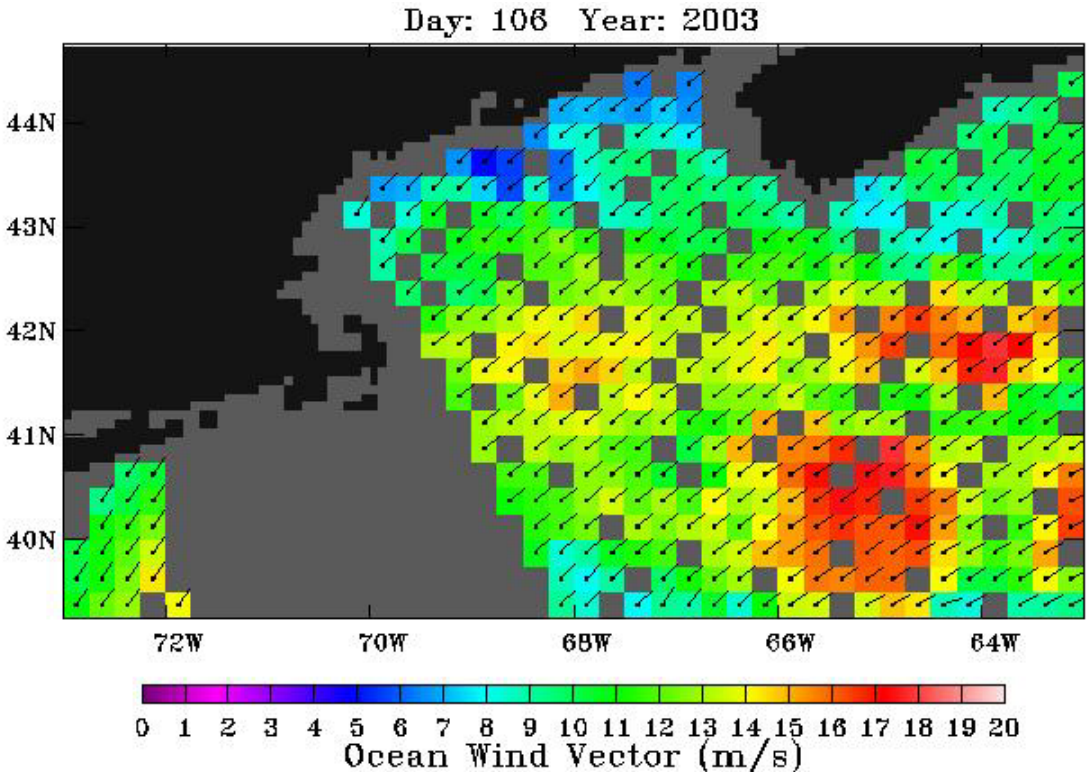

Figure 8-A71. QuikSCAT wind field. Morning satellite overpass on April 16, 2003.

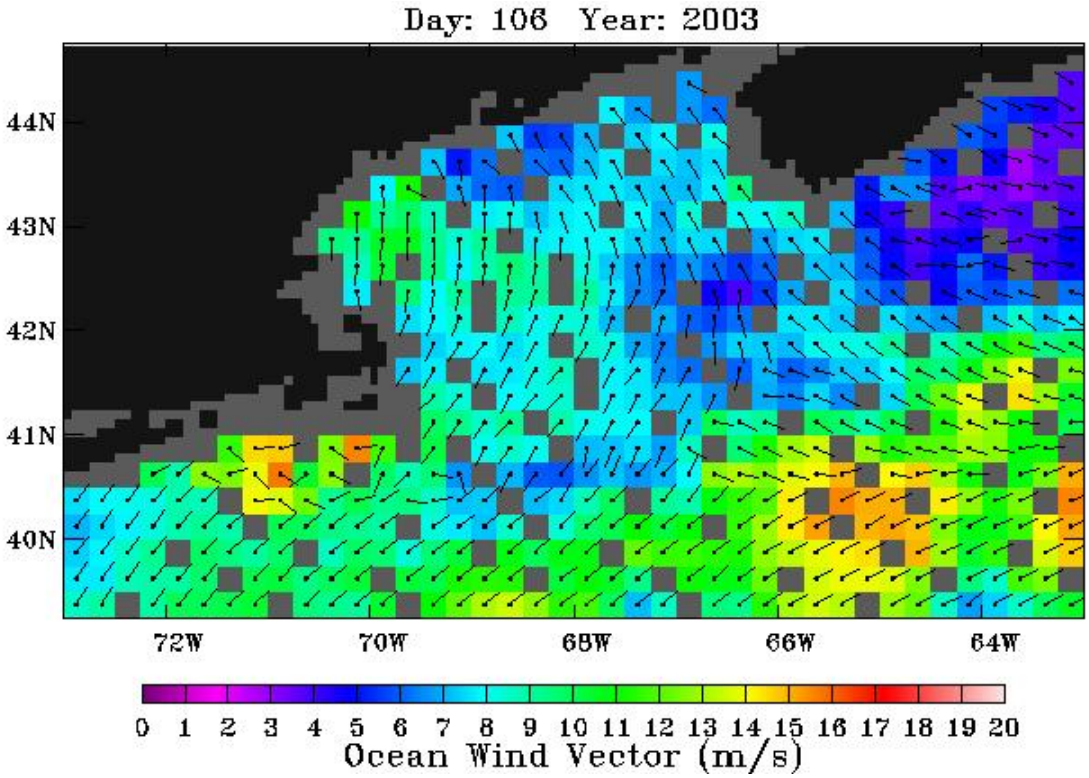

Figure 8-A72. QuikSCAT wind field. Evening satellite overpass on April 16, 2003.

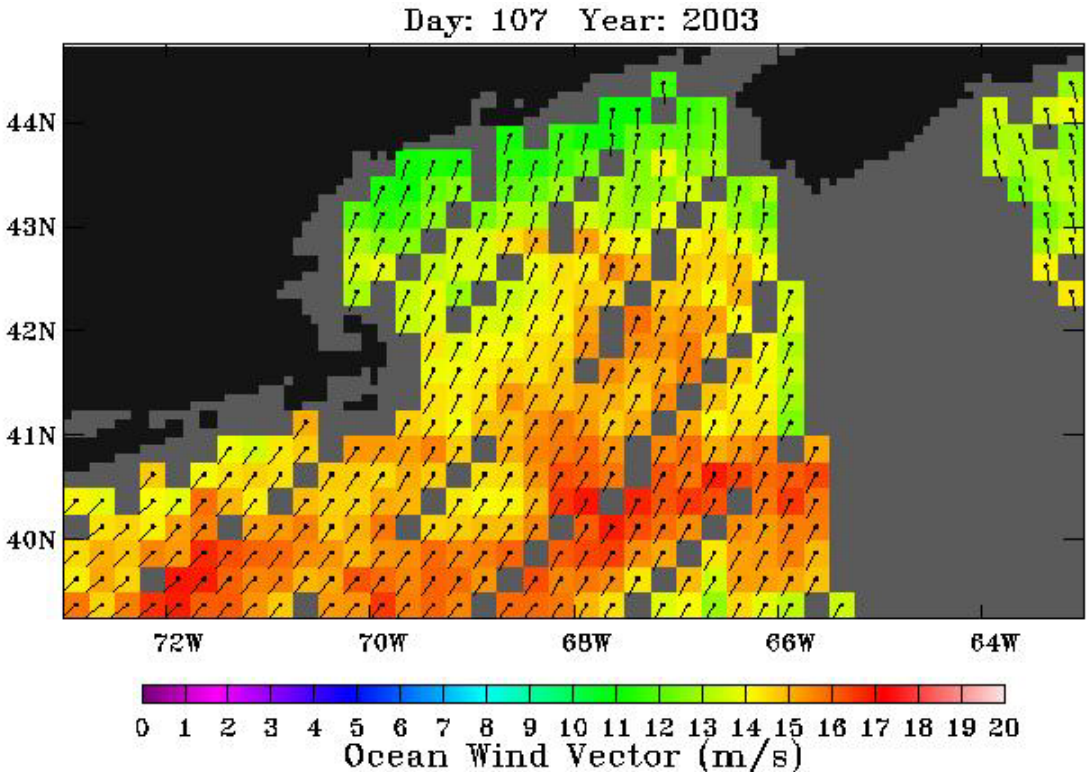

Figure 8-A73. QuikSCAT wind field. Morning satellite overpass on April 17, 2003.

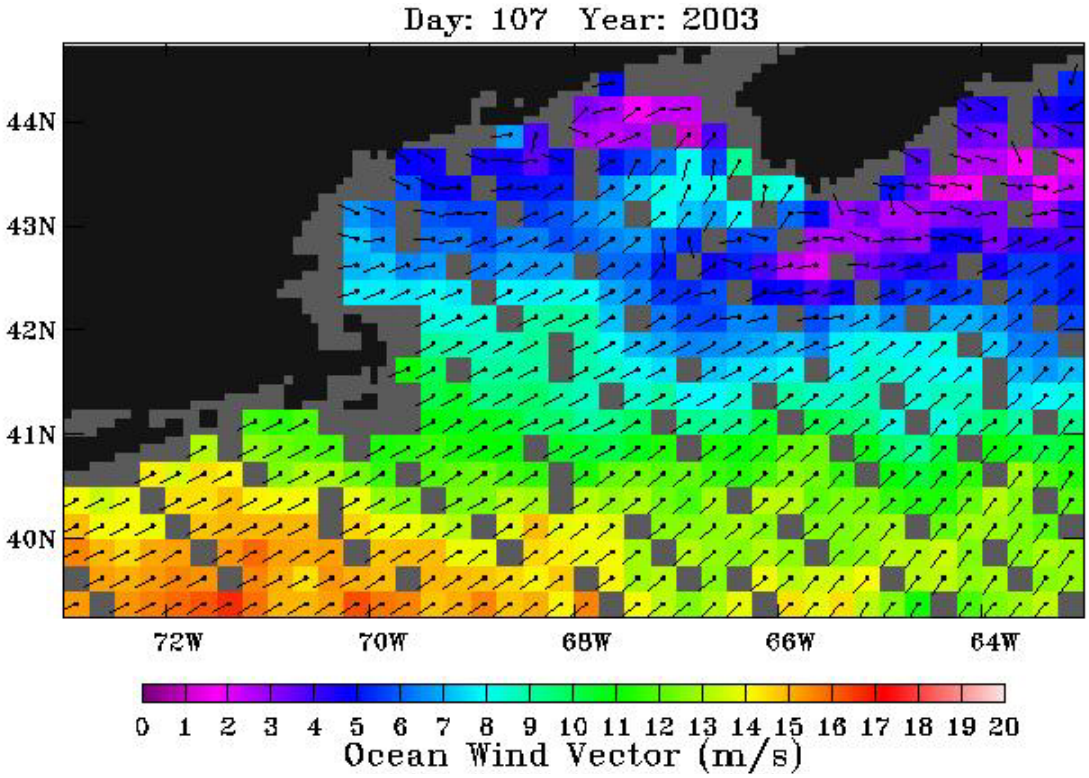

Figure 8-A74. QuikSCAT wind field. Evening satellite overpass on April 17, 2003.

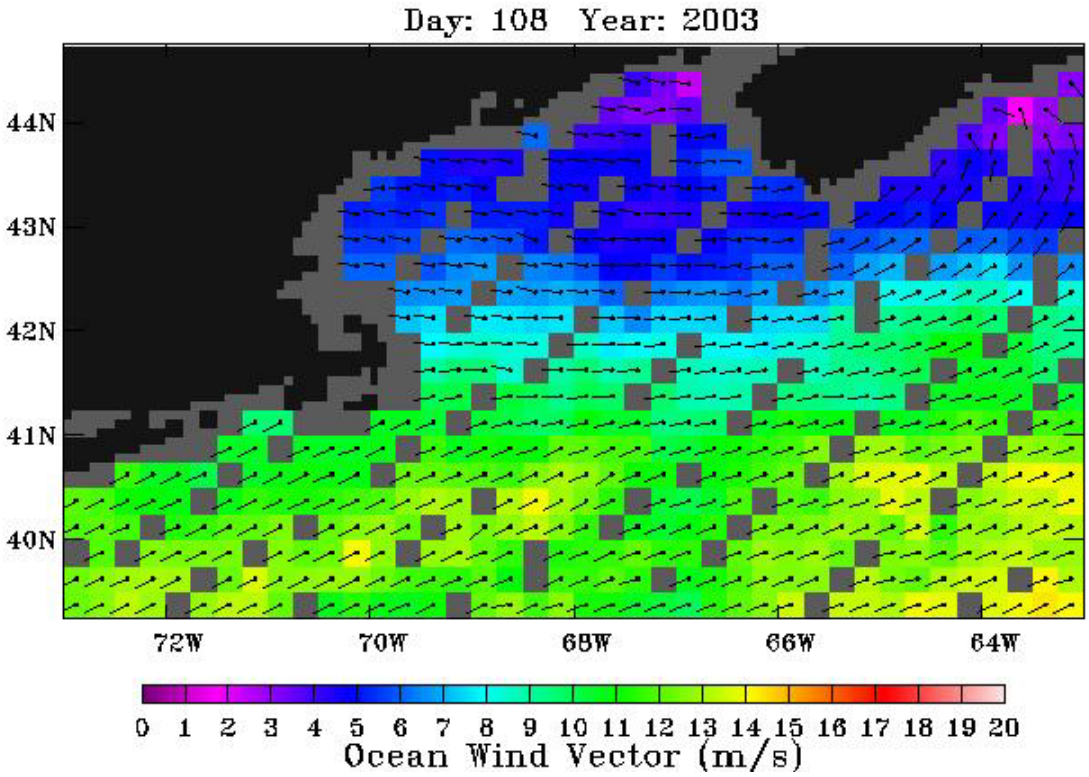

Figure 8-A75. QuikSCAT wind field. Morning satellite overpass on April 18, 2003.

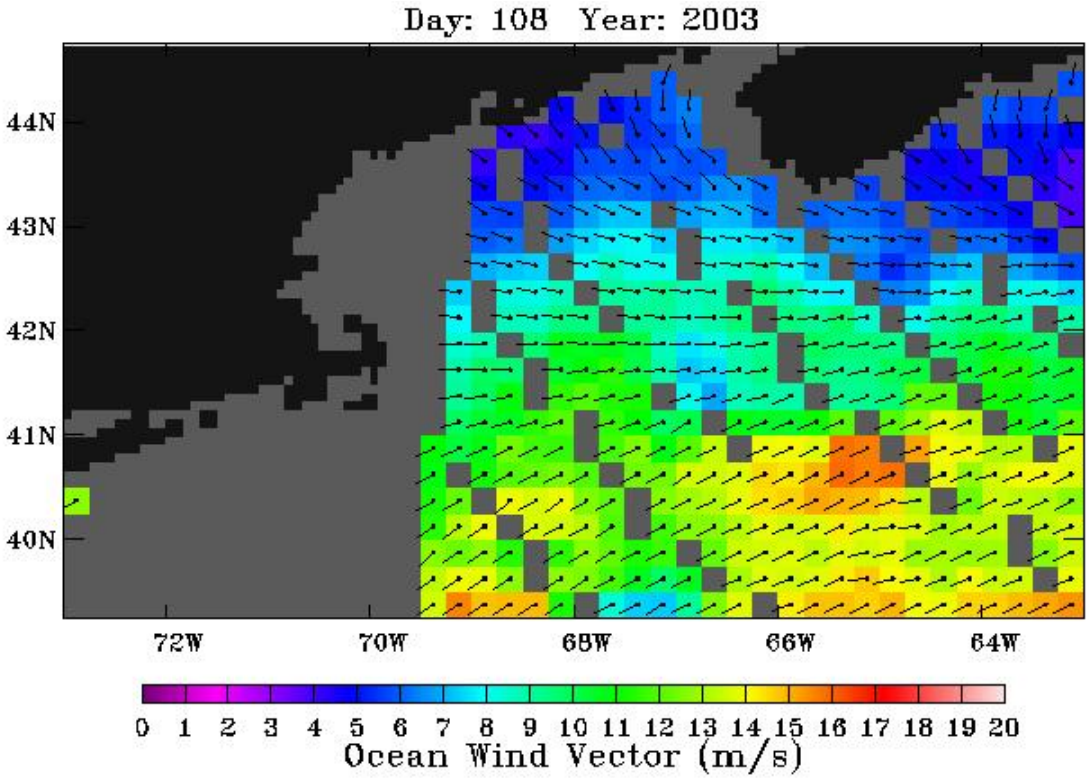

Figure 8-A76. QuikSCAT wind field. Evening satellite overpass on April 18, 2003.

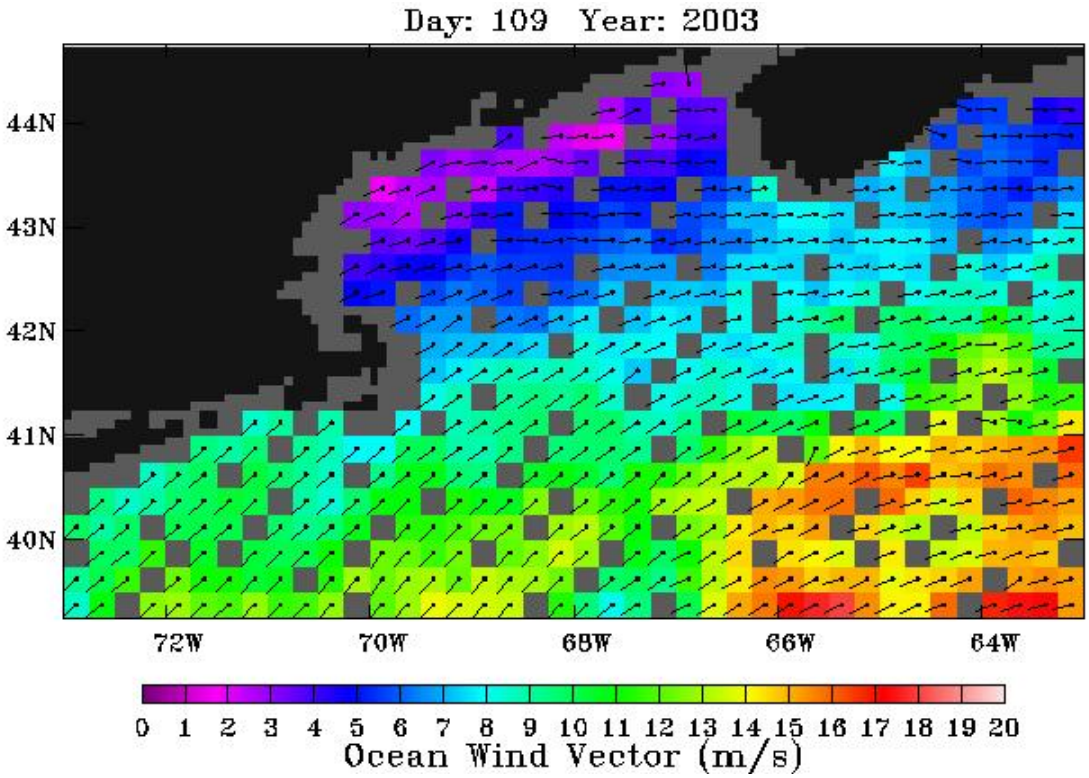

Figure 8-A77. QuikSCAT wind field. Morning satellite overpass on April 19, 2003.

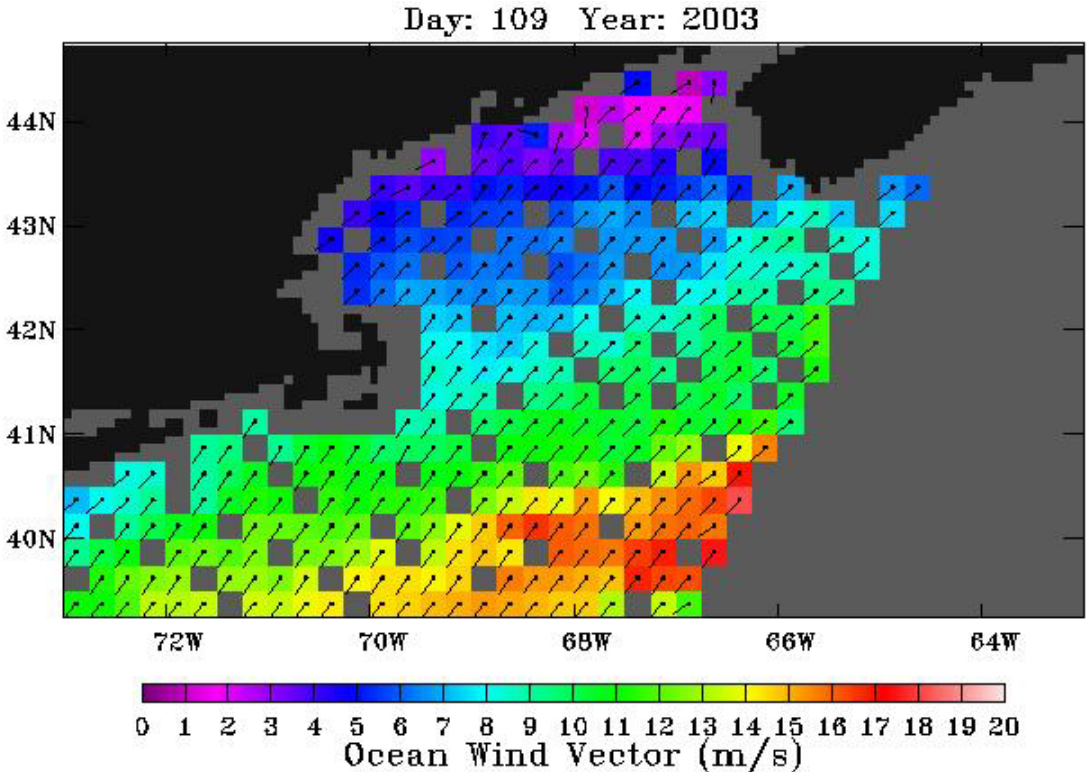

Figure 8-A78. QuikSCAT wind field. Evening satellite overpass on April 19, 2003.

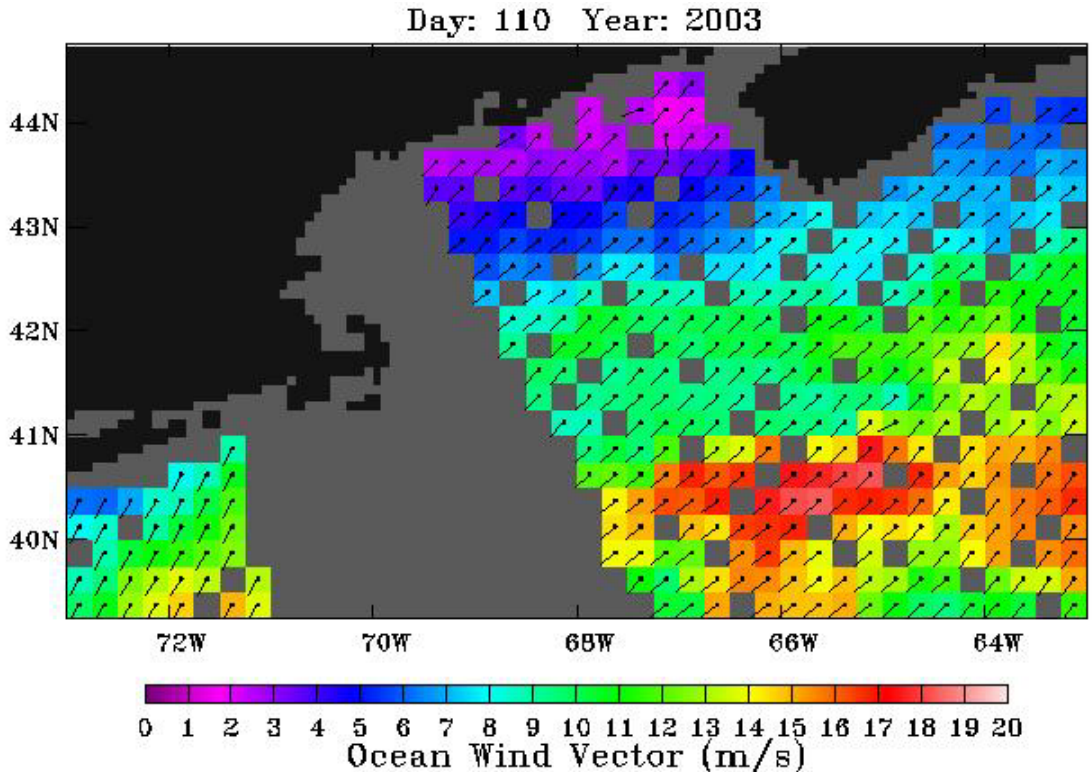

Figure 8-A79. QuikSCAT wind field. Morning satellite overpass on April 20, 2003.

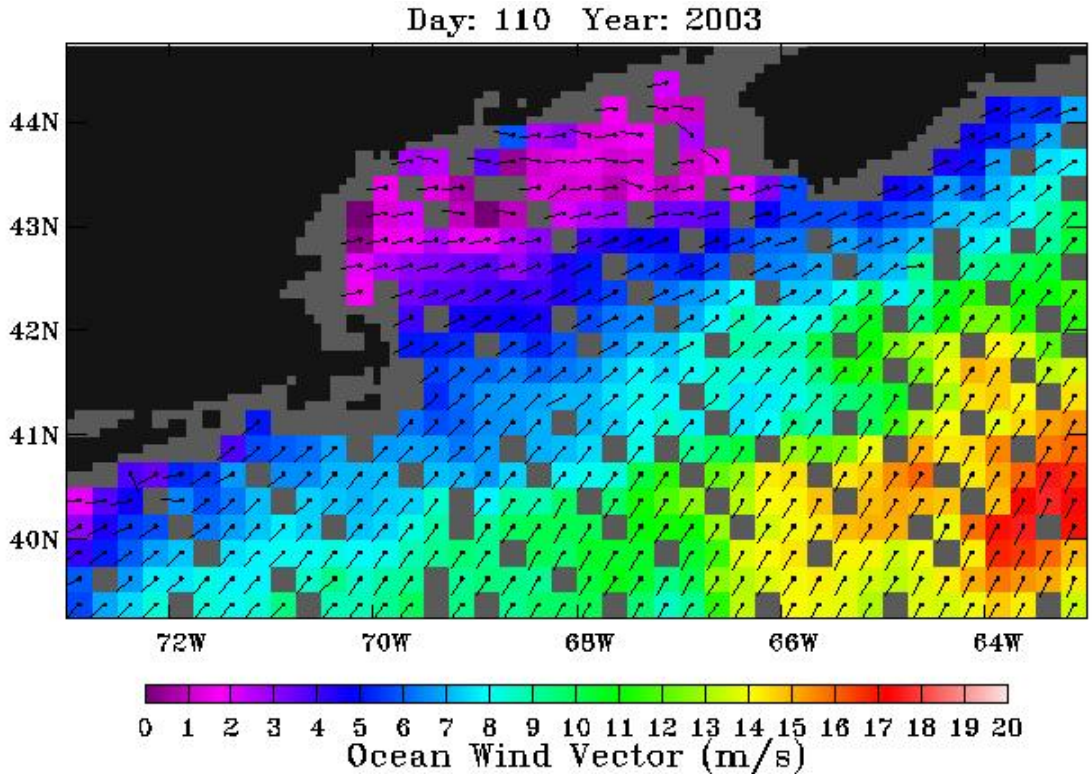

Figure 8-A80. QuikSCAT wind field. Evening satellite overpass on April 20, 2003.

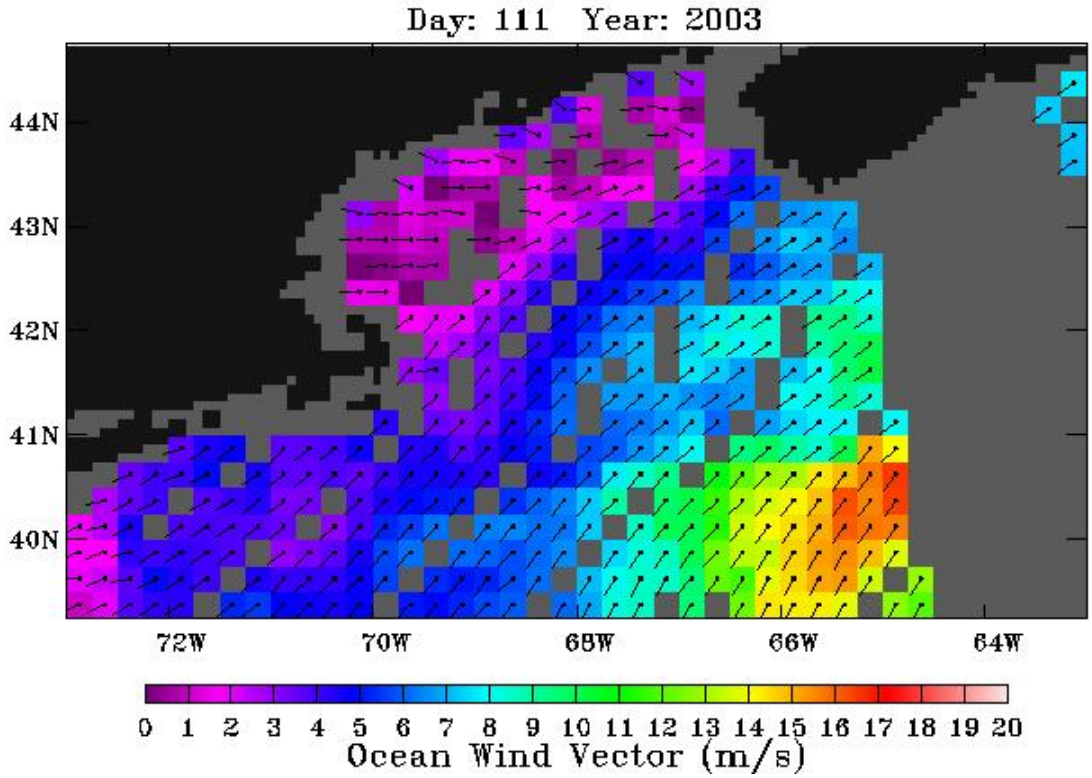

Figure 8-A81. QuikSCAT wind field. Morning satellite overpass on April 21, 2003.

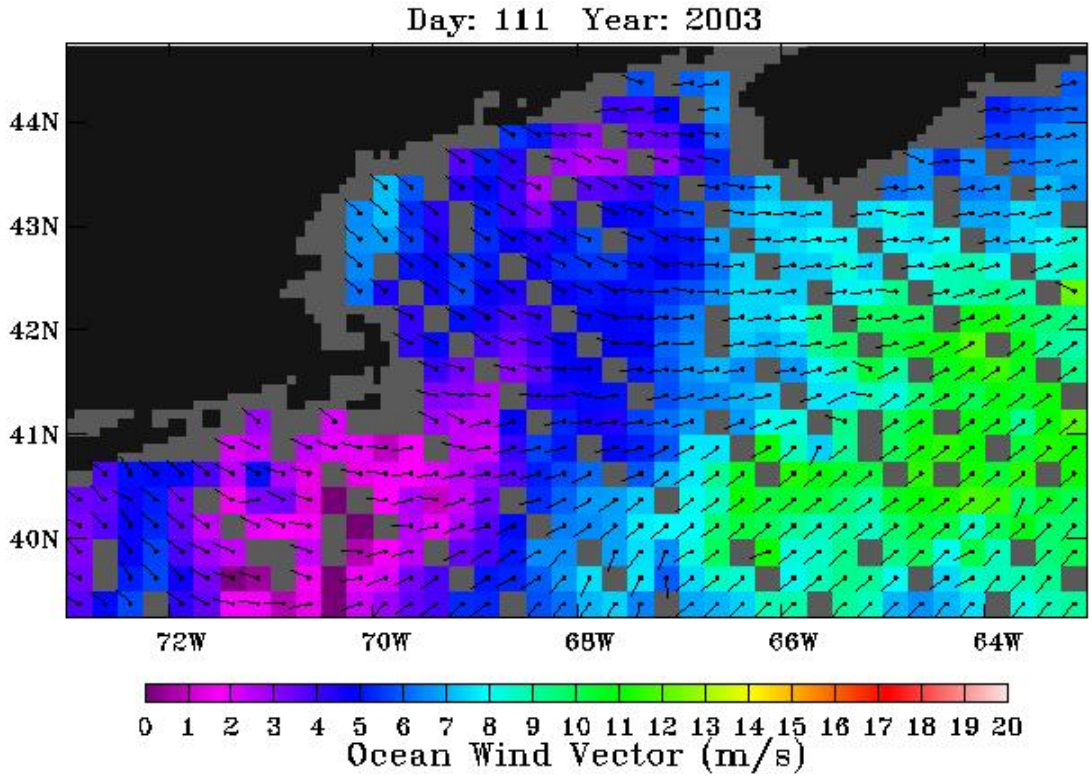

Figure 8-A82. QuikSCAT wind field. Evening satellite overpass on April 21, 2003.

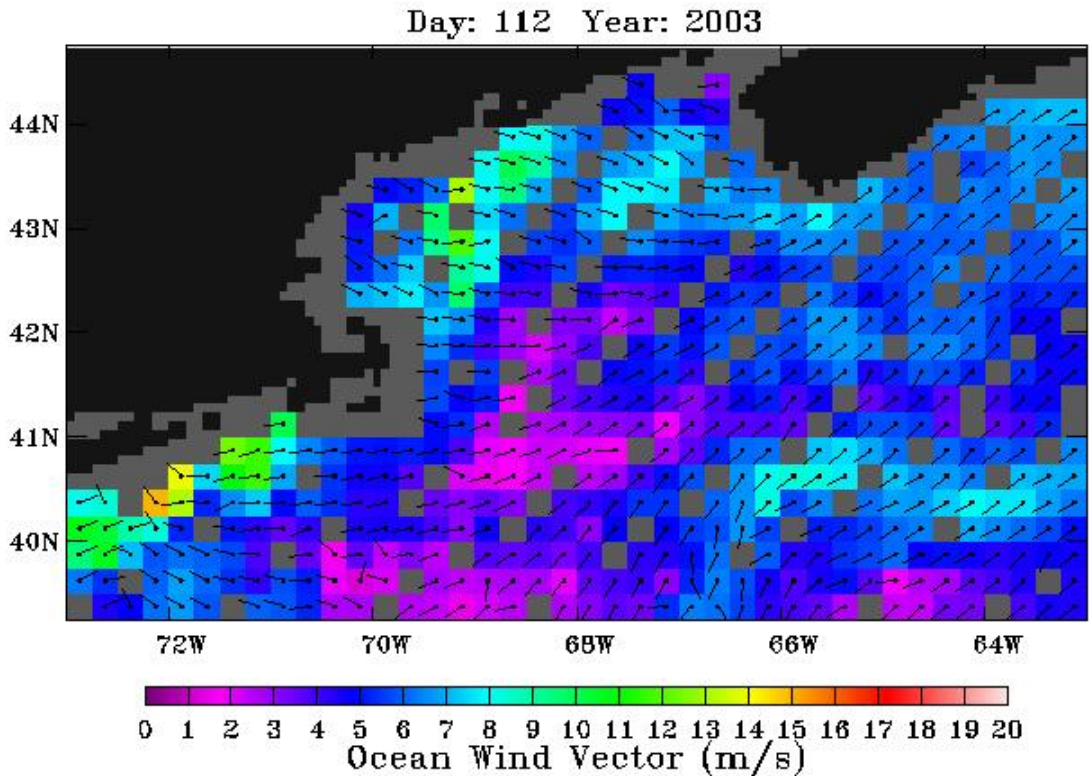

Figure 8-A83. QuikSCAT wind field. Morning satellite overpass on April 22, 2003.

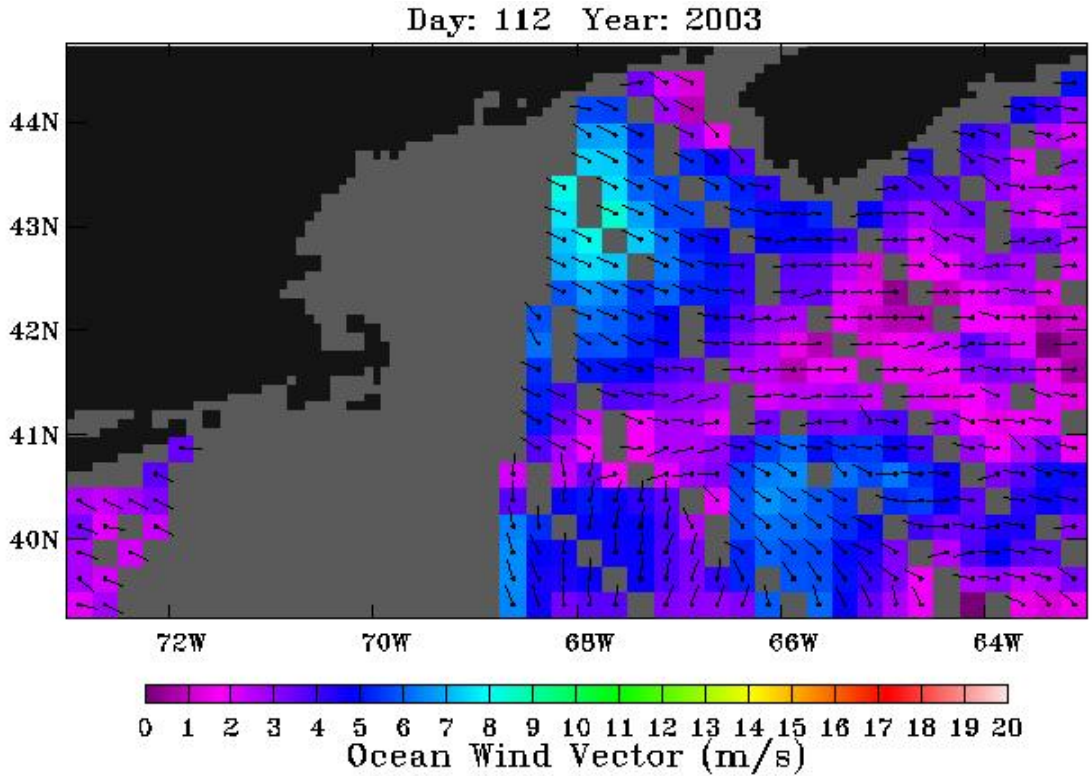

Figure 8-A84. QuikSCAT wind field. Evening satellite overpass on April 22, 2003.

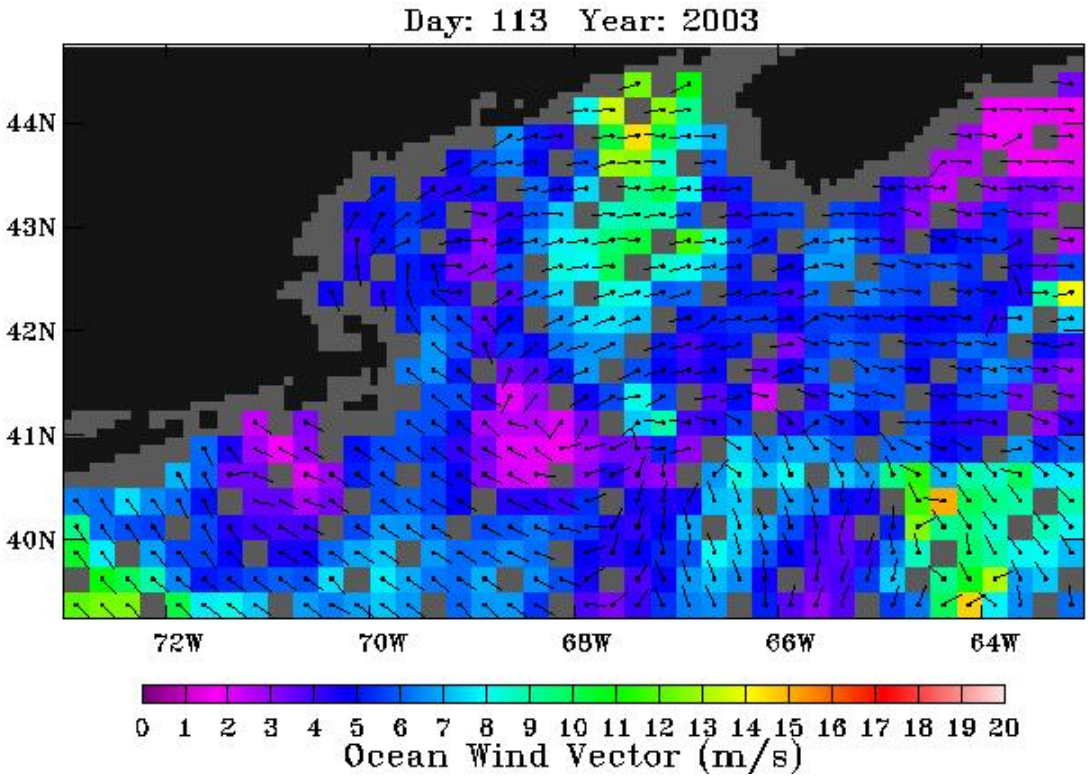

Figure 8-A85. QuikSCAT wind field. Morning satellite overpass on April 23, 2003.

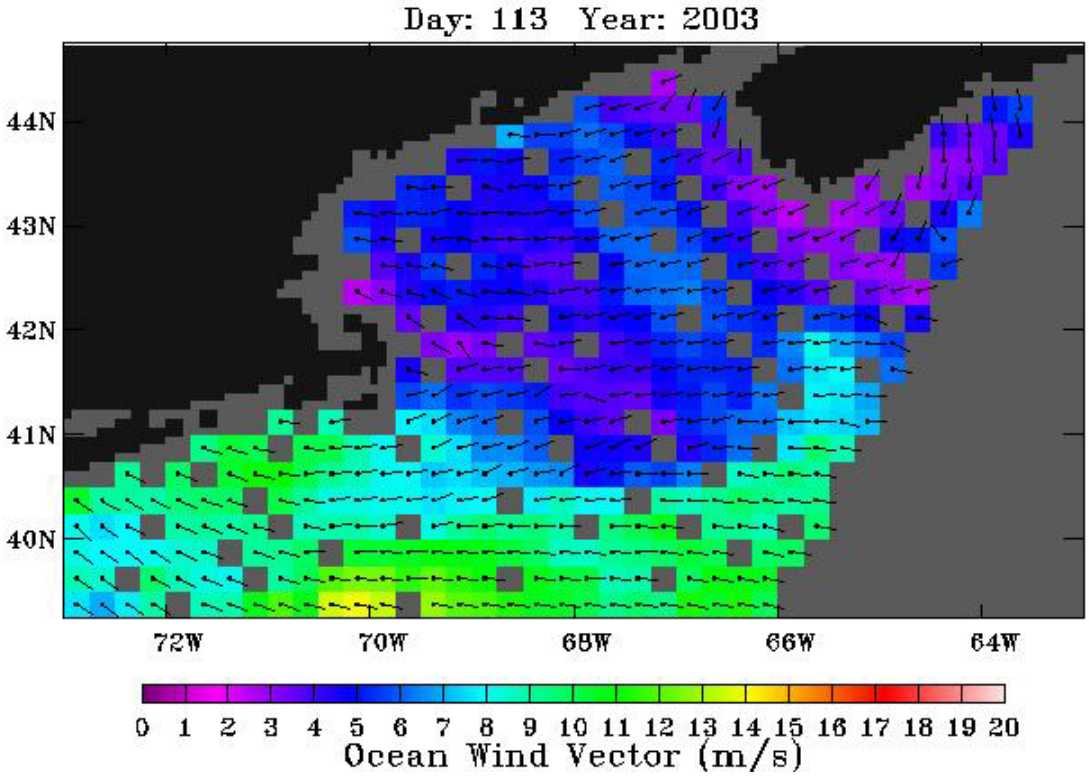

Figure 8-A86. QuikSCAT wind field. Evening satellite overpass on April 23, 2003.

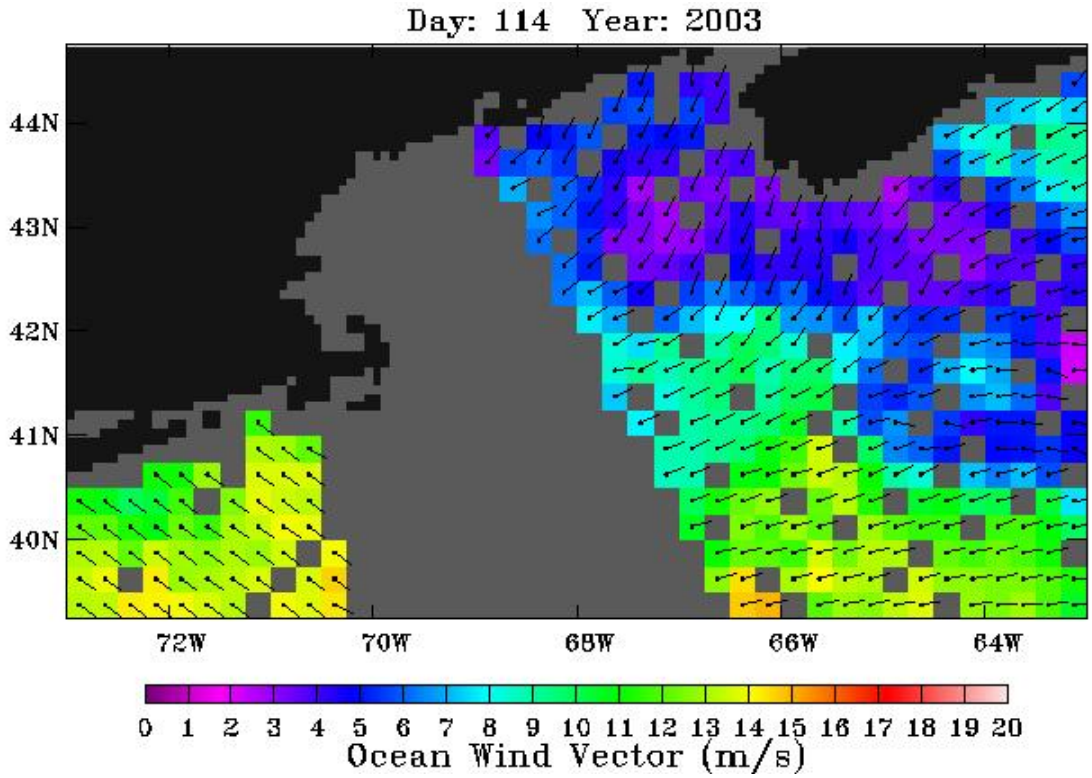

Figure 8-A87. QuikSCAT wind field. Morning satellite overpass on April 24, 2003.

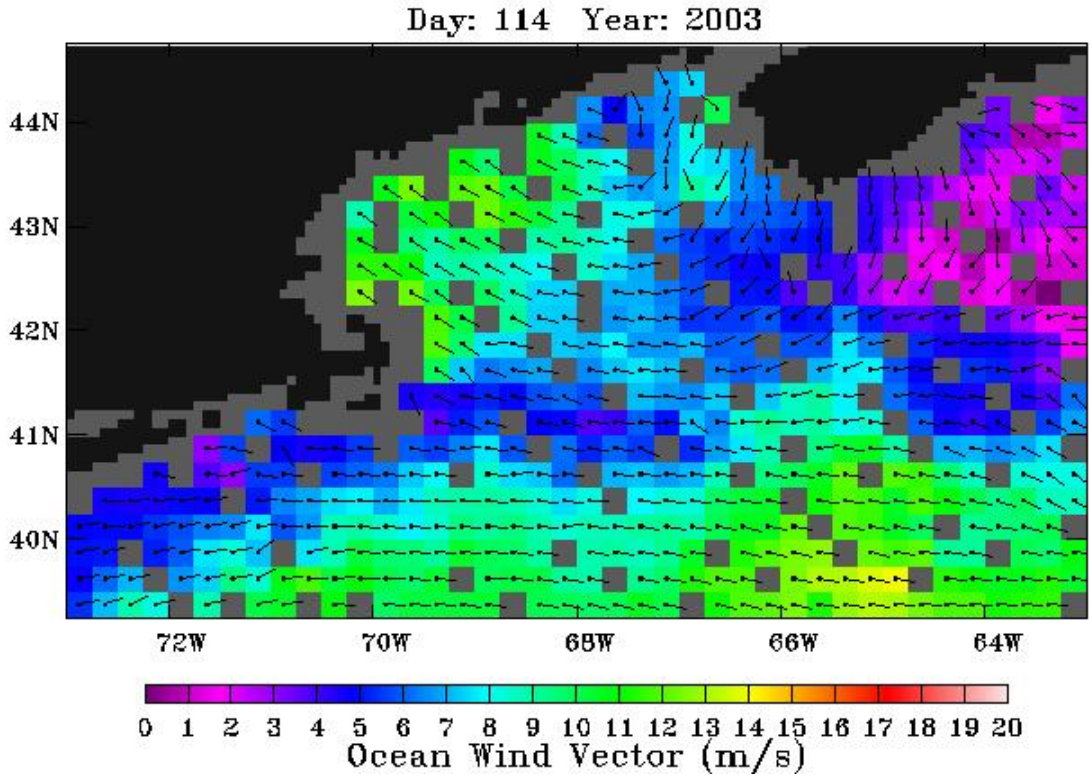

Figure 8-A88. QuikSCAT wind field. Evening satellite overpass on April 24, 2003.

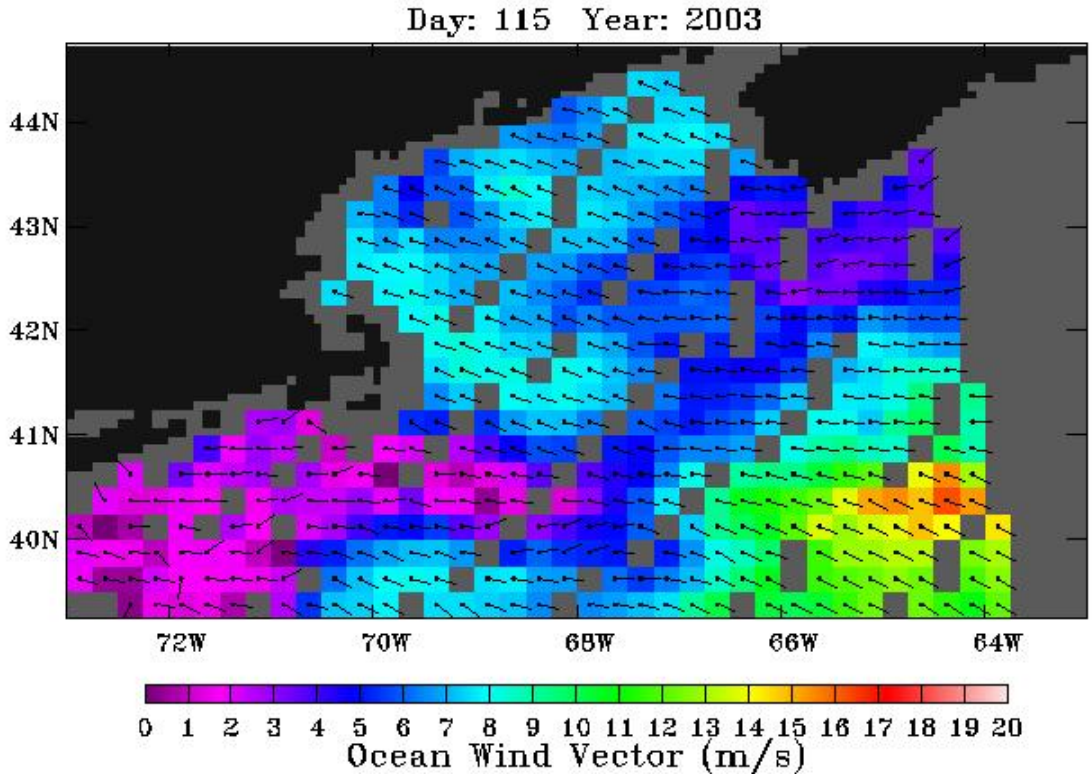

Figure 8-A89. QuikSCAT wind field. Morning satellite overpass on April 25, 2003.

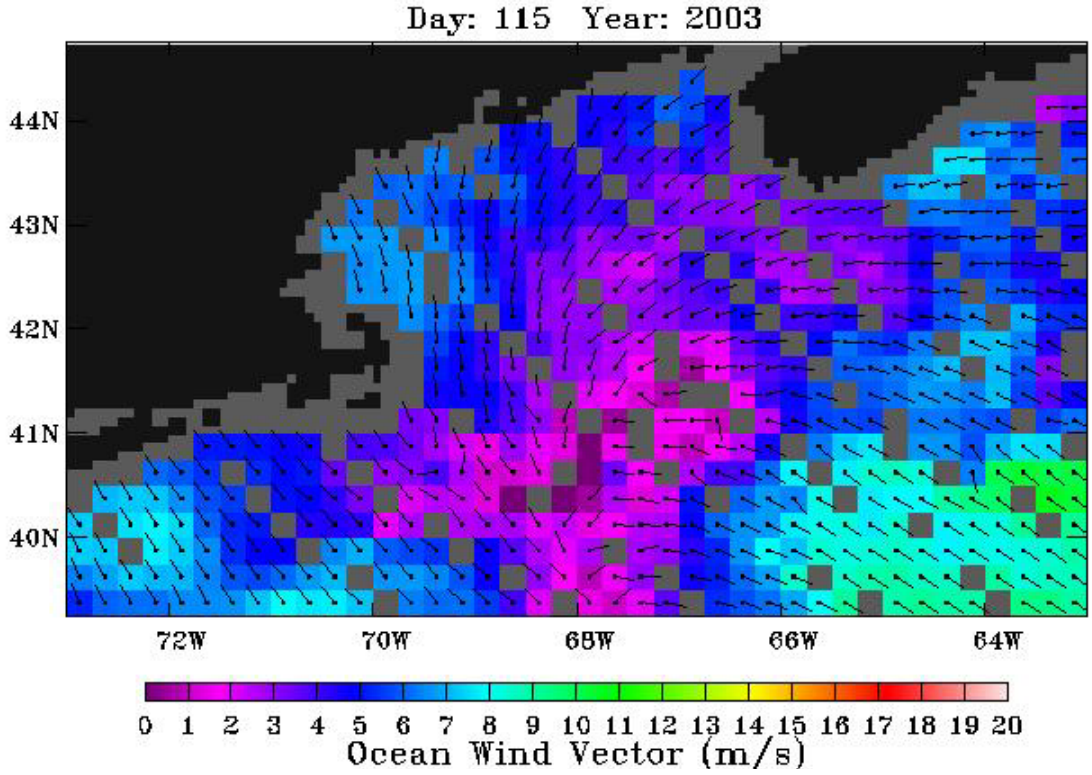

Figure 8-A90. QuikSCAT wind field. Evening satellite overpass on April 25, 2003.

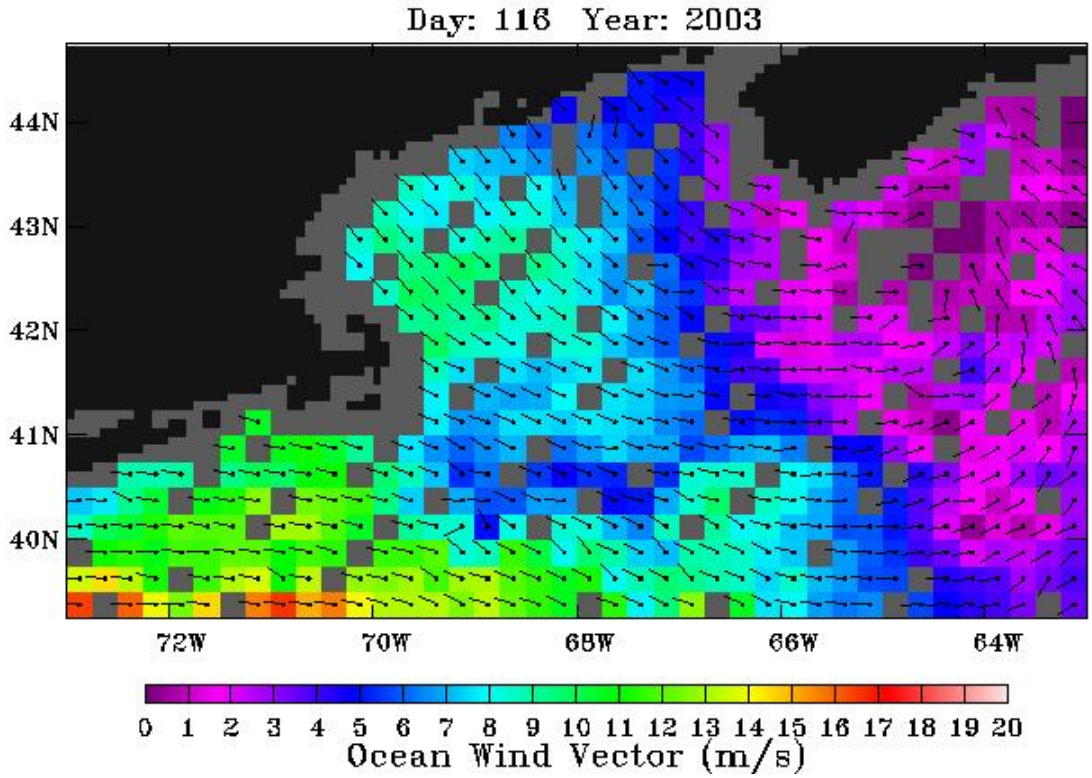

Figure 8-A91. QuikSCAT wind field. Morning satellite overpass on April 26, 2003.

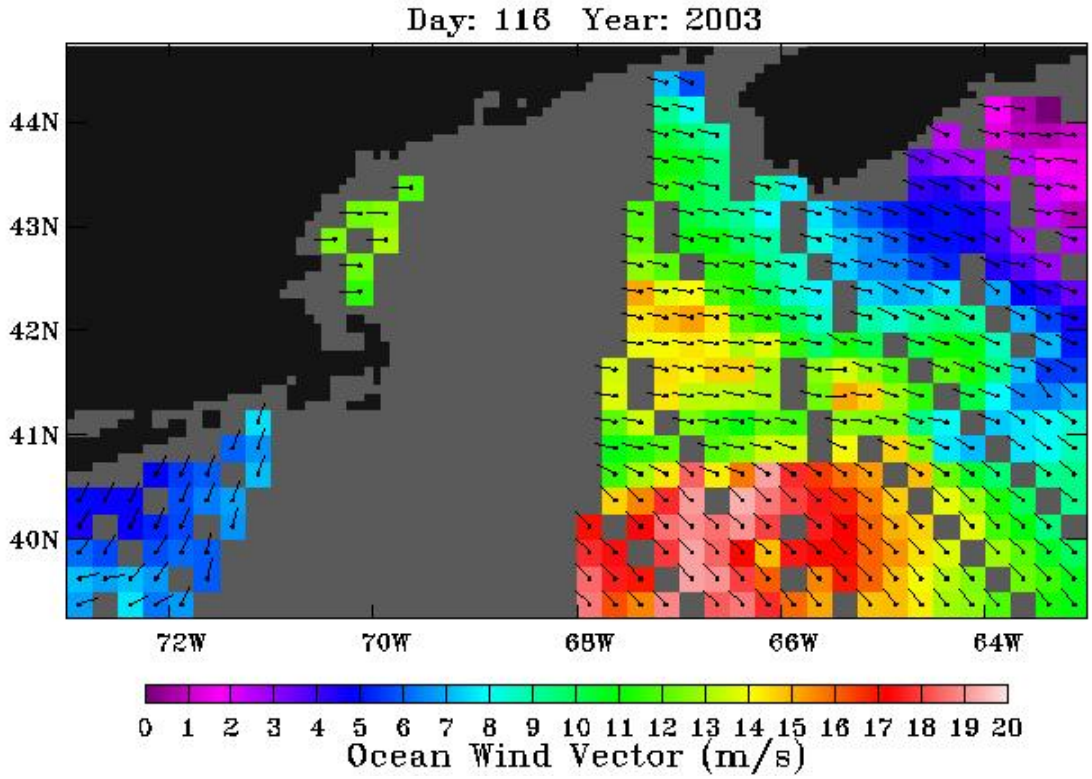

Figure 8-A92. QuikSCAT wind field. Evening satellite overpass on April 26, 2003.

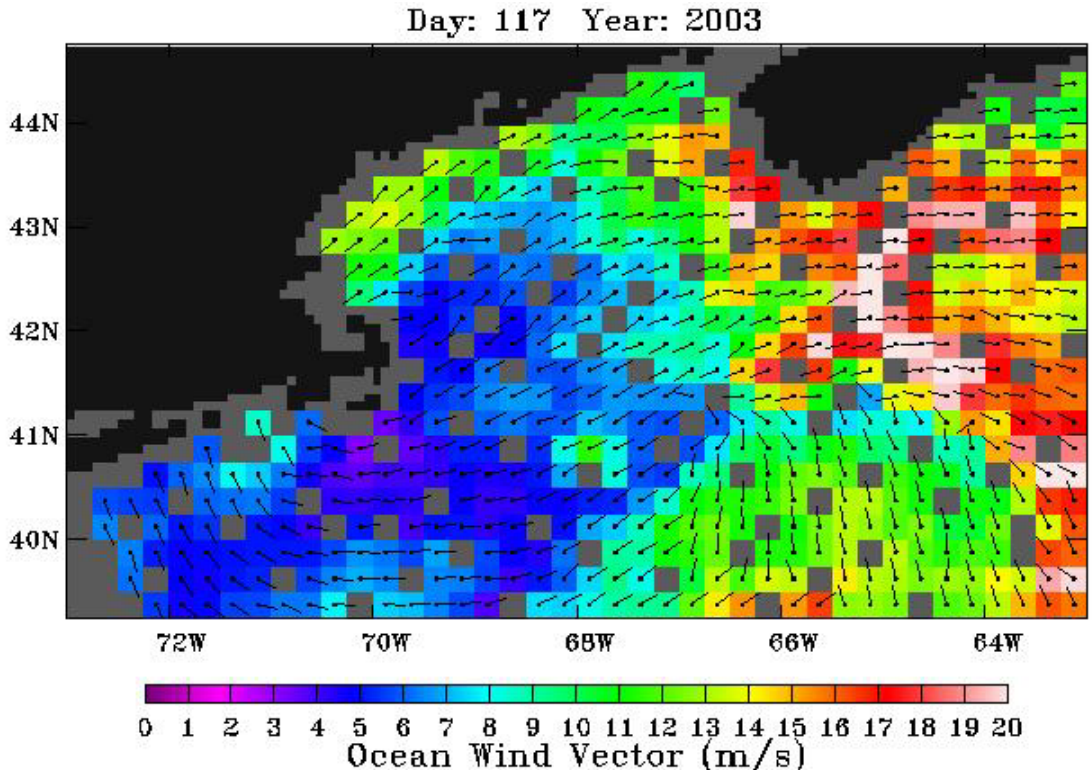

Figure 8-A93. QuikSCAT wind field. Morning satellite overpass on April 27, 2003.

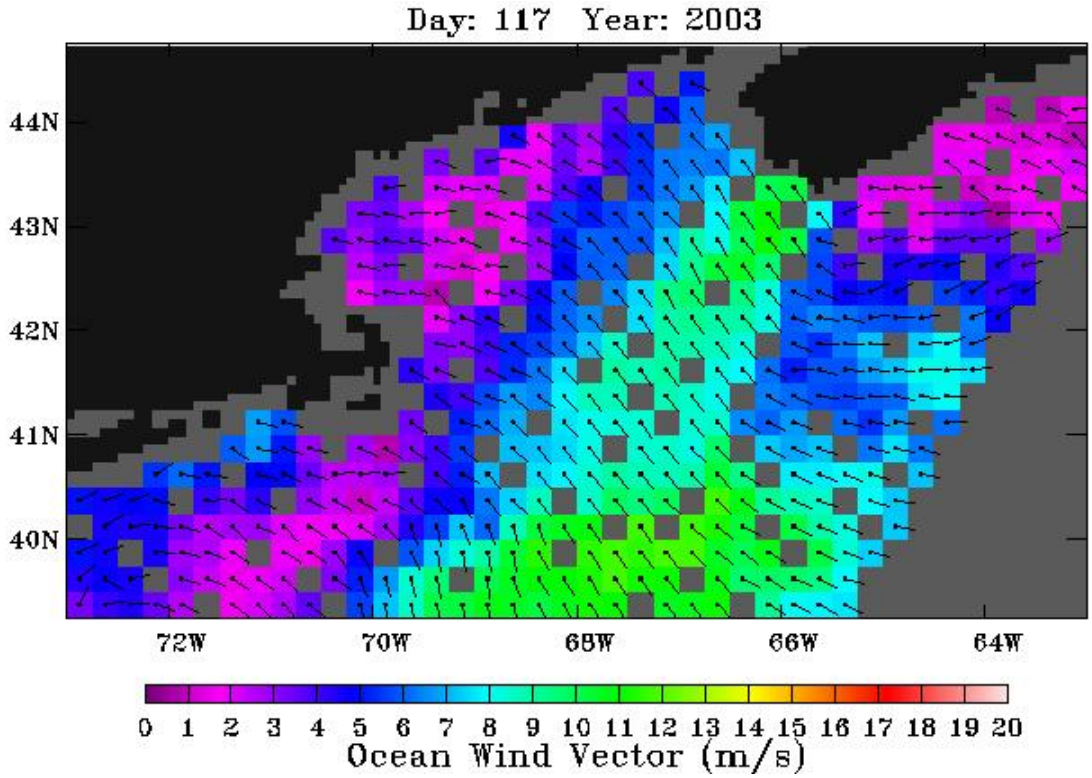

Figure 8-A94. QuikSCAT wind field. Evening satellite overpass on April 27, 2003.

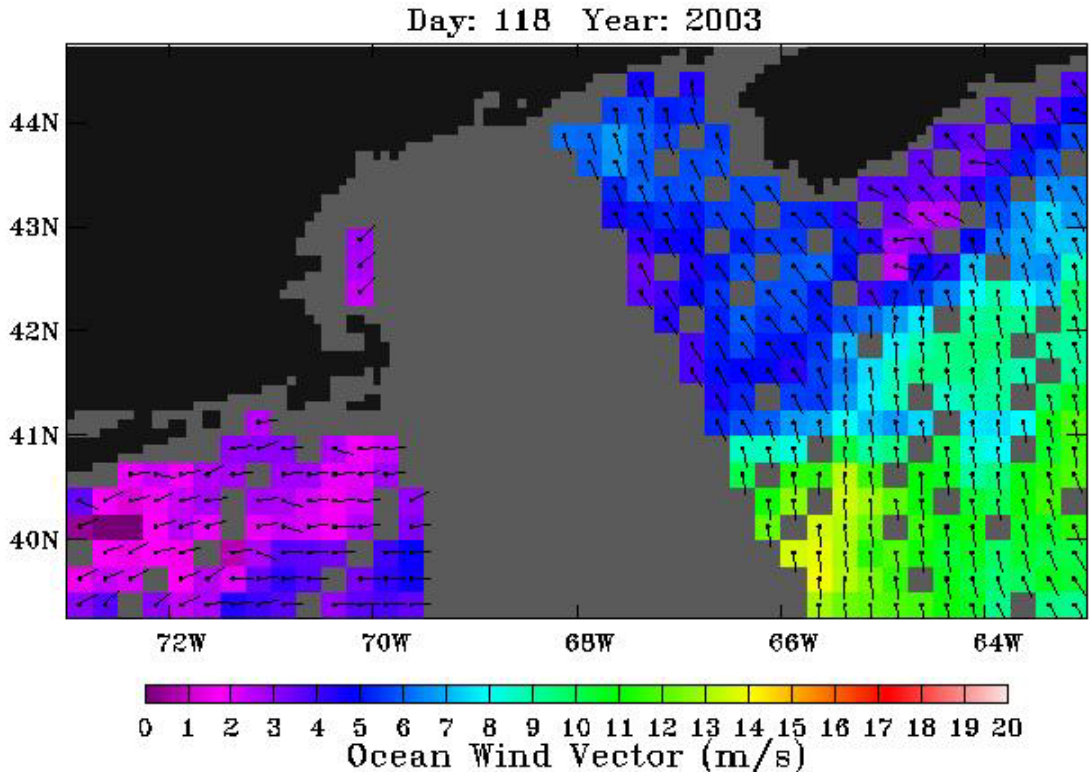

Figure 8-A95. QuikSCAT wind field. Morning satellite overpass on April 28, 2003.

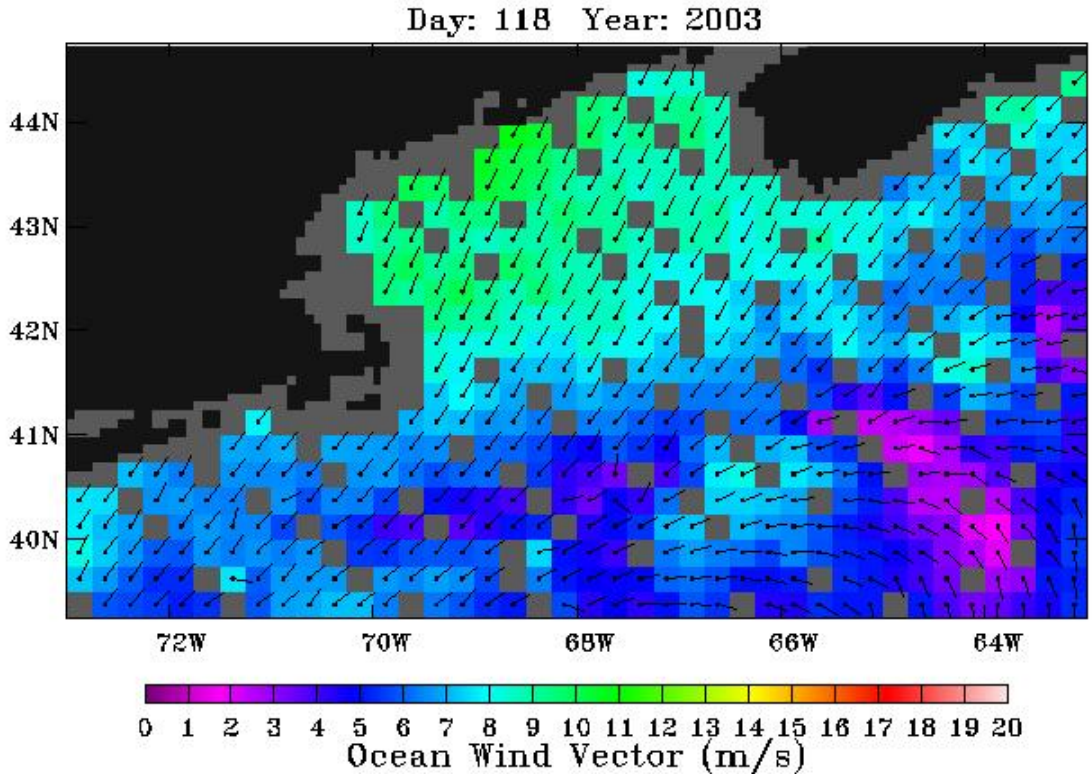

Figure 8-A96. QuikSCAT wind field. Evening satellite overpass on April 28, 2003.

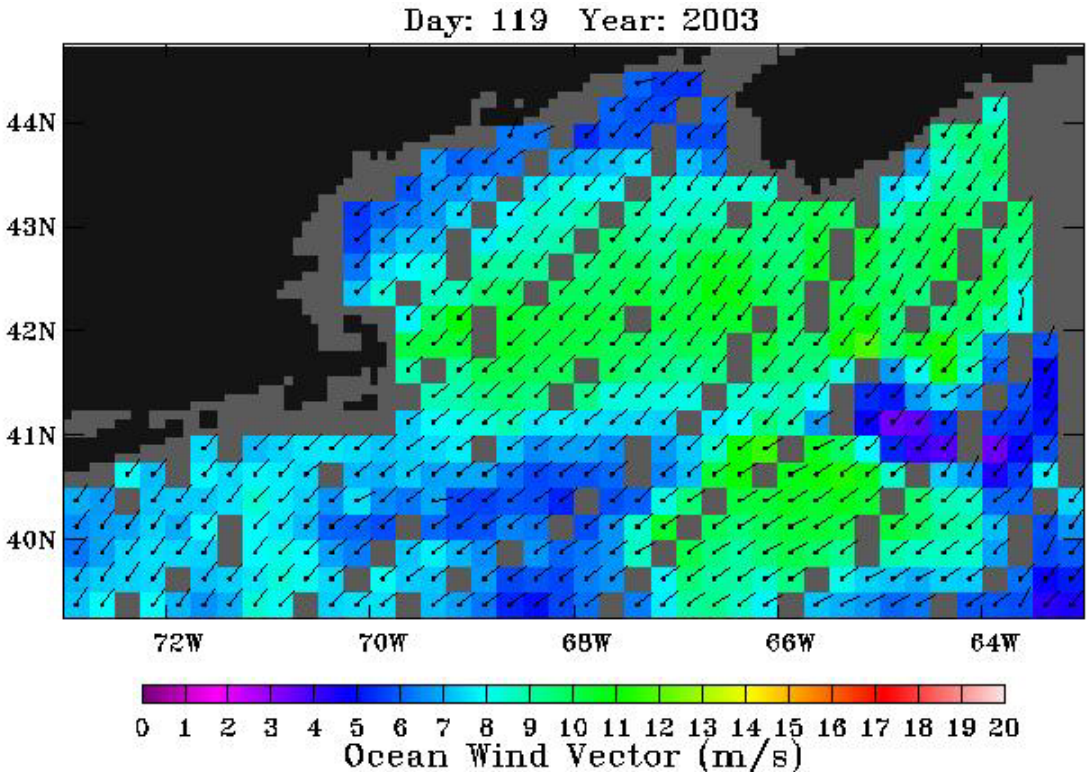

Figure 8-A97. QuikSCAT wind field. Morning satellite overpass on April 29, 2003.

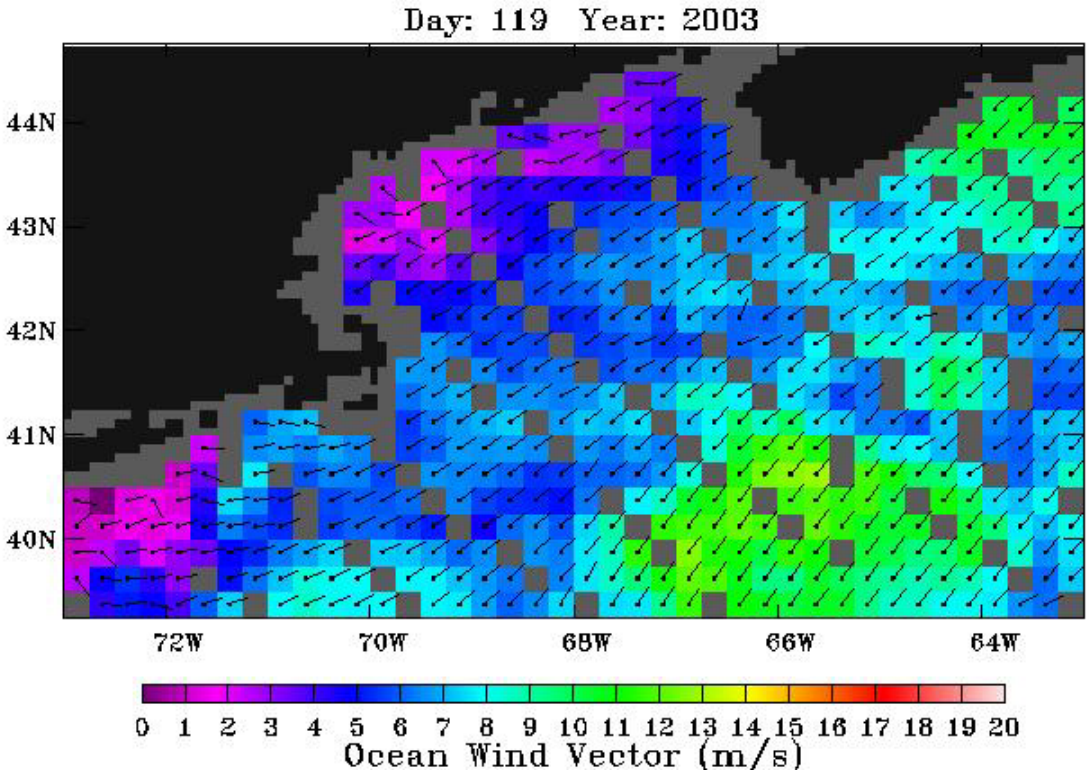

Figure 8-A98. QuikSCAT wind field. Evening satellite overpass on April 29, 2003.

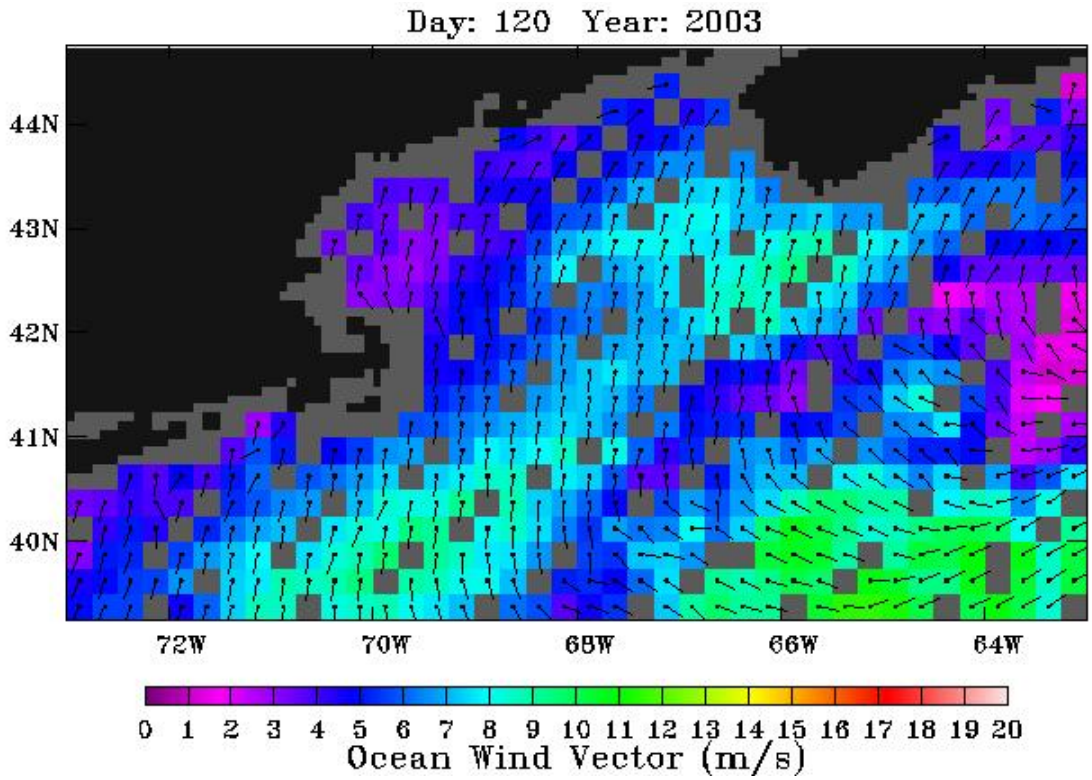

Figure 8-A99. QuikSCAT wind field. Morning satellite overpass on April 30, 2003.

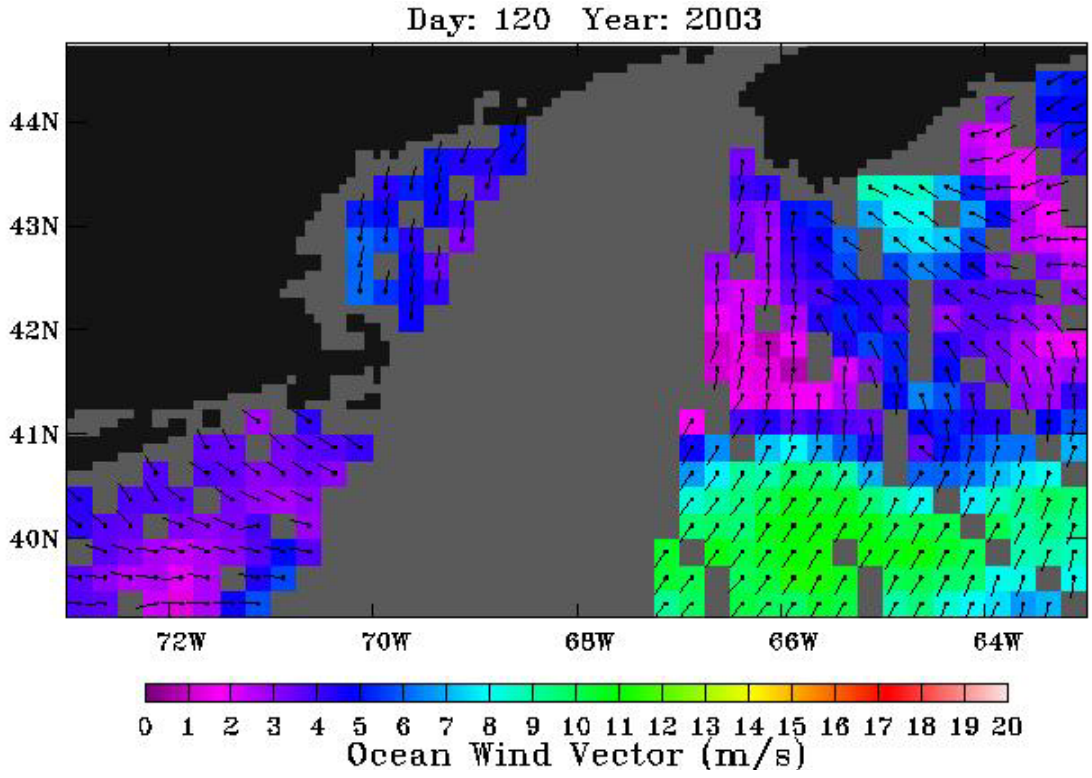

Figure 8-A100. QuikSCAT wind field. Evening satellite overpass on April 30, 2003.

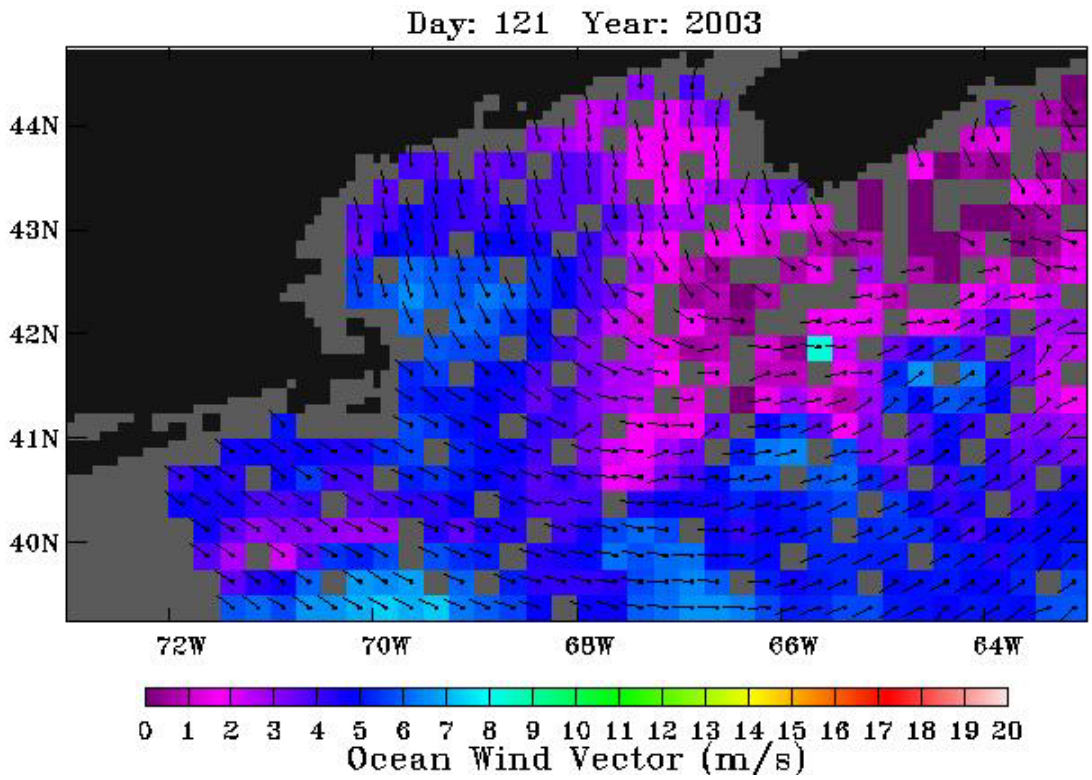

Figure 8-A101. QuikSCAT wind field. Morning satellite overpass on May 1, 2003.

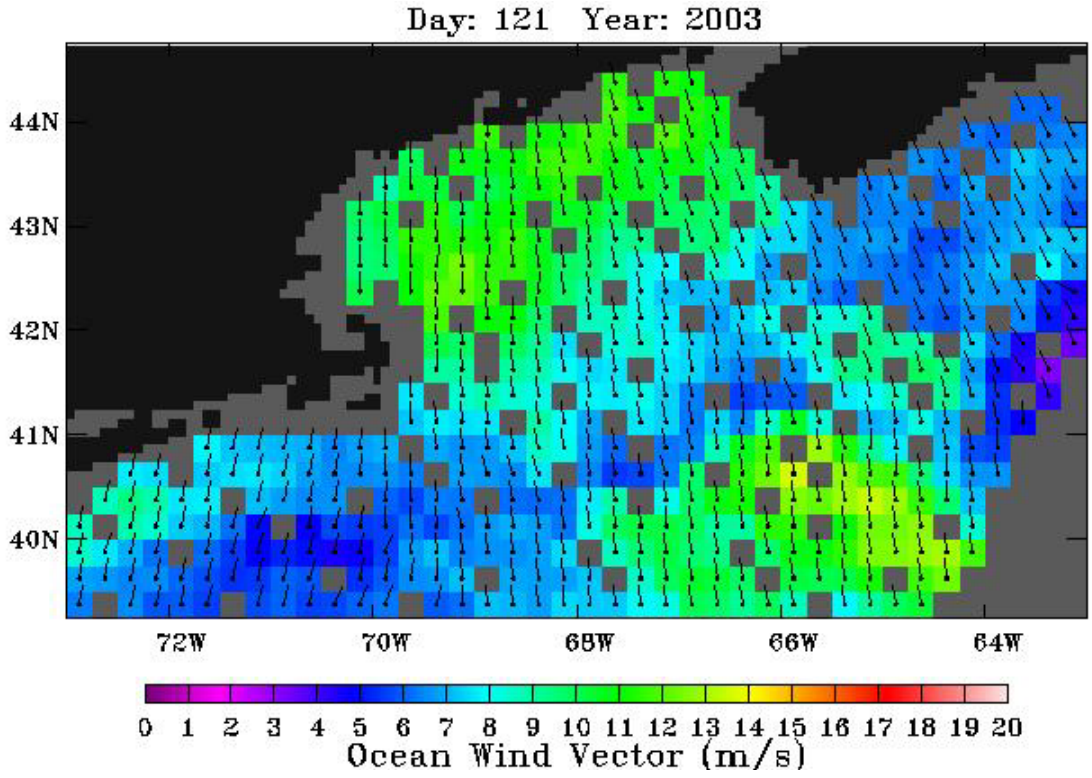

Figure 8-A102. QuikSCAT wind field. Evening satellite overpass on May 1, 2003.

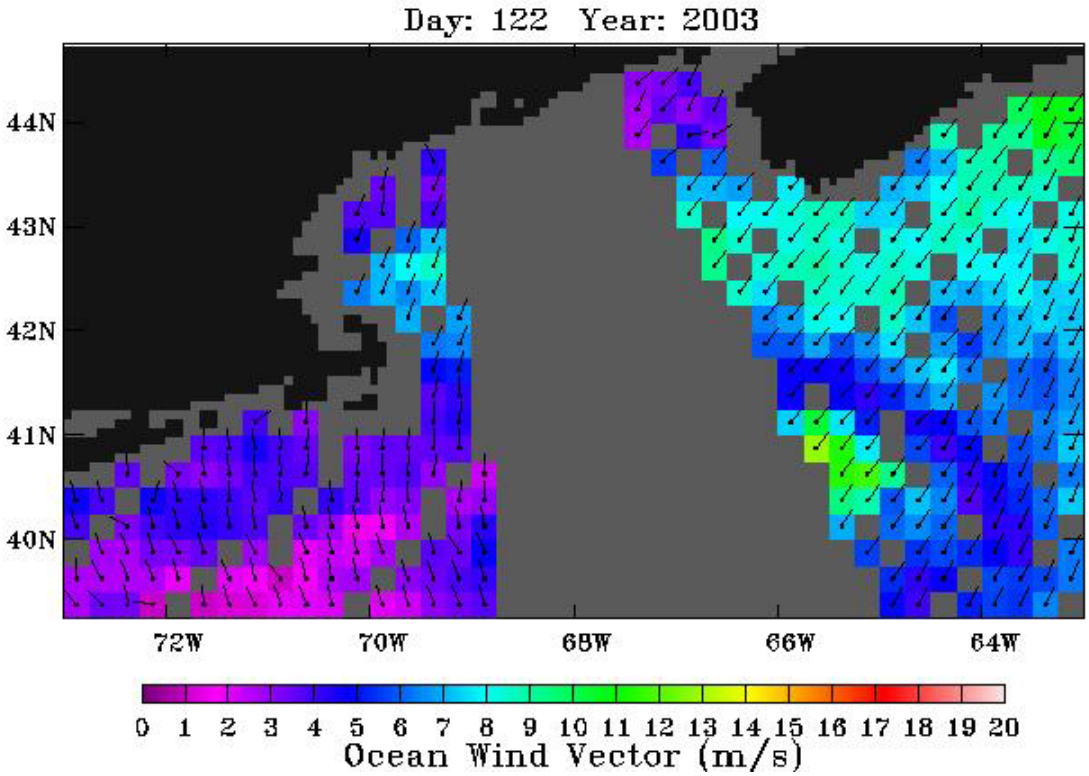

Figure 8-A103. QuikSCAT wind field. Morning satellite overpass on May 2, 2003.

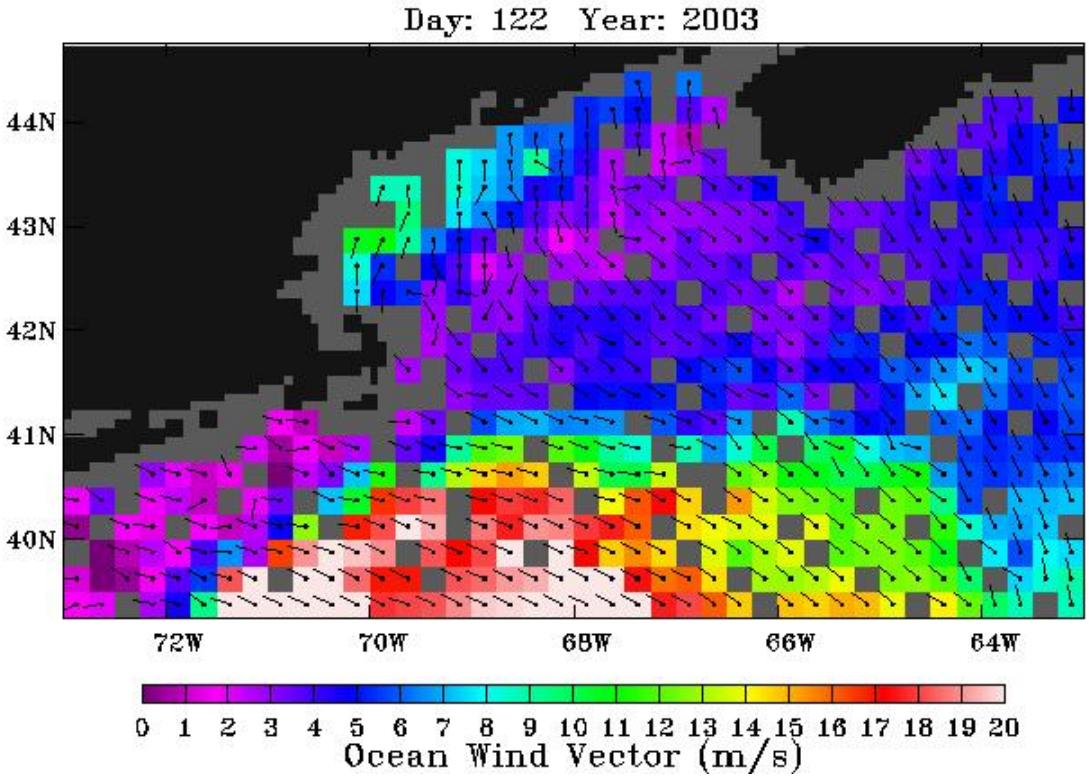

Figure 8-A104. QuikSCAT wind field. Evening satellite overpass on May 2, 2003.

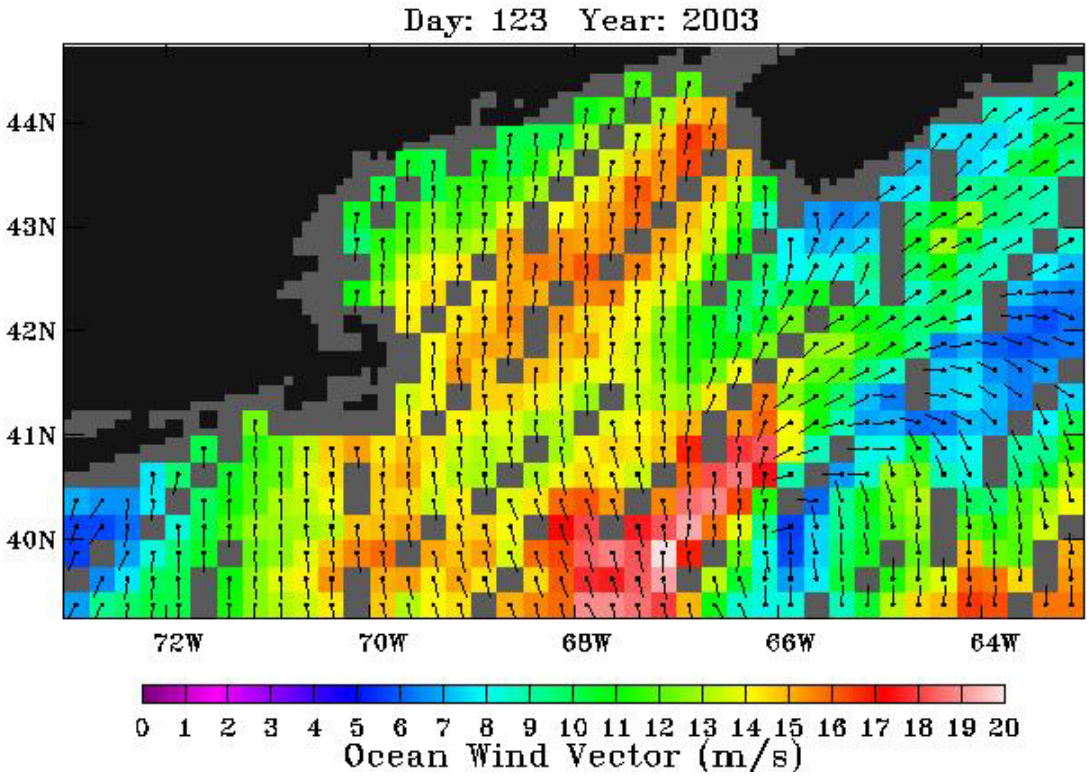

Figure 8-A105. QuikSCAT wind field. Morning satellite overpass on May 3, 2003.

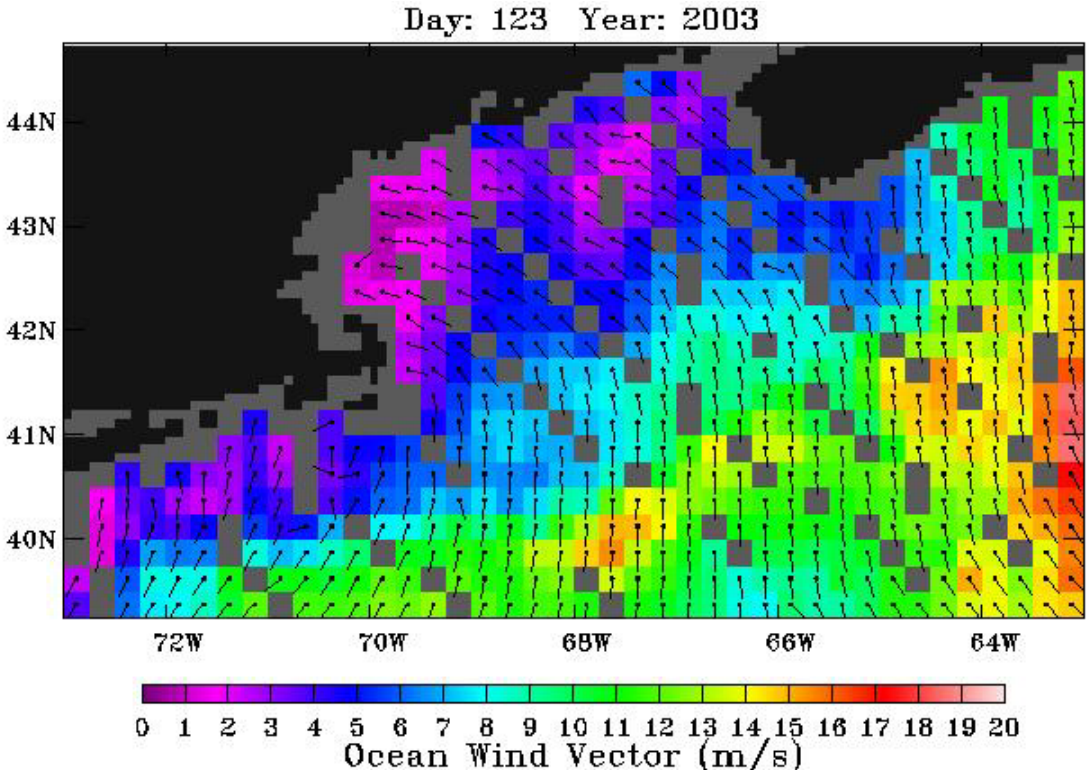

Figure 8-A106. QuikSCAT wind field. Evening satellite overpass on May 3, 2003.

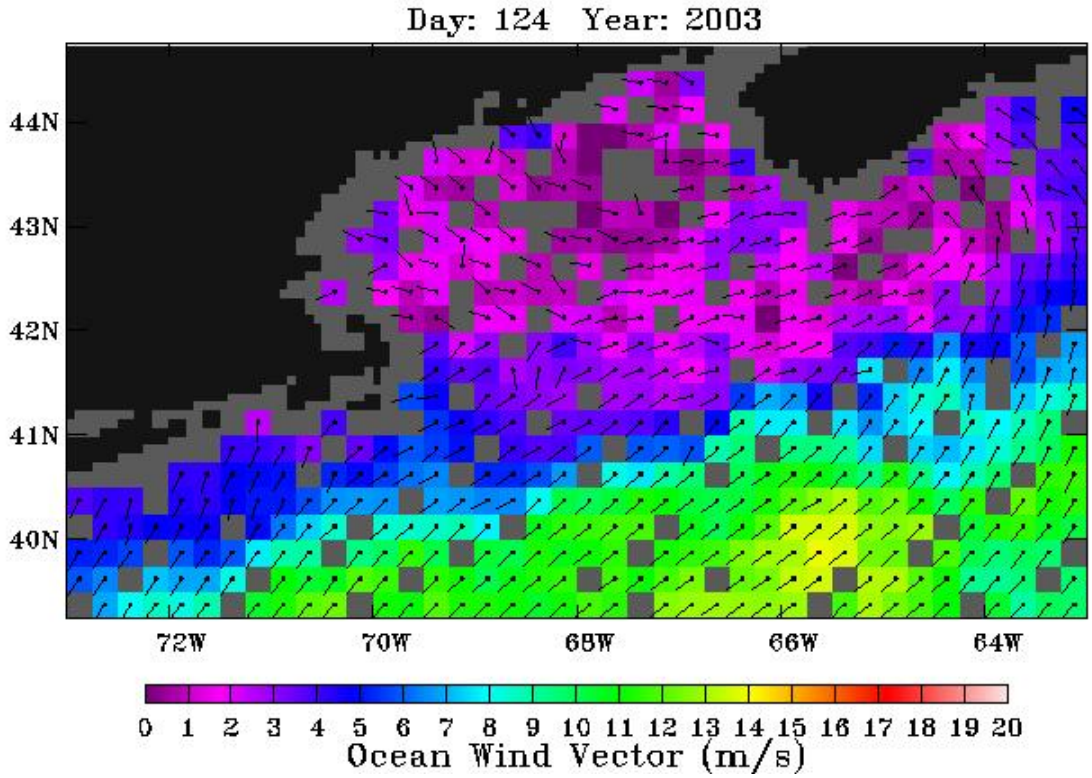

Figure 8-A107. QuikSCAT wind field. Morning satellite overpass on May 4, 2003.

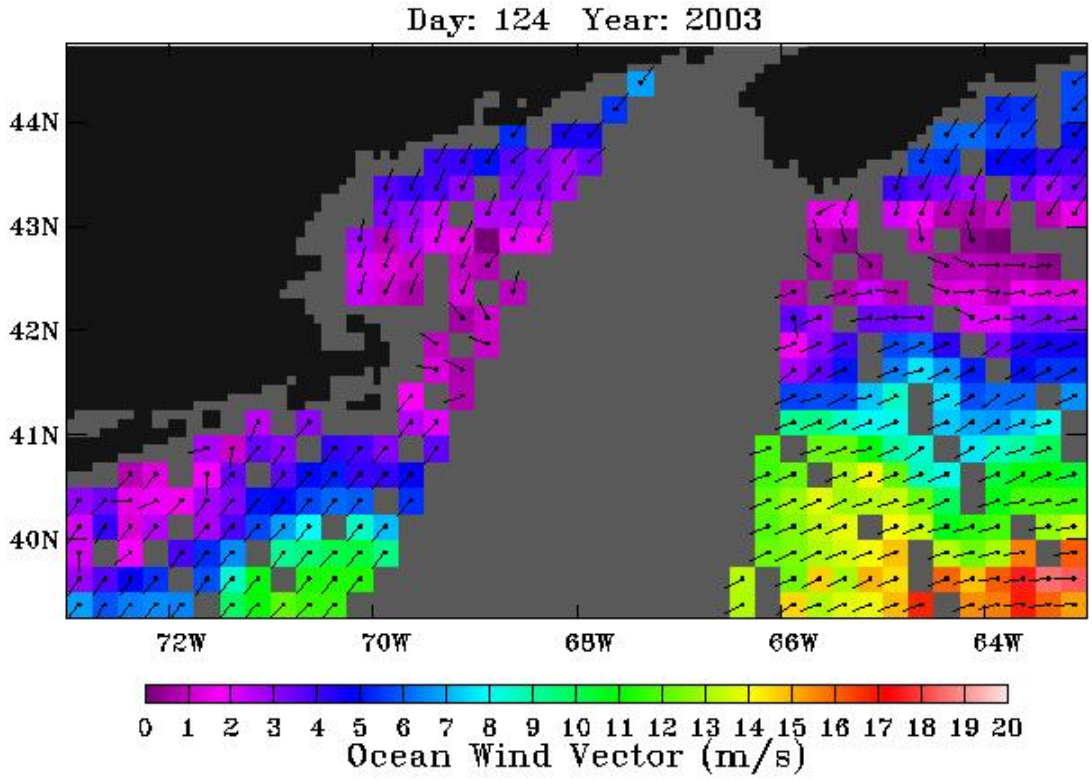

Figure 8-A108. QuikSCAT wind field. Evening satellite overpass on May 4, 2003.

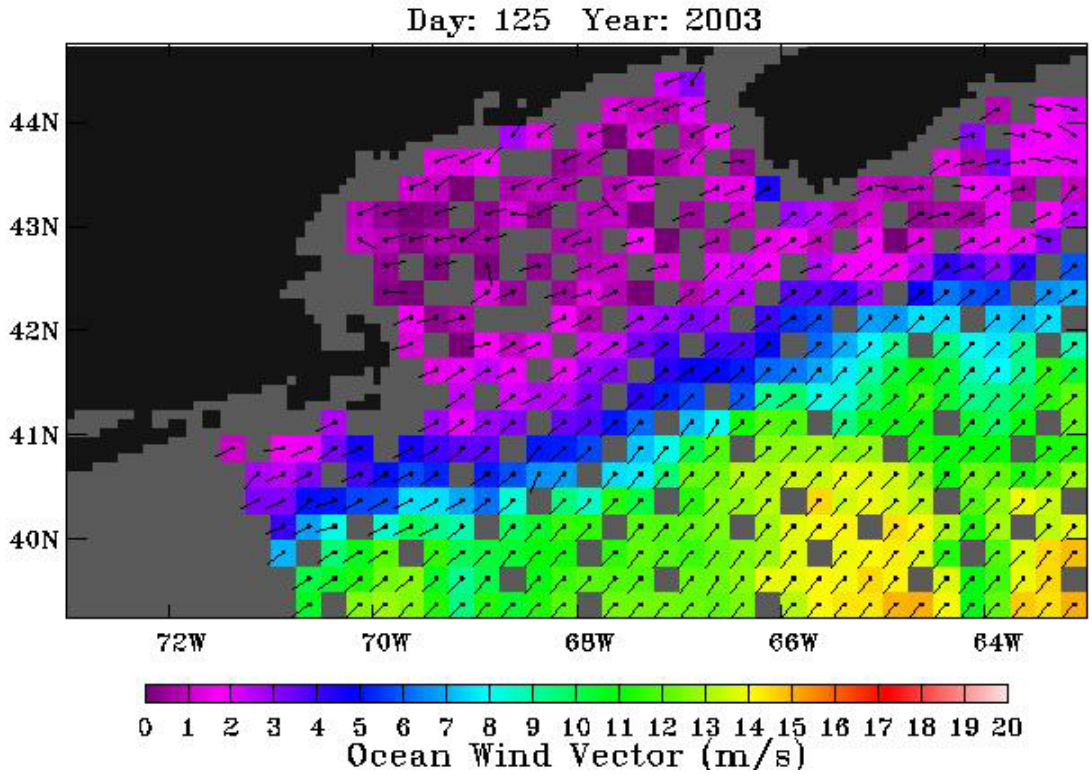

Figure 8-A109. QuikSCAT wind field. Morning satellite overpass on May 5, 2003.

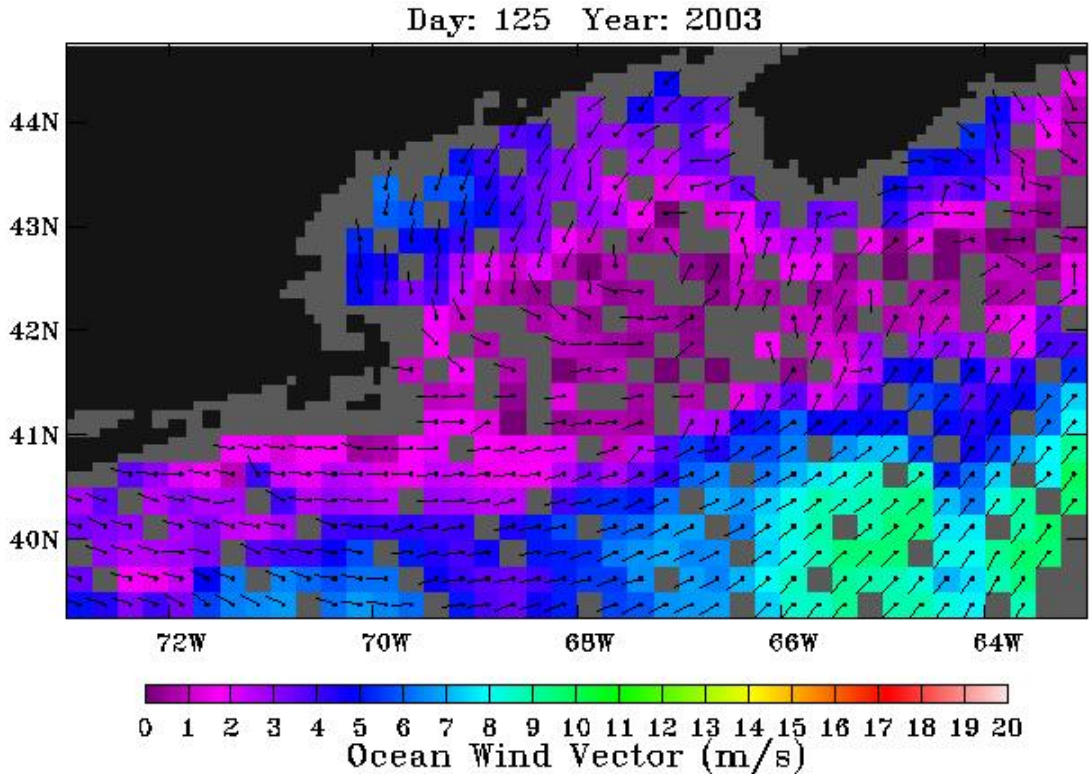

Figure 8-A110. QuikSCAT wind field. Evening satellite overpass on May 5, 2003.

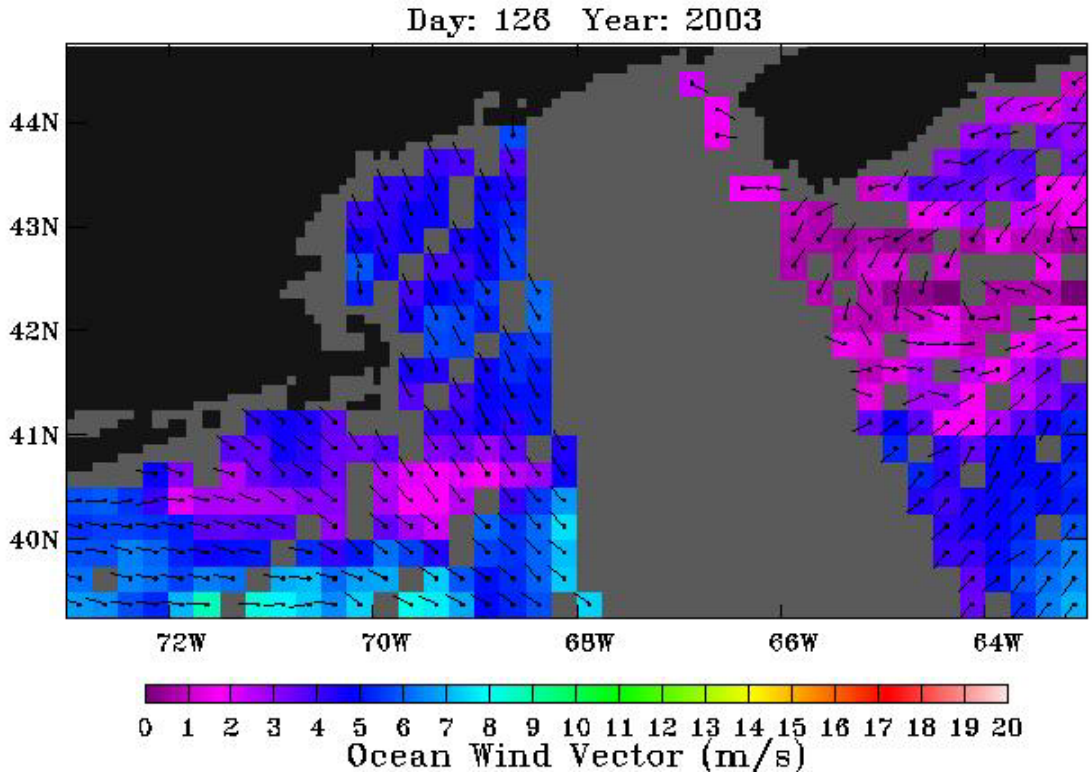

Figure 8-A111. QuikSCAT wind field. Morning satellite overpass on May 6, 2003.

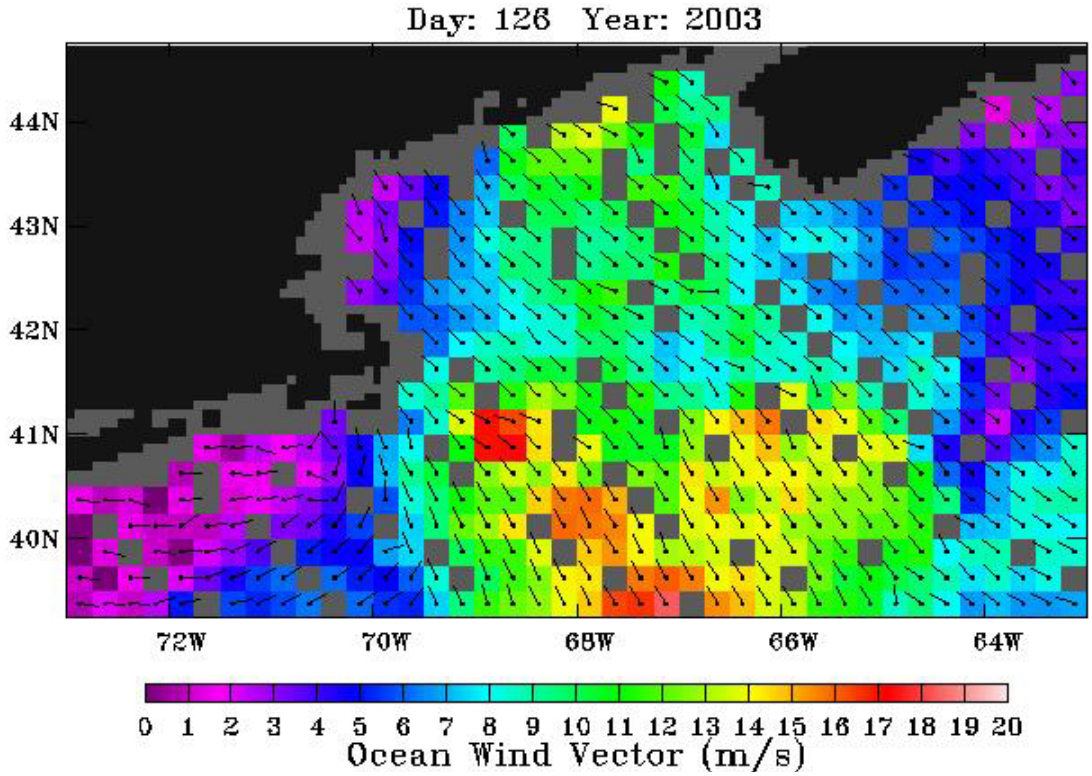

Figure 8-A112. QuikSCAT wind field. Evening satellite overpass on May 6, 2003.

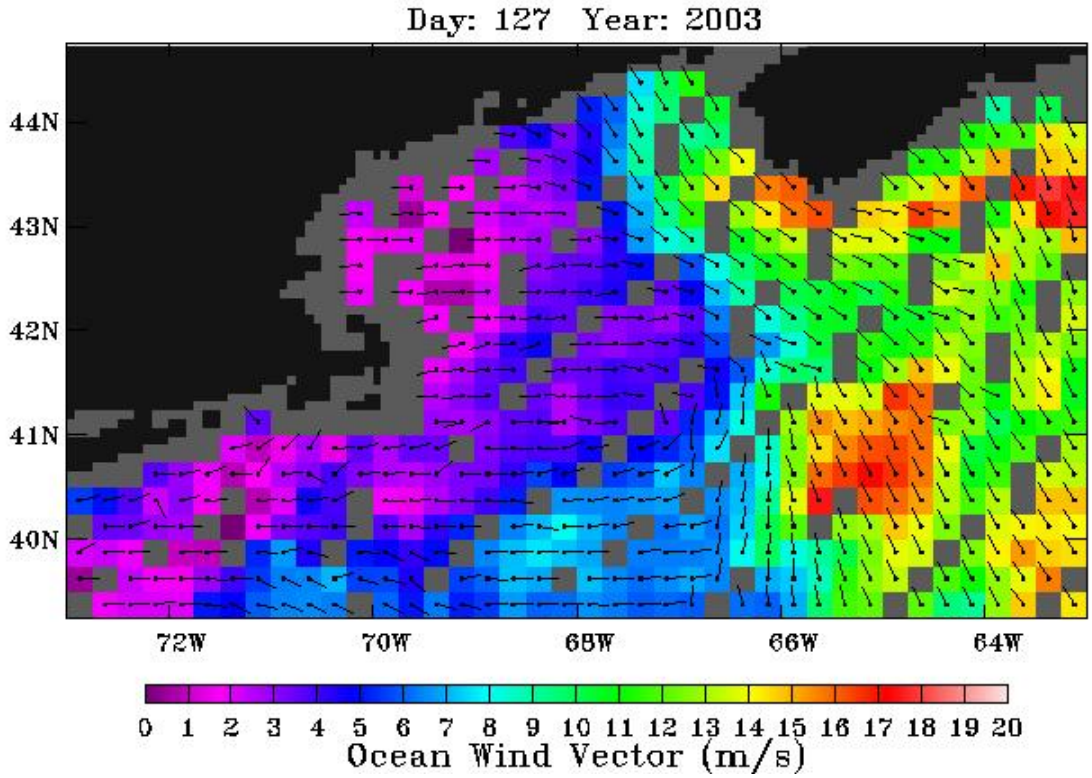

Figure 8-A113. QuikSCAT wind field. Morning satellite overpass on May 7, 2003.

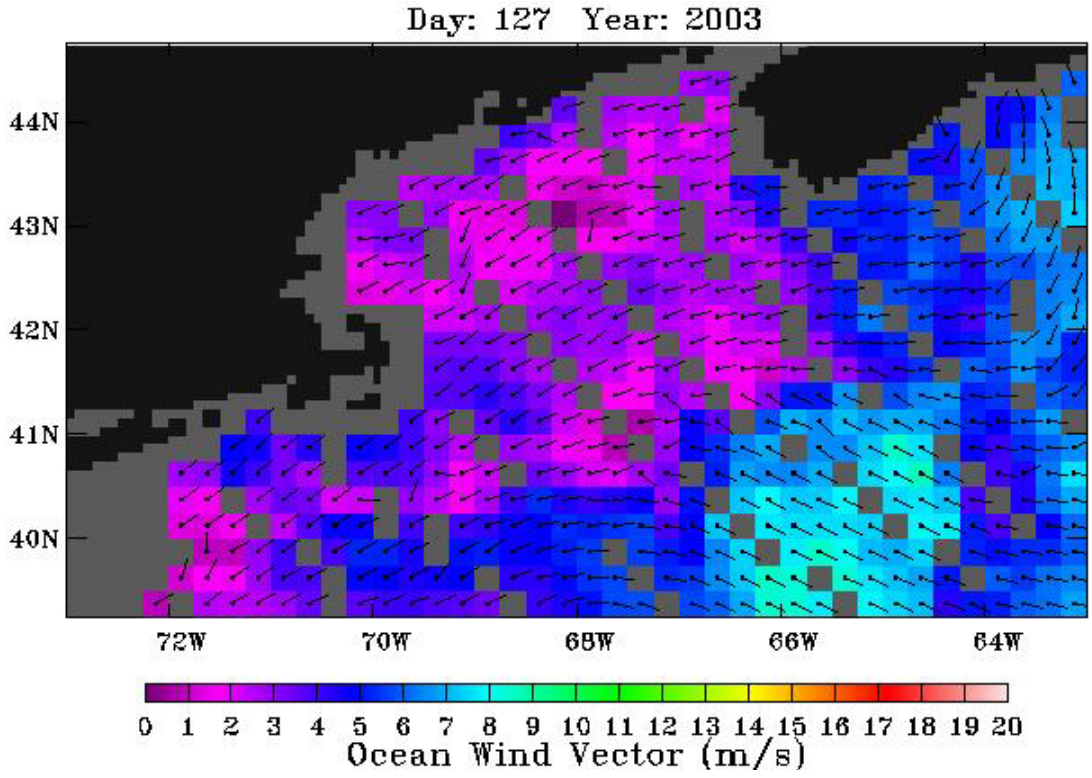

Figure 8-A114. QuikSCAT wind field. Evening satellite overpass on May 7, 2003.

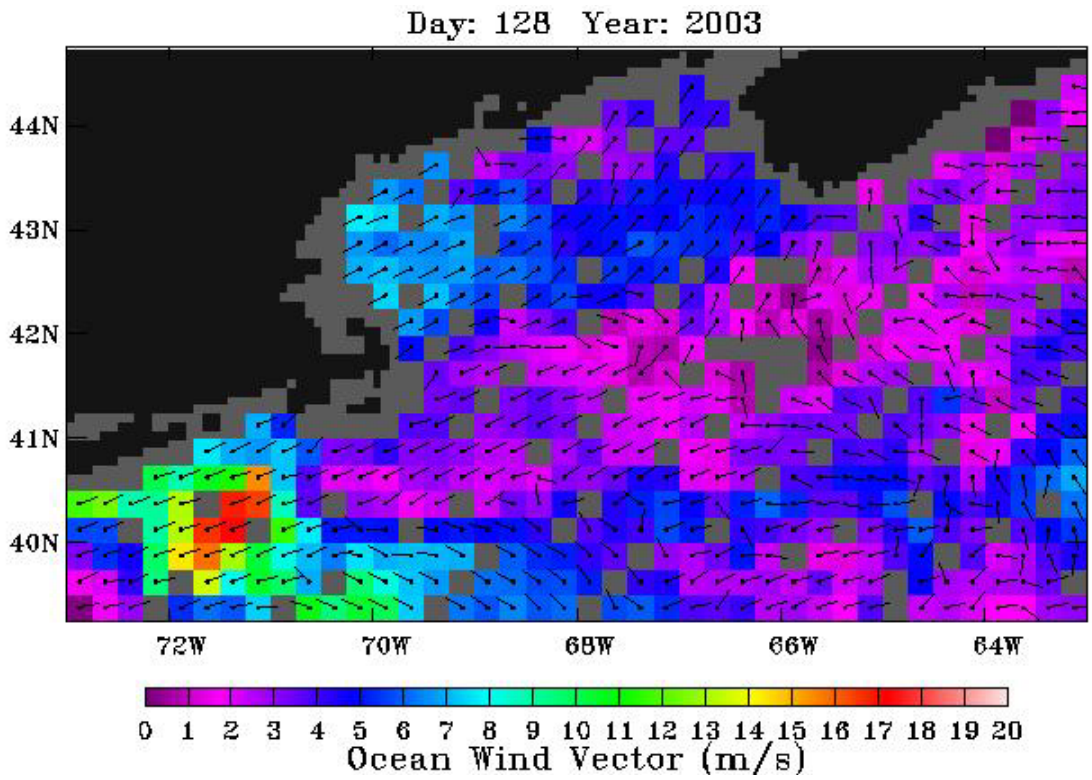

Figure 8-A115. QuikSCAT wind field. Morning satellite overpass on May 8, 2003.

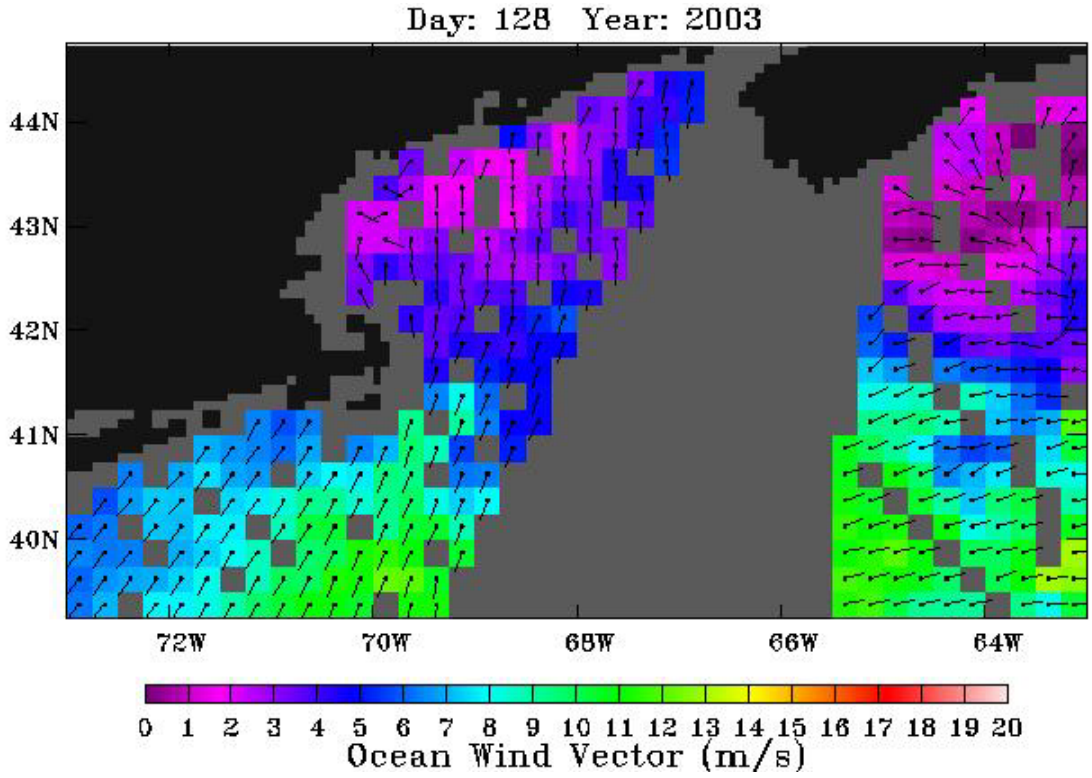

Figure 8-A116. QuikSCAT wind field. Evening satellite overpass on May 8, 2003.

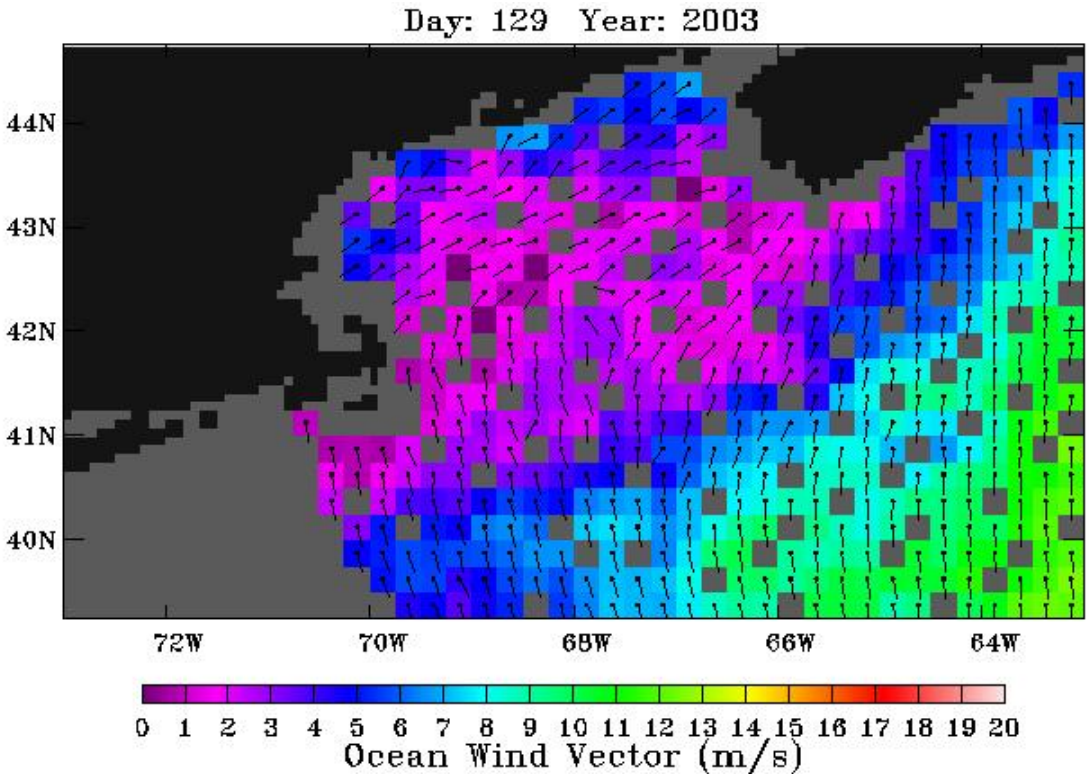

Figure 8-A117. QuikSCAT wind field. Morning satellite overpass on May 9, 2003.

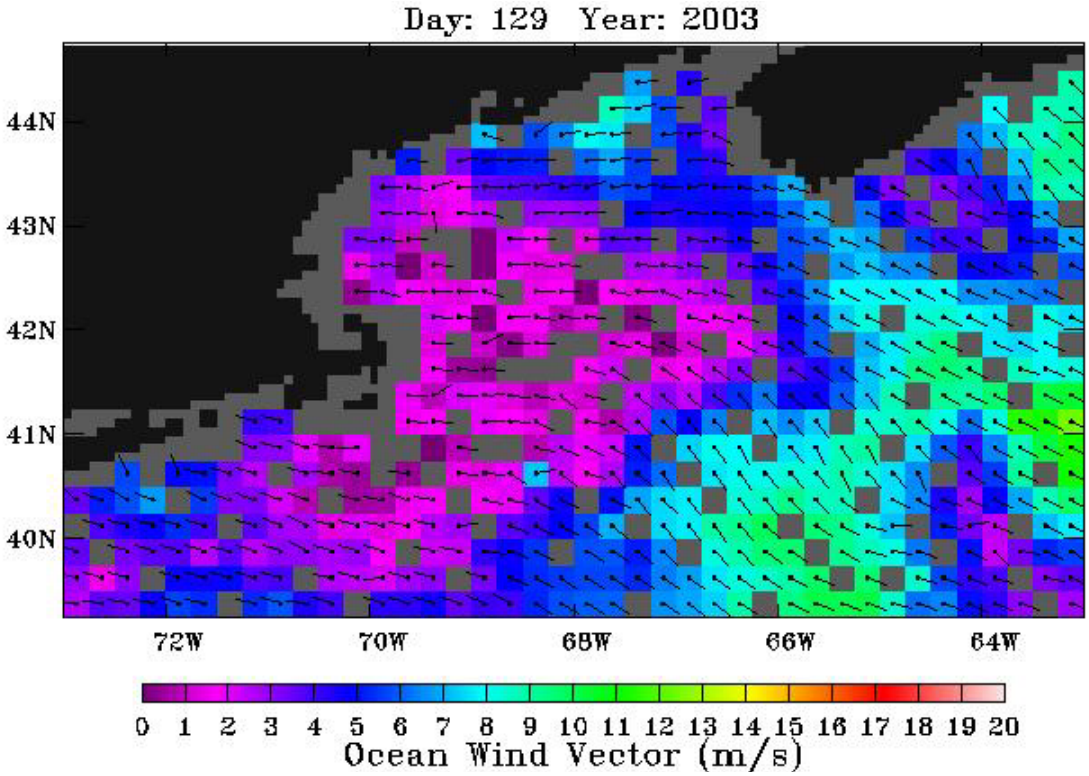

Figure 8-A118. QuikSCAT wind field. Evening satellite overpass on May 9, 2003.

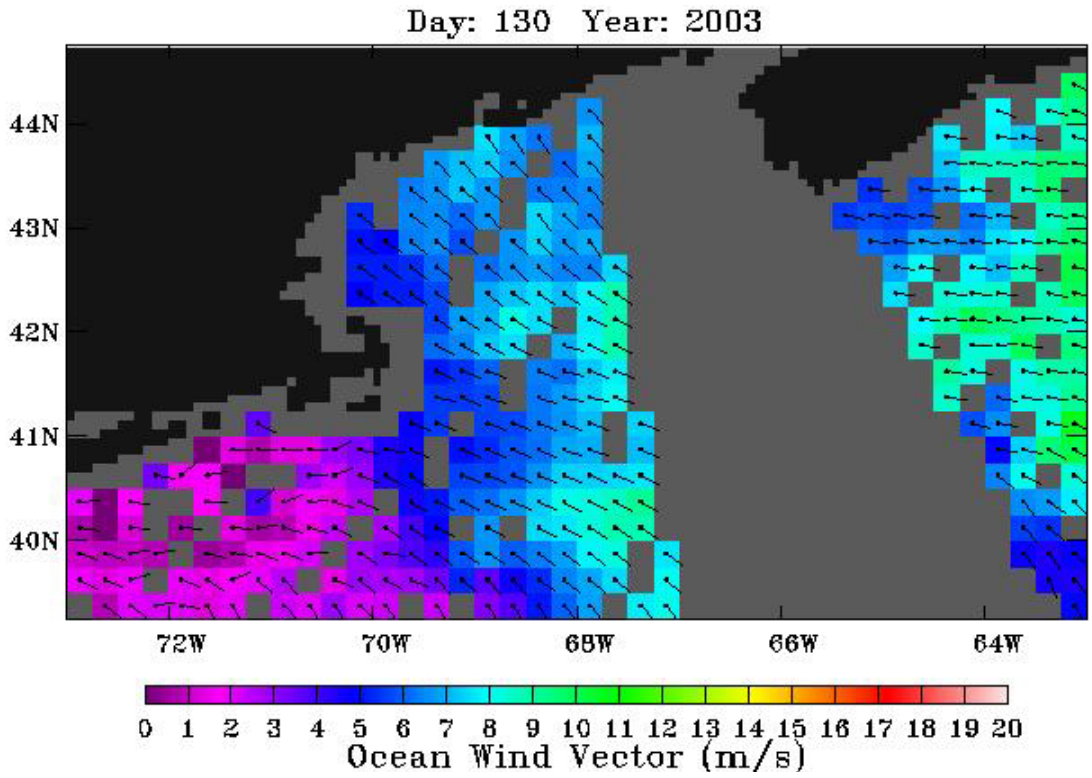

Figure 8-A119. QuikSCAT wind field. Morning satellite overpass on May 10, 2003.

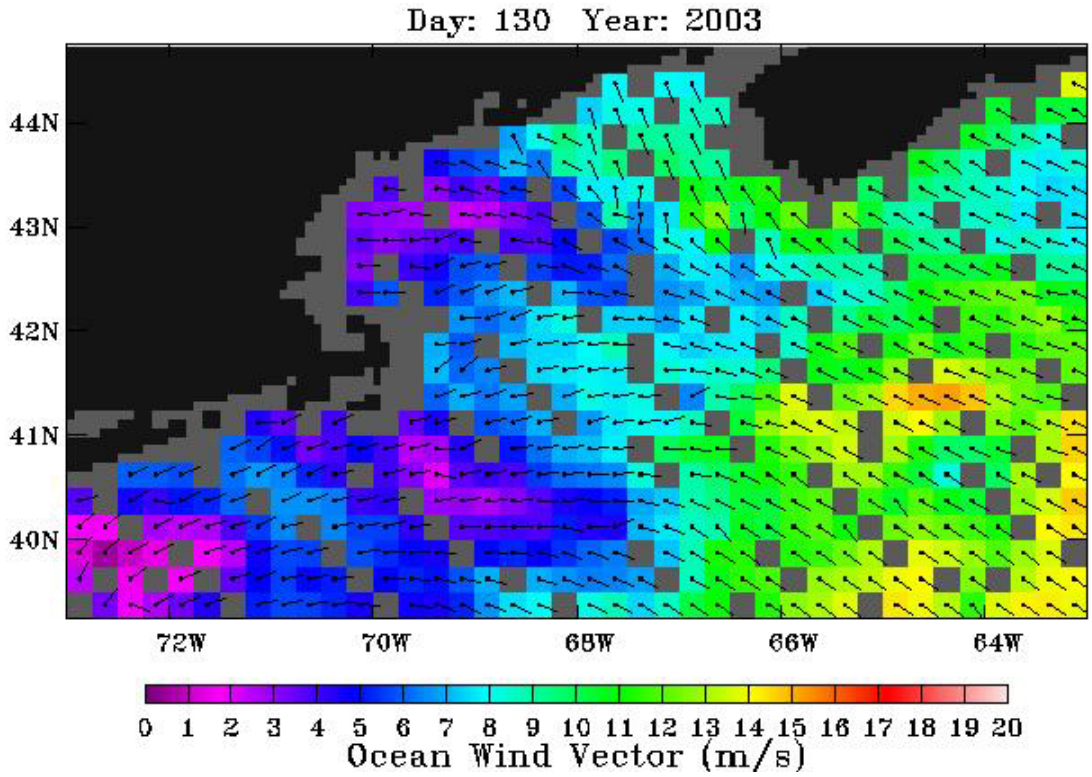

Figure 8-A120. QuikSCAT wind field. Evening satellite overpass on May 10, 2003.

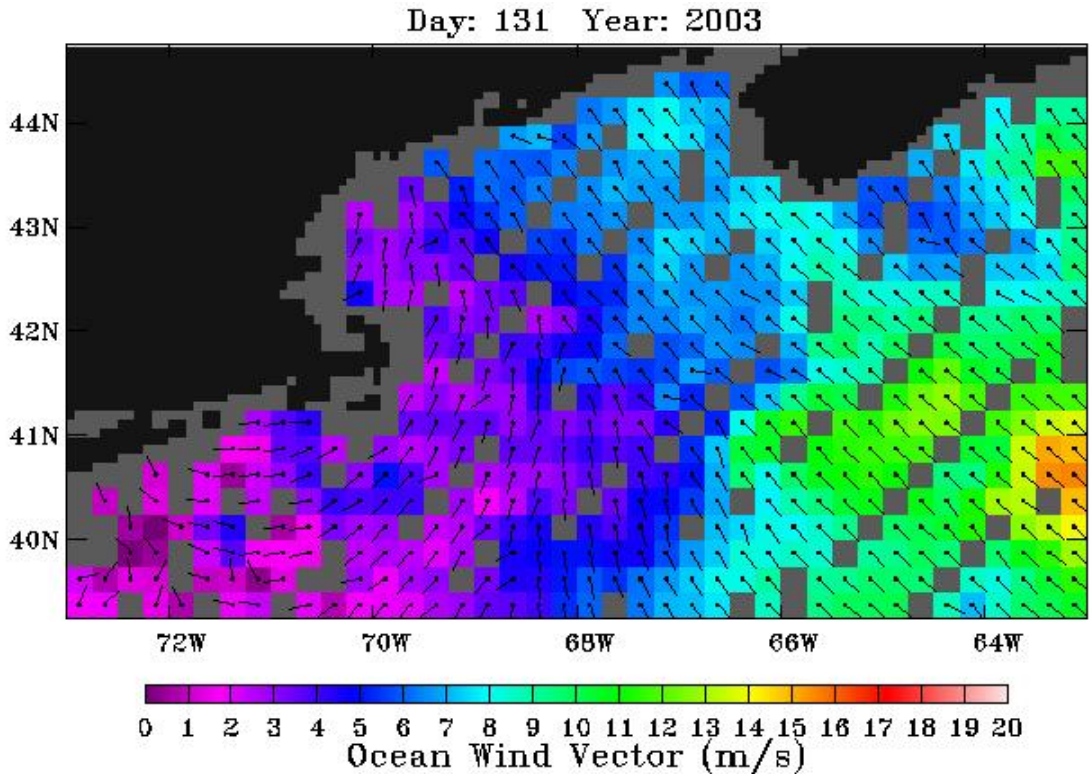

Figure 8-A121. QuikSCAT wind field. Morning satellite overpass on May 11, 2003.

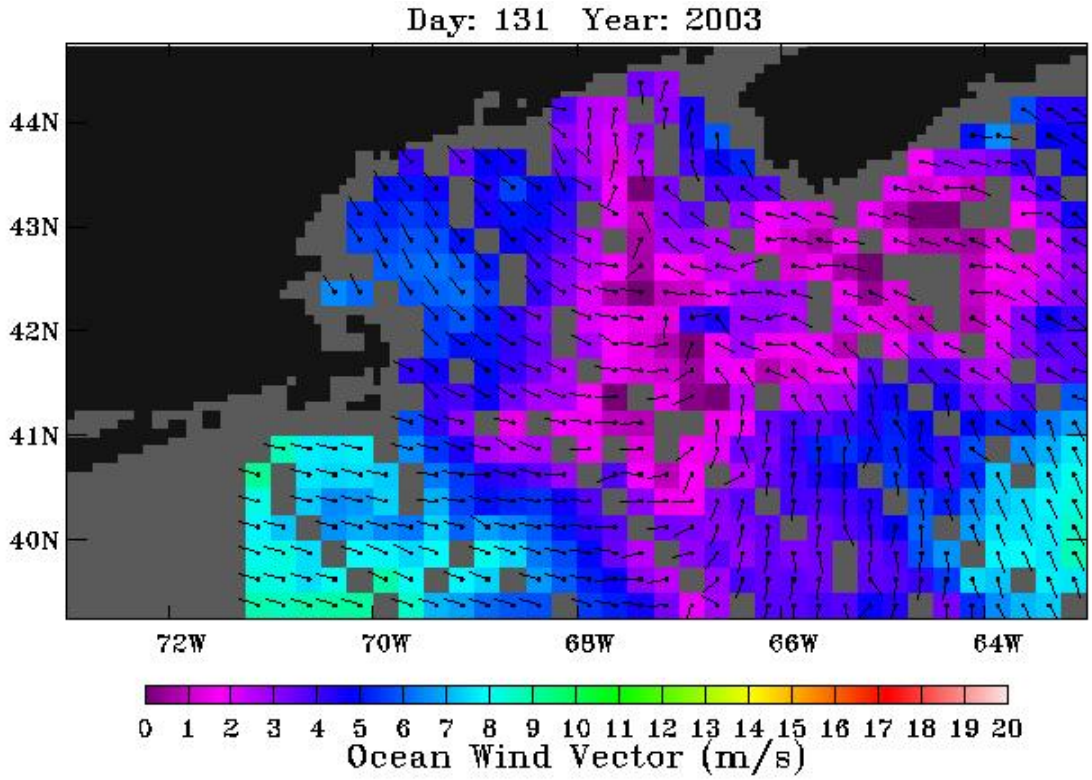

Figure 8-A122. QuikSCAT wind field. Evening satellite overpass on May 11, 2003.

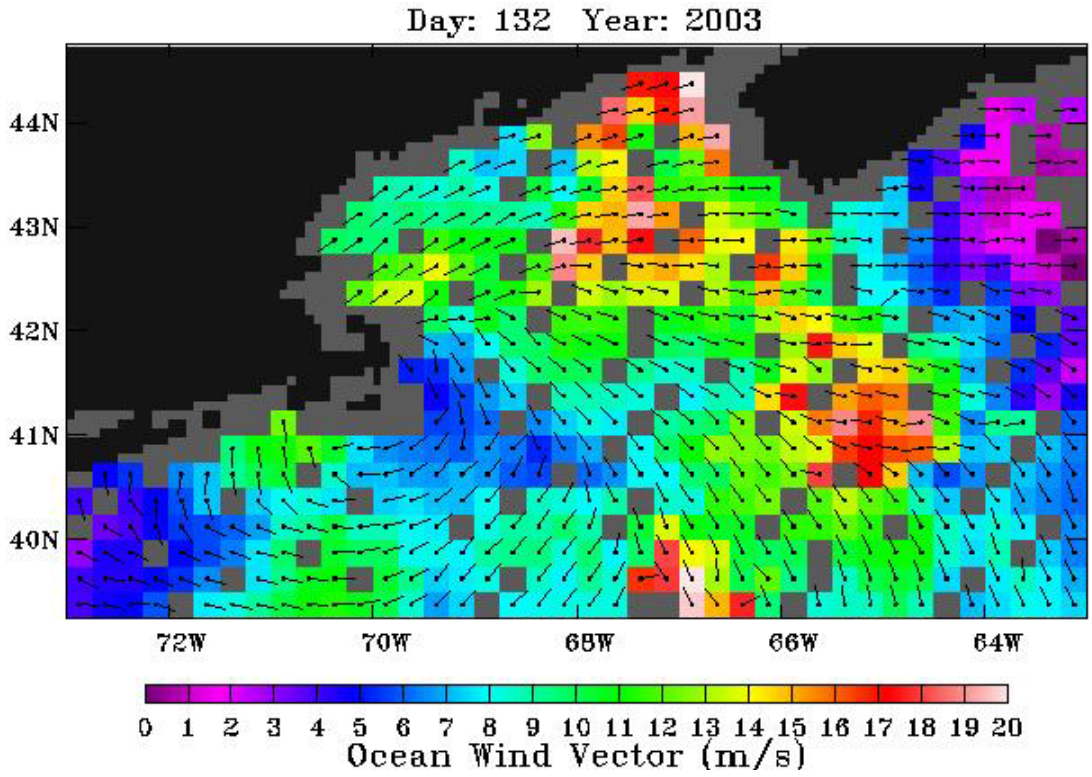

Figure 8-A123. QuikSCAT wind field. Morning satellite overpass on May 12, 2003.

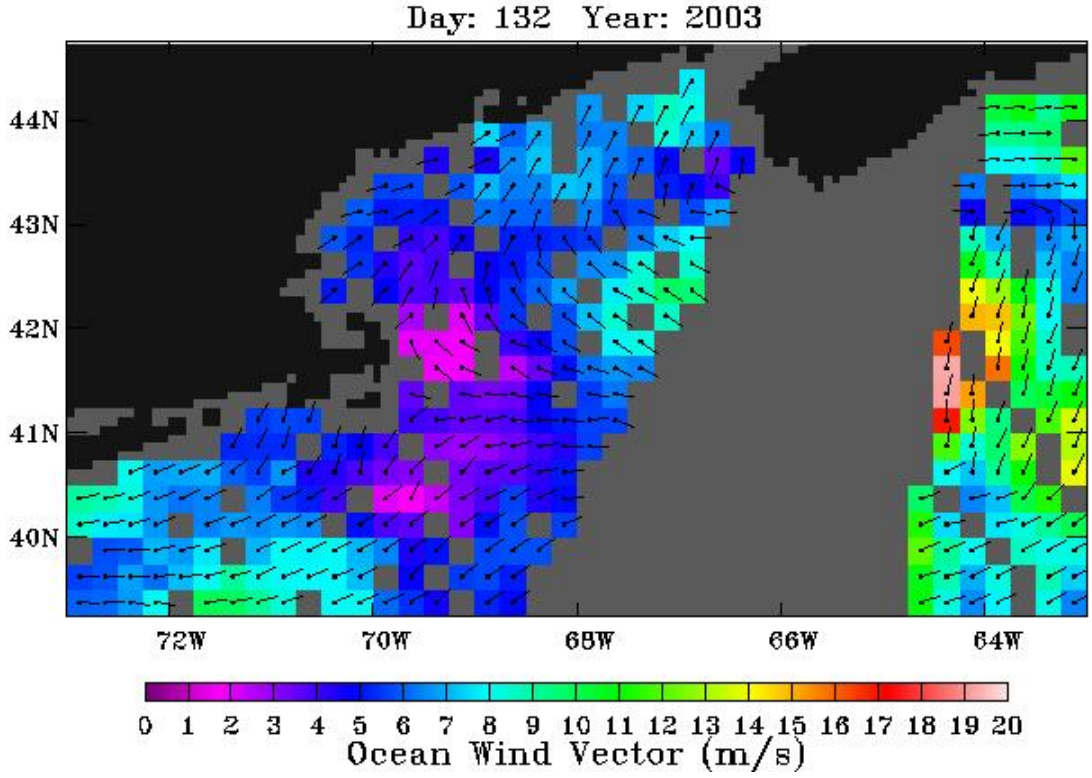

Figure 8-A124. QuikSCAT wind field. Evening satellite overpass on May 12, 2003.

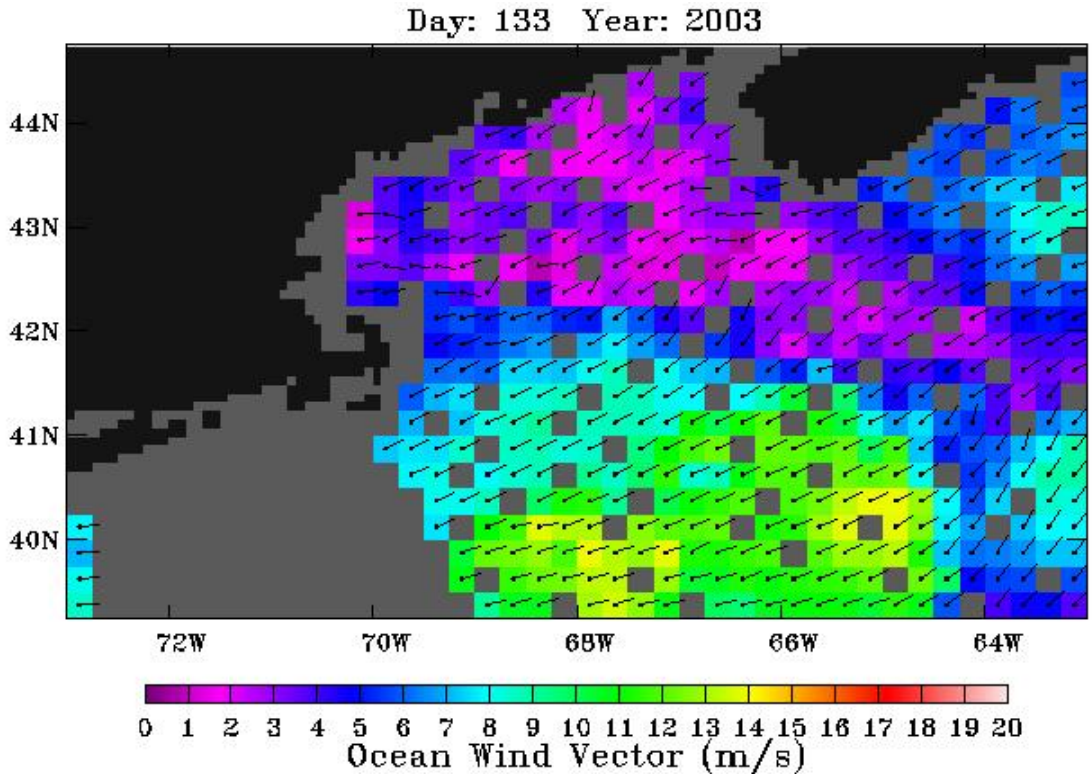

Figure 8-A125. QuikSCAT wind field. Morning satellite overpass on May 13, 2003.

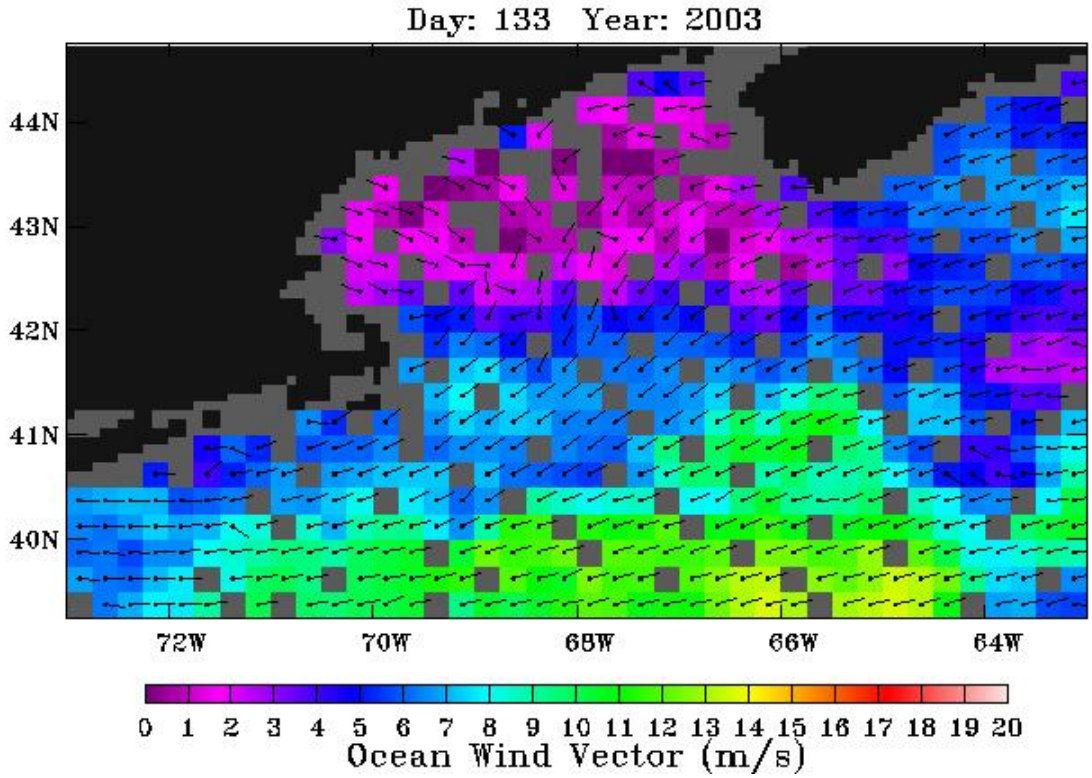

Figure 8-A126. QuikSCAT wind field. Evening satellite overpass on May 13, 2003.

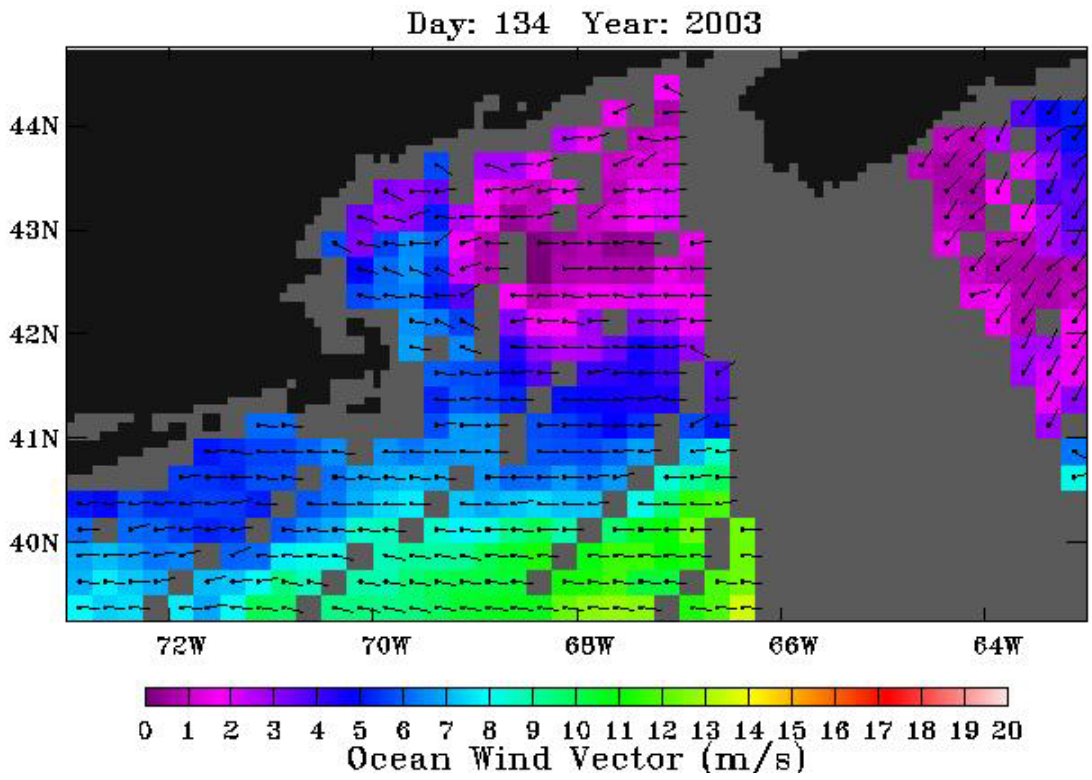

Figure 8-A127. QuikSCAT wind field. Morning satellite overpass on May 14, 2003.

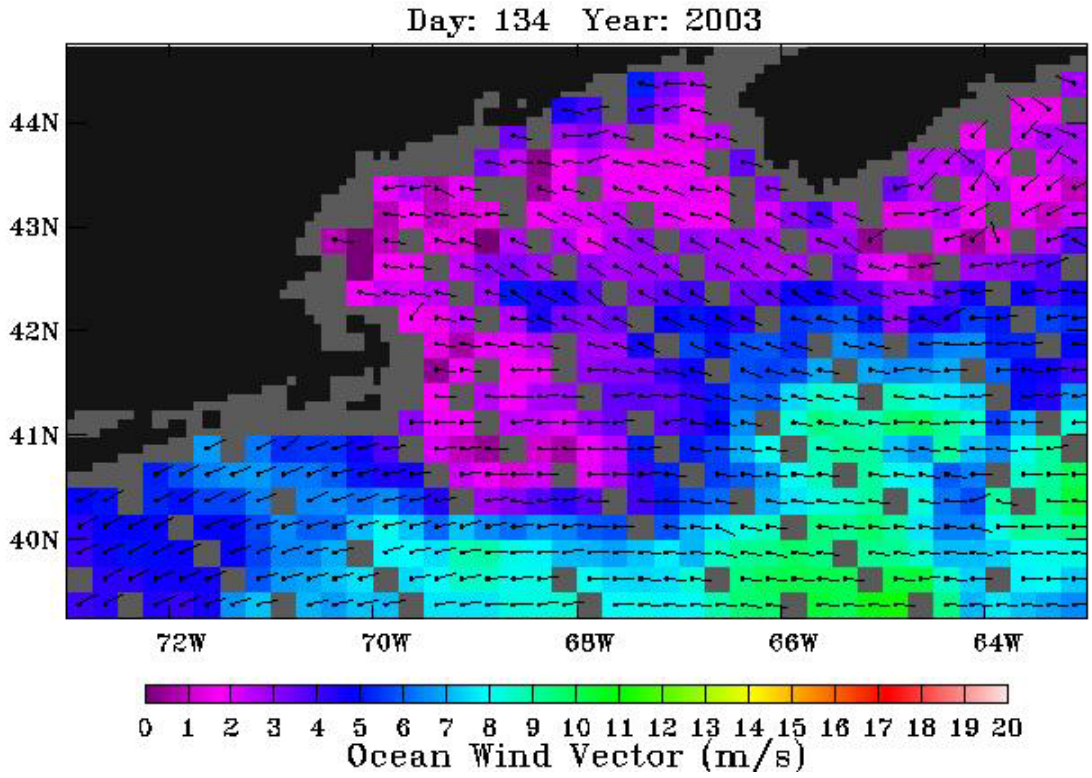

Figure 8-A128. QuikSCAT wind field. Evening satellite overpass on May 14, 2003.

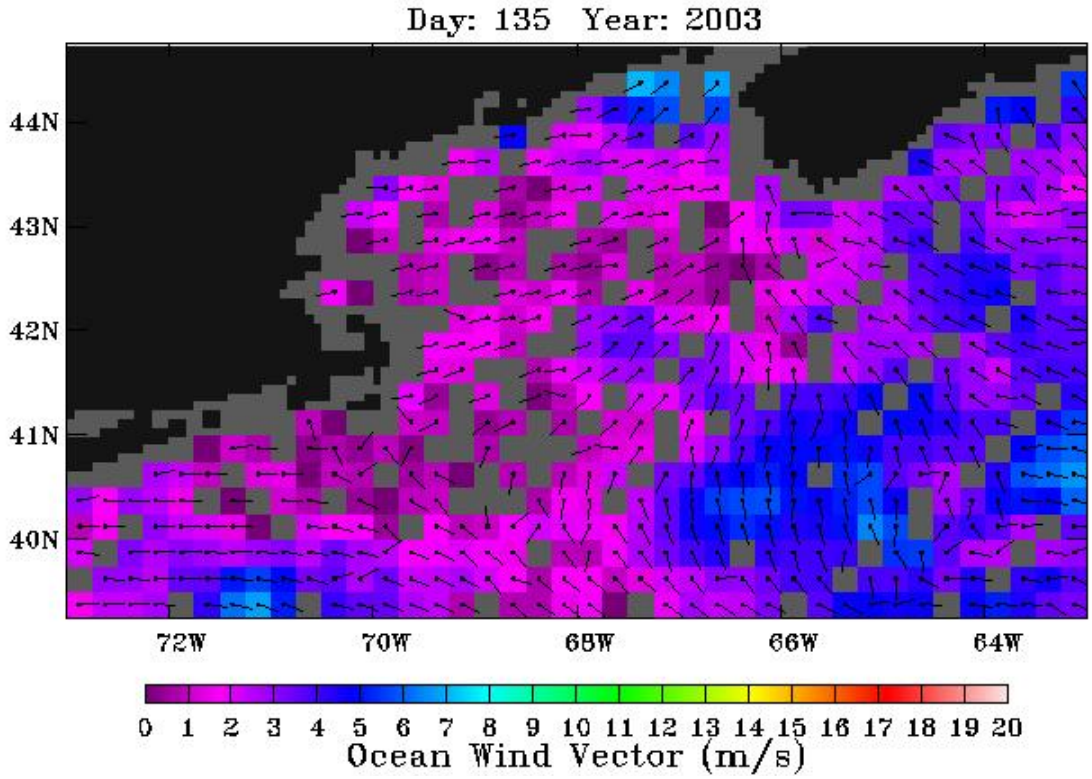

Figure 8-A129. QuikSCAT wind field. Morning satellite overpass on May 15, 2003.

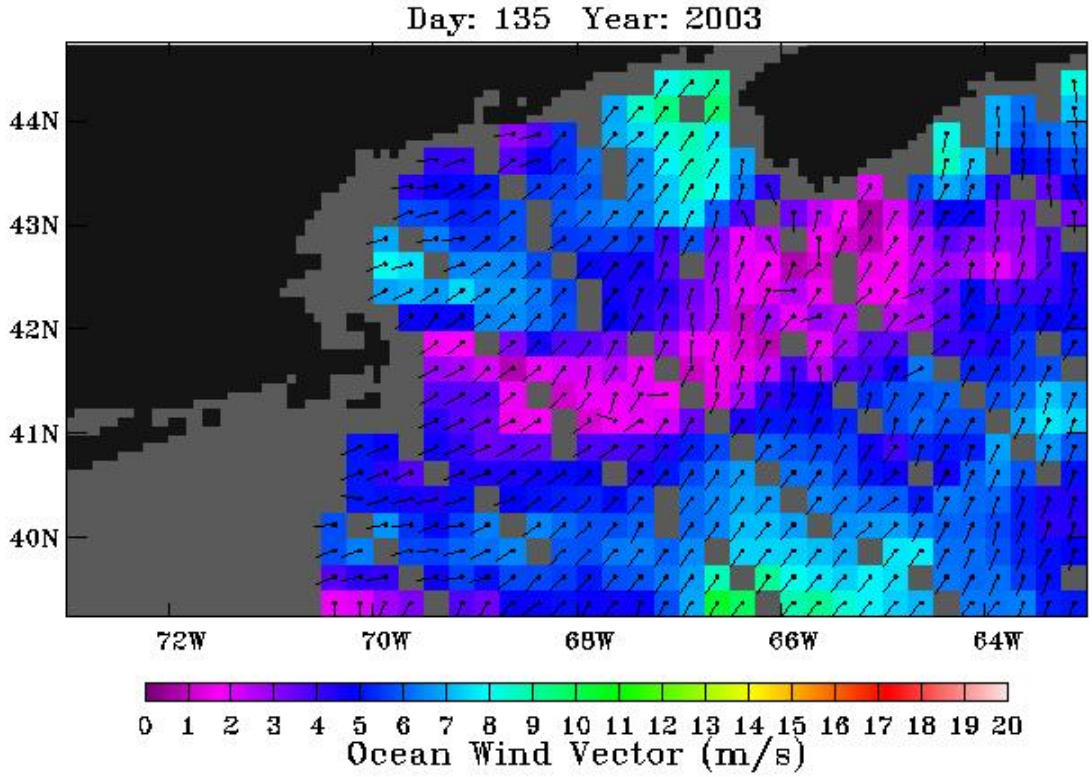

Figure 8-A130. QuikSCAT wind field. Evening satellite overpass on May 15, 2003.

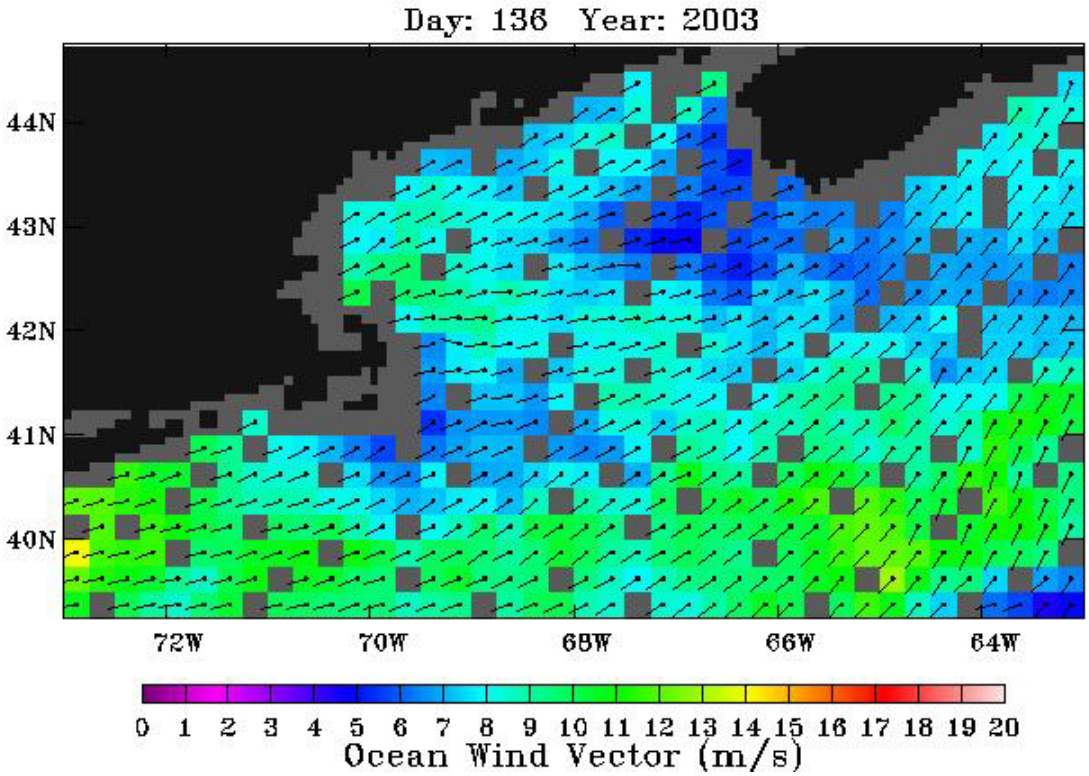

Figure 8-A131. QuikSCAT wind field. Morning satellite overpass on May 16, 2003.

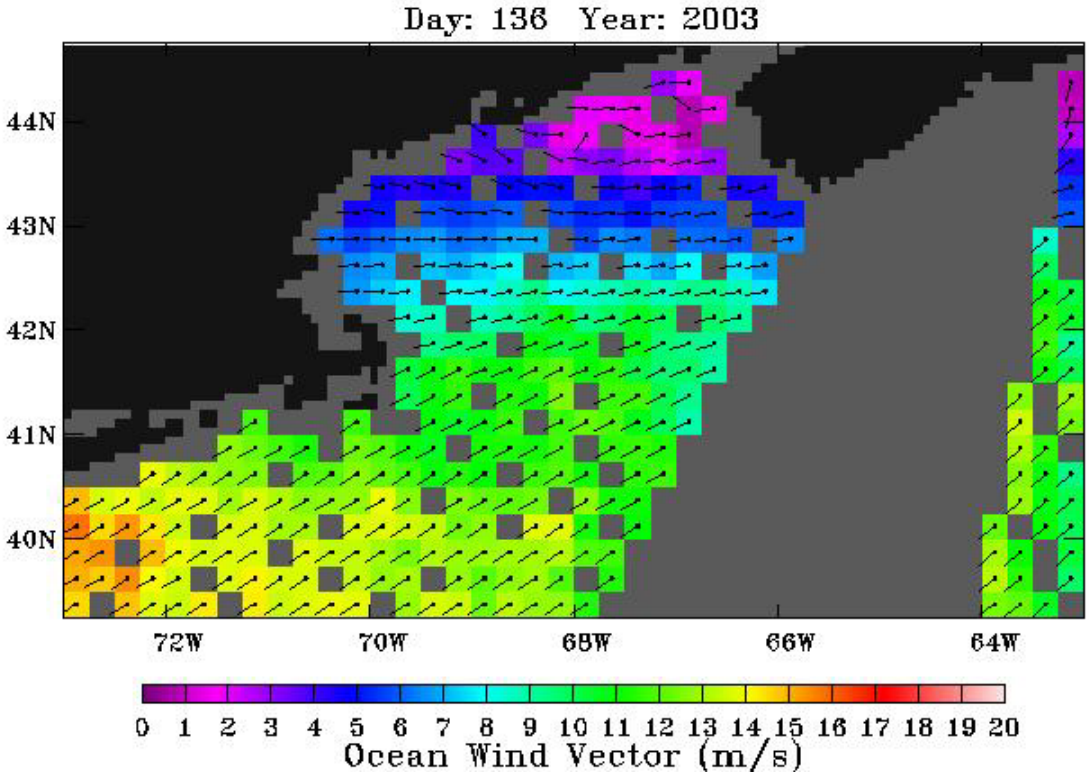

Figure 8-A132. QuikSCAT wind field. Evening satellite overpass on May 16, 2003.

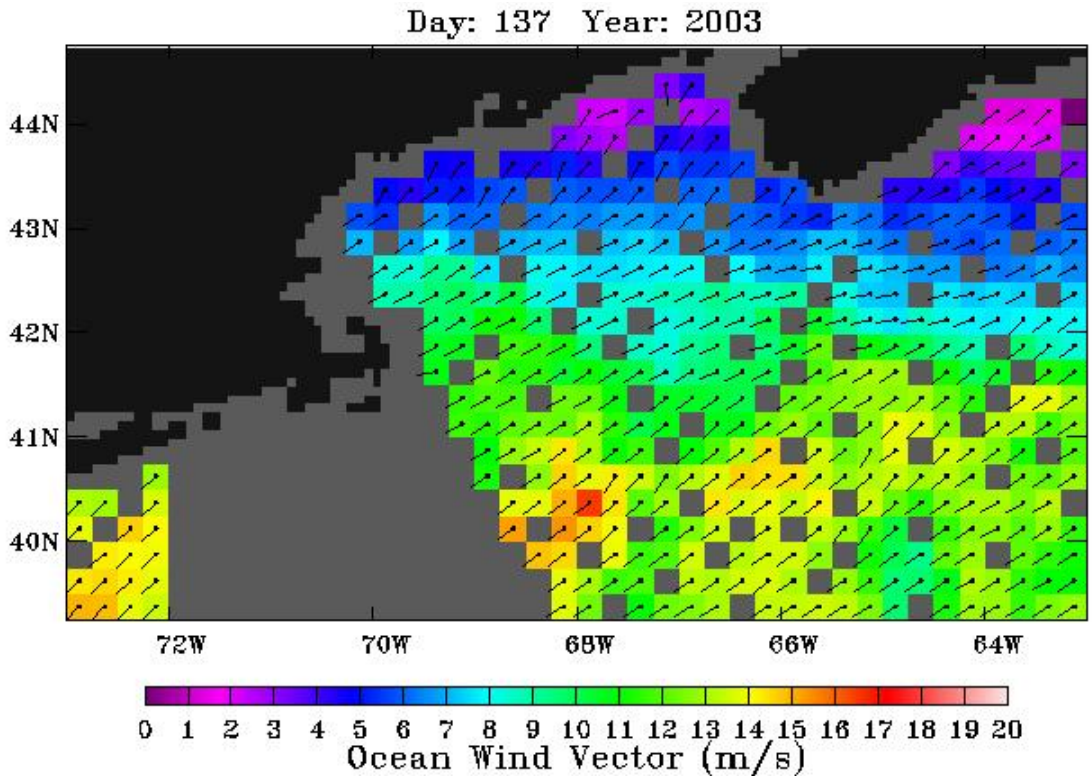

Figure 8-A133. QuikSCAT wind field. Morning satellite overpass on May 17, 2003.

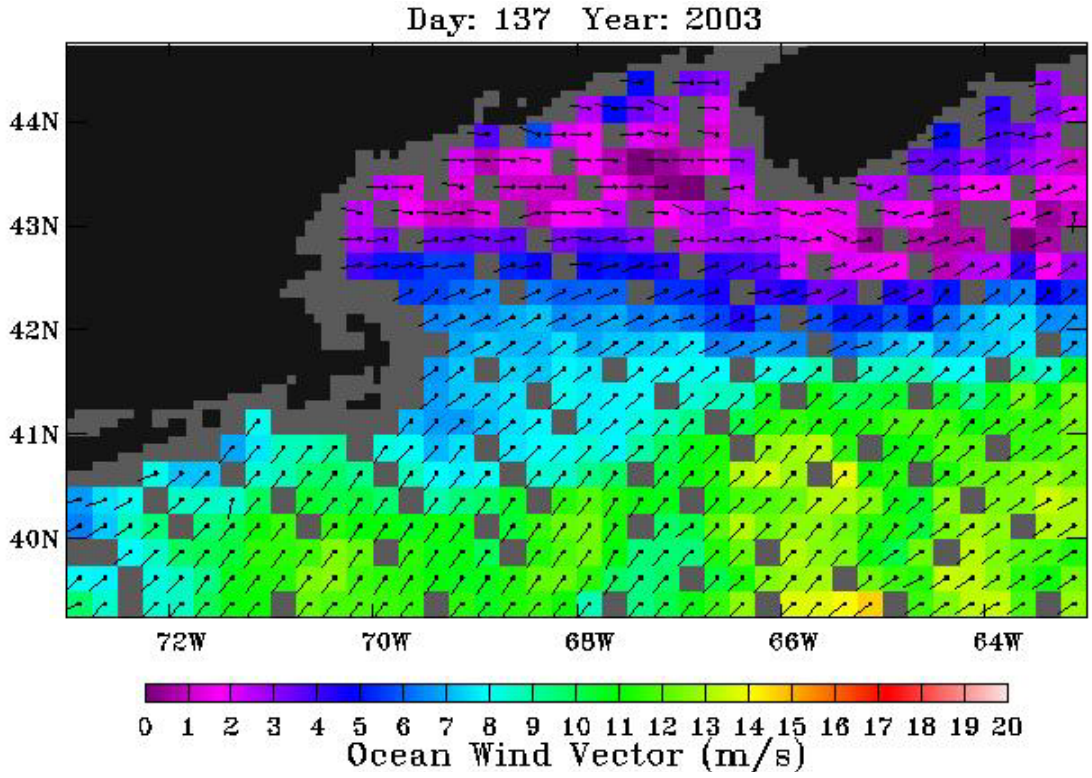

Figure 8-A134. QuikSCAT wind field. Evening satellite overpass on May 17, 2003.

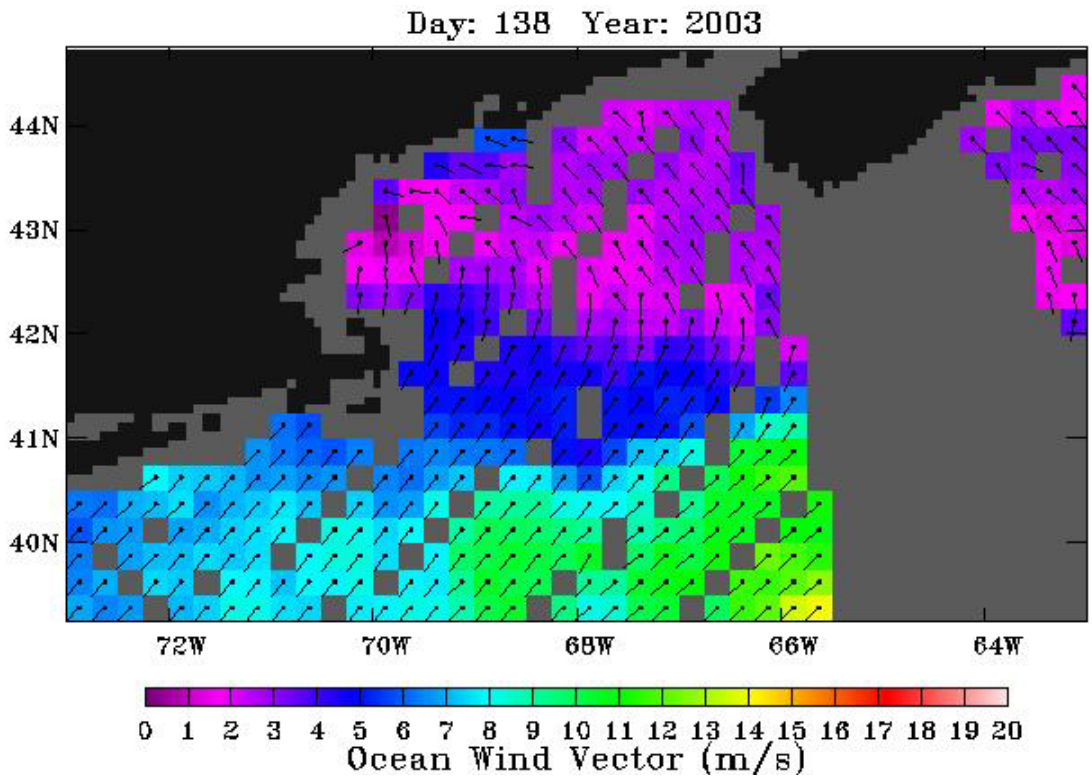

Figure 8-A135. QuikSCAT wind field. Morning satellite overpass on May 18, 2003.

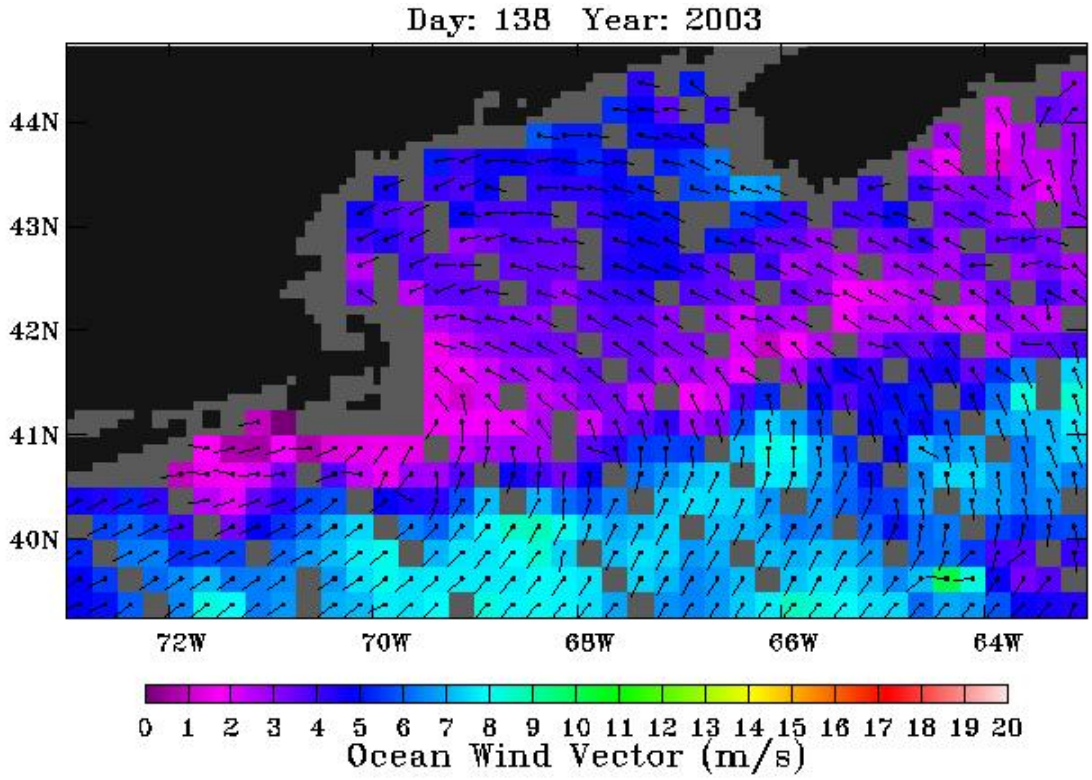

Figure 8-A136. QuikSCAT wind field. Evening satellite overpass on May 18, 2003.

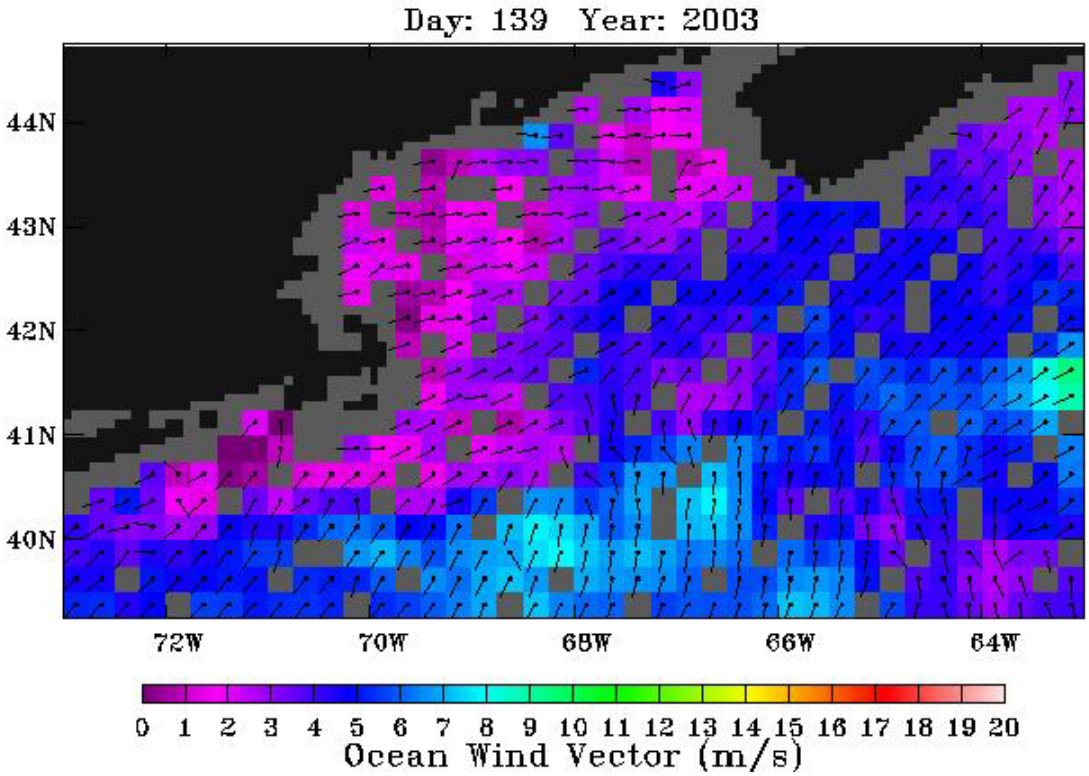

Figure 8-A137. QuikSCAT wind field. Morning satellite overpass on May 19, 2003.

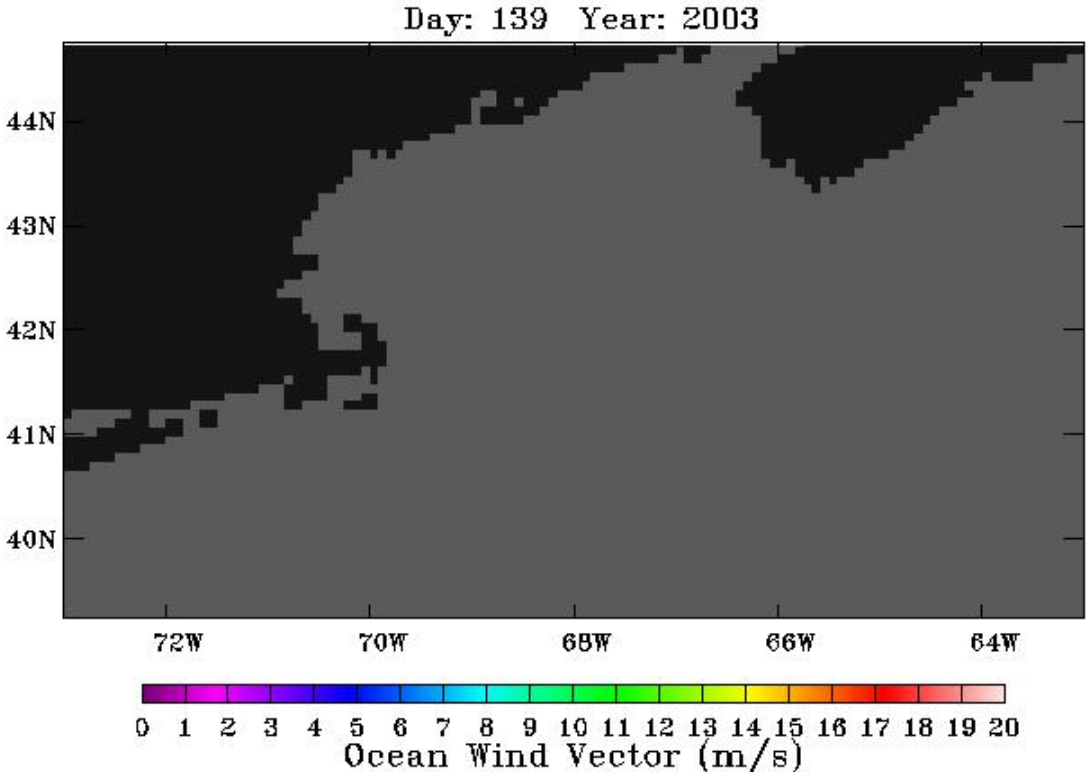

Figure 8-A138. QuikSCAT wind field. Evening satellite overpass on May 19, 2003.

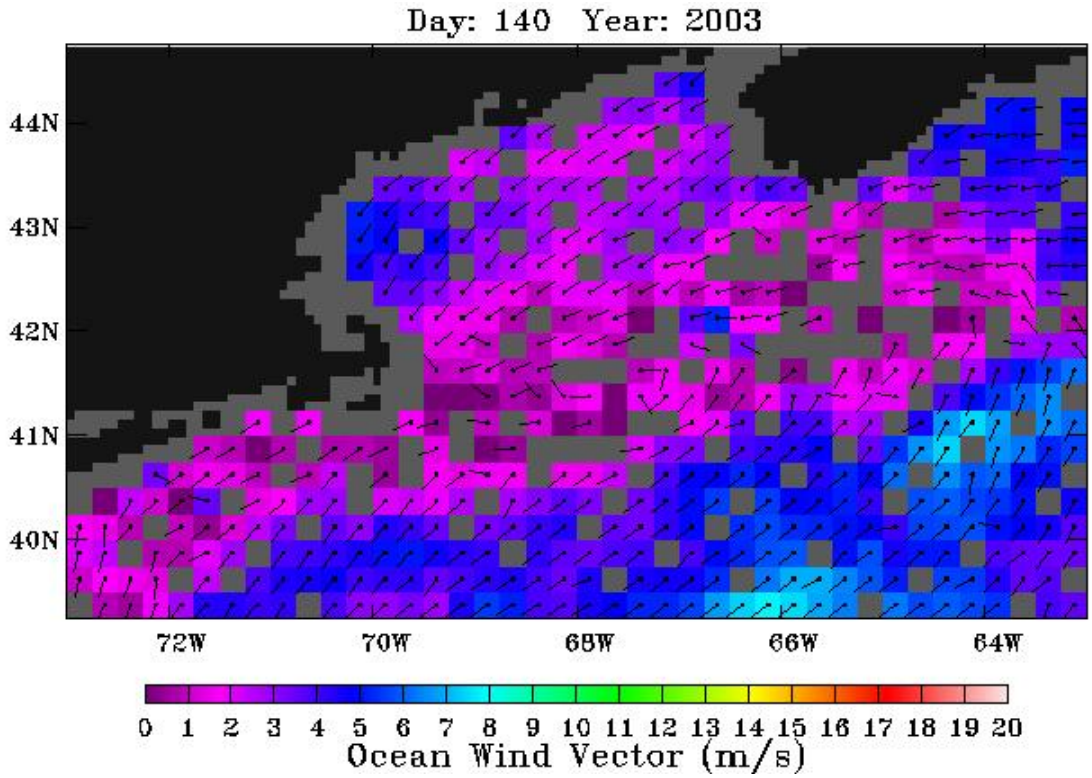

Figure 8-A139. QuikSCAT wind field. Morning satellite overpass on May 20, 2003.

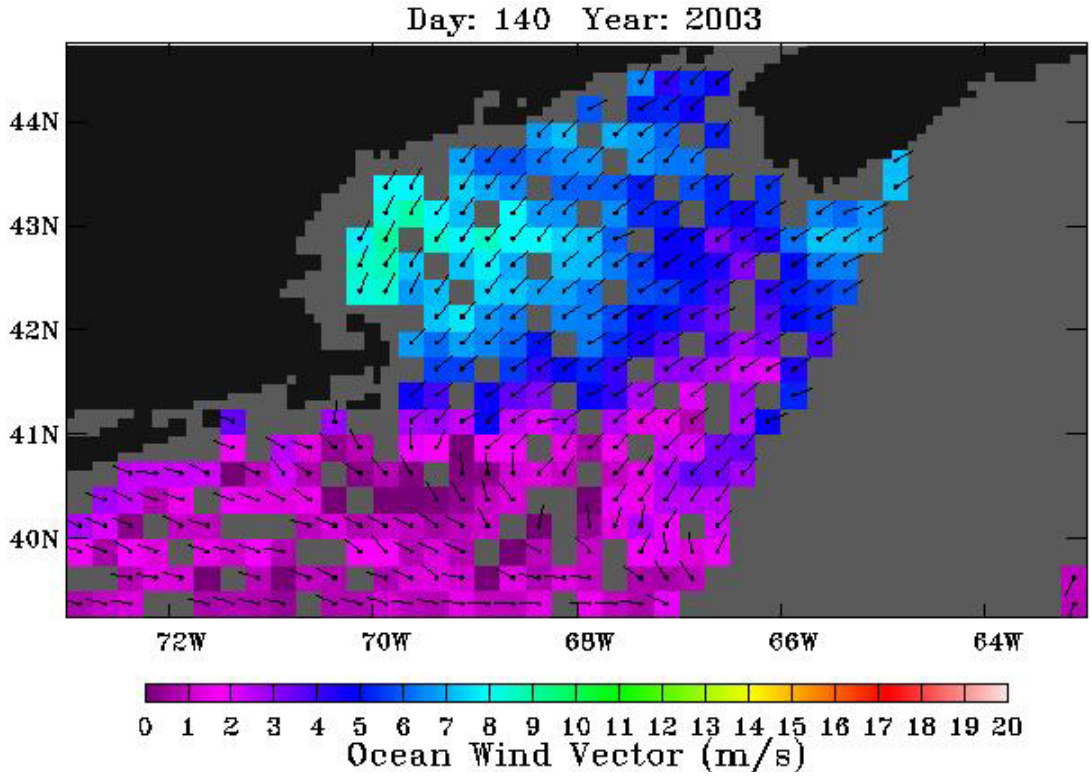

Figure 8-A140. QuikSCAT wind field. Evening satellite overpass on May 20, 2003.

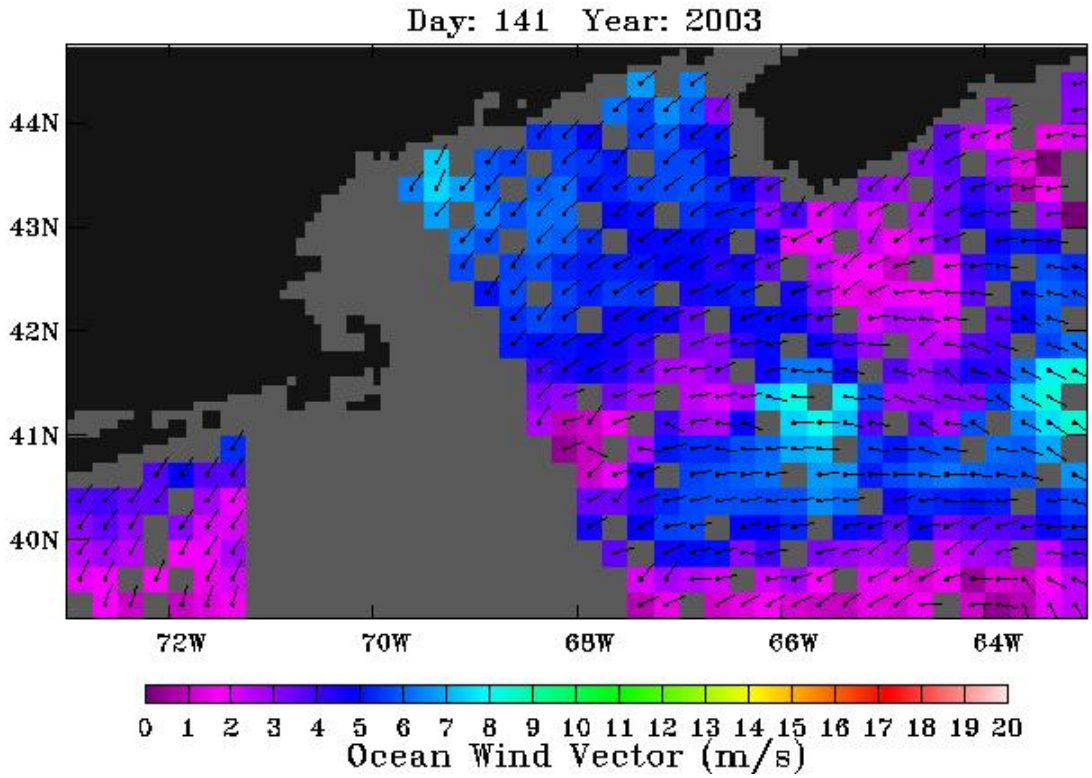

Figure 8-A141. QuikSCAT wind field. Morning satellite overpass on May 21, 2003.

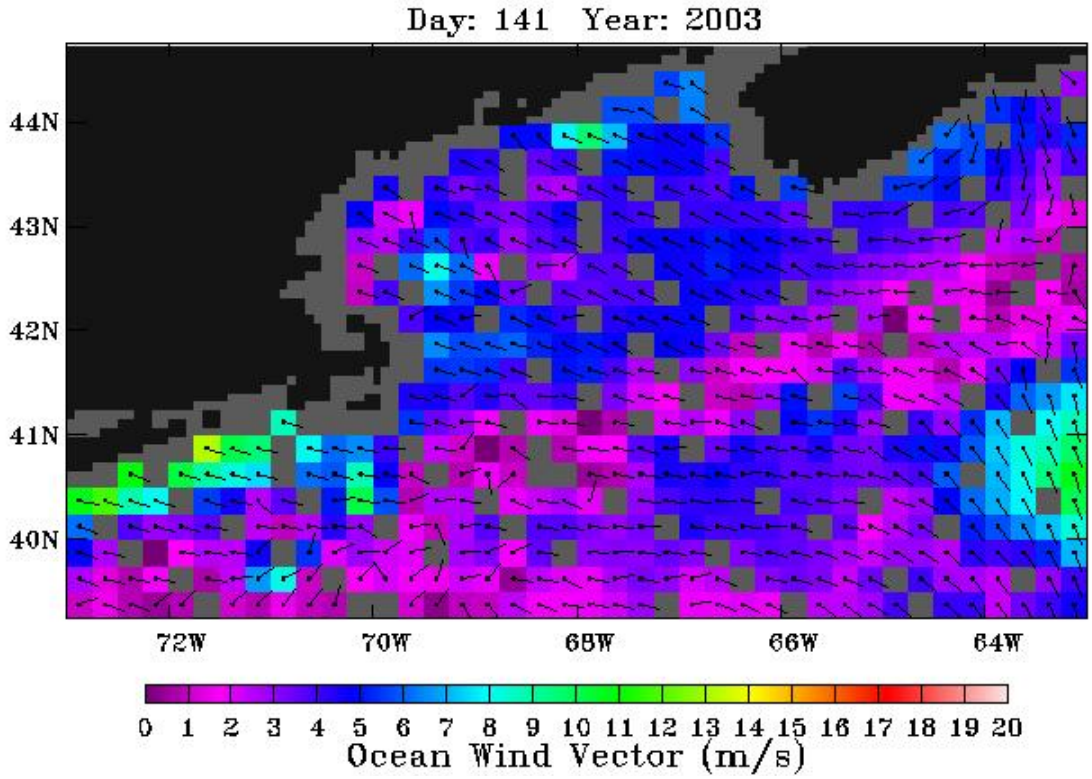

Figure 8-A142. QuikSCAT wind field. Evening satellite overpass on May 21, 2003.

APPENDIX 9-A

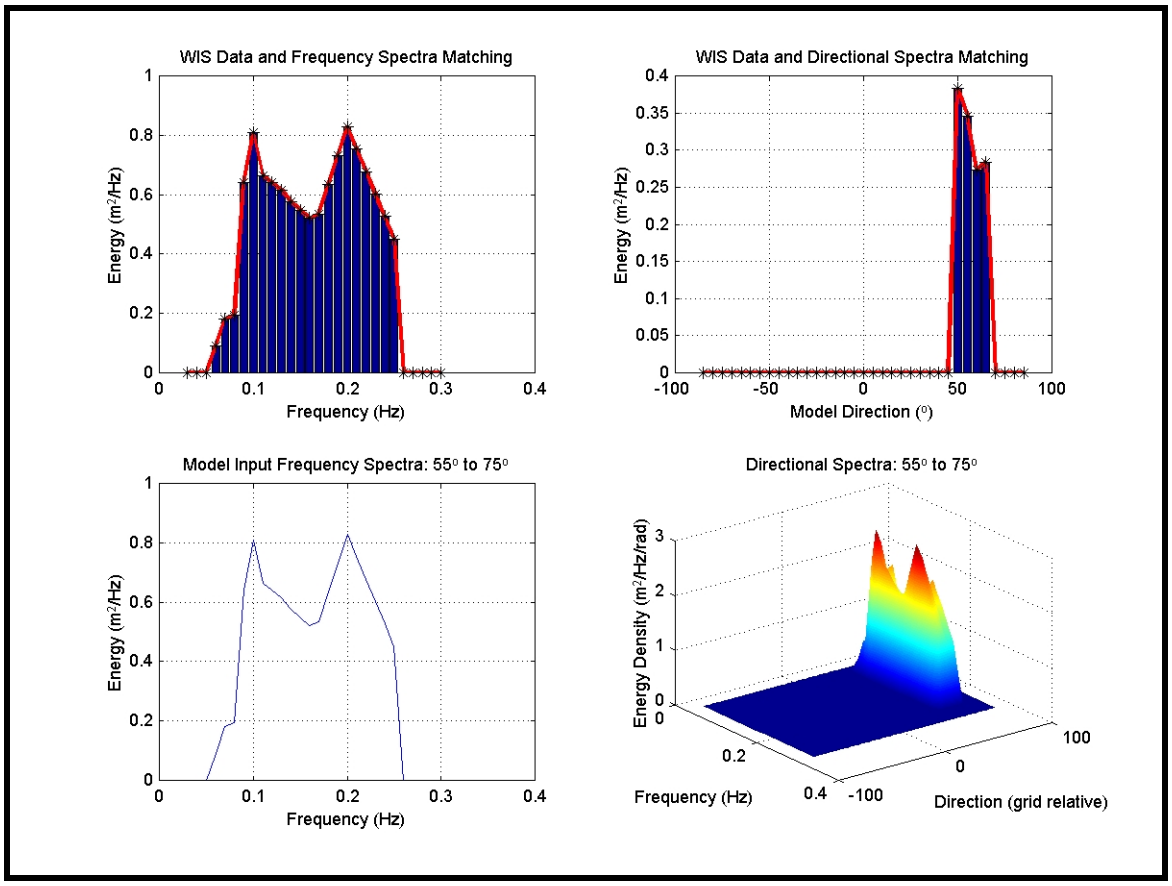

Figure 9-A1. Two-dimensional spectra input into STWAVE for a northeast (55 to 75 degree bin) approach directional spectra bin. The upper left panel shows the actual frequency distribution of the WIS data (blue bars) and the matching model input (red line) for the frequency spectra. The upper right panel shows the actual directional distribution of the WIS data (blue bars) and the matching model input (red line) for the directional spectra. The bottom left panel shows the model input frequency spectra (same as red line in the upper left panel). The lower right panel presents the combined frequency-directional spectra input into the model.

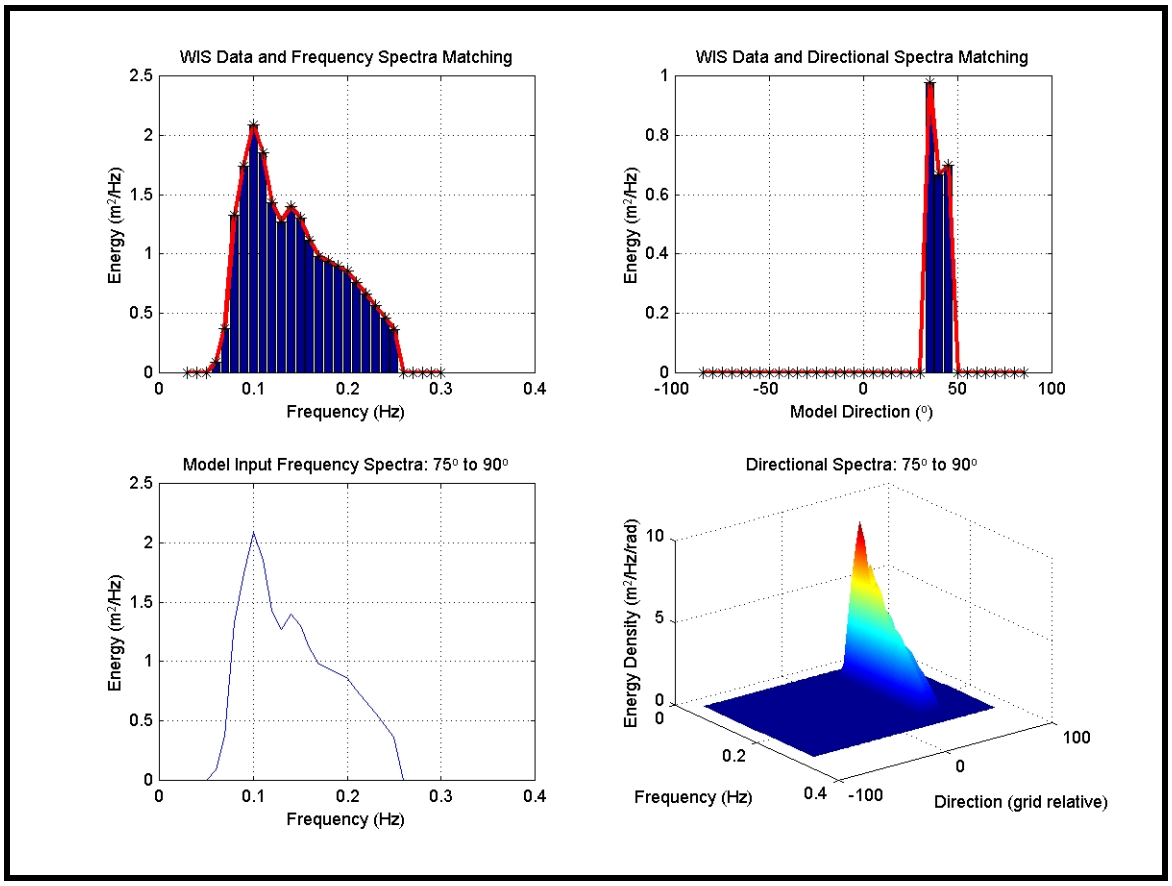

Figure 9-A2. Two-dimensional spectra input into STWAVE for an east-northeast (75 to 90 degree bin) approach directional spectra bin. The upper left panel shows the actual frequency distribution of the WIS data (blue bars) and the matching model input (red line) for the frequency spectra. The upper right panel shows the actual directional distribution of the WIS data (blue bars) and the matching model input (red line) for the directional spectra. The bottom left panel shows the model input frequency spectra (same as red line in the upper left panel). The lower right panel presents the combined frequency-directional spectra input into the model.

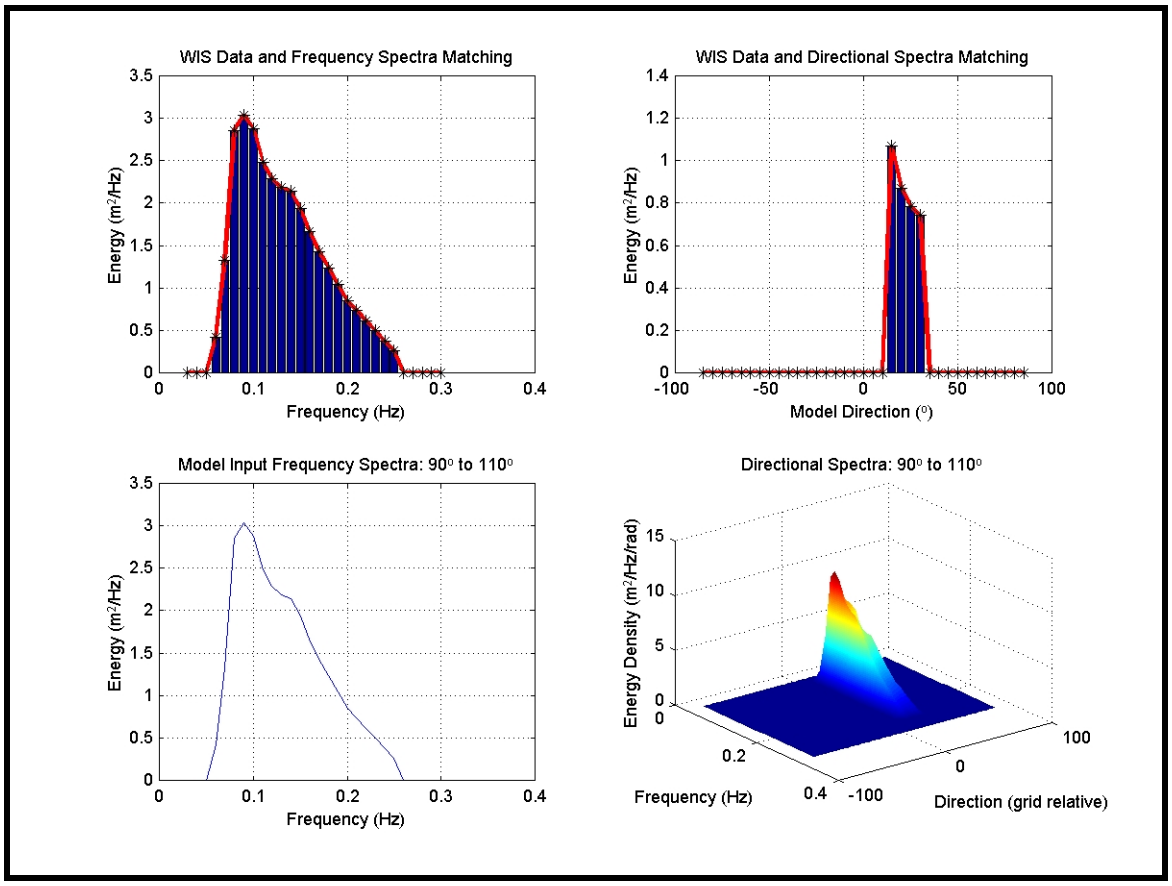

Figure 9-A3. Two-dimensional spectra input into STWAVE for an east (90 to 110 degree bin) approach directional spectra bin. The upper left panel shows the actual frequency distribution of the WIS data (blue bars) and the matching model input (red line) for the frequency spectra. The upper right panel shows the actual directional distribution of the WIS data (blue bars) and the matching model input (red line) for the directional spectra. The bottom left panel shows the model input frequency spectra (same as red line in the upper left panel). The lower right panel presents the combined frequency-directional spectra input into the model.

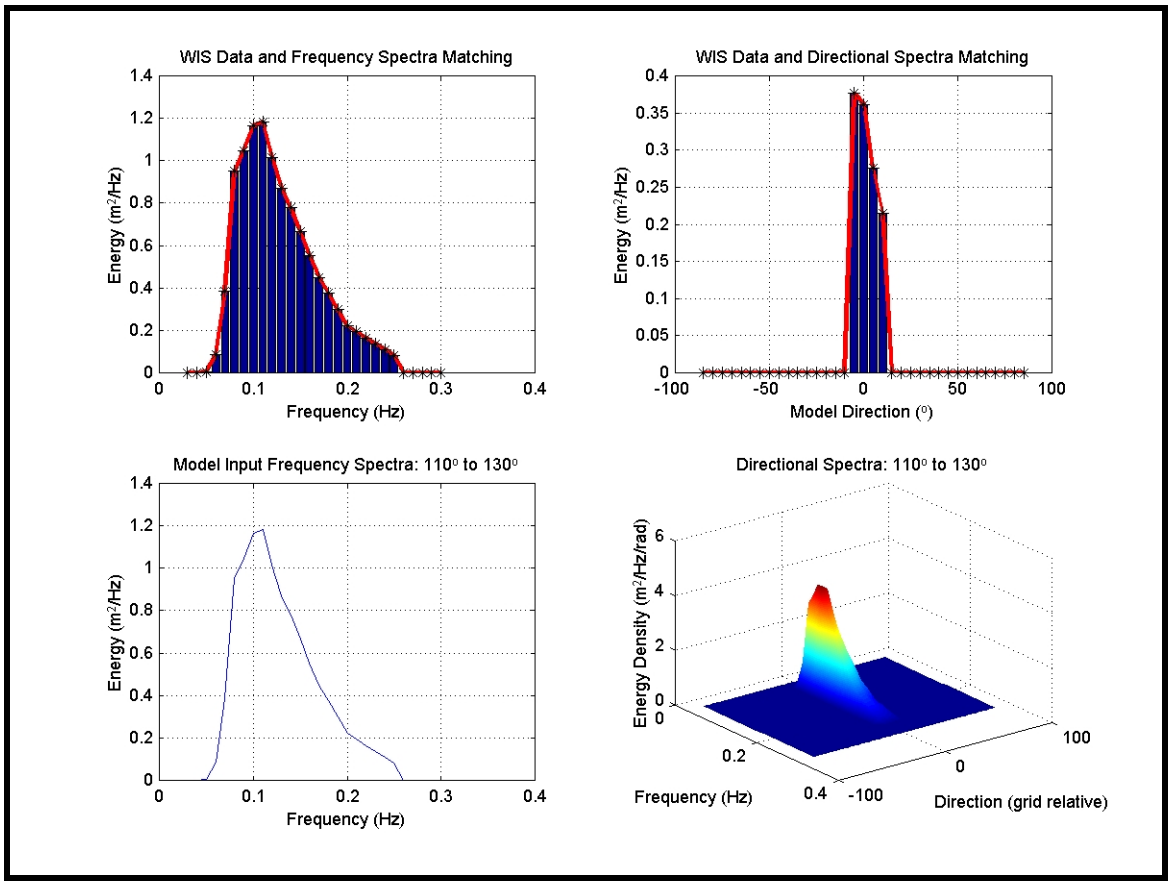

Figure 9-A4. Two-dimensional spectra input into STWAVE for an east-southeast (110 to 130 degree bin) approach directional spectra bin. The upper left panel shows the actual frequency distribution of the WIS data (blue bars) and the matching model input (red line) for the frequency spectra. The upper right panel shows the actual directional distribution of the WIS data (blue bars) and the matching model input (red line) for the directional spectra. The bottom left panel shows the model input frequency spectra (same as red line in the upper left panel). The lower right panel presents the combined frequency-directional spectra input into the model.

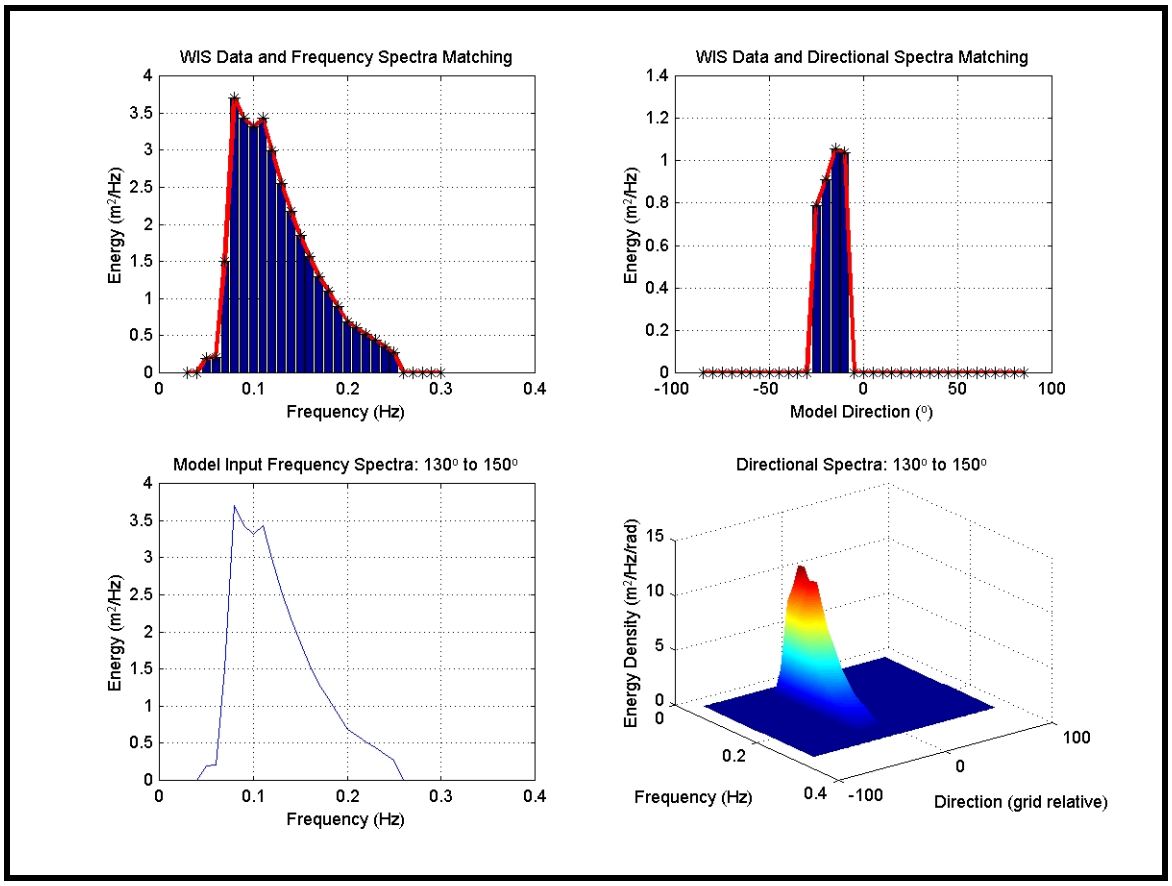

Figure 9-A5. Two-dimensional spectra input into STWAVE for a southeast (130 to 150 degree bin) approach directional spectra bin. The upper left panel shows the actual frequency distribution of the WIS data (blue bars) and the matching model input (red line) for the frequency spectra. The upper right panel shows the actual directional distribution of the WIS data (blue bars) and the matching model input (red line) for the directional spectra. The bottom left panel shows the model input frequency spectra (same as red line in the upper left panel). The lower right panel presents the combined frequency-directional spectra input into the model.

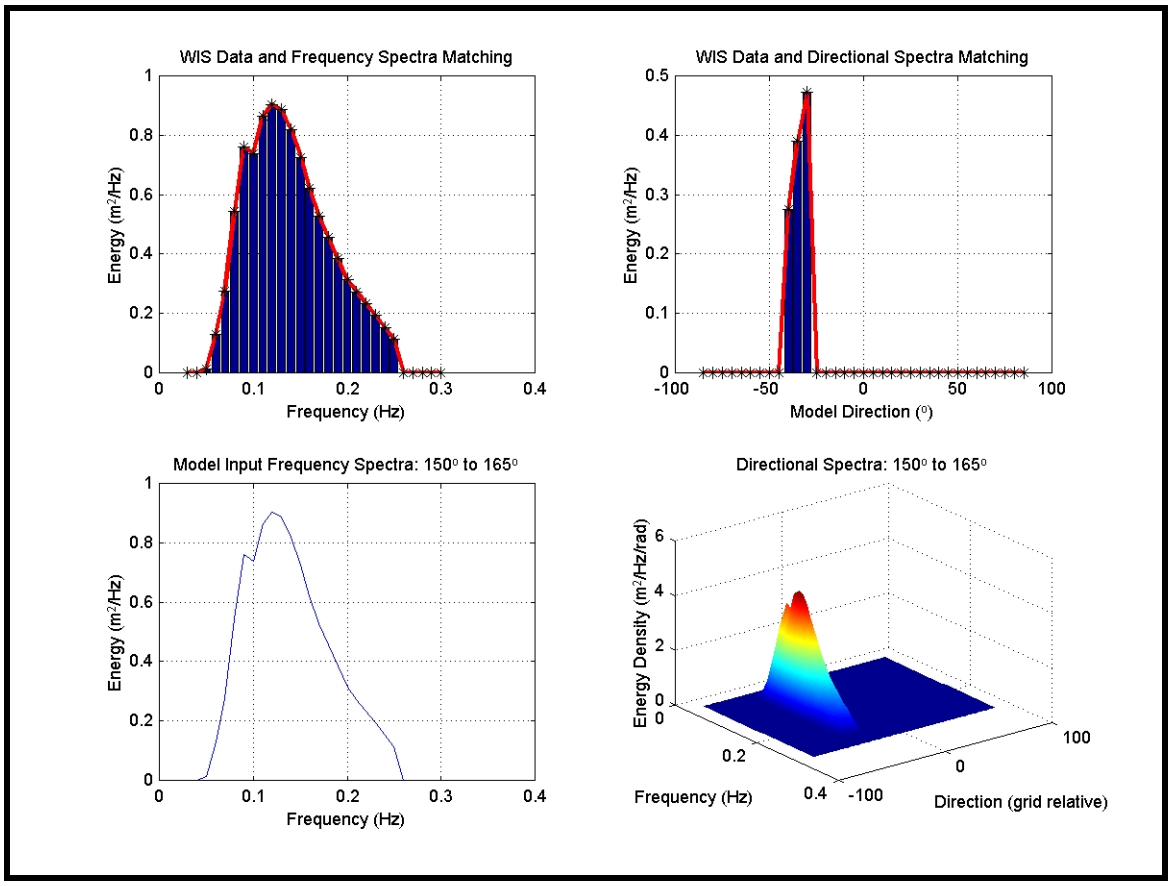

Figure 9-A6. Two-dimensional spectra input into STWAVE for a south-southeast (150 to 165 degree bin) approach directional spectra bin. The upper left panel shows the actual frequency distribution of the WIS data (blue bars) and the matching model input (red line) for the frequency spectra. The upper right panel shows the actual directional distribution of the WIS data (blue bars) and the matching model input (red line) for the directional spectra. The bottom left panel shows the model input frequency spectra (same as red line in the upper left panel). The lower right panel presents the combined frequency-directional spectra input into the model.

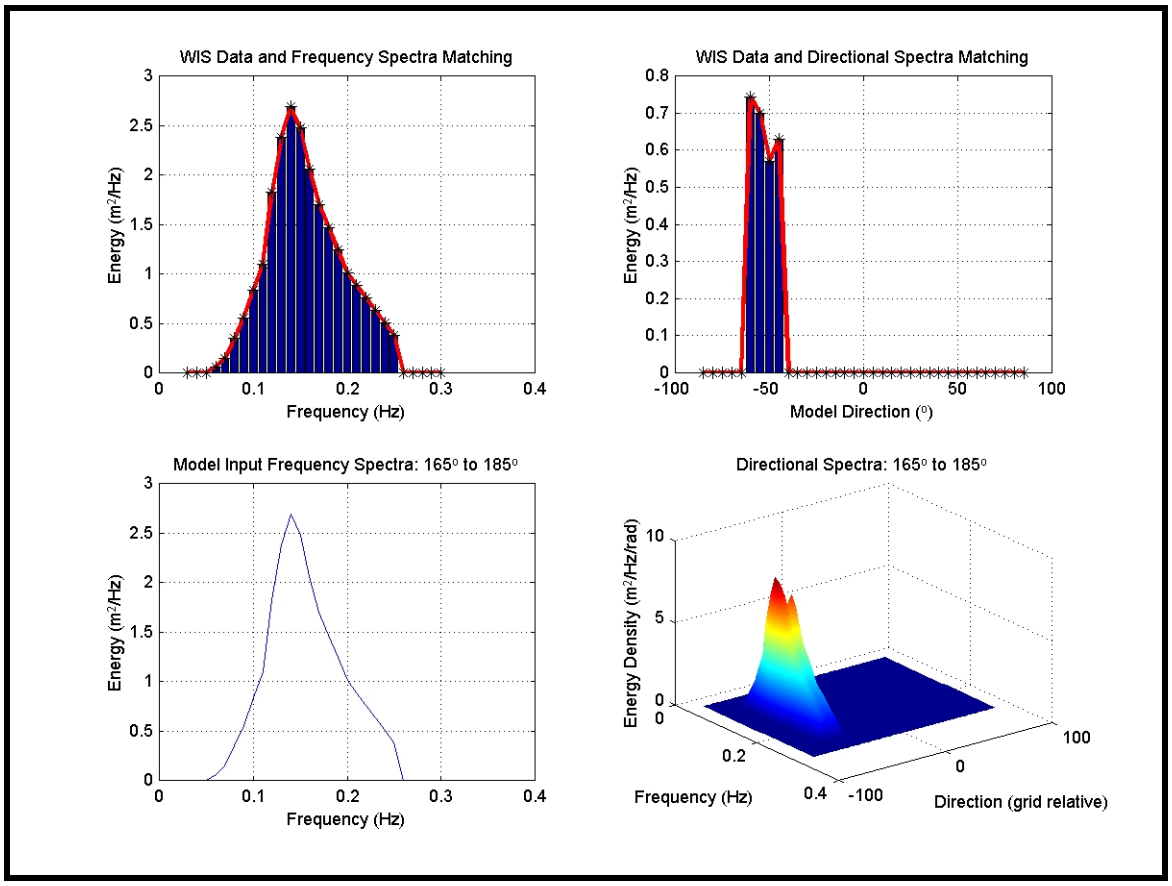

Figure 9-A7. Two-dimensional spectra input into STWAVE for a south (165 to 185 degree bin) approach directional spectra bin. The upper left panel shows the actual frequency distribution of the WIS data (blue bars) and the matching model input (red line) for the frequency spectra. The upper right panel shows the actual directional distribution of the WIS data (blue bars) and the matching model input (red line) for the directional spectra. The bottom left panel shows the model input frequency spectra (same as red line in the upper left panel). The lower right panel presents the combined frequency-directional spectra input into the model.

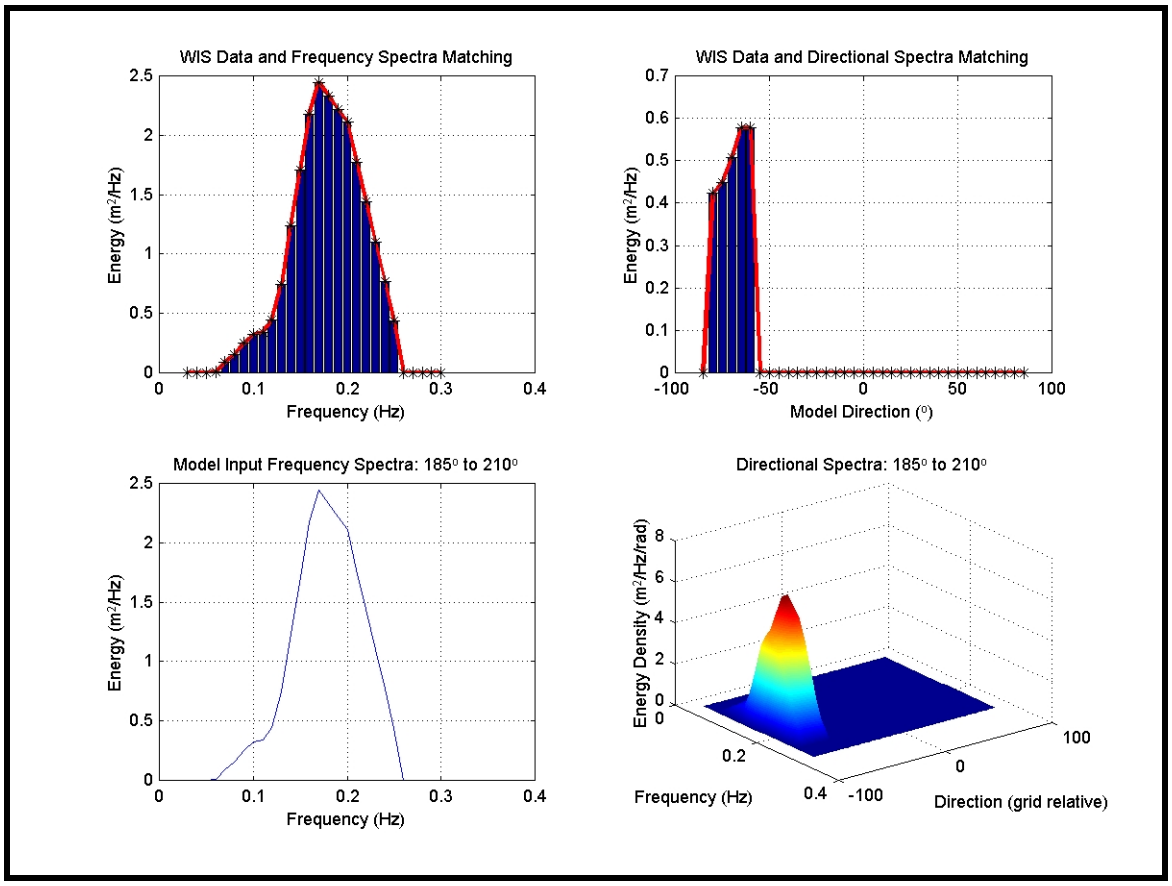

Figure 9-A8. Two-dimensional spectra input into STWAVE for a south-southwest (185 to 210 degree bin) approach directional spectra bin. The upper left panel shows the actual frequency distribution of the WIS data (blue bars) and the matching model input (red line) for the frequency spectra. The upper right panel shows the actual directional distribution of the WIS data (blue bars) and the matching model input (red line) for the directional spectra. The bottom left panel shows the model input frequency spectra (same as red line in the upper left panel). The lower right panel presents the combined frequency-directional spectra input into the model.

APPENDIX 11-A

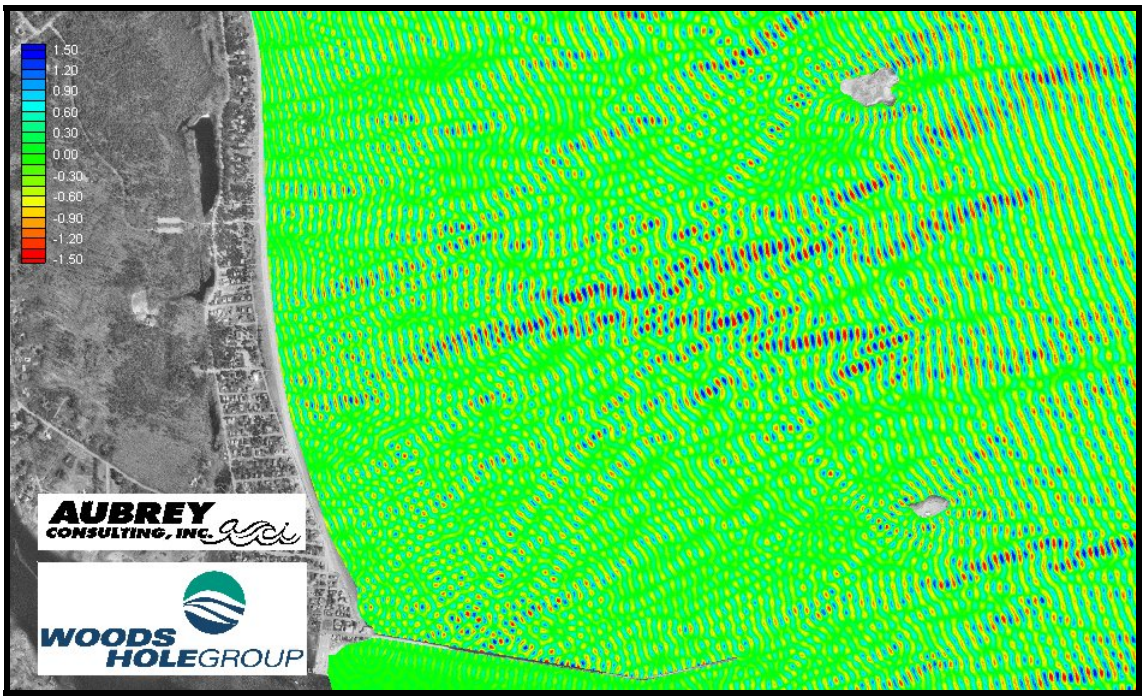

Figure 11-A1. Sea surface results from the nearshore wave model for existing conditions using a northeast (55 to 75 degree bin) approach directional spectra bin. Blues indicate wave crests, while reds and yellows indicate wave troughs. Scale in meters.

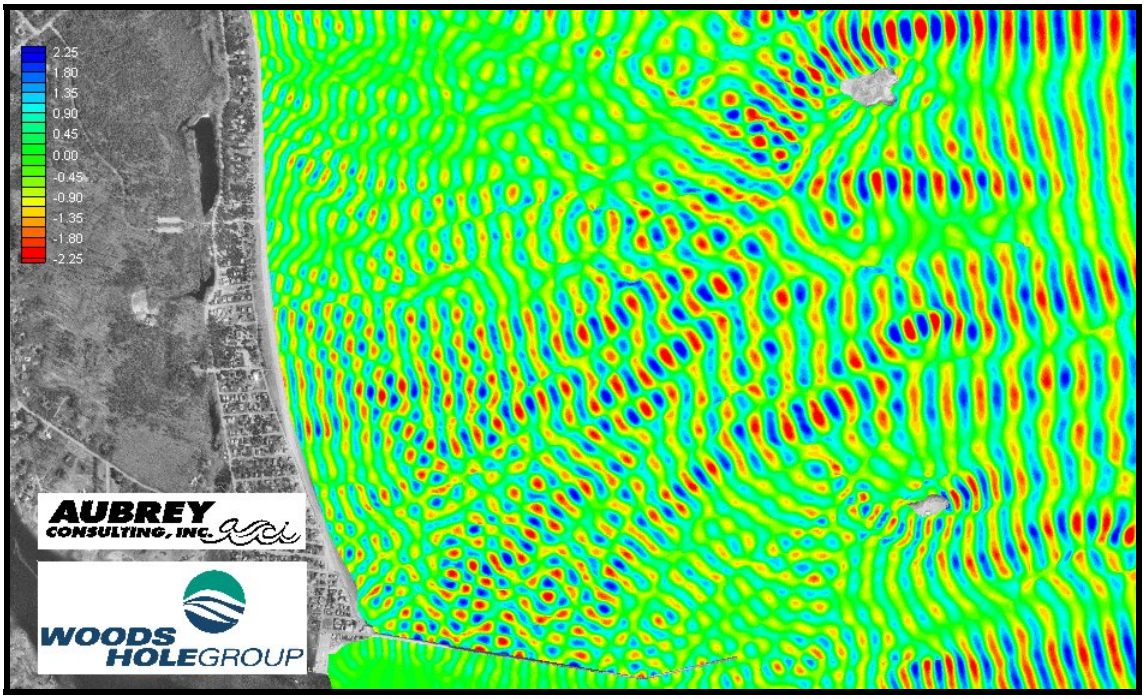

Figure 11-A2. Sea surface results from the nearshore wave model for existing conditions using an east-northeast (75 to 90 degree bin) approach directional spectra bin. Blues indicate wave crests, while reds and yellows indicate wave troughs. Scale in meters.

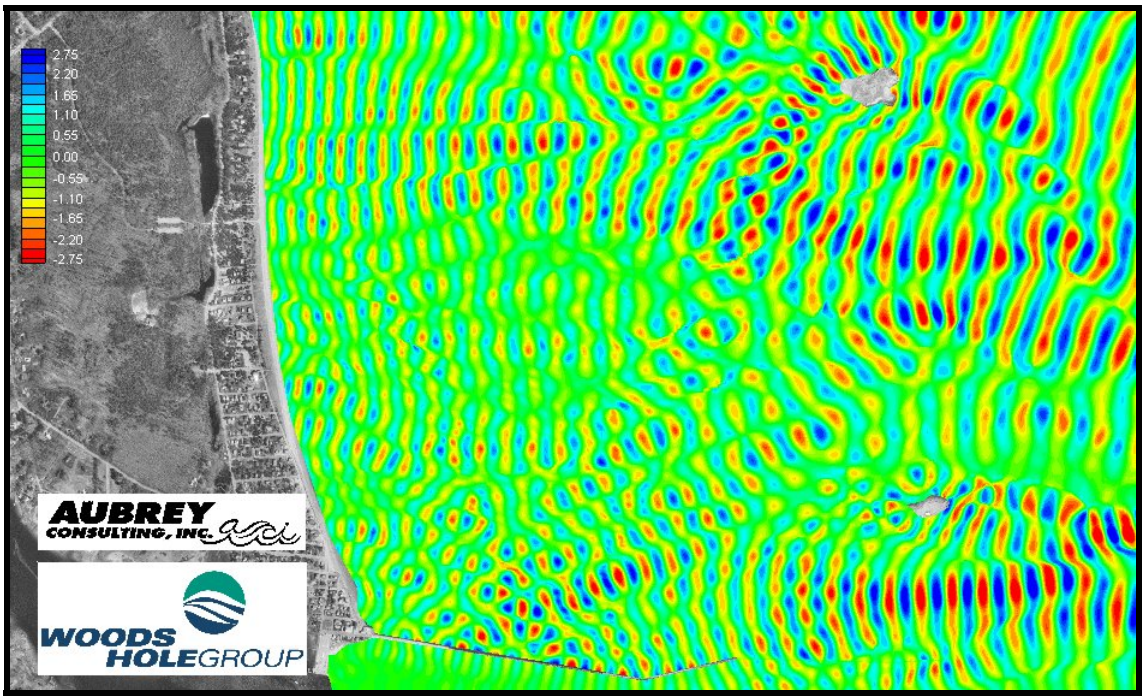

Figure 11-A3. Sea surface results from the nearshore wave model for existing conditions using an east (90 to 110 degree bin) approach directional spectra bin. Blues indicate wave crests, while reds and yellows indicate wave troughs. Scale in meters.

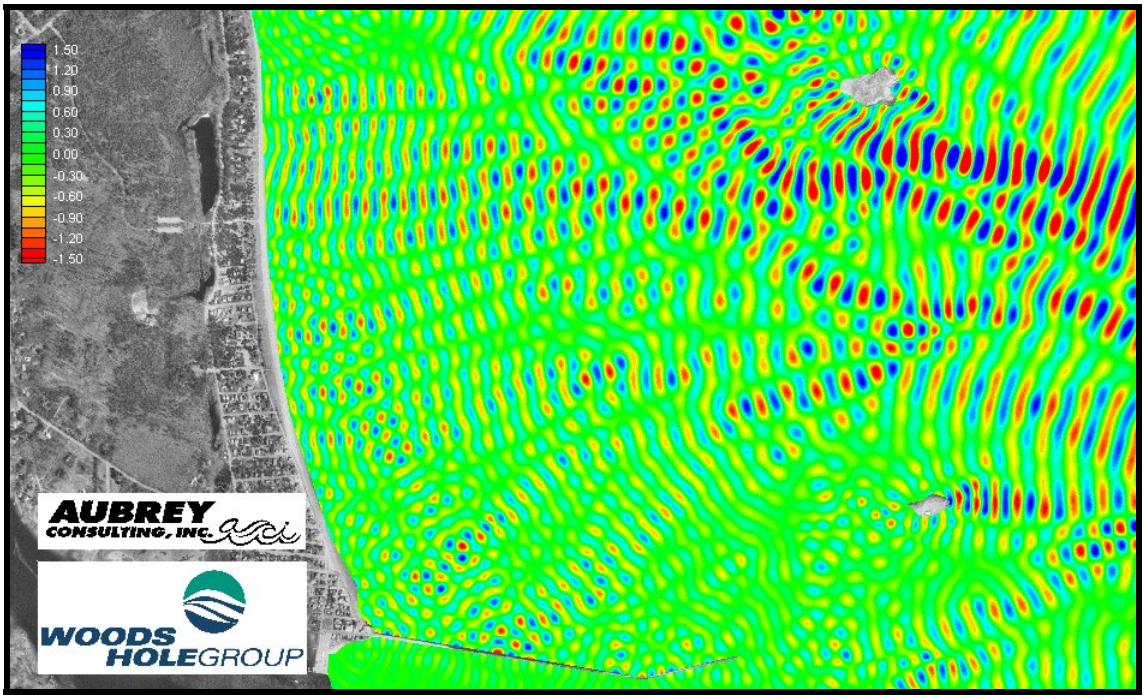

Figure 11-A4. Sea surface results from the nearshore wave model for existing conditions using an east-southeast (110 to 130 degree bin) approach directional spectra bin. Blues indicate wave crests, while reds and yellows indicate wave troughs. Scale in meters.

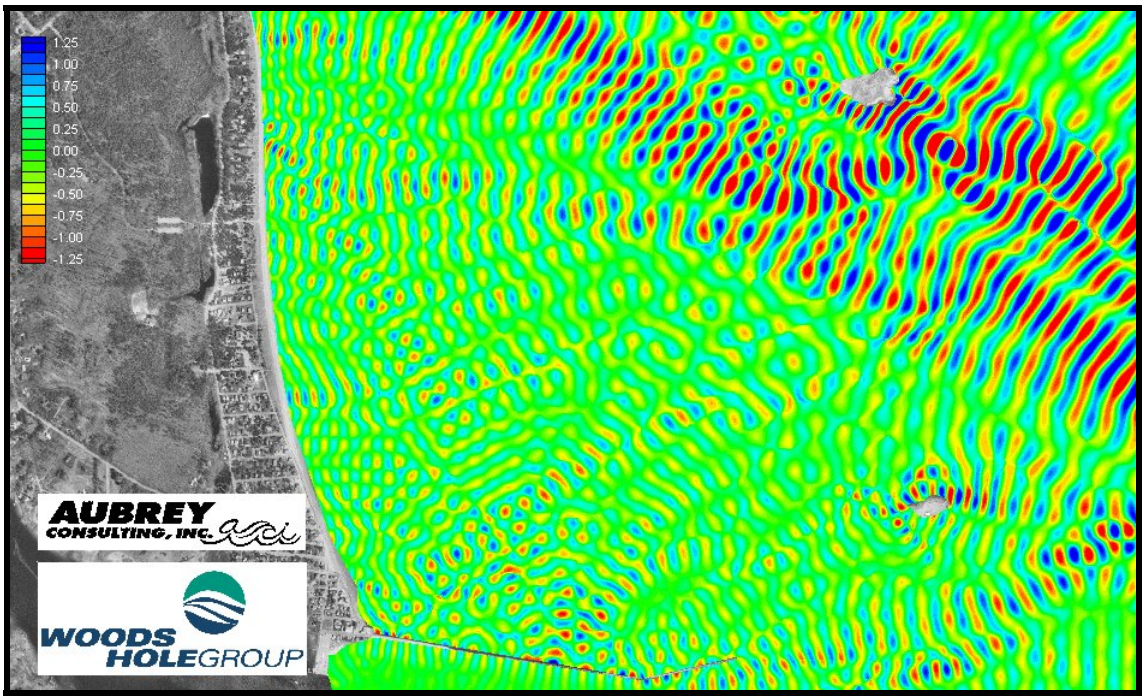

Figure 11-A5. Sea surface results from the nearshore wave model for existing conditions using a southeast (130 to 150 degree bin) approach directional spectra bin. Blues indicate wave crests, while reds and yellows indicate wave troughs. Scale in meters.

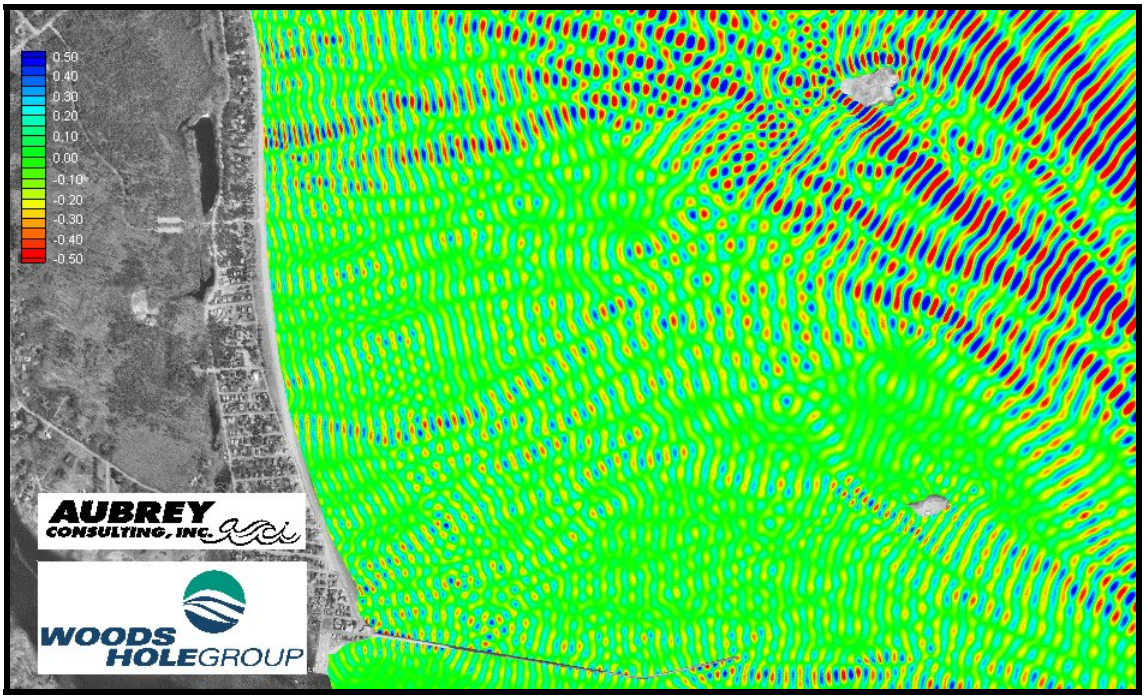

Figure 11-A6. Sea surface results from the nearshore wave model for existing conditions using a south-southeast (150 to 165 degree bin) approach directional spectra bin. Blues indicate wave crests, while reds and yellows indicate wave troughs. Scale in meters.

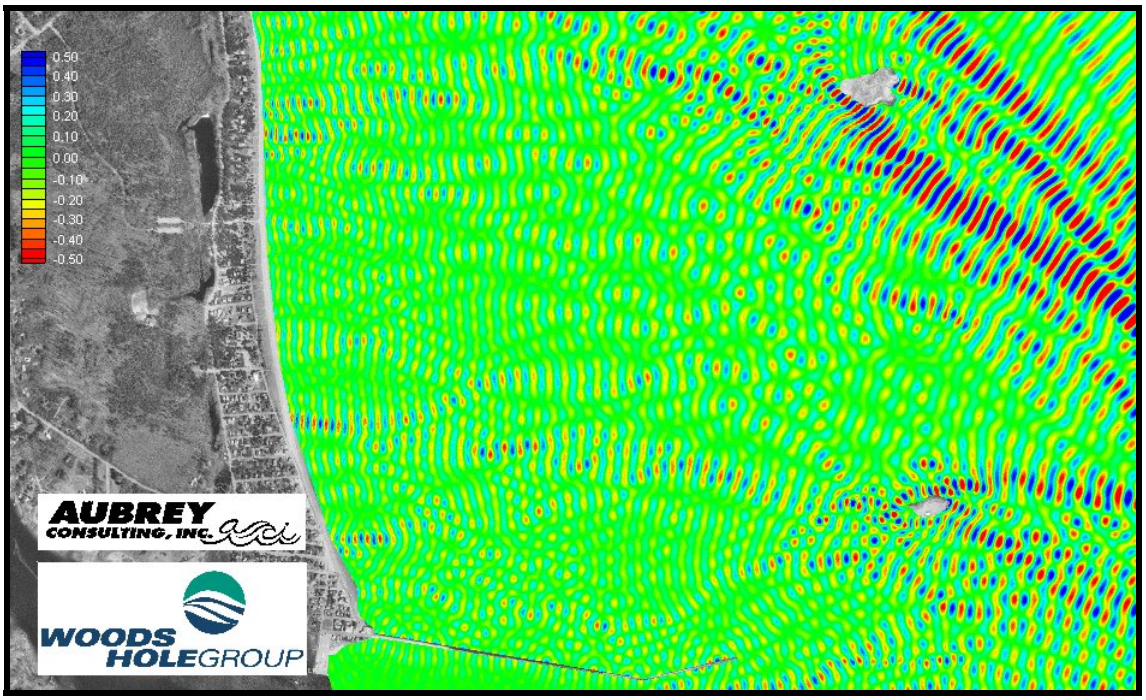

Figure 11-A7. Sea surface results from the nearshore wave model for existing conditions using a south (165 to 185 degree bin) approach directional spectra bin. Blues indicate wave crests, while reds and yellows indicate wave troughs. Scale in meters.

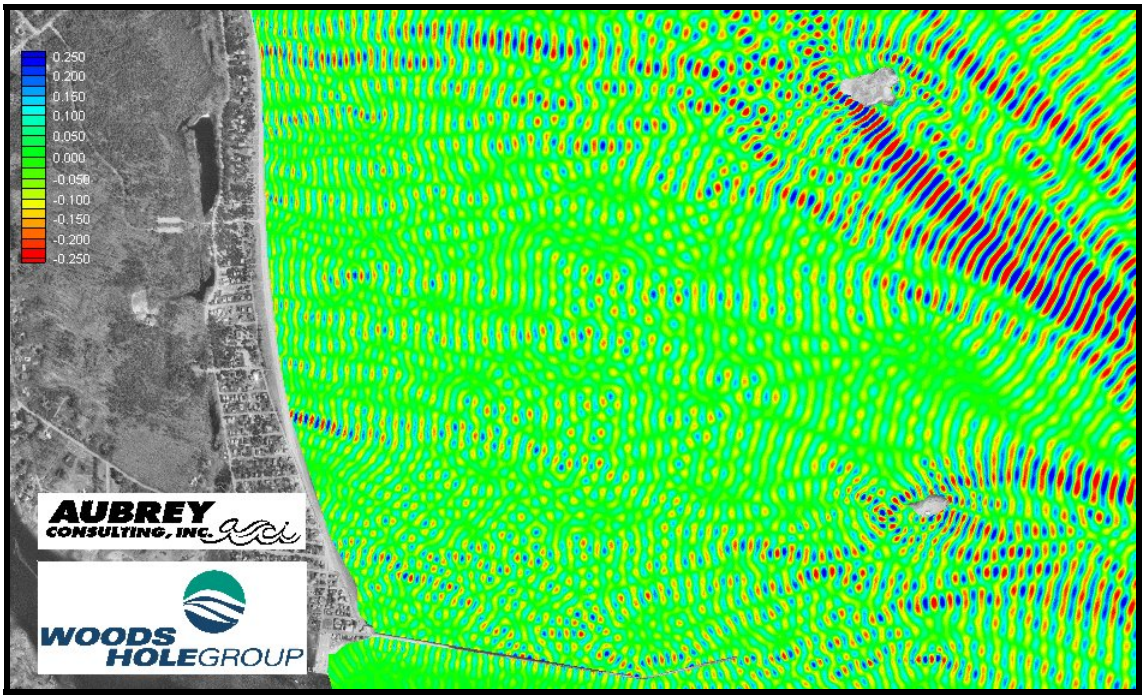

Figure 11-A8. Sea surface results from the nearshore wave model for existing conditions using a south-southwest (185 to 210 degree bin) approach directional spectra bin. Blues indicate wave crests, while reds and yellows indicate wave troughs. Scale in meters.

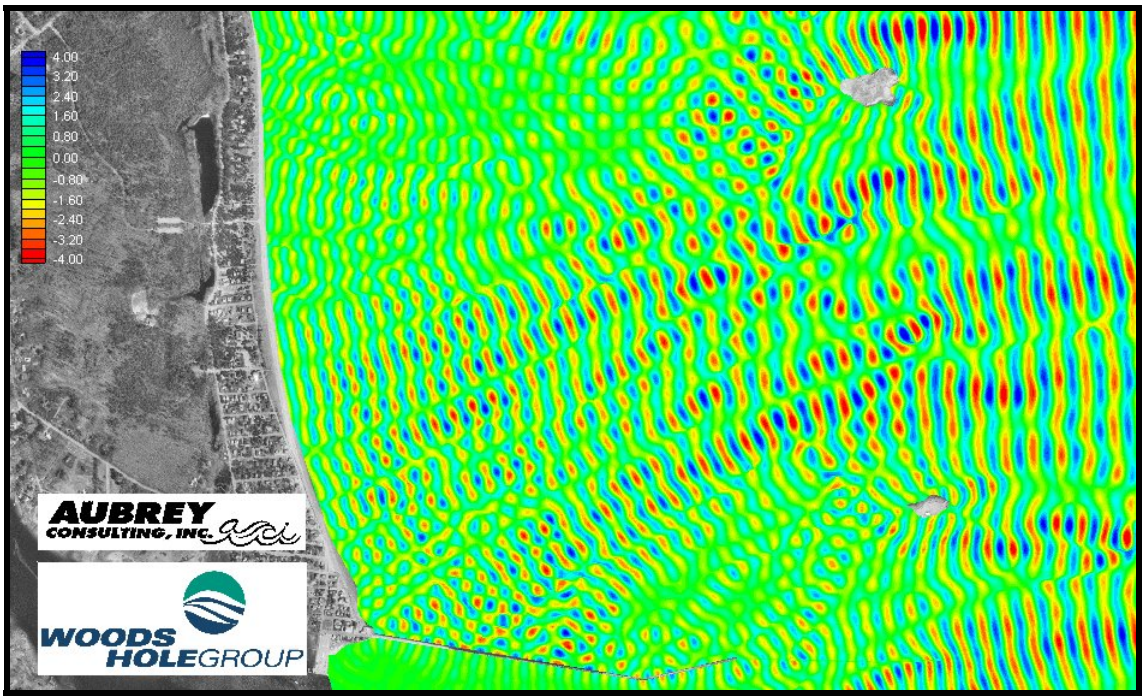

Figure 11-A9. Sea surface results from the nearshore wave model for existing conditions for a 10-yr return period storm. Scale in meters.

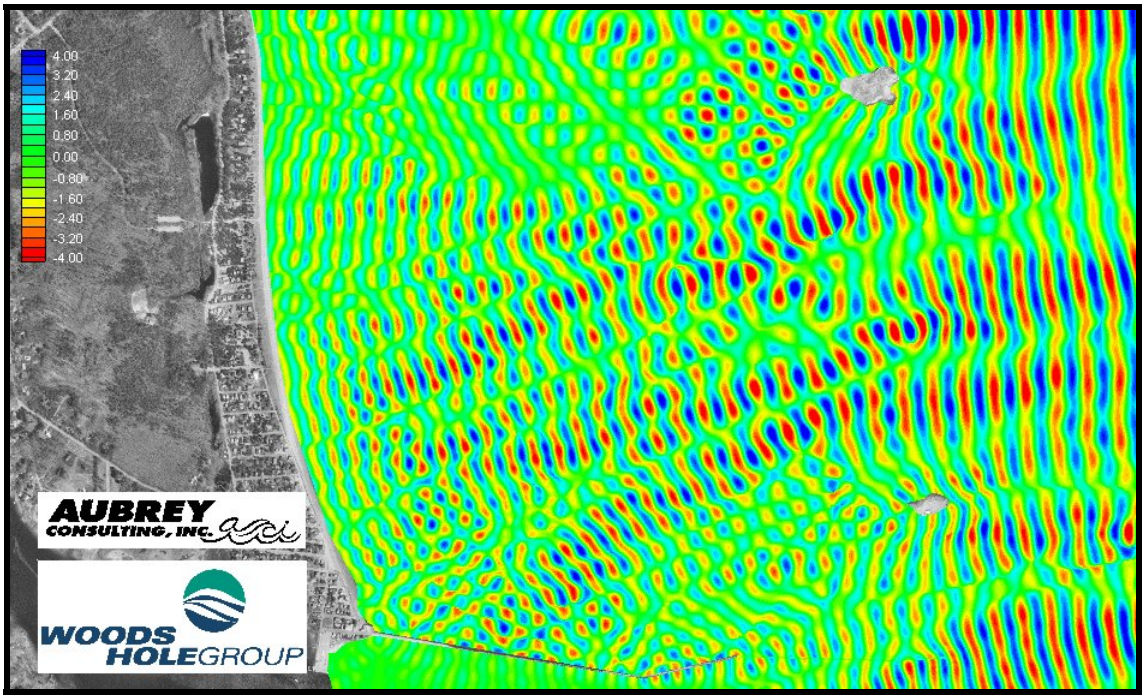

Figure 11-A10. Sea surface results from the nearshore wave model for existing conditions for a 50-yr return period storm. Scale in meters.

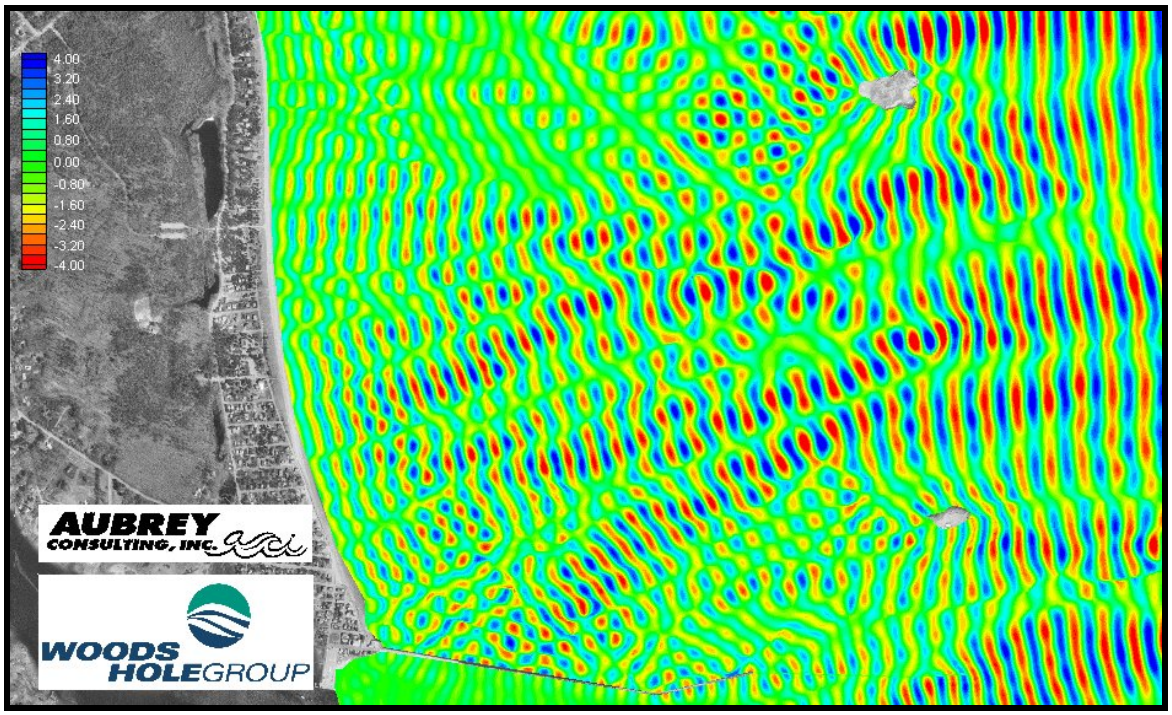

Figure 11-A11. Sea surface results from the nearshore wave model for existing conditions for a 100-yr return period storm. Scale in meters.

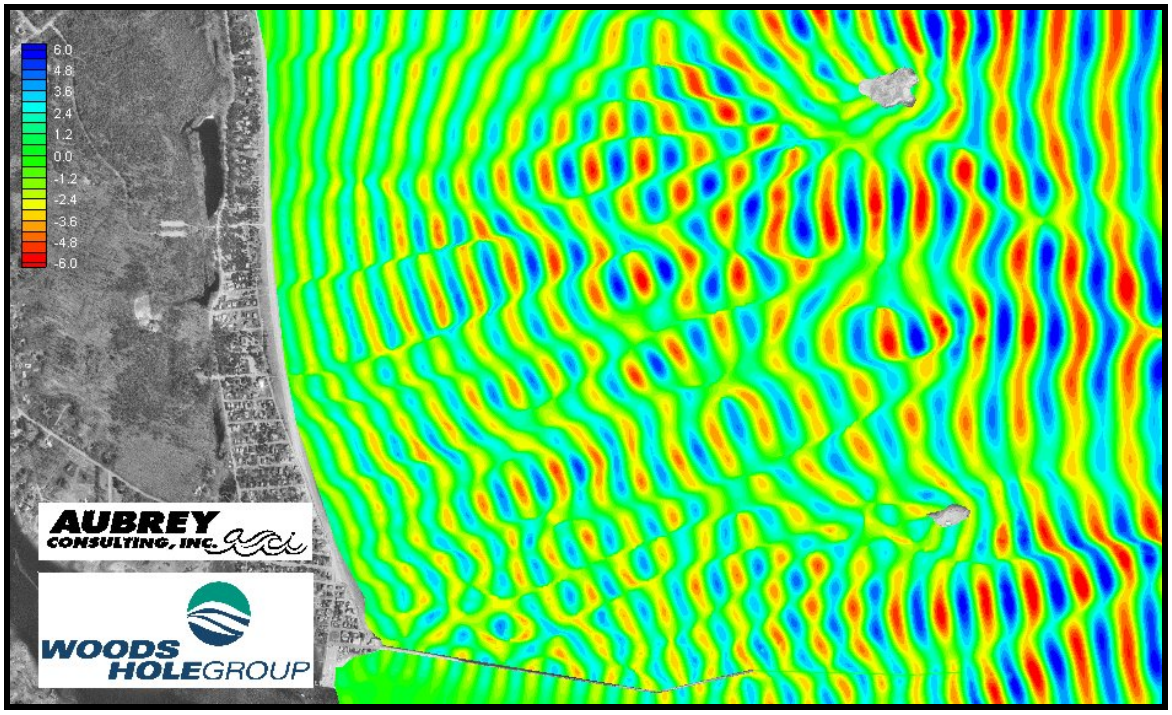

Figure 11-A12. Sea surface results from the nearshore wave model for existing conditions for Perfect Storm (10/31/1991). Scale in meters.

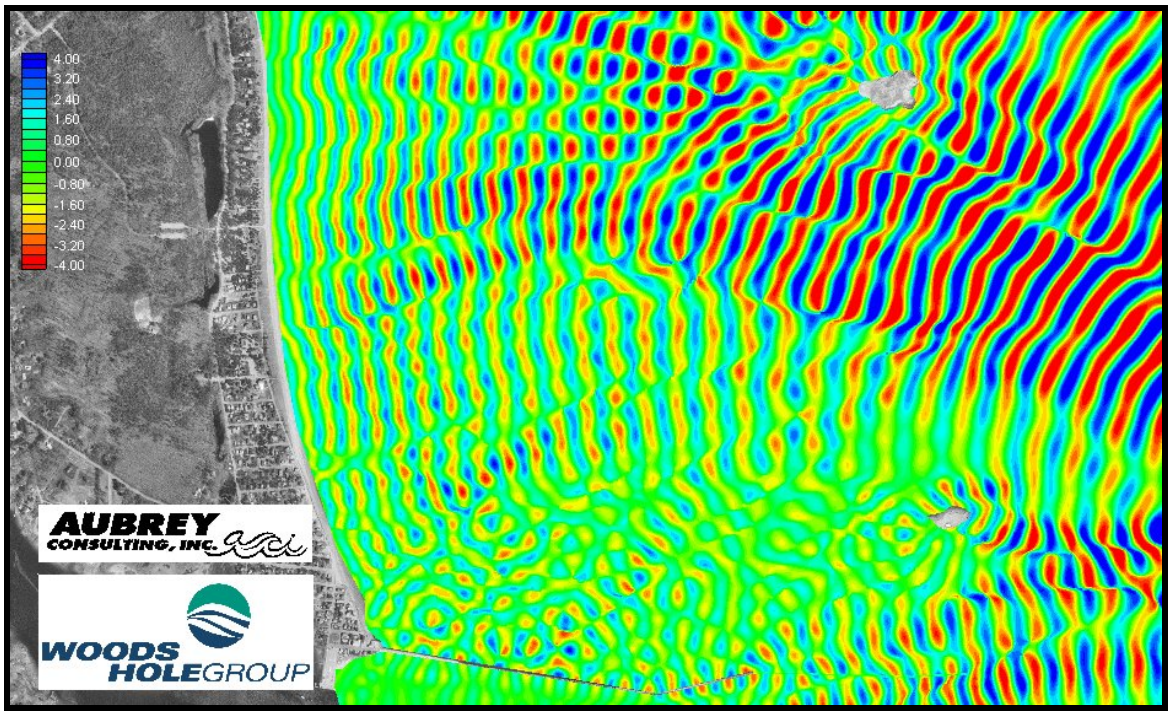

Figure 11-A13. Sea surface results from the nearshore wave model for existing conditions for Hurricane Bob (8/20/1991). Scale in meters.

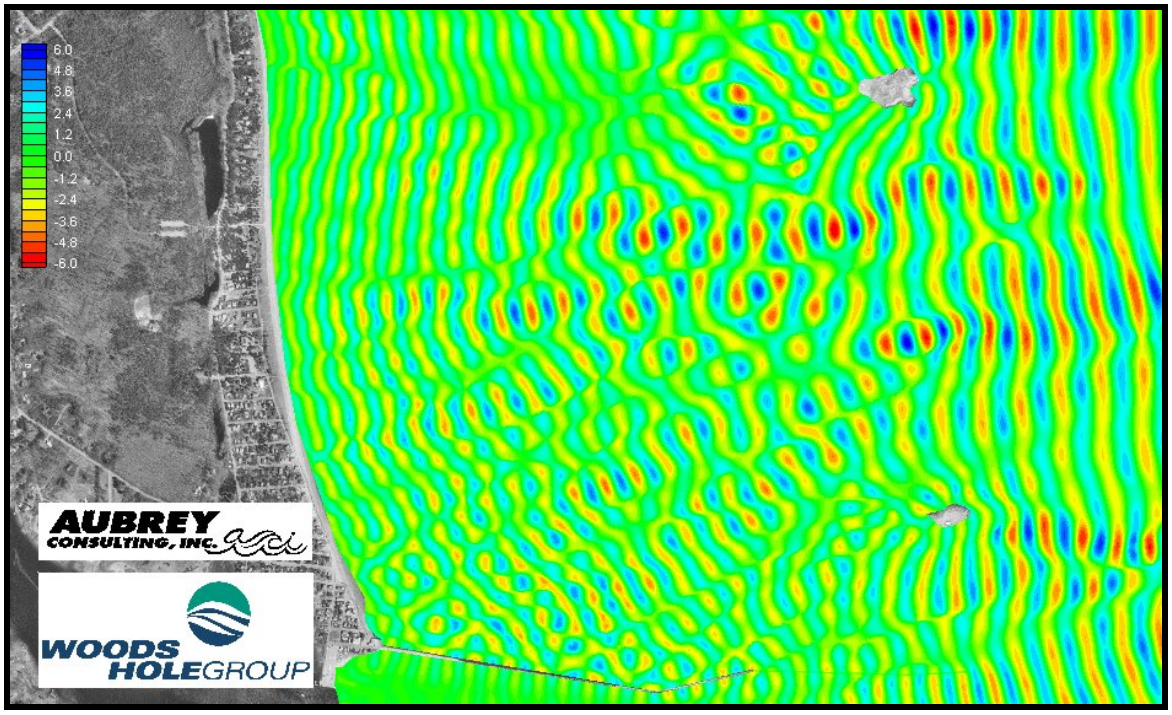

Figure 11-A11. Sea surface results from the nearshore wave model for existing conditions for Northeaster (March 6-7, 2001). Scale in meters.

APPENDIX 13-A

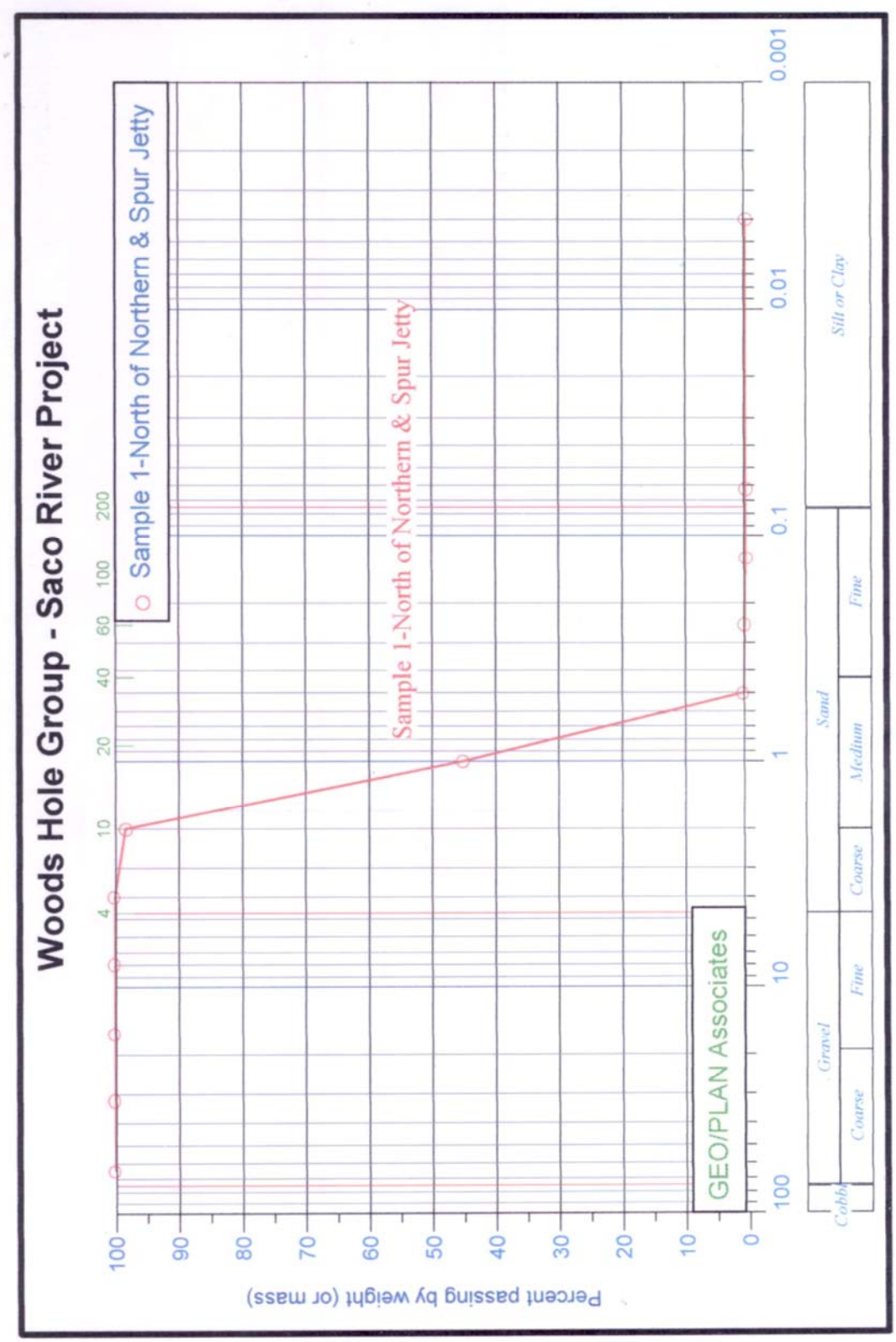

Figure 13A-1. Grain size distribution for sediment grab sample along Saco Bay shoreline, location 1.

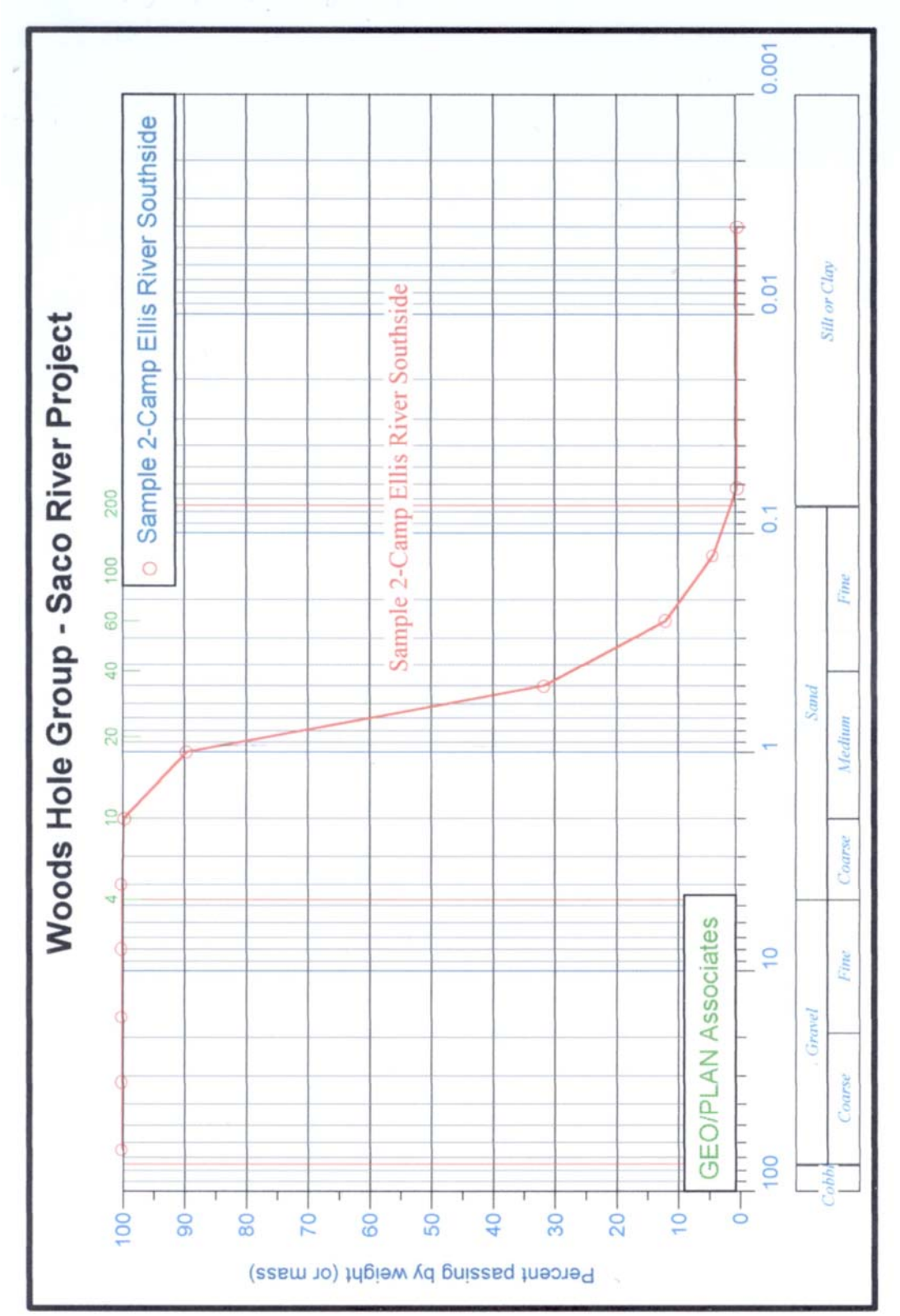

Figure 13A-2. Grain size distribution for sediment grab sample along Saco Bay shoreline, location 2.

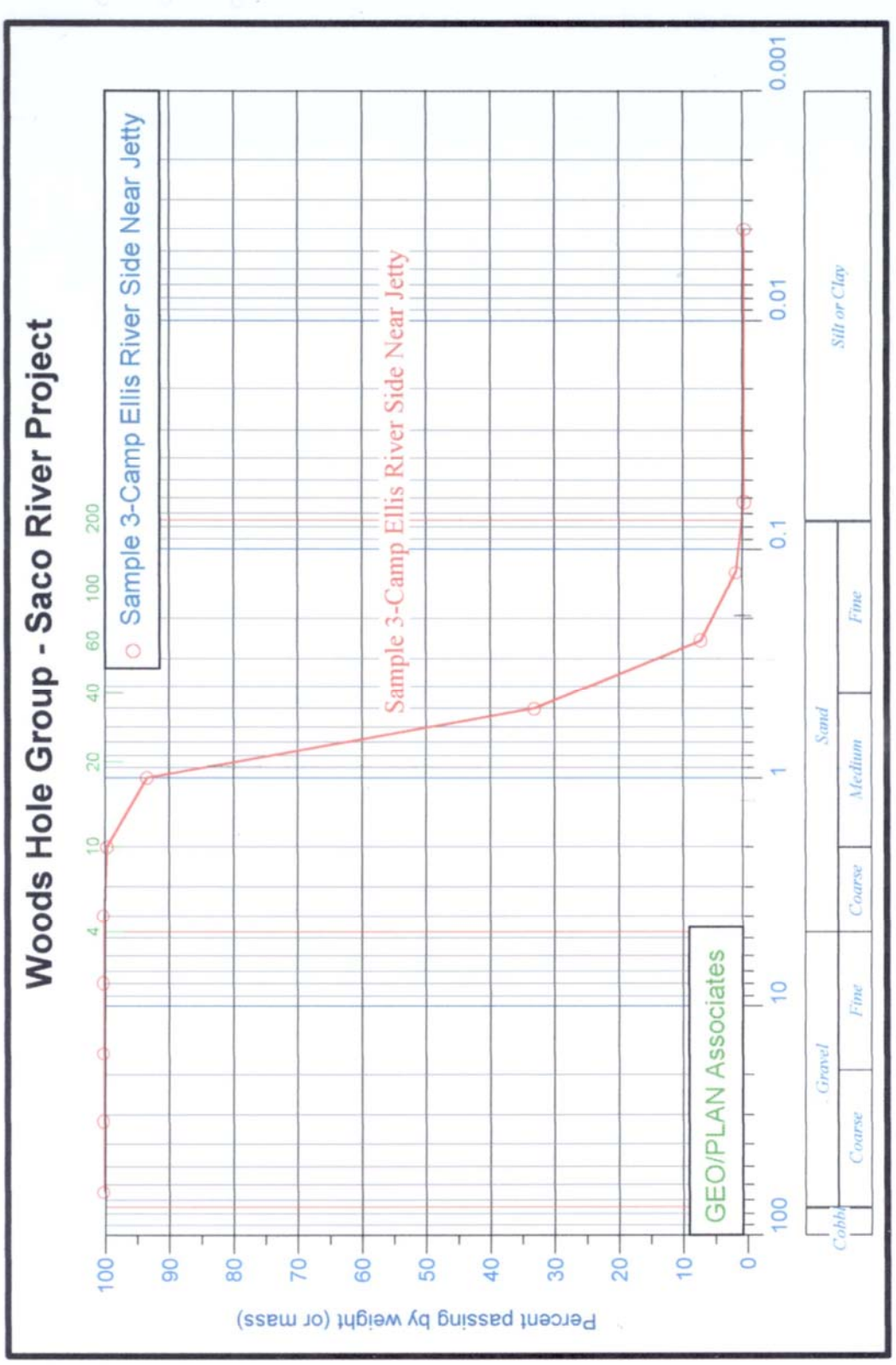

Figure 13A-3. Grain size distribution for sediment grab sample along Saco Bay shoreline, location 3.

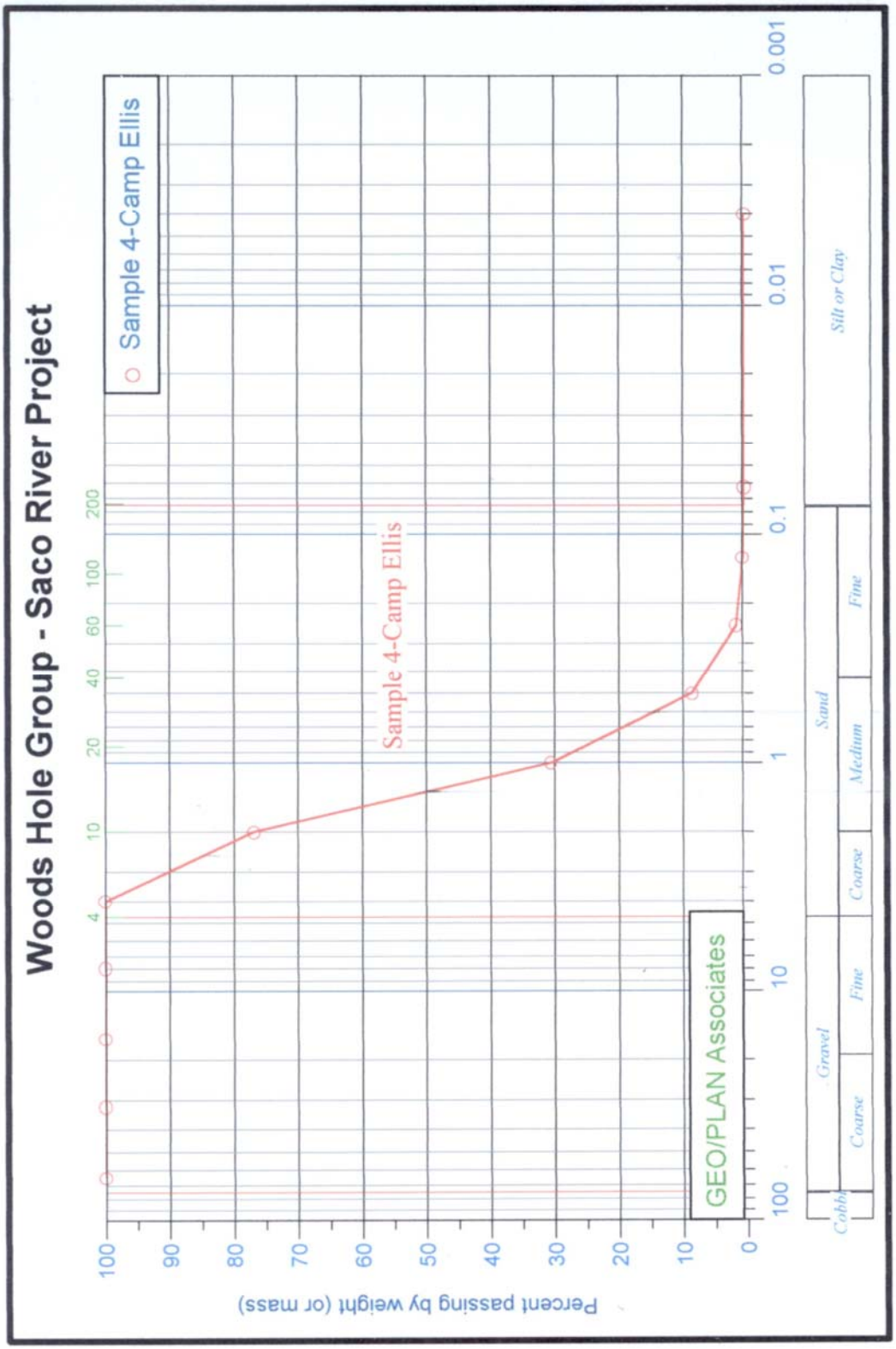

Figure 13A-4. Grain size distribution for sediment grab sample along Saco Bay shoreline, location 4.

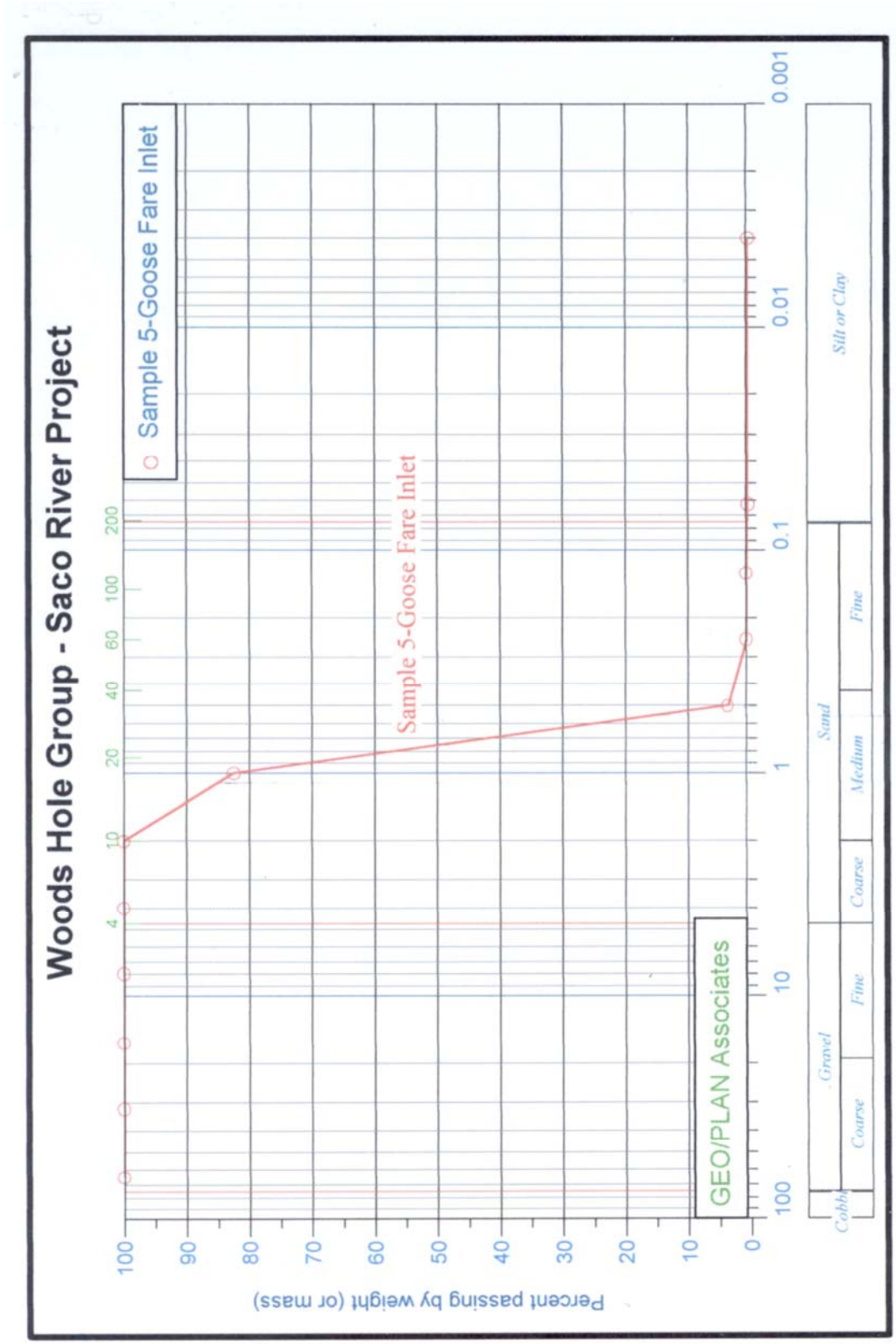

Figure 13A-5. Grain size distribution for sediment grab sample along Saco Bay shoreline, location 5.

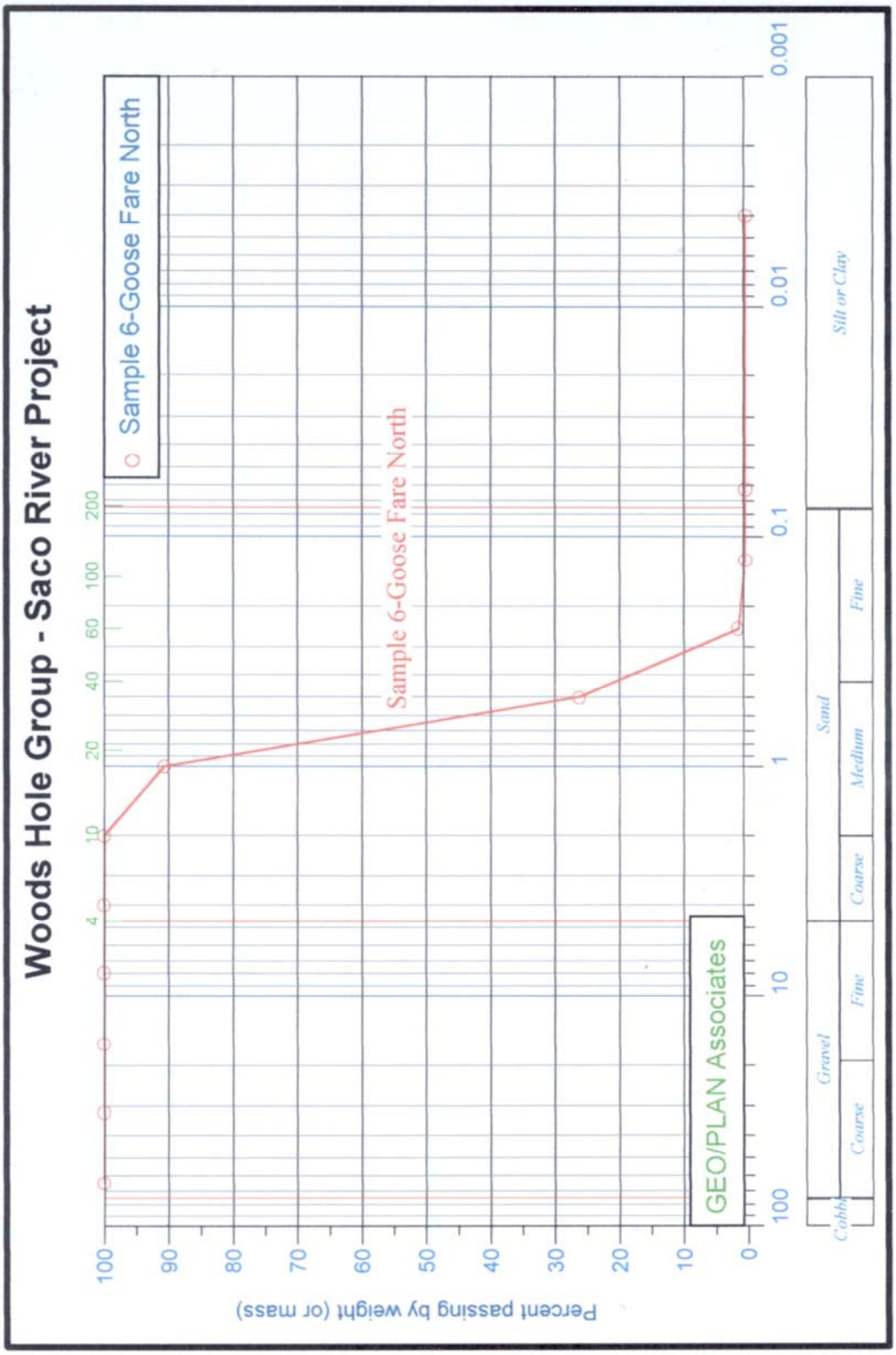

Figure 13A-6. Grain size distribution for sediment grab sample along Saco Bay shoreline, location 6.

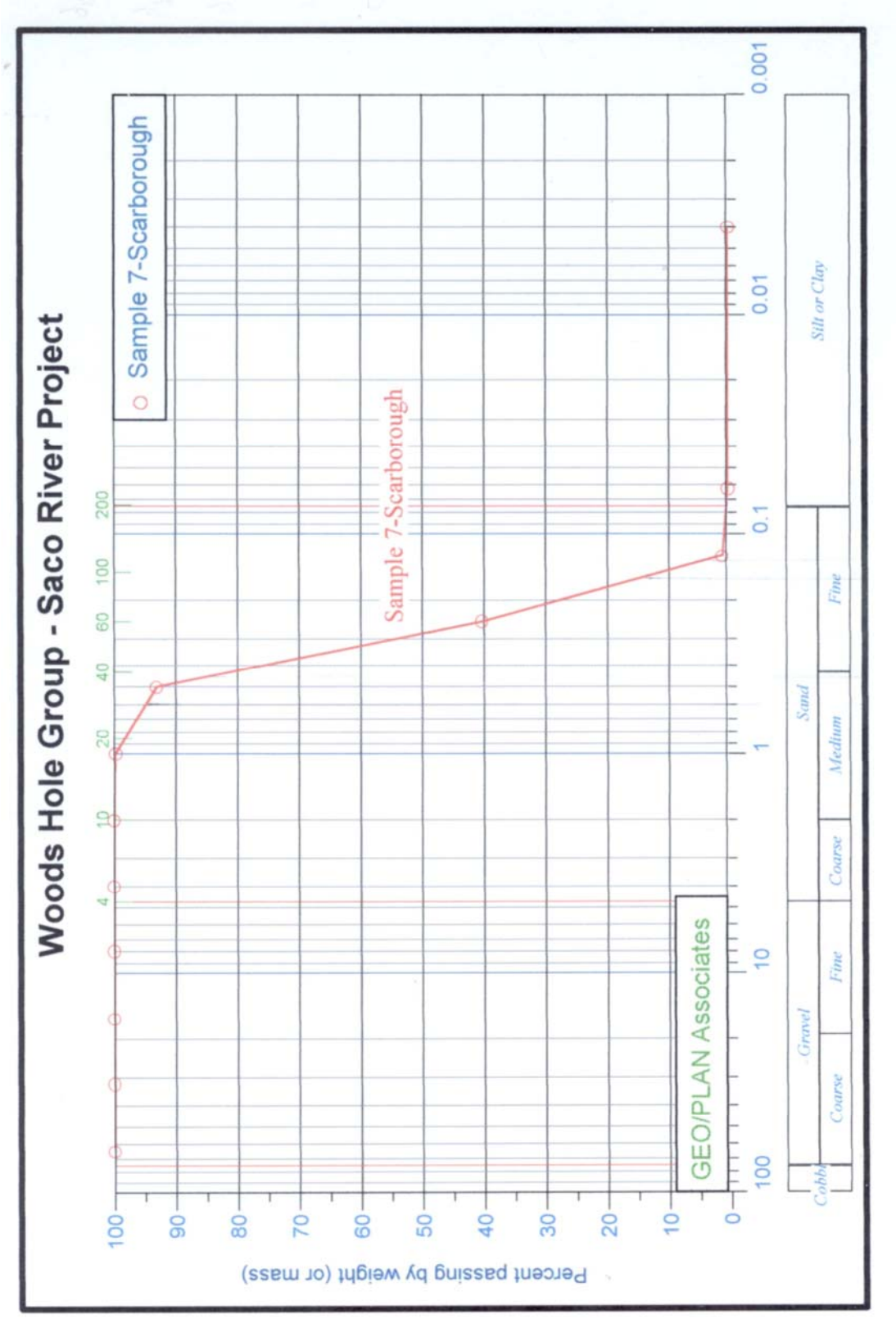

Figure 13A-7. Grain size distribution for sediment grab sample along Saco Bay shoreline, location 7.

APPENDIX 3-B

Appendix 3-B. Shoreline Change Rates (ft/yr) for Saco Bay, Maine

	Incremental Rates (end point method)														
Transect	**1864--1944**	**1864--1977**	**1864-1986**	**1864--1995**	**1864--1998**	**1944--1977**	**1944-1986**	**1944--1995**	**1944--1998**	**1977-1986**	**1977--1995**	**1977--1998**	**1986-1995**	**1986--1998**	**1995--1998**
1	-1.6076067														
2	-1.2139071														
3	-0.3936996														
4	0.1312332														
5	0.1312332														
6	-0.6889743														
7	-0.7217826														
8	-1.1154822														
9	1.312332														
10	-1.1482905			0.2296581				2.4278142							
11	-1.0498656			0.2624664				2.3621976							
12	-0.1640415			0.656166				1.9356897							
13	0.8858241			1.0170573				1.2139071							
14	1.8372648			1.1154822				0.0328083							
15	2.5262391			0.3608913				-3.0511719							
16	2.9199387	-0.1640415		0.2952747	0.2296581	-7.6443339		-3.7729545	-3.7401462		3.2152134	2.3293893			-3.1167885
17	1.5419901	-0.5577411		0.0656166	0.0328083	-5.6758359		-2.1981561	-2.1981561		4.1010375	3.2152134			-2.3950059
18	0.6233577	-0.6889743		-0.2624664	-0.2624664	-3.9041877		-1.6076067	-1.6076067		2.5262391	2.0013063			-1.2139071
19	-0.2624664	-0.8202075		-0.4593162	-0.4265079	-2.2309644		-0.7545909	-0.6889743		1.9356897	1.7388399			0.4265079
20	-0.7873992	-0.9514407		-0.5249328	-0.4265079	-1.2795237		-0.0656166	0.0984249		2.1653478	2.2637727			3.0511719
21	-1.1154822	-1.1482905		-0.5577411	-0.4921245	-1.2795237		0.3608913	0.4265079		3.28083	3.0511719			1.4763735
22	-1.312332	-1.0826739		-0.6889743	-0.6233577	-0.5905494		0.328083	0.3608913		1.968498	1.8372648			1.1810988
23	-1.5747984	-1.1154822		-0.6889743	-0.5577411	0		0.7545909	0.9514407		2.0997312	2.4606225			4.6587786
24	-1.4763735	-1.0498656		-0.5905494	-0.4921245	-0.0984249		0.7873992	0.9186324		2.3950059	2.5262391			3.3464466
25	-1.312332	-0.8202075		-0.5249328	-0.3936996	0.328083		0.7217826	0.9514407		1.4763735	1.9356897			4.8884367
26	-1.2467154	-0.7545909		-0.3936996	-0.2296581	0.4593162		0.9186324	1.2795237		1.7060316	2.5262391			7.4802924
27	-1.0826739	-0.656166		-0.4265079	-0.1640415	0.3608913		0.5905494	1.1810988		1.0498656	2.4606225			11.2532469
28	-0.8202075	-0.6233577		-0.0984249	-0.0656166	-0.0984249		1.0826739	1.0498656		3.1824051	2.8543221			0.8530158
29	-0.656166	-0.656166		0.1968498	0.2952747	-0.656166		1.5419901	1.7060316		5.5117944	5.4133695			4.7900118
30	-0.656166	-0.5249328		0.3936996	0.4921245	-0.1640415		2.0341146	2.2309644		6.0039189	5.9711106			5.8398774
31	-0.5577411	-0.2624664		0.656166	0.6889743	0.4265079		2.5590474	2.5262391		6.4632351	5.8398774			1.9028814
32	-0.1968498	0.0656166		0.8530158	0.9186324	0.7217826		2.4934308	2.5590474		5.6758359	5.4133695			3.7729545
33	-0.0984249	0.5577411		1.0170573	1.1482905	2.0669229		2.7887055	2.9855553		4.0354209	4.4291205			6.7585098
34	0.0656166	1.0498656		1.4107569	1.4107569	3.5104881		3.5104881	3.3792549		3.5432964	3.2152134			1.2467154
35	0.4921245	1.5747984		1.8372648	1.7388399	4.1994624		3.936996	3.608913		3.4448715	2.6574723			-2.296581
36	1.4435652	2.2309644		2.624664	2.4934308	4.1994624		4.4619288	4.0354209		4.921245	3.7729545			-3.4120632
37	2.4278142	3.1495968		3.4448715	3.3136383	4.8556284		5.0524782	4.593162		5.4461778	4.1666541			-3.6417213
38	3.2480217	4.1666541		4.3306956	4.1994624	6.3648102		6.0039189	5.577411		5.3477529	4.3963122			-1.7060316
39	3.6745296														
40		-4.265079													
41	-4.921245	-4.0682292	-4.0354209	-3.3136383	-3.3136383	-2.0013063	-2.3621976	-0.7873992	-0.9186324	-3.6417213	1.4435652	0.8202075	6.3976185	4.1338458	-3.0511719
42	-4.3963122	-3.6417213	-3.6417213	-2.8871304	-2.9199387	-1.8372648	-2.1653478	-0.5249328	-0.7217826	-3.3136383	1.8700731	1.0498656	6.9225513	4.265079	-4.1010375
43	-3.8385711	-3.0511719	-3.1495968	-2.6902806	-2.5262391	-1.0826739	-1.7716482	-0.8530158	-0.5577411	-4.2322707	-0.3608913	0.328083	3.4120632	3.6745296	4.5603537
44	-3.3792549	-2.624664	-2.7558972	-2.3293893	-2.1981561	-0.7873992	-1.5747984	-0.656166	-0.4921245	-4.4947371	-0.4593162	-0.0328083	3.4776798	3.28083	2.6574723
45	-2.8215138	-2.3621976	-2.5262391	-2.0997312	-1.8700731	-1.2795237	-1.968498	-0.984249	-0.5249328	-4.4291205	-0.3936996	0.7217826	3.608913	4.5603537	7.5787173
46	-2.4606225	-2.2637727	-2.1981561	-1.5747984	-1.6076067	-1.8044565	-1.6732233	-0.1968498	-0.328083	-1.1154822	2.7230889	2.0013063	6.4632351	4.2978873	-2.5918557
47	-2.0013063	-1.9028814	-1.9356897	-1.2139071	-1.312332	-1.6732233	-1.7716482	0	-0.2624664	-2.0669229	3.0511719	1.968498	8.0380335	4.9540533	-4.7900118
48	-1.6732233	-1.640415	-1.6732233	-1.0826739	-1.0170573	-1.5747984	-1.6076067	-0.1312332	0	-1.7716482	2.4934308	2.3950059	6.6928932	5.5117944	1.8044565
49	-1.4435652	-1.5419901	-1.4107569	-0.9514407	-0.8858241	-1.7716482	-1.3779486	-0.1968498	-0.0328083	0.1312332	2.6902806	2.6574723	5.2165197	4.5603537	2.5590474
50	-1.1482905	-1.2467154	-1.1154822	-0.7873992	-0.7545909	-1.4763735	-1.0170573	-0.1968498	-0.1312332	0.7545909	2.0997312	1.968498	3.4448715	2.8871304	1.1482905
51	-0.8858241	-1.0170573	-0.8858241	-0.5577411	-0.4921245	-1.312332	-0.8858241	-0.0328083	0.0656166	0.656166	2.3293893	2.2309644	4.0026126	3.4120632	1.5747984
52	-0.5249328	-0.7545909	-0.6233577	-0.2952747	-0.1968498	-1.2467154	-0.7873992	0.0984249	0.328083	0.9514407	2.5262391	2.7558972	4.0682292	4.1010375	4.1994624
53	-0.1640415	-0.4921245	-0.3936996	-0.0984249	0	-1.2795237	-0.8202075	0	0.2624664	0.8530158	2.3293893	2.7230889	3.7729545	4.1010375	5.1509031
54	0.1640415	-0.328083	-0.1968498	0.0656166	0.1640415	-1.5091818	-0.9186324	-0.0656166	0.1968498	1.2139071	2.5918557	2.8543221	3.9698043	4.0682292	4.3306956
55	0.4921245	-0.1312332	0.0328083	0.2952747	0.3608913	-1.640415	-0.8202075	0	0.1968498	2.296581	3.0183636	3.0511719	3.7073379	3.6417213	3.4120632
56	0.7873992	0.0656166	0.2624664	0.5249328	0.5577411	-1.7060316	-0.7545909	0.1640415	0.1968498	2.7558972	3.5432964	3.2152134	4.2978873	3.5432964	1.2139071
57	1.1154822	0.2296581	0.4921245	0.7217826	0.7217826	-1.9028814	-0.656166	0.0984249	0.0984249	3.9698043	3.7401462	3.28083	3.5432964	2.7558972	0.2952747
58	1.5747984	0.4265079	0.7217826	0.9186324	0.8858241	-2.3293893	-0.9186324	-0.0984249	-0.1640415	4.265079	3.9041877	3.2480217	3.5761047	2.4606225	-0.984249
59	1.968498	0.6889743	0.8858241	1.1482905	1.0498656	-2.4934308	-1.1810988	-0.1968498	-0.3608913	3.7073379	3.9698043	2.9855553	4.2322707	2.4278142	-3.2480217
60	1.9028814	0.6889743	0.9514407	1.1482905	1.0826739	-2.1981561	-0.8530158	0	-0.1312332	4.1010375	4.0026126	3.0839802	3.9041877	2.296581	-2.7558972
61	1.7060316	0.7217826	1.0498656	1.1810988	1.1154822	-1.7388399	-0.2624664	0.3608913	0.1968498	5.1837114	4.1994624	3.2152134	3.2152134	1.7716482	-2.7558972
62	1.8700731	0.7545909	1.0170573	1.2467154	1.1482905	-1.9356897	-0.5905494	0.328083	0.1312332	4.3963122	4.3963122	3.3464466	4.3963122	2.5590474	-3.2480217
63	1.9028814	0.8202075	1.0826739	1.312332	1.2467154	-1.8700731	-0.4593162	0.3608913	0.2296581	4.7243952	4.4291205	3.5104881	4.1338458	2.624664	-2.1653478
64	2.0669229	0.8530158	1.0170573	1.2467154	1.2467154	-2.0997312	-1.0170573	0	0	2.952747	3.8057628	3.28083	4.593162	3.5432964	0.1640415
65	2.1325395	0.8530158	1.0498656	1.1810988	1.1810988	-2.3293893	-1.0826739	-0.328083	-0.1968498	3.5104881	3.28083	3.0839802	3.0839802	2.7887055	1.8044565
66	2.1325395	0.8530158	0.984249	1.1482905	1.1482905	-2.2637727	-1.2795237	-0.4265079	-0.328083	2.3293893	2.9199387	2.6902806	3.5104881	2.952747	1.1810988
67	1.968498	0.8858241	1.0826739	1.1154822	1.0826739	-1.7388399	-0.5905494	-0.2624664	-0.2296581	3.5761047	2.4606225	2.1653478	1.3779486	1.1482905	0.3936996
68	1.9028814	0.9186324	1.1482905	1.0498656	1.0170573	-1.4435652	-0.3608913	-0.2624664	-0.2952747	3.6745296	1.8372648	1.5091818	0.0656166	-0.0984249	-0.6233577
69	2.0013063	0.9186324	1.0826739	1.1154822	1.0826739	-1.7388399	-0.5905494	-0.2624664	-0.2296581	3.5761047	2.4606225	2.1653478	1.3779486	1.1482905	0.3936996
70	2.0669229	0.7545909	0.9514407	0.8530158	0.8202075	-2.3950059	-1.2467154	-1.0170573	-1.0498656	3.0511719	1.4763735	1.0826739	-0.0656166	-0.3936996	-1.3451403
71	1.8700731	0.656166	0.7873992	0.7217826	0.656166	-2.2309644	-1.312332	-1.0498656	-1.1482905	2.1325395	1.0826739	0.5905494	0.0656166	-0.5577411	-2.5590474
72	1.640415	0.5577411	0.656166	0.656166	0.4921245	-2.0669229	-1.2467154	-0.9186324	-1.1810988	1.8044565	1.1810988	0.2296581	0.5905494	-0.9514407	-5.7742608
73	1.4107569	0.4265079	0.5905494	0.5249328	0.4265079	-1.968498	-1.0170573	-0.8858241	-1.0170573	2.4606225	1.1154822	0.4593162	-0.1968498	-1.0170573	-3.7073379
74	1.2139071	0.328083	0.4265079	0.4265079	0.3608913	-1.8044565	-1.0498656	-0.7873992	-0.9186324	1.8044565	1.1154822	0.5249328	0.4593162	-0.3936996	-3.0839802
75	1.1482905	0.1312332	0.1640415	0.2952747	0.2624664	-2.2637727	-1.7060316	-1.0498656	-1.0498656	0.3608913	1.1482905	0.8858241	1.9356897	1.2795237	-0.8530158
76	0.9186324	0.0328083	-0.0656166	0.0984249	0.1312332	-2.1325395	-1.968498	-1.1810988	-1.0498656	-1.3779486	0.5577411	0.6889743	2.4934308	2.2637727	1.5091818
77	0.8202075	0.0984249	-0.1312332	0.1312332	0.1312332	-1.640415	-1.9356897	-0.9186324	-0.8858241	-3.0511719	0.3936996	0.2624664	3.7729545	2.7230889	-0.656166
78	0.6889743	0.0984249	-0.2624664	0.1312332	0.0984249	-1.3451403	-2.0669229	-0.7873992	-0.8202075	-4.6587786	0.2296581	0.0656166	4.9868616	3.5432964	-0.9514407
79	0.5577411	0.0984249	-0.2624664	0.0984249	0	-0.984249	-1.8372648	-0.5905494	-0.8530158	-4.921245	0.0984249	-0.5905494	5.0524782	2.5918557	-5.0524782
80	0.5905494	0.2296581	-0.2296581	0.1312332	-0.0656166	-0.656166	-1.7716482	-0.5577411	-1.0498656	-5.8398774	-0.3936996	-1.640415	4.9540533	1.4763735	-9.5472153
81	0.7873992	0.2296581	-0.1312332	0.1968498	-0.0328083	-1.0826739	-1.9028814	-0.7217826	-1.2467154	-4.921245	-0.0656166	-1.4435652	4.7243952	1.1154822	-10.170573
82	0.984249	0.2296581	-0.0984249	0.2624664	0.0328083	-1.5419901	-2.0997312	-0.8858241	-1.3451403	-4.1994624	0.328083	-1.0826739	4.7572035	1.2467154	-9.8096817
83	1.0826739	0.2296581	-0.0328083	0.2952747	0.1640415	-1.8372648	-2.2309644	-0.984249	-1.2467154	-3.608913	0.5577411	-0.328083	4.6587786	2.1325395	-5.7742608
84	1.0826739	0.2296581	0.0328083	0.3608913	0.2296581	-1.8372648	-1.968498	-0.7873992	-1.0826739	-2.5262391	1.0826739	0.0984249	4.6259703	2.0341146	-6.1679604
85	1.1482905	0.2296581	0	0.4265079	0.1968498	-2.0669229	-2.2309644	-0.7545909	-1.2139071	-2.8215138	1.640415	0.1640415	6.0367272	2.3621976	-9.2191323
86	1.0170573	0.1640415	0.0328083	0.3608913	0.1968498	-1.9356897	-1.8372648	-0.6889743	-1.0170573	-1.4763735	1.6076067	0.4593162	4.6259703	1.8700731	-6.8241264
87	0.7873992	0.1312332	0.0328083	0.3608913	0.2624664	-1.5091818	-1.4107569	-0.328083	-0.5577411	-1.1154822	1.8044565	0.9186324	4.6915869	2.4278142	-4.6259703
88	0.6889743	0.1640415	-0.0328083	0.3608913	0.328083	-1.1482905	-1.3779486	-0.1640415	-0.1968498	-2.2637727	1.640415	1.2467154	5.4789861	3.8385711	-1.2795237
89	0.4921245	0.1640415	0.0328083	0.4265079	0.3936996	-0.6889743	-0.8858241	0.2952747	0.2296581	-1.6076067	2.1325395	1.7060316	5.7742608	4.1338458	-1.0170573
90	0.5249328	0.2296581	0.0656166	0.5249328	0.5249328	-0.5249328	-0.8202075	0.4921245	0.5577411	-1.8372648	2.3293893	2.2309644	6.3976185	5.2821363	1.7388399
91	0.6233577	0.1312332	0.1968498	0.656166	0.656166	-1.0826739	-0.6233577	0.6889743	0.7217826	1.0826739	3.9041877	3.5761047	6.6272766	5.4133695	1.5419901
92	0.7217826	0.2952747	0.2296581	0.5905494	0.656166	-0.7217826	-0.7217826	0.3608913	0.5577411	-0.8530158	2.3293893	2.5262391	5.4133695	5.0196699	3.7401462
93	0.9514407	0.2624664	0.1640415	0.6233577	0.6889743	-1.3779486	-1.3451403	0.0984249	0.328083	-1.2467154	2.7887055	2.952747	6.6928932	6.0367272	3.9698043
94	0.9514407	0.3608913	0.1968498	0.6889743	0.7545909	-1.1154822	-1.2467154	0.2952747	0.4265079	-1.7716482	2.8543221	2.8215138	7.4146758	6.233577	2.4934308
95	0.984249	0.3608913	0.1312332	0.8530158	0.8202075	-1.1810988	-1.4763735	0.6233577	0.5905494	-2.5590474	3.936996	3.3792549	10.2689979	7.7755671	-0.0656166
96	1.2139071	0.3936996	0.2952747	1.0170573	1.0170573	-1.5419901	-1.4435652	0.7217826	0.7217826	-1.0498656	4.8228201	4.265079	10.5642726	8.2348833	0.9186324
97	1.5419901	0.5577411	0.4593162	1.1482905	1.1482905	-1.8372648	-1.6076067	0.5249328	0.5577411	-0.7545909	4.8228201	4.3306956	10.3018062	8.0708418	1.1154822
98	1.9028814	0.6889743	0.6889743	1.2139071	1.2139071	-2.296581	-1.6732233	0.1312332	0.2296581	0.5905494	4.4947371	4.1666541	8.3333082	6.8241264	2.0997312
99	1.968498	0.7545909	0.656166	1.1810988	1.2139071	-2.1981561	-1.8372648	-0.0656166	0.0984249	-0.5249328	3.7729545	3.6417213	8.0052252	6.7257015	2.7887055
100	1.8700731	0.7545909	0.6889743	1.0826739	1.1810988	-2.0013063	-1.5419901	-0.1312332	0.1312332	0.1312332	3.28083	3.4776798	6.3976185	5.9711106	4.6915869

Appendix 3-B. Shoreline Change Rates (ft/yr) for Saco Bay, Maine

	Incremental Rates (end point method)														
Transect	**1864--1944**	**1864--1977**	**1864-1986**	**1864--1995**	**1864--1998**	**1944--1977**	**1944-1986**	**1944--1995**	**1944--1998**	**1977-1986**	**1977--1995**	**1977--1998**	**1986-1995**	**1986--1998**	**1995--1998**
100	1.8700731	0.7545909	0.6889743	1.0826739	1.1810988	-2.0013063	-1.5419901	-0.1312332	0.1312332	0.1312332	3.28083	3.4776798	6.3976185	5.9711106	4.6915869
101	1.8044565	0.8858241	0.656166	1.0826739	1.1482905	-1.312332	-1.5091818	-0.0984249	0.1640415	-2.2637727	2.0997312	2.4606225	6.3320019	5.9383023	4.7243952
102	1.8700731	0.8530158	0.6889743	1.0826739	1.1482905	-1.5747984	-1.5419901	-0.0984249	0.1312332	-1.3451403	2.5918557	2.7887055	6.4304268	5.8726857	4.1338458
103	1.968498	0.8530158	0.656166	1.1154822	1.1482905	-1.7716482	-1.8700731	-0.2296581	-0.0328083	-2.1653478	2.624664	2.6902806	7.3162509	6.2991936	3.1167885
104	2.0341146	0.9514407	0.6889743	1.1810988	1.1482905	-1.640415	-1.8372648	-0.1640415	-0.1312332	-2.624664	2.4934308	2.2309644	7.4802924	5.8726857	0.7873992
105	2.0341146	1.1154822	0.7545909	1.1154822	1.2467154	-1.1810988	-1.640415	-0.2952747	0.0984249	-3.4448715	1.2795237	2.0997312	5.8726857	6.233577	7.2834426
106	1.968498	1.1810988	0.7545909	1.2139071	1.3451403	-0.7873992	-1.5747984	0.0328083	0.3936996	-4.4291205	1.4763735	2.2309644	7.2834426	7.1522094	6.8241264
107	2.1653478	0.984249	0.8530158	1.3451403	1.3451403	-1.8700731	-1.6076067	0.0656166	0.1640415	-0.6889743	3.5761047	3.3464466	7.7099505	6.3320019	1.9356897
108	2.1653478	1.0498656	0.9186324	1.5419901	1.5419901	-1.6732233	-1.4107569	0.5577411	0.5905494	-0.5577411	4.5603537	4.0682292	9.5800236	7.5131007	1.0826739
109	2.4934308	1.312332	1.1154822	1.7060316	1.640415	-1.5091818	-1.4763735	0.5249328	0.3936996	-1.4107569	4.2322707	3.3464466	9.7112568	6.8569347	-2.0997312
110	2.8543221	1.7716482	1.4435652	2.1325395	2.1325395	-0.8858241	-1.2139071	1.0170573	1.0826739	-2.4606225	4.4619288	4.1994624	11.2204386	9.1207074	2.4934308
111	3.4120632	2.1981561	1.8372648	2.4606225	2.5262391	-0.7873992	-1.1482905	0.9514407	1.1810988	-2.4278142	4.0682292	4.2322707	10.4330394	9.1535157	5.2165197
112	3.608913	2.4278142	1.9356897	2.6574723	2.7558972	-0.4593162	-1.2795237	1.1482905	1.5091818	-4.2978873	4.0026126	4.5275454	12.139071	11.0563971	7.7755671
113	4.9540533	3.28083	3.1824051	3.5432964	3.4776798	-0.7873992	-0.2296581	1.3779486	1.2795237	1.8044565	5.2821363	4.4947371	8.6613912	6.4960434	-0.2952747
114	4.8556284	3.5104881	3.608913	3.8713794	3.6417213	0.2624664	1.2139071	2.296581	1.8700731	4.7243952	5.9711106	4.4291205	7.1850177	4.1994624	-5.249328
115	5.0196699	2.7887055	3.0183636	3.5104881	2.952747	-2.6902806	-0.8530158	1.1482905	-0.1312332	5.8726857	8.0380335	3.8385711	10.170573	2.296581	-22.4736855
116	4.1338458	2.3950059	2.6902806	3.2480217	2.624664	-1.8044565	0	1.8700731	0.4265079	6.5288517	8.530158	3.8713794	10.498656	1.9028814	-25.1639661
117	4.1338458	2.3293893	2.7887055	3.0839802	2.5918557	-2.0669229	0.2624664	1.4435652	0.3608913	8.6941995	7.7755671	4.1010375	6.8569347	0.6889743	-18.7663476
118	4.0354209	2.3621976	2.5918557	3.0511719	2.5918557	-1.7060316	-0.1640415	1.4435652	0.4593162	5.4461778	7.1522094	3.8385711	8.858241	2.6574723	-16.8306579
119	3.7401462	2.3293893	2.3950059	2.8543221	2.4934308	-1.0826739	-0.1312332	1.4107569	0.656166	3.28083	5.9711106	3.3464466	8.5957746	3.3792549	-13.0248951
120	3.3792549	2.1981561	2.1653478	2.6574723	2.3950059	-0.6889743	-0.0984249	1.5091818	0.9514407	2.0341146	5.5117944	3.5761047	8.8910493	4.6915869	-8.4973497
121	3.2480217	1.8372648	2.0669229	2.4278142	2.2309644	-1.6076067	-0.1968498	1.1810988	0.7545909	5.0196699	6.2007687	4.4291205	7.3818675	3.9698043	-6.7257015
122	2.9855553	1.4107569	1.7716482	2.2309644	1.968498	-2.3621976	-0.5249328	1.0826739	0.4921245	6.2007687	7.3162509	4.921245	8.3989248	3.9698043	-9.9409149
123	2.8543221	1.2795237	1.640415	2.1325395	1.8700731	-2.5262391	-0.656166	1.0170573	0.4265079	6.1023438	7.4474841	4.9540533	8.7598161	4.1338458	-10.4002311
124	2.8215138	1.0826739	1.5747984	2.1325395	1.7716482	-3.1167885	-0.8202075	1.0170573	0.1968498	7.6115256	8.4973497	5.3477529	9.3503655	3.6745296	-14.2059939
125	2.7558972	1.0170573	1.5419901	1.968498	1.7388399	-3.2480217	-0.8202075	0.7545909	0.1968498	8.0708418	7.9396086	5.577411	7.8083754	3.7073379	-9.2191323
126	2.6902806	0.9514407	1.4107569	1.9028814	1.7060316	-3.28083	-1.0170573	0.656166	0.2624664	7.2834426	7.8083754	5.8070691	8.3333082	4.7243952	-6.6928932
127	2.5918557	0.8530158	1.2795237	1.8372648	1.6732233	-3.3464466	-1.2139071	0.656166	0.328083	6.6272766	7.9724169	6.1023438	9.2847489	5.7086442	-5.5117944
128	2.4934308	0.7873992	1.2139071	1.8372648	1.640415	-3.4448715	-1.2795237	0.7873992	0.3608913	6.5944683	8.4317331	6.2991936	10.2033813	6.0695355	-6.9881679
129	2.4278142	0.8202075	1.1810988	1.7716482	1.6076067	-3.1167885	-1.2139071	0.7545909	0.3936996	5.6430276	7.7099505	5.8398774	9.7440651	6.0039189	-5.8398774
130	2.2309644	0.656166	1.1482905	1.7716482	1.5747984	-3.1824051	-0.9514407	1.0170573	0.5577411	7.217826	8.6613912	6.3976185	10.1049564	5.7742608	-7.873992
131	2.0669229	0.6889743	1.1810988	1.7716482	1.5091818	-2.7230889	-0.5577411	1.2795237	0.656166	7.3490592	8.4645414	5.9383023	9.5472153	4.8556284	-9.9737232
132	2.0669229	0.5905494	1.1154822	1.7388399	1.4763735	-2.9199387	-0.7217826	1.2139071	0.656166	7.3818675	8.7270078	6.233577	10.0721481	5.3805612	-9.3175572
133	2.0341146	0.5905494	1.1482905	1.7388399	1.4763735	-2.8543221	-0.5249328	1.2795237	0.656166	7.9724169	8.7598161	6.1023438	9.514407	4.7243952	-10.3346145
134	2.0341146	0.5905494	1.0826739	1.7060316	1.4763735	-2.9199387	-0.7545909	1.2139071	0.6889743	7.1522094	8.6285829	6.2991936	10.0721481	5.6758359	-8.2348833
135	2.0669229	0.5249328	1.0498656	1.7060316	1.5091818	-3.1824051	-0.8858241	1.1810988	0.7217826	7.545909	9.0878991	6.8241264	10.6298892	6.2991936	-7.2834426
136	2.1325395	0.5249328	1.0826739	1.7716482	1.5747984	-3.3464466	-0.9514407	1.2139071	0.7217826	7.8411837	9.4159821	7.0865928	10.9907805	6.5288517	-7.4802924
137	2.1325395	0.5577411	1.0826739	1.8372648	1.5747984	-3.2480217	-0.9186324	1.3779486	0.7545909	7.6443339	9.7440651	6.9881679	11.7781797	6.4632351	-10.2033813
138	1.968498	0.5249328	1.0498656	1.8044565	1.5747984	-2.952747	-0.6889743	1.5747984	0.984249	7.545909	9.7440651	7.1194011	11.9094129	6.7913181	-9.3831738
139	1.8044565	0.4265079	0.984249	1.8044565	1.5747984	-2.952747	-0.5249328	1.8372648	1.2467154	8.3333082	10.4658477	7.8083754	12.5983872	7.4474841	-8.8254327
140	1.8372648	0.2952747	0.984249	1.7716482	1.5747984	-3.4120632	-0.656166	1.7060316	1.2467154	9.4487904	10.9579722	8.4973497	12.467154	7.7755671	-7.0209762
141	1.8372648	0.328083	1.0170573	1.7716482	1.6076067	-3.3464466	-0.5249328	1.7060316	1.2795237	9.8752983	10.9251639	8.4645414	11.9094129	7.4146758	-6.6928932
142	1.7060316	0.328083	0.984249	1.8044565	1.6076067	-2.9855553	-0.3936996	1.968498	1.4435652	9.1535157	10.9907805	8.3661165	12.795237	7.8083754	-7.9396086
143	1.8044565	0.3936996	1.0170573	1.8044565	1.5747984	-2.9855553	-0.4921245	1.8372648	1.2467154	8.6285829	10.5642726	7.873992	12.467154	7.3162509	-8.9238576
144	1.9028814	0.4265079	1.0170573	1.5419901	1.5419901	-3.1495968	-0.6889743	1.0170573	1.0498656	8.2348833	8.5629663	7.5787173	8.858241	7.0865928	1.5091818
145	1.9356897	0.4593162	1.1154822	1.4435652	1.5747984	-3.1495968	-0.4593162	0.656166	1.0170573	9.3503655	7.6115256	7.545909	5.8726857	6.1679604	7.0865928
146	1.968498	0.5249328	1.1154822	1.4435652	1.6076067	-2.9855553	-0.5577411	0.656166	1.0498656	8.3661165	7.2506343	7.3490592	6.1023438	6.5944683	8.1036501
147	2.0013063	0.5577411	1.1482905	1.4435652	1.640415	-2.9199387	-0.5577411	0.5249328	1.0826739	8.1364584	6.7913181	7.2834426	5.4789861	6.6600849	10.4330394
148	2.0341146	0.656166	1.1810988	1.4107569	1.6076067	-2.7558972	-0.4593162	0.4593162	0.984249	7.9724169	6.233577	6.8241264	4.5603537	5.9711106	10.4658477
149	2.0341146	0.6233577	1.2139071	1.4763735	1.6076067	-2.8215138	-0.3608913	0.5905494	0.984249	8.6285829	6.7257015	6.9225513	4.8884367	5.6430276	8.0052252
150	2.0341146	0.656166	1.2139071	1.4763735	1.5747984	-2.6902806	-0.328083	0.6233577	0.9514407	8.2676916	6.56166	6.5944683	4.8884367	5.3149446	6.6272766
151	1.9356897	0.656166	1.1482905	1.4107569	1.5419901	-2.4606225	-0.3936996	0.5249328	0.9186324	7.1850177	5.9383023	6.1679604	4.6915869	5.3805612	7.5787173
152	1.8372648	0.656166	1.1810988	1.3779486	1.5091818	-2.2309644	-0.0656166	0.6889743	1.0826739	7.9068003	6.0039189	6.233577	4.1338458	4.9868616	7.6115256
153	1.7716482	0.656166	1.1154822	1.3451403	1.5091818	-2.0669229	-0.0984249	0.6889743	1.1482905	7.0865928	5.7086442	6.1351521	4.3635039	5.4133695	8.6941995
154	1.7388399	0.6233577	1.1154822	1.3451403	1.5091818	-2.1325395	-0.1312332	0.6889743	1.1154822	7.1522094	5.7742608	6.1679604	4.4291205	5.4461778	8.6285829
155	1.7716482	0.6233577	1.0826739	1.312332	1.4763735	-2.1653478	-0.2296581	0.6233577	1.0498656	6.7913181	5.6102193	6.0367272	4.4291205	5.4789861	8.7270078
156	1.7060316	0.5249328	1.0170573	1.2467154	1.4435652	-2.3293893	-0.3608913	0.5249328	1.0498656	6.889743	5.6758359	6.3320019	4.4619288	5.905494	10.4002311
157	1.5747984	0.4921245	0.9186324	1.1482905	1.3779486	-2.1981561	-0.3936996	0.4921245	1.0826739	6.2663853	5.3477529	6.2007687	4.4291205	6.1351521	11.4172884
158	1.4763735	0.3608913	0.9514407	1.1154822	1.3451403	-2.296581	-0.0328083	0.5905494	1.1482905	8.1692667	5.7742608	6.4632351	3.4448715	5.2165197	10.826739
159	1.3451403	0.2296581	0.9186324	1.0826739	1.2795237	-2.5262391	0.0656166	0.656166	1.2139071	9.5800236	6.4304268	7.0209762	3.3464466	5.1180948	10.7939307
160	1.1810988	-0.0984249	0.9186324	1.0498656	1.2795237	-3.28083	0.3608913	0.7873992	1.4107569	13.6154445	8.1692667	8.6941995	2.8215138	5.0524782	12.1062627
161	0.984249	-0.0328083	0.8858241	0.984249	1.2795237	-2.5590474	0.656166	0.9514407	1.7060316	12.4015374	7.3490592	8.3333082	2.4278142	5.3149446	14.4028437
162	0.9514407	0.0328083	0.8858241	0.984249	1.2795237	-2.2637727	0.7217826	1.0170573	1.7388399	11.6797548	6.9553596	7.9724169	2.3293893	5.2165197	14.3044188
163	1.0170573	0	0.9186324	1.0170573	1.312332	-2.4278142	0.7545909	1.0170573	1.7716482	12.3359208	7.2834426	8.3333082	2.296581	5.3805612	15.0262014
164	1.1154822	0.0328083	0.9514407	1.0498656	1.3779486	-2.5590474	0.6233577	0.984249	1.7388399	12.2046876	7.3490592	8.4317331	2.624664	5.6430276	15.1902429
165	1.2139071	0.1312332	0.984249	1.0826739	1.4107569	-2.4606225	0.4921245	0.8530158	1.7060316	11.4172884	6.9225513	8.2348833	2.5262391	5.905494	16.5025749
166	1.312332	0.1640415	0.9514407	1.1154822	1.4763735	-2.6902806	0.2296581	0.7873992	1.7060316	11.0235888	7.1194011	8.5629663	3.28083	6.6928932	17.5196322
167	1.2795237	0.2952747	0.9514407	1.0826739	1.4435652	-2.0341146	0.328083	0.7545909	1.640415	9.0550908	5.7742608	7.4146758	2.5918557	6.2007687	17.6180571
168	1.2795237	0.2952747	0.984249	1.0826739	1.3779486	-2.0997312	0.3936996	0.7217826	1.5091818	9.514407	5.8726857	7.1522094	2.3293893	5.3805612	15.0590097
169	1.3451403	0.1968498	0.9186324	1.0498656	1.312332	-2.5590474	0.0656166	0.6233577	1.312332	9.7440651	7.3818675	3.2152134	5.6102193	13.0905117	
170	1.312332	0.1640415	0.9186324	1.0170573	1.2795237	-2.624664	0.2296581	0.5577411	1.2467154	10.6626975	6.3320019	7.2506343	2.0669229	4.7243952	13.12332
171	1.2467154	0.1312332	0.8530158	0.9514407	1.2139071	-2.5262391	0.1312332	0.4921245	1.2139071	9.7440651	6.0039189	6.9881679	2.296581	4.9540533	13.3201698
172	1.1154822	0.0656166	0.7873992	0.8858241	1.1482905	-2.4934308	0.1640415	0.4921245	1.1810988	9.8752983	5.905494	6.9225513	2.0013063	4.7243952	13.3529781
173	0.9186324	0.0656166	0.6889743	0.7873992	1.0826739	-2.0669229	0.2624664	0.5249328	1.312332	8.7270078	5.249328	6.6272766	1.8372648	5.0524782	15.1902429
174	0.9514407	0.0328083	0.7545909	0.7873992	1.1154822	-2.1981561	0.3608913	0.4921245	1.3779486	9.7440651	5.3805612	6.9225513	1.0826739	4.8228201	16.6009998
175	1.1482905	0	0.7545909	0.8530158	1.1810988	-2.7558972	0.0328083	0.3608913	1.2467154	10.2361896	5.9711106	7.4802924	1.7716482	5.4133695	16.8962745
176	1.3779486	0.1312332	0.8530158	0.9186324	1.2467154	-2.9199387	-0.1640415	0.1640415	1.0826739	9.84249	5.7414525	7.2834426	1.7388399	5.3805612	16.8634662
177	1.640415	0.2952747	0.9186324	0.9514407	1.2795237	-2.952747	-0.4593162	-0.0656166	0.7873992	8.6613912	5.0852865	6.6272766	1.6076067	5.1180948	16.1744919
178	1.8044565	0.4593162	0.9514407	0.984249	1.3451403	-2.7887055	-0.656166	-0.2624664	0.6233577	7.1194011	4.265079	5.9383023	1.4763735	5.0524782	16.2073002
179	1.9356897	0.9514407	1.0498656	1.0826739	1.4107569	-1.4435652	-0.656166	-0.1968498	0.656166	2.1981561	2.0341146	3.9041877	1.8700731	5.1837114	15.6495591
180	2.0341146	1.0826739	1.1482905	1.2795237	1.5419901	-1.2467154	-0.5577411	0.0984249	0.7873992	2.0013063	2.5262391	3.9041877	3.0839802	5.3149446	12.3687291
181	2.2637727	1.2467154	1.2467154	1.4435652	1.6732233	-1.2467154	-0.6889743	0.1968498	0.8202075	1.2467154	2.8215138	4.0026126	4.3306956	6.0367272	11.4500967
182	2.5262391	1.3779486	1.4763735	1.640415	1.8044565	-1.4107569	-0.5249328	0.2624664	0.7545909	2.6574723	3.2480217	4.1338458	3.8385711	5.249328	9.6784485
183	2.7558972	1.6076067	1.6732233	1.7388399	2.0013063	-1.1482905	-0.3936996	0.1312332	0.8858241	2.4278142	2.4934308	4.0682292	2.5590474	5.2821363	13.8451026
184	2.9855553	1.8044565	2.0997312	1.9028814	2.296581	-1.0826739	0.4265079	0.2296581	1.2795237	5.8726857	2.5262391	4.921245	-0.7217826	4.2322707	19.8818298
185	3.1495968	1.968498	2.2309644	2.0013063	2.4278142	-0.8858241	0.4593162	0.1968498	1.3779486	5.3805612	2.1325395	4.8884367	-1.0498656	4.5275454	22.1127942
186	3.3464466	2.1325395	2.3293893	2.0997312	2.4934308	-0.8202075	0.4265079	0.1312332	1.2467154	5.0196699	1.9028814	4.4947371	-1.1482905	4.0682292	20.6036124
187	3.5104881	2.2309644	2.4606225	2.1325395	2.5590474	-0.8202075	0.4921245	-0.0328083	1.1482905	5.2165197	1.3451403	4.1994624	-2.4606225	3.4448715	22.1127942
188	3.6745296	2.296581	2.4278142	2.1981561	2.5918557	-1.0170573	0.0328083	-0.1312332	1.0170573	3.936996	1.4435652	4.1666541	-0.984249	4.3306956	21.0301203
189	3.5104881	2.2309644	2.3950059	2.1325395	2.4934308	-0.8202075	0.2952747	0	0.984249	4.3963122	1.5091818	3.8057628	-1.312332	3.4120632	18.2414148
190	3.5104881	2.0997312	2.2637727	2.0669229	2.3621976	-1.3451403	-0.1312332	-0.1968498	0.6889743	4.2322707	1.9028814	3.8385711	-0.3608913	3.5104881	15.7807923
191	3.5432964	2.0013063	2.2309644	2.0013063	2.2637727	-1.7716482	-0.328083	-0.4593162	0.3608913	4.9540533	1.8700731	3.6417213	-1.1154822	2.6902806	14.7309267
192	3.3792549	1.9356897	2.1325395	1.9356897	2.1981561	-1.6076067	-0.2624664	-0.328083	0.4265079	4.6259703	1.968498	3.608913	-0.5905494	2.8543221	13.779486
193	3.2152134	1.8372648	2.0341146	1.9028814	2.0997312	-1.5091818	-0.2296581	-0.1968498	0.4265079	4.3963122	2.1981561	3.4448715	0.0328083	2.7558972	11.3844801
194	3.1495968	1.8044565	2.0341146	1.7388399	2.0341146	-1.4763735	-0.0656166	-0.4593162	0.3608913	5.1180948	1.4107569	3.2152134	-2.1981561	1.7716482	14.3372271
195	3.2152134	1.8044565	2.0341146	1.7716482	2.0013063	-1.6732233	-0.2952747	-0.4921245	0.1968498	4.8228201	1.6076067	3.1495968	-1.5091818	1.9356897	12.6968121
196	2.9855553	1.5091818	1.7716482	1.5419901	1.7388399	-2.0669229	-0.5905494	-0.7217826	-0.1312332	4.7572035	1.7388399	2.8871304	-1.1810988	1.5419901	10.1049564

Appendix 3-B. Shoreline Change Rates (ft/yr) for Saco Bay, Maine

Incremental Rates (end point method)

Transect	1864--1944	1864--1977	1864-1986	1864--1995	1864--1998	1944--1977	1944-1986	1944--1995	1944--1998	1977-1986	1977--1995	1977--1998	1986-1995	1986--1998	1995--1998
197	2.7558972	1.312332	1.4763735	1.3779486	1.4435652	-2.1981561	-0.984249	-0.8202075	-0.4921245	3.4448715	1.7060316	2.1325395	0.0328083	1.1810988	4.7900118
198	2.4278142	1.0826739	1.312332	1.1810988	1.1482905	-2.2637727	-0.8530158	-0.7545909	-0.7545909	4.2322707	1.968498	1.6076067	-0.2296581	-0.328083	-0.656166
199	2.1325395	0.9514407	1.1482905	1.0826739	1.0498656	-1.9356897	-0.7873992	-0.6233577	-0.5905494	3.4448715	1.7716482	1.5419901	0.0984249	0.0984249	0.1312332
200	1.9356897	0.8202075	0.984249	0.9514407	0.984249	-1.9356897	-0.8530158	-0.6233577	-0.4593162	3.1824051	1.7716482	1.8044565	0.3936996	0.7873992	2.0997312
201	1.8372648	0.656166	0.8530158	0.8530158	0.8858241	-2.1653478	-0.984249	-0.7217826	-0.5249328	3.2152134	1.9028814	2.0341146	0.6233577	1.1482905	2.7887055
202	1.6732233	0.5577411	0.7545909	0.7545909	0.7873992	-2.1653478	-1.0170573	-0.7545909	-0.5249328	3.2152134	1.8700731	2.0341146	0.5249328	1.1482905	3.1495968
203	1.4763735	0.4265079	0.5905494	0.6233577	0.6889743	-2.0997312	-1.0826739	-0.6889743	-0.4921245	2.624664	1.8700731	2.0341146	1.1154822	1.5747984	2.952747
204	1.2139071	0.3936996	0.5249328	0.5249328	0.5905494	-1.5747984	-0.7545909	-0.5577411	-0.328083	2.1653478	1.312332	1.6076067	0.4593162	1.1810988	3.3792549
205	0.9514407	0.2952747	0.4921245	0.4593162	0.4921245	-1.2795237	-0.3608913	-0.2624664	-0.1640415	3.0183636	1.5419901	1.5419901	0.0656166	0.4265079	1.640415
206	0.8202075	0.2952747	0.5577411	0.4921245	0.5249328	-0.984249	0.0656166	-0.0328083	0.0984249	4.0354209	1.7060316	1.8372648	-0.5577411	0.1968498	2.5590474
207	0.8858241	0.3936996	0.6233577	0.5249328	0.5577411	-0.7545909	0.1312332	0	0.0984249	3.3792549	1.3779486	1.4435652	-0.5905494	0	1.9356897
208	0.8858241	0.4265079	0.5249328	0.5249328	0.5577411	-0.656166	-0.1968498	0	0.0656166	1.5091818	1.1810988	1.2139071	0.8530158	0.984249	1.3779486
209	0.9186324	0.4921245	0.5249328	0.5905494	0.6233577	-0.5577411	-0.1968498	0.0984249	0.1640415	1.1810988	1.312332	1.3451403	1.4435652	1.4763735	1.640415
210	1.0498656	0.5577411	0.5577411	0.6233577	0.6889743	-0.6233577	-0.328083	-0.0328083	0.1640415	0.7873992	1.0826739	1.4435652	1.4107569	1.9356897	3.6417213
211	1.1810988	0.6233577	0.5577411	0.7217826	0.7873992	-0.8202075	-0.6889743	-0.6556166	0.1640415	-0.1968498	1.312332	1.7060316	2.8215138	3.1167885	4.0682292
212	1.3779486	0.6233577	0.6889743	0.6889743	0.7873992	-1.2139071	-0.656166	-0.3608913	-0.0656166	1.312332	1.1482905	1.7060316	0.984249	1.968498	5.1180948
213	1.4107569	0.5905494	0.656166	0.656166	0.7545909	-1.4763735	-0.8202075	-0.5577411	-0.2624664	1.6076067	1.0826739	1.6732233	0.5905494	1.7388399	5.3477529
214	1.3451403	0.5577411	0.7545909	0.6233577	0.8202075	-1.3779486	-0.3936996	-0.4921245	0.0328083	3.1167885	1.1154822	2.2309644	-0.8530158	1.5747984	9.2191323
215	1.2139071	0.4921245	0.6233577	0.5905494	0.8858241	-1.2139071	-0.4593162	-0.3608913	0.3936996	2.296581	1.1810988	2.9199387	0.0984249	3.3792549	13.7466777
216	1.0498656	0.4921245	0.4593162	0.5905494	0.9514407	-0.8858241	-0.656166	-0.0984249	0.7545909	0.2296581	1.312332	3.3464466	2.3621976	5.6430276	16.0104504
217	1.0498656	0.4921245	0.5577411	0.6889743	1.0498656	-0.8202075	-0.3608913	0.1312332	1.1154822	1.1810988	1.8372648	4.0682292	2.4606225	6.2007687	17.9789484
218	1.0826739	0.5249328	0.6233577	0.8202075	1.2139071	-0.8858241	-0.2624664	0.3936996	1.4435652	2.1325395	2.6902806	5.0524782	3.28083	7.2506343	19.7834049
219	1.1810988	0.5577411	0.7873992	0.984249	1.4107569	-0.9514407	0	0.656166	1.7388399	3.5104881	3.5761047	5.8726857	3.608913	7.6443339	20.341146
220	1.2795237	0.656166	1.0170573	1.1810988	1.6076067	-0.8530158	0.4593162	0.984249	2.0997312	5.3149446	4.3306956	6.6928932	3.3792549	7.7099505	21.3910116
221	1.2139071	0.7873992	1.1154822	1.4435652	1.8044565	-0.2296581	0.9514407	1.8044565	2.6902806	5.2821363	5.4789861	7.217826	5.7086442	8.6613912	17.9461401
222	1.0826739	0.9186324	1.2139071	1.6076067	1.968498	0.4921245	1.4435652	2.4278142	3.2480217	4.8884367	5.9383023	7.545909	6.9225513	9.5472153	17.7492903
223	1.0170573	1.0170573	1.3779486	1.8044565	2.0997312	0.9514407	2.0341146	3.0183636	3.7401462	5.9711106	6.7913181	8.0380335	7.6115256	9.5800236	15.8792172
224	0.8530158	1.0826739	1.3451403	1.8372648	2.1325395	1.640415	2.296581	3.3464466	4.0682292	4.6259703	6.3976185	7.8083754	8.1036501	10.2033813	16.7650413
225	0.6889743	0.984249	1.3779486	1.8372648	2.0997312	1.7716482	2.6902806	3.6417213	4.2322707	6.1023438	7.0209762	8.0708418	7.9068003	9.514407	14.5996935
226	0.8858241	1.0826739	1.6076067	1.968498	2.2637727	1.5091818	2.9855553	3.608913	4.2978873	8.3989248	7.4474841	8.5957746	6.5288517	8.7598161	15.8464089
227	1.312332	1.2139071	2.0013063	2.2309644	2.4934308	0.984249	3.28083	3.7073379	4.265079	11.7125631	8.6285829	9.3831738	5.6430276	7.6443339	14.0419524
228	1.5747984	1.4107569	2.2309644	2.4278142	2.6574723	0.984249	3.4448715	3.7729545	4.265079	12.467154	8.7598161	9.3831738	5.1509031	7.1194011	13.3529781
229	1.6732233	1.5091818	2.3621976	2.5262391	2.6902806	1.0826739	3.6745296	3.8385711	4.1994624	13.1561283	8.8910493	9.0550908	4.6915869	6.0039189	10.1049564
230	1.640415	1.4435652	2.2637727	2.4278142	2.624664	0.984249	3.4120632	3.608913	4.0354209	12.3031125	8.3989248	8.858241	4.593162	6.2663853	11.5813299
231	1.4763735	1.4107569	2.1981561	2.4278142	2.5262391	1.1810988	3.5104881	3.8713794	4.1010375	12.0734544	8.7270078	8.6285829	5.4461778	6.0367272	7.873992
232	1.2795237	1.3779486	2.1653478	2.3621976	2.4278142	1.6076067	3.8385711	4.0682292	4.1666541	11.9094129	8.4973497	8.1364584	5.1837114	5.3149446	5.6758359
233	0.984249	1.2139071	1.9356897	2.2309644	2.2637727	1.7716482	3.8057628	4.1994624	4.1666541	11.2204386	8.5629663	7.9396086	5.9711106	5.4789861	4.0026126
234	1.0498656	1.3779486	2.0013063	2.296581	2.296581	2.1325395	3.8385711	4.2322707	4.1666541	10.0393398	8.0380335	7.3162509	6.0695355	5.2821363	2.7887055
235	1.0170573	1.5091818	2.1325395	2.3950059	2.3621976	2.6574723	4.265079	4.4947371	4.2978873	10.2033813	7.8083754	6.8569347	5.4461778	4.3963122	1.0498656
236	0.8858241	1.6732233	2.296581	2.5262391	2.3950059	3.608913	4.9868616	5.1180948	4.6915869	9.9737232	7.9068003	6.3648102	5.8726857	3.6745296	-3.28083
237	0.4921245	1.8044565	2.3621976	2.6574723	2.4278142	4.9868616	5.8726857	6.0039189	5.2821363	9.1535157	7.8411837	5.7414525	6.56166	3.2152134	-7.3162509
238	0.2952747	1.8044565	2.296581	2.5590474	2.3293893	5.4461778	6.1679604	6.1023438	5.3477529	8.7270078	7.3162509	5.2165197	5.9383023	2.5918557	-8.0052252
239	0.2624664	1.8044565	2.3293893	2.5262391	2.296581	5.5446027	6.233577	6.0695355	5.3149446	8.7598161	7.0537845	4.9540533	5.4133695	2.1325395	-8.202075
240	0.3608913	2.1325395	2.3950059	2.624664	2.3293893	6.4304268	6.2663853	6.1351521	5.249328	5.7086442	5.6102193	3.4448715	5.5117944	1.7388399	-10.1049564
241	0.7545909	2.3950059	2.7887055	2.9199387	2.5590474	6.3320019	6.6272766	6.2991936	5.1837114	7.7099505	6.233577	3.4448715	4.7900118	0.2296581	-14.0747607
242	1.2139071	2.5918557	3.28083	3.2152134	2.7558972	5.9383023	7.2506343	6.3320019	5.0524782	12.0734544	7.0209762	3.6417213	2.0997312	-2.624664	-17.5196322
243	1.8700731	3.3136383	3.5432964	3.5104881	2.9855553	6.7913181	6.6928932	6.6095355	4.6587786	6.3648102	4.7243952	1.312332	3.1495968	-2.4278142	-19.9802547
244	2.6902806	3.8385711	3.8057628	3.936996	3.3792549	6.6600849	5.9711106	5.8726857	4.4291205	3.4448715	4.4619288	0.8858241	5.4461778	-1.0170573	-21.3910116
245	2.8215138	4.0682292	3.9041877	4.1338458	3.5104881	7.1522094	6.0039189	6.1679604	4.593162	1.8372648	4.4291205	0.5905494	6.9881679	-0.328083	-23.4251262
246	2.3950059	4.1010375	3.8385711	4.0026126	3.4448715	8.3333082	6.6272766	6.56166	5.0196699	0.3608913	3.3464466	-0.1312332	6.2663853	-0.5249328	-21.9159444
247	2.3293893	4.0682292	3.936996	3.9041877	3.3464466	8.3333082	7.0209762	6.3976185	4.8884367	2.3293893	2.8871304	-0.4921245	3.4448715	-2.5590474	-21.4894365
248	2.4606225	4.2322707	4.0354209	3.7401462	3.2480217	8.530158	7.0537845	5.7414525	4.4619288	1.6076067	0.656166	-1.9356897	-0.2624664	-4.5603537	-18.1757982
249	3.0183636	4.0682292	3.8385711	3.4448715	3.1824051	6.5944683	5.3477529	4.1010375	3.3792549	0.7873992	-0.4265079	-1.6076067	-1.640415	-3.4120632	-9.0550908
250	3.6745296	4.0682292	3.7401462	3.3464466	3.1167885	4.9868616	3.8713794	2.8543221	2.296581	-0.2296581	-1.0498656	-1.9028814	-1.8700731	-3.1167885	-7.0537845
251	4.6259703	4.3963122	4.0354209	3.4448715	3.4448715	3.7729545	2.8871304	1.5419901	1.7060316	-0.2952747	-2.4934308	-1.5419901	-4.6259703	-2.4606225	4.3963122
252	5.7742608	4.7572035	4.5603537	3.7401462	3.936996	2.3293893	2.2637727	0.5577411	1.2139071	1.968498	-2.6902806	-0.5249328	-7.217826	-2.3950059	12.7624287
253	6.889743	5.0852865		4.2322707	4.3963122	0.7545909		0.0984249	0.7545909		-1.0826739	0.7545909			12.139071
254	8.3004999	5.905494		5.0852865	5.2165197	0.0656166		0.0656166	0.656166		0.0984249	1.5419901			10.4658477
255	9.84249	6.9553596		6.1023438	6.2007687	-0.0328083		0.2624664	0.7873992		0.8530158	2.0997312			9.9737232
256					0			0			0.0656166				
257	1.9028814	1.1810988		1.0498656	0	-0.6233577		-0.2952747			0.3608913				
258	0.1312332	0.3936996		0.6233577	0.9514407	1.0498656		1.3451403	2.1981561		1.9356897	3.9698043			16.6994247
259	-0.4921245	-0.0656166		0.2624664	0.5577411	1.0170573		1.4435652	2.0997312		2.1981561	3.8057628			13.7466777
260	-0.8202075	-0.3608913		0.0984249	0.1312332	0.7873992		1.5091818	1.5091818		2.7887055	2.624664			1.4763735
261	-1.0170573	-0.328083		0.0328083	-0.2624664	1.312332		1.7060316	0.8530158		2.3950059	0.1640415			-13.8451026
262	-0.984249	0.1312332		-0.0656166	-0.4265079	2.8871304		1.3451403	0.4265079		-1.4107569	-3.3792549			-15.6495591
263	-0.6889743	0.5249328		-0.2624664	-0.3936996	3.5104881		0.4265079	0.0984249		-5.1509031	-5.249328			-5.905494
264	-0.5905494	0.7217826		-0.2952747	-0.3608913	3.936996		0.0984249	-0.0328083		-6.7913181	-6.2007687			-2.4278142
265	-0.5577411	0.9514407		-0.2952747	-0.328083	4.6587786		0.1640415	0.0328083		-7.9396086	-7.1850177			-2.5262391
266	-0.5577411	1.1482905		0.0656166	-0.2624664	5.249328		1.0170573	0.1640415		-6.5944683	-7.7427588			-14.7965433
267	-0.3608913			0.3936996	-0.1312332			1.5747984	0.2296581						-23.4251262
268	-0.2624664			0.4921245	0.0328083			1.6732233	0.5249328						-19.4881302
269	-0.2952747			0.5577411	0.3936996			1.9028814	1.4107569						-7.5787173
270	-0.1640415			0.6889743	0.5577411			2.0341146	1.640415						-5.4461778
271	0.0984249				0.9186324				2.1981561						
272	0.2296581				1.3451403				3.0511719						
273	-0.0656166				1.5747984				4.0026126						
274	-0.656166														
275	-0.984249														
276	-0.656166														

Appendix 3-B. Long-Term Rates (ft/yr) for Saco Bay, Maine			
Long-Term Rates (regression method)			
Transect	1864-1998		
1			
2			
3			
4			
5			
6			
7			
8			
9			
10			
11			
12			
13			
14			
15			
16	-0.0328083		
17	-0.1968498		
18	-0.4265079		
19	-0.5249328		
20	-0.5249328		
21	-0.5905494		
22	-0.6889743		
23	-0.656166		
24	-0.5577411		
25	-0.4593162		
26	-0.328083		
27	-0.2952747		
28	-0.1312332		
29	0.1312332		
30	0.328083		
31	0.5905494		
32	0.7873992		
33	1.0826739		
34	1.4435652		
35	1.8372648		
36	2.5590474		
37	3.4120632		
38	4.2978873		
39			
40			
41	-3.4120632		
42	-3.0183636		
43	-2.6574723		
44	-2.296581		
45	-2.0669229		
46	-1.7388399		
47	-1.4435652		
48	-1.2139071		
49	-1.0826739		

Appendix 3-B. Long-Term Rates (ft/yr) for Saco Bay, Maine			
Long-Term Rates (regression method)			
Transect	**1864-1998**		
50	-0.8858241		
51	-0.6233577		
52	-0.3608913		
53	-0.1640415		
54	-0.0328083		
55	0.1968498		
56	0.3936996		
57	0.5577411		
58	0.7217826		
59	0.8858241		
60	0.9186324		
61	1.0170573		
62	1.0170573		
63	1.1154822		
64	1.0498656		
65	1.0170573		
66	0.9514407		
67	0.984249		
68	0.9514407		
69	0.9186324		
70	0.7217826		
71	0.5905494		
72	0.4921245		
73	0.3936996		
74	0.2952747		
75	0.1312332		
76	-0.0328083		
77	0		
78	-0.0328083		
79	-0.0656166		
80	-0.0656166		
81	-0.0328083		
82	0		
83	0.0656166		
84	0.1312332		
85	0.1312332		
86	0.1312332		
87	0.1640415		
88	0.1968498		
89	0.2624664		
90	0.3608913		
91	0.4921245		
92	0.4593162		
93	0.4593162		
94	0.5249328		
95	0.5905494		

Appendix 3-B. Long-Term Rates (ft/yr) for Saco Bay, Maine			
Long-Term Rates (regression method)			
Transect	**1864-1998**		
96	0.7545909		
97	0.8530158		
98	0.9514407		
99	0.9186324		
100	0.8858241		
101	0.9186324		
102	0.9186324		
103	0.8858241		
104	0.9514407		
105	0.984249		
106	1.0826739		
107	1.1154822		
108	1.2467154		
109	1.4107569		
110	1.8700731		
111	2.1981561		
112	2.3950059		
113	3.2480217		
114	3.5761047		
115	2.9199387		
116	2.6902806		
117	2.624664		
118	2.5590474		
119	2.4606225		
120	2.296581		
121	2.0997312		
122	1.8372648		
123	1.7060316		
124	1.640415		
125	1.5747984		
126	1.5091818		
127	1.4435652		
128	1.4107569		
129	1.3779486		
130	1.3451403		
131	1.3451403		
132	1.312332		
133	1.312332		
134	1.2795237		
135	1.2795237		
136	1.312332		
137	1.3451403		
138	1.3451403		
139	1.3451403		
140	1.312332		
141	1.312332		

Appendix 3-B. Long-Term Rates (ft/yr) for Saco Bay, Maine			
Long-Term Rates (regression method)			
Transect	**1864-1998**		
142	1.3451403		
143	1.3451403		
144	1.2139071		
145	1.2139071		
146	1.2467154		
147	1.2467154		
148	1.2795237		
149	1.2795237		
150	1.2795237		
151	1.2467154		
152	1.2467154		
153	1.2139071		
154	1.2139071		
155	1.1810988		
156	1.1154822		
157	1.0498656		
158	1.0170573		
159	0.984249		
160	0.9186324		
161	0.9186324		
162	0.9514407		
163	0.984249		
164	1.0170573		
165	1.0498656		
166	1.0498656		
167	1.0498656		
168	1.0498656		
169	0.984249		
170	0.9514407		
171	0.8858241		
172	0.8202075		
173	0.7545909		
174	0.7873992		
175	0.8202075		
176	0.8858241		
177	0.9186324		
178	0.9514407		
179	1.0826739		
180	1.2467154		
181	1.3779486		
182	1.5419901		
183	1.7060316		
184	1.968498		
185	2.0997312		
186	2.1653478		
187	2.2309644		

Appendix 3-B. Long-Term Rates (ft/yr) for Saco Bay, Maine			
Long-Term Rates (regression method)			
Transect	**1864-1998**		
188	2.2637727		
189	2.2309644		
190	2.0669229		
191	2.0013063		
192	1.9356897		
193	1.8700731		
194	1.7716482		
195	1.7716482		
196	1.5091818		
197	1.2795237		
198	1.0498656		
199	0.9514407		
200	0.8530158		
201	0.7217826		
202	0.656166		
203	0.5249328		
204	0.4593162		
205	0.4265079		
206	0.4593162		
207	0.5249328		
208	0.4921245		
209	0.5249328		
210	0.5905494		
211	0.6233577		
212	0.656166		
213	0.5905494		
214	0.656166		
215	0.6233577		
216	0.656166		
217	0.7545909		
218	0.8530158		
219	1.0170573		
220	1.2139071		
221	1.4435652		
222	1.6076067		
223	1.8044565		
224	1.8372648		
225	1.8372648		
226	1.968498		
227	2.2309644		
228	2.4278142		
229	2.4934308		
230	2.3950059		
231	2.3621976		
232	2.3293893		
233	2.1653478		

Appendix 3-B. Long-Term Rates (ft/yr) for Saco Bay, Maine			
Long-Term Rates (regression method)			
Transect	**1864-1998**		
234	2.2309644		
235	2.3293893		
236	2.4606225		
237	2.5918557		
238	2.5262391		
239	2.5262391		
240	2.624664		
241	2.8871304		
242	3.1824051		
243	3.4448715		
244	3.8057628		
245	3.9698043		
246	3.936996		
247	3.9041877		
248	3.8385711		
249	3.5432964		
250	3.4120632		
251	3.5761047		
252	3.936996		
253			
254			
255			
256			
257			
258	0.7545909		
259	0.3936996		
260	0.0656166		
261	-0.0984249		
262	-0.1312332		
263	-0.1312332		
264	-0.0984249		
265	-0.0328083		
266	0.1640415		
267			
268			
269			
270			
271			
272			
273			
274			
275			
276			

APPENDIX 6-B

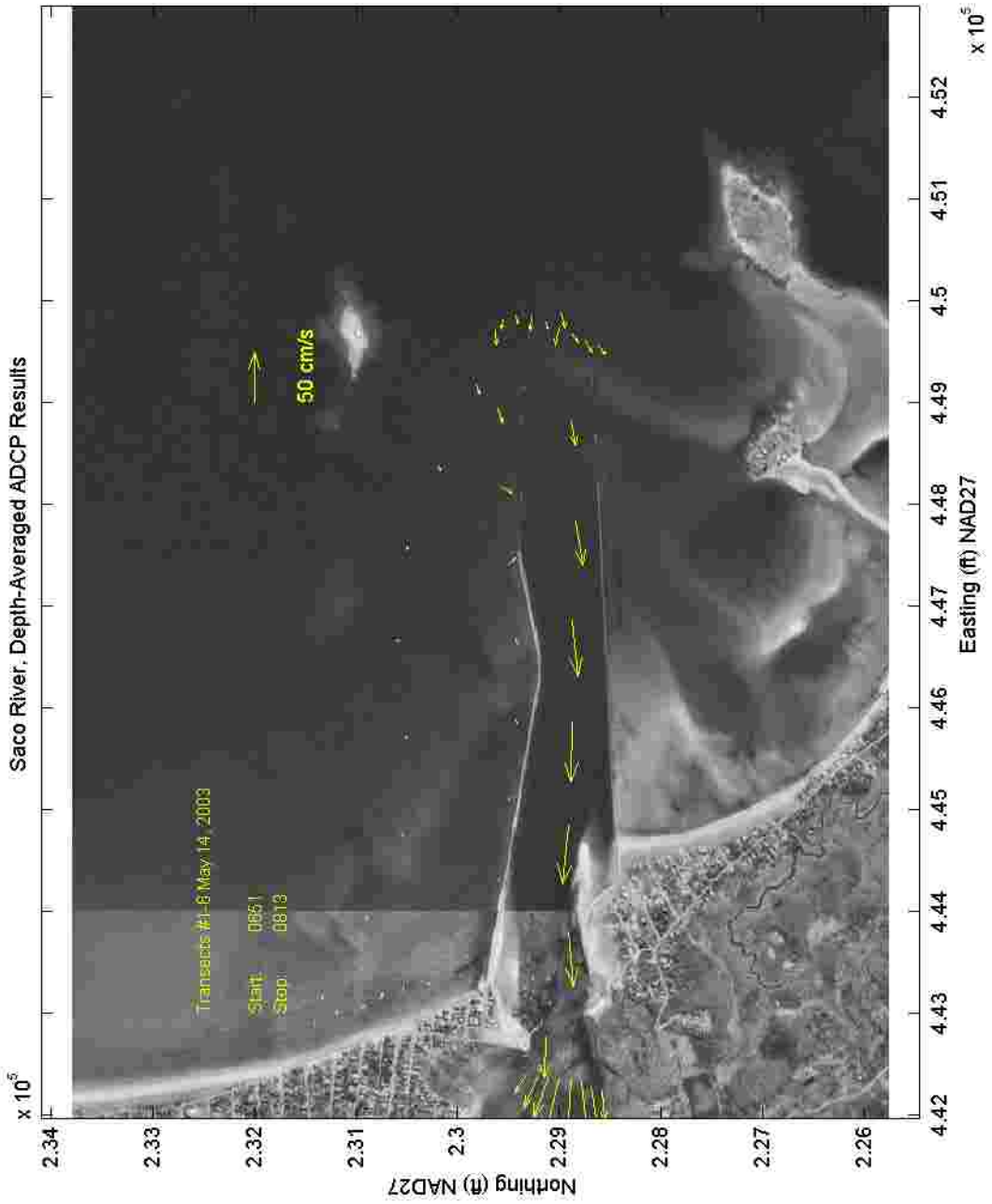

Figure 6-B1. Plan view of depth-averaged currents observed at all six (6) transects during a flood tide.

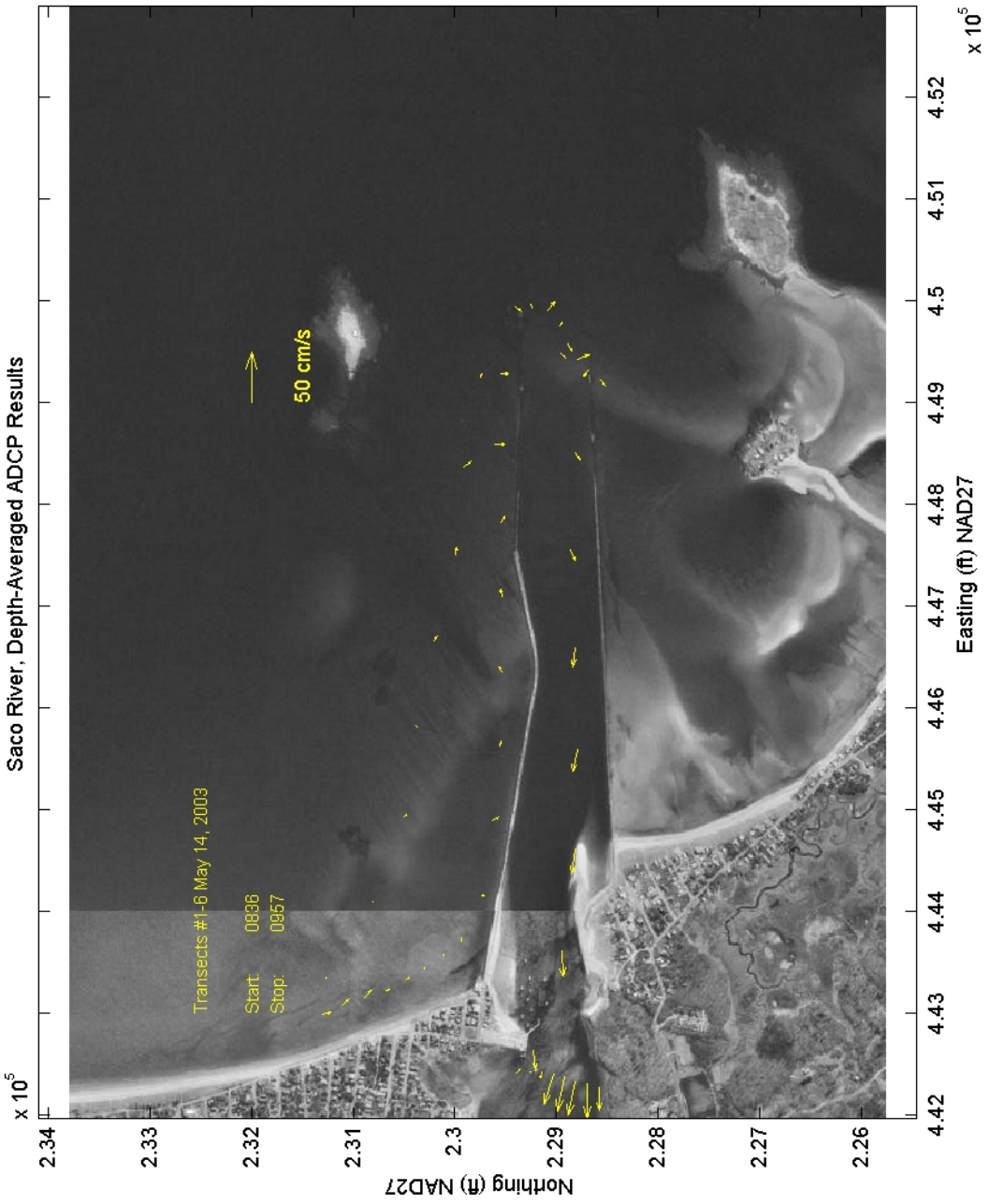

Figure 6-B2. Plan view of depth-averaged currents observed at all six (6) transects at the end of a flood tide.

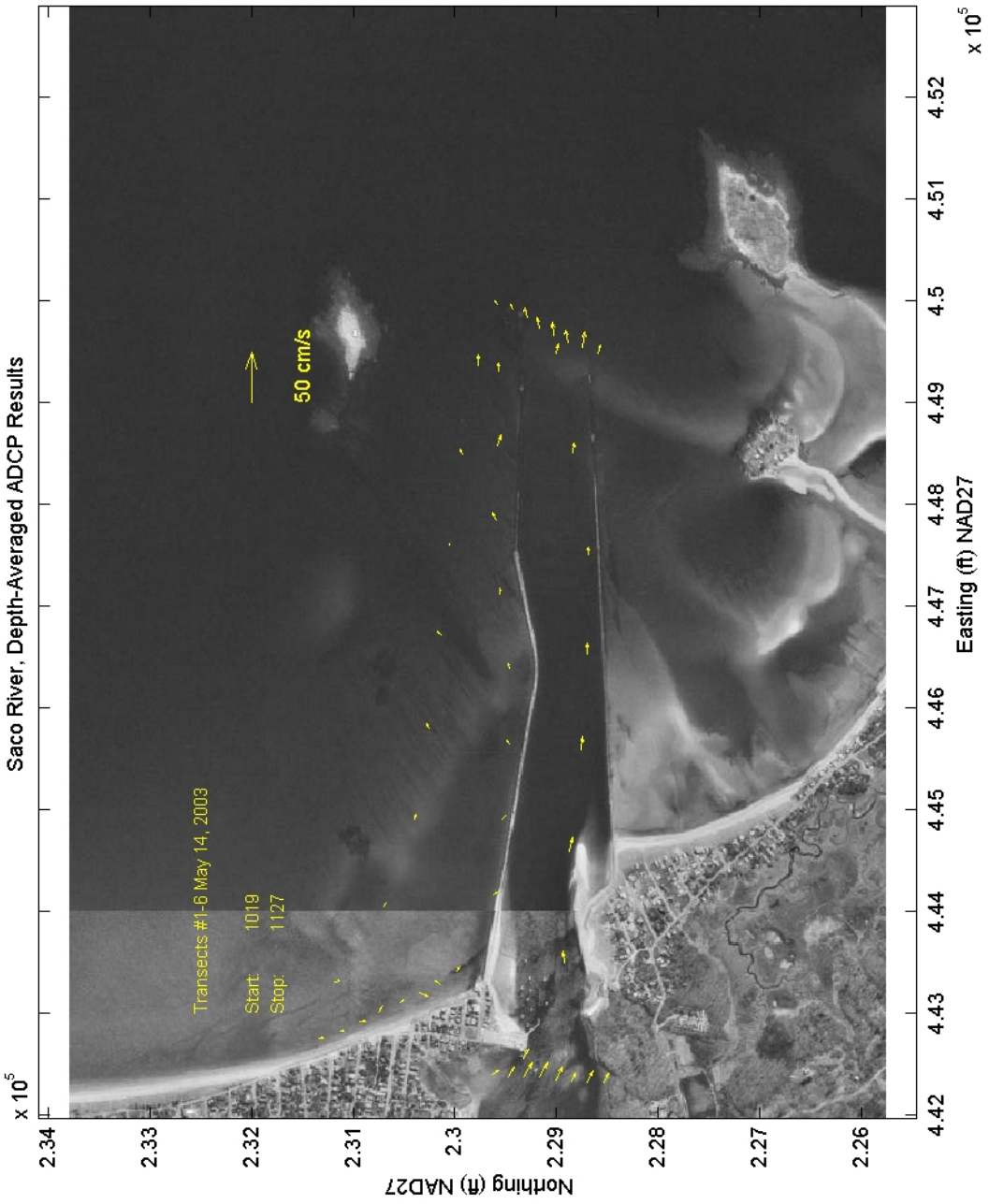

Figure 6-B3. Plan view of depth-averaged currents observed at all six (6) transects during the start of an ebb tide.

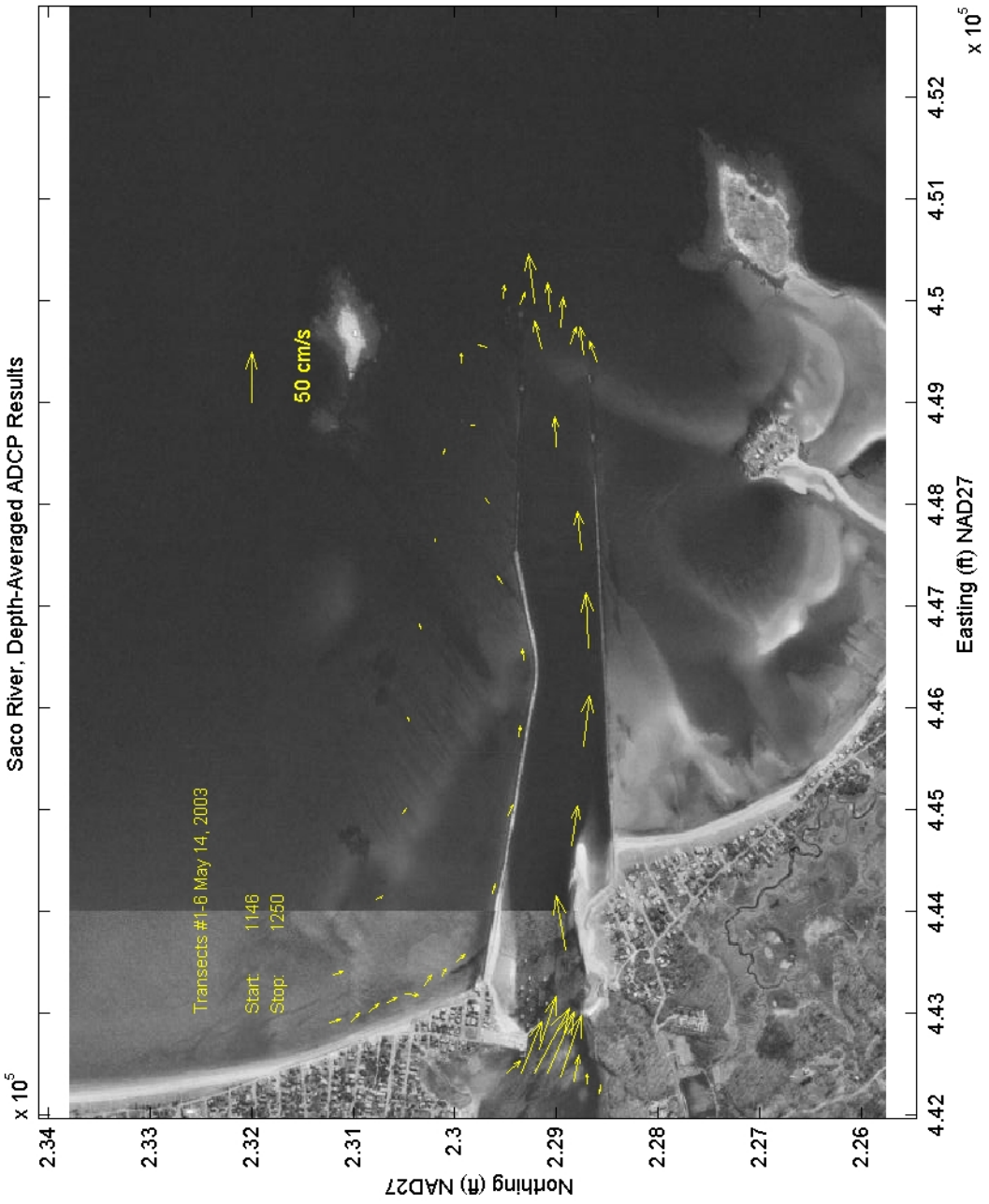

Figure 6-B4. Plan view of depth-averaged currents observed at all six (6) transects during an ebb tide.

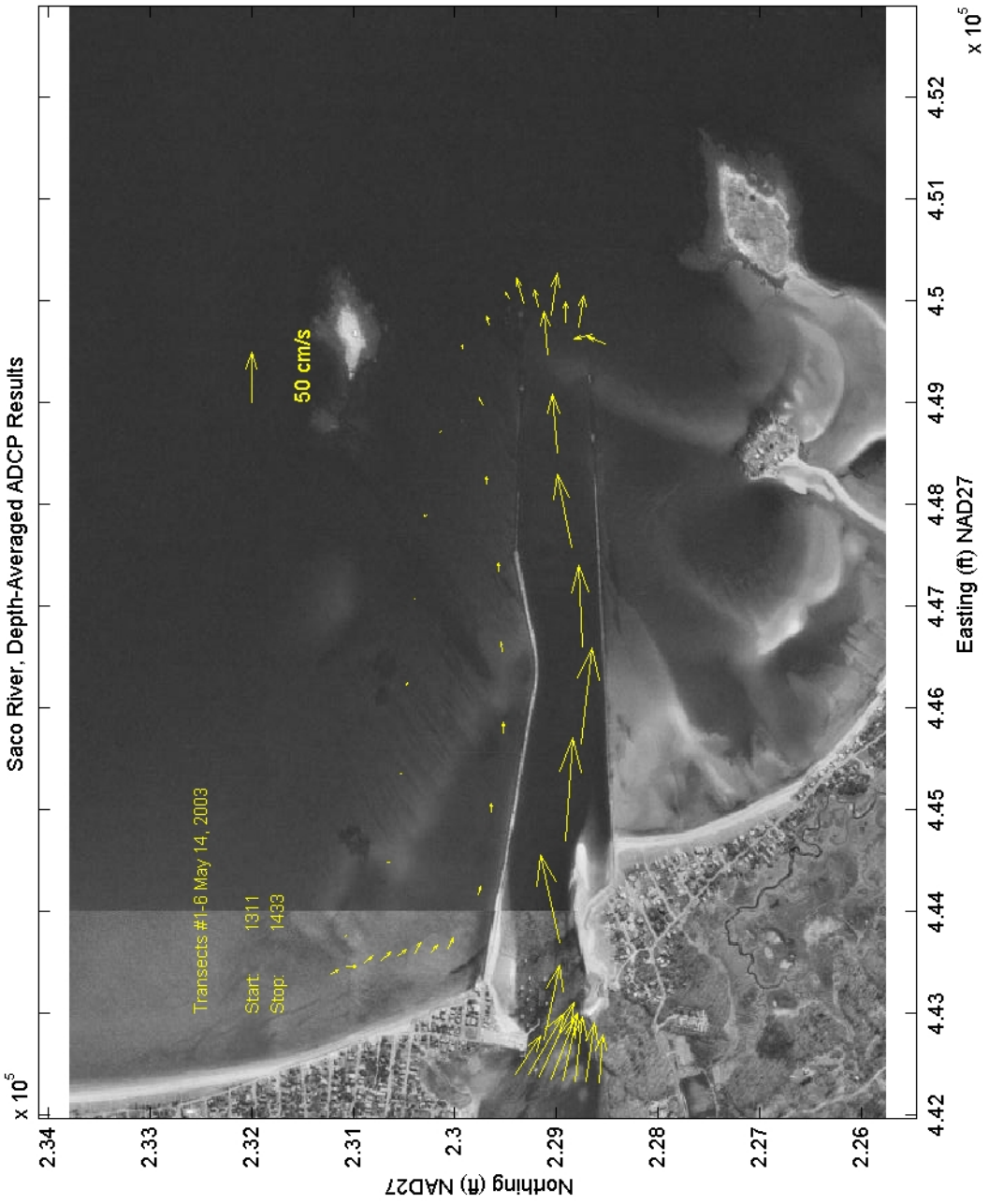

Figure 6-B5. Plan view of depth-averaged currents observed at all six (6) transects during an ebb tide.

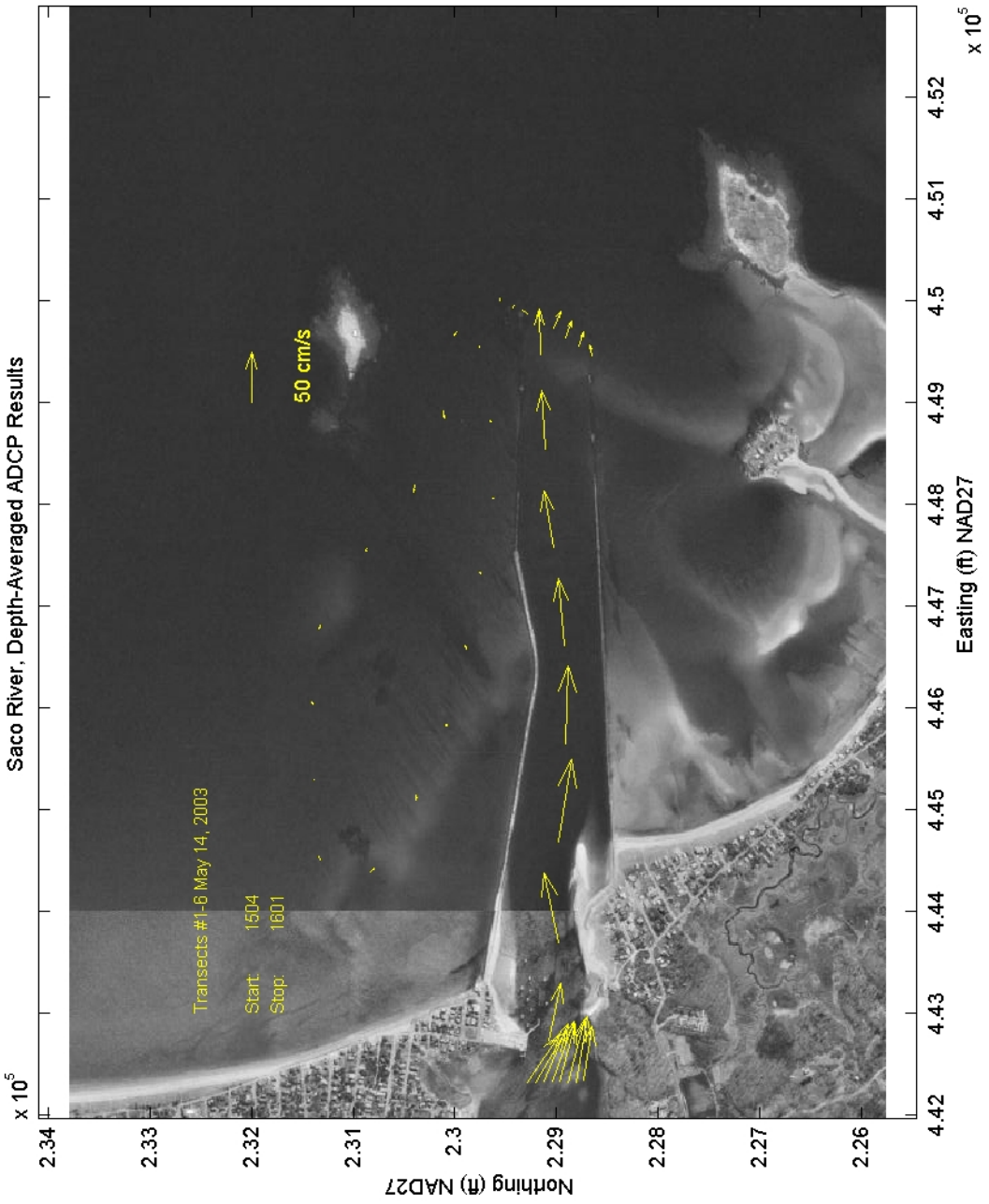

Figure 6-B6. Plan view of depth-averaged currents observed at Transects 1, 2, 3, 5 and 6 during an ebb tide.

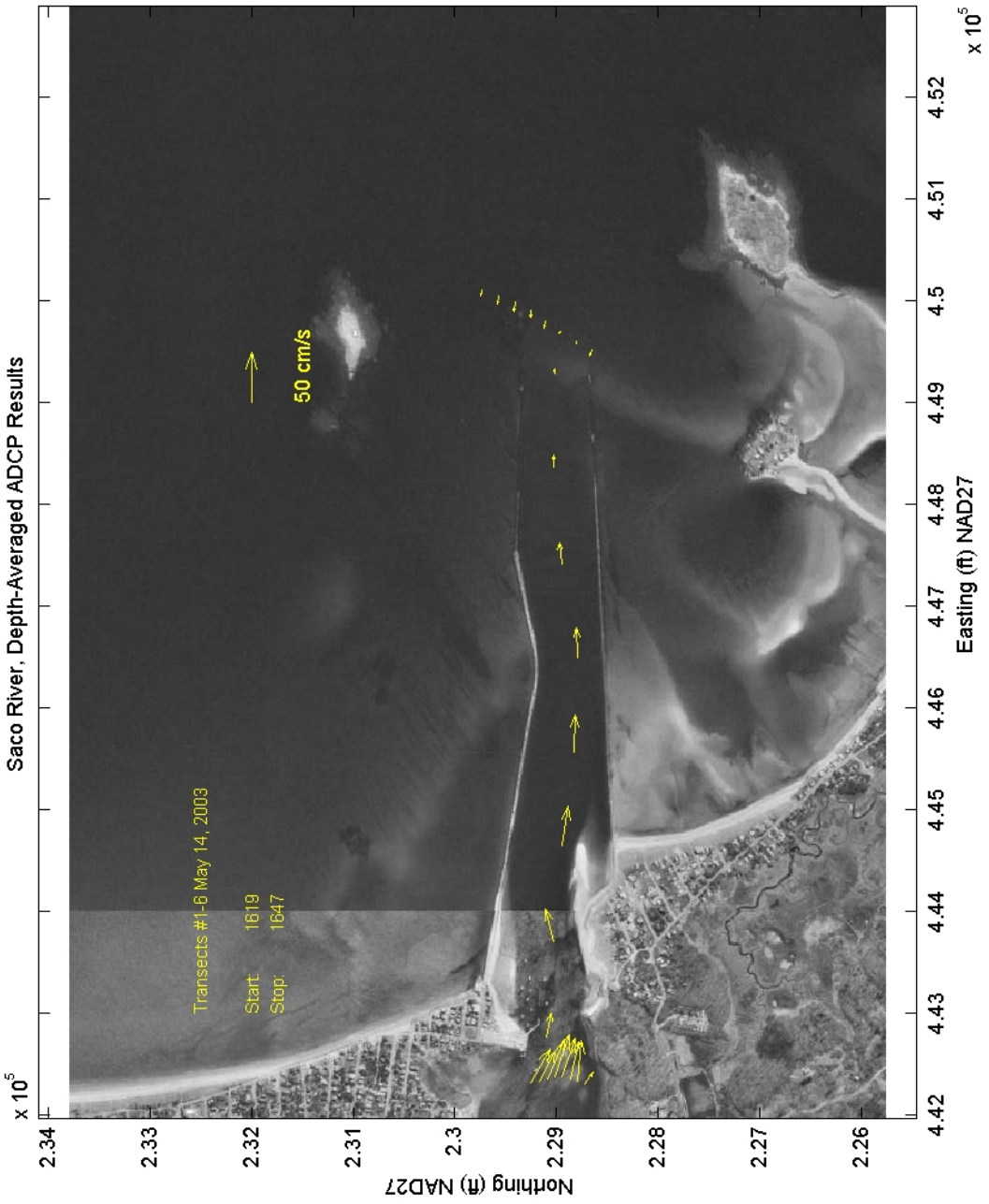

Figure 6-B7. Plan view of depth-averaged currents observed at Transects 1, 2 and 6 as the tide is changing from ebb to flood.

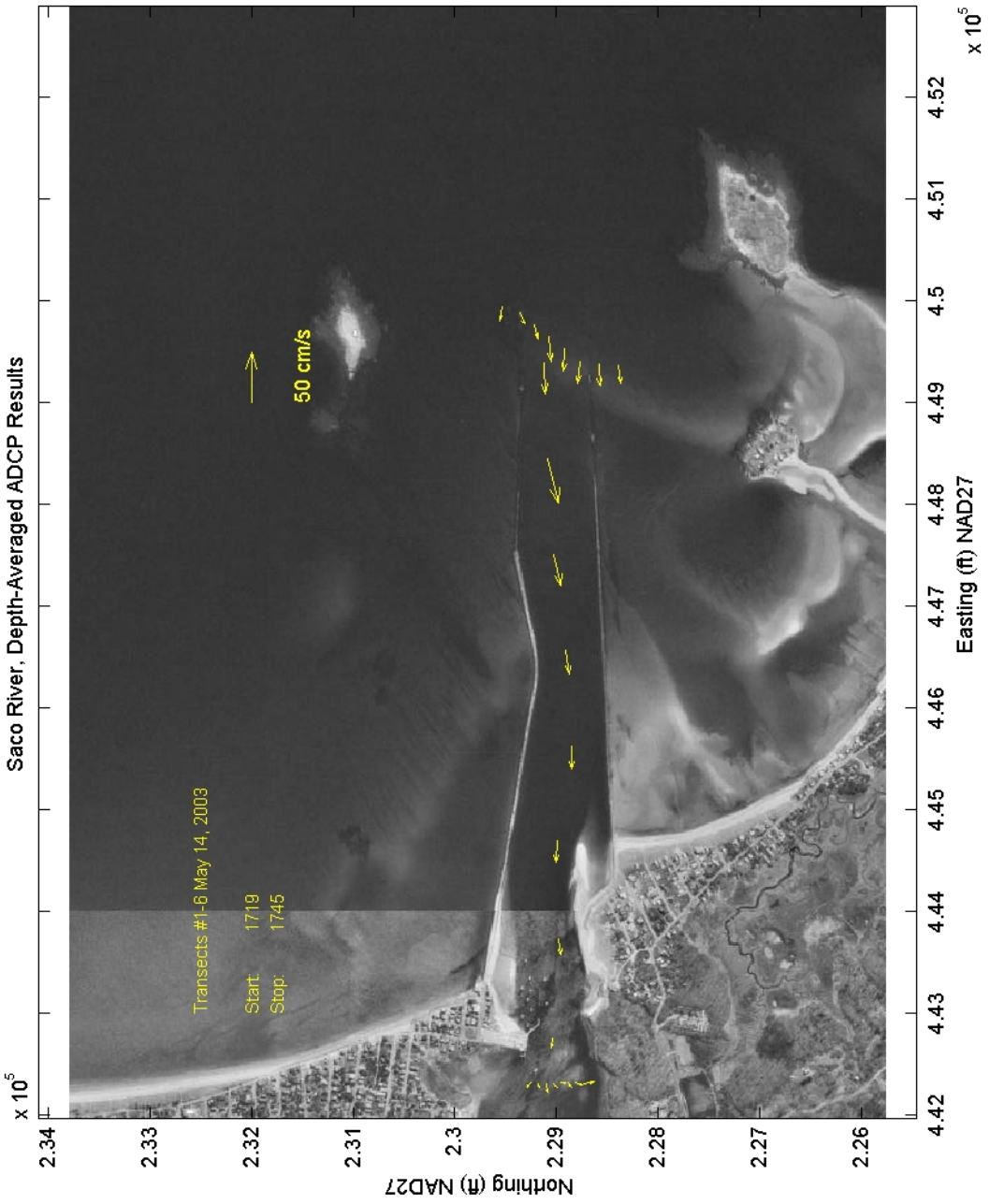

Figure 6-B8. Plan view of depth-averaged currents observed at Transects 1, 2 and 6 during a flood tide.

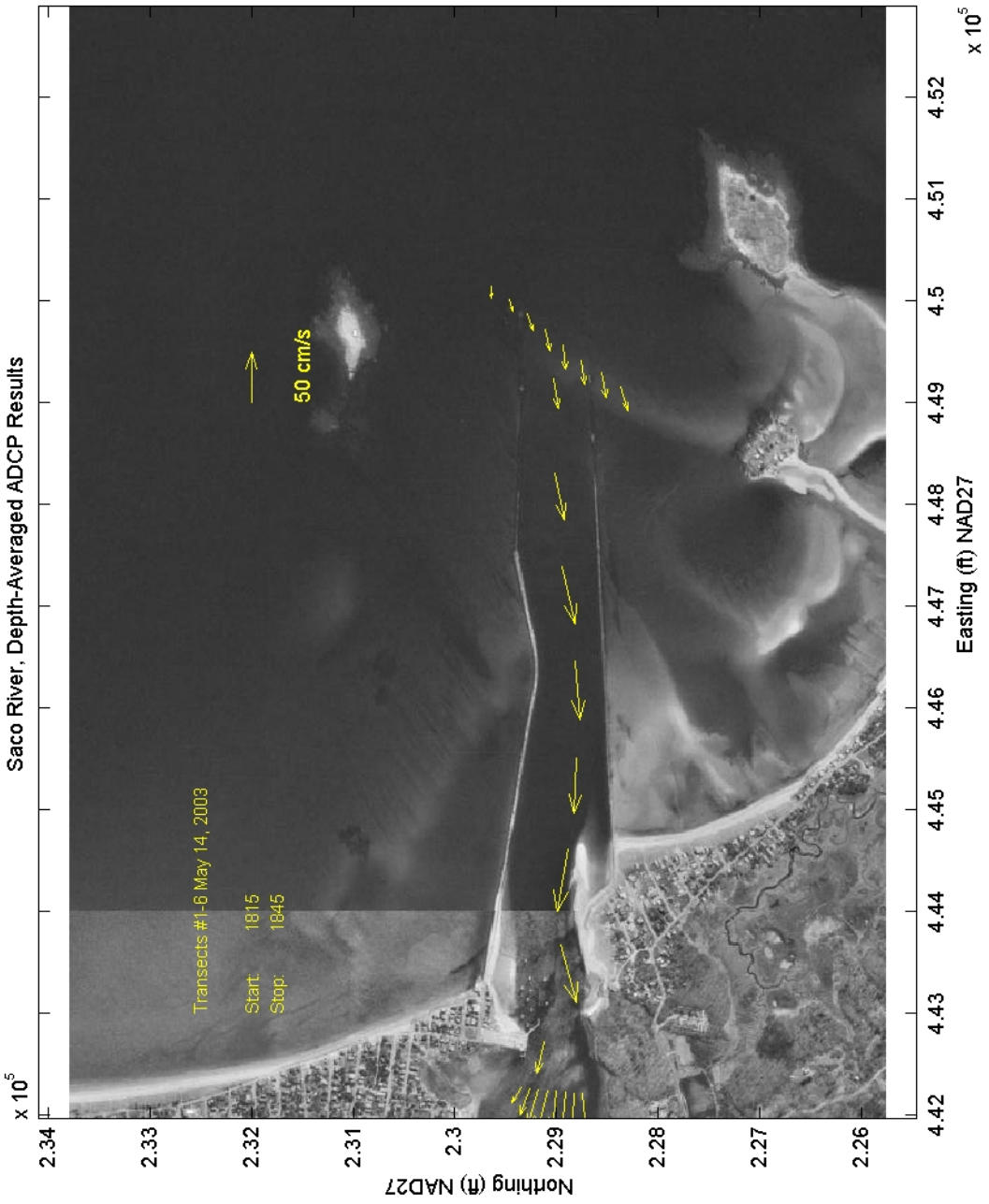

Figure 6-B9. Plan view of depth-averaged currents observed at Transects 1, 2 and 6 during a flood tide.

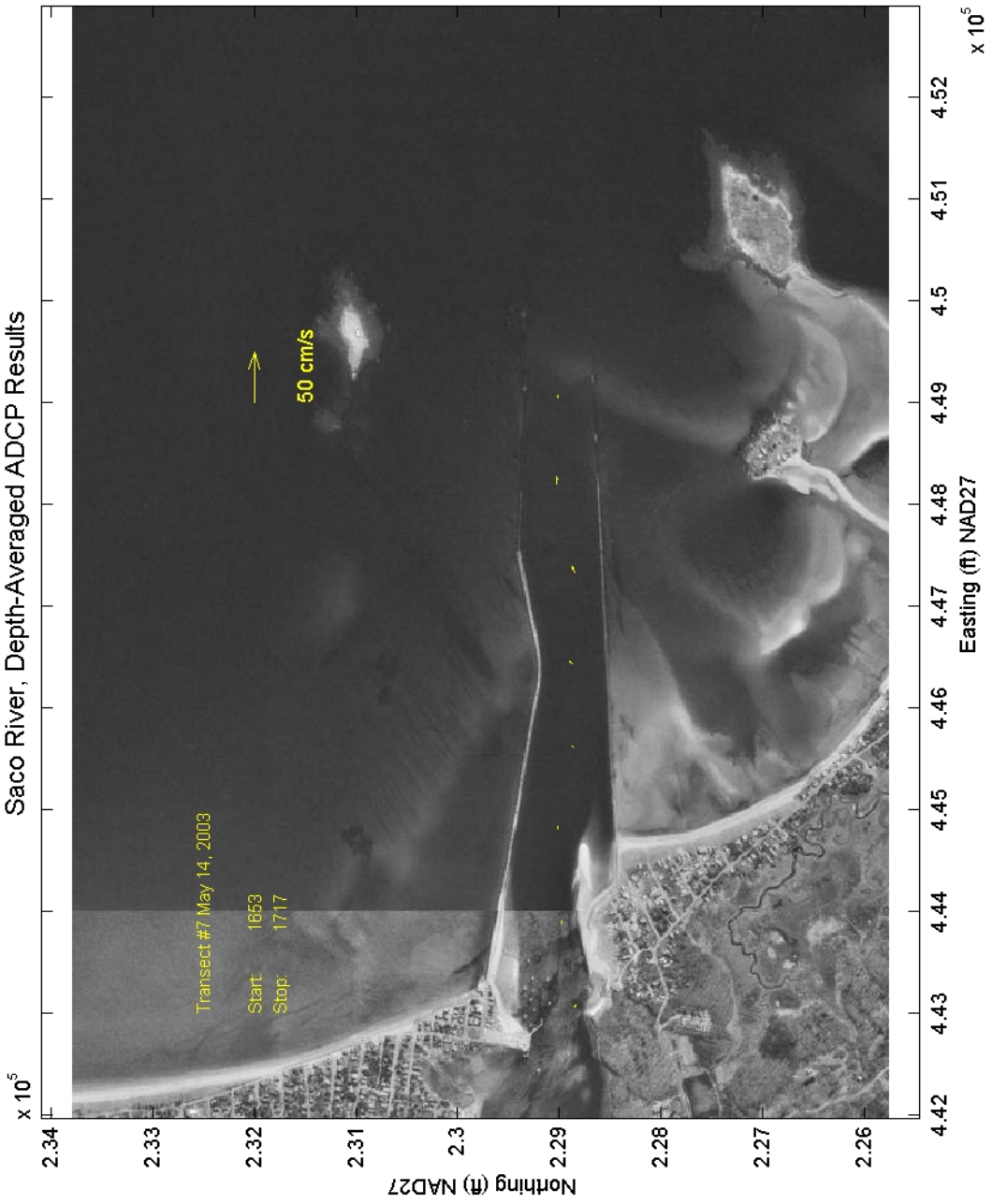

Figure 6-B10. Plan view of depth-averaged currents observed at Transect 7 prior to flood tide.

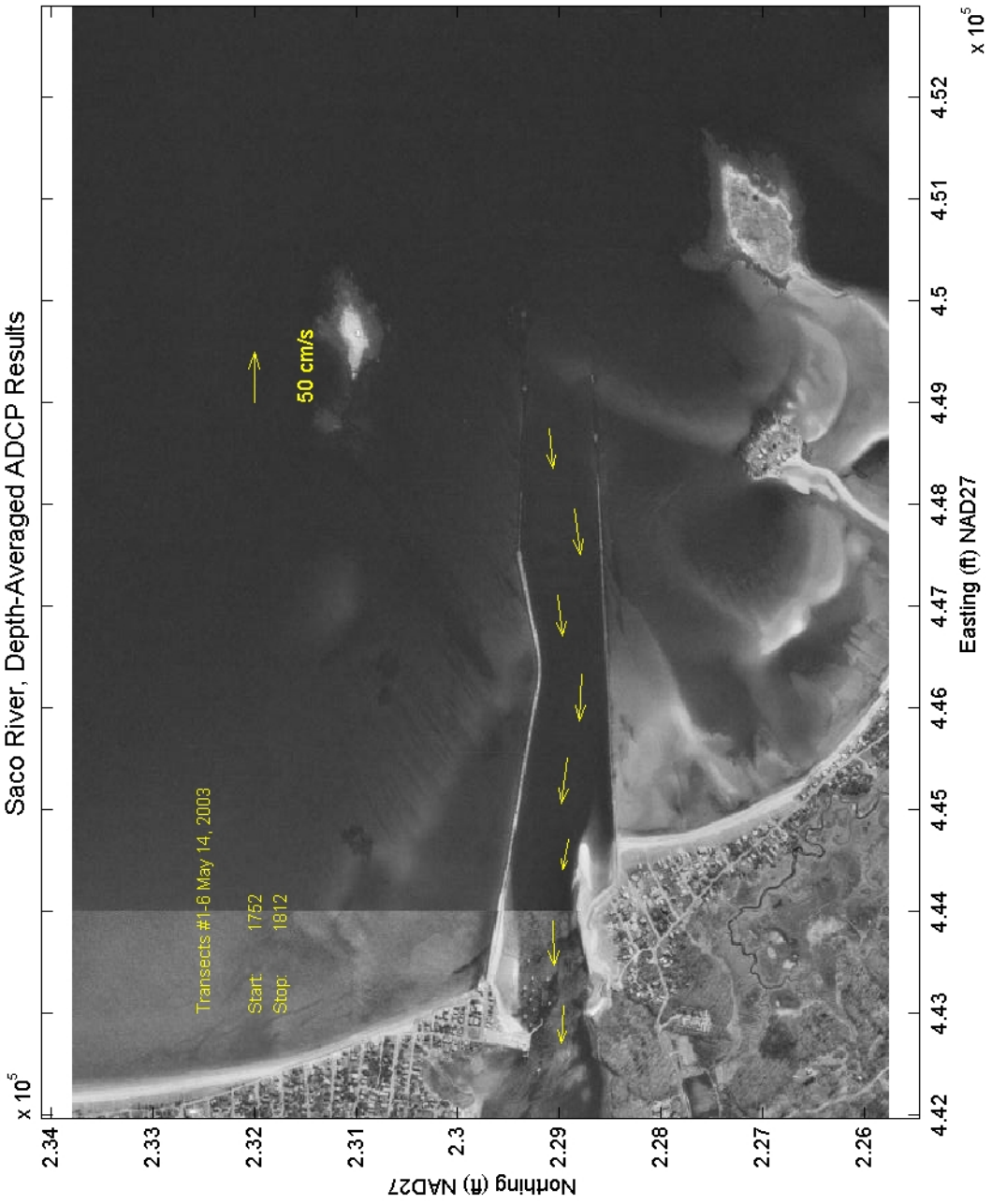

Figure 6-B11. Plan view of depth-averaged currents observed at Transect 7 during flood tide.

APPENDIX 9-B

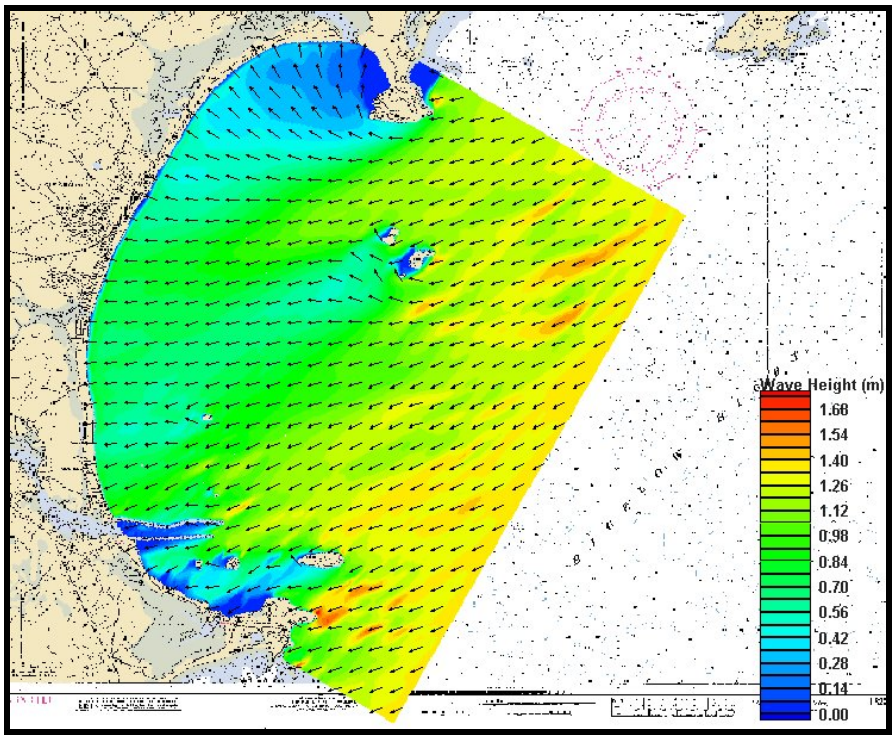

Figure 9-B1. STWAVE modeling results for existing conditions using a northeast (55 to 75 degree bin) approach directional spectra bin.

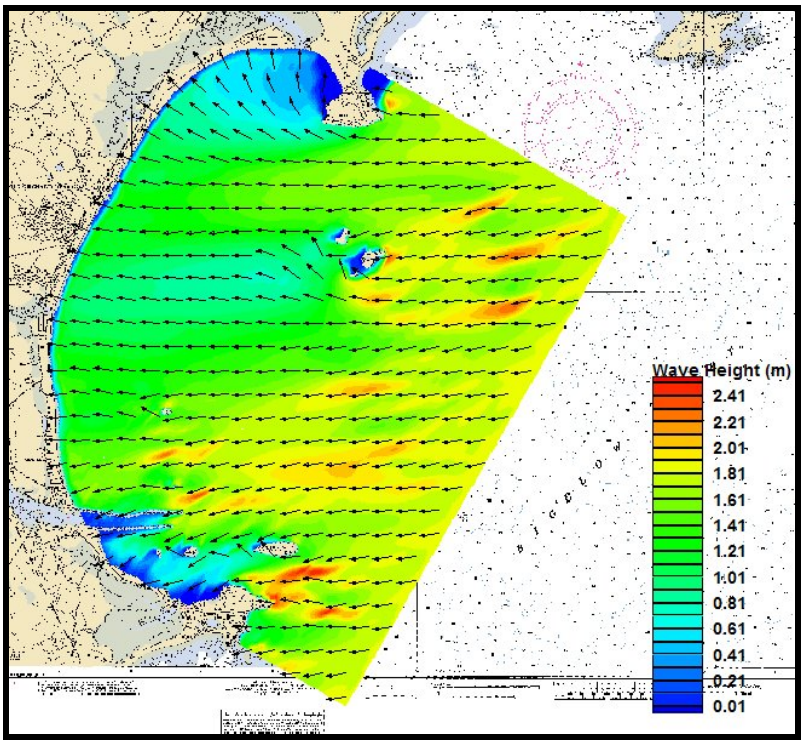

Figure 9-B2. STWAVE modeling results for existing conditions using an east-northeast (75 to 90 degree bin) approach directional spectra bin.

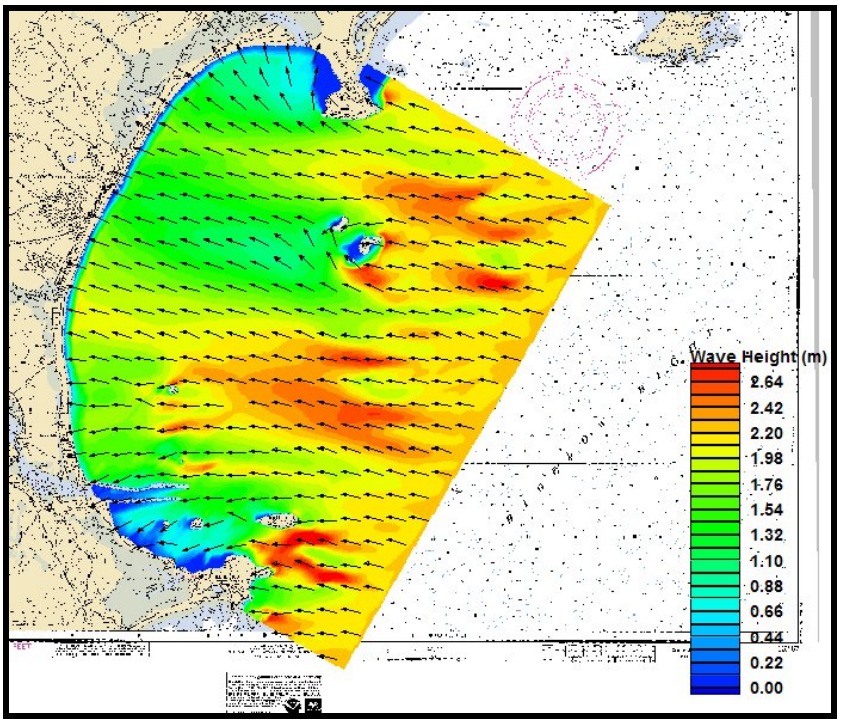

Figure 9-B3. STWAVE modeling results for existing conditions using an east (90 to 110 degree bin) approach directional spectra bin.

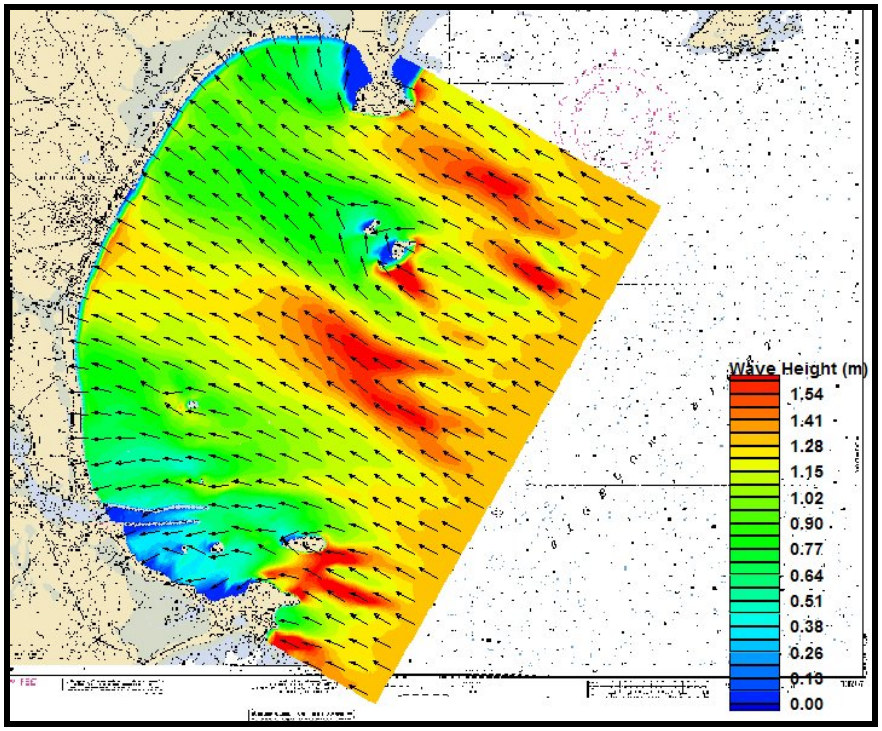

Figure 9-B4. STWAVE modeling results for existing conditions using an east-southeast (110 to 130 degree bin) approach directional spectra bin.

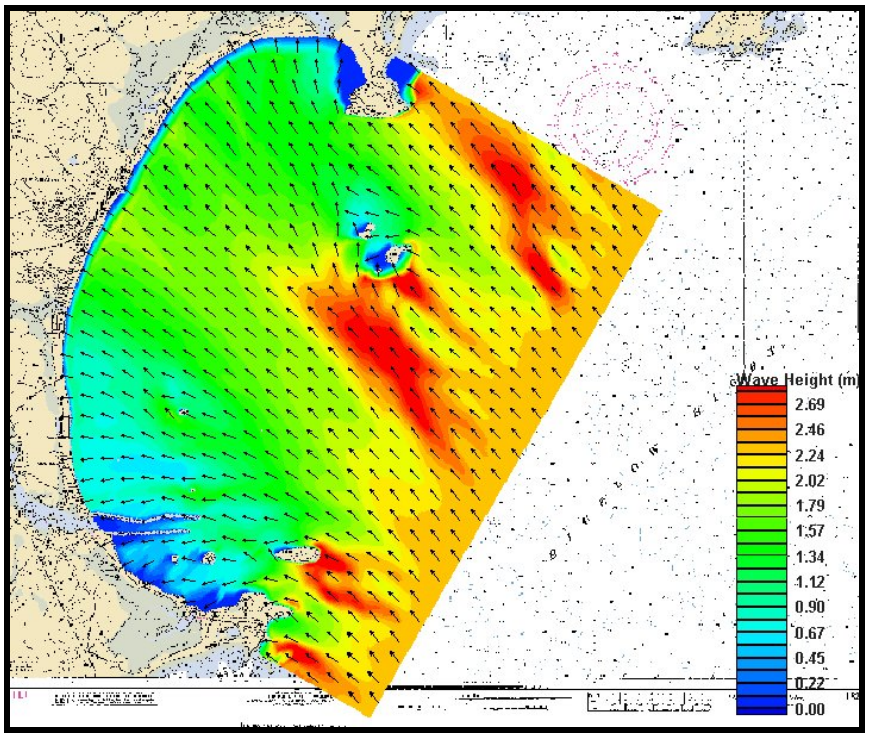

Figure 9-B5. STWAVE modeling results for existing conditions using a southeast (130 to 150 degree bin) approach directional spectra bin.

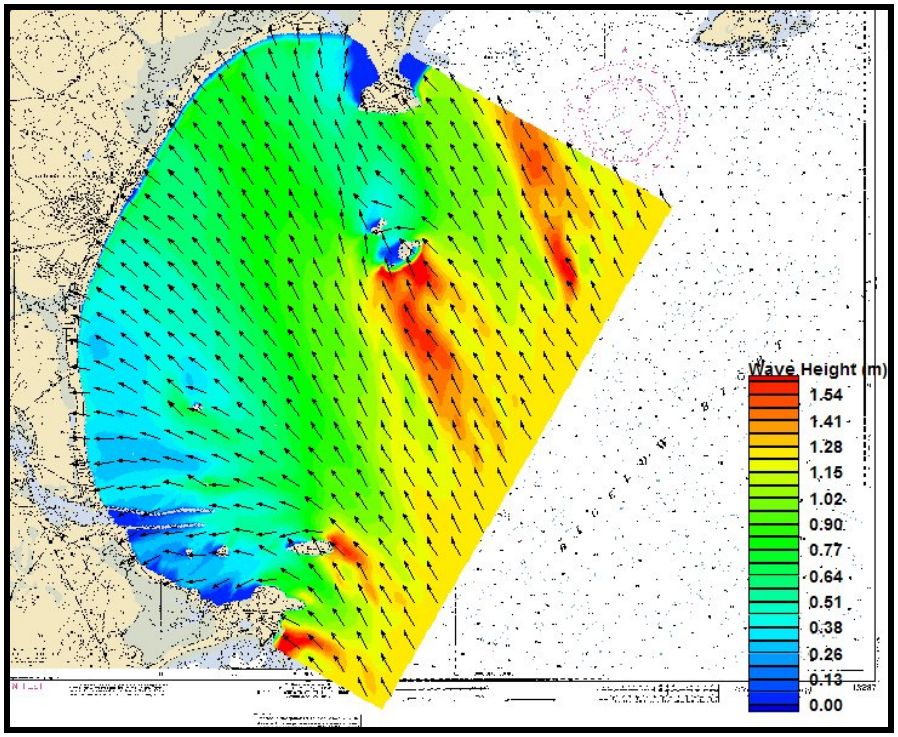

Figure 9-B6. STWAVE modeling results for existing conditions using a south-southeast (150 to 165 degree bin) approach directional spectra bin.

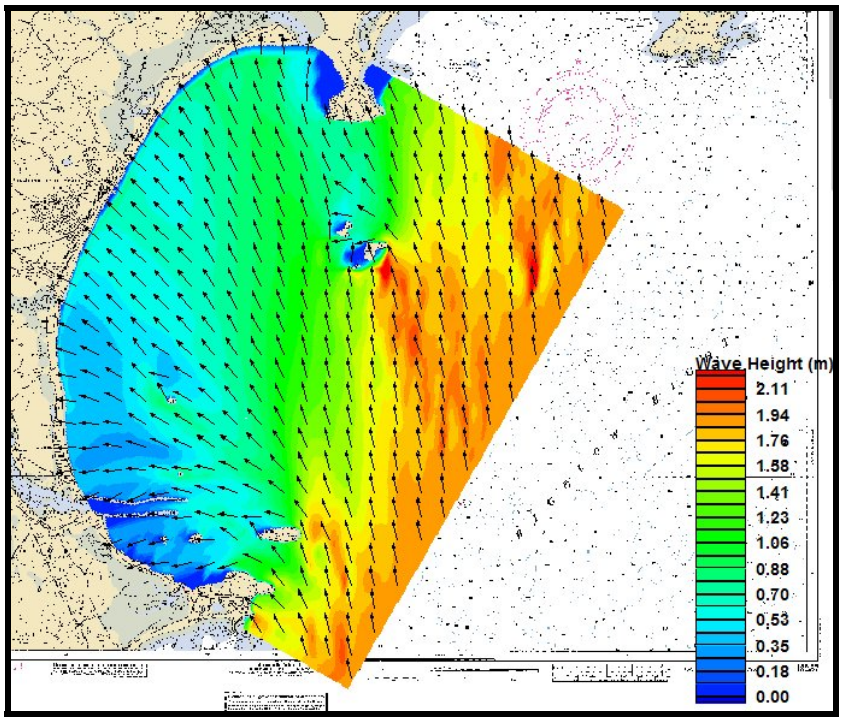

Figure 9-B7. STWAVE modeling results for existing conditions using a south (165 to 185 degree bin) approach directional spectra bin.

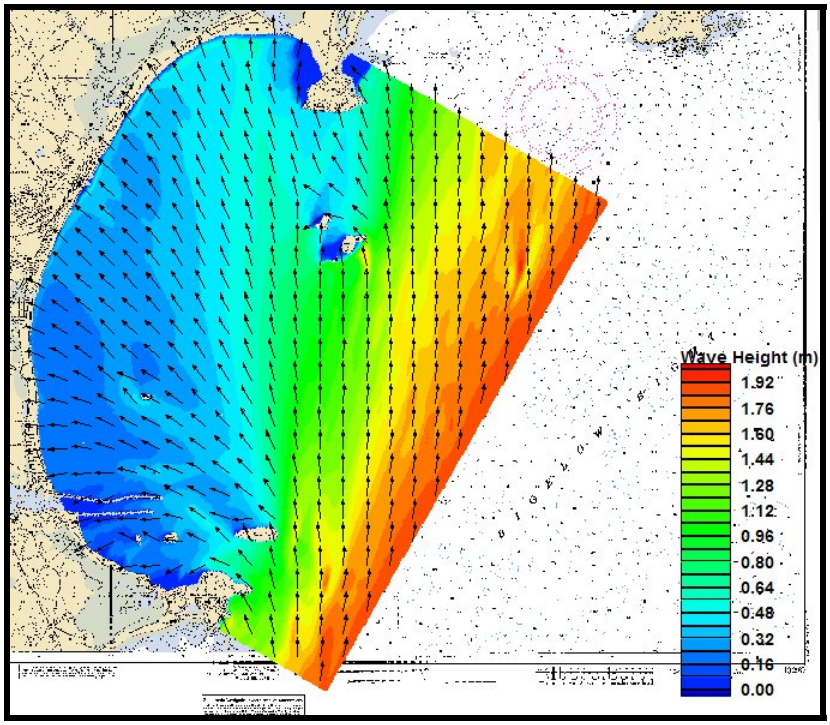

Figure 9-B8. STWAVE modeling results for existing conditions using a south-southwest (185 to 210 degree bin) approach directional spectra bin.

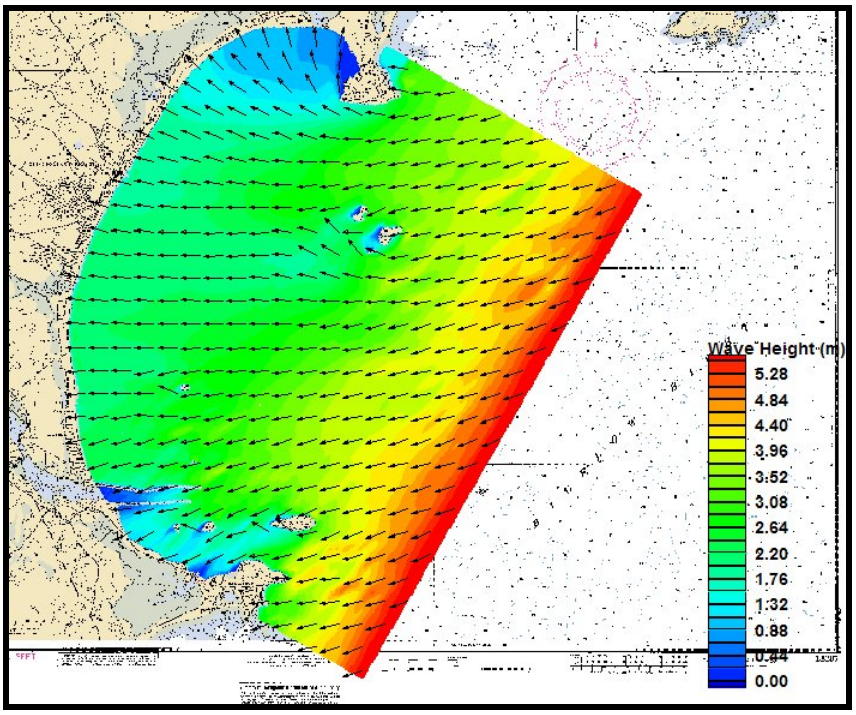

Figure 9-B9. STWAVE modeling results for a 10-yr return period storm.

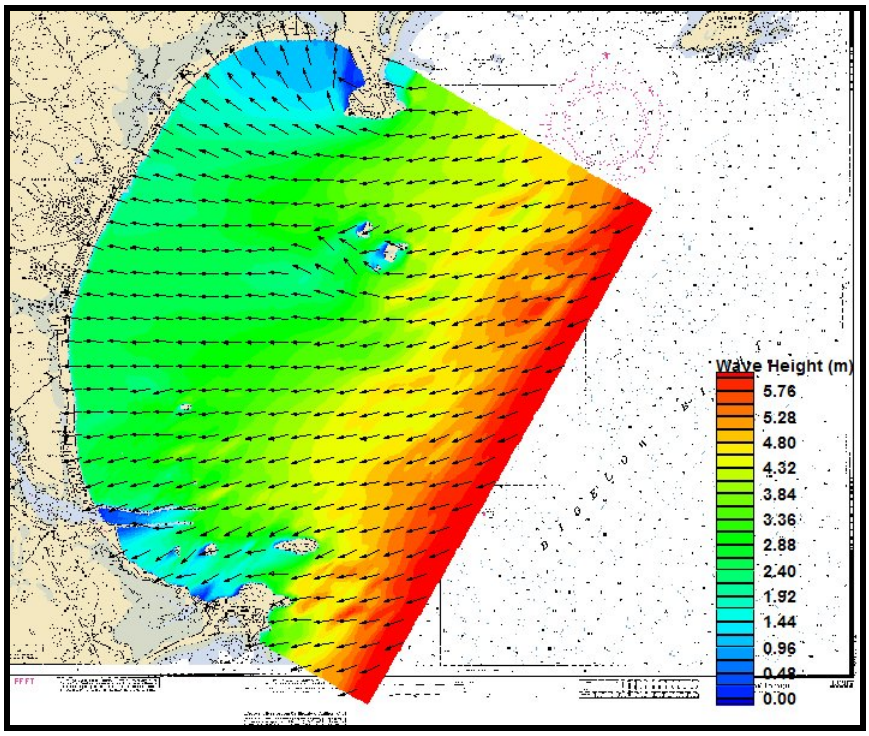

Figure 9-B10. STWAVE modeling results for a 50-yr return period storm.

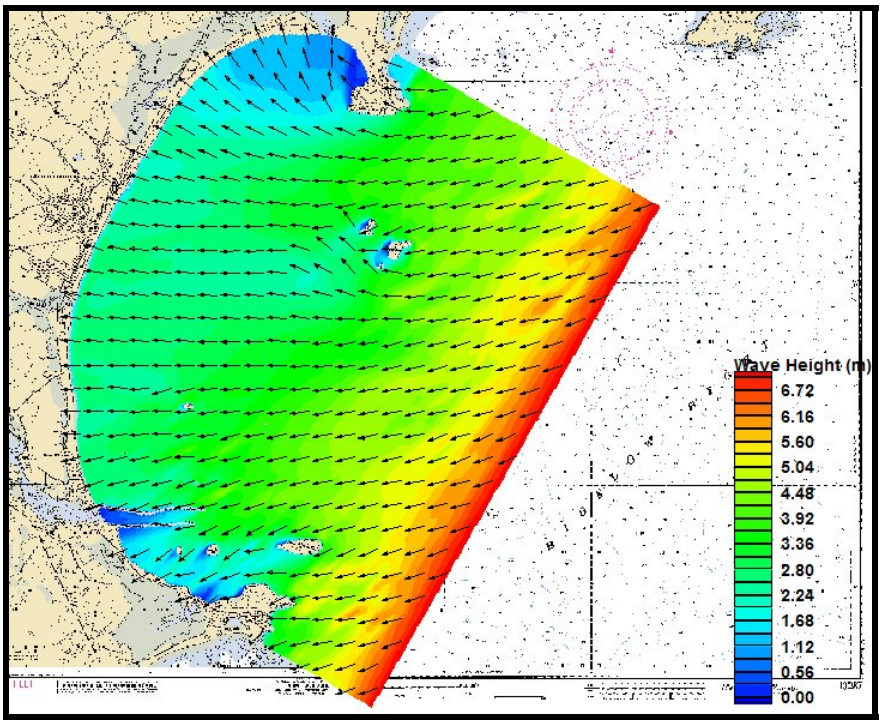

Figure 9-B11. STWAVE modeling results for a 100-yr return period storm

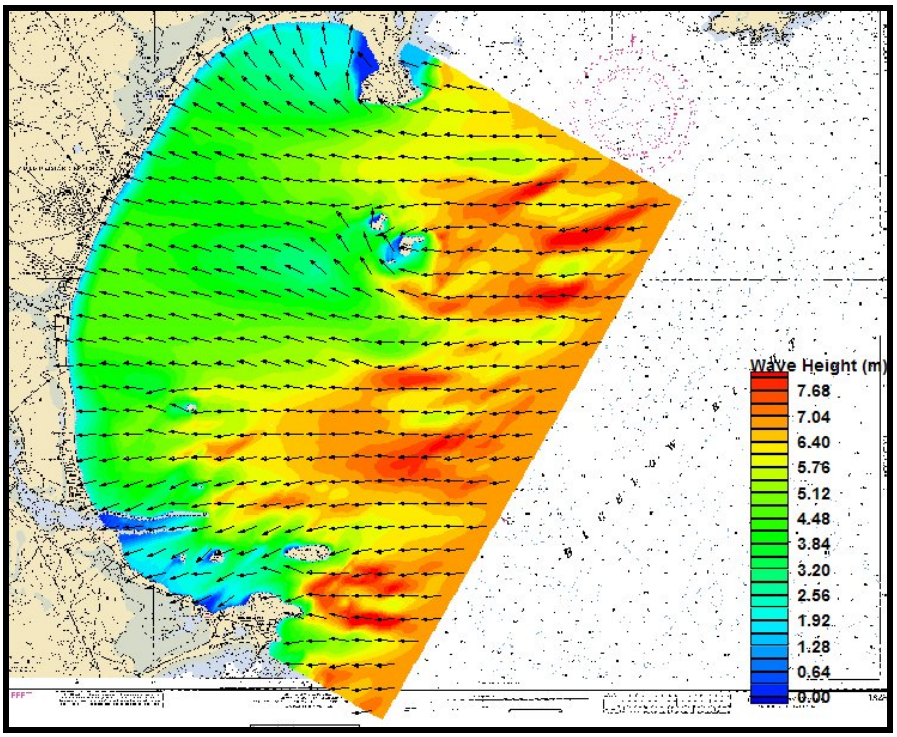

Figure 9-B12. STWAVE modeling results for Perfect Storm approach (10/31/1991).

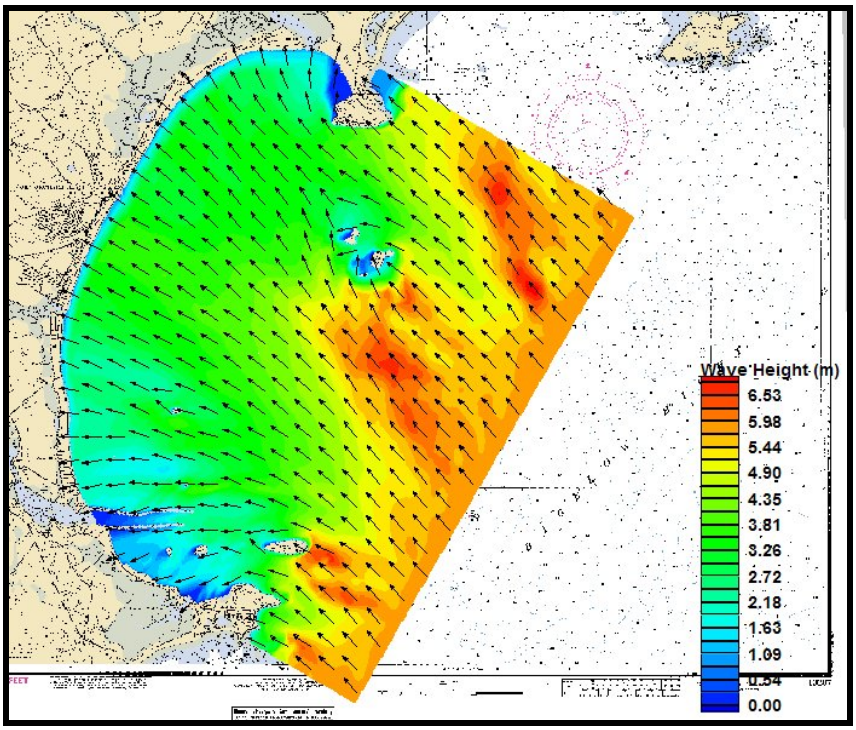

Figure 9-B13. STWAVE modeling results for Hurricane Bob approach (8/20/1991).

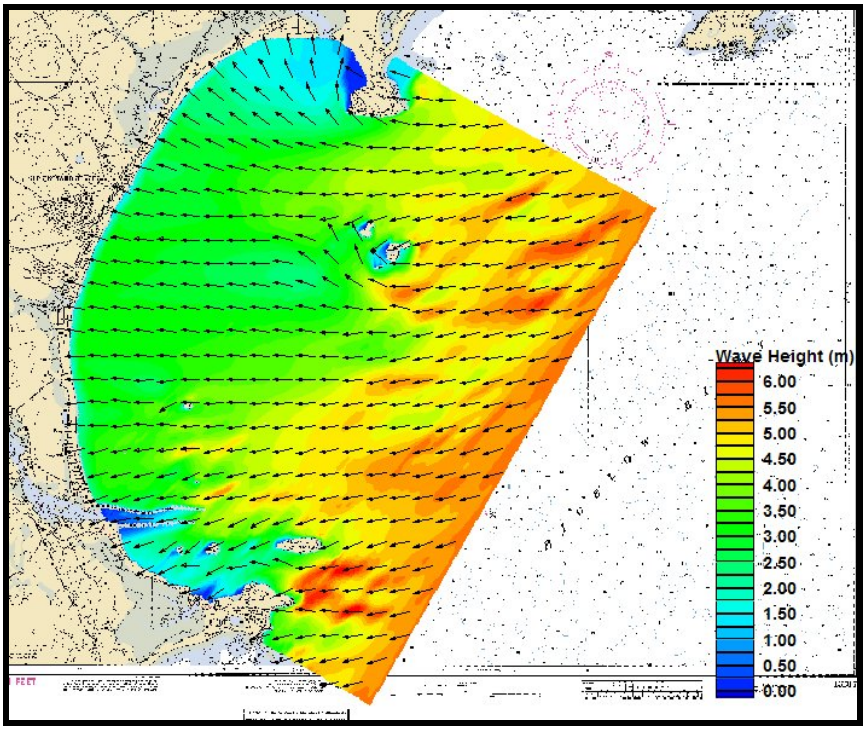

Figure 9-B14. STWAVE modeling results for Northeaster (March 6-7, 2001).

APPENDIX 11-B

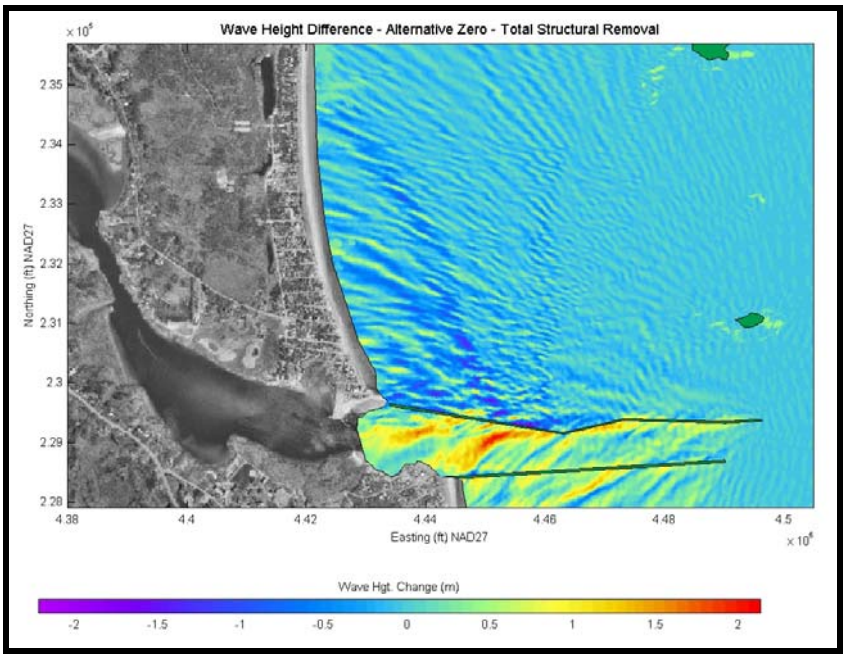

Figure11-B1. Wave height changes for Alternate 0 for an Eastern (90-110 degree) wave approach bin. A negative wave height change indicates a reduction in wave height, while a positive wave height change indicates an increase in wave height.

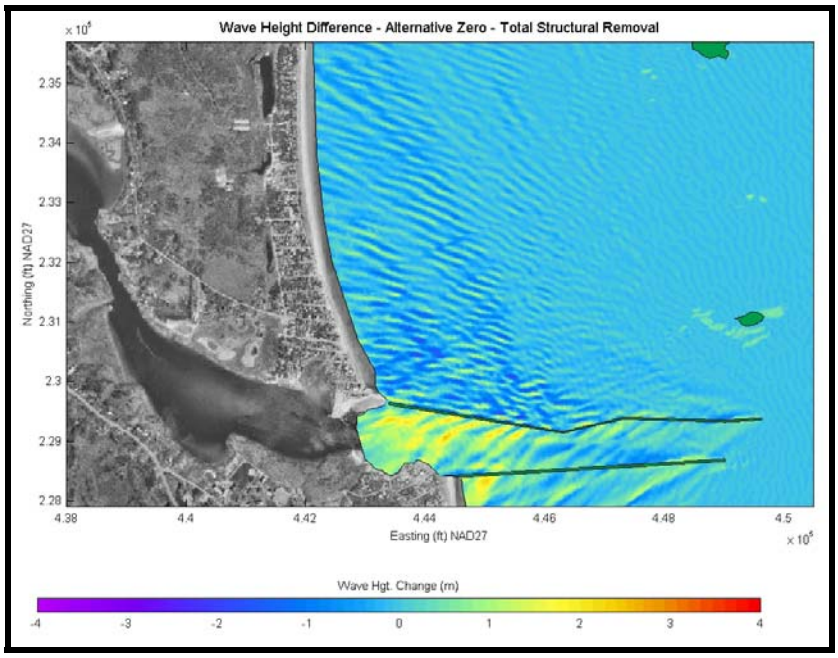

Figure 11-B2. Wave height changes for Alternative 0 for a 10-yr return period storm. A negative wave height change indicates a reduction in wave height, while a positive wave height change indicates an increase in wave height.

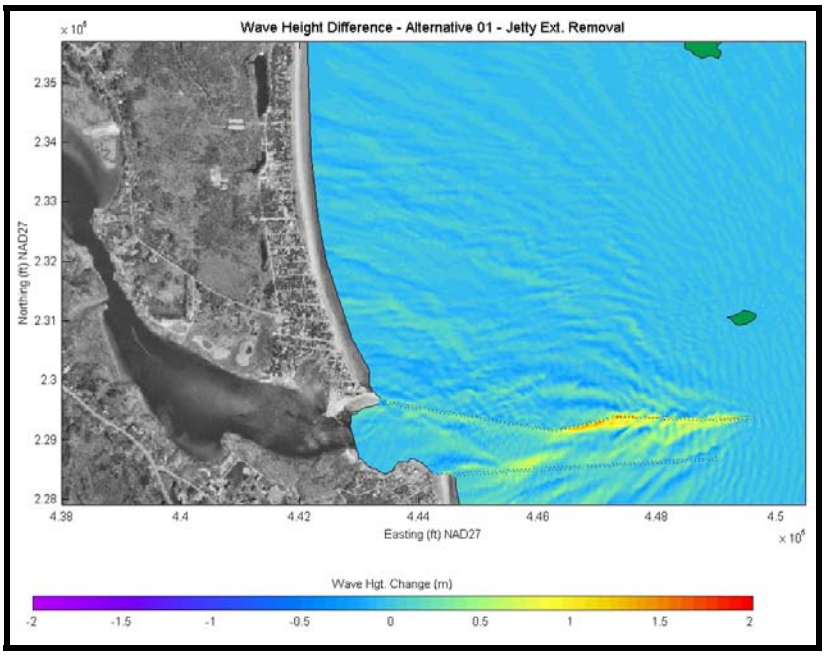

Figure11-B3. Wave height changes for Alternate 01 for an Eastern (90-110 degree) wave approach bin. A negative wave height change indicates a reduction in wave height, while a positive wave height change indicates an increase in wave height.

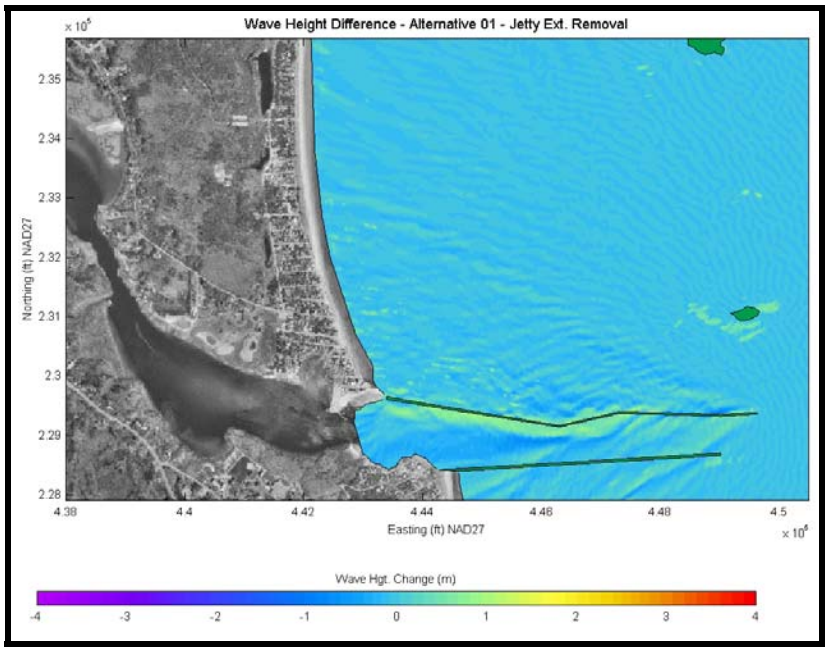

Figure 11-B4. Wave height changes for Alternative 01 for a 10-yr return period storm. A negative wave height change indicates a reduction in wave height, while a positive wave height change indicates an increase in wave height.

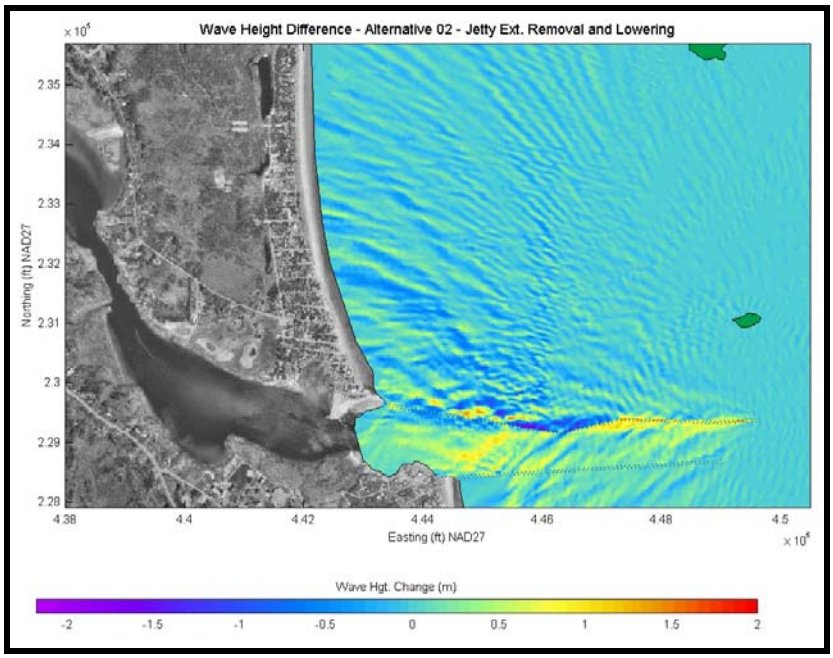

Figure11-B5. Wave height changes for Alternate 02 for an Eastern (90-110 degree) wave approach bin. A negative wave height change indicates a reduction in wave height, while a positive wave height change indicates an increase in wave height.

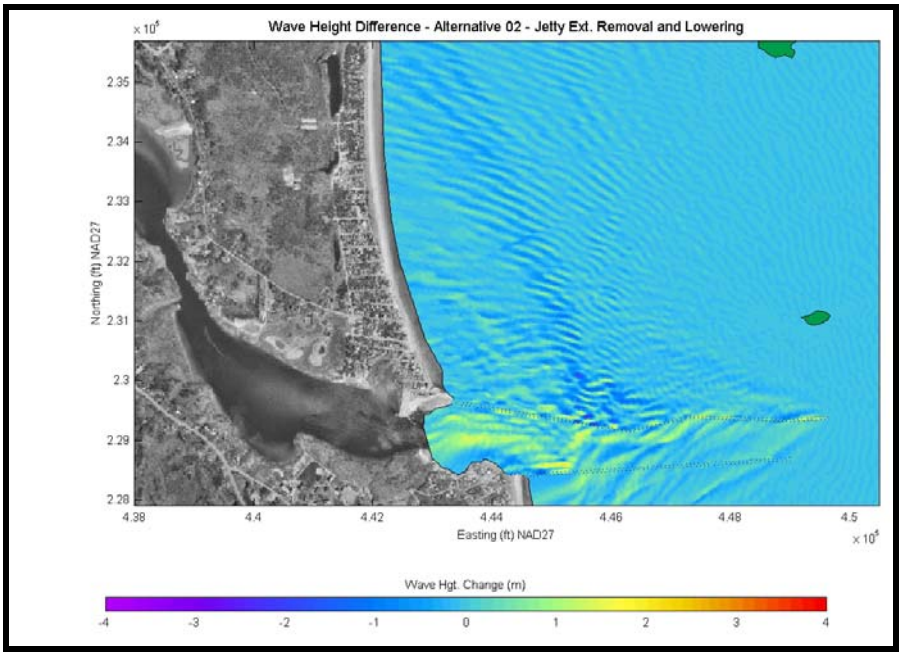

Figure 11-B6. Wave height changes for Alternative 02 for a 10-yr return period storm. A negative wave height change indicates a reduction in wave height, while a positive wave height change indicates an increase in wave height.

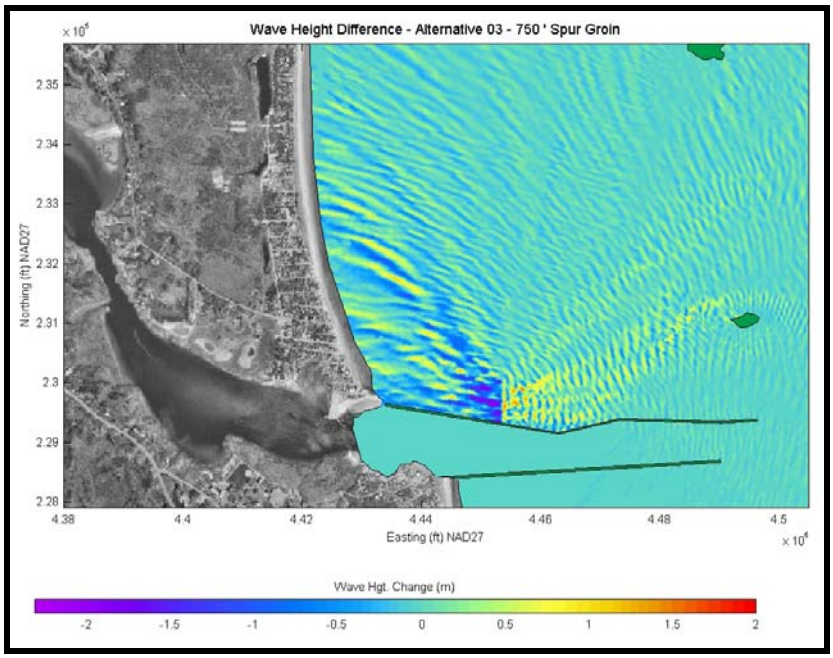

Figure11-B7. Wave height changes for Alternate 03 for an Eastern (90-110 degree) wave approach bin. A negative wave height change indicates a reduction in wave height, while a positive wave height change indicates an increase in wave height.

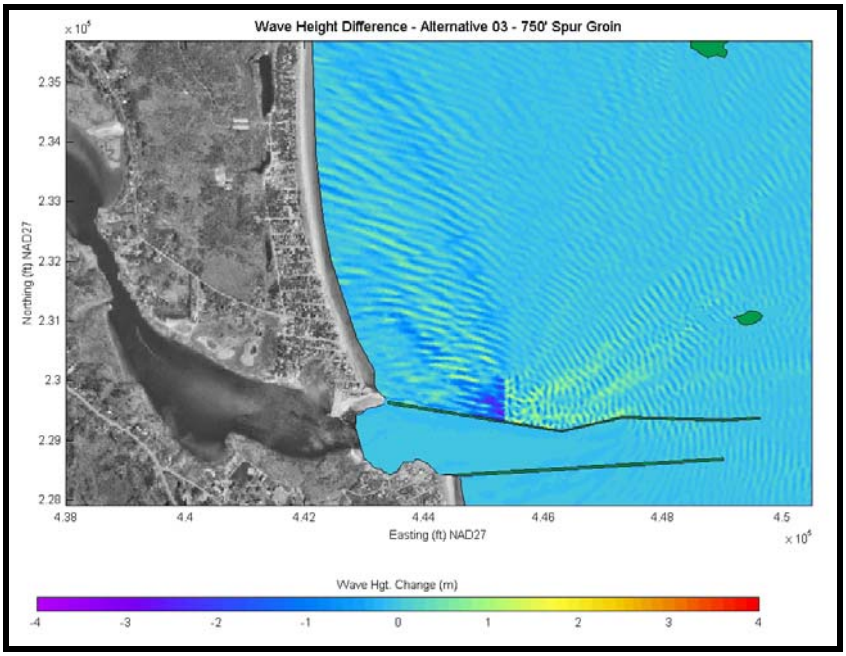

Figure 11-B8. Wave height changes for Alternative 03 for a 10-yr return period storm. A negative wave height change indicates a reduction in wave height, while a positive wave height change indicates an increase in wave height.

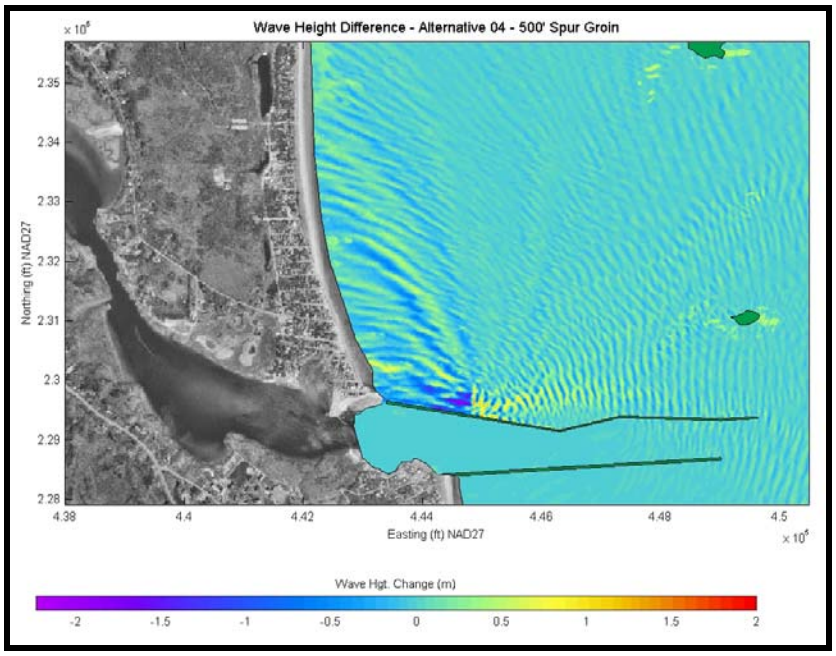

Figure11-B9. Wave height changes for Alternate 04 for an Eastern (90-110 degree) wave approach bin. A negative wave height change indicates a reduction in wave height, while a positive wave height change indicates an increase in wave height.

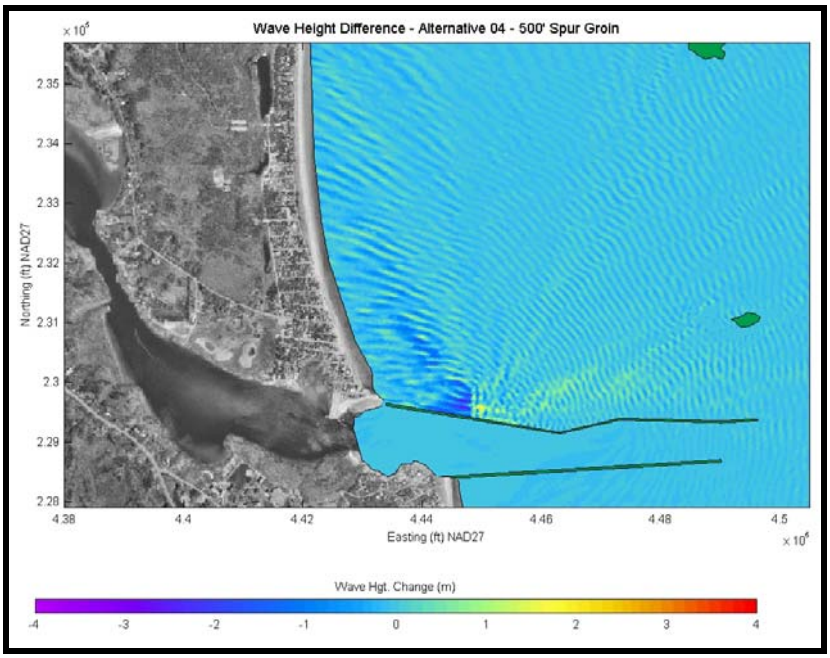

Figure 11-B10. Wave height changes for Alternative 04 for a 10-yr return period storm. A negative wave height change indicates a reduction in wave height, while a positive wave height change indicates an increase in wave height.

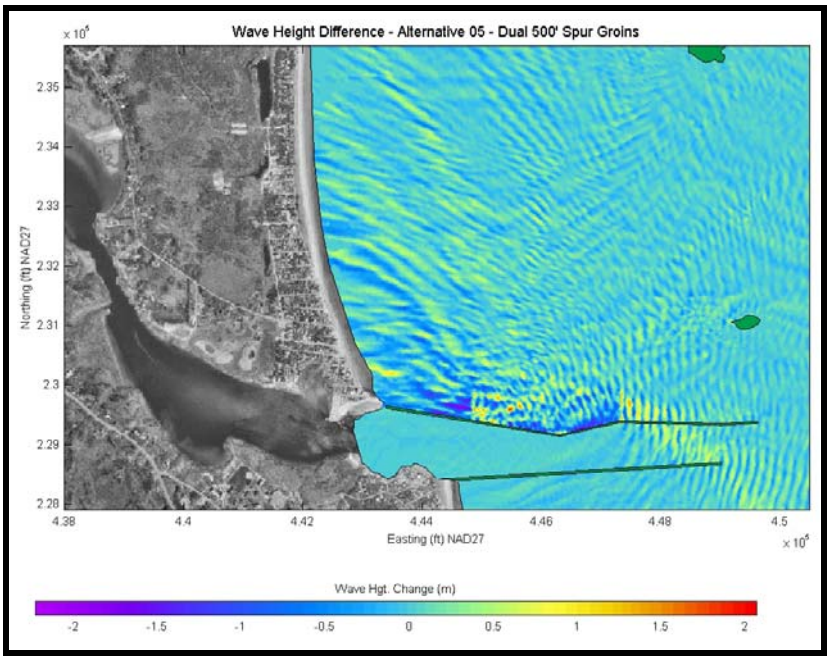

Figure11-B11. Wave height changes for Alternate 05 for an Eastern (90-110 degree) wave approach bin. A negative wave height change indicates a reduction in wave height, while a positive wave height change indicates an increase in wave height.

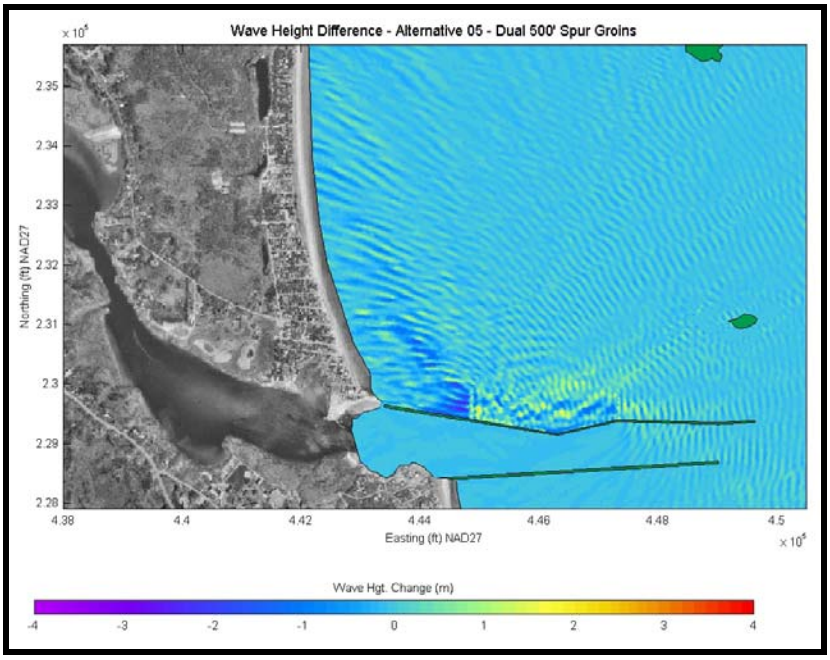

Figure 11-B12. Wave height changes for Alternative 05 for a 10-yr return period storm. A negative wave height change indicates a reduction in wave height, while a positive wave height change indicates an increase in wave height.

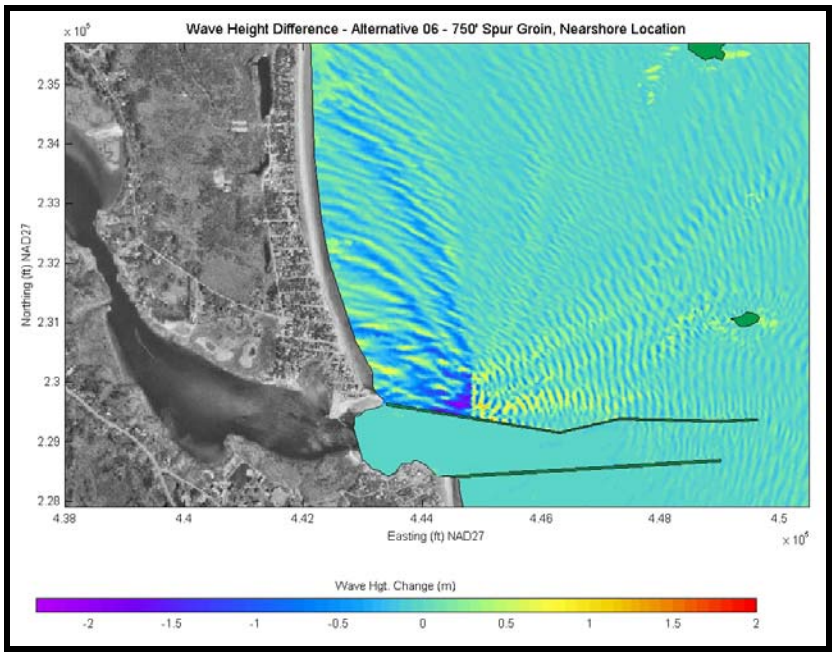

Figure11-B13. Wave height changes for Alternate 06 for an Eastern (90-110 degree) wave approach bin. A negative wave height change indicates a reduction in wave height, while a positive wave height change indicates an increase in wave height.

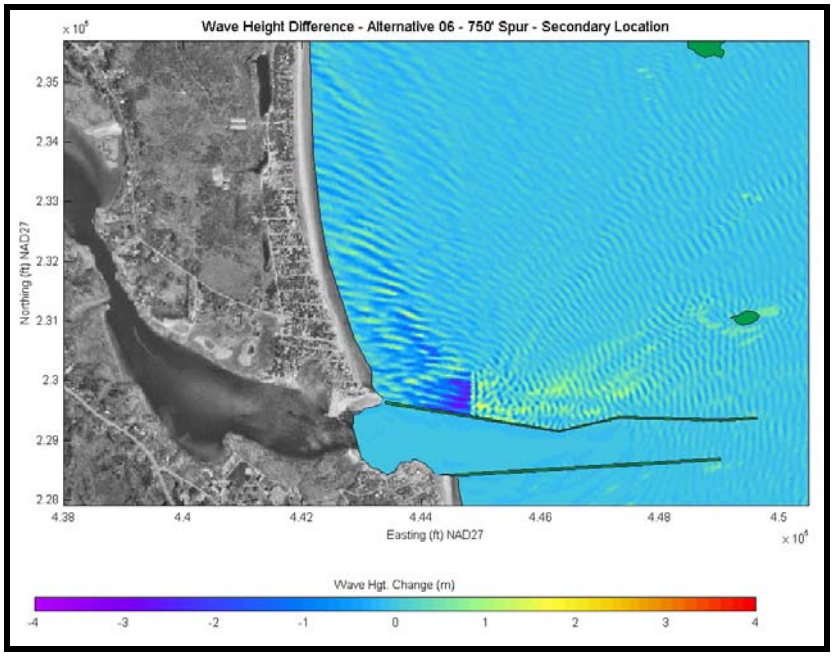

Figure 11-B14. Wave height changes for Alternative 06 for a 10-yr return period storm. A negative wave height change indicates a reduction in wave height, while a positive wave height change indicates an increase in wave height.

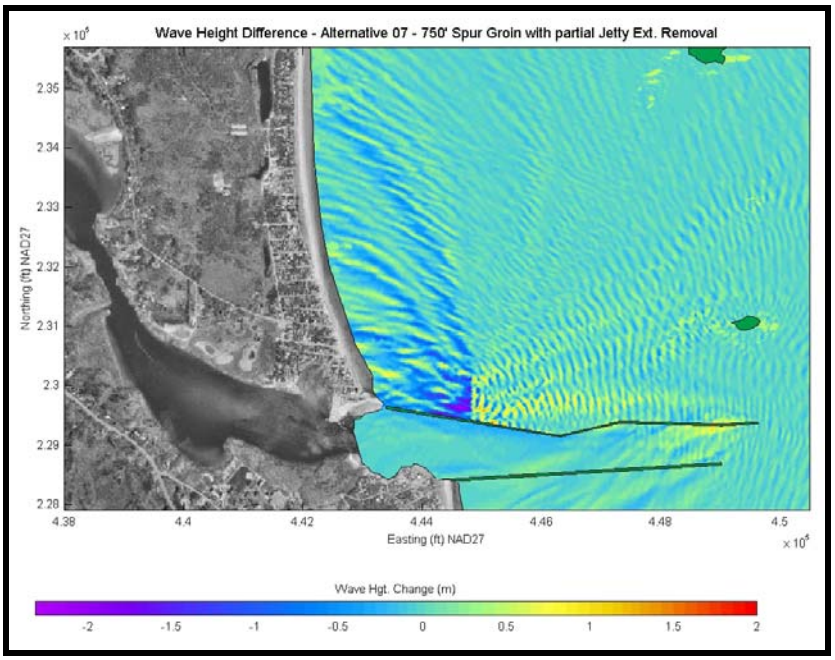

Figure11-B15. Wave height changes for Alternate 07 for an Eastern (90-110 degree) wave approach bin. A negative wave height change indicates a reduction in wave height, while a positive wave height change indicates an increase in wave height.

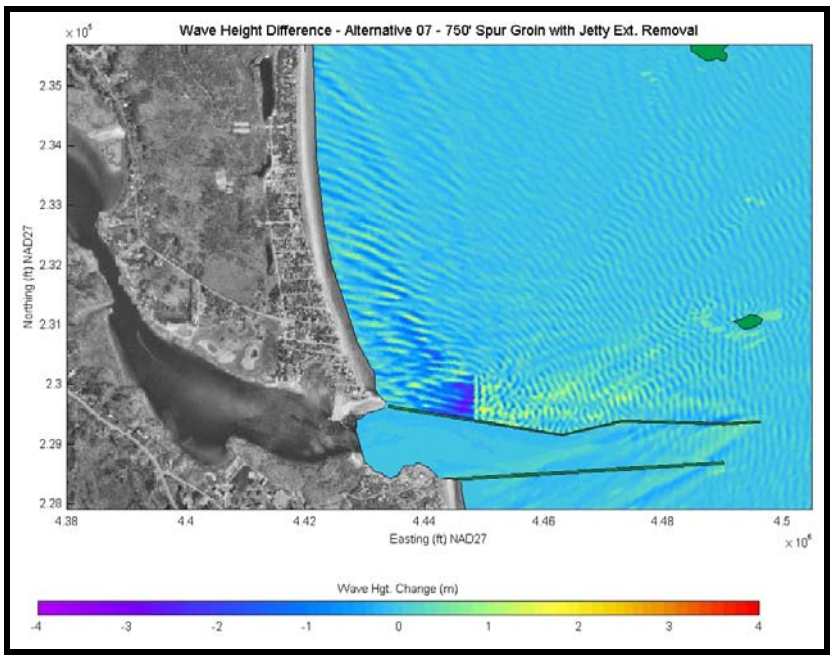

Figure 11-B16. Wave height changes for Alternative 07 for a 10-yr return period storm. A negative wave height change indicates a reduction in wave height, while a positive wave height change indicates an increase in wave height.

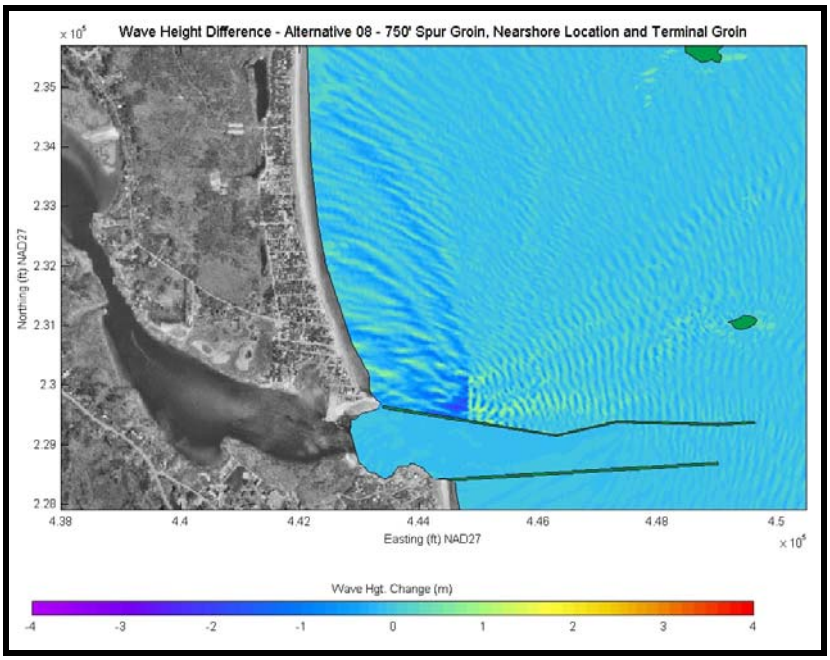

Figure11-B17. Wave height changes for Alternate 08 for an Eastern (90-110 degree) wave approach bin. A negative wave height change indicates a reduction in wave height, while a positive wave height change indicates an increase in wave height.

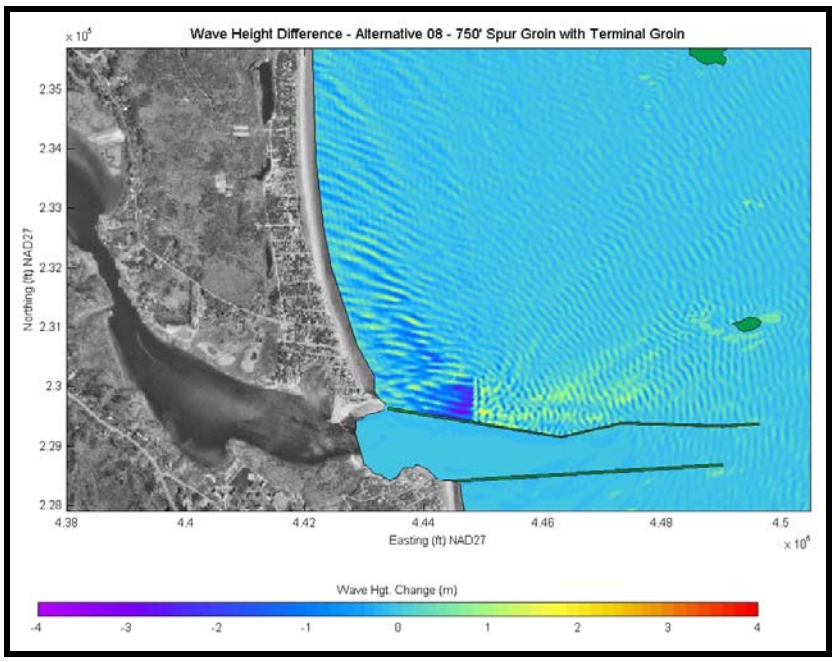

Figure 11-B18. Wave height changes for Alternative 08 for a 10-yr return period storm. A negative wave height change indicates a reduction in wave height, while a positive wave height change indicates an increase in wave height.

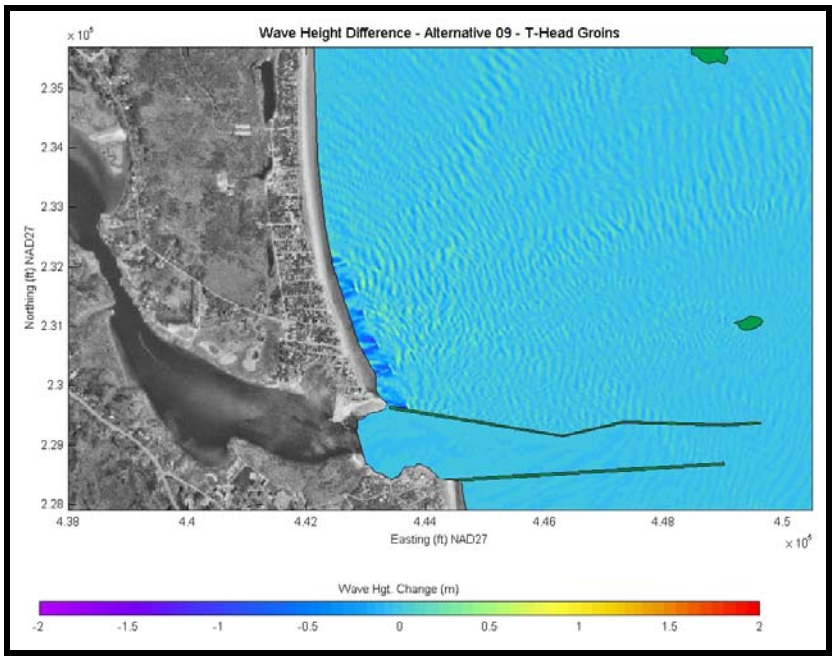

Figure11-B19. Wave height changes for Alternate 09 for an Eastern (90-110 degree) wave approach bin. A negative wave height change indicates a reduction in wave height, while a positive wave height change indicates an increase in wave height.

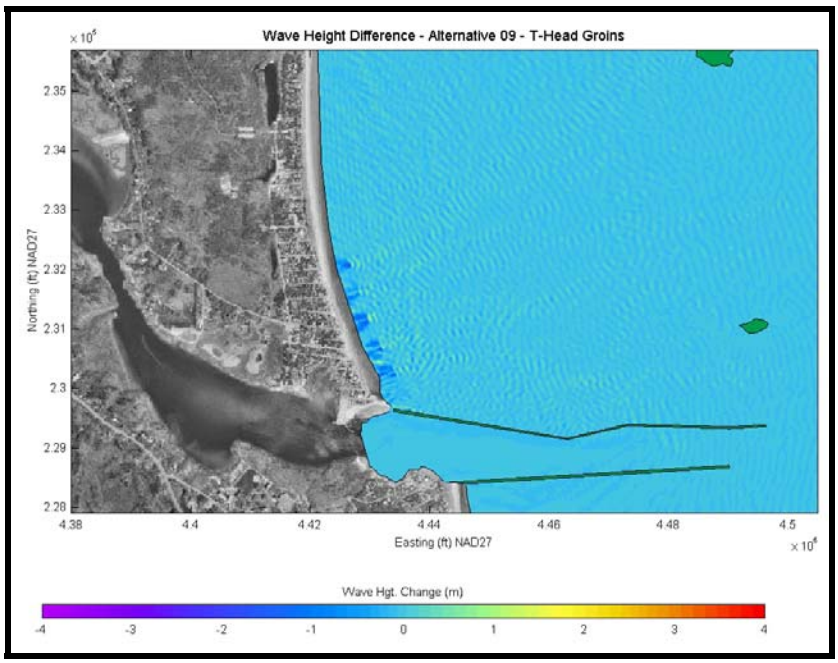

Figure 11-B20. Wave height changes for Alternative 09 for a 10-yr return period storm. A negative wave height change indicates a reduction in wave height, while a positive wave height change indicates an increase in wave height.

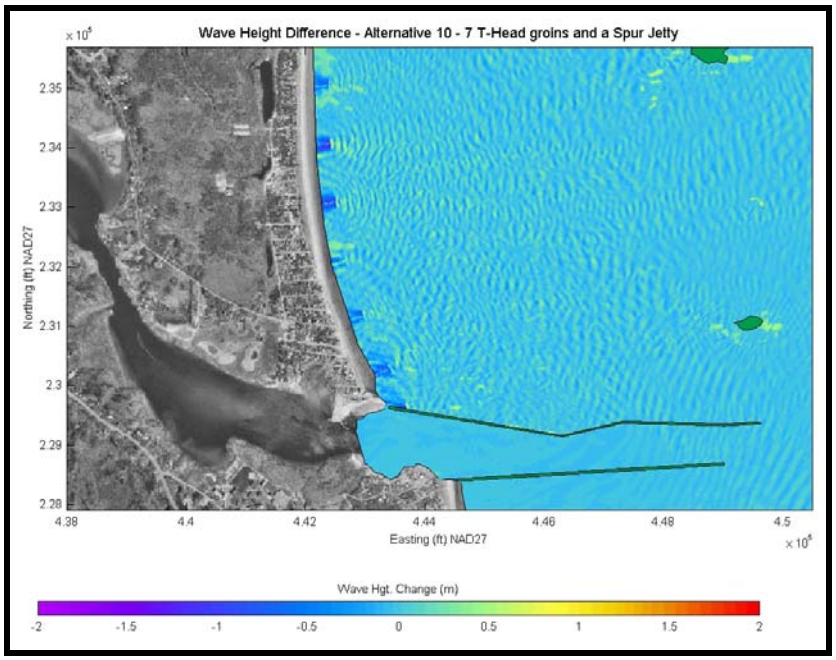

Figure11-B21. Wave height changes for Alternate 10 for an Eastern (90-110 degree) wave approach bin. A negative wave height change indicates a reduction in wave height, while a positive wave height change indicates an increase in wave height.

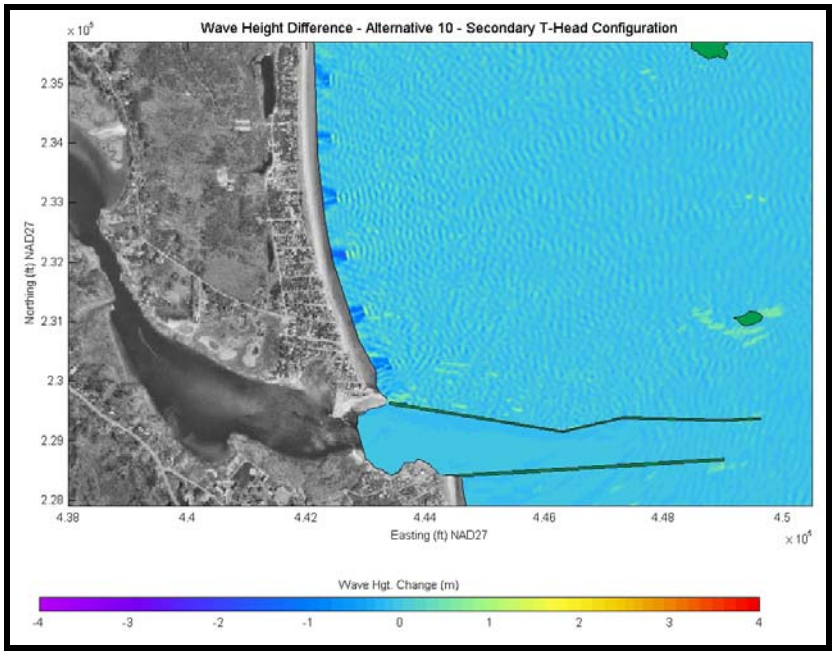

Figure 11-B22. Wave height changes for Alternative 10 for a 10-yr return period storm. A negative wave height change indicates a reduction in wave height, while a positive wave height change indicates an increase in wave height.

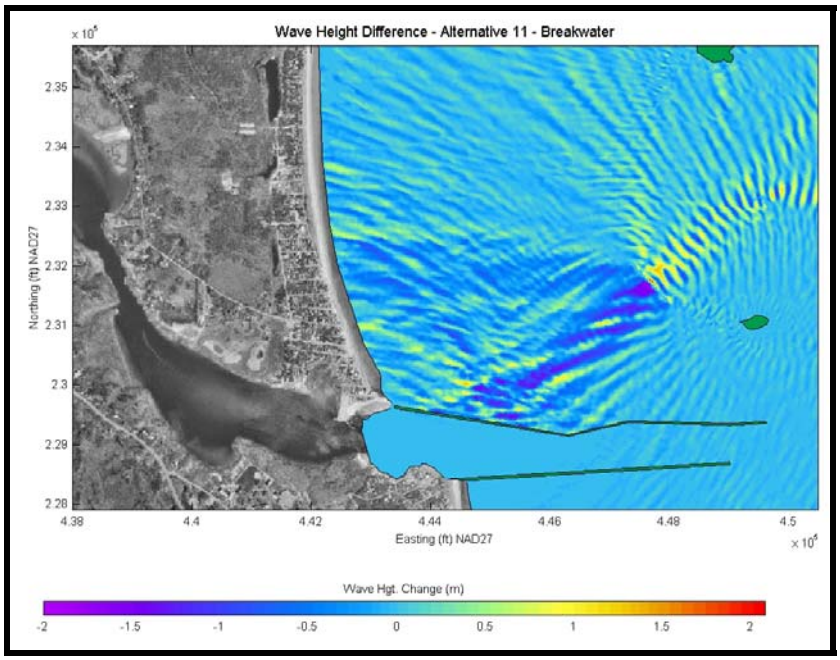

Figure11-B23. Wave height changes for Alternate 11 for an Eastern (90-110 degree) wave approach bin. A negative wave height change indicates a reduction in wave height, while a positive wave height change indicates an increase in wave height.

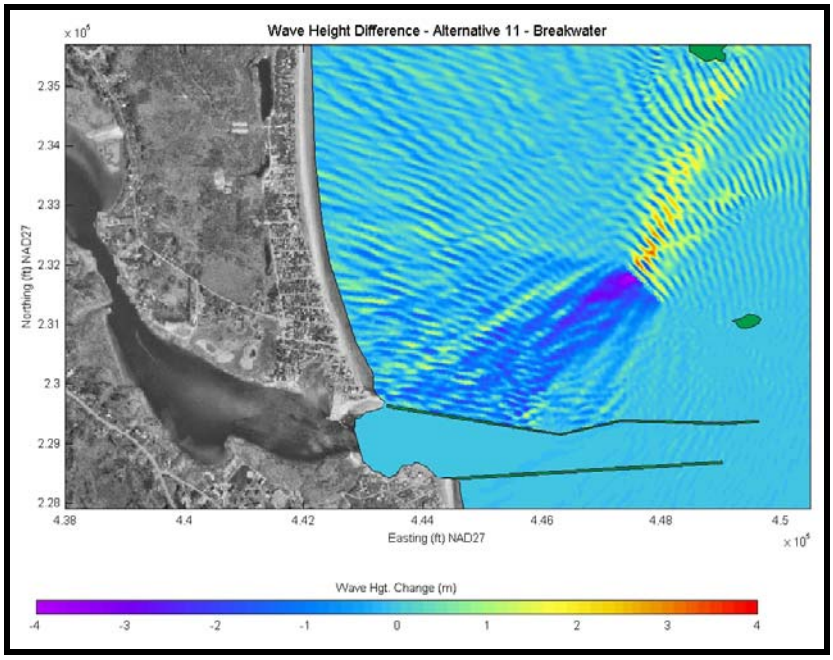

Figure 11-B24. Wave height changes for Alternative 11 for a 10-yr return period storm. A negative wave height change indicates a reduction in wave height, while a positive wave height change indicates an increase in wave height.

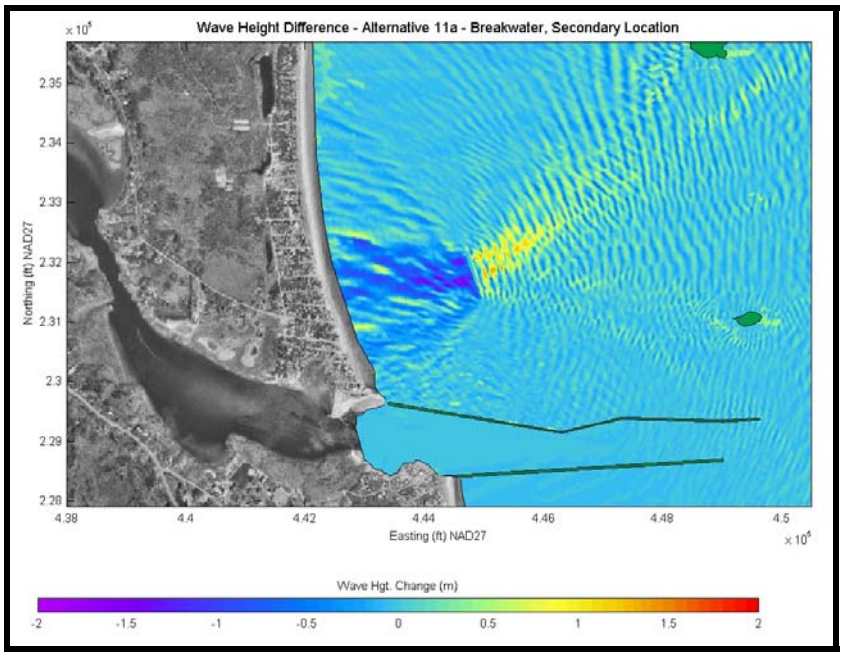

Figure11-B25. Wave height changes for Alternate 11a for an Eastern (90-110 degree) wave approach bin. A negative wave height change indicates a reduction in wave height, while a positive wave height change indicates an increase in wave height.

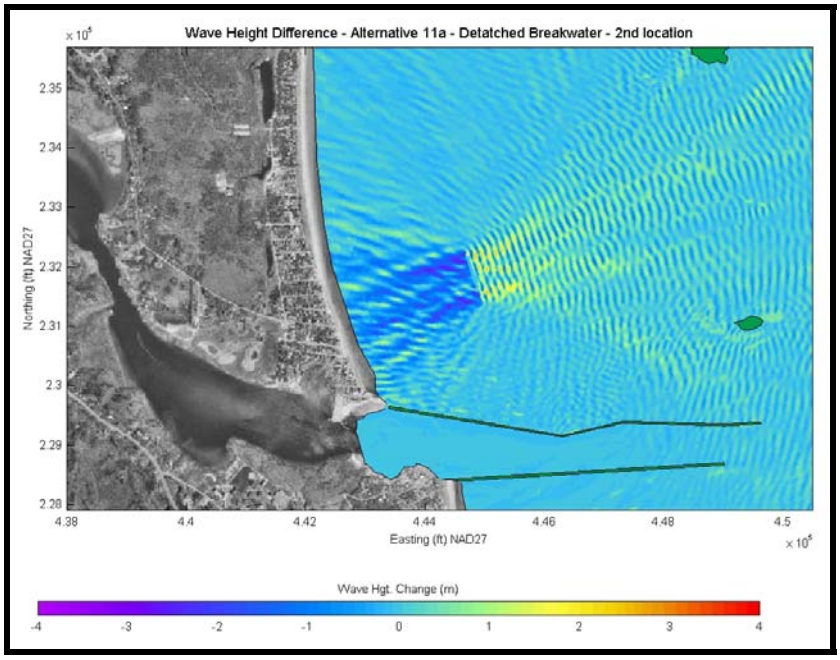

Figure 11-B26. Wave height changes for Alternative 11a for a 10-yr return period storm. A negative wave height change indicates a reduction in wave height, while a positive wave height change indicates an increase in wave height.

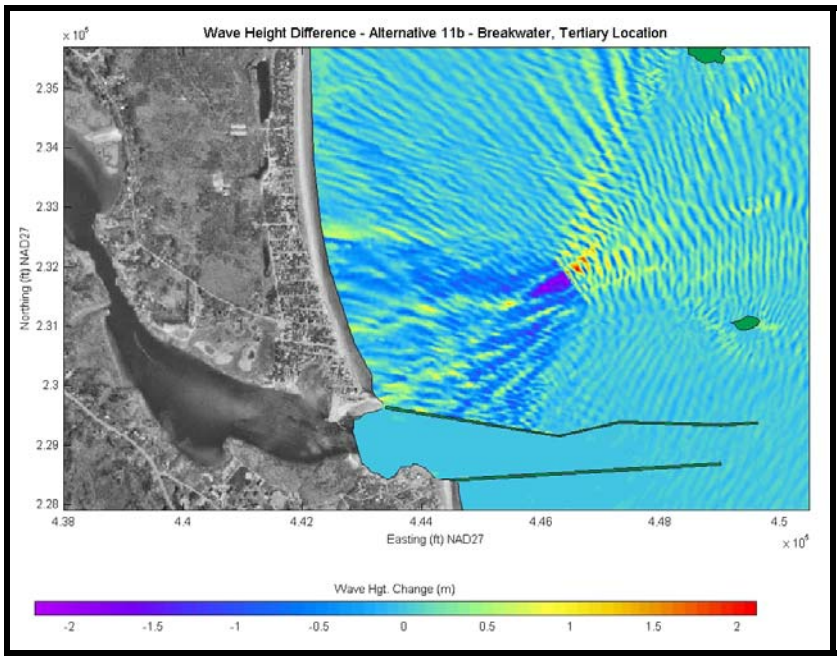

Figure11-B27. Wave height changes for Alternate 11b for an Eastern (90-110 degree) wave approach bin. A negative wave height change indicates a reduction in wave height, while a positive wave height change indicates an increase in wave height.

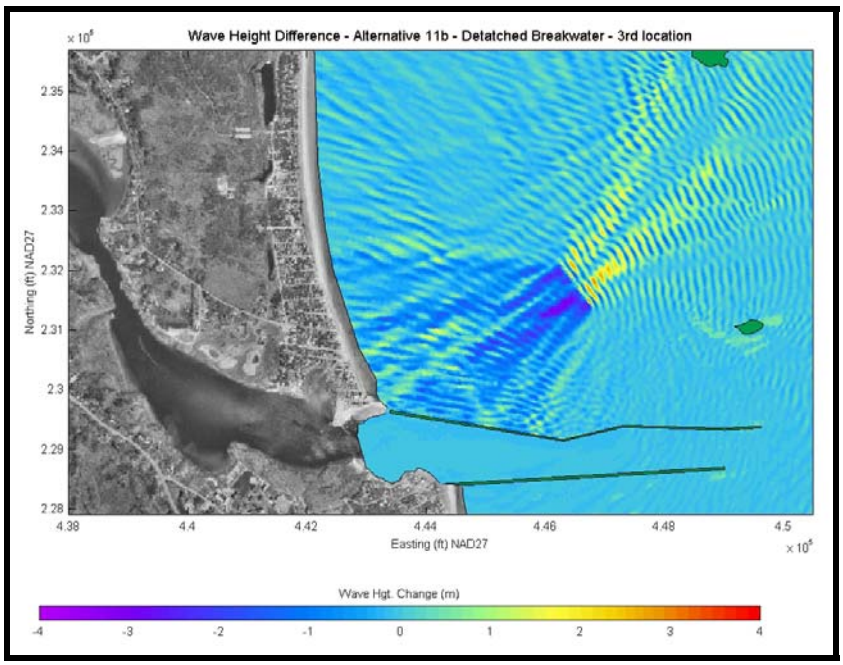

Figure 11-B28. Wave height changes for Alternative 11b for a 10-yr return period storm. A negative wave height change indicates a reduction in wave height, while a positive wave height change indicates an increase in wave height.

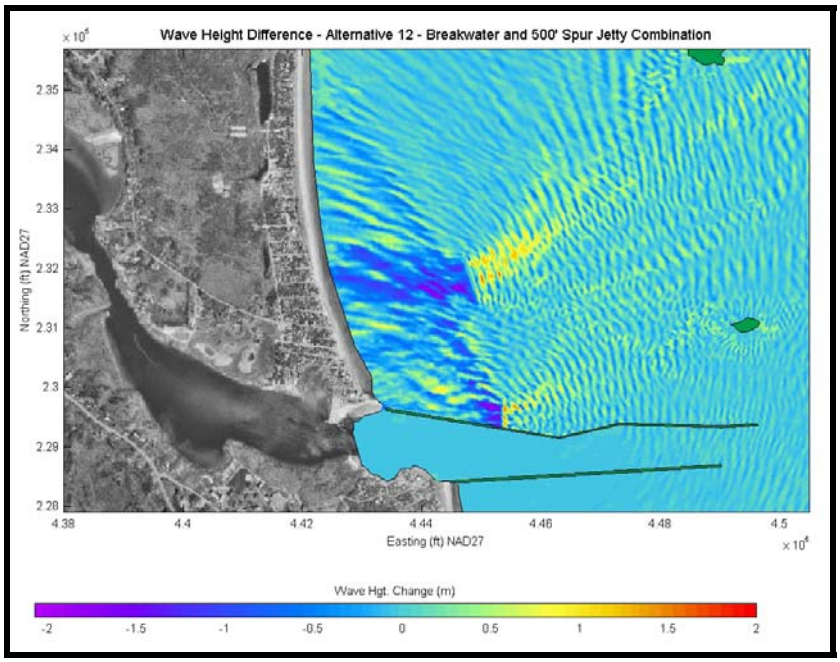

Figure11-B29. Wave height changes for Alternate 12 for an Eastern (90-110 degree) wave approach bin. A negative wave height change indicates a reduction in wave height, while a positive wave height change indicates an increase in wave height.

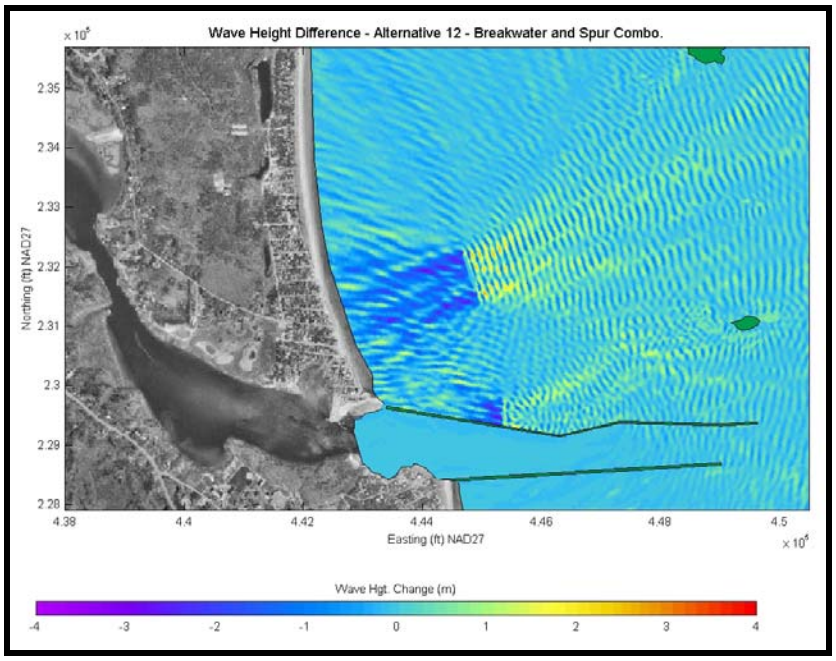

Figure 11-B30. Wave height changes for Alternative 12 for a 10-yr return period storm. A negative wave height change indicates a reduction in wave height, while a positive wave height change indicates an increase in wave height.

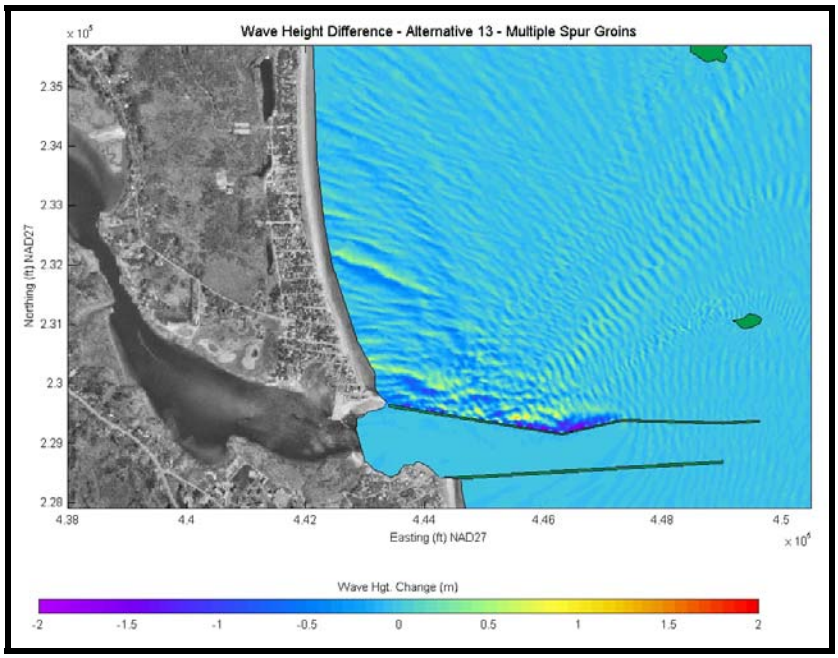

Figure11-B31. Wave height changes for Alternate 13 for an Eastern (90-110 degree) wave approach bin. A negative wave height change indicates a reduction in wave height, while a positive wave height change indicates an increase in wave height.

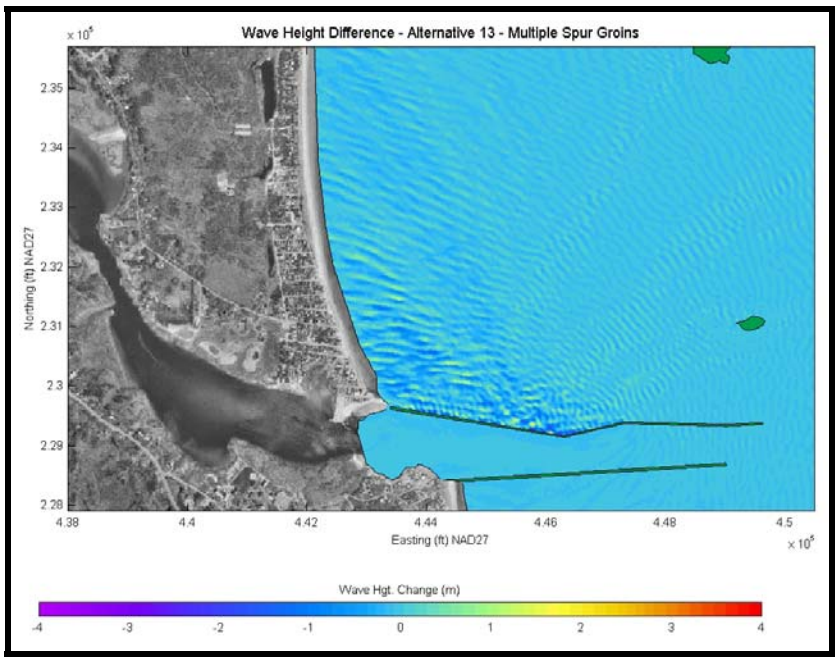

Figure 11-B32. Wave height changes for Alternative 13 for a 10-yr return period storm. A negative wave height change indicates a reduction in wave height, while a positive wave height change indicates an increase in wave height.

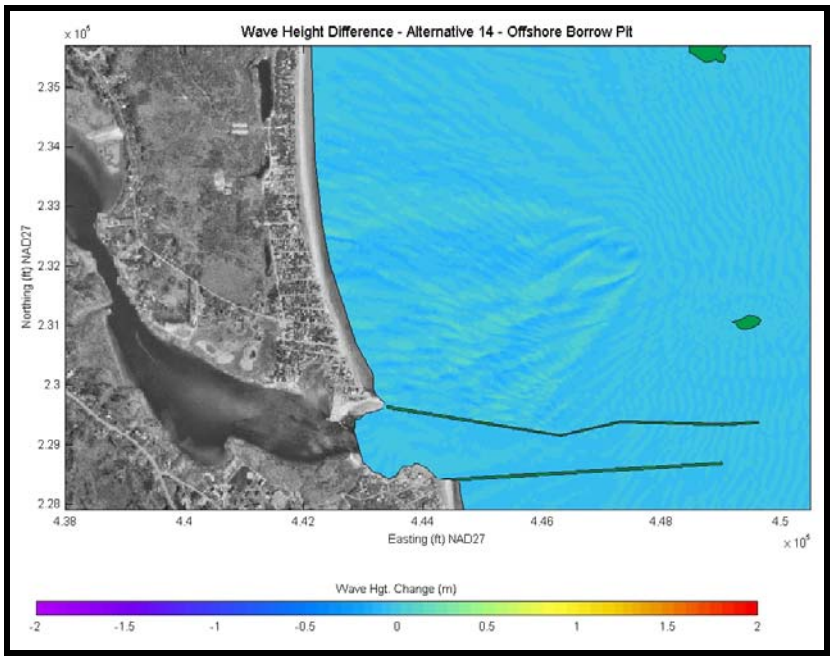

Figure11-B33. Wave height changes for Alternate 14 for an Eastern (90-110 degree) wave approach bin. A negative wave height change indicates a reduction in wave height, while a positive wave height change indicates an increase in wave height.

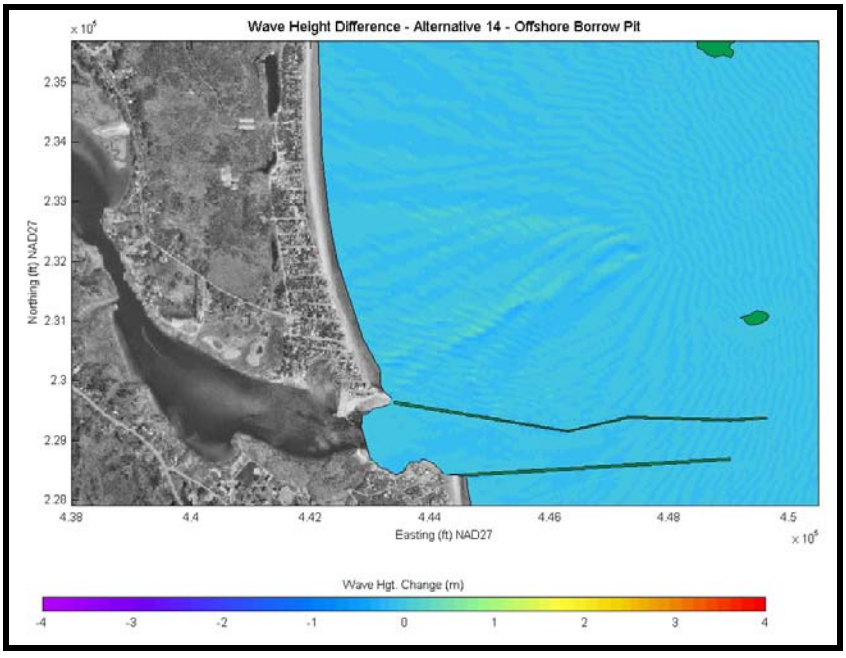

Figure 11-B34. Wave height changes for Alternative 14 for a 10-yr return period storm. A negative wave height change indicates a reduction in wave height, while a positive wave height change indicates an increase in wave height.

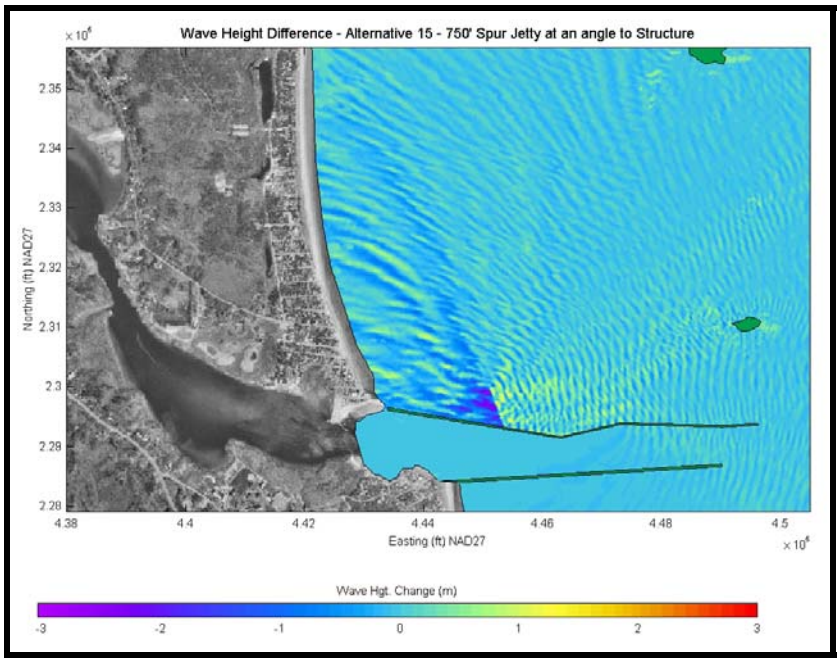

Figure 11-B35. Wave height changes for Alternative 15 for a 10-yr return period storm. A negative wave height change indicates a reduction in wave height, while a positive wave height change indicates an increase in wave height.

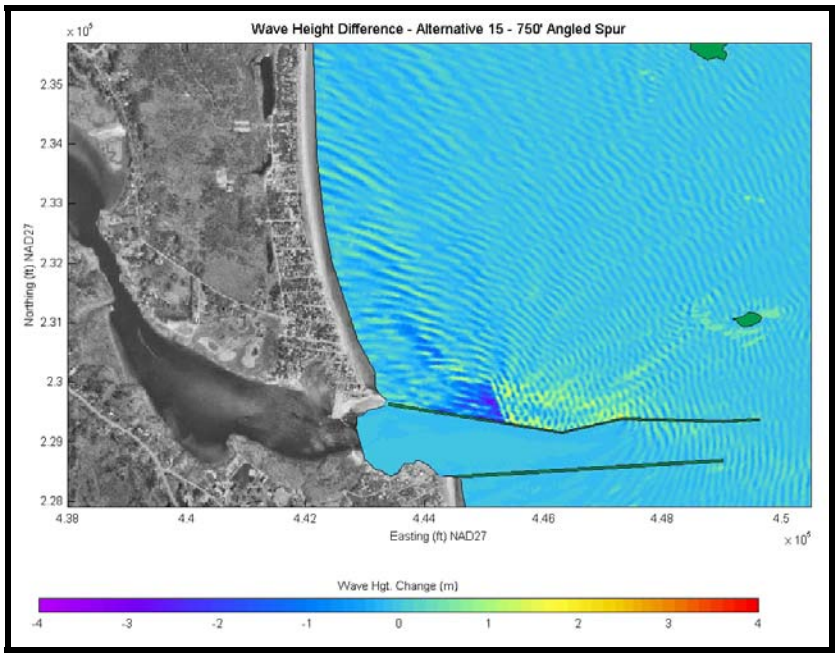

Figure11-B36. Wave height changes for Alternate 15 for an Eastern (90-110 degree) wave approach bin. A negative wave height change indicates a reduction in wave height, while a positive wave height change indicates an increase in wave height.

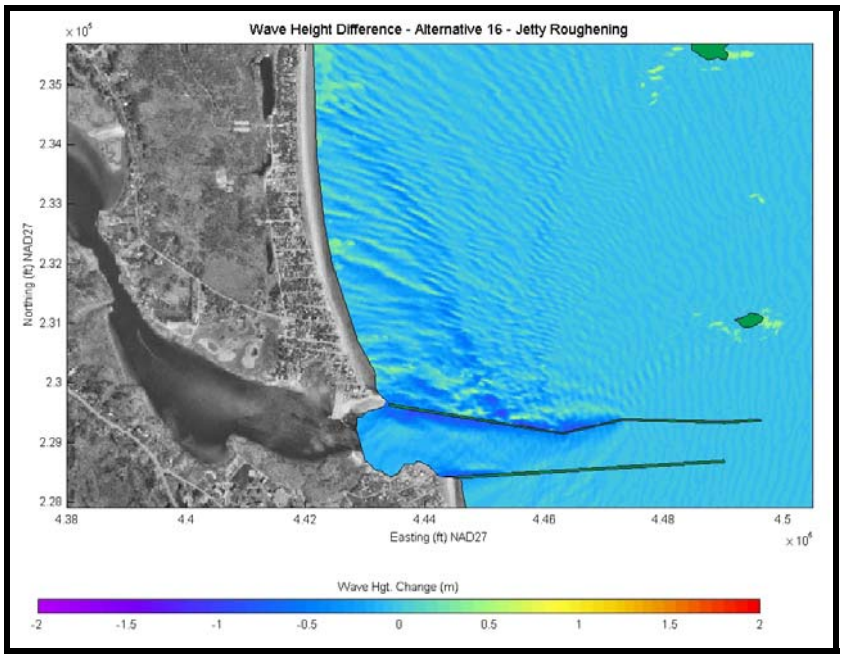

Figure 11-B37. Wave height changes for Alternative 16 for a 10-yr return period storm. A negative wave height change indicates a reduction in wave height, while a positive wave height change indicates an increase in wave height.

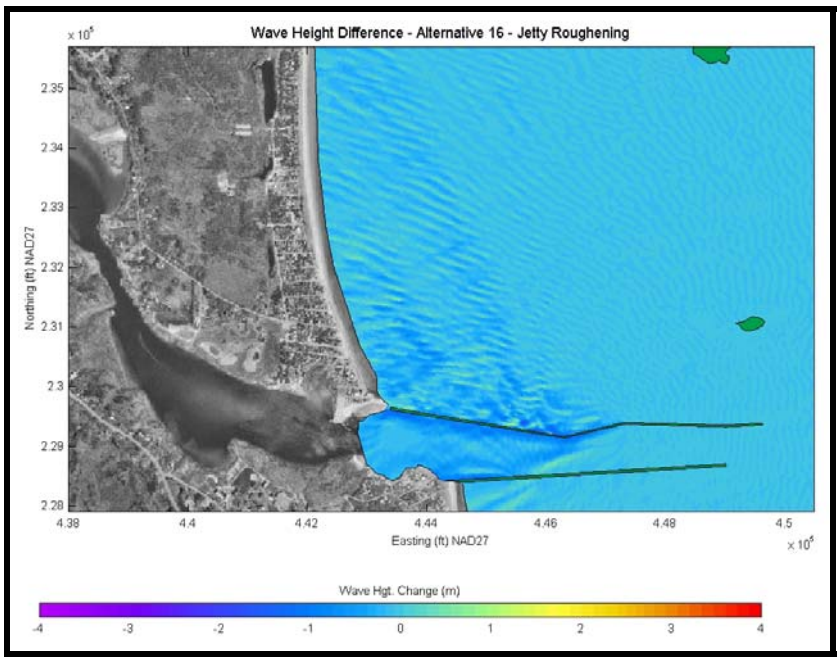

Figure11-B38. Wave height changes for Alternate 16 for an Eastern (90-110 degree) wave approach bin. A negative wave height change indicates a reduction in wave height, while a positive wave height change indicates an increase in wave height.

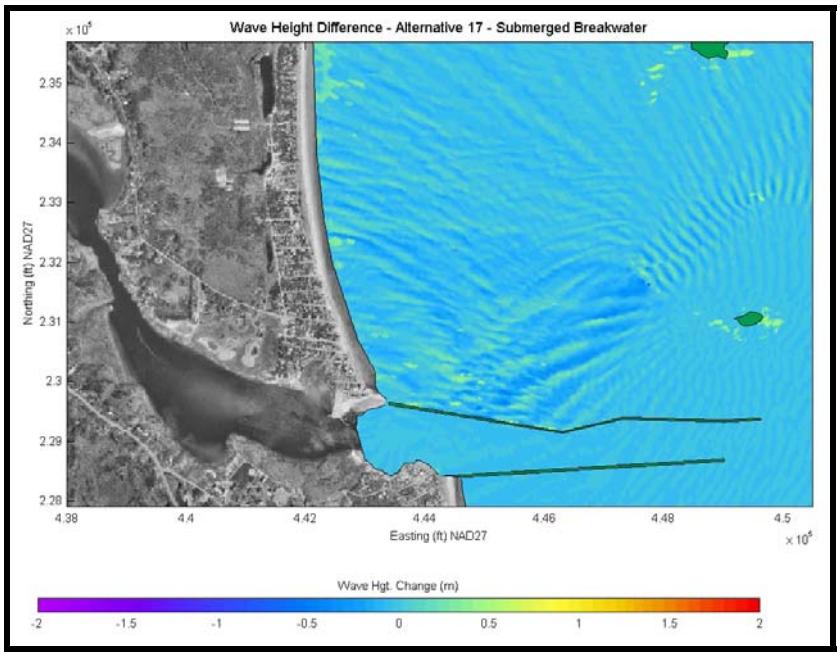

Figure 11-B39. Wave height changes for Alternative 17 for a 10-yr return period storm. A negative wave height change indicates a reduction in wave height, while a positive wave height change indicates an increase in wave height.

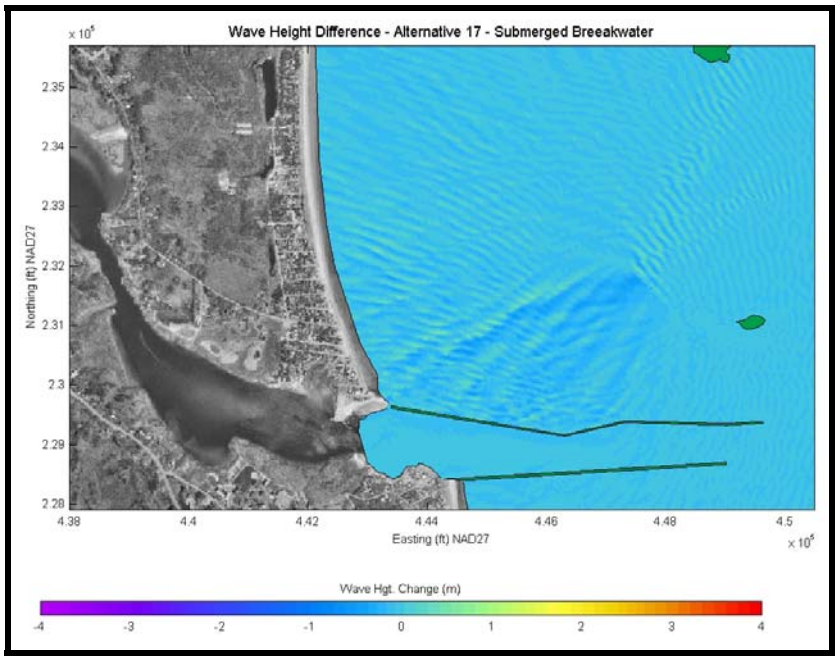

Figure11-B40. Wave height changes for Alternate 17 for an Eastern (90-110 degree) wave approach bin. A negative wave height change indicates a reduction in wave height, while a positive wave height change indicates an increase in wave height.

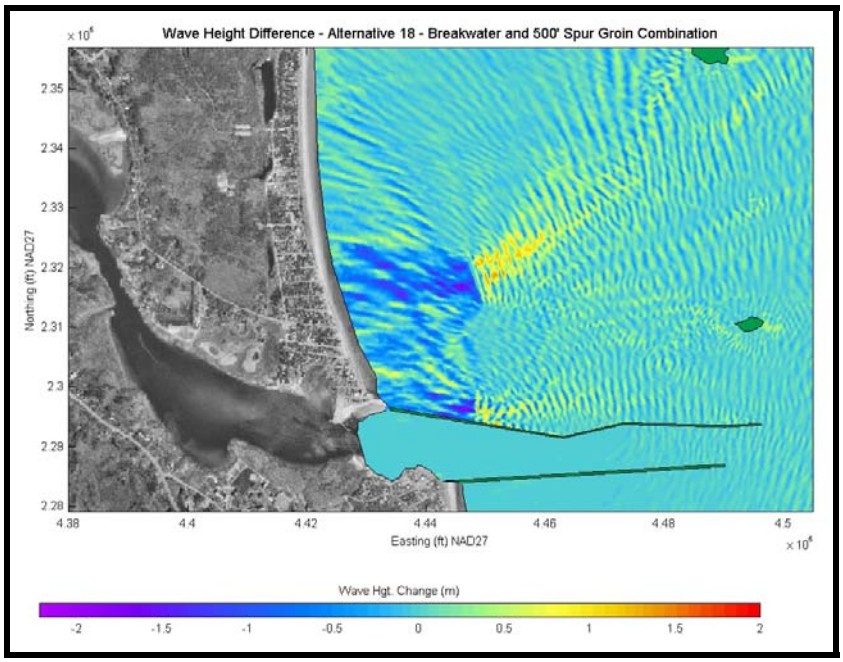

Figure 11-B41. Wave height changes for Alternative 18 for a 10-yr return period storm. A negative wave height change indicates a reduction in wave height, while a positive wave height change indicates an increase in wave height.

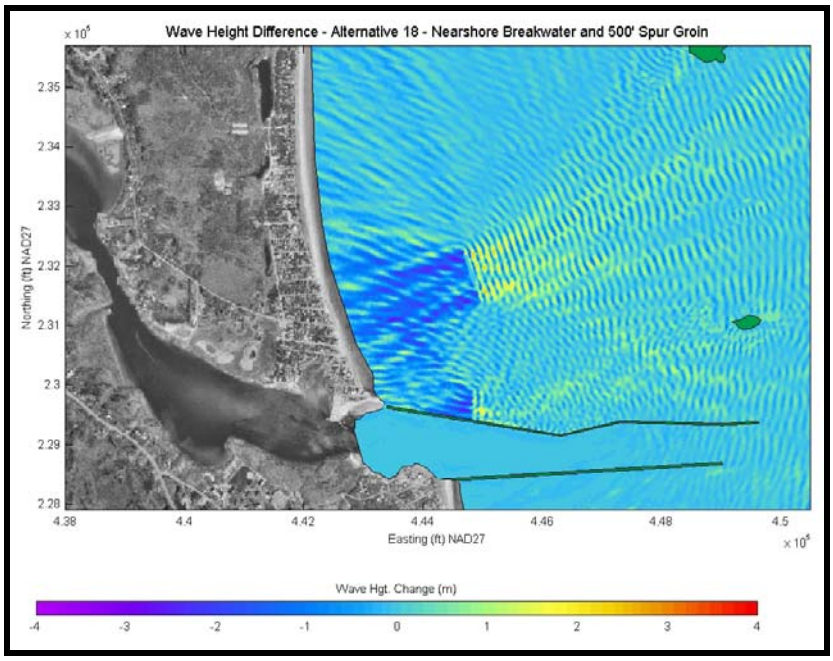

Figure11-B42. Wave height changes for Alternate 18 for an Eastern (90-110 degree) wave approach bin. A negative wave height change indicates a reduction in wave height, while a positive wave height change indicates an increase in wave height.

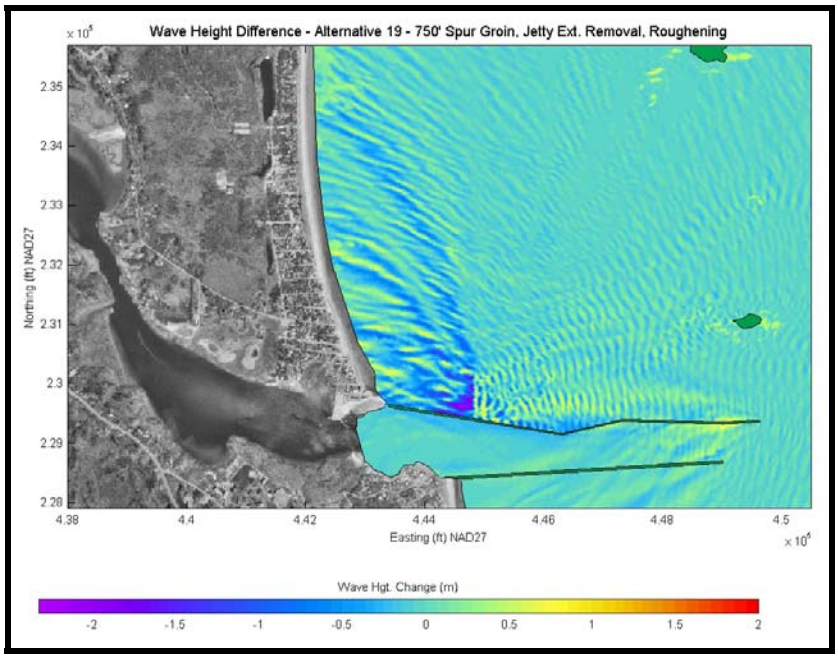

Figure 11-B43. Wave height changes for Alternative 19 for a 10-yr return period storm. A negative wave height change indicates a reduction in wave height, while a positive wave height change indicates an increase in wave height.

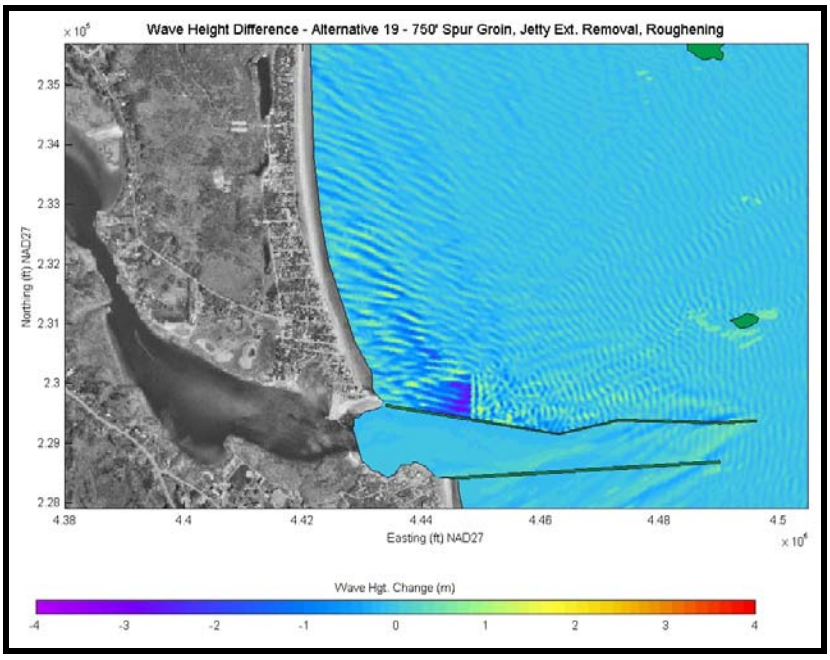

Figure11-B44. Wave height changes for Alternate 19 for an Eastern (90-110 degree) wave approach bin. A negative wave height change indicates a reduction in wave height, while a positive wave height change indicates an increase in wave height.

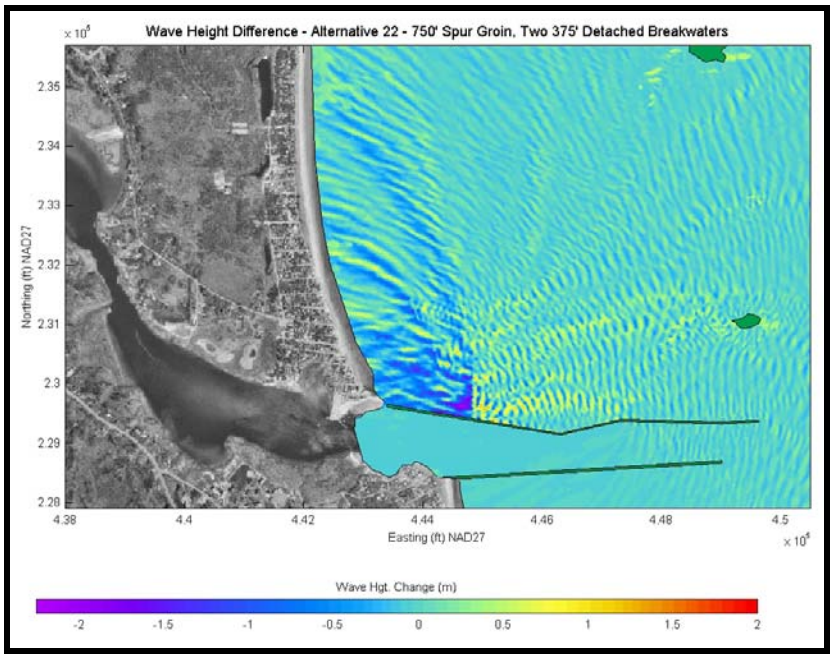

Figure 11-B45. Wave height changes for Alternative 22 for a 10-yr return period storm. A negative wave height change indicates a reduction in wave height, while a positive wave height change indicates an increase in wave height.

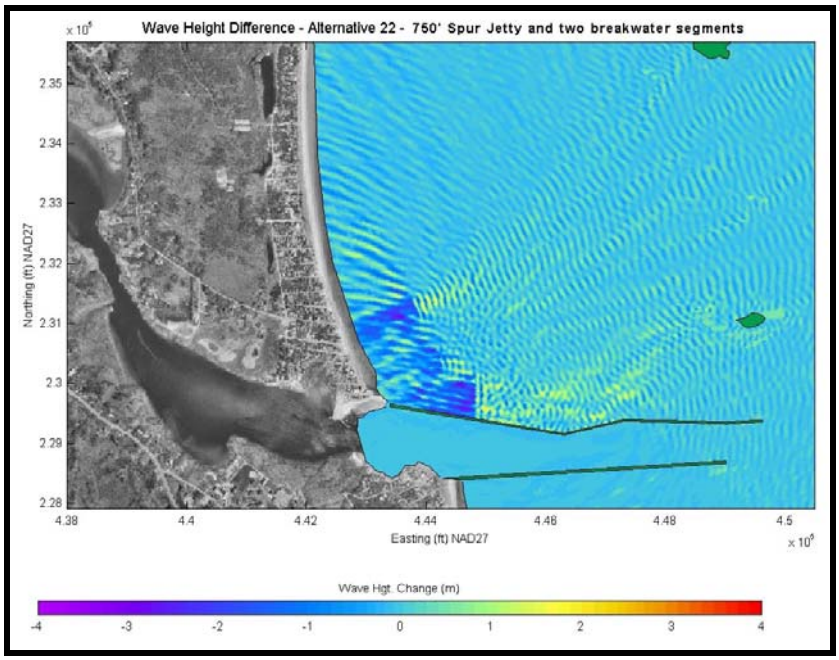

Figure11-B46. Wave height changes for Alternate 22 for an Eastern (90-110 degree) wave approach bin. A negative wave height change indicates a reduction in wave height, while a positive wave height change indicates an increase in wave height.

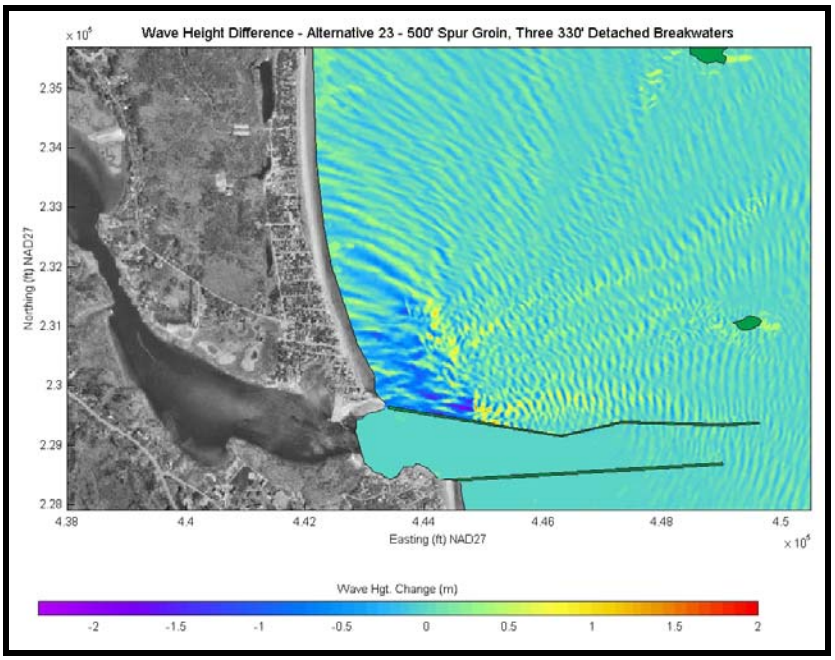

Figure 11-B47. Wave height changes for Alternative 23 for a 10-yr return period storm. A negative wave height change indicates a reduction in wave height, while a positive wave height change indicates an increase in wave height.

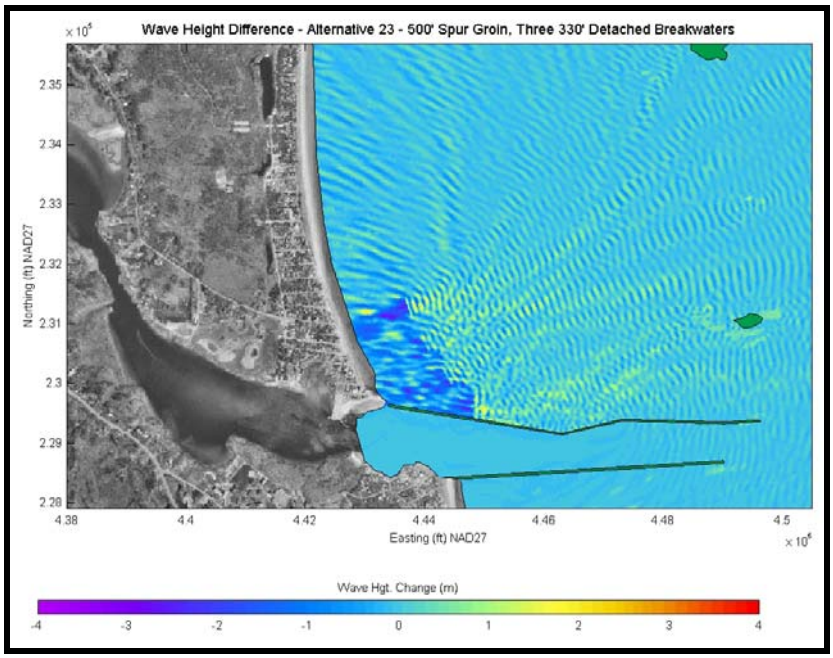

Figure11-B48. Wave height changes for Alternate 23 for an Eastern (90-110 degree) wave approach bin. A negative wave height change indicates a reduction in wave height, while a positive wave height change indicates an increase in wave height.

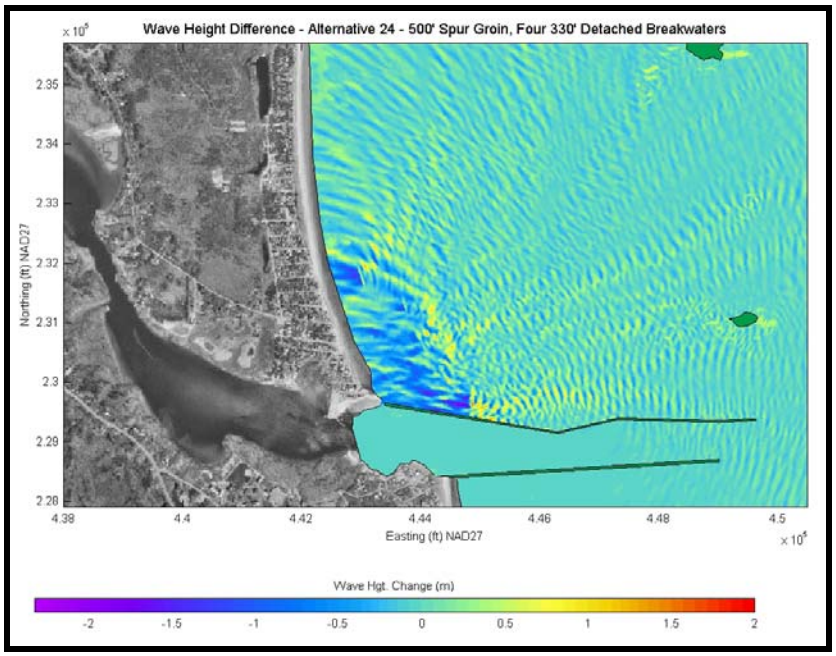

Figure 11-B49. Wave height changes for Alternative 24 for a 10-yr return period storm. A negative wave height change indicates a reduction in wave height, while a positive wave height change indicates an increase in wave height.

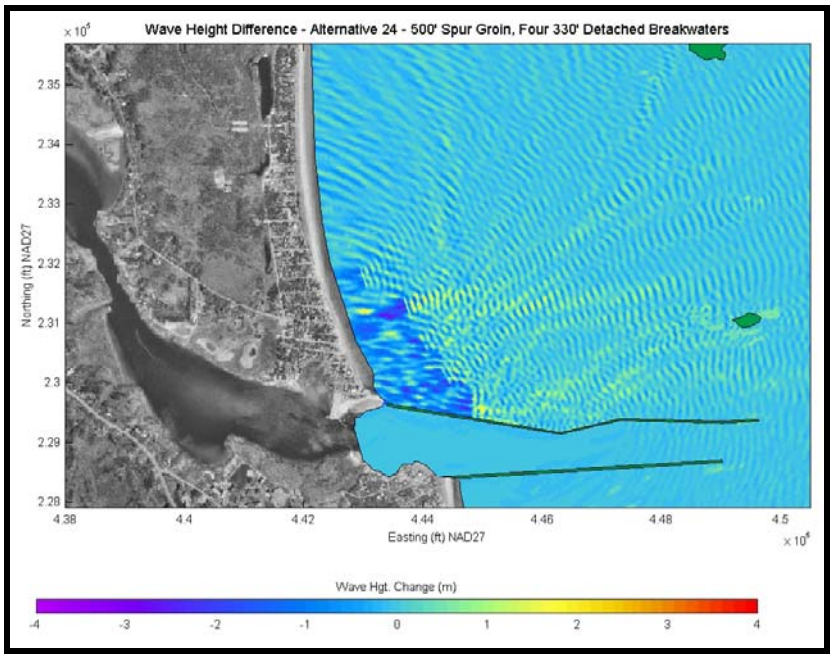

Figure11-B50. Wave height changes for Alternate 24 for an Eastern (90-110 degree) wave approach bin. A negative wave height change indicates a reduction in wave height, while a positive wave height change indicates an increase in wave height.

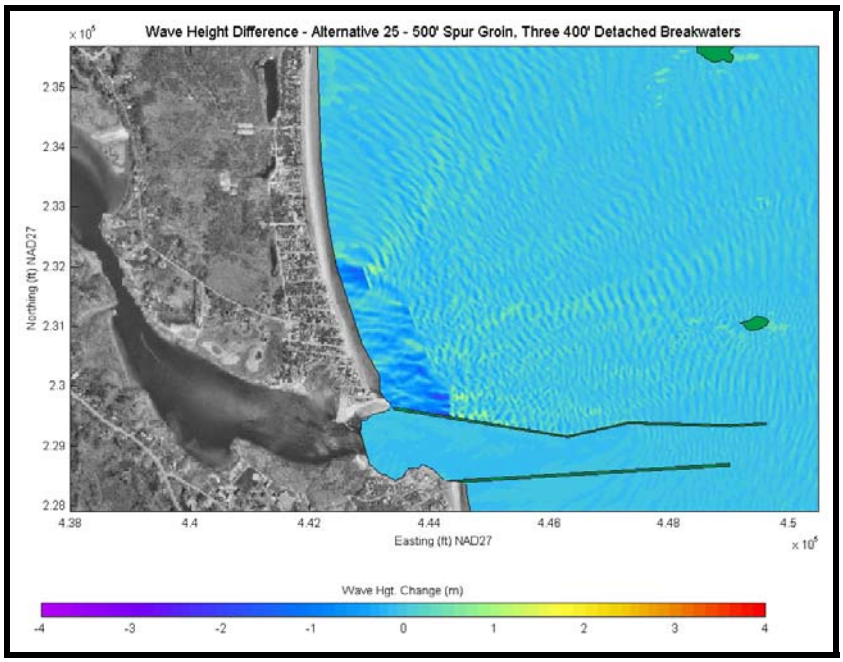

Figure 11-B51. Wave height changes for Alternative 25 for a 10-yr return period storm. A negative wave height change indicates a reduction in wave height, while a positive wave height change indicates an increase in wave height.

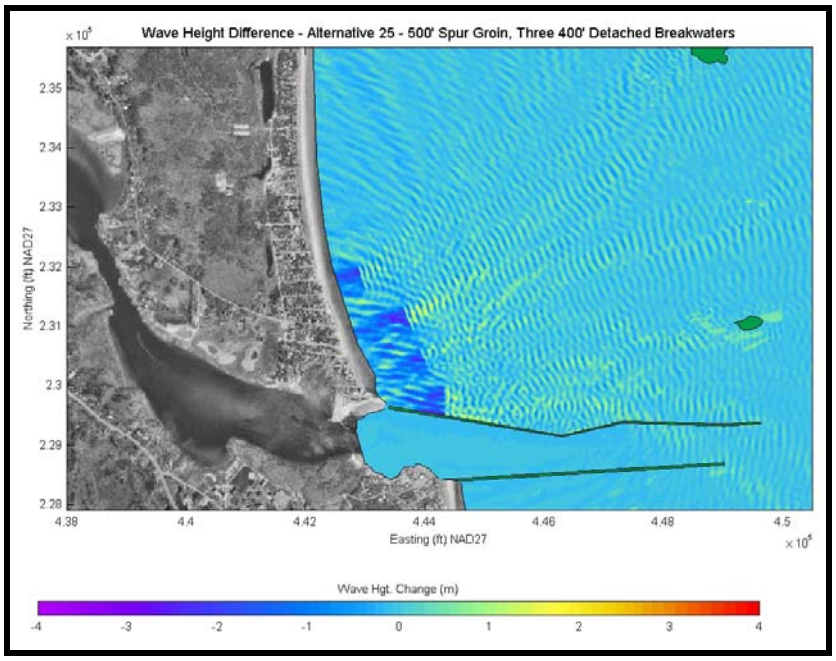

Figure11-B52. Wave height changes for Alternate 25 for an Eastern (90-110 degree) wave approach bin. A negative wave height change indicates a reduction in wave height, while a positive wave height change indicates an increase in wave height.

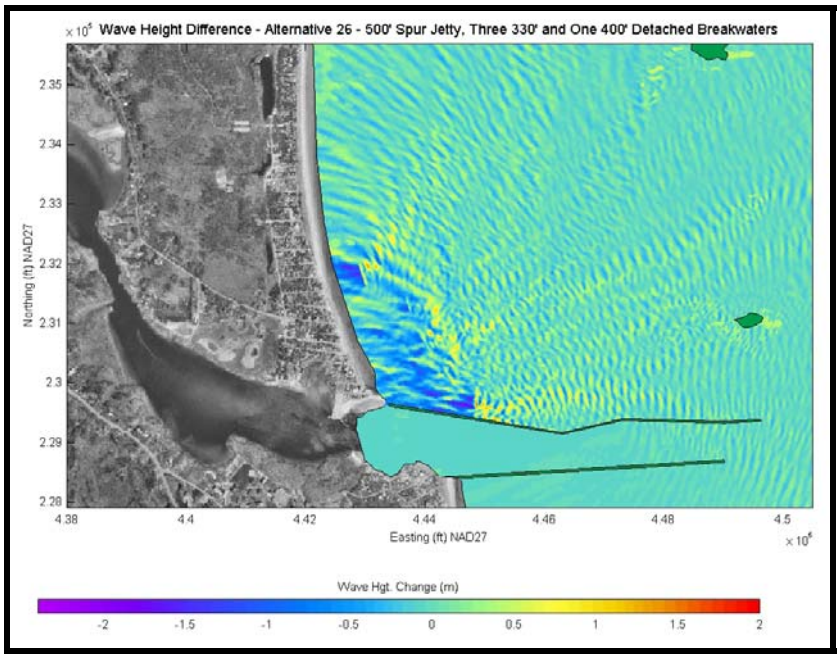

Figure 11-B53. Wave height changes for Alternative 26 for a 10-yr return period storm. A negative wave height change indicates a reduction in wave height, while a positive wave height change indicates an increase in wave height.

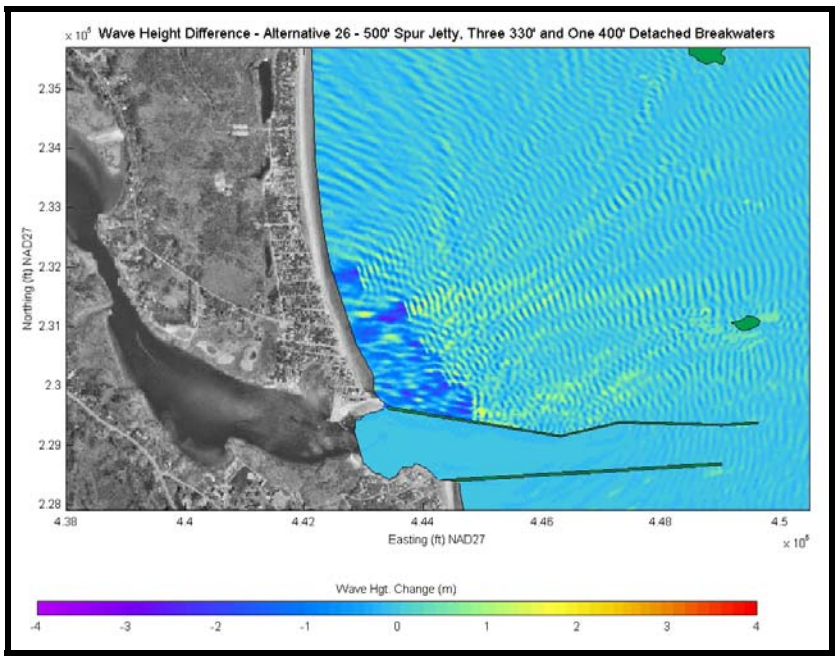

Figure 11-B54. Wave height changes for Alternative 26 for a 10-yr return period storm. A negative wave height change indicates a reduction in wave height, while a positive wave height change indicates an increase in wave height.

APPENDIX 13-B

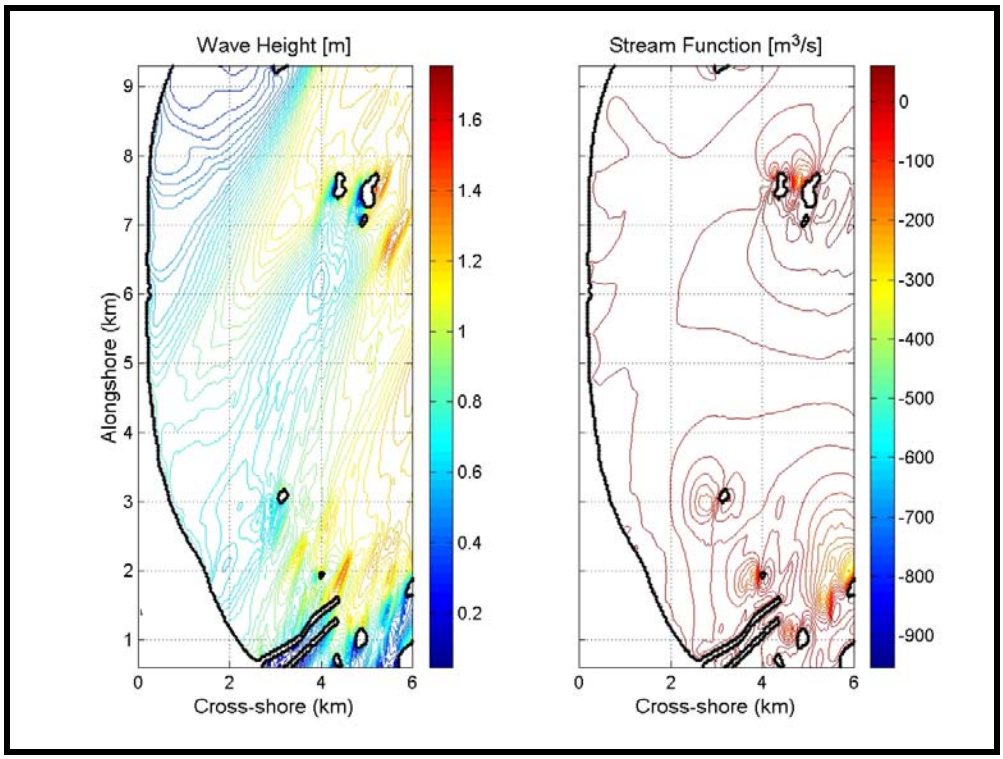

Figure 13-B1. Wave height and stream function for a northeast (55 to 75 degree) approach condition.

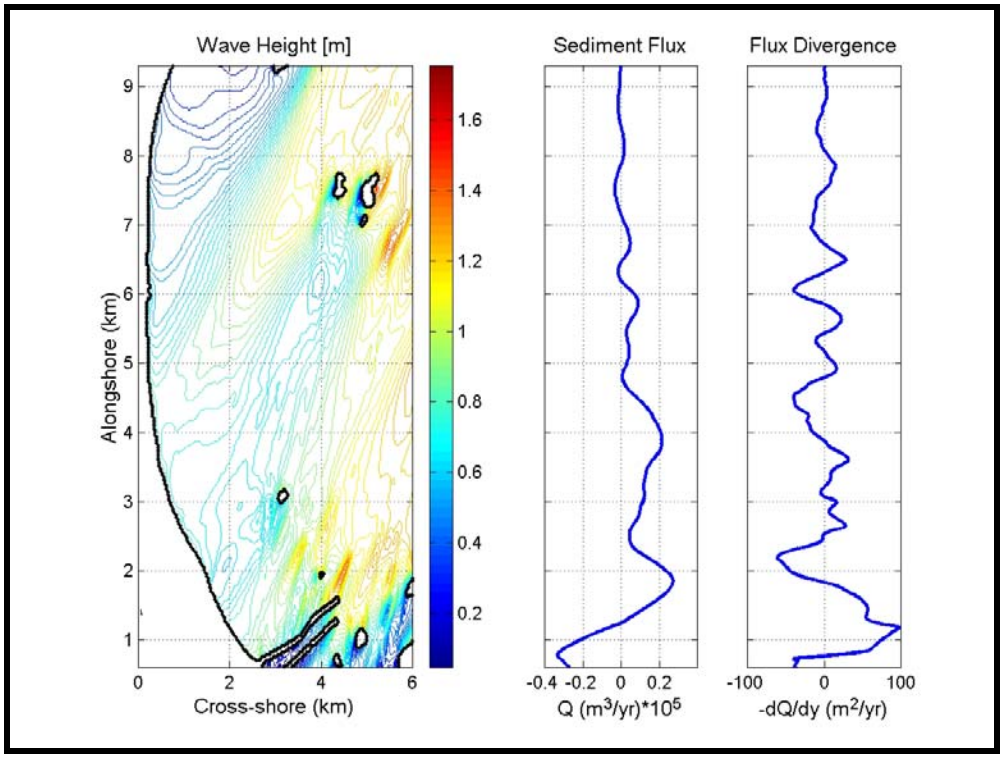

Figure 13-B2. Sediment flux and flux divergence for a northeast (55 to 75 degree) wave directional approach simulation.

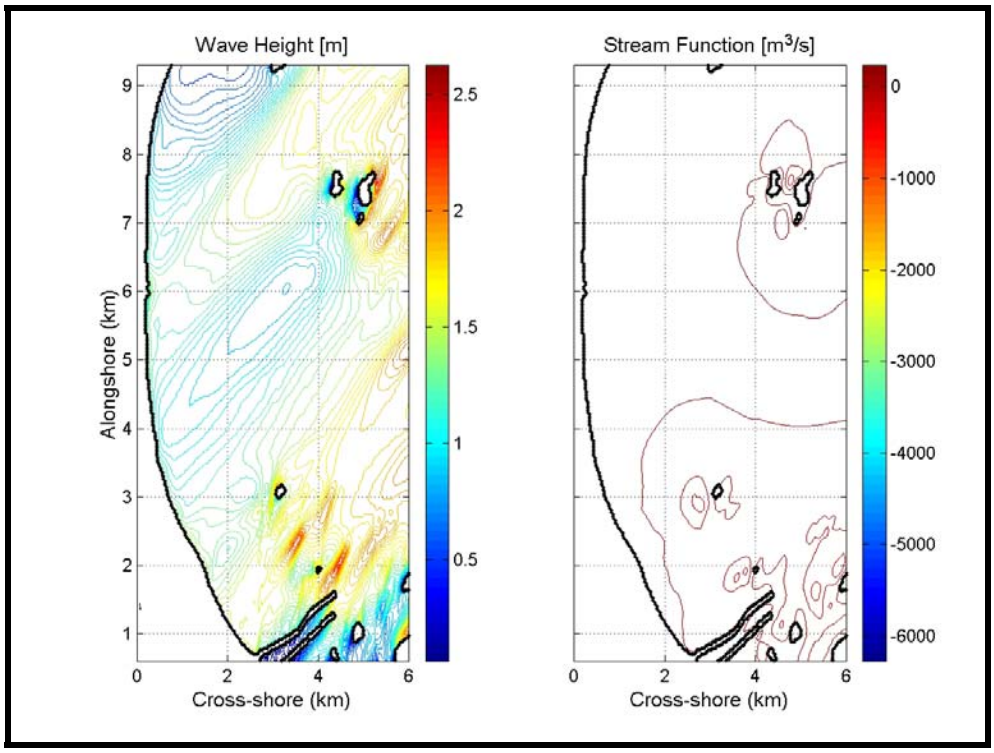

Figure 13-B3. Wave height and stream function for an east-northeast (75 to 90 degree) approach condition.

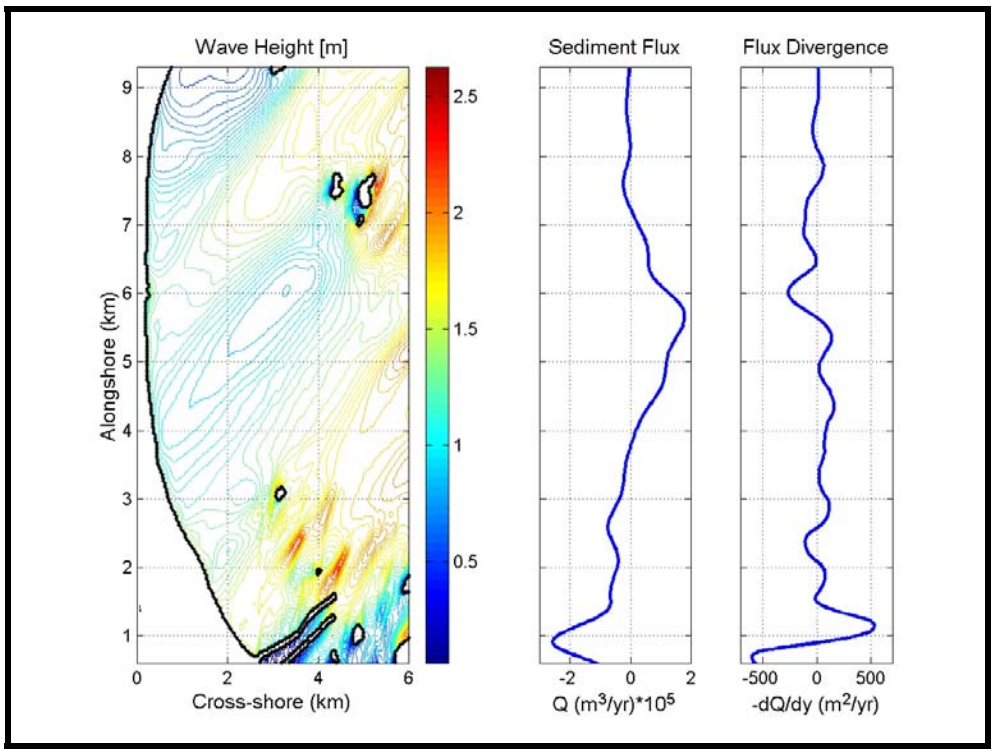

Figure 13-B4. Sediment flux and flux divergence for an east-northeast (75 to 90 degree) wave directional approach simulation.

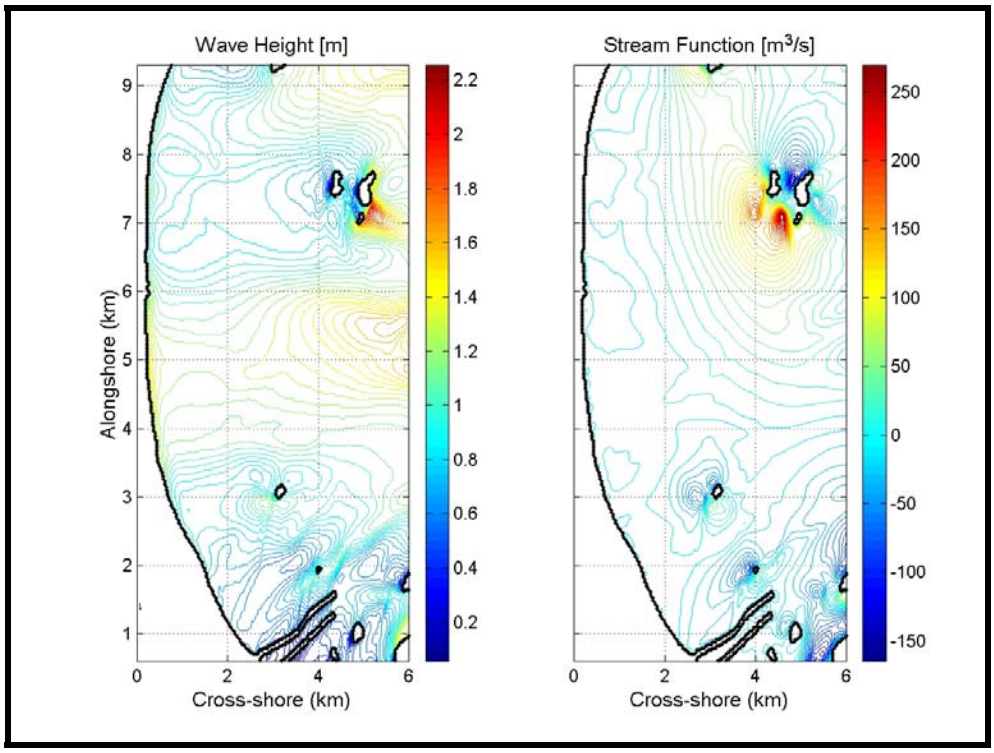

Figure 13-B5. Wave height and stream function for an east-southeast (110 to 130 degree) approach condition.

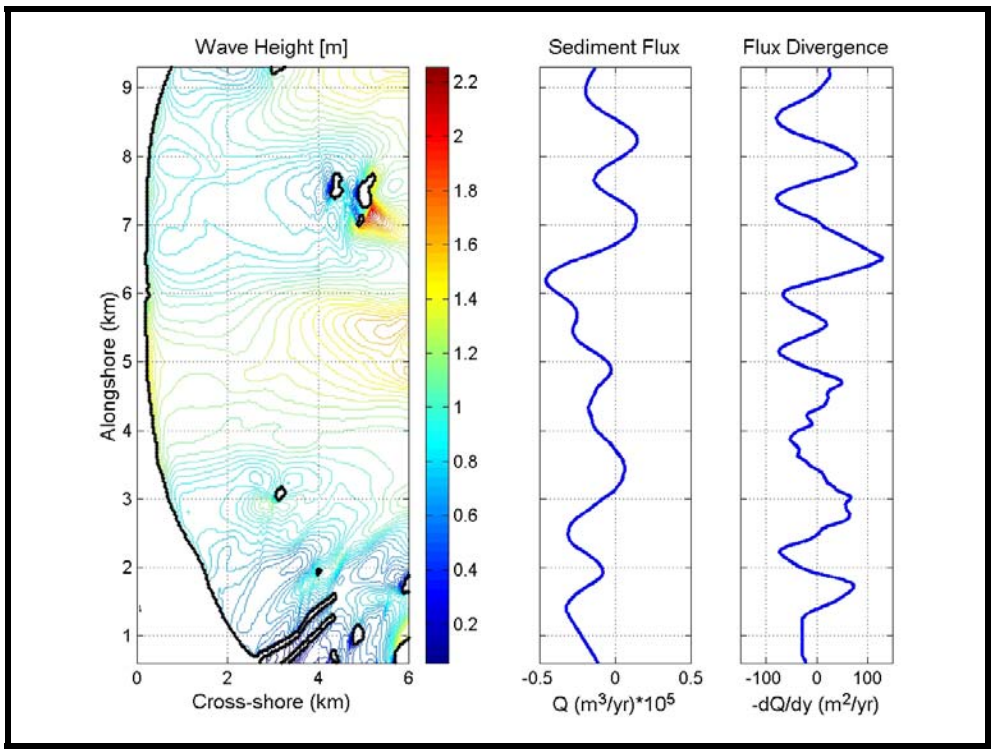

Figure 13-B6. Sediment flux and flux divergence for an east-southeast (110 to 130 degree) wave directional approach simulation.

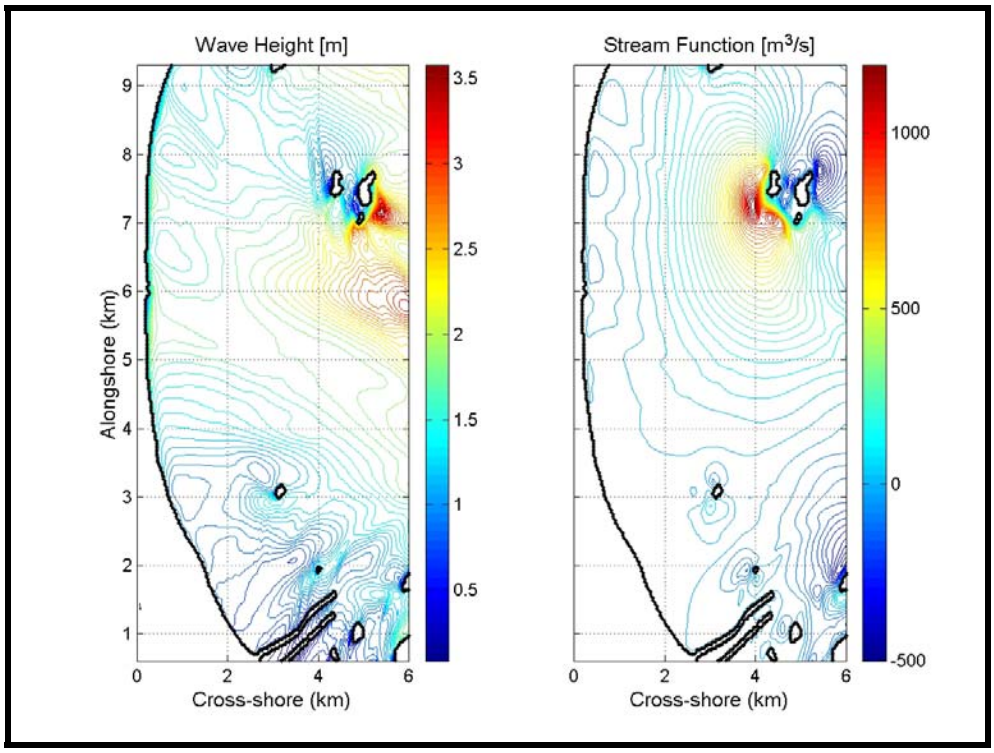

Figure 13-B7. Wave height and stream function for a southeast (130 to 150 degree) approach condition.

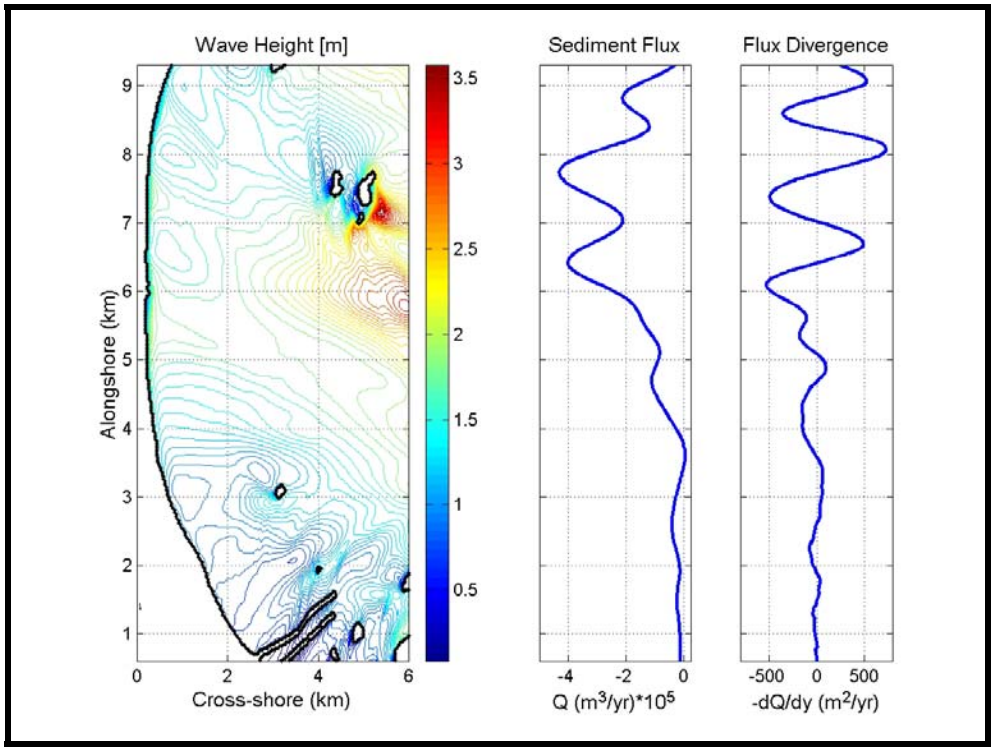

Figure 13-B8. Sediment flux and flux divergence for a southeast (130 to 150 degree) wave directional approach simulation.

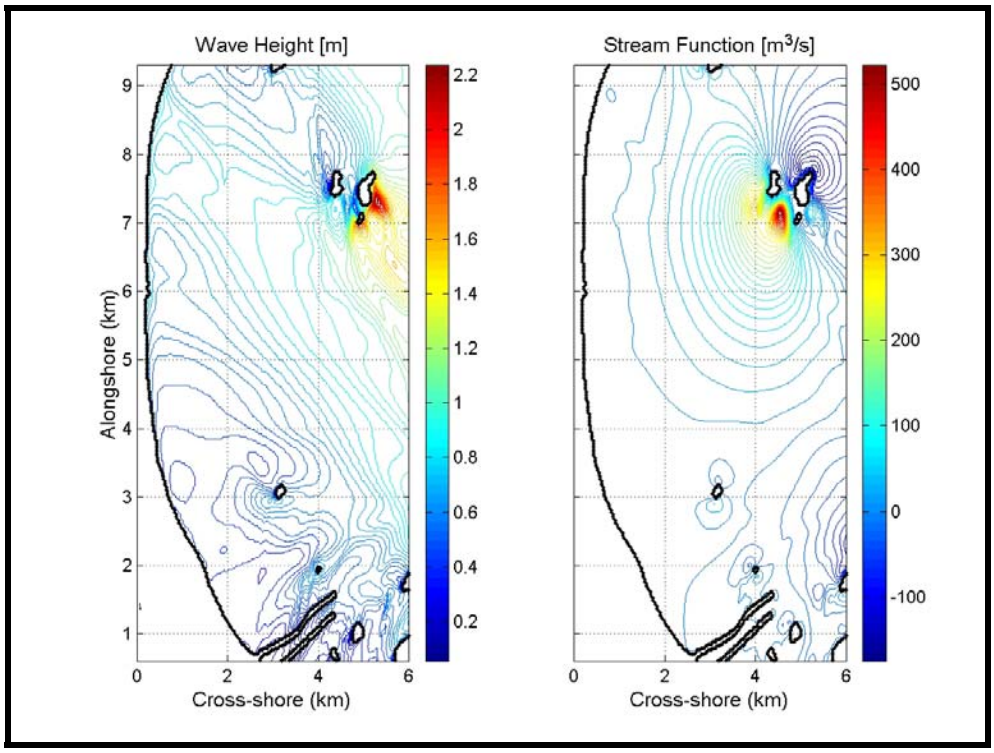

Figure 13-B9. Wave height and stream function for a south-southeast (150 to 165 degree) approach condition.

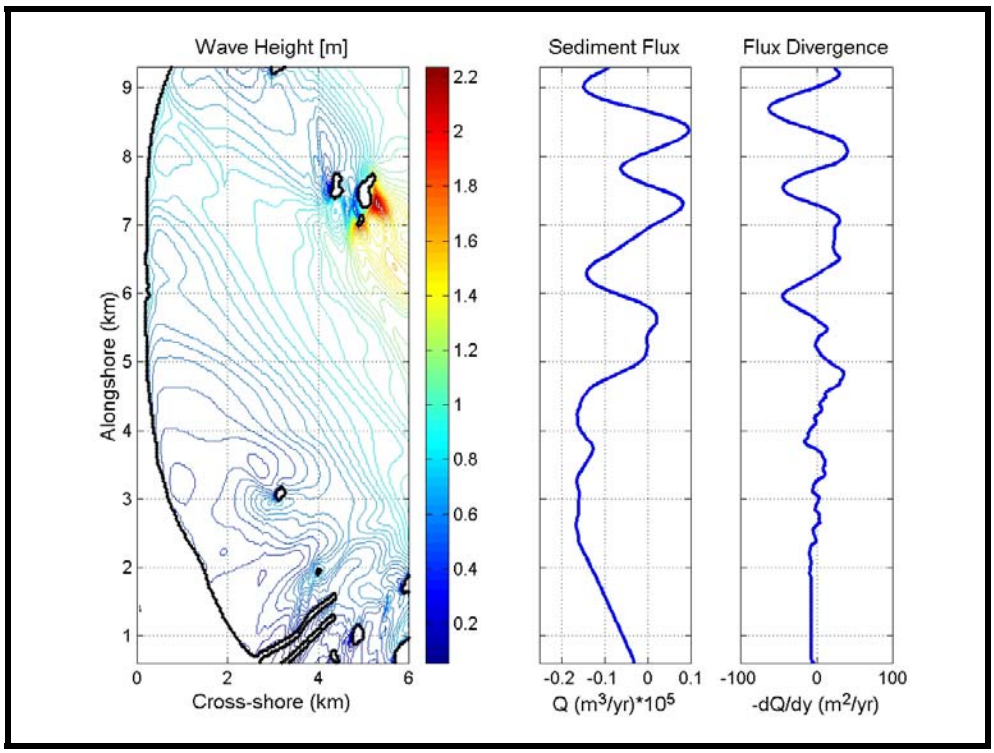

Figure 13-B10. Sediment flux and flux divergence for a south-southeast (150 to 165 degree) wave directional approach simulation.

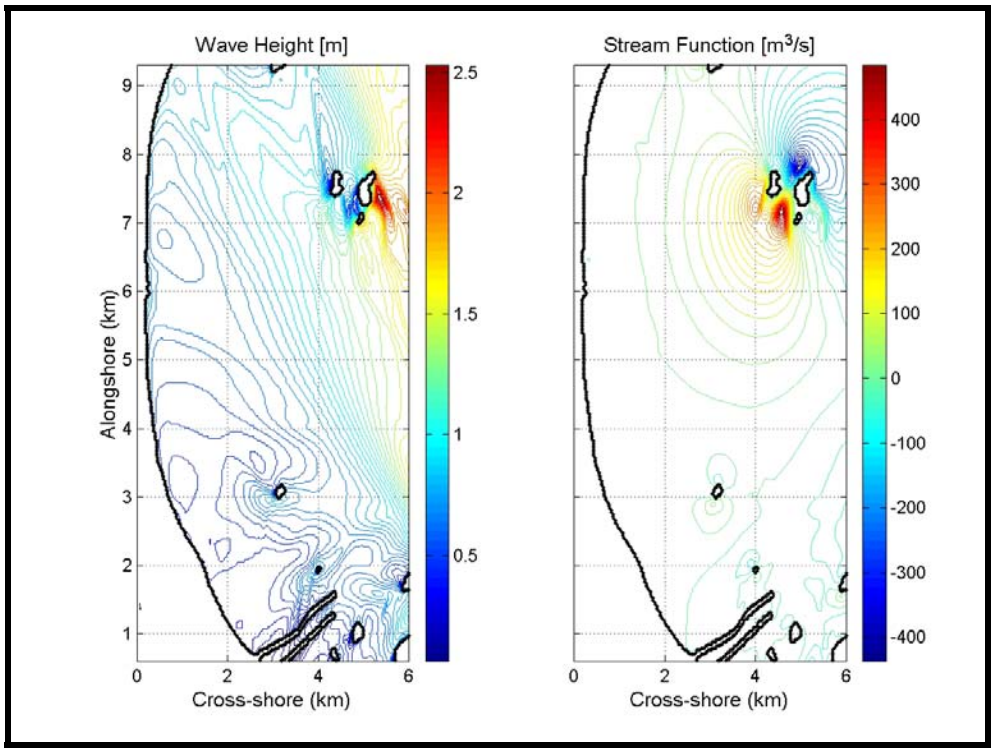

Figure 13-B11. Wave height and stream function for a south (165 to 185 degree) approach conditions.

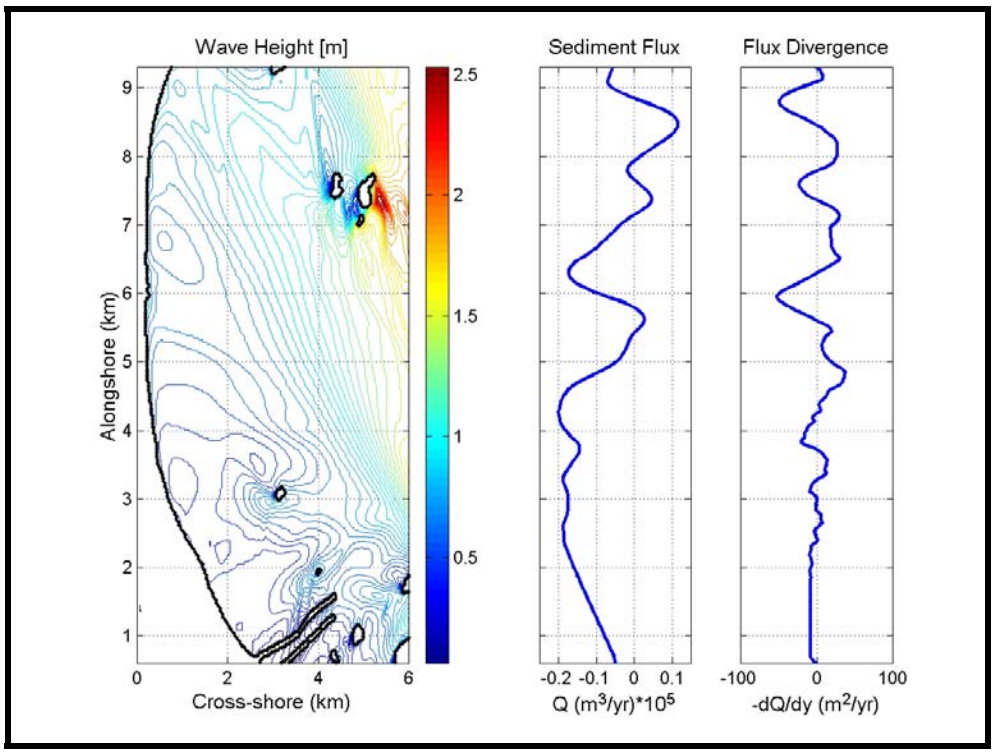

Figure 13-B12. Sediment flux and flux divergence for a south (165 to 185 degree) wave directional approach simulation.

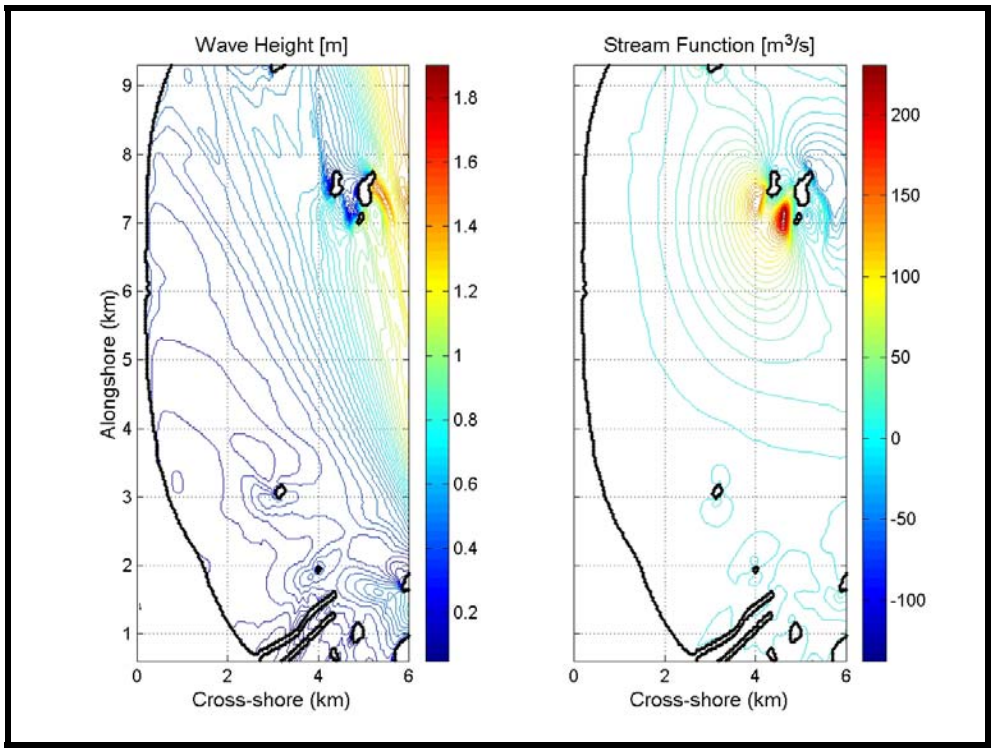

Figure 13-B13. Wave height and stream function for a south-southwest (185 to 210 degree) approach conditon.

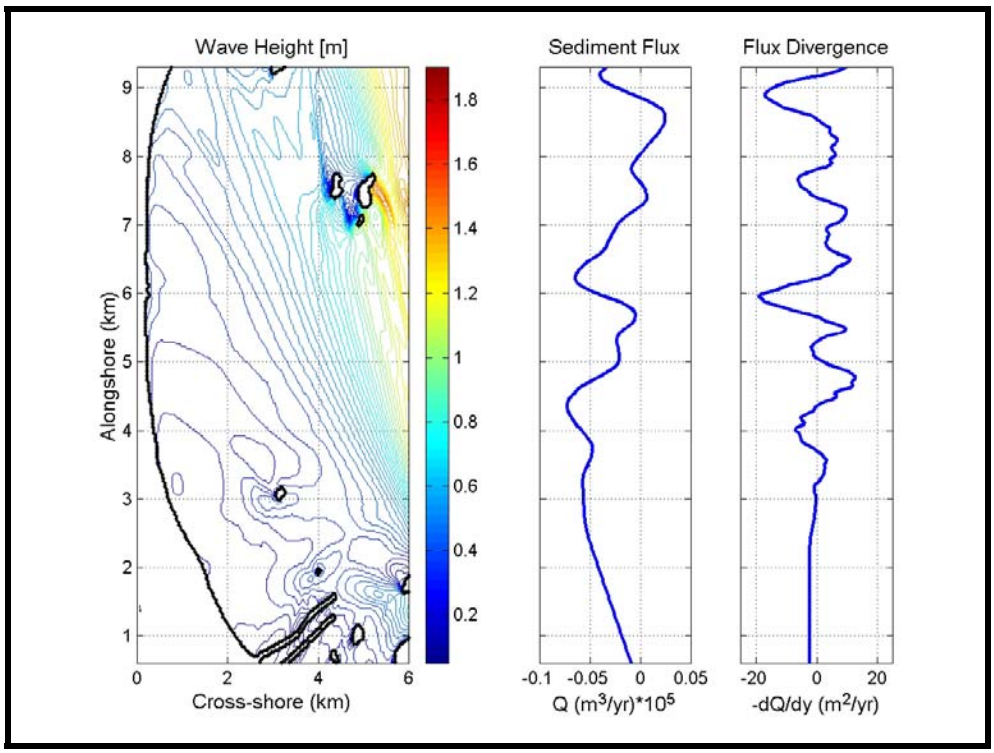

Figure 13-B14. Sediment flux and flux divergence for a south-southwest (185 to 210 degree) wave directional approach simulation.

APPENDIX 11-C

Appendix 11-C. Energy Changes in Camp Ellis Alternatives

Annual Eastern (90-110 degree) approach bin

Alt.	Description	Area	Existing		Alternative		% Change	
1	Jetty Extension Removal		Avg WH	Energy	Avg WH	Energy	% Energy	WH %
	Nearshore region from structure	A	1.17	1617.97	1.16	1605.57	-0.77	-0.85
	Nearshore region from A to erosion end	B	1.11	1475.78	1.14	1529.35	3.63	2.70
	Nearshore region - Ferry Beach	C	1.18	3381.22	1.18	3390.25	0.27	0.00
	Along Structure - Nearshore	D	1.47	2769.20	1.47	2777.89	0.31	0.00
	Along Structure - to first bend	E	1.69	6264.07	1.71	6343.65	1.27	1.18
	Along Structure - to second bend	F	1.44	2836.09	1.54	3253.91	14.73	6.94
	Along Structure - Jetty Extension	G	1.87	9668.63	1.92	10049.54	3.94	2.67
	Entrance Channel	H	1.25	3589.86	1.50	5126.87	42.82	20.00
	Offshore	I	1.27	19857.73	1.27	20037.78	0.91	0.00
2	Jetty Ext. Removal and Lowering		Avg WH	Energy	Avg WH	Energy	% Energy	WH %
	Nearshore region from structure	A	1.17	1617.97	1.22	1753.60	8.38	4.27
	Nearshore region from A to erosion end	B	1.11	1475.78	1.07	1290.64	-12.55	-3.60
	Nearshore region - Ferry Beach	C	1.18	3381.22	1.15	3213.69	-4.95	-2.54
	Along Structure - Nearshore	D	1.47	2769.20	1.41	2646.68	-4.42	-4.08
	Along Structure - to first bend	E	1.69	6264.07	1.57	5482.62	-12.48	-7.10
	Along Structure - to second bend	F	1.44	2836.09	1.40	2753.96	-2.90	-2.78
	Along Structure - Jetty Extension	G	1.87	9668.63	1.91	10026.55	3.70	2.14
	Entrance Channel	H	1.25	3589.86	1.50	5127.69	42.84	20.00
	Offshore	I	1.27	19857.73	1.23	18676.95	-5.95	-3.15
3	750' Spur at offshore location, straight		Avg WH	Energy	Avg WH	Energy	% Energy	WH %
	Nearshore region from structure	A	1.17	1617.97	1.10	1468.94	-9.21	-5.98
	Nearshore region from A to erosion end	B	1.11	1475.78	1.10	1343.63	-8.95	-0.90
	Nearshore region - Ferry Beach	C	1.18	3381.22	1.18	3341.00	-1.19	0.00
	Along Structure - Nearshore	D	1.47	2769.20	1.33	2270.30	-18.02	-9.52
	Along Structure - to first bend	E	1.69	6264.07	1.63	6117.69	-2.34	-3.55
	Along Structure - to second bend	F	1.44	2836.09	1.57	3420.60	20.61	9.03
	Along Structure - Jetty Extension	G	1.87	9668.63	1.90	9973.76	3.16	1.60
	Entrance Channel	H	1.25	3589.86	1.26	3617.85	0.78	0.80
	Offshore	I	1.27	19857.73	1.25	19648.85	-1.05	-1.57
4	500' Spur at inshore location, straight		Avg WH	Energy	Avg WH	Energy	% Energy	WH %
	Nearshore region from structure	A	1.17	1617.97	1.10	1497.02	-7.48	-5.98
	Nearshore region from A to erosion end	B	1.11	1475.78	1.10	1410.65	-4.41	-0.90
	Nearshore region - Ferry Beach	C	1.18	3381.22	1.20	3502.93	3.60	1.69
	Along Structure - Nearshore	D	1.47	2769.20	1.21	1921.52	-30.61	-17.69
	Along Structure - to first bend	E	1.69	6264.07	1.78	7008.33	11.88	5.33
	Along Structure - to second bend	F	1.44	2836.09	1.51	3142.83	10.82	4.86
	Along Structure - Jetty Extension	G	1.87	9668.63	1.89	9859.29	1.97	1.07
	Entrance Channel	H	1.25	3589.86	1.26	3633.04	1.20	0.80
	Offshore	I	1.27	19857.73	1.26	19886.39	0.14	-0.79
5	Dual 500' Spurs		Avg WH	Energy	Avg WH	Energy	% Energy	WH %
	Nearshore region from structure	A	1.17	1617.97	1.09	1430.69	-11.57	-6.84
	Nearshore region from A to erosion end	B	1.11	1475.78	1.10	1381.15	-6.41	-0.90
	Nearshore region - Ferry Beach	C	1.18	3381.22	1.19	3492.46	3.29	0.85
	Along Structure - Nearshore	D	1.47	2769.20	1.18	1807.43	-34.73	-19.73
	Along Structure - to first bend	E	1.69	6264.07	1.70	6356.48	1.48	0.59
	Along Structure - to second bend	F	1.44	2836.09	1.31	2439.12	-14.00	-9.03
	Along Structure - Jetty Extension	G	1.87	9668.63	1.92	10357.69	7.13	2.67
	Entrance Channel	H	1.25	3589.86	1.33	4089.03	13.90	6.40
	Offshore	I	1.27	19857.73	1.30	20937.66	5.44	2.36

6	750' Spur at inshore location, straight		Avg WH	Energy	Avg WH	Energy	% Energy	WH %
	Nearshore region from structure	A	1.17	1617.97	1.05	1335.81	-17.44	-10.26
	Nearshore region from A to erosion end	B	1.11	1475.78	1.11	1399.64	-5.16	0.00
	Nearshore region - Ferry Beach	C	1.18	3381.22	1.15	3211.49	-5.02	-2.54
	Along Structure - Nearshore	D	1.47	2769.20	1.00	1318.22	-52.40	-31.97
	Along Structure - to first bend	E	1.69	6264.07	1.80	7242.38	15.62	6.51
	Along Structure - to second bend	F	1.44	2836.09	1.52	3193.90	12.62	5.56
	Along Structure - Jetty Extension	G	1.87	9668.63	1.89	9866.65	2.05	1.07
	Entrance Channel	H	1.25	3589.86	1.26	3633.79	1.22	0.80
	Offshore	I	1.27	19857.73	1.25	19457.19	-2.02	-1.57
7	750' Spur at inshore location, straight with Jetty Ext. Removal		Avg WH	Energy	Avg WH	Energy	% Energy	WH %
	Nearshore region from structure	A	1.17	1617.97	1.04	1312.08	-18.91	-11.11
	Nearshore region from A to erosion end	B	1.11	1475.78	1.11	1403.06	-4.93	0.00
	Nearshore region - Ferry Beach	C	1.18	3381.22	1.15	3237.25	-4.26	-2.54
	Along Structure - Nearshore	D	1.47	2769.20	0.97	1246.82	-54.98	-34.01
	Along Structure - to first bend	E	1.69	6264.07	1.79	7275.95	16.15	5.92
	Along Structure - to second bend	F	1.44	2836.09	1.56	3345.96	17.98	8.33
	Along Structure - Jetty Extension	G	1.87	9668.63	1.92	10105.64	4.52	2.67
	Entrance Channel	H	1.25	3589.86	1.37	4290.34	19.51	9.60
	Offshore	I	1.27	19857.73	1.25	19431.90	-2.14	-1.57
8	750' Spur at inshore location, straight with Terminal Groin		Avg WH	Energy	Avg WH	Energy	% Energy	WH %
	Nearshore region from structure	A	1.17	1617.97	1.05	1333.51	-17.58	-10.26
	Nearshore region from A to erosion end	B	1.11	1475.78	1.11	1412.71	-4.27	0.00
	Nearshore region - Ferry Beach	C	1.18	3381.22	1.15	3227.84	-4.54	-2.54
	Along Structure - Nearshore	D	1.47	2769.20	1.00	1315.47	-52.50	-31.97
	Along Structure - to first bend	E	1.69	6264.07	1.80	7259.66	15.89	6.51
	Along Structure - to second bend	F	1.44	2836.09	1.52	3218.59	13.49	5.56
	Along Structure - Jetty Extension	G	1.87	9668.63	1.90	9920.18	2.60	1.60
	Entrance Channel	H	1.25	3589.86	1.27	3646.77	1.59	1.60
	Offshore	I	1.27	19857.73	1.25	19557.66	-1.51	-1.57
9	T-Heads, 1st Configuration		Avg WH	Energy	Avg WH	Energy	% Energy	WH %
	Nearshore region from structure	A	1.17	1617.97	1.02	1406.62	-13.06	-12.82
	Nearshore region from A to erosion end	B	1.11	1475.78	1.05	1462.80	-0.88	-5.41
	Nearshore region - Ferry Beach	C	1.18	3381.22	1.19	3415.55	1.02	0.85
	Along Structure - Nearshore	D	1.47	2769.20	1.48	2803.14	1.23	0.68
	Along Structure - to first bend	E	1.69	6264.07	1.69	6319.70	0.89	0.00
	Along Structure - to second bend	F	1.44	2836.09	1.44	2858.04	0.77	0.00
	Along Structure - Jetty Extension	G	1.87	9668.63	1.88	9699.20	0.32	0.53
	Entrance Channel	H	1.25	3589.86	1.25	3598.26	0.23	0.00
	Offshore	I	1.27	19857.73	1.28	20205.92	1.75	0.79
10	T-Heads, 2nd Configuration		Avg WH	Energy	Avg WH	Energy	% Energy	WH %
	Nearshore region from structure	A	1.17	1617.97	1.09	1586.43	-1.95	-6.84
	Nearshore region from A to erosion end	B	1.11	1475.78	1.07	1503.86	1.90	-3.60
	Nearshore region - Ferry Beach	C	1.18	3381.22	1.16	3464.85	2.47	-1.69
	Along Structure - Nearshore	D	1.47	2769.20	1.49	2877.33	3.90	1.36
	Along Structure - to first bend	E	1.69	6264.07	1.70	6442.91	2.85	0.59
	Along Structure - to second bend	F	1.44	2836.09	1.45	2893.40	2.02	0.69
	Along Structure - Jetty Extension	G	1.87	9668.63	1.88	9731.17	0.65	0.53
	Entrance Channel	H	1.25	3589.86	1.26	3637.23	1.32	0.80
	Offshore	I	1.27	19857.73	1.28	20327.02	2.36	0.79

11	Breakwater, Offshore Location		Avg WH	Energy	Avg WH	Energy	% Energy	WH %
	Nearshore region from structure	A	1.17	1617.97	1.18	1633.88	0.98	0.85
	Nearshore region from A to erosion end	B	1.11	1475.78	0.96	1058.26	-28.29	-13.51
	Nearshore region - Ferry Beach	C	1.18	3381.22	1.16	3211.84	-5.01	-1.69
	Along Structure - Nearshore	D	1.47	2769.20	1.46	2763.89	-0.19	-0.68
	Along Structure - to first bend	E	1.69	6264.07	1.44	4441.30	-29.10	-14.79
	Along Structure - to second bend	F	1.44	2836.09	1.38	2599.72	-8.33	-4.17
	Along Structure - Jetty Extension	G	1.87	9668.63	1.87	9613.30	-0.57	0.00
	Entrance Channel	H	1.25	3589.86	1.25	3559.85	-0.84	0.00
	Offshore	I	1.27	19857.73	1.15	16356.55	-17.63	-9.45
11a	Breakwater, Nearshore Location		Avg WH	Energy	Avg WH	Energy	% Energy	WH %
	Nearshore region from structure	A	1.17	1617.97	1.09	1419.33	-12.28	-6.84
	Nearshore region from A to erosion end	B	1.11	1475.78	0.78	706.64	-52.12	-29.73
	Nearshore region - Ferry Beach	C	1.18	3381.22	1.16	3298.00	-2.46	-1.69
	Along Structure - Nearshore	D	1.47	2769.20	1.49	2877.75	3.92	1.36
	Along Structure - to first bend	E	1.69	6264.07	1.69	6371.58	1.72	0.00
	Along Structure - to second bend	F	1.44	2836.09	1.44	2874.94	1.37	0.00
	Along Structure - Jetty Extension	G	1.87	9668.63	1.88	9786.75	1.22	0.53
	Entrance Channel	H	1.25	3589.86	1.26	3625.88	1.00	0.80
	Offshore	I	1.27	19857.73	1.29	20990.31	5.70	1.57
11b	Breakwater, Middle Location		Avg WH	Energy	Avg WH	Energy	% Energy	WH %
	Nearshore region from structure	A	1.17	1617.97	1.21	1720.27	6.32	3.42
	Nearshore region from A to erosion end	B	1.11	1475.78	0.94	1019.38	-30.93	-15.32
	Nearshore region - Ferry Beach	C	1.18	3381.22	1.18	3363.16	-0.53	0.00
	Along Structure - Nearshore	D	1.47	2769.20	1.44	2670.26	-3.57	-2.04
	Along Structure - to first bend	E	1.69	6264.07	1.52	5132.83	-18.06	-10.06
	Along Structure - to second bend	F	1.44	2836.09	1.42	2767.69	-2.41	-1.39
	Along Structure - Jetty Extension	G	1.87	9668.63	1.86	9562.50	-1.10	-0.53
	Entrance Channel	H	1.25	3589.86	1.26	3607.57	0.49	0.80
	Offshore	I	1.27	19857.73	1.14	17094.75	-13.91	-10.24
12	Breakwater, Nearshore Location and 500' Spur at Offshore Location		Avg WH	Energy	Avg WH	Energy	% Energy	WH %
	Nearshore region from structure	A	1.17	1617.97	1.09	1410.38	-12.83	-6.84
	Nearshore region from A to erosion end	B	1.11	1475.78	0.76	651.52	-55.85	-31.53
	Nearshore region - Ferry Beach	C	1.18	3381.22	1.13	3091.69	-8.56	-4.24
	Along Structure - Nearshore	D	1.47	2769.20	1.48	2814.68	1.64	0.68
	Along Structure - to first bend	E	1.69	6264.07	1.67	6329.36	1.04	-1.18
	Along Structure - to second bend	F	1.44	2836.09	1.51	3156.23	11.29	4.86
	Along Structure - Jetty Extension	G	1.87	9668.63	1.90	9966.21	3.08	1.60
	Entrance Channel	H	1.25	3589.86	1.27	3681.53	2.55	1.60
	Offshore	I	1.27	19857.73	1.27	20725.49	4.37	0.00
13	Comb Spur Groins		Avg WH	Energy	Avg WH	Energy	% Energy	WH %
	Nearshore region from structure	A	1.17	1617.97	1.08	1443.49	-10.78	-7.69
	Nearshore region from A to erosion end	B	1.11	1475.78	1.06	1320.47	-10.52	-4.50
	Nearshore region - Ferry Beach	C	1.18	3381.22	1.16	3260.38	-3.57	-1.69
	Along Structure - Nearshore	D	1.47	2769.20	1.40	2621.26	-5.34	-4.76
	Along Structure - to first bend	E	1.69	6264.07	1.62	5937.90	-5.21	-4.14
	Along Structure - to second bend	F	1.44	2836.09	1.34	2601.69	-8.26	-6.94
	Along Structure - Jetty Extension	G	1.87	9668.63	1.87	9699.19	0.32	0.00
	Entrance Channel	H	1.25	3589.86	1.26	3604.62	0.41	0.80
	Offshore	I	1.27	19857.73	1.25	19351.34	-2.55	-1.57
14	Offshore Borrow Location		Avg WH	Energy	Avg WH	Energy	% Energy	WH %
	Nearshore region from structure	A	1.17	1617.97	1.17	1629.66	0.72	0.00
	Nearshore region from A to erosion end	B	1.11	1475.78	1.10	1428.31	-3.22	-0.90
	Nearshore region - Ferry Beach	C	1.18	3381.22	1.18	3375.72	-0.16	0.00
	Along Structure - Nearshore	D	1.47	2769.20	1.46	2740.91	-1.02	-0.68
	Along Structure - to first bend	E	1.69	6264.07	1.69	6291.28	0.43	0.00
	Along Structure - to second bend	F	1.44	2836.09	1.42	2778.73	-2.02	-1.39
	Along Structure - Jetty Extension	G	1.87	9668.63	1.87	9623.88	-0.46	0.00
	Entrance Channel	H	1.25	3589.86	1.25	3578.33	-0.32	0.00
	Offshore	I	1.27	19857.73	1.26	19832.21	-0.13	-0.79

15	750' Spur at offshore location, angled		Avg WH	Energy	Avg WH	Energy	% Energy	WH %
	Nearshore region from structure	A	1.17	1617.97	1.10	1471.79	-9.03	-5.98
	Nearshore region from A to erosion end	B	1.11	1475.78	1.09	1353.90	-8.26	-1.80
	Nearshore region - Ferry Beach	C	1.18	3381.22	1.16	3294.05	-2.58	-1.69
	Along Structure - Nearshore	D	1.47	2769.20	1.21	1867.50	-32.56	-17.69
	Along Structure - to first bend	E	1.69	6264.07	1.61	6303.87	0.64	-4.73
	Along Structure - to second bend	F	1.44	2836.09	1.57	3462.67	22.09	9.03
	Along Structure - Jetty Extension	G	1.87	9668.63	1.92	10189.60	5.39	2.67
	Entrance Channel	H	1.25	3589.86	1.28	3759.22	4.72	2.40
	Offshore	I	1.27	19857.73	1.25	19593.22	-1.33	-1.57
16	Jetty Roughening		Avg WH	Energy	Avg WH	Energy	% Energy	WH %
	Nearshore region from structure	A	1.17	1617.97	1.08	1426.50	-11.83	-7.69
	Nearshore region from A to erosion end	B	1.11	1475.78	1.05	1275.96	-13.54	-5.41
	Nearshore region - Ferry Beach	C	1.18	3381.22	1.15	3210.26	-5.06	-2.54
	Along Structure - Nearshore	D	1.47	2769.20	1.26	2204.29	-20.40	-14.29
	Along Structure - to first bend	E	1.69	6264.07	1.49	5122.72	-18.22	-11.83
	Along Structure - to second bend	F	1.44	2836.09	1.34	2500.76	-11.82	-6.94
	Along Structure - Jetty Extension	G	1.87	9668.63	1.87	9647.12	-0.22	0.00
	Entrance Channel	H	1.25	3589.86	1.26	3611.62	0.61	0.80
	Offshore	I	1.27	19857.73	1.22	18376.15	-7.46	-3.94
17	Submerged Breakwater		Avg WH	Energy	Avg WH	Energy	% Energy	WH %
	Nearshore region from structure	A	1.17	1617.97	1.17	1646.32	1.75	0.00
	Nearshore region from A to erosion end	B	1.11	1475.78	1.09	1420.38	-3.75	-1.80
	Nearshore region - Ferry Beach	C	1.18	3381.22	1.19	3417.44	1.07	0.85
	Along Structure - Nearshore	D	1.47	2769.20	1.49	2862.69	3.38	1.36
	Along Structure - to first bend	E	1.69	6264.07	1.64	5933.71	-5.27	-2.96
	Along Structure - to second bend	F	1.44	2836.09	1.41	2730.17	-3.73	-2.08
	Along Structure - Jetty Extension	G	1.87	9668.63	1.87	9611.64	-0.59	0.00
	Entrance Channel	H	1.25	3589.86	1.26	3596.35	0.18	0.80
	Offshore	I	1.27	19857.73	1.23	18830.74	-5.17	-3.15
18	Breakwater, Nearshore Location with 500' straight spur at inshore location		Avg WH	Energy	Avg WH	Energy	% Energy	WH %
	Nearshore region from structure	A	1.17	1617.97	0.99	1186.01	-26.70	-15.38
	Nearshore region from A to erosion end	B	1.11	1475.78	0.74	644.91	-56.30	-33.33
	Nearshore region - Ferry Beach	C	1.18	3381.22	1.16	3264.09	-3.46	-1.69
	Along Structure - Nearshore	D	1.47	2769.20	1.21	1940.69	-29.92	-17.69
	Along Structure - to first bend	E	1.69	6264.07	1.77	7007.52	11.87	4.73
	Along Structure - to second bend	F	1.44	2836.09	1.51	3160.85	11.45	4.86
	Along Structure - Jetty Extension	G	1.87	9668.63	1.90	9954.83	2.96	1.60
	Entrance Channel	H	1.25	3589.86	1.27	3649.59	1.66	1.60
	Offshore	I	1.27	19857.73	1.28	21040.80	5.96	0.79
19	750' Spur with Jetty Roughening from spur to bend and partial ext. removal		Avg WH	Energy	Avg WH	Energy	% Energy	WH %
	Nearshore region from structure	A	1.17	1617.97	1.03	1296.44	-19.87	-11.97
	Nearshore region from A to erosion end	B	1.11	1475.78	1.09	1344.18	-8.92	-1.80
	Nearshore region - Ferry Beach	C	1.18	3381.22	1.14	3176.85	-6.04	-3.39
	Along Structure - Nearshore	D	1.47	2769.20	0.94	1173.35	-57.63	-36.05
	Along Structure - to first bend	E	1.69	6264.07	1.66	6230.22	-0.54	-1.78
	Along Structure - to second bend	F	1.44	2836.09	1.46	2943.93	3.80	1.39
	Along Structure - Jetty Extension	G	1.87	9668.63	1.90	9924.89	2.65	1.60
	Entrance Channel	H	1.25	3589.86	1.35	4122.11	14.83	8.00
	Offshore	I	1.27	19857.73	1.22	18505.48	-6.81	-3.94
20	Case 11a with a salient formation		Avg WH	Energy	Avg WH	Energy	% Energy	WH %
	Nearshore region from structure	A	1.17	1617.97	1.09	1404.62	-13.19	-6.84
	Nearshore region from A to erosion end	B	1.11	1475.78	0.67	526.88	-64.3	-39.64
	Nearshore region - Ferry Beach	C	1.18	3381.22	1.1	2920.44	-13.63	-6.78
	Along Structure - Nearshore	D	1.47	2769.2	1.49	2866.4	3.51	1.36
	Along Structure - to first bend	E	1.69	6264.07	1.69	6383.04	1.9	0.00
	Along Structure - to second bend	F	1.44	2836.09	1.45	2885.26	1.73	0.69
	Along Structure - Jetty Extension	G	1.87	9668.63	1.88	9800.45	1.36	0.53
	Entrance Channel	H	1.25	3589.86	1.26	3629.09	1.09	0.80
	Offshore	I	1.27	19857.73	1.28	20881.62	5.16	0.79
21	Case 11a with partial salient formation		Avg WH	Energy	Avg WH	Energy	% Energy	WH %
	Nearshore region from structure	A	1.17	1617.97	1.09	1421.06	-12.17	-6.84
	Nearshore region from A to erosion end	B	1.11	1475.78	0.78	697.83	-52.71	-29.73
	Nearshore region - Ferry Beach	C	1.18	3381.22	1.15	3248.99	-3.91	-2.54
	Along Structure - Nearshore	D	1.47	2769.2	1.49	2890.67	4.39	1.36
	Along Structure - to first bend	E	1.69	6264.07	1.69	6387.92	1.98	0.00
	Along Structure - to second bend	F	1.44	2836.09	1.44	2881.82	1.61	0.00
	Along Structure - Jetty Extension	G	1.87	9668.63	1.88	9798.57	1.34	0.53
	Entrance Channel	H	1.25	3589.86	1.27	3635.23	1.26	1.60
	Offshore	I	1.27	19857.73	1.29	21085.43	6.18	1.57

22	750' Spur with Segmented BW (2)		Avg WH	Energy	Avg WH	Energy	% Energy	WH %
	Nearshore region from structure	A	1.17	1617.97	0.87	899.19	-44.42	-25.64
	Nearshore region from A to erosion end	B	1.11	1475.78	1.09	1325.47	-10.19	-1.80
	Inshore region of area B	B2	1.1	622.77	1.09	596.4268	-4.23	-0.91
	Nearshore region - Ferry Beach	C	1.18	3381.22	1.16	3252.22	-3.82	-1.69
	Along Structure - Nearshore	D	1.47	2769.2	0.94	1203.24	-56.55	-36.05
	Along Structure - to first bend	E	1.69	6264.07	1.81	7306.9	16.65	7.10
	Along Structure - to second bend	F	1.44	2836.09	1.53	3237.09	14.14	6.25
	Along Structure - Jetty Extension	G	1.87	9668.63	1.9	9957.5	2.99	1.60
	Entrance Channel	H	1.25	3589.86	1.27	3654.75	1.81	1.60
	Offshore	I	1.27	19857.73	1.27	20330.36	2.38	0.00
23	500' Spur with Segmented BW (3)		Avg WH	Energy	Avg WH	Energy	% Energy	WH %
	Nearshore region from structure	A	1.17	1617.97	0.85	891.5	-44.90	-27.35
	Nearshore region from A to erosion end	B	1.11	1475.78	1.05	1251.04	-15.23	-5.41
	Inshore region of area B	B2	1.1	622.77	1.09	583.4	-6.32	-0.91
	Nearshore region - Ferry Beach	C	1.18	3381.22	1.2	3491.54	3.26	1.69
	Along Structure - Nearshore	D	1.47	2769.2	1.11	1716.94	-38.00	-24.49
	Along Structure - to first bend	E	1.69	6264.07	1.79	7087.69	13.15	5.92
	Along Structure - to second bend	F	1.44	2836.09	1.51	3181.2	12.17	4.86
	Along Structure - Jetty Extension	G	1.87	9668.63	1.9	9932.63	2.73	1.60
	Entrance Channel	H	1.25	3589.86	1.27	3656.09	1.85	1.60
	Offshore	I	1.27	19857.73	1.29	20926.96	5.38	1.57
24	Alt. 23 with additional northern BW		Avg WH	Energy	Avg WH	Energy	% Energy	WH %
	Nearshore region from structure	A	1.17	1617.97	0.86	896.24	-44.61	-26.50
	Nearshore region from A to erosion end	B	1.11	1475.78	0.97	1171.37	-20.63	-12.61
	Inshore region of area B	B2	1.1	622.77	0.84	348.82	-43.99	-23.64
	Nearshore region - Ferry Beach	C	1.18	3381.22	1.21	3547.47	4.92	2.54
	Along Structure - Nearshore	D	1.47	2769.2	1.11	1711.06	-38.21	-24.49
	Along Structure - to first bend	E	1.69	6264.07	1.79	7083.37	13.08	5.92
	Along Structure - to second bend	F	1.44	2836.09	1.51	3177.74	12.05	4.86
	Along Structure - Jetty Extension	G	1.87	9668.63	1.89	9895.67	2.35	1.07
	Entrance Channel	H	1.25	3589.86	1.27	3643.11	1.48	1.60
	Offshore	I	1.27	19857.73	1.3	21122.41	6.37	2.36
25	Spur moved landward and 3 BW		Avg WH	Energy	Avg WH	Energy	% Energy	WH %
	Nearshore region from structure	A	1.17	1617.97	0.84	867.77	-46.37	-28.21
	Nearshore region from A to erosion end	B	1.11	1475.78	0.97	1213.69	-17.76	-12.61
	Inshore region of area B	B2	1.1	622.77	0.77	310.42	-50.16	-30.00
	Nearshore region - Ferry Beach	C	1.18	3381.22	1.2	3500.14	3.52	1.69
	Along Structure - Nearshore	D	1.47	2769.2	1.23	2370.35	-14.4	-16.33
	Along Structure - to first bend	E	1.69	6264.07	1.75	6780.83	8.25	3.55
	Along Structure - to second bend	F	1.44	2836.09	1.49	3075.69	8.45	3.47
	Along Structure - Jetty Extension	G	1.87	9668.63	1.9	9938.53	2.79	1.60
	Entrance Channel	H	1.25	3589.86	1.27	3658.37	1.91	1.60
	Offshore	I	1.27	19857.73	1.3	21151.58	6.52	2.36
26	Case 24 with add. longer northern BW		Avg WH	Energy	Avg WH	Energy	% Energy	WH %
	Nearshore region from structure	A	1.17	1617.97	0.85	892.42	-44.84	-27.35
	Nearshore region from A to erosion end	B	1.11	1475.78	0.95	1166.39	-20.96	-14.41
	Inshore region of area B	B2	1.1	622.77	0.75	293.62	-52.85	-31.82
	Nearshore region - Ferry Beach	C	1.18	3381.22	1.21	3524.65	4.24	2.54
	Along Structure - Nearshore	D	1.47	2769.2	1.11	1727.43	-37.62	-24.49
	Along Structure - to first bend	E	1.69	6264.07	1.78	7048.76	12.53	5.33
	Along Structure - to second bend	F	1.44	2836.09	1.51	3157.93	11.35	4.86
	Along Structure - Jetty Extension	G	1.87	9668.63	1.89	9896.74	2.36	1.07
	Entrance Channel	H	1.25	3589.86	1.27	3652.77	1.75	1.60
	Offshore	I	1.27	19857.73	1.3	21110.64	6.31	2.36
Positive Value = Increase ; Negative Value = Decrease								
WH = Wave Height in Meters, Energy in Meters Squared								

Appendix 11-C. Energy Changes in Camp Ellis Alternatives

10 Year Storm

Alt.	Description	Area	Existing		Alternative		% Change	
1	Jetty Extension Removal		Avg WH	Energy	Avg WH	Energy	% Energy	WH %
	Nearshore region from structure	A	1.93	4360.84	1.98	4626.02	6.08	2.59
	Nearshore region from A to erosion end	B	2.11	4899.04	2.14	5078.01	3.65	1.42
	Nearshore region - Ferry Beach	C	1.81	7635.26	1.83	7878.10	3.18	1.10
	Along Structure - Nearshore	D	2.30	6690.00	2.42	7350.45	9.87	5.22
	Along Structure - to first bend	E	2.20	10517.06	2.28	11201.76	6.51	3.64
	Along Structure - to second bend	F	1.50	3352.42	1.56	3707.18	10.58	4.00
	Along Structure - Jetty Extension	G	1.69	8167.80	1.71	8373.25	2.52	1.18
	Entrance Channel	H	2.24	11600.55	2.38	13004.02	12.10	6.25
	Offshore	I	2.30	63712.47	2.31	64051.60	0.53	0.43
2	Jetty Ext. Removal and Lowering		Avg WH	Energy	Avg WH	Energy	% Energy	WH %
	Nearshore region from structure	A	1.93	4360.84	1.89	4190.59	-3.90	-2.07
	Nearshore region from A to erosion end	B	2.11	4899.04	2.11	4937.67	0.79	0.00
	Nearshore region - Ferry Beach	C	1.81	7635.26	1.81	7663.71	0.37	0.00
	Along Structure - Nearshore	D	2.30	6690.00	2.38	7042.80	5.27	3.48
	Along Structure - to first bend	E	2.20	10517.06	2.02	8941.57	-14.98	-8.18
	Along Structure - to second bend	F	1.50	3352.42	1.47	3322.43	-0.89	-2.00
	Along Structure - Jetty Extension	G	1.69	8167.80	1.71	8331.47	2.00	1.18
	Entrance Channel	H	2.24	11600.55	2.36	12808.52	10.41	5.36
	Offshore	I	2.30	63712.47	2.26	60965.25	-4.31	-1.74
3	750' Spur at offshore location, straight		Avg WH	Energy	Avg WH	Energy	% Energy	WH %
	Nearshore region from structure	A	1.93	4360.84	1.90	4237.73	-2.82	-1.55
	Nearshore region from A to erosion end	B	2.11	4899.04	2.04	4557.90	-6.96	-3.32
	Nearshore region - Ferry Beach	C	1.81	7635.26	1.83	7819.47	2.41	1.10
	Along Structure - Nearshore	D	2.30	6690.00	2.22	6246.08	-6.64	-3.48
	Along Structure - to first bend	E	2.20	10517.06	2.07	9867.55	-6.18	-5.91
	Along Structure - to second bend	F	1.50	3352.42	1.72	4238.89	26.44	14.67
	Along Structure - Jetty Extension	G	1.69	8167.80	1.77	8770.93	7.38	4.73
	Entrance Channel	H	2.24	11600.55	2.26	11763.45	1.40	0.89
	Offshore	I	2.30	63712.47	2.29	62769.68	-1.48	-0.43
4	500' Spur at inshore location, straight		Avg WH	Energy	Avg WH	Energy	% Energy	WH %
	Nearshore region from structure	A	1.93	4360.84	1.84	3952.84	-9.36	-4.66
	Nearshore region from A to erosion end	B	2.11	4899.04	2.02	4464.02	-8.88	-4.27
	Nearshore region - Ferry Beach	C	1.81	7635.26	1.77	7350.76	-3.73	-2.21
	Along Structure - Nearshore	D	2.30	6690.00	1.93	4914.66	-26.54	-16.09
	Along Structure - to first bend	E	2.20	10517.06	2.32	11574.29	10.05	5.45
	Along Structure - to second bend	F	1.50	3352.42	1.65	3886.56	15.93	10.00
	Along Structure - Jetty Extension	G	1.69	8167.80	1.77	8820.78	7.99	4.73
	Entrance Channel	H	2.24	11600.55	2.24	11644.67	0.38	0.00
	Offshore	I	2.30	63712.47	2.31	63915.93	0.32	0.43
5	Dual 500' Spurs		Avg WH	Energy	Avg WH	Energy	% Energy	WH %
	Nearshore region from structure	A	1.93	4360.84	1.84	3977.23	-8.80	-4.66
	Nearshore region from A to erosion end	B	2.11	4899.04	2.05	4591.19	-6.28	-2.84
	Nearshore region - Ferry Beach	C	1.81	7635.26	1.78	7439.00	-2.57	-1.66
	Along Structure - Nearshore	D	2.30	6690.00	1.91	4808.01	-28.13	-16.96
	Along Structure - to first bend	E	2.20	10517.06	2.30	11353.58	7.95	4.55
	Along Structure - to second bend	F	1.50	3352.42	1.59	3599.76	7.38	6.00
	Along Structure - Jetty Extension	G	1.69	8167.80	1.79	9183.55	12.44	5.92
	Entrance Channel	H	2.24	11600.55	2.28	11987.75	3.34	1.79
	Offshore	I	2.30	63712.47	2.31	64425.33	1.12	0.43

6	750' Spur at inshore location, straight		Avg WH	Energy	Avg WH	Energy	% Energy	WH %
	Nearshore region from structure	A	1.93	4360.84	1.84	4028.83	-7.61	-4.66
	Nearshore region from A to erosion end	B	2.11	4899.04	2.05	4624.98	-5.59	-2.84
	Nearshore region - Ferry Beach	C	1.81	7635.26	1.78	7417.89	-2.85	-1.66
	Along Structure - Nearshore	D	2.30	6690.00	1.59	3698.86	-44.71	-30.87
	Along Structure - to first bend	E	2.20	10517.06	2.41	12693.06	20.69	9.55
	Along Structure - to second bend	F	1.50	3352.42	1.74	4311.40	28.61	16.00
	Along Structure - Jetty Extension	G	1.69	8167.80	1.81	9162.28	12.18	7.10
	Entrance Channel	H	2.24	11600.55	2.28	11951.42	3.02	1.79
	Offshore	I	2.30	63712.47	2.29	63230.97	-0.76	-0.43
7	750' Spur at inshore location, straight with Jetty Ext. Removal		Avg WH	Energy	Avg WH	Energy	% Energy	WH %
	Nearshore region from structure	A	1.93	4360.84	1.85	4050.96	-7.11	-4.15
	Nearshore region from A to erosion end	B	2.11	4899.04	2.05	4627.21	-5.55	-2.84
	Nearshore region - Ferry Beach	C	1.81	7635.26	1.77	7381.68	-3.32	-2.21
	Along Structure - Nearshore	D	2.30	6690.00	1.59	3717.54	-44.43	-30.87
	Along Structure - to first bend	E	2.20	10517.06	2.41	12692.61	20.69	9.55
	Along Structure - to second bend	F	1.50	3352.42	1.74	4316.32	28.75	16.00
	Along Structure - Jetty Extension	G	1.69	8167.80	1.80	9107.39	11.50	6.51
	Entrance Channel	H	2.24	11600.55	2.34	12692.38	9.41	4.46
	Offshore	I	2.30	63712.47	2.29	63121.14	-0.93	-0.43
8	750' Spur at inshore location, straight with Terminal Groin		Avg WH	Energy	Avg WH	Energy	% Energy	WH %
	Nearshore region from structure	A	1.93	4360.84	1.84	4017.47	-7.87	-4.66
	Nearshore region from A to erosion end	B	2.11	4899.04	2.05	4624.88	-5.60	-2.84
	Nearshore region - Ferry Beach	C	1.81	7635.26	1.77	7404.60	-3.02	-2.21
	Along Structure - Nearshore	D	2.30	6690.00	1.59	3704.65	-44.62	-30.87
	Along Structure - to first bend	E	2.20	10517.06	2.41	12682.66	20.59	9.55
	Along Structure - to second bend	F	1.50	3352.42	1.74	4311.16	28.60	16.00
	Along Structure - Jetty Extension	G	1.69	8167.80	1.80	9140.16	11.90	6.51
	Entrance Channel	H	2.24	11600.55	2.28	11956.57	3.07	1.79
	Offshore	I	2.30	63712.47	2.29	63220.11	-0.77	-0.43
9	T-Heads, 1st Configuration		Avg WH	Energy	Avg WH	Energy	% Energy	WH %
	Nearshore region from structure	A	1.93	4360.84	1.78	4080.92	-6.42	-7.77
	Nearshore region from A to erosion end	B	2.11	4899.04	1.95	4697.30	-4.12	-7.58
	Nearshore region - Ferry Beach	C	1.81	7635.26	1.82	7744.82	1.43	0.55
	Along Structure - Nearshore	D	2.30	6690.00	2.31	6729.75	0.59	0.43
	Along Structure - to first bend	E	2.20	10517.06	2.21	10560.38	0.41	0.45
	Along Structure - to second bend	F	1.50	3352.42	1.52	3431.10	2.35	1.33
	Along Structure - Jetty Extension	G	1.69	8167.80	1.70	8234.29	0.81	0.59
	Entrance Channel	H	2.24	11600.55	2.25	11671.76	0.61	0.45
	Offshore	I	2.30	63712.47	2.32	64468.36	1.19	0.87
10	T-Heads, 2nd Configuration		Avg WH	Energy	Avg WH	Energy	% Energy	WH %
	Nearshore region from structure	A	1.93	4360.84	1.86	4448.92	2.02	-3.63
	Nearshore region from A to erosion end	B	2.11	4899.04	1.98	4903.03	0.08	-6.16
	Nearshore region - Ferry Beach	C	1.81	7635.26	1.78	7799.50	2.15	-1.66
	Along Structure - Nearshore	D	2.30	6690.00	2.36	7136.37	6.67	2.61
	Along Structure - to first bend	E	2.20	10517.06	2.23	10875.81	3.41	1.36
	Along Structure - to second bend	F	1.50	3352.42	1.53	3485.58	3.97	2.00
	Along Structure - Jetty Extension	G	1.69	8167.80	1.71	8308.73	1.73	1.18
	Entrance Channel	H	2.24	11600.55	2.27	11867.97	2.31	1.34
	Offshore	I	2.30	63712.47	2.33	64925.46	1.90	1.30

11	Breakwater, Offshore Location		Avg WH	Energy	Avg WH	Energy	% Energy	WH %
	Nearshore region from structure	A	1.93	4360.84	1.74	3529.09	-19.07	-9.84
	Nearshore region from A to erosion end	B	2.11	4899.04	2.03	4459.74	-8.97	-3.79
	Nearshore region - Ferry Beach	C	1.81	7635.26	1.79	7511.67	-1.62	-1.10
	Along Structure - Nearshore	D	2.30	6690.00	1.78	3991.58	-40.34	-22.61
	Along Structure - to first bend	E	2.20	10517.06	1.58	5512.87	-47.58	-28.18
	Along Structure - to second bend	F	1.50	3352.42	1.32	2599.81	-22.45	-12.00
	Along Structure - Jetty Extension	G	1.69	8167.80	1.70	8185.05	0.21	0.59
	Entrance Channel	H	2.24	11600.55	2.23	11558.32	-0.36	-0.45
	Offshore	I	2.30	63712.47	1.94	47419.02	-25.57	-15.65
11a	Breakwater, Nearshore Location		Avg WH	Energy	Avg WH	Energy	% Energy	WH %
	Nearshore region from structure	A	1.93	4360.84	1.68	3396.76	-22.11	-12.95
	Nearshore region from A to erosion end	B	2.11	4899.04	1.67	3059.83	-37.54	-20.85
	Nearshore region - Ferry Beach	C	1.81	7635.26	1.83	7825.27	2.49	1.10
	Along Structure - Nearshore	D	2.30	6690.00	2.32	6923.62	3.49	0.87
	Along Structure - to first bend	E	2.20	10517.06	2.21	10775.79	2.46	0.45
	Along Structure - to second bend	F	1.50	3352.42	1.52	3452.18	2.98	1.33
	Along Structure - Jetty Extension	G	1.69	8167.80	1.76	8862.88	8.51	4.14
	Entrance Channel	H	2.24	11600.55	2.27	11905.15	2.63	1.34
	Offshore	I	2.30	63712.47	2.33	67958.71	6.66	1.30
11b	Breakwater, Middle Location		Avg WH	Energy	Avg WH	Energy	% Energy	WH %
	Nearshore region from structure	A	1.93	4360.84	1.87	4036.25	-7.44	-3.11
	Nearshore region from A to erosion end	B	2.11	4899.04	1.88	3874.78	-20.91	-10.90
	Nearshore region - Ferry Beach	C	1.81	7635.26	1.81	7726.56	1.20	0.00
	Along Structure - Nearshore	D	2.30	6690.00	1.97	4959.26	-25.87	-14.35
	Along Structure - to first bend	E	2.20	10517.06	1.98	8395.99	-20.17	-10.00
	Along Structure - to second bend	F	1.50	3352.42	1.49	3366.43	0.42	-0.67
	Along Structure - Jetty Extension	G	1.69	8167.80	1.70	8182.18	0.18	0.59
	Entrance Channel	H	2.24	11600.55	2.26	11823.41	1.92	0.89
	Offshore	I	2.30	63712.47	2.07	55529.77	-12.84	-10.00
12	Breakwater, Nearshore Location and 500' Spur at Offshore Location		Avg WH	Energy	Avg WH	Energy	% Energy	WH %
	Nearshore region from structure	A	1.93	4360.84	1.70	3488.04	-20.01	-11.92
	Nearshore region from A to erosion end	B	2.11	4899.04	1.56	2739.14	-44.09	-26.07
	Nearshore region - Ferry Beach	C	1.81	7635.26	1.81	7717.25	1.07	0.00
	Along Structure - Nearshore	D	2.30	6690.00	2.29	6634.24	-0.83	-0.43
	Along Structure - to first bend	E	2.20	10517.06	2.13	10239.12	-2.64	-3.18
	Along Structure - to second bend	F	1.50	3352.42	1.70	4179.66	24.68	13.33
	Along Structure - Jetty Extension	G	1.69	8167.80	1.82	9352.06	14.50	7.69
	Entrance Channel	H	2.24	11600.55	2.28	12031.09	3.71	1.79
	Offshore	I	2.30	63712.47	2.31	67181.01	5.44	0.43
13	Comb Spur Groins		Avg WH	Energy	Avg WH	Energy	% Energy	WH %
	Nearshore region from structure	A	1.93	4360.84	1.75	3645.95	-16.39	-9.33
	Nearshore region from A to erosion end	B	2.11	4899.04	2.06	4666.69	-4.74	-2.37
	Nearshore region - Ferry Beach	C	1.81	7635.26	1.80	7562.86	-0.95	-0.55
	Along Structure - Nearshore	D	2.30	6690.00	2.15	6043.52	-9.66	-6.52
	Along Structure - to first bend	E	2.20	10517.06	2.04	9307.21	-11.50	-7.27
	Along Structure - to second bend	F	1.50	3352.42	1.48	3319.52	-0.98	-1.33
	Along Structure - Jetty Extension	G	1.69	8167.80	1.71	8282.46	1.40	1.18
	Entrance Channel	H	2.24	11600.55	2.25	11674.42	0.64	0.45
	Offshore	I	2.30	63712.47	2.29	62889.80	-1.29	-0.43

14	Offshore Borrow Location		Avg WH	Energy	Avg WH	Energy	% Energy	WH %
	Nearshore region from structure	A	1.93	4360.84	1.95	4428.21	1.54	1.04
	Nearshore region from A to erosion end	B	2.11	4899.04	2.11	4883.80	-0.31	0.00
	Nearshore region - Ferry Beach	C	1.81	7635.26	1.80	7621.68	-0.18	-0.55
	Along Structure - Nearshore	D	2.30	6690.00	2.28	6566.79	-1.84	-0.87
	Along Structure - to first bend	E	2.20	10517.06	2.20	10511.90	-0.05	0.00
	Along Structure - to second bend	F	1.50	3352.42	1.51	3371.16	0.56	0.67
	Along Structure - Jetty Extension	G	1.69	8167.80	1.70	8175.66	0.10	0.59
	Entrance Channel	H	2.24	11600.55	2.24	11606.88	0.05	0.00
	Offshore	I	2.30	63712.47	2.31	63985.77	0.43	0.43
15	750' Spur at offshore location, angled		Avg WH	Energy	Avg WH	Energy	% Energy	WH %
	Nearshore region from structure	A	1.93	4360.84	1.91	4325.17	-0.82	-1.04
	Nearshore region from A to erosion end	B	2.11	4899.04	2.05	4596.08	-6.18	-2.84
	Nearshore region - Ferry Beach	C	1.81	7635.26	1.81	7665.56	0.40	0.00
	Along Structure - Nearshore	D	2.30	6690.00	2.06	5461.25	-18.37	-10.43
	Along Structure - to first bend	E	2.20	10517.06	2.17	10941.99	4.04	-1.36
	Along Structure - to second bend	F	1.50	3352.42	1.77	4547.90	35.66	18.00
	Along Structure - Jetty Extension	G	1.69	8167.80	1.81	9268.72	13.48	7.10
	Entrance Channel	H	2.24	11600.55	2.31	12269.47	5.77	3.12
	Offshore	I	2.30	63712.47	2.30	63355.13	-0.56	0.00
16	Jetty Roughening		Avg WH	Energy	Avg WH	Energy	% Energy	WH %
	Nearshore region from structure	A	1.93	4360.84	1.74	3597.66	-17.50	-9.84
	Nearshore region from A to erosion end	B	2.11	4899.04	2.04	4551.12	-7.10	-3.32
	Nearshore region - Ferry Beach	C	1.81	7635.26	1.77	7370.39	-3.47	-2.21
	Along Structure - Nearshore	D	2.30	6690.00	2.05	5575.18	-16.66	-10.87
	Along Structure - to first bend	E	2.20	10517.06	1.88	8067.29	-23.29	-14.55
	Along Structure - to second bend	F	1.50	3352.42	1.37	2773.35	-17.27	-8.67
	Along Structure - Jetty Extension	G	1.69	8167.80	1.70	8171.59	0.05	0.59
	Entrance Channel	H	2.24	11600.55	2.24	11640.97	0.35	0.00
	Offshore	I	2.30	63712.47	2.26	61089.62	-4.12	-1.74
17	Submerged Breakwater		Avg WH	Energy	Avg WH	Energy	% Energy	WH %
	Nearshore region from structure	A	1.93	4360.84	1.92	4329.96	-0.71	-0.52
	Nearshore region from A to erosion end	B	2.11	4899.04	2.08	4785.27	-2.32	-1.42
	Nearshore region - Ferry Beach	C	1.81	7635.26	1.82	7772.16	1.79	0.55
	Along Structure - Nearshore	D	2.30	6690.00	2.27	6511.88	-2.66	-1.30
	Along Structure - to first bend	E	2.20	10517.06	2.12	9841.36	-6.42	-3.64
	Along Structure - to second bend	F	1.50	3352.42	1.45	3134.16	-6.51	-3.33
	Along Structure - Jetty Extension	G	1.69	8167.80	1.69	8153.93	-0.17	0.00
	Entrance Channel	H	2.24	11600.55	2.24	11630.22	0.26	0.00
	Offshore	I	2.30	63712.47	2.26	61579.32	-3.35	-1.74
18	Breakwater, Nearshore Location with 500' straight spur at inshore location		Avg WH	Energy	Avg WH	Energy	% Energy	WH %
	Nearshore region from structure	A	1.93	4360.84	1.51	2831.69	-35.07	-21.76
	Nearshore region from A to erosion end	B	2.11	4899.04	1.47	2412.61	-50.75	-30.33
	Nearshore region - Ferry Beach	C	1.81	7635.26	1.78	7419.35	-2.83	-1.66
	Along Structure - Nearshore	D	2.30	6690.00	1.90	4841.72	-27.63	-17.39
	Along Structure - to first bend	E	2.20	10517.06	2.34	12059.55	14.67	6.36
	Along Structure - to second bend	F	1.50	3352.42	1.66	3977.10	18.63	10.67
	Along Structure - Jetty Extension	G	1.69	8167.80	1.84	9575.33	17.23	8.88
	Entrance Channel	H	2.24	11600.55	2.27	11968.20	3.17	1.34
	Offshore	I	2.30	63712.47	2.32	67856.43	6.50	0.87
19	750' Spur with Jetty Roughening from spur to bend and partial ext. removal		Avg WH	Energy	Avg WH	Energy	% Energy	WH %
	Nearshore region from structure	A	1.93	4360.84	1.84	4035.39	-7.46	-4.66
	Nearshore region from A to erosion end	B	2.11	4899.04	2.05	4590.81	-6.29	-2.84
	Nearshore region - Ferry Beach	C	1.81	7635.26	1.77	7348.04	-3.76	-2.21
	Along Structure - Nearshore	D	2.30	6690.00	1.57	3659.76	-45.30	-31.74
	Along Structure - to first bend	E	2.20	10517.06	2.18	10468.45	-0.46	-0.91
	Along Structure - to second bend	F	1.50	3352.42	1.55	3545.98	5.77	3.33
	Along Structure - Jetty Extension	G	1.69	8167.80	1.73	8483.92	3.87	2.37
	Entrance Channel	H	2.24	11600.55	2.33	12614.57	8.74	4.02
	Offshore	I	2.30	63712.47	2.26	61544.58	-3.40	-1.74

20	Case 11a with a salient formation		Avg WH	Energy	Avg WH	Energy	% Energy	WH %
	Nearshore region from structure	A	1.93	4360.84	1.57	2891.55	-33.69	-18.65
	Nearshore region from A to erosion end	B	2.11	4899.04	1.41	2267.42	-53.72	-33.18
	Nearshore region - Ferry Beach	C	1.81	7635.26	1.74	7085.42	-7.2	-3.87
	Along Structure - Nearshore	D	2.3	6690	2.25	6416.55	-4.09	-2.17
	Along Structure - to first bend	E	2.2	10517.06	2.19	10520.38	0.03	-0.45
	Along Structure - to second bend	F	1.5	3352.42	1.51	3384.38	0.95	0.67
	Along Structure - Jetty Extension	G	1.69	8167.8	1.76	8788.36	7.6	4.14
	Entrance Channel	H	2.24	11600.55	2.22	11568.71	-0.27	-0.89
	Offshore	I	2.3	63712.47	2.31	67272.19	5.59	0.43
22	750' Spur with Segmented BW (2)		Avg WH	Energy	Avg WH	Energy	% Energy	WH %
	Nearshore region from structure	A	1.93	4360.84	1.51	2789.32	-36.04	-21.76
	Nearshore region from A to erosion end	B	2.11	4899.04	1.96	4208.78	-14.09	-7.11
	Inshore region of area B	B2	1.94	1792.8	1.9	1721.088	-1.04	-2.06
	Nearshore region - Ferry Beach	C	1.81	7635.26	1.77	7353.55	-3.69	-2.21
	Along Structure - Nearshore	D	2.3	6690	1.51	3324.53	-50.31	-34.35
	Along Structure - to first bend	E	2.2	10517.06	2.42	12785.64	21.57	10.00
	Along Structure - to second bend	F	1.5	3352.42	1.76	4411.44	31.59	17.33
	Along Structure - Jetty Extension	G	1.69	8167.8	1.8	9074.75	11.1	6.51
	Entrance Channel	H	2.24	11600.55	2.28	11953.9	3.05	1.79
	Offshore	I	2.3	63712.47	2.34	66519.31	4.41	1.74
23	500' Spur with Segmented BW (3)		Avg WH	Energy	Avg WH	Energy	% Energy	WH %
	Nearshore region from structure	A	1.93	4360.84	1.39	2314.89	-46.92	-27.98
	Nearshore region from A to erosion end	B	2.11	4899.04	1.96	4292.71	-12.38	-7.11
	Inshore region of area B	B2	1.94	1792.8	1.91	1776.55	-0.91	-1.55
	Nearshore region - Ferry Beach	C	1.81	7635.26	1.77	7397.55	-3.11	-2.21
	Along Structure - Nearshore	D	2.3	6690	1.78	4353.57	-34.92	-22.61
	Along Structure - to first bend	E	2.2	10517.06	2.37	12284.14	16.8	7.73
	Along Structure - to second bend	F	1.5	3352.42	1.69	4103.02	22.39	12.67
	Along Structure - Jetty Extension	G	1.69	8167.8	1.8	9112.94	11.57	6.51
	Entrance Channel	H	2.24	11600.55	2.27	11886.64	2.47	1.34
	Offshore	I	2.3	63712.47	2.38	68939.26	8.2	3.48
24	Alt. 23 with additional northern BW		Avg WH	Energy	Avg WH	Energy	% Energy	WH %
	Nearshore region from structure	A	1.93	4360.84	1.4	2336.16	-46.43	-27.46
	Nearshore region from A to erosion end	B	2.11	4899.04	1.88	4153.92	-15.21	-10.90
	Inshore region of area B	B2	1.94	1792.8	1.66	1373.21	-23.4	-14.43
	Nearshore region - Ferry Beach	C	1.81	7635.26	1.77	7393.11	-3.17	-2.21
	Along Structure - Nearshore	D	2.3	6690	1.79	4365.93	-34.74	-22.17
	Along Structure - to first bend	E	2.2	10517.06	2.37	12246.46	16.44	7.73
	Along Structure - to second bend	F	1.5	3352.42	1.68	4051.58	20.86	12.00
	Along Structure - Jetty Extension	G	1.69	8167.8	1.8	9116.2	11.61	6.51
	Entrance Channel	H	2.24	11600.55	2.27	11870.7	2.33	1.34
	Offshore	I	2.3	63712.47	2.4	69657.02	9.33	4.35
25	Spur moved landward and 3 BW		Avg WH	Energy	Avg WH	Energy	% Energy	WH %
	Nearshore region from structure	A	1.93	4360.84	1.44	2494.3	-42.8	-25.39
	Nearshore region from A to erosion end	B	2.11	4899.04	1.72	3691.35	-24.65	-18.48
	Inshore region of area B	B2	1.94	1792.8	1.35	1054.51	-41.18	-30.41
	Nearshore region - Ferry Beach	C	1.81	7635.26	1.78	7467.25	-2.2	-1.66
	Along Structure - Nearshore	D	2.3	6690	1.99	5831.52	-12.83	-13.48
	Along Structure - to first bend	E	2.2	10517.06	2.3	11549.86	9.82	4.55
	Along Structure - to second bend	F	1.5	3352.42	1.64	4016.47	19.81	9.33
	Along Structure - Jetty Extension	G	1.69	8167.8	1.77	8871.04	8.61	4.73
	Entrance Channel	H	2.24	11600.55	2.29	12086.47	4.19	2.23
	Offshore	I	2.3	63712.47	2.38	68735.59	7.88	3.48
26	Case 24 with add. longer northern BW		Avg WH	Energy	Avg WH	Energy	% Energy	WH %
	Nearshore region from structure	A	1.93	4360.84	1.39	2305.89	-47.12	-27.98
	Nearshore region from A to erosion end	B	2.11	4899.04	1.76	3905.17	-20.29	-16.59
	Inshore region of area B	B2	1.94	1792.8	1.38	1075.55	-40.01	-28.87
	Nearshore region - Ferry Beach	C	1.81	7635.26	1.78	7416.41	-2.87	-1.66
	Along Structure - Nearshore	D	2.3	6690	1.78	4327.33	-35.32	-22.61
	Along Structure - to first bend	E	2.2	10517.06	2.37	12258.03	16.55	7.73
	Along Structure - to second bend	F	1.5	3352.42	1.69	4090.75	22.02	12.67
	Along Structure - Jetty Extension	G	1.69	8167.8	1.79	9030.57	10.56	5.92
	Entrance Channel	H	2.24	11600.55	2.27	11871.94	2.34	1.34
	Offshore	I	2.3	63712.47	2.41	70211.52	10.2	4.78
Positive Value = Increase ; Negative Value = Decrease								
WH = Wave Height in Meters, Energy in Meters Squared								

APPENDIX 13-C

Table 13-C1. Beach nourishment performance assuming a replenishment of approximately 80,000 cubic yards occurs every 10 years for beach nourishment alone, Alternative 6, Alternative 11a, and Alternative 18.

Years	Beach Nourish. Alone		Alt 6 – Spur jetty		Alt 11 - Breakwater		Alt 18 – Breakwater/Spur	
	% Remaining	*Volume (cy)*	*% Remaining*	*Volume (cy)*	*% Remaining*	*Volume (cy)*	*% Remaining*	*Volume (cy)*
1*	75.07%	225197	81.57%	244718	81.01%	243015	86.26%	258792
2	64.31%	192929	73.37%	220117	72.82%	218467	80.27%	240820
5*	44.99%	134960	56.80%	170412	56.98%	170951	67.94%	203829
10	27.31%	81933	39.56%	118675	41.75%	125251	54.18%	162541
10	*53.98%*	*161933*	*66.23%*	*198675*	*68.42%*	*205251*	*80.85%*	*242541*
11	44.97%	134900	58.89%	176668	61.25%	183757	75.13%	225379
12	39.90%	119708	54.44%	163327	57.14%	171406	71.60%	214805
15	28.91%	86723	44.00%	131993	47.87%	143610	63.17%	189519
20	16.06%	48169	31.05%	93159	37.10%	111312	52.47%	157424
20	*42.72%*	*128169*	*57.72%*	*173159*	*63.77%*	*191312*	*79.14%*	*237424*
21	34.20%	102597	50.86%	152579	57.09%	171273	73.79%	221380
22	29.54%	88620	46.82%	140446	53.38%	160150	70.59%	211772
25	19.42%	58247	37.26%	111770	45.01%	135041	62.89%	188678
30	7.35%	22057	25.14%	75420	35.08%	105237	52.90%	158709
30	*34.02%*	*102057*	*51.81%*	*155420*	*61.75%*	*185237*	*79.57%*	*238709*
31	25.59%	76784	45.05%	135158	55.17%	165517	74.31%	222942
32	21.02%	63067	41.10%	123301	51.56%	154672	71.19%	213575
35	11.10%	33287	31.75%	95259	43.40%	130197	63.68%	191028
40	-0.78%	0	19.84%	59508	33.66%	100994	53.85%	161555
40	*25.89%*	*77665*	*46.50%*	*139508*	*60.33%*	*180994*	*80.52%*	*241555*
41	17.49%	52463	39.77%	119319	53.78%	161349	75.28%	225844
42	12.94%	38806	35.84%	107524	50.19%	150565	72.17%	216521
45	3.05%	9154	26.54%	79606	42.07%	126218	64.68%	194050
50	-8.79%	0	14.64%	43919	32.36%	97088	54.86%	164567

* = Partial Salient formed at year 1, and Full Salient formed at year 5. Gray rows indicate dredging/nourishment (80,000 cy).

Table 13-C2. Beach nourishment performance assuming a replenishment of approximately 80,000 cubic yards occurs every 10 years for beach nourishment alone, Alternative 23, Alternative 25, and Alternative 26.

Years	Beach Nourish. Alone		Alt 23 – Seg. Breakwater 2		Alt 25 – Seg. Breakwater 4		Alt 26 – Seg. Breakwater 5	
	% Remaining	*Volume (cy)*	*% Remaining*	*Volume (cy)*	*% Remaining*	*Volume (cy)*	*% Remaining*	*Volume (cy)*
1*	75.07%	225197	83.38%	250146	88.05%	264151	87.49%	262470
2	64.31%	192929	76.02%	228057	82.83%	248498	82.05%	246141
5*	44.99%	134960	60.93%	182796	72.03%	216099	70.82%	212474
10	27.31%	81933	44.75%	134252	59.54%	178610	58.03%	174077
10	*53.98%*	*161933*	*71.42%*	*214252*	*86.20%*	*258610*	*84.69%*	*254077*
11	44.97%	134900	64.67%	194002	81.09%	243259	79.40%	238197
12	39.90%	119708	60.54%	181615	77.87%	233619	76.11%	228321
15	28.91%	86723	50.75%	152240	70.07%	210220	68.17%	204518
20	16.06%	48169	38.49%	115469	59.90%	179709	57.95%	173859
20	*42.72%*	*128169*	*65.16%*	*195469*	*86.57%*	*259709*	*84.62%*	*253859*
21	34.20%	102597	58.86%	176567	81.74%	245234	79.65%	238945
22	29.54%	88620	55.11%	165330	78.79%	236359	76.64%	229907
25	19.42%	58247	46.17%	138509	71.57%	214719	69.34%	208026
30	7.35%	22057	34.72%	104155	61.98%	185943	59.75%	179252
30	*34.02%*	*102057*	*61.39%*	*184155*	*88.65%*	*265943*	*86.42%*	*259252*
31	25.59%	76784	55.19%	165565	83.90%	251694	81.53%	244583
32	21.02%	63067	51.53%	154599	81.00%	243014	78.59%	235759
35	11.10%	33287	42.80%	128397	73.94%	221812	71.45%	214358
40	-0.78%	0	31.54%	94625	64.47%	193406	62.00%	186005
40	*25.89%*	*77665*	*58.21%*	*174625*	*91.14%*	*273406*	*88.67%*	*266005*
41	17.49%	52463	52.03%	156104	86.40%	259192	83.79%	251379
42	12.94%	38806	48.40%	145196	83.51%	250538	80.86%	242588
45	3.05%	9154	39.70%	119108	76.45%	229362	73.74%	221234
50	-8.79%	0	28.46%	85382	66.96%	200876	64.28%	192827

* = Partial Salient formed at year 1, and Full Salient formed at year 5. Gray rows indicate dredging/nourishment (80,000 cy).

Table 13-C3. Required beach replenishment time frames to ensure minimal amount of beach for storm damage protection. Beach is replenished to 100% (300,000 cubic yards) when only 30% (approximately) of the original nourishment remains. Re-nourishment is included in Year 50 to return the beach to 100% independent of the amount of material remaining. All of the final alternatives are presented (including Alternative 23 and beach nourishment alone, for comparative purposes).

Alternative	Years after initial fill	Volume required (cubic yards)
Beach Nourishment Alone	Year 9	209,461
	Year 18	209,461
	Year 27	209,461
	Year 36	209,461
	Year 45	209,461
	Year 50	149,569
Alt. 6 – Spur Jetty	Year 14	210,903
	Year 28	210,903
	Year 42	210,903
	Year 50	163,380
Alt. 11a - Breakwater	Year 15	208,908
	Year 30	208,908
	Year 45	208,908
	Year 50	134,022
Alt. 18 – Breakwater and Spur Jetty	Year 22	204,915
	Year 44	204,915
	Year 50	112,044
Alt. 23 – Segmented Breakwaters, Configuration 3	Year 17	211,253
	Year 34	211,253
	Year 50	205,643
Alt. 25 – Segmented Breakwaters, Configuration 4	Year 31	209,981
	Year 50	167,436
Alt. 26 – Segmented Breakwaters, Configuration 5	Year 30	210,898
	Year 50	176,127

Table 13-C4. Estimated downdrift impacts and nourishment requirements for Alternative 9 (T-Head groins). Assumes no replenishment in T-Head groin field, and based on 100,000 cubic yards of material for neighboring beaches.

Year after instillation of Alt. 9	Volume required on downdrift beaches (cubic yards)
Year 6	Approx. 100,000
Year 12	Approx. 100,000
Year 18	Approx. 100,000
Year 24	Approx. 100,000
Year 30	Approx. 100,000
Year 36	Approx. 100,000
Year 42	Approx. 100,000
Year 48	Approx. 100,000
Year 50	Approx. 100,000